

# TMD Handbook

A modern introduction to the physics of  
Transverse Momentum Dependent distributions



Renaud Boussarie  
Matthias Burkardt  
Martha Constantinou  
William Detmold  
Markus Ebert  
Michael Engelhardt  
Sean Fleming  
Leonard Gamberg  
Xiangdong Ji  
Zhong-Bo Kang  
Christopher Lee  
Keh-Fei Liu  
Simonetta Liuti  
Thomas Mehen  
Andreas Metz  
John Negele  
Daniel Pitonyak  
Alexei Prokudin  
Jian-Wei Qiu  
Abha Rajan  
Marc Schlegel  
Phiala Shanahan  
Peter Schweitzer  
Iain W. Stewart  
Andrey Tarasov  
Raju Venugopalan  
Ivan Vitev  
Feng Yuan  
Yong Zhao

Preprint numbers:  
JLab-Thy-2018-#  
MIT-CTP 5386  
LA-UR-21-20798



Renaud Boussarie<sup>11,20</sup>, Matthias Burkardt<sup>1</sup>, Martha Constantinou<sup>2</sup>, William Detmold<sup>3</sup>, Markus Ebert<sup>3</sup>, Michael Engelhardt<sup>1</sup>, Sean Fleming<sup>4</sup>, Leonard Gamberg<sup>5</sup>, Xiangdong Ji<sup>6</sup>, Zhong-Bo Kang<sup>7</sup>, Christopher Lee<sup>8</sup>, Keh-Fei Liu<sup>9</sup>, Simonetta Liuti<sup>14</sup>, Thomas Mehen<sup>10</sup>, Andreas Metz<sup>2</sup>, John Negele<sup>3</sup>, Daniel Pitonyak<sup>17,5,12</sup>, Alexei Prokudin<sup>5,16</sup>, Jian-Wei Qiu<sup>16,21</sup>, Abha Rajan<sup>12</sup>, Marc Schlegel<sup>1</sup>, Phiala Shanahan<sup>3</sup>, Peter Schweitzer<sup>15</sup>, Iain W. Stewart<sup>3</sup>, Andrey Tarasov<sup>18,19</sup>, Raju Venugopalan<sup>11</sup>, Ivan Vitev<sup>8</sup>, Feng Yuan<sup>13</sup>, Yong Zhao<sup>3,11,22</sup>

<sup>1</sup>*Department of Physics, New Mexico State University, Las Cruces, NM 88003*

<sup>2</sup>*Department of Physics, Temple University, Philadelphia, PA 19122 - 1801, USA*

<sup>3</sup>*Center for Theoretical Physics, Massachusetts Institute of Technology, Cambridge, MA 02139*

<sup>4</sup>*Department of Physics and Astronomy, University of Arizona, Tucson, AZ 85721*

<sup>5</sup>*Division of Science, Penn State University Berks,  
Reading, PA 19610*

<sup>6</sup>*University of Maryland*

<sup>7</sup>*University of California at Los Angeles*

<sup>8</sup>*Theoretical Division, Los Alamos National Laboratory, Los Alamos, NM 87545*

<sup>9</sup>*University of Kentucky*

<sup>10</sup>*Department of Physics, Duke University, Durham, NC 27708*

<sup>11</sup>*Physics Department, Brookhaven National Laboratory, Upton, NY 11973*

<sup>12</sup>*Old Dominion University*

<sup>13</sup>*Lawrence Berkeley National Laboratory*

<sup>14</sup>*University of Virginia*

<sup>15</sup>*Department of Physics, University of Connecticut, Storrs, CT 06269*

<sup>16</sup>*Theory Center, Jefferson Lab, Newport News, Virginia 23606*

<sup>17</sup>*Department of Physics, Lebanon Valley College, Annville, Pennsylvania 17003*

<sup>18</sup>*Department of Physics, The Ohio State University, Columbus, OH 43210*

<sup>19</sup>*Joint BNL-SBU Center for Frontiers in Nuclear Science (CFNS) at Stony Brook University, Stony Brook, NY 11794*

<sup>20</sup>*Centre de Physique Theorique, Ecole polytechnique, CNRS, I.P. Paris, F-91128 Palaiseau, France*

<sup>21</sup>*Department of Physics, William & Mary, Williamsburg, Virginia 23187*

<sup>22</sup>*Physics Division, Argonne National Laboratory, Lemont, IL 60439*

# Contents

<b>1</b>	<b>Introduction</b>	<b>8</b>
1.1	Hadrons, Partons and QCD . . . . .	9
1.2	Structure of the Nucleon . . . . .	13
1.3	Matching Cross Section to the Structure . . . . .	15
1.4	Calculation of Hadron Structure in Lattice QCD . . . . .	20
1.5	Guide to Reading the Handbook . . . . .	21
<b>2</b>	<b>Definition of TMDs</b>	<b>25</b>
2.1	Basic Ideas from the Parton Model . . . . .	25
2.2	TMD Factorization Theorem for Drell-Yan . . . . .	33
2.3	Basic Definition of TMD PDFs . . . . .	37
2.4	Definitions with Rapidity Regulators . . . . .	41
2.4.1	Overview of rapidity regulators . . . . .	42
2.4.2	Illustration at one loop . . . . .	45
2.5	Additional TMD PDF definitions . . . . .	53
2.6	TMD Fragmentation Functions . . . . .	56
2.7	Quark and Gluon Spin Dependent TMDs and FFs . . . . .	59
2.7.1	Universality of TMD PDFs and TMD FFs . . . . .	61
2.7.2	Leading Quark TMD PDFs . . . . .	63
2.7.3	Leading Quark TMD FFs . . . . .	67
2.7.4	Leading Gluon TMD PDFs . . . . .	70
2.7.5	Leading Gluon TMD FFs . . . . .	72
2.8	TMD PDFs and TMD FFs at small $b_T$ . . . . .	74
2.9	Relating Integrated TMDs to Collinear Functions . . . . .	79
2.10	Connection to Lattice QCD . . . . .	82
2.10.1	Lorentz-invariant approach . . . . .	83
2.10.2	Large-momentum effective theory . . . . .	85
2.10.3	Relations between lattice and continuum TMDs . . . . .	87
2.11	Complete TMD Factorization for DY, SIDIS, and $e^+e^-$ . . . . .	87
2.11.1	Polarized Drell-Yan cross section . . . . .	87
2.11.2	Higgs production in gluon fusion . . . . .	91
2.11.3	Polarized SIDIS cross section . . . . .	93
2.11.4	Back-to-back hadron production in $e^+e^-$ . . . . .	96
2.11.5	TMD cross sections for other processes . . . . .	98
<b>3</b>	<b>Factorization Theorems</b>	<b>99</b>
3.1	Factorization Basics . . . . .	99
3.2	Elements of Factorization . . . . .	99
3.2.1	Region analysis . . . . .	100
3.2.2	Approximations . . . . .	101
3.2.3	The Glauber region . . . . .	102

3.2.4	Inclusivity of processes . . . . .	103
3.2.5	Last steps . . . . .	103
3.3	Process Dependence . . . . .	103
3.4	Factorization Violations . . . . .	104
3.5	Factorization in SCET . . . . .	105
<b>4</b>	<b>Evolution and Resummation</b>	<b>109</b>
4.1	Introduction . . . . .	109
4.1.1	Historical overview . . . . .	110
4.2	TMD Evolution and Resummation . . . . .	111
4.2.1	The goal of resummation . . . . .	111
4.2.2	A first glance at resummation from evolution . . . . .	113
4.3	TMD Evolution . . . . .	114
4.3.1	One-loop examples . . . . .	118
4.4	CSS Formalism . . . . .	120
4.4.1	The CSS Solution . . . . .	120
4.4.2	Ji-Ma-Yuan scheme . . . . .	123
4.5	Evolution in SCET . . . . .	124
4.5.1	RG and RRG . . . . .	125
4.5.2	Combined TMD PDF evolution . . . . .	127
4.5.3	RG and RRG solutions . . . . .	128
4.6	Two-Dimensional Evolution . . . . .	131
4.7	Connecting Resummation to Fixed Order . . . . .	133
4.8	Resummation in Momentum Space . . . . .	139
4.9	Summary and Outlook . . . . .	147
<b>5</b>	<b>Phenomenology and Extraction of TMDs</b>	<b>149</b>
5.1	Introduction: Historical Perspective . . . . .	149
5.2	Unpolarized Observables . . . . .	151
5.2.1	SIDIS multiplicities . . . . .	151
5.2.2	Drell-Yan and weak gauge boson production . . . . .	159
5.3	Polarized Observables . . . . .	161
5.3.1	Sivers effect in SIDIS and DY . . . . .	161
5.3.2	Collins effect in SIDIS and $e^+e^-$ annihilation . . . . .	167
5.3.3	$A_N$ in proton-proton collision . . . . .	171
5.4	Boer-Mulders Effect . . . . .	174
5.5	Worm-gear $g_{1T}^\perp$ and $h_{1L}^\perp$ and Pretzelosity $h_{1T}^\perp$ TMD PDFs . . . . .	176
5.6	Observables for Gluon TMDs . . . . .	179
5.6.1	Gluon TMDs from proton-proton collisions . . . . .	180
5.6.2	Gluon TMDs in lepton-nucleon collisions . . . . .	184
5.7	TMDs in Nuclei . . . . .	185
5.8	Importance of QED Corrections to SIDIS for Extracting TMDs . . . . .	186
5.9	Outlook and Future Work . . . . .	188

<b>6 Lattice QCD calculations of TMDs and related aspects of hadron structure</b>	<b>190</b>
6.1 Lattice QCD . . . . .	190
6.2 Lattice Hadron Structure . . . . .	193
6.2.1 Static structure of hadrons . . . . .	193
6.2.2 Decomposition of the proton momentum and spin . . . . .	195
6.3 Structure Functions and PDFs . . . . .	199
6.3.1 Hadronic tensor . . . . .	199
6.3.2 Quasi-PDFs in large-momentum effective theory approach . . . . .	203
6.3.3 Pseudo-distributions . . . . .	212
6.3.4 Current-current correlator . . . . .	213
6.3.5 Good lattice cross sections . . . . .	214
6.3.6 Comparison of methods . . . . .	215
6.4 Lattice QCD Calculations of TMD Observables . . . . .	216
6.4.1 Lorentz-invariant approach . . . . .	216
6.4.2 Calculation of TMD soft function and TMDPDF . . . . .	227
6.4.3 Lattice QCD input to TMD evolution . . . . .	229
6.4.4 Summary . . . . .	231
<b>7 Models</b>	<b>233</b>
7.1 Why Models? . . . . .	233
7.2 The Brodsky-Hwang-Schmidt Calculation of a Transverse SSA . . . . .	233
7.3 Limits in QCD . . . . .	235
7.3.1 The parton model . . . . .	235
7.3.2 The large- $N_c$ limit . . . . .	236
7.3.3 Non-relativistic limit . . . . .	236
7.4 Modelling of T-even TMD PDFs . . . . .	237
7.4.1 Covariant parton model . . . . .	237
7.4.2 Bag model . . . . .	239
7.4.3 Lightfront constituent quark models . . . . .	239
7.4.4 Spectator models . . . . .	240
7.4.5 NJL framework . . . . .	240
7.4.6 AdS/QCD inspired models . . . . .	240
7.4.7 Chiral quark soliton model . . . . .	241
7.4.8 Predictions from quark models for T-even TMD PDFs . . . . .	241
7.5 Modelling of T-odd TMDs PDFs . . . . .	246
7.5.1 A no-go theorem . . . . .	246
7.5.2 Including gauge field degrees of freedom . . . . .	246
7.5.3 Quark-target model . . . . .	246
7.5.4 Lensing function . . . . .	247
7.5.5 Augmented LCWFs, eikonal methods, instantons and other approaches	247
7.5.6 Predictions from quark models for T-odd TMD PDFs . . . . .	248
7.6 Gluon TMDs . . . . .	249
7.7 Quark TMD Fragmentation Functions . . . . .	250
7.7.1 Spectator models for TMDFFs . . . . .	250
7.7.2 Models for multi-step fragmentation process . . . . .	252

7.7.3	Combining models for FFs . . . . .	253
7.7.4	Universality of TMD fragmentation functions . . . . .	254
7.8	Formal Constraints on TMD Functions . . . . .	255
7.8.1	Positivity constraints . . . . .	255
7.8.2	Burkardt sum rule . . . . .	256
7.8.3	Schäfer-Teryaev sum rule . . . . .	257
7.9	Relations in Models . . . . .	257
7.9.1	Independence of TMD PDFs in QCD . . . . .	257
7.9.2	Quark-model Lorentz-invariance relations . . . . .	258
7.9.3	Relations among TMDs in quark models . . . . .	259
7.9.4	Connection of pretzelosity to orbital angular momentum . . . . .	261
7.10	Summary and Outlook . . . . .	261
<b>8</b>	<b>Small-<math>x</math> TMDs</b>	<b>263</b>
8.1	Gluon Saturation and TMDs at Small $x$ . . . . .	263
8.2	Weizsäcker-Williams and Dipole Gluon Distributions . . . . .	268
8.3	TMD Evolution and Resummation . . . . .	270
8.4	Spin-dependent TMDs . . . . .	272
8.5	Saturation and Multiple Scattering Effects for TMDs . . . . .	277
8.6	Outlook . . . . .	279
<b>9</b>	<b>Jet Fragmentation</b>	<b>281</b>
9.1	Jets as Probes of TMD PDFs . . . . .	282
9.2	Jet Substructure and Jet Fragmentation . . . . .	286
9.3	Hadron longitudinal distribution inside jets: $z_h$ dependence . . . . .	287
9.4	Hadron transverse momentum distribution inside jets: $j_{\perp}$ -dependence . . . . .	289
9.4.1	Polarized jet fragmentation functions . . . . .	290
9.5	Jets with Heavy Quarkonium . . . . .	291
9.6	Transverse Energy-Energy Correlations . . . . .	293
9.7	Medium Modification of Jets . . . . .	296
9.7.1	Jet cross sections . . . . .	300
9.7.2	Jet substructure . . . . .	302
9.8	Outlook . . . . .	306
<b>10</b>	<b>Subleading TMDs</b>	<b>308</b>
10.1	Introduction . . . . .	308
10.2	Observables for Subleading TMDs . . . . .	309
10.3	Subleading TMD Distribution Functions . . . . .	310
10.3.1	Quark-gluon-quark correlators . . . . .	310
10.3.2	Quark-quark correlators and equations of motion . . . . .	310
10.4	Factorization for SIDIS with Subleading Power TMDs . . . . .	312
10.4.1	Status of SIDIS factorization at next-to-leading power . . . . .	313
10.4.2	SIDIS structure functions in terms of next-to-leading power TMDs . . . . .	313
10.5	Experimental Results for NLP TMD Observables . . . . .	316
10.6	Estimating Subleading TMDs and Related Observables . . . . .	317

10.6.1	Generalized scalar charge from lattice QCD . . . . .	317
10.6.2	Model calculations of subleading TMDs . . . . .	318
10.6.3	Model calculations of subleading-power observables . . . . .	321
10.7	Summary and Outlook . . . . .	322
<b>11</b>	<b>Generalized TMDs and Wigner Phase Space Distributions</b>	<b>331</b>
11.1	Wigner Distributions . . . . .	332
11.2	Momentum Space Definition – Generalized TMDs (GTMDs) . . . . .	335
11.3	Observables for GTMDs . . . . .	337
11.4	Connection with Orbital Angular Momentum of Partons . . . . .	340
11.5	GTMD observables from LQCD: quark orbital angular momentum in the proton	345
11.6	Model results and their interpretation . . . . .	347
<b>12</b>	<b>Summary and Outlook</b>	<b>350</b>
<b>13</b>	<b>Acknowledgement</b>	<b>351</b>
<b>A</b>	<b>Glossary</b>	<b>352</b>
<b>B</b>	<b>Feynman rules</b>	<b>352</b>
<b>C</b>	<b>Fourier transforms</b>	<b>353</b>
C.1	Conventions for the TMD PDF . . . . .	353
C.2	Conventions for the TMD FF . . . . .	355
<b>D</b>	<b>Explicit definitions of TMD PDFs</b>	<b>356</b>
<b>E</b>	<b>Expansions for evolution kernels</b>	<b>360</b>
<b>List of acronyms</b>		<b>363</b>
<b>Erratum and Chapter Contact Emails</b>		<b>364</b>
<b>Index</b>		<b>365</b>

# 1 - Introduction

Nucleons are the fundamental building blocks of all atomic nuclei and make up essentially all the visible matter in the universe, including the stars, the planets, and us. However, the nucleon is not static but has a complex and dynamic internal structure, the details of which are only beginning to be revealed in modern experiments. A deeper understanding of this building block of matter therefore requires that we understand the nucleon's internal structure in terms of its constituents.

In Quantum Chromodynamics (QCD), the theory of the strong interactions, the nucleon emerges as a strongly interacting, relativistic bound state of quarks and gluons (referred to collectively as partons). Fifty years of experimental investigations into the nucleon's internal structure have provided remarkable insight into the dynamics of quarks and gluons [2]. However, many outstanding questions remain. This is largely because of the *color confinement* – a fundamental property of QCD. Even the most advanced detector can not see quarks and gluons in isolation as they are forever bound inside nucleons, or in general, in all hadrons. It is an unprecedented intellectual challenge to probe the quark-gluon dynamics, quantify the quark-gluon structure of hadrons, and study the emergence of hadrons from quarks and gluons, given that we can not see quarks and gluons directly by any modern tools.

On the other hand, QCD has another equally important and fundamental property, *asymptotic freedom* – the strong force is weakly coupled if it is probed at a sufficiently short-distance [3, 4]. It is asymptotic freedom that makes it possible for us to develop the powerful theoretical formalism, known as QCD factorization [5], that links the quarks and gluons at sub-femtometer scales to the hadrons measured by modern detectors in high energy experiments with a set of well-defined and fundamental distribution functions that encode rich information on nucleon's internal structure. It is the universality of these distribution functions and the precision that we can achieve in determining them from known experimental data that ensures the predictive power of QCD and allows us to explore and study the dynamics of quarks and gluons and the structure of the nucleon by performing experiments in which the nucleon receives large momentum transfers, even though we never "see" quarks and gluons directly. QCD along with its factorization formalism has been extremely successful in interpreting all available data from high energy scatterings when probing distances less than 0.1 fermi (fm) (or equivalently, with larger than 2 GeV momentum transfer in the collision), which has provided us the confidence and the tools to discover the Higgs particle at the LHC and to explore the new physics beyond QCD and the Standard Model in high energy hadronic collisions.

Interestingly, many typical hard probes for distance scales less than 0.1 fm in high energy scattering are not very sensitive to the confined spatial landscape and motion of quarks and gluons inside the bound nucleon with a radius about one fermi. For this reason, the results of generations of experiments have only provided one-dimensional snapshots of the longitudinal momentum distributions of quarks and gluons inside a colliding nucleon, utilizing the well-developed collinear QCD factorization formalism to encode them in universal parton distribution functions (PDFs). In recent years we have begun to capture more detailed information about nucleon structure due to our ability to precisely measure new types of observables in high energy scattering with two distinctive momentum scales: one hard scale with a large momentum transfer to pin down the particle nature of quarks and gluons along

with one soft scale to be sensitive to the confined motion and the spatial landscape of the quarks and gluons inside the nucleon. Most importantly, theoretical advances over the past decade have resulted in the development of a powerful transverse momentum dependent (TMD) QCD factorization formalism that enables us to extract the 3-dimensional (3D) motion of quarks and gluons inside a colliding nucleon. Information from these new and precise data enables the determination of universal transverse momentum dependent parton distributions (or simply, TMDs). With additional data from experiments around the world and the future Electron-Ion Collider (EIC) [15], a much sharper and detailed picture of the nucleon's internal landscape will become available to shed light on the dynamics of confined quarks and gluons that form the nucleon - the building block of our visible world.

In this TMD Handbook, we provide a modern introduction to the physics of transverse momentum dependent distributions – the TMDs, which encode the quantum correlations between hadron polarization and the motion and polarization of quarks and gluons inside it, as sketched in Fig. 1.1. We cover the precise definition of these fundamental and universal TMDs and their properties, the TMD factorization formalisms to match these quantum distributions to physical observables measured in high energy scattering experiments, and phenomenological approaches for extracting them from precise experimental data. We introduce new advances in ab initio lattice QCD (LQCD) calculations, as well as various model calculations of the TMDs. We discuss what we can learn from the TMDs to understand better how the dynamics of QCD determines the properties of the nucleon and its internal landscape. This TMD handbook is a project of the TMD Collaboration – a Topical Collaboration in Nuclear Theory for the Coordinated Theoretical Approach to Transverse Momentum Dependent Hadron Structure in QCD [<https://sites.google.com/a/lbl.gov/tmdwiki/>], supported by the Office of Nuclear Physics of the U.S. Department of Energy.

In the rest of this Chapter, we provide an intuitive introduction to the TMDs and their role in describing the hadron's internal structure, and the role of lattice QCD for calculating these intrinsically non-perturbative but fundamental distribution functions. An outline for the material in the remaining chapters of this handbook can be found in Sec. 1.5.

## 1.1 Hadrons, Partons and QCD

The discovery of the neutron by Chadwick in 1932 heralded the strong interactions, as a force much stronger than the electromagnetic Coulomb repulsion between the protons in a nucleus was needed to keep atomic nuclei together. In the twenty years following this discovery tremendous progress was made in understanding the interactions between two nucleons, however particle physics was still rather simple with the only additions being the pions ( $\pi$ ) as expected from Yukawa theory and the muons ( $\mu$ ) ("Who ordered that?" [6]). In the next decade this simple state of affairs was blown apart by the proliferate discovery of different particles, which led to the development of the eight-fold way by Gell-Mann and Ne'eman that put light hadrons and mesons into multiplets of flavor  $SU(3)$ ,

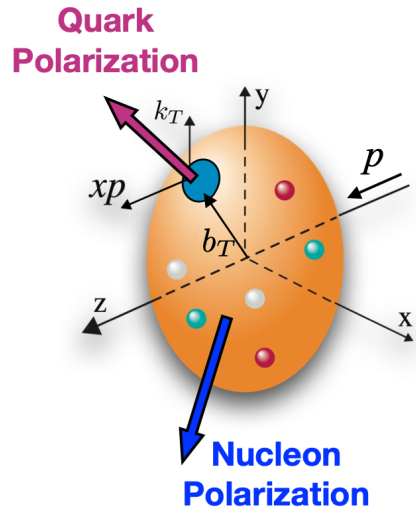


Figure 1.1: Illustration of the momentum and spin variables probed by TMD parton distributions.

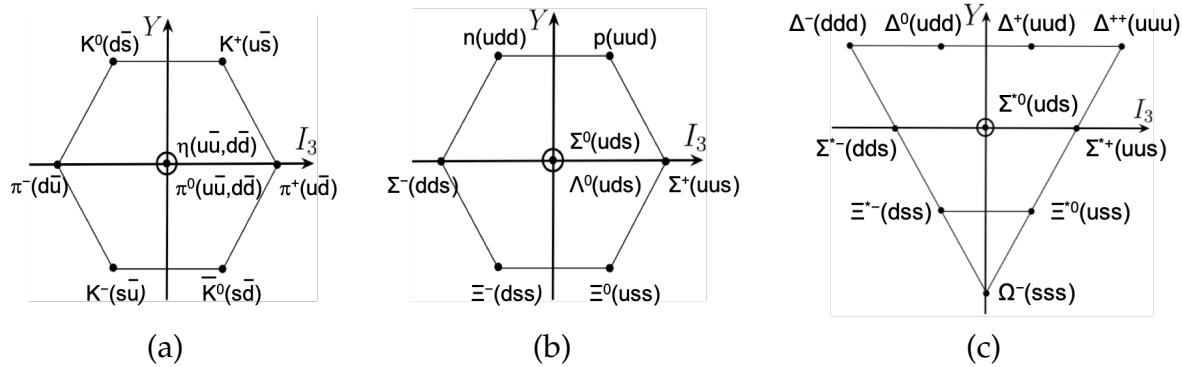


Figure 1.2: The Quark Model of hadrons in the eight-fold way. (a) mesons (flavor 8 representation); (b) baryons (flavor 8 representation); and (c) baryons (flavor 10 representation).

as shown in Fig. 1.2. The eight-fold way was given deeper meaning by Gell-Mann and Zweig with the introduction of the quark model (QM) of hadrons: mesons were bound states of quark-antiquark pairs and baryons bound states of three quarks.

Quarks with spin- $\frac{1}{2}$  and fractional charges were not taken seriously as fundamental particles at that time, but rather were regarded as a convenient bookkeeping device. Taking the quarks as real degrees of freedom requires understanding how the  $\Delta^{++}(1232)$  could be a low-lying state. In the original QM, this particle is a bound state of three “up” quarks,  $uuu$  as shown in Fig. 1.2(c). If it were presumed to be the product of three S-wave quarks to make it the lowest lying state, its wave function would be symmetric under the interchange of any two quarks, which is not allowed for fermions. The puzzle was resolved after the color of quarks was introduced. In 1964 O. W. Greenberg proposed adding to the quarks a new quantum number called color that could take on  $N_c$  values, where  $N_c$  is the number of colors. Choosing  $N_c = 3$  made the  $\Delta^{++}(1232)$  wave function antisymmetric under interchange of two quarks with different colors as required by fermi statistics. Thus was born the seed of QCD.

The discovery that the nucleon is composed of spin- $\frac{1}{2}$  point-like particles from the experimental measurements of inclusive electron-proton deep-inelastic scattering (DIS) cross section,  $e(l) + p(P) \rightarrow e(l') + X$ , performed at SLAC over 50 years ago, confirmed the existence of quarks [7]. By measuring the scattered lepton momentum  $l'$  to define the momentum transfer of the collision,  $q = l - l'$ , as sketched in Fig. 1.3(a), and keeping  $Q \equiv \sqrt{-q^2} \gg 1/R$ , where  $R$  is the proton radius, the DIS experiments provided a short-distance electromagnetic probe for the charged point-like particles inside the proton. With the momentum transfer,  $Q \gg 1/R$ , and the effective size of the hard collision  $\sim \mathcal{O}(1/Q) \ll R$ , pulling two or more point-like particles out from the same hard collision would be penalized by powers of  $1/(QR)$ , and therefore, the DIS cross section is dominated by the scattering off a single point-like particle, as indicated in Fig. 1.3(b). Furthermore, the time of the hard collision  $\sim 1/Q$  is much shorter than the characteristic time scale  $R$  for the dynamics inside the proton, implying that interactions inside the proton are effectively frozen during the hard collision. Although the inclusive DIS cross section  $E' d\sigma_{ep \rightarrow e'X} / d^3l'$  is invariant under boosts along the collision axis, the scattering is best pictured in the infinite momentum frame in which the proton moves very fast and all point-like particles inside it move in parallel. The momentum of the active point-like particle is  $k \approx \xi P \sim Q$  with a momentum fraction  $\xi$ , while its typical transverse

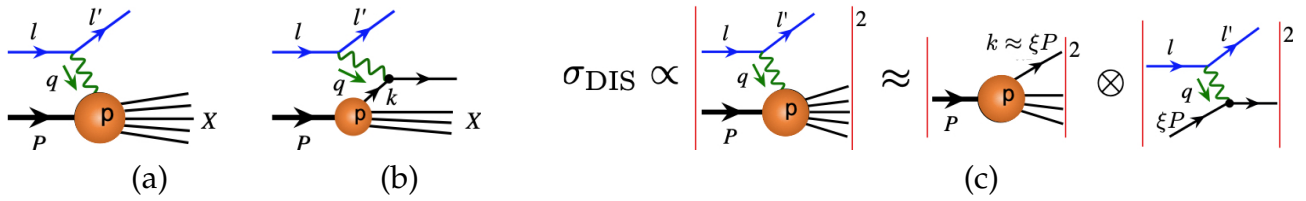


Figure 1.3: Inelastic electron-proton DIS with one-photon exchange (a), via a single point-like particle (b), and the DIS cross section in the parton model (c).

momentum  $k_T \sim 1/R \ll Q$ . Let  $f_{i/p}(\xi)$  be the probability distribution density to find a type “*i*” point-like particle inside the fast moving proton carrying momentum fraction  $\xi$ , then the DIS cross section on the proton can be approximated as sketched in Fig. 1.3(c), and expressed as

$$\begin{aligned} E' \frac{d\sigma_{ep \rightarrow e'X}}{d^3 l'} &\approx \sum_i \int d\xi f_{i/p}(\xi) E' \frac{d\hat{\sigma}_{ei \rightarrow e'X}}{d^3 l'} = \sum_i e_i^2 \left\{ \frac{2\alpha^2}{Q^2 s} \left[ \frac{1 + (1 - y)^2}{y^2} \right] \right\} f_{i/p}(x) \\ &\equiv \sum_i f_{i/p} \otimes \hat{\sigma}_i . \end{aligned} \quad (1.1)$$

Here  $\alpha = e^2/4\pi$  is the electromagnetic fine structure constant,  $\sum_i$  sums over all possible types of point-like particles weighted by the fractional charge squared  $e_i^2$ ,  $s = (l + P)^2 \simeq 2P \cdot l$  is the center of mass energy squared,  $y = P \cdot q/P \cdot l$  is the fractional energy loss of the electron in the proton rest frame, and  $x = Q^2/2P \cdot q$  is the Bjorken variable. The  $\hat{\sigma}_i$  in the abstract notation of Eq. (1.1) represents the partonic cross section,  $E' d\hat{\sigma}_{ei \rightarrow e'X}/d^3 l'$  and  $\otimes$  refers to the convolution over momentum fraction  $\xi$ . Eq. (1.1) is Feynman’s parton model formula [8] for the inclusive DIS cross section, where  $f_{i/p}(\xi = x)$  are the parton distribution functions (PDFs), and the partons are spin- $\frac{1}{2}$  point-like particles, which are now identified as quarks. The parton model formula in Eq. (1.1) shows that other than the lepton-parton scattering,  $E' d\hat{\sigma}_{ei \rightarrow e'X}/d^3 l'$ , the rest of DIS cross section on the proton is independent of  $Q^2$  and depends only on  $x$ . This phenomenon is known as Bjorken scaling, and was verified by the early SLAC experiments.

The success of the parton model formula in Eq. (1.1) to interpret the DIS data verifies the existence of spin- $\frac{1}{2}$  point-like particles inside the proton and provides a way to extract the PDFs. However, it does not provide an independent test of this parton picture. The inclusive production of massive lepton pairs in hadron-hadron collisions,  $H_a(P_a) + H_b(P_b) \rightarrow \gamma^*(q)[\rightarrow l\bar{l}(q)] + X$ , known as the Drell-Yan process [9], provided the much needed test. With the invariant mass of the lepton pair  $Q^2 \equiv q^2 \gg 1/R^2$ , the inclusive cross section should be dominated by the probability to find a quark in one hadron and an antiquark in another hadron convolved with the annihilation of the quark-antiquark pair into the observed lepton pair, as sketched in Fig. 1.4,

$$\frac{d\sigma_{H_a+H_b \rightarrow l\bar{l}+X}}{dQ^2 dY} \approx \sum_{i,j} f_{i/H_a} \otimes f_{j/H_b} \otimes \hat{\sigma}_{ij} = \frac{4\pi\alpha^2}{3N_c Q^2 s} \sum_i e_i^2 f_{i/H_a}(x_a) f_{\bar{i}/H_b}(x_b) . \quad (1.2)$$

Here  $Y = \frac{1}{2} \ln(x_a/x_b)$  is the rapidity of the lepton pair,  $\sum_i$  sums over all possible types of quark and antiquark, the parton momentum fractions are given by  $x_a = Q e^Y/\sqrt{s}$  and  $x_b = Q e^{-Y}/\sqrt{s}$

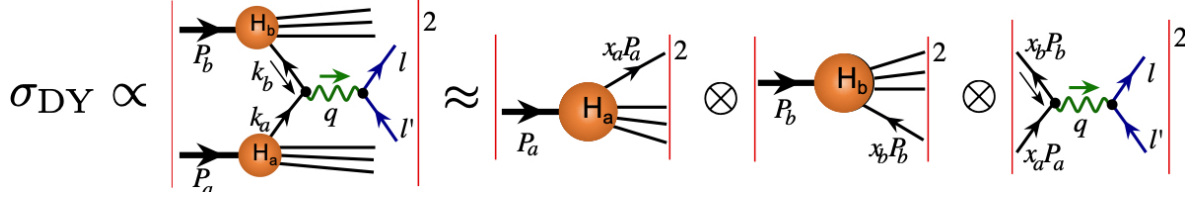


Figure 1.4: The Drell-Yan cross section in the parton model.

with total center of mass collision energy squared  $s = (P_a + P_b)^2$ , and  $1/N_c = 1/3$  is the color factor, which was missing in the original Drell-Yan formula since it predated QCD. With PDFs extracted from the DIS measurements, the Drell-Yan formula in Eq. (1.2) has effectively no free parameter for predicting the massive lepton pair production in hadronic collisions including its dependence on  $Q^2$ ,  $Y$  and collision energy  $\sqrt{s}$ . However, a somewhat large  $K_{\text{factor}} = \sigma_{\text{Exp}}/\sigma_{\text{Thy}} \sim 2$  was found [?], which indicates that the normalization of the predicted cross section is off by roughly a factor of 2.

A better microscopic picture of the strong interactions emerged in the form of QCD, and the quarks are held together by the strong color force via gluons. As a quantum field theory, the QCD Lagrange density is constructed from two types of particle fields: spin- $\frac{1}{2}$  Dirac fields (quarks),  $\psi_f^i$  with color  $i = 1, 2, 3 = N_c$  and flavor  $f = u, d, s, c, b, t$  for up, down, strange, charm, bottom, and top quarks, respectively, and massless spin-1 vector fields (gluons),  $A_\mu^a$  with color  $a = 1, 2, \dots, 8 = N_c^2 - 1$ , with SU(3) local color gauge symmetry,

$$\mathcal{L}_{\text{QCD}}(\psi_f, A_\mu) = -\frac{1}{4}G_{\mu\nu,a}^2[A] + \sum_f \bar{\psi}_f (iD_\mu[A]\gamma^\mu - m_f) \psi_f. \quad (1.3)$$

Here the gluon field strength  $G_{\mu\nu,a}[A] = \partial_\mu A_{\nu,a} - \partial_\nu A_{\mu,a} - g f_{abc} A_{\mu,b} A_{\nu,c}$ , the covariant derivative  $D_\mu[A] = \partial_\mu + ig A_{\mu,a} t_a$ , the generator  $t_a$  and structure constant  $f_{abc}$  define the SU(3) color algebra,  $[t_a, t_b] = if_{abc} t_c$ , and  $g$  is the strong coupling constant. Symbolically, the elementary interaction between quark (solid-line) and gluon (curly-line) can be represented by the Feynman diagram in Fig. 1.5(a), and three-gluon and four-gluon interactions in Fig. 1.5(b) and (c), respectively, with corresponding Feynman rules given in the Appendix [10]. QCD is a renormalizable quantum field theory and its effective interaction strength is characterized by a running coupling  $\alpha_s(\mu) = g^2(\mu)/(4\pi)$ , depending on the renormalization scale  $\mu$  which corresponds with the scale at which the interaction was probed. At the lowest order,  $\alpha_s(\mu) = 4\pi/\beta_0 \ln(\mu^2/\Lambda_{\text{QCD}}^2)$

with  $\beta_0 = \frac{11}{3}C_A - \frac{4}{3}T_F n_f$ , where  $C_A = N_c$ ,  $T_F = \frac{1}{2}$ ,  $n_f$  is number of active quark flavors, and the fundamental strong interaction scale  $\Lambda_{\text{QCD}} \sim 1/R$  depends on  $n_f$ . Unlike the electromagnetic force,  $\alpha_s(\mu)$  decreases as the  $\mu$  increases, that is, the strong interaction becomes weaker at a shorter distance or with a larger momentum transfer. This property is called asymptotic freedom, and makes it possible to perform controlled perturbative evaluation of strong interaction dynamics at short distances using QCD perturbation theory.

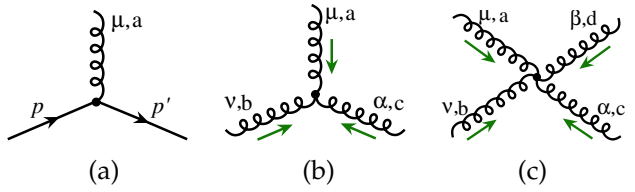


Figure 1.5: QCD interactions: quark-gluon (a), three-gluon (b) and four-gluon (c).

However, the nucleon (in general, all hadrons) has internal strong dynamics taking place at the characteristic scale of  $1/R \sim 200$  MeV  $\sim \Lambda_{\text{QCD}}$ . At these scales the strong coupling is so large that QCD perturbation theory is not applicable. That is, any high energy scattering cross section with identified hadron(s), even with a large momentum transfer  $Q$ , can not be fully calculated in QCD perturbation theory. In the parton model, as shown in Eqs. (1.1) and (1.2), the leading non-perturbative information of the hadron is embedded into the universal PDFs. Using QCD, we can identify the parton constituents  $i$  that are probed by  $f_{i/p}$  as the quarks, antiquarks and gluons, and define PDFs in terms of matrix elements of gauge invariant quark or gluon operators (see Eqs. (2.17) and (2.18) below). It is QCD factorization that allows us to consistently separate physics taking place at different momentum scales, to organize the leading process-*independent* non-perturbative contributions to high energy scattering cross sections with identified hadron(s) into universal distribution functions, such as PDFs, combined with perturbatively calculable short-distance partonic cross sections  $\hat{\sigma}(Q)$ , and to justify that all process-*dependent* non-perturbative information can be neglected as power suppressed corrections. On the other hand, physically observed cross sections should not depend on the precise scale at which short and long distance contributions are factorized from each other, which leads naturally to renormalization group improved QCD factorization and the scale-dependence of the factorized universal distribution functions, including PDFs and TMDs (as discussed in Sec. 4 of this handbook). That is, like the strength of strong interaction,  $\alpha_s$ , the PDFs, and in general, the factorized universal distribution functions depend on the scale at which they are probed. The renormalization group improved QCD factorization formalism allows us to calculate the partonic cross section  $\hat{\sigma}(Q)$  order-by-order in perturbation theory to improve its precision, to extract the non-perturbative, but, universal PDFs from experimental data, to predict the scale dependence of the PDFs, and to test QCD dynamics and factorization by verifying the universality of these PDFs. As discussed in Chapters 2 and 3 of this handbook, the parton model formulas in Eqs. (1.1) and (1.2) can be derived from QCD as the leading power contribution in both  $\alpha_s$  and  $1/Q$  to the corresponding QCD processes. Furthermore, corrections from higher orders in  $\alpha_s$  can be systematically included. The non-perturbative PDFs can also be studied and extracted from lattice QCD calculations of hadron matrix elements of quark and gluon correlators, as discussed in the Sec. 1.4, complementary to what can be extracted from experimental data.

## 1.2 Structure of the Nucleon

As a relativistic bound state of quarks and gluons, the nucleon's internal structure can not be described by any kind of “still picture” that is often used to describe atomic or molecular structure. As shown in Eqs. (1.1) and (1.2), the leading structure information of the nucleon, which we can extract from experimental data of high energy scattering with a large momentum transfer  $Q$ , is embedded in the PDFs as the probability densities to find a collinear quark, or antiquark, or gluon carrying a momentum fraction  $\xi$  inside a colliding nucleon. This is pictured in Fig. 1.3 or Fig. 1.4. In QCD, the nucleon's rich internal structure can be described by its matrix elements of gauge-invariant partonic operators composed of quark and gluon fields with various spin projections, similar to the definition of quark distribution in Eqs. (2.17) and (2.18). Although none of these matrix elements are direct physical observables, owing to the fact that no quark and gluon can be seen in isolation, the QCD factorization formalism does link these matrix elements to physically measured cross sections with power suppressed

$$\begin{aligned}
f_{q/h}(\xi) &= \frac{1}{2} \left[ \left| \frac{\vec{S}}{P} \right|^2 + \left| \frac{\vec{S}}{P} - \frac{\vec{\xi}P}{P} \right|^2 \right] \\
\Delta f_{q/h}(\xi) &= \frac{1}{2} \left[ \left| \frac{\vec{S}}{P} \right|^2 - \left| \frac{\vec{S}}{P} - \frac{\vec{\xi}P}{P} \right|^2 \right] \\
\delta f_{q/h}(\xi) &= \frac{1}{2} \left[ \left| \frac{\vec{S}}{P} \right|^2 - \left| \frac{\vec{S}}{P} + \frac{\vec{\xi}P}{P} \right|^2 \right]
\end{aligned}$$

Figure 1.6: Graphic representation of leading order collinear quark distributions of hadron  $h$ :  $f_{q/h}(\xi)$  (unpolarized),  $\Delta f_{q/h}(\xi)$  (longitudinally polarized) and  $\delta f_{q/h}(\xi)$  (transversely polarized). The red and black arrow represent spin direction of the quark and hadron, respectively. See the text for more details.

and controllable approximations.

When a spin-1/2 quark of longitudinal momentum fraction  $\xi$  is probed in a scattering experiment with polarized nucleons, we can access four possible quark polarization states, which are often referred as unpolarized, longitudinally polarized and two transversely polarized states. With a spin- $\frac{1}{2}$  nucleon, we can define the unpolarized collinear quark distribution of an unpolarized nucleon  $f_{q/h}(\xi)$ , the collinear quark helicity distribution of a longitudinally polarized nucleon  $\Delta f_{q/h}(\xi)$ , and the collinear transversity distribution of a transversely polarized nucleon with the direction of quark transverse polarization parallel to the direction of nucleon's polarization  $\delta f_{q/h}(\xi)$  (equivalent to the notations  $h_1(\xi)$  or  $\delta q(\xi)$  that are also used in the literature) as sketched in Fig. 1.6. Similarly, we have three collinear antiquark distributions for the nucleon. However, the nucleon has only two collinear gluon distributions: the unpolarized collinear gluon distribution of a unpolarized nucleon  $f_{g/h}(\xi)$  and the collinear gluon helicity distribution of a longitudinally polarized nucleon  $\Delta f_{g/h}(\xi)$ . Transverse spin-flip of a spin- $\frac{1}{2}$  nucleon can not generate a two-unit spin-flip needed to define the collinear gluon transversity of the nucleon, and therefore the nucleon does not have a gluon transversity distribution. Unpolarized collinear PDFs have been well-determined from experimental data on QCD factorizable high energy scattering observables with large momentum transfers [11]. Helicity distributions and transversity distributions are expected to be better determined from future precision data from Jefferson Lab and the EIC.

With a large momentum transfer  $Q \gg 1/R$ , the scattering takes place at such a short time  $\sim 1/Q$  that the hard probe is not very sensitive to the physics at the scale of  $\Lambda_{QCD} \sim 1/R$ , including the active parton's confined transverse motion ( $k_T$ ) in momentum space and its spatial distribution ( $b_T$ ) in position space, as shown in Fig. 1.1. On the other hand, both the confined motion and the spatial distribution of quarks and gluons inside a bound nucleon are important part of the nucleon's 3D internal structure, which is an immediate consequence of QCD dynamics. To probe such 3D internal structure, we need a new type of *two-scale* “hard-probes”, which are physical observables with a large momentum transfer  $Q_1 \gg \Lambda_{QCD} \sim 1/R$  to localize the probe to see the particle nature of quarks and gluons, while they also have an additional well-measured soft momentum scale,  $Q_2 \ll Q_1$ , so that they are much more sensitive to the details of hadron's internal structure. For example, as described in Chapter 2, the Drell-Yan cross section is an ideal two-scale observable if we measure the differential cross section as a function of the pair's transverse momentum  $q_T = |\mathbf{q}_T|$  in addition to measuring the invariant mass of the lepton pair,  $Q$ , in particular because the production rates are dominated by the region where  $q_T \ll Q$ . In terms of the parton model picture in Fig. 1.4, the pair's

transverse momentum is a sum of the transverse momentum of the active quark and antiquark,  $\mathbf{q}_T = \mathbf{k}_{aT} + \mathbf{k}_{bT}$ . The parton model formula in Eq. (1.2) is then modified as,

$$\begin{aligned} \frac{d\sigma_{H_a+H_b \rightarrow l\bar{l}+X}}{dQ^2 dY d^2\mathbf{q}_T} &= \frac{4\pi\alpha^2}{3N_c Q^2 s} \sum_i e_i^2 \int d^2\mathbf{k}_{aT} d^2\mathbf{k}_{bT} \delta^{(2)}(\mathbf{q}_T - \mathbf{k}_{aT} - \mathbf{k}_{bT}) \\ &\quad \times f_{1(i/H_a)}(x_a, \mathbf{k}_{aT}) f_{1(\bar{i}/H_b)}(x_b, \mathbf{k}_{bT}) \\ &= \hat{\sigma}_{q\bar{q} \rightarrow l\bar{l}} \otimes f_1 \widetilde{\otimes} f_1. \end{aligned} \quad (1.4)$$

where  $f_1(x_a, \mathbf{k}_{aT})$  is the TMD version of the collinear quark distribution  $f(\xi = x_a)$ , and  $\widetilde{\otimes}$  represents the convolution of both longitudinal momentum fraction and transverse momenta of the active quark and antiquark, different from  $\otimes$  that represents only the convolution of longitudinal momentum fraction as in Eq. (1.2). The transverse momenta, which are expected to be much smaller than the hard scale  $Q$ , are neglected in evaluating the hard part  $\hat{\sigma}_{q\bar{q} \rightarrow l\bar{l}}$ .

That is, the  $q_T$ -distribution of Drell-Yan cross section is directly sensitive to the transverse momentum of the active partons, and a good probe for the TMD PDFs (or simply, TMDs).

Like the collinear PDFs, the TMDs are distribution densities to find a quark or a gluon carrying a longitudinal momentum fraction  $\xi$  and transverse momentum  $\mathbf{k}_T$  inside a colliding nucleon. The detailed definitions of TMDs in QCD will be given in Chapter 2. With the dependence on the active parton's transverse momentum, the TMDs carry much more information on hadron structure than what longitudinal PDFs can provide. The TMDs provide the leading information on quantum correlation between nucleon's spin and active parton's polarization as well as its motion. Instead of three independent quark PDFs in Fig. 1.6, we will have eight independent and non-vanishing quark TMDs because of the quark's transverse motion, as summarized in Fig. 1.7. Here the TMDs are organized in terms of the correlation between polarization states of quark and nucleon: unpolarized ( $U$ ), longitudinally polarized ( $L$ ), and transversely polarized ( $T$ ). Similarly, we have TMDs for gluons and antiquarks, introduced in Chapter 2.

Like the unpolarized quark PDF,  $f_{q/h}(\xi)$  in Fig. 1.6, its TMD version,  $f_1(\xi, \mathbf{k}_T)$  in Fig. 1.7 represents the probability density to find an unpolarized quark carrying collinear momentum fraction  $\xi$  and transverse momentum  $\mathbf{k}_T$  inside an unpolarized nucleon. On the other hand, some TMDs have no correspondence to collinear PDFs. For example, the Sivers function  $f_{1T}^\perp$  represents a quantum correlation between the transverse spin direction of the nucleon and the strength and direction of transverse motion of an unpolarized active quark, as well as its flavor dependence. Another interesting TMD, with no collinear correspondence, is the pretzelosity  $h_{1T}^\perp$  that represents how the correlation of nucleon spin and quark spin can influence the quark's transverse motion, and approximately, its moment in a model dependent way can be interpreted as quark orbital angular momentum contribution to the proton's spin [12–14], see Chapter 7.

In summary, TMDs are fundamental distributions which carry novel information about the nucleon's internal momentum and spin structure, beyond what is known from high precision determinations of the classic PDFs.

### 1.3 Matching Cross Section to the Structure

The TMDs, and in general any parton distributions or correlation functions, can not be directly measured in physical experiments since we can not directly detect quarks and gluons

		Quark Polarization		
		Un-Polarized (U)	Longitudinally Polarized (L)	Transversely Polarized (T)
Nucleon Polarization	U	$f_1 = \text{○} \bullet$ Unpolarized		$h_1^\perp = \text{○} \bullet - \text{○} \bullet$ Boer-Mulders
	L		$g_1 = \text{○} \bullet \rightarrow - \text{○} \bullet \rightarrow$ Helicity	$h_{1L}^\perp = \text{○} \bullet \rightarrow - \text{○} \bullet \rightarrow$ Worm-gear
	T	$f_{1T}^\perp = \text{○} \uparrow - \text{○} \downarrow$ Sivers	$g_{1T}^\perp = \text{○} \uparrow - \text{○} \downarrow$ Worm-gear	$h_1 = \text{○} \uparrow \bullet - \text{○} \uparrow \bullet$ Transversity $h_{1T}^\perp = \text{○} \uparrow \bullet - \text{○} \uparrow \bullet$ Pretzelosity

Figure 1.7: Leading power spin dependent quark TMDPDFs. The red dot and black circle represent the quark and nucleon, while the red and black arrow represent their spin direction, respectively.

in isolation. We need QCD factorization formulas to relate TMDs to physical observables, such as cross sections or spin asymmetries defined in terms of ratios of polarized and unpolarized cross sections. Like the parton model formula for inclusive Drell-Yan cross section in Eq. (1.2), sketched in Fig. 1.4, we have an extended parton model factorization formula in Eq. (1.4) to express the differential Drell-Yan cross section,  $d\sigma/d^4q$ , in terms of TMDs when  $q_T \ll Q$ . A similar and more rigorous QCD factorization formula for the differential Drell-Yan cross section will be introduced in Chapter 2.

However, with the Drell-Yan process alone in Eq. (1.4), it is impossible to extract and disentangle various quark TMDs listed in Fig. 1.7, not to mention the antiquark and gluon TMDs. We need more well-defined and factorizable two-scale observables to be able to probe all TMDs. By detecting a hadron (or jet) of momentum  $P_h$  in the final state of electron-proton DIS in addition to the scattered electron, as sketched in Fig. 1.8, this semi-inclusive DIS (SIDIS) process provides more well-defined two-scale observables, where the hard scale  $Q \gg \Lambda_{\text{QCD}}$  and the soft scale is the transverse momentum of the observed final-state hadron  $P_{hT}$  in the photon-hadron frame where the exchanged virtual photon and the colliding hadron define the  $z$ -axis. In this virtual photon-hadron frame, the produced leading hadron in the most events of SIDIS is very likely to go in the direction opposite to the colliding hadron and to have a very small  $P_{hT}$ . So that, the  $P_{hT}$ -distribution of lepton-hadron SIDIS is another natural *two-scale* observable. In particular, it forms an important part of the physics program at a future electron-ion collider [15], where it will be fully explored.

In the parton model picture, the lepton-proton SIDIS cross section can be factorized, as

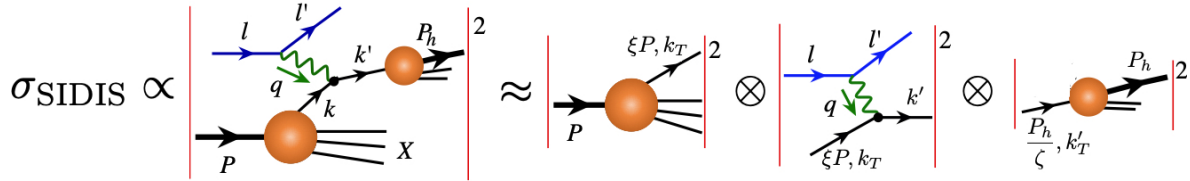


Figure 1.8: The semi-inclusive DIS cross section in the parton model.

sketched in Fig. 1.8, when  $Q \gg P_{hT}/z_h \gtrsim \Lambda_{\text{QCD}}$  with  $z_h = P \cdot P_h / P \cdot q$ ,

$$E'E_h \frac{d\sigma_{ep \rightarrow e'hX}}{d^3 l' d^3 P_h} \approx \hat{\sigma}_{eq \rightarrow e'q'} \otimes f_1 \tilde{\otimes} D_{h/q'}, \quad (1.5)$$

where  $f_1(\xi, k_T)$  is defined in Fig. 1.7 and  $D_{h/q}(\zeta, \mathbf{k}'_T)$  is a new type of TMDs, which are quark TMD fragmentation functions (FFs) for a quark of flavor  $q$  to hadronize into an observed hadron  $h$  carrying the momentum fraction  $\zeta$  of the fragmenting quark momentum, as sketched in Fig. 1.8. Like the quark TMD PDFs in Fig. 1.7, the quark TMD FFs are also organized in terms of the correlation between the polarization and transverse momentum of the fragmenting quark and the properties of the hadron observed in the final-state, as summarized in Fig. 2.6. With well-defined antiquark and gluon TMD FFs, these distributions provide the fundamental information on how hadrons with measured transverse momentum emerge from energetic quarks and gluons. In Eq. (1.5),  $\tilde{\otimes}$  represents the convolution of both momentum fraction  $\xi$  and  $k_T$  or  $\zeta$  and  $k'_T$  in case of FFs. Like the Drell-Yan  $q_T$  distribution, the lepton-proton SIDIS cross section can also be factorized in QCD in terms of TMDs [74]. More detailed formulae for the SIDIS factorization theorem are given in Chapter 2, and more detailed arguments for this factorization are given in Chapter 3.

With SIDIS, we obtain a new type of two-scale observables that are sensitive to the TMD PDFs in addition to the Drell-Yan process. However, SIDIS also introduces the capability to probe a new type of TMD physics encoded in the universal TMD FFs. In order to extract these TMDs from experimental data, clearly, we need to identify more factorizable two-scale observables that are sensitive to the same TMDs, including both TMD PDFs and TMD FFs. Another natural two-scale observable is the di-hadron production in  $e^+e^-$  collisions:  $e^+ + e^- \rightarrow H_1(P_1) + H_2(P_2) + X$ . In the region where the two produced high momentum hadrons are almost back-to-back, the momentum imbalance,  $\bar{p} \equiv |\vec{P}_1 + \vec{P}_2| \ll |\vec{P}_1 - \vec{P}_2|/2 \equiv \bar{P}$ , defines a soft momentum scale  $\bar{p}$  together with a hard scale  $\bar{P}$ . A TMD factorization theorem can then be derived to express the di-hadron production in this region in terms of two TMD FFs together with a perturbatively calculable hard part [16]

$$E_1 E_2 \frac{d\sigma_{e^+e^- \rightarrow H_1 H_2 X}}{d^3 P_1 d^3 P_2} \approx \sum_{i,j} \hat{\sigma}_{e^+e^- \rightarrow ij} \otimes D_{H_1/i} \tilde{\otimes} D_{H_2/j}. \quad (1.6)$$

In Fig. 1.9, we summarize how TMD PDFs and TMD FFs are connected to the three classical two-scale factorizable observables with parton model factorization formalisms in Eqs. (1.4), (1.5) and (1.6), respectively. Corresponding QCD factorization formalisms are presented in the later Chapters in this Handbook.

Much of the predictive power of perturbative QCD factorization approach to experimentally measured cross sections relies on the universality of these TMDs and our ability to

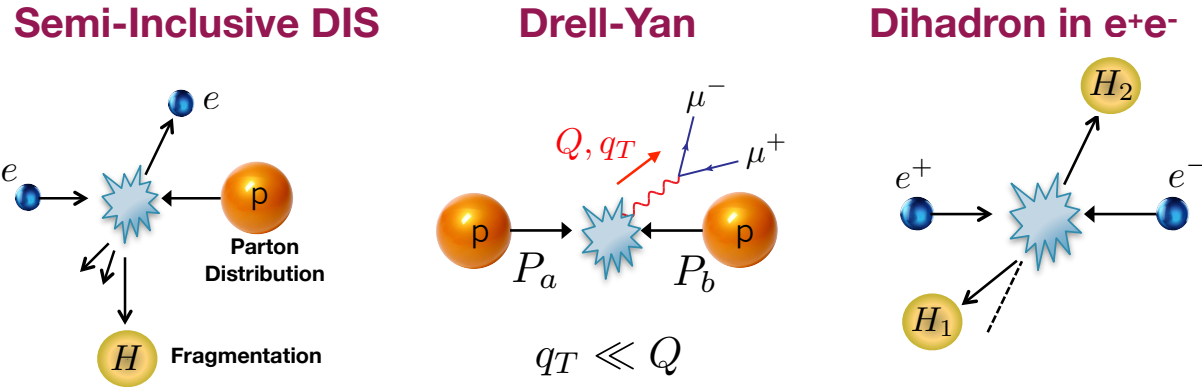


Figure 1.9: Schematic illustration of TMD parton distributions and fragmentation functions which appear in key cross sections.

calculate the short-distance hard parts  $\hat{\sigma}$ 's. However, extracting the 3D hadronic structure information, encoded in these TMDs, from experimentally measured data of these cross sections requires to solve an inverse problem to deconvolute TMDs from the factorization formalisms, such as those in Eqs. (1.4), (1.5) and (1.6). As discussed in Chapter 5, with the experimental data of these two-scale observables we can extract these TMDs simultaneously by QCD global analysis of all available data [17]. A typical procedure for global analysis involves following necessary steps:

1. Identify good “two-scale” observables, such as cross sections or spin asymmetries that are defined as ratios of polarized and unpolarized cross sections, that can be factorized into convolution of TMDs along with perturbatively calculable short-distance hard parts, like those three classical examples in Fig. 1.9;
2. Make a choice of experimental data sets for these good observables, such that the data set can give the best constraints on a close set of TMDs;
3. Calculate and/or verify the perturbative short-distance hard parts for these good observables;
4. Develop a program for solving the scale dependence of the TMDs, which depend on the hard scale at which they are probed, just like PDFs;
5. Choose an algorithm to minimize the difference between the data and theoretical calculations based on the factorization formalisms to extract the set of universal TMDs that can best describe the data within the experimental uncertainties.

However, with the limited data on the “two-scale” observables, our knowledge on the TMDs is still limited [17]. More detailed methods and procedures for extracting TMDs from QCD global analysis are given in Chapter 5.

With the large number of independent TMD PDFs and TMD FFs, and the rich information of TMD physics, it is a challenge to find more two-scale observables and new approaches to isolate different TMDs. Since all TMDs are classified in terms of the correlation of hadron

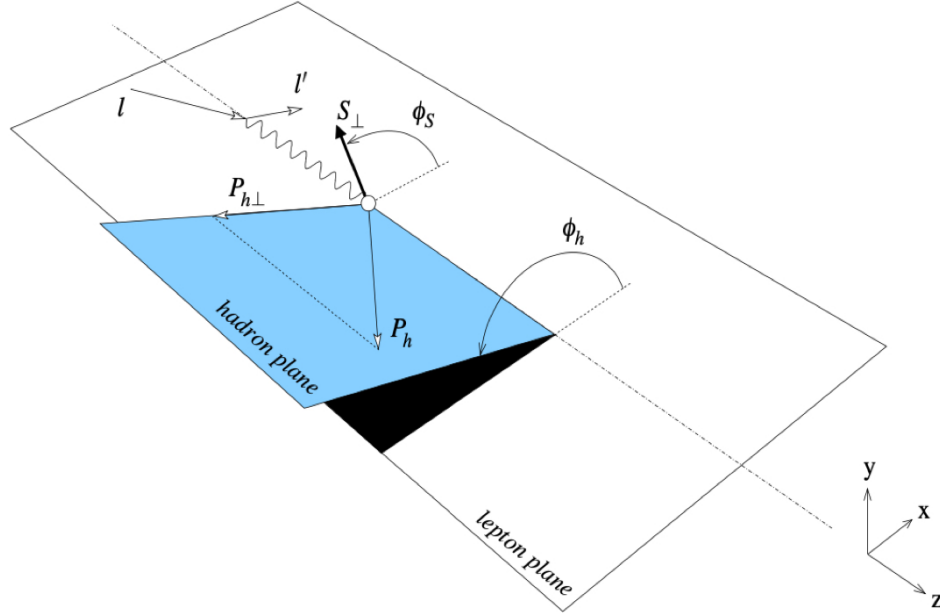


Figure 1.10: The Trento convention for the “photon-hadron” frame of SIDIS [18].

polarization and the polarization of quarks and gluons, spin asymmetries of cross sections with polarized beams can provide many more independent observables from the three classical two-scale observables alone. In addition, with the well-defined leptonic plane, defined by the colliding and scattered lepton, and the hadronic plane, in terms of the colliding hadron and the observed final-state hadron, as shown in Fig. 1.10, we can measure the lepton-hadron SIDIS cross section as a function of the angle  $\phi_h$  between these two planes, and the angle  $\phi_s$  between the direction of hadron spin and the leptonic plane. Measuring various angular modulations of these two planes in SIDIS provides a unique way to isolate the information on various combinations of TMDs, as demonstrated in Chapter 5. For example, for SIDIS with an unpolarized electron beam scattered off a transversely polarized proton ( $S_{\perp}$ ), we can define the single transverse spin asymmetry as  $A_{UT} = [\sigma_{UT}(S_{\perp}) - \sigma_{UT}(-S_{\perp})]/[\sigma_{UT}(S_{\perp}) + \sigma_{UT}(-S_{\perp})]$  which is a function of the angle between the leptonic and hadronic plane and the direction of hadron spin. By measuring different angular modulations,

$$\begin{aligned} A_{UT}^{Collins} &\propto \langle \sin(\phi_h + \phi_s) \rangle_{UT} \propto h_1 \tilde{\otimes} H_1^{\perp}, \\ A_{UT}^{Sivers} &\propto \langle \sin(\phi_h - \phi_s) \rangle_{UT} \propto f_{1T}^{\perp} \tilde{\otimes} D_1, \\ A_{UT}^{Pretzelosity} &\propto \langle \sin(3\phi_h - \phi_s) \rangle_{UT} \propto h_{1T}^{\perp} \tilde{\otimes} H_1^{\perp}, \end{aligned} \quad (1.7)$$

where TMD PDFs and TMD FFs are defined in Figs. 1.7 and 2.6, respectively, we can obtain enhanced sensitivities to different TMDs. With experiments carried out at HERMES and COMPASS, the on-going experiments at Jefferson Lab and more at the future EIC, lepton-hadron SIDIS experiments with various beam polarizations will provide rich information on the TMDs and the 3D hadron structure in momentum space.

However, above angular modulations rely on our ability to determine the “photon-hadron ( $\gamma^*P$ )” frame where the TMD factorization and the lepton and hadron planes are defined. The large momentum transfer between the colliding lepton and hadron can trigger QED photon radiation from the colliding and scattering leptons to make it difficult, if not impossible, to

fully determine the momentum of the exchanged virtual photon and the photon-hadron frame, which immediately impact the meaning of above angular modulations as well as the measured value of  $P_{hT}$  [524, 525]. More discussion on the role of QED radiation in extracting TMDs from SIDIS will be given in Sec. 5.8 of Chapter 5.

## 1.4 Calculation of Hadron Structure in Lattice QCD

Hadron structure, encoded in the universal PDFs, TMDs and other quark-gluon correlation functions of the hadron, can not be calculated in QCD perturbation theory. The numerical technique of lattice QCD in principle provides a way in which to calculate nonperturbative QCD information about the properties of hadrons by directly evaluating the QCD path integrals that define such quantities. For many years, this technique has been used to access static and quasi-static quantities such as magnetic moments and electroweak form factors of the proton. Calculations of some of these quantities are now reaching a level of sophistication where the small effects of QED and isospin-breaking must be included in the LQCD calculations and a community consensus of such results is maintained by the Flavour Lattice Averaging Group [19].

PDFs and TMDs and related objects are defined precisely in QCD by operators that involve correlations of quark and gluon fields with light-like separations in spacetime. It is therefore very natural to ask whether given sufficient computing power we could calculate the PDFs and TMDs, and in general, the leading quark-gluon correlations inside a bound nucleon *directly* in LQCD. If it were possible, the quantum correlations between a hadron's mass and spin and the motion of quarks and gluons inside it could be determined, shedding light on how quarks and gluons are confined inside the hadrons. However for these partonic quantities, an impediment to LQCD calculations is raised by the light-cone nature of their definition. Since LQCD is most practically formulated in Euclidean space, direct determinations of such light-like separated correlations are not possible. For that reason, most QCD studies of partonic physics have concentrated on the  $x^n$  weighted Mellin moments of PDFs. However for technical reasons, these calculations have been restricted to the lowest few moments,  $n \in \{1, 2, 3\}$ .

Despite the challenges, various approaches to go beyond calculations of moments and extract quark-gluon correlation functions from lattice QCD have been proposed and investigated over the years [20–27]. Stimulated by the quasi-PDFs approach introduced in Ref. [28] (the approach was later formulated in a large-momentum effective field theory [29, 30]), many new ideas and approaches have been proposed for the extraction of PDFs, TMDs and other quark-gluon correlation functions from LQCD calculations. These approaches include the pseudo-PDFs [31], current-current correlators in momentum space [32] and current-current correlators in position space [33]. The central idea of all these new approaches is to identify quantities that can be reliably calculated in LQCD as well as being objects from which the PDFs, TMDs or other quark-gluon correlation functions can be extracted with controllable approximations [34]. While calculations of these quantities are still being refined, tremendous progress has been made and these developments hold the exciting potential for accurate, model-independent determinations of (TMD) PDFs directly from QCD.

In Chapter 6, the recent developments in LQCD calculations of the PDFs and TMDs will be covered. Although extracting the fundamental PDFs, TMDs and other quark-gluon correlation functions from LQCD calculations is analogous to extracting such distributions from observables that are measured precisely in experiments and factorizable in QCD, LQCD

calculations may provide additional complementary information on hadrons that is difficult to extract from experiment. For example, calculations can cover parameter values and kinematics that are difficult for experiments to reach. Moreover in LQCD, we have the freedom to choose the combinations of operators that are calculated in order to determine aspects of hadron structure that might not be readily accessible in experiments. Despite the so-far insurmountable challenges for *direct* LQCD calculations of PDFs, TMDs and other leading quark-gluon correlation functions, the various LQCD approaches that will be discussed below definitively enhance our ability to explore the rich, non-perturbative structure of hadrons and the dynamics of quarks and gluons at the QCD scale.

## 1.5 Guide to Reading the Handbook

As this handbook is quite comprehensive, a guide to the reader that goes beyond the section titles in the table of contents is likely to be of benefit to all readers. With that in mind we will introduce various subjects in the chapters, making editorial comments regarding each section with the aim of guiding a reader in the desired direction.

If there is one chapter that lies at the heart of this document it is Chapter 2 “Definitions of TMDs”, which should not be skipped, though some sections may be omitted depending on the depth of knowledge that is being sought. Keep in mind that studying the definition of TMDs is like peeling off the layers of an onion with each new layer exposing further subtle facts. It would not be inappropriate to take this metaphor literally as well and there is no shame in keeping some tissues handy. The layers start with an overview based on the parton model in Sec. 2.1 and become successively more detailed. The complexity of the later sections is softened by explicit examples that are worked out in the text. We recommend that everyone read Secs. 2.1–2.3, 2.6, 2.7.1, 2.7.2, 2.10, and 2.11. Those interested in getting to the core of the onion should also read Secs. 2.4, 2.5, the remaining parts of Sec. 2.7, and Secs. 2.8 and 2.9. In Sec. 2.2 the factorization theorem for Drell-Yan is covered, which is important because it introduces many of the concepts and much of the notation that is used later. Section 2.3 introduces the high-level definitions of the TMD functions, including the two broad categories of definitions widely used in the literature. Section 2.4 covers the concept of rapidity regulators in TMDs. The need to regulate rapidity divergences is an important feature of TMD functions and they can not be fully understood without an understanding of this topic. This section also contains an explicit one-loop example that illustrates rapidity regulation in action. Section 2.5 connects the main definition of the TMD PDF used in this handbook to some others in the literature. Section 2.6 introduces the TMD fragmentation functions. Section 2.7 discusses the universality of TMDs for different processes and introduces the full complement of spin dependent TMDs. The connection between TMDs and PDFs at perturbative transverse momentum is discussed in Sec. 2.8, and the extent to which integrating TMDs over their transverse momentum results in longitudinal PDFs is taken up in Sec. 2.9. The connection of continuum TMDs and lattice friendly definitions for TMD correlators is introduced in Sec. 2.10, including the Lorentz invariance and large momentum effective theory (LaMET) approaches. Finally, Sec. 2.11 dives into TMD factorization for DY, SIDIS and  $e^+e^-$  cross sections including the definitions of kinematic variables that are used throughout the handbook.

Chapter 3 provides a broad view of the ideas behind proofs of factorization for TMD processes, without diving too deep into the details. Readers interested in more technical details are referred to the referenced literature, while those seeking to get an intuitive understanding

of the key concepts will find what they are looking for. A novel aspect of this section is the simultaneous treatment of both the traditional QCD factorization approach of Collins-Soper-Sterman and the more recent SCET approach, with parallels also drawn.

Chapter 4 covers evolution and resummation of large logarithms in TMD physics. Again this chapter peels like an onion with the broadest view being the outer layer, and successive layers zooming in on the details. An effort is made to cover and connect approaches from QCD factorization and SCET. Section 4.1 gives a historical overview of the development of TMD evolution starting with QCD factorization and then the SCET approach. In Sec. 4.2 one finds an overview of what the goal of resummation is and what can be achieved, while in Sec. 4.3 gets into the beautiful nitty-gritty of resummation, and also provides a short one-loop example. Section 4.4 covers solutions of the evolution equations used in the CSS formalism, while the path followed to solve evolution equations in SCET is taken up in Sec. 4.5. Sec. 4.6 on “Two-dimensional evolution” reviews novel insights that can be gained from treating simultaneously the evolution in invariant mass and rapidity and is a recommended read. Section 4.7 is a small but important section on how the resummed results can be smoothly matched onto fixed order results, so that final cross sections are accurate in regions where resummation is or is not important. Finally, Sec. 4.8 revisits evolution but this time with all or parts of the evolution in momentum space, rather than only using position space as in the previous sections.

Chapter 5 is a thorough tour of the phenomenology involved in the extraction of TMDs. Section 5.1 gives a historical overview of the rich phenomenology of extracting TMD functions. Not only is this section interesting reading it also will really help readers make sense of the current state of affairs, and hence is recommended. Sections 5.2–5.5 give an overview of phenomenology for TMD functions ranging from the unpolarized distributions, to the important Sivers and Collins functions, to the interesting Boer-Mulders and worm-gear distributions. These sections all involve processes that are dominated by the quark substructure of hadrons, where the wealth of available data means that we are currently very capable of probing the strong interactions. Gluon TMDs are not nearly as well probed by experimental measurements, as described in Sec. 5.6. Experimental analysis of nuclear TMDs are also in their infancy, with plenty of open opportunities, as described in Sec. 5.7. In Sec. 5.8 we discuss the importance of accounting for QED radiation when extracting TMD functions, and Sec. 5.9 gives a glimpse into future phenomenological directions for TMD physics.

Chapter 6 focuses on how nonperturbative knowledge about TMDs can be obtained from first principles with lattice QCD. We begin in Sec. 6.1 with a brief review of lattice QCD techniques, to paint the stage for those unfamiliar with lattice calculations, albeit with broad brush strokes. The goal of lattice QCD calculations in the context of this handbook is to determine various aspects of TMDs. To build up to this challenging endeavor we discuss several topics that serve as important stepping stones. Section 6.2 broadly covers the structure of the proton on the lattice, including the current status of classic results like the analysis of moments of PDFs, and the decomposition of the proton’s spin. This is followed by Sec. 6.3 which gives an extensive overview of the currently very active program of determining longitudinal PDFs and structure functions on the lattice. This section sets the stage for lattice extractions of TMD functions, for example by reviewing work on the LaMET approach involving quasi-PDFs. Section 6.4 then dives into lattice and TMD functions, including the Lorentz Invariants approach, calculation of TMD soft functions, and Lattice QCD information for TMD evolution.

This section will be of interests to those planning to do research on TMD functions on the lattice, as well as non-experts looking for a good overview of what information can currently be determined by lattice QCD calculations, as well as prospects for the future.

Chapter 7 covers models of hadronic physics applied to TMDs. This is well worth reading as models have played an important role in the development of this field. In particular a significant result was a model calculation by Brodsky, Hwang and Schmidt [58] of the single spin asymmetry (SSA) that demonstrated a nonzero transverse SSA in SIDIS, as discussed in Sec. 7.2. Sections 7.3–7.5 cover frameworks for both T-even and T-odd TMDs, including various types of parton and quark models, the bag model, Nambu–Jona-Lasinio models, AdS/QCD models, and soliton models, and we also cover models for gluons TMDs (Sec. 7.6) and for fragmentation functions (Sec. 7.7). We also discuss in Sec. 7.8 more general results for TMDs that so-far lack QCD derivations, namely positivity constraints and sum rules. Finally, we contrast relations derived from models with results obtained from QCD in Sec. 7.9.

Chapter 8 focuses on the small- $x$  kinematic region of TMDs with important implications for our understanding of QCD. An overview of why this region is of such interest, and the connection between TMDs and saturation phenomena for hadronic systems is given in Sec. 8.1. It also gives a foundation to the sections that follow and is recommended reading for anyone interested in the small- $x$  regime. Section 8.2 takes a closer look at the gluon distribution functions at small  $x$ , including both the Weizäcker-Williams and dipole distributions. In Sec. 8.3 we discuss the evolution of TMD distributions when simultaneously accounting for small- $x$  resummation. Section 8.4 concentrates on the more advanced topic of spin-dependent TMDs at small- $x$ . Finally, Sec. 8.5 leads us to the frontier of the field in terms of the physics of saturation and multiple scattering effects. A road map of future research that needs to be done is given in Sec. 8.6.

Chapter 9 takes a different approach to the extraction of TMD functions by considering measurements of jet observables; specifically jet fragmentation. The chapter begins with an overview of jets to a level that is needed to understand subsequent sections. Sec. 9.1 considers jets as probes of TMD PDFs, which while more complicated than the processes already considered can provide a wealth of data from hadron colliders. The following sections are refinements on this idea: Sec. 9.2 considers jet substructure, Sec. 9.5 studies jets with heavy quarkonium and Sec. 9.6 introduces transverse energy-energy correlators. Sec. 9.7 takes jets into the realm of in-medium effects as applied to either cold QCD matter or the QGP. This is a rich field so that this section only provides a broad view.

Chapter 10 is recommended for anyone interested in azimuthal asymmetry observables whose structure functions enable us to probe novel subleading-power TMDs, such as quark-gluon-quark correlators. These observables depend on sixteen new TMD PDFs and four new TMD FFs, in addition to those that already appeared at leading power, making the subject somewhat daunting. After an introduction in Sec. 10.1, we describe in Sec. 10.2 to discussing observables, focussing on terms in the SIDIS cross section that are sensitive to subleading TMDs, and giving their general decomposition in terms of hadronic structure functions. Historically SIDIS provided our first view of these asymmetries. In Sec. 10.3 we define the subleading power TMD distributions as operator matrix elements, and then in Sec. 10.4 we present the factorization formula that relates the structure functions to leading and subleading TMDs. In Sec. 10.5 we give a review of experimental measurements of subleading power TMD observables. Section 10.6 discusses both lattice and model based methods for estimating the

contribution of subleading TMDs to different processes. Many things remain to be worked out for the subject of subleading power TMDs, and Sec. 10.7 gives a summary and outlook.

In Chapter 11 we zoom out to consider a more general class of multidimensional functions which probe quark substructure, of which the TMDs are just an important case. Section 11.1 introduces the Wigner distribution and how it reduces to more familiar TMD PDFs, impact parameter-dependent parton distributions, PDFs, and form factors. Section 11.2 introduces generalized TMDs (GTMDs) through a Fourier transform in transverse position space of the Wigner distribution. Section 11.3 discusses observables which can be used to measure the GTMDs. Section 11.4 connects the GTMDs and associated GPDs (generalized parton distributions) to the orbital angular momentum of partons. Section 11.5 discusses the measurement of GTMDs on the lattice, while Sec. 11.6 considers the evaluation of the GTMDs and Wigner distributions in specific models.

## 2 - Definition of TMDs

In this chapter we introduce theoretical background as well as complete definitions of transverse momentum distribution functions. For simplicity, we focus on the Drell-Yan process in proton-proton collisions,  $pp \rightarrow \gamma^*/ZX \rightarrow \ell^+\ell^-X$  with unpolarized protons, as a physical example that connects TMD PDFs to experiment. Here  $X$  is the hadronic debris from the deeply inelastic collision. We also consider SIDIS,  $e^-p \rightarrow e^-HX$ , where  $H$  is the fragmentation hadron. We start with basic ideas from the parton model in Sec. 2.1, followed by an overview of results obtained from TMD factorization in Sec. 2.2. In Sec. 2.3 we discuss the basic ingredients necessary for the most popular definition of TMD PDFs, which can be constructed using various different rapidity regulators, as reviewed in Sec. 2.4. In Sec. 2.5 we discuss alternate definitions where both the TMD PDFs and the short distance part of the Drell-Yan factorization theorem depend on an additional rapidity variable.

Next, we generalize the discussion to include polarized protons which gives us access to the full range of spin dependent leading power TMD functions, displayed in Fig. 1.7, and the analogous TMD fragmentation functions. The complete field theory definitions for leading power spin dependent TMD PDFs and TMD FFs for both quarks and gluons are given in Sec. 2.7. We then consider two theoretical methods to obtain insight into these distributions. For perturbative  $k_T \gg \Lambda_{\text{QCD}}$ , connections between these TMD PDFs and longitudinal PDFs are discussed in Sec. 2.8. In Sec. 2.9 we discuss the relationship between collinear PDFs and TMD PDFs. Then in Sec. 2.10 we discuss the use of matrix elements employed in Lattice QCD computations that can be connected to TMD PDFs, providing an introduction to the more detailed discussion in Sec. 6.

Finally, in Sec. 2.11 we give full leading power results for TMD cross sections with polarized protons, discussing the Drell-Yan process, semi-inclusive deep inelastic scattering (SIDIS)  $e^-p \rightarrow e^-HX$  which involves both a TMD PDF for the proton  $p$  and a TMD FF for the hadron  $H$ , and  $e^+e^-$  collisions with the back-to-back production of two identified hadrons  $H_1$  and  $H_2$ ,  $e^+e^- \rightarrow H_1H_2X$ , which involves two TMD FFs.

Some fundamental aspects of our notation are also introduced in this chapter. A summary of our notation including relations to alternates used in the literature can also be found in appendix A.

### 2.1 Basic Ideas from the Parton Model

Before turning to the modern definitions of TMD PDFs, we start with a historical review with the goal of building intuition about the physics encoded in TMDs. The intuitive concepts of both parton distributions and TMD parton distributions significantly predate QCD, by a number of years [35]. They arise naturally whenever the kinematics of a process, viewed from a parton model perspective, imply sensitivity to the longitudinal momentum fraction that the colliding partons have relative to the bound state that contains them, as well as their small intrinsic transverse motion in the bound state. In this section we base our discussion on the generalized parton model, which allows for the presence of gluon radiation.

### 2.1.1 Drell-Yan in the Parton Model

To facilitate discussion of this parton model (and its generalization to include transverse momentum dependence), we first consider the unpolarized Drell-Yan process, where two protons collide to produce a lepton pair,

$$p(P_A) + p(P_B) \rightarrow \ell^+ + \ell^- + X. \quad (2.1)$$

Here  $X$  denotes all the other final-state particles, including the proton remnants and those produced along with the leptons. In this process, the measurement of the leptonic momentum probes the kinematics of the colliding quark and anti-quark partons in the protons through the hard process  $q\bar{q} \rightarrow \gamma^*(q)/Z(q) \rightarrow \ell^+\ell^-$ . Here  $P_A^\mu$  and  $P_B^\mu$  are the proton momenta, and  $q^\mu$  is the momentum of the virtual photon or  $Z$ -boson. The nature of this probe is made precise through factorization formulas which describe the cross section for the hadronic collisions.

Let us start by reviewing the intuition embodied in the most basic collinear version for inclusive Drell-Yan integrated over all transverse momenta:

$$\frac{d\sigma}{dQ^2 dY} = \sum_{i,j} \int_{x_a}^1 d\xi_a \int_{x_b}^1 d\xi_b f_{i/H_a}(\xi_a) f_{j/H_b}(\xi_b) \frac{d\hat{\sigma}_{ij}(\xi_a, \xi_b)}{dQ^2 dY} \left[ 1 + O\left(\frac{\Lambda_{\text{QCD}}^2}{Q^2}\right) \right]. \quad (2.2)$$

Here  $Q^2 = q^2$  is the invariant mass of the  $\ell^+\ell^-$  pair,  $Y$  is their rapidity, a variable that is related to their polar angle from the collision axis (precise definitions can be found in Sec. 2.2), and

$$x_a = Q e^{+Y}/\sqrt{s}, \quad x_b = Q e^{-Y}/\sqrt{s}, \quad (2.3)$$

where  $s = (P_A + P_B)^2$  is the invariant mass for the incoming pair of hadrons. Equation (2.2) expresses the natural classical intuition for scattering of composite particles with point-like constituents for  $Q^2 \gg \Lambda_{\text{QCD}}^2$ , and has corrections suppressed by  $O(\Lambda_{\text{QCD}}^2/Q^2)$  as indicated. The total cross section  $d\sigma$  contains the cross section  $d\hat{\sigma}_{ij}$  for the partonic process

$$i(p_a) + j(p_b) \rightarrow \ell^+ + \ell^- + X. \quad (2.4)$$

Here, we scatter partons of type  $i$  and  $j$  with momenta  $p_a^\mu$  and  $p_b^\mu$ , and these momenta have longitudinal momentum fractions  $\xi_a$  and  $\xi_b$  relative to the longitudinal components of  $P_A$  and  $P_B$  respectively. In Eq. (2.2), this partonic cross section is multiplied by a probability density  $f_{i/H_a}(\xi_a)$  for finding a parton  $i$  in hadron  $H_a$  with momentum fraction  $\xi_a$ , times a probability density  $f_{j/H_b}(\xi_b)$  for finding a parton  $j$  in hadron  $H_b$  with momentum fraction  $\xi_b$ . These are combined with an integral over all possible momentum fractions and a sum over all parton types, which includes both quarks and antiquarks of various flavors, and gluons. In an observable like (2.2), that has been averaged over the large allowed physical range for the transverse momentum of the dilepton pair, it is reasonable that the exact transverse momentum dependence of the partons in the convolution integral is not numerically important. Thus it is sensible that what appears is the average of the small transverse momentum within the target structures, so that the densities  $f_{i/H_a}(\xi_a)$  and  $f_{j/H_b}(\xi_b)$  are functions of only the longitudinal momentum components.

The situation changes if one considers a more detailed cross section, differential in the transverse momentum  $\mathbf{q}_T$  of the dilepton pair. Here a measurement of  $Q$ ,  $Y$ , and  $\mathbf{q}_T$  is equivalent to a measurement of the full dilepton four-momentum  $q$ . If the transverse momentum is large (e.g.,  $q_T \sim Q$ ), the simplest generalization of (2.2) is adequate, with the partonic cross section made differential in the transverse momentum,

$$\frac{d\sigma}{d^4q} = \sum_{i,j} \int_{x_a}^1 d\xi_a \int_{x_b}^1 d\xi_b f_{i/H_a}(\xi_a) f_{j/H_b}(\xi_b) \frac{d\hat{\sigma}_{ij}(\xi_a, \xi_b)}{d^4q} \left[ 1 + O\left(\frac{\Lambda_{\text{QCD}}^2}{q_T^2}, \frac{\Lambda_{\text{QCD}}^2}{Q^2}\right) \right]. \quad (2.5)$$

(Large  $q_T$ )

Since the transverse momentum is large, the comparatively small transverse momentum generated by bound state effects inside the targets can still be ignored in calculations of the differential partonic cross section. Thus, the distribution functions still depend only on longitudinal components of momentum,  $\xi_A$  and  $\xi_B$ .

As smaller transverse momenta are considered, this becomes less reasonable, and in the vicinity of  $q_T \sim \Lambda_{\text{QCD}}$ , it becomes clear from momentum conservation alone that the differential cross section is very sensitive to the small transverse momentum inside the colliding bound states. For the regime where  $\Lambda_{\text{QCD}} \lesssim q_T \ll Q$  a different partonic picture is needed, wherein the probability densities describing the incoming colliding bound states include dependence on the small transverse momenta. This TMD version of the parton model is

$$\frac{d\sigma}{d^4q} = \frac{1}{s} \sum_{i \in \text{flavors}} \hat{\sigma}_{ii}^{\text{TMD}}(Q) \int d^2\mathbf{k}_T f_{i/H_a}(x_a, \mathbf{k}_T) f_{\bar{i}/H_b}(x_b, \mathbf{q}_T - \mathbf{k}_T) \left[ 1 + O\left(\frac{q_T^2}{Q^2}, \frac{\Lambda_{\text{QCD}}^2}{Q^2}\right) \right]. \quad (2.6)$$

(Small  $q_T$ )

This equation again represents a natural model rooted in classical intuition. A partonic cross section (represented by  $\hat{\sigma}_{ii}^{\text{TMD}}$ ) multiplies a product of probability densities  $f_{i/H_a}$  and  $f_{\bar{i}/H_b}$  for finding partons  $i$  and  $\bar{i}$ . Now, however, these densities depend on both longitudinal momentum fractions ( $x_a$  and  $x_b$ ) and transverse ( $\mathbf{k}_T$  and  $\mathbf{q}_T - \mathbf{k}_T$ ) components of the incoming parton momenta. Since we impose that  $q_T \ll Q$ , all other particles (denoted as  $X$  in Eq. (2.1)) must themselves have small transverse momentum. These restrictions imply that the longitudinal momentum fractions are fixed to  $x_a$  and  $x_b$  and there is no longer an integral over the fractions  $\xi_{a,b}$ , but there is now an integral over transverse momenta which are constrained to add up to  $\mathbf{q}_T$ . Due to the restriction to the leading terms in the small  $q_T$  limit, the parton types  $i$  and  $\bar{i}$  in the sum in Eq. (2.6) are restricted to quarks and anti-quarks of the same flavor ( $\bar{i}$  being the charge conjugate of  $i$ ). This region of small transverse momentum is evidently more sensitive to details of the target structure than either the large transverse momentum region described by (2.5) or the transverse integrated cross section in (2.2).

In practice, one often works with the Fourier-transformed TMD PDF, which is defined as

$$\tilde{f}_{i/H}(x, \mathbf{b}_T) = \int d^2\mathbf{k}_T e^{-i\mathbf{b}_T \cdot \mathbf{k}_T} f_{i/H}(x, \mathbf{k}_T). \quad (2.7)$$

Here,  $\mathbf{b}_T$  is Fourier-conjugate to the transverse momentum  $\mathbf{k}_T$ , and  $\tilde{f}_{i/H}(x, \mathbf{b}_T)$  is referred to as the transverse position space or coordinate space distribution. We provide some additional

details on the Fourier transform in appendix C. Inserting Eq. (2.7) into Eq. (2.6), one obtains the equivalent result

$$\frac{d\sigma}{d^4q} = \frac{1}{s} \sum_{i \in \text{flavors}} \hat{\sigma}_{i\bar{i}}^{\text{TMD}}(Q) \int \frac{d^2\mathbf{b}_T}{(2\pi)^2} e^{i\mathbf{b}_T \cdot \mathbf{q}_T} \tilde{f}_{i/H_a}(x_a, \mathbf{b}_T) \tilde{f}_{\bar{i}/H_b}(x_b, \mathbf{b}_T) \left[ 1 + O\left(\frac{q_T^2}{Q^2}, \frac{\Lambda_{\text{QCD}}^2}{Q^2}\right) \right]. \quad (2.8)$$

Compared to Eq. (2.6), we have traded the convolution integral in  $\mathbf{p}_T$  for the inverse Fourier transform in  $\mathbf{b}_T$ , which in practice is more convenient to work with and thus the preferred choice for most phenomenological applications. Note however that despite working in  $\mathbf{b}_T$  space, Eq. (2.8) receives the same corrections in  $q_T/Q$  and  $\Lambda_{\text{QCD}}/Q$  as Eq. (2.6), and thus is valid only at small  $q_T \ll Q$ .

Eqs. (2.2-2.6) alone are already useful as phenomenological models, even without the introduction of field theoretic concepts. We will see that when we treat the problem field-theoretically, there is more than one type of leading-order TMD PDF, even in the situation discussed here with unpolarized hadrons  $H_{A,B}$ , cf. Fig. 1.7. It is worth pausing to remark on several points of interpretation. First, the parton densities are understood here to be intrinsic to the structure of the colliding hadrons, insensitive to the type of process, and thus universal. This will be important, as the universality is a major part of the predictive power of the parton model. Second, the differential cross section  $\hat{\sigma}_{i\bar{i}}$  for partonic scattering is of course very sensitive to the specific type of overall cross section of which it is a part. However, it also involves a large  $Q$ , and this ultimately ensures that it is sensitive only to the dynamics of small time and distance scales of order  $\sim Q^{-1}$ . This turns out to make it ideal for calculations in perturbation theory, made possible by the asymptotic freedom of QCD.

The study of TMDs is the study of the small  $q_T$  behavior in Eq. (2.6), motivated largely by the expectation that the small transverse momentum dependence in the TMD PDFs,  $f_{i/H_a}(x_a, \mathbf{k}_T)$  and  $f_{j/H_b}(x_b, \mathbf{q}_T - \mathbf{k}_T)$ , carries more information about nucleon structure than the more standard collinear PDFs  $f_{i/H_A}(\xi_a)$  and  $f_{j/H_b}(\xi_b)$ .

## 2.1.2 SIDIS in the Parton Model

In addition to the parton distributions  $f_{i/h}$ , another important set of distribution functions for probing hadronic structure are the fragmentation functions  $D_{h/j}$ , which describe the process whereby a parton  $j$  is converted to a final state hadron  $h$ . To introduce them we consider the semi-inclusive DIS (SIDIS) process where an electron and proton collide inelastically, with a measured final state hadron  $h$ ,

$$e^-(l) + p(P) \rightarrow e^-(l') + h(P_h) + X. \quad (2.9)$$

Here,  $l^\mu$  and  $l'^\mu$  are the initial and final electron momenta,  $P^\mu$  is the proton momentum, and  $P_h^\mu$  is the final hadron's momentum. Once again  $X$  denotes hadronic debris from this deep inelastic collision. This process probes the short distance scattering of the electron and a quark of flavor  $i$  in the proton,  $e^- i \rightarrow e^- i$ , through exchange of a virtual photon or Z-boson with spacelike momentum  $q^\mu$ , so that

$$q^\mu = l^\mu - l'^\mu, \quad q^2 = -Q^2 < 0. \quad (2.10)$$

The final state quark  $i$  then fragments to the hadron  $h$ . Key variables for describing the SIDIS cross section include

$$x = \frac{Q^2}{2P \cdot q}, \quad y = \frac{P \cdot q}{P \cdot l}, \quad z_h = \frac{P \cdot P_h}{P \cdot q}. \quad (2.11)$$

Here,  $x$  is the standard DIS Bjorken scaling variable. In the proton rest frame,  $y$  is the fractional energy loss of the electron, and  $z_h$  is the ratio of the energy of the hadron to that of the  $\gamma^*/Z^*$  in the proton rest frame.

Again we start with the basic collinear version of the fragmentation process, with an unpolarized proton and without a measurement of final state transverse momentum:

$$\frac{d\sigma}{dx dy dz_h} = \sum_{i,j} \int_x^1 d\xi \int_{z_h}^1 d\zeta f_{i/p}(\xi) D_{h/j}(\zeta) \frac{d\hat{\sigma}_{ij}(\xi, \zeta)}{dx dy dz_h} \left[ 1 + O\left(\frac{\Lambda_{\text{QCD}}^2}{Q^2}\right) \right]. \quad (2.12)$$

Here,  $d\hat{\sigma}_{ij}$  is the cross section for scattering a parton of type  $i$  into a parton of type  $j$ , i.e., it corresponds to the partonic process

$$e^-(l) + i(k) \rightarrow e^-(l') + j(p) + X. \quad (2.13)$$

For the incoming parton  $i$  with momentum  $k^\mu$ , the momentum fraction  $\xi$  is defined as the ratio of the longitudinal momentum component of  $k^\mu$  relative to the proton momentum  $P^\mu$ . For the outgoing parton  $j$  with momentum  $p^\mu$ , the momentum fraction  $\zeta$  is defined as the ratio of the longitudinal momentum component of  $P_h^\mu$  relative to  $p^\mu$ . In Eq. (2.12) the partonic cross section  $d\hat{\sigma}_{ij}$  is combined with a probability density  $f_{i/p}(\xi)$  for finding the parton  $i$  in the proton with momentum fraction  $\xi$ . In addition it is combined with  $D_{h/j}(\zeta)$  for the fragmentation process, which is the probability density for the parton  $j$  to fragment to a hadron  $h$ , where  $h$  has a fraction  $\zeta$  of the parton's momentum. Equation (2.12) is the direct analog of the Drell-Yan cross section in Eq. (2.2), except with one parton distribution function and one fragmentation function, rather than two parton distribution functions.

To make the process more differential, we consider measuring in addition the transverse momentum  $\mathbf{P}_{hT}$  of the hadron  $h$ . We choose to define  $\mathbf{P}_{hT}$  in the  $\gamma^* p$  center of mass frame, with 3-momenta  $\mathbf{q}$  and  $\mathbf{P}$  aligned along the  $z$ -axis, such that it satisfies  $\mathbf{q} \cdot \mathbf{P}_{hT} = \mathbf{P} \cdot \mathbf{P}_{hT} = 0$ . (For further details about this frame, see the extended discussion in Sec. 2.11.) For simplicity, we continue to consider unpolarized protons and measure only the magnitude of the transverse momentum,  $P_{hT} = |\mathbf{P}_{hT}|$ .

For large  $P_{hT} \sim Q$  the transverse momentum of the hadron is inherited from the transverse momentum of the parton  $j$  at leading order in  $\Lambda_{\text{QCD}}^2/P_{hT}^2 \ll 1$ . This yields a parton model cross section that is similar in form to Eq. (2.12), but with the cross section  $d\hat{\sigma}_{ij}(\xi, \zeta)/dx dy dz_h dP_{hT}^2$  in the integrand. This is the exact analog of the Drell-Yan generalization, in going from Eq. (2.2) to Eq. (2.5).

On the other hand, for small  $P_{hT}$  we begin to probe transverse momentum in the fragmentation process, while at the same time becoming sensitive to the transverse momentum of the initial state parton inside the proton. In particular for  $\Lambda_{\text{QCD}} \lesssim P_{hT} \ll Q$  the TMD version of

the parton model cross section is

$$\frac{d\sigma}{dxdydz_h d^2\mathbf{P}_{hT}} = \sum_i \hat{\delta}_{ii}^{\text{TMD}}(Q, x, y) \int d^2\mathbf{p}_T d^2\mathbf{k}_T \delta^{(2)}(\mathbf{P}_{hT} - z_h \mathbf{k}_T - \mathbf{p}_T) f_{i/p}(x, \mathbf{k}_T) D_{h/i}(z_h, \mathbf{p}_T) \\ \times \left[ 1 + O\left(\frac{P_{hT}^2}{Q^2}, \frac{\Lambda_{\text{QCD}}^2}{Q^2}\right) \right] \quad (\text{Small } P_{hT}). \quad (2.14)$$

Once again with the parton model description, we have a factor  $\hat{\delta}_{ii}^{\text{TMD}}$  determined by the partonic cross section multiplying probability densities  $f_{i/p}$  and  $D_{h/i}$ , which now depend on both longitudinal momentum fractions ( $x$  and  $z_h$ ) and transverse momenta. The restrictions on final state radiation fix the longitudinal momentum fractions appearing in the TMDs, and imply that it is the same parton flavor  $i$  appearing in both TMD functions in Eq. (2.14). Here the TMD fragmentation function  $D_{h/i}(z_h, \mathbf{p}_T)$  gives the probability of parton  $i$  fragmenting to hadron  $h$  with longitudinal momentum fraction  $z_h$ , where the hadron  $h$  has a transverse momentum  $\mathbf{p}_T$  relative to the direction of motion of the parton  $i$ . In the frame where it is the proton and outgoing hadron that are aligned along the  $z$ -direction, the transverse momentum conservation is given by the partonic formula  $\mathbf{k}_T + \mathbf{q}_T = -\mathbf{p}_T/z_h$ . In the  $\gamma^* p$  rest frame used here, we replace  $\mathbf{q}_T \rightarrow -\mathbf{P}_{hT}/z_h$ , which yields the  $\delta$ -function in Eq. (2.14).

Once again it is useful to work with the Fourier-transformed TMD FF,

$$\tilde{D}_{h/i}(z, \mathbf{b}_T) = \frac{1}{z^2} \int d^2\mathbf{p}_T e^{-i\mathbf{b}_T \cdot \mathbf{p}_T/z} D_{h/i}(z, \mathbf{p}_T) \\ = \int d^2\mathbf{p}'_T e^{+i\mathbf{b}_T \cdot \mathbf{p}'_T} D_{h/i}(z, -z\mathbf{p}'_T). \quad (2.15)$$

Here we see that for the fragmentation function  $\tilde{D}_{h/i}(z, \mathbf{b}_T)$  the transverse position  $\mathbf{b}_T$  is defined as the Fourier conjugate variable to  $\mathbf{p}'_T$ , the momentum of the incoming quark in a frame where the transverse momentum of the hadron  $h$  vanishes.

Together with Eq. (2.7), this enables us to write Eq. (2.14) in an equivalent fashion as

$$\frac{d\sigma}{dxdydz_h dP_{hT}^2} = \sum_{i \in \text{flavors}} \hat{\delta}_{ii}^{\text{TMD}}(Q, x, y) \int_0^{2\pi} d\phi_h \int d^2\mathbf{b}_T e^{+i\mathbf{b}_T \cdot \mathbf{P}_{hT}/z_h} \tilde{f}_{i/p}(x, \mathbf{b}_T) \tilde{D}_{h/i}(z_h, \mathbf{b}_T) \\ \times \left[ 1 + O\left(\frac{P_{hT}^2}{Q^2}, \frac{\Lambda_{\text{QCD}}^2}{Q^2}\right) \right]. \quad (2.16)$$

Here  $\phi_h$  is the transverse angle of the vector  $\mathbf{P}_{hT}$ . We will take up an extended version of this formula, which is derived from QCD and applies for polarized protons and with additional angular measurements, in Sec. 2.11.

### 2.1.3 Beyond the Parton Model

With this introduction of the concepts, several key points need to be addressed. Parton model descriptions like Eqs. (2.2-2.6) need to be justified in QCD. This is the topic of factorization theorems, to be discussed in Sec. 3. A related question that must be addressed is exactly how to define the PDFs and TMD PDFs (and similar objects) in quantum field theory. While

many aspects of the parton picture remain valid, there are a number of important caveats that arise, such as the dependence on parameters associated with the renormalization scheme, like the renormalization scale  $\mu$ . A central goal of the next few sections will be to flesh out in detail the quantum field theory definition of TMD PDFs and TMD FFs that arise from the proof of factorization theorems for TMD sensitive cross sections.

As a prelude to some of the extra ingredients that appear, we will briefly review the field theory definition of the unpolarized collinear PDF for a parton of flavor  $i$  in a hadron  $H$ . The definition for these PDFs is much simpler than the corresponding definition for TMD PDFs. In quantum field theory the starting point is the definition of a bare parton distribution

$$f_{i/H}^0(\xi) = \int \frac{dw^-}{2\pi} e^{-i\xi P^+ w^-} \langle H(P) | \bar{\psi}_i^0(0, w^-, \mathbf{0}_T) \frac{\gamma^+}{2} W_{n_a}(w^-, 0) \psi_i^0(0, 0, \mathbf{0}_T) | H(P) \rangle. \quad (2.17)$$

This formula involves a Wilson line operator  $W_{n_a}(w^-, 0)$  connecting the points 0 and  $w^-$  along the light-cone, which ensures gauge invariance (see Eq. (2.43), explicit definitions of the notation used here are left to Secs. 2.2 and 2.3). The 0 superscripts in Eq. (2.17) denote bare quantities. The bare fields obey canonical commutation relations and thus give a true number density interpretation. (In a free field theory we can set  $W_{n_a} = 1$  and Eq. (2.17) becomes a literal number density.) Implicit in this definition is the presence of an ultraviolet regulator, like dimensional regularization. Of course, for a renormalizable interacting theory like QCD, this bare definition needs to be replaced by something involving renormalized quantities for it to be useful. In the most commonly used  $\overline{\text{MS}}$  scheme, this process is carried out by (minimal) removal of ultraviolet divergences with a renormalization factor  $Z_{ij}^{\text{PDF}}$ , and introduces dependence on the renormalization scale  $\mu$ , yielding

$$f_{i/H}(\xi, \mu) = \sum_j \int_\xi^1 \frac{dz}{z} Z_{ij}^{\text{PDF}}(z, \mu) f_{j/H}^0(\xi/z). \quad (2.18)$$

Since the renormalization involves a mixing of parton types, it contains a sum over  $j$ . We see that the renormalized PDF  $f_{i/H}(\xi, \mu)$  is obtained by a type of generalized multiplicative renormalization of the bare PDF. Here the parameter  $\mu$  plays the role of a momentum cutoff on the fluctuations from quantum fields that are retained in the PDF. It is effectively speaking akin to a cutoff on invariant mass,  $|p^2| \lesssim \mu^2$ , but where the cutoff  $\mu$  has been introduced in a gauge invariant manner.

The renormalization procedure also introduces a dependence on  $\mu$  into the short distance partonic cross section, such as  $d\hat{\sigma}_{ij}(\xi_a, \xi_b, \mu)/d^4q$  in Eq. (2.5). Ultimately, the choice of  $\mu$  is dictated by the requirement that the partonic scattering cross sections are well-behaved perturbatively (with no large logarithms in  $d\hat{\sigma}_{ij}$ ). Therefore the PDFs are not literally process independent, since different processes will require different choices of  $\mu$ . However, the dependence on  $\mu$  can be systematically calculated with perturbative evolution equations, which for the PDF are known as the DGLAP equations [36–39]. Once this is accounted for, the PDFs can be understood to be effectively universal.

For the TMD PDFs (and fragmentation functions) extra subtleties enter beyond the need for ultraviolet renormalization, both formally and in their interpretation, and these issues are among the main topics of sections 2.2–2.5 in this chapter. Here we give a brief review of

the historical landmarks that characterized the development of the current rigorous understanding. It was realized by the late 1990s or early 2000s that existing definitions were not adequate for some applications, especially those associated with hadron structure. (Readers reviewing the relevant literature from the 1970s-1990s should be aware that terminology has evolved significantly since that time and, for example, the “TMD” label only became pervasive comparatively recently. In some parts of this earlier literature, terms like “unintegrated” PDF are used interchangeably with “TMD PDF.”) A useful review of the status of TMD PDF definitions and associated open problems as they were understood around 2003 is found in [40], and it provides a useful context for the last two decades of development. An issue highlighted there that will be relevant to the discussions below is the appearance of so-called rapidity (or light-cone) divergences in the most natural candidate definitions for TMD PDFs. Rapidity divergences correspond to configurations of partons moving with infinite rapidity in a direction *opposite* the direction of motion of the parent hadron. They are regulated by neither the non-perturbative infrared physics nor by the ultraviolet regulators, and so they signal a significant challenge to any proposed definition. Ways of dealing with them will be discussed in much more detail in coming sections. The basic problem of light-cone divergences and the need to regulate them was recognized very early on. For example, Refs. [41] and [42] pointed out that an extra parameter they called  $\zeta = (2P \cdot n)^2 / (-n^2)$  appears in some QCD calculations, where the “ $\zeta$ ” notation is meant to be reminiscent of the Mandelstam  $s$  and thereby evoke a kind of evolution with collision energy. In their definition of  $\zeta$ ,  $P$  is a target hadron four-momentum and  $n$  is a non-light-like gauge fixing vector with  $n^2 \neq 0$ . The  $\zeta$  acts effectively as a rapidity regulator and the need to fix it ultimately becomes associated with a new type of evolution. Collins derived the corresponding evolution for the Sudakov form factor in Ref. [43], and in the Collins-Soper-Sterman (CSS) formalism the analogous behavior appears as the Collins-Soper (CS) equation. Fundamentally, the rapidity divergences are artifacts of approximations at the level of the factorization derivations that place the Wilson lines appearing in the gauge invariant form of TMD definitions exactly on the light cone. Therefore, regulating them while maintaining explicit gauge invariance in definitions amounts to shifting the Wilson lines slightly off the light cone, see Refs. [44, 45] for early discussions of Wilson lines in TMD PDFs. The importance of including a transverse gauge link at light-cone infinity to obtain fully gauge invariant results was pointed out in Ref. [46].

The role of Wilson lines was also important in early discussions concerning the use of TMD correlation functions for describing nontrivial polarization dependence, and it was one of the motivating factors that led to later refinements to TMD definitions. A now famous TMD mechanism called the Sivers effect [47] was proposed in 1990 to explain the larger than expected transverse single spin asymmetries in experiments like [48–54].<sup>1</sup> An argument presented in [57], however, appeared to show using the time-reversal and parity ( $TP$ ) invariance of QCD that the Sivers TMD must be zero. A later model calculation in 2002 by Brodsky, Hwang, and Schmidt (BHS) [58] showed that a Sivers-like asymmetry *does* arise at leading power in processes like SIDIS, and they interpreted this as indicating a conflict with factorization. A more detailed description of this influential calculation can be found in Sec. 7.2. Work in [59] addressing the BHS result demonstrated that TMD factorization actually does hold, and is not in contradiction with the definition of a Sivers TMD, despite the earlier proof appearing to

---

<sup>1</sup>See also Ref. [55, 56]

show it must vanish by  $TP$  invariance. The loophole is that the  $TP$ -based argument neglected a non-trivial role for the Wilson lines in TMD correlation functions. Once they are taken into account in the factorization derivation,  $TP$  invariance shows not that the Sivers function vanishes, but that it acquires a process-dependent overall sign [59]. In other words, the apparent proof that the Sivers function vanishes by  $TP$  invariance is the consequence of an overly literal interpretation of the TMD PDF as a simple number density.

While the Wilson lines in collinear correlation functions can sometimes appear to be largely formalistic, the examples above, of the light-cone divergences and the process-dependent sign on some TMD PDFs, highlight the central role Wilson line structures play in TMD factorization (see chapter 3). Another driving motivation to revisit the issue of TMD PDF definitions in the early 2000s was that their domain of practical application began to broaden. The focus of early applications was to a handful of specific processes at collider energies, where the role played by intrinsic non-perturbative transverse structure was of less direct interest, and could possibly even be viewed as a nuisance in some applications. However, the TMD concept was being used increasingly in hadron structure studies. (An extensive classification of the various polarization structures allowable in a TMD approach was developed by Boer, Mulders, and Tangerman in the mid 1990s in, for example, Refs. [60–62].) Some of the work needed to orient CSS-based treatments more toward hadron structure was simply organizational. For example, in the practical cross section formulas like Eq. (1.1) of Ref. [63], tracing the various factors back to the separate operator definitions for specific TMD correlation functions is non-obvious. (Indeed, non-perturbative transverse momentum contributions are only explicitly introduced later in Eq. (5.6).) It was pointed out in Refs. [64, 65] that the original CSS-like organization placed process dependent perturbative contributions not in an overall explicitly factorized hard part, but in exponential factors that resemble evolution contributions for separate TMD functions. In the context of resummation approaches to transverse momentum distributions, later work reorganized these non-universal perturbative contributions into explicitly separate hard factors [66–70].

Other complications appeared to be more fundamental, such as the nontrivial dependence on the structure of Wilson lines structures discussed above, and the realization that CSS-type factorization might break in cases where it is reasonable to conjecture that it might hold (see Sec. 3.4 for more on this).

Proposals for refining the TMD definitions during this period can be found in, for example, Refs. [40, 46, 71–82]. The treatment that has since been settled upon was provided in the textbook of Collins in 2011 [10], and an application to hadron structure phenomenology was presented in Ref. [83].

## 2.2 TMD Factorization Theorem for Drell-Yan

In this section we give a basic introduction to the TMD factorization theorems that describe the Drell-Yan process,  $pp \rightarrow \gamma^*/Z \rightarrow \ell^+\ell^-$  with unpolarized protons, which serves to set up basic notation and concepts for TMD factorization.

For the analysis of hard scattering processes it is useful to use light-cone coordinates since the hadronic dynamics are always preferentially probed along the collision axis and involve partons whose dynamics are described by fluctuations near the light-cone. We choose the  $\hat{z}$ -axis for the incoming protons in the  $pp$  collision and in terms of  $(t, x, y, z)$  components

define the light-like basis vectors

$$n_a^\mu = \frac{1}{\sqrt{2}}(1, 0, 0, 1), \quad n_b^\mu = \frac{1}{\sqrt{2}}(1, 0, 0, -1), \quad (2.19)$$

with  $n_a^2 = n_b^2 = 0$  and  $n_a \cdot n_b = 1$ . Any four vector can then be decomposed in terms of these basis vectors as

$$p^\mu = (n_b \cdot p)n_a^\mu + (n_a \cdot p)n_b^\mu + p_T^\mu \equiv (p^+, p^-, \mathbf{p}_T). \quad (2.20)$$

In the second equation, we introduced a common short-hand notation for the light-cone decomposition. Its components are defined as

$$p^+ \equiv n_b \cdot p = \frac{1}{\sqrt{2}}(p^0 + p^z), \quad p^- \equiv n_a \cdot p = \frac{1}{\sqrt{2}}(p^0 - p^z), \quad \mathbf{p}_T = (p_x, p_y). \quad (2.21)$$

Note that  $\mathbf{p}_T$  is treated as a standard two-dimensional vector in Euclidean space, as opposed to the corresponding Minkowski vector  $p_T^\mu = (0, p_x, p_y, 0)$ . This leaves an ambiguity in defining its magnitude, which we define as

$$p_T \equiv |\mathbf{p}_T| = \sqrt{-p_T \cdot p_T}, \quad (2.22)$$

where only the latter expression involves a scalar product in Minkowskian signature.

In lightcone coordinates, Lorentz-invariant scalar products take the simple form

$$p \cdot b = p^+ b^- + p^- b^+ - \mathbf{p}_T \cdot \mathbf{b}_T, \quad p^2 = 2p^+ p^- - \mathbf{p}_T^2 = 2p^+ p^- - p_T^2. \quad (2.23)$$

These coordinates are particularly convenient to discuss energetic hadrons. For example, the momenta  $P_A$  and  $P_B$  of the incoming protons in the Drell-Yan process are given by

$$P_A^\mu = P_A^+(1, e^{-2Y_A}, \mathbf{0}_T), \quad P_B^\mu = P_B^-(e^{+2Y_B}, 1, \mathbf{0}_T), \quad (2.24)$$

where the components are  $p^\mu = (p^+, p^-, \mathbf{p}_T)$  and the proton rapidities are defined as

$$Y_A = \frac{1}{2} \ln \frac{P_A^+}{P_A^-} = \frac{1}{2} \ln \frac{2(P_A^+)^2}{m_p^2}, \quad Y_B = \frac{1}{2} \ln \frac{P_B^+}{P_B^-} = \frac{1}{2} \ln \frac{m_p^2}{2(P_B^-)^2}. \quad (2.25)$$

Eq. (2.24) makes it clear that the momenta  $P_{A,B}$  are aligned along the  $n_{a,b}$  directions. In the limit of taking the protons massless,  $m_p \rightarrow 0$ , we have  $Y_{A,B} \rightarrow \pm\infty$  and the protons are exactly aligned along  $n_{a,b}$ .

Consider the production of a Drell-Yan pair  $\ell^+ \ell^-$  with total momentum  $q^\mu$ , and invariant mass  $Q^2 = q^2$ . Decomposing  $q^\mu$  in light cone coordinates we can then define the lepton pair's rapidity  $Y$  and transverse momentum  $q_T$  by

$$Y = \frac{1}{2} \ln \left( \frac{n_b \cdot q}{n_a \cdot q} \right) = \frac{1}{2} \ln \left( \frac{q^+}{q^-} \right), \quad q_T^\mu = q^\mu - n_a^\mu n_b \cdot q - n_b^\mu n_a \cdot q = (0, q_T^x, q_T^y, 0). \quad (2.26)$$

We denote the Euclidean transverse momentum as  $\mathbf{q}_T$ , and also use a plain  $q_T$  to denote the magnitude of the Euclidean vector  $q_T = |\mathbf{q}_T|$ , but write the magnitude squared as  $\mathbf{q}_T^2 = (q_T^x)^2 + (q_T^y)^2$ . (This avoids the notational issue of using  $q_T^2$ , which can be mistaken as a four-vector squared.) We assume  $Q^2 \gg \Lambda_{\text{QCD}}^2$ , but for the transverse momentum we allow both  $q_T \sim \Lambda_{\text{QCD}}$  and  $q_T \gg \Lambda_{\text{QCD}}$ . We decompose the cross section as

$$\frac{d\sigma}{dQdYd^2\mathbf{q}_T} = \left( \frac{d\sigma^W}{dQdYd^2\mathbf{q}_T} + \frac{d\sigma^Y}{dQdYd^2\mathbf{q}_T} \right) \left[ 1 + \mathcal{O}\left(\frac{\Lambda_{\text{QCD}}^2}{Q^2}\right) \right]. \quad (2.27)$$

Here,  $d\sigma^W$  denotes the most singular part of the cross section, which dominates at small  $q_T$ . It is defined such that at any order in a strict  $\alpha_s$  expansion it includes all terms that exhibit  $1/q_T^2$  behavior as  $q_T \rightarrow 0$ . In practice this singular behavior is tamed by the resummation of large logarithms, see Chapter 4. We use the superscript  $W$  since these contributions are often referred to as the  $W$  term. In contrast, the  $Y$  term, denoted  $d\sigma^Y$ , are non-singular terms that are suppressed by  $\mathcal{O}(q_T^2/Q^2)$  relative to  $d\sigma^W$ .<sup>2</sup> These non-singular components of the cross section are necessary to reproduce the full results for the partonic cross sections  $d\hat{\sigma}_{ij}/dQdYd^2\mathbf{q}_T$  in a fixed order  $\alpha_s$  expansion, and are often referred to as the  $Y$  term [16, 63, 86]. Methods for carrying out the resummation of large logarithms in  $d\sigma^W$  sometime incorporate non-singular terms, with a compensating modification to  $d\sigma^Y$ . As indicated both contributions receive corrections in  $\Lambda_{\text{QCD}}^2/Q^2$ , analogous to the collinear factorization result in Eq. (2.2). In this chapter, we only discuss  $d\sigma^W$ , whose factorization into a piece describing physics at the hard scale  $Q$  and universal TMD PDFs describing physics at the low scale  $q_T$  is well understood, and neglect corrections from  $d\sigma^Y$ . A dedicated discussion of the  $d\sigma^Y$  contributions can be found in Sec. 4.7.

TMD factorization was originally derived by Collins, Soper and Sterman (CSS) in [16, 63, 86]. Refs. [5, 87–90] showed the cancellation of potentially factorization-violating Glauber modes, and the factorization was further elaborated on and extended in [65, 66, 89, 91]. It has also been considered in the framework of Soft-Collinear Effective Theory (SCET) [92–95] by various authors [96–102]. For a relation of the different approaches to each other, see e.g. [103, 104]. In the original formulation by Collins and Soper [16, 63, 86] and its modification by Ji, Ma and Yuan [74],  $\sigma^W$  is written as

$$\frac{d\sigma^W}{dQdYd^2\mathbf{q}_T} = \sum_{\text{flavors } i} H_{i\bar{i}}(Q^2, \mu; \rho) \int d^2\mathbf{b}_T e^{i\mathbf{b}_T \cdot \mathbf{q}_T} \tilde{f}_{i/p}(x_a, \mathbf{b}_T, \mu, \tilde{\zeta}_a; \rho) \tilde{f}_{\bar{i}/p}(x_b, \mathbf{b}_T, \mu, \tilde{\zeta}_b; \rho), \quad (2.28)$$

where the  $\tilde{\zeta}$  and  $\rho$  variables are discussed below. In the modern definition by Collins [89], which yields a factorization theorem that is equivalent to many SCET based definitions [96–

---

<sup>2</sup>More generally, fiducial experimental cuts on the phase space of the final state leptons will induce linear  $\mathcal{O}(q_T/Q)$  corrections [84], but these can be computed with the same leading-power factorization technology [85].

102, 105], the singular cross section can be written as

$$\frac{d\sigma^W}{dQ dY d^2\mathbf{q}_T} = \sum_{\text{flavors } i} H_{i\bar{i}}(Q^2, \mu) \int d^2\mathbf{b}_T e^{i\mathbf{b}_T \cdot \mathbf{q}_T} \tilde{f}_{i/p}(x_a, \mathbf{b}_T, \mu, \zeta_a) \tilde{f}_{\bar{i}/p}(x_b, \mathbf{b}_T, \mu, \zeta_b) \quad (2.29a)$$

$$= \sum_{\text{flavors } i} H_{i\bar{i}}(Q^2, \mu) \int d^2\mathbf{b}_T e^{i\mathbf{b}_T \cdot \mathbf{q}_T} \tilde{B}_{i/p}(x_a, \mathbf{b}_T, \mu, \zeta_a/v^2) \tilde{B}_{\bar{i}/p}(x_b, \mathbf{b}_T, \mu, \zeta_b/v^2) \\ \times \tilde{S}_{n_a n_b}(b_T, \mu, v). \quad (2.29b)$$

In Eqs. (2.28) and (2.29) we use the notation  $f = f_1$  and  $\tilde{f} = \tilde{f}_1$  for the unpolarized TMD PDF, and this should be understood as the case in what follows, unless otherwise indicated. We will start by describing the most important ingredients common to Eqs. (2.28, 2.29a, 2.29b), and then return to comparisons between these three equivalent expressions for the cross section. In both Eqs. (2.28) and (2.29), the factorization is written in Fourier space, with  $\mathbf{b}_T$  being Fourier-conjugate to the measured transverse momentum  $\mathbf{q}_T$ , and in both cases the hard function  $H_{i\bar{i}}$  encodes virtual corrections to the underlying hard process  $q_i q_{\bar{i}} \rightarrow \gamma^*/Z \rightarrow l^+ l^-$ , with the quark flavors  $i, \bar{i}$  being summed over. Here  $i$  is a quark flavor and  $\bar{i}$  is the charge conjugate of  $i$ , since other flavor combinations and cases involving gluons occur only in  $d\sigma^Y$ . Note that, whenever possible, we will neglect target mass corrections from  $m_P^2 \ll Q^2$ , together with other  $\Lambda_{\text{QCD}}^2/Q^2$  power corrections.

Compared to our parton model discussion in Eq. (2.6), the TMD PDFs in Eq. (2.29) have dependence on two additional variables, the renormalization scale  $\mu$  and Collins-Soper scales  $\zeta_{a,b}$  [16, 86]. These dependences arise from defining the renormalized TMD PDFs in quantum field theory, while being careful about the treatment of rapidity dependence. A more detailed discussion of the relation between bare and renormalized TMD PDFs is given below in Sec. 2.3, while methods of handling rapidity divergences that appear in intermediate steps of the TMD PDF definitions, and which are related to the appearance of  $\zeta_{a,b}$ , are treated in Sec. 2.4. The dependences of the TMD PDFs on both  $\mu$  and  $\zeta$  are governed by evolution equations, which are discussed in Sec. 4. In particular this enables a TMD PDF  $f_{i/H}(x, \mathbf{b}_T, \mu_0, \zeta_0)$  to be evolved from initial scales  $\mu_0$  and  $\zeta_0$  to final scales  $\mu$  and  $\zeta$ , yielding  $f_{i/H}(x, \mathbf{b}_T, \mu, \zeta)$ . In this context the scales appearing in Eq. (2.29) can be interpreted as the final scales after this evolution. Taking a  $\mu \sim Q$  then minimizes large logarithms in  $H_{i\bar{i}}(Q, \mu)$ . Likewise, the final Collins-Soper scales  $\zeta_{a,b}$  are given by

$$\zeta_a = 2(x_a P_A^+)^2 e^{-2y_n} = x_a^2 m_p^2 e^{2(Y_A - y_n)}, \quad \zeta_b = 2(x_b P_B^-)^2 e^{2y_n} = x_b^2 m_p^2 e^{-2(Y_B - y_n)}, \quad (2.30)$$

such that their product yields the invariant mass of the hard process,

$$\zeta_a \zeta_b = (2x_a x_b P_A^+ P_B^-)^2 = Q^4. \quad (2.31)$$

Here  $2P_A^+ P_B^- \approx (P_A + P_B)^2 = s$  is the center-of-mass energy of the proton-proton collision, while  $Y_A$  and  $Y_B$  are the rapidities of the two protons (which are equal in the center-of-momentum frame,  $Y_A = Y_B = y_P$ ). The rapidity variable  $y_n$  in Eq. (2.30) controls an additional scheme dependence which cancels between the two TMD PDFs. While this allows one to derive evolution equations with respect to  $\zeta_{a,b}$ , there does not appear to be a great benefit from exploiting the  $y_n$  dependence otherwise, and often the simplest choice  $y_n = 0$  is adopted.

In Eqs. (2.28) and (2.29a), the result is written in terms of renormalized TMD PDFs  $f_{i/p}$  and  $f_{\bar{i}/p}$  which give rise to the transverse momentum  $\mathbf{q}_T$ . In contrast, in Eq. (2.29b) it arises from three renormalized functions, namely two beam functions  $B_{i/p}$  and  $B_{\bar{i}/p}$  [106] which describe collinear radiation close to the proton, and the soft function  $S_{n_a n_b}$  encoding soft exchange between the colliding partons  $i$  and  $\bar{i}$ , but which is independent of the quark flavors  $i$  and  $\bar{i}$ . The two cases can be trivially related through

$$\tilde{f}_{i/p}(x, \mathbf{b}_T, \mu, \zeta) = \tilde{B}_{i/p}(x, \mathbf{b}_T, \mu, \zeta/\nu^2) \sqrt{\tilde{S}_{n_a n_b}(b_T, \mu, \nu)}, \quad (2.32)$$

where the so-called rapidity renormalization scale  $\nu$  cancels between  $B_{i/p}$  and  $S_{n_a n_b}$ . The relation in Eq. (2.32) is common in the SCET based constructions in Refs. [96–102, 105], since renormalized beam and soft functions are constructed before combining them into renormalized TMD PDFs. In contrast, in the modern Collins construction [89] only the bare analogs of  $B_{i/p}$  and  $S_{n_a n_b}$  appear, which are directly used to define the renormalized TMD PDFs. Further discussion of these various constructions can be found in Sec. 2.4. In the discussion in Sec. 2.3 we will treat Eqs. (2.29a) and (2.29b) on the same footing.

Finally, we return to discussing the differences between Eqs. (2.28) and (2.29). Here the crucial difference is the scheme employed for the hard function  $H_{i\bar{i}}$ , which from the scheme independence of  $d\sigma^W$  automatically defines the scheme for the product of the two  $f_{i/p}$ s, or the product of the two  $B_{i/p}$ s and  $S_{n_a n_b}$ . Thus two categories of definitions of TMD PDFs can be identified according to the definition of  $H_{i\bar{i}}$  appearing in their associated factorization theorems. In Eq. (2.29),  $H_{i\bar{i}}$  is defined purely in the  $\overline{\text{MS}}$  scheme, and thus only depends on the hard scale  $Q$  and the renormalization scale  $\mu$ . In particular, this  $H_{i\bar{i}}(Q, \mu)$  can be computed by a partonic form factor calculation in dimensional regularization with  $d = 4 - 2\epsilon$ , by simply using  $\overline{\text{MS}}$  subtractions for  $1/\epsilon$  poles. We will refer to approaches that fit within this framework as the  $\overline{\text{MS}}$  class of schemes. In contrast, in Eq. (2.28)  $H_{i\bar{i}}(Q, \mu; \rho)$  also depends on an additional rapidity scale  $\rho$ , and the TMDs use different definitions for the Collins-Soper scales, which are therefore denoted by  $\tilde{\zeta}_{a,b}$ .

In the following we will focus on the most popular TMD PDF schemes, corresponding to the category involving the  $\overline{\text{MS}}$  hard function  $H_{i\bar{i}}(Q, \mu)$ . This includes the discussion in Secs. 2.3 and 2.4. A complete description of the alternate schemes involving  $H_{i\bar{i}}(Q, \mu; \rho)$ , including definitions of the variables  $\rho, \tilde{\zeta}_{a,b}$ , will then be taken up in Sec. 2.5.

## 2.3 Basic Definition of TMD PDFs

The goal of this section is to provide basic rigorous field theory definitions of the TMD PDFs with an emphasis on aspects that are universal across all approaches to handling issues associated with regulating so-called rapidity singularities, leaving differences to the discussion in Sec. 2.4. We focus here entirely on constructions which yield the factorization theorem in Eq. (2.29).

The construction of complete TMD definitions is driven by the following constraints [89], which all of the definitions discussed here will satisfy (up to any exceptions which we will note explicitly):

1. The definition should follow from, and be constrained by, the steps needed to factorize a class of physical processes. In our case, this includes at least those processes for which TMD factorization theorems are most easily derivable:

- $e^+e^-$ -annihilation into a pair of nearly back-to-back hadrons.
  - hadron-hadron production of lepton pairs (Drell-Yan scattering) or weak bosons.
  - Semi-inclusive deep inelastic scattering.
2. It should work at both perturbative and non-perturbative levels. Namely, it should be possible to use it with non-perturbative models of partons, and provide rigorous connections of the definition to calculations done with fundamental non-perturbative methods like lattice QCD.
  3. Gauge invariance should be preserved, ideally before regulators (UV or rapidity) are removed.
  4. Unphysical contributions not present in the unfactorized physical processes should cancel naturally in the definition. These include, for example, Wilson line self energies or interactions with the Wilson line at  $\infty$  [81].
  5. Renormalization is multiplicative and evolution equations are exactly homogeneous in the power expansion which yields Eqs. (2.28) and (2.29).
  6. A final practical consideration is that definitions should simplify multi-loop fixed order partonic calculations, in order to make it easier to build in the transition between the nonperturbative and perturbative  $k_T$  regimes.

In some cases these conditions may clash, such as 2. and 6., which makes apparent the importance of having available multiple constructions that can be demonstrated to be equivalent for the final TMD PDFs.

The small transverse momentum described by a TMD PDF  $f_{i/p}$  arises from two physical sources. Firstly, it arises from energetic radiation close to each proton, which is described by a proton matrix element, which is equivalently referred to as either an unsubtracted TMD PDF  $f_{i/p}^{(u)}$  or as an unsubtracted beam function. Secondly, one has to consider soft exchange between the two partons  $i$  and  $j$  involved in the hard collision, which is encoded in a soft vacuum matrix element  $S_{n_a n_b}$ . Unlike in the inclusive factorization theorem leading to Eq. (2.2), these soft radiation effects do not cancel out, and encode important eikonal soft dynamics between the two directions defined by identified hadrons. In practice, there can also be a double counting between the two matrix elements, which is removed by dividing by a soft subtraction factor  $S_{n_a n_b}^{\text{subt}}$ . As indicated by the notation, this factor is closely related to the soft function itself.<sup>3</sup> The generic definition for a TMD PDF can thus be written as

$$\tilde{f}_{i/p}(x, \mathbf{b}_T, \mu, \zeta) = \lim_{\substack{\epsilon \rightarrow 0 \\ \tau \rightarrow 0}} Z_{\text{uv}}^i(\mu, \zeta, \epsilon) \frac{\tilde{f}_{i/p}^{0(u)}(x, \mathbf{b}_T, \epsilon, \tau, xP^+)}{\tilde{S}_{n_a n_b}^{0 \text{ subt}}(b_T, \epsilon, \tau)} \sqrt{\tilde{S}_{n_a n_b}^0(b_T, \epsilon, \tau)}. \quad (2.33)$$

---

<sup>3</sup>In the approach of CSS [45] and Collins [89] these subtractions ensure there is no double counting of momentum regions, and also the proper cancellation of singularities. In SCET these subtractions are known as zero-bin subtractions [107] and arise from ensuring fluctuations encoded by collinear fields do not have singular overlap with those of the soft fields, thus also ensuring there is no double counting of infrared regions.

Here, the superscript  $^0$  denotes that the functions on the right hand side of Eq. (2.33) are bare quantities. They suffer from both ultraviolet (UV) divergences, which can be regulated using dimensional regularization with  $d = 4 - 2\epsilon$  dimensions, and so-called rapidity divergences which require a dedicated regulator [41, 81, 86, 96, 99, 102, 108, 109], which in Eq. (2.33) is generically denoted as  $\tau$ . The rapidity divergences cancel between the various factors in the right hand side of Eq. (2.33), such that the renormalization counterterm  $Z_{\text{uv}}^i$  in Eq. (2.33) only subtracts divergences in  $\epsilon$ . As usual, the UV divergences give rise to the renormalization scale  $\mu$ , which is defined in the  $\overline{\text{MS}}$  scheme. Likewise, the rapidity divergences give rise to sensitivity to the Collins-Soper scale  $\zeta$  [16, 86], whose precise definition depends on the employed regulator  $\tau$ . Note that in the definition in Eq. (2.33), one effectively absorbs half of the soft function into the TMD PDF  $f_{i/p}$ , while the other half is absorbed into the TMD PDF  $f_{j/p}$  for the other proton. The ratio  $f_{i/p}^{0(\text{u})}/S_{n_a n_b}^{0 \text{subt}}$  is constructed such that it describes collinear radiation, as discussed above.

Before giving explicit definitions of the functions in Eq. (2.33), we briefly connect to TMD factorization as given in Eq. (2.29b). In this approach, one separately constructs renormalized beam and soft functions, which can either be used to directly give the cross section (or combined as in Eq. (2.32) to give the TMD PDF). In this case, one has to renormalize both UV and rapidity divergences, which is achieved through

$$\begin{aligned} \tilde{B}_{i/p}(x, \mathbf{b}_T, \mu, \zeta/v^2) &= \lim_{\substack{\epsilon \rightarrow 0 \\ \tau \rightarrow 0}} \tilde{Z}_B^i(b_T, \mu, \nu, \epsilon, \tau, xP^+) \tilde{B}_{i/p}^0(x, \mathbf{b}_T, \epsilon, \tau, xP^+) \\ &= \lim_{\substack{\epsilon \rightarrow 0 \\ \tau \rightarrow 0}} \tilde{Z}_B^i(b_T, \mu, \nu, \epsilon, \tau, xP^+) \frac{\tilde{f}_{i/p}^{0(\text{u})}(x, \mathbf{b}_T, \epsilon, \tau, xP^+)}{\tilde{S}_{n_a n_b}^{0 \text{subt}}(b_T, \epsilon, \tau)}, \end{aligned} \quad (2.34)$$

$$\tilde{S}_{n_a n_b}(b_T, \mu, \nu) = \lim_{\substack{\epsilon \rightarrow 0 \\ \tau \rightarrow 0}} \tilde{Z}_S(b_T, \mu, \nu, \epsilon, \tau) \tilde{S}_{n_a n_b}^0(b_T, \epsilon, \tau). \quad (2.35)$$

Here,  $\nu$  is the rapidity renormalization scale arising from subtracting poles in  $\tau$ . The TMD PDF obtained by combining collinear and soft matrix elements can be equivalently defined from Eqs. (2.34) and (2.35) as

$$\tilde{f}_{i/p}(x, \mathbf{b}_T, \mu, \zeta) = \tilde{B}_{i/p}(x, \mathbf{b}_T, \mu, \zeta/v^2) \sqrt{\tilde{S}_{n_a n_b}(b_T, \mu, \nu)}. \quad (2.36)$$

Here, the  $\nu$  dependence cancels between both functions, leaving only the Collins-Soper scale  $\zeta$ , whose precise definition again depends on the definition of the regulator  $\tau$  and thus is scheme dependent (cf. the  $y_n$  dependence in Eq. (2.30)).

We now give explicit definitions of the proton and soft matrix elements relevant for quark TMD PDFs. We consider a proton  $p$  moving close to the  $n_a^\mu = (1, 0, \mathbf{0}_T)$  direction with momentum  $P^\mu = P^+(1, e^{-2y}, \mathbf{0}_T)$ . The corresponding definitions for a proton moving along the  $n_b^\mu = (0, 1, \mathbf{0}_T)$  direction are obtained by exchanging  $n_a \leftrightarrow n_b$ . The bare unsubtracted TMD PDF (or equivalently the bare beam function) and the bare soft function are defined as

$$\tilde{f}_{i/p}^{0(\text{u})}(x, \mathbf{b}_T, \epsilon, \tau, xP^+) = \int \frac{db^-}{2\pi} e^{-ib^-(xP^+)} \langle p(P) | [\bar{\psi}_i^0(b^\mu) W_\square(b^\mu, 0) \frac{\gamma^+}{2} \psi_i^0(0)]_\tau | p(P) \rangle, \quad (2.37)$$

$$\tilde{S}_{n_a n_b}^0(b_T, \epsilon, \tau) = \frac{1}{N_c} \langle 0 | \text{Tr}[W_\gg(b_T)]_\tau | 0 \rangle. \quad (2.38)$$

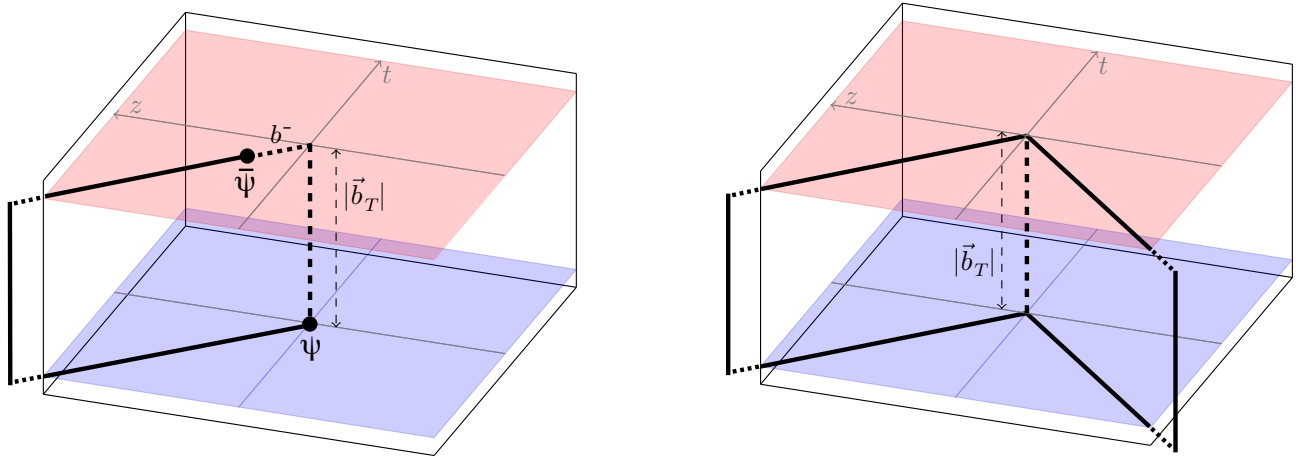


Figure 2.1: Graphs of the Wilson line structure  $W_{\sqsubset}(b^\mu, 0)$  of the unsubtracted TMD PDF  $f_{i/p}^{0(u)}$  (left) and of  $W_{\triangleright}(b_T)$  for the soft function  $S_{n_a n_b}^0$  (right), defined in Eqs. (2.37) and (2.38). The Wilson lines (solid) extend to infinity in the directions indicated. Adapted from [105].

Here the brackets  $[\cdots]_\tau$  denote that the operators inside are considered with an additional rapidity regulator  $\tau$ , where the details on methods for how this is done are left to Sec. 2.4 below. Note that by Poincaré invariance, the proton matrix element in Eq. (2.37) only depends on the difference  $b^\mu - 0 = b^\mu$  of the positions of the quark fields. In parts of the literature, the correlator is defined as  $\bar{\psi}_i^0(0) W_{\sqsubset}(0, b^\mu) \frac{\gamma^+}{2} \psi_i^0(b^\mu)$ , which thus is related to our convention by  $b^\mu \rightarrow -b^\mu$ . In particular, this also reverses the sign in the Fourier transform.

In Eqs. (2.37) and (2.38) we have  $b^\mu = (0, b^-, \mathbf{b}_T)$ , and the staple shaped Wilson lines  $W_{\sqsubset}(b^\mu, 0)$  and  $W_{\triangleright}(b_T)$  are defined by products of straight line segments,

$$\begin{aligned} W_{\sqsubset}(b^\mu, 0) &= W[0 \rightarrow -\infty n_b \rightarrow -\infty n_b + \mathbf{b}_T \rightarrow b] \\ &= W_{n_b}(b^\mu; -\infty, 0) W_{\hat{b}_T}(-\infty n_b; 0, b_T) W_{n_b}(0^\mu; 0, -\infty), \end{aligned} \quad (2.39)$$

$$\begin{aligned} W_{\triangleright}(b_T) &= W[0 \rightarrow -\infty n_b \rightarrow -\infty n_b + \mathbf{b}_T \rightarrow \mathbf{b}_T \rightarrow -\infty n_a + \mathbf{b}_T \rightarrow -\infty n_a \rightarrow 0] \\ &= W_{n_a}(b_T; 0, -\infty) W_{n_b}(b_T; -\infty, 0) W_{\hat{b}_T}(-\infty n_b; 0, b_T) \\ &\quad \times W_{n_b}(0; 0, -\infty) W_{n_a}(0; -\infty, 0) W_{\hat{b}_T}(-\infty n_a; b_T, 0), \end{aligned} \quad (2.40)$$

with  $\hat{b}_T^\mu = b_T^\mu / b_T$ . For later use we also define a generalized version of the first product of Wilson lines, where we take  $x^\mu = (0, x^-, \mathbf{x}_T)$  and  $y^\mu = (0, y^-, \mathbf{y}_T)$  as the two endpoints,

$$\begin{aligned} W_{\sqsubset}(x^\mu, y^\mu) &= W[x \rightarrow -\infty n_b + x \rightarrow -\infty n_b + y \rightarrow y] \\ &= W_{n_b}(x^\mu; -\infty, 0) W_{\hat{\Delta}}(-\infty n_b^\mu + y_T^\mu; 0, |\mathbf{x}_T - \mathbf{y}_T|) W_{n_b}(y^\mu; 0, -\infty), \end{aligned} \quad (2.41)$$

and here  $\hat{\Delta}^\mu = (x_T - y_T)^\mu / |\mathbf{x}_T - \mathbf{y}_T|$ . Here the Wilson line along a generic path  $\gamma$  is defined by the path-ordered exponential

$$W[\gamma] = P \exp \left[ -ig_0 \int_\gamma dx^\mu A_\mu^{c0}(x) t^c \right], \quad (2.42)$$

where  $t^c$  are the generators of SU(3) in the fundamental representation. The individual Wilson lines  $W_n(x; a, b)$  are defined as path-ordered exponentials connecting the point  $x^\mu + an^\mu$  to  $x^\mu + bn^\mu$  along the direction  $n$ ,

$$W_n(x^\mu; a, b) = P \exp \left[ -ig_0 \int_a^b ds n \cdot A^{c0}(x^\mu + sn^\mu) t^c \right]. \quad (2.43)$$

Note that for  $W_n$  the subscript  $n$  is always a four vector. Also note that here  $W[\gamma]$  and  $W_n$  are defined using the bare strong coupling  $g_0$  and bare gluon fields  $A^{c0}$ . The  $P$  in  $W_n(x^\mu; a, b)$  denotes path ordering for the expanded exponential, where the matrices  $t^c$  are ordered by their corresponding values along the path from  $s = a$  to  $s = b$ , starting from right and going to the left. For reference we note that  $W_n(x^\mu; c, b)W_n(x^\mu; a, c) = W_n(x^\mu; a, b)$ , and since  $W_n^\dagger(x^\mu; a, b) = W_n(x^\mu; b, a)$ , we have  $W_n^\dagger(x^\mu; a, b)W_n(x^\mu; a, b) = 1$ . The Wilson line structures appearing in the unsubtracted TMD PDF and soft function are illustrated in Fig. 2.1. Note that the transverse Wilson lines  $W_{b_T}$  follow a straight line path in the transverse plane at light-cone  $-\infty$  as indicated. These segments are needed for the full gauge invariance of the operators. (In perturbative calculations the transverse links can be neglected in nonsingular gauges such as Feynman gauge, where the gluon field strength vanishes at infinity, but are known to be important in certain singular gauges, see [46, 110–112].)

On first encountering the operator definition of the unsubtracted TMD PDF, a reader may be struck by the fact that the simplest straight Wilson line between two points is not what appears in  $f_{i/p}^{0(u)}$ . Instead, the proof of factorization that leads to these objects dictates that it is the staple shaped Wilson line in Eq. (2.37) which connects the quark fields at the two different spacetime points and ensures gauge invariance of the composite operator. To understand physically why it is this staple shape that appears, we note that having a quark field whose color is transported off to spacetime infinity by a Wilson line along the light-cone is the closest approximation to a parton by operators in QCD. This concept is made very explicit in the construction of the soft collinear effective theory [93, 94], where the composite operator obtained by attaching a quark to this type of Wilson line plays a fundamental role. Thus the staple shaped Wilson line is the natural QCD consequence of taking partons at the spacetime points 0 and  $b^\mu$  and connecting them by a transverse Wilson line to obtain a gauge invariant operator.

## 2.4 Definitions with Rapidity Regulators

In the previous section, the basic definition of TMD PDFs has been given. As indicated there, definitions of TMD PDFs not only require the specification of a UV renormalization scheme, which we take to be the standard  $\overline{\text{MS}}$  scheme, but also to define an additional rapidity regularization for individual ingredients. A large variety of such rapidity regulators have been suggested in the literature, giving rise to various different constructions of TMD factorization. Here, we will briefly summarize these definitions for TMD PDFs in the  $\overline{\text{MS}}$  class of schemes, while TMD PDF defined in additional schemes will be discussed in Sec. 2.5. For more details on results with the different rapidity regulators, we refer to appendix D.

The origin of rapidity divergences is intimately connected to the derivation of TMD factorization, which will be discussed in more detail in Sec. 3. Roughly speaking, TMD factorization is based on organizing the cross section into hard, collinear and soft regions. At the pertur-

bative level, this corresponds to expanding Feynman diagrams in these regions. For example, one would expand

$$\underbrace{\int_{q_T}^Q \frac{dk}{k}}_{\text{full}} = \lim_{\tau \rightarrow 0} \left[ \underbrace{\int_0^Q \frac{dk}{k} R_c(k, \tau)}_{\text{collinear}} + \underbrace{\int_{q_T}^\infty \frac{dk}{k} R_s(k, \tau)}_{\text{soft}} \right] = \ln \frac{Q}{q_T}. \quad (2.44)$$

Here, the full theory contains the integral on the left hand side of Eq. (2.44). In the collinear region, one expands away the transverse momentum  $q_T$ , which is considered small compared to  $Q$ ,  $q_T \ll Q$ , while in the soft region the large momentum  $Q \rightarrow \infty$  is expanded away. These expansions are unavoidable, since they are necessary to derive the factorization theorem. This renders the collinear and soft integrals logarithmically divergent, and their separate evaluation requires the introduction of a regulating function  $R(k, \tau)$ , for which  $R_c(k, \tau)$  and  $R_s(k, \tau)$  are the versions appropriate for the collinear and soft calculations. Upon combining the two contributions, one can remove the regulator,  $\tau \rightarrow 0$ , and obtain the correct final result.

In the following, we first give an overview of the rapidity regulators employed in the literature, before explicitly illustrating the application of such a regulator at one loop.

### 2.4.1 Overview of rapidity regulators

Here, we collect key properties of the different rapidity regulators encountered in the literature. The different notations for the rapidity-regularized unsubtracted TMD PDF and soft functions in each case are summarized in table 2.1. We also collect explicit expressions for the corresponding one-loop results of the quark TMD PDF in appendix D, which explicitly illustrates their equivalence.

- **Space-like Wilson-lines:** The modern definition by Collins [89] plays a key role in the all order proof of TMD factorization discussed in Sec. 3. Here the lightlike directions  $n_a$  and  $n_b$ , for the paths of the Wilson lines in the definitions in Eqs. (2.37) and (2.38), are replaced by spacelike reference vectors

$$\begin{aligned} n_a^\mu &\rightarrow n_A^\mu(y_A) \equiv n_a^\mu - e^{-2y_A} n_b^\mu = (1, -e^{-2y_A}, \mathbf{0}_T), \\ n_b^\mu &\rightarrow n_B^\mu(y_B) \equiv n_b^\mu - e^{+2y_B} n_a^\mu = (-e^{+2y_B}, 1, \mathbf{0}_T), \end{aligned} \quad (2.45)$$

which ensures maximum universality for the TMD PDF definitions [10, 83]. With this rapidity regulator the limit  $\tau \rightarrow 0$  corresponds to  $y_A \rightarrow \infty$  and  $y_B \rightarrow -\infty$ . The ratio of bare soft function and soft subtractions appearing in Eq. (2.33) is given by [89]

$$\frac{\sqrt{\tilde{S}_{JC}^0}}{\tilde{S}_{JC}^{0\text{subt}}} = \sqrt{\frac{\tilde{S}_{n_A n_B}^0(b_T, \epsilon, y_A - y_n)}{\tilde{S}_{n_A n_B}^0(b_T, \epsilon, y_A - y_B) \tilde{S}_{n_A n_B}^0(b_T, \epsilon, y_n - y_B)}}. \quad (2.46)$$

Here, the additional rapidity  $y_n$  governs how the split of the soft function is made when combining it with each of the two TMDs appearing in the factorized cross section. This combination can be simplified into a single Wilson line using [113]

$$\lim_{y_A \rightarrow \infty} \frac{\sqrt{\tilde{S}_{JC}^0}}{\tilde{S}_{JC}^{0\text{subt}}} = \frac{1}{\sqrt{\tilde{S}_{n_A(y_n) n_B(y_B)}^0(b_T, \epsilon, 2y_n - 2y_B)}}. \quad (2.47)$$

In addition, the rapidity regulator is implemented in the bare unsubtracted TMD PDF by replacing  $n_b \rightarrow n_B(y_B)$  in the staple shaped Wilson line, so that  $[\cdots]_\tau$  in Eq. (2.37) is enforced by using

$$W_{\square}^{n_B}(b^\mu, 0) = W_{n_B}(b^\mu; -\infty, 0) W_{b_T}(-\infty n_B; 0, 1) W_{n_B}(0; 0, -\infty), \quad (2.48)$$

and this then gives  $\tilde{f}_{i/p}^{0(u)}(x, \mathbf{b}_T, \epsilon, y_B, xP^+)$ . The final renormalized TMD PDF is then obtained as

$$\tilde{f}_{i/p}(x, \mathbf{b}_T, \mu, \zeta) = \lim_{\epsilon \rightarrow 0} Z_{uv}(\mu, \zeta, \epsilon) \lim_{y_B \rightarrow -\infty} \frac{\tilde{f}_{i/p}^{0(u)}(x, \mathbf{b}_T, \epsilon, y_B, xP^+)}{\sqrt{\tilde{S}_{n_A(y_n)n_B(y_B)}^0(b_T, \epsilon, 2y_n - 2y_B)}}, \quad (2.49)$$

and here the Collins-Soper scale arises as  $\zeta = 2(xP^+e^{-y_n})^2$ .

- The  **$\delta$  regulator** was introduced in [99, 100] by Echevarria, Idilbi and Scimemi (EIS) and later modified in [114–116]. The regulator modifies the Feynman rules of the Wilson lines  $W_{n_a}$  and  $W_{n_b}$ . At one loop this simply shifts the eikonal propagators ( $n_a \cdot k + i0$ ) and ( $n_b \cdot k + i0$ ) by an infinitesimal amount  $i\delta^+$  and  $i\delta^-$ , respectively. In this scheme the bare regulated soft function is split into two parts to associate with the two TMD PDFs as

$$\tilde{S}_{\text{EIS}}^0(b_T, \epsilon, \sqrt{\delta^+\delta^-}) = \sqrt{\tilde{S}_{\text{EIS}}^0(b_T, \epsilon, \delta^+e^{-y_n})} \sqrt{\tilde{S}_{\text{EIS}}^0(b_T, \epsilon, \delta^-e^{+y_n})}, \quad (2.50)$$

where  $y_n$  regulates the amount of the soft function combined with each of the unsubtracted TMD PDFs. Here the subtraction factor is equal to the corresponding soft function component,  $\tilde{S}_{\text{EIS}}^{0\text{subt}}(b_T, \epsilon, \delta^+e^{-y_n}) = \tilde{S}_{\text{EIS}}^0(b_T, \epsilon, \delta^+e^{-y_n})$  so the physical TMD PDF is obtained as

$$\tilde{f}_{i/p}(x, \mathbf{b}_T, \mu, \zeta) = \lim_{\substack{\epsilon \rightarrow 0 \\ \delta^+ \rightarrow 0}} Z_{uv}^i(\mu, \zeta, \epsilon) \frac{\tilde{f}_{i/p}^{0(u)}(x, \mathbf{b}_T, \epsilon, \delta^+/(xP^+))}{\sqrt{\tilde{S}_{\text{EIS}}^0(b_T, \epsilon, \delta^+e^{-y_n})}}. \quad (2.51)$$

The Collins-Soper scale in this approach is given by  $\zeta = 2(xP^+e^{-y_n})^2$ , which is the same as in the modern Collins construction.

- The  **$\eta$  regulator** due to Chiu, Jain, Neill and Rothstein (CJNR) in [102, 109] separately modifies the Feynman rules of Wilson lines appearing in the unsubtracted TMD PDF and soft function. It introduces regulating factors of  $|k^+/\nu|^{-\eta}$  in the Wilson lines appearing in  $W_{\square}(b^\mu, 0)$ , and regulating factors  $|k^z/\nu|^{-\eta/2}$  in the Wilson lines appearing in  $S_{n_a n_b}$ . Amplitudes are expanded in the limit  $\eta \rightarrow 0$ , and Rapidity divergences become manifest as poles in  $\eta$ , similar to UV divergences that arise as poles in  $\epsilon$ . This regulator is commonly applied by separately renormalizing the unsubtracted TMD PDF and soft functions, giving rise to renormalized beam functions and renormalized soft functions. Here, poles in  $\eta$  are cancelled by a rapidity renormalization factor, giving rise to a (dimension-1) rapidity scale  $\nu$  (which is analogous to  $\mu$  in the  $\overline{\text{MS}}$  scheme). In this

construction the TMD PDF is obtained in either one of two ways, from the bare or renormalized quantities:

$$\begin{aligned}\tilde{f}_{i/p}(x, \mathbf{b}_T, \mu, \zeta) &= \lim_{\substack{\epsilon \rightarrow 0 \\ \eta \rightarrow 0}} Z_{uv}^i(\mu, \zeta, \epsilon) \tilde{f}_{i/p}^{0(u)}(x, \mathbf{b}_T, \epsilon, \eta, xP^+) \sqrt{\tilde{S}_{\text{CJNR}}^0(b_T, \epsilon, \eta)} \\ &= \tilde{B}_{i/p}^{\text{CJNR}}(x, \mathbf{b}_T, \mu, \sqrt{\zeta}/\nu) \sqrt{\tilde{S}_{\text{CJNR}}^0(b_T, \mu, \nu)}.\end{aligned}\quad (2.52)$$

In this construction  $\zeta = 2(xP^+)^2$ , corresponding to taking  $y_n = 0$  in the modern Collins result. Note that in this regulator, there is no zero-bin subtraction factor, so  $S_{\text{CJNR}}^{0\text{subt}} = 1$ .

- The **exponential regulator** due to Li, Neill and Zhu (LNZ) [105] inserts an  $\exp[-\tau e^{-\gamma_E} k^0]$  factor into the phase space of each real emission, where  $k^0$  is the energy of the emission. Since the energies of the emissions are additive, this can be viewed as utilizing the fully differential distribution function in  $(x, k^0, \mathbf{k}_T)$  and then performing a Laplace transform over  $k^0$  with an infinitesimal  $\tau$ . Thus this regulator is defined at the operator level without modifying the Wilson lines and is clearly gauge invariant at intermediate stages. Similar to the  $\eta$  regulator, it can be used to define separately renormalized beam and soft functions, so the final renormalized TMD PDF can either be obtained from bare or renormalized quantities

$$\begin{aligned}\tilde{f}_{i/p}(x, \mathbf{b}_T, \mu, \zeta) &= \lim_{\substack{\epsilon \rightarrow 0 \\ \tau \rightarrow 0}} Z_{uv}^i(\mu, \zeta, \epsilon) \frac{\tilde{f}_{i/p}^{0(u)}(x, \mathbf{b}_T, \epsilon, \tau, xP^+)}{\sqrt{\tilde{S}_{\text{LNZ}}^0(b_T, \epsilon, \tau)}} \\ &= \tilde{B}_{i/p}^{\text{LNZ}}(x, \mathbf{b}_T, \mu, \sqrt{\zeta}/\nu) \sqrt{\tilde{S}_{\text{LNZ}}^0(b_T, \mu, \nu)},\end{aligned}\quad (2.53)$$

where here again  $\zeta = 2(xP^+)^2$ . Since for this construction the soft function is equal to the subtraction  $\tilde{S}_{\text{LNZ}}^{0\text{subt}} = \tilde{S}_{\text{LNZ}}^0$ , it enters on the first line in the denominator, while in the second line a factor of  $1/\tilde{S}_{\text{LNZ}}^{0\text{subt}}$  is already contained inside the rapidity-renormalized beam function  $\tilde{B}_{i/p}^{\text{LNZ}}$ .

- The **analytic regulator** was first introduced by Becher and Neubert (BN) [96]. So far this regulator has been primarily considered for Drell-Yan, so we focus on that case here. In the modified version due to Becher and Bell [117], one inserts a factor  $(\nu/k^+)^{\alpha}$  for each real emission. In this regulator, the soft function is absent,  $\tilde{S}_{\text{BN}}^0 = 1$ , and subtractions are also absent  $\tilde{S}_{\text{BN}}^{0\text{subt}} = 1$ . Due to the asymmetry of the regulator under  $n_a \leftrightarrow n_b$ , one has different constructions for the  $n_a$ -collinear and  $n_b$ -collinear unsubtracted TMD PDFs, which can be combined to obtain the product of the renormalized TMD PDFs,

$$\begin{aligned}&\lim_{\substack{\epsilon \rightarrow 0 \\ \alpha \rightarrow 0}} \left[ \tilde{f}_{i/p}^{0(u), \text{BN}}(x_1, \mathbf{b}_T, \epsilon, \alpha, x_a P_A^+) \tilde{f}_{j/p}^{0(u), \text{BN}}(x_2, \mathbf{b}_T, \epsilon, \alpha, x_b P_B^-) \right] \\ &= \left( \frac{b_T^2 Q^2}{b_0^2} \right)^{-\gamma_\zeta^q(\mu, b_T)} \left[ \tilde{f}_{i/p}^{\text{BN}}(x_1, \mathbf{b}_T, \mu, \zeta = b_0^2/b_T^2) \tilde{f}_{j/p}^{\text{BN}}(x_2, \mathbf{b}_T, \mu, \zeta = b_0^2/b_T^2) \right],\end{aligned}\quad (2.54)$$

where  $b_0 = 2e^{-\gamma_E} = 1.12292$ . In this definition one exponentiates the dependence on  $\zeta_1 \zeta_2 = Q^4$  through the CS kernel  $\gamma_\zeta$  (see Sec. 4) and correspondingly fixes  $\zeta = b_0^2/b_T^2$  in the remaining TMD PDFs. For this reason there is often no  $\zeta$  variable written in the renormalized TMD PDFs. Note that this definition does not suffice to separately define  $\tilde{f}_{i/p}^{\text{BN}}$  and  $\tilde{f}_{j/p}^{\text{BN}}$  uniquely, and hence is on a different footing compared to other constructions.

- The **pure rapidity regulator** was introduced by Ebert, Moult, Stewart, Tackmann, Vita, and Zhu (EMSTVZ) [118]. It is defined similarly to the analytic regulator by inserting a factor  $|k^+/k^-|^{-\eta/2}$  for each real emission, but is analogous to the eta and exponential regulators in that renormalized  $n_a$  and  $n_b$ -collinear TMD PDFs can be defined separately. It shares the feature that the soft function and subtraction function are absent,  $\tilde{S}_{\text{EMSTVZ}}^0 = \tilde{S}_{\text{EMSTVZ}}^{0\text{subt}} = 1$ . Here the  $n_a$  and  $n_b$ -collinear TMD PDFs are simply related by  $\eta \leftrightarrow -\eta$ , so although they may be defined separately, only the product of renormalized TMD PDFs is the same as this product in the eta and exponential regulator constructions. This pure rapidity regulator has been used to study power corrections to TMD factorization at one loop, since the regulator itself does not induce power suppressed contributions [118].

## 2.4.2 Illustration at one loop

In this section, we study the quark TMD PDF perturbatively at one loop, which will show concretely how rapidity divergences arise and how they are regulated in practice. As shown in Eq. (2.33), we need to consider both the unsubtracted quark TMD PDF and the soft function, which we can then combine into the TMD PDF. Since the unsubtracted TMD PDF is defined with an external hadronic state and thus is genuinely nonperturbative, we need to replace the external hadron with a parton, which allows us to use standard Feynman rules to perturbatively study this matrix element. In Sec. 2.8, we will see that this calculation is of practical relevance, as it allows us to perturbatively relate the TMD PDF to the standard PDF whenever  $q_T \gg \Lambda_{\text{QCD}}$  is a perturbative scale.

Regulator	Unsubtracted TMD PDF	Soft function	Subtracted TMD PDF $f_{i/p}$	CS scale
Space-like Wilson lines [89]	$\tilde{f}_{i/p}^{0(\text{u})}(y_B)$	$\tilde{S}_{n_A n_B}^0(2y_n - 2y_B)$	$\lim_{y_B \rightarrow -\infty} \frac{\tilde{f}_{i/p}^{0(\text{u})}(y_B)}{\sqrt{\tilde{S}_{n_A n_B}^0(2y_n - 2y_B)}}$	$\zeta = 2(xP^+ e^{-y_n})^2$
$\delta$ regulator [100]	$\tilde{f}_{i/p}^{0(\text{u})}(\delta^+)$	$\tilde{S}_{n_A n_B}^0(\sqrt{\delta^+ \delta^-})$	$\lim_{\delta^+ \rightarrow 0} \frac{\tilde{f}_{i/p}^{0(\text{u})}(\delta^+)}{\sqrt{\tilde{S}^0(\delta^+ e^{-y_n})}}$	$\zeta = 2(xP^+ e^{-y_n})^2$
$\eta$ regulator* [102]	$\tilde{f}_{i/p}^{0(\text{u})}(\eta)$	$\tilde{S}_{n_A n_B}^0(\eta)$	$\lim_{\eta \rightarrow 0} \tilde{f}_{i/p}^{0(\text{u})}(\eta) \sqrt{\tilde{S}^0(\eta)}$	$\zeta = 2(xP^+)^2$
Exponential regulator* [105]	$\tilde{f}_{i/p}^{0(\text{u})}(\tau)$	$\tilde{S}_{n_A n_B}^0(\tau)$	$\lim_{\tau \rightarrow 0} \frac{\tilde{f}_{i/p}^{0(\text{u})}(\tau)}{\sqrt{\tilde{S}^0(\tau)}}$	$\zeta = 2(xP^+)^2$

Table 2.1: Summary of different schemes for defining a TMD PDF  $\tilde{f}_{i/p}(x, \mathbf{b}_T, \mu, \zeta)$  as in Eq. (2.33). In all functions, we drop all arguments except for the regulator. In the subtracted TMD PDF, we only show the limit of taking the rapidity regulator to zero, but not the UV subtraction. Schemes denoted with an asterisk (\*) are also defined with renormalized beam and soft functions.

**Unsubtracted TMD PDF.** We begin our calculation with the unsubtracted TMD PDF at NLO, and as discussed calculate its matrix element with the hadron state replaced by an external quark of lightlike momentum  $p^\mu = (p^+, 0, \mathbf{0})$ . Here we consider

$$\tilde{f}_{q/q'}^{0(u)}(x, \mathbf{b}_T, \epsilon, \tau) = \int \frac{db^-}{2\pi} e^{-ib^-(xp^+)} \langle q'(p) | [\bar{\psi}_q^0(b^\mu) W_{\square}(b^\mu, 0) \frac{\gamma^+}{2} \psi_q^0(0)]_\tau | q'(p) \rangle. \quad (2.55)$$

Here, the subscript on  $f_{q/q'}$  indicates that we analyze the contribution from an external parton of flavor  $q'$  to the quark TMD PDF of flavor  $q$ . At one loop,  $q = q'$  of identical flavor, while starting at two loops, one can also have different flavors  $q \neq q'$ . There can also be contributions from quarks mixing with gluons at one loop, which we will not consider in this section. To ensure that gluon contributions drop out, we can consider  $q$  to be a non-singlet combination of quark flavors.

At one loop, there are only four types of diagrams and their mirror diagrams, which are shown in Fig. 2.2. In these diagrams, the  $\otimes$  denotes the quark fields, with the left field positioned at the origin and the right field located at  $b^\mu$ . The two double lines represent the Wilson line segments along  $n_b$ . Note that we do not consider the transverse gauge links, as they do not contribute in a physical gauge such as Feynman gauge (in general gauges they do matter, see e.g. [46, 110–112]). Physically, this reflects that the Wilson line at infinite distance does not impact the physics at the finite distance  $b^\mu$ .

The different diagrams in Fig. 2.2 arise from different ways to exchange a gluon between the quark fields and Wilson lines in Eq. (2.55). To evaluate these diagrams, we need to know the Feynman rules for the connection of a gluon to a Wilson line. They are given by

$$\begin{aligned} W_{n_b}(b^\mu; -\infty, 0) : & \quad \overline{\text{---}} \overset{b^\mu}{\text{---}}_{k, \mu} = -g_0 n_b^\mu t^a \frac{e^{-ik \cdot b}}{n_b \cdot k + i0}, \\ W_{n_b}^\dagger(0; -\infty, 0) : & \quad \overset{0^\mu}{\text{---}} \overline{\text{---}}_{k, \mu} = +g_0 n_b^\mu t^a \frac{1}{n_b \cdot k - i0}. \end{aligned} \quad (2.56)$$

As indicated, the first line gives the Feynman rule for the Wilson line stretching from  $b^\mu$  to lightcone infinite, while the second line shows the Feynman rule for the Wilson line stretching back from lightcone infinite to the origin. In both cases, the gluon momentum  $k$  is incoming, and the gluon has color index  $a$  and polarization vector  $\epsilon^\mu$ . Note that a gluon exchange between these two segments is proportional to  $n_b^2 = 0$ , and thus vanishes. For this reason, Fig. 2.2 does not contain a diagram where the gluon is exchanged between the Wilson line segments.

In our calculation, we will regulate both infrared (IR) and UV divergences by extending spacetime to  $d = 4 - 2\epsilon$  dimensions. The quark momentum is chosen as  $p^\mu = (p^+, 0, 0)$ , which simplifies the calculation due to  $p^2 = 0$ . We are now ready to write down the explicit

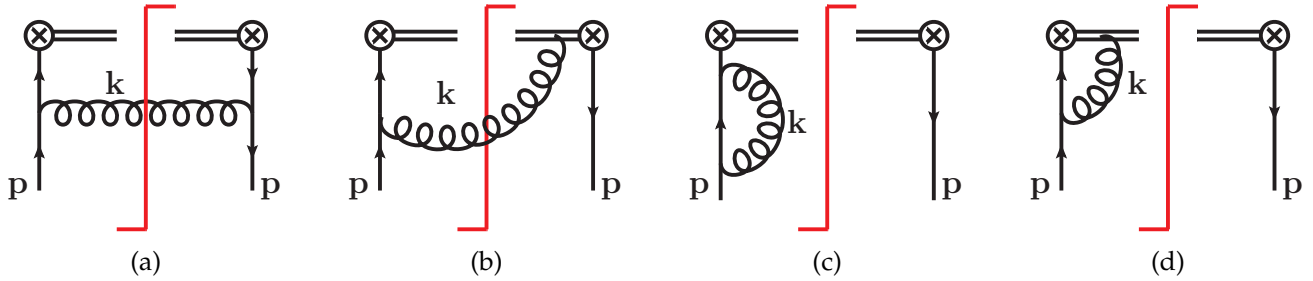


Figure 2.2: One-loop contribution to the unsubtracted quark-TMD PDF. The  $\otimes$  denote the two quark fields, the double line the staple shaped Wilson lines connecting the quark fields, and the red line the on-shell cut. The diagrams (b)–(d) have mirror diagrams that are not explicitly shown. In pure dimensional regularization, the virtual diagrams (c) and (d) are scaleless and vanish.

expressions for the diagrams in Fig. 2.2:

$$\mathcal{M}_a = -ig_0^2 C_F \int \frac{d^d k}{(2\pi)^d} \int \frac{db^-}{2\pi} e^{-ib^-(xp^+)} e^{i(p-k)\cdot b} \frac{\bar{u}(p)\gamma^\mu(\not{p}-\not{k})\gamma^+(\not{p}-\not{k})\gamma_\mu u(p)}{2[(p-k)^2 + i0]^2(k^2 + i0)}, \quad (2.57)$$

$$\mathcal{M}_b = -2ig_0^2 C_F \int \frac{d^d k}{(2\pi)^d} \int \frac{db^-}{2\pi} e^{-ib^-(xp^+)} e^{i(p-k)\cdot b} \frac{\bar{u}(p)\gamma^+(\not{p}-\not{k})\gamma^+ u(p)}{2(k^+ + i0)[(p-k)^2 + i0](k^2 + i0)}. \quad (2.58)$$

Note that the quark field sitting at  $b^\mu$  induces a phase  $e^{iq\cdot b}$ , where  $q^\mu$  is the momentum flowing out of the right vertex  $\otimes$ . We have not given diagrams (c) and (d), as they vanish in dimensional regularization, i.e. they involve scaleless integrals of the type  $\int d^d k f(k^2) = 0$  in dimensional regularization. The overall factor of 2 in  $\mathcal{M}_b$  arises from the mirror diagram.

To proceed, we evaluate the  $b^-$  integral as

$$\int \frac{db^-}{2\pi} e^{-ib^-(xp^-)} e^{i(p-k)\cdot b} = \int \frac{db^-}{2\pi} e^{-ib^-[(1-x)p^+ - k^+] + i\mathbf{b}_T \cdot \mathbf{k}_T} = \delta[(1-x)p^+ - k^+] e^{i\mathbf{b}_T \cdot \mathbf{k}_T}, \quad (2.59)$$

where we used that  $b^+ = p^- = 0$ , such that the remaining phase arises purely from the transverse momentum. This result has a simple interpretation: the emitted gluon carries away the longitudinal momentum  $k^+ = (1-x)p^+$ , such that the leftover momentum  $xp^+$  is absorbed by the quark field. In other words, the parton participating in the hard interaction will carry the momentum fraction  $x$  of the external parent hadron.

Using lightcone coordinates, the integration measure becomes  $d^d k = dk^+ dk^- d^{d-2} \mathbf{k}_T$ , whose  $k^+$  integral is already fixed by Eq. (2.59). Performing the standard Dirac algebra in the numerators in Eq. (2.57), we obtain

$$\begin{aligned} \mathcal{M}_a &= ig_0^2 C_F \int \frac{d^{d-2} \mathbf{k}_T}{(2\pi)^d} e^{i\mathbf{b}_T \cdot \mathbf{k}_T} \int dk^- \frac{(2-d)(1-x)p^+}{[(p-k)^2 + i0](k^2 + i0)}, \\ \mathcal{M}_b &= ig_0^2 C_F \int \frac{d^{d-2} \mathbf{k}_T}{(2\pi)^d} e^{i\mathbf{b}_T \cdot \mathbf{k}_T} \int dk^- \frac{-4x/(1-x)p^+}{[(p-k)^2 + i0](k^2 + i0)}. \end{aligned} \quad (2.60)$$

The remaining integral over  $k^-$  can be evaluated using the residue theorem,

$$\begin{aligned} \int dk^- \frac{1}{[(p-k)^2 + i0](k^2 + i0)} &= \int dk^- \frac{1}{[-2xp^+k^- - \mathbf{k}_T^2 + i0][2(1-x)p^+k^- - \mathbf{k}_T^2 + i0]} \\ &= \frac{i\pi}{p^+\mathbf{k}_T^2} \theta(x)\theta(1-x). \end{aligned} \quad (2.61)$$

From the first line, we see that if  $x$  and  $1-x$  have different signs, then the residues of  $k^-$  will lie on the same complex half plane, and one can deform the  $k^-$  contour into the other half plane such that the integral vanishes. (Here, the signs of the Feynman  $i0$  prescription are crucial.) Hence, the only physical contribution arises if  $0 < x < 1$ , the expected physical range of the momentum fraction. We then choose the residue at  $k^- = \mathbf{k}_T^2/(2k^+) > 0$ , which is equivalent to choosing  $k^2 = 0$ . Thus, we can interpret this choice as setting the gluon in Fig. 2.2 on shell. In fact, we could have started with this choice right away by using the Cutkosky rule [? ]

$$\frac{1}{k^2 + i0} \rightarrow 2 \operatorname{Im}\left(\frac{1}{k^2 + i0}\right) = -2\pi i \theta(k^0) \delta(k^2) \equiv -2\pi i \delta_+(k^2). \quad (2.62)$$

Our more exhaustive derivation shows how this constraint naturally arises from the definition of the unsubtracted TMD PDF.

Combining the two matrix elements in Eq. (2.60) with Eq. (2.62), we obtain the one-loop contribution to the bare unsubtracted quark TMD PDF as

$$\mathcal{M}_a + \mathcal{M}_b = \frac{g_0^2 C_F}{2\pi} \left[ \frac{1+x^2}{1-x} - \epsilon(1-x) \right] \int \frac{d^{d-2}\mathbf{k}_T}{(2\pi)^{d-2}} \frac{e^{i\mathbf{b}_T \cdot \mathbf{k}_T}}{\mathbf{k}_T^2}. \quad (2.63)$$

To evaluate the remaining  $\mathbf{k}_T$  integral, we have to fix how we want to treat  $\mathbf{k}_T$  and  $\mathbf{b}_T$  in  $2-2\epsilon$  dimensions. There is no unique choice, but ultimately every choice leads to equivalent TMD PDFs. Following [105] we extend  $\mathbf{b}_T = (b_T, 0, \vec{0}_{-2\epsilon})$  and  $\mathbf{k}_T = k_T(\cos\theta, \sin\theta, \vec{0}_{-2\epsilon})$ , such that the phase only picks out the purely two-dimensional piece. This yields

$$\int \frac{d^{d-2}\mathbf{k}_T}{(2\pi)^{d-2}} \frac{e^{i\mathbf{b}_T \cdot \mathbf{k}_T}}{\mathbf{k}_T^2} = \frac{\Omega_{-2\epsilon}}{(2\pi)^{2-2\epsilon}} \int_0^\infty dk_T k_T^{1-2\epsilon} \int_0^\pi d\theta \sin^{-2\epsilon} \theta \frac{e^{ib_T k_T \cos\theta}}{k_T^2} = \frac{\Gamma(-\epsilon)}{4\pi} (\pi \mathbf{b}_T^2)^\epsilon, \quad (2.64)$$

where  $\Omega_n = 2\pi^{(n+1)/2}/\Gamma[(n+1)/2]$  is the area of a unit  $n$ -sphere. Thus, we finally arrive at

$$\mathcal{M}_a + \mathcal{M}_b = \frac{\alpha_s(\mu) C_F}{2\pi} \left[ \frac{1+x^2}{1-x} - \epsilon(1-x) \right] \Gamma(-\epsilon) \left( \frac{\mathbf{b}_T^2 \mu^2}{4e^{-\gamma_E}} \right)^\epsilon, \quad (2.65)$$

where we also replaced the bare by the renormalized coupling in the  $\overline{\text{MS}}$  scheme,

$$g_0 = Z_g \mu^\epsilon g(\mu) \left( \frac{e^{\gamma_E}}{4\pi} \right)^{\epsilon/2}, \quad \alpha_s(\mu) = \frac{g(\mu)^2}{4\pi}. \quad (2.66)$$

Here  $Z_g = 1 + \mathcal{O}(g^2)$  is the strong coupling counterterm which can be set to one for this one-loop calculation. The inclusion of the factor of  $(e^{\gamma_E}/4\pi)^{\epsilon/2}$  implements the use of the  $\overline{\text{MS}}$  scheme rather than MS scheme.<sup>4</sup>

Eq. (2.66) seems satisfactory, as we apparently only need to expand in  $\epsilon \rightarrow 0$  to obtain the desired bare result. This will yield poles in  $1/\epsilon$  that arise from regulating the  $k_T \rightarrow 0$  region in Eq. (2.65). However, there is still one problem: the result in Eq. (2.66) diverges as  $x \rightarrow 1$ , i.e. in the limit when the struck quark carries all the energy of the parent hadron, or equivalently where the energy of the emitted gluon vanishes,  $k^+ \rightarrow 0$ . This is precisely the manifestation of the rapidity divergence at one loop in the unsubtracted TMD PDF, which will only cancel when combining Eq. (2.66) with the soft function, which has a similar divergence as  $k^\mu \rightarrow 0$ . In order to correctly combine the two results, we need to regulate this divergence. Then, after combination we can remove the regulator and obtain the desired finite result.

To illustrate this in practice, in the following we employ the  $\eta$  regulator [102, 109], which modifies the formula for Wilson lines, and which can be implemented directly at the level of Eq. (2.66). The regulator results in adding the following factor to the integral<sup>5</sup>

$$R_c(k, \tau) = \left| \frac{\sqrt{2}k^+}{\nu} \right|^{-\tau} = \left( \frac{(1-x)p^+}{\nu/\sqrt{2}} \right)^{-\tau}. \quad (2.67)$$

It allows us to regulate the divergent term in Eq. (2.66) through the identity

$$\frac{1+x^2}{1-x}(1-x)^{-\tau} = -\left(\frac{2}{\tau} + \frac{3}{2}\right)\delta(1-x) + \left[\frac{1+x^2}{1-x}\right]_+ + \mathcal{O}(\tau). \quad (2.68)$$

Here, the plus prescription is defined such that

$$[f(x)]_+ = f(x) \text{ for } x \neq 1, \quad \int_0^1 dx [f(x)]_+ = 0, \quad (2.69)$$

such that it only modifies the limit  $x \rightarrow 1$  in a way that yields a well-defined integral up to  $x = 1$ . Applying Eq. (2.68) to Eq. (2.66) and using Eq. (2.69), we finally obtain the bare unsubtracted TMD PDF

$$\begin{aligned} \tilde{f}_{q/q}^{0(u)(1)}(x, \mathbf{b}_T, \epsilon, \tau) &= \frac{\alpha_s(\mu)C_F}{2\pi} \left\{ -\left(\frac{1}{\epsilon} + L_b\right)[P_{qq}(x)]_+ + (1-x) \right. \\ &\quad \left. + \delta(1-x)\left(\frac{1}{\epsilon} + L_b\right)\left(\frac{3}{2} + \frac{2}{\tau} - 2\ln\frac{x p^+}{\nu/\sqrt{2}}\right) + \mathcal{O}(\tau) + \mathcal{O}(\epsilon) \right\}. \end{aligned} \quad (2.70)$$

Here, we introduced the shorthand notation

$$L_b = \ln \frac{\mathbf{b}_T^2 \mu^2}{b_0^2}, \quad \text{with} \quad b_0 = 2e^{-\gamma_E}, \quad (2.71)$$

---

<sup>4</sup>Note that another, slightly less popular, definition of  $\overline{\text{MS}}$  replaces  $e^{\epsilon\gamma_E} \rightarrow 1/\Gamma(1-\epsilon)$  in Eq. (2.67). One must be careful about which convention is being used when examining perturbative results in the literature.

<sup>5</sup>In [102, 109], the regulator is denoted as  $\eta$ . For continuity of the presentation, here we denote it as  $\tau$ . The factor of  $\sqrt{2}$  compensates for a different lightcone convention in [102, 109].

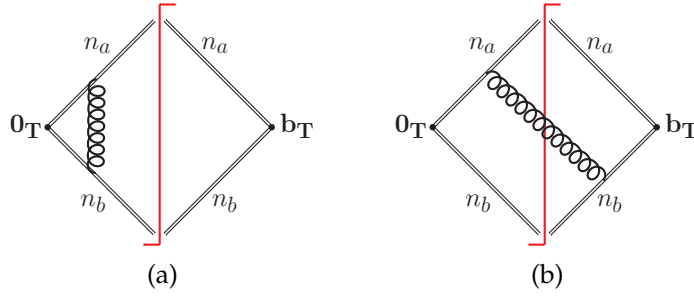


Figure 2.3: One-loop contributions to the soft function, with mirror diagrams obtained by a left-right swap of the exchanged gluon not shown. The double lines denote the Wilson lines from the transverse positions  $0_T$  and  $\mathbf{b}_T$  stretching to lightcone infinity as indicated. The red line denotes the on-shell cut. Diagram (a) is scaleless and vanishes in pure dimensional regularization.

for the canonical logarithm encoding the  $\mathbf{b}_T$ -dependence, and introduced notation for the quark-quark one-loop splitting function which reads

$$P_{qq}(x) = \frac{1+x^2}{1-x}. \quad (2.72)$$

Eq. (2.71) is our desired final result: the divergence as  $x \rightarrow 1$  is regulated through the plus distribution, with the divergence now manifest as a pole in  $1/\tau$ . In addition, it contains a  $1/\epsilon$  pole from the  $k_T \rightarrow 0$  region of the integral in Eq. (2.65). Note that the divergence in the first line in Eq. (2.71) is proportional to the quark-to-quark splitting function  $P_{qq}$ . In fact, one encounters the identical divergence for the collinear PDF itself, illustrating the universality from the collinear limit of QCD.

The bare result in Eq. (2.71) depends somewhat on the employed rapidity regulator, and is not universal. So that results with other regulators can be easily compared, we collect explicit bare results for all regulators discussed above in Sec. 2.4.1 in appendix D.

**Soft function.** Let us now study the corresponding one-loop calculation of the soft function. The relevant diagrams are shown in Fig. 2.3, up to mirror diagrams, and can be evaluated in the same fashion as shown explicitly for the unsubtracted TMD PDF. As before, we first give the generic bare result without any rapidity regulator,

$$\begin{aligned} \mathcal{M}_S &= 2g_0^2 C_F \int \frac{d^d k}{(2\pi)^d} e^{i\mathbf{b}_T \cdot \mathbf{k}_T} \frac{-i}{(2k^+ k^- - \mathbf{k}_T^2 + i0)} \frac{1}{(k^+ - i0)(-k^- + i0)} \\ &= 2g_0^2 C_F \int \frac{d^d k}{(2\pi)^d} e^{i\mathbf{b}_T \cdot \mathbf{k}_T} (2\pi) \delta_+(k^2) \frac{1}{k^+ k^-} \\ &= \frac{g_0^2 C_F}{\pi} \int \frac{d^{2-2\epsilon} \mathbf{k}_T}{(2\pi)^{d-2}} \frac{e^{i\mathbf{b}_T \cdot \mathbf{k}_T}}{k_T^2} \int_0^\infty \frac{dk^-}{k^-}. \end{aligned} \quad (2.73)$$

Since the result from Fig. 2.3(a) is scaleless, here we show only the contribution from Fig. 2.3(b) and its mirror image. With the expression in the first line we can do the  $k^+$  integral by contours,

fixing  $k^+ = \mathbf{k}_T^2/(2k^-) - i0$  with  $k^- > 0$ . This gives an equivalent result to the expression in the second line, which uses Eq. (2.63) to express the integral with the on-shell constraint for the cut graph. Clearly, Eq. (2.74) is divergent as either  $k^- \rightarrow 0$  or  $k^- \rightarrow \infty$ . Since the rapidity of the emission  $k$  is given by  $y_k = \frac{1}{2} \ln(k^+/k^-)$ , these limits correspond to  $y_k \rightarrow \pm\infty$ , which explains the terminology ‘‘rapidity divergence’’. To regulate it in a manner consistent with the above calculation of the unsubtracted TMD PDF, we again use the  $\eta$  regulator [102, 109], which for the soft function inserts the factor

$$R_s(k, \tau) = \left| \frac{k^+ - k^-}{v/\sqrt{2}} \right|^{-\tau} w^2(\tau, v). \quad (2.74)$$

(The absolute value is important.) Here  $w(\tau, v)$  is a bookkeeping parameter for the rapidity divergence, related to a bare parameter by  $w^0 = w(\tau, v)v^{\tau/2}$ . It satisfies  $w(0, v) = 1$  and  $v\partial/\partial v w(\tau, v) = -(\tau/2)w(\tau, v)$ . Thus, the regulated integral becomes

$$\int_0^\infty \frac{dk^-}{k^-} \rightarrow w^2 \left( \frac{v}{\sqrt{2}} \right)^\tau \int_0^\infty \frac{dk^-}{k^-} \left| \frac{\mathbf{k}_T^2}{2k^-} - k^- \right|^{-\tau} = \frac{v^\tau k_T^{-\tau}}{2^\tau \sqrt{\pi}} \Gamma\left(\frac{1}{2} - \frac{\tau}{2}\right) \Gamma\left(\frac{\tau}{2}\right). \quad (2.75)$$

Inserting this into Eq. (2.74), we obtain the bare rapidity-regulated soft function as

$$\begin{aligned} \tilde{S}_q^{0(1)}(b_T, \epsilon, \tau) &= \frac{g_0^2 C_F}{\pi} \frac{v^\tau}{2^\tau \sqrt{\pi}} \Gamma\left(\frac{1}{2} - \frac{\tau}{2}\right) \Gamma\left(\frac{\tau}{2}\right) \int \frac{d^{2-2\epsilon} \mathbf{k}_T}{(2\pi)^{d-2}} \frac{e^{i\mathbf{b}_T \cdot \mathbf{k}_T}}{k_T^{2+\tau}} \\ &= \frac{g_0^2 C_F}{\pi} \frac{v^\tau}{2^\tau \sqrt{\pi}} \Gamma\left(\frac{1}{2} - \frac{\tau}{2}\right) \Gamma\left(\frac{\tau}{2}\right) \frac{\pi^\epsilon \Gamma(-\epsilon - \tau/2)}{4\pi 2^\tau \Gamma(1 + \tau/2)} b_T^{2\epsilon + \tau}, \end{aligned} \quad (2.76)$$

where the integral over  $k_T$  is easily obtained similar to Eq. (2.65). Expanding in  $\tau \rightarrow 0$  and  $\epsilon \rightarrow 0$  and using Eq. (2.67), we obtain

$$\tilde{S}_q^{0(1)}(b_T, \epsilon, \tau) = \frac{\alpha_s(\mu) C_F}{2\pi} \left[ \frac{2}{\epsilon^2} + 4 \left( \frac{1}{\epsilon} + L_b \right) \left( -\frac{1}{\tau} + \ln \frac{\mu}{v} \right) - L_b^2 - \frac{\pi^2}{6} \right] + O(\tau) + O(\epsilon). \quad (2.77)$$

**TMD PDF.** Having calculated the unsubtracted TMD PDF and the soft function at one loop, we can now combine them into the TMD PDF following Eq. (2.33). To do so, we first note that in the  $\eta$  regulator we have chosen for illustration, the soft subtraction factor is equal to unity,  $\tilde{S}_{n_a n_b}^{0\text{subt}} = 1$  [102], so from Eq. (2.33) the physical TMD PDF is constructed as

$$\tilde{f}_{i/H}(x, \mathbf{b}_T, \mu, \zeta) = \lim_{\substack{\epsilon \rightarrow 0 \\ \tau \rightarrow 0}} Z_{uv}^i(\mu, \zeta, \epsilon) \tilde{f}_{i/H}^{0(u)}(x, \mathbf{b}_T, \epsilon, \tau, xP^+) \sqrt{\tilde{S}_{n_a n_b}^0(b_T, \epsilon, \tau)}. \quad (2.78)$$

Comparing the one-loop results Eqs. (2.71) and (2.77), we see that all poles in  $\tau$  precisely cancel in this combination. Taking the product  $f_{q/q}^{0(u)} \sqrt{S_{n_a n_b}^0}$  the final bare result for the physical TMD PDF at one-loop is

$$\begin{aligned} \tilde{f}_{q/q}^{0(1)}(x, \mathbf{b}_T, \epsilon, \zeta) &= \frac{\alpha_s(\mu) C_F}{2\pi} \left[ -\left( \frac{1}{\epsilon} + L_b \right) [P_{qq}(x)]_+ + (1-x) \right] \\ &\quad + \frac{\alpha_s(\mu) C_F}{2\pi} \delta(1-x) \left[ \frac{1}{\epsilon^2} - \frac{L_b^2}{2} + \left( \frac{1}{\epsilon} + L_b \right) \left( \frac{3}{2} + \ln \frac{\mu^2}{\zeta} \right) - \frac{\pi^2}{12} \right] + O(\epsilon). \end{aligned} \quad (2.79)$$

The first line in Eq. (2.80) contains an infrared  $1/\epsilon$  pole, while the second line has ultraviolet  $1/\epsilon$  poles that will be removed by renormalization. Here,  $\zeta \propto (\bar{n} \cdot p)^2 = 2(xP^+)^2$  corresponds to the lightcone momentum carried by the struck quark, and the proportionality factor may be rapidity scheme dependent.

To obtain the renormalized TMD PDF  $f_{q/q}$ , we cancel all  $1/\epsilon$  poles in Eq. (2.80) that are of ultraviolet origin with the counterterm that appears in Eq. (2.33), which in  $\overline{\text{MS}}$  yields

$$Z_{\text{uv}}^q(\mu, \zeta, \epsilon) = 1 - \frac{\alpha_s(\mu)C_F}{2\pi} \left[ \frac{1}{\epsilon^2} + \frac{1}{\epsilon} \left( \frac{3}{2} + \ln \frac{\mu^2}{\zeta} \right) \right] + \mathcal{O}(\alpha_s^2). \quad (2.80)$$

Combining the ingredients in Eq. (2.33) this yields the quark-to-quark contribution to the renormalized TMD PDF at one-loop as

$$\tilde{f}_{q/q}^{(1)}(x, \mathbf{b}_T, \mu, \zeta) = \frac{\alpha_s(\mu)C_F}{2\pi} \left[ -\left( \frac{1}{\epsilon} + L_b \right) [P_{qq}(x)]_+ + (1-x) - \frac{L_b^2}{2} + L_b \left( \frac{3}{2} + \ln \frac{\mu^2}{\zeta} \right) - \frac{\pi^2}{12} \right]. \quad (2.81)$$

Note that the remaining  $1/\epsilon$  pole here is of infrared origin and thus must not be absorbed in the UV counterterm. It is the same collinear divergence that is present for the PDF, which enables the TMD PDF to be matched on to the PDF for perturbative  $b_T$ , see Sec. 2.8. The results in Eqs. (2.80) and (2.82) are independent of the chosen rapidity regulator, and different regulators only differ by the explicit intermediate expressions for the bare unsubtracted TMD PDF and soft function.<sup>6</sup>

In the SCET literature, one often separately renormalizes the unsubtracted TMD PDF, in this case referred to as beam function, and the soft function, see Eqs. (2.34) and (2.35). In this case, one reproduces the same TMD PDF when combining the renormalized beam and soft functions as given in Eq. (2.36). Here, we explicitly illustrate this at one loop. In the  $\eta$  regulator scheme used above,  $S^{0\text{subt}} = 1$ , so the renormalized beam function is given by

$$\tilde{B}_{i/p}(x, \mathbf{b}_T, \mu, \zeta/\nu^2) = \lim_{\substack{\epsilon \rightarrow 0 \\ \tau \rightarrow 0}} \tilde{Z}_B^q(b_T, \mu, \nu, \epsilon, \tau, xP^+) \tilde{f}_{i/p}^{0\text{(u)}}(x, \mathbf{b}_T, \epsilon, \tau, xP^+). \quad (2.82)$$

The counterterm can be easily read off from the result in Eq. (2.64) for the quark-to-quark channel. To do this one expands first in  $\tau \rightarrow 0$ , adding a term to  $\tilde{Z}_B^q$  to cancel the  $1/\tau$  divergence to all orders in  $\epsilon$ , and then expands in  $\epsilon \rightarrow 0$ , adding additional terms to  $\tilde{Z}_B^q$  to cancel  $1/\epsilon$  divergences. This is necessary to ensure that the coefficient of the  $1/\tau$  terms is  $\mu$ -independent, which is important when deriving the corresponding renormalization group evolution equations in  $\mu$  and  $\nu$  [102]. Recall that the  $1/\epsilon$  pole in the first line of Eq. (2.64) is of infrared origin and hence must not be subtracted by the counterterm. This yields,

$$\begin{aligned} \tilde{Z}_B(b_T, \mu, \nu, \epsilon, \tau, xP^+) &= 1 - \frac{\alpha_s(\mu)C_F}{2\pi} \left[ \frac{2w^2(\tau, \nu)}{\tau} \left( \frac{1}{\epsilon} + L_b + \dots \right) + \frac{1}{\epsilon} \left( \frac{3}{2} - 2 \ln \frac{xP^-}{\nu} \right) \right] \\ &\quad + \mathcal{O}(\alpha_s^2). \end{aligned} \quad (2.83)$$

---

<sup>6</sup>When comparing results from the literature, care has to be taken concerning the employed definition of the  $\overline{\text{MS}}$  scheme, see Eq. (2.67) and the following discussion.

Here the ellipsis  $+ \dots$  denotes the fact that all orders in  $\epsilon$  are kept in the function multiplying the  $1/\tau$  divergence in this counterterm (and we have displayed only the expanded form for brevity). Combining Eqs. (2.64) and (2.84) as in Eq. (2.83), we obtain the quark-to-quark contribution to the renormalized beam function in the  $\eta$  regulator scheme,

$$\begin{aligned} \tilde{B}_{q/q}(x, \mathbf{b}_T, \mu, \zeta/v^2) &= \delta(1-x) + \frac{\alpha_s(\mu)C_F}{2\pi} \left[ -\left(\frac{1}{\epsilon} + L_b\right)[P_{qq}(x)]_+ + (1-x) \right. \\ &\quad \left. + \delta(1-x)L_b \left(\frac{3}{2} - 2 \ln \frac{x p^-}{v}\right) \right] + \mathcal{O}(\alpha_s^2). \end{aligned} \quad (2.84)$$

The renormalized soft function is similarly constructed following Eqs. (2.35) and (2.77), from which we can read off the soft function counterterm and the renormalized soft function as

$$\begin{aligned} \tilde{Z}_S(b_T, \mu, v, \epsilon, \tau) &= 1 - \frac{\alpha_s(\mu)C_F}{2\pi} \left[ -\frac{4w^2(\tau, v)}{\tau} \left(\frac{1}{\epsilon} + L_b + \dots\right) + \frac{2}{\epsilon^2} + \frac{4}{\epsilon} \ln \frac{\mu}{v} \right] + \mathcal{O}(\alpha_s^2), \\ \tilde{S}_{n_a n_b}(b_T, \mu, v) &= 1 + \frac{\alpha_s(\mu)C_F}{2\pi} \left[ -L_b^2 + 4L_b \ln \frac{\mu}{v} - \frac{\pi^2}{6} \right] + \mathcal{O}(\alpha_s^2). \end{aligned} \quad (2.85)$$

Again the ellipsis  $+ \dots$  denotes all higher-order terms in  $\epsilon$  which are kept in the  $1/\tau$  coefficient in the  $\tilde{Z}_S^{(1)}$  counterterm. These terms are identical for the counterterms in Eqs. (2.84) and (2.86). Combining the renormalized results for  $\tilde{B}_{q/q}^{(1)}$  and  $\tilde{S}_{n_a n_b}^{(1)}$  from Eqs. (2.85) and (2.86) following Eq. (2.36), one reproduces the renormalized TMD PDF in Eq. (2.82). This illustrates the equality of the two approaches.

## 2.5 Additional TMD PDF definitions

Here we discuss the original CS definition and the JMY definition, which have an extra variable in the renormalized TMD PDF,  $f_{i/p}(x_a, \mathbf{b}_T, \mu, \hat{\zeta}_a; \rho)$ . We also discuss the connection between these definitions and the earlier ones described in Secs. 2.3 and 2.4.

For these definitions, the unsubtracted unpolarized bare quark distribution is again defined as

$$\begin{aligned} \tilde{f}_{i/p}^{0(u)}(x, \mathbf{b}_T, \epsilon, v, x P^+) &= \int \frac{db^-}{2\pi} e^{-ib^-(x P^+)} \langle p(P) | \bar{\psi}_i^0(b^\mu) W_\square^v(b^\mu, 0) \frac{\gamma^+}{2} \psi_i^0(0) | p(P) \rangle, \\ W_\square^v(b^\mu, 0) &= W[0 \rightarrow -\infty v \rightarrow -\infty v + \mathbf{b}_T \rightarrow b] \\ &= W_v(b^\mu; -\infty, 0) W_{\hat{b}_T}(-\infty v; 0, b_T) W_v(0; 0, -\infty), \end{aligned} \quad (2.86)$$

with the Wilson lines defined as in Eq. (2.43). Once again we use here past pointing Wilson lines, as is suitable for Drell-Yan. The key difference compared to the definitions discussed in Secs. 2.3 and 2.4 is the choice of the Wilson line direction  $v$ .

Physically, a parton interpretation is most natural if the gauge link vector  $v$  is chosen along the conjugate light-cone direction to  $P^\mu$ , i.e.,  $v^\mu = n_b^\mu$ . However, as described above, the light-cone gauge link introduces rapidity (or light-cone) singularities for the TMD distribution, where the radiated gluon (virtual or real) has vanishing minus momentum  $\ell^-$ , or large rapidity  $\ln(\ell^+/\ell^-)$ . In the original definition of TMD PDFs by Collins and Soper [86, 119] this problem was circumvented by the use of a physical gauge  $n \cdot A = 0$  for the gauge fields, where  $n \approx n_b$ ,

but one keeps  $n^2 \neq 0$  to regulate the singularities. This procedure induces dependence of the TMD PDF on the Collins-Soper scale

$$\tilde{\zeta}_a^2 = \frac{(2P_A \cdot n)^2}{|n^2|}. \quad (2.87)$$

Note that  $\tilde{\zeta}_a$  has mass dimension-1, and hence differs from the dimension-2 parameter  $\zeta_a$  used in Secs. 2.3 and 2.4. In Refs. [86, 119] a square-root of the hard function,  $\sqrt{H_{ii}(Q, \mu; \rho)}$  displayed in Eq. (2.28) was absorbed into the definition of the TMD PDF, in which case the dependence on  $\rho$  cancels out (for an explicit definition of  $\rho$ , see Eq. (2.93) below). In the modern use of schemes that build off of the original Collins-Soper definitions, this process dependent hard function is instead factored out, and thus enters cross sections as a term that multiplies the TMDs. Ref. [103] derives explicit relations between the original Collins-Soper TMD PDF definition discussed here, and the modern Collins definition [89] with space-like Wilson lines, discussed in Sec. 2.4.1.

The Ji-Ma-Yuan (JMY) scheme [74] builds on the original CS TMD PDF definition by relaxing the restriction to a particular gauge, and instead regulating the rapidity divergences by choosing directions  $v$  in the Wilson lines to be slightly off-light-cone, with

$$v = (v^+, v^-, 0_T), \text{ with } v^- \gg v^+ > 0. \quad (2.88)$$

The use of this  $v$  in Eq. (2.87) implements the analog of the regulator  $\tau$  from Sec. 2.3. Unlike the modern Collins definition, here  $v$  is a time-like vector. Physically, the virtual gluons with rapidity smaller than  $\ln v^+/v^-$  are excluded from the parton distribution. With this definition a dimensionful Collins-Soper scale  $\tilde{\zeta}_a$  emerges as a parameter for the distribution, with<sup>7</sup>

$$\tilde{\zeta}_a^2 = \frac{(2P_A \cdot v)^2}{v^2} \simeq \frac{2v^-(P_A^+)^2}{v^+}. \quad (2.89)$$

The approximation indicated by the  $\simeq$  here is exact only when taking the limit in Eq. (2.89). The limit of entirely lifting the cut-off,  $v^-/v^+ \rightarrow \infty$ , corresponds to  $\tilde{\zeta}_a \rightarrow \infty$ . Similarly, for the TMD distribution for the opposite proton, a Wilson line path parameter  $\bar{v}$  is introduced, and the distribution gains a dependence on an additional parameter  $\tilde{\zeta}_b$ , where

$$\bar{v} = (\bar{v}^+, \bar{v}^-, 0_T), \text{ with } \bar{v}^+ \gg \bar{v}^- > 0, \quad (2.90)$$

$$\tilde{\zeta}_b^2 = \frac{(2\bar{v} \cdot P_B)^2}{\bar{v}^2} \simeq \frac{2\bar{v}^+(P_B^-)^2}{\bar{v}^-}.$$

Again the limit of entirely lifting the cut-off,  $\bar{v}^+/\bar{v}^- \rightarrow \infty$ , corresponds to  $\tilde{\zeta}_b \rightarrow \infty$ .

The corresponding soft function for this scheme is [74]

$$\tilde{S}_{v\bar{v}}^0(b_T, \epsilon, \rho) = \frac{1}{N_c} \langle 0 | \text{Tr}[W_{\gg}^{v\bar{v}}(b_T)] | 0 \rangle, \quad (2.91)$$

$$\begin{aligned} W_{\gg}^{v\bar{v}}(b_T) &= W[0 \rightarrow -\infty\bar{v} \rightarrow -\infty\bar{v} + b_T \rightarrow b_T \rightarrow -\infty v + b_T \rightarrow -\infty v \rightarrow 0] \\ &= W_{\bar{v}}(b_T; 0, -\infty) W_v(b_T; -\infty, 0) W_{\hat{b}_T}(-\infty v; 0, b_T) \\ &\quad \times W_v(0; 0, -\infty) W_{\bar{v}}(0; -\infty, 0) W_{\hat{b}_T}(-\infty\bar{v}; b_T, 0). \end{aligned}$$

<sup>7</sup>Note that we reserve the notation  $\hat{\zeta}_a$  for the dimensionless Collins-Soper scale introduced in Sec. 2.10.1, and hence use  $\tilde{\zeta}_a$  here.

Because of the definitions of  $v$  and  $\bar{v}$  there is an additional invariant

$$\rho^2 = \frac{(2v \cdot \bar{v})^2}{v^2 \bar{v}^2} \simeq \frac{v^- \bar{v}^+}{v^+ \bar{v}^-} \gg 1, \quad (2.92)$$

which appears as a variable in the soft function in Eq. (2.92). The approximation indicated by the  $\simeq$  in Eq. (2.93) is exact only when taking the leading term from the limits in Eqs. (2.89) and (2.91). Furthermore, in this construction the soft overlap subtraction is equal to the soft function,  $S_{v\bar{v}}^{0\text{subt}}(b_T, \epsilon, \rho) = S_{v\bar{v}}^0(b_T, \epsilon, \rho)$ . Using the direct analog of Eq. (2.33) this then gives the renormalized TMD PDF for this construction as

$$\tilde{f}_{i/p}(x_a, \mathbf{b}_T, \mu, x_a \tilde{\zeta}_a; \rho) = \lim_{\epsilon \rightarrow 0} Z_{uv}^i(\mu, \rho, \epsilon) \frac{\tilde{f}_{i/p}^{0(u)}(x_a, \mathbf{b}_T, \epsilon, v, xP^+)}{\sqrt{\tilde{S}_{v\bar{v}}^0(b_T, \epsilon, \rho)}} + O(v^+, \bar{v}^-). \quad (2.93)$$

In this relation the  $O(v^+, \bar{v}^-)$  indicates that the result is expanded in the limits given in Eqs. (2.89) and (2.91). In a similar manner, the other TMD PDF appearing in the Drell-Yan cross section will be  $\tilde{f}_{\bar{i}/p}(x_b, \mathbf{b}_T, \mu, x_b \tilde{\zeta}_b; \rho)$ . Here the analog of the relation  $\zeta_a \zeta_b = Q^4$  from Eq. (2.31) is given by

$$\frac{x_a \tilde{\zeta}_a}{\sqrt{\rho}} \frac{x_b \tilde{\zeta}_b}{\sqrt{\rho}} = Q^2 = \sqrt{\zeta_a \zeta_b}. \quad (2.94)$$

In the JMY scheme the three variables  $x_a \tilde{\zeta}_a$ ,  $x_b \tilde{\zeta}_b$ , and  $\rho$  are all large, but the ratio in Eq. (2.95) is fixed to be  $Q^2$ .

Note that  $\rho$  is an extra variable that is present in the TMD PDF with this JMY definition. In the Drell-Yan cross section the dependence on  $\rho$  in this TMD PDF cancels with the  $\rho$  dependence of the other TMD PDF and the hard function  $H_{i\bar{i}}(\mu, Q; \rho)$  to yield a  $\rho$  independent result, see Eq. (2.28). To relate individual TMD PDFs in the JMY and  $\overline{\text{MS}}$  class of definitions we must simplify the dependence on the extra variable that appears in the JMY case. This can be accomplished by relating the limits in Eqs. (2.89) and (2.91) by choosing  $x_a \tilde{\zeta}_a = x_b \tilde{\zeta}_b$  and  $y_n = 0$  which implies

$$\left( \frac{v^+ \bar{v}^+}{v^- \bar{v}^-} \right)^{1/4} = e^{Y_p + Y} = e^{y_n} = 1, \quad \frac{x_a \tilde{\zeta}_a}{\sqrt{\rho}} = \sqrt{\zeta_a} = \frac{x_b \tilde{\zeta}_b}{\sqrt{\rho}} = \sqrt{\zeta_b} = Q. \quad (2.95)$$

The first equation here implies the last two equations. Note that the first equation is a ratio of two large numbers that is fixed to 1, where  $y_n = 0$  is the rapidity scheme parameter that appeared in Eq. (2.30) for the  $\overline{\text{MS}}$  class of schemes. In this case we still take the limit of  $\tilde{\zeta}_a, \tilde{\zeta}_b, \rho \rightarrow \infty$ , but holding the ratios in Eq. (2.96) fixed. This constraint on the limits reduces the number of variables in the JMY definition by one. Comparing Eqs. (2.28) and (2.29) we see that with the constraint in Eq. (2.96) the relation between the two definitions is given by

$$\tilde{f}_{i/p}(x_a, \mathbf{b}_T, \mu, x_a \tilde{\zeta}_a = \sqrt{\rho} Q, \rho) = \sqrt{\frac{H_{i\bar{i}}(Q^2, \mu)}{H_{i\bar{i}}(Q^2, \mu; \rho)}} \tilde{f}_{i/p}(x_a, \mathbf{b}_T, \mu, \zeta_a = Q^2). \quad (2.96)$$

Here the  $\sqrt{H_{i\bar{i}}(Q^2, \mu)/H_{i\bar{i}}(Q^2, \mu; \rho)}$  prefactor acts as a scheme conversion factor, and can be written out as a perturbative series in  $\alpha_s$  that is dominated by the scale  $\mu \sim Q$ . Since this factor has non-trivial  $\mu$  dependence, we will see in Sec. 4 that the TMD evolution equations differ between the  $\overline{\text{MS}}$  class of schemes discussed in Secs. 2.3 and 2.4, and the schemes discussed here that have  $\rho$  dependence. The evolution equations can also be used to relate these TMDs at different values of  $\tilde{\zeta}_a$  and  $\zeta_a$  than used in Eq. (2.96).

## 2.6 TMD Fragmentation Functions

So far, we have only discussed TMD PDFs in detail, which describe the extraction of a quark from an incoming hadron, where the quark carries a longitudinal momentum fraction  $x$  and a transverse momentum  $\mathbf{k}_T$  relative to the parent hadron. The corresponding final-state process is described by a quark that is produced in a hard interaction and then nonperturbatively fragments into a detected hadron, for example a pion. In this case, the hadron carries a longitudinal momentum fraction  $z$  and a transverse momentum relative to the fragmenting quark. This nonperturbative process is encapsulated in a TMD fragmentation function (TMD FF), the final-state analog of the TMD PDF. In this section, we provide a brief introduction to unpolarized TMD FFs, similar to our general discussion of unpolarized TMD PDFs in Sec. 2.3. In the following Sec. 2.7, we generalize both distributions to polarized processes, allowing for polarizations of both the quark and the hadron state.

To contrast TMD PDFs and FFs, recall the factorization of the Drell-Yan process in Eq. (2.1),

$$p(P_A) + p(P_B) \rightarrow \ell^+(l) + \ell^-(l') + X. \quad (2.97)$$

When measuring the momentum  $q = l + l'$  of the  $\ell^+\ell^-$  final state at small  $q_T$ , the factorization theorem in Eq. (2.29) is appropriate,

$$\frac{d\sigma^W}{dQ dY d^2\mathbf{q}_T} \sim \int d^2\mathbf{b}_T e^{i\mathbf{b}_T \cdot \mathbf{q}_T} \tilde{f}_{i/p}(x_a, \mathbf{b}_T, \mu, \zeta_a) \tilde{f}_{\bar{i}/p}(x_b, \mathbf{b}_T, \mu, \zeta_b), \quad (2.98)$$

where for brevity we focus only on the Fourier integral of Eq. (2.29). Here,  $f_{i/p}$  are the TMD PDFs that describe the extraction of a parton of flavor  $i$  at small transverse momentum from the hadron  $p$ . The SIDIS process discussed in Sec. 2.1,

$$e^-(l) + p(P) \rightarrow e^-(l') + h(P_h) + X, \quad (2.99)$$

is closely related to the Drell-Yan process, as one merely exchanges the roles of the incoming hadron and outgoing lepton, and the momentum transfer is given by  $q = l - l'$ . When the transverse momentum  $P_{Th}$  of the detected hadron is small, the cross section obeys factorization similar to Eq. (2.99),

$$\frac{d\sigma^W}{dx dy dz_h d^2\mathbf{P}_{hT}} \sim \int d^2\mathbf{b}_T e^{i\mathbf{b}_T \cdot \mathbf{P}_{hT}/z} \tilde{f}_{i/p}(x, \mathbf{b}_T, \mu, \zeta_a) \tilde{D}_{h/i}(z_h, \mathbf{b}_T, \mu, \zeta_b), \quad (2.100)$$

where  $x, y, z_h$  are the standard SIDIS observables defined in Eq. (2.11). Compared to Eq. (2.99), here we have a different hard function  $H_{i\bar{i}}^{\text{SIDIS}}$ , which only differs from  $H_{i\bar{i}}$  because  $q^2 > 0$  in SIDIS, while  $q^2 < 0$  for Drell-Yan. The TMD PDF  $\tilde{f}_{i/p}$  in Eq. (2.101) is identical to that in Drell-Yan, as it describes the same physics of extracting a parton at small transverse momentum

from the hadron.<sup>8</sup> In contrast, the second TMD PDF in Eq. (2.99) was replaced by the TMD fragmentation function  $\tilde{D}_{h/i}(z_h, \mathbf{b}_T, \mu, \zeta_b)$ , which precisely encodes the fragmentation of the final-state parton of flavor  $i$  into the hadron  $h$ , where  $h$  carries the longitudinal momentum fraction  $z_h$ , and  $\mathbf{b}_T$  is Fourier conjugate to its transverse momentum.

Before proceeding, let us discuss one important subtlety in the precise definition of transverse momentum. In general, the notion of “transverse” is defined with respect to two reference directions. For Drell-Yan, it is natural to use the proton directions as the reference directions, and consequently it is natural to discuss the transverse momentum of the quark relative to its parent hadron. In contrast, in SIDIS there are two useful choices:

- ① Hadron-Hadron frame: Similar to Drell-Yan, one can define the transverse momentum relative to the directions of the incoming proton  $p$  and outgoing hadron  $h$ , both of which thus have vanishing transverse momentum,  $\mathbf{P}_T = \mathbf{P}_{hT} = 0$ . For the TMD FF, this implies that  $\mathbf{q}_T \neq 0$ , and the fragmenting parton has a nonvanishing transverse momentum  $\mathbf{p}'_T$  relative to the detected hadron. Whenever we use  $\mathbf{q}_T$  or  $\mathbf{p}'_T$ , we refer to this frame. In summary:

$$\text{hadron–hadron frame : specified by } \mathbf{q}_T \neq 0, \quad \mathbf{p}'_T \neq 0. \quad (2.101)$$

If we denote the transverse momentum of the parton from the TMD PDF by  $\mathbf{k}_T$ , then the measured momentum transfer is given by

$$\mathbf{q}_T^{(1)} = -\mathbf{k}_T^{(1)} + \mathbf{p}'_T^{(1)}. \quad (2.102)$$

Here we have included a superscript ① to indicate the frame being used.

- ② Photon-Hadron frame: In the experiment, it is common to define transverse momenta relative to the momenta of the incoming and outgoing leptons, as these can be measured very well. Since this definition does not uniquely specify the angles, the measurements are commonly performed in the so-called Trento frame [18], where  $\mathbf{q}$  is aligned along the  $z$  axes. In this case, the incoming hadron still has vanishing transverse momentum  $\mathbf{P}_T = 0$ , and the same interpretation of the TMD PDF applies. However, the outgoing hadron  $h$  now has transverse momentum  $\mathbf{p}_T \neq 0$  relative to the fragmenting parton. Whenever we use  $\mathbf{p}_T$ , we refer to this frame. In summary:

$$\text{photon–hadron frame : specified by } \mathbf{p}_T \neq 0. \quad (2.103)$$

If we denote the transverse momentum of the parton from the TMD PDF by  $\mathbf{k}_T$ , then the measured hadron momentum is given by

$$\mathbf{P}_{hT}^{(2)} = z_h \mathbf{k}_T^{(2)} + \mathbf{p}_T^{(2)}. \quad (2.104)$$

Again, the superscript ② indicates the frame being used.

---

<sup>8</sup>More precisely, the definition of the TMD PDF in Drell-Yan involves Wilson lines extending to  $-\infty$ , while in SIDIS they extend to  $+\infty$ , but this does not impact the unpolarized TMD PDF. This will be discussed in more detail in Sec. 2.7.

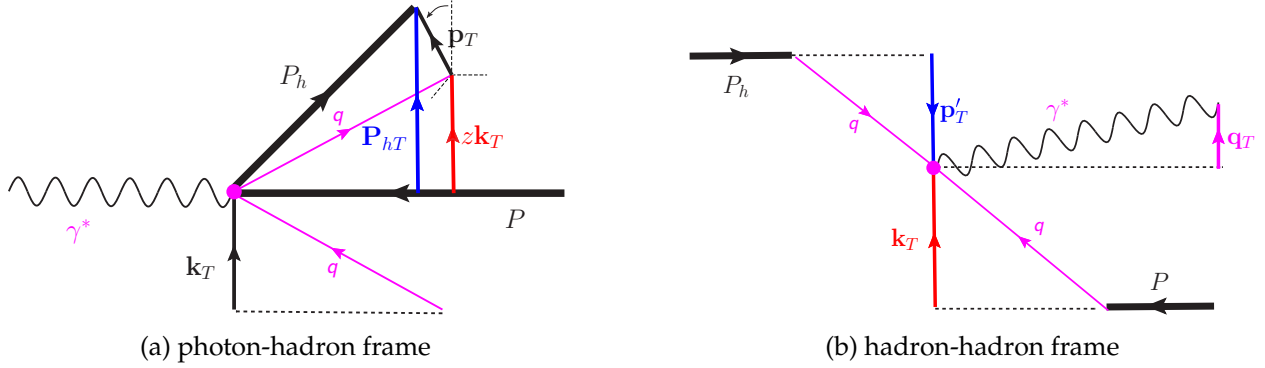


Figure 2.4: Illustration of the different frames used to describe the kinematics of the SIDIS process, as discussed in the text.

These two frames are illustrated in Fig. 2.4. Importantly, these two frames are related by

$$\mathbf{p}_T^{(2)} = -z_h p_T'^{(1)}, \quad \mathbf{P}_{hT}^{(2)} = -z_h \mathbf{q}_T^{(1)}, \quad (2.105)$$

where the second relation follows from the first relation together with Eqs. (2.103) and (2.105). Eq. (2.106) is to be understood in terms of the components in the two different frames. Namely,  $\mathbf{p}_T$  and  $\mathbf{P}_{hT}$  are specified in the parton frame, while  $\mathbf{k}_T$  and  $\mathbf{q}_T$  are specified in the hadron frame. Eq. (2.106) then allows one to easily transform between these two frames [10, 120].

Having clarified this important subtlety in the definition of the transverse direction, we are now in a position to define the TMD FF in analogy to the TMD PDF. We first recall the definition of the unsubtracted TMD PDF in Eq. (2.37),

$$\tilde{f}_{i/p}^{0(u)}(x, \mathbf{b}_T, \epsilon, \tau, xP^+) = \int \frac{db^-}{2\pi} e^{-ib^-(xP^+)} \langle p(P) | [\bar{\psi}_i^0(b^\mu) W_\square(b^\mu, 0) \frac{\gamma^+}{2} \psi_i^0(0)]_\tau | p(P) \rangle, \quad (2.106)$$

where the incoming proton is aligned along the  $n_a$  direction, and  $b^\mu = (0, b^-, \mathbf{b}_T)$ . In the SIDIS process, one still encounters a  $n_a$ -collinear proton, while the outgoing hadron is aligned along the orthogonal direction  $n_b$ . For ease of comparison to Eq. (2.107), here we provide the definition of the TMD FF for a hadron along the  $n_a$  direction with large  $P^+$  momentum. The corresponding definition for an outgoing hadron aligned along the  $n_b$ -direction is easily obtained by replacing  $n_a \leftrightarrow n_b$ , and consequently  $b^- \rightarrow b^+$  and  $P^+ \rightarrow P^-$ .

The bare unsubtracted TMD FF for a parton of flavor  $i$  inside a hadron  $h$  is defined as

$$\begin{aligned} \tilde{\Delta}_{h/i}^{0(u)}(z, \mathbf{b}_T, \epsilon, \tau, P^+/z) &= \frac{1}{4N_c z} \text{Tr} \int \frac{db^-}{2\pi} \sum_X e^{ib^-(P^+/z)} \gamma_{\alpha\alpha'}^+ \\ &\times \langle 0 | [(\bar{W}_\square \psi_i^{0\alpha})(b)]_\tau | h(P), X \rangle \langle h(P), X | [(\bar{\psi}_i^{0\alpha'} W_\square)(0)]_\tau | 0 \rangle. \end{aligned} \quad (2.107)$$

As for the TMD PDF, here  $P$  is the hadron momentum,  $b^\mu = (0, b^-, \mathbf{b}_T)$ , the superscript 0 denotes bare fields, and  $\tau$  is a generic rapidity regulator. The TMD FF is normalized by  $1/z$  and  $1/(4N_c)$ , the latter corresponding to the number of colors and spin states, and the trace is over color and spin indices  $\alpha, \alpha'$ . The key difference between Eqs. (2.107) and (2.108) is that the hadron state appears as an out-state in the matrix element, with  $\sum_X$  denoting the sum

over all additional hadronic final states  $X$ . (In the TMD PDF, the proton appears in the initial state, and the complete sum over  $X$  in the final state can be eliminated by unitarity.)

Recall that Eq. (2.108) is defined in a frame where  $P$  has no transverse momentum, while the quark field  $\psi$  acquires a transverse momentum  $\mathbf{p}'_T$  conjugate to  $\mathbf{b}_T$ . Thus, the corresponding momentum-space TMD FF is given with respect to  $\mathbf{p}'_T$ ,

$$\tilde{\Delta}_{h/i}^{0(u)}(z, \mathbf{b}_T, \epsilon, \tau, P^+/z) = \int d^2\mathbf{p}'_T e^{+i\mathbf{p}'_T \cdot \mathbf{b}_T} \Delta_{h/i}^{0(u)}(z, -z\mathbf{p}'_T, \epsilon, \tau, P^+/z). \quad (2.108)$$

The sign of the Fourier phase is fixed by the corresponding sign in Eq. (2.108). Note that it differs by a sign from the convention for the TMD PDF, compare Eq. (2.7), reflecting that Eqs. (2.107) and (2.108) differ in the sign of their Fourier phase.

The Wilson lines  $W_\nwarrow$  and  $W_\perp$  correspond to “half” of the staple-shaped Wilson line defined in Eq. (2.39), as indicated by their symbols, and again are important for the gauge invariance of the fragmentation function. In the fragmentation functions the transverse link that appears in the TMD PDFs is split in two parts, and as will be discussed in Sec. 2.7.1, the Wilson lines extend to  $+\infty$  as opposed to the  $-\infty$  for TMD PDFs in Drell-Yan, so we can write  $W_{\hat{b}_T}(+\infty n_b; 0, b_T) = W_{\hat{b}_T}(+\infty n_b; +\infty, b_T) W_{\hat{b}_T}(+\infty n_b; 0, +\infty)$ . Explicitly, when taken on the light-cone the Wilson lines appearing in the unsubtracted TMD FFs in Eq. (2.132) are defined as [86, 89]

$$\begin{aligned} W_\perp(b) &= W_{n_b}(b^\mu; +\infty, 0) W_{\hat{b}_T}(+\infty n_b; +\infty, b_T), \\ W_\nwarrow(0) &= W_{\hat{b}_T}(+\infty n_b; 0, +\infty) W_{n_b}(0; 0, +\infty), \end{aligned} \quad (2.109)$$

where the individual Wilson-line segments are defined in Eq. (2.43). As indicated by the brackets  $[\dots]_\tau$  in Eq. (2.132), the same rapidity regulators discussed in Sec. 2.4 must also be implemented for the unsubtracted fragmentation function. As we have seen, most often this modifies the precise definition of the Wilson lines.

Finally, it remains to combine the unsubtracted TMD FF with a soft factor and UV renormalization factor as in Eq. (2.33),

$$\tilde{\Delta}_{h/i}(z, \mathbf{b}_T, \mu, \zeta) = \lim_{\substack{\epsilon \rightarrow 0 \\ \tau \rightarrow 0}} Z_{uv}^i(\mu, \zeta, \epsilon) \frac{\tilde{\Delta}_{h/i}^{0(u)}(z, \mathbf{b}_T, \epsilon, \tau, P^+/z)}{\tilde{S}_{n_a n_b}^{0 \text{ subt}}(b_T, \epsilon, \tau)} \sqrt{\tilde{S}_{n_a n_b}^0(b_T, \epsilon, \tau)}. \quad (2.110)$$

Here  $\zeta = 2(p_h^+)^2 e^{-2y_n}/z^2$  for the fragmentation case, where  $y_n$  is the rapidity cutoff parameter defined (for example) in the Collins approach with space-like Wilson lines for the rapidity regulator in Sec. 2.4. By inverting Eq. (2.109) and employing Eq. (2.106), we thus obtain the desired TMD FF in momentum space in either frame as

$$\Delta_{h/i}(z, \mathbf{p}_T = -z\mathbf{p}'_T, \mu, \zeta) = \int \frac{d^2\mathbf{b}_T}{(2\pi)^2} e^{-i\mathbf{p}'_T \cdot \mathbf{b}_T} \tilde{\Delta}_{h/i}(z, \mathbf{b}_T, \mu, \zeta). \quad (2.111)$$

## 2.7 Quark and Gluon Spin Dependent TMDs and FFs

In this section we provide a number of generalizations of the field theory definition of the unpolarized TMD PDF discussed above. This includes both measuring the quark spin

structure and allowing for the hadron to be polarized, and the corresponding TMD PDFs were summarized above in Fig. 1.7. In addition, we also consider spin-dependent gluon TMD PDFs, as well as spin-dependent TMD fragmentation functions (TMD FFs) that are needed in SIDIS. Note that we limit ourselves to TMD PDFs and TMD FFs at leading power in the transverse momentum (often referred to as leading twist). Their extension at subleading twist will be discussed in Chapter 10.

We will limit our discussion to spin-1/2 hadrons such as the proton. For a review which includes results for hadrons of other spin, see Ref. [? ]. The spinor  $u(P, S)$  for a spin-1/2 hadron with polarization vector  $S^\mu$  satisfies

$$u(P, S)\bar{u}(P, S) = (\not{P} + M)\frac{1}{2}(1 + \gamma_5 \not{S}), \quad (2.112)$$

where  $M$  is the hadron mass. The spin vector can be decomposed in a covariant fashion as

$$S^\mu = S_L \frac{P^+ n_a^\mu - P^- n_b^\mu}{M} + S_T^\mu, \quad S^2 = -(S_L^2 + S_T^2), \quad (2.113)$$

where  $S_L$  and  $S_T^\mu$  denote the longitudinal and transverse spin components. To see the connection between the spin vector  $S^\mu$  and notions that are familiar from the treatment of spin in quantum mechanics, we can work in the hadron rest frame where  $S^\mu = (0, \mathbf{S}) = (0, \mathbf{S}_T, S_L)$ . In this frame Eq. (2.113) can be written in terms of the standard spin density matrix  $\rho$  for a spin-1/2 particle,

$$u(P, S)\bar{u}(P, S) = 2M \begin{pmatrix} \rho & 0 \\ 0 & 0 \end{pmatrix}, \quad \rho = \frac{1}{2}(1 + \boldsymbol{\sigma} \cdot \mathbf{S}), \quad (2.114)$$

where  $\boldsymbol{\sigma}$  is the usual vector of Pauli spin matrices. For a pure spin state we have  $\mathbf{S}^2 = -S^2 = 1$ , whereas for a mixed polarization state one has  $\mathbf{S}^2 < 1$ . In the following sections we will make extensive use of  $S_L$  and  $S_T^\mu$  when discussing the TMDs that are probed by longitudinal and transversely polarized hadronic targets.

For polarized hadrons, there are two distinguished transverse directions, namely  $\mathbf{p}_T$  and  $\mathbf{S}_T$ . To describe all possible transverse structures that can be built out of these quantities, it will be useful to introduce a transverse metric  $g_T^{\alpha\beta}$  and the transverse fully-antisymmetric tensor  $\epsilon_T^{\alpha\beta}$ . Following [121], we define these tensors as

$$g_T^{\alpha\beta} = g^{\alpha\beta} - (n_a^\alpha n_b^\beta + n_a^\beta n_b^\alpha), \quad \epsilon_T^{\alpha\beta} = \epsilon^{\alpha\beta\rho\sigma} n_{a\rho} n_{b\sigma} = \epsilon^{\alpha\beta-+}. \quad (2.115)$$

With our choice of  $n_{a,b}^\mu$  as given in Eq. (2.19), the only nonvanishing components of these tensors are given by

$$g_T^{11} = g_T^{22} = -1, \quad \epsilon_T^{12} = -\epsilon_T^{21} = 1. \quad (2.116)$$

Throughout this section, we will always consider the case of a  $n_a$ -collinear hadron, both for the quark and gluon TMD PDFs and the corresponding TMD fragmentation functions introduced in the following. The corresponding expressions for  $n_b$ -collinear hadrons can

easily obtained by replacing  $n_a \leftrightarrow n_b$ , which also exchanges  $x^\pm \rightarrow x^\mp$  for each four vector  $x^\mu$ . We caution the reader that in principle, this would also affect the definitions of the longitudinal proton spin  $S_L$  in Eq. (2.114) and the transverse tensor  $\epsilon_T^{\alpha\beta}$  in Eq. (2.116). In practice, it is of course more convenient to always use the same definition of  $S_L$  and  $\epsilon_T^{\alpha\beta}$  for both  $n_a$ -collinear and  $n_b$ -collinear hadrons, which can be compensated by a sign flip of all  $S_L$  and  $\epsilon_T^{\alpha\beta}$  appearing in the  $n_b$ -collinear case. This subtle yet important sign is often not stated explicitly in the literature, and has to be kept in mind when comparing explicit expressions.

### 2.7.1 Universality of TMD PDFs and TMD FFs

In the following sections we present suitable generalizations of the definition of TMD PDFs to cases with spin polarization and to processes other than Drell-Yan. We will also give the analogous definitions for TMD FFs. Here we address a key ingredient needed for this generalization, namely the proper treatment of the process dependent incoming or outgoing directions for the Wilson line operators. As discussed above in Sec. 2.1, this dependence is important for obtaining a non-zero Sivers function, since this distribution would otherwise vanish by the  $TP$  invariance of QCD [59].

To generalize our notation to incorporate Wilson line paths that come in from  $-\infty$  or go out to  $+\infty$ , we consider unsubtracted TMD PDFs with the staple shaped Wilson lines

$$\begin{aligned} W_{\square}(b^\mu, 0) &= W_{n_b}(b^\mu; -\infty, 0) W_{\hat{b}_T}(-\infty n_b; 0, b_T) W_{n_b}(0; 0, -\infty), \\ W_{\square}(b^\mu, 0) &= W_{n_b}(b^\mu; +\infty, 0) W_{\hat{b}_T}(+\infty n_b; 0, b_T) W_{n_b}(0; 0, +\infty), \end{aligned} \quad (2.117)$$

where the incoming or outgoing staple is indicated by the subscripts on the LHS. Similarly, soft functions involve Wilson loops with paths that extend to  $\pm$  infinity, given by matrix elements of

$$\begin{aligned} W_{\gg}(b_T) &= W_{n_a}(b_T; 0, -\infty) W_{n_b}(b_T; -\infty, 0) W_{\hat{b}_T}(-\infty n_b; 0, b_T) \\ &\quad \times W_{n_b}(0; 0, -\infty) W_{n_a}(0^\mu; -\infty, 0) W_{\hat{b}_T}(-\infty n_a; b_T, 0), \\ W_{\ll}(b_T) &= W_{n_a}(b_T; 0, +\infty) W_{n_b}(b_T; +\infty, 0) W_{\hat{b}_T}(+\infty n_b; 0, b_T) \\ &\quad \times W_{n_b}(0; 0, +\infty) W_{n_a}(0^\mu; +\infty, 0) W_{\hat{b}_T}(+\infty n_a; b_T, 0). \end{aligned} \quad (2.118)$$

This generalizes the results quoted above in Eq. (2.39) and drawn in Fig. 2.1, where only the cases  $W_{\square}$  and  $W_{\gg}$  were considered. In general the Wilson lines in Eqs. (2.118) and (2.119) also involve additional rapidity regulators, as discussed in detail in Sec. 2.4. The soft function involves a vacuum matrix element of  $W_{\gg}$  or  $W_{\ll}$  and hence is not sensitive to the hadron state, or the quark or gluon operator polarization. It is therefore universal up to the direction for the Wilson lines and their color representation. On the other hand, the unsubtracted TMD PDF does depend on the choice of hadron state, the quark or gluon operator polarization, and in principal on the Wilson line directions.

To be definite we consider the three TMD process of Drell-Yan, SIDIS, and back-to-back hadron production in  $e^+e^-$  annihilation, as illustrated in Fig. 1.9. For the analysis of these processes we follow Refs. [89, 122], where the structure of the Wilson line operators that are consistent with the derivation of factorization have been analyzed using the space-like Wilson line regulator  $n_a \rightarrow n_A$  and  $n_b \rightarrow n_B$  given above in Eq. (2.45). A key ingredient in this

Function	Drell-Yan TMD PDF	SIDIS TMD PDF	SIDIS TMD FF	$e^+e^-$ TMD FF
Wilson lines in $\tilde{S}_{n_a n_b}^{0\pm\infty}$	$W_{\gg}^{-\infty}$	$W_{\ll}^{+\infty}$	$W_{\ll}^{+\infty}$	$W_{\ll}^{+\infty}$
Wilson lines in $\tilde{f}_{i/p_s}^{[\Gamma]0(u)}$ or $\tilde{D}_{i/p_s}^{[\Gamma]0(u)}$	$W_{\sqsubset}$	$W_{\sqsupset}$	$W_{\neg}, W_{\perp}$	$W_{\neg}, W_{\perp}$
TMDs	$\tilde{F}_{i/p_s}^{-\infty}$	$\tilde{F}_{i/p_s}^{+\infty}$	$\tilde{D}_{i/p_s}$	$\tilde{D}_{i/p_s}$
T-even $\tilde{F} = \tilde{f}_1, \tilde{g}_1, \tilde{g}_{1T}^\perp, \tilde{h}_{1L}^\perp, \tilde{h}_1, \tilde{h}_{1T}^\perp$	$\tilde{F}_{i/p_s}^{-\infty}(x, b_T) = \tilde{F}_{i/p_s}^{+\infty}(x, b_T)$		universal	
T-odd $\tilde{F} = \tilde{f}_{1T}^\perp, \tilde{h}_1^\perp$	$\tilde{F}_{i/p_s}^{-\infty}(x, b_T) = -\tilde{F}_{i/p_s}^{+\infty}(x, b_T)$			

Table 2.2: Summary of Wilson line directions for TMD PDFs and TMD FFs in different processes [89, 122]. The TMD FFs are seen to be universal between SIDIS and  $e^+e^- \rightarrow H_1 H_2 X$ . For the TMD PDFs the distributions in Drell-Yan and SIDIS can be related by time-reversal symmetry as indicated.

analysis is considering which directions are consistent with momentum contour deformations out of the so-called Glauber region (see Chapter 3). A summary of the key results is given in Table 2.2. For each TMD appearing in a given process, the  $\pm\infty$  directions are correlated between the soft function and the hadronic matrix elements giving various unsubtracted TMD PDFs  $\tilde{f}_{i/p_s}^{[\Gamma]0(u)}$  or unsubtracted TMD FFs  $\tilde{D}_{i/p_s}^{[\Gamma]0(u)}$ , see Ref. [71]. In particular, for the TMD PDFs the hadronic and vacuum matrix elements are taken to involve different Wilson line paths as follows

$$\begin{aligned} \tilde{F}_{i/p_s}^{-\infty} : & \quad \tilde{f}_{i/p_s}^{[\Gamma]0(u)} \text{ defined using } W_{\sqsubset}, & \tilde{S}_{n_a n_b}^0 \text{ defined using } W_{\gg} \\ \tilde{F}_{i/p_s}^{+\infty} : & \quad \tilde{f}_{i/p_s}^{[\Gamma]0(u)} \text{ defined using } W_{\sqsupset}, & \tilde{S}_{n_a n_b}^0 \text{ defined using } W_{\ll}. \end{aligned} \quad (2.119)$$

Here the first line gives the same definition as in Eqs. (2.37) and (2.38), while the second line modifies the Wilson lines used in these definitions. (For simplicity we do not discuss the freedom in the direction dependence of soft subtractions, and instead refer the interested reader to Ref. [122].) For the Drell-Yan process one obtains Wilson lines from  $-\infty$  in the TMD PDFs, while for SIDIS one finds lines extending out to  $+\infty$ . The results for these two cases can be related by a combination of time-reversal and parity ( $TP$ ) symmetry [59]. This gives equality for the T-even distributions and an extra minus sign for the T-odd distributions, as shown in the last two rows of Table 2.2. A more detailed presentation of the physical argument for this sign flip is given below in Sec. 2.7.2.

The process dependence of the Wilson lines appearing in the fragmentation functions in SIDIS and  $e^+e^-$  annihilation have also been analyzed in Ref. [122]. Here it is found that all lines can be consistently taken to point out to  $+\infty$ , and hence that all leading power fragmentation functions are universal without sign flips. For this reason we postpone giving definitions of the Wilson lines appearing in the unsubtracted TMD FFs, which are denoted by  $W_{\neg}$  and  $W_{\perp}$ , in Sec. 2.7.3 below.

Since all leading power TMD PDFs can be expressed in terms of the same eight functions, the underlying hadronic distributions apply equally well to both Drell-Yan and SIDIS once the extra sign for the T-odd distributions is taken into account, and hence are universal. To keep track of the extra process dependent minus sign in subsequent sections, we define

$$\kappa = \begin{cases} +1 & (\text{Drell-Yan}) \\ -1 & (\text{SIDIS}) \end{cases}, \quad (2.120)$$

and will include factors of  $\kappa$  in front of the TMD PDFs  $h_1^\perp$  and  $f_{1T}^\perp$  in suitable places. This implies that we will always use the relations shown in Table 2.2 to express the TMD PDFs in terms of those defined with Wilson lines that extend from  $-\infty$  as in Drell-Yan. With this choice there is no longer any ambiguity in expressions which require specifying a Wilson line direction. Therefore in subsequent sections we will drop the  $\pm\infty$  superscripts on the Wilson lines that were used for the discussion in this section.

## 2.7.2 Leading Quark TMD PDFs

To generalize the definition in Eq. (2.33) of the unpolarized leading power quark TMD PDF to include other quark spin structures and to include polarized protons, we modify the definition of the unsubtracted TMD PDF  $f_{i/p}^{0(u)}$  in Eq. (2.37) to include a general spin matrix  $\Gamma$ :

$$\tilde{f}_{i/pS}^{[\Gamma]0(u)}(x, \mathbf{b}_T, \epsilon, \tau, xP^+) = \int \frac{db^-}{2\pi} e^{-ib^-(xP^+)} \langle p(P, S) | [\bar{\psi}^i(b^\mu) W_\square(b^\mu, 0) \frac{\Gamma}{2} \psi^i(0)]_\tau | p(P, S) \rangle. \quad (2.121)$$

Here  $S$  in the states indicates the spin of the proton. The full set of TMD PDFs at leading order in small transverse momentum, so-called leading twist, is obtained by considering the Dirac structures

$$\Gamma \in \{ \gamma^+, \gamma^+ \gamma_5, i\sigma^{\alpha+} \gamma_5 \}, \quad (2.122)$$

where  $\sigma^{\mu\nu} = \frac{i}{2}[\gamma^\mu, \gamma^\nu]$ . To see why there are only these three structures at leading power, we note that the leading power operators are built out of the “good-components” of the fermion field [123], which obey  $\frac{1}{2}\gamma^-\gamma^+\psi^i = \psi^i$ . In SCET these projection relations are obeyed by the collinear fermion fields that are used to construct leading power operators, see [124]. It is straightforward to check that any other choices for  $\Gamma$  will either give zero or can be reduced to one of those in Eq. (2.123) when sandwiched between these projectors in  $\bar{\psi}^i(\frac{1}{2}\gamma^+\gamma^-)\Gamma(\frac{1}{2}\gamma^-\gamma^+)\psi^i$ .

Inserting Eq. (2.122) into Eq. (2.33) with the corresponding soft function, subtraction function, and UV renormalization factors yields the renormalized spin-dependent TMD PDF  $\tilde{f}_{i/pS}^{[\Gamma]}(x, \mathbf{b}_T, \mu, \zeta)$ . These TMD PDFs can be affected by whether their Wilson lines point to  $\pm\infty$ , as discussed in Sec. 2.7.1. We work in a convention where symmetry relations are always used to convert TMD PDFs to the versions obtained with Wilson lines from  $-\infty$ , and encode the extra process dependent sign that appears for the time reversal odd TMD PDFs in a coefficient  $\kappa = \pm 1$ , see Eq. (2.121).

For a spin-1/2 particle such as the proton, using the spin vector from Eq. (2.114), the spin-dependent TMD PDFs can be further decomposed into eight independent structures<sup>9</sup> as

---

<sup>9</sup>There exist different notations for the corresponding TMDs, for instance those used by Torino-Cagliari group. The notations and relations to our notations can be found in Refs. [18, 125–127].

		Quark Polarization		
		Un-Polarized (U)	Longitudinally Polarized (L)	Transversely Polarized (T)
Nucleon Polarization	U	$f_1 = \text{Unpolarized}$		$h_1^\perp = \text{Boer-Mulders}$
	L		$g_1 = \text{Helicity}$	$h_{1L}^\perp = \text{Worm-gear}$
	T	$f_{1T}^\perp = \text{Sivers}$	$g_{1T}^\perp = \text{Worm-gear}$	$h_1 = \text{Transversity}$ $h_{1T}^\perp = \text{Pretzelosity}$

Figure 2.5: Leading power quark parton distribution functions for the proton or a spin-1/2 hadron.

follows [60, 61, 128, 129]:

$$\begin{aligned}
f_{i/p_S}^{[\gamma^+]}(x, \mathbf{k}_T, \mu, \zeta) &= f_1(x, k_T) - \frac{\epsilon_T^{\rho\sigma} k_{T\rho} S_{T\sigma}}{M} \kappa f_{1T}^\perp(x, k_T), \\
f_{i/p_S}^{[\gamma^+ \gamma_5]}(x, \mathbf{k}_T, \mu, \zeta) &= S_L g_1(x, k_T) - \frac{k_T \cdot S_T}{M} g_{1T}^\perp(x, k_T), \\
f_{i/p_S}^{[i\sigma^{\alpha+} \gamma_5]}(x, \mathbf{k}_T, \mu, \zeta) &= S_T^\alpha h_1(x, k_T) + \frac{S_L k_T^\alpha}{M} h_{1L}^\perp(x, k_T) \\
&\quad - \frac{\mathbf{k}_T^2}{M^2} \left( \frac{1}{2} g_T^{\alpha\rho} + \frac{k_T^\alpha k_T^\rho}{\mathbf{k}_T^2} \right) S_T \rho h_{1T}^\perp(x, k_T) - \frac{\epsilon_T^{\alpha\rho} k_{T\rho}}{M} \kappa h_1^\perp(x, k_T).
\end{aligned} \tag{2.123}$$

Here for brevity on the right hand side we have dropped the arguments  $\mu$  and  $\zeta$ , as well as the flavor and hadron subscripts  $i/p_S$ . Note that all functions on the right-hand side only depend on the magnitude  $k_T = |\mathbf{k}_T|$ , but that all  $k_T^\mu$  with an explicit Lorentz index or scalar products are evaluated in Minkowskian metric. In Eq. (2.124),  $M$  denotes the nucleon mass, which is inserted such that all distributions on the right-hand side have the same mass dimension. The displayed greek indices are transverse, and the transverse tensors  $g_T^{\alpha\beta}$  and  $\epsilon_T^{\rho\sigma}$  are defined in Eq. (2.116). The spin vector of the proton  $p_S$  is decomposed as given in Eq. (2.114).

Eq. (2.124) gives the eight leading spin-dependent TMDs for a spin- $\frac{1}{2}$  hadron [60, 61, 128, 129] following the conventions of [121]. This general decomposition is obtained by considering the most general decomposition of the correlator in Eq. (2.122) with open spinor indices on the fermion fields that satisfy the good component projection relations  $\frac{1}{2}\gamma^- \gamma^+ \psi^i = \psi^i$ , and which is linear in the hadron spin-polarization vector. The contractions with the Dirac structures

in Eq. (2.123) then suffice to project out all the leading power TMDs, as given in Eq. (2.124). The complete decomposition at subleading-twist, which also contains the Dirac structures not included in Eq. (2.123), can be found in [121, 130, 131], and is discussed further in Chapter 10 below. As summarized in Fig. 2.5, the different structures correspond to specific polarizations for the quark operator and hadron, three of which have collinear counterparts (i.e. integrated over  $\mathbf{k}_T$ ):

- $f_1(x, k_T)$  describes an unpolarized quark inside an unpolarized hadron, similar to the unpolarized collinear distribution  $f_1(x)$ .
- $g_1(x, k_T)$  is the helicity distribution which describes a longitudinally polarized quark inside a longitudinally polarized hadron, similar to the collinear helicity distribution  $g_1(x)$ .
- $h_1(x, k_T)$  is the transversity distribution which describes a transversely polarized quark inside a transversely polarized hadron, similar to the collinear transversity distribution  $h_1(x)$ .

The remaining distributions only arise when measuring transverse momenta and have no collinear counterpart:

- $f_{1T}^\perp(x, k_T)$  is the Sivers function [132] which describes an unpolarized quark inside a transversely polarized hadron. Since it is  $T$ -odd, it was originally believed to vanish due to symmetry arguments [57]. It was later clarified that it is nonvanishing when correctly taking the Wilson lines in the definition of the unsubtracted TMD PDF and soft function into account [58, 59, 133].
- The function  $g_{1T}^\perp(x, k_T)$  describes longitudinally polarized quarks in a transversely polarized hadron, and vice versa  $h_{1L}^\perp(x, k_T)$  describes transversely polarized quarks in a longitudinally polarized hadron [134]. They are referred in the literature as “worm-gear”  $T$  and  $L$  functions or Kotzinian-Mulders [61, 135] functions.
- $h_1^\perp(x, k_T)$  is the Boer-Mulders function [60] which describes a transversely polarized quark in an unpolarized hadron. Like the Sivers function  $f_{1T}^\perp$ , it is time-reversal odd.
- $h_{1T}^\perp(x, k_T)$  is the pretzelosity function, which contributes to the distribution of a transversely polarized quark in a transversely polarized hadron [129], in addition to the transversity  $h_1(x, k_T)$ . Curiously, the name of this function stems from its expected shape [136] published by G. Miller, which was also highlighted in the New York Times [137], exhibiting the unusual shape of the proton due to the presence of this function.

Following the discussion in Ref. [138] we review in detail the argument for the sign change of the Sivers function. Let  $|\alpha\rangle = |p(P, S)\rangle$  and  $\langle\beta|$  be equal to the rest of the matrix element in Eq. (2.122). The definition in Eq. (2.122) is suitable for the Drell-Yan process with past pointing Wilson lines while for SIDIS one defines a similar matrix element with future pointing Wilson lines  $W_\exists(b^u, 0)$  as in Eq. (2.118). From the parity and time-reversal invariance of QCD,  $\langle\alpha_P|\beta_P\rangle = \langle\alpha|\beta\rangle$  and  $\langle\beta_T|\alpha_T\rangle = \langle\alpha|\beta\rangle$ , where  $|\alpha_P\rangle$  and  $|\beta_P\rangle$ , and  $|\alpha_T\rangle$  and  $|\beta_T\rangle$  are the parity and time-reversal transformed states from the states  $|\alpha\rangle$  and  $|\beta\rangle$ , respectively.

Thus one derives [138] that the only difference between  $f_{i/p_S}^{[\gamma^+]}(x, \mathbf{k}_T, \mu, \zeta)$  for SIDIS and Drell-Yan is  $S \rightarrow -S$ . Therefore one immediately concludes that the spin-averaged TMD quark distributions are process independent

$$f_1^{\text{SIDIS}}(x, k_T) = f_1^{\text{DY}}(x, k_T) \quad (2.124)$$

while Sivers function changes the sign

$$f_{1T}^{\perp\text{SIDIS}}(x, k_T) = -f_{1T}^{\perp\text{DY}}(x, k_T) \quad (2.125)$$

The sign change of the Sivers function is a property of the gauge invariant TMD parton distributions. Similar arguments can also be made for the other TMD PDFs listed in Table 2.2. In order to make sure that a single definition (that of Drell-Yan) can be used for both SIDIS and Drell-Yan we previously introduced the coefficient  $\kappa = \pm 1$  in Eq. (2.121) to explicitly account for this sign change in SIDIS processes. In this notation, tests of the sign-flip prediction between SIDIS and DY become tests of  $\kappa^{\text{DY}} = -\kappa^{\text{SIDIS}}$ .

One can obtain the position-space version of Eq. (2.124) by a Fourier transform with respect to  $\mathbf{k}_T$ . In contrast to Eq. (2.124), which is commonly adopted in the literature, there are different conventions for the spin-decomposition in position space. Historically, it was common to simply Fourier-transform Eq. (2.124) as is, and this was used for example in [139] and in the lattice studies in [140–142] (see Sec. 6). In this case, one decomposes  $\tilde{f}$  as [139]<sup>10</sup>

$$\begin{aligned} \tilde{f}_{i/p_S}^{[\gamma^+]}(x, \mathbf{b}_T, \mu, \zeta) &= \tilde{f}_1(x, b_T) + i\epsilon_{\rho\sigma}b_T^\rho S_T^\sigma M \tilde{f}_{1T}^\perp(x, b_T), \\ \tilde{f}_{i/p_S}^{[\gamma^+\gamma_5]}(x, \mathbf{b}_T, \mu, \zeta) &= S_L \tilde{g}_1(x, b_T) + i b_T \cdot S_T M \tilde{g}_{1T}^\perp(x, b_T), \\ \tilde{f}_{i/p_S}^{[i\sigma^{\alpha+}\gamma_5]}(x, \mathbf{b}_T, \mu, \zeta) &= S_T^\alpha \tilde{h}_1(x, b_T) - i S_L b_T^\alpha M \tilde{h}_{1L}^\perp(x, b_T) + i\epsilon^{\alpha\rho} b_{\perp\rho} M \tilde{h}_1^\perp(x, b_T) \\ &\quad + \frac{1}{2} \mathbf{b}_T^2 M^2 \left( \frac{1}{2} g_T^{\alpha\rho} + \frac{b_T^\alpha b_T^\rho}{\mathbf{b}_T^2} \right) S_{\perp\rho} \tilde{h}_{1T}^\perp(x, b_T). \end{aligned} \quad (2.126)$$

Here, the explicit factors of  $i$  ensure that all functions on the right-hand side are manifestly real. Due to the  $\mathbf{k}_T$ -dependent prefactors in Eq. (2.124), the  $\tilde{f}$ ,  $\tilde{g}$  and  $\tilde{h}$  in Eq. (2.127) are now  $\mathbf{b}_T$ -dependent derivatives of Fourier transformations of the corresponding  $f$ ,  $g$  and  $h$  in Eq. (2.124), namely

$$\begin{aligned} \tilde{f}_1(x, b_T) &\equiv \tilde{f}_1^{(0)}(x, b_T), & \tilde{f}_{1T}^\perp(x, b_T) &\equiv \tilde{f}_{1T}^{\perp(1)}(x, b_T), & \tilde{h}_{1T}^\perp(x, b_T) &\equiv \tilde{h}_{1T}^{\perp(2)}(x, b_T), \\ \tilde{g}_{1L}(x, b_T) &\equiv \tilde{g}_{1L}^{(0)}(x, b_T), & \tilde{h}_1^\perp(x, b_T) &\equiv \tilde{h}_1^{\perp(1)}(x, b_T), \\ \tilde{h}_1(x, b_T) &\equiv \tilde{h}_1^{(0)}(x, b_T), & \tilde{g}_{1T}(x, b_T) &\equiv \tilde{g}_{1T}^{(1)}(x, b_T), \\ && \tilde{h}_{1L}^\perp(x, b_T) &\equiv \tilde{h}_{1L}^{\perp(1)}(x, b_T). \end{aligned} \quad (2.127)$$

<sup>10</sup>Note that we have accounted for a relative minus sign in  $b^\mu$  when relating the definition in [139] to our convention. See also [143], and the comment below Eq. (2.37).

The derivatives are defined as

$$\begin{aligned}\tilde{f}^{(n)}(x, b_T, \mu, \zeta) &\equiv n! \left( \frac{-1}{M^2 b_T} \partial_{b_T} \right)^n \tilde{f}(x, b_T, \mu, \zeta) \\ &= \frac{2\pi n!}{(b_T M)^n} \int_0^\infty dk_T k_T \left( \frac{k_T}{M} \right)^n J_n(b_T k_T) f(x, k_T, \mu, \zeta).\end{aligned}\quad (2.128)$$

Note that for real  $f$  this Hankel transform is real as well, and that  $\tilde{f}^{(n)}$  have the same mass dimension for all  $n$ . This convention with the explicit factor of  $n!$  was introduced in [139] such that taking  $b_T \rightarrow 0$  recovers the moments obtained by integrating over  $\mathbf{k}_T$  as defined in [60, 129]. The inverse transformation is given by

$$f^{(n)}(x, k_T, \mu, \zeta) = \frac{M^{2n}}{2\pi n!} \int_0^\infty db_T b_T \left( \frac{b_T}{k_T} \right)^n J_n(b_T k_T) \tilde{f}^{(n)}(x, k_T, \mu, \zeta). \quad (2.129)$$

For more details on deriving these Fourier relations, see appendix C.

In [144], it was proposed to absorb the hadron masses used in the normalization in Eq. (2.124) into the Fourier-transformed distributions. Compared to the above decomposition, in this convention one replaces the distributions  $\tilde{F}(x, b_T)$  by the alternate definitions  $\tilde{F}'(x, b_T)$  where the relationship is

$$b_T^\alpha M \tilde{F}^{(1)} = \frac{b_T^\alpha}{b_T} \tilde{F}'^{(1)}, \quad b_T^\alpha b_T^\rho M^2 \tilde{F}^{(2)} = \frac{b_T^\alpha b_T^\rho}{b_T^2} \tilde{F}'^{(2)}, \quad \tilde{F}^{(n)} = (b_T M^2)^{-n} \tilde{F}'^{(n)}. \quad (2.130)$$

Here the last equality is applied when there are no  $b_T$  dependent factors in front of the distribution  $\tilde{F}^{(n)}$ .

It is natural to ask whether the TMD PDFs are positive definite functions. This has been explored recently in Ref. [145]. For further discussion in the context of phenomenological analyses, see Chapter 5, and for a discussion in the context of various models for TMDs, see Sec. 7.8.1.

### 2.7.3 Leading Quark TMD FFs

We now discuss the generalization of the TMD FFs, introduced in Sec. 2.6 for unpolarized processes, to also allow for polarizations of the fragmenting quark and detected hadron. The generalization of Eq. (2.108) is given by

$$\begin{aligned}\tilde{\Delta}_{h/i}^{[\Gamma]0(u)}(z, \mathbf{b}_T, \epsilon, \tau, P^+/z) &= \frac{1}{4N_c z} \text{Tr} \int \frac{db^-}{2\pi} \sum_X e^{ib^-(P^+/z)} \Gamma_{\alpha\alpha'}^+ \\ &\times \langle 0 | [(W \llcorner \psi_i^{0\alpha})(b)]_\tau | h(P, S), X \rangle \langle h(P, S), X | [(\bar{\psi}_i^{0\alpha'} W \lrcorner)(0)]_\tau | 0 \rangle.\end{aligned}\quad (2.131)$$

Compared to Eq. (2.108), the hadron state now carries the spin  $S$ , and the Dirac structure  $\Gamma$  is chosen analogous to Eq. (2.123) as

$$\Gamma \in \{ \gamma^+, \gamma^+ \gamma_5, i \sigma^{\alpha+} \gamma_5 \}. \quad (2.132)$$

## Leading Quark TMDFFs



		Quark Polarization		
		Un-Polarized (U)	Longitudinally Polarized (L)	Transversely Polarized (T)
Unpolarized (or Spin 0) Hadrons	L	$D_1 = \bullet$ Unpolarized		$H_1^\perp = \bullet - \bullet$ Collins
	T	$D_{1T}^\perp = \bullet - \bullet$ Polarizing FF	$G_{1T}^\perp = \bullet - \bullet$	$H_{1L}^\perp = \bullet - \bullet$ Helicity
Polarized Hadrons	L		$G_1 = \bullet - \bullet$	$H_{1T}^\perp = \bullet - \bullet$
	T		$H_{1L} = \bullet - \bullet$ Transversity	$H_1 = \bullet - \bullet$

Figure 2.6: Leading power quark TMD fragmentation functions for a spin-1/2 (or for an unpolarized or spin 0) hadron.

Eq. (2.132) is combined with the soft function as in Eq. (2.111) to obtain the UV-renormalized and soft-subtracted TMD FF. After taking the Fourier transform with respect to  $\mathbf{b}_T$ , we then obtain the renormalized TMD FF in momentum space,

$$\Delta_{h/i}(z, \mathbf{p}_T = -z\mathbf{p}'_T, \mu, \zeta) = \int \frac{d^2\mathbf{b}_T}{(2\pi)^2} e^{-i\mathbf{p}'_T \cdot \mathbf{b}_T} \tilde{\Delta}_{h/i}(z, \mathbf{b}_T, \mu, \zeta). \quad (2.133)$$

As discussed at length in Sec. 2.6, here  $\mathbf{p}_T$  is the hadron transverse momentum relative to the fragmenting quark in the photon-hadron frame, while  $\mathbf{p}'_T$  is the parton momentum relative to the detected hadron in the hadron-hadron frame.

The spin-dependent TMD FF can be decomposed into eight independent structures in the

same fashion as the spin-dependent TMD PDF,

$$\begin{aligned}\Delta_{h/i}^{[\gamma^+]}(z, -z\mathbf{p}'_T, \mu, \zeta) &= D_1(z, zp'_T) - \frac{\epsilon_T^{\rho\sigma} p'_{T\rho} S_{T\sigma}}{M_h} D_{1T}^\perp(z, zp'_T), \\ \Delta_{h/i}^{[\gamma^+ \gamma_5]}(z, -z\mathbf{p}'_T, \mu, \zeta) &= S_L G_1(z, zp'_T) - \frac{p'_T \cdot S_T}{M_h} G_{1T}^\perp(z, zp'_T), \\ \Delta_{h/i}^{[i\sigma^{\alpha+} \gamma_5]}(z, -z\mathbf{p}'_T, \mu, \zeta) &= S_T^\alpha H_1(z, zp'_T) + \frac{S_L p'^\alpha_T}{M_h} H_{1L}^\perp(z, zp'_T) \\ &\quad - \frac{\mathbf{p}'_T^2}{M_h^2} \left( \frac{1}{2} g_T^{\alpha\rho} + \frac{p'^\alpha_T p'^\rho_T}{\mathbf{p}'_T^2} \right) S_{T\rho} H_{1T}^\perp(z, zp'_T) - \frac{\epsilon_T^{\alpha\rho} p'_{T\rho}}{M_h} H_1^\perp(z, zp'_T).\end{aligned}\tag{2.134}$$

Once again on the right-hand side we suppress the arguments  $\mu$  and  $\zeta$  as well as the subscripts  $h/i$ . This decomposition is analogous to Eq. (2.124), where the TMD FFs are distinguished from the TMD PDFs by using capital symbols, but have similar interpretations in terms of the quark and hadron polarization, as summarized in Fig. 2.6. Note that the functions appearing in Eq. (2.135) are written as a function of  $zp'_T$ , while the prefactors only involve  $\mathbf{p}'_T$ , as is common in the literature, see e.g. [121]. We again encounter two  $T$ -odd functions, namely  $D_{1T}^\perp$  and the Collins function  $H_1^\perp$ .

As before, we can equivalently consider the decomposition of the spin-dependent TMD FF in position space. Following our presentation of the TMD PDF, we write the decomposition analogous to Eq. (2.127) as [139]<sup>11</sup>

$$\begin{aligned}\tilde{\Delta}_{h/i}^{[\gamma^+]}(z, \mathbf{b}_T, \mu, \zeta) &= \tilde{D}_1(z, b_T) - i\epsilon_{T\rho\sigma} b_T^\rho S_T^\sigma M_h \tilde{D}_{1T}^\perp(z, b_T), \\ \tilde{\Delta}_{h/i}^{[\gamma^+ \gamma_5]}(z, \mathbf{b}_T, \mu, \zeta) &= S_L \tilde{G}_1(z, b_T) + i b_T \cdot S_T M_h \tilde{G}_{1T}^\perp(z, b_T), \\ \tilde{\Delta}_{h/i}^{[i\sigma^{\alpha+} \gamma_5]}(z, \mathbf{b}_T, \mu, \zeta) &= S_T^\alpha \tilde{H}_1(z, b_T) + i S_L b_T^\alpha M_h \tilde{H}_{1L}^\perp(z, b_T) - i\epsilon_T^{\alpha\rho} b_{\perp\rho} M_h \tilde{H}_1^\perp(z, b_T) \\ &\quad + \frac{1}{2} \mathbf{b}_T^2 M_h^2 \left( \frac{1}{2} g_T^{\alpha\rho} + \frac{b_T^\alpha b_T^\rho}{\mathbf{b}_T^2} \right) S_{\perp\rho} \tilde{H}_{1T}^\perp(z, b_T).\end{aligned}\tag{2.135}$$

Due to the  $\mathbf{p}'_T$ -dependent prefactors in Eq. (2.135), the  $\tilde{D}$ ,  $\tilde{G}$  and  $\tilde{H}$  in Eq. (2.136) are now  $\mathbf{b}_T$ -dependent derivatives of Fourier transformations of the corresponding  $D$ ,  $G$  and  $H$  in Eq. (2.135). They are given by,

$$\begin{aligned}\tilde{D}_1(z, b_T) &\equiv \tilde{D}_1^{(0)}(z, b_T), & \tilde{D}_{1T}^\perp(z, b_T) &\equiv \tilde{D}_{1T}^{\perp(1)}(z, b_T), & \tilde{H}_{1T}^\perp(z, b_T) &\equiv \tilde{H}_{1T}^{\perp(2)}(z, b_T), \\ \tilde{G}_1(z, b_T) &\equiv \tilde{G}_1^{(0)}(z, b_T), & \tilde{D}_1^\perp(z, b_T) &\equiv \tilde{D}_1^{\perp(1)}(z, b_T), \\ \tilde{H}_1(z, b_T) &\equiv \tilde{H}_1^{(0)}(z, b_T), & \tilde{G}_{1T}(z, b_T) &\equiv \tilde{G}_{1T}^{(1)}(z, b_T), \\ && \tilde{H}_{1L}^\perp(z, b_T) &\equiv \tilde{H}_{1L}^{\perp(1)}(z, b_T),\end{aligned}\tag{2.136}$$

<sup>11</sup>When comparing Eq. (2.136) to the corresponding expression in [139], one has to account for a sign change  $b^\mu \rightarrow -b^\mu$  due to a different definition of the TMD correlator as well as  $\epsilon_T^{\alpha\beta} \rightarrow -\epsilon_T^{\alpha\beta}$  because we consider a  $n_a$ -collinear hadron.

where the derivatives are defined as

$$\begin{aligned}\tilde{D}^{(n)}(z, b_T, \mu, \zeta) &\equiv n! \left( \frac{-1}{M_h^2 b_T} \partial_{b_T} \right)^n \tilde{D}(z, b_T, \mu, \zeta) \\ &= \frac{2\pi n!}{(M_h^2)^n} \int_0^\infty dp'_T p'_T \left( \frac{p'_T}{b_T} \right)^n J_n(b_T p'_T) D(z, z p'_T, \mu, \zeta).\end{aligned}\quad (2.137)$$

## 2.7.4 Leading Gluon TMD PDFs

So far, we have only considered quark TMD PDFs and TMD FFs. One can similarly define the corresponding gluon distributions. The unsubtracted gluon TMD PDF is defined via

$$\tilde{f}_{g/p_S}^{\alpha\beta 0(u)}(x, \mathbf{b}_T, \epsilon, \tau, xP^+) = \frac{1}{xP^+} \int \frac{db^-}{2\pi} e^{-ib^-(xP^+)} \langle p(P, S) | G^{\alpha\beta}(b^\mu) \mathcal{W}_\square(b^\mu, 0) G^{\gamma\delta}(0) | p(P, S) \rangle. \quad (2.138)$$

Compared to the TMD PDF in Eq. (2.37), the quark fields have been replaced by the gluon field strength tensor  $G^{\alpha\beta} = \partial^\alpha A^\beta - \partial^\beta A^\alpha - ig[A^\alpha, A^\beta]$ . In contrast to the quark fields, which transform in the fundamental representation of the QCD gauge group,  $G^{\alpha\beta}$  transforms in the adjoint representation. To compensate for this, the Wilson line  $\mathcal{W}_\square$  in the fundamental representation has been replaced by the Wilson line  $\mathcal{W}_\square$  in the adjoint representation. It is defined as in Eqs. (2.39) and (2.43), up to taking the color matrix in Eq. (2.43) in the adjoint representation. The different mass dimension of  $G^{\alpha\beta}$  compared to  $\psi^i$  is compensated by the overall normalization factor  $1/xP^+$ .

Due to the tensor structure of the gluon field strength  $G^{\alpha\beta}$ , the gluon TMD PDF in Eq. (2.139) carries a tensor structure as well. In principle, due to the presence of two gluon field strengths, it is a rank-four tensor. However, two of the indices are fixed to be +, see Eq. (2.139), as all other choices are power suppressed, leaving only the rank-two TMD PDF  $\tilde{f}_{g/p_S}^{\alpha\beta}$ . In addition,  $\alpha$  and  $\beta$  have to be transverse indices, which is kept implicit in Eq. (2.139).

The TMD PDF is then obtained similar to Eq. (2.33) by combining the unsubtracted gluon TMD PDF with the corresponding gluon soft function,

$$\tilde{f}_{g/p_S}^{\alpha\beta}(x, \mathbf{b}_T, \mu, \zeta) = \lim_{\substack{\epsilon \rightarrow 0 \\ \tau \rightarrow 0}} Z_{uv}^i(\mu, \zeta, \epsilon) \frac{\tilde{f}_{g/p}^{\alpha\beta 0(u)}(x, \mathbf{b}_T, \epsilon, \tau, xP^+)}{\tilde{\mathcal{S}}_{n_a n_b}^0(b_T, \epsilon, \tau)} \sqrt{\tilde{\mathcal{S}}_{n_a n_b}^0(b_T, \epsilon, \tau)}. \quad (2.139)$$

In analogy to Eq. (2.40) but using adjoint Wilson lines, the gluon soft function is defined as

$$\tilde{\mathcal{S}}_{n_a n_b}^0(b_T, \epsilon, \tau) = \frac{1}{N_c^2 - 1} \langle 0 | \text{Tr}[\mathcal{W}_\gg(b_T)]_\tau | 0 \rangle. \quad (2.140)$$

Compared to the quark soft function in Eq. (2.38), we again take all Wilson lines in the adjoint instead of the fundamental representation, and have adjusted the overall normalization factor to  $N_c^2 - 1 = 8$ , the total number of independent generators of the adjoint representation. Note that here we have chosen incoming Wilson lines from  $-\infty$ . The process dependence of gluon TMD PDFs is more complicated than the quark case and has been explored in Ref. [146, 147].

		Leading Gluon TMDPDFs		
		Gluon Operator Polarization		
Nucleon Polarization	U	Un-Polarized	Helicity 0 antisymmetric	Helicity 2
	L	$f_1^g = \text{Unpolarized}$	$g_{1L}^g = \text{Helicity}$	$h_{1L}^{\perp g} = \text{Linearly Polarized}$
	T	$f_{1T}^{\perp g} = \text{Transversity}$	$g_{1T}^{\perp g} = \text{Transversity}$	$h_{1T}^g = \text{Transversity}$

Nucleon Spin → Nucleon Spin ↑↓ Gluon Operator Helicities ↑↓

Figure 2.7: Leading power gluon TMD parton distribution functions for a spin-1/2 hadron (or unpolarized hadron).

As for the quark TMD PDF, we can decompose the spin-dependent gluon TMD PDF  $f_{g/p}^{\alpha\beta}$  into independent structures. Due to the spin-1 nature of the gluon, this has a different structure than for the spin- $\frac{1}{2}$  quark. The decomposition in momentum space was first given in [148]. Here we follow the conventions of [149], with lower case  $f_X^g$ ,  $g_X^g$  and  $h_X^g$  functions, which parallels the notation used for the quark TMD PDFs, and enables us to reserve capital letters for TMD FFs. Thus we write the spin decomposition as

$$\begin{aligned}
 f_{g/p}^{\alpha\beta}(x, \mathbf{k}_T, \mu, \zeta) &= \frac{1}{2} \left[ -g_T^{\alpha\beta} f_1^g(x, k_T) + \frac{\mathbf{k}_T^2}{M^2} \left( \frac{g_T^{\alpha\beta}}{2} + \frac{k_T^\alpha k_T^\beta}{\mathbf{k}_T^2} \right) h_1^{\perp g}(x, k_T) \right] \\
 &\quad + \frac{S_L}{2} \left[ -i\epsilon_T^{\alpha\beta} g_{1L}^g(x, k_T) - \frac{k_\rho \epsilon_T^{\rho\{\alpha} k_T^{\beta\}}}{2M^2} h_{1L}^{\perp g}(x, k_T) \right] \\
 &\quad + \frac{1}{2} \left\{ g_T^{\alpha\beta} \frac{k_{T\rho} S_{T\sigma} \epsilon_T^{\rho\sigma}}{M} f_{1T}^{\perp g}(x, k_T) - i\epsilon_T^{\alpha\beta} \frac{k_T \cdot S_T}{M} g_{1T}^g(x, k_T) \right. \\
 &\quad \left. + \frac{k_{T\rho} \epsilon_T^{\rho\{\alpha} k_T^{\beta\}}}{2M^2} \frac{k_T \cdot S_T}{M} h_{1T}^{\perp g}(x, k_T) - \frac{k_{T\rho} \epsilon_T^{\rho\{\alpha} S_T^{\beta\}} + S_{T\rho} \epsilon_T^{\rho\{\alpha} k_T^{\beta\}}}{4M} h_{1T}^g(x, k_T) \right\}.
 \end{aligned} \tag{2.141}$$

Here, the notation  $a^{\{\alpha} b^{\beta\}} = a^\alpha b^\beta + a^\beta b^\alpha$  indicates symmetrization in the indices. As we have done previously, for brevity we suppress the  $\mu$  and  $\zeta$  scales and the subscript  $g/p$  on the right hand side of Eq. (2.142). The function  $f_{g/p}^{\alpha\beta}$  has two transverse indices,  $\alpha, \beta = 1, 2$ . Denoting basis vectors by  $\hat{e}_1$  and  $\hat{e}_2$ , they can be decomposed into the  $\pm 1$  gluon helicities, denoted by  $\uparrow = (\hat{e}_1 + i\hat{e}_2)/\sqrt{2}$  and  $\downarrow = (\hat{e}_1 - i\hat{e}_2)/\sqrt{2}$ . The irreducible representations are simple products of

helicities, for which it is convenient to form symmetric and antisymmetric combinations (see also Ref. [150]). This is summarized in Fig. 2.7. The symmetric helicity 0 combination  $\uparrow\downarrow + \downarrow\uparrow$  gives the unpolarized configurations that appear for unpolarized and transversely polarized hadrons, with distributions  $f_1^g$  and  $f_{1T}^{\perp g}$ . The antisymmetric helicity 0 combination  $\uparrow\downarrow - \downarrow\uparrow$  yields the helicity distributions  $g_{1L}^g$  and  $g_{1T}^{\perp g}$  for longitudinally and transversely polarized hadrons, respectively. Finally, the helicity 2 combinations  $\uparrow\uparrow + \downarrow\downarrow$  and  $\uparrow\uparrow - \downarrow\downarrow$  are given in Eq. (2.142) by the  $h_1^{\perp g}$ ,  $h_{1L}^{\perp g}$ ,  $h_{1T}^g$  and  $h_{1T}^{\perp g}$  terms for the spin-1/2 hadron polarizations indicated in Fig. 2.7. They are symmetric and traceless combinations of  $\alpha, \beta = 1, 2$ . In Fig. 2.7 the orientation of gluon helicity arrows indicates the degree to which they are correlated with the direction of the momentum  $p_T$  or hadron spin.

The corresponding expression in position space was first given in [151].<sup>12</sup> Here, we deviate from their notation to use the same conventions as in the quark case presented in Sec. 2.7.2. Namely, we define the Fourier transform and its inverse by Eqs. (2.129) and (2.130), allowing us to use the explicit expressions in appendix C. This yields

$$\begin{aligned} f_{g/p}^{\alpha\beta}(x, \mathbf{b}_T, \mu, \zeta) &= \frac{1}{2} \left[ -g_T^{\alpha\beta} \tilde{f}_1^g(x, b_T) - \frac{1}{2} b_T^2 M^2 \left( \frac{g_T^{\alpha\beta}}{2} + \frac{b_T^\alpha b_T^\beta}{\mathbf{b}_T^2} \right) \tilde{h}_1^{\perp g}(x, b_T) \right] \\ &\quad + \frac{S_L}{2} \left[ -i \epsilon_T^{\alpha\beta} \tilde{g}_{1L}^g(x, b_T) + \frac{M^2}{4} b_{T\rho} \epsilon_T^{\rho\{\alpha} b_T^{\beta\}} \tilde{h}_{1L}^{\perp g}(x, b_T) \right] \\ &\quad + \frac{1}{2} \left[ -i M g_T^{\alpha\beta} b_{T\alpha} S_{T\beta} \epsilon_T^{\alpha\beta} \tilde{f}_{1T}^{\perp g}(x, b_T) - M \epsilon_T^{\alpha\beta} b_T \cdot S_T \tilde{g}_{1T}^g(x, b_T) \right. \\ &\quad \left. + \frac{i M^3}{12} b_{T\rho} \epsilon_T^{\rho\{\alpha} b_T^{\beta\}} b_T \cdot S_T \tilde{h}_{1T}^{\perp g}(x, b_T) \right. \\ &\quad \left. + \frac{i}{4} M (b_{T\rho} \epsilon_T^{\rho\{\alpha} S_T^{\beta\}} + S_{T\rho} \epsilon_T^{\rho\{\alpha} b_T^{\beta\}}) \tilde{h}_{1T}^g(x, b_T) \right]. \end{aligned} \quad (2.142)$$

The relation between the functions in momentum and position space is given by

$$\begin{aligned} \tilde{f}_1^g(x, b_T) &\equiv \tilde{f}_1^{g(0)}(x, b_T), & \tilde{f}_{1T}^{\perp g}(x, b_T) &\equiv \tilde{f}_{1T}^{\perp g(1)}(x, b_T), & \tilde{h}_{1L}^{\perp g}(x, b_T) &\equiv \tilde{h}_{1L}^{\perp g(2)}(x, b_T), \\ \tilde{g}_{1L}^g(x, b_T) &\equiv \tilde{g}_{1L}^{g(0)}(x, b_T), & \tilde{g}_{1T}^g(x, b_T) &\equiv \tilde{g}_{1T}^{g(1)}(x, b_T), & \tilde{h}_1^{\perp g}(x, b_T) &\equiv \tilde{h}_1^{\perp g(2)}(x, b_T), \\ \tilde{h}_{1T}^g(x, b_T) &\equiv \tilde{h}_{1T}^{g(1)}(x, b_T) & \tilde{h}_{1T}^{\perp g}(x, b_T) &\equiv \tilde{h}_{1T}^{\perp g(3)}(x, b_T), \end{aligned} \quad (2.143)$$

where the  $\tilde{f}^{(n)}$  are defined in Eq. (2.129).

## 2.7.5 Leading Gluon TMD FFs

We now discuss the definition of polarized gluon TMD FFs. Similar to quark TMD FFs, the gluon TMD FF  $\Delta_{h/g}^{\mu\nu}(z, \mathbf{p}_T)$  encodes the fragmentation of a gluon produced in the underlying hard scattering into a hadron of type  $h$ , carrying the longitudinal momentum  $z$  and transverse momentum  $\mathbf{p}_T$  relative to the fragmenting gluon.

<sup>12</sup>Compared to Eq. (2.142), the expression in [151] is missing a factor 1/2 in all terms involving  $S_T$ , which we have restored. They also have a typo in their  $\tilde{h}_{1T}^{\perp g(2)}(x, b_T)$ , which should read  $\tilde{h}_{1T}^{\perp g(3)}(x, b_T)$ .

		Leading Gluon TMDFFs		
		Gluon Operator Polarization		
		Un-Polarized	Helicity 0 antisymmetric	Helicity 2
Unpolarized (or Spin 0) Hadrons		$D_1^g = \text{circle with dot}$ Unpolarized		$H_1^{\perp g} = \text{circle with dot} + \text{circle with cross}$ Linearly Polarized
Polarized Hadrons	L		$G_{1L}^g = \text{circle with dot} \rightarrow - \text{circle with cross}$ Helicity	$H_{1L}^{\perp g} = \text{circle with dot} \rightarrow + \text{circle with cross} \rightarrow$
	T	$D_{1T}^{\perp g} = \text{circle with dot} \uparrow - \text{circle with dot} \downarrow$	$G_{1T}^{\perp g} = \text{circle with dot} \uparrow \rightarrow - \text{circle with cross} \uparrow$	$H_{1T}^g = \text{circle with dot} \uparrow + \text{circle with cross} \uparrow$ Transversity $H_{1T}^{\perp g} = \text{circle with dot} \uparrow + \text{circle with cross} \uparrow$

Figure 2.8: Leading power gluon TMD fragmentation functions for an unpolarized or spin-0 hadron or a polarized spin-1/2 hadron.

To contrast TMD FFs and TMD PDFs, we first recall the definition of the spin-dependent unsubtracted TMD PDF in Eq. (2.139),

$$\tilde{f}_{g/h}^{\alpha\beta 0(u)}(x, \mathbf{b}_T, \epsilon, \tau, xP^+) = \frac{1}{xP^+} \int \frac{db^-}{2\pi} e^{-ib^-(xP^+)} \langle h(P, S) | G^{+\alpha}(b^\mu) \mathcal{W}_\square(b^\mu, 0) G^{+\beta}(0) | h(P, S) \rangle. \quad (2.144)$$

Here, the incoming proton is aligned along the  $n_a$  direction,  $b^\mu = (0, b^-, \mathbf{b}_T)$ , and  $\alpha$  and  $\beta$  are transverse indices. The corresponding unsubtracted TMD FF is defined as

$$\begin{aligned} \tilde{\Delta}_{h/g}^{\alpha\beta 0(u)}(z, \mathbf{b}_T, \epsilon, \tau, zP^+) &= \frac{1}{z} \frac{1}{zP^+} \int \frac{db^-}{2\pi} \sum_X e^{ib^-(zP^+)} \langle 0 | G^{+\alpha}(b) \mathcal{W}_\perp(b) | h(P, S), X \rangle \\ &\quad \times \langle h(P, S), X | G^{+\beta}(0) \mathcal{W}_\perp(0) | 0 \rangle. \end{aligned} \quad (2.145)$$

As for the quark TMD FF, the matrix element is normalized by an additional factor of  $1/z$  and  $1/2$ , the latter accounting for the gluon spin states. The hadron  $h$  appears as an out-state in the matrix element, with  $\sum_X$  denoting the sum over all additional hadronic final states  $X$ , which in contrast to the TMD PDF can not be eliminated by unitarity. In Eq. (2.146), the Wilson lines  $\mathcal{W}_\perp$  and  $\mathcal{W}_\square$  are defined as in Eq. (2.110), up to replacing the fundamental Wilson lines  $W_n$  by Wilson lines  $\mathcal{W}_n$  in the adjoint representation.

The gluon TMD FF is obtained by combining Eq. (2.146) with the soft function and UV renormalization as in Eq. (2.140). In momentum space, the TMD FF can be decomposed

analogously to Eq. (2.142) as

$$\begin{aligned} \Delta_{h/g}^{\alpha\beta}(z, -z\mathbf{p}'_T, \mu, \zeta) = & \frac{1}{2} \left[ -g_T^{\alpha\beta} D_1^g(z, zp'_T) + \frac{\mathbf{p}'_T^2}{M^2} \left( \frac{g_T^{\alpha\beta}}{2} + \frac{p'_T{}^\alpha p'_T{}^\beta}{\mathbf{p}'_T^2} \right) H_1^{\perp g}(z, zp'_T) \right] \\ & + \frac{S_L}{2} \left[ -i\epsilon_T^{\alpha\beta} G_{1L}^g(z, zp'_T) - \frac{p'_T{}^\rho \epsilon_T^{\rho\{\alpha} p'_T{}^{\beta\}}}{2M^2} H_{1L}^{\perp g}(z, zp'_T) \right] \\ & + \frac{1}{2} \left\{ g_T^{\alpha\beta} \frac{p'_T{}^\rho S_{T\sigma} \epsilon_T^{\rho\sigma}}{M} D_{1T}^{\perp g}(z, zp'_T) - i\epsilon_T^{\alpha\beta} \frac{p'_T \cdot S_T}{M} G_{1T}^g(z, zp'_T) \right. \\ & \left. + \frac{p'_T{}^\rho \epsilon_T^{\rho\{\alpha} p'_T{}^{\beta\}}}{2M^2} \frac{p'_T \cdot S_T}{M} H_{1T}^{\perp g}(z, zp'_T) - \frac{p'_T{}^\rho \epsilon_T^{\rho\{\alpha} S_T^{\beta\}} + S_{T\rho} \epsilon_T^{\rho\{\alpha} p'_T{}^{\beta\}}}{4M} H_{1T}^g(z, zp'_T) \right\}. \end{aligned} \quad (2.146)$$

As in Eq. (2.142), the notation  $a^{\{\alpha} b^{\beta\}} = a^\alpha b^\beta + a^\beta b^\alpha$  indicates symmetrization in the indices, and on the right hand side we suppress explicit  $\mu$  and  $\zeta$  scales and the subscript  $g/h$ . The relation of the different structures to the gluon and hadron spin is summarized in Fig. 2.8.

Taking the Fourier transform of Eq. (2.147), we obtain the decomposition in position space,

$$\begin{aligned} \tilde{\Delta}_{h/g}^{\alpha\beta}(z, \mathbf{b}_T, \mu, \zeta) = & \frac{1}{2} \left[ -g_T^{\alpha\beta} \tilde{D}_1^g(z, b_T) - \frac{1}{2} b_T^2 M^2 \left( \frac{g_T^{\alpha\beta}}{2} + \frac{b_T^\alpha b_T^\beta}{\mathbf{b}_T^2} \right) \tilde{H}_1^{\perp g}(z, b_T) \right] \\ & + \frac{S_L}{2} \left[ -i\epsilon_T^{\alpha\beta} \tilde{G}_{1L}^g(z, b_T) + \frac{M^2}{4} b_{T\rho} \epsilon_T^{\rho\{\alpha} b_T^{\beta\}} \tilde{H}_{1L}^{\perp g}(z, b_T) \right] \\ & + \frac{1}{2} \left[ -iM g_T^{\alpha\beta} b_{T\alpha} S_{T\beta} \epsilon_T^{\alpha\beta} \tilde{F}_{1T}^{\perp g}(z, b_T) - M \epsilon_T^{\alpha\beta} b_T \cdot S_T \tilde{G}_{1T}^g(z, b_T) \right. \\ & \left. + \frac{iM^3}{12} b_{T\rho} \epsilon_T^{\rho\{\alpha} b_T^{\beta\}} b_T \cdot S_T \tilde{H}_{1T}^{\perp g}(z, b_T) \right. \\ & \left. + \frac{i}{4} M \left( b_{T\rho} \epsilon_T^{\rho\{\alpha} S_T^{\beta\}} + S_{T\rho} \epsilon_T^{\rho\{\alpha} b_T^{\beta\}} \right) \tilde{H}_{1T}^g(z, b_T) \right]. \end{aligned} \quad (2.147)$$

The relation between the functions in momentum and position space is given by

$$\begin{aligned} \tilde{D}_1^g(z, b_T) &\equiv \tilde{D}_1^{g(0)}(z, b_T), & \tilde{D}_{1T}^{\perp g}(z, b_T) &\equiv \tilde{D}_{1T}^{\perp g(1)}(z, b_T), & \tilde{H}_{1L}^{\perp g}(z, b_T) &\equiv \tilde{H}_{1L}^{\perp g(2)}(z, b_T), \\ \tilde{G}_{1L}^g(z, b_T) &\equiv \tilde{G}_{1L}^{g(0)}(z, b_T), & \tilde{G}_{1T}^g(z, b_T) &\equiv \tilde{G}_{1T}^{g(1)}(z, b_T), & \tilde{H}_1^{\perp g}(z, b_T) &\equiv \tilde{H}_1^{\perp g(2)}(z, b_T), \\ \tilde{H}_{1T}^g(z, b_T) &\equiv \tilde{H}_{1T}^{g(1)}(z, b_T) & & & \tilde{H}_{1T}^{\perp g}(z, b_T) &\equiv \tilde{H}_{1T}^{\perp g(3)}(z, b_T), \end{aligned} \quad (2.148)$$

where the  $f^{(n)}$  are defined in Eq. (2.138).

## 2.8 TMD PDFs and TMD FFs at small $b_T$

Much of the focus of our discussion is on the case where  $q_T$ , or equivalently  $b_T$ , are non-perturbative scales, i.e.  $q_T \sim b_T^{-1} \sim \Lambda_{\text{QCD}}$ , where TMD PDFs and TMD FFs are genuinely non-perturbative objects encoding nonperturbative transverse-momentum distributions of quarks and gluons inside hadrons. However, it turns out that contributions from perturbative scales

$q_T \sim b_T^{-1} \gg \Lambda_{\text{QCD}}$  also often play an important role in predictions for colliders. Hence, in this section we investigate this regime where the dependence on transverse variables can be computed perturbatively in QCD. In general, we will need to smoothly connect the non-perturbative and perturbative regimes to make phenomenological predictions.

For the perturbative regime,  $q_T \sim b_T^{-1} \gg \Lambda_{\text{QCD}}$ , one can relate the unpolarized TMD PDFs to collinear PDFs through a type of operator expansion [63, 119],

$$\tilde{f}_{1i}(x, b_T, \mu, \zeta) = \sum_j \int_x^1 \frac{dy}{y} \tilde{C}_{ij}\left(\frac{x}{y}, b_T, \mu, \zeta\right) f_j(y, \mu) + O(b_T^2 \Lambda_{\text{QCD}}^2). \quad (2.149)$$

In Eq. (2.150), the sum runs over all parton flavors  $j$ , and the  $\tilde{C}_{ij}$  are perturbative matching kernels, such that the only nonperturbative input on the right hand side of Eq. (2.150) is given by the collinear PDF  $f_j(y, \mu)$ . As indicated, this equation holds up to corrections in  $b_T^2 \Lambda_{\text{QCD}}^2$ . Taking the Fourier transform yields an equivalent result in transverse momentum space,

$$f_{1i}(x, k_T, \mu, \zeta) = \sum_j \int_x^1 \frac{dy}{y} C_{ij}\left(\frac{x}{y}, k_T, \mu, \zeta\right) f_j(y, \mu) \times \left[1 + O(\Lambda_{\text{QCD}}^2/k_T^2)\right]. \quad (2.150)$$

Relations similar to Eqs. (2.150) and (2.151) also hold for the other polarized TMD PDFs and for the TMD FFs, which can be related to polarized collinear PDFs and FFs, as discussed below.

Eq. (2.151) can be understood by noting that for perturbative  $q_T$ , both Eqs. (2.5) and (2.6) are valid descriptions of the Drell-Yan process, where Eq. (2.5) should be used when  $q_T \sim Q$  and Eq. (2.6) should be used when  $q_T \ll Q$ . In a strict perturbative expansion of the cross section in terms of the strong coupling constant  $\alpha_s$ , Eqs. (2.5) and (2.6) yield identical results when expanded for small  $q_T \ll Q$ . This can be used to calculate the perturbative matching kernels  $C_{ij}$ , and Refs. [68, 152] used this approach to obtain these kernels at NNLO.

Alternatively, one can calculate the matching kernels  $\tilde{C}_{ij}$  directly from the matrix element definitions in Eqs. (2.37) and (2.38). In this approach, one replaces the proton state in Eq. (2.37) with a quark state  $\psi_j$  of flavor  $j$  or a gluon state  $j = g$ . Since the soft function is defined as a vacuum matrix element without hadronic states, it can be straightforwardly calculated perturbatively from Eq. (2.38). The construction of the TMD PDFs for parton  $i$  is then either achieved by combining the bare unsubtracted TMD PDF and bare soft function, as in Eq. (2.33), or by combining renormalized beam and soft functions as in Eq. (2.36). As explained in Sec. 2.4, the bare perturbative results require the use of a dedicated rapidity regulator  $\tau$ , which cancels upon combining the bare unsubtracted TMD PDF and bare soft function in Eq. (2.33). Likewise, the individual renormalized beam and soft functions depend on a rapidity renormalization scale  $\nu$ , which cancels out when these functions are combined in Eq. (2.36) to obtain the renormalized TMD PDF. Finally we subtract the perturbative results for the longitudinal PDF  $f_{j/P}(y, \mu)$  itself, thus obtaining the desired kernels  $\tilde{C}_{ij}$  and  $\tilde{C}_{ig}$ . This calculation was explicitly illustrated at one loop for the quark TMD PDF using the  $\eta$  regulator in Sec. 2.4.2.

This strategy was employed in [83, 89] using Wilson lines off the lightcone at NLO. NNLO results were first obtained in [153] using the analytic regulator, and later also in [115, 116] and [154] using the  $\delta$  and  $\eta$  regulator, respectively. Recently, N<sup>3</sup>LO results were independently

obtained by two groups in [155–158] employing the exponential regulator. The calculations in [157] were based on a hybrid approach, where the full QCD cross section was expanded in the collinear limit, which was then combined with the exponential regulator to obtain the TMD PDFs. We remark that calculations based on the exponential or  $\eta$  regulator are often used to separately calculate renormalized beam and soft functions.

For illustration, we show how to obtain the perturbative matching of the quark TMD PDF onto the quark PDF, omitting contributions from matching onto the gluon TMD PDF. The required perturbative result for the TMD PDF was calculated in Sec. 2.4.2, with the final result given in Eq. (2.82). The corresponding perturbative result for the collinear quark PDF is given by

$$f_{q/q}(x, \mu) = \delta(1 - x) - \frac{\alpha_s(\mu) C_F}{2\pi} \frac{1}{\epsilon} [P_{qq}(x)]_+ + O(\alpha_s^2), \quad (2.151)$$

where the displayed  $1/\epsilon$  pole is of infrared (collinear) origin. Comparing Eq. (2.152) to Eq. (2.82), one sees that this term exactly cancels between the perturbative results for the TMD PDF and PDF. The remaining terms then yield the matching kernel

$$\begin{aligned} \tilde{C}_{qq}(x, b_T, \mu, \zeta) &= \delta(1 - x) + \frac{\alpha_s(\mu) C_F}{2\pi} \left\{ -L_b [P_{qq}(x)]_+ + (1 - x) \right. \\ &\quad \left. + \delta(1 - x) \left[ -\frac{1}{2} L_b^2 + L_b \left( \frac{3}{2} + \ln \frac{\mu^2}{\zeta} \right) - \frac{\pi^2}{12} \right] \right\} + O(\alpha_s^2), \end{aligned} \quad (2.152)$$

where  $L_b$  and  $P_{qq}(x)$  are given in Eqs. (2.72) and (2.73), respectively. As discussed in Sec. 2.3 and appendix D, the final results for definitions of the TMD PDF agree across many choices of the rapidity regulators that are used at intermediate steps, and hence Eq. (2.153) holds for all rapidity regulators discussed in Sec. 2.4.1. A different result for  $\tilde{C}_{qq}$  is obtained if one uses one of the TMD PDF definitions discussed in Sec. 2.5, since these TMD PDFs and the corresponding  $\tilde{C}_{qq}$  depend on the different parameter  $\zeta$  and an extra parameter  $\rho$ .

**Matching of spin-dependent TMD PDFs and TMD FFs.** In a similar fashion, one can match all spin-dependent quark and gluon TMDs onto their collinear counterparts for perturbative  $q_T \sim b_T^{-1} \gg \Lambda_{\text{QCD}}$ . For example, the quark helicity distribution  $g_1(x, b_T, \mu, \zeta)$  can be matched onto the collinear helicity distribution  $g_1(x, \mu)$ , instead of the collinear PDF  $f_1(x, \mu)$ . The collinear distributions that a TMD PDF matches onto are classified by so-called twist, related to the twist of operators defining the collinear distribution. In particular, the non-local operator defining the collinear distributions can be expanded in terms of a tower of local operators, for example for a pair of quarks of flavor  $i$

$$P_{S,N}^{\mu_0 \mu_1 \cdots \mu_N} \bar{\psi}_i^0 \Gamma_{\mu_0} iD_{\mu_1} \cdots iD_{\mu_N} \psi_i^0, \quad (2.153)$$

where we have an infinite set of local operators indexed by  $N$ , and  $P_{S,N}$  is a dimensionless projector onto the spin- $S$  combination of the Lorentz indices  $\mu_0 \cdots \mu_N$ . The operator in Eq. (2.154) has dimension  $D = 3 + N$ , and twist  $t = D - S$ . Typically, the contributions from longitudinal distributions are suppressed with increasing twist, such that one only needs to consider the lowest values of twist. For example, the longitudinal PDF  $f_1(x, \mu)$  is twist 2,

which is thus also referred to as leading twist. Other twist 2 longitudinal PDFs include the helicity  $g_1(x)$  and transversity  $h_1(x)$ . For small  $b_T$ , some TMD distributions do not match onto twist 2 distributions, but obtain their first contribution at twist 3, where the so-called Qiu-Sterman function [159]  $T(x_1, x_2, x_3)$  plays the role of the unpolarized twist-2 PDF, and also has a chiral-odd counterpart  $\delta T_\epsilon(x_1, x_2, x_3)$ . See for example [160] for a discussion of twist-3 PDFs.

In tables 2.3 and 2.4, we summarize the knowledge, at the time of this writing, of these matching relations for quark TMD PDFs and gluon TMD PDFs. For each TMD distribution function, the table shows which collinear distributions that they match onto (up to twist 3), the perturbative order to which the matching is known, and a list of references for these matching calculations. Care has to be taken when using these results due to a variety of different conventions used in the literature, including whether results are expressed in momentum or position space, how the different distributions are normalized (cf. Eq. (2.127) for the convention used here), and the precise definition of the  $\overline{\text{MS}}$  scheme.

The unpolarized TMD PDFs have the simplest structure, and their matching is already known at  $N^3\text{LO}$  [156–158, 161]. Much less is known for the other TMDs, in particular those matching onto subleading-twist PDFs. For the quark TMD PDF, recently a comprehensive calculation of the twist-3 matching at LO was presented in [162].

For TMD FFs the situation is more complicated, as a similar relation between TMD FFs and collinear FFs by means of an operator product expansion (OPE) can not be established in the same way, see e.g. [162, 163] for a detailed discussion. However, at a perturbative level, one can relate the two objects by demanding that the cross sections calculated within TMD and collinear factorization are consistent. This has been used to obtain a matching of the unpolarized TMD FF onto the collinear FF up to  $N^3\text{LO}$  [114, 116, 158, 161, 164]. There is also an interesting relation between TMD PDFs and TMD FFs through analytic continuation [165], which so far has only been employed for the unpolarized TMDs [158].

Name	Function	Twist-2 matching	Twist-3 matching	Known order	Refs.
unpolarized	$\tilde{f}_1(x, b_T)$	$f_1(x)$	–	$N^3LO(\alpha_s^3)$	[68, 83, 89, 153] [116, 154, 156–158, 164]
helicity	$\tilde{g}_1(x, b_T)$	$g_1(x)$	$\mathcal{T}_g(x)$	$NLO(\alpha_s^1)$	[144, 166]
worm-gear $T$	$\tilde{g}_{1T}^\perp(x, b_T)$	$g_1(x)$	$\mathcal{T}_g(x)$	$LO(\alpha_s^0)$	[143, 167]
Sivers	$\tilde{f}_{1T}^\perp(x, b_T)$	–	$T(-x, 0, x)$	$NLO(\alpha_s^1)$	[72, 168–174]
transversity	$\tilde{h}_1(x, b_T)$	$h_1(x)$	$\mathcal{T}_h(x)$	$NNLO(\alpha_s^2)$	[144, 166, 175]
worm-gear $L$	$\tilde{h}_{1L}^\perp(x, b_T)$	$h_1(x)$	$\mathcal{T}_h(x)$	$LO(\alpha_s^0)$	[143, 167]
Boer-Mulders	$\tilde{h}_1^\perp(x, b_T)$	–	$\delta T_\epsilon(-x, 0, x)$	$NLO(\alpha_s^0)$	[143]
pretzelosity	$\tilde{h}_{1T}^\perp(x, b_T)$	–	$\mathcal{T}_h(x)$	$LO(\alpha_s^0)$	[162]

Table 2.3: Collinear matching of the quark TMD PDFs up to collinear twist 3 at perturbative  $b_T^{-1} \gg \Lambda_{\text{QCD}}$ . For brevity, the renormalization scale  $\mu$  and the Collins-Soper scale  $\zeta$  are suppressed. The upper four rows of the table show chiral-even TMDs, while the bottom four rows show chiral-odd TMDs.  $\mathcal{T}_g(x)$  and  $\mathcal{T}_h(x)$  are abbreviations for specific combinations of the twist-3 distributions. Table adapted from Ref. [162], to which we refer for further details.

Name	Function	Twist-2 matching	Twist-3 matching	Known order	Refs.
unpolarized	$\tilde{f}_1(x, b_T)$	$f_1(x)$	–	$N^3LO(\alpha_s^3)$	[116, 152–154] [157, 158, 176]
linearly polarized	$\tilde{h}_1^{\perp g}(x, b_T)$	$f_1(x)$	–	$NNLO(\alpha_s^2)$	[98, 102, 152] [144, 151, 176, 177]
helicity	$\tilde{g}_{1L}^g(x, b_T)$	$g_1(x)$		$NLO(\alpha_s^1)$	[151]
	$\tilde{g}_{1T}^g(x, b_T)$				
Sivers	$\tilde{f}_{1T}^{\perp g}(x, b_T)$	–			
	$\tilde{h}_{1T}^g(x, b_T)$				
	$\tilde{h}_{1L}^{\perp g}(x, b_T)$				
	$\tilde{h}_{1T}^{\perp g}(x, b_T)$				

Table 2.4: Collinear matching of the gluon TMD PDFs up to collinear twist 3 at perturbative  $b_T^{-1} \gg \Lambda_{\text{QCD}}$ . For brevity, the renormalization scale  $\mu$  and the Collins-Soper scale  $\zeta$  are suppressed. The upper four rows of the table show chiral-even TMDs, while the bottom four rows show chiral-odd TMDs. Empty entries indicate that for most gluon TMDs the matching has not yet been considered in the literature, and these rows presumably obtain their first contributions at twist 3.

## 2.9 Relating Integrated TMDs to Collinear Functions

An interesting question to ask about TMD PDFs is how they relate to longitudinal PDFs. Naively they might be thought of as simply more differential TMDs that yield the longitudinal PDFs upon integration. One might thus expect that

$$\int d^2\mathbf{k}_T f_{i/H}^{0(u)}(x, \mathbf{k}_T) \stackrel{?}{=} f_{i/H}^0(x). \quad (2.154)$$

Indeed, it is easy to see that this expectation is fulfilled at the *bare* level,

$$\begin{aligned} \int d^2\mathbf{k}_T f_{i/H}^{0(u)}(x, \mathbf{k}_T, \epsilon, \tau, xP^+) &= \int d^2\mathbf{k}_T \int \frac{d^2\mathbf{b}_T}{(2\pi)^2} e^{i\mathbf{b}_T \cdot \mathbf{k}_T} \tilde{f}_{i/H}(x, \mathbf{b}_T) \\ &= \tilde{f}_{i/H}^{0(u)}(x, \mathbf{b}_T = \mathbf{0}, \epsilon, \tau, xP^+) \\ &= f_{i/H}^0(x, \epsilon). \end{aligned} \quad (2.155)$$

In the first step, we inserted the definition of the Fourier transform in Eq. (2.7), and then used the standard identity  $\int d^2\mathbf{k}_T e^{i\mathbf{b}_T \cdot \mathbf{k}_T} = (2\pi)^2 \delta(\mathbf{b}_T)$  to evaluate the bare TMD PDF at  $\mathbf{b}_T = \mathbf{0}$ . With this choice, the Wilson lines in Eq. (2.37) can be simplified using  $W_n(a, b)W_n^\dagger(b, a) = 1$ , such that the staple-shaped Wilson line  $W_\square$  in Eq. (2.39) reduces to the straight Wilson line encountered in the definition of the PDF in Eq. (2.17). Similarly, one can show that the bare TMD soft function defined in Eq. (2.38) reduces to unity when integrated over all  $\mathbf{k}_T$ ,

$$\int d^2\mathbf{k}_T S_{n_a n_b}^0(k_T, \epsilon, \tau) = \tilde{S}_{n_a n_b}^0(\mathbf{b}_T = \mathbf{0}, \epsilon, \tau) = 1. \quad (2.156)$$

Thus, at the bare level both unsubtracted and subtracted TMD PDF recover the longitudinal PDF when integrated over all  $\mathbf{k}_T$ .<sup>13</sup>

However, after renormalization the naive expectation of Eq. (2.155) is broken, i.e.

$$\int d^2\mathbf{k}_T f_{i/p}(x, \mathbf{k}_T, \mu, \zeta) \neq f_i(x, \mu). \quad (2.157)$$

This is easy to see from the scale dependence on the two sides of Eq. (2.158). Evolution equations for the TMDs are discussed in detail in Sec. 4. We have

$$\begin{aligned} \mu \frac{d}{d\mu} f_{i/p}(x, \mathbf{k}_T, \mu, \zeta) &= \gamma_\mu^i(\mu, \zeta) f_{i/p}(x, \mathbf{k}_T, \mu, \zeta), \\ \mu \frac{d}{d\mu} f_i(x, \mu) &= \sum_j \int_x^1 \frac{dx'}{x'} P_{ij}(x', \mu) f_j\left(\frac{x}{x'}, \mu\right). \end{aligned} \quad (2.158)$$

Importantly, the  $\mu$  evolution of the TMD PDF is diagonal both in flavor  $i$  and momentum fraction  $x$ , while for the PDF it sums over all flavors  $j$  and involves a convolution in  $x$ . Even

<sup>13</sup>Note that there are many more spin-dependent TMD PDFs than longitudinal PDFs. However, most of these are proportional to  $\mathbf{b}_T$ , see e.g. Eq. (2.127) and thus vanish exactly at the bare level for  $\mathbf{b}_T = \mathbf{0}$ . Thus, only the unpolarized ( $f_1$ ), helicity ( $g_1$ ) and transversity ( $h_1$ ) distributions remain, for which there are corresponding longitudinal PDFs.

more strikingly, only the TMD PDF depends on the CS scale  $\zeta$ , while the PDF is independent of it. Clearly, these observations forbid a simple relation between TMD PDF and PDF at the renormalized level, and thus break Eq. (2.155).

It is then natural to ask why Eq. (2.155) holds at the bare level, but not at the renormalized level, see e.g. Refs. [74, 89, 99]. The fundamental reason is that the limit  $b_T \rightarrow 0$  that is the source of the simple relation in Eq. (2.156) corresponds to large momenta  $k_T \sim 1/b_T \rightarrow \infty$ , and thus an ultraviolet region. When defining the renormalized TMDs, this ultraviolet region has been regulated by a UV regulator, and UV divergences are removed yielding results in the  $\overline{\text{MS}}$  scheme. The act of renormalization, taking  $\epsilon \rightarrow 0$  and absorbing UV divergences into counterterms, does not commute with taking the limit  $b_T \rightarrow 0$ .

This fact was nicely illustrated in Ref. [99], where the integral in Eq. (2.155) was carried out using perturbative one-loop results, similar to those presented in Sec. 2.4.2. In this case, one actually has to perform the  $\mathbf{k}_T$  integral in  $d - 2 = 2 - 2\epsilon$  dimensions, cf. Eq. (2.65). Only then does one find that all perturbative corrections to the TMD PDF vanish up to terms identical to the longitudinal distribution, thereby confirming Eq. (2.156) at the one-loop order.

Since the above argument is based on integrating the TMD PDF into the UV region  $k_T \rightarrow \infty$ , one can also ask what happens if one limits the integral in Eq. (2.155) to some large but finite value,  $|\mathbf{k}_T| \leq k_T^{\text{cut}} \gg \Lambda_{\text{QCD}}$ . Intuitively this should avoid some of the issues with the UV region, and one can hope to at least find a good *approximation* of the form

$$\int_{k_T \leq k_T^{\text{cut}}} d^2\mathbf{k}_T f_{i/p}(x, \mathbf{k}_T, \mu, \zeta) \stackrel{?}{\approx} f_i(x, \mu). \quad (2.159)$$

Technically, the integral in Eq. (2.160) is sensitive to both nonperturbative  $k_T \sim \Lambda_{\text{QCD}}$  and to perturbative  $k_T \sim k_T^{\text{cut}}$ . The nonperturbative region is expected to have little impact for large  $k_T^{\text{cut}}$ , which can be tested numerically by suitable models. In contrast, the perturbative region is calculable in terms of longitudinal PDFs, as explained in Sec. 2.8. This makes Eq. (2.160) a reasonable guess, and studies of this relation have been performed for example in Refs. [166, 178, 179].

The formalism for carrying out such an analysis was taken a step further in Ref. [180] by developing a method to carry out the  $k_T \leq k_T^{\text{cut}}$  integration in Eq. (2.160) in a model-independent way by using a position space cutoff  $b_T \leq b_T^{\text{cut}}$ . This provides control over the required approximations since the long-distance contributions from  $b_T \sim 1/\Lambda_{\text{QCD}}$  are organized into a systematic expansion in  $1/(b_T^{\text{cut}} k_T^{\text{cut}}) \ll 1$  by inducing higher-order surface terms at the cutoff. This approach yields a method for evaluating the integral of renormalized TMD functions where all sources of uncertainty can be determined. These sources include perturbative uncertainty from missing higher order terms in the  $\alpha_s$  expansion at small  $b_T$ , non-perturbative TMD effects that appear as coefficients in a  $(b_T^{\text{cut}} \Lambda_{\text{QCD}})^2$  expansion, and the overall impact of the precise choice for the cutoffs  $k_T^{\text{cut}}$  and  $b_T^{\text{cut}}$ . To test this setup, one can examine unpolarized TMDs and use the state-of-the-art OPE result with Eq. (2.150) evaluated at three-loop logarithmic accuracy [180]. (These orders of renormalization group improved perturbation theory are explained in Chapter 4.) In Fig. 2.9, Eq. (2.160) is tested by plotting the relative deviation between the cumulative integral over  $k_T \leq k_T^{\text{cut}}$  and the longitudinal PDF. The plot uses a  $d$ -quark with fixed  $x = 0.01$  and  $k_T^{\text{cut}} = 10$  GeV, and then varies the renormalization scale  $\mu$  and Collins-Soper scale  $\zeta$ . Astonishingly, one finds that even in the

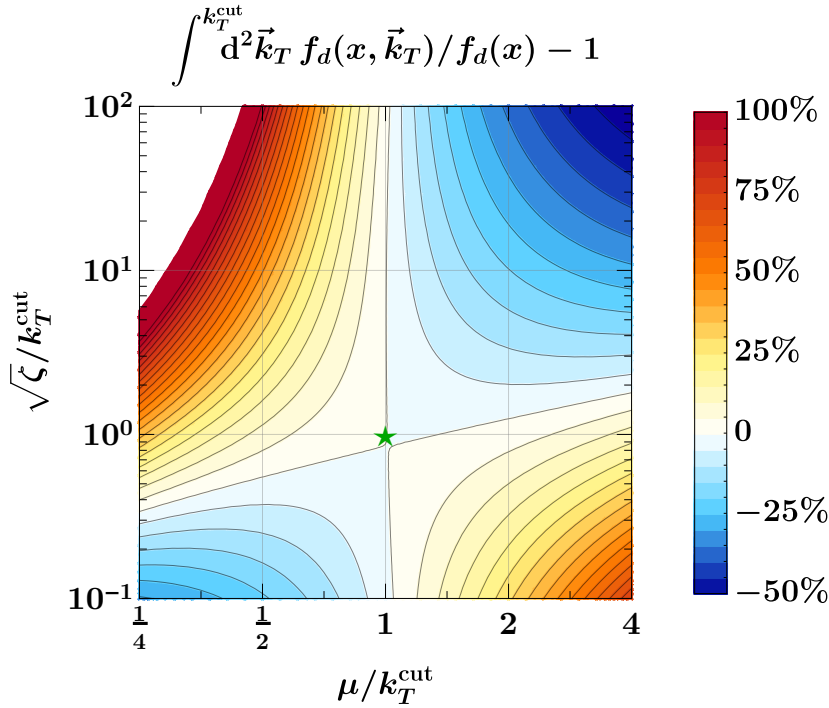


Figure 2.9: Comparison of the cumulative integral of the TMD PDF over  $k_T \leq k_T^{\text{cut}}$  to the longitudinal PDF for the  $d$ -quark with  $x = 0.01$  and  $k_T^{\text{cut}} = 10 \text{ GeV}$  as a function of both  $\mu$  and  $\zeta$ . The star denote the special point  $\mu = \sqrt{\zeta} = k_T^{\text{cut}}$ . The contours increase in steps of 5%, such that the innermost shaded regions indicate deviations of  $\pm 5\%$ . Taken from Ref.[180].

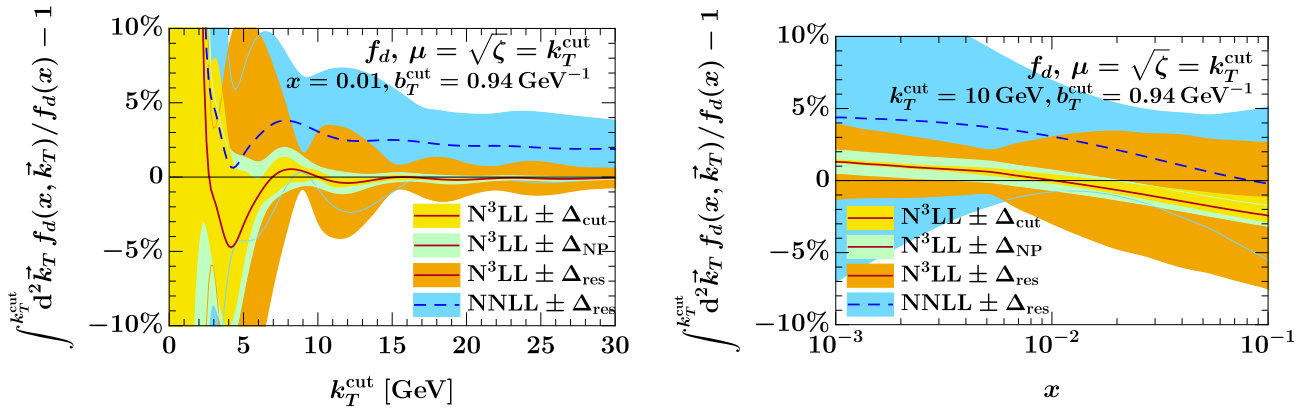


Figure 2.10: Comparison of the cumulative integral of the TMD PDF over  $k_T \leq k_T^{\text{cut}}$  to the longitudinal PDF for the  $d$ -quark as a function of  $k_T^{\text{cut}}$  (left) and  $x$  (right). Taken from Ref.[180].

presence of perturbative corrections and renormalization group running the TMD PDF and PDF agree extremely well; for the natural choice for the two renormalization scale parameters

$\mu = \sqrt{\zeta} = k_T^{\text{cut}}$  the agreement is at the percent level. Thus we can conclude that

$$\int_{k_T \leq k_T^{\text{cut}}} d^2\mathbf{k}_T f_{i/p}(x, \mathbf{k}_T, \mu = k_T^{\text{cut}}, \sqrt{\zeta} = k_T^{\text{cut}}) \simeq f_i(x, \mu = k_T^{\text{cut}}). \quad (2.160)$$

This gives justification to the original physical picture underlying Eq. (2.160). The contour bands in Fig. 2.9 also illustrate that the dependence on variations of either  $\zeta$  or  $\mu$  around  $k_T^{\text{cut}}$  is quite moderate, while there is a rather large effect of varying both scales simultaneously. As explained in Chapter 4, a simultaneous variation, such as along the diagonal directions, induces large double logarithms predicted by the hard evolution, which can not be compensated by evolution of the collinear PDF.

To verify that the above observation is not an accidental feature of the values  $x = 0.01$  and  $k_T^{\text{cut}} = 10 \text{ GeV}$  used so far, in Fig. 2.10 results for the comparison as a function of  $k_T^{\text{cut}}$  (left figure) and  $x$  (right figure) are given. Here the various sources of uncertainty are also assessed, as indicated by the different colored bands. The yellow band shows very small uncertainties from terms beyond third order in the  $1/(b_T^{\text{cut}} k_T^{\text{cut}})$  expansion, which are assessed by varying the choice of  $b_T^{\text{cut}}$  used in the analysis. The green band shows the quite small uncertainties from treating the leading  $\mathcal{O}(b_T^{\text{cut}} \Lambda_{\text{QCD}}^2)$  nonperturbative corrections as unknowns, and varying them in the analysis. Finally, the largest uncertainties are from the truncation of perturbation theory, which can be observed to decrease fairly significantly when going from second order (blue band at NNLL) to third order (orange band at N<sup>3</sup>LL). Overall, for all  $x$  values and for  $k_T^{\text{cut}} \geq 10 \text{ GeV}$  one sees that Eq. (2.161) is satisfied as an equality within the uncertainties. Furthermore, these uncertainties are only  $\mathcal{O}(5\%)$  for a large range of  $x$  and  $k_T^{\text{cut}}$  values. For the small  $k_T^{\text{cut}}$  region it is not surprising that the relation in Eq. (2.161) breaks down since the result becomes sensitive to the non-perturbative nature of the  $k_T$  distribution. To conclude, we observe that Eq. (2.161) holds to an excellent approximation over a large range of  $x$  and  $k_T^{\text{cut}}$ , and thus can be understood as a practical version of the naive expectation in Eq. (2.155).

While this method was discussed here only in the context of the unpolarized TMD, the strategy is completely general and thus also applies to spin-dependent TMDs. For example, Ref. [166] already studied the  $k_T^{\text{cut}}$  dependence of the helicity and transversity distributions at one loop. For those TMDs that vanish at bare level, i.e. at  $b_T = 0$ , the method provides a way to test model-independently how fast they vanish as a function of  $k_T^{\text{cut}}$ . This approach therefore holds potential for determining the extent to which bare relations, like the TMD positivity constraints discussed in Sec. 7.8.1, can be extended to formulas for renormalized distributions in QCD. It should also enable more rigorous treatment of the Burkardt and Schäfer-Teryaev sum rules discussed in Secs. 7.8.2 and 7.8.3, including assessing the precise conditions under which they are valid and the size of power corrections to these results.

## 2.10 Connection to Lattice QCD

Lattice QCD is the only currently available method to obtain nonperturbative hadron structure information from the underlying field theory, QCD, without uncontrolled model assumptions. It is therefore important to develop methods for calculating TMD observables within Lattice QCD.

Since the Euclidean space-time signature employed in Lattice QCD does not straightforwardly accommodate real-time separations, the TMDs defined using light-like Wilson-line

operators are not directly calculable on the Euclidean lattice. One method to circumvent this problem is to use space-like Wilson lines in the definition of the TMD correlators in Eq. (2.87) and exploit Lorentz covariance to relate their matrix elements to equal-time ones on the lattice [27, 140–142, 181, 182]. Since this method does not apply to the soft factor, most often ratios of matrix elements are considered where the soft factors drop out. Another method that has led to much progress in the lattice calculation of collinear PDFs is the large-momentum effective theory (LaMET) [28–30], extensions of which to TMDs have been constructed over the past few years [104, 183–191].

### 2.10.1 Lorentz-invariant approach

For use in lattice calculations, the correlator from which the unsubtracted TMD PDFs are obtained after Fourier transformation is generalized in several ways,

$$\tilde{\Phi}_i^{[\Gamma]}(b, P', P, S, v, \eta, a) = \frac{1}{2} \langle p(P', S) | \bar{\psi}_i^0(b^\mu/2) \Gamma W_{\square\eta}^v(b^\mu/2, -b^\mu/2) \psi_i^0(-b^\mu/2) | p(P, S) \rangle. \quad (2.161)$$

On the lattice, the UV regulator (previously denoted by  $\epsilon$ ) is realized by the lattice spacing  $a$ . Since in a concrete lattice calculation the Wilson lines attached to the quark operators  $\bar{\psi}, \psi$  can not extend to infinity, a staple-shaped gauge connection of finite extent  $\eta$  is used,

$$W_{\square\eta}^v(b^\mu/2, -b^\mu/2) = W_v^\dagger(b^\mu/2; 0, \eta) W_{\hat{v}}(\eta v - b/2; 0, |b|) W_v(-b^\mu/2; 0, \eta). \quad (2.162)$$

This gauge connection is shown in Fig. 2.11, which corresponds to a generalization of the illustration given in Fig. 2.1 (left) above in order to include finite length and to introduce more flexible variables for the endpoints. Apart from the quark operator separation  $b^\mu$ , the staple link is described by the direction of the staple  $v^\mu$  and the length of the staple  $\eta$ . In a concrete lattice calculation, an extrapolation  $\eta \rightarrow -\infty$  (Drell-Yan) or  $\eta \rightarrow +\infty$  (SIDIS) must be performed from data obtained at finite  $\eta$ . (See Sec. 2.7.1 for discussion on the two cases  $\eta = \pm\infty$ .) The staple direction  $v$  is taken off the light cone into the space-like region. This specification is crucial in order to make the definition amenable to lattice computation; the reason is that standard Lattice QCD methods to calculate matrix elements of the form in Eq. (2.162) are restricted to operators that are defined at a single time. As already indicated further above, the temporal lattice direction is Euclidean, and therefore no operators with a real, Minkowski time extent can be accommodated. Consequently, it is imperative that all separations in the operator, i.e.,  $b$  and  $\eta v$ , be space-like. For this reason we take

$$\frac{v^+}{v^-} = -e^{2y_v} < 0. \quad (2.163)$$

Only then is there no obstacle to boosting the problem to a Lorentz frame in which the operator in Eq. (2.162) exists at a single time, with  $y_v = 0$ . The lattice calculation is then carried out in that particular frame.

The correlator (2.162) furthermore depends on the momenta  $P, P'$  of the in- and outgoing states as well as their spin  $S$ . TMDs are obtained in the forward limit,  $P = P'$ , which we will assume for the remainder of the discussion in this section. (The generalization to nonzero momentum transfer yields the Generalized Transverse Momentum-Dependent parton distributions (GTMDs) discussed in Chapter 11.) A useful parameter to characterize the rapidity

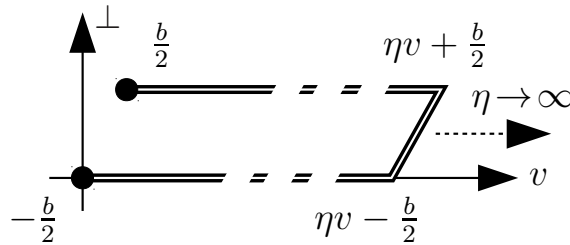


Figure 2.11: Staple-shaped path for the gauge connection  $W_{\square\eta}^v$  in Eq. (2.162).

of the staple link direction  $v$  relative to the hadron is the dimensionless Collins-Soper type evolution parameter

$$\hat{\zeta} = \frac{v \cdot P}{\sqrt{|v^2|P^2}}. \quad (2.164)$$

This parameter characterizes the staple link connecting the quark operators. It therefore differs from the variable  $\zeta_a$  defined in Eq. (2.30), which involves a combination of variables inherited from the proton matrix element ( $m_p$  and  $y_A$ ) and the TMD soft factor ( $y_n$ ).

Using Lorentz covariance, the matrix element in Eq. (2.162) can be decomposed into independent tensors constructed from  $P^\mu$ ,  $b^\mu$  and  $v^\mu$ , with the coefficients (or amplitudes) uniquely determined by the Lorentz scalars  $P \cdot b$ ,  $b^2$ ,  $\hat{\zeta}$ ,  $v \cdot b / \sqrt{-v^2}$ , and  $\eta^2 v^2$  [140]. (Following standard conventions, we do not treat the dependence on  $m_p^2 = P^2$  as a variable.) Such decompositions will be presented in Sec. 6.4.1. In Table 2.5 we list these Lorentz scalars, together with their values in two reference frames for comparison. TMD PDFs are originally defined in a frame where  $b^+ = 0$  and  $v_T = P_T = 0$ . This constrains one of the five Lorentz scalars, since it implies the relation, expressed in Lorentz-invariant form,

$$\frac{v \cdot b}{v \cdot P} = \frac{P \cdot b}{m_N^2} \left[ 1 - \sqrt{1 + \hat{\zeta}^{-2}} \right]. \quad (2.165)$$

In Table 2.5 the column labeled Modern CS ( $y_B$ ) corresponds to the frame choice used in the modern Collins-Soper definition with space-like Wilson lines of infinite extent, Eq. (2.48) inserted into Eq. (2.37), with finite but large  $|y_B|$ . The column labeled Euclidean Lattice gives the values in the frame where  $v^\mu$  has no time component ( $y_v = 0$ ), in which the lattice calculation is performed. Since all the Lorentz scalars can be determined in this Euclidean frame, one can obtain full information about the unsubtracted TMD PDF. In order to make full contact with the modern Collins definition of the unsubtracted TMD PDF, which is considered in the limit  $\eta \rightarrow \infty$  and eventually with large  $y_B \rightarrow -\infty$ , the lattice results obtained at finite values must ultimately be extrapolated towards a large rapidity difference  $\hat{\zeta} \rightarrow \infty$  and large  $\eta \rightarrow \infty$ .

An important corollary of this discussion is that the soft factor (2.38), cf. Fig. 2.1 (right), cannot be straightforwardly calculated in Lattice QCD in a completely analogous fashion. Since it contains two staple directions with two different rapidities, there exists no Lorentz transformation that simultaneously renders both directions purely spatial. In the modern Collins

Lorentz Invariant	Modern CS ( $y_B$ )	Euclidean Lattice
$P \cdot b$	$P^+ b^-$	$-P_z b_z$
$b^2$	$-\mathbf{b}_T^2$	$-b_z^2 - \mathbf{b}_T^2$
$\hat{\zeta} = \frac{v \cdot P}{m_p \sqrt{-v^2}}$	$\sinh(y_P - y_B)$	$\hat{\zeta} = \frac{-v_z P_z}{m_p \sqrt{v_z^2 + v_T^2}}$
$\frac{v \cdot b}{\sqrt{-v^2}}$	$\frac{-e^{y_B} b^-}{\sqrt{2}}$	$\frac{-v_z b_z - \mathbf{v}_T \cdot \mathbf{b}_T}{\sqrt{v_z^2 + v_T^2}}$
$\eta^2 v^2$	$-\infty$	$-\eta^2 (v_z^2 + v_T^2)$

Table 2.5: Comparison in position space of the Lorentz invariant variables between the Euclidean lattice approach and the modern CS definition prior to taking the  $y_B \rightarrow -\infty$  limit. In modern CS we have  $b^\mu = (0, b^-, b_T)$  in light-cone coordinates where  $v = n_B(y_B)$  from Eq. (2.45). The Euclidean lattice construction takes  $b^\mu = (0, b_T^x, b_T^y, b^z)$  in Cartesian coordinates.

definition the soft function is combined with the unsubtracted TMD PDF as in Eq. (2.49), which is necessary for the  $y_B \rightarrow -\infty$  limit that yields the full TMD PDF to exist. One way to deal with this obstacle is to circumvent it by constructing observables in the form of ratios in which soft factors cancel. These may be, e.g., ratios between matrix elements with different Dirac structures  $\Gamma$ , allowing one to access spin physics, or ratios between matrix elements with different external momenta, allowing one to access nonperturbative TMD evolution. Examples of suitable spin physics observables are given in Sec. 6.4.1. There, the Lorentz-invariant calculational scheme is laid out in further detail, and an overview is given of the numerical results obtained in the computational program based on this approach. The systematic dependence of lattice TMD observables with respect to various parameters, e.g., the staple length  $\eta$  and the evolution parameter  $\hat{\zeta}$  is exhibited using selected twist-2 TMD observables. Initial results pertaining to twist-3 TMDs are presented in Sec. 10.6.1, and results for GTMDs, yielding, in particular, quark orbital angular momentum in the proton, are discussed in Sec. 11.5.

## 2.10.2 Large-momentum effective theory

The idea of large-momentum effective theory (LaMET) is to approximate light-cone correlations for parton physics by the equal-time correlations in a boosted hadron state. In the TMD case, one starts from the matrix element in (2.162) where both the hadron momentum  $P^\mu$  and Wilson line direction  $v^\mu$  are along the  $z$  direction [104, 183, 184], as shown in Fig. 2.12a, and studies

$$\hat{f}_i(b^z, \mathbf{b}_T, a, P^z, \eta) = \frac{1}{2} \left\langle p(P, S) \left| \bar{\psi}_i^0(b^\mu/2) \Gamma W_{\square\eta}^z(b^\mu/2, -b^\mu/2) \psi_i^0(-b^\mu/2) \right| p(P, S) \right\rangle. \quad (2.166)$$

The Wilson line  $W_{\square\eta}^z(b^\mu/2, -b^\mu/2)$  closes in the transverse direction at the end of the staple, along  $b_T^\mu$ , which is different from that in the Lorentz-invariant approach, as the latter requires the Wilson line be parallel to the full  $b^\mu$ . (The use of  $b^\mu$  provides more symmetries that are used to reduce the number of independent amplitudes.) Here  $\hat{f}_i(b^z, \mathbf{b}_T, a, P^z, \eta)$  is referred to as the unsubtracted quasi TMD [183, 184] or quasi beam function [104]. The renormalized

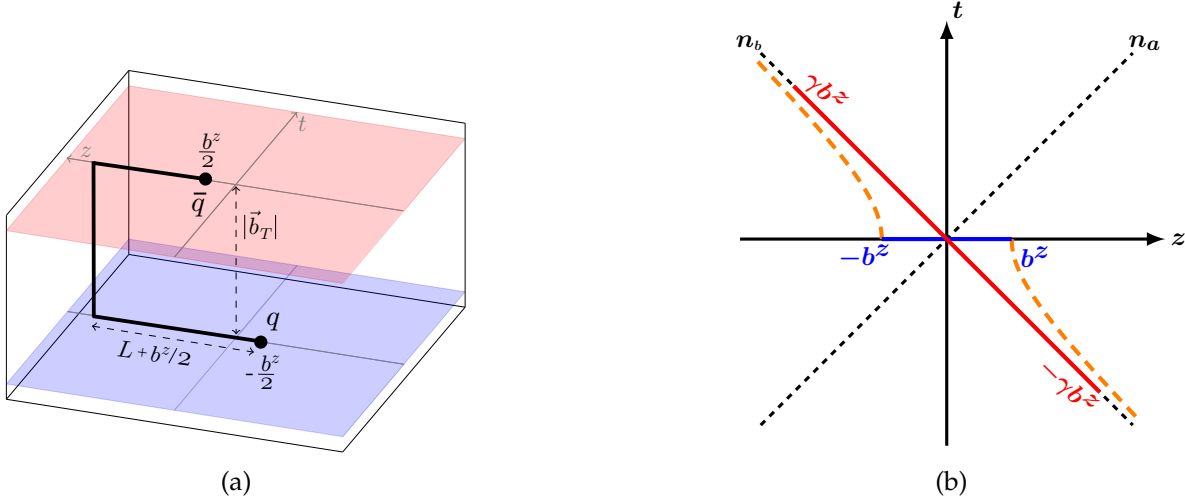


Figure 2.12: (a) Staple-shaped path for the gauge connection used in the LaMET calculation of TMD PDFs. (b) The behavior of the longitudinal separation under a Lorentz boost along the  $z$  direction. Here  $\gamma b^z$  is the length of the projection of the boosted Wilson line along the  $n_b$  light-cone direction.

quasi TMD PDF in  $x$  space is defined with the inclusion of a quasi soft function  $\tilde{S}^i(b_T, a, \eta)$

$$\hat{f}_i^{\text{TMD}}(x, \mathbf{b}_T, \mu, P^z) = \int \frac{db^z}{2\pi} e^{ib^z(xP^z)} \tilde{Z}'_i(b^z, \mu, \tilde{\mu}) \tilde{Z}_{uv}^i(b^z, \tilde{\mu}, a) \\ \times \hat{f}_i(b^z, \mathbf{b}_T, a, P^z, \eta) / \sqrt{\tilde{S}^i(b_T, a, \eta)}, \quad (2.167)$$

where  $\tilde{S}^i$  cancels the large  $\eta$  dependence in the quasi beam function.  $\tilde{Z}_{uv}$  is the lattice renormalization factor, and  $\tilde{Z}'$  converts from the lattice renormalization scheme with scheme parameter  $\tilde{\mu}$ , to the  $\overline{\text{MS}}$  scheme with  $\overline{\text{MS}}$  renormalization scale  $\mu$ .

Instead of using Lorentz covariance, in LaMET one boosts the equal-time correlator to the light-cone direction by calculating in a large-momentum hadron state. A picture of the Lorentz boost is shown in Fig. 2.12b. When  $P^z \gg m_p$ , one can perform a large-momentum expansion of the lattice construction to extract the parton physics, where the leading power contribution includes short distance matching and scale running [30]. In Fourier space, the distribution defined by boosting the matrix element of the equal-time correlator is also called the unsubtracted quasi TMD [183] or the quasi beam function [104]. After inclusion of the quasi soft function and renormalization [186, 192], one can take the  $\eta \rightarrow \infty$  limit and obtain the quasi TMD PDF.

The corresponding quasi soft function has the same issue as encountered in the Lorentz-invariant approach, namely, no single Lorentz boost can transform it into the soft function used in TMD factorization. Therefore, the difference between the quasi and physical TMD PDFs includes a perturbative matching coefficient and a nonperturbative contribution from the mismatch of the soft functions [104]. Nevertheless, one can still form ratios of the quasi TMD PDFs in different hadron states or for different spin structures to obtain information on TMD evolution or ratios of TMD PDFs in  $x$ -space [104, 185, 190]. Recently, methods have been proposed to calculate this nonperturbative contribution [187], which is called the reduced soft

function, from lattice QCD. With this development, a full determination of the TMD PDF as well as the Drell-Yan cross section appears within reach in lattice QCD [188].

A more detailed discussion of developments in the LaMET approach is given in Sec. 6.4.2.

### 2.10.3 Relations between lattice and continuum TMDs

Since both the Lorentz-invariant approach, or the Musch-Hägler-Engelhardt-Negele-Schäfer (MHENS) scheme, and the quasi TMD use off-the-light-cone Wilson lines, they are closely related to the Collins scheme. In fact, using Lorentz invariance, one can show that both the MHENS [140] and quasi [? ] beam functions with infinite Wilson lines are equivalent to that in the Collins scheme. Therefore, the Collins soft function can be used to subtract the rapidity divergences in the MHENS and quasi beam functions to define the relevant TMDs. In lattice QCD calculations, the light-cone limit in the MHENS and quasi TMDs are achieved by boosting the hadron momentum  $P^z$  to infinity. Since the lattice theory has a natural UV momentum cutoff, the  $P^z \rightarrow \infty$  limit has to be taken after the UV regularization, which, however, is opposite to the Collins scheme where the UV regularization is done before the light-cone limit (see Eq. (2.49)). Therefore, the lattice TMDs correspond to a new scheme, which is called the large-rapidity (LR) scheme [? ], and differs from the Collins scheme by the order of  $\epsilon \rightarrow 0$  and  $y_B \rightarrow -\infty$  limits.

Due to the asymptotic freedom of QCD, the large rapidity or momentum limit only affects the UV region, so changing the order of  $\epsilon \rightarrow 0$  and  $y_B \rightarrow -\infty$  limits leave infrared physics intact. Using the LaMET formalism [28–30], behind which is the general principle for effective field theories, one can relate the two different orders of limits with a factorization formula or perturbative matching [? ], which has been proposed in Refs. [104, 185, 187, 188]. Moreover, the matching is diagonal in the parton flavor space and independent of the spin structure, and there is no mixing between the gluon and quark channels [? ], which makes their individual lattice calculations easier.

Besides, the JMY scheme is related to the LR scheme by replacing the spacelike Wilson lines with timelike ones, so one can derive the matching coefficients for the JMY and LR schemes to the Collins scheme from one another through such an analytical continuation [? ]. The relations of both lattice and continuum off-the-light-cone schemes are shown in Fig. 2.13.

## 2.11 Complete TMD Factorization for DY, SIDIS, and $e^+e^-$

In this section, we extend our previous discussion of TMD factorization for the unpolarized Drell-Yan process to polarized Drell-Yan in Sec. 2.11.1, to Higgs production at hadron colliders in Sec. 2.11.2, to polarized Semi-Inclusive Deep-Inelastic Scattering (SIDIS) in Sec. 2.11.3, and to dihadron production at  $e^+e^-$  colliders in Sec. 2.11.4.

### 2.11.1 Polarized Drell-Yan cross section

We now consider the polarized Drell-Yan process,

$$H_1(P_1, S_1) + H_2(P_2, S_2) \rightarrow \gamma^*/Z \rightarrow \ell^+\ell^-, \quad (2.168)$$

where the hadrons  $H_{1,2}$  have momenta  $P_{1,2}$  and spin  $S_{1,2}$ . By measuring the angular distributions of the detected lepton pair, one can study the polarization of the struck quarks, which in turn allows one to study correlations of the quark and hadron polarizations. After some preliminaries, below we will specialize to the special case of Drell-Yan for a pion-proton collision,  $H_1 = \pi$  and  $H_2 = p$ .

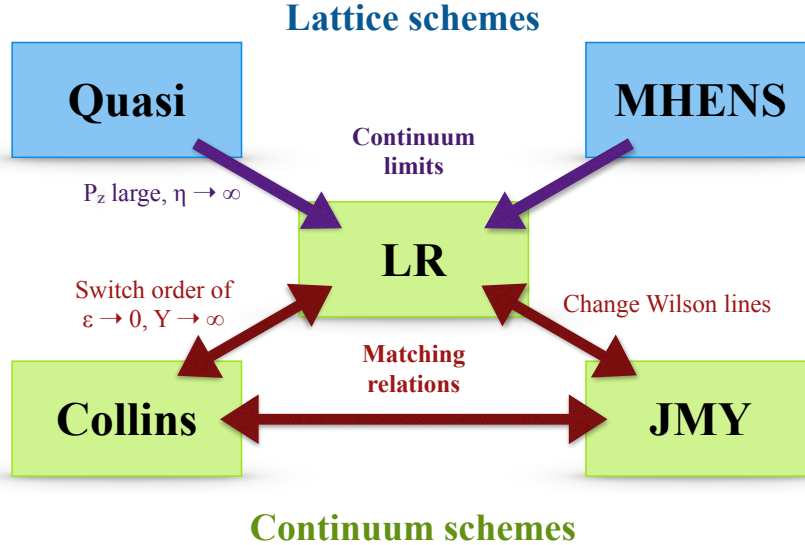


Figure 2.13: An overview of lattice and continuum TMD schemes and their relationships, including the MHENS scheme and the LR scheme introduced in Ref. [? ].

One needs to define a reference frame in which to measure the leptonic angles, which is commonly achieved in the Collins-Soper frame [193]. It can be obtained from the lab frame, where the incoming pion is aligned along the  $z$  axis, by first boosting along  $z$  such that the virtual boson has vanishing longitudinal momentum. Subsequently, one performs a transverse boost such that the virtual boson has vanishing transverse momentum, i.e. is produced at rest. In such a rest frame, the two leptons are produced back-to-back with transverse momenta  $\pm \mathbf{q}_T/2$ . In the Collins-Soper frame, the lepton momenta span the  $(x, z)$ -plane, and one defines the angle  $\phi$  as the inclination of the hadron to the lepton plane. Likewise, one defines the angle  $\phi_s$  as the azimuthal angle of the proton spin vector with respect to the lepton plane. These kinematics are illustrated in Fig. 2.14 for pion-proton scattering.

Following [195], we write the Drell-Yan cross section in the one-photon approximation as

$$\sigma = \int \frac{d^3 \vec{l}}{l^0} \frac{d^3 \vec{l'}}{l'^0} \frac{\alpha_{em}^2}{\mathcal{F} Q^4} L_{\mu\nu} W^{\mu\nu}, \quad (2.169)$$

where  $l$  and  $l'$  are the lepton momenta,

$$\mathcal{F} = 4 \sqrt{(P_1 \cdot P_2)^2 - M_1^2 M_2^2}, \quad (2.170)$$

is the flux factor of the incoming hadrons, and  $Q^2 = q^2$  with  $q = l + l'$  is the photon virtuality. The kinematics of the lepton pair are described by the spin-averaged leptonic tensor

$$L^{\mu\nu} = \sum_{\lambda, \lambda'} [\bar{u}(l, \lambda) \gamma^\mu v(l', \lambda')] [v(l', \lambda') \gamma^\nu u(l, \lambda)] = 4 \left( l^\mu l'^\nu + l^\nu l'^\mu - \frac{Q^2}{2} g^{\mu\nu} \right). \quad (2.171)$$

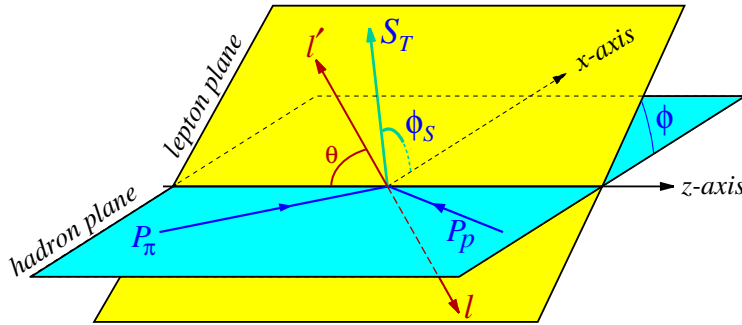


Figure 2.14: The DY process in the Collins-Soper frame where the pion and the proton come in with different momenta  $P_\pi, P_p$ , but each carries the same transverse momentum  $\frac{1}{2} q_T$ , and the produced lepton pair is at rest. The angle  $\phi$  describes the inclination of the leptonic frame with respect to the hadronic plane, and  $\phi_S$  is the azimuthal angle of the transverse-spin vector of the proton. Here  $\theta$  is the angle between the final state lepton and  $z$ -axis, where the  $z$ -axis is defined by the intersection of the hadron and lepton planes. The figure is from Ref. [194].

The hadronic physics is encoded in the hadronic tensor

$$W^{\mu\nu} = \int \frac{d^4x}{(2\pi)^4} e^{iq\cdot x} \langle P_1, S_1; P_2, S_2 | J_{em}^\mu(0) J_{em}^\nu(0) | P_1, S_1; P_2, S_2 \rangle, \quad (2.172)$$

where  $J_{em}^\mu$  is the electromagnetic current. By decomposing the Lorentz tensors  $L^{\mu\nu}$  and  $W^{\mu\nu}$  into all independent angular and spin structures, one can derive the most general decomposition of the Drell-Yan cross section. In the most general case with two arbitrarily polarized hadrons, there are a total of 48 independent structures [195], out of which 24 are suppressed at small  $q_T$ .

For brevity of our discussion, we only focus on the case of pions scattering off polarized protons,  $\pi p \rightarrow \gamma^* \rightarrow \ell^+ \ell^-$ , as measured by the COMPASS Collaboration [196], and refer to [195] for the fully generic result. We also neglect contributions from  $Z$  exchange, which are suppressed at low energies. At small  $q_T$ , this process is described by only six independent structures, and can be written as [195]

$$\begin{aligned} \frac{d\sigma}{d^4q d\Omega} = & \frac{\alpha_{em}^2}{\mathcal{F} Q^2} \left\{ \left[ (1 + \cos^2 \theta) F_{UU}^1 + \sin^2 \theta \cos(2\phi) F_{UU}^{\cos 2\phi} \right] \right. \\ & + S_L \sin^2 \theta \sin(2\phi) F_{UL}^{\sin 2\phi} \\ & + S_T (1 - \cos^2 \theta) \sin \phi_S F_{UT}^{\sin \phi_S} \\ & \left. + S_T \sin^2 \theta [\sin(2\phi + \phi_S) F_{UT}^{\sin(2\phi + \phi_S)} + \sin(2\phi - \phi_S) F_{UT}^{\sin(2\phi - \phi_S)}] \right\}, \end{aligned} \quad (2.173)$$

where  $\Omega$  is the solid angle of the dilepton system in the Collins-Soper frame, with the angles  $\phi$ ,  $\theta$  and  $\phi_S$  defined accordingly, see Fig. 2.14. The first subscript on the structure functions  $F$  indicates that the pion is unpolarized ( $U$ ), while the second subscript corresponds to the proton polarization, which can be unpolarized ( $U$ ), longitudinally ( $L$ ) or transversely ( $T$ )

polarized. It is also common to measure the individual structure functions normalized to the unpolarized case, i.e.,

$$A_{XY}^{\text{weight}}(x_\pi, x_p, q_T, Q^2) = \frac{F_{XY}^{\text{weight}}(x_\pi, x_p, q_T, Q^2)}{F_{UU}^1(x_\pi, x_p, q_T, Q^2)}. \quad (2.174)$$

As made explicit here, all structure functions only depend on the longitudinal momentum fractions  $x_\pi$  and  $x_p$ , as well as the transverse momentum  $q_T^2$  and photon virtuality  $Q^2$ .

The structure functions in Eq. (2.174) can be expressed in terms of the spin-dependent TMDs introduced in Sec. 2.7 as follows [195]:

$$\begin{aligned} F_{UU}^1 &= C[f_{1,\pi} f_{1,p}], \\ F_{UU}^{\cos 2\phi} &= C \left[ \frac{2(\hat{\mathbf{h}} \cdot \mathbf{p}_{T\pi})(\hat{\mathbf{h}} \cdot \mathbf{p}_{Tp}) - \mathbf{p}_{T\pi} \cdot \mathbf{p}_{Tp}}{M_\pi M_p} h_{1,\pi}^\perp h_{1,p}^\perp \right], \\ F_{UL}^{\sin 2\phi} &= -C \left[ \frac{2(\hat{\mathbf{h}} \cdot \mathbf{p}_{T\pi})(\hat{\mathbf{h}} \cdot \mathbf{p}_{Tp}) - \mathbf{p}_{T\pi} \cdot \mathbf{p}_{Tp}}{M_\pi M_p} h_{1,\pi}^\perp h_{1L,p}^\perp \right], \\ F_{UT}^{\sin \phi_s} &= C \left[ \frac{\hat{\mathbf{h}} \cdot \mathbf{p}_{Tp}}{M_p} f_{1,\pi} f_{1T,p}^\perp \right], \\ F_{UT}^{\sin(2\phi - \phi_s)} &= -C \left[ \frac{\hat{\mathbf{h}} \cdot \mathbf{p}_{T\pi}}{M_\pi} h_{1,\pi}^\perp h_{1,p} \right], \\ F_{UT}^{\sin(2\phi + \phi_s)} &= -C \left[ \frac{2(\hat{\mathbf{h}} \cdot \mathbf{p}_{Tp})[2(\hat{\mathbf{h}} \cdot \mathbf{p}_{T\pi})(\hat{\mathbf{h}} \cdot \mathbf{p}_{Tp}) - \mathbf{p}_{T\pi} \cdot \mathbf{p}_{Tp}] - \mathbf{p}_{Tp}^2 (\hat{\mathbf{h}} \cdot \mathbf{p}_{T\pi})}{2 M_\pi M_p^2} h_{1,\pi}^\perp h_{1T,p}^\perp \right]. \end{aligned} \quad (2.175)$$

Here,  $\hat{\mathbf{h}} = \mathbf{q}_T/q_T$  points along the  $x$ -axis in the CS frame,  $M_{\pi,p}$  are the pion and proton masses, and the convolution integrals are defined as

$$\begin{aligned} C[\omega f_\pi f_p] &= \sum_i H_{i\bar{i}}(Q^2, \mu) \int d^2 \mathbf{p}_{T\pi} d^2 \mathbf{p}_{Tp} \delta^{(2)}(\mathbf{q}_T - \mathbf{p}_{T\pi} - \mathbf{p}_{Tp}) \\ &\quad \times \omega(\mathbf{q}_T, \mathbf{p}_{T\pi}, \mathbf{p}_{Tp}, \dots) f_{i/p}(x_a, p_{TN}, \mu, \zeta_a) f_{\bar{i}/\pi}(x_b, p_{T\pi}, \mu, \zeta_b), \end{aligned} \quad (2.176)$$

where the sum runs over all quark flavors  $i = u, \bar{u}, d, \bar{d}, \dots$ , the hard function  $H_{i\bar{i}}$  encodes physics at the hard scale  $Q$ , and  $\omega$  is a kinematic weight function given by the prefactors in Eq. (2.176). For a virtual photon up to two-loop order, its only flavor dependence is given by the quark charges  $e_i$  which are each proportional to the electromagnetic coupling  $|e|$ , so

$$H_{i\bar{i}}(Q^2, \mu) = e_i^2 H(Q^2, \mu) + \mathcal{O}(\alpha_s^3). \quad (2.177)$$

The convolution variables  $\mathbf{p}_{T\pi}$  and  $\mathbf{p}_{Tp}$  correspond to the momenta of struck quarks in the pion and proton, respectively. We have also restored all arguments of the TMD functions, where as usual the Collins-Soper scales obey  $\zeta_\pi \zeta_N = Q^4$ .

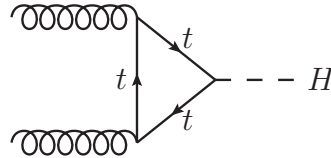


Figure 2.15: Higgs-boson production in gluon fusion mediated by a top-quark loop. Contributions from lighter quarks are suppressed by their quark masses.

Similar to our treatment of unpolarized Drell-Yan in Sec. 2.2, one can also express Eq. (2.176) more compactly in  $b_T$  space as [139, 194]

$$\begin{aligned} F_{UU}^1 &= \mathcal{B}[\tilde{f}_{1,\pi}^{(0)} \tilde{f}_{1,p}^{(0)}], \\ F_{UU}^{\cos 2\phi} &= M_\pi M_p \mathcal{B}[\tilde{h}_{1,\pi}^{\perp(1)} \tilde{h}_{1,p}^{\perp(1)}], \\ F_{UL}^{\sin 2\phi} &= -M_\pi M_p \mathcal{B}[\tilde{h}_{1,\pi}^{\perp(1)} \tilde{h}_{1L,p}^{\perp(1)}], \\ F_{UT}^{\sin \phi_s} &= M_p \mathcal{B}[\tilde{f}_{1,\pi}^{(0)} \tilde{f}_{1T,p}^{\perp(1)}], \\ F_{UT}^{\sin(2\phi-\phi_s)} &= -M_\pi \mathcal{B}[\tilde{h}_{1,\pi}^{\perp(1)} \tilde{h}_{1,p}^{(0)}], \\ F_{UT}^{\sin(2\phi+\phi_s)} &= -\frac{M_\pi M_p^2}{4} \mathcal{B}[\tilde{h}_{1,\pi}^{\perp(1)} \tilde{h}_{1T,p}^{\perp(2)}]. \end{aligned} \quad (2.178)$$

Here, the analog of the convolution integral in Eq. (2.177) is the Bessel transform

$$\mathcal{B}[\tilde{f}_\pi^{(m)} \tilde{f}_p^{(n)}] \equiv \sum_i H_{ii}(Q, \mu) \int_0^\infty \frac{db_T}{2\pi} b_T b_T^{m+n} J_{m+n}(q_T b_T) \tilde{f}_{i/p}^{(m)}(x_a, b_T, \mu, \zeta_a) \tilde{f}_{i/\pi}^{(n)}(x_b, b_T, \mu, \zeta_b), \quad (2.179)$$

where  $J_{m+n}(x)$  is the Bessel function of the first kind of order  $m+n$ , and the  $\tilde{f}^{(n)}$  are derivatives of the Fourier transform of  $f$ , as defined in Eq. (2.129).

## 2.11.2 Higgs production in gluon fusion

So far, we have only discussed the (polarized) Drell-Yan process, which is a key benchmark for both low-energy experiments such as JLab or COMPASS as well as for high-energy colliders such as Tevatron or the LHC. A key property of the Drell-Yan process is that it is initiated by quark annihilation, but does not directly probe the gluonic structure of the proton. Gluon-induced scatterings become much more important at high-energy colliders, in particular for the production of Higgs bosons.

While the Higgs boson does not directly couple to gluons, it can be produced in gluon fusion through a closed quark loop, as depicted in Fig. 2.15. Since the Yukawa coupling of the Higgs boson to a quark is proportional to the quark mass, this process is dominated by a virtual top loop, while contributions from lighter quarks such as the  $b$  quark are suppressed.

The transverse momentum distribution of the Higgs boson is a key observable for probing its production mechanism, and thus has been extensively measured at the LHC [197–207]. At small transverse momentum  $q_T \ll m_H$  of the Higgs boson, its theoretical description requires

the use of TMD factorization. The analog of Eq. (2.29) for a gluon-induced process in the collision of unpolarized protons reads

$$\frac{d\sigma^W}{dQdYd^2\mathbf{q}_T} = 2H_{\rho\sigma\rho'\sigma'}(Q, \mu) \int d^2\mathbf{b}_T e^{i\mathbf{b}_T \cdot \mathbf{q}_T} \tilde{f}_{g/p}^{\rho\sigma}(x_a, \mathbf{b}_T, \mu, \zeta_a) \tilde{f}_{g/p}^{\rho'\sigma'}(x_b, \mathbf{b}_T, \mu, \zeta_b) \quad (2.180a)$$

$$= 2H_{\rho\sigma\rho'\sigma'}(Q, \mu) \int d^2\mathbf{b}_T e^{i\mathbf{b}_T \cdot \mathbf{q}_T} \tilde{B}_{g/p}^{\rho\sigma}(x_a, \mathbf{b}_T, \mu, \zeta_a/v^2) \tilde{B}_{g/p}^{\rho'\sigma'}(x_b, \mathbf{b}_T, \mu, \zeta_b/v^2) \\ \times \tilde{\mathcal{S}}_{n_a n_b}(b_T, \mu, v). \quad (2.180b)$$

As in Eq. (2.29), we present this result both using the approach of renormalized TMD PDFs  $f_{g/p}^{\rho\sigma}$  and by separately considering renormalized beam functions  $B_{g/p}^{\rho\sigma}$  and the soft function  $\tilde{\mathcal{S}}_{n_a n_b}$ . Here the soft function has Wilson lines in the adjoint representation, and hence differs from the soft function  $S_{n_a n_b}$  in quark-initiated Drell-Yan. The definition of the corresponding bare gluon soft function  $\tilde{\mathcal{S}}_{n_a n_b}^0(b_T, \epsilon, \tau)$  is given above in Eq. (2.141). As before, these functions depend on the transverse separation  $\mathbf{b}_T$ , which is Fourier-conjugate to  $\mathbf{q}_T$ , the longitudinal momentum fractions  $x_{a,b}$ , the renormalization scale  $\mu$  and the Collins-Soper scale  $\zeta_{a,b}$ . The latter obeys  $\zeta_a \zeta_b = Q^4$ , where for on-shell Higgs production  $Q^2 = m_H^2$ . The beam and soft functions also depend on the rapidity renormalization scale  $v$ , which cancels exactly between them.

The key difference between Eq. (2.29), the TMD factorization for unpolarized Drell-Yan, and Eq. (2.181) is the Lorentz structure of the TMD PDFs (or beam functions). This arises because even in an unpolarized proton, the spin-1 nature of the gluon induces a nontrivial Lorentz structure, as was pointed out in [208], see also [91]. From Eq. (2.142), the gluon TMD PDF in an unpolarized hadron reads

$$\tilde{f}_{g/p}^{\rho\sigma}(x, \mathbf{b}_T, \mu, \zeta) = -\frac{g_T^{\rho\sigma}}{2} \tilde{f}_1^g(x, b_T, \mu, \zeta) + \left(\frac{g_T^{\rho\sigma}}{2} + \frac{b_T^\rho b_T^\sigma}{\mathbf{b}_T^2}\right) \tilde{h}_1^{\perp g}(x, b_T, \mu, \zeta), \quad (2.181)$$

where  $g_T^{\rho\sigma}$  is the transverse metric and  $b_T$  on the right-hand side is a Minkowskian four-vector.

Eq. (2.181) holds for generic gluon-induced processes, where the process-dependence is carried by the hard function  $H_{\rho\sigma\rho'\sigma'}$ . For the case of Higgs production discussed here, the spin-0 nature of the Higgs boson forbids any nontrivial spin correlations, such that the hard function simplifies to

$$H^{\rho\sigma\rho'\sigma'}(Q, \mu) = H_{ggH}(Q, \mu) g_T^{\rho\sigma} g_T^{\rho'\sigma'}, \quad (2.182)$$

such that the cross section only depends on the combination

$$\tilde{f}_{g/p}^{\rho\sigma}(x_a, \mathbf{b}_T) \tilde{f}_{g/p}^{\rho\sigma}(x_b, \mathbf{b}_T) = \frac{1}{2} \left[ \tilde{f}_1^g(x_a, \mathbf{b}_T) \tilde{f}_1^g(x_b, \mathbf{b}_T) + \tilde{h}_1^{\perp g}(x_a, \mathbf{b}_T) \tilde{h}_1^{\perp g}(x_b, \mathbf{b}_T) \right], \quad (2.183)$$

where we suppressed the scales for brevity. Inserting this into Eq. (2.181a), one obtains the simple result

$$\frac{d\sigma^W}{dQdYd^2\mathbf{q}_T} = H_{ggH}(Q, \mu) \int d^2\mathbf{b}_T e^{i\mathbf{b}_T \cdot \mathbf{q}_T} \left[ \tilde{f}_1^g(x_a, \mathbf{b}_T, \mu, \zeta_a) \tilde{f}_1^g(x_b, \mathbf{b}_T, \mu, \zeta_b) \right. \\ \left. + \tilde{h}_1^{\perp g}(x_a, \mathbf{b}_T, \mu, \zeta_a) \tilde{h}_1^{\perp g}(x_b, \mathbf{b}_T, \mu, \zeta_b) \right], \quad (2.184)$$

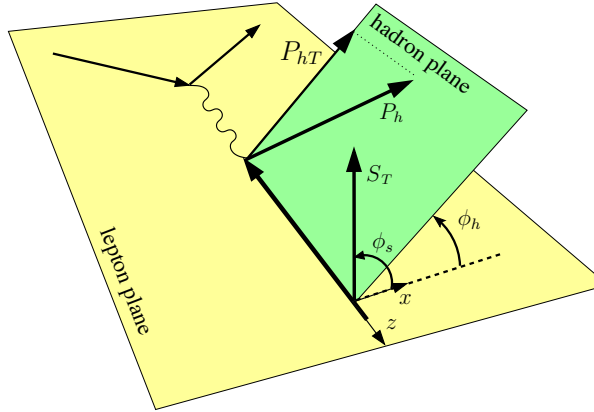


Figure 2.16: Semi Inclusive Deep Inelastic Scattering process (SIDIS) in  $\gamma^* p$  center of mass frame. The plot is from Ref. [209], adapted to the notation used here.

and similarly for the form in Eq. (2.181b).

Finally, we remark that Higgs production at the LHC is dominated by perturbative  $\Lambda$ -QCD  $\ll q_T \ll m_H$ , in which case one can relate the gluon TMD PDFs to collinear PDFs as discussed in Sec. 2.8, supplemented by resummation of large logarithms as outlined in Chapter 4.

### 2.11.3 Polarized SIDIS cross section

We now consider Semi-Inclusive Deep-Inelastic Scattering (SIDIS),

$$\ell(l) + p(P) \rightarrow \ell(l') + h(P_h) + X , \quad (2.185)$$

where the incoming lepton (an electron, positron or muon) with momentum  $l$  scatters off a proton with momentum  $P$ , both of which can be polarized. One measures both the outgoing lepton with momentum  $l'$  and a hadron of type  $h$  (such as a pion or kaon) and momentum  $P_h$ , but is inclusive over any additional hadronic radiation  $X$ .

As in the case of polarized Drell-Yan discussed in Sec. 2.11.1, we are interested in measuring angular correlations in order to extract correlations between the polarization of the struck quark and the spin of the proton. This requires defining a reference frame in which to specify angular measurements, which is commonly chosen according to the Trento conventions [18]. In this frame, the spacelike momentum  $q$  defines the  $z$  axis, which together with the lepton momenta defines the  $(x, z)$ -plane, with respect to which all angles are defined. This is illustrated in Fig. 2.16.

We are interested in measuring the momentum component  $P_{hT}$  and azimuthal angle  $\phi_h$  of the detected hadron in this frame. In addition, there is an azimuthal angle  $\psi_l$  characterizing the overall orientation of the lepton scattering plane around the incoming lepton direction. The angle is calculated with respect to an arbitrary reference axis, which in the case of transversely polarized targets is chosen to be the direction of the polarization vector  $S_T$ . In the DIS limit  $\psi_l \approx \phi_s$ , where the latter is the azimuthal angle of the spin-vector of the struck hadron. These observables are also illustrated in Fig. 2.16.

In the limit that  $Q \ll m_{W,Z}$ , the SIDIS process can be described in the single-photon exchange approximation, and is characterized by 18 independent structure functions [121]. At leading order in a  $1/Q$  expansion, only a subset of 8 structure functions contributes, and the

SIDIS cross section can be written as [121, 210]

$$\frac{d^6\sigma}{dx dy dz_h d\phi_S d\phi_h dP_{hT}^2} = \frac{\alpha_{em}^2}{x y Q^2} \left(1 - y + \frac{1}{2}y^2\right) \left[ F_{UU,T} + \cos(2\phi_h) p_1 F_{UU}^{\cos(2\phi_h)} \right. \\ + S_L \sin(2\phi_h) p_1 F_{UL}^{\sin(2\phi_h)} + S_L \lambda p_2 F_{LL} \\ + S_T \sin(\phi_h - \phi_S) F_{UT,T}^{\sin(\phi_h - \phi_S)} \\ + S_T \sin(\phi_h + \phi_S) p_1 F_{UT}^{\sin(\phi_h + \phi_S)} + \lambda S_T \cos(\phi_h - \phi_S) p_2 F_{LT}^{\cos(\phi_h - \phi_S)} \\ \left. + S_T \sin(3\phi_h - \phi_S) p_1 F_{UT}^{\sin(3\phi_h - \phi_S)} \right], \quad (2.186)$$

Up to corrections suppressed as  $1/Q^2$ , the kinematic prefactors  $p_i$  in Eq. (2.187) are given by [210]

$$p_1 = \frac{1-y}{1-y+\frac{1}{2}y^2}, \quad p_2 = \frac{y(1-\frac{1}{2}y)}{1-y+\frac{1}{2}y^2}, \quad p_3 = \frac{(2-y)\sqrt{1-y}}{1-y+\frac{1}{2}y^2}, \quad p_4 = \frac{y\sqrt{1-y}}{1-y+\frac{1}{2}y^2}. \quad (2.187)$$

The factors  $p_3$  and  $p_4$  are listed here for completeness, but only appear in the subleading power cross sections, given for SIDIS in Eq. (10.17).

The structure functions  $F_{XY}^{\text{weight}}$  in Eq. (2.187) implicitly depend on  $x, z_h, P_{hT}^2$  and  $Q^2 \simeq xyS$ . Their superscripts indicate the azimuthal dependence, while the subscripts encode the beam and target polarizations. The first subscript  $U$  ( $L$ ) denotes the unpolarized beam (longitudinally polarized beam with twice helicity  $\lambda$ ). The second subscript  $U$  ( $L$  or  $T$ ) refers to the target, which can be unpolarized (longitudinally ( $S_L$ ) or transversely ( $S_T$ ) polarized with respect to virtual photon).  $F_{UU,T}$  is the structure function due to transverse polarization of the virtual photon (indicated by the third sub-index  $T$ ). The subleading terms in the SIDIS cross section can be found in Ch. 10 in Eq. (10.17).

The structure functions in Eq. (2.187) are described in terms of convolutions of TMDs and FFs, similar to the case of polarized Drell-Yan, see Eqs. (2.174) and (2.176). They are given at leading power by [121]

$$F_{UU,T} = C[f_1 D_1], \\ F_{UU}^{\cos 2\phi_h} = C \left[ \frac{2(\hat{h} \cdot \mathbf{p}_T)(\hat{h} \cdot \mathbf{k}_T) - \mathbf{p}_T \cdot \mathbf{k}_T}{z_h M_N M_h} h_1^\perp H_1^\perp \right], \\ F_{UL}^{\sin 2\phi_h} = C \left[ \frac{2(\hat{h} \cdot \mathbf{p}_T)(\hat{h} \cdot \mathbf{k}_T) - \mathbf{p}_T \cdot \mathbf{k}_T}{z_h M_N M_h} h_{1L}^\perp H_1^\perp \right], \\ F_{LL} = C[g_1 D_1], \\ F_{LT}^{\cos(\phi_h - \phi_S)} = C \left[ \frac{\hat{h} \cdot \mathbf{k}_T}{M_N} g_{1T}^\perp D_1 \right], \\ F_{UT}^{\sin(\phi_h + \phi_S)} = C \left[ \frac{\hat{h} \cdot \mathbf{p}_T}{z_h M_h} h_1 H_1^\perp \right], \\ F_{UT}^{\sin(\phi_h - \phi_S)} = C \left[ -\frac{\hat{h} \cdot \mathbf{k}_T}{M_N} f_{1T}^\perp D_1 \right],$$

$$F_{UT}^{\sin(3\phi_h - \phi_s)} = C \left[ \frac{4(\hat{\mathbf{h}} \cdot \mathbf{p}_T)(\hat{\mathbf{h}} \cdot \mathbf{k}_T)^2 - 2(\hat{\mathbf{h}} \cdot \mathbf{k}_T)(\mathbf{k}_T \cdot \mathbf{p}_T) - (\hat{\mathbf{h}} \cdot \mathbf{p}_T)\mathbf{k}_T^2}{2z_h M_N^2 M_h} h_{1T}^\perp H_1^\perp \right], \quad (2.188)$$

where we always abbreviate  $F_{XY}^{\text{weight}} \equiv F_{XY}^{\text{weight}}(x, z_h, P_{hT}, Q^2)$ , and  $\hat{\mathbf{h}} = \mathbf{P}_{hT}/P_{hT}$  is the unit vector along the  $x$ -axis. The convolution is defined analogously to Eq. (2.177) as [121]

$$\begin{aligned} C[\omega f D] &= x \sum_i H_{ii}(Q^2, \mu) \int d^2 \mathbf{k}_T d^2 \mathbf{p}_T \delta^{(2)}(z_h \mathbf{k}_T + \mathbf{p}_T - \mathbf{P}_{hT}) \\ &\quad \times \omega f_{i/N}(x, k_T, \mu, \zeta_1) D_{h/i}(z_h, p_T, \mu, \zeta_2), \end{aligned} \quad (2.189)$$

where  $\omega$  is a weight function, which in general depends on  $\mathbf{k}_T$  and  $\mathbf{p}_T$ , and the sum runs over all quark and anti-quark flavors  $i = u, \bar{u}, d, \bar{d}$ , etc. Here, the hard function for the SIDIS process is denoted by  $H_{ii}(Q^2, \mu)$ , and is related to that for the Drell-Yan process by

$$H_{ii}(Q^2, \mu) = H_{i\bar{i}}(-Q^2, \mu). \quad (2.190)$$

One can also express the convolutions in Eq. (2.189) through Fourier transforms of products of TMDs in  $b_T$  space [139],

$$\begin{aligned} F_{UU}(x, z_h, P_{hT}, Q^2) &= \mathcal{B}[\tilde{f}_1^{(0)} \tilde{D}_1^{(0)}], \\ F_{UU}^{\cos 2\phi_h}(x, z_h, P_{hT}, Q^2) &= M_N M_h \mathcal{B}[\tilde{h}_1^{\perp(1)} \tilde{H}_1^{\perp(1)}], \\ F_{UL}^{\sin 2\phi_h}(x, z_h, P_{hT}, Q^2) &= M_N M_h \mathcal{B}[\tilde{h}_{1L}^{\perp(1)} \tilde{H}_1^{\perp(1)}], \\ F_{LL}(x, z_h, P_{hT}, Q^2) &= \mathcal{B}[\tilde{g}_1^{(0)} \tilde{D}_1^{(0)}], \\ F_{LT}^{\cos(\phi_h - \phi_s)}(x, z_h, P_{hT}, Q^2) &= M_N \mathcal{B}[\tilde{g}_{1T}^{\perp(1)} \tilde{D}_1^{(0)}], \\ F_{UT}^{\sin(\phi_h + \phi_s)}(x, z_h, P_{hT}, Q^2) &= M_h \mathcal{B}[\tilde{h}_1^{(0)} \tilde{H}_1^{\perp(1)}], \\ F_{UT}^{\sin(\phi_h - \phi_s)}(x, z_h, P_{hT}, Q^2) &= -M_N \mathcal{B}[\tilde{f}_{1T}^{\perp(1)} \tilde{D}_1^{(0)}], \\ F_{UT}^{\sin(3\phi_h - \phi_s)}(x, z_h, P_{hT}, Q^2) &= \frac{M_N^2 M_h}{4} \mathcal{B}[\tilde{h}_{1T}^{\perp(2)} \tilde{H}_1^{\perp(1)}], \end{aligned} \quad (2.191)$$

where the Fourier transform corresponding to Eq. (2.190) is given analogously to Eq. (2.180) as

$$\begin{aligned} \mathcal{B}[\tilde{f}^{(m)} \tilde{D}^{(n)}] &\equiv x \sum_i e_i^2 \mathcal{H}_{ii}(Q^2, \mu) \int_0^\infty \frac{db_T}{2\pi} b_T b_T^{m+n} J_{m+n}(q_T b_T) \\ &\quad \times \tilde{f}_{i/N}^{(m)}(x, b_T, \mu, \zeta_1) \tilde{D}_{h/i}^{(n)}(z_h, b_T, \mu, \zeta_2). \end{aligned} \quad (2.192)$$

The Fourier-transformed TMD PDFs  $\tilde{f}$  and their derivatives  $\tilde{f}^{(n)}$  are defined in Eqs. (2.127) and (2.129), and the corresponding definitions for the TMD FFs  $\tilde{D}$  and their derivatives  $\tilde{D}^{(n)}$  are given in Eqs. (2.136) and (2.138).

### 2.11.4 Back-to-back hadron production in $e^+e^-$

The first process where TMD factorization was proven is back-to-back hadron production in  $e^+e^-$  annihilation [86],

$$e^+(P_{e^+}) + e^-(P_{e^-}) \rightarrow h_1(P_{h_1}) + h_2(P_{h_2}) + X, \quad (2.193)$$

where  $h_{1,2}$  are the identified hadrons with momenta  $P_{h_{1,2}}$ , and one is inclusive over additional hadronic final states  $X$ . Similar to the detected outgoing hadron in SIDIS, see Sec. 2.11.3, these hadrons arise from the fragmentation of quarks in the underlying partonic process, and are described by fragmentation functions characterized by the longitudinal momentum fractions

$$z_{h1} = \frac{2|\mathbf{P}_{h1}|}{Q}, \quad z_{h2} = \frac{2|\mathbf{P}_{h2}|}{Q}, \quad (2.194)$$

where the center-of-mass energy  $Q^2 = (P_{e^+} + P_{e^-})^2$  defines the hard scale of the process.

At leading order, the hadrons are produced exactly back to back, which is spoiled at higher orders due to the additional radiation  $X$ , which thus gives rise to an imbalance between the hadron momenta. The near back-to-back region is characterized by a small transverse momentum of the dihadron system compared to  $Q$ , which is the realm of TMD factorization.

As before, measuring angular distributions of the final-state hadrons can give access to spin correlations in the fragmenting hadrons, most famously in the form of the Collins effect that gives rise to an azimuthal asymmetry of the form  $\cos(2\phi)$  [57]. To define the azimuthal angle  $\phi$ , two different reference frames have been proposed in the literature [211]:

1. One defines the thrust axis of the  $e^+e^-$  annihilation and measures the relative azimuthal angular correlation between the two hadrons in the two back-to-back jets. In this case, one has to measure two azimuthal angles  $\phi_1$  and  $\phi_2$ , and the Collins effect manifests itself as a  $\cos(\phi_1 + \phi_2)$  asymmetry, and is referred to as the  $A_{12}$  asymmetry.
2. One aligns the  $z$  axis along one of the detected hadrons, and measures the azimuthal angle  $\phi_0$  of the other hadron with respect to this axis and the lepton plane, as illustrated in Fig. 2.17. The Collins effect then appears as a  $\cos(2\phi_0)$  asymmetry, and is referred to as the  $A_0$  asymmetry.

The  $A_{12}$  asymmetry can not be directly described within TMD factorization, as one needs to define the jet directions, which goes beyond standard TMD factorization. Hence, we will only consider the second approach of the  $A_0$  asymmetry, which is described within TMD factorization in terms of the Collins function.

In the limit of small transverse momentum  $P_{h\perp}$ , the cross section as predicted by TMD factorization reads [212, 213]

$$\frac{d^5\sigma^{e^+e^- \rightarrow h_1h_2+X}}{dz_{h1}dz_{h2}d^2\mathbf{q}_T d\cos\theta} = \frac{N_c \pi \alpha_{\text{em}}^2}{2Q^2} z_{h1}^2 z_{h2}^2 \left[ (1 + \cos^2\theta) F_{UU} + \sin^2\theta \cos(2\phi_0) F_{UU}^{\cos 2\phi_0} \right]. \quad (2.195)$$

As illustrated in Fig. 2.17, the transverse momentum  $\mathbf{P}_{h\perp}$  is defined as the component of  $P_{h1}$  transverse to  $P_{h2}$ , its azimuthal angle  $\phi_0$  is measured relative to the lepton plane, and  $\theta$  is the polar angle between the hadron  $h_2$  and the  $e^+e^-$  beam.

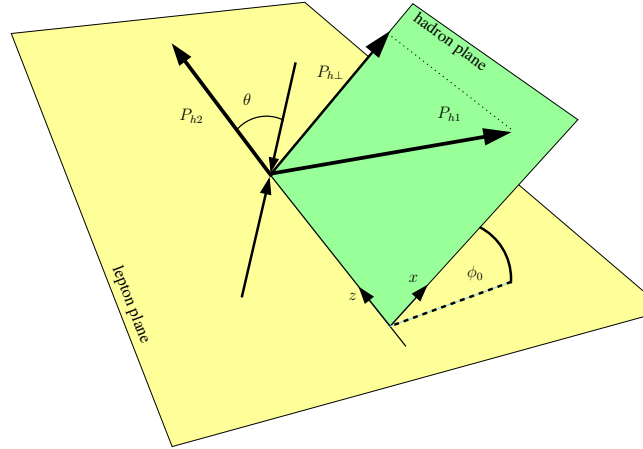


Figure 2.17:  $e^+ + e^- \rightarrow h_1 + h_2 + X$  process in the frame of method (2). The figure is from [209].

Here the structure function  $F_{UU}$  is a convolution of unpolarized TMD fragmentation functions for a quark and an anti-quark, and the polarized structure function  $F_{UU}^{\cos 2\phi}$  is a convolution of Collins fragmentation functions for a quark and an anti-quark.

$$\begin{aligned} F_{UU} &= C_{ee}[D_1 \bar{D}_1], \\ F_{UU}^{\cos 2\phi} &= -C_{ee} \left[ \frac{2(\hat{h} \cdot \mathbf{k}_{T1})(\hat{h} \cdot \mathbf{k}_{T2}) - \mathbf{k}_{T1} \cdot \mathbf{k}_{T2}}{z_{h1} z_{h2} M_{h1} M_{h2}} H_1^\perp \bar{H}_1^\perp \right] \end{aligned} \quad (2.196)$$

where the operation  $C_{ee}$  is defined by

$$\begin{aligned} C_{ee} \left[ w(k_{T1}, k_{T2}) D_1 \bar{D}_2 \right] &= \sum_q e_q^2 \mathcal{H}_{q\bar{q}}(Q^2, \mu) \int \frac{d^2 \mathbf{k}_{T1}}{z_{h1}^2} \frac{d^2 \mathbf{k}_{T2}}{z_{h2}^2} \delta^{(2)} \left( -\frac{\mathbf{k}_{T1}}{z_{h1}} - \frac{\mathbf{k}_{T2}}{z_{h2}} - \mathbf{q}_T \right) w(k_{T1}, k_{T2}) \\ &\times \left[ D_1^{h_1/q}(z_{h1}, k_{T1}, \mu, \zeta_1) D_2^{h_2/\bar{q}}(z_{h2}, k_{T2}, \mu, \zeta_2) + D_1^{h_1/\bar{q}}(z_{h1}, k_{T1}, \mu, \zeta_1) D_2^{h_2/q}(z_{h2}, k_{T2}, \mu, \zeta_2) \right]. \end{aligned} \quad (2.197)$$

so that

$$\begin{aligned} F_{UU}(z_{h1}, z_{h2}, q_T, Q^2) &= \mathcal{B}[\tilde{D}_1^{(0)} \tilde{\bar{D}}_1^{(0)}], \\ F_{UU}^{\cos 2\phi_0}(z_{h1}, z_{h2}, q_T, Q^2) &= -M_{h1} M_{h2} \mathcal{B}[\tilde{H}_1^{\perp(1)} \tilde{\bar{H}}_1^{\perp(1)}], \end{aligned} \quad (2.198)$$

where

$$\begin{aligned} \mathcal{B}[\tilde{D}_1^{(n)} \tilde{\bar{D}}_2^{(m)}] &\equiv \sum_a e_a^2 \mathcal{H}^{(e^+ e^-)}(Q, \mu_Q) \int_0^\infty \frac{db_T b_T}{2\pi} b_T^{n+m} J_{n+m}(q_T b_T) \\ &\times \left( \tilde{D}_1^{(n)\bar{a}}(z_{h1}, b_T, \mu, \zeta_1) \tilde{D}_2^{(m)a}(z_{h2}, b_T, \mu, \zeta_2) + \tilde{D}_1^{(n)a}(z_{h1}, b_T, \mu, \zeta_1) \tilde{D}_2^{(m)\bar{a}}(z_{h2}, b_T, \mu, \zeta_2) \right). \end{aligned} \quad (2.199)$$

## 2.11.5 TMD cross sections for other processes

In this chapter we have discussed TMD PDFs which describe the distribution of light partons (up, down, and strange, which can be treated as massless) within an initial state hadron and TMD FFs which describe the hadronization of a light parton to a final state hadron. The simplest and most frequently considered cross sections that are sensitive to these TMD distributions have been described in Secs. 2.11.1 to 2.11.4. These distributions will be the focus of the next several chapters of the handbook.

In particular, note that we will discuss phenomenology of TMD PDFs and FFs in Chapter 5. We discuss in detail unpolarised observables both for SIDIS in Sec. 5.2.1 and DY in Sec. 5.2.2. In Sec. 5.3, Sec. 5.4, and Sec. 5.5 we will discuss the progress in understanding polarised TMDs from SIDIS, DY and  $e^+e^-$  data. We will discuss observables in proton-proton scattering in twist-3 formalism in Sec. 5.3.3. Observables and corresponding cross-sections for gluon TMDs will be considered in Sec. 5.6.

Beginning in Chapter 9 we will discuss important generalizations involving heavy quarks (typically charm or bottom quarks) and final states involving jets. Jets are collimated showers of energetic hadrons that are frequently observed in high energy collisions. The concept of jets and some of the algorithms that are used to define them are discussed in Chapter 9. Sec. 9.1 shows how cross sections with final state jets can be used to extract TMD PDFs. Jet fragmentation and substructure involving the measurement of an identified hadron and its momentum transverse to the jet axis is an important new application of the TMD formalism and is discussed in Sec. 9.2. Applications to the theory of the production of heavy quarkonium (bound states of heavy quarks and antiquarks) are the subject of Sec. 9.5. Transverse energy-energy correlations, which provide a new method to study TMD dynamics, are described in Sec. 9.6. Sec. 9.7 discusses the medium modification of jets, which requires the TMD formalism, and can be used to probe both cold nuclear matter as well as the quark gluon plasma.

# 3 - Factorization Theorems

## 3.1 Factorization Basics

Ultimately, intuitive partonic pictures (like many of those discussed in the Introduction) need to be justified or derived in real QCD. The challenge is that borders separating effects that are genuinely intrinsic to bound-state particles (the hadrons) from effects specific to the interactions between them is ambiguous in relativistic quantum field theories like QCD. In QCD, the notion of a parton as a nearly freely propagating point-like quantum of the quark or gluon field is most meaningful in contexts where asymptotic freedom applies. To put partonic intuition on a firm theoretical footing, therefore, it is important to be able to isolate a short-distance part of an interaction and calculate it with small-coupling techniques, independently of non-perturbative details of physics at large distance scales. Complications can arise because actual physical processes generally involve a complicated interplay between large-distance, non-perturbative dynamics and short-distance, process-specific dynamics. For maintaining predictive power it is necessary, if possible, to factor these different categories of QCD physics into pieces that can be calculated and interpreted independently, and then to reassemble them into calculations of physical observables. This is what QCD factorization theorems aim to do.

Factorization theorems have many important practical consequences. For instance, they constrain the possible definitions of parton densities and similar non-perturbative objects, and they ultimately lead to the evolution equations that relate objects at different scales. Below we will summarize some of the main issues that must be confronted in a factorization derivation generally, with a focus on aspects specific to TMD factorization.

For the majority of this chapter, including Secs. 3.2-3.4, we follow the CSS methods for deriving factorization, as in Refs. [10, 63, 86, 89], since this provides foundational and complete results for factorization proofs. In Sec. 3.5 we discuss factorization and factorization violation from the point of view of SCET following Ref. [214], and also make direct correspondences between ingredients in the CSS and SCET formalisms.

It should be understood that the discussion of factorization in this section is only an outline, and many important subtleties can not be discussed in the limited space of a handbook. There remain many open questions related to understanding the applications, limits, and interpretation of factorization theorems, especially for processes with sensitivity to the details of hadron structure or non-perturbative effects.

## 3.2 Elements of Factorization

The starting point for deriving factorization is a study of the asymptotic behavior in general graphical structures at arbitrary order in perturbation theory as some particular hard scale (we will always call it  $Q$ ) approaches infinity. In principle, this needs to be done separately for different processes, and the details of a specific process can be important, as will be discussed in more detail below. The factorization derivation for Drell-Yan scattering (already analyzed in detail in Chapter 2) is a prototypical example, and we will continue to refer to it for illustrative purposes. For Drell-Yan scattering, the hard scattering scale  $Q$  is the invariant mass of the produced lepton-antilepton pair. For definiteness, let us assume that the cross section is differential in the transverse momentum  $q_T$  of the produced dilepton pair, and we will further

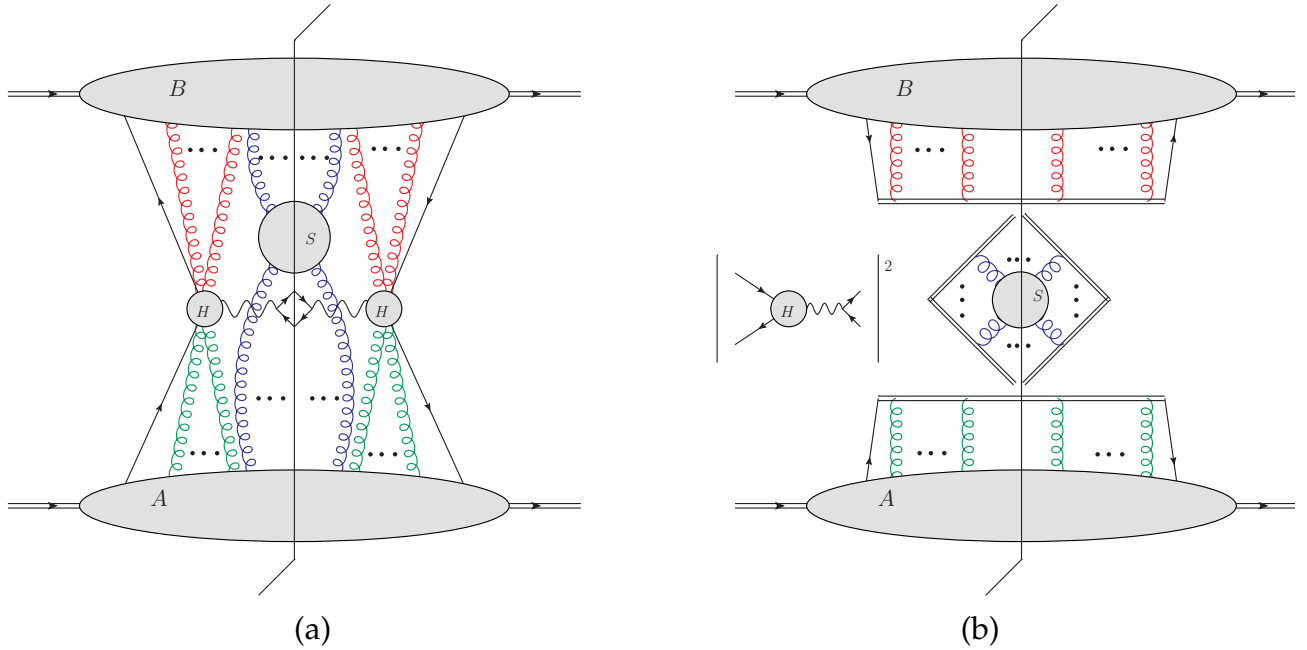


Figure 3.1: (a) Graphical structure corresponding to leading regions in Drell-Yan scattering, before factorization. Green gluons are collinear to lines in the  $A$ -blob, red gluons are collinear to lines in the  $B$ -blob, and blue gluons have nearly zero momentum (soft). (b) Separation into hard, soft, and collinear parts after approximations and Ward identities—see Sec. 3.2.5.

assume that  $q_T \sim \Lambda_{QCD}$  so that the relevant factorization is TMD factorization with sensitivity to non-perturbative hadron structure. The basic steps for deriving the factorization formula in the large  $Q$  limit, both for the Drell-Yan example and for those other processes for which factorization theorems exist, can be summarized according to the following steps:

### 3.2.1 Region analysis

For an arbitrary Feynman graph contributing to a specific process, certain configurations of internal momentum for internal parton lines dominate in the asymptotically large  $Q$  limit. The first step, then, is to identify and catalogue all these “leading regions.” A systematic approach to region analysis was developed by Libby and Sterman [215], (also see [10, Chapter 5]), and its key ideas are that: i.) there is a correspondence between mass divergences in Feynman graphs and their  $Q \rightarrow \infty$  asymptotes and ii.) the mass divergences correspond to surfaces in the higher dimensional space of the momentum of all lines in a general graph that are trapped between propagator poles. These “pinched singular surfaces” (PSSs) can not be deformed away from the poles that trap them. In the Libby-Sterman approach, the identification and characterization of PSSs becomes a largely geometric problem, and they are often summarized in graphical form as in Fig. 3.1(a) for Drell-Yan scattering at small transverse momentum for the produced lepton pair. The  $H$  blobs contain lines that are off shell by at least order  $Q$ , while the  $A$  and  $B$  blobs contain parton lines that are collinear to one or the other incoming hadron momentum. The  $S$  blob represents lines with nearly zero momenta in the center-of-mass system. The gluon lines shown attaching  $A$  and  $B$  to  $H$  represent gluons collinear to  $A$  and  $B$  respectively and attaching to the interior lines of  $H$ . The gluon lines attaching  $S$  to  $A$  and

Leading regions	Momentum scaling	CSS QFT blobs	SCET objects
Hard	$p^2 \gg Q^2 \lambda^2$	$H$	offshell, $C$
Collinear-a	$p^\mu \sim Q(\lambda^2, \lambda^0, \lambda)$	$A$	$\xi_{n_a}, A_{n_a}^\mu$
Collinear-b	$p^\mu \sim Q(\lambda^0, \lambda, \lambda)$	$B$	$\xi_{n_b}, A_{n_b}^\mu$
Soft	$p^\mu \sim Q(\lambda, \lambda, \lambda)$	$S$	$\psi_s, A_s^\mu$
Glauber	$p^+ p^- \ll \mathbf{p}_\perp^2 \sim Q^2 \lambda^2$		offshell, $\mathcal{L}_G^{(0)}$

Table 3.1: Summary of the leading momentum regions for the classic TMD observables (Drell-Yan, SIDIS, and back-to-back hadron production in  $e^+e^-$ ) and their corresponding QFT blobs in the CSS formalism and objects in SCET. Matrix elements of the SCET fields in the last column yield functions equivalent to the evaluation of the final  $A, B, S$  blobs in CSS. In the momentum scaling column the parentheses refer to  $(p^+, p^-, p_\perp)$  components, and  $\lambda \ll 1$  is a small expansion parameter.

$B$  are soft, having nearly zero momentum in the center-of-mass system. To summarize, an arbitrary Feynman graph contributing at leading power in  $\Lambda_{QCD}/Q$  to Drell-Yan scattering at low  $q_T$  matches the structure of Fig. 3.1(a) if it contributes to a PSS. The leading regions for TMD factorization of classic processes are summarized in Table 3.1.

It needs to be emphasized that, while Fig. 3.1(a) corresponds to a mass divergence, the lines in actual Feynman graphs are integrated over all momenta. Therefore, different regions can overlap in non-trivial ways, and this creates additional work in the factorization derivation. Ultimately, however, the  $H$  subgraphs will correspond roughly to hard factors, and the  $A, B$ , and  $S$  factors will be factored away. The extra gluon lines shown entangling the  $H, A, B$ , and  $S$  blobs represent additional collinear-to- $A$  (green) and collinear-to- $B$  (red) gluon lines that can attach inside  $H$ , as well as soft lines (blue) that can attach inside both collinear  $A$  and  $B$  blobs. These “extra” lines also indicate that more work is needed before factorization is achieved.

### 3.2.2 Approximations

Identifying the graphical structures that contribute to leading regions does not immediately produce factorization, but it does suggest the necessary approximations. Within each leading region, a specific power-law expansion in  $1/Q$  applies, giving region-specific approximations. These approximations allow the internal kinematics of different parts of a graph to be disentangled. (Note that, without approximations, all components of a parton’s four-momentum can flow through both  $A$  and  $B$  in 3.1(a)). The exact details of the physical observable under consideration generally play a role in determining which power-law approximations are applicable. In the Drell-Yan example with  $q_T \sim \Lambda_{QCD}$ , for instance, the power-law expansion includes an expansion in powers of  $q_T/Q$ . If instead  $q_T \sim Q$ , a different expansion applies.

These approximations allow the “extra” gluon attachments to  $H$  in 3.1(a), which appear at first to spoil factorizability, be identified with eikonal attachments, after application of Ward identities. Ultimately, the eikonal attachments are to be identified with Wilson line operators in soft and collinear factors.

As an example, consider the single gluon connecting the  $A^\mu$  and  $B^\nu$  blobs via the  $S^{\mu\nu}$  blob in Fig. 3.2(a), where the  $\mu$  and  $\nu$  are the Lorentz indices associated with the gluon coupling.

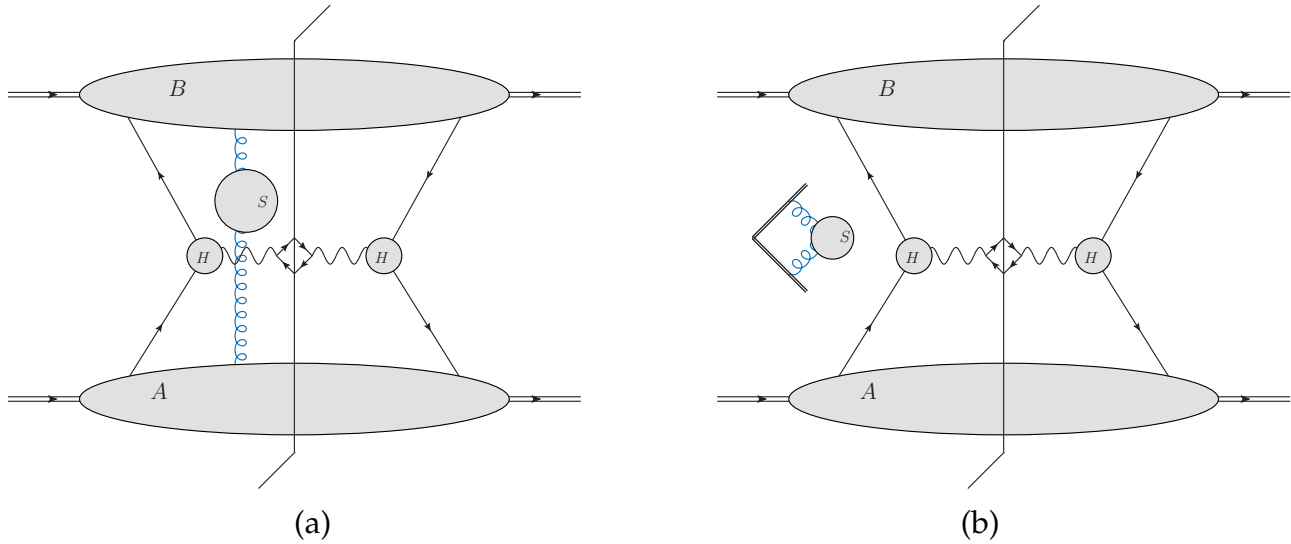


Figure 3.2: Example of a soft gluon being factorized. See Eq. (3.2).

Assume the momentum carried by this gluon is soft In the center of mass system,  $l \sim (0, 0, \mathbf{0}_T)$ . Also, in the center of mass frame  $A^+$  and  $B^-$  are the largest components of the collinear blobs. So the contraction of factors in the integrand has the leading behavior:

$$A^\mu B^\nu S_{\mu\nu} \approx A^+ B^- S^{+-}, \quad (3.1)$$

with errors being power suppressed. There are further simplifications if we multiply by 1 by including a factor of  $(l^+ l^-)/(l^+ l^-)$ . Then,

$$A^\mu B^\nu S_{\mu\nu} \approx A^+ l^- B^- l^+ \frac{S^{+-}}{(l^+ + i\epsilon)(l^- - i\epsilon)} \approx A^\mu l_\mu B^\nu l_\nu \frac{n_{b,\mu} n_{a,\nu} S^{\mu\nu}}{(l^+ + i\epsilon)(l^- - i\epsilon)}. \quad (3.2)$$

Here  $n_a$  and  $n_b$  are the auxiliary vectors defined in Chapter 2, Eqs. 2.19. Note that after the second  $\approx$ , we have had to assume that all components of  $l^\mu$  are of comparable size, and we have inserted the  $\pm i\epsilon$  in the denominator without comment. These steps will be discussed more below. Now that  $l$  four-momenta are contracted exactly with  $A^\mu$  and  $B^\nu$ , Ward identities reduce  $l_\mu A^\mu$  and  $l_\nu B^\nu$  to simple blobs independent of any “extra” external gluon momentum. The only memory of the soft gluon is in the last factor involving the “eikonal” propagators  $1/(l^+ + i\epsilon)$  and  $1/(l^- - i\epsilon)$ , and all of this has been factored away from the rest of the graph. These last factors are denoted by the  $S$  blob with the double lines in Fig. 3.2(b).

(Note carefully that none of the momentum integrals, including the integrals over  $l$  components, have been made explicit in (3.2).)

### 3.2.3 The Glauber region

One relies on the sorts of approximations discussed in the last subsection to convert extra gluon attachments into eikonal lines when the gluons are collinear or soft. In cases where they are soft, there is also a requirement that the longitudinal components are not small relative to the transverse components. If a soft gluon momentum  $l$  is pinched in a region where  $|l^+ l^-| \ll |l_\perp|^2$ , then it is said to be trapped in the “Glauber region.” (Note that multiple Glauber

gluon interactions between spectator remnants are reminiscent of the multiple nucleon interactions that give rise to shadowing in the classic Glauber model [216] of high energy nuclear scattering.) Glauber gluons create complications for factorization derivations because, when a gluon is pinched in the Glauber region, the Ward identities that would normally disentangle it from  $A$  or  $B$ , as in the example of 3.2 do not apply. If  $l^+$  or  $l^-$  is small relative to  $l_T$ , the approximation in the last  $\approx$  of Eq. (3.2) fails.

In processes like semi-inclusive deep inelastic scattering, with at most one hadron in the initial state, the Glauber region can be avoided by an appropriate choice of integration contours. This is related to the choice of  $\pm i\epsilon$  in Eq. (3.2). In hadron-hadron collisions, the situation is more complicated, and the importance of Glauber gluons depends on the details of the process. In Drell-Yan scattering, there are in fact Glauber pinches graph by graph. The solution to the Glauber gluon problem for more complicated processes like Drell-Yan scattering is discussed below.

### 3.2.4 Inclusivity of processes

The kinds of factorization theorems that emerge (or fail to emerge) from a derivation are sensitive to the level of inclusivity of the process under consideration. The above Drell-Yan example includes a sum over all final states, excluding the momentum of the lepton pair. This ultimately leads to the cancellation of the Glauber pinches discussed above, and so is critical to the derivation. (Useful reviews of this cancellation can be found in [10, Chs.14.3-14.5], and see also [217] and the introduction to [90].)

### 3.2.5 Last steps

After the cancellation of Glauber poles, the approximations discussed in Sec. 3.2.2 can finally be applied, and a cross section separates into factors. This step is often represented graphically as in Fig. 3.1(b). The double lines with gluon attachments represent Wilson line operators in hadronic matrix elements for  $A$  and  $B$  and for a vacuum matrix element for  $S$ . To finalize the factorization derivation, the overlap of momentum in integrals from one region to another need to be accounted for. The important aspects of the final form of factorization are that the hard part be calculable to fixed order in perturbative QCD, while the non-perturbative factors should be identifiable with interpretable matrix elements like PDFs. In Fig. 3.1(b), the separate soft factor connecting  $A$  and  $B$  is awkward for a TMD factorization formula, and the formulas for Fig. 3.1(b) generally include an array of arbitrary cutoffs. For this and other reasons, there is generally still room for refinement and optimization, which has led to a lot of work on this topic. These topics go beyond the scope of this section, and are largely the topic of Chapter 2.

## 3.3 Process Dependence

Even when there are no Glauber pinches in a process, the necessity to avoid the Glauber region places constraints on the types of contour deformations that can be used to derive factorization, and this translates into constraints on the Wilson lines that can be used to define TMD PDFs. As a consequence, there can be interesting instances of non-trivial process dependence. The most well-known case of this is the Sivers function in Drell-Yan scattering (at small  $q_T$ ) and SIDIS. The gluon attachments that ultimately correspond to Wilson lines require contour deformations in opposite directions in the complex plane to avoid the Glauber region. The end result is a future-pointing Wilson line in the TMD PDF for SIDIS and a past-pointing

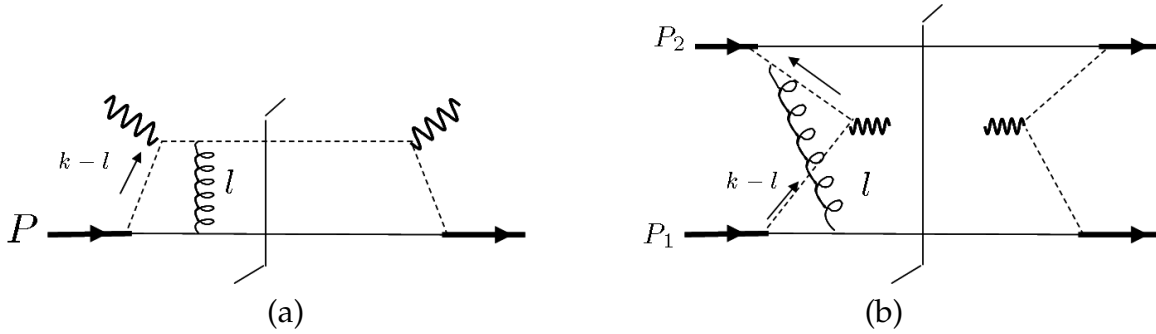


Figure 3.3: A single “extra” gluon attachment as it appears in (a) SIDIS and (b) the Drell-Yan process. (Figures taken from [224].)

Wilson line for TMD PDFs in Drell-Yan scattering. The different directions for the Wilson lines amounts to an overall minus sign change for the Sivers function when comparing Drell-Yan scattering and SIDIS. See Secs. 2.7.1 and 2.7.2 for further details.

### 3.4 Factorization Violations

Factorization can be violated for a number of reasons. Since the derivations are based on power-law expansions in ratios of invariant scales (e.g.,  $\Lambda_{\text{QCD}}/Q$  or  $q_T/Q$ ), then factorization can fail if hard scales like  $Q$  become too small and power corrections are important or the power expansion fails outright. Understanding quantitatively which combinations of scales allow for the safe application of particular factorization theorems is an important practical task, especially given that many of the experiments designed to probe hadronic structure correspond to rather small  $Q$ . Much research remains to be done in this area.

Particularly interesting cases of factorization breaking occur when final states are made too exclusive, so that Glauber gluons fail to cancel. This can lead to very large phenomenological consequences, as in diffractive hard scattering [218–221]. In hadron-hadron collisions with measured transverse momentum for hadrons in the final state, the contour deformations analogous to those discussed above in Sec. 3.3 that avoid the Glauber region do not lead to separate Wilson lines for separate TMD PDFs or fragmentation functions [222, 223]. Instead of a simple sign change for a single TMD PDF, the process dependence involves the details of the whole process.

This type of factorization breaking and/or process dependence arises from complications in the Ward identity arguments needed to separate long-distance interactions into gauge invariant correlation functions with appropriate Wilson line structures. The sign dependence of the Sivers function, for example, can be understood at the level of Feynman graphs by noting that the extra collinear gluon attachments that result in a Wilson line attached to a quark coming in from the distant past in the case of Drell-Yan scattering while they attach to an outgoing quark in the SIDIS case. (See Fig. 3.3). The fact that attachments are to an *incoming* line in the Drell-Yan process is critical in determining the shape of the Wilson line in (2.39). In the case of SIDIS, the same Wilson line is used, but pointing in the “+”-infinity rather than the “-”-infinity directions. In much of the original work on process dependence, the Wilson line in a TMD PDF definition was therefore notated with a “[+]” or “[−]” superscript to indicate which direction was relevant to a particular process [73]. The quantum-mechanical

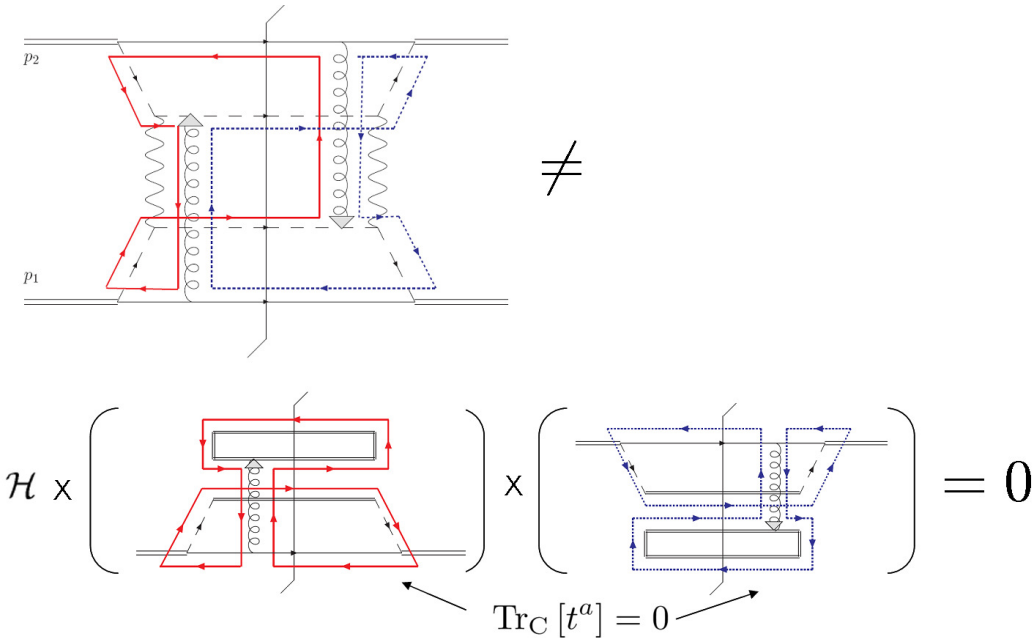


Figure 3.4: A visualization of the failure of color flow to factorize into independent Wilson line structures for separate hadrons in a process involving color in both the initial and final states of the hard part. The Wilson loop structures in the second line vanish due to the traceless single color matrices. (Figure taken from Ref. [224].)

phase of the quark wavefunction is shifted in an opposite way depending on whether the quark propagates in from the distant past or out to the distance future—see [81] for an optical analogy.

One notes that it is the direction of flow of the color charge (incoming or outgoing) that determines the Wilson line direction, and this suggests that factorization theorems for more complicated TMD processes can be constructed, with increasingly complex Wilson line structures for the TMD correlation functions [76]. However, this tends to fail for somewhat interesting reasons [225] that can be visualized in the Feynman diagram shown in Fig. 3.4. There, two hadrons collide and a colorless particle is exchanged in the hard part. The graph before factorization is nonzero, but after factorization, the only possible Wilson line structure for each PDF is a Wilson loop. With a single gluon attachment, however, each Wilson loop gives a factor of zero. The right side of the graph thus fails to reproduce the non-vanishing unfactorized graph. In other words, the quantum-mechanical phase shift associated with extra collinear gluon attachments is a consequence of the presence of *both* hadrons simultaneously, and not a simple sum of Wilson line phase shifts associated with each hadron. (This captures the essence of the problem with color flow arguments, though more details are needed to show that it represents an unavoidable problem for factorization—see, for example, Ref. [225].)

### 3.5 Factorization in SCET

In the SCET [92–95, 124] approach to factorization, an effective field theory is set up with fields that describe the infrared momentum regions of QCD, which typically have either collinear or soft scaling. The effective Lagrangian encodes self interactions of these fields,

as well as their interaction with each other and with the hard region of momentum space encoded in Wilson coefficients.

For the classic TMD processes described in Sec. 2.11 the relevant modes are soft,  $n_a$ -collinear, and  $n_b$ -collinear, in one-to-one correspondence with the regions  $S$ ,  $A$ , and  $B$  discussed in Sec. 3.2.1. Indeed, although the formal setup is different, there is a close parallel between many items appearing in the CSS formalism and SCET formalism. In our brief review of factorization in SCET we will highlight these parallels. The relevant SCET Lagrangian for TMD observables involving at most two energetic jets or hadrons is

$$\mathcal{L} = \mathcal{L}_{n_a}^{(0)} + \mathcal{L}_{n_b}^{(0)} + \mathcal{L}_S^{(0)} + \mathcal{L}_{\text{hard}}^{(0)} + \mathcal{L}_G^{(0)} + \mathcal{O}(\lambda), \quad (3.3)$$

where  $\lambda \sim q_T/Q \ll 1$  is the TMD power counting parameter, and only leading power terms are kept for the discussion here as denoted by the superscripts (0). The term  $\mathcal{L}_{n_a}^{(0)}$  describes interactions between  $n_a$ -collinear quark and gluon fields describing momenta with the scaling  $(n_a \cdot p, n_b \cdot p, p_\perp) \sim Q(\lambda^2, 1, \lambda)$ ,  $\mathcal{L}_{n_b}^{(0)}$  does the same for  $n_b$ -collinear fields where  $(n_b \cdot p, n_a \cdot p, p_\perp) \sim Q(\lambda^2, 1, \lambda)$ , and  $\mathcal{L}_S^{(0)}$  describes interactions between soft quark and gluon fields with momenta scaling as  $p^\mu \sim Q\lambda$ . Each of the Lagrangians  $\mathcal{L}_{n_a}^{(0)}$ ,  $\mathcal{L}_{n_b}^{(0)}$ , and  $\mathcal{L}_S^{(0)}$  is equivalent to a copy of the QCD Lagrangian for its fields, up to the fact that the fields are setup so that they induce subtractions that enable them to correctly capture their momentum region while avoiding double counting of other infrared regions [107]. In SCET these induced subtractions are referred to as zero-bin contributions, while in the CSS approach they are referred to as soft subtractions. In SCET for TMDs the leading power interactions between modes in different momentum regions are entirely contained in the Lagrangians  $\mathcal{L}_{\text{hard}}^{(0)}$  and  $\mathcal{L}_G^{(0)}$ , which describe the offshell short-distance hard scattering process and offshell long-distance Glauber interactions respectively. A summary of the way that the leading momentum regions for classic TMD observables are described by objects in SCET is given in Table 3.1.

For TMD cross sections in Drell-Yan, SIDIS, or back-to-back hadron production in  $e^+e^-$  collisions, the QCD current  $\bar{\psi}\Gamma\psi$  is matched onto SCET to obtain a leading power hard interaction which involves a quark current with Wilson lines

$$\mathcal{L}_{\text{hard}}^{(0)} = \int d\omega_a d\omega_b C^{(0)}(\omega_a, \omega_b) \bar{\chi}_{n_a, \omega_a} \Gamma(S_{n_a}^\dagger S_{n_b}) \chi_{n_b, \omega_b}. \quad (3.4)$$

Here the  $n_a$ -collinear field  $\chi_{n_a, \omega_a} = \delta(\omega_a - i n_b \cdot \partial)(W_{n_a}^\dagger [n_b \cdot A_{n_a}] \xi_{n_a})$  involves a quark field  $\xi_{n_a}$  attached to a Wilson line built from collinear gluon fields  $A_{n_a}$  that extends to infinity in the direction  $n_b$ , and this product of fields has minus-momentum  $\omega_a$ . The description is then directly analogous for  $\chi_{n_b, \omega_b}$ . For intuition these  $\chi_{n_a, \omega_a}$  fields are the closest possible analog of fields for partons in the parton model. From the SCET point of view, the presence of the Wilson lines is necessary in order to satisfy the full structure of gauge transformations allowed in this effective theory. The  $S_{n_a}[n_a \cdot A_s]$  and  $S_{n_b}[n_b \cdot A_s]$  in Eq. (3.4) are Wilson lines involving soft gluon fields  $A_s$ . They describe the fact that soft interactions with an energetic color source in direction  $n$  and a given overall color representation are described by a Wilson line in this representation along  $n$ . These soft Wilson lines encode the eikonal soft interactions, as discussed for CSS in Sec. 3.2.2. Finally the Wilson coefficient  $C^{(0)}$  encodes contributions from the hard momentum region. The SCET hard scattering Lagrangian in Eq. (3.4) is derived

by integrating out off-shell momentum regions with  $p^2 \gg \lambda^2$ , which is done to all orders in perturbation theory. Integrating out hard fluctuations with  $p^2 \sim Q^2$  and hard-collinear fluctuations with  $p^2 \sim Q^2\lambda$  leads to the  $W_{n_a}, W_{n_b}, S_{n_a}, S_{n_b}$  Wilson lines and the hard Wilson coefficient  $C^{(0)}$ . The structure of the resulting terms is also constrained by gauge symmetries of the effective theory. Since the hard interaction Lagrangian encodes the coupling to the leptonic currents, it is always included perturbatively, namely once for each hard interaction.

In SCET all interactions that can potentially spoil factorization are encoded in the Glauber Lagrangian  $\mathcal{L}_G^{(0)}$ , whose detailed form can be found in Ref. [214]. It contains leading power long-distance interactions between both  $n_a$ - $n_b$ -soft,  $n_a$ -soft, and  $n_b$ -soft modes, all of which are forward scattering in nature with  $1/p_\perp^2$  type potentials. Since insertions of this Lagrangian are not suppressed it can be inserted an arbitrary number of times at leading power, and these interactions have the potential to spoil factorization since they recouple collinear and soft regions in a non-trivial manner. Thus the influence of  $\mathcal{L}_G^{(0)}$  must be shown to be either of a form which can be absorbed into a soft or collinear matrix element, or to fully cancel out. In SCET both the soft and collinear Wilson lines along a direction  $n_i$  can be chosen to extend either from  $-\infty n_i^\mu + x^\mu$  to  $x^\mu$ , or from  $x^\mu$  to  $x^\mu + \infty n_i^\mu$ . This affects the signs  $\pm i\epsilon$  of eikonal propagators like those shown in Eq. (3.2). In SCET the subtractions from the Glauber region guarantee that results are independent of this choice. However, sometimes the only non-trivial impact of the Glauber region is to influence the direction of collinear and soft Wilson lines, and in that case their effects can be absorbed into collinear and soft matrix elements with precisely specified Wilson line directions.<sup>14</sup> For TMD factorization both occur, the cancellation of certain  $\mathcal{L}_G^{(0)}$  contributions and the absorption of other  $\mathcal{L}_G^{(0)}$  effects. In particular, Glauber interactions between so-called active partons can be absorbed into the direction of soft Wilson lines, forcing them to extend out to either  $+\infty$  or  $-\infty$ , while analogously the interactions between active and spectator partons can be absorbed into the direction of the collinear Wilson lines [214]. In the CSS formalism the same result is obtained but in a different manner, since the Glauber and soft regions are not separated from the start. Instead certain propagators are left in a form that can handle simultaneously the Glauber and soft contributions. The results for collinear and soft regions are determined by contour deformations that are done to put these contributions in the collinear and soft regions (that end up in their matrix elements), and expansions are carried out at this point. These contour deformations are done in order to avoid the Glauber region when possible. Finally, there are spectator-spectator Glauber interactions which cancel out due to unitarity and the inclusive sum over hadronic states in TMD observables, which has been worked out in detail in CSS [10, 88] and also occurs in SCET [226]. See Sec. 3.2.3 for further discussion in context of CSS. With these considerations in hand,  $\mathcal{L}_G^{(0)}$  can be dropped for the remaining analysis of TMD factorization in SCET.

To derive the form of the TMD factorization, for example for Drell-Yan  $pp \rightarrow X\ell^+\ell^-$ , one considers the hadronic matrix elements  $\langle p | \mathcal{L}_{\text{hard}}^{(0)\dagger} | X \rangle \langle X | \mathcal{L}_{\text{hard}}^{(0)} | p \rangle$ . Since the decoupled Lagrangians  $\mathcal{L}_{n_a}^{(0)}, \mathcal{L}_{n_b}^{(0)}$ , and  $\mathcal{L}_S^{(0)}$  enter as a direct sum, the state  $|X\rangle$  can be factorized into soft and collinear components and the dynamics of the soft and collinear matrix elements factorizes. Finally Eq. (3.4) involves a simple product of fields from the different sectors. This

<sup>14</sup>Technically this amounts to simultaneously not considering certain Glauber interactions, nor corresponding soft and collinear Glauber-region subtractions. These are in 1-to-1 correspondence, such that the sum of the direct Glauber interactions and Glauber-region subtractions give zero.

enables the cross section to be factorized without relying on perturbation theory, leading to the TMD factorization theorems discussed in Sec. 2.11. The  $n_a$ -collinear quark fields and Wilson lines lead to the operators with the staple-shaped path giving the bare beam function  $\tilde{B}_{i/p}^0$ , with another  $\tilde{B}_{\bar{i}/p}^0$  from the  $n_b$ -collinear sector, while the soft Wilson lines give the soft function  $\tilde{S}_{n_a n_b}^0$ , which is the vacuum matrix element of the closed loop given in Eq. (2.38) and Fig. 2.1 (right panel). The beam functions can be further written as unsubtracted TMDPDFs and soft subtractions,  $\tilde{B}_{i/p}^0 = \tilde{f}_{i/p}^0 / \tilde{S}_{n_a n_b}^{0\text{subt}}$ , where  $\tilde{f}_{i/p}^0$  is given in Eq. (2.37) and Fig. 2.1 (left panel), and  $\tilde{S}_{n_a n_b}^{0\text{subt}}$  encodes the zero-bin subtractions which stop the unsubtracted TMDPDF matrix element from double counting the soft regime.

While this discussion is only at the broad outline level, and hence leaves out many of the details and subtleties associated with actually carrying out the derivation of the TMD factorization theorems (such as the rapidity regularization), it provides the basic picture of how the factorization comes about in SCET.

# 4 - Evolution and Resummation

## 4.1 Introduction

In this Handbook, in Chapters 2 and 3, we have introduced the theoretical tools to investigate hadrons as a dynamical system of quarks and gluons (partons) from QCD field theory in the context of TMD observables. In this chapter we continue this field theoretic treatment and cover the subject of TMD evolution. We will emphasize how the QCD definitions of TMDs, coupled with TMD factorization theorems yield the TMD evolution equations. We will review two general classes of approaches to TMD evolution. One class of approaches formulated more directly in traditional QCD, and another in the language of Effective Field Theory, i.e. Soft Collinear Effective Theory (SCET). In both, evolution of TMDs follows from the methods to regulate and define them as reviewed in Chapter 2.

Having established the QCD field theory definitions of the TMD PDFs that arise from the modern proofs of factorization [10, 40, 74, 75, 81, 99, 100, 103] we find that the TMDs depend on two auxiliary variables. One is the renormalization scale  $\mu$ , arising from renormalizing the UV divergence, which separates high and low energy or mass scales from one another. The second is the rapidity evolution scale,  $\nu$  or  $\zeta$ , associated with regulating rapidity divergences, separating soft and collinear momentum regions from one another. Thus, what is unique about TMD evolution is that it takes place in *two* dimensions, as opposed to one for usual collinear DGLAP evolution.

As we saw in Chapter 2 the interplay of these scales makes it possible to use QCD factorization to express TMD observables as a convolution of a hard scattering cross section and renormalized TMDs at leading power in the hard scale. We refer to this as the  $W$  term, Eq. (2.29). The requirement of independence of the  $W$  term on these regulator scales leads to renormalization group (RG) and *rapidity renormalization group* (RRG) evolution equations—the Collins-Soper (CS) equations—relating TMD PDFs and other ingredients at different scales.<sup>15</sup>

The solutions of the TMD evolution equations will generically lead to solutions for transverse position space (Fourier transform) TMD PDFs of the schematic form:

$$\tilde{f}_{i/P}(x, \mathbf{b}_T, \mu, \zeta) = \tilde{f}_{i/P}(x, \mathbf{b}_T, \mu_0, \zeta_0) U_{\text{RG}}(\mu_0, \mu; \zeta_0) V_{\text{RRG}}(\zeta_0, \zeta; b_T, \mu), \quad (4.1)$$

where  $U_{\text{RG}}$  evolves the TMD PDF from an energy/mass scale  $\mu_0$  to another scale  $\mu$ , and  $V_{\text{RRG}}$  evolves it from a rapidity scale  $\zeta_0$  to another scale  $\zeta$ . (See Fig. 4.1.) Explicit forms for these evolution kernels, and methods to obtain them, are the topic of the rest of this Chapter. Such evolution is essential to relate the TMD PDFs at a hadronic or low scale, to cross sections measured at large collision energies  $Q$ . In Chapter 5 the status of predictions and tests of the TMD formalism from phenomenological studies is covered. Central to the phenomenology of extracting TMDs from SIDIS, Drell-Yan, weak gauge boson production,  $e^+e^-$  annihilation into hadron pairs, including corresponding azimuthal and spin modulations of cross sections, is the implementation of TMD evolution. This technology provides much of the predictive power of TMD factorization.

<sup>15</sup>We note that the RRG encompasses a more general class of evolution that includes not only TMD evolution but also other types of evolution such as BFKL evolution [214, 227].

Another powerful consequence of evolution is the possibility to resum large logs of ratios of scales such as  $q_T/Q$ , or  $Qb_T$  that appear in the perturbative expansion of the  $W$  term. We review this connection here in this Chapter, in particular in Sec. 4.2. Before doing so, we present a short historical overview.

### 4.1.1 Historical overview

Much of the literature on TMD factorization and evolution was pioneered by Collins, Soper, and Sterman (CSS) [63, 86, 119], was expanded upon in recent years [10, 74, 83, 228], and further elaborated upon and extended in [65, 66, 89, 91]. It has also been cast in the framework of Soft Collinear Effective Theory (SCET) [92–95] by numerous authors [96–102]. For a relation of the different approaches to each other, see e.g. [103], and for a historical review on TMD PDFs we refer the reader to [89].

The CSS based construction of TMD PDFs satisfy the property of maximum universality [10, 122, 229], meaning that the same correlation functions appear in a large number of processes. This universality provides the predictive power of the TMD formalism. Modern treatments in SCET [96–102, 186] cast factorization and evolution in the framework of effective field theory and the matching and running of EFT operators and matrix elements, and have proven to be useful for obtaining higher order perturbative results for anomalous dimensions and resummed cross sections. The equivalence between various constructions which leads to a factorized cross section like Eq. (2.29) has been reviewed in Chapters 2 and 3.

We remark that it is somewhat common to refer loosely to the CSS formalism [10, 40, 46, 81] and its modern implementations [10, 74, 75, 99, 100] as a  $q_T$  resummation method. Resummation methods however, generally do not take into account the non-perturbative physics that becomes important in regimes where logarithms are so large that perturbative expansions break down and non-perturbative physics becomes relevant (see Sec. 4.2). However, TMD factorization formalisms exploit the renormalization group and the CS equation to calculate the cross section such that point by point in  $b_T, \forall b_T$  (and  $q_T$  via the Fourier transform) asymptotic freedom is exploited to maintain a small  $\alpha_s$  and a valid perturbative expansion in the hard scattering cross section. These methods are more powerful than resummation methods since they constitute a true TMD factorization formalism using a pQCD perturbation expansion for all  $b_T$ , even well into the non-perturbative large  $b_T$  region [63] where details of hadron structure become important. We will review this approach and its correspondence to the SCET formulation in Sec. 4.3.

Below, we will review the derivation of the TMD evolution equations both from the “direct” QCD approaches like CSS, and from the EFT framework of SCET. Both routes to the evolution equations are ultimately equivalent, but highlight complementary aspects of TMD evolution and inspire various methods to obtain their explicit solutions.

Before delving into the details of TMD evolution equations and their solutions, we proceed next to an introductory discussion of resummation of large logarithms in perturbative expansions of TMD cross sections. We will concentrate on the Drell-Yan process Eq. (2.27) as the physical example connecting TMD PDFs to experiments, as the methods illustrated here easily carry over to other TMD processes.

## 4.2 TMD Evolution and Resummation

We emphasize, once again, evolution serves two primary purposes. The first is to relate the TMD PDFs themselves at nonperturbative scales to cross sections measured at large energies. The second equally important, is to provide a route to the summation of large perturbative logs appearing in the fixed-order expansions of TMD cross sections in QCD. The tools and approaches we review in this Chapter aim at achieving both purposes. The actual extraction, computation, or modeling of nonperturbative TMD PDFs are the focus of later Chapters, and we will dive into the technology of TMD evolution itself in the next Section. Before doing so, we take the opportunity in this Section to present a bit more general introduction to the connection between evolution and perturbative resummation, whose history of development and application in QCD is long and impressive.

The relation of Sudakov resummation to factorization was emphasized in the early works of [43, 86, 230, 231]. It was further developed and given a unified treatment in the work of [232], which derived the resummation of Sudakov logarithms from factorization properties of QCD cross sections and renormalization group evolution of the factorized contributions. This approach ties very naturally to the framework of effective field theories like SCET, which soon emerged, with their built-in tools of matching and running between scales.

Early work on resumming large logs in the context of evolution and transverse momentum factorization was carried out by Collins, Soper, and Sterman (the CSS approach) [16, 63, 86]. For early work on summation of large perturbative logs in the context of the transverse momentum distribution of the Drell-Yan cross section at moderate to high transverse momentum, see Refs. [233, 234], and for a review of the topic, see Refs. [235].

### 4.2.1 The goal of resummation

Let us introduce now the relation between evolution of TMD PDFs, or more generally of elements of a factorized cross section in QCD, and the resummation of large logs that arise in perturbative QCD predictions of cross sections that depend on more than one physical scale, separated by a hierarchy.

The large logs that appear in the perturbative expansion of the Drell-Yan cross section are in the “W-term” of Eq. (2.29), and are easiest to count in  $b_T$  space. Expressing the cross section,

$$\frac{d\sigma^W}{dQ dY d^2\mathbf{q}_T} = \int d^2\mathbf{b}_T e^{i\mathbf{b}_T \cdot \mathbf{q}_T} \tilde{\sigma}^W(\mathbf{b}_T), \quad (4.2)$$

for perturbative values of  $q_T \sim b_T^{-1} \gg \Lambda_{\text{QCD}}$ , we can schematically express the perturbative expansion of  $\tilde{\sigma}$  as

$$\begin{aligned} \tilde{\sigma}^W(\mathbf{b}_T) = f_i(x_1)f_j(x_2) & \left\{ 1 + \frac{\alpha_s}{4\pi} (c_{12}L_b^2 + c_{11}L_b + c_{10}) \right. \\ & + \left( \frac{\alpha_s}{4\pi} \right)^2 (c_{24}L_b^4 + c_{23}L_b^3 + c_{22}L_b^2 + c_{21}L_b + c_{20}) \\ & \left. + \left( \frac{\alpha_s}{4\pi} \right)^3 (c_{36}L_b^6 + c_{35}L_b^5 + c_{34}L_b^4 + c_{33}L_b^3 + c_{32}L_b^2 + c_{31}L_b + c_{30}) \right\} + \dots, \end{aligned} \quad (4.3)$$

where the ellipses indicate terms of higher order in  $\alpha_s$ , and where we suppress for the moment the scale dependence of PDFs and  $\alpha_s$  for our heuristic illustration here (but which are

accounted for in the methods described below). At every order, powers of  $\alpha_s^n$  are accompanied by logs of order up to  $L_b^{2n}$ , where  $L_b = \ln(Qb_T/b_0)$ , where  $b_0 = 2e^{-\gamma_E}$ . These logs become prohibitively large for  $b_T \gg 1/Q$  (equivalently,  $q_T \ll Q$ ). In this case the standard perturbative expansion in small  $\alpha_s \ll 1$  breaks down, thus requiring their resummation to all orders in  $\alpha_s$ , which requires predicting the coefficients  $c_{nm}$  systematically. It turns out to be much more straightforward and systematic to predict logs in the *logarithm* of the perturbative cross section Eq. (4.3):

$$\begin{aligned} \tilde{\sigma}^W(\mathbf{b}_T) = f_q(x_1)f_{\bar{q}}(x_2)C[\alpha_s] \exp & \left\{ \frac{\alpha_s}{4\pi} \left( d_{12}L_b^2 + d_{11}L_b \right) \right. \\ & + \left( \frac{\alpha_s}{4\pi} \right)^2 \left( d_{23}L_b^3 + d_{22}L_b^2 + d_{21}L_b \right) \\ & \left. + \left( \frac{\alpha_s}{4\pi} \right)^3 \left( d_{34}L_b^4 + d_{33}L_b^3 + d_{32}L_b^2 + d_{31}L_b \right) \right\} + \dots , \end{aligned} \quad (4.4)$$

LL      NLL    NNLL    N<sup>3</sup>LL

where  $C[\alpha_s]$  collects the constant coefficients:

$$C[\alpha_s] = 1 + \sum_{n=1}^{\infty} \left( \frac{\alpha_s}{4\pi} \right)^n C_n , \quad (4.5)$$

and the logs in Eq. (4.4) now organize themselves into exponentiated towers beginning with the leading log (LL) tower of terms  $\alpha_s^n L_b^{n+1}$ , then next-to-leading log (NLL)  $\alpha_s^n L_b^n$ , then NNLL  $\alpha_s^n L_b^{n-1}$ , etc. Heuristically, if one counts a large log as  $L_b \sim 1/\alpha_s$ , these towers correspond to terms of order  $1/\alpha_s$  (LL), order 1 (NLL), order  $\alpha_s$  (NNLL), etc. The constant coefficients  $C_n$  may be included according the same heuristic counting, or included to one higher order of accuracy, which is sometimes called “primed” counting [236, 237]. It is the coefficients  $d_{nm}$  that turn out to be most simply related to coefficients in the perturbative expansions of anomalous dimensions of objects in factorization theorems written in Chap. 2. Achieving resummation of each tower of logs requires knowing these anomalous dimensions in TMD evolution to appropriate orders, shown later in Table 4.2.

The logs in Eq. (4.4) arise from ratios of widely separated energy or rapidity scales that contribute to the Drell-Yan cross section. The power of factorization as reviewed in Chapters 2 and 3 is to separate the logs  $L_b$  into separate, single-scale contributions, e.g.

$$\ln^2(Qb_T) = \ln^2 \frac{\mu}{Q} + \left[ \ln^2(\mu b_T) + 2 \ln(\mu b_T) \ln \frac{\nu}{\mu} \right] - 2 \ln(\mu b_T) \ln \frac{\nu}{Q} , \quad (4.6)$$

where for illustration we have organized the logs into contributions to the double log that come from hard, soft, and beam functions in the factorized form of the cross section in Eq. (2.29b). The factorized logs are now of ratios of the arbitrary scale or rapidity boundaries  $\mu, \nu$  and physical scales  $Q$  or  $b_T$ . Logs of  $\mu/Q$  or  $\mu b_T$  are associated with regulation of UV divergences in hard functions and the TMD PDFs, at high and low scales  $Q$  and  $1/b_T$ . Logs of  $\nu/\mu$  and  $\nu/Q$  are associated with regulation of rapidity divergences and separation of collinear ( $\nu \sim Q$ ) and soft ( $\nu \sim \mu \sim 1/b_T$ ) degrees of freedom contributing to TMD PDFs. The evolution equations of TMD PDFs in these scales that we review in this Chapter admit solutions that take exponentiated forms that achieve the resummation of logs in Eq. (4.4).

## 4.2.2 A first glance at resummation from evolution

Before going into the full details of TMD evolution and resummation of all the logs in a TMD cross section in Sec. 4.3 we begin with a simplified discussion of scale evolution, focusing only on the single-scale hard function describing physics above the hard scale  $Q$ , to illustrate the basic idea of resummation from evolution. First, recall Eq. (2.29),

$$\frac{d\sigma^W}{dQ dY d^2\mathbf{q}_T} = \sum_{\text{flavors } i} H_{i\bar{i}}(Q^2, \mu) \int d^2\mathbf{b}_T e^{i\mathbf{b}_T \cdot \mathbf{q}_T} \tilde{f}_{i/p}(x_a, \mathbf{b}_T, \mu, \zeta_a) \tilde{f}_{\bar{i}/p}(x_b, \mathbf{b}_T, \mu, \zeta_b). \quad (4.7)$$

In the following, we will focus on the role of the UV renormalization scale  $\mu$ , while the evolution in the Collins-Soper scale  $\zeta_{a,b}$  is discussed below. A priori,  $\mu$  is completely arbitrary, and formally cancels exactly between the ingredients on the right-hand side. In practice, both the hard function and the TMD PDFs are known only at a certain (perturbative) order, and the choice of  $\mu$  becomes important. To understand how one chooses it in practice, let us inspect the first-order perturbative result of the hard function, which is given by

$$H_{i\bar{i}}(Q^2, \mu) = \delta_{i\bar{i}} \sigma_0 H(Q^2, \mu) \quad (4.8)$$

$$H(Q^2, \mu) = \left[ 1 + \frac{\alpha_s(\mu)}{4\pi} \left( -2\Gamma_0 \ln^2 \frac{Q}{\mu} - \gamma_0 \ln \frac{Q}{\mu} + H_1 \right) \right] + \mathcal{O}(\alpha_s^2).$$

Here,  $\sigma_0$  is the Born cross section,  $\Gamma_0$  and  $\gamma_0$  are coefficients of the so-called cusp and noncusp anomalous dimensions, while  $H_1$  is a process-dependent constant. Here, a precise definition of these quantities is not needed; we only need to know that they are fixed numeric constants. In order to truncate Eq. (4.8) at  $\mathcal{O}(\alpha_s)$ , or more generally at some finite perturbative order  $\mathcal{O}(\alpha_s^n)$ , we *must* ensure that the coefficient in square brackets is small, such that an expansion in  $\alpha_s \ll 1$  is justified. Clearly, this can not be fulfilled for any arbitrary choice of  $\mu$ . When  $Q/\mu \sim 1$ , the logarithmic terms in Eq. (4.8) are indeed small, and the expansion in  $\alpha_s \ll 1$  is applicable. This suggests that in order for perturbation theory to be reliable, we must choose  $\mu \sim Q$ .

We can repeat the same strategy for the TMD PDFs in Eq. (4.7). Since the expressions are rather cumbersome, we will not do so explicitly. However, it is quite intuitive that since the TMD PDFs are sensitive to the scale  $b_T$ , one needs to set  $\mu \sim 1/b_T$ . Recalling that intuitively  $q_T \sim 1/b_T$ , this implies  $\mu \sim q_T$ . However, this choice leads to a problem for the hard function, since the expansion in Eq. (4.8) breaks down for  $\mu \sim q_T$  in the region we are interested in, namely  $q_T \ll Q$  for which  $\ln(Q/q_T) \gg 1$ .

Fortunately, we can use evolution equations to solve this apparent conundrum. Anticipating later results in this chapter, we note that the hard function obeys the simple renormalization group equation (RGE)

$$\frac{d}{d \ln \mu} \ln H(Q, \mu) = \gamma_\mu^H(Q, \mu) = 4\Gamma_{\text{cusp}}[\alpha_s(\mu)] \ln \frac{Q}{\mu} + \gamma_\mu^H[\alpha_s(\mu)], \quad (4.9)$$

which follows from studying the factorization of the cross section Eq. (4.7) as a function of the arbitrary separation scale  $\mu$  between high- and low-scale physics. Here,  $\Gamma_{\text{cusp}}$  and  $\gamma_\mu^H$  are the cusp and noncusp anomalous dimensions, whose one-loop coefficients we already noted in

Eq. (4.8).  $\Gamma_{\text{cusp}}$  appears universally in QCD as the coefficient of the log-enhanced piece of the anomalous dimension of operators built out of Wilson lines meeting at an angle, or, “cusp”, as in the matrix elements defining TMD PDFs or soft functions, to which the hard function is related through invariance of the factorized cross section as a function of  $\mu$ .

Now, Eq. (4.9) can be easily solved as

$$H(Q, \mu) = H(Q, \mu_0) \exp \left[ \int_{\mu_0}^{\mu} \frac{d\mu'}{\mu'} \gamma_{\mu}^H(Q, \mu') \right], \quad (4.10)$$

where  $\mu_0$  is an *arbitrary* reference scale. Eq. (4.10) is the solution to our above problem: we can simply set  $\mu_0 \sim Q$ , such that  $H(Q, \mu_0)$  is reliably calculable as discussed above, while choosing  $\mu \sim q_T$  as required for the calculation of the TMD PDFs. To see how the apparent problem of large logarithms has disappeared, we can evaluate the integral in Eq. (4.10). For simplicity, we set  $\mu_0 = Q$  and neglect the  $\mu$  dependence of the running coupling  $\alpha_s(\mu)$ , which yields

$$\begin{aligned} H(Q, \mu) &= H(Q, Q) \exp \left[ \int_Q^{\mu} \frac{d\mu'}{\mu'} \gamma_{\mu}^H(Q, \mu') \right] \\ &\approx H(Q, Q) \exp \left[ -2\Gamma_{\text{cusp}}(\alpha_s) \ln^2 \frac{Q}{\mu} - \gamma_{\mu}^H(\alpha_s) \ln \frac{Q}{\mu} \right]. \end{aligned} \quad (4.11)$$

If we were to re-expand this exponential, we would recover the potentially large double logarithms  $\alpha_s \ln^2(Q/\mu)$  in Eq. (4.8) we were worried about spoiling perturbation theory. However, as they now appear only in the exponential, they do not deteriorate our perturbative results, and we are free to set  $\mu \sim q_T$  as desired. (Note the overall minus in the exponential, which guarantees exponential suppression as  $q_T/Q \rightarrow 0$ .) This is referred to as *resummation*, as a whole class of logarithms  $\alpha_s^n L^{2n}$  have been summed to all orders in perturbation theory as anticipated in Eq. (4.4).

In the following sections we will complete the discussion of evolution of the TMD PDF factors in Eq. (4.7) and the summation of all logs of  $q_T/Q$  or  $Q b_T$  appearing in the perturbative expansions of the TMD cross section Eq. (4.2).

### 4.3 TMD Evolution

In this section we will review the derivation of the TMD evolution equations both from the “direct” QCD approaches like CSS, and from the EFT framework of SCET. Both routes to the evolution equations are ultimately equivalent, but highlight complementary aspects of TMD evolution and inspire various methods to obtain their explicit solutions.

In Chapter 2 the quantum field theory definitions of TMD PDFs as composite operators were established with the unique role played by the soft factors which are essential for the consistency of TMD definitions and their validity in a factorization formula like Eq. (2.29). Essential to these definitions are the subtraction of UV and rapidity divergences resulting in the renormalized TMD PDFs. As a consequence (as stated earlier), the TMD PDFs depend on two auxiliary parameters, the rapidity and renormalization scales,  $\zeta$  and  $\mu$  respectively. For removal of rapidity divergences, various schemes were summarized in Sec. 2.4 with corresponding scheme dependent rapidity scales; mainly depending on the implementation

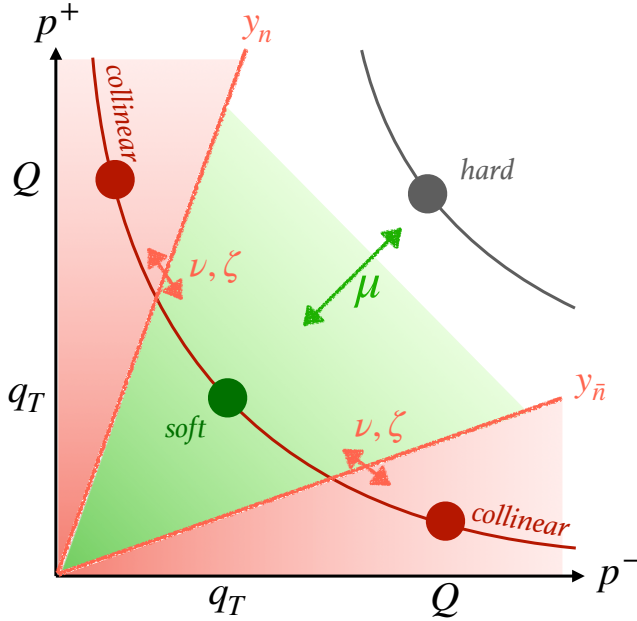


Figure 4.1: Momentum regions for TMD factorization and evolution. UV regulators like  $\overline{\text{MS}}$  separate hard momentum regions from IR collinear/soft regions. The variation of this arbitrary boundary leads to the  $\mu$ -RGEs. Rapidity regulators such as those reviewed in Chapter 2 define schemes for separating collinear and soft regions from one another (e.g.  $\nu, \zeta, y_{n,\bar{n}}$ ), and variation of these boundaries leads to rapidity RGEs, i.e., Collins-Soper equation. The rapidity evolution kernel has its own  $\mu$ -RGE, capturing variation of the scale  $\mu$  where the rapidity factorization/evolution occurs. Solutions of the  $\mu$  and rapidity RGEs sum large logs of ratios of mass and rapidity scales of these separated regions that appear in perturbative expansions of TMD cross sections.

of rapidity subtraction through the soft factor. For a summary of the various rapidity regulator schemes, see Table 2.1 in Sec. 2.4.1, and appendix D. The role of these regulators in separating UV/IR and soft/collinear momentum regions is illustrated schematically in Fig. 4.1. The invariance of factorized cross section  $d\sigma^W$  with respect to these scales results in a system of differential equations that determines the scale dependence of the TMDs. These are the TMD evolution equations.

Both the CSS [10, 83, 86, 119] and SCET [96–102, 186] formalisms lead to a common set of evolution equations for the generic TMD PDF defined in Eq. (2.33):

$$\frac{d \ln \tilde{f}_{i/p}(x, \mathbf{b}_T; \mu, \zeta)}{d \ln \mu} \stackrel{\text{CSS}}{=} \gamma_q[\alpha_s(\mu); \zeta/\mu^2] \stackrel{\text{SCET}}{=} \gamma_\mu^q(\mu, \zeta), \quad (4.12a)$$

$$\frac{\partial \ln \tilde{f}_{i/p}(x, \mathbf{b}_T; \mu, \zeta)}{\partial \ln \sqrt{\zeta}} = \tilde{K}(b_T; \mu) \stackrel{=} \gamma_\zeta^q(\mu, b_T), \quad (4.12b)$$

$$\frac{d \tilde{K}(b_T; \mu)}{d \ln \mu} = -\gamma_K[\alpha_s(\mu)] \stackrel{=} -2\Gamma_{\text{cusp}}^q[\alpha_s(\mu)], \quad (4.12c)$$

where we have shown typical names given to each anomalous dimension in much of the CSS- and SCET-based literature. These and some other common notations are summarized in Table 4.1. These equations are for quark TMD PDFs of flavor  $q$ ; analogous equations, with appropriate anomalous dimensions, hold for gluon TMD PDFs.

<i>Anomalous dimensions:</i>	TMD PDF $\mu$ RG (4.12a)	CS kernel/RRG (4.12b)	Cusp (4.12c)
CSS	$\gamma_q[\alpha_s(\mu); \zeta/\mu^2]$	$\tilde{K}(b_T; \mu)$	$-\gamma_K[\alpha_s(\mu)]$
SCET RRG [102, 109]	$\gamma_\mu^q(\mu, \zeta)$	$\gamma_\zeta^q(\mu, b_T) = -\gamma_v^q(b_T, \mu)$	$-2\Gamma_{\text{cusp}}^q[\alpha_s(\mu)]$
EIS [99, 238]	$\gamma_F^q(\mu, \zeta)$	$-2\mathcal{D}^q(\mu, b_T)$	$-2\Gamma_{\text{cusp}}^q(\mu)$
BN [96]	$-\Gamma_{\text{cusp}}^q[\alpha_s]L_\perp + 2\gamma^q[\alpha_s]$	$-F_{q\bar{q}}(L_\perp, \alpha_s)$	$-2\Gamma_{\text{cusp}}^q[\alpha_s]$
<i>Alternate organization:</i>	Eq. (4.35)	Eq. (4.38)	Eq. (4.39)
JMY [74]	$2\gamma_F[\alpha_s(\mu)] - \gamma_S(\mu, \rho)$	$2[K(\mu, b_T) + G(\mu, \zeta)]$	$-\gamma_K[\alpha_s(\mu)]$

Table 4.1: Common notations for anomalous dimensions of quark TMD PDFs in TMD evolution, Eq. (4.12). The first column of anomalous dimensions are for  $\mu$ -RG from UV renormalization of the TMD PDFs in Eq. (4.12a). The second column is the Collins-Soper kernel or rapidity anomalous dimension of the TMD PDFs in Eq. (4.12b). The final column gives different names for the “cusp” anomalous dimension, which appears in Eq. (4.12c) as the  $\mu$ -RG anomalous dimension of the CS kernel itself, i.e., the mixed  $\mu, \sqrt{\zeta}$  derivative of the TMD PDF. For the BN row,  $L_\perp = \ln(\mathbf{b}_T^2 \mu^2 / b_0^2)$ , and the  $\zeta$  dependence in the evolution is not actually explicit, see comments below Eq. (2.54). For the JMY row, note that the pieces of the evolution are organized slightly differently, as expressed in Eqs. (4.35) and (4.38), and the results are given for the subtracted TMD PDF in Eq. (2.94), which also has dependence on an extra scheme parameter  $\rho$ . The universal anomalous dimension  $\gamma_K$  of the CS kernel is the same in Eqs. (4.12c) and (4.39). (A similar table can be made for gluon TMDs, with  $q \rightarrow g$  where appropriate and CS kernel for gluons.)

The first equation (4.12a) expresses the usual RG evolution in  $\mu$  from UV renormalization. The second equation Eq. (4.12b), is the Collins-Soper equation, which expresses the evolution in the Collins-Soper scale  $\zeta$  resulting from regulating rapidity divergences.  $\tilde{K}$ , or  $\gamma_\zeta^q$ , the rapidity anomalous dimension is the Collins-Soper kernel. It is independent of  $x$  and  $\zeta$  and the flavor of the parton and the hadron in the PDF, however it does depend on the color representation for the parton; there is one for quarks and another for the gluon [239]. Noting that the only dependence of  $\tilde{f}_{i/p}(x, \mathbf{b}_T; \mu, \zeta)$  on  $\zeta$  (or  $y_n$ ) (see Eq. (2.30)) is through the soft factor, from the definition of  $\tilde{f}_{i/p}(x, \mathbf{b}_T; \mu, \zeta)$  one obtains by direct computation [10, 83],

$$\tilde{K}(b_T; \mu) = \lim_{\substack{y_A \rightarrow +\infty \\ y_B \rightarrow -\infty}} \frac{1}{2} \frac{\partial}{\partial y_n} \ln \left( \frac{\tilde{S}_{n_A n_B}^0(b_T, \epsilon, y_n - y_B)}{\tilde{S}_{n_A n_B}^0(b_T, \epsilon, y_A - y_n)} \right) + \text{UV counterterm}. \quad (4.13)$$

In SCET these equations will arise similarly from RG and rapidity RG evolution of beam and soft functions. The third equation expresses the  $\mu$ -RG evolution of the Collins-Soper kernel  $\tilde{K}$  or rapidity anomalous dimension  $\gamma_\zeta$ . Taking the derivative of (4.12a) with respect to  $\ln \zeta$  and using that the mixed  $\mu, \zeta$  second derivatives of the TMD PDF are equal, we immediately find,

$$\frac{\partial \gamma_q[\alpha_s(\mu); \zeta/\mu^2]}{\partial \ln \sqrt{\zeta}} = -\gamma_K[\alpha_s(\mu)]. \quad (4.14)$$

This imposes a consistency condition on the anomalous dimensions in Eqs. (4.12a) and (4.12b). They imply a relation between  $\gamma_q, \gamma_K$  (i.e.,  $\gamma_\mu^q, \gamma_\zeta^q$ ). Now one can easily integrate this equation

with respect to  $\zeta$ , where we choose  $\zeta_0 \sim \mu^2$ . As a result the anomalous dimension of the TMD PDF  $\gamma_q$  has linear dependence on  $\ln(\zeta/\mu^2)$ ; expressing this in terms of the CSS and SCET notation from Table 4.1 one obtains,

$$\gamma_q[\alpha_s(\mu); \zeta/\mu^2] = -\frac{1}{2}\gamma_K[\alpha_s(\mu)] \ln \frac{\zeta}{\mu^2} + \gamma_q[\alpha_s(\mu); 1], \quad (4.15a)$$

or

$$\gamma_\mu^q(\mu, \zeta) = -\Gamma_{\text{cusp}}^q[\alpha_s(\mu)] \ln \frac{\zeta}{\mu^2} + \gamma_\mu^q[\alpha_s(\mu)], \quad (4.15b)$$

that is, the coefficient of the log in the UV anomalous dimension of the TMD PDF is the anomalous dimension  $\gamma_K$  or  $\Gamma_{\text{cusp}}^q$  of the Collins-Soper kernel in Eq. (4.12c).

Further, from (4.12c) we can straightforwardly integrate with respect to  $\mu$  and thus, the Collins-Soper kernel or rapidity anomalous dimension itself take the form,

$$\tilde{K}(b_T; \mu) = - \int_{1/\bar{b}_T}^\mu \frac{d\mu'}{\mu'} \gamma_K[\alpha_s(\mu')] + \tilde{K}(b_T, 1/\bar{b}_T), \quad (4.16a)$$

or

$$\gamma_\zeta^q(\mu, b_T) = -2 \int_{1/\bar{b}_T}^\mu \frac{d\mu'}{\mu'} \Gamma_{\text{cusp}}^q[\alpha_s(\mu')] + \gamma_\zeta^q[\alpha_s(1/\bar{b}_T)]. \quad (4.16b)$$

where  $\bar{b}_T = b_T/b_0$ , recalling  $b_0 = 2e^{-\gamma_E}$ . The first terms on the right-hand side of each expression in Eq. (4.16) are predicted by the RGE Eq. (4.12c) of the Collins-Soper kernel, while the latter term is a boundary condition, which is not predicted by the RGE itself. It can in principle be specified at any scale  $\mu_0$  but it is conventional to choose it at  $\mu_0 = 1/\bar{b}_T$  as in Eq. (4.16). With this choice, explicit logs of  $\mu_0 \bar{b}_T$  in the perturbative expansion of the non-cusp anomalous dimension are eliminated, hence its sole dependence on  $\alpha_s(1/\bar{b}_T)$  in the form Eq. (4.16b).<sup>16</sup> For perturbative values of  $1/\bar{b}_T$ , it can be predicted in fixed-order perturbation theory. For nonperturbative  $1/\bar{b}_T$ , it should be obtained via a nonperturbative model via ab initio calculations such as by lattice QCD, nonperturbative models, and global analyses of related experimental data. The latter program is the topic of Chap. 5. Identical relations to the above hold for gluon TMD PDF anomalous dimensions.

The cusp anomalous dimension  $\Gamma_{\text{cusp}}$  in Eq. (4.16), to which  $\gamma_K$  is equivalent, is a universal object appearing ubiquitously in QCD (see, e.g., [? ? ? ? ]). It appears due to divergences in matrix elements of operators built out of Wilson lines in different directions meeting at an angle, forming a “cusp”, such as between two jets or hadronic beams. The angle may be  $\pi$  for back-to-back configurations. The hard function, for example, in Eq. (4.9) is associated with Wilson lines in the fundamental representation of SU(3) in two light-like directions, and has an anomalous dimension whose log-enhanced piece is known to have the coefficient  $\Gamma_{\text{cusp}}$ . It is known to two [? ], three [1114], and recently even four-loop [? ] order in QCD. The consistency

<sup>16</sup>There is an unfortunate historical convention in much of the SCET literature that the full anomalous dimension, as on the LHS of Eq. (4.16b), and its non-cusp piece, as on the RHS of the same equation, are given the same symbolic name, e.g.  $\gamma_\zeta^q$ , but distinguished by the form of their argument, i.e. the non-cusp piece being specified  $\gamma_\zeta^q[\alpha_s]$  signifying that it is given by an expansion in  $\alpha_s$  with pure numerical coefficients, Eq. (E.2).

relations between anomalous dimensions of hard and TMD PDF pieces of the cross section Eq. (4.7), as well as between UV and rapidity evolution of the TMD PDFs expressed in Eq. (4.7), guarantee the further universality between the cusp anomalous dimension and the rapidity anomalous dimension.

Finally, we obtain the generic solution for the evolved TMD PDF in Eq. (4.1) by performing integration on the rapidity parameter  $\zeta$  in Eq. (4.12b), and integration on the renormalization scale  $\mu$  in Eq. (4.12a), where we have evolved the TMD PDF from the pair of initial to final scales  $\{\mu_0, \zeta_0\} \rightarrow \{\mu, \zeta\}$ , and illustrated by Fig. 4.2,

$$\tilde{f}_{i/P}(x, \mathbf{b}_T, \mu, \zeta) = \tilde{f}_{i/P}(x, \mathbf{b}_T, \mu_0, \zeta_0) \exp \left\{ \int_{\mu_0}^{\mu} \frac{d\mu'}{\mu'} \gamma_q [\alpha_s(\mu'); \zeta_0/\mu'^2] \right\} \exp \left\{ \tilde{K}(b_T; \mu) \ln \sqrt{\frac{\zeta}{\zeta_0}} \right\}, \quad (4.17)$$

which gives definitions to the RG and RRG evolution kernels  $U$  and  $V$  in Eq. (4.1). The RG evolution between scales  $\mu_0, \mu$  is governed by the anomalous dimension  $\gamma_q$ , and the rapidity evolution between the rapidity scales  $\zeta_0, \zeta$  by the Collins-Soper kernel  $\tilde{K}$ .

Below we will review how the evolution equations Eq. (4.12), and solutions (4.17) are applied to exploit the universality properties of the non-perturbative content which emphasize the intrinsic properties associated with hadronic structure in (4.17), as well as the perturbative content which are optimized to have no large logarithms in their expansion in powers of  $\alpha_s$ . First we consider the treatment in the CSS formalism, in which the Wilson lines in the definition of the TMD PDF are tilted away from the lightcone. Then we cover the treatment in the SCET framework, in which the TMD PDFs are factored into beam and soft functions, each with their own RG and rapidity RG evolution equations, which combine to give the same TMD evolution equations Eq. (4.12). We will also review how explicit forms for the solutions of these equations can be written, first in  $\mathbf{b}_T$  space and then transformed to momentum space, and also directly in momentum space. The difference in various prescriptions or approaches to doing this amounts to alternative choices (implicit or explicit) for the low scales from which the TMD PDFs are evolved.

First, however in Table 4.2 we summarize the orders of accuracy to which the anomalous dimensions and other relevant quantities (the beta function for running of  $\alpha_s$  and fixed-order coefficient functions in, e.g., Eq. (4.30)), need to be known, in powers  $k$  of  $\alpha_s^k$ , to achieve the orders of accuracy in resummed logs illustrated in Eq. (4.4). In the next section we illustrate the calculations to leading order in  $\alpha_s$ .

### 4.3.1 One-loop examples

From the calculations of quark TMD PDFs in perturbation theory in Sec. 2.4.2, we can illustrate how to obtain their UV and rapidity anomalous dimensions to one-loop order. For higher-order results, see appendix E.

We recall that the UV anomalous dimension is associated with the behavior of the TMD PDF as the arbitrary boundary between hard scales  $Q$  and low scales  $q_T$  or  $1/b_T$  is varied, while the rapidity anomalous dimension is associated with its behavior as the (arbitrary) boundaries between forward/backward and central rapidities is varied. At one-loop order, the variation with respect to these boundaries can be obtained from the soft and collinear divergences in the one-loop graphs shown in Fig. 2.2. From the one-loop result for the bare TMD PDF in Eq. (2.71)

$\gamma_K(\alpha_s(\mu))$	$\beta[\alpha_s(\mu)]$	$\gamma_q(\alpha_s(\mu); 1)$	$\tilde{K}(\bar{b}_T; 1/\bar{b}_T)$	$\tilde{C}_{j/j'}$	accuracy	accuracy (SCET)
—	—	—	—	0	QPM	
1	1	—	—	0	LO-LL	LL
2	2	1	1	0	LO-NLL	NLL
3	3	2	2	0	LO-NNLL	
2	2	1	1	1	NLO-NLL	NLL'
3	3	2	2	1	NLO-NNLL	NNLL
3	3	2	2	2	NNLO-NNLL	NNLL'
4	4	3	3	2	NNLO- $N^3LL$	$N^3LL$

Table 4.2: Orders of accuracy needed for evolution of TMD PDFs and other ingredients entering the transverse momentum dependent W term needed to achieve given orders of logarithmic accuracy (LL, NLL, NNLL). The numbers refer to the loop order  $k$  to which the quantity needs to be computed, e.g.  $k = n + 1$  in terms of the coefficients in the expansions Eqs. (E.2) and (E.6) of the anomalous dimensions or beta function. (A dash “—” indicates the quantity does not exist at  $\alpha_s^0$ .) The names of anomalous dimensions are those in the CSS row of Table 4.1, same counting applies to other rows. We also include the needed accuracies for coefficient functions  $\tilde{C}$  that will appear in Eq. (4.30) (which corresponds to perturbative expansions of beam and soft functions in SCET in Eq. (4.43).) “QPM” refers to the *quark parton model*, i.e., Born-level. This table describes the accuracy of the resummed W term; a full prediction for a TMD cross section will include matching to a fixed-order “Y” term whose accuracy is specified separately, see Sec. 4.7.

using  $\overline{\text{MS}}$  to regulate the UV divergences and the  $\eta$  regulator for rapidity divergences, one obtains the UV renormalization factor Eq. (2.81), from which the anomalous dimension of the renormalized TMD PDF in Eq. (2.82) can be obtained by the condition of  $\mu$ -independence of the bare TMD PDF,

$$\gamma_\mu^q(\mu, \zeta) = -(Z_{\text{uv}}^q)^{-1} \mu \frac{d}{d\mu} Z_{\text{uv}}^q, \quad (4.18)$$

which to one loop gives

$$\gamma_\mu^q(\mu, \zeta) = \frac{\alpha_s(\mu) C_F}{\pi} \left( \frac{3}{2} + \ln \frac{\mu^2}{\zeta} \right), \quad (4.19)$$

where in evaluating the  $\mu$  derivative in Eq. (4.18) it is important to remember the relation Eq. (2.67) between the bare and renormalized coupling constants. Equivalently one can just take the  $d/d \ln \mu$  derivative of the renormalized TMD PDF itself, Eq. (2.82).

Meanwhile the Collins-Soper kernel, or equivalently the rapidity anomalous dimension, is obtained from the  $\ln \sqrt{\zeta}$  derivative of the renormalized TMD PDF in Eq. (2.82), which gives to one loop

$$\gamma_\zeta^q(\mu, b_T) = -\frac{2\alpha_s(\mu) C_F}{\pi} \ln \frac{\mu b_T}{b_0}, \quad (4.20)$$

so that at one loop in perturbation theory the non-cusp part of the Collins-Soper kernel is zero.

(It begins at two loops.) Alternatively, the anomalous dimension  $\gamma_\zeta$  can be reconstructed from those of the beam and soft functions in Eq. (2.85) and Eq. (2.86). For these pieces, the anomalous dimensions can be obtained from the rapidity renormalization in the RRG, differentiating the  $\tilde{Z}_{B,S}$  renormalization factors in Eq. (2.84) and Eq. (2.86) with respect to  $\ln v$ , keeping in mind the  $v$  dependence of the bookkeeping parameter  $w(\tau, v)$  appearing in Eq. (2.75). We leave the explicit formulae for the anomalous dimensions  $\gamma_v^{B,S}$  for Sec. 4.5.1.

We see also at one loop the consistency relation Eq. (4.12c) between mixed derivatives of the TMD PDFs, giving the RG evolution of the Collins-Soper kernel itself, is explicitly satisfied,

$$\sqrt{\zeta} \frac{d}{d\sqrt{\zeta}} \gamma_\mu^q = \mu \frac{d}{d\mu} \gamma_\zeta^q = -\frac{2\alpha_s(\mu)C_F}{\pi} = -2\Gamma_{\text{cusp}}[\alpha_s]. \quad (4.21)$$

Results to two loops are given in appendix E.

In the next subsections we review how to solve the TMD evolution equations in general, to arbitrary orders in the perturbative expansions of anomalous dimensions, in both CSS and SCET formalisms.

## 4.4 CSS Formalism

In this section we will consider rapidity regularization based on TMD factorization of Collins [10, 83, 103, 240] and also the earlier scheme of Ji, Ma, and Yuan [74, 75]. We take as a starting point the Drell-Yan cross section in terms of the TMD  $d\sigma^W$  term. In Collins' formulation [10], TMD factorization is carried out in  $\mathbf{b}_T$  configuration space<sup>17</sup>, where the cross section is expressed in terms of Fourier transforms of the TMD PDFs, (4.7).

### 4.4.1 The CSS Solution

Here we present the solution optimized for perturbative calculations [10, 83, 240]. We begin with Eq. (4.7). Since the solution to the evolution equation is independent of the path traced out in the  $\{\mu, \zeta\}$  phase space of rapidity and energy, other choices are also possible [102, 238]; for a discussion, see section 4.6.

First, we point out that if we insert the solution (4.17) into the W term, Eq. (4.7) and perform the Fourier integral where  $b_T$  extends from  $b_T = [0, \infty)$ , one can not avoid using the parton densities and TMD evolution kernel in the non-perturbative large  $b_T$  region. Furthermore, a fixed order perturbative expansion of  $\tilde{K}(b_T, \mu)$  will encounter large logarithmic contributions from higher order terms and thus, a perturbative treatment of  $b_T$  is not reliable. For these reasons, Collins, et. al. [10, 63, 240] provided a prescription that aims to maximize the the use of perturbation theory for small  $b_T$  and at the same time, combine nonperturbative information; that is to match perturbative and non-perturbative properties of the TMD factorization formulation. A widely used scheme to separate perturbative and non-perturbative contributions partitions the large and small  $b_T$  via a function  $b_*$  that freezes above some  $b_{\max}$  and equals  $b_T$  for small  $b_T$ :

$$b_*(b_T) \longrightarrow \begin{cases} b_T & b_T \ll b_{\max} \\ b_{\max} & b_T \gg b_{\max}. \end{cases} \quad (4.22)$$

Here we adopt the  $b_*$  prescription [240] by replacing  $\mathbf{b}_T$  in the solution to the evolution

---

<sup>17</sup>See Sec. 4.8 for some methods to perform resummation in momentum space.

equations by the function

$$\mathbf{b}_* \equiv \mathbf{b}_*(\mathbf{b}_T) = \frac{\mathbf{b}_T}{\sqrt{1 + b_T^2/b_{max}^2}}. \quad (4.23)$$

Note that  $b_*$  freezes at  $b_{max}$  when  $b_T$  is large so that  $b_*$  is always small (i.e., in the perturbative region). Other choices can be found in [247, 248]. This definition is constructed so that it equals  $\mathbf{b}_T$  for small values and smoothly approaches the upper cutoff  $b_{max}$  when  $\mathbf{b}_T$  becomes large. Typical values of  $b_{max} \sim 1 \text{ GeV}^{-1}$  and can be thought of as characterizing a boundary between the perturbative and non-perturbative  $\mathbf{b}_T$ -dependence [10, 83]. We can now use this to match the perturbative and non-perturbative pieces of the TMD PDF. To do this, we partition the left-hand side of Eq. (4.17) into the part of  $\tilde{f}$  at  $\mathbf{b}_*$  through the identity,

$$\tilde{f}_{i/p}(x, \mathbf{b}_T, \mu, \zeta) = \tilde{f}_{i/p}(x, \mathbf{b}_*, \mu, \zeta) \frac{\tilde{f}_{i/p}(x, \mathbf{b}_T, \mu, \zeta)}{\tilde{f}_{i/p}(x, \mathbf{b}_*, \mu, \zeta)} \quad (4.24)$$

which we calculate perturbatively and a part that we deem "intrinsically non-perturbative".

At large  $\mathbf{b}_T$  the expression for the evolved TMD PDFs are defined by the deviation of  $f_{j/p}(x, \mathbf{b}_T, \mu, \zeta)$  and  $\tilde{K}(b_T; \mu)$  between  $\mathbf{b}_T$  and  $\mathbf{b}_*$  in terms of the non-perturbative universal and scale independent functions  $g_{j/p}(x, b_T, b_{max})$  and  $g_k(b_T; b_{max})$ . They are defined through the ratio in Eq. (4.24),

$$\begin{aligned} \frac{\tilde{f}_{i/p}(x, \mathbf{b}_T, \mu, \zeta)}{\tilde{f}_{i/p}(x, \mathbf{b}_*, \mu, \zeta)} &= \frac{\tilde{f}_{i/p}(x, \mathbf{b}_T, \mu_0, \zeta'_0)}{\tilde{f}_{i/p}(x, \mathbf{b}_*, \mu_0, \zeta'_0)} \exp \left[ \ln \sqrt{\frac{\zeta}{\zeta'_0}} (\tilde{K}(b_T, \mu) - \tilde{K}(b_*, \mu)) \right] \\ &= \exp [-g_{i/p}(x, b_T)] \exp \left[ -\ln \sqrt{\frac{\zeta}{\zeta'_0}} g_k(b_T; b_{max}) \right], \end{aligned} \quad (4.25)$$

where RRG and RG transformations are performed,  $\zeta \rightarrow \zeta'_0$  and  $\mu \rightarrow \mu_0$  [10] respectively (*n.b.* the effects of anomalous dimension,  $\gamma_q$ , cancel), and where the non-perturbative part of the Collins Soper kernel  $g_k(b_T; b_{max})$  is,

$$g_k(b_T; b_{max}) = \tilde{K}(b_*, \mu_0) - \tilde{K}(b_T, \mu_0), \quad (4.26)$$

and the intrinsic transverse momentum distribution (in Fourier space) is given by the exponent of  $g_{i/p}(x, b_T)$ . The arbitrary reference scale,  $\zeta'_0$  determines how much of the TMD density is in  $g_{i/p}(x, b_T)$  and how much is put into the exponential of  $g_k$  times the log in Eq. (4.24) [240]. From Eq. (4.25) both  $g_{i/p}$  and  $g_k$  vanish as  $b_T \rightarrow 0$  [63, 240]. Also, both functions are independent of  $\zeta$  and  $\mu$  because there is an exact cancellation in terms obtained by applying  $\mu$ -RG and  $\zeta$ -RRG transformations to Eqs. (4.26) and (4.25). Now substituting

Eqs. (4.25) and (4.26) and using (4.15a) in (4.24), Eq. (4.17) can be expressed as,

$$\begin{aligned} \tilde{f}_{i/p}(x, \mathbf{b}_T, \mu, \zeta) &= \tilde{f}_{i/p}(x, \mathbf{b}_*, \mu_0, \zeta_0) \\ &\times \exp \left[ \ln \sqrt{\frac{\zeta}{\zeta_0}} \tilde{K}(b_*, \mu_0) + \int_{\mu_0}^{\mu} \frac{d\mu'}{\mu'} \left( \gamma_q[\alpha_s(\mu')]; 1] - \ln \frac{\sqrt{\zeta}}{\mu'} \gamma_K[\alpha_s(\mu')] \right) \right] \\ &\times \exp \left[ -g_{i/p}(x, b_T) - \ln \left( \sqrt{\frac{\zeta}{\zeta_0}} \right) g_k(b_T; b_{\max}) \right]. \end{aligned} \quad (4.27)$$

Finally to optimize the solution for perturbative calculations, RG and RRG transformations are performed,  $\mu_0 \rightarrow 1/b_*$  and  $\zeta_0 \rightarrow 1/b_*^2$  respectively, permitting perturbative calculations of  $\tilde{K}$  and  $\tilde{f}$  [10], where now (4.27) becomes

$$\begin{aligned} \tilde{f}_{i/p}(x, \mathbf{b}_T, \mu, \zeta) &= \tilde{f}_{i/p}(x, \mathbf{b}_*, \mu_{b_*}, \mu_{b_*}^2) \\ &\times \exp \left[ \ln \frac{\sqrt{\zeta}}{\mu_{b_*}} \tilde{K}(b_*, \mu_{b_*}) + \int_{\mu_{b_*}}^{\mu} \frac{d\mu'}{\mu'} \left( \gamma_q[\alpha_s(\mu')]; 1] - \ln \frac{\sqrt{\zeta}}{\mu'} \gamma_K[\alpha_s(\mu')] \right) \right] \\ &\times \exp \left[ -g_{i/p}(x, b_T) - \ln \left( \sqrt{\frac{\zeta}{\zeta_0}} \right) g_k(b_T; b_{\max}) \right], \end{aligned} \quad (4.28)$$

with

$$\mu_{b_*} \equiv \frac{C_1}{b_*}, \quad (4.29)$$

where  $C_1/b_*$  is the hard scale. It is chosen to allow perturbative calculations of  $b_*$ -dependent quantities and where  $C_1$  is a constant of order unity chosen to allow for perturbative calculations without large logarithms [10, 240].

Thus, we can express the TMD parton densities at small  $\mathbf{b}_T$  in terms of the integrated PDFs using an operator product expansion as expressed in Sec. 2.8, where now, Eq. (2.150) takes the form,

$$\tilde{f}_{i/p}(x, \mathbf{b}_*, \mu_{b_*}, \mu_{b_*}^2) = \sum_j \int_x^1 \frac{d\hat{x}}{\hat{x}} \tilde{C}_{i/j}(x/\hat{x}, b_T; \mu_{b_*}, \mu_{b_*}^2, \alpha_s(\mu_{b_*})) f_{j/p}(\hat{x}; \mu_{b_*}) + O((m b_*(b_T))^p). \quad (4.30)$$

Thus, the first line of (4.28) is expressed in terms of the collinear pdfs using an OPE in terms of collinear PDFs [10, 83, 240],

$$\tilde{f}_{i/p}(x, \mathbf{b}_T, \mu, \zeta) = \sum_j \int_x^1 \frac{d\hat{x}}{\hat{x}} \tilde{C}_{i/j}(x/\hat{x}, b_T; \mu_{b_*}, \mu_{b_*}^2, \alpha_s(\mu_{b_*})) f_{j/p}(\hat{x}; \mu_{b_*}) \quad (4.31)$$

$$\begin{aligned} &\times \exp \left[ \ln \frac{\sqrt{\zeta}}{\mu_{b_*}} \tilde{K}(b_*, \mu_{b_*}) + \int_{\mu_{b_*}}^{\mu} \frac{d\mu'}{\mu'} \left( \gamma_q[\alpha_s(\mu')]; 1] - \ln \frac{\sqrt{\zeta}}{\mu'} \gamma_K[\alpha_s(\mu')] \right) \right] \\ &\times \exp \left[ -g_{i/p}(x, b_T) - \ln \left( \sqrt{\frac{\zeta}{\zeta_0}} \right) g_k(b_T; b_{\max}) \right]. \end{aligned} \quad (4.32)$$

The sum is over all flavors  $j$  of partons: quarks, anti-quarks and gluons and  $f_j(\hat{x}; \mu_{b_*})$  is understood to be renormalized at the scale  $\mu_{b_*}$ .

Finally, we mention that there are some alternatives in the literature to the  $b_*$ -prescription. Here, we sketch out the approach proposed by Qiu and Zhang. In Refs. [178, 243] the authors separate the perturbative and non-perturbative contribution through the parameter  $b_{max}$  such that,

$$d\tilde{W}(b_T, Q) = d\tilde{W}(b_T, Q), \text{ for } b_T \leq b_{max}, \quad (4.33)$$

and

$$d\tilde{W}(b_T, Q) = d\tilde{W}(b_{max}, Q) d\tilde{W}_{QZ}^{NP}(b_T, Q; b_{max}), \quad \text{for } b_T > b_{max}, \quad (4.34)$$

where  $d\tilde{W}_{QZ}^{NP}(b_T, Q; b_{max})$  includes power corrections to improve the matching between the perturbative and non-perturbative regions of  $d\tilde{W}(b_T, Q)$ . This approach attempts to minimize the influence of the non-perturbative piece of  $d\tilde{W}(b_T, Q)$ , which contains several parameters and does not have a fixed functional form, at small  $b_T$  where one should be driven by perturbatively calculable effects. In the context of the “resummation approach” [251, 252], one avoids the Landau pole encountered in performing Fourier transforms ( $b$ -space integrations) by extending  $b_T$  to the complex plane and exploiting the analytic structure of the running coupling. Phenomenological parameters then appear only as non-perturbative power corrections.

#### 4.4.2 Ji-Ma-Yuan scheme

The Ji-Ma-Yuan (JMY) scheme [74] is similar to that proposed by Collins-Soper [86], i.e., off-light-front gauge link is applied to regulate the rapidity divergence. Instead of a space-like gauge link used in Collins-Soper [86], a time-like off-light-front gauge is adopted in JMY scheme. The rapidity regulator is defined as  $\tilde{\zeta}^2 = (v \cdot P)/v^2$ , where  $v$  is the direction of the Wilson line with  $v^2$  a small parameter but positive. See Sec. 2.5 for a detailed review of the definition of TMD PDFs in this scheme.

There is a UV evolution equation for TMD PDFs with respect to the factorization scale  $\mu_F$ . For example, for the un-subtracted momentum-space TMD quark distribution, the renormalization group equation becomes very simple,

$$\mu \frac{df_q^{(unsub.)}(x, \mathbf{k}_T, \mu, \zeta)}{d\mu} = 2\gamma_F[\alpha_s(\mu)] f_q^{(unsub.)}(x, \mathbf{k}_T, \mu, \zeta), \quad (4.35)$$

where  $\gamma_F$  is the anomalous dimension of the quarks in the axial gauge and at one-loop order  $\gamma_F = (3\alpha_s/4\pi)C_F$ . The subtracted TMD distribution in Eq. (2.94), then, satisfies

$$\mu \frac{df_q^{(sub.)}(x, \mathbf{k}_T, \mu, \zeta, \rho)}{d\mu} = \{2\gamma_F[\alpha_s(\mu)] - \gamma_S(\mu, \rho)\} f_q^{(sub.)}(x, \mathbf{k}_T, \mu, \zeta, \rho), \quad (4.36)$$

where  $\gamma_S(\mu, \rho)$  is the anomalous dimension of the soft factor,

$$\mu \frac{\partial S(b_T, \mu, \rho)}{\partial \mu} = \gamma_S(\mu, \rho) S(b_T, \mu, \rho), \quad (4.37)$$

where this  $S$  is the renormalized version of Eq. (2.92), see [74] for details. The  $\rho$  dependence of  $\gamma_S$  in Eq. (4.37) cancels against  $\rho$  dependence that appears in the hard function in the factorized hard-scattering cross sections in this formalism, see e.g. Eqs. (2.28) and (2.97).

The evolution of the TMD PDF, now in  $\mathbf{b}_T$  space, with respect to  $\zeta$  takes the form,

$$\tilde{\zeta} \frac{\partial}{\partial \tilde{\zeta}} \tilde{f}_q^{(sub.)}(x, \mathbf{b}_T, \mu, x\tilde{\zeta}, \rho) = (K(\mu, b_T) + G(\mu, x\tilde{\zeta})) \tilde{f}_q^{(sub.)}(x, \mathbf{b}_T, \mu, x\tilde{\zeta}, \rho) \quad (4.38)$$

where  $K$  depends on UV renormalization scale  $\mu$  and infrared impact parameter  $b_T$ , and is non-perturbative when  $b_T$  is large;  $G$  is perturbative for large  $\mu$  and  $\zeta$ ; and both are free of gluon and quark mass singularity. The sum  $K + G$ , however, is independent of explicit dependence on the UV scale  $\mu$  and hence,

$$\mu \frac{d}{d\mu} K = -\gamma_K[\alpha_s(\mu)] = -\mu \frac{d}{d\mu} G \quad (4.39)$$

where  $\gamma_K$  is the cusp anomalous dimension and is a perturbation series in  $\alpha_s(\mu)$  free of infrared singularities. The one-loop anomalous dimension  $\gamma_K$  is given by  $\gamma_K = \frac{\alpha_s}{\pi} 2C_F$ . Using the above renormalization group equation Eq. (4.39), one can sum over large logarithms  $\ln \zeta^2 b_T^2$  in  $K + G$  when  $b$  is small (otherwise  $K$  is non-perturbative). Substituting the result into Eq. (4.38), one finds an expression that resums double-leading logarithms in  $\zeta b_T$ .

Solving the evolution equations also resums the large logarithms in the TMDs. The procedure follows Collins-Soper 81 [86, 119], and later Collins-Soper-Sterman 85 [63]. First of all, there are large logarithms in  $K + G$  (which is independent of the renormalization scale). To sum it, we solve the renormalization group equation to get

$$K(b_T, \mu) + G(x\zeta, \mu) = K(b_T, \mu_L) + G(x\zeta, \mu_H) - \int_{\mu_L}^{\mu_H} \frac{d\mu}{\mu} \gamma_K(\alpha(\mu)) . \quad (4.40)$$

To isolate the large logarithms, one has to choose  $\mu_L$  to be on the order of  $\Lambda_{\text{QCD}}$  and  $\mu_H$  to be on the order of  $\zeta$ . Therefore, we let

$$\mu_L = C_1 M_p; \quad \mu_H = C_2 x \zeta = C_2 Q \sqrt{\rho} . \quad (4.41)$$

Substituting the above into the Collins-Soper equation for  $\tilde{f}_q^{(sub.)}$ , the large logarithms in  $\zeta$  can be factorized,

$$\begin{aligned} \tilde{f}_q^{(sub.)}(x, \mathbf{b}_T, \mu, x\zeta, \rho) &= \exp \left\{ - \int_{\mu_L}^{C_2 x \zeta} \frac{d\mu}{\mu} \left[ \ln \left( \frac{C_2 x \zeta}{\mu} \right) \gamma_K(\alpha(\mu)) - K(b_T, \mu_L) - G(\mu/C_2, \mu) \right] \right\} \\ &\times \tilde{f}_q^{(sub.)}(x, \mathbf{b}_T, \mu, x\zeta_0 = \mu_L/C_2, \rho) , \end{aligned} \quad (4.42)$$

where the exponential factor contains the entire dependence on  $\zeta$ , in particular, the large Sudakov double logarithms. However, the above expression contains much more than just the leading double logarithms; it contains all the sub-leading logs as well.

## 4.5 Evolution in SCET

In this section we review the formulation and derivation of TMD PDF evolution equations, and their solutions, in the framework of Soft Collinear Effective Theory, using the tools of RG evolution and rapidity RG evolution of beam and soft functions describing the dynamics of collinear and soft modes in the EFT.

### 4.5.1 RG and RRG

Let us take as a starting point the Drell-Yan cross section given in Eq. (2.29b), in terms of separate beam and soft functions, with a clear separation of the rapidity evolution of the two pieces in  $\nu$ . We work for now with the expression in  $\mathbf{b}_T$  space, and for simplicity keep one flavor channel in this section, that is,

$$\frac{d\sigma^W}{dQdYd^2\mathbf{q}_T} = \int d^2\mathbf{b}_T e^{i\mathbf{b}_T \cdot \mathbf{q}_T} \tilde{\sigma}(\mathbf{b}_T) \\ \tilde{\sigma}(\mathbf{b}_T) = H(Q, \mu) \tilde{B}(x_a, \mathbf{b}_T, \mu, \zeta_a/\nu^2) \tilde{B}(x_b, \mathbf{b}_T, \mu, \zeta_b/\nu^2) \tilde{S}(b_T, \mu, \nu), \quad (4.43)$$

which is related to the form Eq. (2.29a) through the relation Eq. (2.36) between beam/soft functions and the TMD PDFs. In this section we are suppressing all flavor indices. The UV and rapidity divergences in these functions are renormalized according to Eqs. (2.34) and (2.35). Anomalous dimensions for  $\mu$  and  $\nu$  evolution of the beam and soft functions are defined by

$$\begin{aligned} \gamma_\mu^B(\mu, \zeta/\nu^2) &= -(\tilde{Z}_B)^{-1} \mu \frac{d}{d\mu} \tilde{Z}_B(\mathbf{b}_T, \mu, \nu, xP) & \gamma_\mu^S(\mu, \mu/\nu) &= -(\tilde{Z}_S)^{-1} \mu \frac{d}{d\mu} \tilde{Z}_S(b_T, \mu, \nu) \\ \gamma_\nu^B(b_T, \mu) &= -(\tilde{Z}_B)^{-1} \nu \frac{d}{d\nu} \tilde{Z}_B(\mathbf{b}_T, \mu, \nu, xP) & \gamma_\nu^S(b_T, \mu) &= -(\tilde{Z}_S)^{-1} \nu \frac{d}{d\nu} \tilde{Z}_S(b_T, \mu, \nu). \end{aligned} \quad (4.44)$$

where  $x = x_a$  or  $x_b$  and  $P = P_a^+$  or  $P_b^-$  as appropriate for each beam function. The dependences on regulators  $\epsilon, \tau$  and the limits  $\epsilon, \tau \rightarrow 0$  that appear in Eqs. (2.34) and (2.35) are also implicit here. The exact relation of the Collins-Soper scale  $\zeta$  to  $xP$  depends on the regulator used, as explained in Sec. 2.4. The hard function has only a  $\mu$  anomalous dimension,

$$\gamma_\mu^H = -(Z_H)^{-1} \mu \frac{d}{d\mu} Z^H(Q, \mu), \quad (4.45)$$

where  $Z_H$  is the UV renormalization counterterm for the hard function. We can define it here in terms of  $Z_{B,S}$ :

$$Z_H(Q, \mu) = [\tilde{Z}_B(b_T, \mu, \nu, x_a P_a^+) \tilde{Z}_B(b_T, \mu, \nu, x_b P_b^-) \tilde{Z}_S(b_T, \mu, \nu)]^{-1}, \quad (4.46)$$

where the  $b_T, \nu$  dependences on the right-hand side will cancel, and  $Z_H$  will also depend only on the combination  $2x_a P_a^+ x_b P_b^- = Q^2$  in Eq. (2.31).

The renormalized functions all then satisfy the RG and rapidity RG (RRG) equations,

$$\mu \frac{d}{d\mu} \tilde{B}(x, \mathbf{b}_T, \mu, \zeta/\nu^2) = \gamma_\mu^B(\mu, \zeta/\nu^2) \tilde{B}(x, \mathbf{b}_T, \mu, \zeta/\nu^2) \quad (4.47a)$$

$$\nu \frac{d}{d\nu} \tilde{B}(x, \mathbf{b}_T, \mu, \zeta/\nu^2) = \gamma_\nu^B(b_T, \mu) \tilde{B}(x, \mathbf{b}_T, \mu, \zeta/\nu^2) \quad (4.47b)$$

for the beam functions, and

$$\mu \frac{d}{d\mu} \tilde{S}(b_T, \mu, \nu) = \gamma_\mu^S(\mu, \mu/\nu) \tilde{S}(b_T, \mu, \nu) \quad (4.48a)$$

$$\nu \frac{d}{d\nu} \tilde{S}(b_T, \mu, \nu) = \gamma_\nu^S(b_T, \mu) \tilde{S}(b_T, \mu, \nu) \quad (4.48b)$$

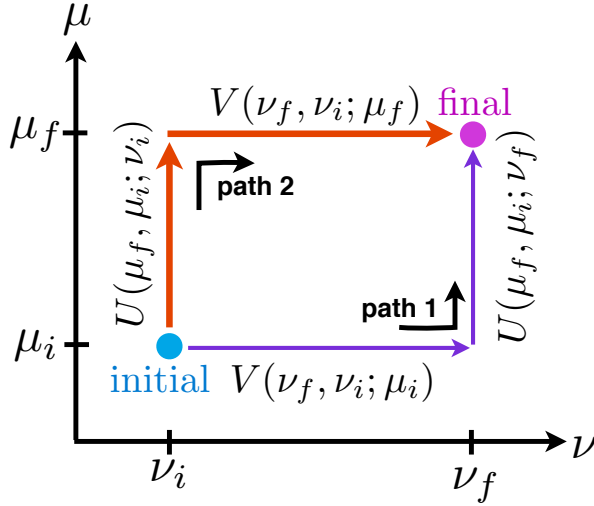


Figure 4.2: Two equivalent paths of RG and RRG evolution. The beam and soft functions in Eqs. (4.63) and (4.64) can be along either path, with Eq. (4.51) guaranteeing path independence of the combined evolution. Figure taken from [102].

for the soft function. The hard function just satisfies the RG equation

$$\mu \frac{d}{d\mu} H(Q, \mu) = \gamma_\mu^H(Q, \mu) H(Q, \mu). \quad (4.49)$$

The independence of the physical cross section Eq. (2.29b) on  $\mu, \nu$  imposes constraints on the beam, soft, and hard anomalous dimensions:

$$0 = \gamma_\mu^H(Q, \mu) + \gamma_\mu^S(\mu, \mu/\nu) + \gamma_\mu^B(\mu, \zeta_a/\nu^2) + \gamma_\mu^B(\mu, \zeta_b/\nu^2) \quad (4.50a)$$

$$0 = \gamma_\nu^S(b_T, \mu) + 2\gamma_\nu^B(b_T, \mu). \quad (4.50b)$$

Since Eq. (4.50b) requires  $\gamma_\nu^B = -\gamma_\nu^S/2$ , we will speak of a single “rapidity anomalous dimension”  $\gamma_\nu = \gamma_\nu^B$ . The commutativity of  $\mu$  and  $\nu$  derivatives also imposes a very powerful constraint on the beam and soft anomalous dimensions, namely,

$$\mu \frac{d}{d\mu} \gamma_\nu = \nu \frac{d}{d\nu} \gamma_\mu^B = 2\Gamma_{\text{cusp}}, \quad (4.51)$$

Here  $\Gamma_{\text{cusp}} = \Gamma_{\text{cusp}}^{q,g}$  depending on the flavor channel. These equations Eq. (4.51) guarantee that RG evolution along the two paths shown in Fig. 4.2 is equivalent. In Sec. 4.6 we will review an interpretation of Eq. (4.51) as the evolution of a conservative vector field.

The appearance of  $\Gamma_{\text{cusp}}$  on the RHS of Eq. (4.51) follows from the consistency condition Eq. (4.50a) with the hard anomalous dimension, which takes the form

$$\gamma_\mu^H(\mu) = -4\Gamma_{\text{cusp}}[\alpha_s(\mu)] \ln \frac{\mu}{Q} + \gamma_\mu^H[\alpha_s(\mu)], \quad (4.52)$$

with the coefficient of the log being proportional to  $\Gamma_{\text{cusp}}$  [102]. The  $\mu$ -anomalous dimensions

of the beam and soft functions take similar forms:

$$\gamma_\mu^B(\mu, \zeta/v^2) = \Gamma_{\text{cusp}}[\alpha_s(\mu)] \ln \frac{\nu^2}{\zeta} + \gamma_\mu^B[\alpha_s(\mu)] \quad (4.53a)$$

$$\gamma_\mu^S(\mu, \mu/v) = 4\Gamma_{\text{cusp}}[\alpha_s(\mu)] \ln \frac{\mu}{v} + \gamma_\mu^S[\alpha_s(\mu)], \quad (4.53b)$$

which imply the form for  $\gamma_\mu^i$  for the TMD PDF in Eq. (4.15b).

As for the rapidity anomalous dimensions, obtaining their all-orders form requires some care. At one loop, the (quark) beam and soft functions take the forms Eqs. (2.85) and (2.86), implying the one-loop values for the anomalous dimensions,

$$\gamma_\nu(b_T, \mu) = \frac{\alpha_s(\mu)}{4\pi} 2\Gamma_0 \ln \frac{\mu b_T}{b_0}, \quad (4.54)$$

recalling  $b_0 = 2e^{-\gamma_E}$ . The “non-cusp” parts are zero at one loop. Evaluated at a low scale  $\mu \sim b_T^{-1}$ , it is sufficient to evaluate the rapidity anomalous dimension at a fixed order. However, at a larger scale  $\mu$ , the  $\gamma_\nu$ ’s themselves contain large logs that need to be resummed. The resummed form can be obtained by integrating the consistency conditions Eq. (4.51):

$$\gamma_\nu(b_T, \mu) = 2 \int_{b_0/b_T}^\mu \frac{d\mu'}{\mu'} \Gamma_{\text{cusp}}[\alpha_s(\mu')] + \gamma_\nu[\alpha_s(b_0/b_T)], \quad (4.55)$$

where  $\gamma_\nu[\alpha_s(\mu)]$  is the “non-cusp” piece, and is the constant of integration at  $\mu = b_0/b_T$ , the scale where the log in the anomalous dimension vanishes, i.e.

$$\gamma_\nu[\alpha_s(b_0/b_T)] \equiv \gamma_\nu(b_T, \mu = b_0/b_T). \quad (4.56)$$

Perturbatively this non-cusp piece is nonzero starting at two loops.

In the next subsection we proceed to derive evolution of the TMD PDF  $\tilde{f}$  from the above evolution equations for beam and soft functions in SCET.

### 4.5.2 Combined TMD PDF evolution

In SCET it is natural to keep track of the evolution of the separate beam and soft functions each associated with a separate mode in the effective Lagrangian. However their evolution equations, Eqs. (4.47a) and (4.47b) for the beam function and Eqs. (4.48a) and (4.48b) for the soft function can also be recombined to give the evolution equations Eq. (4.12b) for the combined TMD PDF Eq. (2.36), which we repeat here:

$$\tilde{f}_j(x, \mathbf{b}_T, \mu, \zeta) = \tilde{B}_j(x, \mathbf{b}_T, \mu, \zeta/v^2) \sqrt{\tilde{S}(b_T, \mu, v)}. \quad (4.57)$$

It now obeys the evolution equations:

$$\mu \frac{d}{d\mu} \tilde{f}_j(x, \mathbf{b}_T, \mu, \zeta) = \gamma_\mu^j(\mu, \zeta) \tilde{f}_j(x, \mathbf{b}_T, \mu, \zeta) \quad (4.58a)$$

$$\zeta \frac{d}{d\zeta} \tilde{f}_j(x, \mathbf{b}_T, \mu, \zeta) = \frac{1}{2} \gamma_\zeta^j(\mu, b_T) \tilde{f}_j(x, \mathbf{b}_T, \mu, \zeta), \quad (4.58b)$$

where  $j = q, g$  as appropriate. The TMD PDF anomalous dimensions are given in terms of the beam and soft anomalous dimensions Eqs. (4.53a) and (4.53b), first for the  $\mu$ -anomalous dimension:

$$\begin{aligned}\gamma_\mu^j(\mu, \zeta) &= \gamma_\mu^{B_j}(\mu, \zeta/\nu^2) + \frac{1}{2}\gamma_\mu^S(\mu, \mu/\nu) \\ &= \Gamma_{\text{cusp}}^i[\alpha_s(\mu)] \ln \frac{\mu^2}{\zeta} + \gamma_\mu^j[\alpha_s(\mu)],\end{aligned}\quad (4.59)$$

where the non-cusp part of the anomalous dimension is given by

$$\gamma_\mu^j[\alpha_s(\mu)] = \gamma_\mu^{B_j}[\alpha_s(\mu)] + \frac{1}{2}\gamma_\mu^S[\alpha_s(\mu)] = -\frac{1}{2}\gamma_\mu^H[\alpha_s(\mu)].\quad (4.60)$$

In the rapidity evolution, the  $\nu$  evolution cancels between  $B$  and  $S$ , but the  $\zeta$  evolution of  $f$  is inherited from the beam function in Eq. (4.47b), giving

$$\begin{aligned}\gamma_\zeta^j(\mu, b_T) &= -\gamma_\nu(b_T, \mu) \\ &= -2 \int_{1/\bar{b}_T}^\mu \frac{d\mu'}{\mu'} \Gamma_{\text{cusp}}^j[\alpha_s(\mu')] + \gamma_\zeta^j[\alpha_s(1/\bar{b}_T)],\end{aligned}\quad (4.61)$$

using the resummed form given in Eq. (4.55), and where the non-cusp piece here is given by

$$\gamma_\zeta^j[\alpha_s] = \gamma_\nu^{B_j}[\alpha_s] + \frac{1}{2}\gamma_\nu^{S_j}[\alpha_s] = -\gamma_\nu[\alpha_s].\quad (4.62)$$

The evolution equations Eq. (4.58) coincide with the universal forms given at the beginning of the Chapter, Eq. (4.12).

### 4.5.3 RG and RRG solutions

Now we turn to solving the above evolution equations. The solutions to the RG and RRG evolution equations Eqs. (4.47a) and (4.47b) for the beam function and Eqs. (4.48a) and (4.48b) for the soft function can be obtained in straightforward manner. Evolution along the two equivalent paths illustrated in Fig. 4.2 allows us to write:

$$\tilde{B}(x, \mathbf{b}_T, \mu, \zeta/\nu^2) = \tilde{B}(x, \mathbf{b}_T, \mu_L, \zeta/\nu_H^2) U_B(\mu_L, \mu; \nu) V_B(\nu_H, \nu; \mu_L) \quad (4.63a)$$

$$= \tilde{B}(x, \mathbf{b}_T, \mu_L, \zeta/\nu_H^2) V_B(\nu_H, \nu; \mu) U_B(\mu_L, \mu; \nu_H), \quad (4.63b)$$

and

$$\tilde{S}(b_T, \mu, \nu) = \tilde{S}(b_T, \mu_L, \nu_L) U_S(\mu_L, \mu; \nu) V_S(\nu_L, \nu; \mu_L) \quad (4.64a)$$

$$= \tilde{S}(b_T, \mu_L, \nu_L) V_S(\nu_L, \nu; \mu) U_S(\mu_L, \mu; \nu_L), \quad (4.64b)$$

evolving both  $B, S$  from their “natural” scales where fixed-order logs in their expansions are small. The RG evolution kernels are given by:

$$U_B(\mu_L, \mu; \nu) = \exp \left[ \int_{\mu_L}^\mu \frac{d\mu'}{\mu'} \gamma_\mu^B(\mu', \zeta/\nu^2) \right], \quad U_S(\mu_L, \mu; \nu) = \exp \left[ \int_{\mu_L}^\mu \frac{d\mu'}{\mu'} \gamma_\mu^S(\mu', \mu'/\nu) \right] \quad (4.65)$$

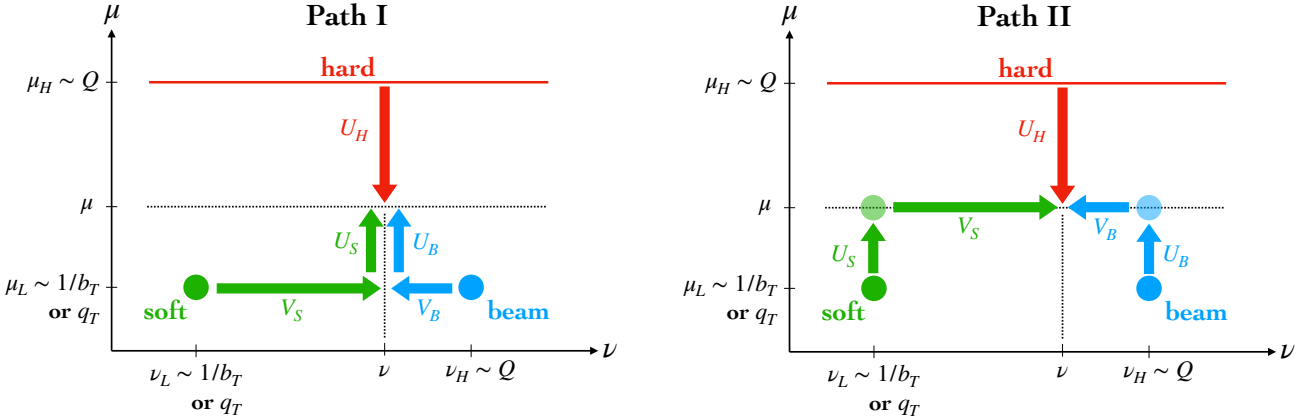


Figure 4.3: Two possible paths for RG and RRG evolution of ingredients of DY cross section for  $b_T$  or  $q_T$  resummation, from their “natural” scales to arbitrary scales  $\mu, \nu$ . The simplest path arises from choosing  $\mu \sim \mu_L$  and  $\nu \sim \nu_H$ , the natural scales for the beam function. Then we only need to RG evolve the hard function to  $\mu_L$  and RRG evolve the soft function to  $\nu_H$ .

In appendix E we give formulae for evaluating the integral over the anomalous dimensions in an explicit form at given orders of perturbative accuracy, in particular accounting for integrating the functions  $\alpha_s(\mu')$  that will appear in the expansions of the integrands. Meanwhile the RRG evolution kernels in Eqs. (4.63) and (4.64) are given by:

$$V_B(\nu_H, \nu; \mu) = \exp \left[ \int_{\nu_H}^{\nu} \frac{d\nu'}{\nu'} \gamma_v^B(b_T, \mu) \right] = \exp \left\{ \left[ 2\eta_\Gamma(b_0/b_T, \mu) + \gamma_v^B[\alpha_s(b_0/b_T)] \right] \ln \frac{\nu}{\nu_H} \right\} \quad (4.66)$$

$$V_S(\nu_L, \nu; \mu) = \exp \left[ \int_{\nu_L}^{\nu} \frac{d\nu'}{\nu'} \gamma_v^S(b_T, \mu) \right] = \exp \left\{ \left[ -4\eta_\Gamma(b_0/b_T, \mu) + \gamma_v^S[\alpha_s(b_0/b_T)] \right] \ln \frac{\nu}{\nu_L} \right\}.$$

The  $\nu'$  integrals are actually trivial to evaluate since the anomalous dimensions  $\gamma_v$  in Eq. (4.55) have no explicit  $\nu$  dependence. We have expressed the integral over the cusp piece in a resummed form  $\eta_\Gamma(b_0/\bar{b}_T, \mu)$ , where

$$\eta_\Gamma(\mu_L, \mu) = \int_{\mu_L}^{\mu} \frac{d\mu'}{\mu'} \Gamma_{\text{cusp}}[\alpha_s(\mu')], \quad (4.67)$$

whose explicit forms at specific orders of perturbative accuracy are also given in appendix E. It is imperative to use its resummed form when  $\mu b_T/b_0 \gg 1$ , e.g. when  $\mu$  is taken near the hard scale. Near  $\mu \sim b_0/b_T$  one could use a fixed-order truncation of  $\eta_\Gamma$ .

The hard function, meanwhile, just undergoes  $\mu$  evolution, with the solution

$$H(Q, \mu) = H(Q, \mu_H) U_H(\mu_H, \mu), \quad (4.68)$$

where

$$U_H(\mu_H, \mu) = \exp \left\{ \int_{\mu_H}^{\mu} \frac{d\mu'}{\mu'} \gamma_H[\alpha_s(\mu')] \right\}, \quad (4.69)$$

again whose explicit form at given orders of perturbative accuracy is given in appendix E.

In total then, the resummed Drell-Yan cross section in  $b_T$  space Eq. (4.43) can be written

$$\begin{aligned}\tilde{\sigma}(\mathbf{b}_T, x_a, x_b, Q; \mu_{L,H}, \nu_{L,H}) &= U_{\text{tot}}(\mu_{L,H}, \nu_{L,H}; \mu, \nu) H(Q^2, \mu_H) \tilde{S}(b_T, \mu_L, \mu_L/\nu_L) \\ &\quad \times \tilde{B}(x_a, \mathbf{b}_T, \mu_L, \zeta_a/\nu_H^2) \tilde{B}(x_b, \mathbf{b}_T, \mu_L, \zeta_b/\nu_H^2).\end{aligned}\quad (4.70)$$

Note on the LHS of Eq. (4.70) we have indicated the cross section should be independent of  $\mu, \nu$  that appear in the combination of all evolution kernels  $U_{\text{tot}}$ . In principle it is also independent of  $\mu_{L,H}, \nu_{L,H}$ , but in practice this is only true if summed to all orders in  $\alpha_s$ ; at a truncated resummed order, it retains subleading numerical dependence on these scale choices, which represents the freedom in choosing how to deal with the subleading terms at a given order of resummed accuracy. This variation is also a standard measure of the perturbative uncertainty at a given order of resummed accuracy, as varying the scales  $\mu_{L,H}, \nu_{L,H}$  probes the size of the missing subleading terms.

We can express  $U_{\text{tot}}$  in two ways, corresponding to the two equivalent paths in Fig. 4.3:

$$U_{\text{tot}}(\mu_{L,H}, \nu_{L,H}; \mu, \nu) \stackrel{\text{I}}{=} U_H(\mu_H, \mu) U_S(\mu_L, \mu; \nu) V_S(\nu_L, \nu; \mu_L) U_B^2(\mu_L, \mu; \nu) V_B^2(\nu_H, \nu; \mu_L) \quad (4.71\text{a})$$

$$\stackrel{\text{II}}{=} U_H(\mu_H, \mu) V_S(\nu_L, \nu; \mu) U_S(\mu_L, \mu; \nu_L) V_B^2(\nu_H, \nu; \mu) U_B^2(\mu_L, \mu; \nu_H) \quad (4.71\text{b})$$

Using our freedom to choose  $\mu, \nu$ , the simplest choices arise from choosing  $\mu = \mu_L$  and  $\nu = \nu_H$ , requiring only the hard function to be RG evolved down to  $\mu_L$  and the soft function RRG evolved to  $\nu_H$ :

$$U_{\text{tot}}(\mu_{L,H}, \nu_{L,H}) = U_H(\mu_H, \mu_L) V_S(\nu_L, \nu_H; \mu_L). \quad (4.72)$$

Of course the total evolution should be independent of the path chosen in Eq. (4.71).

At this point exactly where  $\mu_{H,L}$  and  $\nu_{H,L}$  are chosen is unspecified. The natural choices are that  $\mu_H, \nu_H \sim Q$  and  $\mu_L \sim \nu_L \sim b_0/b_T$  in  $b_T$  space. Making exactly these choices and performing the inverse transform in Eq. (2.29) to momentum space leads to correspondence with the more traditional picture presented in Sec. 4.3. With these scale choices and the exponentiated forms of  $U_H, V_S$  in Eqs. (4.69) and (4.66), we recognize that the solution in Eq. (4.70) achieves the resummation of the towers of fixed-order logs illustrated in Eq. (4.4), tower by tower, determined by the order of anomalous dimensions included according to Table 4.2. By using the forms of evolution kernels  $K_{\Gamma,\gamma}, \eta_\Gamma$  given in appendix E, each tower is captured in a simple, closed form in terms of ratios of the running coupling at different scales.

With such scale choices in  $b_T$  space, the inverse transform over  $b_T$  in Eq. (2.29) requires a prescription (such as  $b_*$  in Eq. (4.23)) to regulate the integral over large  $b_T$ . In the SCET picture, we are led to consider the scales of the hard, collinear, and soft modes to be freely variable to start with, and in particular  $\mu_L, \nu_L$  do not need to be chosen as functions of  $b_T$  prior to doing the integral. This leads to alternate methods to perform the resummation directly in momentum space (e.g. [255, 256]) or to a hybrid scheme to choose the scales partially in  $b_T$  and partially in  $q_T$  space [257], see Sec. 4.8.

## 4.6 Two-Dimensional Evolution

The two-dimensional nature of the TMD evolution equations Eq. (4.58) allows for a nice interpretation with analogues to electromagnetism and other fields of physics, as first presented by [238], in which Eq. (4.58) is expressed as a vector differential equation. First, we define the vectors of evolution variables and anomalous dimensions:

$$\boldsymbol{\nu} = (\ln \mu, \ln \zeta), \quad \mathbf{E}(\boldsymbol{\nu}, b_T) = \left( \gamma_\mu(\boldsymbol{\nu}), \frac{1}{2} \gamma_\zeta(\boldsymbol{\nu}, b_T) \right). \quad (4.73)$$

The RG and RRG equations in Eq. (4.58) are then expressed as the single vector equation

$$\nabla f(x, \mathbf{b}_T, \boldsymbol{\nu}) = \mathbf{E}(\boldsymbol{\nu}, b_T) f(x, \mathbf{b}_T, \boldsymbol{\nu}), \quad (4.74)$$

where  $\nabla = d/d\boldsymbol{\nu} = (d/d\ln \mu, d/d\ln \zeta)$ . The consistency relations in Eq. (4.51) are then equivalent to the property that  $\mathbf{E}$  is a conservative vector field, which is the gradient of a potential:

$$\nabla \times \mathbf{E} = 0 \Rightarrow \mathbf{E}(\boldsymbol{\nu}, b_T) = \nabla U(\boldsymbol{\nu}, b_T). \quad (4.75)$$

In terms of  $U$ , the solution of the vector RGE Eq. (4.74) for the TMD  $f$  can be expressed:

$$\ln \frac{f(x, \mathbf{b}_T, \boldsymbol{\nu}_f)}{f(x, \mathbf{b}_T, \boldsymbol{\nu}_i)} = \int_{\boldsymbol{\nu}_i}^{\boldsymbol{\nu}_f} d\boldsymbol{\nu} \cdot \mathbf{E}(\boldsymbol{\nu}, b_T) = \int_{\boldsymbol{\nu}_i}^{\boldsymbol{\nu}_f} d\boldsymbol{\nu} \cdot \nabla U(\boldsymbol{\nu}, b_T) = U(\boldsymbol{\nu}_f) - U(\boldsymbol{\nu}_i). \quad (4.76)$$

An explicit solution for  $U$  takes the form:

$$U(\boldsymbol{\nu}, b_T) = \frac{\ln \zeta}{2} \gamma_\zeta(\mu, b_T) + \int^\mu d \ln \mu' \left\{ \Gamma_{\text{cusp}}[\alpha_s(\mu')] \ln \mu'^2 + \gamma_\mu[\alpha_s(\mu')] \right\} + F(b_T), \quad (4.77)$$

where  $F$  is a function of only  $b_T$ . Using the resummed form Eq. (4.61) for  $\gamma_\zeta$ , and taking the difference of potentials in Eq. (4.76), we obtain for the total TMD evolution between  $\boldsymbol{\nu}_i$  and  $\boldsymbol{\nu}_f$ :

$$\begin{aligned} U(\boldsymbol{\nu}_f) - U(\boldsymbol{\nu}_i) &= \int_{\mu_i}^{\mu_f} d \ln \mu \left\{ \Gamma_{\text{cusp}}[\alpha_s(\mu)] \ln \frac{\mu^2}{\zeta_f} + \gamma_\mu[\alpha_s(\mu)] \right\} \\ &\quad + \left\{ - \int_{1/\bar{b}_T}^{\mu_i} d \ln \mu \Gamma_{\text{cusp}}[\alpha_s(\mu)] + \frac{1}{2} \gamma_\zeta[\alpha_s(1/\bar{b}_T)] \right\} \ln \frac{\zeta_f}{\zeta_i} \\ &= \int_{\mu_i}^{\mu_f} d \ln \mu \left\{ \Gamma_{\text{cusp}}[\alpha_s(\mu)] \ln \frac{\mu^2}{\zeta_i} + \gamma_\mu[\alpha_s(\mu)] \right\} \\ &\quad + \left\{ - \int_{1/\bar{b}_T}^{\mu_f} d \ln \mu \Gamma_{\text{cusp}}[\alpha_s(\mu)] + \frac{1}{2} \gamma_\zeta[\alpha_s(1/\bar{b}_T)] \right\} \ln \frac{\zeta_f}{\zeta_i}, \end{aligned} \quad (4.78)$$

in which we recognize the two forms that come from the one-dimensional evolution along the two equivalent straight-line paths in Fig. 4.4 or Eq. (4.71).

The 2-D picture affords another cute way to illustrate this evolution. We can consider the *equipotential* lines, which are always orthogonal to the evolution field  $\mathbf{E}$ , along which there is zero evolution. Parameterizing such a line in  $\boldsymbol{\nu}$  space by

$$\boldsymbol{\omega}(t; \boldsymbol{\nu}_0) = (t, \ln \zeta_{\text{equi}}(t))|_{\boldsymbol{\nu}_0}, \quad (4.79)$$

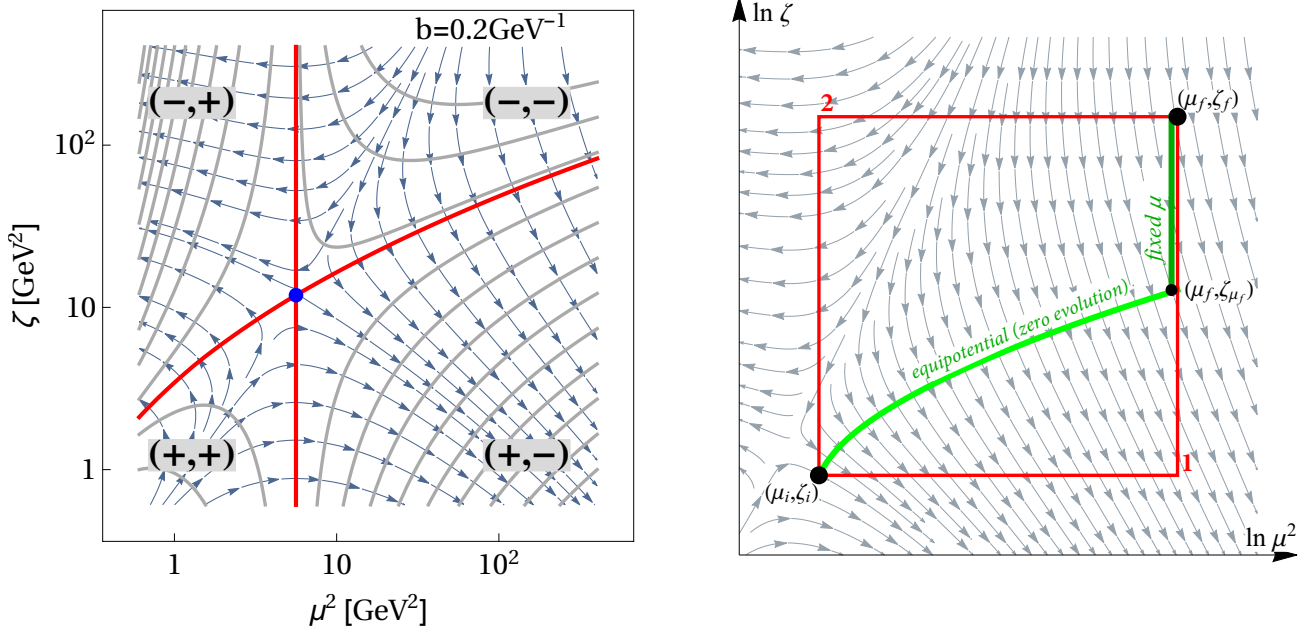


Figure 4.4: 2-D evolution field for TMD evolution. *Left:* Field lines for 2-D anomalous dimensions Eq. (4.73) and equipotential lines in grey. The two red lines pass through the saddle point. *Right:* TMD evolution along the straight line paths similar to Fig. 4.3 in red, and along a path incorporating an equipotential line in green. Figures taken/modifies from [238].

with the equipotential line passing through a specified point  $\nu_0 = (\ln \mu_0, \ln \zeta_0)$  and  $t = \ln \mu$ , we solve the equation for an equipotential line,

$$\frac{d\omega}{d \ln \mu} \cdot \nabla U(\nu, b_T) = 0 \quad \Rightarrow \quad \frac{\partial U}{\partial \ln \mu} + \frac{d \ln \zeta_{\text{equi}}}{d \ln \mu} \frac{\partial U}{\partial \ln \zeta} = 0. \quad (4.80)$$

whose solution is,

$$\ln \zeta_{\text{equi}}(\mu; \mu_0, \zeta_0) = \frac{-2 \int_{\mu_0}^{\mu} d \ln \mu' \left\{ \Gamma_{\text{cusp}}[\alpha_s(\mu')] \ln \mu'^2 + \gamma_\mu[\alpha_s(\mu')] \right\} + \gamma_\zeta(\mu_0) \ln \zeta_0}{\gamma_\zeta(\mu, b_T)}. \quad (4.81)$$

Along the line  $(\mu, \zeta_{\text{equi}}(\mu; \mu_0, \zeta_0))$ , the total evolution from  $(\mu_0, \zeta_0)$  is zero, and  $f(x, \mathbf{b}_T, \nu)$  is the same everywhere on this line. This lets us envision evolution along the green path shown in Fig. 4.4, so the nonzero evolution is only along the vertical segment from  $\zeta_f$  to  $\zeta_{\text{equi}}$  at  $\mu_f$ :

$$U(\nu_f) - U(\nu_i) = \frac{1}{2} \gamma_\zeta(\mu_f, b_T) \ln \frac{\zeta_f}{\zeta_{\text{equi}}(\mu_f; \mu_0, \zeta_0)}, \quad (4.82)$$

which is a nice, compact expression. Plugging in Eq. (4.81), however, we see it is perfectly equivalent to the expressions Eq. (4.78), encoding the evolution in the horizontal  $\mu$  direction instead in the exact location of  $\zeta_{\text{equi}}$  as a function of the initial  $\mu_0, \zeta_0$ . At any finite order of resummed accuracy, these scales (or at least the final location of  $\zeta_{\text{equi}}(\mu_f; \nu_0)$ ) should still be varied to probe the residual theoretical uncertainty.

## 4.7 Connecting Resummation to Fixed Order

A primary goal of transverse-momentum-dependent (TMD) factorization theorems [10, 63, 74, 75, 86, 99, 114, 119, 122, 241], is to describe the cross section as a function of the transverse momentum  $\mathbf{q}_T$  point-by-point, from small  $q_T \sim m$  (where  $m$  is a typical hadronic mass scale), to large  $q_T \sim Q$ , where  $Q$  is a large momentum or mass in the reaction and sets the hard scale [178, 235, 242, 243]. In order to achieve this, Collins, Soper and Sterman organized the cross section in the additive form  $W + Y$  [10, 83, 86, 119] (see Eq. (2.27)). As detailed in Section 2.2 the  $W$ -term is valid for  $q_T \ll Q$  and involves the TMD PDFs. They depend on intrinsic transverse momentum as well as the usual momentum fraction variables and since TMD factorization is necessary to describe processes that are sensitive to transverse momentum, that is small compared to the hard scale. They are the natural quantities that describe the partonic content of target and produced hadrons in deep inelastic (DIS) processes. The  $Y$ -term, which involves collinear PDFs serves as a correction for larger  $q_T$  values and is the difference between the collinear cross section for  $q_T \sim Q$  beginning at a fixed order in the strong coupling, and its small transverse momentum asymptotic limit for  $m \ll q_T \ll Q$  [63, 244, 245]. The latter is called the asymptotic term (AY) [10, 63, 249].

Various methods are in use to ensure the two terms match or interpolate smoothly [63, 66, 249, 250, 260, 1232? ? ]. For large  $q_T$ , the resummed  $W$  term is re-expanded in fixed-order, yielding the singular log terms at a given order  $\alpha_s^n$ , the AY term, and the  $Y$  term matches it onto the correct full QCD result at this fixed order. The latter is the fixed order term (FO). To do this properly, two things need to be done, for both of which there are multiple valid approaches. First, the resummation in the  $W$  term should be “turned off” for large  $q_T$  so it gets truncated at a fixed order in  $\alpha_s$ ; in this region, logs and non-logs are of similar size and the former no longer should be resummed to all orders in  $\alpha_s$ . Second, since the fixed-order expansion of  $W$  will be missing the non-logs at the desired fixed order in  $\alpha_s$ , the missing terms must be added back in the  $Y$  term. The transition between resummation and fixed-order regions and the matching onto the full fixed-order QCD result should be achieved in a smooth, well-defined manner.

### 4.7.1 Matching in the CSS formalism

We begin with a synopsis of the  $W + Y$  construction  $q_T$ -differential cross section, Eq. (2.27) which we abbreviate as,

$$\Gamma(\mathbf{q}_T, Q, S) \equiv \frac{d\sigma}{dQ dY d^2\mathbf{q}_T} = W(\mathbf{q}_T, Q, S) + Y(\mathbf{q}_T, Q, S) + O((m/Q)^c), \quad (4.83)$$

where  $\mathbf{q}_T$  and  $Q^2$  are the transverse momentum and virtuality, respectively, of the virtual photon. In Eq. (4.83), the  $W$ -term factorizes into TMD PDFs (and FFs in SIDIS and SIA) and is valid for  $q_T \ll Q$ , while the  $Y$ -term serves as a correction for larger  $q_T$  values and uses collinear PDFs and FFs.

The construction of the cross section in Eq. (4.83) as the sum of  $W(\mathbf{q}_T, Q, S)$  and  $Y(\mathbf{q}_T, Q, S)$  results from applying so-called “approximators” in the context of factorization, to  $\Gamma(\mathbf{q}_T, Q, S)$  [5, 10, 249] that are designed to be valid for the corresponding momentum regions of  $q_T$ .

The  $W$  term is defined from the TMD approximator,  $T_{\text{TMD}}$

$$W(q_T, Q) \equiv T_{\text{TMD}}\Gamma(q_T, Q), \quad (4.84)$$

where for the purposes of this discussion, we consider the  $W$  term for the unpolarized case. The  $T_{\text{TMD}}$  “approximator” is an instruction to replace the object to its right by an approximation that is designed to be good in the  $q_T \ll Q$  momentum region where the approximation has fractional errors of the order  $(q_T/Q)^a$  or  $(m/Q)^{a'}$ . That is, it replaces the exact  $\Gamma(q_T, Q)$  by the approximate  $W(q_T, Q)$ :

$$T_{\text{TMD}}\Gamma(q_T, Q) = \Gamma(q_T, Q) + O\left(\frac{q_T}{Q}\right)^a \Gamma(q_T, Q) + O\left(\frac{m}{Q}\right)^{a'} \Gamma(q_T, Q), \quad (4.85)$$

with where  $a, a' > 0$ .

Another approximator,  $T_{\text{coll}}$ , handles the large  $q_T \sim Q$  region. It replaces  $\Gamma(q_T, Q)$  with an approximation that is good when  $q_T \sim Q$  with a fractional error of  $(m/q_T)^b$ . That is,

$$T_{\text{coll}}\Gamma(q_T, Q) = \Gamma(q_T, Q) + O\left(\frac{m}{q_T}\right)^b \Gamma(q_T, Q), \quad (4.86)$$

where  $b > 0$ . Since  $T_{\text{coll}}$  is to be applied to the  $q_T \sim Q$  region, one only needs collinear factorization at a fixed order [63, 233] and with a hard scale  $\mu \sim Q$ .

If  $m \lesssim q_T$  and  $q_T \sim Q$  were the only regions of interest, then the  $T_{\text{TMD}}$  and  $T_{\text{coll}}$  approximators would be sufficient. One could simply calculate using fixed order collinear factorization for the large  $q_T$ -dependence and TMD factorization for small  $q_T$ -dependence. A reasonable description of the full transverse momentum dependence would be obtained by simply interpolating between the two descriptions [??].

However, the region between large and small  $q_T$  needs special treatment if errors are to be power suppressed point-by-point in  $q_T$ . The standard method is to construct a sequence of nested subtractions [10]. The smallest-size region is a neighborhood of  $q_T = 0$ , where  $T_{\text{TMD}}$  gives a very good approximation. So, one starts by adding and subtracting the  $T_{\text{TMD}}$  approximation:

$$\Gamma(q_T, Q) = T_{\text{TMD}}\Gamma(q_T, Q) + \left[ \Gamma(q_T, Q) - T_{\text{TMD}}\Gamma(q_T, Q) \right]. \quad (4.87)$$

From Eq. (4.85), the error term in the square brackets is order  $(q_T/Q)^a$  and is only unsuppressed at  $q_T \gg m$ . Thus, one can apply  $T_{\text{coll}}$  and then use a fixed-order perturbative expansion in collinear factorization:

$$\begin{aligned} \Gamma(m \lesssim q_T \lesssim Q, Q) &= T_{\text{TMD}}\Gamma(q_T, Q) + T_{\text{coll}}[\Gamma(q_T, Q) - T_{\text{TMD}}\Gamma(q_T, Q)] \\ &\quad + O\left(\left(\frac{m}{q_T}\right)^b \left(\frac{q_T}{Q}\right)^a\right) \Gamma(q_T, Q) \\ &\quad + O\left(\left(\frac{m}{q_T}\right)^b \left(\frac{m}{Q}\right)^{a'}\right) \Gamma(q_T, Q) \\ &= W(q_T, Q) + T_{\text{coll}}\Gamma(q_T, Q) - T_{\text{coll}}T_{\text{TMD}}\Gamma(q_T, Q) \\ &\quad + O\left(\frac{m}{Q}\right)^c \Gamma(q_T, Q), \end{aligned} \quad (4.88)$$

where  $c = \min(a, a', b)$ . Thus, the cross section is determined point-by-point in the mid- $q_T$  region, up to powers of  $m/Q$ , by a combination of TMD and collinear correlation functions.

This construction of  $W + Y$  defines  $W$ , Eq. (4.84), the first term, and  $Y$ , to be the second and third terms after the second equality in Eq. (4.88): that is,

$$Y(q_T, Q) \equiv T_{\text{coll}}\Gamma(q_T, Q) - T_{\text{coll}}T_{\text{TMD}}\Gamma(q_T, Q). \quad (4.89)$$

The specific definitions of  $T_{\text{coll}}$  and  $T_{\text{TMD}}$  allowed Eq. (4.88) to work only in the  $m \lesssim q_T \lesssim Q$  region, which we emphasize by the argument on the left side of Eq. (4.88).

In common terminology, the first term in braces in Eq. (4.89) is called the “fixed order” (FO) contribution, while the second term is the “asymptotic” (AY) contribution. We will use the notation

$$\text{FO}(q_T, Q) \equiv T_{\text{coll}}\Gamma(q_T, Q) \quad (4.90)$$

$$\text{AY}(q_T, Q) \equiv T_{\text{coll}}T_{\text{TMD}}\Gamma(q_T, Q). \quad (4.91)$$

This corresponds to the terminology in, for example, Ref. [244]. The term “fixed order” is meant to imply that the calculation of  $\Gamma$  is done entirely with collinear factorization with hard parts calculated to low order in perturbation theory using  $\mu = Q$  and with collinear PDFs (and in the case of SIDIS or SIA, FFs) calculated using  $\mu = Q$ . That is, the hard part and the parton correlation functions are evaluated at the same scale.

The resulting cross section is accurate up to an error that is of order  $(m/Q)^c$ , where  $c$  is a positive power, and  $m$  is a typical hadronic mass scale. We note that the actual value for  $c$  in the error term  $O((m/Q)^c)$  depends on which structure function we look at in  $\Gamma(\mathbf{q}_T, Q, S)$ .

In the next subsection we provide some details on the implementation of the approximators and the and we will examine some of the complications involved when combining (matching) TMD factorization with collinear factorization to allow accurate predictions over the whole range of measured transverse momentum in a process like Drell-Yan [240, 262]... [other refs]. We review some improved methods for combining the two types of factorization [249, 261].

#### 4.7.2 Improved Matching TMD and Collinear Factorization

The error estimates in Eq. (4.88) are inapplicable outside this range, i.e., they must not be applied when  $q_T \gg Q$  or  $q_T \ll m$ . This is because they were extracted from the leading power of expansions in relatively small kinematic variables  $q_T/Q$  and  $m/q_T$  to give Eqs. (4.85) and (4.86). The issues are illustrated by Eq. (4.86). The  $(m/q_T)^b$  estimate is obtained from an expansion in powers of mass with respect to the smallest scale in the collinear hard-scattering; it is of the order of the first omitted term in the expansion. But once  $q_T$  gets much smaller, the error can be arbitrarily larger.

The above observations do not represent a fundamental breakdown of the formalism. They merely indicate that some extra care is needed to construct a formalism valid also for  $q_T \lesssim m$  and  $q_T \gtrsim Q$ .

Let’s consider first,  $q_T \lesssim m$ : Clearly collinear factorization is certainly not applicable for the differential cross section. But this region is actually where the  $W$ -term in Eq. (4.85) has its highest validity. So one simply must ensure that the would-be  $Y$ -term

$$T_{\text{coll}}\Gamma(q_T, Q) - T_{\text{coll}}T_{\text{TMD}}\Gamma(q_T, Q) \quad (4.92)$$

is sufficiently suppressed in Eq. (4.88) for  $q_T \lesssim m$ . Therefore, we will modify the usual definition of  $Y$  by inserting a suppression factor at low  $q_T$ :

$$\begin{aligned} Y(q_T, Q) &\equiv \{T_{\text{coll}} [\Gamma(q_T, Q) - W(q_T, Q)]\} X(q_T/\lambda) \\ &= \{T_{\text{coll}} \Gamma(q_T, Q) - T_{\text{coll}} T_{\text{TMD}} \Gamma(q_T, Q)\} X(q_T/\lambda). \end{aligned} \quad (4.93)$$

The smooth cutoff function  $X(q_T/\lambda)$  approaches zero for  $q_T \lesssim \lambda$  and unity for  $q_T \gtrsim \lambda$ . It ensures that the  $Y$ -term is a correction for  $q_T \gtrsim m$  only. As long as  $\lambda = O(m)$ , any  $\lambda$ -dependence must be weak. This is analogous to the introduction of a  $Q_T^{\min}$  in Ref. [63, Eq. (2.8)].

The exact functional form of  $X(q_T/\lambda)$  is arbitrary, but is most useful in calculations if it sharply suppresses  $q_T \ll m$  contributions while not affecting  $q_T \gtrsim m$ . While a step function is acceptable, we suggest using a slightly smoother function since one expects the transition from perturbative to non-perturbative physics to be relatively smooth. One possible choice is

$$X(q_T/\lambda) = 1 - \exp \{-(q_T/\lambda)^{a_X}\}. \quad (4.94)$$

This is what is used in sample calculations in [249]. A large value for the power  $a_X$  makes the switching function more like a step function.

So, now,

$$Y(q_T, Q) \equiv \{\text{FO}(q_T, Q) - \text{AY}(q_T, Q)\} X(q_T/\lambda). \quad (4.95)$$

The term “fixed order” here is meant to imply that the calculation of  $\Gamma$  is done entirely with collinear factorization with hard parts calculated to low order in perturbation theory using  $\mu = Q$  and with collinear pdfs (and ffs in the case of SIDIS and SIA) calculated using  $\mu = Q$ . That is, the hard part and the parton correlation functions are evaluated at the same scale.

Now one can extend the power suppression error estimate in Eq. (4.88) down to  $q_T = 0$  to recover Eq. (4.83). Equation Eq. (4.88) becomes

$$\Gamma(q_T \lesssim Q, Q) = W(q_T, Q) + Y(q_T, Q) + \mathcal{O}\left(\frac{m}{Q}\right)^c \Gamma(q_T, Q), \quad (4.96)$$

which is Eq. (4.83), but restricted to  $q_T \lesssim Q$ .

So far, aside from introducing an explicit  $X(q_T/\lambda)$ , we have only reviewed the standard  $W+Y$  construction. The  $q_T \lesssim Q$  restriction on the left of Eq. (4.96) should be emphasized. Since we rely on strict power counting in  $q_T/Q$  and  $m/q_T$ , the region of  $q_T \gtrsim Q$  is not guaranteed to be well-described by the above  $W+Y$  construction.

Also, these modifications to the transition to the  $q_T/Q \gtrsim 1$  region will leave the standard treatment of TMD factorization [10] in the  $q_T/Q \ll 1$  region only slightly modified. In particular, the operator definitions for transverse-coordinate-space TMD functions, along with their evolution properties, are exactly the same as in the usual formalism. This is an important aspect of these modifications [249].

Next, a modification of the definition of  $W$  was carried out. This is to provide a convenient solution to the problem that with the definition of the  $W$  term, the integral over all  $\mathbf{q}_T$  of  $W(q_T)$  is zero, because  $\hat{W}(b_T)$  is zero at  $b_T = 0$  [249].

It would be preferable for the integral to have a normal collinear expansion in terms of pdfs and ffs at scale  $\mu_Q$ ; the lowest order term then reproduces the lowest order collinear

factorization result for the integrated cross section. At the same time, we wish to preserve the results for the Fourier transform of  $\tilde{W}(b_T)$ , since these embody the derived factorization and evolution properties. Most importantly, the modified  $W$  term must still approximate the cross section at low  $q_T$  to the same accuracy as in Eq. (4.85). One can achieve the modified  $W$  in two stages.

The first is to modify the Fourier transform of the  $W$  term where by  $\tilde{W}(b_T, Q)$  we refer to the integrand of Eq. (4.7) to read

$$W_a(q_T, Q; \eta, C_5) = \int \frac{d^2 \mathbf{b}_T}{(2\pi)^2} e^{i \mathbf{q}_T \cdot \mathbf{b}_T} \tilde{W}(b_c(b_T), Q). \quad (4.97)$$

where

$$b_c(b_T) = \sqrt{b_T^2 + b_0^2 / (C_5 Q)^2}. \quad (4.98)$$

That is,  $\tilde{W}(b_T, Q)$  is replaced by  $\tilde{W}(b_c(b_T), Q)$ . The function  $b_c(b_T)$  is arranged to agree with  $b_T$  when  $b_T \gg 1/Q$ , but to be of order  $1/Q$  when  $b_T = 0$ , thereby providing a cutoff at small  $b_T$ . Then, when Eq. (4.97) is integrated over  $\mathbf{q}_T$ , we get  $\tilde{W}(b_0/(C_5 Q), Q)$ , instead of the previous value  $\tilde{W}(0, Q) = 0$ . We have included an explicit numerical factor of  $b_0 \equiv 2 \exp(-\gamma_E)$ . We have chosen the value of  $b_c(0)$  to be proportional to  $1/Q$ , so that,  $\tilde{W}(b_0/(C_5 Q), Q)$  has a normal collinear factorization property. The numerical constant  $C_5$  fixes the exact proportionality between  $b_c(0)$  and  $1/Q$ .

Note that the integrand in (4.97) is non-singular at  $b_T = 0$ , unlike the unmodified  $\tilde{W}(b_T, Q)$ . Thus the large  $q_T$  behavior is exponentially damped. Even so, the function still extends to arbitrarily large  $q_T$ .

The second and final stage of modification for  $W$  is to make an explicit cutoff at large  $q_T$ , to give:

$$W_{\text{New}}(q_T, Q; \eta, C_5) \equiv \Xi\left(\frac{q_T}{Q}, \eta\right) \int \frac{d^2 \mathbf{b}_T}{(2\pi)^2} e^{i \mathbf{b}_T \cdot \mathbf{q}_T} \tilde{W}(b_c(b_T), Q). \quad (4.99)$$

Here  $\Xi(q_T/(Q\eta))$  is a cutoff function that we introduce to ensure that  $W_{\text{New}}(q_T, Q; \eta, C_5)$  vanishes for  $q_T \gtrsim Q$ , and  $\eta$  is a parameter to control exactly where the suppression of large  $q_T$  begins.  $\Xi(q_T/Q, \eta)$  should approach unity when  $q_T \ll Q$  and should vanish for  $q_T \gtrsim Q$ . This preserves the required approximation property of  $W_{\text{New}}(q_T, Q; \eta, C_5)$  at small  $q_T$ . At the same time, since the changes are dominantly at large  $q_T$ , the integral over all  $\mathbf{q}$  still has a normal collinear expansion, as we will make more explicit below.

A simple  $\Theta(Q - q_T)$  step function is acceptable for  $\Xi$ . When we combine  $W_{\text{New}}(q_T, Q; \eta, C_5)$  with a  $Y$  one introduce methods to minimize sensitivity to the exact form of  $\Xi(q_T/Q, \eta)$ . However, a smoother function is preferred since the domain of validity of the  $W$ -term approximation does not end at a sharp point in  $q_T$ , and thus a smooth function characterizes general physical expectations. A reasonable choice is

$$\Xi\left(\frac{q_T}{Q}, \eta\right) = \exp\left[-\left(\frac{q_T}{\eta Q}\right)^{a_\Xi}\right], \quad (4.100)$$

with  $a_\Xi > 2$ .

The only differences between the old and new  $W$ -term are: i) the use of  $b_c(b_T)$  rather than  $b_T$  in  $\tilde{W}$ , and ii) the multiplication by  $\Xi(q_T/Q, \eta)$ . (The second modification was proposed by Collins [10]. There  $\Xi$  is called  $F(q_T/Q)$ .) Equation (4.99) matches the standard definition in the limit that  $C_5$  and  $\eta$  approach infinity.

### 4.7.3 SCET: profile scales

In SCET the  $W$  in Eq. (4.83) may be viewed as the part of the cross section predicted using the leading-power effective theory Lagrangian, resummed using all the technology reviewed in Sec. 4.5. The  $T$  approximator in Eq. (4.84) can be viewed as the set of instructions that describes how to match QCD onto leading-power SCET and compute with it, with power corrections being contained in the corresponding terms of Eq. (4.85). The  $Y$  term would be described in SCET as the difference between the prediction of fixed-order perturbative calculation in full QCD with the truncated fixed-order expansion of the resummed leading-power SCET prediction, called the “non-singular function” or “remainder function”. A smooth interpolation that combines the resummed prediction with this fixed-order remainder is then needed.

In SCET the matching of the resummed result ( $W$ ) onto the fixed-order result for large  $q_T$  ( $Y$ ) is naturally achieved by the use of so-called “profile scales”, see, e.g., [236, 253, 263]. The  $W$ -term cross section Eq. (4.70) sums logs of  $\mu_L/\mu_H$  or  $\nu_L/\nu_H$ , where  $\mu_L, \nu_L \sim 1/b_T$  or  $q_T$ , and  $\mu_H, \nu_H \sim Q$ . These logs are large and must be resummed when the low and high scales are actually well separated. However, for  $1/b_T$  or  $q_T \sim Q$ , the logs are no longer large, and equally important as the non-singular terms in the  $Y$ -term part of the cross section. The resummation of logs in the  $W$  term can be smoothly turned off, and properly matched with the non-singular  $Y$  term, by choosing  $\mu_L, \nu_L$  to be functions of  $1/b_T$  or  $q_T$  such that for some value  $1/b_T, q_T \lesssim Q$ , the low and high scales merge, that is,

$$\mu_L = \mu_{\text{run}}(q_T), \quad \nu_L = \nu_{\text{run}}(q_T), \quad (4.101)$$

(or, alternatively, as functions of  $1/b_T$ ), where  $\mu_{\text{run}}, \nu_{\text{run}}$  are *profile functions*, which must have the behavior

$$\mu_{\text{run}}(q_T), \nu_{\text{run}}(q_T) \sim \begin{cases} \mu_0, \nu_0 & \Lambda_{\text{QCD}} \lesssim q_T \ll Q \\ q_T & \Lambda_{\text{QCD}} \ll q_T \ll Q \\ \mu_H & 1/b_T, q_T \gtrsim Q, \end{cases} \quad (4.102)$$

which freezes the scales at  $\mu_0, \nu_0 \gtrsim \Lambda_{\text{QCD}}$  for very low  $q_T$ , to allow for matching onto a nonperturbative model (a key difference to the  $b^*$  prescription is that this only freezes out the scales, not  $b_T$  itself); achieves perturbative resummation of logs of  $q_T/Q$  in the region where these logs are large; and turns off the resummation in the  $W$  term by setting all scales equal  $\mu_L, \nu_L = \mu_H, \nu_H$  for large  $q_T$ , automatically turning it into a fixed-order expansion of the log terms. Then in the large  $q_T$  region, the  $W$  and  $Y$  terms automatically combine to give the correct full QCD prediction at a fixed order in  $\alpha_s$ , where  $W$  and  $Y$  satisfy the relation

$$\sigma_{\text{FO}(n)}^{\text{QCD}} = \sigma^W|_{\text{FO}(n)} + \sigma_{(n)}^Y, \quad (4.103)$$

with the subscript  $(n)$  indicating the  $\alpha_s^n$  term in the fixed-order expansion of the full QCD prediction, the expanded  $W$  term, or the nonsingular  $Y$  term.

Exactly how the profile scales interpolate between the regions indicated in Eq. (4.102) is a matter of choice. A simple example (by no means unique) from [257] interpolating between

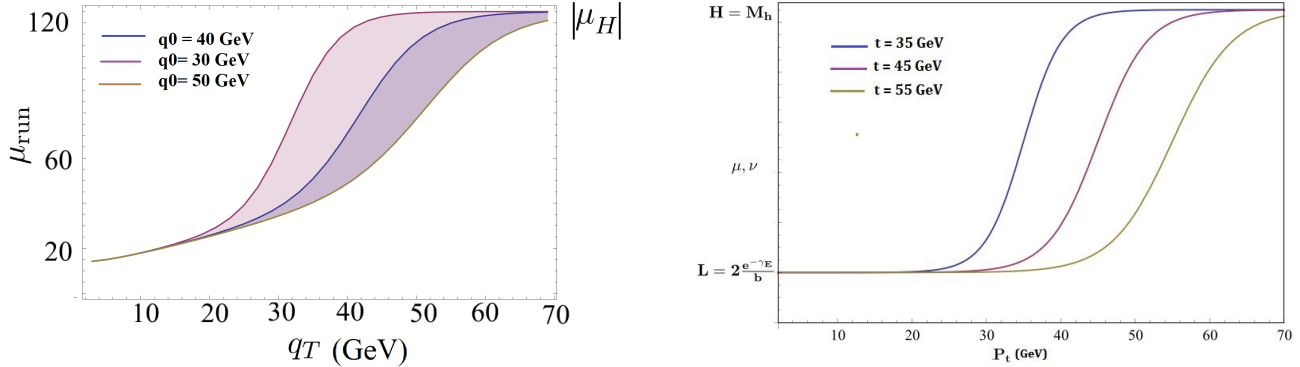


Figure 4.5: Examples of profile functions for scales  $\mu_L, \nu_L$  interpolating between resummation region for small  $q_T$  or  $1/b_T$  and high  $q_T \sim Q$  [257, 264].

the resummation and fixed-order region is:

$$\mu_{\text{run}}(q_T), \nu_{\text{run}}(q_T) = q_T^{1-\zeta(q_T)} \mu_H^{\zeta(q_T)}, \quad \zeta(q_T) = \frac{1}{2} \left\{ 1 + \tanh \left\{ \rho \left( \frac{q_T}{q_0} - 1 \right) \right\} \right\}, \quad (4.104)$$

where  $\rho$  controls the rate of the rise of the profile from low to high values, and  $q_0$  controls the transition point. This point should be chosen to occur close the region where nonsingular terms become comparable in size to the logs in the singular part, see Fig. 4.5 (left). Another example from [264] is:

$$\mu_{\text{run}}, \nu_{\text{run}} = \frac{L}{2} \left\{ 1 - \tanh \left[ s \left( \frac{4q_T}{t} - 4 \right) \right] \right\} + \frac{H}{2} \left\{ 1 + \tanh \left[ s \left( \frac{4q_T}{t} - 4 \right) \right] \right\}, \quad (4.105)$$

with  $L, H$  the initial (low) and final (high) values of the scales and  $s, t$  determining the rate and location of the transition, respectively, see Fig. 4.5 (right).

Many other choices for functional forms of profile scales are possible. Variations in profile parameters can form part of the estimate of theoretical uncertainty. All of this is to illustrate the flexibility afforded by the variable and various scales in the effective field theory framework allowing smooth connections of resummed, fixed-order, and nonperturbative regimes, and robust estimations of theoretical uncertainties.

In the notation of Table 4.2, when a resummed  $W$  term at a given accuracy is matched onto a  $Y$  term at a given fixed-order accuracy, the literature will normally refer to the accuracy of such a matched cross section as  $N^k \text{LL}' + N^n \text{LO}$  or  $N^k \text{LL}' + O(\alpha_s^m)$ , as the case may be. Recall that the primed ' accuracies of the resummed part indicate that the finite coefficient functions  $\tilde{C}$  in Table 4.2 are kept to one higher power of accuracy in  $\alpha_s$  than the unprimed. This is often beneficial when matching an  $N^k \text{LL}'$  resummed calculation with a fixed-order calculation to the same accuracy to which  $\tilde{C}$  is known.

## 4.8 Resummation in Momentum Space

The renormalization group and rapidity evolution equations are simplest when expressed in  $b_T$  space. In this form they are ordinary differential equations and can be solved using standard techniques. After the evolution equations are solved, a Fourier integral of a product of the TMDs must be computed in order to obtain the  $p_T$  dependence of the cross section. This

integration must be done numerically and can be technically challenging. The integral is over all values of  $b_T$ , including large  $b_T$  where perturbation theory is no longer valid. Therefore the resummed expressions involve the running coupling  $\alpha_s(\mu)$  evaluated at a scale  $\mu \sim 1/b_T$ , in which case one will run into the Landau pole where  $\alpha_s$  diverges. Earlier we described the most commonly used prescription for dealing with these issues in Eq. 4.23. In this section, we review some recent attempts to avoid these difficulties by formulating the evolution equations directly in momentum space so that one can evolve only between perturbative scales.

### 4.8.1 Distributional momentum-space scheme

When solving the RGE and RRGE in  $b_T$ -space one necessarily has to perform scale setting in  $b_T$ -space. For example, in the last section we evolved the scales  $\mu, \nu$  from the scale  $Q$  to the scale  $b_0/b_T$ . This resums logs of  $Qb_T$  in the Fourier transform of the cross section. The goal of Ref. [256] is to resum logs of the form  $[\ln^2(k_T^2/Q^2)/k_T^2]_+$  directly in momentum space. As we will see below, in momentum space the perturbative evaluation of the elements of the factorization theorem leads to distribution functions like  $\delta(k_T)$  and  $[\theta(k_T)/k_T]_+$ . For ordinary functions, RGE is run between the high and low scales to resum logarithms and then in the perturbative part of the calculation  $\mu$  is set to a scale that minimizes the logarithms in the perturbative part. Something similar can be done directly in momentum space, but this requires a procedure to set scales in the presence of distributions, as shown in Ref. [256].

The work of Ref. [256] is based on the SCET formalism as presented in Sec. 4.5. In momentum space, the evolution in  $\mu$  takes the same simple form as in Eqs. (4.47a) and (4.48a), as the corresponding anomalous dimensions are independent of  $b_T$ ,

$$\mu \frac{d}{d\mu} B(x, \mathbf{k}_T, \mu, \zeta/\nu^2) = \gamma_\mu^B(\mu, \zeta/\nu^2) B(x, \mathbf{k}_T, \mu, \zeta/\nu^2) \quad (4.106a)$$

$$\mu \frac{d}{d\mu} S(k_T, \mu, \nu) = \gamma_\mu^S(\mu, \mu/\nu) S(k_T, \mu, \nu). \quad (4.106b)$$

In contrast, the anomalous dimensions in the  $\nu$  evolution in Eqs. (4.47b) and (4.48b) depend on  $b_T$ , and upon Fourier transform the simple product in  $b_T$  space turns into a convolution in momentum space,

$$\nu \frac{d}{d\nu} B(x, \mathbf{k}_T, \mu, \zeta/\nu^2) = \int d^2 \mathbf{k}'_T \gamma_\nu^B(\mathbf{k}'_T, \mu) B(x, \mathbf{k}_T - \mathbf{k}'_T, \mu, \zeta/\nu^2) \quad (4.107a)$$

$$\nu \frac{d}{d\nu} S(k_T, \mu, \nu) = \int d^2 \mathbf{k}'_T \gamma_\nu^S(\mathbf{k}'_T, \mu) S(|\mathbf{k}_T - \mathbf{k}'_T|, \mu, \nu). \quad (4.107b)$$

The  $\nu$ -independence of cross section requires  $\gamma_\nu(\mathbf{k}_T, \mu) \equiv \gamma_\nu^S(\mathbf{k}_T, \mu) = -2\gamma_\nu^B(\mathbf{k}_T, \mu)$ , and commutativity of  $\mu$  and  $\nu$  derivatives requires

$$\mu \frac{d}{d\mu} \gamma_\nu^S(\mathbf{k}_T, \mu) = \nu \frac{d}{d\nu} \gamma_\mu^S(\mu, \nu) \delta(\mathbf{k}_T) = -4\Gamma_{\text{cusp}}[\alpha_s(\mu)] \delta(\mathbf{k}_T). \quad (4.108)$$

Eq. (4.108) clearly illustrates that anomalous dimensions, and consequently the beam and soft functions themselves, are distributions in momentum space. This complicates the solution of

their (R)RGEs compared to Fourier space. For example, the formal solution of Eq. (4.108) is easily obtained as

$$\gamma_v^S(\mathbf{k}_T, \mu) = -4\delta(\mathbf{k}_T) \int_{\mu_0}^{\mu} \frac{d\mu'}{\mu'} \Gamma_{\text{cusp}}[\alpha_s(\mu')] + \gamma_v^S(\mathbf{k}_T, \mu_0). \quad (4.109)$$

Here, we expect the boundary term to contain logarithms  $\ln(k_T/\mu_0)$ , suggesting to choose  $\mu_0 = k_T$  to minimize these. Clearly, this choice clashes with Eq. (4.109), as the  $\delta(\mathbf{k}_T)$  makes it mathematically ill-defined to set the lower scale of the integral to  $\mu_0 = k_T$ . This is in sharp contrast to Fourier space, where the  $\delta(\mathbf{k}_T)$  becomes unity, and one can straightforwardly set  $\mu_0 = b_0/b_T$  to minimize all logarithms resulting in the simple solution in Eq. (4.55).

To circumvent the above problem, Ref. [256] developed a method to solve differential equations such as Eq. (4.108) directly in distribution space. For the simpler case of a one-dimensional distribution, their prescription is given by

$$D(k, \mu = k|_+) = \frac{d}{dk} \int^k dk' D(k', \mu = k), \quad (4.110)$$

where the  $\mu = k|_+$  denotes the *distributional scale setting*. In essence, the prescription is to first take the cumulant of the distribution, which turns it into a regular function, then set the scale as usual, and finally take the derivative to go back to distribution space. In the two-dimensional case relevant for TMD factorization, this becomes

$$D(\mathbf{p}_T, \mu = p_T) \equiv \frac{1}{2\pi p_T} \frac{d}{dp_T} \left[ \int_{|\mathbf{k}_T| \leq p_T} d^2 \mathbf{k}_T D(\mathbf{k}_T, \mu = p_T) \right], \quad (4.111)$$

where the cumulant and derivative are taken in two dimensions.

Applying this method to Eq. (4.108), we obtain

$$\begin{aligned} \gamma_v^S(\mathbf{p}_T, \mu) &= \left\{ -4\delta(\mathbf{p}_T) \int_{\mu_0}^{\mu} \frac{d\mu'}{\mu'} \Gamma_{\text{cusp}}[\alpha_s(\mu')] + \gamma_v^S(\mathbf{p}_T, \mu_0) \right\}_{\mu_0=p_T|_+} \\ &= \frac{1}{2\pi p_T} \frac{d}{dp_T} \left\{ -4\theta(p_T) \int_{p_T}^{\mu} \frac{d\mu'}{\mu'} \Gamma_{\text{cusp}}[\alpha_s(\mu')] + \theta(p_T) \gamma_v^S[\alpha_s(p_T)] \right\} \\ &= \left[ \frac{4\Gamma_{\text{cusp}}[\alpha_s(p_T)]}{2\pi p_T^2} \right]_+^\mu + \left[ \frac{1}{2\pi p_T^2} \frac{d\gamma_v[\alpha_s(p_T)]}{d \ln p_T} \right]_+^\mu + \delta(p_T) \gamma_v^S[\alpha_s(\mu)]. \end{aligned} \quad (4.112)$$

In the second step,  $\theta(p_T)$  is the Heaviside function which is crucial for the correct distributional behavior after taking the derivative, and the boundary term is denoted as  $\gamma_v^S[\alpha_s(p_T)]$ , as it only depends on the scale  $p_T$ . In the last step, we have taken the derivative; the resulting two-dimensional distributions are defined as

$$[f(\mathbf{p}_T)]_+^\mu = f(\mathbf{p}_T) \quad \text{for } p_T > 0, \quad \int_{|\mathbf{p}_T| \leq \mu} d^2 \mathbf{p}_T [f(\mathbf{p}_T)]_+^\mu = 0. \quad (4.113)$$

One can check that the  $\mu$  dependence of the first term in the last line of Eq. (4.112) precisely obeys Eq. (4.108), while the  $\mu$  dependence cancels between the last two terms. Nevertheless,

these two terms have a nontrivial structure, showing that the boundary term in momentum space is not only located at  $p_T = 0$ , but spread throughout  $p_T$  space.

Eq. (4.112) illustrates a few key features of the solution in momentum space, and how it relates to the solution Fourier space. First, we see that the strong coupling in Eq. (4.112) is evaluated at  $\alpha_s(p_T)$  and thus exhibits a Landau pole at  $p_T \lesssim \Lambda_{\text{QCD}}$ , similar to the result in Fourier space becoming nonperturbative for  $b_0/b_T \lesssim \Lambda_{\text{QCD}}$ . Due to this divergence, one can not Fourier transform Eq. (4.112). However, upon expanding Eq. (4.112) in  $\alpha_s(\mu)$ , one can Fourier transform  $\gamma_\nu^S$  order by order in  $\alpha_s(\mu)$ . From this, Ref. [256] observed that the fixed-order expansions of  $\gamma_\nu^S(\mathbf{p}_T, \mu)$  and  $\tilde{\gamma}_\nu^S(\mathbf{b}_T, \mu)$  agree order by order, up to different boundary terms in their solutions. This implies that to a given resummation accuracy, both approaches are formally equivalent, despite differing by formally higher-order terms of nonperturbative origin.

Let us now turn to the solution of the more complicated evolution in  $\nu$ . Focusing on the soft function, the formal solution of Eq. (4.107b) is

$$S(\mathbf{p}_T, \mu, \nu_B) = \int d^2\mathbf{k}_T V(\mathbf{p}_T - \mathbf{k}_T, \mu, \nu_B, \nu_S) S(\mathbf{k}_T, \mu, \nu_S). \quad (4.114)$$

where the the rapidity evolution kernel is given by

$$V(\mathbf{p}_T, \mu, \nu_B, \nu_S) = \delta(\mathbf{p}_T) + \ln \frac{\nu_B}{\nu_S} \gamma_\nu(\mathbf{p}_T, \mu) + \frac{1}{2} \ln^2 \frac{\nu_B}{\nu_S} \int d^2\mathbf{k}_T \gamma_\nu(\mathbf{k}_T, \mu) \gamma_\nu(\mathbf{p}_T - \mathbf{k}_T, \mu) + \dots \quad (4.115)$$

where higher order terms involve multiple convolutions. Similar to the case of  $\gamma_\nu^S$ , the correct solution in momentum space is obtained by distributionally setting  $\nu_S = p_T|_+$ . This can not be achieved in closed form, and one has to resort to numerical methods, which so far have not been developed.

The authors of Ref. [255] developed a numerical resummation of TMD distributions in momentum space based on the general methods of [265, 266] which do not begin from factorization and RGEs per se, but can be applied even to observables that do not manifestly factorize. A full review of these methods is outside the scope of this Handbook, and we refer to [267] for more details on their method. In the following, we briefly discuss their method at NLL accuracy, following the presentation of Ref. [255]. Their starting point is the cumulant of the  $q_T$  distribution, which at NLL accuracy can be written as follows:

$$\begin{aligned} \Sigma(q_T) &= \int_0^{q_T} dk_T \frac{d\sigma(k_T)}{dk_T} \\ &= \sigma_0 \int_0^\infty \langle dk_1 \rangle R'(k_1) e^{-R(\epsilon k_1)} \sum_{n=0}^\infty \frac{1}{n!} \prod_{i=2}^{n+1} \int_{\epsilon k_1}^{k_1} \langle dk_i \rangle R'(k_i) \theta\left(|\mathbf{q}_T| - \left|\sum_j \mathbf{k}_j\right|\right). \end{aligned} \quad (4.116)$$

Here, the  $k_i$  are the real emissions recoiling against the color-singlet final state, and the largest emission  $k_1$  has been singled out. Each emission comes with a measure  $\langle dk_i \rangle = \frac{dk_i}{k_T} \frac{d\phi}{2\pi}$ . The parameter  $\epsilon \ll 1$  indicates that emissions with momenta below  $\epsilon k_1$  are unresolved, i.e. do not contribute to the observable  $q_T$ , up to small corrections in  $\epsilon$ . Thus, they can be neglected in

the calculation of  $q_T$ , and have already been integrated over, with their effect being encoded by the so-called radiator [268],

$$R(\epsilon k_T) = \int_{\epsilon k_T}^Q \frac{d\mu'}{\mu'} \gamma_\mu^H(Q, \mu') . \quad (4.117)$$

Its derivative  $R'(k_i)$  approximates the full matrix element at NLL, and is corrected at higher orders. In essence, Eq. (4.116) thus constitutes the calculation of the cumulant in  $q_T$  by explicitly summing over all possible real emissions weighted by an approximate matrix element. By working in cumulant space, this can be implemented numerically via a parton-shower approach. The  $q_T$  spectrum is then obtained by a (numerical) derivative with respect to  $q_T$ .

Naively, in order to resum logarithms of  $\ln(Q/q_T)$ , where  $Q$  is the hard scale, one would like to expand  $R(\epsilon k_1)$  and  $R'(k_i)$  around  $k_i \sim q_T$ . However, this leads to a well known singularity [?], see Eq. (4.120) below. To circumvent this problem, [255] proposes to expand around the hardest emission  $k_1$  instead, such that

$$R(\epsilon k_1) = R(k_1) + R'(k_1) \ln \frac{1}{\epsilon} + \dots , \quad R'(k_i) = R'(k_1) + \dots . \quad (4.118)$$

Effectively, this approach thus resums logarithms  $\ln(Q/k_1)$  rather than  $\ln(Q/q_T)$  in momentum space, and leads to a stable prediction. On the other hand, it is argued that small  $q_T$  can be dominated by large  $k_i$  due to kinematic cancellations in  $\mathbf{q}_T = \sum_i \mathbf{k}_i$ , and thus  $k_1$  is a more appropriate resummation scale than  $q_T$  itself.

The structure of Eq. (4.116) is similar to the convolution structure in Eq. (4.115), but with the critical difference of scales being set to  $k_1$  rather than distributionally. In Ref. [267], their approach was also compared to conventional resummation in Fourier space. Similar to the discussion above, it was found that formally both approaches are equivalent, up to different terms entering the boundary conditions of the resummation. Finally, we remark that Eq. (4.117) also suffers from the Landau pole when the scales entering the radiator  $R(k_1)$  become nonperturbative. This region is simply excluded in the direct-space approach, and it has not been established yet how to supplement their numerical approach with a nonperturbative model.

### 4.8.2 Hybrid schemes

Another set of approaches take what we call a *hybrid* approach. Namely, in the expression Eq. (4.43) for the momentum-space  $q_T$  spectrum, one does still choose the low rapidity  $v$  scale in the soft function to be a function of  $b_T$  but chooses the low  $\mu$  scale in the beam and soft functions to be purely in momentum space. In [97, 98], an early version of this was introduced, with an implicit choice of  $v_L \sim 1/b_T$  already made but without an actual rapidity scale that can be varied (to properly probe uncertainties). The  $\mu_L$  scale was left to be chosen in momentum space, thus avoiding an explicit Landau pole in transforming from  $b_T$  to  $q_T$  space. In [264], the full power of SCET and the RRG was implemented, though with all low scales chosen in  $b_T$  space as  $\sim 1/b_T$ . However, the variable RG and rapidity scales were also made functions of  $q_T$  (i.e., profile scales) in such a way as to achieve a smooth matching of the momentum-space cross section onto the fixed-order result for large  $q_T$ . This paved a path to a more fully “hybrid” scheme using SCET and the RRG in [257], where the  $\mu_L$  scale was chosen fully in momentum

space while  $\nu_L$  was left in  $b_T$  space. The choice of  $\mu_L$  paralleled the choices of [97, 98] while maintaining full variable dependence on the rapidity scale  $\nu_L$  as in [264]. Without making any attempt to compare the advantages of any of these approaches, we will review the hybrid approach of [257] in some detail here, for its pedagogical value.

In [257], the natural, central choices for the scales are slightly modified from the naive choices  $\nu_L \sim 1/b_T$  and  $\mu_L \sim q_T$ . The Fourier transform integral in Eq. (4.43) can then either be done numerically, but much faster than typical in a purely  $b_T$ -space scale-setting scheme, or be done after a very good approximation to the  $b_T$  integrand in Eq. (4.43) that makes it *analytically* integrable.

After evolution from their natural scales, the  $b_T$  integrand of Eq. (4.43) takes the form Eq. (4.70). With the form of the evolution factor in Eq. (4.71), the integral that must be done to bring the cross section back to momentum space is:

$$\begin{aligned} \frac{d\sigma^W}{dq_T^2} &\sim \int db_T b_T J_0(bq_T) S(b_T; \mu_L, \mu_L/\nu_L) B(x_a, b_T, \mu_L, \zeta_a/\nu_H^2) B(x_B, b_T, \mu_L, \zeta_b/\nu_H^2) \\ &\quad \times \exp\left[-\Gamma_0 \frac{\alpha_s(\mu_L)}{\pi} \ln \frac{\nu_H}{\nu_L} \ln \frac{\mu_L b_T}{b_0}\right], \end{aligned} \quad (4.119)$$

where we have truncated the rapidity evolution kernel for now to NLL accuracy (and displayed only terms that have  $b_T$  dependence). The high rapidity scale  $\nu_H$  here can be considered to be the standard choice  $\sim Q$ , but the low scale  $\nu_L, \mu_L$  are not yet specified. We can try to evaluate the integral in Eq. (4.119) explicitly at NLL accuracy (setting  $S$  and  $B$  to tree level):

$$\frac{d\sigma^W}{dq_T^2} \sim e^{-2\omega_S \gamma_E} \frac{\Gamma(1 - \omega_S)}{\Gamma(\omega_S)} \frac{1}{\mu_L^2} \left(\frac{\mu_L^2}{q_T^2}\right)^{1-\omega_S} f(x_a, \mu_L) f(x_B, \mu_L), \quad \text{where } \omega_S = \Gamma_0 \frac{\alpha_s(\mu_L)}{2\pi} \ln \frac{\nu_H}{\nu_L}, \quad (4.120)$$

which is a nice simple analytic result, but has a divergence at  $\omega_S = 1$ . This is a problem since  $\omega_S > 0$ , and typically we do have  $\omega_S \sim 1$ . This divergence comes from the  $\ln \mu_L b_T$  in Eq. (4.119), or from small values of  $b_T$ , not large, as we would have otherwise expected. This problem was first noted and studied in [? ]. Normally choosing  $\mu_L \sim b_0/b_T$  solves this issue (while large  $b_T$  still requires a regulator/cutoff like those described earlier), but we would like here to leave  $\mu_L$  unspecified for now and be free to choose it in momentum space. What we need, then, is a way to regulate the integral in Eq. (4.119) for both small and large  $b_T$ .

In [257] it was observed that in the low-scale soft function  $S(b_T; \mu_L, \mu_L/\nu_L)$ , there are terms which if exponentiated would naturally provide a regulator for both the low- and high- $b_T$  regions of the integral. Namely, we would like to include the terms in  $S$  that organize themselves into the form:

$$S_{\text{exp}}(b_T) = \exp\left[-\frac{\alpha_s(\mu_L)}{2\pi} \Gamma_0 \ln^2(\mu_L b_T/b_0) - \frac{\alpha_s^2(\mu_L)}{4\pi^2} \Gamma_0 \beta_0 \ln^2(\mu_L b_T/b_0) \ln \frac{\nu_H}{\nu_L}\right], \quad (4.121)$$

which do in fact exist as part of its all-orders expansion. We can shift these terms from the fixed-order expansion of  $S$  in Eq. (4.119) into the exponent of the rapidity evolution kernel by making a shift in the natural choice of scale  $\nu_L$ , namely, instead of starting the evolution of  $S$  at  $\nu_L \sim \mu_L$ , we choose to evaluate it instead at the scale:

$$\nu_L \rightarrow \nu_L^* = \nu_L (\mu_L b_T/b_0)^{-1+p}, \quad p = \frac{1}{2} \left[1 - \frac{\alpha_s(\mu_L) \beta_0}{2\pi} \ln \frac{\nu_H}{\nu_L}\right], \quad (4.122)$$

This factor now naturally regulates the large (and small)  $b_T$  regions of the integral in Eq. (4.119). With  $\nu_L$  replaced by  $\nu_L^*$  in Eq. (4.119), one can choose  $\mu_L$  as a function of a momentum, not of  $b_T$ , and evaluate the  $b_T$  integral numerically fairly quickly, without encountering a Landau pole in  $\alpha_s(\mu_L)$ . There is an optimal choice of  $\mu_L$  which is not exactly  $q_T$  as one might naively expect but is slightly higher. See [257] for details (cf. also [97, 98]).

One can go further in this approach and obtain an analytic result for the integral in Eq. (4.119) that is a very close approximation to the exact numerical result. The approach tackles integrals of the form

$$I_b^0 = \int_0^\infty db b J_0(b q_T) e^{-A \ln^2 \Omega b}, \quad (4.123)$$

in which Eq. (4.119) can be put with the choice  $\nu_L \rightarrow \nu_L^*$  in Eq. (4.122).  $A, \Omega$  are functions of the various scales [257]. By using the Mellin-Barnes representation of the Bessel function,

$$J_0(z) = \frac{1}{2\pi i} \int_{c-i\infty}^{c+i\infty} dt \frac{\Gamma[-t]}{\Gamma[1+t]} \left(\frac{z}{2}\right)^{2t}, \quad (4.124)$$

where  $c$  lies to the left of all poles of the Gamma function, we obtain a form of  $I_b^0$  that is amenable to a series expansion of part of the integrand and an analytic integration:

$$I_b^0 = \frac{2}{\pi q_T^2 \sqrt{\pi A}} \text{Im} \left\{ e^{-A(L-i\pi/2)^2} \int_{-\infty}^\infty dx \Gamma[-c - ix]^2 e^{-\frac{1}{A}[x+A\pi/2-i(c-t_0)]^2} \right\}, \quad (4.125)$$

where  $L = \ln(2\Omega/q_T)$  and  $t_0 = -1+AL$ .  $c = -1$  turns out to be a stable choice for the integration contour, and the Gamma function admits a useful series expansion in Hermite polynomials:

$$\Gamma(1 - ix)^2 = e^{-A_0 x^2} \sum_{n=0}^{\infty} c_{2n} H_{2n}(\alpha x) + \frac{i\gamma_E}{\beta} e^{-B_0 x^2} \sum_{n=0}^{\infty} c_{2n+1} H_{2n+1}(\beta x), \quad (4.126)$$

$A_0, B_0$  are numerical coefficients chosen so the right-hand side most closely approximates the Gaussian nature of  $\Gamma(1 - ix)^2$ , and  $\alpha, \beta$  are also coefficients that are chosen to speed up convergence of the series expansion, while maintaining accuracy of the expansion over a wide enough range in  $x$  to capture the range of the Gaussian factor in Eq. (4.125). There is not a unique best choice, but in [257] some suggested choices are given. In terms of these choices, the series coefficients  $c_{2n,2n+1}$  in Eq. (4.126) are uniquely determined. Typically only the first three or so of the even and the odd coefficients are needed for sufficient accuracy. In terms of these coefficients, the result of the integral  $I_b^0$  (and thus, the  $q_T$  spectrum in momentum space) can be expressed in the explicit form:

$$I_b^0 = \frac{2}{\pi q_T^2} \sum_{n=0}^{\infty} \text{Im} \left[ c_{2n} \mathcal{H}_{2n}(\alpha, A_0) + \frac{i\gamma_E}{\beta} c_{2n+1} \mathcal{H}_{2n+1}(\beta, B_0) \right], \quad (4.127)$$

where

$$\mathcal{H}_n(\alpha, A_0) = \mathcal{H}_0(\alpha, A_0) \frac{(-1)^n n!}{(1+A_0 A)^n} \sum_{m=0}^{\lfloor n/2 \rfloor} \frac{1}{m!} \frac{1}{(n-2m)!} \left\{ [A(\alpha^2 - A_0) - 1](1+A_0 A) \right\}^m (2\alpha z_0)^{n-2m}, \quad (4.128)$$

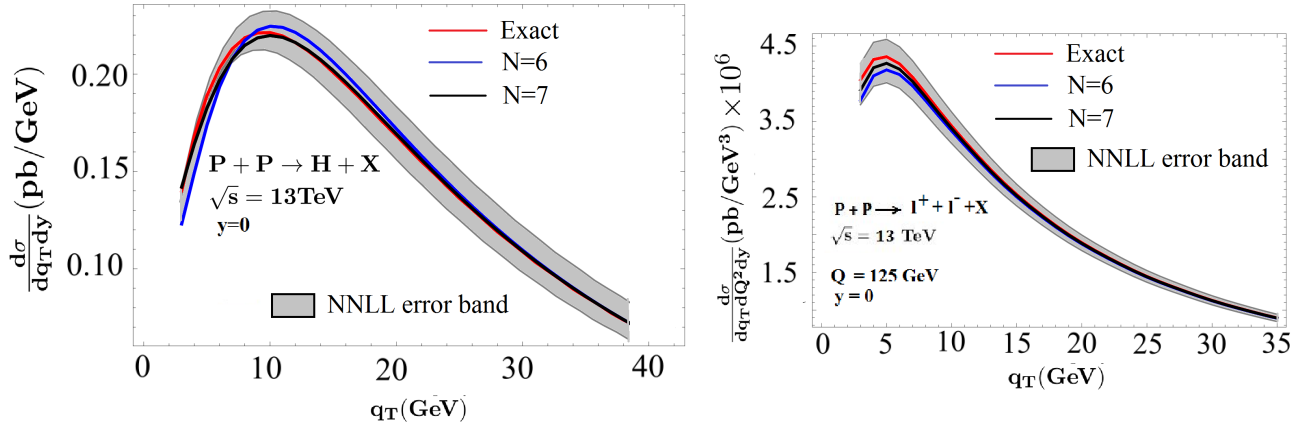


Figure 4.6: Systematic improvement in the accuracy of Higgs (left) and DY (right)  $q_T$  cross sections with increasing number of terms, with increasing number of terms in the Hermite polynomial expansion used in Eq. (4.126). “Exact” (red) gives resummed cross section without Hermite expansion (i.e. numerical  $b$  integration).  $N = 6$  (blue) is the result with six terms in this expansion, three each for real and imaginary terms.  $N = 7$  (black) is the result with one more real term. Here we plot only the purely

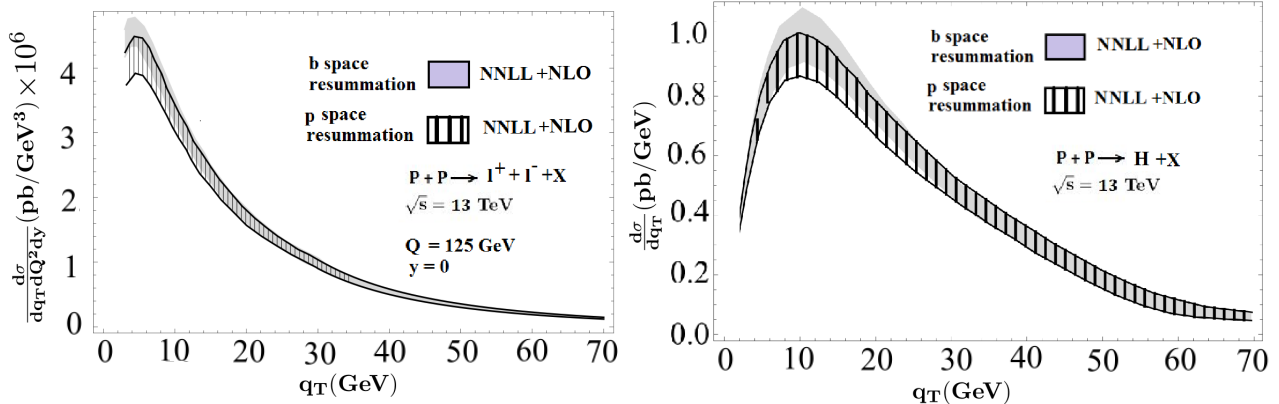


Figure 4.7: Comparison of  $q_T$  distributions at NNLL accuracy matched to fixed-order  $\mathcal{O}(\alpha_s)$ , in a  $b$ -space scheme numerically integrated with a cutoff in  $b_T$  to Fourier transform to momentum space (gray solid band) vs. in the hybrid scheme of [257]. The overlap shows the consistency of the methods with one another. The fixed-order matching is done with the method of profile scales similar to that described in Sec. 4.7 and [264].

where  $z_0 = A(\pi/2 + iL)$ , the prefactor is

$$\mathcal{H}_0(\alpha, A_0) = e^{\frac{-A(L-i\pi/2)^2}{1+A_0A}} \frac{1}{\sqrt{1+A_0A}}, \quad (4.129)$$

and the same formulas hold for odd  $n$  with  $\alpha \rightarrow \beta, A_0 \rightarrow B_0$ . Though these expressions are a bit involved, they represent forms of the momentum-space result for the inverse Fourier transform of the  $b_T$ -space integrand of the form appearing in the cross section Eq. (4.119), retaining the full analytic dependence on all resummation and momentum scales. They are useful for a fast and efficient evaluation of the resummed momentum-space spectrum.

In Fig. 4.6 we show results from [257] for the  $q_T$  spectrum in Higgs production or Drell-Yan at the LHC, comparing the exact numerical result from evaluating Eq. (4.119) numerically, versus the method of Hermite polynomials outlined above, with a total of six or seven basis

terms used in the expansion. The discrepancies are smaller than the perturbative uncertainty in the NNLL result. In Fig. 4.7 we then compare the result of computing the NNLL resummed cross section matched to a fixed-order  $\mathcal{O}(\alpha_s)$  prediction, in this hybrid scheme vs. a  $b$ -space resummation scheme as implemented in [264].

## 4.9 Summary and Outlook

In this chapter, we reviewed evolution and resummation for TMDs which arise as consequences of the renormalization and definitions of TMD PDFs discussed in depth in Chapter 2 and factorization of TMD cross sections whose demonstration was reviewed in Chapter 3. Sec. 4.1 gave the primary motivations to study evolution for TMDs: to compare TMDs extracted at different scales and to resum large logarithms to all orders in perturbation theory. We also presented a brief historical review of work on deriving the evolution equations. In Sec. 4.2 we schematically displayed the all orders form of the fixed-order expansion of the perturbative cross section, as well as the reorganized exponentiated form it takes in the resummed perturbative expansion. This was crucial to obtain a well-behaved perturbative expansion for the TMD cross section for small  $q_T$ . This schematic description also allows the reader to understand which terms are captured by LL, NLL, NNLL, etc. accuracy and the order to which individual ingredients in the factorized cross section need to be computed to achieve these accuracies. This section also showed how to solve evolution equations and obtain resummed expressions for the hard function, as an illustrative example. In Sec. 4.3 the full TMD evolution was studied. The full form of the CSS equations is given, as well the form of the evolution equations in other approaches including SCET. The anomalous dimensions are extracted at one-loop order from the one-loop calculation of the TMD PDF in Sec. 2.4.2. The CSS formalism was further discussed in Sec. 4.4, where the need for a nonperturbative treatment of the large  $b_T$  region is explained along with the commonly used  $b_*$  prescription for freezing  $b_T$  to perturbative scales in the cross section. The perturbative and nonperturbative contributions to the TMD PDF are defined.

Beginning in Sec. 4.5 the SCET approach to evolution is described in detail. The SCET factorization theorems emphasize beam and soft functions, which correspond to matrix elements of collinear and soft operators in the effective theory Lagrangian. Using the relations derived in Chapter 2 between these beam and soft functions and the TMD PDFs, we were able to derive RG and RRG evolution equations for TMD PDFs that are equivalent to those found in the CSS formalism. Solutions to RG and RRG evolution equations were given and path independence of the solutions was emphasized. This property motivates the full two-dimensional picture of TMD evolution reviewed in Sec. 4.6, leading to an intuitive geometrical interpretation and analogies to equipotential lines, along which evolution vanishes. In addition to the resummed expression for the  $W$  term it is important to be able to interpolate between regions in which resummation is needed and regions where fixed order calculations are appropriate. This is the subject of matching the  $W$  term onto large  $q_T$  collinear factorized cross section. This was the subject of Sec. 4.7, where both CSS and SCET approaches are again reviewed in parallel. In the former approach,  $W + Y$  construction is reviewed, where matching of the  $W$  term onto the fixed order term is implemented thru the asymptotic term supplemented with cutoff functions designed to respect the errors of the approximators that designate the TMD and collinear momentum regions. In the latter approach, profile functions, which allow one to turn on and turn off resummation as needed, are introduced. Sec. 4.8 describes recent proposals to

formulate the evolution equations and their corresponding solutions directly in momentum space, or in a hybrid of  $b_T$  and momentum spaces, in an attempt to get around some of the issues encountered in resumming in  $b_T$  space, e.g., Landau poles. This is an area in which we expect more work to be done in coming years.

Evolution and resummation will play a crucial role in subsequent chapters. The following Chapter 5 gives a broad and thorough overview of the phenomenology of TMDs, and detailed comparison of the predictions TMD formalism with Drell-Yan, SIDIS, and di-hadron production will be discussed. As we will see, early fits used naive gaussians multiplying collinear PDFs and did not incorporate evolution. As more detailed information about TMDs has become available, the TMD evolution discussed in this chapter has become essential for properly interpreting and extracting the TMDs.

# 5 - Phenomenology and Extraction of TMDs

## 5.1 Introduction: Historical Perspective

TMD phenomenology plays an important role in testing theoretical ideas about the properties of TMDs, the applicability of QCD factorization theorems, the interplay between perturbative and non-perturbative regimes; and, ultimately, in the analysis of the existing experimental data and predictions for future measurements.

The importance of the transverse motion of partons confined inside the nucleon was pointed out in the 70's by Feynman, Field, and Fox [269, 270], who realized that the origin of transverse momentum of the produced lepton pair in Drell-Yan processes could be either due to the non-zero *intrinsic* transverse momentum of partons confined in the nucleon (non-perturbative effect) or due to the gluon radiation off active partons (perturbative effect). These studies were precursors of the naive TMD picture such as the Generalized Parton Model, Sec. 7.3.1, developed by the Torino-Cagliari group in pioneering studies of asymmetries in hadron-hadron scattering [271–274], and to the rigorous QCD factorization proofs by Collins-Soper-Sterman (CSS) [10, 63, 86]. The modern TMD factorization theorems with well-defined TMDs are discussed in Chapters 2- 4.

Azimuthal asymmetries in unpolarized reactions, Drell-Yan, and SIDIS, can be used to test the perturbative and non-perturbative aspects of strong interactions, as recognized in early work by Georgi and Politzer [275], Mendez [276], and Kane, Pumplin, and Repko [277]. It was Robert Cahn [278, 279] who first pointed out that intrinsic quark motion can generate an azimuthal  $\cos \phi_h$  asymmetry in unpolarized SIDIS, where  $\phi_h$  is the azimuthal angle of the hadron plane with respect to the lepton scattering plane. This  $\cos \phi_h$  or “Cahn effect” in SIDIS is a subleading TMD effect and presented in Chapter 10.

The systematic description of SIDIS cross sections in terms of TMD functions has began in 1995, when Kotzinian [280] and later Mulders and Tangerman [281], Boer and Mulders [60] expressed the unpolarized and polarized SIDIS cross sections in terms of structure functions that are, at tree level, described by convolutions of TMDs. See Ref. [121] and Sec. 2.11.3 for the modern description of SIDIS in terms of TMDs. The polarized Drell-Yan process was parametrized in terms of TMDs by Mulders and Tangerman in Ref. [61] and recently the description was completed by Arnold, Metz, and Schlegel in Ref. [195], see also Sec. 2.11.1. Boer, Jakob, and Mulders investigated asymmetries in polarized hadron production in  $e^+e^-$  annihilation, see Sec. 2.11.4, Ref. [211], and Pitonyak, Schlegel, and Metz extended upon this work in Ref. [213].

Simultaneously, the description of asymmetries in terms of multi-parton quantum mechanical correlations, or twist-3 functions, a well-known example being the Efremov-Teryaev-Qiu-Sterman matrix element [159, 282–284], was formulated for processes with only one large hard scale. These correlations are suppressed relative to the leading power contribution to the unpolarized cross-sections, but can be dominant in spin asymmetries. They are key ingredients in collinear approach to factorization [159, 285]. It was later realized that TMD and twist-3 approaches are intimately related [168]. The first phenomenological demonstration of the common origin of the transverse single spin asymmetries in various processes was performed in Ref. [17].

In the 90's two very important TMD functions encoding correlations of transverse motion and spin were proposed by Sivers [132, 286] and Collins [57]. In order to describe the large (left-right) single spin asymmetries (SSAs) of pion production in hadron-hadron scattering, Sivers suggested that they could originate, at leading power, from the intrinsic motion of quarks in the colliding hadrons generating an inner asymmetry of unpolarised quarks in a transversely polarized hadron, the so-called "Sivers effect". He proposed a new TMD function, now commonly called the Sivers function ( $f_{1T}^\perp$ ), which represents the number density of unpolarized partons inside a transversely polarized nucleon. This mechanism was criticized at first [57] as it seemed to violate time-reversal invariance of QCD, however Brodsky, Hwang and Schmidt proved by an explicit calculation that initial-state interactions in Drell-Yan processes [133, 711] and final-state interactions in SIDIS [58], arising from gluon exchange between the struck quark and the nucleon remnants, can generate a leading (not power suppressed) transverse spin asymmetry. This model calculation is reviewed in Sec. 7.2. The situation was further clarified by Collins [59] who pointed out that this transverse spin asymmetry is due to the Sivers function which, taking correctly into account the gauge links in the TMDs, is not forbidden by time-reversal but rather enters the descriptions of SIDIS and Drell-Yan processes with opposite signs.

Collins proposed a mechanism based on a spin asymmetry in the fragmentation of transversely polarized quarks into a spinless hadron [57], which involved a TMD fragmentation function, called the Collins function ( $H_1^\perp$ ), which generates a typical azimuthal correlation, later denoted as the "Collins effect". This work was preceded by other proposed methods to measure the polarization state of a parton coming out of a hard scattering process. Nachtmann suggested a parity-odd three-particle correlation within a jet to determine the longitudinal polarization of a parton [287], and Dalitz, Goldstein and Marshall discussed how to probe the helicity of heavy quarks in  $e^+e^-$  annihilation [288, 289]. Efremov, Mankiewicz and Törnqvist showed how to probe *transverse* polarization of partons using the concept of "jet handedness" and showed how it can be used to measure transversity [290]. This concept was later independently elaborated by Collins, Heppelmann and Ladinsky in Ref. [291]. (For completeness, it should be mentioned that transversity can also be accessed in a collinear factorization approach in terms of the so-called interference fragmentation functions. We refer the interested reader to [292–295].)

The definition of TMDs is gauge invariant and follows from QCD factorization theorems, see the discussion in Chapters 2 and 3. A generic unpolarized TMD PDF  $f$  in momentum  $k_T$ -space is related to TMD  $\tilde{f}$  in configuration  $b_T$ -space via the inverse Fourier transform. Note that theoretically TMDs are usually studied in  $b_T$ -space, for instance, in studies of the operator definition and evolution of  $\tilde{f}(x, b_T)$ , see Chapters 2 and 3, while experimental measurements are carried out in momentum space. Experimentally measured observables, such as cross-sections, are related to the structure functions that encode the dynamics of confined partons and can be expressed in the TMD approximation as convolutions. The convolution in momentum space implies an integration over the unobserved parton momenta, while in configuration space the convolution becomes a simple product [139] of TMDs in  $b_T$ -space. Thus, experimentally measured cross-sections are not a direct measure of TMDs and global QCD fits have to deal with the model dependence and shape bias of TMD parametrizations. In addition, the extraction of the hadron structure relies on the precise reconstruction of the

$\gamma^*P$  frame of SIDIS events. The QED radiation distorts the  $\gamma^*P$  frame and therefore impacts precise extraction of the underlying hadron structure. The formalism that incorporates both QED and TMD physics will be discussed in Sec. 5.8.

In this Chapter we will review phenomenological predictions and extractions of TMDs from SIDIS, Drell-Yan, weak gauge boson production,  $e^+e^-$  annihilation into hadron pairs, proton-proton scattering, including corresponding azimuthal and spin modulations of cross sections at leading power. The subleading effects will be discussed in Chapter 10. We will also discuss open questions in modern phenomenological studies and outline future directions.

We refer the reader to Chapter 9 for discussions of jets in QCD and the corresponding phenomenology. Ref. [296] is a review on parton fragmentation functions. The 3-D Structure of the nucleon is discussed in a topical issue of the European Physical Journal A [? ]. The way to obtaining a multi-dimensional “picture” of the proton is discussed in Ref. [297], an overview on the current experimental and phenomenological status of transverse single-spin asymmetries (tSSAs) in proton-proton collisions is presented in Ref. [298], phenomenology of transverse spin is in Ref. [299], and experimental results on TMDs are discussed in Ref. [300].

## 5.2 Unpolarized Observables

### 5.2.1 SIDIS multiplicities

Perhaps one of the most fundamental measurements in SIDIS related to TMD physics is the study of the unpolarized  $P_{hT}$  differential cross section obtained by integrating Eq. (2.187) over the angle  $\phi_h$ :

$$\frac{d^4\sigma_{\text{SIDIS}}}{dx dy dz_h dP_{hT}} = 4\pi P_{hT} \frac{\alpha_{em}^2}{x y Q^2} \left(1 - y + \frac{1}{2}y^2\right) F_{UU,T}. \quad (5.1)$$

This cross section contains dependence on  $P_{hT}$  and is thus sensitive to transverse momentum dependence of TMDs <sup>18</sup>. The study of  $P_{hT}$  differential cross section (5.1) in a wide range of  $P_{hT}$  will be crucial for modern and future phenomenology of TMD physics.

Two experimental collaborations, HERMES and COMPASS, reported the measurements of the  $P_{hT}$  differential cross section [301, 302]. Both collaborations presented their results in terms of multiplicities. HERMES experiment measured pion or kaon production in the scattering of 27.6 GeV positrons from the HERA polarized positron storage ring at DESY off proton and deuteron targets in the SIDIS kinematics  $Q^2 > 1 \text{ GeV}^2$ ,  $W^2 \equiv (P + q)^2 > 10 \text{ GeV}^2$ ,  $0.023 < x < 0.4$ ,  $y < 0.85$ ,  $0.2 < z_h < 0.7$ . The measured multiplicity [301] is defined as

$$M_n^h \equiv \frac{d^4\sigma_{\text{SIDIS}}/dx dQ^2 dz_h dP_{hT}}{d^2\sigma_{\text{DIS}}/dx dQ^2}, \quad (5.2)$$

where the DIS cross section in the denominator is

$$\frac{d^2\sigma_{\text{DIS}}}{dx dQ^2} = \frac{4\alpha_{em}^2}{x Q^4} \left[ \left(1 - y + \frac{1}{2}y^2\right) F_2(x, Q^2) \right]. \quad (5.3)$$

---

<sup>18</sup>Notice that if one keeps  $1/Q^2$  suppressed terms, then an additional contribution  $p_1 F_{UU,L}$  is present in Eq. (5.1), see Eq. (10.17), and Eq. (5.3) contains an additional structure function  $F_L(x, Q^2)$  [121].

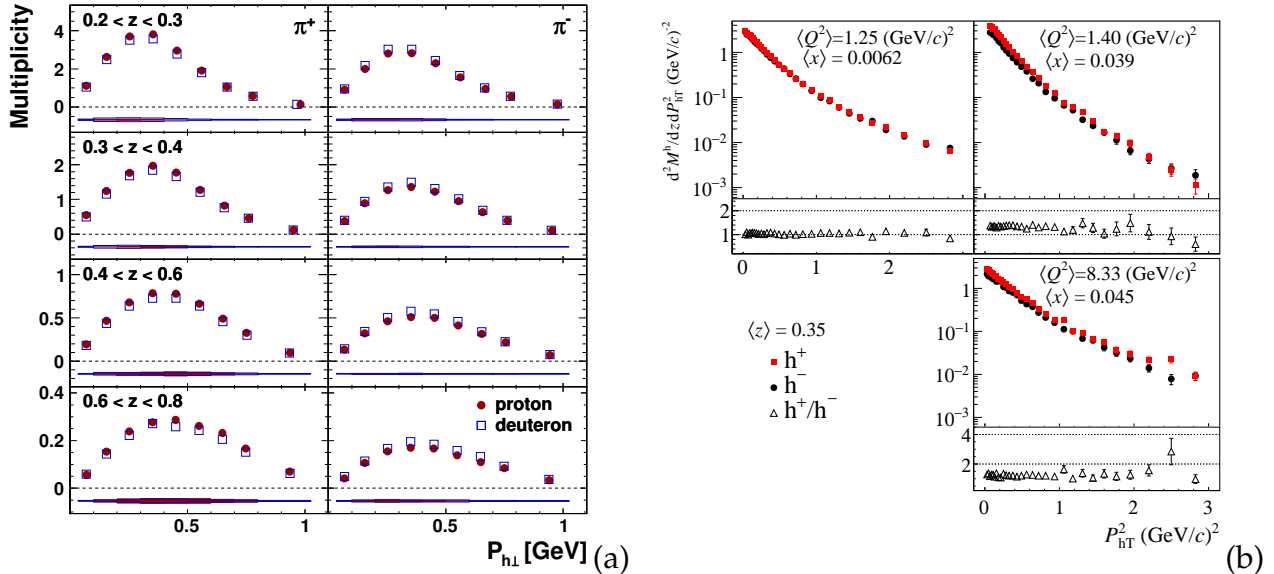


Figure 5.1: (a) HERMES multiplicities [301] of  $\pi^\pm$  pions for the proton and the deuteron as a function of  $P_{hT}$  in four  $z_h$  bins. Positive charge is on the left and negative charge is on the right of each panel. The figure is from Ref. [301].

(b) COMPASS results [302]. Top row: Upper panels: Multiplicities of positively (full squares) and negatively (full circles) charged hadrons as a function of  $P_{hT}^2$  at fixed  $Q^2$ , i.e.  $\langle Q^2 \rangle \simeq 1.3 (\text{GeV}/c)^2$ , for lower (left) and higher (right)  $x$  bins. Lower panels: Ratio of multiplicities of positively and negatively charged hadron. Right column: Same at fixed  $x$ , i.e.  $\langle x \rangle \simeq 0.04$ , for lower (top) and higher (bottom)  $Q^2$  bins. All measured at  $\langle z_h \rangle = 0.35$ . Only statistical uncertainties are shown. Figures from Ref. [302]

Results of HERMES measurements for charged pions are presented in Fig. 5.1(a). Notice the kinematical zero at  $P_{hT} = 0$  and the typical shape of the multiplicity which could in principle be described by the TMD approach, provided that TMD approximations hold, for instance  $q_T/Q \ll 1$ , where  $q_T \simeq P_{hT}/z_h$ .

The COMPASS collaboration performed measurements of charged pions, kaons, or charged hadrons produced in collisions of 160 GeV longitudinally polarized muons scattered off proton and deuteron targets in the typical SIDIS kinematics  $Q^2 > 1 \text{ GeV}^2$ ,  $W > 5 \text{ GeV}$ ,  $0.003 < x < 0.7$ ,  $0.1 < y < 0.9$ ,  $0.2 < z_h < 1$ . The COMPASS multiplicity [302] is defined as

$$M^h \equiv \frac{d^4\sigma_{\text{SIDIS}}/dx dQ^2 dz_h dP_{hT}^2}{d^2\sigma_{\text{DIS}}/dx dQ^2} \quad (5.4)$$

and shown in Fig. 5.1(b). One can see that HERMES and COMPASS definitions of multiplicity are related by:  $M_n^h(x, z_h, Q^2, P_{hT}) = 2P_{hT} M^h(x, z_h, Q^2, P_{hT}^2)$ .

### Parton model approximation

The early attempts to describe the unpolarized multiplicities in SIDIS were made in parton model-like approximations to TMDs in Refs. [303–306].

Here we will discuss the analyses performed in the parton model approximation for TMDs, also known as Generalized Parton Model (GPM). Refs. [303–305] assumed factorization of  $x(z_h)$  and  $k_T(p_T)$  dependencies, and the  $k_T$  and  $p_T$  dependencies were assumed to be Gaussian,

as historically was done for instance in Ref. [35], with one free parameter which fixes the Gaussian width,

$$f_{1q/N}(x, k_T) = f_{1q/N}(x) \frac{e^{-k_T^2/\langle k_\perp^2 \rangle}}{\pi \langle k_\perp^2 \rangle} \quad (5.5)$$

$$D_{1h/q}(z_h, p_T) = D_{1h/q}(z_h) \frac{e^{-p_T^2/\langle p_\perp^2 \rangle}}{\pi \langle p_\perp^2 \rangle}. \quad (5.6)$$

The collinear PDFs,  $f_{1q/N}(x)$  and  $D_{1h/q}(z_h)$ , were taken from the available fits of the world data. The widths of the Gaussians could depend on  $x$  or  $z_h$  and might be different for different flavours, and Ref. [306] explored flavour dependence of TMDs.

Ref. [305] assumes flavour independence and one obtains

$$F_{UU,T} = x \sum_q e_q^2 f_{1q/N}(x) D_{1h/q}(z_h) \frac{e^{-P_{hT}^2/\langle P_T^2 \rangle}}{\pi \langle P_T^2 \rangle} \quad (5.7)$$

where

$$\langle P_T^2 \rangle = \langle p_\perp^2 \rangle + z_h^2 \langle k_\perp^2 \rangle. \quad (5.8)$$

The Gaussian parameterization of TMDs, used in the GPM, is supported by a number of experimental observations [304] as well as by dedicated lattice simulations [307, 308]. It has the advantage that the intrinsic transverse momentum dependence of the cross section can be integrated out analytically. The GPM is a very simple model, which successfully describes a vast body of data and is useful for estimating the outcome of experimental measurements; however, it is not the right model for description of TMD physics. Factorization of collinear and transverse momentum dependence as in Eq. (5.6) is certainly violated in full TMD evolution beyond the lowest  $C^{(0)}$  coefficient function. Also, recent TMD analyses found that more complicated functional forms of intrinsic TMDs are needed to describe the experimental data, see the next Subsection.

Nevertheless, this simple TMD Gaussian parameterization, with constant and flavour independent widths, delivers a satisfactory description [17, 304, 305] of the HERMES and COMPASS data points over large ranges of  $x$ ,  $z_h$ ,  $P_{hT}$  and  $Q^2$ . These analyses used the following data selection cuts:

$$0.2 < z_h < 0.6, Q^2 > 1.63 \text{ GeV}^2, \text{ and } 0.2 < P_{hT} < 0.9 \text{ (GeV)}. \quad (5.9)$$

Notice that from the point of view of power counting the conditions  $q_T \ll Q$ , where  $\mathbf{q}_T$  is the transverse momentum of the virtual photon in a frame in which both the target particle and the final-state hadron have no transverse momentum, and  $P_{hT} \ll Q$ , where  $P_{hT}$  is the transverse momentum of the produced hadron in  $\gamma^*P$  frame, are equivalent since  $q_T \simeq P_{hT}/z_h$ . However, depending on the numerical value for  $z_h$ , data which satisfy  $P_{hT} \ll Q$  may not satisfy  $q_T \ll Q$  and therefore be difficult to describe in a TMD approach. Examples of description of HERMES multiplicities from Ref. [305] are shown in Fig. 5.2.

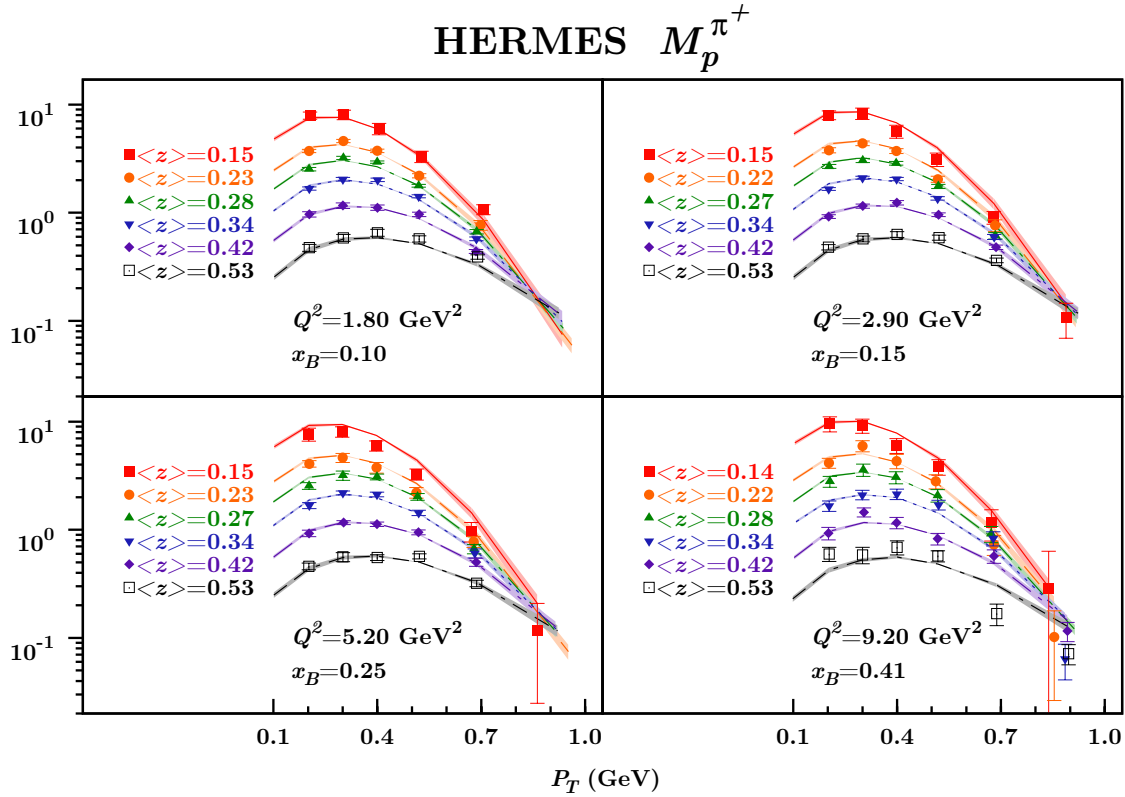


Figure 5.2: The multiplicities  $M_p^{\pi^+}$  obtained from Eq. (5.2), with the parameters of Eq. (5.8), are compared with HERMES measurements for  $\pi^+$  SIDIS production off a proton target [301]. The shaded uncertainty bands correspond to a 5% variation of the total  $\chi^2$ . Plot from Ref. [305].

### Analyses with TMD evolution

In order to go beyond a simple parton model and implement QCD evolution to connect the different  $Q$  scales, one needs to solve the evolution equations, introduce perturbative and non-perturbative Sudakov form factors, and a non-perturbative shape of intrinsic TMDs, see Chapter 4.

Fits of experimental data from high-energy experiments have been well developed in the literature, in particular, in the publications of the Brock-Laundry-Nadolsky-Yan (BLNY)-type of parameterizations [309, 310] utilizing the  $b_*$  prescription, see Chapter 4. Other choices, other than  $b_*$  to avoid the Landau pole, have been made in the literature, see, for example, Refs. [66, 178, 243, 252, 262, 311–314].

The HERMES and COMPASS SIDIS data were used for an NLL TMD extraction (in conjunction with Drell-Yan, and Z-boson production data) in Ref. [248] and also partly used in NLL analysis of Ref. [310]. An  $N^3LO$  description of the SIDIS data was achieved in Ref. [314].

One of the important nonperturbative functions,  $g_K$ , encodes the information on large  $b_T$  behavior of the evolution kernel  $\tilde{K}$ . This function does not depend on the particular process, it does not depend on the scale and has no dependence on the momentum fractions  $x, z_h$ . The large- $b_T$  behavior of the CS evolution kernel,  $\tilde{K}$ , can be related [315] to properties of QCD

vacuum and therefore is an important object of study in its own right.

This function should be parametrized phenomenologically and an often-used [244, 309, 316] parametrization is

$$g_K(b_T; b_{max}) = g_2 b_T^2, \quad (5.10)$$

which proved to be very reliable to describe Drell-Yan data and  $W^\pm, Z$  boson production. It is often referred to as the BLNY-type of parameterization [244, 309, 316]. This Gaussian-type parametrization,  $\exp(-g_K(b_T; b_{max}) \log(Q^2/Q_0^2))$ , suggests that large  $b_T$  region is strongly suppressed [317] and in principle can be unreliable to describe data at lower energies which are more sensitive to moderate-to-high values of  $b_T$ . Other parametrizations were proposed in Refs. [317] and [310] and have the form:

$$g_K(b_T; b_{max}) = g_2 \ln\left(\frac{b_T}{b_*}\right), \quad (5.11)$$

and allows one to describe simultaneously unpolarized multiplicities from SIDIS measurements by HERMES, low energy Drell-Yan as well as  $Z$  boson production up to LHC energies [310]. It was suggested in Ref. [240] that  $g_K(b_T; b_{max})$  becomes a constant at large values of  $b_T$ .

In Ref. [314] a global analysis of a large set of DY and SIDIS data, including precision LHC measurements, was performed with  $N^3LO$  TMD evolution and NNLO matching to the collinear distributions. The unpolarized TMD PDFs for the pion were extracted in the same framework in Ref. [318]. In these extractions the Collins-Soper kernel is parameterized as

$$\mathcal{D}(b_T, \mu) = \mathcal{D}_{\text{resum}}(b_*, \mu) + c_0 b_T b_*, \quad (5.12)$$

where  $\mathcal{D} \equiv -\tilde{K}/2$ , see Table 4.1, and  $\mathcal{D}_{\text{resum}}$  is the resummed  $N^3LO$  expression for the perturbative part of the Collins-Soper kernel, see Ref. [319], and  $c_0$  is a free parameter, so that

$$g_K(b_T; b_{max}) = -2c_0 b_T b_*, \quad (5.13)$$

in our notations. The linear behavior at large- $b_T$  of Eq. (5.12) is in agreement with the predicted nonperturbative behavior [240, 315] and coefficient  $c_0$  can be related to the gluon condensate and therefore is exclusively sensitive [315] to the structure of QCD vacuum.

The comparison of extractions of the Collins-Soper kernel from the data are shown in Fig. 5.3. Notice that results differ at large values of  $b_T$  because the contribution from this region is additionally suppressed by the intrinsic TMD shape, see Eq. (4.27), therefore more experimental data is needed to explore the large- $b_T$  behavior of the Collins-Soper kernel. Studies of the Collins-Soper kernel will become increasingly important in future for the understanding [315] of the universal properties of TMDs and the QCD vacuum.

The first extraction of unpolarized TMDs from a simultaneous fit of available data measured in SIDIS, Drell-Yan and  $Z$  boson production was reported in Ref. [248]. To connect data at different scales, the authors used TMD evolution at NLL accuracy. The authors of Ref. [248] extracted unpolarized TMDs using 8059 data points with 11 free parameters. Ref. [248] used the following data selection criteria:

$$\begin{aligned} Q^2 &> 1.4 \text{ GeV}^2, \quad 0.2 < z_h < 0.74, \\ P_{hT} &< \min[0.2Q, 0.7z_hQ] + 0.5 \text{ GeV}. \end{aligned} \quad (5.14)$$

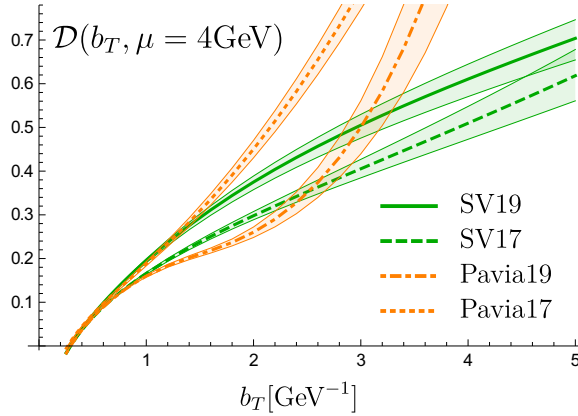


Figure 5.3: Comparison of extracted values of  $\mathcal{D}$ . The lines labeled as SV19, SV17, Pavia19 and Pavia17 correspond to Refs.[314],[320],[321], and [248]. Plot from Ref. [315].

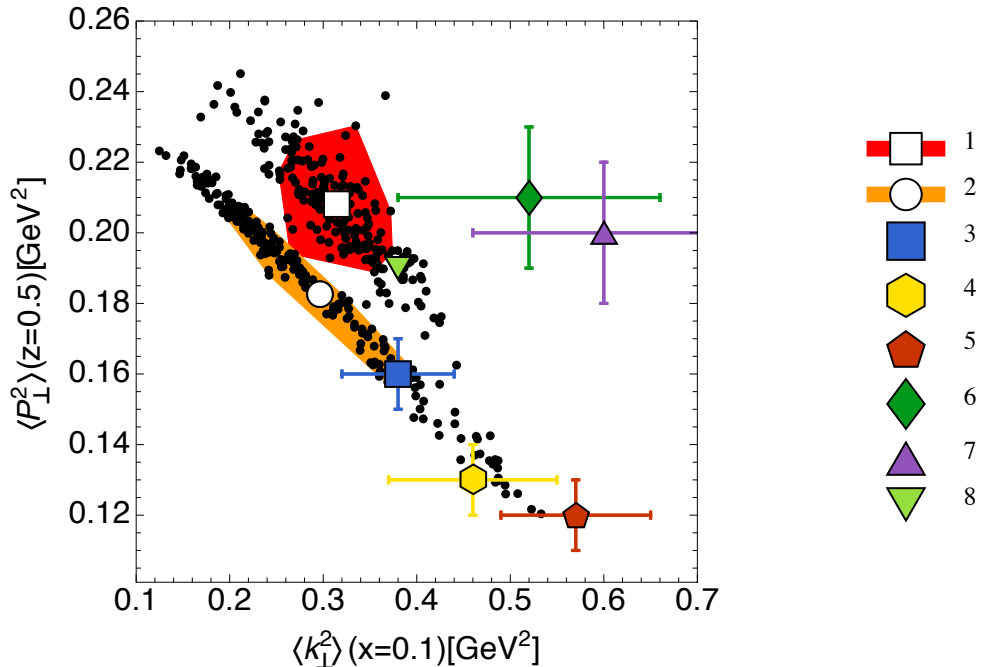


Figure 5.4: Correlation between transverse momenta in TMD FFs,  $\langle P_\perp^2 \rangle(z = 0.5)$ , and in TMD PDFs,  $\langle k_\perp^2 \rangle(x = 0.1)$ , in different phenomenological extractions. (1): average values (white square) obtained in Ref. [248], values obtained from each replica (black dots) and 68% C.L. area (red); (2) results from Ref. [306], (3) results from Ref. [304], (4) results from Ref. [305] for HERMES data, (5) results from Ref. [305] for HERMES data at high  $z$ , (6) results from Ref. [305] for normalized COMPASS data, (7) results from Ref. [305] for normalized COMPASS data at high  $z$ , (8) results from Ref. [322]. Plot from Ref. [248]

The average  $\chi^2/\text{d.o.f.}$  is  $1.55 \pm 0.05$  and can be improved up to 1.02 by restricting the kinematic cuts, without changing the parameters.

The authors used a more complicated shape of intrinsic TMDs compared to the simple

Gaussian parameterizations used in Eq. (5.6)

$$f_{1\text{NP}}^a(x, \mathbf{k}_\perp^2) = \frac{1}{\pi} \frac{(1 + \lambda \mathbf{k}_\perp^2)}{g_{1a} + \lambda g_{1a}^2} e^{-\frac{\mathbf{k}_\perp^2}{g_{1a}}} , \quad (5.15)$$

$$D_{1\text{NP}}^{a \rightarrow h}(z, \mathbf{p}_\perp^2) = \frac{1}{\pi} \frac{1}{g_{3a \rightarrow h} + (\lambda_F/z^2) g_{4a \rightarrow h}^2} \left( e^{-\frac{\mathbf{p}_\perp^2}{g_{3a \rightarrow h}}} + \lambda_F \frac{\mathbf{p}_\perp^2}{z^2} e^{-\frac{\mathbf{p}_\perp^2}{g_{4a \rightarrow h}}} \right) . \quad (5.16)$$

Resulting widths of TMDs are shown in Fig. 5.4. The horizontal axis shows the value of the average transverse momentum squared for the incoming parton,  $\langle \mathbf{k}_\perp^2 \rangle$  at  $\langle x \rangle = 0.1$ . The vertical axis shows the value of  $\langle \mathbf{p}_\perp^2 \rangle$  at  $\langle z \rangle = 0.5$ , the average transverse momentum squared acquired during the fragmentation process. The white square (label 1) indicates the average values of the two quantities obtained in the analysis of Ref. [248] at  $Q^2 = 1 \text{ GeV}^2$ . Each black dot around the white square is an outcome of one replica. The replica approach consists in creating several replicas of the data points. In each replica each data point in the data set is shifted by a Gaussian noise with the same variance as the measurement and therefore, represents a possible outcome of an independent experimental measurement. After these replicas are used in the data analysis.

The red region around the white square contains the 68% of the replicas that are closest to the average value. The same applies to the white circle and the orange region around it (label 2), related to the flavor-independent version of the analysis in Ref. [306], obtained by fitting only HERMES SIDIS data at an average  $\langle Q^2 \rangle = 2.4 \text{ GeV}^2$  and neglecting QCD evolution. A strong anticorrelation between the transverse momenta is evident in this older analysis. In Ref. [248], the inclusion of Drell-Yan and Z production data adds physical information about TMD PDFs, free from the influence of TMD FFs. This reduces significantly the correlation between  $\langle \mathbf{k}_\perp^2 \rangle$  at  $\langle x \rangle = 0.1$  and  $\langle \mathbf{p}_\perp^2 \rangle$  at  $\langle z \rangle = 0.5$ . The 68% confidence region is smaller than in the older analysis in Ref. [306]. The average values of  $\langle \mathbf{k}_\perp^2 \rangle$  at  $\langle x \rangle = 0.1$  are similar and compatible within error bands. The values of  $\langle \mathbf{p}_\perp^2 \rangle$  at  $\langle z \rangle = 0.5$  in Ref. [248] analysis turn out to be larger than in the older Ref. [306] analysis by the same group, an effect that is due mainly to COMPASS data.

The first NNLO and N<sup>3</sup>LO analysis of a large body of SIDIS and DY data, see Fig. 5.5, was presented in Ref. [314]. In Ref. [314] the hard coefficient function is taken at  $\alpha_s^3$ -order, the anomalous dimensions are at  $\alpha_s^3$ -order, and the double-logarithm part ( $\Gamma_{\text{cusp}}$ ) is at  $\alpha_s^4$ -order. It gives N<sup>3</sup>LO perturbative precision. In the resummation nomenclature, Chapter 4, the perturbative input of Ref. [314] can be mapped as NNLO-N<sup>3</sup>LL, see Table 4.2 indicating that the order of small- $b_T$  matching for the unpolarized distributions is  $\alpha_s^2$ . Altogether the authors of Ref. [314] obtain the global value of  $\chi^2/N_{pt} = 0.95$  and 1.06 for NNLO and N<sup>3</sup>LO respectively of the simultaneous fits of Drell-Yan and SIDIS data, see Fig. 5.5, with the following cuts to select the data:

$$Q > 2 \text{ (GeV)}, \quad q_T/Q < 0.25 \quad (5.17)$$

where  $q_T = P_{hT}/z_h$  in SIDIS or  $q_T$  in Drell-Yan.

The TMD distribution  $F(x, b_T; \mu, \zeta_\mu)$  with  $\zeta_\mu$  is expressed in the  $\zeta$ -prescription [314], see Sec. 4.6, as a function of  $\mu$  and Collins-Soper kernel  $\mathcal{D}$ . The resulting expression for the

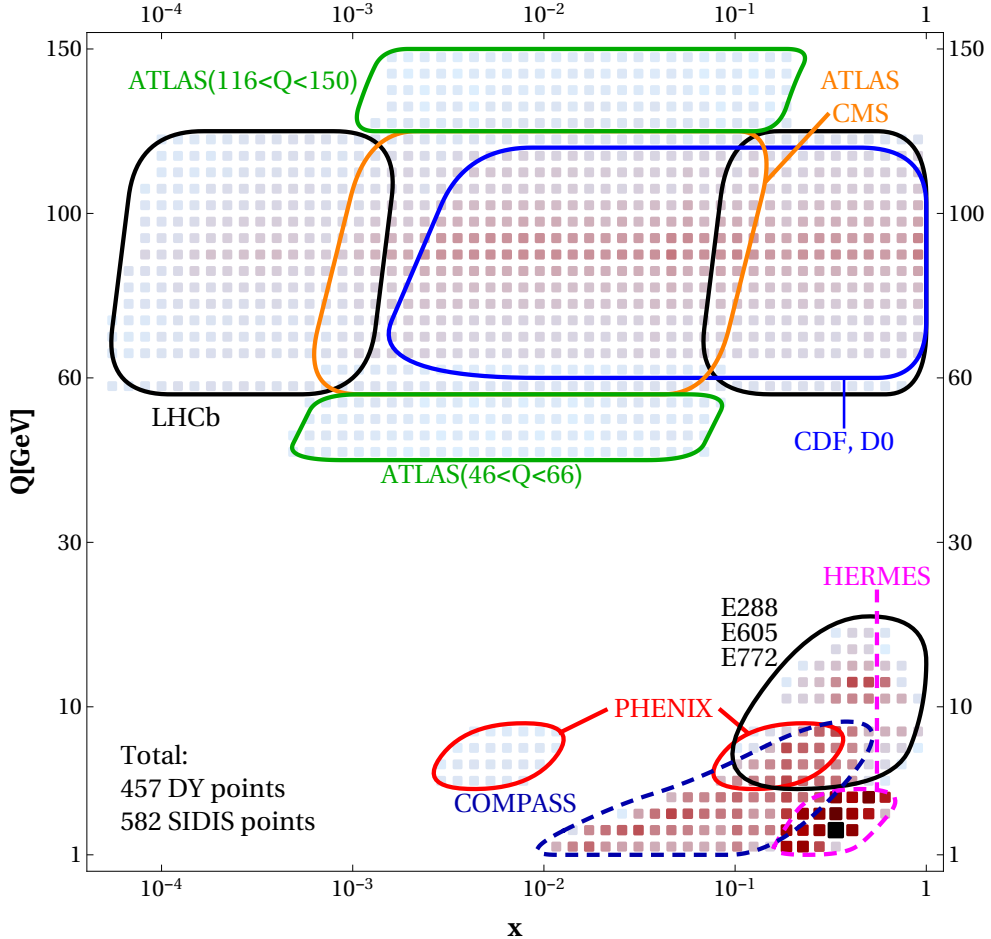


Figure 5.5: Data used in analysis of Ref. [314] (a darker color corresponds to a higher density). Plot from Ref. [314].

evolved TMD distributions reads

$$F(x, b_T; Q, Q^2) = \left( \frac{Q^2}{\zeta_Q(b_T)} \right)^{-\mathcal{D}(b_T, Q)} F(x, b_T) , \quad (5.18)$$

where the function  $F(x, b_T)$  is the so-called “optimal” TMD distribution. The prescription consists in defining the TMD distribution on a null-evolution line  $\zeta_Q(b_T)$ , see appendix C2 of Ref. [314], that makes evolution factor for TMD distributions to be equal one for all values of the impact parameter  $b_T$  such that  $F(x, b_T; Q, \zeta_Q(b_T)) = F(x, b_T)$  becomes independent of any perturbative parameter. This function is completely non-perturbative and one can freely parameterize it without any reference to perturbative order. Another important feature of the  $\zeta$ -prescription used in Eq. (5.18) is that the nonperturbative Soper-Collins kernel  $\mathcal{D}$  with its arbitrary functional form at large  $b_T$  is the argument of  $\zeta_Q(b_T)$ . Therefore the evolution can be defined unambiguously in both perturbative and most importantly, the nonperturbative regions. Lastly, no integration is involved in the computation of the evolution exponent and it speeds up numerical computations.

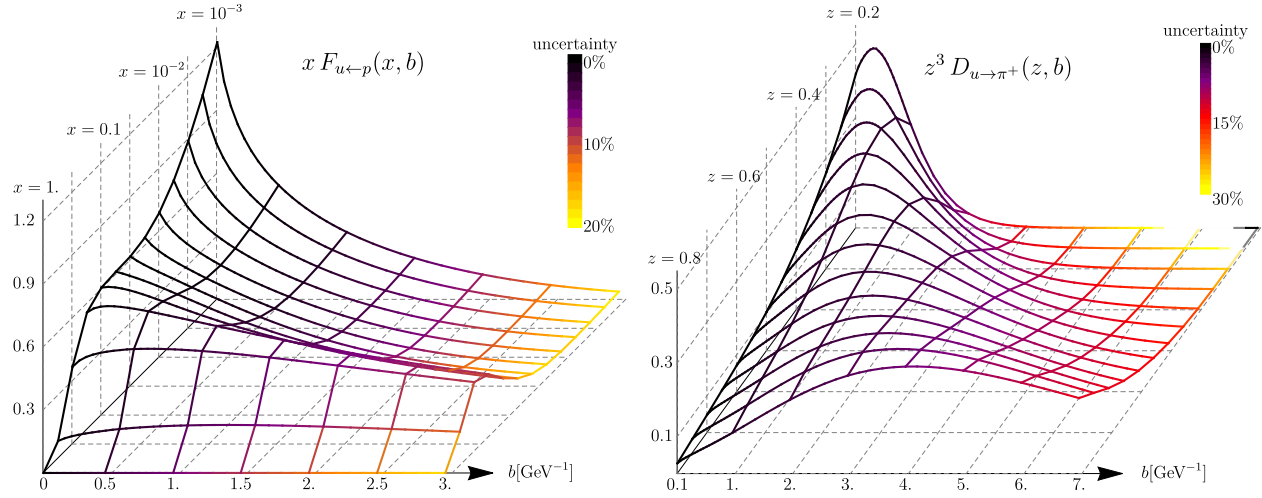


Figure 5.6: Example of extracted (optimal) unpolarized TMD distributions. The color indicates the relative size of the uncertainty band. Plot from Ref. [314].

The TMD distributions show a non-trivial intrinsic structure. The authors of Ref. [314] use the following parameterizations for intrinsic shapes of TMDs

$$f_{NP}(x, b_T) = \exp\left(-\frac{\lambda_1(1-x) + \lambda_2x + x(1-x)\lambda_5 b_T^2}{\sqrt{1+\lambda_3 x^{\lambda_4} b_T^2}}\right), \quad (5.19)$$

$$D_{NP}(z, b_T) = \exp\left(-\frac{\eta_1 z + \eta_2(1-z)}{\sqrt{1+\eta_3(b_T/z)^2}} \frac{b_T^2}{z^2}\right) \left(1 + \eta_4 \frac{b_T^2}{z^2}\right), \quad (5.20)$$

and extract  $\lambda_i$  and  $\eta_i$ . This functional form of  $f_{NP}$  was also used in [313]. It has five free parameters which grant a sufficient flexibility in  $x$ -space as needed for the description of the precise LHC data. An example of distributions in  $(x, b_T)$ -plane is presented in Fig. 5.6. Depending on the value of  $x$ , the  $b_T$ -behavior apparently changes. The authors of Ref. [314] observe (the same observation was made in Ref. [248]) that the unpolarized TMD FF gains a large  $b_T^2$ -term in the nonperturbative part. It could indicate non-trivial consequences of hadronization physics, or a tension between collinear and TMD distributions.

## 5.2.2 Drell-Yan and weak gauge boson production

Drell-Yan lepton pair production via either virtual photon or Z boson served in prior chapters of this handbook to set up the basic notation and concepts for TMD factorization. Factorized in terms of a convolution of two TMD PDFs from each incoming proton at the small transverse momentum  $q_T$  as shown in Eq. (2.29a), Drell-Yan production in unpolarized proton-proton collisions is one of the most important processes for extracting unpolarized quark TMD PDFs.

There is a tremendous amount of experimental data for Drell-Yan production, ranging from lower energy Fermilab experiments to the highest energy data at the LHC. The lower-energy fixed-target Fermilab data include E605 [323] and E288 [324], while the higher-energy Fermilab

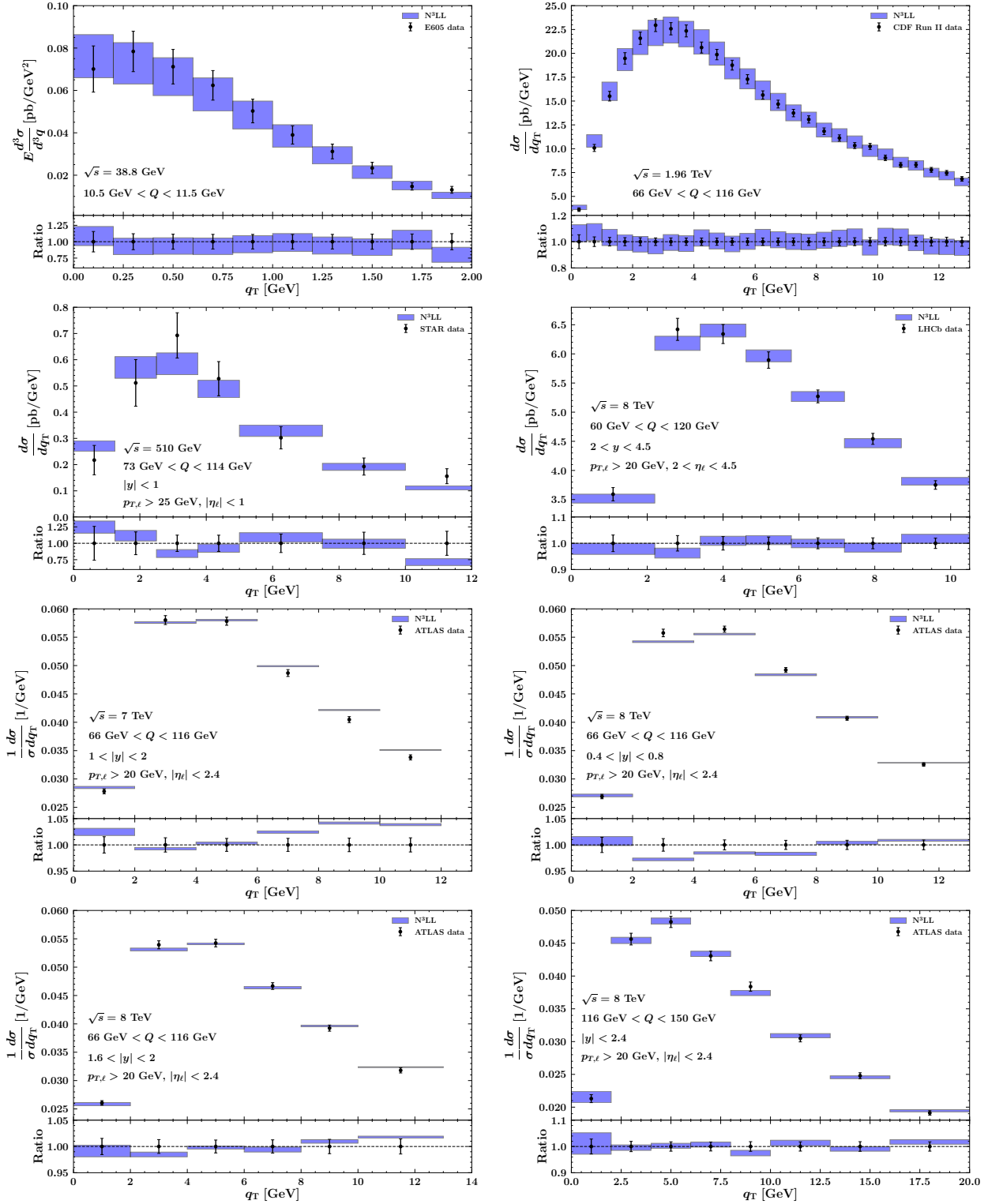


Figure 5.7: Comparison between experimental data and theoretical predictions from the TMD formalism at  $N^3LL$  accuracy. Plot from Ref. [321].

data from collider Tevatron include CDF Run I [325] and Run II [326], and D0 Run I [327] and Run II [328, 329]. LHC data include forward Z-production data from the LHCb experiment at 7 [330], 8 [331], and 13 [332] TeV, Z-production data from the CMS experiment at 7 [333] and 8 [334] TeV, Z-production data differential in rapidity from the ATLAS experiment at 7 [333] and 8 [335] TeV, and off-peak (low- and high-mass) Drell-Yan data from the ATLAS experiment at 8 TeV [335]. Finally, there is also preliminary Z production data from the STAR experiment at 510 GeV.

Earlier description of the small- $q_T$  Drell-Yan data from both fixed-target and collider Fermilab data within the Collins Soper Sterman (CSS) framework has been performed by several groups in, e.g. [178, 243, 309, 310], where different ways of implementing nonperturbative contributions have been explored. In recent years, the perturbative precision for the resummation of logarithms of the transverse momentum of the vector boson have been further increased up to the  $N^3LL$  order. At the same time, a more stringent cut of  $q_T/Q \lesssim 0.2$  has been implemented to ensure the data is in the domain of the TMD factorization region. The most recent extractions of the TMD PDFs have been performed by two groups in [314] and [321] independently. Ref. [314] includes both SIDIS and Drell-Yan data, and thus allows simultaneous extraction of both TMD PDFs and TMD FFs. On the other hand, Ref. [321] excludes SIDIS data but extends the Drell-Yan data sets, and improves the logarithmic accuracy to the  $N^3LL$  order.

It is also important to keep in mind that these two groups use slightly different TMD evolution schemes and also different nonperturbative contributions. Nevertheless, both groups have achieved very good description of the available data. The global analysis of Drell-Yan experimental data generally leads to very good  $\chi^2/N_{\text{data}} \sim 1$ , indicating very good quality of the fit. Although not available at the moment, it would be highly desirable to compare the extracted unpolarized TMD PDFs from these two groups. Instead here we show in Fig. 5.7 a comparison between experimental data and theoretical predictions from the TMD formalism at  $N^3LL$  accuracy.

## 5.3 Polarized Observables

### 5.3.1 Sivers effect in SIDIS and DY

The Sivers function  $f_{1T}^\perp$  [132] encodes the correlation between the partonic intrinsic motion and the transverse spin of the nucleon, and it generates a dipole deformation in momentum space and could not exist without the contribution of orbital angular momentum of partons to the spin of the nucleon. It arises from interaction of the initial or final state quark with the remnant of the nucleon and thus, many of its features reveal the gauge link structure that reflects the kinematics of the underlining process [46]. Above all, the difference between initial and final state gauge link contours leads to the opposite signs for Sivers functions in SIDIS and DY kinematics [58, 59, 133, 711], see Eq. (2.121)

$$f_{1T}^\perp(x, k_T)_{[\text{SIDIS}]} = -f_{1T}^\perp(x, k_T)_{[\text{DY}]} \quad (5.21)$$

In the limit of the large transverse momentum the Sivers function is related [168] to the key ingredient of collinear factorization of SSAs, the Qiu-Sterman (QS) function [159, 282–284], which describes the correlation of quarks with the null-momentum gluon field. Therefore, the measurement of Sivers function and the exploration of its properties is a crucial test of our understanding of the strong force, and one of the goals of polarized SIDIS and DY

experimental programs of future and existing experimental facilities such as the Electron Ion Collider [15, 336], Jefferson Lab 12 GeV Upgrade [337], RHIC [338] at BNL, and COMPASS [339, 340] at CERN. It has so far received the widest attention, from both phenomenological and experimental points of view. The Sivers function has been extracted from SIDIS data by several groups, with consistent results [322, 341–350].

The Sivers asymmetry in SIDIS,  $A_{UT,T}^{\sin(\phi_h - \phi_S)}$ , is

$$A_{UT,T}^{\sin(\phi_h - \phi_S)} \equiv \frac{F_{UT,T}^{\sin(\phi_h - \phi_S)}}{F_{UU,T}} = -M_N \frac{\mathcal{B}[\tilde{f}_{1T}^{\perp(1)} \tilde{D}_1^{(0)}]}{\mathcal{B}[\tilde{f}_1^{(0)} \tilde{D}_1^{(0)}]} . \quad (5.22)$$

where  $M_N$  is the mass of the nucleon.

In Drell-Yan process  $(h_1(P_1, S) + h_2(P_2) \rightarrow l^+(l) + l^-(l') + X)$  the experimentally measured transverse spin asymmetry is

$$A_{TU}^{\sin(\phi_h - \phi_S)} \equiv \frac{F_{TU}^{\sin(\phi_h - \phi_S)}}{F_{UU}^1} = -M \frac{\mathcal{B}[\tilde{f}_{1T}^{\perp(1)} \tilde{f}_1^{(0)}]}{\mathcal{B}[\tilde{f}_1^{(0)} \tilde{f}_1^{(0)}]} , \quad (5.23)$$

where  $M$  is the mass of the polarised hadron  $h_1$ .

The Sivers asymmetry has been measured in SIDIS and DY [196, 351–356], Figs. 5.8, 5.9. In particular, these are SIDIS measurements collected in  $\pi^\pm$  and  $K^\pm$  production off polarized proton target at HERMES [352], off a deuterium target from COMPASS [353], Fig. 5.8(a), and  ${}^3\text{He}$  target from JLab [355, 357],  $h^\pm$  data on the proton target from COMPASS [358]. In Drell-Yan the data exist from DY measurements of  $W^\pm/Z$  production from STAR [356], Fig. 5.9, and pion-induced DY from COMPASS [196], Fig. 5.8(b).

### Parton model approximation

Extractions [341–347, 360] of the Sivers functions that utilize parton model approximation, including the Generalized Parton Model, generically use the Gaussian model for the  $k_T$ -dependence and generically parametrize the Sivers function as

$$f_{1T}^{\perp a}(x, k_T^2) = f_{1T}^{\perp(1)a}(x) \frac{2M^2}{\pi \langle k_T^2 \rangle_{f_{1T}^{\perp}}^2} e^{-k_T^2 / \langle k_T^2 \rangle_{f_{1T}^{\perp}}} , \quad (5.24)$$

where the first moment of the Sivers function  $f_{1T}^{\perp(1)a}(x)$ , is, in  $k_T$ -space and within the Gaussian model approximation, simply defined according to

$$f_{1T}^{\perp(n)a}(x) = \int d^2 k_T f_{1T}^{\perp(n)a}(x, k_T) , \quad f_{1T}^{\perp(n)a}(x, k_T) = \left( \frac{k_T^2}{2M^2} \right)^n f_{1T}^{\perp a}(x, k_T) . \quad (5.25)$$

The exact QCD definition in terms of renormalized functions in  $b_T$ -space is given in Chapter 2 in Eq. (2.130), see also appendix C. Since here the meaning of the scales  $\mu$  and  $\zeta$  is undefined, typically no scale dependence is indicated in parton model expressions. It is implicitly understood that parameters, like Gaussian width, refer to the typical  $Q^2$  at which the investigated data was taken. Some of these early Sivers function extractions also explored the connection to the QS function (defined below in Eq. 5.43, see also footnote 19).

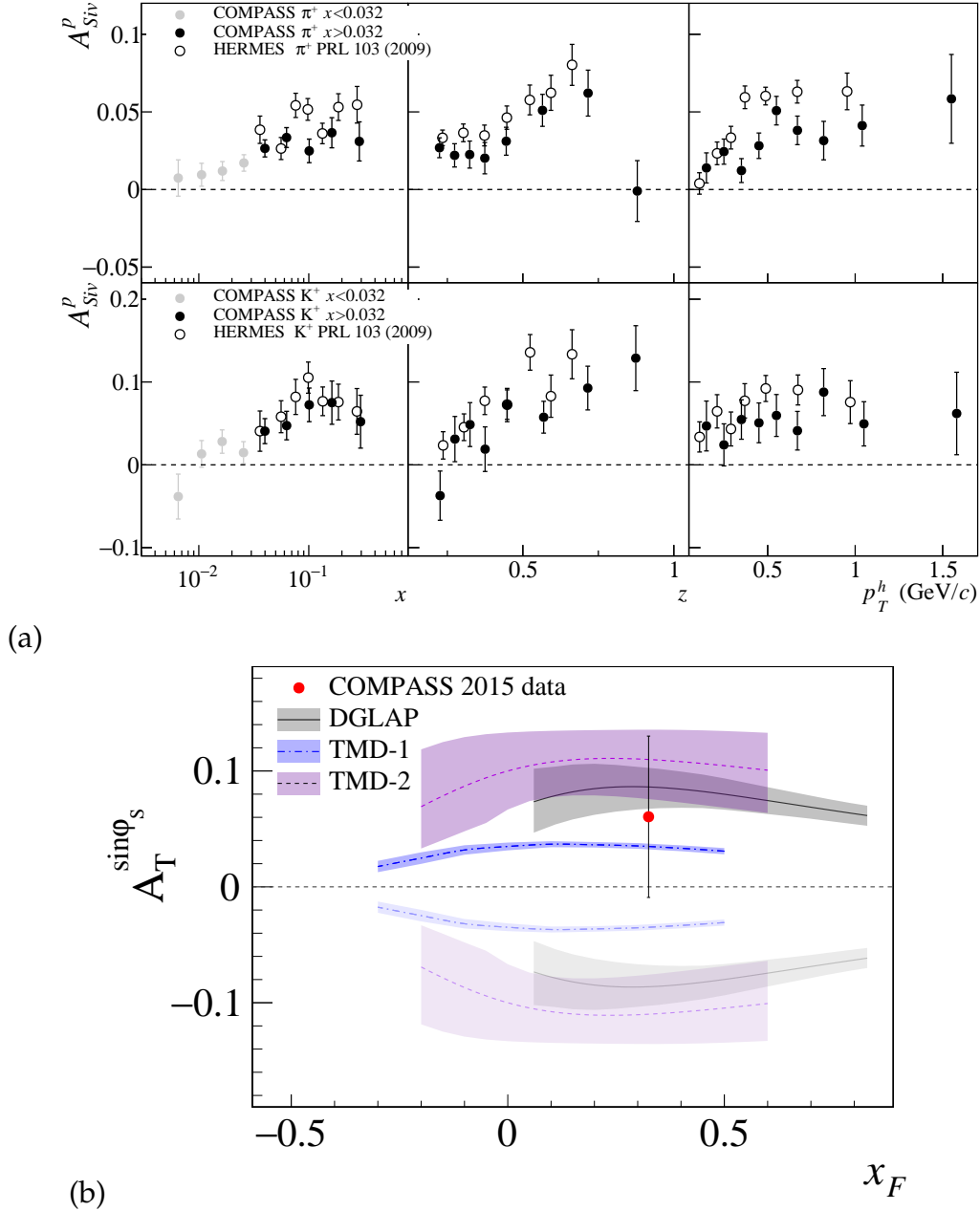


Figure 5.8: **(a)** COMPASS results of Ref. [354] on the Sivers asymmetries for positive pions (top) and kaons (bottom) on proton as a function of  $x$ ,  $z_h$  and  $P_{hT}$ , requiring  $x > 0.032$ . The asymmetries are compared to HERMES results [351]. The plot is from Ref. [354].

**(b)** COMPASS experimental result [196] for the Sivers asymmetry in Drell-Yan and the theoretical predictions for different  $Q^2$  evolution schemes from Refs. [359] (DGLAP), [322] (TMD1) and [172] (TMD2). The dark-shaded (light-shaded) predictions are evaluated with (without) the sign-change prediction. The error bar represents the total experimental uncertainty. The plot is from Ref. [196].

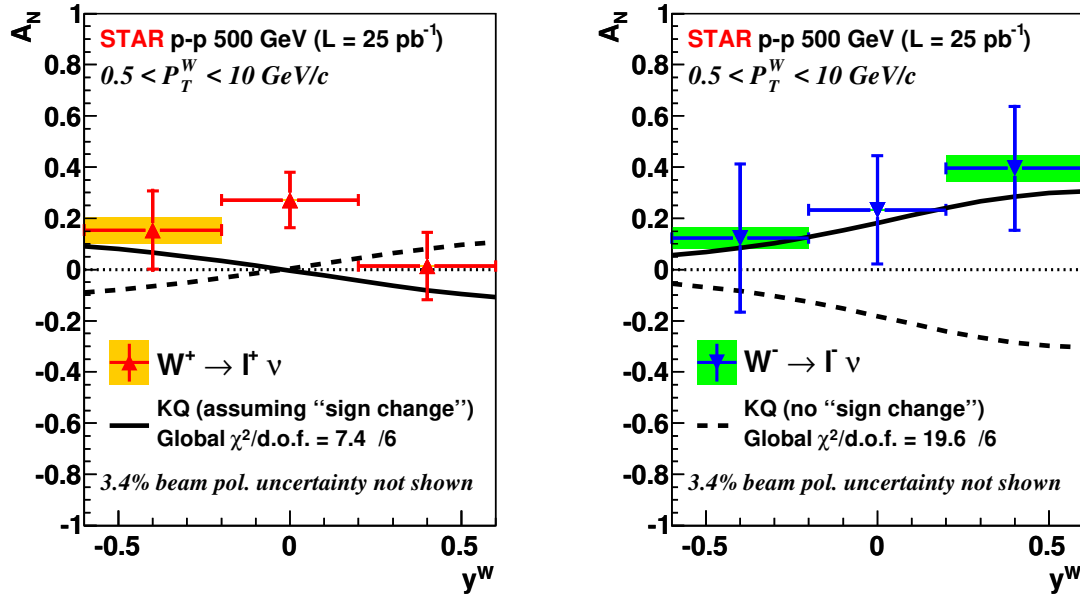


Figure 5.9: STAR results [356] for transverse single-spin asymmetry for  $W^+$  (left plot) and  $W^-$  (right plot) versus  $y^W$  compared with the non TMD-evolved KQ [138] model, assuming (solid line) or excluding (dashed line) a sign change in the Sivers function. The plot from Ref. [356].

### Extractions with TMD evolution

Many analyses [322, 348, 349] that utilize TMD evolution employ the small- $b_T$  operator product expansion of the Sivers function via the QS function and parametrize the QS function.<sup>19</sup> This approach avoids possible complications of the integral relations [362] however the QS function is not an autonomous function, but mixes with other twist-3 distributions [160], and therefore taking into account the correct twist-3 evolution becomes troublesome in these analyses. Ref. [349] uses NNLL resummation while Ref. [348] uses NLL resummation.

The  $N^3LO$  global analysis of SIDIS and DY data including  $W^\pm/Z$  boson production data and extraction of the Sivers function [350, 361] uses a novel method of inverting the OPE relation and reconstructs QS function from the Sivers functions in a model independent way circumventing the problem of implementation of twist-3 evolution:

$$T_q(-x, 0, x; \mu_b) = -\frac{1}{\pi} \left( 1 + C_F \frac{\alpha_s(\mu_b)}{4\pi} \frac{\pi^2}{6} \right) f_{1T;q \leftarrow h}^\perp(x, b_T) - \frac{\alpha_s(\mu_b)}{4\pi^2} \int_x^1 \frac{dy}{y} \left[ \frac{\bar{y}}{N_c} f_{1T;q \leftarrow h}^\perp \left( \frac{x}{y}, b_T \right) + \frac{3y^2 \bar{y}}{2x} G^{(+)} \left( -\frac{x}{y}, 0, \frac{x}{y}; \mu_b \right) \right] + O(a_s^2, b_T^2), \quad (5.26)$$

where  $\bar{y} = 1 - y$ ,  $\alpha_s$  is the strong coupling constant,  $T_q$  and  $G^{(+)}$  are QS quark and gluon functions. This expression is valid only for small (non-zero) values of  $b_T$ .

<sup>19</sup> The definitions of the QS function vary in different analyses. The following relations can be found for the QS functions used:  $-\pi T_q(-x, 0, x; \mu)|_{[350, 361]} = f_{1T}^{\perp(1)}(x, \mu)|_{[348]} = -\frac{T_F(x, x; \mu)}{2M}|_{[349]} = \pi F_{FT}(x, x; \mu)|_{[17]}$ .

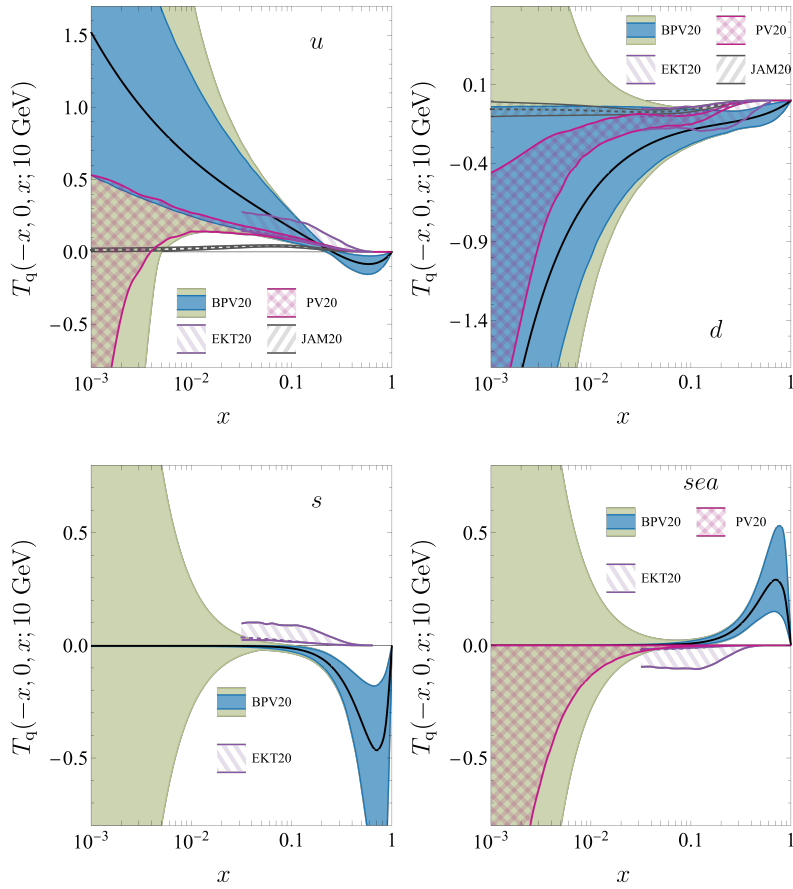


Figure 5.10: Qiu-Sterman function from Ref. [361] at  $\mu = 10$  GeV for different quark flavors, derived from the Sivers function (5.26). Ref. [361] results are labeled as BPV20. The black line shows the central value. Blue band shows 68%CI without gluon contribution added. The green band shows the band obtained by adding the gluon contribution estimated to be  $G^{(+)} = \pm(|T_d| + |T_u|)$ . The results are compared to JAM20 [17] (gray dashed line with the error corridor hatched), PV20 [348] (magenta hatched region), EKT20 [349] (violet hatched region, dashed line). Figure from Ref. [361].

Ref. [350] uses  $b_T \simeq 0.11 \text{ GeV}^{-1}$  such that  $\mu_b = 10 \text{ GeV}$ . The resulting QS-functions are shown in Fig. 5.10. To estimate the uncertainty due to the gluon contribution, the gluon contribution is varied as  $G^{(+)} = \pm(|T_u| + |T_d|)$ . The resulting 68% confidence interval uncertainty band and comparison to Refs. [17, 348, 349] are also shown in Fig. 5.10.

The only global QCD analysis to date that uses SIDIS, DY,  $W^\pm/Z$  production data, and  $pp \rightarrow \pi X$  data on  $A_N$  asymmetries is presented in Ref. [17] and uses the parton model approximation. This analysis shows universality of the mechanism for spin asymmetries in various processes and extracts the Sivers functions, transversity, and the Collins fragmentation functions from the available experimental data.

The magnitude of the Sivers function extracted in our fit is generally much smaller than the unpolarized TMD PDF. To present the distortion effect on the unpolarized quarks driven

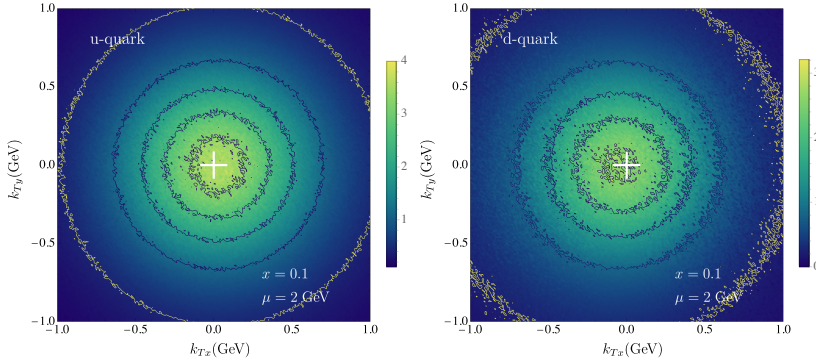


Figure 5.11: Tomographic scan of the nucleon via the momentum space quark density function  $\rho_{1;q \leftarrow h^\uparrow}(x, \vec{k}_T, \vec{S}_T, \mu)$  defined in Eq. (5.27) at  $x = 0.1$  and  $\mu = 2$  GeV. Panels are for  $u$  and  $d$  quarks. The variation of color in the plot is due to variation of replicas and illustrates the uncertainty of the extraction. The nucleon polarization vector is along the  $\hat{y}$ -direction. The figures are from Ref. [361].

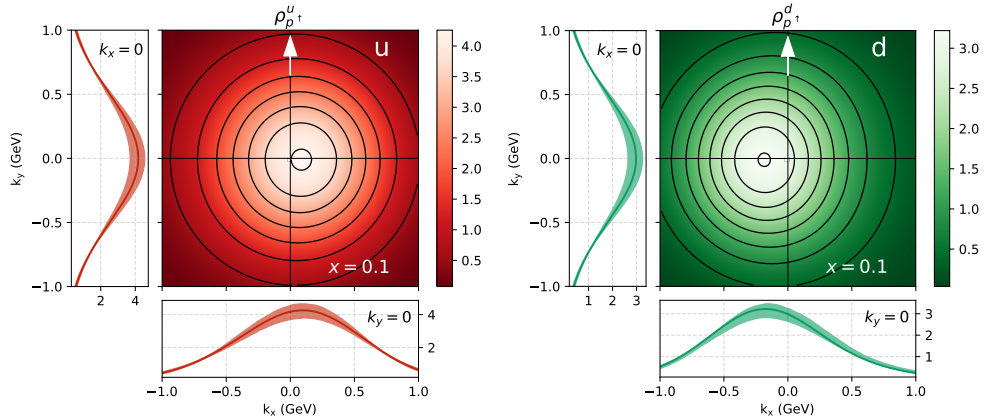


Figure 5.12: The density distribution  $\rho_p^a$  of an unpolarized quark with flavor  $a$  in a proton polarized along the  $+y$  direction and moving towards the reader, as a function of  $(k_x, k_y)$  at  $Q^2 = 4$  GeV $^2$ . The figures are from Ref. [348].

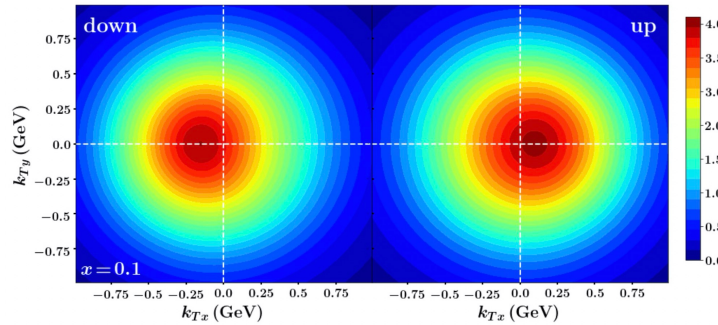


Figure 5.13: The density distribution of an unpolarized up and down quarks using Sivers functions from Ref. [17].

by the hadron polarization, we introduce the momentum space quark density function

$$\rho_{1;q \leftarrow h^\uparrow}(x, \vec{k}_T, \vec{S}_T, \mu) = f_{1;q \leftarrow h}(x, k_T; \mu, \mu^2) - \frac{k_{Tx}}{M} f_{1T;q \leftarrow h}^\perp(x, k_T; \mu, \mu^2), \quad (5.27)$$

where  $\vec{k}_T$  is a two-dimensional vector  $(k_{Tx}, k_{Ty})$ . This function reflects the TMD density of unpolarized quark  $q$  in the spin-1/2 hadron totally polarized in  $\hat{y}$ -direction, **PS:**  $\vec{S}_T = (S_x, S_y)$ , where  $S_x = 0, S_y = 1$   $\vec{S}_T = (0, 1)$ . [?] In Figs. 5.11, 5.12, 5.13 we plot  $\rho$  from Refs. [17, 348, 361] at  $x = 0.1$  and  $\mu = 2$  GeV. To present the uncertainty in unpolarized and Sivers function, we randomly select one replica for each point of a figure. Thus, the color fluctuation roughly reflects the uncertainty band of our extraction. The presented pictures have a shift of the maximum in  $k_{Tx}$ , which is the influence of Sivers function that introduces a dipole modulation of the momentum space quark densities. This shift corresponds to the correlation of the Orbital Angular Momentum (OAM) of quarks and the nucleon's spin. One can see from Figs. 5.11, 5.12, 5.13 that  $u$  quark has a negative correlation and  $d$  quark has a positive correlation. Without OAM of quarks, such a correlation and the Sivers function are zero, and thus we can observe in Figs. 5.11, 5.12, 5.13 the evidence of the presence of OAM of  $u$  and  $d$  quarks in the wave function of the nucleon.

### 5.3.2 Collins effect in SIDIS and $e^+e^-$ annihilation

Transversity,  $h_1$ , measures the probability to find a quark in an eigenstate of the transversely projected Pauli-Lubanski operator  $s \cdot \gamma_\perp \gamma_5$  in a transversely polarized nucleon [363]. The “transversity” basis was introduced in hadron-hadron scattering by Goldstein and Moravcsik in Ref [364]. Transversity or  $h_1(x)$  as a structure function was introduced for the first time by Ralston and Soper in Ref. [128] in their systematic study of the polarized Drell-Yan process. The transversity PDF together with unpolarized and helicity PDFs, describes the structure of a spin-1/2 hadron in the leading-power collinear description. The possibility of accessing transversity in double polarized Drell-Yan process and a careful study of its properties and sum rules was explored by Jaffe and Ji in Ref. [363]. The  $Q^2$  evolution of transversity was investigated by Artru and Mekhi in Ref. [365] at leading order (LO) in QCD. Soffer derived a positivity bound for transversity in Ref. [366] and it was shown by Barone that Soffer inequality is preserved by QCD evolution at LO in Ref. [367]. Vogelsang studied NLO evolution of transversity in Ref. [368] and showed that Soffer inequality is preserved at NLO QCD.

Being chiral-odd,  $h_1(x)$  can not be directly accessed in DIS, as another chiral-odd function is needed to form a chiral even observable. Such a function can be a chiral-odd fragmentation function of transversely polarized quark into an unpolarized nucleon, the so-called Collins fragmentation function [57], and transversity can be accessed in SIDIS. The Collins FF  $H_1^\perp$  decodes the fundamental correlation between the transverse spin of a fragmenting quark and the transverse momentum of the produced final hadron [57]. The measurements that access Collins FF were discussed in Ref. [291]. The description of SIDIS in terms of TMD functions was performed by Kotzinian in Ref. [280] and by Mulders and Tangerman in Ref. [129]. See Ref. [121] for the modern description of SIDIS in terms of TMDs.

The Collins asymmetry in SIDIS is  $A_{UT}^{\sin(\phi_h + \phi_S)}$  and given by the expression

$$A_{UT}^{\sin(\phi_h + \phi_S)} \equiv \frac{F_{UT}^{\sin(\phi_h + \phi_S)}}{F_{UU,T}} = M_h \frac{\mathcal{B}[\tilde{h}_1^{(0)} \tilde{H}_1^{\perp(1)}]}{\mathcal{B}[\tilde{f}_1^{(0)} \tilde{D}_1^{(0)}]}, \quad (5.28)$$

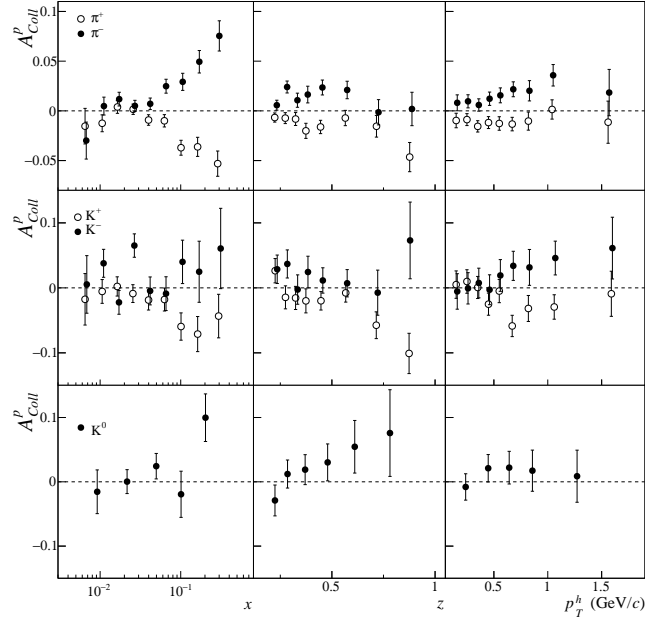


Figure 5.14: COMPASS results of Ref. [354] on the Collins asymmetries for charged pions (top), charged kaons (middle) and neutral kaons (bottom) on proton as a function of  $x$ ,  $z_h$  and  $P_{hT}$ . The plot from Ref. [354].

The  $F_{UT}^{\sin(\phi_h + \phi_s)}$  structure function of the SIDIS cross section is given by the convolution of the transversity distribution  $h_1$  and the Collins FF  $H_1^\perp$ , (2.189),(2.192),

$$F_{UT}^{\sin(\phi_h + \phi_s)} = C \left[ \frac{\hat{h} \cdot \mathbf{p}_T}{z M_h} h_1 H_1^\perp \right] = M_h \mathcal{B}[\tilde{h}_1^{(0)} \tilde{H}_1^{\perp(1)}]. \quad (5.29)$$

The Collins function generates the  $\cos 2\phi_0$  modulation in the  $e^+e^-$  cross-section, see Eq. (2.196), and therefore by combining the data from  $e^+e^-$  and SIDIS processes in a global analysis one is able to constrain both transversity and Collins TMD FF.

The HERMES Collaboration measured Collins asymmetries in electron proton scattering at the laboratory electron beam energy 27.5 GeV in production of  $\pi^+$ ,  $\pi^-$ , and  $\pi^0$  [352, 369]. The data are presented in bins of  $x$ ,  $z_h$ , and  $P_{hT}$  respectively. Clear non-zero asymmetries were found for both  $\pi^+$  and  $\pi^-$ . Large negative asymmetry for  $\pi^-$  suggest that unfavored Collins fragmentation function is big and not suppressed with respect to the favored one. Recall that isospin and charge conjugation symmetries suggest that

$$\begin{aligned} H_{1\pi^+/u}^\perp &= H_{1\pi^+/\bar{d}}^\perp = H_{1\pi^-/\bar{u}}^\perp = H_{1\pi^-/d}^\perp \equiv H_{1\text{fav}}^\perp \\ H_{1\pi^+/\bar{u}}^\perp &= H_{1\pi^+/d}^\perp = H_{1\pi^-/u}^\perp = H_{1\pi^-/\bar{d}}^\perp \equiv H_{1\text{unf}}^\perp \end{aligned} \quad (5.30)$$

3D binned data are presented by HERMES in Ref. [352]. The favored Collins functions describe valence quarks fragmenting to the pion while unfavored correspond to nonvalence quarks.

HERMES [351, 352] and JLab HALL A [355] include the kinematic factor  $p_1$  from Eq. (2.188) in the measured asymmetry,

$$A_{UT}^{\sin(\phi_h + \phi_s)}|_{\text{HERMES}} \equiv \langle \sin(\phi_h + \phi_s) \rangle = p_1 A_{UT}^{\sin(\phi_h + \phi_s)}. \quad (5.31)$$

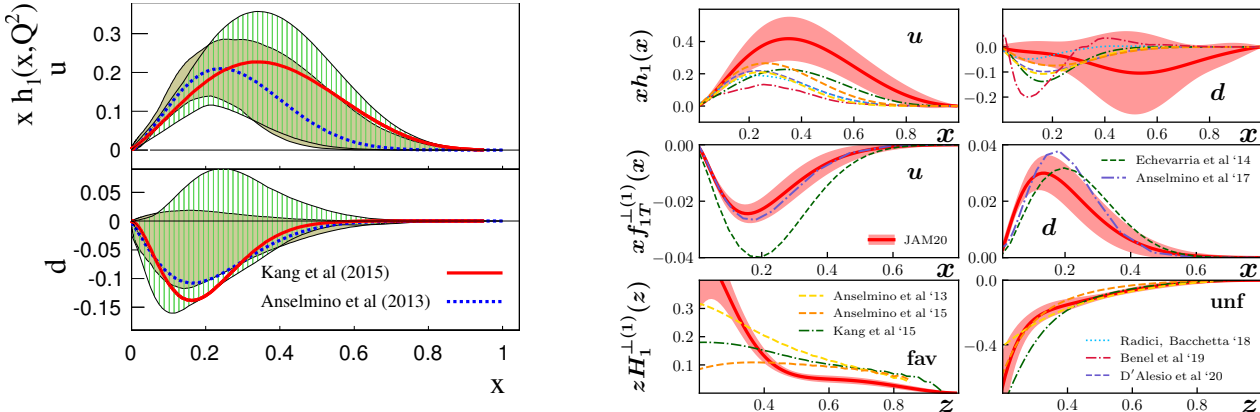


Figure 5.15: Left panel: Comparison of extracted transversity from Refs. [209, 370] (solid lines and vertical-line hashed region) at  $Q^2 = 2.4 \text{ GeV}^2$  with Torino-Cagliari-JLab 2013 extraction [371] (dashed lines and shaded region). Right panel: The extracted functions  $h_1(x)$ ,  $f_{1T}^{(1)}(x)$ , and  $H_1^{(1)}(z)$  at  $Q^2 = 4 \text{ GeV}^2$  from JAM20 global analysis [17] (red solid curves with 1- $\sigma$  CL error bands). The functions from other groups [209, 322, 359, 371–375] are also shown. Plot from Ref. [17]

The COMPASS Collaboration uses muon beam of energy 160 GeV and have measured Collins asymmetries on both NH<sub>3</sub> (proton) [354], see Fig. 5.14, and LiD (deuterium) [353] targets. The data are presented as function of  $x_B$ ,  $z_h$ , and  $P_{h\perp}$ . Results on the proton target are compatible with HERMES findings and asymmetries are found to be compatible with zero on the deuterium target. The beam energy of COMPASS is higher than the energy of HERMES and thus COMPASS reaches lower values of  $x \sim 10^{-3}$ . For each point in  $x$  the scale  $Q^2$  is higher at COMPASS as one has  $Q^2 \simeq sxy$ . Both experiments consider  $Q^2 > 1 \text{ GeV}^2$  in order to be in DIS region and center-of-mass energy of the  $\gamma^*p$  system,  $W^2 > 10 \text{ GeV}^2$  for HERMES and  $W^2 > 25 \text{ GeV}^2$  for COMPASS in order to be outside of the resonance region.

The COMPASS Collaboration considers  $z_h > 0.2$  region and the HERMES Collaboration uses  $0.2 < z_h < 0.7$  in order to minimize both target fragmentation effects and exclusive reaction contributions. All other experimental cuts are described in Refs. [351, 353, 354]. The definition of azimuthal angle  $\phi_S$  of COMPASS experiment is such that

$$A_{UT}^{\text{Collins}}|_{\text{COMPASS}} = -A_{UT}^{\sin(\phi_h + \phi_S)}. \quad (5.32)$$

due to a different convention the notation of the Collins angle  $\phi_C$  used by the COMPASS Collaboration, see Ref. [376].

Jefferson Lab's HALL A published data on  $\pi^\pm$  pion production in 5.9 GeV electron scattering on <sup>3</sup>He (effective neutron) target [355]. Jefferson Lab operates at relatively low energy and reaches higher values of  $x \sim 0.35$ .

Information on Collins fragmentation functions is contained in data from  $e^+e^-$  collisions at the energy  $\sqrt{s} \simeq 10.6 \text{ GeV}$  of the BELLE [377] and the BABAR [378] Collaborations. Both BELLE and BABAR Collaborations require the momentum of the virtual photon  $P_{h\perp}/z_{h1} < 3.5 \text{ GeV}$  in order to remove contributions from hadrons assigned to the wrong hemisphere and it also helps to remove contributions from gluon radiation.

The analysis of BELLE is performed in  $(z_{h1}, z_{h2})$  bins with boundaries at  $z_{hi} = 0.2, 0.3, 0.5, 0.7$  and 1.0. The BABAR Collaboration chooses 6  $z_{hi}$ -bins:  $[0.15 - 0.2]$ ,  $[0.2 - 0.3]$ ,  $[0.3 - 0.4]$ ,

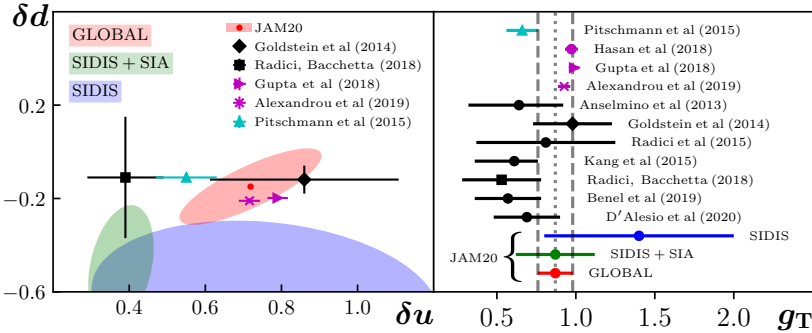


Figure 5.16: Figure from Ref. [17] of the tensor charges  $g_T^u$ ,  $g_T^d$ , and  $g_T^{u-d}$ . Note that Ref. [17] uses  $\delta u$ ,  $\delta d$ , and  $g_T$ , respectively, to denote these quantities. The JAM20 result refers to that obtained in Ref. [17] at  $Q^2 = 4 \text{ GeV}^2$ . Also shown are other results from phenomenology (black) [209, 371, 373–375, 381, 382], lattice QCD (purple) [383–385], and Dyson-Schwinger (cyan) [386] at the same scale.

[0.4 – 0.5], [0.5 – 0.7], [0.7 – 0.9]. A characteristic feature of the asymmetry is growth with  $z_{hi}$  which is compatible with the kinematical zero in the limit  $z_{hi} \rightarrow 0$ .

A recent study presented in Ref. [379] considered the  $\cos 2\phi_h$  azimuthal asymmetry in  $e^+e^-$  due to Collins functions and the acoplanarity to the azimuthal asymmetry due to the digluon radiation. The authors found that in the region  $q_T \ll Q$  region, the asymmetry is dominated by the Collins effect, while the acoplanarity effect dominates in the large  $q_T$  region ( $q_T/Q > 0.5$ ) and is negligible in the small  $q_T$  region. In the intermediate region the two contributions are comparable.

There are many extractions of  $h_1$  and  $H_1^\perp$  from combined fits of SIDIS and  $e^+e^-$  data, for instance those of Refs. [17, 209, 345, 370–372, 380]. In the extractions in Refs. [17, 345, 370–372, 380] the parton model approximation is used and TMDs are parametrized as

$$h_1^q(x, k_T) = h_1^q(x) \frac{1}{\pi \langle k_T^2 \rangle_{h_1}} \exp \left[ -\frac{k_T^2}{\langle k_T^2 \rangle_{h_1}} \right], \quad (5.33)$$

$$H_1^{\perp h/q}(z, p_T) = \frac{2z^2 M_h^2}{\langle p_T^2 \rangle_{H_1^\perp}} H_{1h/q}^{\perp(1)}(z) \frac{1}{\pi \langle p_T^2 \rangle_{H_1^\perp}} \exp \left[ -\frac{p_T^2}{\langle p_T^2 \rangle_{H_1^\perp}} \right], \quad (5.34)$$

while in Refs. [209, 370] the OPE is used for TMDs and the extraction is performed at NLL accuracy.

For completeness we remark that the definition of the transverse moment of the Collins function in (5.34) in terms of renormalized functions in  $b_T$ -space, see Chap. 2 and appendix C, simplifies within the Gaussian model similarly to (5.25) as follows

$$H_1^{\perp(n)a}(z) = \int d^2 p_T H_1^{\perp(n)a}(z, p_T), \quad H_1^{\perp(n)a}(z, p_T) = \left( \frac{p_T^2}{2M_h^2} \right)^n H_1^{\perp a}(z, p_T), \quad (5.35)$$

where  $\mathbf{p}_T = -z \mathbf{p}'_T$ .

A quantity of interest that can be calculated from extractions of the transversity function are the presently still not well-known tensor charges  $g_T^q$  [128, 363, 387–389]. The tensor charges

play an important role for the understanding of the nucleon spin structure, and are important for the nucleon tomography in momentum space. Unlike the axial charge of the nucleon, which is related by the Bjorken sum rule to the axial coupling constant through which the nucleon couples to weak interactions, the tensor charge is not a conserved charge and has no practical application within the Standard Model. However, certain hypothetical beyond the Standard Model (BSM) particles could couple to the nucleon through the tensor charges. For this reason,  $g_T^q$  plays a role for BSM physics, see, e.g., Refs. [390–393].

The tensor charges are computed from the following integrals of  $h_1^q(x)$  [128, 363, 387–389] over the parton momentum fraction  $x$ :

$$g_T^u = \int_0^1 dx (h_1^u(x) - h_1^{\bar{u}}(x)), \quad g_T^d = \int_0^1 dx (h_1^d(x) - h_1^{\bar{d}}(x)), \quad (5.36)$$

where  $u$  and  $d$  represent up and down quarks, respectively. The isovector combination  $g_T^{u-d} \equiv g_T^u - g_T^d$  is also of particular focus. The quantities  $g_T^u$ ,  $g_T^d$ , and  $g_T^{u-d}$  have all been computed in lattice QCD [383–385, 394]. Some results for the tensor charges are collected in Fig. 5.16. The JAM20 results from Ref. [17] show what happens to the extracted values for  $g_T^u$ ,  $g_T^d$ , and  $g_T^{u-d}$  if one includes only SIDIS data (blue), SIDIS and  $e^+e^-$  semi-inclusive annihilation (SIA) data (green), and then a global analysis of SIDIS,  $e^+e^-$ , and  $A_N$  data (red). (See Sec. 5.3.3 for more details about the  $A_N$  observable in proton-proton collisions.) Notice how only after a global analysis do the phenomenological values for  $g_T^u$ ,  $g_T^d$ , and  $g_T^{u-d}$  agree with lattice QCD.

### 5.3.3 $A_N$ in proton-proton collision

#### Cross Section Formulas

Let us consider the production of a single hadron from the collision of two protons  $A$  and  $B$ :

$$p_A(P) + p_B(P') \rightarrow h(P_h) + X. \quad (5.37)$$

The differential cross section  $d\sigma$  for this reaction can be written in a twist expansion,

$$d\sigma = d\sigma_{t2} + d\sigma_{t3} + \dots, \quad (5.38)$$

where  $d\sigma_{t2}$  ( $d\sigma_{t3}$ ) represents the twist-2 (twist-3) term. This reaction can be analyzed within collinear factorization so long as the hard scale, set by the transverse momentum of the produced hadron  $P_{hT}$ , satisfies  $P_{hT} \gg \Lambda_{QCD}$ .

For the case that the initial state protons are unpolarized, the leading-power term in the cross section  $d\sigma_{t2}$  is given at leading-order (in the strong coupling  $\alpha_s$ ) by

$$E_h \frac{d\sigma}{d^3 P_h} = \frac{\alpha_s^2}{S} \sum_i \sum_{a,b,c} \int_0^1 \frac{dz}{z^2} \int_0^1 \frac{dx'}{x'} \int_0^1 \frac{dx}{x} \delta(\hat{s} + \hat{t} + \hat{u}) f_1^a(x) f_1^b(x') D_1^{h/c}(z) \mathcal{H}_U^i, \quad (5.39)$$

where  $\sum_i$  is a sum over all partonic interaction channels,  $a$  can be a quark, anti-quark, or gluon (and likewise for  $b, c$ ), and  $f_1$  ( $D_1$ ) is the usual unpolarized PDF (FF). The well-known hard factors for the unpolarized cross section are denoted by  $\mathcal{H}_U^i$  [395–397] and can be found in, e.g., appendix A of Ref. [396]. They are functions of the partonic Mandelstam variables  $\hat{s} = xx'S$ ,  $\hat{t} = xT/z$ , and  $\hat{u} = x'U/z$ , where  $S = (P + P')^2$ ,  $T = (P - P_h)^2$ , and  $U = (P' - P_h)^2$ .

If any of the particles in (5.37) carry a transverse polarization  $S_T$ , one can then define the SSA  $A_N$ ,

$$A_N \equiv \frac{d\Delta\sigma(S_T)}{d\sigma}, \quad (5.40)$$

where  $d\Delta\sigma(S_T) \equiv \frac{1}{2} [d\sigma(S_T) - d\sigma(-S_T)]$  and  $d\sigma \equiv \frac{1}{2} [d\sigma(S_T) + d\sigma(-S_T)]$ . The leading-power contribution to  $A_N$  is twist 3, and the relevant non-perturbative functions are now twist-3 multi-parton correlators (e.g., quark-gluon-quark or tri-gluon) [159, 282, 284, 285, 396, 398–403]. From an experimental standpoint, recent focus has been on pion production where one of the initial-state protons is transversely polarized. Schematically, we can write  $d\Delta\sigma(S_T)$  as

$$\begin{aligned} d\Delta\sigma(S_T) = & \mathcal{H}_A \otimes f_{a(3)} \otimes f_{b(2)} \otimes D_{h/c(2)} \\ & + \mathcal{H}_B \otimes f_{a(2)} \otimes f_{b(3)} \otimes D_{h/c(2)} \\ & + \mathcal{H}_h \otimes f_{a(2)} \otimes f_{b(2)} \otimes D_{h/c(3)}, \end{aligned} \quad (5.41)$$

where  $f_{a(t)}$  is the twist- $t$  PDF associated with parton  $a$  in proton  $A$  (similarly for  $f_{b(t)}$ ), while  $D_{h/c(t)}$  is the twist- $t$  FF associated with the hadron  $h$  in parton  $c$ . The hard parts are different for each term, depending on which non-perturbative function is kept at twist 3, and are denoted by  $\mathcal{H}_A$ ,  $\mathcal{H}_B$ , and  $\mathcal{H}_h$ . In the case of  $p^\uparrow p \rightarrow \pi X$ , all three terms in Eq. (5.41) enter into the analysis.

Specifically, one receives twist-3 contributions from (a) the transversely polarized proton, (b) the unpolarized proton, and (c) the (unpolarized) final-state pion. For (a), there are two types of terms that arise, a so-called soft-gluon pole (SGP) term and a soft-fermion pole (SFP) term. These are so named because, since SSAs are a naïve time-reversal odd (T-odd) effect, one must pick up a pole in the hard scattering. This pole causes the momentum fraction of either a gluon or quark in the multi-parton correlator to vanish, which leads, respectively, to a SGP or SFP. The SGP term was calculated in Refs. [284, 396] for  $qgq$  correlators and Ref. [403] for tri-gluon ( $ggg$ ) ones, while the SFP term was computed in Ref. [401].

The contribution from the  $qgq$  SGP function  $F_{FT}(x, x)$ , called the Qiu-Sterman (QS) function,<sup>20</sup> to the spin-dependent cross section reads [284, 396]

$$\begin{aligned} E_h d\sigma_{(T)}^{SGP_{qgq}}(S_T) = & -\frac{4\alpha_s^2 M}{S} \epsilon_{\mu\nu\rho\sigma} P'^\mu P^\nu P_h^\rho S_T^\sigma \sum_i \sum_{a,b,c} \int_0^1 \frac{dz}{z^3} \int_0^1 dx' \int_0^1 dx \delta(\hat{s} + \hat{t} + \hat{u}) \\ & \times \frac{\pi}{\hat{s}\hat{u}} f_1^b(x') D_1^{\pi/c}(z) \left[ F_{FT}^a(x, x) - x \frac{dF_{FT}^a(x, x)}{dx} \right] \mathcal{H}_{F_{FT}}^i, \end{aligned} \quad (5.42)$$

where the Levi-Civita tensor is defined with  $\epsilon^{0123} = +1$ . The hard factors are denoted by  $\mathcal{H}_{F_{FT}}^i$  and can be found in Ref. [396]. The notation used for the cross section indicates that this is the  $qgq$  SGP term for the transversely polarized proton. The QS function has an important, model-independent relation to the TMD Sivers function [132]  $f_{1T}^\perp(x, k_T)$  that enters SSAs in processes like SIDIS and Drell-Yan (DY), see Sec. 5.3.1. The identity reads [72]

$$\pi F_{FT}(x, x) = f_{1T}^{\perp(1)}(x)|_{SIDIS} = -f_{1T}^{\perp(1)}(x)|_{DY}. \quad (5.43)$$

---

<sup>20</sup>There are several notations used in the literature for the QS function, e.g.,  $T_F(x, x)$  and  $G_F(x, x)$ .

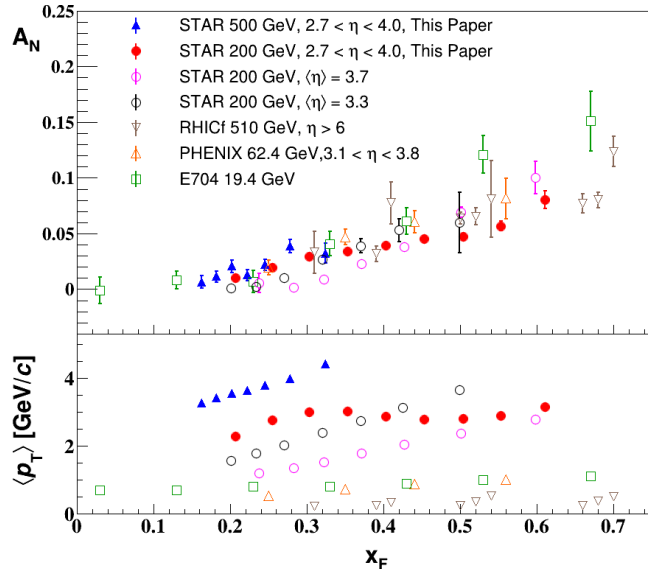


Figure 5.17: Summary of  $A_N$  data for  $\pi^0$  production from Ref. [404].

The Sivers function is also connected to the QS function through the OPE [405], see Eq. (5.26).

The case of twist-3 effects in the unpolarized proton was analyzed many years ago in Ref. [406] and they were found to be negligible. The twist-3 effects due to the final-state pion were computed in Ref. [402] and re-written in Ref. [407] using Lorentz invariance and equation of motion relations [167]. The result reads

$$\frac{E_h d\sigma^{Frag}(S_T)}{d^3 \vec{p}_h} = -\frac{4\alpha_s^2 m_h}{S} \epsilon_{\mu\nu\rho\sigma} P^\mu P^\nu P_h^\rho S_T^\sigma \sum_i \sum_{a,b,c} \int_0^1 \frac{dz}{z^3} \int_0^1 dx' \int_0^1 dx \delta(\hat{s} + \hat{t} + \hat{u}) \frac{1}{\hat{s}} \\ \times h_1^a(x) f_1^b(x') \left\{ \left[ H_{1,\pi/c}^{\perp(1)}(z) - z \frac{dH_{1,\pi/c}^{\perp(1)}(z)}{dz} \right] \mathcal{H}_1^i + \left[ -2H_{1,\pi/c}^{\perp(1)}(z) + \frac{1}{z} \tilde{H}^{\pi/c}(z) \right] \mathcal{H}_2^i \right\}, \quad (5.44)$$

where  $m_h$  is the pion mass,  $h_1$  is the standard twist-2 transversity function, and the hard factors for each term are given by  $\mathcal{H}_1^i$  and  $\mathcal{H}_2^i$ , which can be found in Ref. [407]. In Ref. [407], the notation  $\tilde{S}_{H_1^\perp}^i$  and  $\tilde{S}_H^i$  is used for the hard factors, and one has  $\mathcal{H}_1^i = \tilde{S}_{H_1^\perp}^i$  and  $\mathcal{H}_2^i = \tilde{S}_H^i$ . The notation for the cross section indicates that this is the entire fragmentation term. The functions  $H_1^{\perp(1)}$  and  $\tilde{H}$  are unpolarized twist-3 FFs connected to  $qgq$  matrix elements [167]. The function  $H_1^{\perp(1)}$  is the first moment of the TMD Collins FF  $H_1^\perp(z, p_T)$  that enters SSAs in SIDIS and electron-positron annihilation  $e^+e^- \rightarrow h_1 h_2 X$ . The Collins TMD FF  $H_1^\perp(z, p_T)$  can also be written in terms of  $H_1^{\perp(1)}(z)$  using the OPE [209].

## Phenomenology

The experimental measurements of  $A_N$  span several decades [48, 53, 404, 408–421] and show a characteristic rise at large  $x_F$ , as one sees for the  $\pi^0$  production data in Fig. 5.17. Recent phenomenology found that the fragmentation piece is dominant [17, 407, 422]. The results from the most recent work in Ref. [17] are presented in Fig. 5.18, which included only

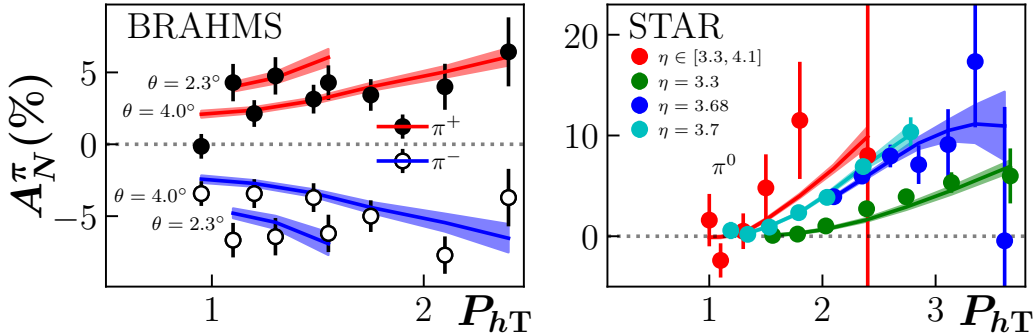


Figure 5.18: Results for the fit in Ref. [17] to the  $A_N$  data in [408–411].

$A_N$  data where  $P_{hT} > 1 \text{ GeV}$ . The analysis exploited the relationships between moments of TMDs and twist-3 functions along with a Gaussian ansatz for the TMD transversity, Sivers, and Collins functions, see Ref. [17] for details. A Monte Carlo framework was used to reliably sample the Bayesian posterior distribution for the parameters. Such an approach allows the relevant regions in parameter space to be determined, and gives state-of-the-art uncertainty quantification, for the hadronic functions that best describe the data.

## 5.4 Boer-Mulders Effect

The Boer-Mulders function  $h_1^\perp$  [60], describing the distribution of transversely polarized quarks in an unpolarized target, can be considered the counterpart of the Sivers function  $f_{1T}^\perp$  discussed in Sec. 5.3.1. Both functions are T-odd and therefore vanish if the gauge-link is not taken into account in their field-theoretic definition. In other words, their existence requires initial and/or final state interactions between the active partons of a process and the target remnants. Both TMDs change sign when going from SIDIS to the Drell-Yan process [59], see Sec. 5.3.1. Since the Boer-Mulders function is chiral-odd, it is generally harder to measure than the Sivers function, even though no target polarization is required.

Let us first discuss the case of the Boer-Mulders function in the Drell-Yan process. It was argued that  $h_1^\perp$  could be essential for a full understanding of the data for the angular distribution of the unpolarized Drell-Yan process [423]. To be more specific, the structure of the Drell-Yan cross section is given by (see [424] and references therein)

$$\frac{1}{\sigma_{DY}} \frac{d\sigma_{DY}}{d\Omega} = \frac{3}{4\pi} \frac{1}{\lambda + 3} \left( 1 + \lambda \cos^2 \theta + \mu \sin 2\theta \cos \phi + \frac{\nu}{2} \sin^2 \theta \cos 2\phi \right), \quad (5.45)$$

the angles  $\theta$  and  $\phi$  characterizing the lepton-pair orientation in a dilepton rest frame like the Collins-Soper frame [193]. In comparison to Eq. (2.174), in Eq. (5.45) all variables but the Collins-Soper angles have been integrated over, while power corrections (for small transverse momenta of the di-lepton pair) have been kept. Of particular interest in this context is the so-called Lam-Tung relation between the coefficients  $\lambda$  and  $\nu$  [425–427],

$$\lambda + 2\nu = 1, \quad (5.46)$$

which is exact at  $\mathcal{O}(\alpha_s)$  in the standard collinear pQCD framework. Even at  $\mathcal{O}(\alpha_s^2)$  the numerical violation of (5.46) was originally reported to be small [428]. This was also studied at

NNLO (i.e.  $\mathcal{O}(\alpha_s^3)$ ) in [429]. Measurements of the angular coefficients are now available over a wide kinematical range, from fixed-target energies [430–434] to collider Tevatron [435] and LHC [436] kinematics. Various beams and targets have been used in the fixed-target regime — data exist for pion beams scattering off tungsten targets [430–432], as well as  $pp$  and  $pd$  collisions [433, 434]. Some of the mentioned data sets show a clear violation of the Lam-Tung relation where, in particular, a large  $\cos 2\phi$  term was observed. Different explanations of this experimental result were then put forward where the most popular one is based on intrinsic transverse motion of partons leading to the Boer-Mulders effect [423]. The product of two Boer-Mulders functions — one for each initial-state hadron — generates a  $\cos 2\phi$  term at leading order in  $1/Q$  [423]. First extractions of the Boer-Mulders function, based on fixed-target data from Fermilab [433, 434] were then reported in Refs. [437, 438]. In Ref. [439] the collinear pQCD calculation of the angular dependence was revisited, and it was argued that the data could actually be largely explained in this framework, including the results from the fixed-target experiments. Extractions of the Boer-Mulders function should take those results into account. A geometric picture that has been invoked to explain the angular dependence of the unpolarized Drell-Yan process [440] is in qualitative agreement with the finding in Ref. [439]. More work on this geometric approach and higher-order pQCD calculations, extended to the production of weak gauge bosons, where the cross section has a richer angular dependence, can be found in Refs. [441–444].

The Boer-Mulders function can also be studied in SIDIS where it appears in combination with the chiral-odd Collins function, giving rise to a  $\cos 2\phi_h$ -modulation of the unpolarized cross section [60]. The relevant structure function takes the generic form (2.189)

$$F_{UU}^{\cos 2\phi_h} = C \left[ \frac{2(\hat{h} \cdot p_T)(\hat{h} \cdot k_T) - p_T \cdot k_T}{z M_N M_h} h_1^{\perp q} H_1^{\perp q} \right] + \frac{4M_N^2}{Q^2} C \left[ \frac{2(\hat{h} \cdot k_T)^2 - k_T^2}{2M_N^2} f_1 D_1 \right] + \dots \quad (5.47)$$

The second term on the r.h.s of Eq. (5.47) is the so-called Cahn effect [278, 279], which is also caused by intrinsic transverse parton motion, but related to unpolarized TMDs. The Cahn effect is a kinematic twist-4 contribution and as such suppressed by a factor  $1/Q^2$  relative to the first term. On the other hand, since  $f_1^q \otimes D_1^q$  is clearly larger than  $|h_1^{\perp q} \otimes H_1^{\perp q}|$ , suppressing the Cahn effect requires very large  $Q^2$ . It should also be noted that the Cahn effect does not represent the entire twist-4 term of a QCD analysis, even though numerically it is most likely the dominant contribution. The SIDIS structure function  $F_{UU}^{\cos 2\phi_h}$  has already been measured in Hall B and Hall A at Jefferson Lab [445, 446], at DESY by the HERMES Collaboration [447], and at CERN by the COMPASS Collaboration [448, 449]. A first extraction of the Boer-Mulders function based on SIDIS data was reported in Ref. [450]. The results were also used to obtain information about the Boer-Mulders function for antiquarks from the early fixed-target measurements of the angular distribution of the Drell-Yan cross section [451]. More recent attempts to pin down the Boer-Mulders function for the nucleon from SIDIS were presented in Refs. [452–454]. For the currently available SIDIS data, the Cahn effect is indeed quite large and can even dominate the  $\cos 2\phi_h$  term of the cross section. Similar to the above discussion for the Drell-Yan process, a thorough higher-order collinear pQCD calculation for SIDIS is mandatory in order to be able to draw definite quantitative conclusions about the Boer Mulders function from this process. Also, new data would be very helpful, where the EIC with

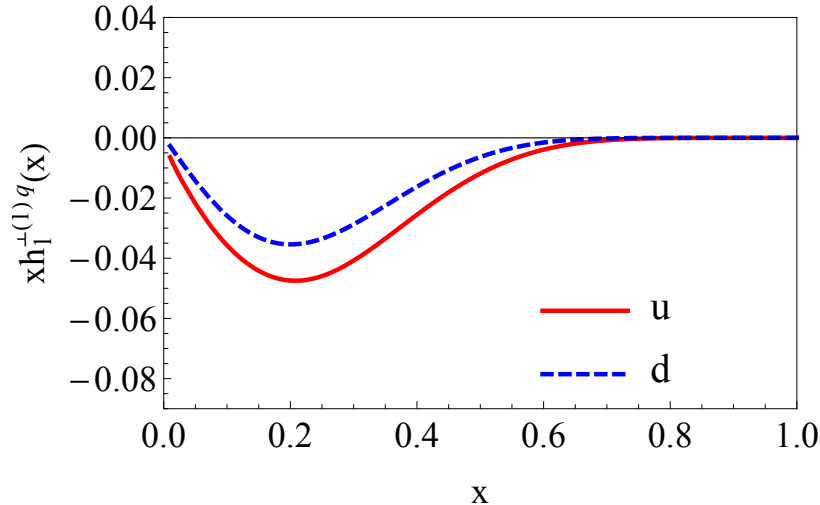


Figure 5.19: The first moment of Boer-Mulders functions  $h_1^{\perp a}$  Ref. [450]

its large kinematical coverage could play a crucial role. The pion and nucleon Boer-Mulders functions were studied intensively in lattice QCD and models, see Chap. 6 and 7.

Fig. 5.19 shows the first moments of Boer-Mulders functions for up and down quarks extracted from the experimental data in Ref. [450].

## 5.5 Worm-gear $g_{1T}^\perp$ and $h_{1L}^\perp$ and Pretzelosity $h_{1T}^\perp$ TMD PDFs

In this section, we review several other TMDs for which presently the information from experiment is still sparse, yet they are as important as the TMDs discussed above in this chapter for obtaining a complete understanding of the transverse-momentum-dependent nucleon structure and fragmentation process. Specifically, we consider the worm-gear functions  $g_{1T}^\perp$  and  $h_{1L}^\perp$ , and the pretzelosity TMD  $h_{1T}^\perp$ .

### Worm-gear TMD PDFs $g_{1T}^\perp$ and $h_{1L}^\perp$

Let us begin with the worm-gear function  $g_{1T}^\perp$ , which describes the distribution of longitudinally polarized quarks in a transversely polarized nucleon. Very recently, this function was extracted for the first time from a global analysis of SIDIS data using Monte Carlo techniques [455]. To this end, the asymmetry (see Eq. (2.189), (2.192))

$$A_{LT}^{\cos(\phi_h - \phi_S)} \equiv \frac{F_{LT}^{\cos(\phi_h - \phi_S)}}{F_{UU,T}} = M \frac{\mathcal{B}[\tilde{g}_{1T}^{\perp(1)} \tilde{D}_1^{(0)}]}{\mathcal{B}[\tilde{f}_1^{(0)} \tilde{D}_1^{(0)}]} . \quad (5.48)$$

was considered for which data from COMPASS [456, 457], HERMES [458], and Jefferson Lab [459] exist. A Gaussian ansatz was made for  $g_{1T}^\perp(x, k_T)$ , and the  $k_T$ -moment

$$g_{1T}^{\perp(1)}(x) = \int d^2 k_T \frac{k_T^2}{2M^2} g_{1T}^\perp(x, k_T) \quad (5.49)$$

was fitted for the up quark and down quark, with the results of the fit shown in Fig. 5.20.

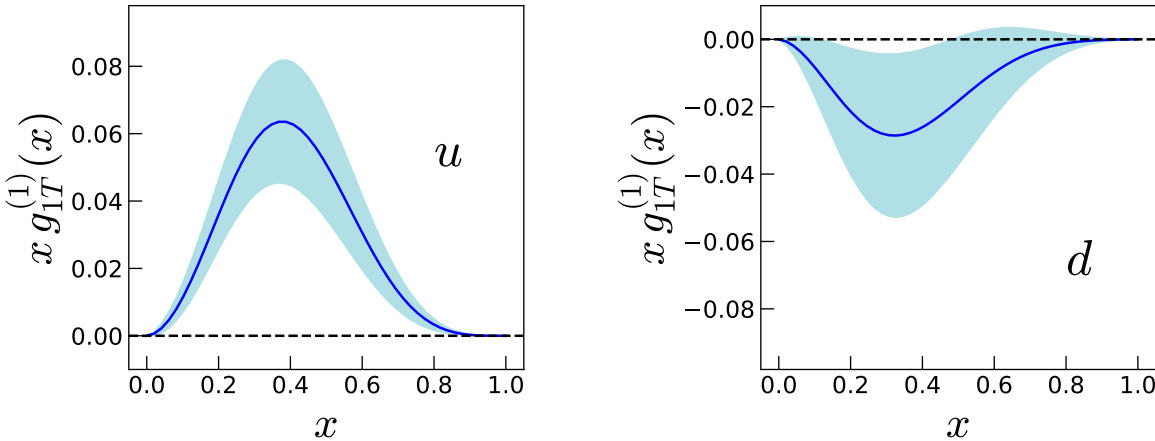


Figure 5.20: Results of global fit for  $x g_{1T}^{(1)}(x)$  at  $Q^2 = 4$  GeV $^2$  for up quarks (left) and down quarks (right). The figures are from Ref. [455].

Estimates for the worm-gear TMDPDFs can be obtained using the so-called Wandzura-Wilczek-type (WW-type) approximation which is based on the QCD equations of motion and consistently neglecting quark-gluon and current quark mass terms [129, 134, 135, 460–464]. This allows one to approximate  $g_{1T}^{(1)}(x)$  (and  $h_{1L}^{(1)}(x)$ ) in terms of integral relations involving twist-2 PDFs. In the case of  $g_{1T}^\perp$  one has

$$g_{1T}^{(1)}(x) \stackrel{\text{WW-type}}{\approx} x \int_x^1 \frac{dy}{y} g_1(y), \quad (5.50)$$

where  $g_1(x)$  is the helicity PDF. The WW-type relations become exact in the parton model and are discussed in Sec. 7.4.1. The fit results of Ref. [455] are compatible with the WW-type approximation in Eq. (5.50), which is in line with the general finding in Ref. [210] that the WW-type approximation for the worm-gear functions is compatible with available data on the pertinent asymmetries regarding sign and magnitude. The extracted results for  $g_{1T}^{(1)}$  in Ref. [455] also agree within errors with information from lattice QCD [142]. Furthermore, it was shown that at present the data for the asymmetry  $A_{LT}^{\cos(\phi_h - \phi_S)}$  can not rule out the strict large- $N_c$  approximation, according to which  $g_{1T}^{1u} = -g_{1T}^{1d}$  [465]; see also Sec. 7.3.2. More precise data are needed in order to move the phenomenology of  $g_{1T}^\perp$  to the next level.

The Kotzinian-Mulders or worm-gear distribution  $h_{1L}^\perp(x, k_T)$  [280] describes the probability of finding a transversely polarized quark but inside a longitudinally polarized nucleon. Since  $h_{1L}^\perp$  is chiral odd, it has to be coupled to another chiral-odd function to manifest its effects in semi-inclusive processes. In SIDIS, this can be achieved via a  $\sin 2\phi_h$  azimuthal asymmetry [134, 280] when  $h_{1L}^\perp$  is combined with the chiral-odd Collins function  $H_1^\perp$  [57], see Eqs. (2.189), (2.192):

$$A_{UL}^{\sin 2\phi_h} \equiv \frac{F_{UL}^{\sin 2\phi_h}}{F_{UU,T}} = M_N M_h \frac{\mathcal{B} [\tilde{h}_{1L}^{(1)} \tilde{H}_1^{(1)}]}{\mathcal{B} [\tilde{f}_1^{(0)} \tilde{D}_1^{(0)}]}. \quad (5.51)$$

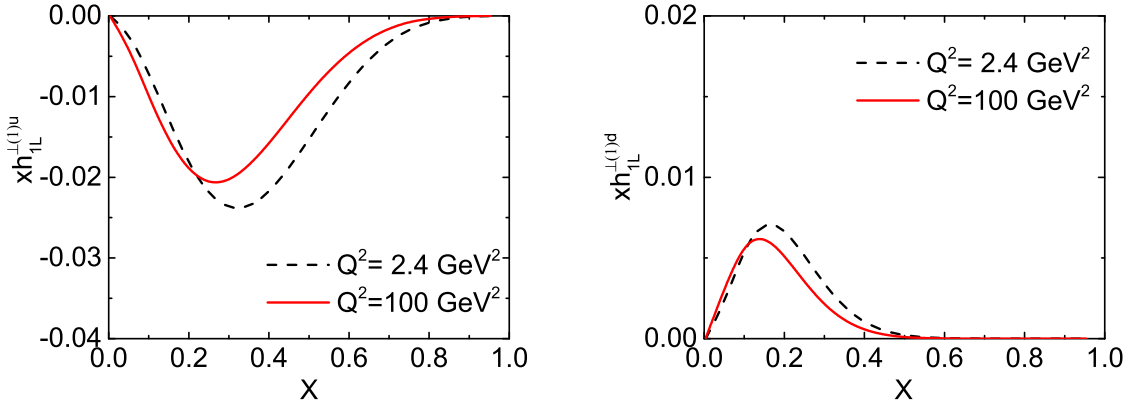


Figure 5.21: Left panel:  $xh_{1L}^{\perp(1)}(x, Q^2)$  of the proton for up quark at  $Q^2 = 2.4 \text{ GeV}^2$  and  $Q^2 = 100 \text{ GeV}^2$ . Right panel: similar to the left panel, but for the down quark. Plots from Ref. [474].

The early work on the  $\sin 2\phi_h$  asymmetry in the longitudinally polarized SIDIS process have been performed in Refs. [210, 466–473], showing that the asymmetry is around several percent.

There are no extractions of  $h_{1L}^\perp$  from the experimental data, however a few analyses used the WW-approximation in which one can write  $h_{1L}^{\perp(1)}(x)$  in terms of an integral relation involving the transversity distribution  $h_1(x)$  as follows

$$h_{1L}^{\perp(1)}(x) \stackrel{\text{WW-type}}{\approx} -x^2 \int_x^1 \frac{dy}{y^2} h_1^a(y). \quad (5.52)$$

In particular, Ref. [474] used NLL TMD factorization formalism to study the  $\sin 2\phi_h$  asymmetry in SIDIS process at the kinematical configuration of HERMES, CLAS and CLAS12. Good agreement with the existing data was found.

In Fig. 5.21, we plot the  $xh_{1L}^{\perp(1)}(x, Q^2)$  from Ref. [474] for up and down quarks at the initial scale  $Q^2=2.4 \text{ GeV}^2$  as well as the evolved scale  $Q^2 = 100 \text{ GeV}^2$ . The plots show that the  $h_{1L}^{\perp(1)}(x, Q^2)$  for the up quark is larger than the one for the down quark in size, and with the opposite sign.

### Pretzelosity TMD PDF, $h_{1T}^\perp$

The pretzelosity distribution function  $h_{1T}^\perp$  [475] describes transversely polarized quarks inside a transversely polarized nucleon. The measured asymmetry in SIDIS contains the convolution of pretzelosity  $h_{1T}^\perp$  and the Collins FF  $H_1^\perp$ , Eqs. (2.189), (2.192):

$$A_{UT}^{\sin(3\phi_h-\phi_S)} \equiv \frac{F_{UT}^{\sin(3\phi_h-\phi_S)}}{F_{UU,T}} = \frac{M_N^2 m_h}{4} \frac{\mathcal{B} [\tilde{h}_{1T}^{\perp(2)} \tilde{H}_1^{\perp(1)}]}{\mathcal{B} [\tilde{f}_1^{(0)} \tilde{D}_1^{(0)}]}. \quad (5.53)$$

Notice that the knowledge of the Collins FF is needed for the extraction of pretzelosity.  $h_{1T}^\perp$  was extracted in parton model approximation in Ref. [475] and the results are shown in Fig. 5.22. Weighted SIDIS asymmetries and predictions for the EIC can be found in Ref [476]. One interesting aspect of pretzelosity is that it is the only leading TMD PDF which is related to

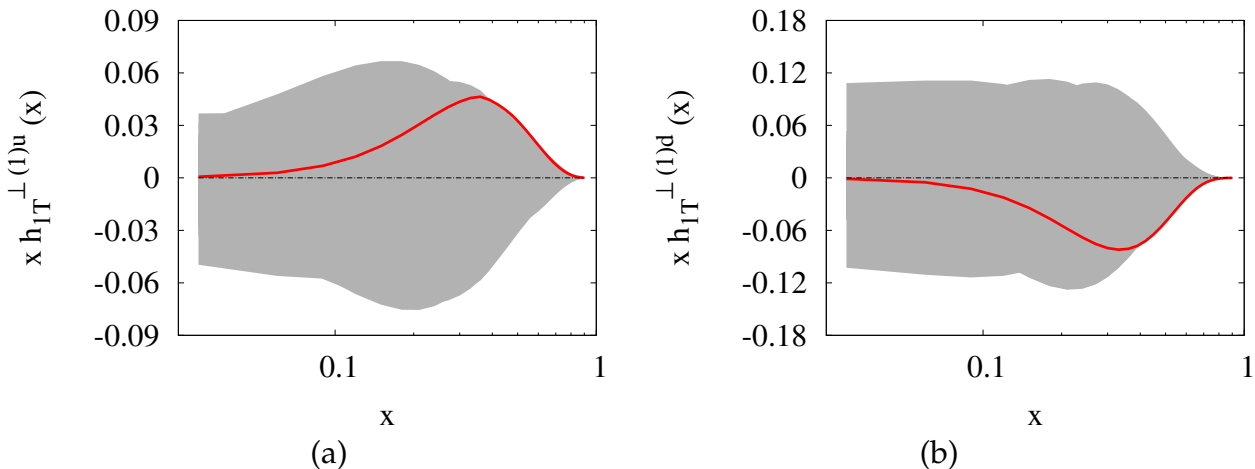


Figure 5.22: First moment of the pretzelosity distribution for up (a) and down (b) quarks at  $Q^2 = 2.4$  GeV $^2$ . The solid line corresponds to the best fit and the shadowed region corresponds to the error corridor.

orbital angular momentum of quarks, even though this relation only holds in quark models, see Sec. 7.9.

## 5.6 Observables for Gluon TMDs

This section is devoted to presenting an overview on the work that has been done on TMD analyses of experimental observables that may provide information on gluon TMDs. We review the present status on where we stand with respect to gluon TMD phenomenology (see also a fairly recent review [477]). At the same time we want to emphasize that the theoretical and experimental research on gluon TMDs is an ongoing endeavor. At present, the TMD theory for gluon distributions is less developed compared to their quark counterparts. While precise all-order definitions of gluon TMDs were discussed in the literature (see, e.g., [151]) rigorous TMD factorization of physical observables involving gluon TMDs has been suggested only for a small number of very simple final states in proton collisions, such as Higgs boson production [151] or  $\eta_{c,b}$ -production [478]. Nonetheless, several spin-independent and spin-dependent observables sensitive to gluon TMDs have been investigated at tree-level (LO) or to one-loop accuracy (NLO) *under the working assumption* that rigorous TMD factorization for those observables would hold and be proved in the future. Possible observables sensitive to gluon TMDs have been identified both for lepton-nucleon and proton-proton collisions. Experimentally, a future EIC will be suitable to perform measurements on gluon TMD observables in lepton-nucleon collisions. A limited amount of data for gluon TMD observables in proton collisions has been generated at the LHC. Thus, in principle, one may be able to learn about (unpolarized) gluon TMDs from existing LHC data – even if this information is rather limited at the moment due to a small number of LHC data points. In future, the knowledge of gluon TMDs can be improved through precise EIC measurements.

Several (color-singlet) final states have been identified in proton collisions that may provide insight into gluon TMDs: photon pair production [479–481], Higgs boson production [151,

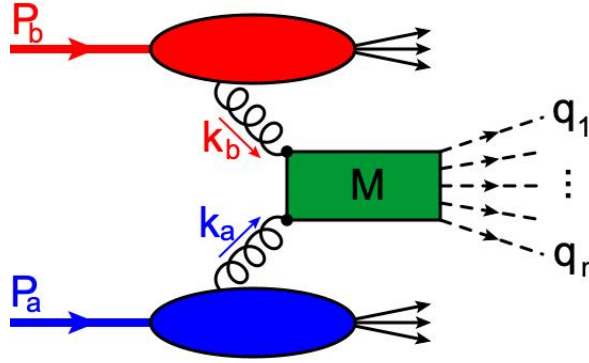


Figure 5.23: General setup of a hard process in proton collisions that is sensitive to gluon TMDs.

482–484], single quarkonium production [485–487], associated quarkonium - photon pair production [488], associated quarkonium - dilepton pair production [489] and quarkonium pair production [490, 491]. For proton collisions it is important to keep in mind that TMD factorization breaking effects – the so-called *color entanglement* – may occur for colored final states like jets of hadrons produced within a fragmentation process (see Refs. [222, 223] and the following section). Therefore, if TMD factorization is considered for final states in proton collisions that involve quarkonia, those quarkonia need to be produced as color singlet states rather than color octet states [492]. We again emphasize that TMD factorization has not been rigorously proven for the associated quarkonium and quarkonium pair final states listed above, even for color singlet quarkonia. On the other hand TMD factorization has not been shown to fail either for color singlet quarkonium final states (except for single  $\chi$  production [487]), and one may consider it as a *working hypothesis*. The correct definition of TMD parton distribution has been discussed in detail in previous sections. Here, we focus on the various gluon TMDs that are relevant for TMD observables. This concerns in particular the TMD distribution of unpolarized gluons in the unpolarized nucleon,  $f_1^g(x, k_T^2)$ , the TMD distribution of linearly polarized gluons in the unpolarized nucleon,  $h_1^{\perp g}(x, k_T^2)$ , and the TMD distribution of unpolarized gluons in a transversely polarized nucleon,  $f_{1T}^{\perp g}(x, k_T^2)$  – the gluonic counterpart to the quark Sivers function. Those functions were introduced in earlier sections.

### 5.6.1 Gluon TMDs from proton-proton collisions

The following subsection is devoted to observables in proton-proton collisions that are sensitive to gluon TMDs. The general formalism of how these observables emerge theoretically has been described in Ref. [489]. Let us consider a general final state of  $n$  particles carrying momenta  $q_1, \dots, q_n$  that has been produced in a collision of two protons of momenta  $P_a$  and  $P_b$ , see Fig. 5.23. The overall 4-momentum of the final state is labelled as  $q^\mu = \sum_{i=1}^n q_i^\mu$ . We assume that the production mechanism of the final state is via gluon fusion in a hard scattering amplitude  $\mathcal{M}$ . The application of TMD factorization to this general process demands (at least) two necessary conditions:

- The transverse momentum of the final state,  $|q_T|$  is much smaller than its invariant mass  $Q = \sqrt{q^2}$ , i.e.,  $|q_T| \ll Q$ . Ideally,  $|q_T|$  is of the order of some hadronic scale in order to maximize the effect of the intrinsic transverse gluonic motion. At the same time, this

condition forbids the production of unobserved partons in the hard scattering amplitude  $\mathcal{M}$ . In other words, all particles  $1, \dots, n$  in the final state must be detected. Otherwise, the final state may recoil against an unobserved parton, such as a radiated gluon. This situation would be described within collinear factorization.

- The particles in the final state need to be color singlets, such as leptons, photons, Z-bosons, Higgs bosons, but also quarkonium states like  $\eta$ ,  $J/\psi$  or  $\Upsilon$  in a color singlet mode. Final state events that are sensitive to color, such as jets, fragmenting hadrons, quarkonia in color octet modes, etc., should be treated with great care as the aforementioned color entanglement may potentially spoil TMD factorization.

If these conditions are met one may analyze a general process as in Fig. 5.23. According to Ref. [489] the fully differential cross section for a general process then acquires the following form,

$$\frac{d\sigma(|q_T| \ll Q)}{dPS_n} = \frac{(2\pi)^4}{4x_a x_b s^2} \left( \hat{F}_1 C[f_1^g f_1^g] + \hat{F}_2 C[w_2 h_1^{\perp g} h_1^{\perp g}] \right. \\ \left. + \hat{F}_{3a} C[w_{3a} h_1^{\perp g} f_1^g] + \hat{F}_{3b} C[w_{3b} f_1^g h_1^{\perp g}] \right. \\ \left. + \hat{F}_4 C[w_4 h_1^{\perp g} h_1^{\perp g}] \right) + O(M/Q). \quad (5.54)$$

In this formula,  $s = (P_a + P_b)^2$  denotes the center-of-mass energy. In addition, there are two kinematical scaling variables  $x_{a/b} = q \cdot P_{b/a} / P_a \cdot P_b$ . The  $3n$ -dimensional phase space element for an  $n$ -particle final state is denoted by  $dPS_n$ . Notice that we consider unpolarized collisions. The structures like, e.g.,  $h_1^{\perp g} f_1^g$  are possible because both TMDs are chiral-even, since the gluon Boer-Mulders function is not chiral-odd as in quark case. The TMD formula (5.54) contains four different convolution integrals of the gluon TMDPDFs  $f_1^g$  and  $h_1^{\perp g}$ , with the general form of the TMD convolution,

$$C[w f g] = \int d^2 k_{aT} \int d^2 k_{bT} \delta^{(2)}(\mathbf{k}_{aT} + \mathbf{k}_{bT} - \mathbf{q}_T) w(\mathbf{k}_{aT}, \mathbf{k}_{bT}, \mathbf{q}_T) f(x_a, \mathbf{k}_{aT}^2) g(x_b, \mathbf{k}_{bT}^2). \quad (5.55)$$

The TMD weights  $w_i$  in (5.54) read (with  $M_N$  being the nucleon mass),

$$w_2 = \frac{2(\mathbf{k}_{aT} \cdot \mathbf{k}_{bT})^2 - \mathbf{k}_{aT}^2 \mathbf{k}_{bT}^2}{4M_N^4}, \\ w_{3a/b} = \frac{\mathbf{k}_{a/bT}^2 \mathbf{q}_T^2 - 2(\mathbf{q}_T \cdot \mathbf{k}_{a/bT})^2}{2M_N^2 \mathbf{q}_T^2}, \\ w_4 = 2 \left[ \frac{\mathbf{k}_{aT} \cdot \mathbf{k}_{bT}}{2M_N^2} - \frac{(\mathbf{k}_{aT} \cdot \mathbf{q}_T)(\mathbf{k}_{bT} \cdot \mathbf{q}_T)}{M_N^2 \mathbf{q}_T^2} \right]^2 - \frac{\mathbf{k}_{aT}^2 \mathbf{k}_{bT}^2}{4M_N^4}. \quad (5.56)$$

The beauty of the "master formula" (5.54) is that the TMD convolution integrals that we are ultimately after are completely independent of the final state, and universal up to the caveats discussed earlier. This, in principle, allows for a combined analysis of gluon induced

processes with various final states, each of which have their own peculiarities, advantages and disadvantages.

The factors  $\hat{F}_i$  in (5.54) are partonic functions that can be calculated in pQCD. In fact, they can be written in terms of helicity amplitudes  $\mathcal{M}_{\lambda_a \lambda_b; I}(k_{a/b} = x_{a/b} P_{a/b})$  where  $k_{a/b}, \lambda_{a/b}$  are the momenta and helicities of the two fusing gluons, respectively (cf. Fig. 5.23). Those helicity amplitudes have been well studied in collinear factorization and are often known to higher orders in perturbation theory for a specific final state. According to Ref. [489] the factors  $\hat{F}_i$  acquire the following form,

$$\begin{aligned}\hat{F}_1 &= \frac{1}{(N_c^2 - 1)^2} \sum_{\lambda_a, \lambda_b = \pm 1} \sum_I \mathcal{M}_{\lambda_a, \lambda_b; I}^{ab}(k_{a/b} = x_{a/b} P_{a/b}) (\mathcal{M}_{\lambda_a, \lambda_b; I}^{ab})^*(k_{a/b} = x_{a/b} P_{a/b}), \\ \hat{F}_2 &= \frac{1}{(N_c^2 - 1)^2} \sum_{\lambda = \pm 1} \sum_I \mathcal{M}_{\lambda, \lambda; I}^{ab}(k_{a/b} = x_{a/b} P_{a/b}) (\mathcal{M}_{-\lambda, -\lambda; I}^{ab})^*(k_{a/b} = x_{a/b} P_{a/b}), \\ \hat{F}_{3a} &= \frac{1}{(N_c^2 - 1)^2} \sum_{\lambda_a, \lambda_b = \pm 1} \sum_I \mathcal{M}_{\lambda_a, \lambda_b; I}^{ab}(k_{a/b} = x_{a/b} P_{a/b}) (\mathcal{M}_{-\lambda_a, \lambda_b; I}^{ab})^*(k_{a/b} = x_{a/b} P_{a/b}), \\ \hat{F}_{3b} &= \frac{1}{(N_c^2 - 1)^2} \sum_{\lambda_a, \lambda_b = \pm 1} \sum_I \mathcal{M}_{\lambda_a, \lambda_b; I}^{ab}(k_{a/b} = x_{a/b} P_{a/b}) (\mathcal{M}_{\lambda_a, -\lambda_b; I}^{ab})^*(k_{a/b} = x_{a/b} P_{a/b}), \\ \hat{F}_4 &= \frac{1}{(N_c^2 - 1)^2} \sum_{\lambda = \pm 1} \sum_I \mathcal{M}_{\lambda, -\lambda; I}^{ab}(k_{a/b} = x_{a/b} P_{a/b}) (\mathcal{M}_{-\lambda, \lambda; I}^{ab})^*(k_{a/b} = x_{a/b} P_{a/b}).\end{aligned}\quad (5.57)$$

In these equations,  $a, b$  are the color indices of the two fusing gluons, and  $N_c = 3$  the number of colors. The index  $I$  combines all of the quantum numbers of the final state that are summed over.

Equation (5.54) becomes particularly simple for a one-particle final state. In this case the partonic factors  $\hat{F}_{3a,b}$  and  $\hat{F}_4$  vanish. The prefactor  $\hat{F}_1$ , together with the convolution  $C[f_1^g f_1^g]$ , leads to the typical  $q_T$ -transverse momentum spectrum of the final state particle that one would also expect from collinear factorization (using CSS resummation techniques [63]). This  $q_T$ -spectrum may be modified by the factor  $\hat{F}_2$ , together with the convolution integral  $C[w_2 h_1^{\perp g} h_1^{\perp g}]$  of linearly polarized gluon distributions. This modification has been discussed for the production of a Higgs boson [482] and for the production of color-singlet quarkonia  $\eta_{c,b}$  and  $\chi_{c,b;0,2}$  [485]. The scale evolution of the modification of the  $q_T$ -spectrum from linearly polarized gluons has been studied in Ref. [493]. It was estimated in Ref. [493] that the effect of linearly polarized gluons becomes negligible for large scales while it may play a non-negligible role for lower scales in quarkonium production.

One disadvantage of a one-particle final state, from the point of view of extracting the TMD convolution integrals from experimental data, is that its invariant mass is simply the particle's mass,  $Q = M$ , so that it can not be tuned. This is however possible for particle pair production. For a two-particle final state one may conveniently work out the partonic prefactors  $\hat{F}_i$  in (5.57) in the Collins-Soper frame [86], i.e., a specific realization of a pair center-of-mass frame where the spatial orientation of the two particles is described by the Collins-Soper angles  $\theta$  and  $\phi$ . In particular the angle  $\phi$  is of interest as it describes azimuthal modulations of the differential cross section. It turns out that the partonic factors  $\hat{F}_1$  and  $\hat{F}_2$  are azimuthally independent

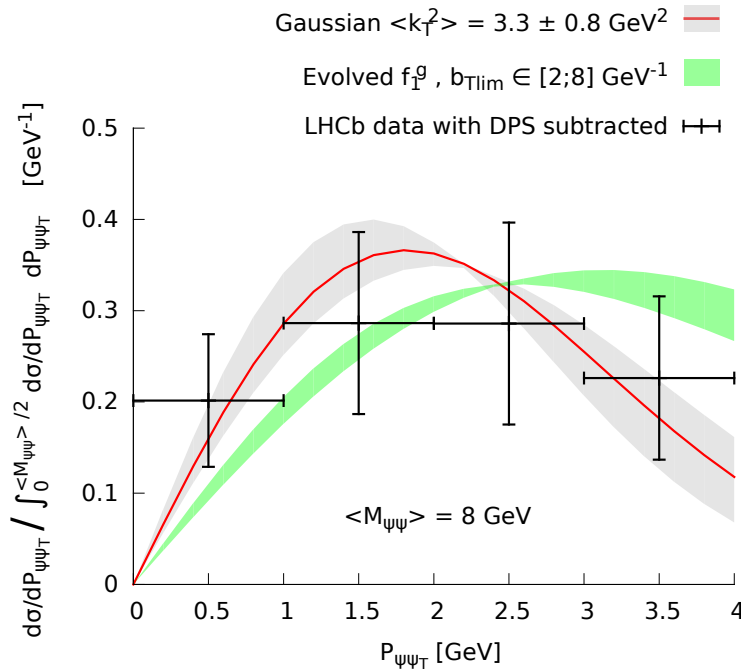


Figure 5.24: Fit of the azimuthally independent term of the  $J/\psi$ -pair production cross section to LHCb data [494]. Plot is from Ref. [491].

while  $\hat{F}_{3a/b}$  and  $\hat{F}_4$  show a  $\cos(2\phi)$  and  $\cos(4\phi)$  dependence [489], respectively<sup>21</sup>. The physical explanation for this behaviour is that  $\hat{F}_{3a/b}(\phi) \equiv F_3 \cos(2\phi)$  is generated by a single gluon helicity flip whereas  $\hat{F}_4(\phi) \equiv F_4 \cos(4\phi)$  is related to a double gluon helicity flip, see Eq. (5.57).

Several 2-particle final states have been investigated with the aim of gaining information on gluon TMDs: "background" photon pair production [481], photon pairs as a decay channel of the Higgs boson [482, 484], quarkonium-photon pairs [488], quarkonium-dilepton pairs [489] and quarkonium pairs [490, 491]. In particular the last final state, i.e.,  $J/\psi$  pairs, has some advantages over the others. First of all, there exist LHC data on the  $q_T$ -spectrum of  $J/\psi$ -pairs, from LHCb [494, 495], CMS [496] and ATLAS [497], as well as from D0 at FermiLab [498]. In fact, in Refs. [490, 491] LHCb data was used to fit the convolution integral  $C[f_1^g f_1^g]$  in order to extract the TMD distribution of unpolarized gluons for the first time (see Fig. 5.24).

Even though experimental data is presently not available on the azimuthal dependencies of the differential  $J/\psi$ -pair cross section, one may theoretically estimate the maximum possible size of the  $\cos(2\phi)$  and  $\cos(4\phi)$  modulations by assuming the saturation of positivity bounds for gluon TMDs, in particular for the distribution of linearly polarized gluons [499]. It again turns out that the final state of  $J/\psi$  or  $\Upsilon$  pairs is exceptionally suitable (compared to other 2-particle final states) for the experimental exploration of the  $\cos(2\phi)$  and  $\cos(4\phi)$  dependence as the partonic factors  $F_{3a/b}$ ,  $F_4$  can become – in certain kinematical regions – as large as the one accompanying the unpolarized gluon TMDs,  $F_1$  (cf. Eq. (5.54)). For details we refer the reader to Refs. [490, 491].

<sup>21</sup>Strictly speaking, this statement is only true if the interactions entering the partonic amplitude  $\mathcal{M}$  are CP-conserving. If CP symmetry is not conserved one may also find  $\sin(2\phi)$  and  $\sin(4\phi)$  modulations [484].

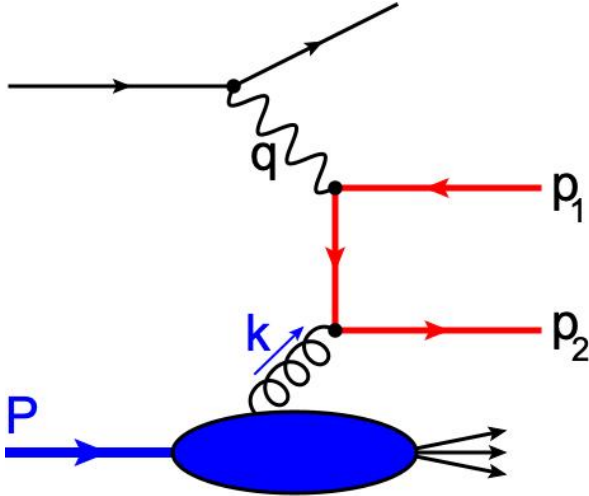


Figure 5.25: Tree-level diagram for heavy back-to-back jet pair production in lepton-nucleon collisions.

In summary, various final states have been identified theoretically in proton collisions that may be utilized to learn about gluon TMDs, in particular about the gluon TMDs  $f_1^g$  and  $h_1^{\perp g}$ . At present, the lack of experimental data on the  $\cos(2\phi)$  and  $\cos(4\phi)$  modulations slows down our progress on the exploration of those functions. This will change in the future after the high-luminosity upgrade of the LHC when more precise LHC data can be expected.

The study of polarized gluon TMDs like the gluon Sivers function  $f_{1T}^{\perp g}$  (and others) through spin asymmetries in proton collisions requires either a polarized nuclear target or a polarized proton beam. The latter option has been realized at RHIC, while future polarized targets are being discussed at the LHC, in particular the implementation of such a target at AFTER@LHC [500, 501] or at LHCb [502]. For more details about the gluon Sivers function we refer the reader to a recent review on that function [147].

### 5.6.2 Gluon TMDs in lepton-nucleon collisions

In this subsection we will briefly discuss observables in lepton-nucleon collisions that are sensitive to gluon TMDs. The exploration of the gluonic structure of the nucleon is an important part of the experimental program at the future Electron-Ion Collider, and we will see that this experiment is well suited for the study of gluon TMDs.

The theoretically cleanest process at an EIC that may be used to study gluon TMDs is the production of two back-to-back jets. The two jets need to be produced by two heavy quarks. This process,  $ep \rightarrow e + \text{jet} + \text{jet} + X$ , has been first analyzed in the TMD framework at tree-level in Ref. [503]. For more formal aspects about TMD factorization of heavy dijet production beyond tree-level we refer the reader to Refs. [504–506].

At tree-level, the only diagram (+ crossed) that contributes in the TMD framework for heavy dijet production in lepton-nucleon collisions, i.e.,  $\gamma^*(q) + n(P) \rightarrow \text{jet}(p_1) + \text{jet}(p_2) + X$  is shown in Fig. 5.25. Its calculation is straight-forward. If the dijet momentum is labeled as  $p \equiv p_1 + p_2$ , then TMD factorization can be applied if the dijet transverse momentum  $p_T$  is much smaller than the hard scale of the process, typically the virtuality of the exchanged photon,  $Q$ . A small  $|p_T|$  may be viewed as a small transverse momentum imbalance of the two jets. In other words, the jets are almost back-to-back in transverse space. In the kinematical

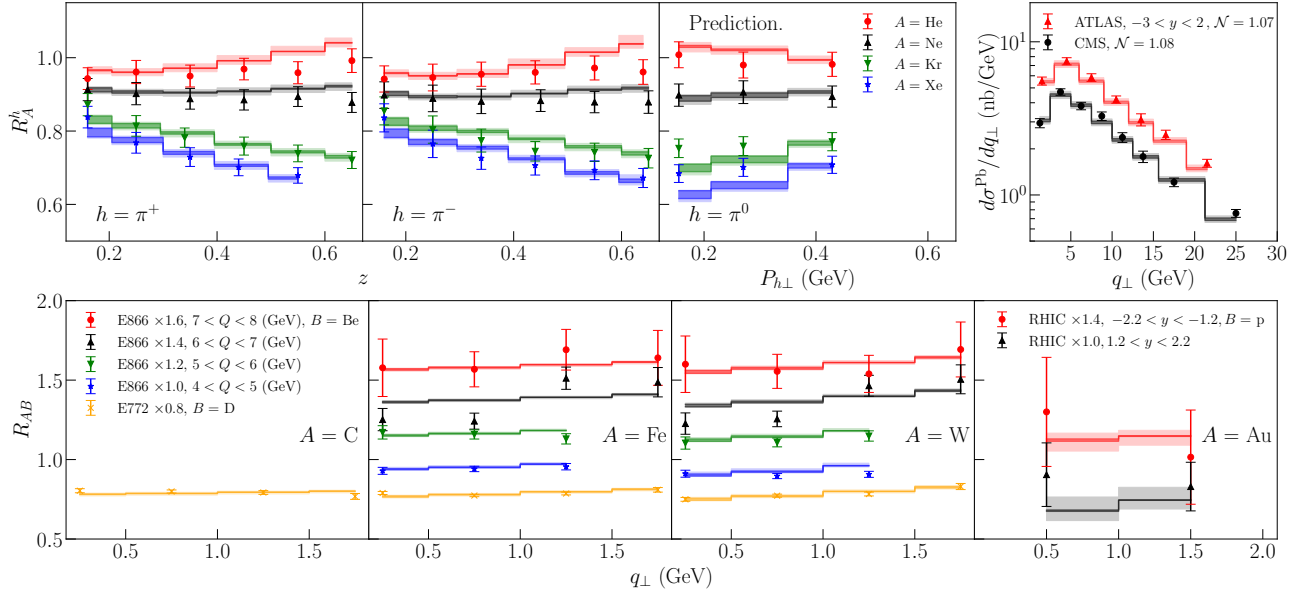


Figure 5.26: Theoretical description of selected experimental data for SIDIS process in lepton-nucleus collisions and DY process in proton-nucleus scatterings. Plot from Ref. [523].

region  $p_T \ll Q$ , the differential cross section for dijet production then reads according to Ref. [503],

$$\frac{d\sigma(|p_T| \ll Q)}{dPS_3} = A f_1^g(x, p_T^2) + B h_1^{\perp g}(x, p_T^2) \cos(2\phi). \quad (5.58)$$

In this schematic formula,  $A$  and  $B$  are partonic factors given in Ref. [503], while  $\phi$  is the azimuthal angle between lepton plane and the dijet transverse momentum. It is quite remarkable that in Eq. (5.58) the gluon TMDs  $f_1^g$  and  $h_1^{\perp g}$  do not show up in a convolution integral combined with other gluon TMDs as they do in proton collisions (see previous section). Instead, formula in Eq. (5.58) suggests that one can probe the support of those functions, in principle point-by-point. In particular the intrinsic transverse gluon momentum  $k_T$  is replaced by the heavy dijet transverse momentum imbalance  $p_T$ . This is truly a unique feature of this process, and makes it an ideal candidate to be investigated at a future EIC. Since the EIC will also allow for polarized proton beams, this process also offers the opportunity to study polarized gluon TMDs like the gluon Sivers function [504, 507].

Certainly, heavy dijet production is not the only final state that can be used to probe gluon TMDs in lepton-nucleon production. As for proton collisions, the production of quarkonium states can also shed information on the gluonic transverse motion in the nucleon. This has been studied recently in a series of papers, see Refs. [508–511].

## 5.7 TMDs in Nuclei

Significant progress has been made in extracting TMDs for free nucleons from experimental data. On the other hand, the corresponding TMDs in a heavy nucleus is still at a primitive stage. Identifying the partonic structure of quarks and gluons in nuclei has remained as one of the most important challenges confronting the nuclear physics community since the

pioneering EMC measurements in 1980s [512], and has been regarded as one of the major goals at the future EIC [15, 513].

The determination of nuclear TMD PDFs and nuclear TMD FFs (collectively called nTMDs) relies on the corresponding TMD QCD factorization. At the moment, experimental data are available from the SIDIS process on a nuclear target, and the Drell-Yan process in proton-nucleus (pA) and pion-nucleus collisions. For a compilation of Drell-Yan data prior to 1993 we refer to the review [514]. More recent nTMD measurements were reported by HERMES [515], JLab [337, 516, 517], Fermilab [518, 519], RHIC [520] and the LHC [521, 522], and will be further measured by the future EIC with unprecedented precision.

The first simultaneous global QCD extraction of the TMD parton distribution functions and the TMD fragmentation functions in nuclei was performed in Ref. [523]. The world set of data from semi-inclusive electron-nucleus deep inelastic scattering and Drell-Yan dilepton production was considered. In total, this data set consists of 126 data points from HERMES, Fermilab, RHIC and LHC. Working at next-to-leading order and next-to-next-to-leading logarithmic accuracy, a very good  $\chi^2/\text{d.o.f.} = 1.045$  was achieved. In this analysis, the broadening of TMDs in nuclei was quantified for the first time .

In Fig. 5.26, we plot the result of the fit and the experimental data. In the top row of this figure, we plot the comparison against: the multiplicity ratio measurement at HERMES [515] as a function of  $z$  (left two columns) and  $P_{h\perp}$  (third column from the left), and the DY  $q_\perp$  distribution from the LHC (right column). We note that the  $P_{h\perp}$  dependent data in the third column is a prediction for those data points. Furthermore, for the LHC data [521, 522], we have provided the  $N_i$  for each of the data sets. In the left three columns of the second row, we plot the comparison against the  $R_{AB}$  ratio for the E866 [518] and E772 [519] experiments. Finally, in the right column of this row, we plot the  $R_{AB}$  at RHIC [520]. In each subplot, we have provided the uncertainty from our fit as a dark band, and the uncertainty from the collinear distributions as a light band.

In the right panel of Fig. 5.27, we plot the ratio of the  $u$ -quark TMDPDF of a bound proton in a gold nucleus and that in a free proton as a function of  $x$  and  $k_\perp$ . The curve along the plane for  $k_\perp = 1 \text{ GeV}$  demonstrates the shadowing, anti-shadowing, and the EMC effect which originate from the collinear distribution. The curves which lie in planes of constant  $x$  increase with increasing  $k_\perp$ , which indicates the transverse momentum broadening effect, with a suppression at low  $k_\perp$  and an enhancement at high  $k_\perp$ . In the second panel of this figure, we plot the ratio of the nTMDFF for  $u \rightarrow \pi^+$  in a Xe nucleus and that in vacuum as a function of  $z$  and  $p_\perp$ . Analogous to the nTMDPDFs, we see that as  $p_\perp$  grows, this ratio becomes larger, indicating that hadrons originating from fragmentation in the presence of a nuclear medium will tend to have a broader distribution of transverse momentum relative to vacuum TMDFFs.

## 5.8 Importance of QED Corrections to SIDIS for Extracting TMDs

By evaluating various angular modulations of the angles  $\phi_h$  and  $\phi_S$ , as defined in Fig. 2.16, the lepton-hadron SIDIS has a unique advantage in separating contributions from different TMDs, as reviewed in this Chapter. However, lepton scattering at large momentum transfer can be a source of considerable photon radiation, which can significantly distort the inferred hadron structure if it is not properly accounted for. The collision induced radiation can not only affect the momentum transfer  $q$  from the colliding lepton to the hadron, preventing a

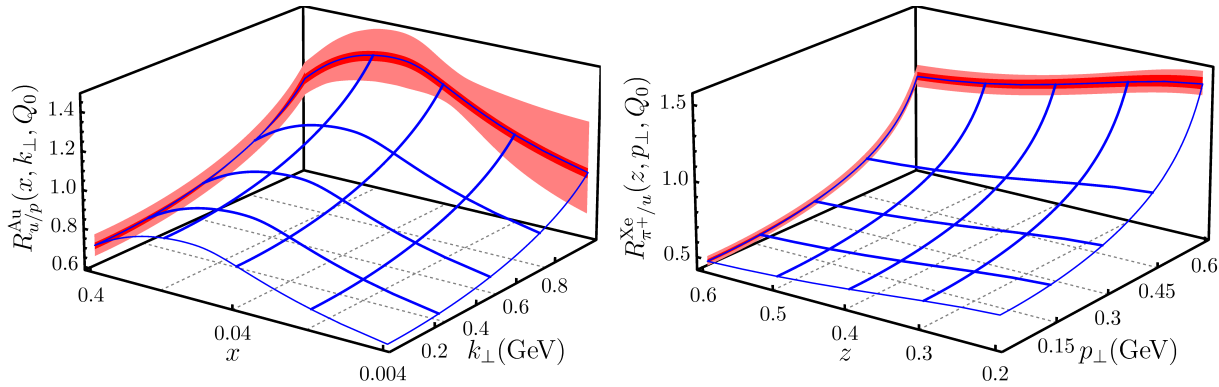


Figure 5.27: The extracted nuclear ratio for the TMDPDF (left) and the TMDFF (right).

well-defined  $\gamma^*(q)P$  frame in Fig. 2.16 where the TMD factorization is defined, it can also alter the angular modulation between the lepton and hadron planes, making it problematic to define the transverse momentum of the produced hadron,  $P_{hT}$ , in the “true”  $\gamma^*P$  frame. This in turn can induce angular modulations which can mimic those arising from the true hadron structure effects encoded by the TMDs.

With a large momentum transfer, the collision-induced QED radiation is an integral part of the experimentally measured cross section for deep-inelastic lepton-hadron scattering. Historically, tremendous efforts have been devoted to isolate and remove collision-induced QED contributions from measured cross sections, which would enable one to focus purely on QCD effects in lepton-hadron scattering, by adding a radiative correction factor to the “Born” cross section that does not include any collision-induced QED radiation effect. However, such QED radiative corrections factors that aim to “correct” for this QED contamination are necessarily sensitive to the very hadronic physics that we aim to explore in SIDIS reactions [524, 525]. This is because the colliding hadron has to experience a range of momentum transfer after we sum over the collision-induced QED radiation. Instead of the single value of momentum transfer  $q$  for the Born cross section, QED radiation changes the kinematic variables ( $x = Q^2/2P \cdot q$ ,  $Q^2 = -q^2$ ) for the Born cross section to ( $x \in [Q^2/2P \cdot q, 1]$ ,  $Q^2 \in [Q_{\min}^2, Q_{\max}^2]$ ) for the SIDIS cross section with the approximation of one-photon exchange. With  $Q_{\min}^2 = Q^2(1 - y)/(1 - x)y$  and  $Q_{\max}^2 = Q^2/(1 - (1 - x)y)$ , the radiative corrections factors could be sensitive to non-perturbative hadron physics if  $Q_{\min}^2$  is sufficiently small even if  $Q^2$  is a hard scale.

The lepton-hadron SIDIS cross section is effectively an inclusive cross section to observe one lepton and one hadron in the final state. It is a well-defined two-scale observable when  $Q^2$  is much larger than the momentum imbalance between the observed final-state lepton and hadron, and the imbalance is sensitive to the collision-induced QED and QCD radiation and transverse momentum of the active partons and leptons. Instead of dealing with a full TMD factorization for all four observed particles (the two leptons and two hadrons) in both QED and QCD, which is likely to be violated [222], a hybrid factorization approach was proposed for treating lepton-hadron SIDIS with collinear factorization for the two leptons and TMD factorization for two hadrons when the SIDIS cross section is in the two-scale regime [524, 525]. Such a hybrid factorization approach to SIDIS is possible because the amount of transverse momentum broadening generated by the collision-induced QED and QCD radiation from a

“point-like” lepton is much smaller than the typical transverse momentum of a colliding parton (which could be further enhanced by QCD radiation from its intrinsic value) for all foreseeable energies of lepton-hadron scattering experiments [525]. The momentum imbalance between the observed lepton and hadron in the final state is therefore dominated by the transverse momentum dependence of the hadron TMDs, which ensures SIDIS to be a useful process for extraction of TMDs. The key impact of QED radiation on the SIDIS cross section is from the change of the momentum transfer to the colliding hadron, in both its direction and invariant mass, caused mainly by the logarithmic-enhanced collinear QED radiation.

With this hybrid factorization approach, the SIDIS cross section for a colliding lepton of momentum  $l$  and helicity  $\lambda_l$  and a nucleon of momentum  $P$  and spin  $S$  can be factorized as [525, 526]

$$E_{l'} E_{P_h} \frac{d\sigma_{l(\lambda_l)P(S) \rightarrow l'P_h X}}{d^3 l' d^3 P_h} \approx \sum_{ij\lambda_k} \int_{\zeta_{\min}}^1 \frac{d\zeta_l}{\zeta_l^2} D_{l'/j}(\zeta_l) \int_{\xi_{\min}}^1 d\xi_l f_{i(\lambda_k)/l(\lambda_l)}(\xi_l) \\ \times \left[ E_{k'} E_{P_h} \frac{d\hat{\sigma}_{k(\lambda_k)P(S) \rightarrow k'P_h X}}{d^3 k' d^3 P_h} \right]_{k=\xi_l l, k'=l'/\zeta_l}, \quad (5.59)$$

where  $D_{l'/j}(\zeta_l)$  and  $f_{i(\lambda_k)/l(\lambda_l)}(\xi_l)$  are lepton FFs and lepton PDFs, respectively, the  $\zeta_l$  and  $\xi_l$  are corresponding lepton momentum fractions, and the integration limits  $\zeta_{\min} = 1 - (1 - x)y$  and  $\xi_{\min} = (1 - y)/(\zeta_{\min} - xy)$  [525]. In Eq. (5.59), the  $\hat{\sigma}_{k(\lambda_k)P(S) \rightarrow k'P_h X}$  is infrared-safe as lepton mass  $m_e \rightarrow 0$  with all infrared sensitive collinear radiative contributions along the direction of colliding and observed lepton resummed into the lepton PDFs and lepton FFs, respectively. In the Born approximation in QED for the  $\hat{\sigma}_{k(\lambda_k)P(S) \rightarrow k'P_h X}$ , which is the LO contribution in  $\alpha$ , the differential SIDIS cross section in the presence of QED effects can be written in the TMD regime as [525]

$$\frac{d\sigma_{l(\lambda_l)P(S) \rightarrow l'P_h X}}{dx dy d\psi dz_h d\phi_h dP_{hT}^2} = \sum_{ij\lambda_k} \int_{\zeta_{\min}}^1 \frac{d\zeta_l}{\zeta_l^2} \int_{\xi_{\min}}^1 \frac{d\xi_l}{\xi_l} f_{i(\lambda_k)/l(\lambda_l)}(\xi_l) D_{l'/j}(\zeta_l) \\ \times \frac{\hat{x}}{x \xi_l \zeta_l} \left[ \frac{\alpha^2}{\hat{x} \hat{y} \hat{Q}^2} \frac{\hat{y}^2}{2(1 - \hat{\varepsilon})} \left( 1 + \frac{\hat{\gamma}^2}{2\hat{x}} \right) \sum_n \hat{w}_n F_n^h(\hat{x}, \hat{Q}^2, \hat{z}_h, \hat{P}_{hT}^2) \right], \quad (5.60)$$

where the kinematic variables with carets in the factorized expression are defined in the same way as those in [121] without carets, except the momentum  $q = l - l'$  of the exchanged virtual photon (or vector boson in general) is replaced by  $\hat{q}(\xi_l, \zeta_l) \equiv \xi_l l - l'/\zeta_l$ , and the produced hadron transverse momentum  $\hat{P}_{hT}$  is defined in the virtual  $\gamma^*(\hat{q})P$  frame. In Eq. (5.60), the expression in the square brackets is the one without the presence of collision-induced QED effects with the usual 18 SIDIS structure functions,  $F_n^h$  with  $n = 1, \dots, 18$ , weighted by factors  $\hat{w}_n$  that are functions of the kinematic variables [121], and the factor in front of the square brackets is a Jacobian between the  $\gamma^*(q)P$  and  $\gamma^*(\hat{q})P$  frame for corresponding variables [525].

## 5.9 Outlook and Future Work

Phenomenology of TMDs have made a huge leap from partonic model approximations to high precision fits up to N<sup>3</sup>LO in the last decade. Universal QCD fits including data from SIDIS, DY,  $W^\pm/Z$  and  $pp$  scattering have been successfully performed.

Phenomenology of TMDs will evolve into global QCD analyses of data at high order perturbative precision and will utilize data from various processes and facilities. Machine learning and AI techniques have been already employed in these types of fits and will continue to be developed and utilized. The 3D structure of the nucleon encoded in TMDs is very intimately related to 1D structure encoded in collinear distributions including twist-3 distributions and in the coming years we will see merging of 1D and 3D phenomenology. We will see increasing impact from ab-initio calculations using lattice QCD on phenomenological studies of the nucleon structure, see Chapter 6. New precise experimental data will allow studies of other TMDs including subleading TMD functions, see Chapter 10. Other observables and measurements will become available that will allow the phenomenology to go beyond the 3D picture and utilize Wigner 5D distributions, see Chapter 11. Gluon and sea-quark structure of the nucleon as well as nuclear modifications to TMDs will be explored with the advent of new experimental measurements, see Chapter 8.

Experimental programs of future and existing experimental facilities such as the Electron Ion Collider [15, 336], Jefferson Lab 12 GeV Upgrade [337], RHIC [338] at BNL, COMPASS [339, 340] at CERN, BELLE II at KEK, BES III in Beijing, and the LHC at CERN will contribute immensely to our understanding of the hadron structure and progress of phenomenology in general and 3D structure in particular.

# 6 - Lattice QCD calculations of TMDs and related aspects of hadron structure

## 6.1 Lattice QCD

As discussed in Chapter 1, many aspects of hadron structure can not be addressed using perturbative QCD. In Chapter 5 experimental data is used to determine the non-perturbative contributions to the TMD PDFs and FFs. However, aspects of hadron structure can also be calculated from the underlying theory of QCD using lattice field theory techniques, referred to as lattice QCD (LQCD). There are many excellent introductions to LQCD, see for example Refs. [527, 528], to which the reader is referred for full details. In this brief overview, we present relevant aspects of LQCD as they impact the discussion of TMD and hadron structure studies.

LQCD was introduced by Wilson in Ref. [1], and in this approach, physical information is extracted from QCD correlation functions that are evaluated from their functional integral representation. At an intermediate stage, a Euclidean spacetime lattice is used to regulate the theory, rendering the functional integral finite-dimensional. The theory is formulated on a discrete, spacetime geometry which in almost all cases is taken to be a regular four-dimensional hypercubic lattice,  $\Lambda_4 = \{n_\mu = (n_1, n_2, n_3, n_4) | n_i \in a[0, 1, \dots, L_i - 1]\}$  where  $a$  is the lattice spacing and  $L_i$  is the lattice extent in the  $i$  direction. Periodic spatial boundary conditions are typically imposed on all fields, and periodic temporal boundary conditions on the gauge fields and anti-periodic temporal boundary conditions for fermions are used. In some cases an anisotropy is introduced, providing a finer discretization in the temporal direction; furthermore, other geometries have been considered in the past [529] but are not in current use. Noting that the exponential of the discretized QCD action is a Boltzmann probability distribution, importance sampling Monte-Carlo methods are then used to stochastically evaluate the requisite integrals. Physics is recovered in the limit that the lattice regulator is removed (the *continuum limit*) and the spacetime volume is taken to infinity (the *infinite volume limit*).

The QCD action must be implemented approximately on the lattice geometry, with derivatives replaced by finite differences. For the gauge fields, the simplest action is the Wilson action

$$S_{\text{gauge}} = \frac{2}{g^2} \sum_{x \in \Lambda_4} \sum_{\mu < \nu} (1 - \text{Re Tr}[P_{\mu\nu}(x)]), \quad (6.1)$$

where  $P_{\mu\nu}(x)$  defines the elementary plaquette which corresponds to products of gauge link variables  $U_\mu(x)$  around a  $1 \times 1$  elementary cell,

$$P_{\mu\nu}(x) = U_\mu(x) U_\nu(x + \hat{\mu}) U_\mu^\dagger(x + \hat{\nu}) U_\nu^\dagger(x).$$

Here, the link variables  $U_\mu(x) = \exp[iaA_\mu(x)]$  are associated with the site  $x$  and extend one lattice spacing to the site  $x + \hat{\mu}$ , where  $\hat{\mu}$  is a unit vector in the  $\mu$  direction. Expanding the LQCD action around the limit  $a \rightarrow 0$  reproduces the continuum QCD action up to  $O(a^2)$  effects. Variants of the action introduce additional terms that can cancel higher powers of  $a$ , providing a closer-to-continuum action [528].

Naive implementations of lattice fermions have multiple zero-modes for massless fermions, corresponding to “doubling” of the light degrees of freedom. These are avoided with the Wilson [1], the Kogut-Susskind [530] and twisted-mass [531] quark actions, but at the expense of explicitly breaking the chiral symmetry of the massless QCD action. Chirally-symmetric fermion formulations such as the domain-wall fermion (DWF) action [532], which avoid this issue by introducing an additional spacetime dimension, and the overlap action [533], maintain a lattice chiral symmetry. As with gauge actions, the fermion actions can also be improved to reduce lattice artifacts; in this case, there is a unique dimension-five operator to add to the action [534],  $i\bar{\psi}\sigma_{\mu\nu}G^{\mu\nu}\psi$ , known as the clover term. Since the (lattice) QCD action is bilinear in the fermion fields,  $S_{\text{fermion}} \sim \int dx \bar{\psi} \mathcal{M} \psi$  where  $\mathcal{M}$  depends on the choice of action and on the gauge field. For the given action encoded in  $\mathcal{M}$ , this results in an effective action  $S_{\text{fermion}} = \text{Tr Ln}[\mathcal{M}]$ .

Given a particular lattice action, LQCD calculations proceed by evaluating the QCD path integrals defining appropriate correlation functions using importance sampling Monte Carlo based on that action. For a generic multi-local operator  $\mathcal{O}(x_1, x_2, \dots)$  built from quark and gluon fields,

$$\langle \mathcal{O}(x_1, x_2, \dots) \rangle = \frac{1}{\mathcal{Z}} \int \mathcal{D}U \tilde{\mathcal{O}}(x_1, x_2, \dots) \det[\mathcal{M}[U]] e^{-S_{\text{gauge}}}, \quad (6.2)$$

where the partition function  $\mathcal{Z} = \int \mathcal{D}U \det[\mathcal{M}[U]] e^{-S_{\text{gauge}}}$ . The field operator  $\tilde{\mathcal{O}}(x_1, x_2, \dots)$  corresponds to the original operator  $\mathcal{O}$  after fermions are integrated out; this integration results in the “contraction” of fermion–anti-fermion pairs in all possible ways, replacing them with quark propagators  $S[U] = \mathcal{M}[U]^{-1}$ . By sampling the gauge fields according to the probability distribution  $\mathcal{P}[U] = \mathcal{Z}^{-1} \det[\mathcal{M}[U]] e^{-S_{\text{gauge}}}$ , this can be approximated as

$$\langle \mathcal{O}(x_1, x_2, \dots) \rangle = \frac{1}{N} \sum_{c=1}^N \tilde{\mathcal{O}}(x_1, x_2, \dots)[U_i] + O\left(1/\sqrt{N}\right), \quad (6.3)$$

where  $\{U_1, \dots, U_N\}$  correspond to a properly sampled set (ensemble) of gauge fields. These requisite configurations are produced with the correct distribution through a Markov chain Monte Carlo process, with the standard algorithm being hybrid Monte Carlo [535]. Before the year 2000, many studies were performed in the quenched version of QCD in which the quark determinant was neglected for computational expediency. This approximation is not typical in modern calculations, although the freedom of using a different quark mass in the quark determinant (referred to as sea quarks in the LQCD context) and the quark propagators (valence quarks in the LQCD context) is sometimes used and referred to as partial quenching.

To undertake a LQCD calculation, the quark masses and the gauge couplings to be used must be specified (along with the values of the coefficients of irrelevant operators used to improve the action) in some way, typically by matching computations of simple quantities such as the pion and kaon masses to their experimental values. Once this is done, other quantities that are computed are predictions of the theory. Having performed a set of simulations at different values of the bare parameters, the continuum and infinite volume limits must be taken before physical results are obtained. In addition to the statistical uncertainties of the simulations, the uncertainties implicit in taking these limits must be carefully investigated

and accounted for. As discussed above, typical LQCD actions differ from the continuum QCD action by terms of  $\mathcal{O}(a)$  or in some cases  $\mathcal{O}(a^2)$ , while for many properties of individual hadrons volume effects are controlled by terms  $\mathcal{O}(e^{-m_\pi L})$  where  $L$  is the smallest dimension of the lattice geometry and  $m_\pi$  is the mass of the lightest hadron. With few exceptions, LQCD calculations are performed ignoring the up and down quark mass splitting and do not include the effects of electromagnetism, as these contributions are small effects in most cases. Precision calculations must account for these additional systematic effects and do so in relevant contexts [536].

An important application of LQCD that is centrally relevant to this review is computing the matrix elements of currents in hadronic states such as the proton. In the continuum, the currents one might consider are operators such as the axial current  $\bar{\psi} \gamma_\mu \gamma_5 \psi$ , twist-two operators  $i^{n-1} \bar{\psi} \gamma_{\{\mu_1} D_{\mu_2} \dots D_{\mu_n\}} \psi$  (where the braces denote symmetrization and trace-subtraction of the enclosed indices), or four-quark operators  $\bar{\psi} \Gamma \psi \bar{\psi} \tilde{\Gamma} \psi$  (where  $\Gamma$  and  $\tilde{\Gamma}$  are Dirac and flavor structures) that typically arise from integrating out physics far above the hadronic scale. As will be discussed below, matrix elements of more complicated nonlocal operators are now also commonly studied. In a discretized lattice theory, these operators must be implemented using the lattice degrees of freedom and differ from the continuum operators by terms  $\mathcal{O}(a)$  (as with the action, improved lattice operators can be constructed that eliminate lattice artifacts to a particular order). Since the operators used in lattice calculations are necessarily formulated in terms of the discretized variables, an additional step that must be undertaken to connect to physics in the continuum limit is renormalization of the operators. Even for operators that are scale-independent, such as the isovector axial charge, a finite renormalization is required. This renormalization can be implemented using lattice perturbation theory (see Ref. [537] for an overview) for the appropriate lattice action. Alternatively, non-perturbative renormalization based on momentum subtraction schemes [538] can also be used and are subject to smaller uncertainties. In such schemes, renormalization constants are fixed by demanding quark and/or gluon two and three point correlation functions take their tree-level values at a particular kinematic point. Ultimately, continuum perturbation theory is then used to convert to standard perturbative schemes such as  $\overline{\text{MS}}$ . This non-perturbative approach is now standard for local operators and the effects of mixing between operators with the same quantum numbers, such as isoscalar quark operators and corresponding gluon operators, can be incorporated (the more intricate problem of renormalization of nonlocal operators is discussed below).

To define the notation used below and further introduce LQCD methods, it is useful to overview the calculation of the proton mass. In particular, the proton mass can be determined from the calculations of the two-point correlation function, which can be expressed (assuming an infinite temporal extent of the lattice geometry for simplicity and making use of translational invariance) as

$$C_{\alpha\beta}(t, \mathbf{p}) = a^3 \sum_{\mathbf{x}} e^{-i\mathbf{p}\cdot\mathbf{x}} C_{\alpha\beta}(t, \mathbf{x}) = a^3 \sum_{\mathbf{x}} e^{-i\mathbf{p}\cdot\mathbf{x}} \langle 0 | \chi_\alpha(\mathbf{x}, t) \bar{\chi}_\beta(\mathbf{0}, 0) | 0 \rangle, \quad (6.4)$$

where

$$\chi_\alpha(\mathbf{x}, t) = \epsilon^{ijk} u_\alpha^i(\mathbf{x}, t) u_\gamma^j(\mathbf{x}, t) [C^{-1} \gamma_5]_{\gamma\delta} d_\delta^k(\mathbf{x}, t) \quad (6.5)$$

is an interpolating operator with the quantum numbers of the proton and  $C = \gamma_0 \gamma_2$  is the

charge conjugation matrix ( $C\gamma_0^T C^{-1} = -\gamma_0$ ). In the above expressions, greek indices refer to the Dirac structure while roman indices label color components.

After integrating out the quark fields in the path integral formulation, this correlator is expressed in terms of products of the inverse of the Dirac operator

$$\begin{aligned} C_{\alpha\beta}(t, \mathbf{p}) &= -a^3 \sum_{\mathbf{x}} e^{-i\mathbf{p}\cdot\mathbf{x}} \epsilon^{ijk} \epsilon^{i'j'k'} [C^{-1}\gamma_5]_{\alpha'\alpha''} [\gamma_5 C]_{\beta'\beta''} \\ &\times \left\langle \left[ \mathcal{M}_d^{-1} \right]_{\alpha''\beta'}^{ki'} \left\{ \left[ \mathcal{M}_u^{-1} \right]_{\alpha'\beta''}^{jj'} \left[ \mathcal{M}_u^{-1} \right]_{\alpha\beta}^{ik'} - \left[ \mathcal{M}_u^{-1} \right]_{\alpha\beta''}^{ij'} \left[ \mathcal{M}_u^{-1} \right]_{\alpha'\beta}^{jk'} \right\} \right\rangle, \end{aligned} \quad (6.6)$$

where the quark propagator  $\mathcal{M}_f^{-1} = \mathcal{M}_f^{-1}(x, 0)$  is the inverse of the Dirac operator for flavor  $f$ . This correlation function can be evaluated as an average over representative gluon field configurations as discussed above.

Inserting a complete set of states<sup>22</sup> between the interpolating operators in Eq. (6.4), it is straightforward to see that the two-point correlator has time dependence governed by the energies of states with the quantum numbers of the proton and with three-momentum  $\mathbf{p}$ :

$$C_{\alpha\beta}(t, \mathbf{p}) = a^3 \sum_{n,\sigma} \frac{e^{-E_n(\mathbf{p})t}}{2E_n(\mathbf{p})} \langle 0 | \chi_\alpha | n; \mathbf{p}, \sigma \rangle_c \langle n; \mathbf{p}, \sigma | \bar{\chi}_\beta | 0 \rangle \quad (6.7)$$

$$= a^3 Z(\mathbf{p}) \sum_{\sigma} u_{\alpha}(n=0, \mathbf{p}, \sigma) \bar{u}_{\beta}(n=0, \mathbf{p}, \sigma) \frac{e^{-E_n(\mathbf{p})t}}{2E_n(\mathbf{p})} + \dots \quad (6.8)$$

where  $Z(\mathbf{p})$  is an overlap factor<sup>23</sup> and higher excited states are ignored. Tracing this correlator against a given Dirac structure, often chosen to be  $\Gamma^+ = \frac{1}{2}(1 + \gamma_4)$ , leads to<sup>24</sup>

$$C_{\Gamma^+}(t, \mathbf{p}) = \Gamma_{\beta\alpha}^+ C_{\alpha\beta}(t, \mathbf{p}) \xrightarrow{t \rightarrow \infty} C e^{-E_n(\mathbf{p})t}, \quad (6.9)$$

where  $C$  is a time-independent constant. Given the discrete time series  $C_{\Gamma}(t, \mathbf{p})$  from the Monte Carlo sampling, the proton mass dispersion relation can be extracted from fits to the time dependence of Eq. (6.9), either in the asymptotic region where the lowest energy state dominates, or from more general time ranges where excited states must also be accounted for.

## 6.2 Lattice Hadron Structure

### 6.2.1 Static structure of hadrons

While the focus of this handbook is on transverse momentum dependent hadron structure, we begin by discussing lattice calculations of hadron structure in a more general context. Since its early days, LQCD has been used as a tool with which to investigate the structure of the proton

<sup>22</sup>Continuum infinite volume states are normalized as  ${}_c\langle n, \mathbf{p}, \sigma | n, \mathbf{p}, \sigma \rangle_c = 2E(\mathbf{p})\delta^3(p-p')$ , with the lattice states defined from these as  $|n, \mathbf{p}, \sigma\rangle = \sqrt{2V_3 E_n(\mathbf{p})}|n, \mathbf{p}, \sigma\rangle_c$  where  $V_3$  is the spatial volume and  $n$  labels excitations.

<sup>23</sup>Defining spinors such that  $\bar{u}(n, \mathbf{p}, \sigma)u(n, \mathbf{p}, \sigma') = 2M_n\delta_{\sigma\sigma'}$ , the overlap matrix elements are given by  $\langle 0 | \chi_{\alpha} | n; \mathbf{p}, \sigma \rangle_c = \sqrt{Z(\mathbf{p})}u_{\alpha}(n, \mathbf{p}, \sigma)e^{i\mathbf{p}\cdot\mathbf{x}}$ .

<sup>24</sup>Here, Euclidean  $\gamma$ -matrices  $\gamma_i^E = -i\gamma_i^M$  for  $i \in \{1, 2, 3\}$  and  $\gamma_4 = \gamma_0^M$ , written in terms of Minkowski space matrices, are used and satisfy  $\{\gamma_{\mu}^E, \gamma_{\nu}^E\} = 2\delta_{\mu\nu}I$ .

and other hadrons. Early works focused on static properties such as the magnetic moment [539] and axial charge [540], but methods with which to study more complex quantities such as the electromagnetic form factors were initially developed in the 1980s [541–543]. By now, form factors of the vector and axial currents have been studied quite precisely, and state-of-the-art calculations make use of the physical values of the quark masses and include multiple lattice spacings and volumes in the calculations [544]. Recent calculations [545] are also providing important insights into understanding weak current interactions of nucleons that are relevant in long-baseline neutrino experiments.

The collinear PDFs are another key pillar of hadron structure. As discussed above, these are extracted from global fits to experimental data and are known with remarkable precision for the unpolarized and helicity PDFs, but are less well constrained in the case of the transversity distributions. As an independent theory approach, LQCD has the potential to provide complimentary information to experimental measurements and even has the potential to improve constraints on global fits [546]. For partonic structure, the Euclidean metric of LQCD imposes a challenge for direct evaluation of lightlike separated operators. To evade this issue, LQCD studies have i) made use of the operator product expansion (OPE), or more recently ii) considered off-lightcone quantities that can be connected to lightcone physics perturbatively as will be discussed in detail in Sec. 6.3.

The traditional LQCD approach based on the OPE expands nonlocal operators (such as the current-current correlator relevant in DIS) in terms of an infinite sum of local operators

$$J_\mu(x) J_\nu(0) = \sum_{i,n} C_{i,n}(x, \mu) x_{\rho_1} \dots x_{\rho_n} O_i^{\mu\nu\rho_1\dots\rho_n}(\mu), \quad (6.10)$$

where  $C_{i,n}(x, \mu)$  are Wilson coefficients and  $O_i(\mu)$  are local operators involving quark and gluon fields and covariant derivatives. Hadronic matrix elements of the local operators on the right-hand side are calculable in Euclidean space, and their analytic continuation back to Minkowski space is straightforward. While the Wilson coefficients and the operator matrix elements separately depend on the renormalization scale  $\mu$ , their product does not. Based on their relevance in high-energy processes such as DIS, the tower of operators is usually expressed in terms of operators of fixed twist (mass dimension minus spin), with the leading twist (twist-two) operators dominating. In particular, the Mellin moments of the leading-twist collinear quark PDFs are given by matrix elements of local gauge-covariant twist-two operators,

$$\langle x^n \rangle_{i/H} \equiv \int_{-1}^1 dx x^n f_{i/H}(x) \iff \langle H | O_{i,n}(0) | H \rangle = \langle x^n \rangle_{i/H} (p_H \cdot n)^{n+1}, \quad (6.11)$$

where  $H$  labels a hadron state of momentum  $p_H$ , and the leading twist operators

$$O_{i,n}(x) = n^{\mu_0} n^{\mu_1} \dots n^{\mu_n} \bar{\psi}_i \gamma_{\{\mu_0} i \overleftrightarrow{D}_{\mu_1} \dots i \overleftrightarrow{D}_{\mu_n\}} \psi_i \quad (6.12)$$

as in Eq. (2.154). Here,  $n_\mu$  is a light-like vector such that  $n^2 = 0$ ,  $\overleftrightarrow{D}_\mu = (\overrightarrow{\partial}_\mu - \overleftarrow{\partial}_\mu)/2 + igA_\mu$ , and  $\{\dots\}$  indicates symmetrization and trace subtraction of the included Lorentz indices (note that the contraction with the  $n$  vectors implies this). Similarly, local twist-2 gluonic operators define

moments of gluon PDFs and the off-forward matrix elements of the same sets of operators define the generalized form factors that describe the Mellin moments of generalized parton distributions (GPDs) [551, 1281, 1282, 1286? ? ? ?, 1287].

Following the pioneering approach of Refs. [541, 547], matrix elements of these operators can be determined from three-point correlation functions (suppressing operator indices)

$$C_{\alpha\beta}^O(t, \tau, \mathbf{p}, \mathbf{q}) = a^6 \sum_{\mathbf{x}} \sum_{\mathbf{y}} e^{-i\mathbf{p}\cdot\mathbf{x}} e^{-i\mathbf{q}\cdot\mathbf{y}} \langle 0 | \chi_\alpha(\mathbf{x}, t) O(\mathbf{y}, \tau) \bar{\chi}_\beta(\mathbf{0}, 0) | 0 \rangle. \quad (6.13)$$

By inserting complete sets of energy eigenstates, this quantity can be expressed in terms of the desired hadronic matrix elements, eigenenergies and overlap factors that can be determined from corresponding two-point functions (Eq. (6.4)). Fits to the time dependencies of Eqs. (6.4) and (6.13) allow the matrix elements to be extracted.

In the context of Eq. (6.11), the LQCD approach is limited to operators of low Lorentz spin because the lattice geometry is invariant under only hypercubic symmetry transformations, elements of  $H(4)$ , rather than under those of  $O(4)$  symmetry [25, 541, 547, 548]. Consequently, the operators  $O_{i,n}(\mu)$  for  $n > 3$  mix with lower dimensional operators in the same  $H(4)$  irreducible representation with coefficients that diverge with inverse powers of the lattice spacing as the continuum limit is approached. In order to relate the matrix elements  $\langle p | O_{i,n}(\mu) | p \rangle$  to the moments of PDFs, the power divergences must be removed which is a significant challenge for  $n > 3$  operators [549]. A method to improve this approach through an approximate restoration of the full symmetry has been proposed in Ref. [550]. Additionally, matrix elements of twist-two operators are statistically more difficult to determine as the number of Lorentz indices, and therefore derivatives, increases. Recent calculations are reviewed in Refs. [536, 546].

### 6.2.2 Decomposition of the proton momentum and spin

The low moments of PDFs that are accessible in LQCD calculations are already useful to understand various aspects of hadron structure. In particular the  $n = 1$  moments correspond to matrix elements of the energy momentum tensor (EMT) and provide insight into the decomposition of the momentum and spin of the proton into its constituent contributions. Understanding these decompositions is a central question in nuclear physics and a major goal for the EIC [513]. As shown in Ref. [551], the matrix elements of the quark and gluon contributions to the EMT in the Belinfante form

$$\mathcal{T}_q^{\mu\nu} = \frac{i}{4} \sum_f \bar{\psi}_f \gamma^{\{\mu} \overset{\leftrightarrow}{D}^{\nu\}} \psi_f = \frac{i}{4} \sum_f \bar{\psi}_f (\overset{\rightarrow}{D}^\mu \gamma^\nu + \overset{\rightarrow}{D}^\nu \gamma^\mu - \overset{\leftarrow}{D}^\mu \gamma^\nu - \overset{\leftarrow}{D}^\nu \gamma^\mu) \psi_f \quad (6.14)$$

$$\mathcal{T}_g^{\mu\nu} = -G^{\mu\alpha} G_\alpha^\nu + \frac{1}{4} g^{\mu\nu} G^{\alpha\beta} G_{\alpha\beta}, \quad (6.15)$$

between nucleon states can be written in terms of gravitational form factors as

$$\begin{aligned} \langle p(P', S') | \mathcal{T}_{q,g}^{\mu\nu} | p(P, S) \rangle &= \bar{u}(P', S') [T_{1,q,g}(q^2) \gamma^{\{\mu} \bar{P}^{\nu\}} + \frac{i}{2m} T_{2,q,g}(q^2) \bar{P}^{\{\mu} \sigma^{\nu\}\alpha} q_\alpha \\ &+ D_{q,g}(q^2) \frac{q^\mu q^\nu - g^{\mu\nu} q^2}{m} + \bar{C}_{q,g}(q^2) g^{\mu\nu} m] u(P, S), \end{aligned} \quad (6.16)$$

where  $P$  and  $P'$  are the initial and final momenta of the nucleon, respectively, and  $\bar{P} = \frac{1}{2}(P' + P)$ . The sum of  $\bar{C}_q$  and  $\bar{C}_g$  is zero, but not so individually. The momentum transfer to the nucleon is  $q = P' - P$ .<sup>25</sup> In the  $q^2 \rightarrow 0$  limit, one obtains

$$\langle x \rangle_{q,g} = T_{1_{q,g}}(0), \quad (6.17)$$

$$J_{q,g} = \frac{1}{2} [T_{1_{q,g}}(0) + T_{2_{q,g}}(0)]. \quad (6.18)$$

where  $\langle x \rangle_{q,g}$ , the second moment of unpolarized PDF, is the momentum fraction carried by the quarks or gluons inside a nucleon. The other form factor,  $T_{2_{q,g}}(0)$ , can be interpreted as anomalous gravitomagnetic moment for quarks and gluons in an analogy to the anomalous magnetic moment [552]. The combination in Eq. (6.18) is the total angular momentum  $J_{q,g}$  carried by the quarks or gluons.

There are two widely-used formulations of the decomposition of the total angular momentum of the proton.

- The Jaffe and Manohar (JM) decomposition [553] is

$$J = J_q + J_g = \frac{1}{2}\Delta\Sigma + L_q^{JM} + \Delta G + L_g, \quad (6.19)$$

where  $\frac{1}{2}\Delta\Sigma$  and  $\Delta G$  are the quark and gluon spin contributions, and  $L_q^{JM}$  and  $L_g$  are the quark and gluon orbital angular momentum (OAM) contributions. In this case, the energy momentum tensor is defined in the canonical form, not the Belinfante form in Eq. (6.14). This form is derived in the infinite momentum frame in light-cone gauge where  $A^+ = 0$ . Furthermore, while  $\Delta G$  can be extracted from high energy experiments, it can not be obtained from a matrix element based on a local operator, rather only as a nonlocal lightcone-separated correlation. The OAM contributions can be determined from GTMDs [554–556] and a corresponding lattice calculation is discussed in Sec. 11.5, cf. also Refs. [556, 557].

- The Ji decomposition [551] is

$$J = \frac{1}{2}\Delta\Sigma + L_q^{Ji} + J_g, \quad (6.20)$$

where  $\frac{1}{2}\Delta\Sigma$  is the same quark spin as in Eq. (6.19),  $L_q^{Ji}$  is the quark OAM which can be obtained from subtracting the quark spin from the quark angular momentum  $J_q$  in Eq. (6.18), and  $J_g$  is the total gluon angular momentum contribution. Both  $J_q$  and  $J_g$  can be obtained from the gravitational form factors in Eq. (6.18) with the Belinfante energy-momentum tensor in Eq. (6.14). Each term in Eq. (6.20) is gauge invariant and defined covariantly by a local operator. The quark OAM can also be calculated as a GTMD observable, which is discussed in Secs. 11.4 and 11.5, cf. also Refs. [556, 557]; the GTMD approach allows for a continuous, gauge-invariant interpolation between the Jaffe-Manohar and Ji definitions of OAM.

---

<sup>25</sup>The nucleon spinor,  $u(P, S)$ , satisfies the following normalization conditions  $\bar{u}(P, S) u(P, S) = 2m$ ,  $\sum_S u(P, S) \bar{u}(P, S) = \not{P} + m$ .

Except for the quark spin, these two decompositions have different operators for the quark and gluon angular momenta. This has lead the community to explore their physical meanings, possible relations among them, and respective realizations in experiments for many years. See Refs. [558, 559] for an overview and Ref. [560] for a recent review.

The so-called “proton spin crisis” arose from the experimental observation in DIS experiments [561] that the quark spin  $\Delta\Sigma$ , defined through

$$\langle p(P, S) | A_i^0 | p(P, S) \rangle = S_i \Delta\Sigma, \quad (6.21)$$

where  $A_i^0$  is the flavor-singlet axial-vector current  $A_i^0 = \sum_{f=u,d,s} \bar{\psi}_f \gamma_i \gamma_5 \psi_f$  contributes only  $\sim 30 - 40\%$  to the total proton spin [562]. This result is at odds with expectation of the quark model where the proton spin is saturated by the sum of the quark spins.

Several LQCD calculations of the forward flavor-singlet axial-vector current matrix element in Eq. (6.21) have been carried out. Because of the flavor-singlet nature, these calculations necessarily involve the disconnected insertion of the current in nucleon three-point functions which is numerically challenging and is usually undertaken using a stochastic noise estimator such as in Ref. [563]. For a recent compilation and evaluation of lattice calculations of  $\Delta\Sigma$  and the individual flavor contributions  $\Delta u$ ,  $\Delta d$  and  $\Delta s$ , see Refs. [536, 546]. It is found that the disconnected insertion contributions are negative which makes the total  $g_A^0$  to be  $\sim 0.3 - 0.4$ .

Analyses [564, 565] of the high-statistics 2009 STAR [566] and PHENIX [567] experiments at RHIC showed evidence of non-zero gluon helicity distribution,  $\Delta g(x, Q^2)$ , in the proton. For  $Q^2 = 10 \text{ GeV}^2$ , the gluon helicity distribution was found to be positive over the region  $0.05 \leq x \leq 0.2$ . However, outside this region the results have very large uncertainties that preclude definitive conclusions on  $\Delta G = \int_0^1 dx \Delta g(x, Q^2)$ .

The gap between the light-front formulation of  $\Delta G$  and the Euclidean metric of lattice calculations has prevented direct calculation. However, it has been shown in Ref. [568] that the matrix elements of appropriate equal-time local operator, when boosted to the infinite momentum frame, are the same as those of the gauge-invariant but nonlocal operator on the light-cone that defines  $\Delta G$ . However, it is found [569] that the infinite boost ( $P_z \rightarrow \infty$ ) and infinite loop momentum ( $k_\mu \rightarrow \infty$ ) limit in the renormalization of the operator do not commute. Since lattice calculation can only be carried out at finite nucleon momentum  $P_z$ , the large momentum effective field theory (LaMET) [29, 568, 570] is formulated to match the finite  $P_z$  matrix elements to those at the infinite momentum frame perturbatively. In particular, a lattice calculation of large momentum matrix elements of the local operator  $\vec{S}_G = \int d^3x \text{Tr}(\vec{E} \times \vec{A}_{\text{phys}})$  is needed, where  $\vec{A}_{\text{phys}}$  satisfies the non-Abelian transverse condition  $\mathcal{D}^i A_{\text{phys}}^i = 0$  [571]. Noting that  $A_{\text{phys}}^i$  is related to  $A_c^i$  in the Coulomb gauge via a gauge transformation [555], matrix elements of the gluon spin operator

$$\vec{S}_G = \int d^3x \text{Tr}(\vec{E} \times \vec{A}_{\text{phys}}) = \int d^3x \text{Tr}(\vec{E}_c \times \vec{A}_c) \quad (6.22)$$

can be calculated with both  $\vec{E}$  and  $\vec{A}$  in the Coulomb gauge. A first lattice calculation in Ref. [572], when extrapolated to the infinite momentum limit, determined  $\Delta G = 0.251(47)(16)$ , which suggests that the gluon spin contributes about half of the proton spin. However in this calculation, the finite piece in the one-loop LaMET matching coefficient is very large, which

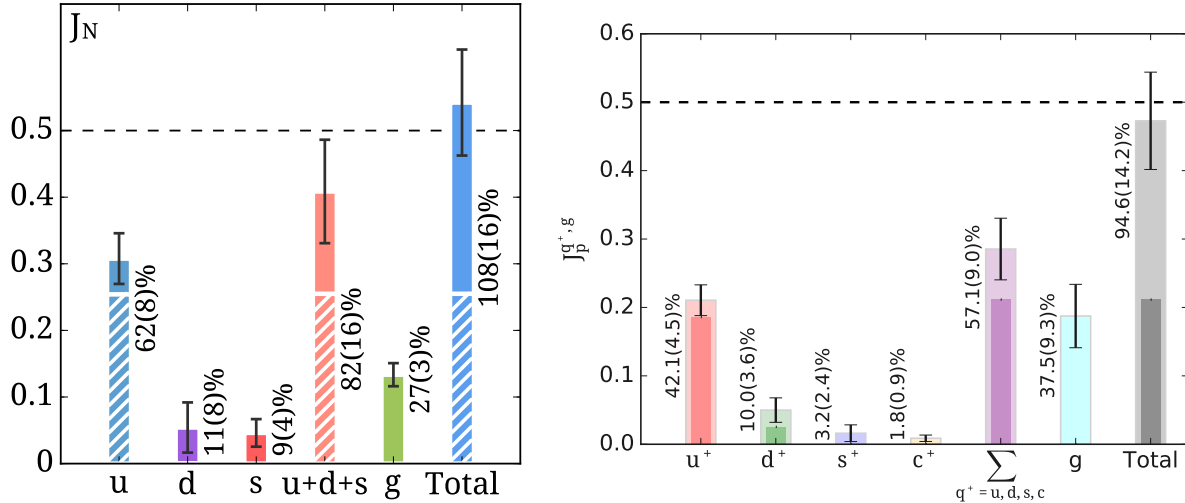


Figure 6.1: Proton spin decomposition in terms of the angular momentum  $J_q$  for the  $u, d$  and  $s$  quarks and the gluon angular momentum  $J_g$  in Ji's decomposition. Left panel is for  $n_f = 2$  calculation [577] and right panel is for  $n_f = 2 + 1 + 1$  calculation. Plot taken from Ref. [578].

indicates a convergence problem for the perturbative series even after resummation of large logarithms and further investigation is required.

An alternative way to determine  $\Delta G$  is to calculate the polarized gluon distribution function  $\Delta g(x, Q^2)$  through the quasi-PDF approach that is discussed below and then integrate to obtain  $\Delta G$ .

Besides the quark and glue spins, there are quark and gluon orbital angular momenta (OAM) as part of the proton spin. The OAM can be extracted experimentally from GPDs and GTMDs [559]. Ji's quark OAM  $L_q^{ji}$  can be obtained from the form factors of the energy-momentum tensor (EMT) by subtracting the spin from  $J_q^{ji}$  in Eq. (6.18) [573–575], and the calculation of Jaffe-Manohar's  $L_q^{JM}$  and  $L_g$  on the lattice from GTMDs has been formulated in Refs. [555, 556]. More details on OAM and lattice calculations of TMD and GTMD observables are discussed in Secs. 6.4 and 11.5.

When the normalized and renormalized quark angular momentum  $Z_{T,q} J_q^{\overline{MS}}$  is calculated, the quark OAM can be obtained by subtracting the quark spin from it. The non-perturbative renormalization of the EMT operator has been carried out in the context of proton mass decomposition [576] where the quark and gluon momentum fractions  $\langle x \rangle_q$  and  $\langle x \rangle_g$  are calculated. It would be essential to have lattice calculations of the momentum and angular momentum fractions of the quarks and gluons in the nucleon with both renormalization and normalization taken into account.

There have been lattice calculations to tackle Ji's proton spin decomposition in Eq. (6.20). The quark angular momenta  $J_q^{ji}$  for the  $u, d$  and  $s$  quarks and the gluon angular momentum  $J_g$  are plotted in the left panel of Fig. 6.1 for the  $n_f = 2$  case [577] and right panel for the  $n_f = 2 + 1 + 1$  case [578].

The momentum fractions  $\langle x \rangle$  for the quarks and gluons are plotted in the left panel of Fig. 6.2. The quark spins for the  $u, d, s$  flavors, the total quark spin  $\Delta \Sigma$ , the gluon angular

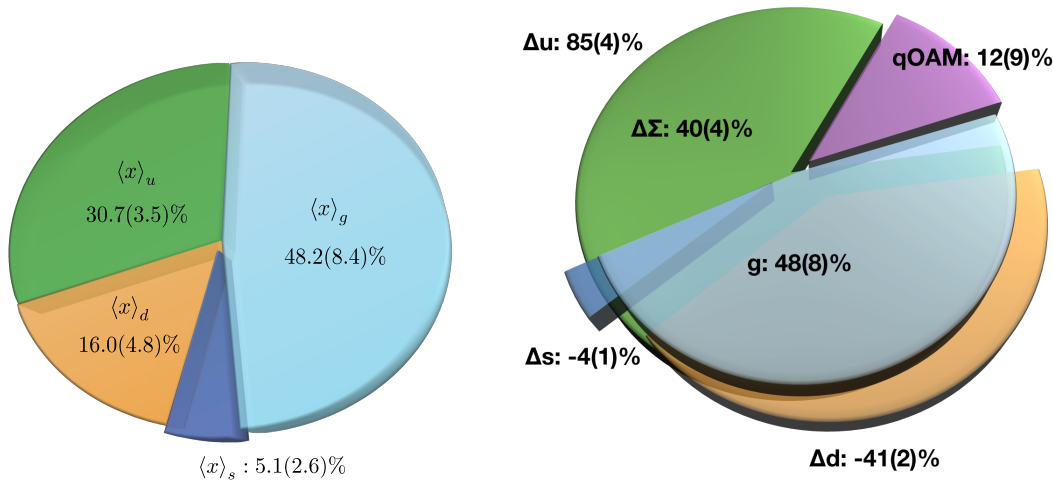


Figure 6.2: Left panel: The momentum fractions for the  $u, d, s$  quarks and the gluon at  $\mu = 2$  GeV from a lattice calculation of  $n_f = 2 + 1$  [576]. Right panel: The quark spins  $\Delta u, \Delta d, \Delta s$ , the total quark spin  $\Delta \Sigma$ , the gluon angular momentum  $J_g$ , and quark orbital angular momentum  $L_q^{ji}$  from the same  $n_f = 2 + 1$  configurations. Plot taken from Ref. [579].

momentum  $J_g$ , and the quark orbital angular momentum  $L_q^{ji}$  are plotted in the right panel. They are from lattice calculations with 2 + 1 flavors [576, 579]

### 6.3 Structure Functions and PDFs

There are several approaches to calculating the structure functions and PDFs on the lattice. Calculating the structure from the hadronic tensor [20–22, 25, 580, 581] or from the Compton amplitude [32, 582] require solving an inverse problem, either through a Laplace transform or from reconstruction of the moments. Over the past few years, several new approaches have been proposed to directly extract the  $x$ -dependence of PDFs on the lattice. In this section, these approaches are reviewed since methods to access TMDs and TMD related quantities are built upon them. When the PDFs are successfully calculated with these approaches, their moments can be cross-checked against those from the three-point functions as discussed in Sec. 6.2.

#### 6.3.1 Hadronic tensor

Since deep inelastic scattering measures the absorptive part of the Compton scattering, i.e. the hadronic tensor  $W_{\mu\nu}$ , it is the imaginary part of the forward amplitude –  $W_{\mu\nu} = \frac{1}{\pi} T_{\mu\nu}$  and can be expressed in terms of the current-current commutator in the nucleon,

$$W_{\mu\nu} = \frac{1}{4\pi} \int d^4x e^{iq\cdot x} \langle p(P, S) | [J_\mu(x), J_\nu(0)] | p(P, S) \rangle \quad (6.23)$$

Being an inclusive reaction, it includes all intermediate states

$$W_{\mu\nu}(q^2, \nu) = \frac{1}{4\pi} \sum_n \int \prod_{i=1}^n \left[ \frac{d^3 p_i}{(2\pi)^3 2E_{pi}} \right] \langle p(P, S) | J_\mu(0) | n \rangle \langle n | J_\nu(0) | p(P, S) \rangle (2\pi)^3 \delta^{(4)}(p_n - P - q). \quad (6.24)$$

It has been shown [20–22, 25, 32, 580, 581, 583] that the hadronic tensor  $W_{\mu\nu}(q^2, \nu)$  can be obtained from the Euclidean path-integral formalism which involves an inverse problem. In this case, one first defines an Euclidean hadronic tensor  $W_{\mu\nu}^E(\vec{q}, \tau)$  which involves a 3-momentum transfer and is defined from a ratio of a 4-point function to a 2-point function

$$\begin{aligned} W_{\mu\nu}^E(\vec{q}, \tau) &= \frac{E_p}{m_N} \frac{\text{Tr}(\Gamma^+ G_{pWp})}{\text{Tr}(\Gamma^+ G_{pp})} \Big|_{t_f - t_2, t_1 - t_0 \gg 1/\Delta E_p} \\ &= \frac{1}{2} \sum_S \left\langle p(P, S) \left| \sum_{\vec{x}} \frac{e^{-i\vec{q}\cdot\vec{x}}}{4\pi} J_\mu(\vec{x}, \tau) J_\nu(0, 0) \right| p(P, S) \right\rangle, \end{aligned} \quad (6.25)$$

where  $G_{pWp}$  is the 4-pt function for the current-current correlator in the nucleon and  $G_{pp}$  is the 2-pt function for the nucleon correlator.  $\Gamma^+$  is the projector for the positive parity nucleon state as before, and where  $t_0$  and  $t_f$  are the source and sink times of the nucleon interpolation field,  $t_1$  and the  $t_2$  are the current insertion time slices, and  $\tau = t_2 - t_1$ .  $\Delta E_p$  is the energy gap between the nucleon energy  $E_p$  and that of the first excited state with the same quantum numbers (i.e., the threshold of a nucleon and a pion in the  $p$ -wave). Inserting intermediate states,  $W_{\mu\nu}^E(\vec{q}, \tau)$  becomes

$$W_{\mu\nu}^E(\vec{q}^2, \tau) = \frac{1}{2} \sum_S \frac{1}{4\pi} \sum_n \left( \frac{m_N}{E_n} \right) \langle p(P, S) | J_\mu(0) | n \rangle \langle n | J_\nu(0) | p(P, S) \rangle \delta(\vec{p}_n - \vec{P} - \vec{q}) e^{-(E_n - E_p)\tau}. \quad (6.26)$$

This approach does not require the initial nucleon momentum  $\vec{P}$  to be large, and no renormalization is needed for the hadronic tensor constructed from conserved currents.

Formally, to recover the delta function  $\delta(E_n - E_p - \nu)$  in Eq. (2.65) in Minkowski space, one can consider the inverse Laplace transform with  $\tau$  being treated as a dimensionful continuous variable

$$W_{\mu\nu}(q^2, \nu) = \frac{1}{2m_N i} \int_{c-i\infty}^{c+i\infty} d\tau e^{\nu\tau} W_{\mu\nu}^E(\vec{q}, \tau), \quad (6.27)$$

with  $c > 0$ . However, there is no lattice data on the integration contour parallel to the imaginary  $\tau$  axis, this can not be done. Instead, one can consider solving it through an inverse problem with Laplace transform. The task is to “solve” the inverse problem in order to find the spectral density  $\rho(\omega)$  from its spectral representation in the Laplace integral

$$W_{\mu\nu}^E(\vec{q}, \tau) = \int e^{-\nu\tau} W_{\mu\nu}(q^2, \nu) d\nu. \quad (6.28)$$

Some favorite approaches to this inverse problem include the Maximum Entropy Method (MEM) [584, 585], the Bayesian Reconstruction (BR) [586] and the Backus-Gilbert Method (BG) [587]. All three approaches have been investigated in Ref. [588].

In order to study parton physics, another challenge of this approach is to access energy transfers such that the calculation can access the DIS region. To determine how large a  $\nu$  is needed for DIS, one can look at  $W$ , the total invariant mass of the hadronic state for the nucleon target at rest

$$W^2 = (q + p)^2 = m_p^2 - Q^2 + 2m_p\nu \quad (6.29)$$

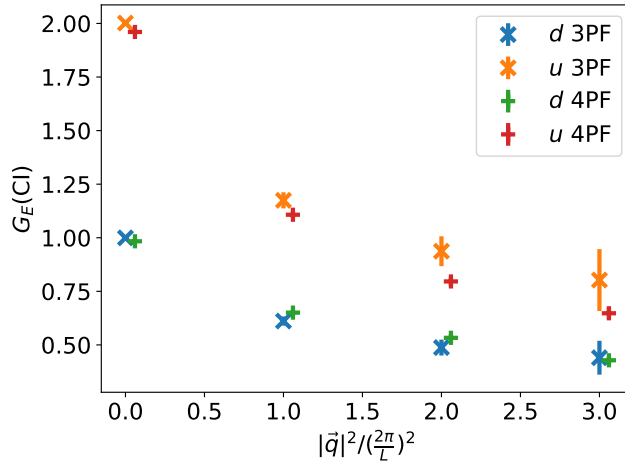


Figure 6.3: Comparison of the electric form factors (connected insertions only) calculated by using three-point functions and four-point functions for the lowest four momentum transfers (including zero) and for both  $u$  and  $d$  quarks. Plot taken from Ref. [588].

The global analyses of the high energy lepton-nucleon and Drell-Yan experiments to extract the parton distribution functions (PDFs) usually make a cut with  $W^2 > 10 \text{ GeV}^2$  to avoid the elastic and inelastic regions. Thus, to be qualified in the DIS region, the energy transfer  $v > 7 \text{ GeV}$  is needed for  $Q^2 = 4 \text{ GeV}^2$ . It is shown recently in a lattice calculation that small lattice spacing (e.g.  $a \leq 0.04 \text{ fm}$ ) is needed to reach such high energy excitations on the lattice [588]. Another aspect of the hadronic tensor is that it is valid in all the energy ranges (from elastic scattering to inelastic scattering and on to deep inelastic scattering). It can be employed to study the neutrino-nucleon scattering cross section at low energies, such as at neutrino energies relevant to the DUNE experiments.

For the elastic scattering, the structure function from the hadronic tensor, a 4-point function, is the sum of the products elastic nucleon form factors for the currents involved [588]. The elastic form factors can be calculated in the nucleon 3-pt functions. As a check of the lattice calculation, the structure function for the  $J_4 J_4$  correlator is calculated for the elastic scattering case which can be obtained from the ground state of  $W_{44}^E$  in Eqs. (6.26) and (6.28) with  $E_n - E_p = \sqrt{m_N^2 + |\vec{q}|^2}$  for  $\vec{P} = 0$ . This should correspond to the product to the electric form factor  $G_E(q^2)$ . Fig. 6.3 shows the lattice calculation of the electric form factors (connected insertions only) calculated by means of the 3-point functions for both  $u$  and  $d$  quarks and compared that those from the corresponding structure functions of the elastic scattering from the hadronic tensor. We see that they agree for the  $u$  and  $d$  quark within errors.

### Auxiliary heavy quark

Another method to access PDFs is via fermion bilinear currents which couple light quarks with a purely fictitious valence heavy quark [25, 589, 590], and have the form:

$$J_{\Psi,\psi}^\mu(x) = \bar{\Psi}(x)\Gamma^\mu\psi(x) + \bar{\psi}(x)\Gamma^\mu\Psi(x), \quad (6.30)$$

with  $\psi(x)$  ( $\Psi(x)$ ) the light (fictitious heavy) quark field, and a general Dirac structure  $\Gamma^\mu$ . This approach has the advantage that in the continuum limit it removes power divergent mixing with lower-dimensionality operators, which is unavoidable with standard techniques. Also, the presence of the heavy fictitious quark results in suppression of the long-range correlations between the currents and higher-twist contamination. One of the technical constraints of this method is the requirement of small lattice spacings (considerably smaller than 0.1 fm), so that heavy quark discretization effects are controllable.

In this approach, the Euclidean Compton tensor with heavy quark currents is written as

$$\begin{aligned} T_{\Psi,\psi}^{\mu\nu}(P, q) &\equiv \sum_S \langle p(P', S) | t_{\Psi,\psi}^{\mu\nu}(q) | p(P, S) \rangle \\ &= \sum_S \int d^4x e^{iq \cdot x} \langle p(P', S) | T \left[ J_{\Psi,\psi}^\mu(x) J_{\Psi,\psi}^\nu(0) \right] | p(P, S) \rangle, \end{aligned} \quad (6.31)$$

with certain constraints on the momenta so that the momentum transfer  $q$  is  $\simeq O(m_\Psi)$ , and  $(p_M + q_M)^2 < (m_\Psi + \Lambda_{\text{QCD}})^2$ , the latter in Minkowski space as indicated by the subscript  $M$ . With such constraints, analytic continuation of the hadronic tensor to Euclidean spacetime is achieved with  $q_4 \rightarrow iq_0$ . LQCD calculations of the tensor  $T_{\Psi,\psi}^{\mu\nu}$  can be extrapolated to the continuum and then related to moments of the PDFs via the OPE. The Wilson coefficients entering this OPE depend on the heavy quark mass and are presented in Ref. [590].

This approach has been recently studied in Ref. [591, 592] for the pion distribution amplitude (DA), using three quenched ensembles at different lattice spacings so that the continuum limit can be taken. The Euclidean hadronic tensor defined by

$$U_A^{[\mu\nu]}(q, p) = \int_{\tau_{\min}}^{\tau_{\max}} d\tau e^{iq_4\tau} R_3^{[\mu\nu]}(\tau, \vec{q}, \vec{p}), \quad (6.32)$$

where the quantity  $R_3^{\mu\nu}(\vec{p}, \vec{q}, \tau)$  is accessed by spatial Fourier transform of three-point functions of two heavy-light currents separated in spacetime with temporal separation of  $\tau$ . One can then obtain the moments of the DA by variation of  $q_4$ .

### OPE without OPE

An alternative method to access hadronic structure functions is proposed in Refs. [32, 582] and uses elements of earlier ideas [23, 547]. In such an approach one calculates the time-ordered product of two currents, which have a small enough spacetime separation for perturbation theory to be valid, but at the same time large enough to suppress discretization effects.

In this method one utilizes the forward Compton amplitude,  $T_{\mu\nu}$ , which can be decomposed into the structure functions  $F_1$  and  $F_2$ . For example, the  $\mu = \nu = 3$  component of the

$$T_{33}(p, q) = \sum_{n=2,4,\dots}^{\infty} 4\omega^n \int_0^1 dx x^{n-1} F_1(x, q^2) = 4\omega \int_0^1 dx \frac{\omega x}{1 - (\omega x)^2} F_1(x, q^2), \quad (6.33)$$

where  $\omega = 2p \cdot q / q^2$ . This can be used to extract the moments of  $F_1(x, q^2)$ . By construction, the computation of  $T_{33}$  requires four-point functions, which makes the calculation computationally

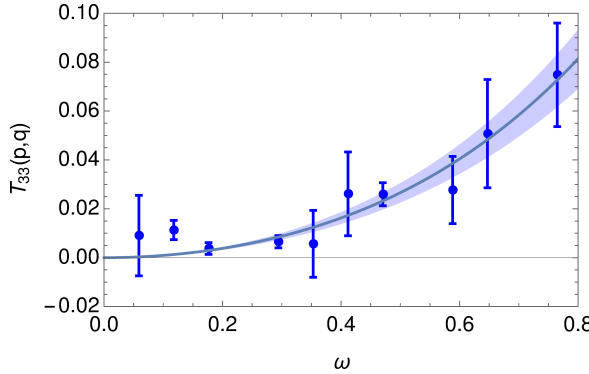


Figure 6.4: Compton amplitude obtained from the lattice computation of Ref. [32] (blue points), fitted to a sixth order polynomial (solid line). Plot taken from Ref. [32].

very demanding. To avoid such difficulties, the Feynman-Hellmann method [593] is utilized in Ref. [32], which adds a term  $\lambda \mathcal{J}_{3f}(x; q)$  in the QCD Lagrangian, where  $\lambda$  is a parameter which is treated perturbatively, and  $\mathcal{J}_{3f}(x; q) = Z_V \cos(\vec{q} \cdot \vec{x}) e_f \bar{\psi}_f(x) \gamma_3 \psi_f(x)$ . Taking the derivative of the nucleon energy with respect to  $\lambda$  gives  $T_{33}$  as shown in Ref. [32]:

$$T_{33}(p, q) = -2E_\lambda(p, q) \frac{\partial^2}{\partial \lambda^2} E_\lambda(p, q) |_{\lambda=0}. \quad (6.34)$$

Note that the addition of the extra term in the Lagrangian requires dedicated simulations for each value of  $\lambda$ , with multiple values needed in order to take the  $\lambda \rightarrow 0$  limit. This approach has been investigated numerically in Refs. [32, 582, 583]; Fig. 6.4 shows an example of the hadronic tensor and fits to it to extract moments of the structure function  $F_1(x)$ .

### 6.3.2 Quasi-PDFs in large-momentum effective theory approach

As mentioned in Sec. 2.10.2, the large-momentum effective theory (LaMET) has been proposed to calculate the TMD and its soft function from lattice QCD. In fact, LaMET is a generic approach to calculate parton physics on the light-cone from Euclidean LQCD correlation functions (see recent reviews in Refs. [30, 594, 595]). The idea is to approximate a light-cone observable by boosting a static or time-independent quasi observable (a Euclidean space matrix element of a operator) to a large-momentum frame, and then perform a systematic expansion of the latter in inverse powers of the momentum to extract the observable of interest.

One of the first applications of LaMET has been to the lattice calculation of gluon helicity contribution to the proton spin [568, 569, 572], as was discussed in Sec. 6.2.2. A method to calculate the canonical parton orbital angular momentum has also been proposed in Refs. [555, 570] based on the LaMET approach. However, the best-studied development so far is in the lattice calculation of the  $x$ -dependence of collinear PDFs.

We focus first on the unpolarized quark PDF as an illustrative example. One can calculate the so called quasi-PDF which is defined from an equal-time spatial correlator [28],

$$\hat{f}(y, P^z, \Lambda) \equiv \int \frac{dz}{4\pi} e^{iyP^z z} \langle p(P, S) | \tilde{O}_\Gamma(z, 0) | p(P, S) \rangle, \quad (6.35)$$

$$\tilde{O}_\Gamma(z, 0) = \bar{\psi}(z) \Gamma W_{\hat{z}}(0; 0, z) \psi(0), \quad (6.36)$$

where  $\Gamma = \gamma^t$  or  $\gamma^z$ ,  $\Lambda$  is the ultraviolet (UV) momentum cutoff, and the spacelike Wilson line is

$$W_{\hat{z}}(0; 0, z) = P \exp \left( i g_0 \int_0^z dz' A^z(z' \hat{z}) \right). \quad (6.37)$$

Under a Lorentz boost in the longitudinal direction, the spatially separated operator  $\tilde{O}_\Gamma(z, 0)$  will approach the light-cone direction, and the quasi-PDF depends dynamically on the hadron momentum  $P^z$  accordingly. Unlike the light-cone PDF where Bjorken- $x$  is restricted to the interval  $x \in [-1, 1]$ , the quasi-PDF has a support for  $y \in (-\infty, \infty)$ .

In LQCD, the UV divergences are regulated in momentum space by the cutoff  $\Lambda \sim a^{-1}$ , and one can only calculate hadron matrix elements at  $P^z \ll \Lambda$ . The light-cone PDF, however, corresponds to the limit  $P^z \gg \Lambda$  which does not commute with the lattice regularization. Nevertheless, as long as  $P^z \gg \Lambda_{\text{QCD}}$ , the relative magnitudes of  $P^z$  and  $\Lambda \sim 1/a$  do not affect the contributions from infrared (IR) degrees of freedom, thus the difference between them are in the UV region which is under perturbative control. This separation gives rise to a factorization formula relating the PDF and the quasi-PDF, which has been studied extensively in the literature [33, 34, 596, 597]. In the  $\overline{\text{MS}}$  scheme, the factorization formula for the nonsinglet quasi-PDF has been proven [30, 34] and rigorously derived as [597]

$$\hat{f}(y, P^z, \mu) = \int_{-1}^1 \frac{dx}{|x|} C\left(\frac{y}{x}, \frac{\mu}{|x|P^z}\right) f(x, \mu) + \dots, \quad (6.38)$$

where  $\mu$  is the  $\overline{\text{MS}}$  scale, and for  $y < 0$ ,  $q(x) = -\bar{q}(-x)$  with  $\bar{q}$  being the antiquark.  $C$  is the perturbative matching coefficient which depends on the logarithm of the parton momentum. The relative power corrections indicated by the ellipsis include target mass  $M$  corrections which are known to all orders of  $M^2/(P^z)^2$  [598], as well as higher-twist contributions of  $\mathcal{O}(\Lambda_{\text{QCD}}^2/(y^2 P_z^2), \Lambda_{\text{QCD}}^2/((1-y)^2 P_z^2))$ , whose enhancement at  $y = 0$  and  $y = 1$  has been argued in Refs. [599, 600]. Similar factorization formulas have also been rigorously derived for the gluon and singlet quark quasi-PDFs [601], as well as for the quasi-GPDs [602].

The above factorization formula can be inverted order by order in perturbation theory [30],

$$f(x, \mu) = \int_{-\infty}^{\infty} \frac{dy}{|y|} C^{-1}\left(\frac{x}{y}, \frac{\mu}{|y|P^z}\right) \hat{f}(y, P^z, \mu) + \dots, \quad (6.39)$$

where  $C^{-1}$  is the inverse of the matching coefficient  $C$ , and the power corrections take similar forms to Eq. (6.38) except that  $y$  is replaced by  $x$ . Therefore, Eq. (6.39) provides a point-by-point determination of the PDF, which has controlled power corrections within a range of  $x$ , i.e.,  $x \in [x_{\min}, x_{\max}]$ . Based on Eq. (6.39), the systematic procedure to calculate the PDFs can be laid out as the following: 1) calculate the lattice matrix elements for the bare quasi-PDF; 2) renormalize the quasi-PDF and extrapolate to the physical quark mass, continuum and infinite volume limits; 3) perturbatively match to the light-cone PDF in the  $\overline{\text{MS}}$  scheme; 4) estimate the power corrections. For the target mass correction, step 3) can be done before step 4), while for the genuine higher-twist correction, one can extrapolate to the  $P^z \rightarrow \infty$  limit for each  $x$  after matching. The renormalization and matching procedures are closely related to each other, which will be elaborated in the following subsection.

### *Renormalization and matching*

The self-energies of spacelike Wilson lines are subject to linear power divergences with a lattice regulator and must be renormalized before one can take the continuum limit of matrix elements of the operators in Eq. (6.36). The renormalization of Wilson lines has been well studied in the literature [603–605]. For the nonlocal quark bilinear operator  $\tilde{O}_\Gamma(z, 0)$  in Eq. (6.36), it has been rigorously proven [606–608] that it can be multiplicatively renormalized in coordinate space as

$$\tilde{O}_\Gamma^B(z, 0) = \left[ \bar{\psi}_i(z) \Gamma W_{\hat{z}}(0; 0, z) \psi_i(0) \right]^B = Z_{\tilde{O}} e^{-\delta m|z|} \left[ \bar{\psi}_i(z) \Gamma W_{\hat{z}}(0; 0, z) \psi_i(0) \right]^R. \quad (6.40)$$

where  $i$  is the unsummed quark flavor index,  $\delta m$  has mass dimension one and absorbs the linear power divergence from the Wilson-line self-energy, and  $Z_{\tilde{O}}$  includes additional logarithmic divergences associated with the end points as well as the wavefunction renormalizations. The superscripts  $B$  and  $R$  indicate bare and renormalized quantities. Moreover, the renormalization is independent of the quark flavor and Dirac matrix  $\Gamma$ , and there is no mixing between quark and gluon sectors. The proof has also been generalized to the gluon quasi-PDF, as the nonlocal gluon bilinear operator is shown to be multiplicatively renormalizable [609, 610] up to a contact term [609].

Based on Eq. (6.40), one can renormalize the quasi-PDF in lattice perturbation theory or perform a nonperturbative renormalization. In the former case, there have been a number of one-loop studies of the quasi-PDF with lattice regularization [611–613], and then one can match the lattice regularized quasi-PDF to the  $\overline{\text{MS}}$  scheme in continuum theory. However, lattice perturbation theory is known to converge slowly, while renormalization of  $\tilde{O}_\Gamma$  or the quasi-PDF is now available in the  $\overline{\text{MS}}$  scheme up to three loops [614–618].

In order to implement a nonperturbative renormalization, one approach is to determine  $\delta m$  in Eq. (6.40) independently from the static quark-antiquark potential [27, 607, 611, 619–621]. After the nonperturbative subtraction of linear power divergences from the quasi-PDF, one can then renormalize the logarithmic divergences using either lattice perturbation theory [611] or other nonperturbative schemes for local composite operators [607].

As has been mentioned in Sec. 6.1, one can perform a nonperturbative renormalization in the regularization-independent momentum subtraction (RI/MOM) scheme [538], which has been widely used for local composite operators. Since the nonlocal quark bilinear  $\tilde{O}_\Gamma(z, 0)$  is of the lowest mass dimension, it does not have power divergent mixings resulting from the reduced symmetry of the hypercubic lattice. Therefore, it remains multiplicatively renormalizable. A RI/MOM scheme can be implemented as first proposed in Refs. [613, 622], and an independent formalism to renormalize the quasi-PDF in the RI/MOM scheme and match it to the PDF was developed and carried out in Refs. [623, 624]. However, because of the breaking of chiral symmetry in certain fermion actions, there is additional operator mixing between  $\tilde{O}_\Gamma(z, 0)$  [607, 613, 625] for different  $\Gamma$  structures. For  $\Gamma = \gamma^z$ , the operator mixes with the scalar case with  $\Gamma = I$  at  $\mathcal{O}(a^0)$ , while for  $\Gamma = \gamma^t$ , there is no mixing at  $\mathcal{O}(a^0)$ . To avoid such mixing,  $\Gamma = \gamma^t$  should be chosen instead of  $\Gamma = \gamma^z$ .

In the RI/MOM scheme, one defines the renormalization factor  $Z_{\text{OM}}(z, p_z^R, \mu_R, a)$  by imposing a momentum subtraction condition on the matrix element of  $\tilde{O}_{\gamma^t}(z, 0)$  at some kinematic

point for each value of  $z$ ,

$$Z_{\text{OM}}^{-1}(z, p_z^R, \mu_R, a) \langle p | \tilde{O}_{\gamma^t}^B(z, 0) | p \rangle \Big|_{\substack{p^2 = -\mu_R^2 \\ p_z = p_z^R}} = \langle p | \tilde{O}_{\gamma^t}(z, 0) | p \rangle_{\text{tree}}, \quad (6.41)$$

where the condition is defined at an off-shell quark momentum  $p_\mu^R = (p_t^R, p_x^R, p_y^R, p_z^R)$ , and the renormalization scale  $\mu_R^2 = -p_R^2 \gg \Lambda_{\text{QCD}}^2$ . In the LQCD calculation, the momentum  $p_\mu^R = (p_4^R, p_x^R, p_y^R, p_z^R)$  is Euclidean, and  $\mu_R^2 = (p_4^R)^2 + (p_x^R)^2 + (p_y^R)^2 + (p_z^R)^2 \geq (p_z^R)^2$ . The bare matrix element  $\langle p | \tilde{O}_{\gamma^t}^B(z, 0) | p \rangle$  is defined from the amputated Green's function  $\Lambda_{\gamma^t}(p, z)$  of  $\tilde{O}_{\gamma^t}^B(z, 0)$  with a projection operator  $\mathcal{P}$ ,

$$\Lambda_\Gamma(z, p, a) \equiv \left[ S_0^{-1}(p, a) \right]^\dagger \sum_{x,y} e^{ip \cdot (x-y)} \langle 0 | T \left[ \psi_0(x) \tilde{O}_\Gamma^B(z, 0) \bar{\psi}_0(y) \right] | 0 \rangle S_0^{-1}(p, a), \quad (6.42)$$

$$\sum_s \langle p, s | \tilde{O}_{\gamma^t}^B(z, 0) | p, s \rangle = \text{Tr} \left[ \Lambda_{\gamma^t}(z, p) \mathcal{P} \right]. \quad (6.43)$$

Then, the bare hadron matrix element of  $\tilde{O}_{\gamma^t}^B(z, 0)$

$$\tilde{h}_B(z, P_z, a^{-1}) = \frac{1}{2P^t} \langle P | \tilde{O}_{\gamma^t}^B(z, 0) | P \rangle \quad (6.44)$$

is renormalized in coordinate space as

$$\tilde{h}_R(z, P_z, p_z^R, \mu_R) = \lim_{a \rightarrow 0} Z_{\text{OM}}^{-1}(z, p_z^R, a^{-1}, \mu_R) \tilde{h}_B(z, P_z, a^{-1}), \quad (6.45)$$

where  $\tilde{h}_R(z, P_z, p_z^R, \mu_R)$  is the renormalized matrix element. At finite lattice spacing,  $\tilde{h}_R$  still has discretization errors, so calculations at different spacings are required extrapolate to the continuum limit, as indicated in Eq. (6.45).

Given the renormalized matrix elements in position space, the quasi-PDF can be constructed through the Fourier transform of Eq. (6.45). The next step is to match the renormalized quasi-PDF to the  $\overline{\text{MS}}$  PDF. According to UV regularization independence, the RI/MOM matrix elements should be the same in dimensional regularization with  $D = 4 - 2\epsilon$ ,

$$\lim_{a \rightarrow 0} Z_{\text{OM}}^{-1}(z, p_z^R, \mu_R, a^{-1}) \tilde{h}_B(z, P_z, a^{-1}) = \lim_{\epsilon \rightarrow 0} Z_{\text{OM}}^{-1}(z, p_z^R, \mu_R, \mu, \epsilon) \tilde{h}_B(z, P_z, \mu, \epsilon), \quad (6.46)$$

where  $\tilde{h}_B(z, P_z, \mu, \epsilon)$  and  $Z_{\text{OM}}(z, p_z^R, \mu_R, \mu, \epsilon)$  are the bare matrix element and RI/MOM renormalization factor in the continuum theory, and  $\mu$  is the UV scale introduced in dimensional regularization. In this way, the matching coefficients can be computed in continuum perturbation theory, which is much easier than that in lattice regularization.

There are two strategies developed to carry out the matching for the RI/MOM quasi-PDF [613, 623]. One is to convert  $\tilde{h}_R(z, P_z, p_z^R, \mu_R)$  from RI/MOM to the  $\overline{\text{MS}}$  scheme first,

$$\tilde{h}_{\overline{\text{MS}}}(z, P_z, \mu) = \tilde{h}_R(z, P_z, p_z^R, \mu_R) \frac{Z_{\text{OM}}(z, p_z^R, \mu_R, \mu, \epsilon)}{Z_{\overline{\text{MS}}}(\epsilon)}, \quad (6.47)$$

where  $Z_{\overline{\text{MS}}}$  is the  $\overline{\text{MS}}$  renormalization factor, and  $Z_{\text{OM}}$  has been calculated at one-loop order [613] in  $z$ -space and at two-loop order in the Fourier space of  $z$  [617]. Then, one transforms the  $\overline{\text{MS}}$  matrix element  $\tilde{h}_{\overline{\text{MS}}}(z, P_z, \mu)$  into momentum space to obtain the quasi-PDF and match the latter to the  $\overline{\text{MS}}$  PDF using Eq. (6.38), where the matching coefficient has been calculated at two-loop order [614–617]. Since the conversion factor in Eq. (6.47) is logarithmically divergent as  $|z| \rightarrow 0$ , and the  $\overline{\text{MS}}$  quasi-PDF does not satisfy vector current conservation [597], it was also proposed that one can modify the  $\overline{\text{MS}}$  scheme renormalization constant by a perturbative factor that cancels the singular terms in the  $|z| \rightarrow 0$  limit and restores the conservation law. Such schemes include the ratio scheme in Refs. [597, 626] and the modified  $\overline{\text{MS}}$  (MMS) scheme in Ref. [627]. Since the  $\overline{\text{MS}}$  matrix element  $\tilde{h}_{\overline{\text{MS}}}(z, P_z, \mu)$  should be independent of the RI/MOM scales  $\mu_R$  and  $p_z^R$ , its remnant dependence on them can in principle be fitted as polynomial lattice discretization effects [622]. This two-step matching procedure has been implemented in the lattice calculations of iso-vector quark PDFs in Refs. [622, 627–631].

The other strategy for matching the quasi-PDF in the RI/MOM scheme is more straightforward [623]. First, one Fourier transforms the RI/MOM matrix element  $\tilde{h}_R(z, P_z, p_z^R, \mu_R)$  to momentum space to obtain the quasi-PDF  $\tilde{f}(x, P_z, p_z^R, \mu_R)$ , and then directly match it onto the  $\overline{\text{MS}}$  PDF [601, 623, 632, 633] through the formula below,

$$f(x, \mu) = \int_{-\infty}^{\infty} \frac{dy}{|y|} C_{\text{OM}} \left( \frac{x}{y}, \frac{\mu_R}{p_z^R}, \frac{yP_z}{\mu}, \frac{yP_z}{p_z^R} \right) \hat{f}(y, P_z, p_z^R, \mu_R) + \dots, \quad (6.48)$$

where  $C_{\text{OM}}$  is the matching coefficient and  $\dots$  are the power corrections.

This strategy was implemented in the lattice calculations of the isovector quark PDFs in the proton and pion in Refs. [624, 632, 634, 635], as well as recent calculations in Refs. [636–640].

Apart from the RI/MOM scheme, it has also been proposed to renormalize the operator  $\tilde{O}_\Gamma(z, 0)$  by forming ratios of bare matrix elements in different external states, for example, the  $P^z = 0$  hadron state [308] or the vacuum [599, 616] in the denominator, and the corresponding matching coefficients to light-cone PDF has been derived up to two-loop order [616]. Since all these matrix elements become nonperturbative at large  $z$ , such ratio schemes only work at small distances when  $z \ll \Lambda_{\text{QCD}}^{-1}$ . Therefore, they are only applicable in coordinate space based on an equivalent short-distance factorization or OPE of the equal-time correlation in Eq. (6.35), such as the pseudo-distribution approach to be discussed below.

Since the factorization formula for the quasi-PDF is proven in the  $\overline{\text{MS}}$  scheme in momentum space, while the lattice renormalization is performed in the coordinate space, any scheme that can not be perturbatively matched to the  $\overline{\text{MS}}$  scheme will affect the validity of factorization. Actually, both the ratio and RI/MOM schemes suffer from this issue, for their conversion factors to  $\overline{\text{MS}}$  include logarithms of  $z^2$  that become IR at large  $z$  [597, 613]. Besides, ratio and RI/MOM schemes could introduce nonperturbative effects at large  $z$  which can not be controlled systematically. In contrast, the Wilson-line mass-subtraction scheme avoids this issue. Nevertheless, lattice discretization effects at  $z \sim a$  will obscure the continuum limit of the renormalized matrix element to reproduce the divergent  $\ln z^2$  behavior at small  $z$  in the  $\overline{\text{MS}}$  scheme. Such discretization effects, however, are cancelled in the RI/MOM and ratio schemes, which leads to a finite  $z \rightarrow 0$  limit of the renormalized matrix elements.

To reconcile the advantages and disadvantages of the above schemes, the hybrid scheme was proposed in Ref. [600] to renormalize the bare matrix elements at small and large  $z$ . At short distance  $z \leq z_S$  where  $z_S \sim 0.2 - 0.3$  fm  $\ll \Lambda_{\text{QCD}}^{-1}$  is smaller than the distance at which the uncertainty in perturbation theory becomes too large, one uses either the RI/MOM or ratio scheme where the lattice discretization effects cancel; for  $z > z_S$ , one uses the Wilson-line-mass-subtraction scheme, with the logarithmic renormalization factor determined by a continuity condition at  $z = z_S$ . After the subtraction, one needs to match the lattice hybrid scheme to the continuum theory, which can be done using the method developed in Ref. [641]. The  $z_S$ -dependence will be cancelled by the perturbative matching in the final result. The perturbative matching for the hybrid renormalized quasi-PDF with ratio scheme at short distance has been derived at one-loop order [600].

Due to finite lattice size and decreasing signal-to-noise ratios at large  $z$ , the lattice results are only well determined for distances less than a truncation scale,  $z_L$ , which causes difficulties in the Fourier transform required to obtain the quasi-PDF. Since the spacelike correlations in the  $\overline{\text{MS}}$  must decay exponentially at large distance due to confinement in the hadron, a physically motivated extrapolation model beyond  $z_L$  can be used to remove the unphysical oscillations in a truncated Fourier transform. In return this will introduce systematic uncertainties in the small- $x$  region, but it generally does not overlap with the region  $x \in [x_{\min}, x_{\max}]$  where the LaMET expansion in Eq. (6.39) has systematic control. A comparison of ratio, RI/MOM and hybrid scheme analyses is shown in Fig. 6.5.

There is a further way to renormalize the quasi-PDF on lattice, which is based on a redefinition of the quasi-PDF using the gradient flow method [642]. The redefined quasi-PDF remains finite in the continuum limit, which is free from the power divergences on the lattice and can be perturbatively matched onto the  $\overline{\text{MS}}$  PDF [643].

### *Lattice Calculations*

The LaMET methodology has been studied intensively on the lattice soon after the proposal [644–646]. A lot of improvements became available regarding the renormalization, the matching, and the parameters of the ensembles employed. To date, lattice calculations are well beyond the exploratory phase with investigations of twist-2 and twist-3 PDFs, as well as GPDs and TMDs. Systematic uncertainties such as excited-states contamination, volume effects, cutoff effects are being addressed carefully. Also, the  $x$ -dependence of PDFs have been calculated directly at the physical quark masses [628, 629, 647].

The first complete calculations at the physical point for the unpolarized, helicity and transversity isovector PDFs appear in Refs. [628, 629], followed by an analysis of selected sources of systematic uncertainties [627]. These calculations use an  $N_f = 2$  ensemble of the twisted-mass [648, 649] lattice discretization with physical light-quark mass and spatial extent of 4.5 fm. The results for all types of collinear PDFs using quasi-PDFs at  $P_3 = 1.38$  GeV are shown in Fig. 6.6. The helicity PDFs is extracted in Ref. [647] using a mixed action setup of clover fermions on a  $N_f = 2 + 1 + 1$  HISQ ensemble with spatial lattice extent  $L \approx 5.8$  fm and a pion mass  $\approx 135$  MeV are shown in Fig. 6.7.

In the aforementioned calculations at the physical point, various non-perturbative renormalization schemes were applied as discussed above, followed by a matching kernel appro-

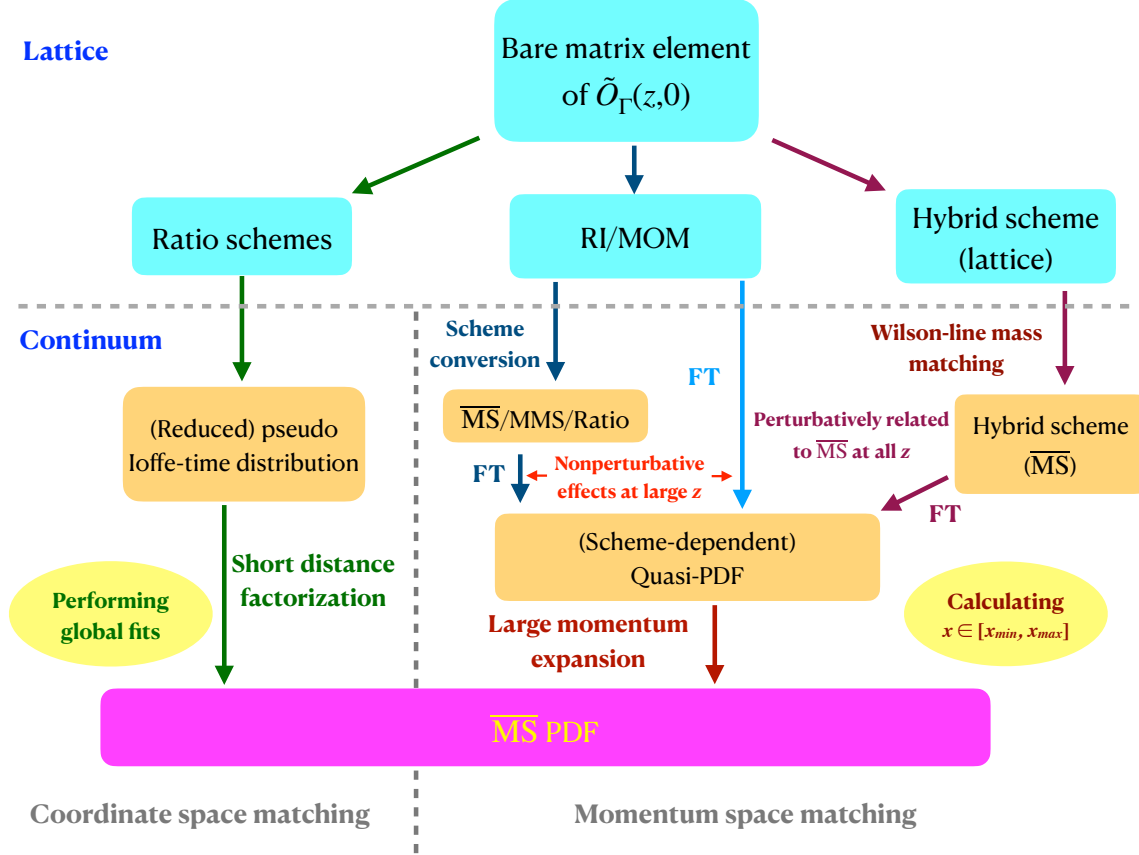


Figure 6.5: Comparison of the ratio, RI/MOM and hybrid renormalization schemes in the lattice calculation of PDFs.

priate for the choice of renormalization. However, the calculations differ in the reconstruction of the  $x$ -dependence. This is an important aspect of the calculation that may introduce systematic uncertainties due to the limited number of lattice data entering the Fourier transform (FT). Refs. [627–629] use a standard discretized FT, while Ref. [647] applies the “derivative method” which relies on integration by parts and neglecting the surface term [634]. While none of the methods overcomes the ill-defined inverse problem, the derivative method has been shown to lead to uncontrolled uncertainties in the small- $x$  region [627, 656].

The quasi-distributions formulation has been used to calculate the PDFs of other particles, such as the pion [636, 639, 657, 658], kaon and  $\Delta^+$  [659]. Sources of systematic uncertainties using ensembles with quark masses larger than their physical values have been studied in Refs. [621, 660]. Another direction is the inclusion of the disconnected diagram contributions for the strange and charm unpolarized PDFs [638] and the up, down and strange unpolarized, helicity and transversity PDFs [631, 661]. The flavor decomposition of the up and down quark PDFs, as well as the strange quark PDFs, are presented in Fig. 6.8 obtained in Ref. [631] using an ensemble leading to a pion mass of 260 MeV. Results for  $|x|\Delta q^+(x) \equiv |x|(\Delta q + \Delta \bar{q})$  and  $|x|\Delta q^-(x) \equiv |x|(\Delta q - \Delta \bar{q})$  are shown for  $q = u, d, s$ , and compared with the JAM17 [653] and NNPDF<sub>POL</sub>1.1 [565, 662] global fits. As can be seen, there is a tension for the case of  $\Delta u^-$ , and a mild disagreement for  $\Delta d^-$ .  $\Delta s^+$  is compatible with the global fits and is more precise,

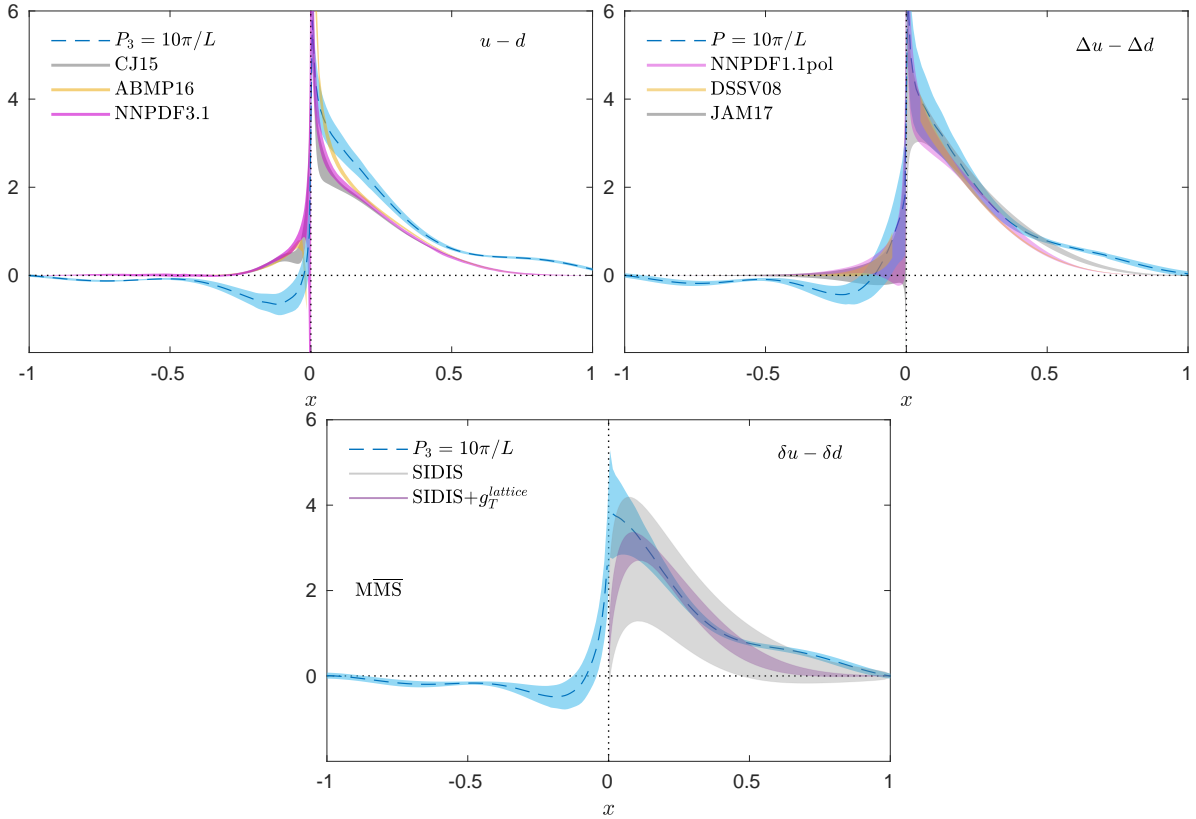


Figure 6.6: The proton unpolarized (top left), helicity (top right) and transversity (bottom) PDFs at the physical point and  $P_3 = 1.38$  GeV from Ref. [627]. A comparison with with global fits [562, 565, 650–654] is also shown. Plot taken from Ref. [655].

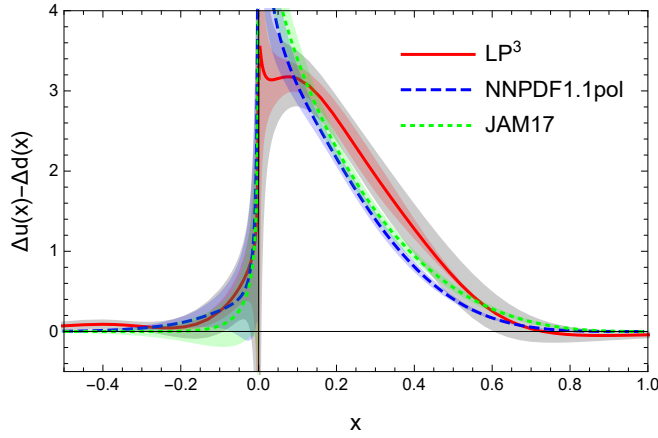


Figure 6.7: The helicity PDF calculated in Ref. [647] using  $P_3 = 3$  GeV (red curve), compared to global fits [564, 565, 653]. Plot taken from Ref. [647].

suggesting a non-zero value for small values of  $x$  which would be valuable input to global fits.

The quasi-PDFs approach has also been extended to the twist-3 PDFs, in particular for

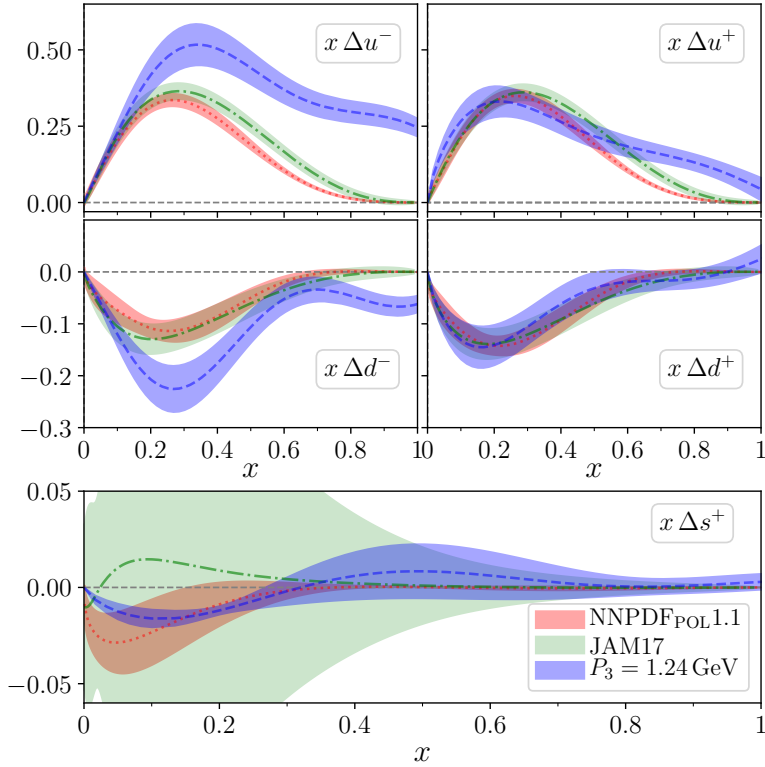


Figure 6.8: Lattice data on the  $|x|\Delta u$  (top),  $|x|\Delta d$  (center), and  $|x|\Delta s^+$  (bottom) quark helicity PDFs (blue) with momentum boost  $P_3 = 1.24$  GeV renormalized in the  $\overline{\text{MS}}$  scheme at a scale of 2 GeV. The global fits JAM17 [653] (green) and NNPDF<sub>POL</sub>1.1 [565, 662] (red) are shown for comparison. Plot taken from Ref. [631].

$g_T(x)$  [630, 663],  $h_L(x)$  [664] and  $e(x)$  [665]. One of the important use of the lattice results is the test of the Wandzura-Wilczek (WW) approximation [666], according to which the twist-3  $g_T(x)$  and its corresponding twist-2  $g_1(x)$  are connected through

$$g_T^{\text{WW}}(x) = \int_x^1 \frac{dy}{y} g_1(y). \quad (6.49)$$

In the WW approximation,  $g_T(x)$  is fully determined by the twist-2  $g_1(x)$ . An analogous relation exists for  $h_L(x)$  [363, 387]. The WW approximation has been implemented for both  $g_T(x)$  and  $h_L(x)$ , which may provide qualitative understanding on the significance of the contribution due to quark-gluon correlations. The results are shown in Fig. 6.9 for the quark region. The actual lattice data for  $g_T(x)$  are consistent with  $g_T^{\text{WW}}(x)$  for a considerable  $x$ -range, even though the uncertainties permit violations up to 40% for  $x \lesssim 0.4$ . Also, the slopes of  $g_T$  and  $g_T^{\text{WW}}$  are the same up to  $x \approx 0.4$ . The lattice results on  $g_T^{\text{WW}}$  are also compared to the estimate obtained using  $g_1$  from global fits by the NNPDF [565] and JAM17 [653] collaborations, and a good agreement is found up to  $x \approx 0.3$ . For the  $h_L(x)$  case, there is an agreement between  $h_L(x)$  and  $h_L^{\text{WW}}(x)$  for  $x \lesssim 0.55$ . Furthermore, the lattice results on  $h_L^{\text{WW}}(x)$  in the region  $0.15 \lesssim x \lesssim 0.55$  are in agreement with  $h_L^{\text{WW}}(x)$  obtained from the JAM17 global fit [17]. It should be mentioned that the lattice calculations on twist-3 PDFs

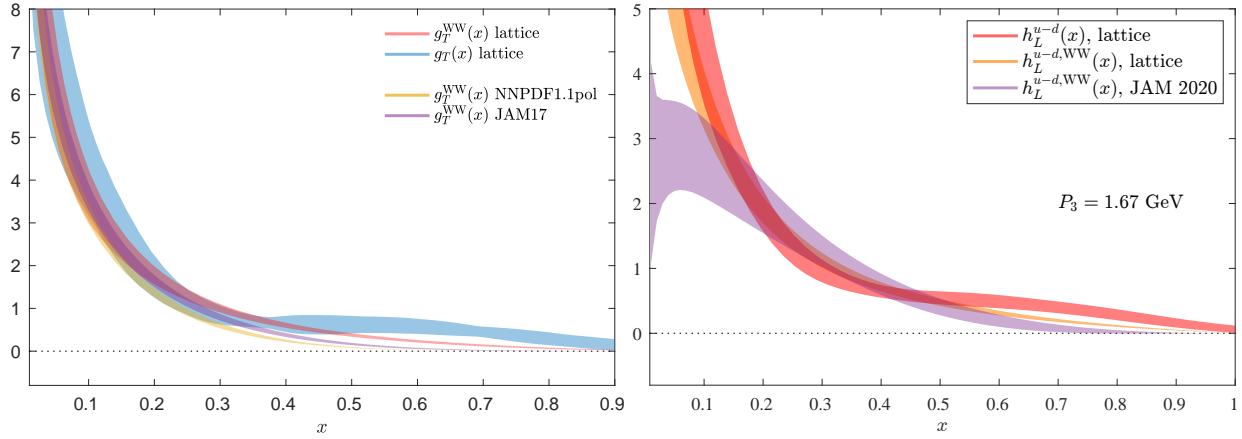


Figure 6.9: Left: Comparison of lattice results on  $g_T(x)$  (blue band) with its WW estimates: lattice-extracted  $g_T^{\text{WW}}$  (red band) and global fits-extracted (NNPDF1.1pol [565] orange band, JAM17 [653] purple band). Plot taken from Ref. [630]. Right: The WW approximation for  $h_L(x)$ , for boosts  $P_3 = 1.67$  GeV. The lattice estimate of  $h_L(x)$  (red band) is compared with its WW-approximation (orange band) extracted on the same gauge ensemble and the one obtained from global fits (violet band) from the JAM collaboration [17]. Plot taken from Ref. [664].

do not consider the mixing with quark-gluon-quark correlators, which requires considerable theoretical development, as well as computational resources. Exploration of twist-3 GPDs is a natural development given the progress in twist-3 PDFs, as well as twist-2 GPDs [667, 668]. Preliminary results can be found in Ref. [669].

### 6.3.3 Pseudo-distributions

An approach closely related to the quasi-distributions, is that of the pseudo-distributions introduced in a series of publications [31, 670, 671]. In this approach, one calculates the same matrix elements as for quasi-distributions, but now views them as functions of two Lorentz invariants, the “Ioffe time” [672],  $\nu = p \cdot z$ , and  $z^2$ . The matrix element is written as  $\mathcal{M}(\nu, z^2) = \langle P | \bar{\psi}(0, z) \gamma_0 W(z, 0) \psi(0, 0) | P \rangle$  and the ratio

$$\mathfrak{M}(\nu, z^2) = \frac{\mathcal{M}(\nu, z^2) / \mathcal{M}(\nu, 0)}{\mathcal{M}(0, z^2) / \mathcal{M}(0, 0)}, \quad (6.50)$$

is called reduced Ioffe time pseudo-distribution (pseudo-ITD), and defines a gauge-invariant renormalization scheme.  $\mathfrak{M}(\nu, z^2)$  is matched to the light-cone ITDs,  $Q(\nu, \mu^2)$  via

$$\begin{aligned} \mathfrak{M}(\nu, z^2) &= Q(\nu, \mu^2) + \frac{\alpha_s C_F}{2\pi} \int_0^1 du \\ &\times \left[ \ln \left( z^2 \mu^2 \frac{e^{2\gamma_E+1}}{4} \right) B(u) + L(u) \right] Q(u\nu, \mu^2), \end{aligned} \quad (6.51)$$

in which the kernel  $B(u)$  evolves the pseudo-ITDs to a common scale  $\mu$  and the part with  $L(u)$  converts to the  $\overline{\text{MS}}$  scheme. For more details see Refs. [597, 673–675]. Note that unlike in the quasi-distributions approach, here one relies on short-distance factorization. The light-cone

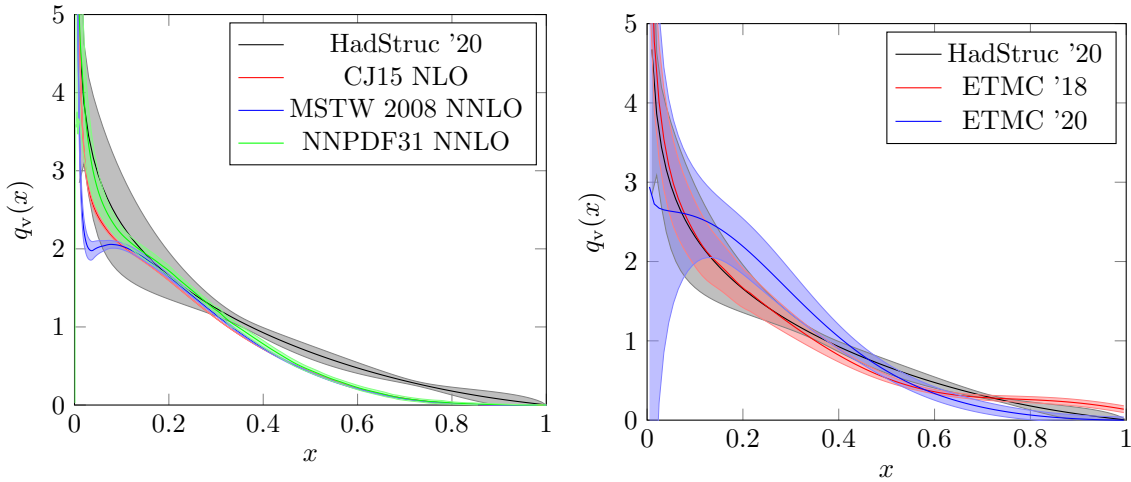


Figure 6.10: Left: The nucleon isovector valence PDF (gray band) and the phenomenological determinations from CJ15 [652] (green), MSTW2008 [682] (red) and NNPDF31 [651] (blue). Plot taken from Ref. [681]. Left: Lattice results on the unpolarized PDF using the quasi-PDFs method [627] (red band) and pseudo-ITDs from Ref. [681] (gray band) and Ref. [683] (blue band).

PDFs may be extracted via a Fourier transform in Ioffe time.

$$q(x, \mu^2) = \int d\nu e^{-i\nu x} Q(\nu, \mu^2), \quad (6.52)$$

The pseudo-distribution approach has been studied in several publications with promising results [308, 656, 673, 676–681]. Results on the nucleon pseudo-PDFs are presented in Ref. [681] for the valence unpolarized PDF. Three ensembles have been used with the lightest quark mass corresponding to a pion mass of 170 MeV. Fig. 6.10 shows the results extrapolated to the physical quark masses compared to the phenomenological fits [651, 652, 682]. Agreement is seen for  $x \sim 0.25$ , with the lattice results being significantly larger than the global fits at intermediate and large  $x$  values. It is interesting to compare data at the physical point from different lattice formulations and/or methodologies. In Fig. 6.10 we show the unpolarized isovector valence PDF for the proton as obtained from the pseudo-PDFs method: HadStruc '20 [681], ETMC '20 [683], and the quasi-PDFs method: ETMC '18 [628]. The results exhibit agreement for a wide range of values for  $x$ . However, systematic effects are not fully quantified that potentially causes some tension in the large  $x$  region.

The full and sea-quark PDFs have been obtained in Ref. [683] using the pseudo-ITD method using one ensemble at the physical quark masses. Three reconstruction methods were implemented, the standard FT, the Backus-Gilbert method, and fitting reconstruction [683]. The latter performs better than the other approaches, and the increase in the uncertainties at small  $x$  reflects the challenges of the inverse problems. The final results are shown in Fig. 6.11, and agreement is found with the phenomenological PDFs for both distributions.

### 6.3.4 Current-current correlator

A different method to extract parton structure was proposed in Ref. [26] using an auxiliary light quark field, and applied for the pion distribution amplitude [684, 685]. The calculation

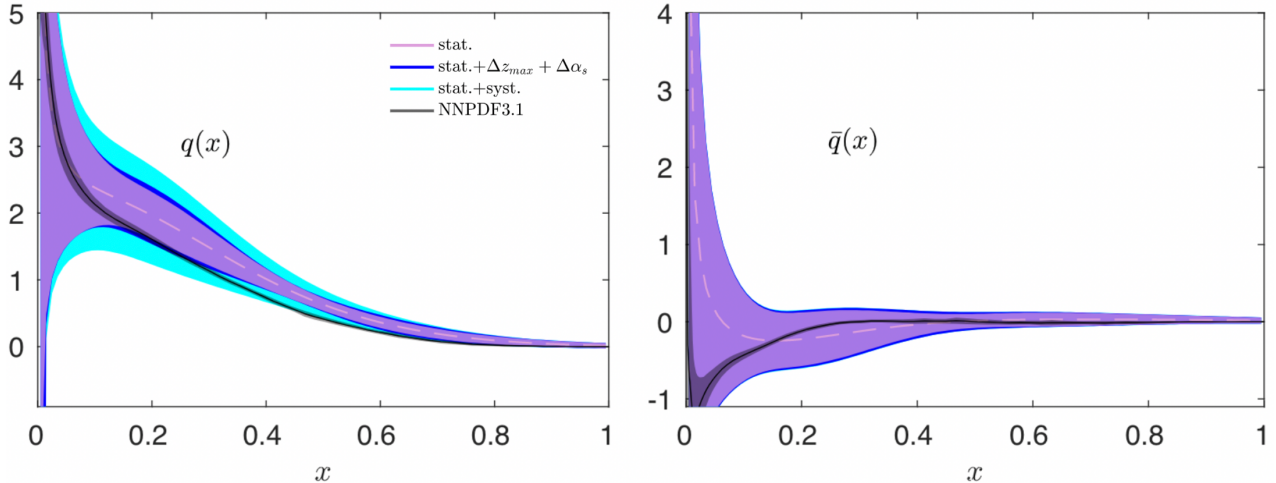


Figure 6.11: Lattice estimates for the unpolarized PDFs for the full (left) and sea (right) contributions [683]. The global fits of NNPDF [651] are shown with a IV: dark grey band. The bands in the lattice data represent: the statistical error (purple), the combination of statistical and systematic due to the choice of  $v_{\max}$  and  $\alpha_s$  (blue), and the total error including also an estimate for the uncertainties related to cutoff effects, finite-volume effects, excited states contamination, truncation and higher-twist effects (cyan). Plot taken from Ref. [683].

relies on current-current correlators, with the currents positioned at points  $z$  and  $-z$  and the pion boosted with momentum  $p$ . An OPE may be used for small values of  $z$  and in such a case the correlator is related to the Fourier transform of the pion DA. The momentum  $p$  can be in any spatial direction, and ideally with a large component in the direction of the current separation ( $z$ ), so that the Ioffe time  $p \cdot z$ , can take large values, which is an important condition to access the full pion DA.

In the work of Ref. [684], a first study is performed using  $N_f=2$  clover fermions and a pion mass of 295 MeV, with a pion momentum  $\sim 2$  GeV, with the pion DA being extracted from the scalar-pseudoscalar channel. From this study, it is seen that there is a need to boost the pion to higher momentum to reach higher values  $p \cdot z$ . Having larger values for  $p$  will allow smaller  $z$  while still keeping the Ioffe time large. This is crucial, as the approach relies on small values of  $z$ , so that the perturbative expansions are meaningful. However,  $p$  can not be increased arbitrarily due to the lattice cutoff, and thus, smaller values of the lattice spacing are needed. In Ref. [685] the pion DA was studied using different channels, that is, vector-vector, axial-axial, vector-axial, axial-vector, scalar-pseudoscalar and pseudoscalar-scalar, and their linear combinations. Given the findings of Refs. [684, 685], the constraint  $|\vec{z}| > 3a$  is imposed to suppress lattice artifacts, and the values used for  $|\vec{z}|$  are relatively small. Results from these exploratory studies show that further investigation is needed to eliminate systematic uncertainties related to the pion mass value, momentum boost, finite lattice spacing, and truncation of the perturbative expansion.

### 6.3.5 Good lattice cross sections

Light-cone distribution functions from LQCD can be related to matrix elements calculable on the lattice using the “lattice cross sections” (LCSs) approach [33, 34, 686]. The main idea of

this approach is to calculate a large class of factorizable matrix elements within LQCD, which can be used in a global fit to extract PDFs, as done with experimental data and phenomenological fits. The matrix elements must be calculable in LQCD, renormalizable, and share the same factorizable logarithmic collinear divergences as the light-cone distribution functions. Quasi-PDFs, pseudo-PDFs and the Compton amplitude  $T_{\mu\nu}$  are examples of good LCSs [33]. In general, good LCSs are related to hadronic matrix elements of operators  $O_n$ , where the hadron  $h$  has momentum  $P$ :

$$\sigma_n(\omega, \xi^2, P^2, S, \mu) = \langle h(P, S) | T\{O_n(\xi, \mu)\} | h(P, S) \rangle, \quad \omega \equiv P \cdot \xi. \quad (6.53)$$

One possibility explored for the operator is a current-current correlators separated by distance  $\xi$  ( $\xi^2 \neq 0$ ), that is

$$O_{J_1 J_2}(\xi) \equiv \xi^{D_{J_1} + D_{J_2} - 2} J_1^R(\xi) J_2^R(0), \quad (6.54)$$

with  $D_{J_i}$  the dimension of the renormalized current  $J_i^R = Z_{J_i} J_i$ , with  $Z_{J_i}$  the renormalization function of  $J_i$ . This particular case is similar to the hadronic tensor approaches discussed above, but more general scenarios can also be considered.

The method was employed in Ref. [687] for an ensemble of  $N_f = 2 + 1$  clover fermions with pion mass of 430 MeV, to calculate current-current correlators for the vector and axial currents, and momentum boost up to  $\sim 1.5$  GeV. The work focuses on the antisymmetric combination of vector and axial-vector operators, which is directly linked to the pion quark distribution. More recently, the calculation improved with four ensembles with three pion masses (278, 358, 413 MeV) and two volumes [688]. A chiral, continuum, volume, and higher-twist extrapolation has been applied, followed by the factorization and a parameterization of the lattice data on the PDF. The fits are in agreement within errors and are shown in the left panel of Fig. 6.12, and are compared with using E615 data [432, 689].

### 6.3.6 Comparison of methods

It is interesting to compare results for the quark distribution in the pion using the various different approaches. Note that some the calculations use different fermion actions and analysis approach, such as the quasi-PDFs [635, 657], pseudo-ITDs [679] and current-current correlators [687].

Ref. [635] uses an  $N_f = 2 + 1 + 1$  mixed-action ensemble of clover on HISQ fermions with a pion mass of 310 MeV and volume  $24^3 \times 64$ . The analysis follows the quasi-PDF approach, and the  $x$ -dependence reconstruction is performed using the derivative method [634]. The derivative method is based on integration by parts of the Fourier transform and neglects the surface term, which introduces uncontrolled uncertainties [678]. Ref. [657] makes use of the quasi-PDFs method on a mixed action of clover fermions in the valence sector and  $N_f = 2 + 1$  HISQ fermions with pion mass 300 MeV. The volume is  $48^3 \times 64$ , corresponding to a spatial extent of 2.9 fm ( $a = 0.06$  fm). Instead of a standard Fourier transform, two types of fits are applied to the lattice data in the coordinate space, similar to the methods of Refs. [679, 687, 688]. Ref. [679] combines two  $N_f = 2 + 1$  ensembles of clover fermions with a pion mass of 415 MeV and different volumes (3 fm and 4 fm). Ref. [687] uses the same large-volume ensemble (4 fm). The comparison of the two calculation is shown in the left panel of Fig. 6.12, where an excellent agreement is observed.

The results from the four different calculations are shown in the right panel of Fig. 6.12. The pseudo and current-current correlators data of Refs. [679, 687] are in reasonable agreement

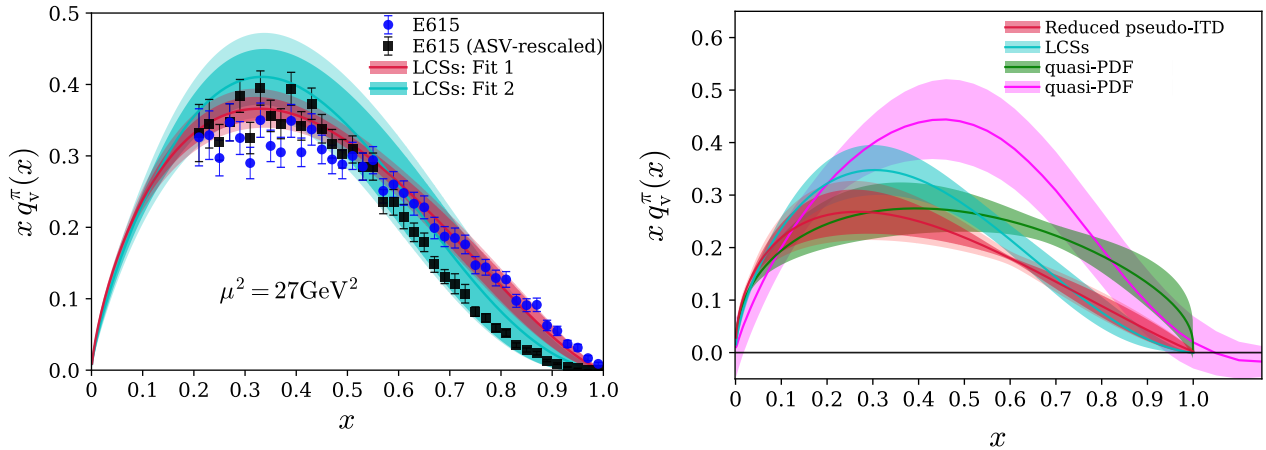


Figure 6.12: Left: Lattice data of pion  $x q_v^\pi(x)$ -distribution using two parameterizations (cyan and red bands), and the E615 data from Ref. [432] (blue) and Ref. [690] (black). Plot taken from Ref. [688]. Right: Lattice data for the pion PDF from Ref. [635] using quasi-PDF (pink band), Ref. [657] also with quasi-PDF (green band), Ref. [679] using pseudo-ITDs (red band), and Ref. [687] using current-current correlators (cyan band). Plot taken from Ref. [679].

with the calculation of Ref. [657]. A tension is observed with the results of Ref. [635], which uses the quasi-PDFs approach. This tension could possibly originate from the use of the derivative method to reconstruct the  $x$ -dependence, which neglects the surface term. Note that the calculations are evolved to different scales. However, the scale dependence is expected to be small for the values used.

## 6.4 Lattice QCD Calculations of TMD Observables

Having presented an overview of progress on understanding the longitudinal momentum dependence of PDFs, a basis has been laid for discussing LQCD approaches to transverse momentum-dependent hadron structure. A number of different aspects have been investigated. They include a longer-established calculational program employing the Lorentz-invariant approach introduced in Sec. 2.10.1, focusing on TMD ratios, as well as calculations of TMD soft functions, and calculations of the Collins-Soper kernel.

### 6.4.1 Lorentz-invariant approach

#### *Calculational scheme*

As already indicated in Sec. 2.10, lattice calculations of TMD (and GTMD) observables are based on the evaluation of the fundamental hadronic matrix elements, cf. Eq. (2.162),

$$\tilde{\Phi}_i^{[\Gamma]}(b, P', P, S, v, \eta, a) = \frac{1}{2} \langle p(P', S) | \bar{\psi}_i^0(b^\mu/2) \Gamma W_{\square\eta}^v(b^\mu/2, -b^\mu/2) \psi_i^0(-b^\mu/2) | p(P, S) \rangle \quad (6.55)$$

in states characterized by their momentum and spin; TMDs are derived from diagonal matrix elements,  $P' = P$ , whereas GTMDs, to be discussed further in Chap. 11, additionally depend on the momentum transfer  $\Delta = P' - P$ .  $\Gamma$  stands for an arbitrary Dirac matrix structure and  $i$  labels the quark flavor. As discussed in detail in Chap. 2, the presence of the gauge connection

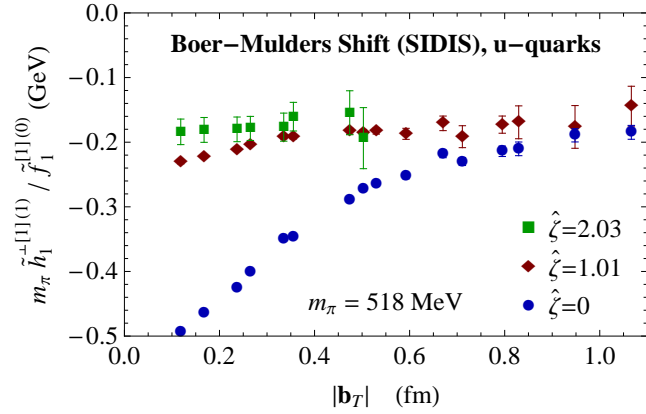


Figure 6.13: Pion  $u$ -quark SIDIS generalized Boer-Mulders shift as a function of  $b_T$ , for several values of  $\hat{\zeta}$ . Only connected contributions to the Boer-Mulders shift were included. Plot taken from Ref. [141].

$W_{\square\eta}^v$  introduces divergences additional to the wave function renormalizations of the quark operators; these can be absorbed into a multiplicative soft factor. In the calculational scheme described in the following, the explicit evaluation of soft factors is avoided by considering appropriate ratios in which they cancel. A method to evaluate soft factors in LQCD, which would allow one to extend lattice calculations beyond ratio observables, is discussed in Sec. 6.4.2.

As laid out in Chap. 2, standard TMDs describing, e.g., the SIDIS and Drell-Yan processes are obtained using a staple-shaped gauge connection path,<sup>26</sup> as exhibited in Fig. 2.11. The path is characterized not only by the separation of the quark operators  $b$ , but also the direction of the staple  $v$ , and the length of the staple  $\eta$ . In a LQCD calculation,  $\eta$  is finite, and one must extrapolate the data to the  $\eta \rightarrow \infty$  limit. In addition,  $v$  is chosen to be space-like, in order to be able to connect the definition in Eq. (6.55) to a Lorentz frame in which  $v$  is purely spatial, and in which therefore the lattice calculation can be performed. As already discussed in Sec. 2.10, a useful parameter characterizing the rapidity of the staple direction  $v$  relative to the average hadron momentum  $\bar{P} = (P' + P)/2$  is the Collins-Soper type evolution parameter  $\hat{\zeta} = v \cdot \bar{P} / (\sqrt{|v^2|} \sqrt{\bar{P}^2})$ . The connection with the modern Collins definition of TMDs is established in the limit  $\hat{\zeta} \rightarrow \infty$ .

In practice, reaching values of  $\hat{\zeta}$  in the range 1–2 in lattice calculations appears to be sufficient to enter a regime in which the data fit a power law behavior that can be extrapolated to the  $\hat{\zeta} \rightarrow \infty$  limit; an illustration is provided by Fig. 6.16 further below. For a light particle such as the pion, this regime has been reached, whereas for the nucleon, current calculations as of this writing are still concentrated at lower values and only beginning to enter the aforementioned regime. The extrapolation  $\hat{\zeta} \rightarrow \infty$  therefore appears feasible with continually improving calculations, but does figure among the chief systematic uncertainties of lattice TMD calculations. It persists as a challenge for future LQCD TMD investigations.

To facilitate the transformation of the results obtained in the Lorentz frame in which the lattice calculation is performed back to the original frame in which TMDs are defined, it is

<sup>26</sup>More complex paths can also become relevant when one extends considerations beyond the simplest processes [691].

useful to employ a decomposition of Eq. (6.55) into Lorentz invariants. Once determined in the lattice frame from the lattice data, these invariants are immediately valid also in the original frame. The full decomposition is discussed in Ref. [140]; it is analogous to the decomposition defining TMDs in momentum space. For a nucleon, at leading twist, one has the forms<sup>27</sup>

$$\frac{1}{2P^+}\tilde{\Phi}^{[\gamma^+]}\ =\ \tilde{A}_{2B} - im_N\epsilon_{ij}b_iS_j\tilde{A}_{12B}, \quad (6.56)$$

$$\frac{1}{2P^+}\tilde{\Phi}^{[\gamma^+\gamma^5]}\ =\ -S_L\tilde{A}_{6B} - i((b\cdot P)S_L - m_N(b_T\cdot S_T))\tilde{A}_{7B}, \quad (6.57)$$

$$\begin{aligned} \frac{1}{2P^+}\tilde{\Phi}^{[i\sigma^{i+}\gamma^5]}\ =\ & -im_N\epsilon_{ij}b_j\tilde{A}_{4B} - S_i\tilde{A}_{9B} + im_NS_Lb_i\tilde{A}_{10B} \\ & +m_N((b\cdot P)S_L - m_N(b_T\cdot S_T))b_i\tilde{A}_{11B}. \end{aligned} \quad (6.58)$$

The Lorentz invariant amplitude combinations  $\tilde{A}_{iB}$  are already suitable linear combinations of the amplitudes one finds in the most general decomposition [140]. They essentially correspond to Fourier-transformed TMDs, cf. also Eq. (2.127). For the following, it is useful to introduce a notation for Mellin moments of Fourier-transformed TMDs, where  $f(x, k_T^2, \dots)$  stands for a generic TMD,

$$\tilde{f}^{[m](n)}(b_T^2, \dots) \equiv n! \left( -\frac{2}{m_N^2} \partial_{b_T^2} \right)^n \int_{-1}^1 dx x^{m-1} \int d^2k_T e^{-ib_T\cdot k_T} f(x, k_T^2, \dots). \quad (6.59)$$

Through the invariant amplitudes  $\tilde{A}_{iB}$ , one can then finally define observables constructed as ratios; for example, for transverse polarization, the following quantities have been studied [140]:

- The generalized Sivers shift

$$\langle k_\perp \rangle_{TU}(b_T^2, \dots) = m_N \frac{\tilde{f}_1^{\perp[1](1)}}{\tilde{f}_1^{[1](0)}} = -m_N \frac{\tilde{A}_{12B}(-b_T^2, b\cdot P = 0, \hat{\zeta}, \eta v\cdot P)}{\tilde{A}_{2B}(-b_T^2, b\cdot P = 0, \hat{\zeta}, \eta v\cdot P)}, \quad (6.60)$$

which formally, in the  $b_T \rightarrow 0$  limit, represents the average transverse momentum  $k_\perp$  of unpolarized (“U”) quarks orthogonal to the transverse (“T”) spin of the proton, normalized to the corresponding number of valence quarks. It is “generalized” in the sense of being defined for arbitrary  $b_T^2$ , not only  $b_T \rightarrow 0$ . This regulates ultraviolet divergences associated with the latter limit; also, the dependence on  $b_T^2$  of course encodes information about the  $k_T$ -dependence of the TMDs appearing in the ratio. Note that, in the numerator, the contributions from quarks and antiquarks are summed over [129], whereas the denominator corresponds to the difference of quark and antiquark contributions (thus, the number of valence quarks in the  $b_T \rightarrow 0$  limit). The generalized Sivers shift is T-odd, i.e., differs in sign between the SIDIS and Drell-Yan limits, cf. Fig. 6.14 (left). A compilation of existing LQCD results for the generalized Sivers shift, compared to a phenomenological extraction, is presented in Fig. 6.15 [142].

<sup>27</sup>Note that the convention for the operator separation  $b$  used here has the opposite sign relative to the convention used in Ref. [140].

- The generalized Boer-Mulders shift

$$\langle k_{\perp} \rangle_{UT}(b_T^2, \dots) = m_N \frac{\tilde{h}_1^{\perp[1](1)}}{\tilde{f}_1^{[1](0)}} = m_N \frac{\tilde{A}_{4B}(-b_T^2, b \cdot P = 0, \hat{\zeta}, \eta v \cdot P)}{\tilde{A}_{2B}(-b_T^2, b \cdot P = 0, \hat{\zeta}, \eta v \cdot P)} \quad (6.61)$$

akin to the Sivers shift, is T-odd and formally, in the  $b_T \rightarrow 0$  limit, represents the average transverse momentum  $k_{\perp}$  of transversely polarized (“T”) quarks in the direction orthogonal to their spin, in an unpolarized (“U”) hadron. It can therefore also be defined for spinless hadrons such as the pion. Fig. 6.13 shows results for the pion generalized Boer-Mulders shift in the SIDIS limit [141]. The generalized Boer-Mulders shift is again normalized to the corresponding number of valence quarks.

- The generalized  $g_{1T}$  worm-gear shift

$$\langle k_{\perp} \rangle_{TL}(b_T^2, \dots) = m_N \frac{\tilde{g}_{1T}^{[1](1)}}{\tilde{f}_1^{[1](0)}} = -m_N \frac{\tilde{A}_{7B}(-b_T^2, b \cdot P = 0, \hat{\zeta}, \eta v \cdot P)}{\tilde{A}_{2B}(-b_T^2, b \cdot P = 0, \hat{\zeta}, \eta v \cdot P)} \quad (6.62)$$

formally, in the  $b_T \rightarrow 0$  limit, represents the average transverse momentum  $k_{\perp}$  of longitudinally polarized (“L”) quarks in the direction of the transverse (“T”) spin of the proton, again normalized to the corresponding number of valence quarks. Unlike the Sivers and the Boer-Mulders shifts, this is a T-even quantity, i.e., the SIDIS and Drell-Yan limits coincide, cf. Fig. 6.14 (right) from Ref. [142]. In the displayed case, the bulk of the  $g_{1T}$  worm-gear shift is induced already in the presence of a straight gauge link, and there is only a moderate modification through the final state interactions encoded in the SIDIS/Drell-Yan staple link structures.

- The generalized tensor charge

$$\frac{\tilde{h}_1^{[1](0)}}{\tilde{f}_1^{[1](0)}} = -\frac{\tilde{A}_{9B}(-b_T^2, b \cdot P = 0, \hat{\zeta}, \eta v \cdot P) - \frac{1}{2}m_N^2 b^2 \tilde{A}_{11B}(-b_T^2, b \cdot P = 0, \hat{\zeta}, \eta v \cdot P)}{\tilde{A}_{2B}(-b_T^2, b \cdot P = 0, \hat{\zeta}, \eta v \cdot P)} \quad (6.63)$$

is also a T-even quantity. In contradistinction to the previous observables, it does not involve any weighting with  $k_T$  and is directly related to the well-known transversity and unpolarized distribution functions. It is interpreted as a generalized tensor charge because, in the formal  $b_T \rightarrow 0$  limit, the numerator corresponds to the integral of the transversity distribution, i.e., the standard tensor charge. It is again normalized to the corresponding number of valence quarks. It should however be emphasized that the additional divergences that arise in the  $b_T \rightarrow 0$  limit require further renormalization, as a consequence of which the ratio of tensor to vector renormalization constants,  $Z_T/Z_V$ , has to be accounted for when connecting the generalized tensor charge to the standard tensor charge.

Note, in particular, that the ratios considered in Eqs. (6.60)-(6.63) cancel any multiplicative renormalization and soft factors associated with the  $\tilde{A}_{iB}$  amplitudes at finite  $b_T$ . It should be emphasized, however, that the multiplicative nature of the renormalization and soft factors

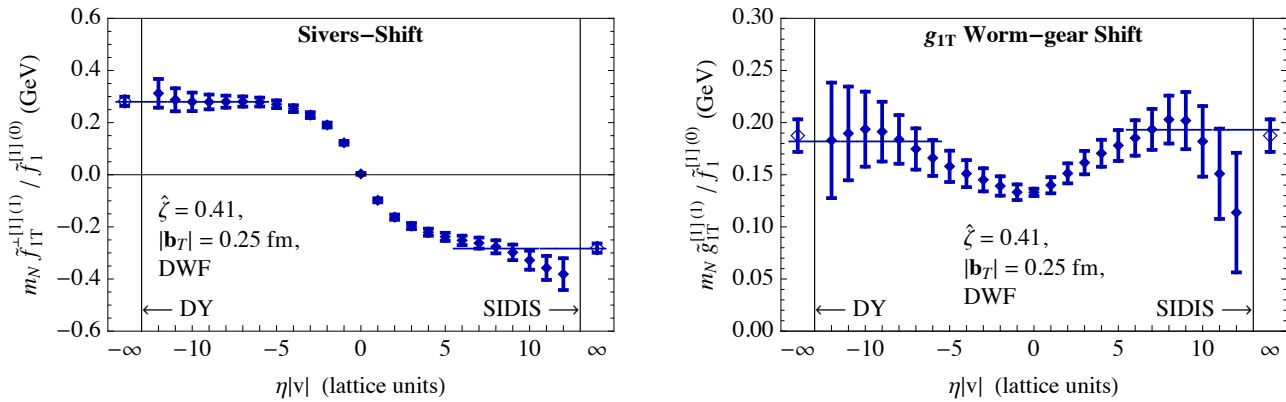


Figure 6.14: Dependence of TMD observables on the staple length. Left: T-odd isovector ( $u - d$  quark) generalized Sivers shift at fixed  $b_T$  and  $\hat{\zeta}$ . Right: T-even isovector generalized  $g_{1T}$  worm-gear shift at fixed  $b_T$  and  $\hat{\zeta}$ . Data were obtained on a domain wall fermion (DWF) ensemble at pion mass  $m_\pi \approx 300$  MeV and lattice spacing  $a = 0.084$  fm. Horizontal lines indicate averages of the data points in the ranges  $\eta|v| \geq 6a$  and  $\eta|v| \leq -6a$ , respectively, where plateau behavior is expected. Extrapolations at  $\eta|v| = \pm\infty$  are obtained as mean values of the aforementioned averages (with a relative minus sign in the case of the Sivers shift). Plot taken from Ref. [142].

obtained in the continuum theory is not immediately guaranteed to transfer to the lattice formulation; the renormalization pattern of the lattice quantities requires separate consideration depending on the concrete discretization employed, as is discussed below in connection with Fig. 6.19.

### *Systematic behavior of lattice TMD observables – numerical studies*

As already indicated in the above discussion, a number of challenges have to be addressed in order to arrive at controlled predictions for TMD observables that can be connected to phenomenology. For one, whereas the extrapolation to infinite staple length  $\eta$  is fairly straightforward, accessing the relevant  $\hat{\zeta}$  regime is more difficult, since it requires data at sufficiently high hadron momenta. Secondly, the purported cancellation of renormalization and soft factors in ratios such as in Eqs. (6.60)-(6.63) requires reexamination in the context of LQCD. Thirdly, progress towards the physical quark masses must be made in lattice TMD calculations; initial studies were performed at artificially large quark masses for reasons of computational cost. In addition, early explorations of TMD observables focused on the point  $b \cdot P = 0$ , see Eqs. (6.60)-(6.63); since the longitudinal component of  $b$  is Fourier conjugate to the longitudinal momentum fraction  $x$ , setting  $b \cdot P = 0$  corresponds to evaluating only the  $x$ -integral of TMDs. To access the  $x$ -dependence of TMD observables, the numerical studies must be extended to include scans of the  $b \cdot P$  direction. Furthermore, it is necessary to buttress these lattice TMD investigations by performing quantitative studies of the scaling with the lattice spacing  $a$ , in order to gain nonperturbative understanding of TMD evolution (lattice calculations of the CS kernel governing rapidity evolution are discussed in Section 6.4.3). In addition, the finite lattice size effects influencing the behavior of nonlocal operators such as the one in Eq. (6.55) remain to be understood, cf. related considerations in Ref. [692].

Significant progress has been made in addressing these challenges. Fig. 6.16 displays a

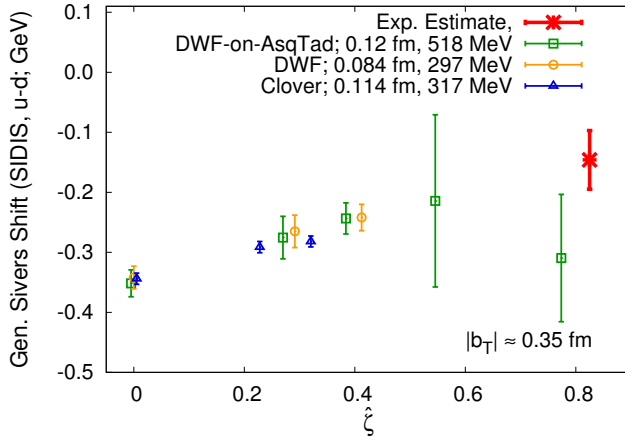


Figure 6.15: Compilation of LQCD results for the Sivers shift, compared to a phenomenological estimate obtained by constructing the Sivers shift from the results of the phenomenological analysis [322], as described in Ref. [142]. Lattice results from several studies combine to a consistent picture, with no significant dependence on the pion mass apparent in the range covered. The trend of the lattice data as a function of the Collins-Soper-type parameter  $\hat{\zeta}$  suggests that agreement between lattice and phenomenological estimates is within reach as lattice studies progress towards larger  $\hat{\zeta}$ . Plot taken from Ref. [142].

result of a dedicated study [141] of the large  $\hat{\zeta}$  regime using the example of the Boer-Mulders shift in the pion. The Boer-Mulders shift measures the average transverse momentum of quarks polarized in the transverse direction orthogonal to the given momentum, in an unpolarized hadron. The pion, by virtue of its lower mass compared with that of the nucleon, allows one to access higher  $\hat{\zeta}$  (note that the hadron mass enters the denominator of  $\hat{\zeta}$ ). This case demonstrates a stable extrapolation to the large  $\hat{\zeta}$  limit, with the signal surviving in the limit. To obtain data of similar quality for the nucleon, it is necessary to employ the momentum smearing method [693]. Lattice TMD studies underway at the time of this writing incorporate this technique.

On the other hand, the question to what extent the multiplicative nature of renormalization and soft factors carries over from the continuum theory to the lattice formulation was investigated empirically in Ref. [142] by varying the lattice discretization scheme. If lattice calculations are beset by deviations from purely multiplicative behavior of the renormalization factors, then the latter would cease to cancel in TMD ratios such as Eqs. (6.60)-(6.63). Being a discretization effect, this would be expected to depend significantly on the type of discretization employed, and therefore manifest itself in a dependence of TMD ratios on the discretization scheme. In Ref. [142], calculations were performed on two ensembles at pion masses close to 300 MeV which differ substantially in discretization: A domain wall fermion ensemble with lattice spacing  $a = 0.084 \text{ fm}$ , and a clover fermion ensemble with  $a = 0.114 \text{ fm}$ . Fig. 6.17 displays a result obtained for the Sivers shift, exhibiting consistent results, corroborating the cancellation of renormalization factors in the ratio in Eq. (6.60) expected from continuum QCD. On the other hand, cf. Fig. 6.18, in the case of the  $g_{1T}$  worm-gear shift, a significant discrepancy is observed at small separations  $b_T$ , which is exacerbated, extending

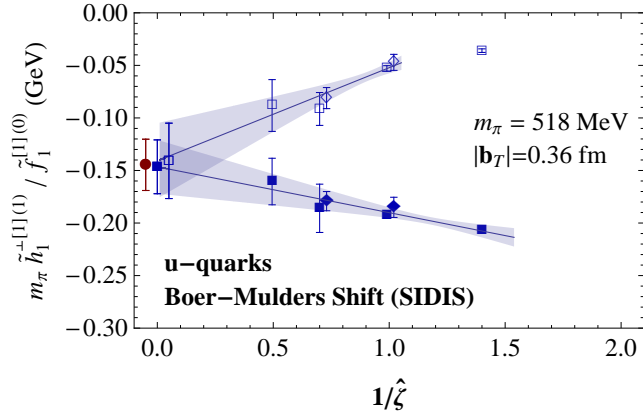


Figure 6.16: Pion  $u$ -quark SIDIS generalized Boer-Mulders shift as a function of  $1/\hat{\zeta}$  at a fixed  $b_T$ . Full symbols show full shift, open symbols a partial contribution that dominates the shift at large  $\hat{\zeta}$ ; extrapolations of the two data sets (blue data points at  $1/\hat{\zeta} = 0$ ) coincide, indicating that a stable description of the large  $\hat{\zeta}$  evolution has been achieved. Red data point at  $1/\hat{\zeta} = 0$  results from a combined fit to both data sets. Only connected contributions to the Boer-Mulders shift were included. Plot taken from Ref. [141].

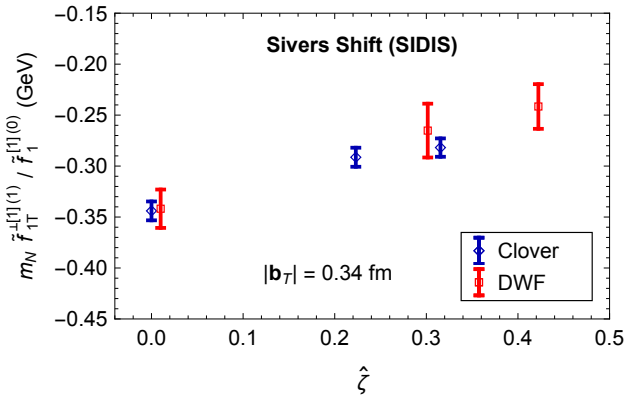


Figure 6.17: Nucleon isovector ( $u - d$  quark) SIDIS generalized Sivers shift as a function of  $\hat{\zeta}$  at a fixed  $b_T$ . Shown are results for an  $a = 0.114$  fm clover ensemble and an  $a = 0.084$  fm domain wall fermion ensemble at pion masses near 300 MeV; the results are compatible with one another, indicating that the effects of renormalization and soft factors are successfully canceled in the Sivers shift ratio in Eq. (6.60). Plot taken from Ref. [142].

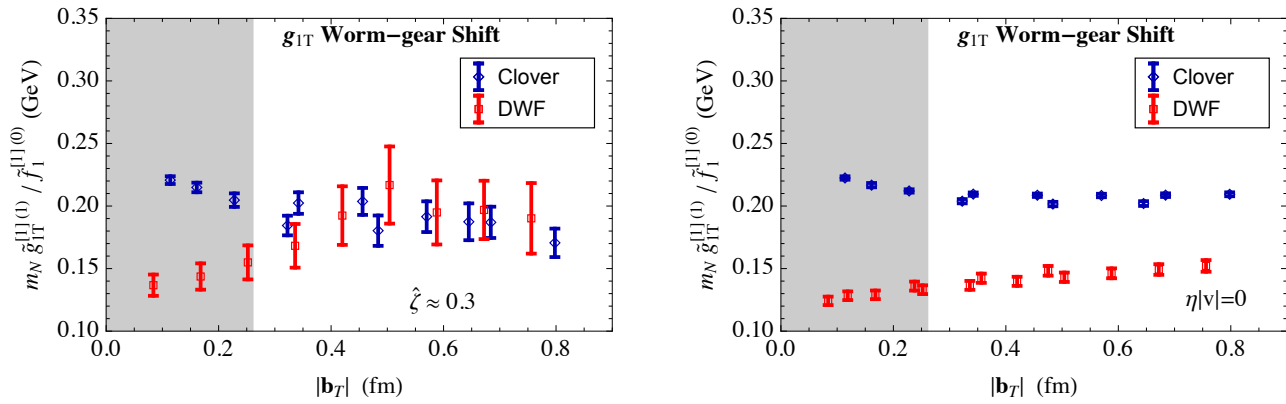


Figure 6.18: Left: Isovector ( $u - d$  quark) SIDIS generalized  $g_{1T}$  worm-gear shift as a function of  $b_T$  at a fixed  $\hat{\zeta}$ , comparing results obtained using clover and domain wall fermions. Right: Isovector straight-link generalized  $g_{1T}$  worm-gear shift as a function of  $b_T$ , comparing results obtained using clover and domain wall fermions; the two panels were obtained using the same nucleon momenta in the lattice calculation. The shaded areas indicate the regions which may be subject to significant lattice artefacts even in the absence of operator mixing. Plot taken from Ref. [142].

to all  $b_T$ , if one instead uses an operator with a straight gauge connection, as employed, e.g., in the PDF studies discussed in Sec. 6.3.

Significant progress has been made in understanding the operator mixing effects underlying these observations in more detail. Triggered by the breaking of chiral symmetry in fermion discretization schemes such as the clover discretization, operator mixing invalidates the simple cancellation of renormalization factors in TMD ratios such as in Eqs. (6.60)-(6.63). The mixing pattern for clover fermions in lattice perturbation theory was derived both for the straight gauge link [613] and the staple-link [694] cases; the fact that a discrepancy between clover fermion and domain wall fermion results is seen specifically in the  $g_{1T}$  worm gear shift, as discussed above and displayed in Fig. 6.18, is consistent with this mixing pattern obtained in lattice perturbation theory. The pattern of mixing can be further understood using an auxiliary field approach to recast bilocal quark operators in terms of local operators, as laid out for straight gauge links in Ref. [607], and extended to staple links in Ref. [620]. The nonperturbative mixing pattern for quark bilinear operators with staple-shaped gauge connections in the RI'/MOM scheme was explored in Ref. [192] where mixing patterns were found that extend beyond those found in one-loop perturbative calculations; a sample result for purely transverse quark operator separation  $b$  is shown in Fig. 6.19. Lattice TMD calculations must take into account these more complex renormalization patterns. One avenue is the use of chirally symmetric formulations such as domain wall fermions in order to avoid certain operator mixings, another is to use a scheme along the lines put forward in Refs. [607, 620] to correctly incorporate mixing effects in clover fermion calculations.

Progress has also been achieved in terms of extending lattice TMD calculations to the physical quark masses. Recent calculations have yielded the first results for TMD observables at the physical values of the quark masses, employing a RBC/UKQCD domain wall fermion ensemble with a lattice spacing  $a = 0.114$  fm [695]. Results from a preliminary analysis are exhibited in Fig. 6.20. Comparing the left panel with the left panel of Fig. 6.14, displayed at similar values of  $b_T$  and  $\hat{\zeta}$ , there appears to be no marked dependence of the isovector

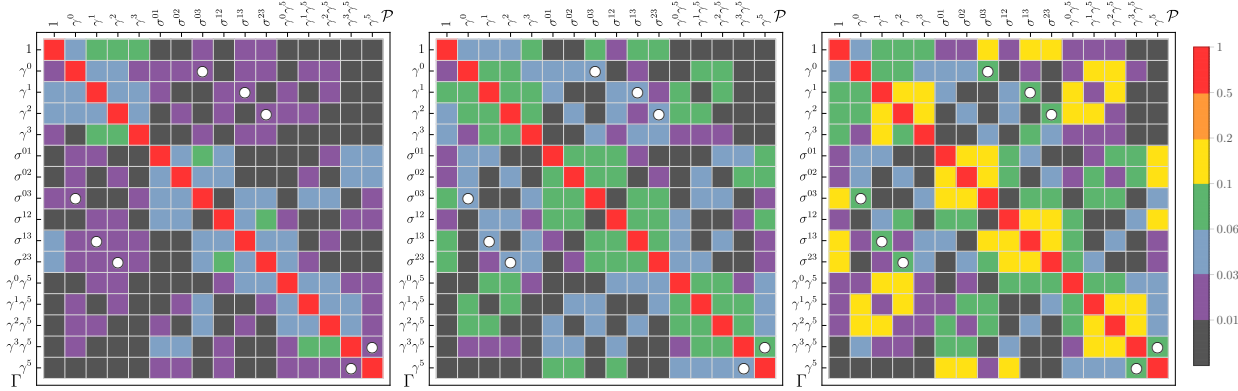


Figure 6.19: Mixing pattern in the RI'/MOM scheme for quark bilinear operators with staple-shaped gauge links constructed using improved Wilson fermions. The quark operator separation  $b$  is purely transverse, with  $b_T/a = 3, 7, 11$  from left to right, where  $a = 0.06$  fm denotes the lattice spacing. The staple length is given by  $\eta/a = 14$ . Colors indicate mixing strengths. White circles indicate mixings already obtained in one-loop lattice perturbation theory [694]. Plot taken from Ref. [192].

generalized Sivers shift on the quark masses in the explored range, extending all the way to the physical quark masses. The right panel of Fig. 6.20 shows results for the generalized tensor charge, cf. Eq. (6.63), in the SIDIS limit as a function of  $b_T$ .

Lattice TMD calculations have also been extended to include the dependence on the longitudinal momentum fraction  $x$ , by performing scans of the matrix element in Eq. (6.55) in the  $b \cdot P$  direction;  $b \cdot P$  is Fourier conjugate to  $x$ . The geometries employed in performing this scan must obey the relation [140]

$$\frac{v \cdot b}{v \cdot P} = \frac{b \cdot P}{m_N^2} \left( 1 - \sqrt{1 + 1/\hat{\zeta}^2} \right), \quad (6.64)$$

which constitutes a Lorentz-invariant expression of the standard TMD kinematics. This forces one to use general off-axis directions on the lattice, which significantly complicates the analysis. On the other hand, an important simplification that arises is that the soft factors depend only on the transverse separation  $b_T$ . This is due to the staple-link structure of the gauge connection for TMDs. Consequently, the soft factors can be factored outside the longitudinal Fourier transformation to  $x$ -space. As a result, the cancellation of soft factors in ratios in  $b$ -space extends to ratios of longitudinal Fourier transforms, i.e., one can obtain renormalized  $x$ - and  $b_T$ -dependent TMD ratios, without having to construct the soft factors explicitly. The results of a preliminary exploration displayed in Fig. 6.21 indicate that it is feasible to obtain the  $x$ -dependence of TMD ratios in this fashion. This has motivated a new calculation underway as of this writing [696].

The above discussion has focused on TMD spin structure, evaluating ratios of TMD moments of different spin content, chiefly for the isovector,  $u - d$ , flavor combination. The reason for the isovector combination being favored in the presentation of results lies in the fact that the computationally expensive contributions from disconnected diagrams, which have hitherto not been evaluated in the lattice TMD program, exactly cancel in the isovector case. Flavor-separated quantities are subject to an additional systematic uncertainty unless these

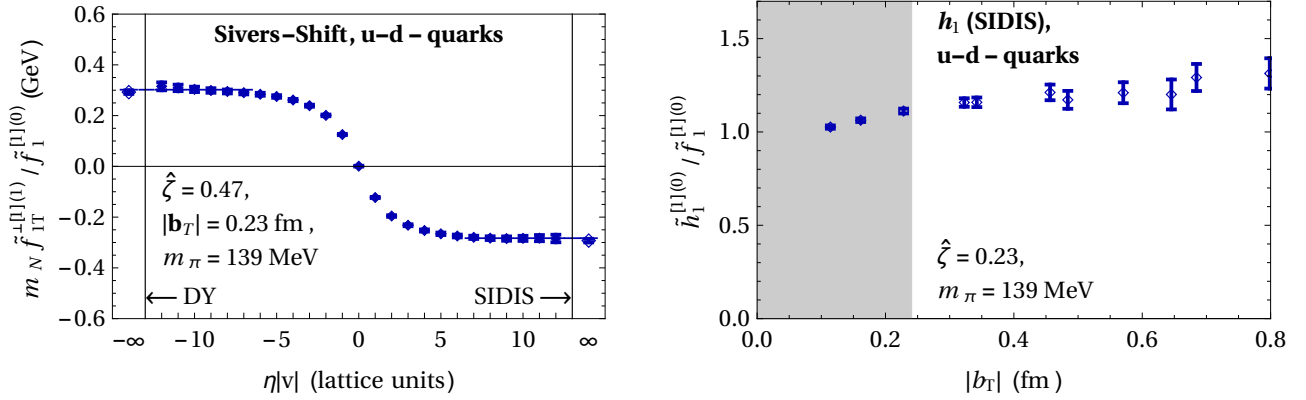


Figure 6.20: Preliminary analysis of nucleon lattice TMD data at the physical quark masses. Left: Isovector generalized Sivers shift as a function of staple length  $\eta$  at fixed  $b_T$  and  $\hat{\zeta}$ . Right: Isovector generalized tensor charge in the SIDIS limit as a function of  $b_T$  for fixed  $\hat{\zeta}$ . Shaded area indicates region which may be subject to significant lattice artefacts. Data were obtained using domain wall fermions at lattice spacing  $a = 0.114$  fm. Plot taken from Ref. [695].

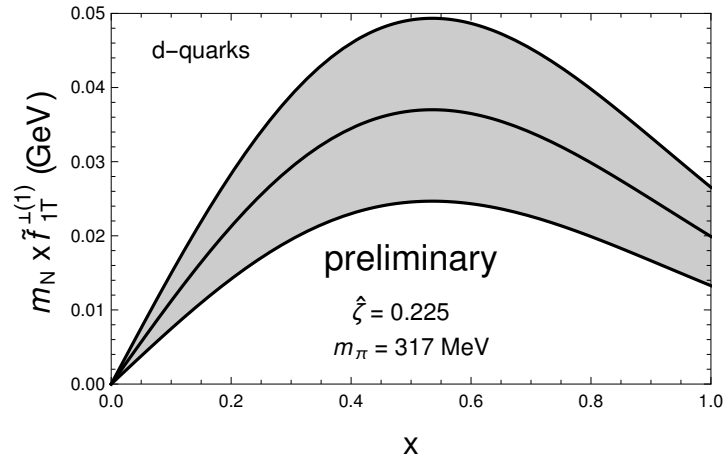


Figure 6.21: Nucleon SIDIS  $d$ -quark generalized Sivers shift as a function of momentum fraction  $x$ , multiplied by  $x$ , evaluated at  $b_T = 0.34$  fm at fixed  $\hat{\zeta} = 0.225$ . Data were obtained using a clover fermion ensemble at  $m_\pi = 317$  MeV. This preliminary analysis, performed at rather low  $\hat{\zeta}$ , still significantly violates constraints such as the limit of support to  $x \leq 1$ ; comprehensive studies in progress as of this writing are anticipated to properly account for these properties.

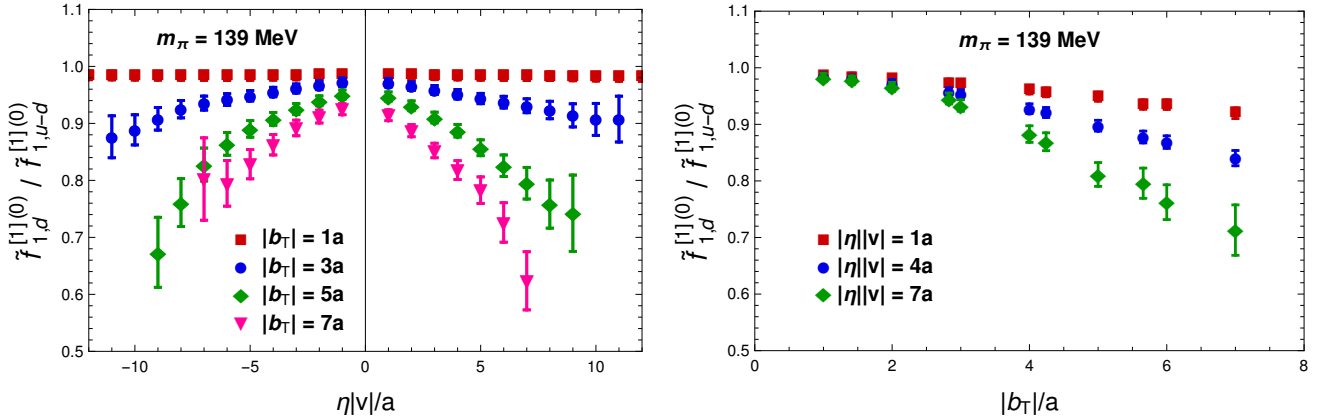


Figure 6.22: Ratio of unpolarized TMD moments of different flavor content  $f_{1,d}^{[1](0)} / f_{1,u-d}^{[1](0)}$  obtained at the physical quark masses for  $\hat{\zeta} = 0.23$ . Left: as a function of staple length  $\eta$ , for selected  $|b_T|$ ; right: as a function of  $|b_T|$  for selected  $|\eta|$ , where for each choice of  $|\eta|$ , the data for  $\eta = \pm|\eta|$  have been averaged. Disconnected contributions to the  $d$ -quark distribution are omitted, cf. main text. Data were obtained using domain wall fermions at lattice spacing  $a = 0.114$  fm [695].

contributions are evaluated. Nonetheless, input on the relative  $u$ -quark vs.  $d$ -quark behavior of TMDs is highly desirable for phenomenological studies [697], and can be presented in the form of ratios of TMD moments of different flavor content rather than spin content. Taking recourse to the recently obtained lattice TMD data at the physical quark masses [695] already highlighted above, obtained using domain wall fermions at lattice spacing  $a = 0.114$  fm, Fig. 6.22 displays preliminary results for the ratio of unpolarized TMD moments  $f_{1,d}^{[1](0)} / f_{1,u-d}^{[1](0)}$ . Note that the ratio  $f_{1,u}^{[1](0)} / f_{1,u-d}^{[1](0)}$  contains no additional independent information, since

$$\frac{f_{1,u}^{[1](0)}}{f_{1,u-d}^{[1](0)}} = \frac{f_{1,d}^{[1](0)}}{f_{1,u-d}^{[1](0)}} + 1 \quad (6.65)$$

Note furthermore that the correction due to the omitted disconnected contributions would be identical for both flavors, such that Eq. (6.65) would continue to hold. Fig. 6.22 implies that the  $d$ -quark distribution is suppressed compared to the  $u$ -quark distribution as either  $|b_T|$  or  $|\eta|$  increases. For  $\eta$  close to zero, i.e., in the absence of final state interactions, the dependence on  $b_T$  appears fairly weak, whereas it strengthens as final state interactions are included. Conversely, in terms of transverse momentum  $k_T$ , one therefore expects the  $d$ -quark distribution to decay more slowly with rising  $k_T$  than the  $u$ -quark distribution. The displayed data were obtained for  $\hat{\zeta} = 0.23$ , but analogous results for  $\hat{\zeta} = 0.47$  and  $\hat{\zeta} = 0.70$  do not differ significantly from those shown. In contrast to ratios with different spin content, the large- $|\eta|$  asymptotic limit is not readily reached in these ratios with different flavor content. This behavior remains to be understood and calls for further investigation.

TMD observables, as discussed in this section, are derived from the matrix element in Eq. (6.55) in the forward limit,  $P' = P$ . On the other hand, lattice studies of the type presented here can also be generalized to nonzero momentum transfer in the transverse direction utilizing largely the same techniques, thus yielding GTMD observables. Such studies have been carried

out, e.g., with a view to extracting information about quark orbital angular momentum in the proton. They are discussed in further detail in Sec. 11.5.

### 6.4.2 Calculation of TMD soft function and TMDPDF

Over the past few years, much progress has been made towards the theoretical development of direct calculations of TMDs using the LaMET approach [104, 183–191]. To calculate TMDPDFs in this approach, one starts by constructing a quasi TMDPDF [104, 183, 184]. For example, for quark of flavor  $i$ , the  $\overline{\text{MS}}$  quasi TMDPDF is defined in Eq. (2.168) as

$$\hat{f}_i^{\text{TMD}}(x, \mathbf{b}_T, \mu, P^z) = \int \frac{db^z}{2\pi} e^{ib^z(xP^z)} \tilde{Z}'_i(b^z, \mu, \tilde{\mu}) \tilde{Z}_{uv}^i(b^z, \tilde{\mu}, a) \\ \times \hat{f}_i(b^z, \mathbf{b}_T, a, P^z, \eta) / \sqrt{\tilde{S}^i(b_T, a, \eta)},$$

where  $b^\mu = (0, \mathbf{b}_T, b^z)$ . Here,  $\hat{f}_i$  and  $\tilde{S}^i$  are the quasi beam and quasi soft functions, which are the analogs of the unsubtracted beam and soft functions. The lattice renormalization factor is  $\tilde{Z}_{uv}^i$ , and  $\tilde{Z}'_i$  converts from the lattice renormalization scheme to the  $\overline{\text{MS}}$  scheme. The lattice renormalization scale  $\tilde{\mu}$  is distinguished from the  $\overline{\text{MS}}$  scale  $\mu$ . In lattice calculations, the Wilson lines that enter  $\hat{f}_i$  and  $\tilde{S}^i$  necessarily have a finite extension  $\eta$  chosen to be in the  $\hat{z}$  direction, which is associated with rapidity regularization and its dependence cancels between  $\hat{f}_i$  and  $\tilde{S}^i$ . Finally,  $\hat{f}_i^{\text{TMD}}$  also depends on the proton momentum  $P^z$  which acts as the analog of the Collins-Soper scale  $\zeta$ , and it was suggested that one can access information of the Collins-Soper evolution through the  $P^z$ -dependence [183].

The quasi beam function is defined in Eq. (2.167) as

$$\hat{f}_i(b^z, \mathbf{b}_T, a, P^z, \eta) = \frac{1}{2} \langle p(P, S) | \bar{\psi}_i^0(b^\mu/2) \Gamma W_{\square\eta}^{\hat{z}}(b^\mu/2, -b^\mu/2) \psi_i^0(-b^\mu/2) | p(P, S) \rangle,$$

where  $\Gamma$  can be chosen as either  $\Gamma = \gamma^0$  or  $\Gamma = \gamma^z$ . As for the quasi soft function, its definition is not unique, and a naive choice is the vacuum matrix element of a rectangle-shaped Wilson loop along the  $z$  direction,

$$\tilde{S}^q(b_T, a, \eta) = \frac{1}{N_c} \langle 0 | \text{Tr} \{ W_{-\hat{z}}(\mathbf{b}_T; 0, -\eta) W_{-\hat{z}}(\mathbf{b}_T; \eta, 0) W_{\hat{b}_T}(\eta\hat{z}; 0, b_T) \\ \times W_{\hat{z}}(0; 0, \eta) W_{\hat{z}}(0; -\eta, 0) W_{\hat{b}_T}(-\eta\hat{z}; b_T, 0) \} | 0 \rangle, \quad (6.66)$$

where the soft Wilson lines  $W_{\pm\hat{z}}$  and  $W_{\hat{b}_T}$  are along the  $\pm z$  and transverse directions respectively.

According to the boost argument in LaMET, the quasi beam function approaches the unsubtracted beam function in the infinite momentum limit, so a perturbative matching is possible between the two. However, the naive quasi soft function fails this argument as it can only be boosted along a single light-cone direction, which is not related to any soft function in TMD factorization. This is demonstrated by an explicit one-loop check [104, 184], where one finds that the quasi and physical TMDPDF differs by an IR logarithm of  $b_T$ , which becomes nonperturbative when  $b_T \sim \Lambda_{\text{QCD}}^{-1}$ . Although by bending the soft Wilson lines by ninety degrees removes this IR logarithm at one loop [104, 183], it was argued that it still exists at two loops due to the mismatch of cusp anomalous dimensions [187].

Nevertheless, with the constraints from RG and Collins-Soper evolutions, as well as from one-loop results [104], it was argued that the non-singlet quasi TMDPDF is related to the physical TMDPDF through

$$\begin{aligned} \hat{f}_{\text{ns}}^{\text{TMD}}(x, \mathbf{b}_T, \mu, P^z) &= C_{\text{ns}}^{\text{TMD}}(\mu, xP^z) g_q^S(b_T, \mu) \exp\left[\frac{1}{2}\gamma_\zeta^q(\mu, b_T) \ln \frac{(2xP^z)^2}{\zeta}\right] \\ &\times f_{\text{ns}}^{\text{TMD}}(x, \mathbf{b}_T, \mu, \zeta) + \mathcal{O}\left(\frac{b_T}{\eta}, \frac{1}{b_T P^z}, \frac{1}{P^z \eta}\right), \end{aligned} \quad (6.67)$$

where  $\gamma_\zeta^q(\mu, b_T)$  is the Collins-Soper evolution kernel, and  $C_{\text{ns}}^{\text{TMD}}$  is a perturbative matching coefficient that is diagonal in  $x$ -space and is also independent of the spin structure [189–191]. The nonperturbative factor  $g_q^S(b_T, \mu)$  reflects the failure of the naive quasi soft function, but is independent of the external hadron state or quark flavor. The power corrections follow from the hierarchy of scales  $b^z \sim 1/P^z \ll b_T \ll \eta$ .

With the above relation, it was proposed that one can calculate the Collins-Soper kernel [185] and ratios of spin-dependent TMDPDFs by forming ratios of the quasi TMDPDFs in different hadron momentum states and with different spin structures [104, 190], as both  $g_q^S(b_T, \mu)$  and the quasi soft function cancel out.

More recently, an important step forward has been made with the proposal [187] to calculate the soft function for TMD PDFs. In this proposal, the rapidity-independent part of the CSS soft function, which is named as the reduced soft factor  $S_r(b_T, \mu)$ , can be calculated through a time-like soft factor in heavy-quark effective theory on the lattice or a pion form factor. The latter method features a form factor defined as

$$F(b_T, P^z) = \langle \pi(-P) | j_1(b_T) j_2(0) | \pi(P) \rangle, \quad (6.68)$$

where  $j_1$  and  $j_2$  are light-quark currents separated in the transverse plane, and the initial- and final-state pions travel with opposite momenta. In the large momentum limit, it is proposed that the above form factor can be factorized as [187]

$$F(b_T, P^z) = S_q^r(b_T, \mu) H(x, \mu) \otimes \Phi^\dagger(x, b_T, P^z, \mu) \otimes \Phi(x, b_T, P^z, \mu) + \dots, \quad (6.69)$$

where  $H(x, \mu)$  is a matching coefficient,  $\Phi$  is a quasi light-cone distribution amplitude defined with the same operator for the quasi beam function, and  $\dots$  are power corrections. The square root of the reduced soft function  $S_r(b_T, \mu)$  can be identified as  $g_q^S(b_T, \mu)$  in Eq. (6.67).

This method has been applied for the first lattice calculation of the reduced soft function in Ref. [698], with the result shown in Fig. 6.23. The result was obtained with tree-level matching at different pion momentum. The agreement with perturbative prediction at small  $b_T$  and insensitivity to the pion momentum  $P^z$  is a promising sign of the effectiveness of this method. A new calculation with reduced operator mixing was carried out in Ref. [699], and similar agreement with perturbation theory has also been observed. Finally, with the calculation of the quasi TMDPDF, the physical TMDPDF as well as the Drell-Yan cross section can be completely determined from LQCD [188]. This has also facilitated the method to calculate phenomenologically interesting TMDs such as the Sivers function [191], as well as light-cone wavefunctions [700].

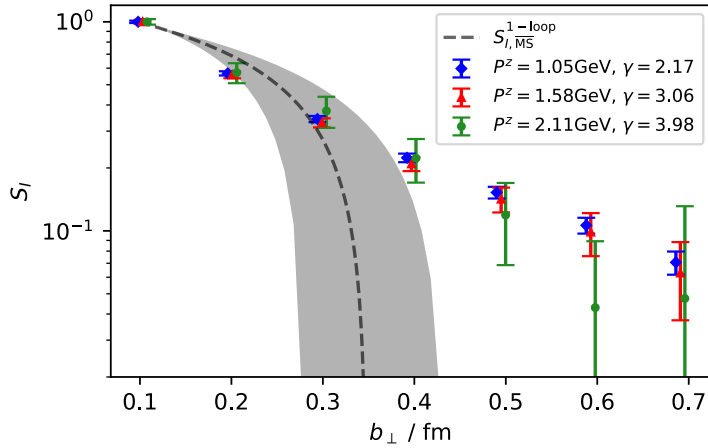


Figure 6.23: The first lattice results of the TMD soft function extracted from the pion form factor at different momentum  $P^z$  with tree-level matching [698]. The dashed line is the one-loop perturbative prediction, which becomes unreliable at  $b_T \sim 0.3$  fm due to reaching the Landau pole. Plot taken from Ref. [698].

#### 6.4.3 Lattice QCD input to TMD evolution

In addition to calculations of key TMD observables, as described in the preceding subsections, LQCD can provide important constraints on the Collins-Soper evolution kernel, also known as the rapidity anomalous dimension, which governs TMD evolution as discussed in Chapter 4. This kernel is nonperturbative for small parton transverse momentum  $q_T \sim \Lambda_{\text{QCD}}$ , and first-principles calculations of this quantity would provide insight into the discrepancies in phenomenological determinations of the kernel in this region [315].

Methods to determine the Collins-Soper kernel from LQCD have been developed in Refs. [104, 185, 186, 189], based on the identification of the kernel with the ratio of quasi TMDPDFs  $\tilde{f}_{\text{ns}}^{\text{TMD}}$ :

$$\gamma_\zeta^q(\mu, b_T) = \frac{1}{\ln(P_1^z/P_2^z)} \ln \frac{C_{\text{ns}}^{\text{TMD}}(\mu, xP_2^z) \tilde{f}_{\text{ns}}^{\text{TMD}}(x, b_T, \mu, P_1^z)}{C_{\text{ns}}^{\text{TMD}}(\mu, xP_1^z) \tilde{f}_{\text{ns}}^{\text{TMD}}(x, b_T, \mu, P_2^z)} + \mathcal{O}\left(1/(b_T P_i^z)\right). \quad (6.70)$$

In this expression,  $P_i^z \gg \Lambda_{\text{QCD}}$  are the  $z$ -components of the hadron momenta and  $C_{\text{ns}}^{\text{TMD}}$  is a perturbative matching coefficient that has been obtained at one-loop order [104, 185]. The quasi TMDPDF  $\tilde{f}_{\text{ns}}^{\text{TMD}}$  is defined as

$$\tilde{f}_i^{\text{TMD}}(x, \vec{b}_T, \mu, P^z) \equiv \lim_{\substack{a \rightarrow 0 \\ \eta \rightarrow \infty}} \int \frac{db^z}{2\pi} e^{-ib^z(xP^z)} \mathcal{Z}_{\gamma^4 \Gamma}^{\overline{\text{MS}}}(\mu, b^z, a) \frac{P^z}{E_P} \tilde{B}_i^\Gamma(b^z, \vec{b}_T, a, \eta, P^z) \tilde{\Delta}_S(b_T, a, \eta). \quad (6.71)$$

Here  $a$  denotes the lattice spacing, the subscript  $i$  is the flavor index, and summation over Dirac structures  $\Gamma$ , is implied. The quasi beam function  $\tilde{B}_i^\Gamma(b^\mu, a, \eta, P^z)$  is defined as the matrix element of a quark bilinear operator with a staple-shaped Wilson line and Dirac structure as in Eq. (6.55), where in this context the space-time coordinates have been shifted and the closure

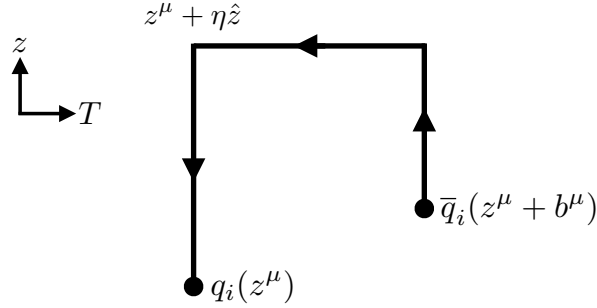


Figure 6.24: Illustration of the staple-shaped Wilson line structure of the nonlocal quark bilinear operators defining quasi beam functions  $\tilde{B}_i^\Gamma(b^\mu, a, \eta, P^z)$ .

of the staple is effected in an asymmetric fashion, as illustrated in Fig. 6.24. The quasi soft factor  $\tilde{\Delta}_S$  [104, 183–185] is also calculable in LQCD, but cancels in the ratio of Eq. (6.70). The factor  $\mathcal{Z}_{\gamma^4 \Gamma}^{\overline{\text{MS}}}(\mu, b^z, a)$  renormalizes the quasi TMDPDF and matches it to the  $\overline{\text{MS}}$ -scheme quasi TMDPDF with Dirac structure  $\gamma^4$  (where ‘4’ indexes the temporal direction) at scale  $\mu$  [186, 192, 694] (the Dirac structure  $\gamma^3$  can also be used to match to the spin-independent TMDPDF in the infinite-momentum limit).

In Refs. [192, 701], an exploratory calculation of the nonperturbative Collins-Soper kernel was undertaken in quenched LQCD, based on the method developed in Refs. [104, 185, 186]. In that calculation, the kernel was extracted over a range of scales  $b_T \in (0.1, 0.8)$  fm. The final results relied on modeling the  $b^z$ -space quasi beam functions to control truncation effects in the Fourier transform; nevertheless, the determination of the Collins-Soper kernel was found to be robust under the variation of models considered. More recently, the calculation of Ref. [702] refined that exploratory study with an updated investigation following the same approach, but using dynamical fermions and more general functional forms as models in  $b^z$ -space.

Complementing the approach of determining the Collins-Soper kernel directly from Eq. (6.70), an alternative strategy using the Mellin moments of the expressions was proposed in Ref. [189] and implemented in a fully-dynamical calculation in Ref. [703] in a study in which the Collins-Soper kernel was determined from three different TMDs ( $f_1, g_{1T}, h_1$ ) for the first time. In that approach, one only needs to calculate the quasi beam function or its derivatives at  $b^z = 0$ . In comparison to the more direct approach of Refs. [104, 185, 186], which requires the numerically-challenging integral over  $b^z$  in the Fourier transform of Eq. (6.71), this reduces the computational cost and has the advantage that renormalization factors cancel in the ratio. However, this approach also requires a nontrivial integration over the TMDPDF that is extracted from experiments, or theory, over a limited kinematic range. Similar methods have been pursued in Ref. [698], which presented the first dynamical calculation of the Collins-Soper kernel, and in Ref. [699], each of which also obtained the kernel via (different) ratios of bare quasi-beam functions at  $b^z = 0$  (i.e., under the assumption that mixing between quasi beam functions with different Dirac structures is negligible, and using leading-order matching). Comparison of results of the various methods will be valuable as calculations advance to phenomenologically-relevant precision; the analysis of Ref. [702] includes an analysis of several approaches, revealing significant systematic differences between the methods even when applied to the same LQCD beam function dataset.

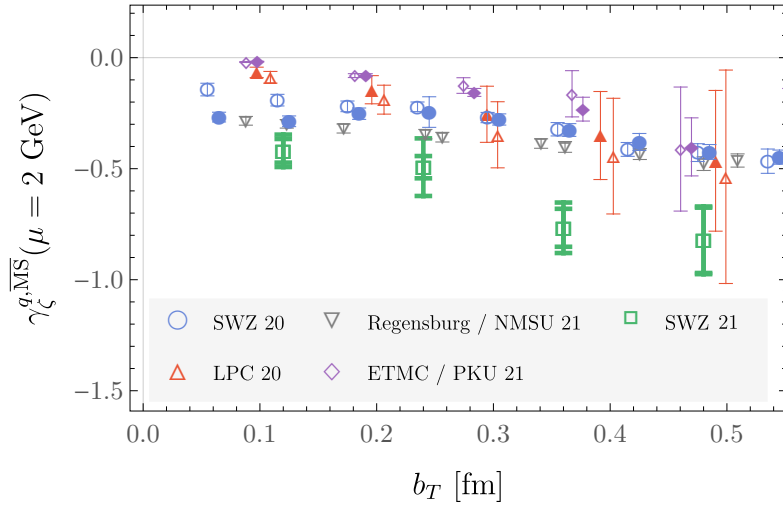


Figure 6.25: Comparison between the Collins-Soper evolution kernel obtained from LQCD calculations in Ref. [701] (SWZ 20), Ref. [698] (LPC 20), Ref. [703] (Regensburg/NMSU 21), and Ref. [699] (ETMC/PKU 21), and Ref. [702] (SWZ 21). Different sets of points with the same color show different sets of results from the same collaboration. Figure adapted from Ref. [702].

Fig. 6.25 summarizes the existing state-of-the-art LQCD calculations of the Collins-Soper kernel. Although the systematic uncertainties remain to be fully controlled, a qualitative conclusion can also already be drawn from the existing results; all LQCD calculations exhibit mild  $b_T$  dependence in the Collins-Soper kernel at large values approaching  $b_T \sim 1$  fm, and it is clear that controlled first-principles calculations of the Collins-Soper kernel at nonperturbative scales as large as  $b_T \sim 1$  fm are tractable with current methods.

#### 6.4.4 Summary

To summarize LQCD approaches to TMDs and the relation of those used to access PDFs, the different methods are compared in Fig. 6.26. With further development, it is expected that lattice QCD will provide systematically controlled predictions for TMD physics.

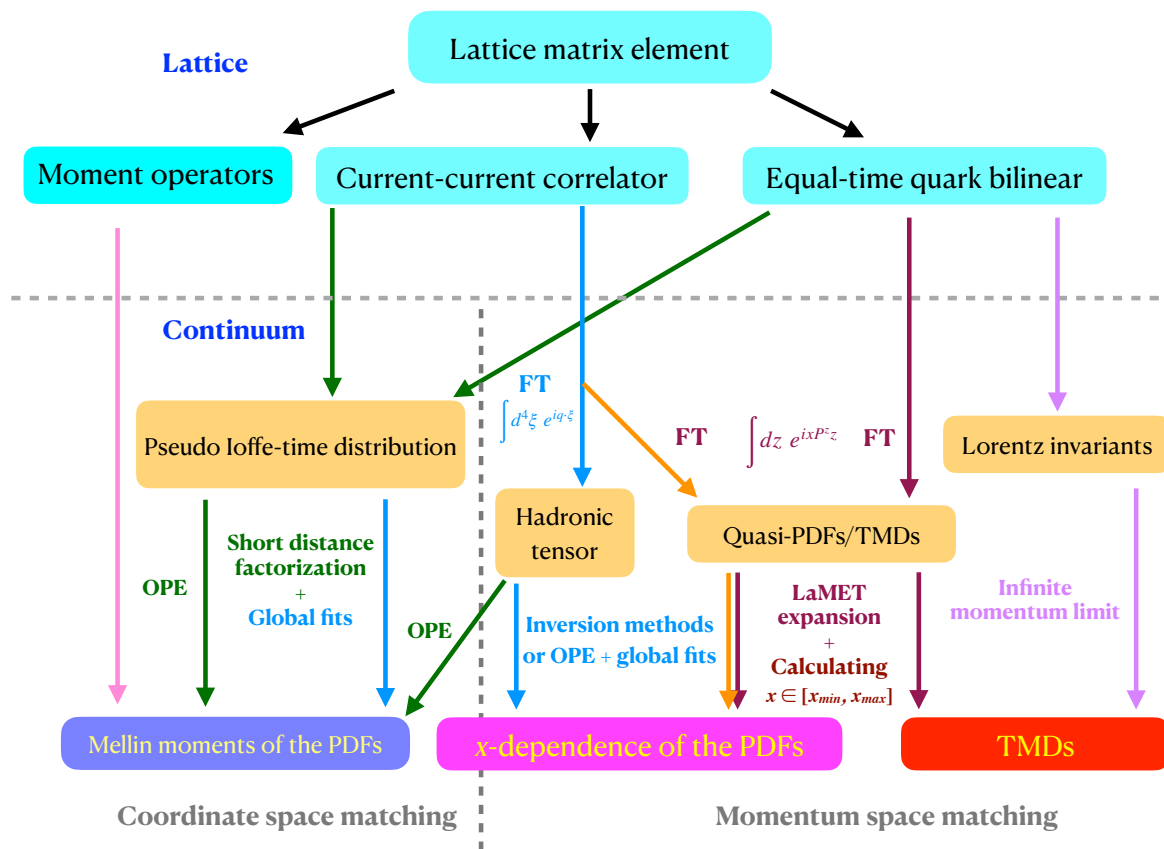


Figure 6.26: Comparison of different approaches to calculate the PDFs and TMDs from lattice QCD.

# 7 - Models

## 7.1 Why Models?

In order to describe the structure of hadrons, it is necessary to solve QCD in the nonperturbative regime. The state-of-the-art first-principle tool for that is LQCD where impressive progress has been made, see Sec. 6. Models are not in competition with lattice studies but provide important complementary tools, and are used in two conceptually different ways.

(i) The first is expository. If there is a point that needs to be made that is independent of the details of the theory, then using a "toy model" can be effective to circumvent technical details of the full theory, and elucidate the underlying physics. Here one often is happy with a "proof-of-principle demonstration" and is not concerned how realistic the used model is, as long as the model shares with QCD the essential features for the considered aspect.

(ii) The second is descriptive. Here the goal is to "approximate QCD" and determine, e.g., the nonperturbative properties of TMD functions as reliably as possible, e.g, in order to produce estimates for cross sections. For that it is important to understand the range of applicability and the limitations of the used models.

Regarding (i), it is worth recalling that model calculations have made a number of important contributions to the understanding of TMD physics. To name a few examples, let us mention the one-loop model calculation in a spectator model with an abelian gauge field [58] which paved the way towards the understanding of T-odd TMDs in QCD [59] and is reviewed in Sec. 7.2. Similarly, model studies of the fragmentation process [704] provided a basis for the understanding of the universality of TMD fragmentation functions [122] which is reviewed in Sec. 7.7.4. As a last example, let us mention that calculations in quark-target models [705] helped to establish that in QCD no relations exist between different TMD functions [706, 707] which will be reviewed in Sec. 7.9.2.

Regarding (ii), let us highlight the many important practical applications of models which range from predictions of new observables, to projections for future experiments, to guiding educated Ansätze for TMD fits, to building Monte Carlo event generators [708]. When phenomenological extractions of TMD functions are available, models allow us to train our physical intuition and interpret the results. If it is possible to explain a certain observation in a model, this can shed valuable light on the underlying physics because in models one can focus on specific aspects of hadronic physics and determine in simplified theoretical frameworks the roles these aspects play for a given process or partonic property.

Progress in TMD physics arises from combined efforts in experiment, perturbative QCD, lattice QCD and phenomenology, and the work in models contributes its share to this.

## 7.2 The Brodsky-Hwang-Schmidt Calculation of a Transverse SSA

In this section, we present a brief discussion of the model calculation by Brodsky, Hwang and Schmidt (BHS) [58] of a transverse SSA, which played an essential role in our understanding of T-odd TMDPDFs and as such had a significant influence on the TMD field. (See also the related discussions in Sec. 2.1 and Sec. 2.7.1.) Specifically, the process

$$\gamma^*(q) + p(P, S_T) \rightarrow q(p) + s(p_s) \quad (7.1)$$

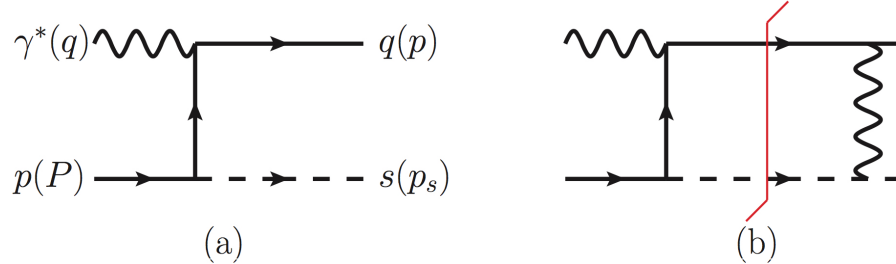


Figure 7.1: Tree-level (left panel) and specific one-loop contribution (right panel) to the process in (7.1). The spectator is indicated by a dashed line. The red line in diagram (b) is the possible on-shell cut, which is essential for generating a transverse SSA. The interaction between the struck quark and the spectator is modeled through the exchange of a single (Abelian) gauge boson. In the model of Ref. [58] the proton carries no electric charge, while the quark charge is  $e_1$  and the spectator charge  $-e_1$ .

was considered, that is, a virtual photon hits a proton producing a quark ( $q$ ) and a spectator ( $s$ ). This reaction was studied in a simple scalar diquark spectator model which, in particular, is characterized by a point-like proton-quark-diquark interaction. The lowest-order diagram of the process is displayed in Fig. 7.1(a). The process in (7.1) can be viewed as a subprocess of SIDIS. Of course, in the real world, the final-state quark will hadronize, where one may consider either semi-inclusive hadron or jet production. However, extending the model to include the hadronization of the quark would not affect the main conclusion of the calculation in Ref. [58], namely, that for the reaction in (7.1) there is a nonzero SSA for a transversely polarized proton. While it had been known since the 1960s that for processes like the one in (7.1) one can have nonzero transverse SSAs [709], the significance of this result for semi-inclusive reactions had not been realized before the BHS paper and a follow-up work by Collins [59].

For definiteness, we consider the Breit frame of the virtual photon, with the photon moving along the negative  $z$ -direction. The proton has the large plus momentum  $Q/\sqrt{2}x$ , where  $x = x_{\text{Bj}} + \mathcal{O}(1/Q^2)$ . The quark carries the large minus momentum  $p^- \approx q^-$  and a small transverse momentum  $\mathbf{p}_T$ . These requirements specify the kinematics according to

$$\begin{aligned} q &= \left( -\frac{Q}{\sqrt{2}}, \frac{Q}{\sqrt{2}}, \mathbf{0}_T \right), & P &= \left( \frac{Q}{\sqrt{2}x}, \frac{xM^2}{\sqrt{2}Q}, \mathbf{0}_T \right), \\ p &= \left( \frac{p_T^2 + m_q^2}{\sqrt{2}Q}, \frac{Q}{\sqrt{2}}, \mathbf{p}_T \right), & p_s &= \left( \frac{Q(1-x)}{\sqrt{2}x}, \frac{x(p_T^2 + m_s^2)}{\sqrt{2}Q(1-x)}, -\mathbf{p}_T \right). \end{aligned} \quad (7.2)$$

The expressions for  $q$  and  $P$  are exact, while for  $p$  and  $p_s$  just the leading terms are listed. The lowest-order diagram in Fig. 7.1(a) alone leads to a vanishing transverse SSA, since this diagram does not have an imaginary part which is a necessary condition for such a spin observable. However, a nonzero transverse SSA can be obtained through the interference of the diagrams in Fig. 7.1(a) and Fig. 7.1(b), with the latter providing the required imaginary part. Averaging over the transverse photon polarizations, summing over the polarizations of the final-state quark and taking a transverse target SSA (with polarization of the proton in the

$y$ -direction) one finds [58]

$$A_{UT,y} = \frac{(e_1)^2}{8\pi} \frac{2(Mx + m_q) p_T^x}{(Mx + m_q)^2 + p_T^2} \frac{p_T^2 + \tilde{M}^2}{p_T^2} \ln \frac{p_T^2 + \tilde{M}^2}{\tilde{M}^2}, \quad (7.3)$$

with  $\tilde{M}^2 = x(1-x)(-M^2 + m_q^2/x + m_s^2/(1-x))$ .<sup>28</sup> The asymmetry vanishes if the transverse momentum of the quark vanishes. We emphasize that  $A_{UT}$  would be zero if there was no interaction between the struck quark and the spectator particle. Initially,  $A_{UT}$  in (7.3) was considered a new leading-twist effect which shows up in the TMD regime of semi-inclusive DIS and which may not even be factorizable [58]. Soon afterwards, however, the non-vanishing asymmetry was shown to be neither a new effect nor in contradiction with QCD factorization [59]. It rather can be understood as a model calculation for the T-odd Sivers function [132, 286], if the gauge link is included in its definition [59]. Therefore, in Ref. [58] it was actually demonstrated for the first time explicitly that T-odd parton distributions can be nonzero. A calculation of the Drell-Yan counterpart of the transverse SSA in Eq. (7.3) showed that this quantity reverses its sign [711],<sup>29</sup> in full agreement with the interpretation of the SSA as a model for the Sivers function and the model-independent prediction of the relative sign of the Sivers function between SIDIS and Drell-Yan [59]. For more discussion of the sign reversal of T-odd TMD PDFs we refer to Secs. 2.1, 2.7.1 and 2.7.2.

## 7.3 Limits in QCD

This section discusses limits in QCD which can be understood as specific models providing guidelines for the understanding of the nonperturbative properties of TMD PDFs.

### 7.3.1 The parton model

Based on Feynman's intuitive ideas [8], the parton model played an important role in establishing QCD as the theory of strong interactions [3, 4]. The formal connection of the parton model to QCD was elucidated in [715]. In many situations, the parton model can be considered the "zeroth order approximation" to QCD although this can not be understood as a rigorous limit. Nevertheless, owing to the asymptotic freedom of QCD, it is not surprising to obtain in this way useful (zeroth order) descriptions of cross sections of many high-energy processes. The calculations of TMD processes in such parton model frameworks are often a good first starting point for phenomenology, see the historical remarks in Secs. 2.1 and 5.1.

One such approach is the generalized parton model of Refs. [125, 127], where, assuming factorization, various processes were studied at tree-level taking into account the transverse motions of partons in the initial hadrons and/or of hadrons originating from a fragmenting parton. Making use of the helicity formalism, the cross sections for the partonic subprocesses were computed at LO with exact (non-collinear) kinematics. This introduces phases in the expressions of the helicity amplitudes describing a process which may lead to cancellations not present when the kinematics in the partonic subprocess is strictly collinear. The purpose of the generalized parton model was not to compute or predict TMD PDFs which were determined by fits to the data. Rather the approach was of value for the phenomenological exploration of

---

<sup>28</sup>The overall sign of the transverse SSA reported in Ref. [58] was incorrect as pointed out in Ref. [710].

<sup>29</sup>The same conclusion was reached in an earlier work [133], but the way the result was obtained could not be justified [711].

TMD processes at early stages when, e.g., the exact TMD PDF definitions were not yet known. A systematic development of parton model concepts is the covariant parton model, Sec. 7.4.1.

### 7.3.2 The large- $N_c$ limit

The limit  $N_c \rightarrow \infty$  is a powerful theoretical tool [716]. In this limit, baryons are described as classical solitons of mesonic fields [717, 718] and their masses grow as  $M \sim N_c$ . While its exact solution in QCD is unknown in 3D, the symmetries of this large- $N_c$  soliton field are known. This information is sufficient [719] to derive relations for the flavor dependence of TMDs [465]. In the situation that  $xN_c$  and  $k_T$  are kept fixed as  $N_c$  grows, the results are summarized in Table 7.1. Analogous relations hold for antiquarks.

In unpolarized (polarized) TMD PDFs, the  $u + d$  ( $u - d$ ) flavor combinations are leading in the large- $N_c$  expansion. Notice that TMD PDFs with a  $\perp$ -label appear with 1 or 2 powers of  $k_T/M$  in the quark correlator, see Eq. (2.124). Due to  $M \sim N_c$  this enhances the large- $N_c$  counting of the corresponding TMD PDFs in Table 7.1. Observables defined as ratios, like spin or azimuthal asymmetries, are generically of order  $N_c^0$ . This is in particular the case for all proton or neutron asymmetries. In the case of the isoscalar deuteron target, however, all spin asymmetries are of order  $1/N_c$ . Even though in nature the number of colors is  $N_c = 3$ , this suppression is seen in experiment, where deuteron spin asymmetries are observed to be systematically smaller than proton (or neutron) spin asymmetries, see Chapter 5.

Let us discuss the prediction  $|f_{1T}^{\perp u} - f_{1T}^{\perp d}|(x, k_T) \sim N_c^3 \gg |f_{1T}^{\perp u} + f_{1T}^{\perp d}|(x, k_T) \sim N_c^2$  from Table 7.1 as an example. Remarkably, in the first extraction of the Sivers function from SIDIS data, where the Sivers effect was clearly seen but the error bars still sizable, this prediction was implemented as a theoretical constraint  $f_{1T}^{\perp u}(x, k_T) = -f_{1T}^{\perp d}(x, k_T)$  neglecting  $1/N_c$ -corrections and gave a very good description of the data [720]. The latest extractions of the Sivers function based on the more precise data support this prediction from [465], see Sec. 5.3.1.

The large- $N_c$  scaling of gluon distribution functions was also discussed in Ref. [721]. For instance, it was shown that  $f_{1T}^{\perp g}(x, k_T) \sim N_c^2$  is suppressed with respect to quark Sivers functions [720], as independently concluded in [722] and supported by phenomenology [723].

### 7.3.3 Non-relativistic limit

Heisenberg's uncertainty principle implies that the constituents of a quantum system move. In systems of the size of  $\mathcal{O}(1 \text{ \AA})$  the motion is non-relativistic to a good approximation. It is instructive to compute the "velocity" and "radius" of a "classical circular orbit" of an electron in Bohr's semi-classical model of hydrogen atom: the "radius" and "velocity" in the  $n^{\text{th}}$  orbit are  $r_n = \frac{1}{\alpha} \lambda_e n$  and  $v_n = \alpha c \frac{1}{n}$  where  $\lambda_e = \hbar/(m_e c)$  is the Compton wavelength of the electron ( $m_e$  is strictly speaking the reduced mass). While not valid in a quantum treatment, such "semi-classical" considerations correctly explain why atoms are relatively large and why they can be treated in non-relativistic quantum mechanics: namely because the electromagnetic

TMD PDF	$f_1^q$	$g_1^q$	$h_1^q$	$f_{1T}^{q\perp}$	$g_{1T}^{\perp q}$	$h_{1L}^{\perp q}$	$h_1^{\perp q}$	$h_{1T}^{\perp q}$
$u + d$	$N_c^2$	$N_c$	$N_c$	$N_c^2$	$N_c^2$	$N_c^2$	$N_c^3$	$N_c^3$
$u - d$	$N_c$	$N_c^2$	$N_c^2$	$N_c^3$	$N_c^3$	$N_c^3$	$N_c^2$	$N_c^4$

Table 7.1: The large- $N_c$  behavior of the  $u \pm d$  flavor combinations of the nucleon TMD PDFs [465].

interaction is relatively weak with  $\alpha \simeq \frac{1}{137}$ . In QCD, for hadrons made of light quarks, like nucleons, one deals with  $\alpha_s(1 \text{ GeV}) = \mathcal{O}(1)$  and a non-relativistic treatment is unjustified.

One may nevertheless ask the question: how would parton distributions look like in a nucleon if the system could be treated in a non-relativistic way? Investigating such questions can give us valuable intuition. For instance, one non-relativistic prediction which gained a lot of popularity, is that transversity and helicity PDFs become equal in the non-relativistic limit,

$$\lim_{\text{non-rel}} h_1^q(x) = \lim_{\text{non-rel}} g_1^q(x). \quad (7.4)$$

This conclusion was derived in Ref. [387] within the bag model (to be discussed below) and has been used to predict observables involving  $h_1^q(x)$  until the first data on this PDF became available, see, e.g., the review article [724] and references therein.

One can introduce a non-relativistic limit for TMD PDFs by working in the constituent quark model limit where quark momenta  $|\mathbf{k}| \ll m_q$  become small, the nucleon size grows, and the constituent quark mass determines the nucleon mass as  $M \rightarrow N_c m_q$  in the limit. Introducing the SU(4) spin-flavor symmetry factors  $N_u = \frac{1}{2}(N_c + 1)$ ,  $N_d = \frac{1}{2}(N_c - 1)$ ,  $P_u = \frac{1}{6}(N_c + 5)$ ,  $P_d = \frac{1}{6}(1 - N_c)$  for general  $N_c$  [725], the non-relativistic limit for the T-even proton TMD PDFs is given by [726]

$$\begin{aligned} \lim_{\text{non-rel}} f_1^q(x, k_T) &= N_q \delta\left(x - \frac{1}{N_c}\right) \delta^{(2)}(\mathbf{k}_T), & \lim_{\text{non-rel}} g_{1T}^{\perp q}(x, k_T) &= P_q N_c \delta\left(x - \frac{1}{N_c}\right) \delta^{(2)}(\mathbf{k}_T), \\ \lim_{\text{non-rel}} g_1^q(x, k_T) &= P_q \delta\left(x - \frac{1}{N_c}\right) \delta^{(2)}(\mathbf{k}_T), & \lim_{\text{non-rel}} h_{1L}^{\perp q}(x, k_T) &= -P_q N_c \delta\left(x - \frac{1}{N_c}\right) \delta^{(2)}(\mathbf{k}_T), \\ \lim_{\text{non-rel}} h_1^q(x, k_T) &= P_q \delta\left(x - \frac{1}{N_c}\right) \delta^{(2)}(\mathbf{k}_T), & \lim_{\text{non-rel}} h_{1T}^{\perp q}(x, k_T) &= -P_q \frac{N_c^2}{2} \delta\left(x - \frac{1}{N_c}\right) \delta^{(2)}(\mathbf{k}_T) \end{aligned} \quad (7.5)$$

If the system is not strictly non-relativistic, the motion of the quarks "smears out" the  $\delta$ -functions. Imagining the transverse motion of quarks to be due to random motion in the transverse plane, one might be tempted to "smear out" the  $\delta^{(2)}(\mathbf{k}_T)$  in terms of Gaussians. While this does not prove anything, it makes the success of the Gaussian Ansatz to some extent plausible. In practical calculations in non-relativistic models the "smearing" of the  $\delta$ -functions in  $x$  and  $\mathbf{k}_T$  is considerable, and we will comment on this below in Sec. 7.5.2.

## 7.4 Modelling of T-even TMD PDFs

T-even TMD PDFs do not require explicit gauge field degrees of freedom in order to be modelled. In this section we will review several such models.

### 7.4.1 Covariant parton model

A consequent exploration of the parton model approach discussed in Sec. 7.3.1 leads to the covariant parton model. In this model, one assumes that the QCD coupling constant  $g(\mu) = 0$  at any scale  $\mu$ . As a consequence, the partons are non-interacting and on-shell making the parton picture, within this model, valid not only in the infinite-momentum frame but in any frame. This is the essence of the covariant parton model [726–731].

In this model, due to the absence of explicit gauge degrees of freedom, the Wilson-lines are replaced by unit matrices in color space, and T-odd TMD PDFs vanish. The quark correlator

entering the definition of TMDs is largely simplified and given, in momentum space, by [730]

$$\Phi^q(k, P, S) = M \Theta(k^0) \delta(k^2 - m^2) (\not{k} + m) (\mathcal{G}^q(P \cdot k) + \mathcal{H}^q(P \cdot k) \gamma^5 \phi). \quad (7.6)$$

Here the notation for the unintegrated quark correlator follows Refs. [60, 61] and is such that from  $\frac{1}{2} \iint dk^+ dk^- \delta(k^+ - xP^+) \text{tr} \Gamma \Phi^q(k, P, S)$  with  $\Gamma = \gamma^+, \gamma^+ \gamma_5, i\sigma^{\alpha+} \gamma_5$ , one recovers the expressions on the right-hand sides of Eq. (2.124). In Eq. (7.6),  $P$  and  $S$  denote the nucleon momentum and polarization vector,  $k$  is the quark momentum with the onshellness of the quarks implemented by  $\Theta(k^0)\delta(k^2 - m^2)$ , and  $\phi = \gamma^\mu \omega_\mu$  with the quark polarization vector  $\omega^\mu$  satisfying  $\omega \cdot k = 0$ ,  $\omega^2 = -1$  and given by

$$\omega^\mu = S^\mu - \frac{M}{m} \frac{k \cdot S}{k \cdot P + mM} k^\mu - \frac{k \cdot S}{k \cdot P + mM} P^\mu. \quad (7.7)$$

The nucleon structure is described in terms of two covariant functions of  $P \cdot k$ :  $\mathcal{G}^q(P \cdot k)$  describes the momentum distribution of unpolarized quarks of flavor  $q = u, d, \dots$  inside the nucleon, and  $\mathcal{H}^q(P \cdot k)$  describes the distribution of polarized quarks. As a result all TMD PDFs are determined in terms of these two functions [726, 729–731].

In the nucleon rest frame,  $P \cdot k = M(\mathbf{k}^2 + m^2)^{1/2}$  and the 3D spherical symmetry becomes apparent which connects longitudinal and transverse quark momenta. As a consequence, in this model it is possible to unambiguously predict TMD PDFs from collinear PDFs [729] which gives predictive power to the approach. The model automatically satisfies the Callan-Gross relation between the unpolarized DIS structure functions, and the Wandzura-Wilczek approximation for the twist-3 collinear PDF  $g_T^a(x)$  becomes exact, namely  $g_T^a(x) = \int_x^1 \frac{dy}{y} g_1^a(y)$  (more on subleading twist in Ch. 10). The Wandzura-Wilczek approximation for  $g_T^a(x)$  is supported by data with a good accuracy, see e.g. Ref. [732] for a brief review. This provides phenomenological support for the covariant parton model. The model can also describe qualitatively the Cahn effect [728], although one of its limitations is that the restriction to onshellness implies unrealistically small transverse parton momenta [728].

The covariant parton model relates the transverse moments of the Kotzinian-Mulders worm-gear functions to the helicity and transversity PDFs as follows [726]

$$g_{1T}^{\perp(1)a}(x) = x \int_x^1 \frac{dy}{y} g_1^a(y), \quad (7.8a)$$

$$h_{1L}^{\perp(1)a}(x) = -x^2 \int_x^1 \frac{dy}{y^2} h_1^a(y), \quad (7.8b)$$

where current quark mass terms are neglected. In QCD these relations are spoiled by the appearance of matrix elements of quark-gluon operators. Assuming these contributions to be small constitutes the WW-type approximation for TMD PDFs. (It is called WW-type approximation to be distinguished from the WW approximation for collinear PDFs because different quark-gluon operators are neglected in both cases.) Based on the positive experience with WW approximation for  $g_T^a(x)$ , one may hope that the approximations (7.8a, 7.8b) are useful for the Kotzinian-Mulders worm-gear functions, though this remains to be tested by data. Presently, little is known about these functions and the WW-type approximations

(7.8a, 7.8b) have been explored for phenomenological applications [210, 461, 462], cf. Sec. 5.5. We stress that in the covariant parton model, the WW-type approximations are exact.

For other studies of transverse parton momentum effects in similar parton model frameworks we refer to Refs. [733–737]. Parton model applications addressing target mass corrections or gluon polarization effects were reported in Refs. [738–741]. The free-quark ensemble model of Ref. [61] is another implementation of the parton model concept.

### 7.4.2 Bag model

This model was introduced in the early 1970s and continues to be useful. In its simplest version, non-interacting quarks are confined inside a spherical cavity with radius  $R$  due to boundary conditions which “simulate” confinement. The nucleon is modelled by placing  $N_c$  quarks in the ground state wave function which has positive parity and is given for massless quarks in momentum space by

$$\Phi_m(\mathbf{k}) = i\sqrt{4\pi}NR^3 \begin{pmatrix} t_0(k)\chi_m \\ \boldsymbol{\sigma} \cdot \hat{\mathbf{k}} t_1(k)\chi_m \end{pmatrix}, \quad N = \frac{\omega^{3/2}}{(2R^3(\omega - 1)\sin^2 \omega)^{1/2}}, \quad \hat{\mathbf{k}} = \mathbf{k}/k, \quad k = |\mathbf{k}|. \quad (7.9)$$

The  $t_i(k)$  are defined as  $t_i(k) = \int_0^1 u^2 du j_i(ukR) j_i(u\omega)$  in terms of spherical Bessel functions,  $\boldsymbol{\sigma}$  denotes the Pauli matrices,  $\chi_m$  the Pauli spinor,  $\omega \approx 2.04$  is the lowest solution of the transcendental bag equation  $\omega_i = (1 - \omega_i) \tan \omega_i$ . The bag model wave function in Eq. (7.9) contains an  $S$ -wave (upper) component with orbital angular momentum  $L = 0$  accompanied by  $t_0$ , and a  $P$ -wave (lower) component with orbital angular momentum  $L = 1$ , accompanied by  $t_1$ . The results for the T-even leading TMD PDFs are given by [13, 742]

$$\begin{aligned} f_1^q(x, k_T) &= N_q A[t_0^2 + 2\hat{k}_z t_0 t_1 + t_1^2], & g_{1T}^{\perp q}(x, k_T) &= P_q A[-2\hat{M}(t_0 t_1 + \hat{k}_z t_1^2)] \\ g_1^q(x, k_T) &= P_q A[t_0^2 + 2\hat{k}_z t_0 t_1 + (2\hat{k}_z^2 - 1)t_1^2], & h_{1L}^{\perp q}(x, k_T) &= P_q A[-2\hat{M}_N(t_0 t_1 + \hat{k}_z t_1^2)] \\ h_1^q(x, k_T) &= P_q A[t_0^2 + 2\hat{k}_z t_0 t_1 + \hat{k}_z^2 t_1^2], & h_{1T}^{\perp q}(x, k_T) &= P_q A[-2\hat{M}_N^2 t_1^2] \end{aligned} \quad (7.10)$$

with the SU(4) spin-flavor symmetry factors as defined below Eq. (7.5) and

$$A = \frac{16\omega^4}{\pi^2(\omega - 1)j_0^2(\omega)M^2}, \quad k = \sqrt{k_z^2 + k_T^2}, \quad k_z = xM - \omega/R, \quad \hat{k}_z = \frac{k_z}{k}, \quad \hat{M} = \frac{M}{k},$$

where  $M$  is the proton mass, and the bag radius is fixed such that  $RM = 4\omega$ . All leading and subleading T-even TMD PDFs were studied in this model, and a complete set of linear and non-linear relations among TMD PDFs was derived [13, 742]. The bag model supports the phenomenologically observed Gaussian  $k_T$ -dependence of TMD PDFs [304].

One drawback of this model is that the bag boundary condition violates chiral symmetry, a feature that can be improved using the so-called cloudy bag model [743]. Another drawback is that it generates unphysical antiquark distributions and the TMD PDFs receive very small but non-zero support for  $x > 1$ . The latter problem can be fixed by employing Peierls-Yoccoz projection techniques, see Ref. [744] for a recent study.

### 7.4.3 Lightfront constituent quark models

In these models, the nucleon structure is modelled in terms of 3-quark lightcone wave functions (LCWFs) which contain information on the bound state properties of the nucleon

in terms of process- and frame-independent amplitudes which are eigenstates of the total quark orbital-angular momentum  $L_z^q$  [745, 746]. The TMD PDFs exhibit multipole patterns [747, 748]: for instance,  $f_1^q$ ,  $g_1^q$ ,  $h_1^q$  are "monopole structures" associated with  $\Delta L_z^q = 0$  (i.e. diagonal in the quark angular momentum components). In contrast,  $g_{1T}^{\perp q}$  and  $h_{1L}^{\perp q}$  correspond to "dipole structures" arising from the interference of S- and P-waves with  $\Delta L_z^q = 1$ , and  $h_{1T}^{\perp q}$  is a "quadrupole structure" associated with  $\Delta L_z^q = 2$  due to the interference of two P-waves or one S-wave and one D-wave [747–750]. Often used approaches for LCWFs include the lightfront constituent quark [747] and chiral quark-soliton [751] models. The lightfront constituent quark model was applied to nucleon and pion TMD PDFs with phenomenological success [471, 752, 753]. Many observables in SIDIS or Drell-Yan were described typically within an accuracy of 10–40 % in the region of  $x \gtrsim 0.1$  where quark models can be expected to work. The approach was extended to subleading functions [754, 755].

#### 7.4.4 Spectator models

The first quark model applied to TMD PDFs was the quark-diquark spectator model [756]. Here the correlator defining TMDs is evaluated by replacing the sum over all intermediate states with a single on-shell spectator thought to be an effective degree of freedom with the nonperturbative effects due to sea quarks and gluons effectively resummed. In models of the nucleon, the spectator can be a spin-0 isoscalar or spin-1 isovector diquark (when modelling pion TMD PDFs, the spectator is another quark or antiquark). The effective nucleon-quark-diquark vertex may be modeled in terms of form factors. Various vertex functions and different choices for diquark masses and axial-vector polarization states have been used in literature [12, 470, 757–761]. The results can be interpreted in terms of the overlap of lightcone wave functions (LCWFs) for the diquark [745]. Several versions of lightcone quark-diquark models were discussed [12, 470, 759, 760]. In these models it is in general not possible to satisfy simultaneously the quark-number and momentum sum rules, a limitation which can be remedied by resolving the internal diquark structure in a dynamical framework [762].

#### 7.4.5 Nambu–Jona–Lasinio framework

The Nambu–Jona–Lasinio model is based on an effective, non-renormalizable 4-quark interaction. The model incorporates one important low-energy aspect of QCD, namely chiral symmetry and its dynamical breaking. Hadronic correlators are evaluated by solving the Faddeev equation in a quark-diquark approximation, including both dynamical scalar and axial vector diquarks. The Nambu–Jona–Lasinio framework can be used to model diquark correlations more realistically. The framework was used to study the transversity parton distribution function [762], and TMD PDFs of  $\rho$ -mesons [763] and pions [764].

#### 7.4.6 AdS/QCD inspired models

The correspondence between 10-dimensional string theories in  $\text{AdS}_5 \times \text{S}^5$  space and conformal  $N = 4$  supersymmetric Yang–Mills theories in 3 + 1 space-time has opened new ways to model QCD in the strong-coupling regime [765]. A lightcone scalar diquark model exploring predictions from a soft-wall AdS/QCD model for the LCWF of the valence quark and the diquark was used to describe TMDs of the pion and nucleon in Refs. [766–768]. The results from this approach met phenomenology with success in Refs. [769, 770].

### 7.4.7 Chiral quark soliton model

This model is based on a low-energy chiral theory describing the interaction of effective quark and antiquark degrees of freedom with Goldstone bosons of the spontaneous chiral symmetry breaking. The Lagrangian is given by  $\mathcal{L} = \bar{\Psi}[i\partial + M \exp(i\gamma_5 \tau^a \pi^a/f_\pi)]\Psi$  in the SU(2) version of the model where  $\pi^a$  denote the pion fields,  $M$  is the dynamically generated quark constituent mass, and  $f_\pi = 93$  MeV the pion decay constant. The UV cutoff of the theory  $\mu_0 \sim \rho^{-1} \sim 600$  MeV is associated with the nonperturbative short-distance scale  $\rho$  at which chiral symmetry breaking occurs. Two distinct nonperturbative scales play important roles for the description of the nucleon structure, namely the scale  $\rho \sim 0.3$  fm associated with chiral symmetry breaking and the scale  $R_{\text{had}} \sim 1$  fm associated with the nucleon size. The interplay of these two distinct nonperturbative scales and their hierarchy,  $\rho \sim 0.3$  fm  $\ll R_{\text{had}} \sim 1$  fm, have profound consequences on TMDs: at a low scale  $\mu_0$  and small  $k_T \lesssim R_{\text{had}}^{-1}$ , valence quarks dominate the  $k_T$ -behavior of TMD PDFs. But in the region  $R_{\text{had}}^{-1} < k_T < \mu_0$  the  $k_T$ -behavior of the TMD PDFs  $f_1^a(x, k_T)$ ,  $g_1^a(x, k_T)$  is dominated by sea quarks, which exhibit slow power-like decays and overwhelm the contribution of valence quarks which decay exponentially in this region [771, 772]. In contrast, the transversity TMD PDF exhibits valence-quark type  $k_T$ -behavior in the entire  $k_T$ -region [771].

### 7.4.8 Predictions from quark models for T-even TMD PDFs

In this section, we discuss results for T-even TMD PDFs from several representative quark models. Let us begin with the  $k_T$ -dependence of the unpolarized TMD PDF. In Chapter 5 we have seen that a lot of phenomenology related to  $k_T$ -effects has been successfully done assuming the Gaussian Ansatz. While there is general consensus that it is merely an approximation, it is a good question to ask why this Gaussian approximation works so well. While we do not know the answer to this question, it is interesting to see what models can teach us.

Let us first stress that no model studied so far exhibits exact Gaussian  $k_T$ -dependence. However, in several models the Gaussian Ansatz appears to be a useful approximation for the exact  $k_T$ -dependence. The Figs. 7.2a and 7.2b show the results from the bag model [13] for  $f_1^u(x, k_T)$  as function of  $k_T$  at selected values of  $0.1 \leq x \leq 0.6$ . The colored lines show exact model results super-imposed on the respective Gaussian approximations. At the low scale of the bag model, the exact numerical results are very well approximated by the Gaussian Ansatz up to  $k_T \lesssim 0.4$  GeV ( $k_T$  larger than that can not be reliably studied in a low energy model with an initial scale of the order of  $\mu_0 \lesssim 0.4$  GeV).

The Gaussian widths used in Figs. 7.2a and 7.2b to depict the Gauss model approximations exhibit a moderate dependence on  $x$  shown in Fig. 7.2c. These widths are defined such that the Gaussian approximations of the true model results is exact in the vicinity of  $k_T = 0$ . One could define the Gaussian widths also as  $\langle k_T^2(x) \rangle = \int d^2 k_T k_T^2 f_1^q(x, k_T) / \int d^2 k_T f_1^q(x, k_T)$ . If the  $k_T$ -dependence in the model was exactly Gaussian, the two definitions would give numerically the same results. The Fig. 7.2c shows that the two definitions of  $\langle k_T^2(x) \rangle$  do not give the same results, but the approximation is very good in the region of  $0.1 \lesssim x \lesssim 0.6$ .

The Gaussian widths of  $f_1^u(x, k_T)$  in Fig. 7.2c are  $\langle k_T^2 \rangle \sim 0.1$  GeV<sup>2</sup>, i.e. about factor 2–3 smaller than what is needed in phenomenology of typical SIDIS experiments [304]. This is to be expected since the model results refer to a low initial scale and evolution broadens the  $k_T$ -dependence. Attempts to implement (approximate or exact)  $k_T$ -evolution starting at low

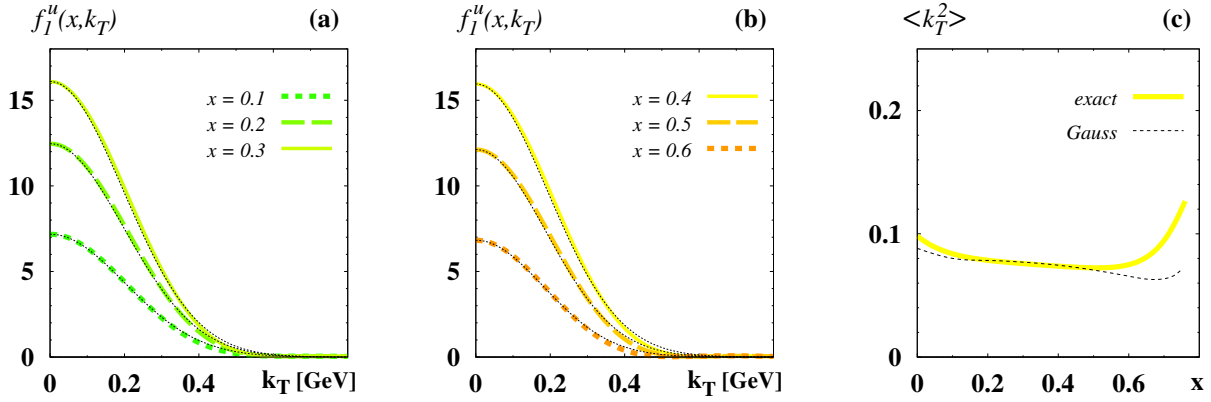


Figure 7.2: The  $k_T$ -dependence of  $f_1^u(x, k_T)$  at (a)  $x = 0.1, 0.2, 0.3$ , and (b)  $x = 0.4, 0.5, 0.6$  in the bag model at a low scale from Ref. [13]. The colored lines are the exact model results. The thin black-dotted lines are the respective Gaussian approximations. (c) The  $x$ -dependence of the exact model results for  $\langle k_T^2 \rangle$  (colored line) vs the Gaussian widths (thin dotted lines) used in parts (a) and (b) of the figure.

initial scales can be found, e.g., in Refs. [471, 730, 752, 753, 773].

In the bag model study of [13], due to SU(4) spin-flavor symmetry,  $f_1^d(x, k_T)$  is exactly one half of  $f_1^u(x, k_T)$ , and exhibits the same  $k_T$ -dependence. The other T-even TMDs  $g_1^q(x, k_T)$ ,  $h_1^q(x, k_T)$ ,  $g_{1T}^{\perp q}(x, k_T)$ ,  $h_{1L}^{\perp q}(x, k_T)$ ,  $h_{1T}^{\perp q}(x, k_T)$  similarly exhibit approximate Gaussian  $k_T$ -behaviors [13]. In conclusion, the relativistic description of the nucleon as a 3-quark bound state in the bag model naturally supports the Gaussian approximation. In other models, the Gaussian  $k_T$ -dependence is also supported to a good approximation, see e.g. [755, 767].

Let us discuss next the  $x$ -dependence of TMD functions. In Figs. 7.3 and 7.4 we show results from 3 different models of the nucleon for  $f_1^q(x)$ ,  $g_1^q(x)$ ,  $h_1^q(x)$ ,  $g_{1T}^{\perp(1)q}(x)$ ,  $h_{1L}^{\perp(1)q}(x)$ ,  $h_{1T}^{\perp(1)q}(x)$ . In models, the integrals over  $k_T$  are convergent or can be simply regularized and, e.g., it is literally  $f_1^q(x) = \int d^2 k_T f_1^q(x, k_T)$ . In QCD, there is no such simple connection between TMD PDFs and collinear PDFs, see Sec. 7.8. Notice that  $f_1^q(x)$ ,  $g_1^q(x)$ ,  $h_1^q(x)$  are collinear PDFs and, especially in the case of  $f_1^q(x)$  and  $g_1^q(x)$ , well known from parametrizations. It is nevertheless interesting to include them in the comparison. As explained in Chapter 5, the usage of transverse moments is convenient in phenomenology (for pretzelosity actually the (2)-transverse moment is more convenient, see Sec. 5.5, but here we prefer to show also the (1)-moment because of its relation to orbital angular momentum in models to be discussed below in Sec. 7.9.4).

The Fig. 7.3 shows the corresponding distributions of  $u$ -quarks in the proton, while in Fig. 7.4 we show the results for  $d$ -quark distributions. The 3 models are the lightcone constituent quark model of Ref. [747], the bag model study of Ref. [13], and the spectator model of Ref. [756]. All results refer to the low initial scales of the models estimated to be around  $\mu_0 \sim (0.3\text{--}0.5)$  GeV. In order to facilitate the comparison of the flavor dependence, we have chosen the same scales for respectively the same TMD PDFs in Figs. 7.3 and 7.4.

It should be stressed that these models have limitations. For instance, they can be expected to be applicable in the valence- $x$  region  $0.1 \lesssim x \lesssim 0.6$  but, e.g., not at small  $x$  where different

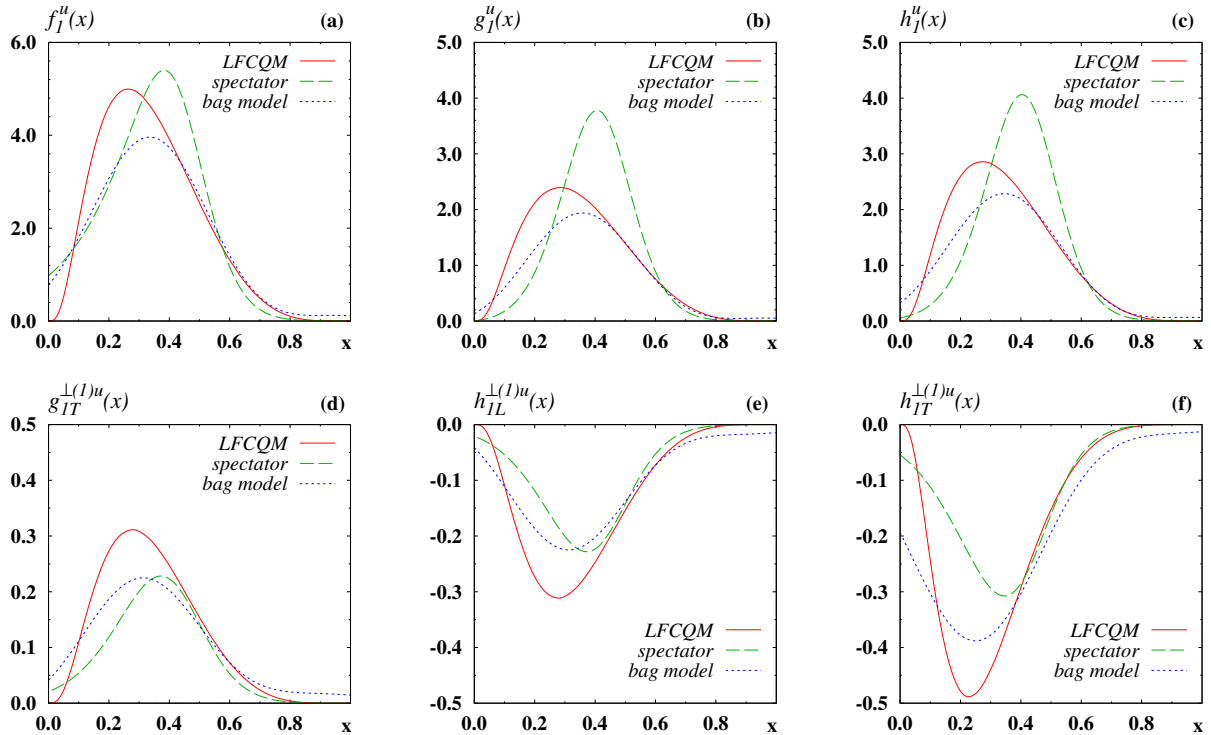


Figure 7.3: T-even TMD PDFs or their (1)-moments for  $u$ -quarks in proton from representative quark models: light-front constituent quark model (LFCQM) [747], spectator model [756], and bag model [13]. The results refer to the low initial scales of the models.

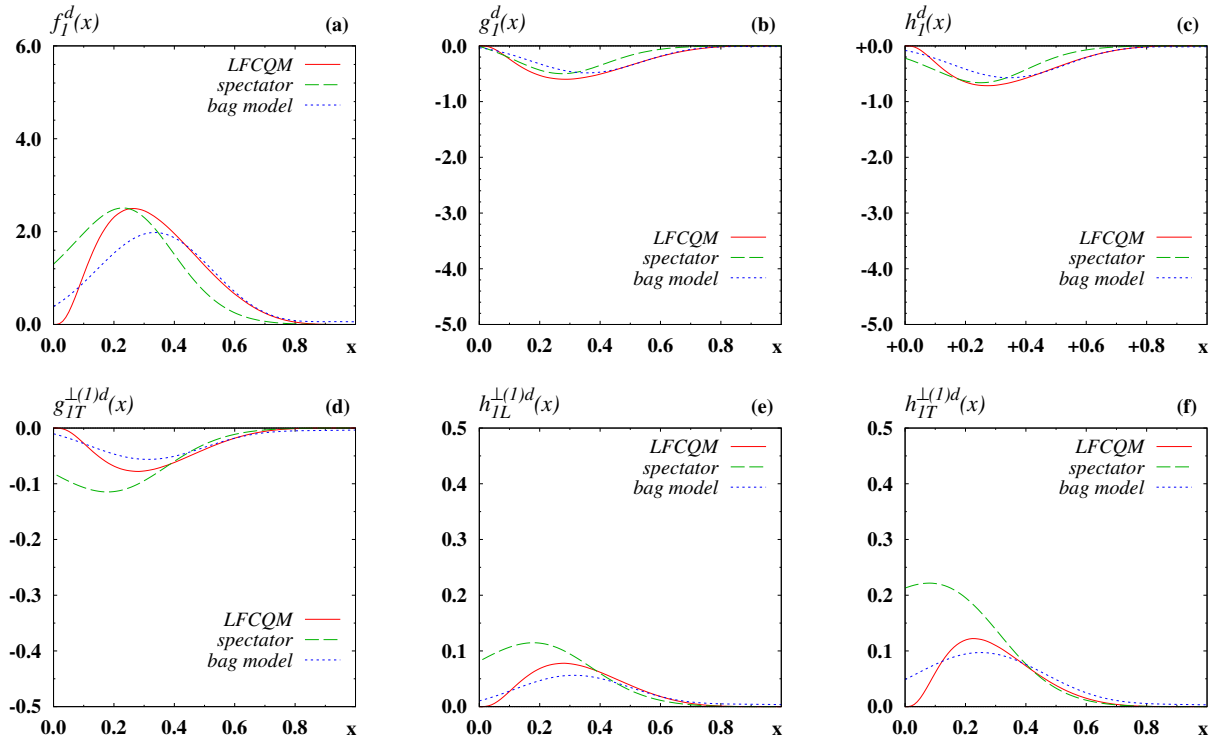


Figure 7.4: T-even TMD PDFs or their (1)-moments for  $d$ -quarks in proton from the same representative quark models as in Fig. 7.3. To facilitate the comparison, the same scales are chosen in both figures.

principles govern the modelling of  $x$ - and  $k_T$ -effects, see Chapter 8.

Clearly, the different models give different results for the TMD distributions in Figs. 7.3 and 7.4. This is to be expected. The models are not precision tools, and each of them has its own limitations. Considering how different these models are, it is remarkable that they agree on many features. E.g., the models agree on the magnitudes and signs of the TMD functions. (We stress that these models are representative. Many other models give results similar to those shown in Figs. 7.3 and 7.4.)

The common features include that transversity  $h_1^q(x)$  is as large as the helicity PDF  $g_1^q(x)$ . This is compatible with information from phenomenology, see Chapter 5, and lattice QCD, see Chapter 6. The Kotzinian-Mulders worm-gear functions  $g_{1T}^{\perp q}$  and  $h_{1L}^{\perp q}$  have the same magnitudes but opposite signs, an interesting observation to which we will come back in more detail in Sec. 7.9). Also, in all 3 models, the pretzelosity function  $h_{1T}^{\perp q}$  is larger than the Kotzinian-Mulders worm-gear function and has opposite sign with respect to transversity. It will be interesting to test these predictions in phenomenology.

The models discussed so far describe quark TMD PDFs. In fact, in some of these models, it is more appropriate to speak about distributions of valence quarks. The chiral quark soliton model is one of the few models where TMD PDFs of quarks and antiquarks can be defined and consistently evaluated [771, 772]. The remarkable prediction of the chiral quark soliton model are the distinctly different valence- and sea-quark  $k_T$ -dependencies.

The Fig. 7.5 shows results on  $f_1^q(x, k_T)$  and  $g_1^q(x, k_T)$  at  $x = 0.1$  from the leading order of the large- $N_c$  expansion at the low scale  $\mu_0 \sim \rho_{\text{av}}^{-1} \sim 0.6 \text{ GeV}$  set by the average instanton size

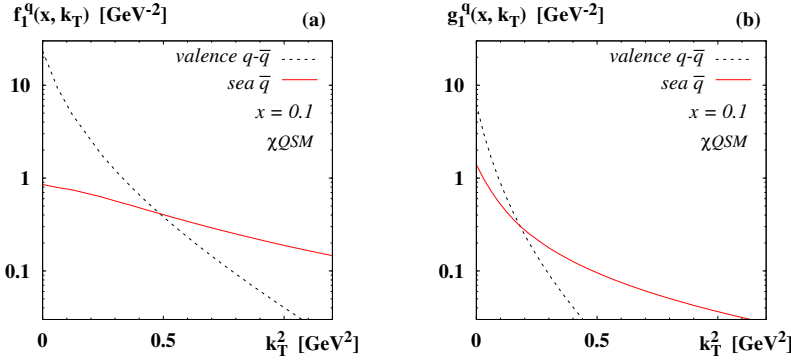


Figure 7.5:  $f_1^q(x, k_T)$  and  $g_1^q(x, k_T)$  at  $x = 0.1$  as functions of  $k_T$  from the chiral quark soliton model ( $\chi$ QSM) at low scale  $\mu_0 = 0.6$  GeV in leading order of large  $N_c$ . Dashed lines: valence quarks. Solid lines: sea quarks. The extended tails of sea quark distributions are due short-range correlations between  $q\bar{q}$ -pairs caused by chiral symmetry breaking. From Ref. [771].

$\rho_{av}$  [771]. In Fig. 7.5, the  $q$  and  $\bar{q}$  stand for the respective leading large- $N_c$  flavor combinations. In the case of  $f_1^q(x, k_T)$  in Fig. 7.5a it is  $q = u + d$  and  $\bar{q} = \bar{u} + \bar{d}$ . In the case of  $g_1^q(x, k_T)$  in Fig. 7.5b it is  $q = u - d$  and  $\bar{q} = \bar{u} - \bar{d}$ . The large- $N_c$  behavior of TMDS PDFs in the chiral quark soliton model is in agreement with general prediction in QCD, see Sec. 7.3.2.

Remarkably, the valence quark distribution,  $q - \bar{q}$ , falls off with  $k_T$  steeply, while the sea quark distribution,  $\bar{q}$ , has an extended power-like tail which in this model is approximately described as  $f_1^{\bar{q}}(x, k_T) \sim f_1^{\bar{q}}(x) / k_T^2$  in the region  $M^2 \ll k_T^2 < \mu_0^2$  where  $M = 350$  MeV is the constituent quark mass. The picture for  $g_1^{\bar{q}}(x, k_T)$  is analogous. This is not accidental but, given the relation of the unpolarized and helicity distributions to vector (V) and axial-vector (A) currents, a consequence of the spontaneous breaking of chiral symmetry. For instance, in the case of transversity — which is not related to the V- or A-currents — the sea quarks exhibit the same  $k_T$ -behavior as valence quarks [771].

The distinct behavior of valence- vs sea-quark distributions at a low scale  $\mu_0$  is an interesting signature of chiral symmetry breaking for the nucleon structure. The  $k_T$ -dependence of valence-quark distributions is governed by the hadronic scale  $R_{had} \sim M^{-1}$  which sets the size of light hadrons  $R_{had} \sim 1$  fm. The valence-quark distributions in the chiral quark soliton model are qualitatively similar to those in the other quark models discussed above. In contrast to this, the  $k_T$ -dependence of sea quarks in the unpolarized and helicity distributions is governed by the much shorter length scale  $\rho_{av} \sim 0.3$  fm which set the scale at which chiral symmetry is spontaneously broken. The sea quarks experience short-range correlations at the length scale  $\rho_{av}$  which cause this characteristic behavior [771]. There is a certain analogy to the short-range nucleon-nucleon correlations observed in nuclear physics [774]. It is interesting to observe in Fig. 7.5 that the  $k_T$  of sea quarks is of more relative importance in the case of polarized as compared to unpolarized sea quarks. It will be interesting to explore the phenomenological consequences from these predictions.

## 7.5 Modelling of T-odd TMDs PDFs

This section is devoted to the modelling of T-odd TMD PDFs where the challenge lies in a consistent inclusion of the final/initial state interactions encoded in the Wilson line.

### 7.5.1 A no-go theorem

In QCD the T-odd character of the Sivers and Boer-Mulders function is ultimately rooted in the process-dependent Wilson line encoding the initial or final state interactions. This means that in order to obtain non-zero results for T-odd TMD PDFs, a model must contain gauge field degrees of freedom. Let us consider a generic quark model, which we define as a model with no explicit gauge field degrees of freedom. Any such realistic model will respect the basic symmetries of QCD, and most notably C, P, and T. Unless one deals with an exotic situation where time-reversal invariance is spontaneously broken (which would be an unrealistic model as this is not the case in QCD), the T-odd TMDs PDFs vanish. A corresponding no-go theorem was explicitly proven in the chiral sigma model in Ref. [775], and it is straightforward to extend this proof to other models with no gauge field degrees of freedom.

### 7.5.2 Including gauge field degrees of freedom

In order to model T-odd TMD PDFs, it is necessary to include gauge field degrees of freedom which can be done in various ways. One way of modelling T-odd TMD PDFs is to consider the one gluon-exchange mechanism which can be an “abelian gluon” or a “QCD-type gluon.” In such model calculations, one takes into account only the contribution from expanding the Wilson line to leading order in the strong coupling and neglects higher orders. As a result, the obtained T-odd TMD PDFs are proportional to the strong coupling constant  $\alpha_s(\mu)$  where  $\mu$  is the low initial scale of the considered model. After the first pioneering calculation of this type within a simple scalar-diquark model framework [58], see Sec. 7.2 for a review, the Sivers and Boer-Mulders functions of the nucleon have been studied in more elaborate versions of spectator [149, 757, 758, 776–779], bag models [780–782], and lightfront constituent quark models [752, 783]. The Boer-Mulders function of the pion was studied in [784–786]. T-odd TMDs were also studied in non-relativistic models [787] (notice that in practical non-relativistic quark model calculations [787] the  $\delta$ -functions of the strict non-relativistic limit in Eq. (7.5) are considerably smeared out).

In these studies, different models are employed for the nucleon structure, but conceptually the same 1-gluon exchange mechanism is invoked to take into account the initial/final state interactions. Common to all these approaches is that the Sivers and Boer-Mulders functions require orbital angular momentum in the nucleon wave function: the matrix elements of these TMD PDFs involve transitions between quark wave functions with orbital angular momentum components which differ by  $\Delta L_z = \pm 1$ .

### 7.5.3 Quark-target model

The Lagrangian of the quark target model is basically the QCD Lagrangian except that it is considered for one single flavor, and the model is solved in perturbative QCD. It is not intended to be a realistic model for a hadron, as the S-matrix contains colored states and the current quark mass terms, which are negligible in QCD, have 100 % strength since the proton state is replaced by a quark. Nevertheless, it is an interesting testing ground, e.g., for relations among TMD PDFs obtained from quark models with no gluonic degrees of freedom. Such relations can be investigated in this model under more realistic conditions thanks to the

QCD-like color structure which includes quark-gluon-quark and three-gluon vertices [149].

#### 7.5.4 Lensing function

An attractive modelling approach is based on the observation that in some models, the same LCWF components enter in the description of T-odd TMD PDFs and certain generalized parton distribution functions [149, 710, 788, 789]. The difference is, of course, that T-odd TMD PDFs contain the effects of initial/final state interactions which, in simple models, can be expressed in terms of so-called "chromodynamic lensing functions." More precisely, this allows one to effectively express the leading T-odd TMD PDFs in terms of convolutions of the lensing functions with generalized parton distribution functions in the impact parameter representation which are introduced in Chapter 11. This connection is rooted in the relations of TMD PDFs and generalized parton distribution functions to the overarching Wigner functions and generalized TMD functions [790, 791], see Chapter 11 for more discussion on these topics.

The generalized parton distribution function needed in this picture to model the Sivers function is not known, but it is related to the known quark contributions to the anomalous magnetic moment of proton and neutron. In this way one can conclude the overall signs of the Sivers function for  $u$ - and  $d$ -flavors. This is possible because the final state interactions, while in detail complicated to describe, can be expected to be attractive on average. The signs of the Sivers function for  $u$ -quarks and  $d$ -quarks concluded in this way are in agreement with phenomenology [792]. In the case of the Boer-Mulders function certain chiral-odd generalized parton distributions enter which are also not known. But on the basis of information from models and lattice QCD, and under the assumption that the final state interactions are on average attractive, one finds also in this case the signs of the  $u$ - and  $d$ -quark Boer-Mulders functions in agreement with phenomenological information [792].

The lensing mechanism is realized to lowest order in spectator or quark-target models [149, 710] but it is not model-independent [707, 785, 793]. Two general conditions needed for the lensing function concept to be applicable are (i) that the coupling between the gauge boson and the spectator system conserves helicity, and (ii) that the model describes the considered hadron as a 2-body system [793]. For instance, the lensing function concept works in conceptually similar models for the Boer-Mulders function of the pion described as a 2-body system in terms of the minimal  $\bar{q}q$  Fock state component, but it does not work for the nucleon whose minimal  $qqq$  Fock-state component constitutes a 3-body system [793]. The lensing function approach was found to work in a recent light-front quark-diquark model study based on a soft wall AdS/QCD model [794].

#### 7.5.5 Augmented LCWFs, eikonal methods, instantons and other approaches

An interesting approach consists in introducing augmented LFWFs which incorporate the initial/final state interaction effects in imaginary process-dependent phases. This approach was worked out in light-front time-ordered perturbation theory in Ref. [795].

The so far discussed approaches were largely based on the 1-gluon rescattering mechanism for initial/final state interactions, i.e., the expansion of the Wilson link to the lowest non-trivial order. Attempts to go beyond that were undertaken in Refs. [778, 786, 796] using nonperturbative eikonal methods to evaluate the Wilson line to all orders in U(1), SU(2), SU(3) gauge groups. The results were used to study T-odd TMDs in the lensing function approach.

Further nonperturbative approaches to T-odd single-spin effects based on the nonperturba-

tive interactions induced by instantons were explored in Ref. [797–799]. A potentially related soft rescattering mechanism was considered in [800] due to the possibility of an anomalous chromomagnetic moment of quarks. Such a Pauli coupling at the vertex between the struck quark and exchanged gluon can be potentially generated by instanton effects [800].

For completeness we remark that a way to circumvent the no-go theorem concerning modelling of T-odd functions in chiral quark models [775] was discussed in [801] where the role of gluons was played by a “hidden vector-meson gauge symmetry.” An attempt to implement this in a practical calculation was present in [802].

### 7.5.6 Predictions from quark models for T-odd TMD PDFs

The aim of this section is to present model results for the leading T-odd TMD PDFs of the nucleon from several representative models. In Fig. 7.6 and 7.7 we show results from the light-front constituent quark model (LFCQM) [783], spectator model [778], and bag model [781, 782]. The signs of the T-odd functions refer to DIS. All model results refer to the low initial scales of the models which are below 0.5 GeV in all cases.

The results from the different models show a significant spread. At the same time, the models also agree on several features. The models predict the same signs and similar flavor dependencies. For instance, the Sivers functions for  $u$ -quarks and  $d$ -quarks have opposite signs and comparable magnitudes. The Boer-Mulders functions for  $u$ -quarks and  $d$ -quarks have the same signs and comparable magnitudes. The sign patterns are compatible with predictions from the large- $N_c$  limit [465] discussed in Sec. 7.3.2.

There is also agreement that, within a given model, the Boer-Mulders function is comparable to the Sivers function or even larger. However, the results on the magnitudes of the functions computed in different models span a wide range: for  $f_{1T}^{\perp u}$ ,  $f_{1T}^{\perp d}$ ,  $h_1^{\perp d}$ , the light-front constituent quark model gives the largest results [783], bag model the smallest results [781, 782], while the spectator model results lie in between — being sometimes closer to one or the other of the above-mentioned models [778]. For  $h_1^{\perp u}$ , the spectator model gives the largest results, and the light-front constituent quark model gives results in-between [783], while the bag model gives consistently the smallest results also in this case [782].

The model results from the models have been compared with phenomenology showing good qualitative agreement. For the Sivers function, the tendency of the light-front constituent quark model results is to be at the upper edge of the uncertainty band of the extractions [783], while the bag model results tend to underestimate the lower bounds of the parametrizations [782] (the extractions are discussed in Secs. 5.3.1 and 5.4).

The comparison to phenomenological extractions for TMD PDFs is not straightforward, because it is necessary to evolve the model results from the low initial scales to the scales of the parametrizations. While there is significant experience with applying DGLAP evolution down to initial scales as low as  $\mu_0 \sim 0.4 \text{ GeV}^2$  (the effective expansion parameter  $\frac{\alpha_s(\mu_0)}{4\pi} \sim 0.1$  may be considered small enough to warrant LO or NLO evolution) [803–807], much less is known about the application of TMD evolution down to such low scales. The comparisons to extractions and phenomenological applications of model results relied on estimates of TMD evolution effects [471, 752, 753, 782] until recently [730, 773].

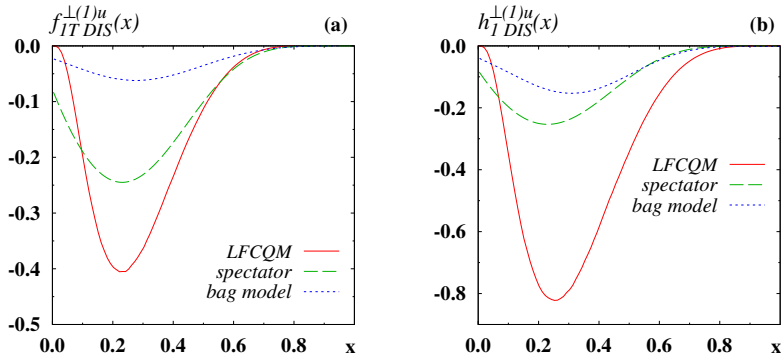


Figure 7.6: Results for (1)-moments of the T-odd Sivers and Boer-Mulders functions for  $u$ -quarks in a proton from representative quark models: light-front constituent quark model (LFCQM) [783], spectator model [778], and bag model [781, 782]. The results refer to the low initial scales of the models.

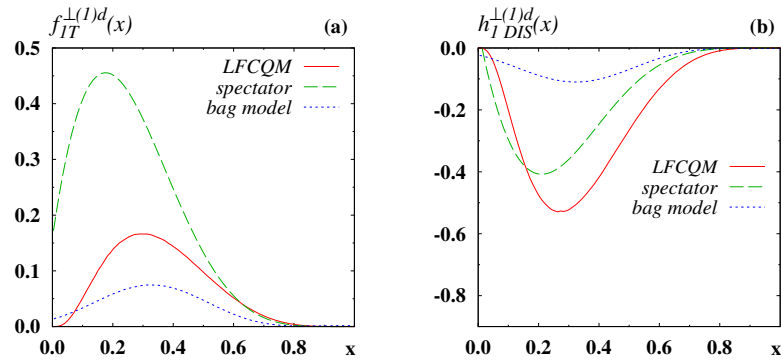


Figure 7.7: Results for (1)-moments of the T-odd Sivers and Boer-Mulders functions for  $d$ -quarks in the same models as in Fig. 7.6. To facilitate the comparison, the same scales are chosen in both figures.

## 7.6 Gluon TMDs

Gluon TMDs can in principle be studied through a variety of processes and at different facilities, see Sec. 5.6. Nevertheless, compared to quark TMDs, very little is presently known about gluon TMDs for moderate parton momentum fractions. The situation is different in the small- $x$  region for which a number of (theoretical) studies exist. Here we will not discuss this regime of gluon saturation but refer to Ch. 8 for more details.

At the present stage, it is important to gather as much information as possible about gluon TMDs through models and also LQCD which could help to guide the experiments. Here we give a very brief account of available model calculations in this field, all of which are concerned with leading-power gluon TMDPDFs. In Ref. [808] a one-loop calculation of the gluon Sivers function in the quark-target model was presented. The result was used to check the Burkardt sum rule [809] for the Sivers function in that model. (The Burkardt sum rule is discussed in Sec. 7.8.2.) Furthermore, in Ref. [149] all gluon TMDs were then computed in the quark-target model. Six out of the eight TMDs are nonzero, while two T-odd gluon TMDs vanish in the one-loop approximation. This result does of course not imply that, in general, those two

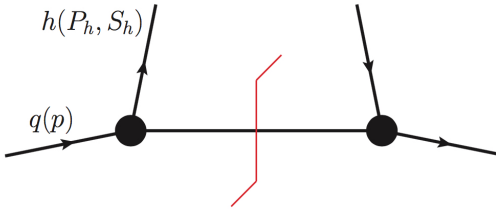


Figure 7.8: Representation of quark fragmentation into a hadron (which is characterized by the four-momentum  $P_h$  and, potentially, the covariant spin vector  $S_h$ ) in a spectator model to leading order in the quark-hadron-spectator coupling. The inclusive system  $X$  is given by a single spectator particle. The red line in the diagram is the on-shell cut.

gluon TMDs vanish or are small. Interestingly, the Burkardt sum rule, in combination with results from a large- $N_c$  analysis, according to which the up-quark and down-quark Sivers functions are almost equal in magnitude but opposite in sign, leads to the prediction that the gluon Sivers function is suppressed relative to the quark Sivers function [720]. Current phenomenology is compatible with this prediction, see also the discussion in Sec. 7.3.2.

A spectator model calculation of the gluon Sivers function of the proton was performed in Ref. [810], leading to results in reasonable agreement with information from experiment. Another spectator model calculation of gluon TMDs can be found in Ref. [811] and, in particular, in the recent work in Ref. [812]. The latter study addresses the four T-even gluon TMDs, where the model parameters are fixed, to the extent possible, by information on the integrated unpolarized and helicity gluon PDFs. Very recently, the same spectator-model approach was extended to the T-odd sector, and results for the gluon Sivers function were reported [813]. The T-even gluon TMDs were also explored in an AdS/QCD approach [814], where the results satisfy the positivity bounds on the gluon TMDs derived previously [148]. In a follow-up study, the same authors addressed the T-odd gluon TMDs, for which they derived a parameterization in terms of light-front wave functions [150]. It is important and encouraging to see those works on models for gluon TMDPDFs in the region of moderate  $x$ . Further developments in this area can be expected for the future.

## 7.7 Quark TMD Fragmentation Functions

Generally, it is difficult to compute (collinear and transverse-momentum-dependent) FFs for light hadrons in nonperturbative approaches. So far it has not been possible to address FFs in lattice QCD because of the state  $|P_h, S_h; X\rangle$  that shows up in their definition. Also, obtaining realistic estimates of FFs in models is more challenging than for PDFs. Nevertheless, a number of model calculations for TMDFFs exist where mostly two classes of models have been explored — spectator models in which a parton fragments into a hadron and a spectator in a single step, and models for multiple-hadron emission. In some recent works the two approaches have been combined. A brief account of those models is given here, with some emphasis on the frequently-used spectator models. At the end of this section we also discuss the universality of (T-odd) TMDFFs in a spectator model.

### 7.7.1 Spectator models for TMDFFs

An early application of a spectator model for quark fragmentation has been discussed in Ref. [756]. The main idea of spectator models for FFs is illustrated in Fig. 7.8: a (time-like

off-shell) quark fragments into a hadron and a single (on-shell) spectator particle. One finds that the squared four-momentum  $p^2$  of the fragmenting quark is given by the transverse quark momentum  $p_T$  (or, equivalently, the transverse hadron momentum) and  $z$  according to

$$p^2 = p_T^2 \frac{z}{1-z} + \frac{m_s^2}{1-z} + \frac{M_h^2}{z}, \quad (7.11)$$

with  $m_s$  denoting the spectator mass. The fragmentation process determines the spectator type. For instance, the spectator is a down quark in the case of fragmentation of an up quark into a  $\pi^+$ . Or the spectator is a  $\bar{u}\bar{d}$  anti-diquark if an up quark fragments into a proton. Let us, as an example, consider the fragmentation of light quarks into pions. For a pseudoscalar interaction between quarks and pions, one finds for the favored  $u \rightarrow \pi^+$  fragmentation [57, 815]

$$D_1^{\pi^+/u}(z, z p_T) = \frac{1}{z} \frac{g_{\pi q}^2}{8\pi^3} \frac{p_T^2 + m_q^2}{\left(p_T^2 + m_q^2 + \frac{1-z}{z^2} m_\pi^2\right)^2}, \quad (7.12)$$

where  $g_{\pi q}$  is the quark-pion coupling constant and  $m_q$  the quark mass. In this model, the fragmenting quark and the spectator have the same mass. Nonzero disfavored FFs can be obtained by considering higher-order diagrams. (For completeness, we remark that the unpolarized TMDFF for a quark into a sigma meson was calculated in the linear sigma model in Ref. [816].)

Integrating the result in Eq. (7.12) upon  $k_T$  provides  $D_1^{\pi^+/u}(z)$ , a function that is rather well known from fits to data. This integral leads to a logarithmic divergence which, according to Eq. (7.11), may be avoided by putting a cut-off on the virtuality of the fragmenting quark. The numerical result shows the right qualitative feature in that it decreases with increasing  $z$ , but there is no quantitative agreement with FF parametrizations based on data [817]. In an attempt to improve the phenomenology also the pseudo-vector quark-pion coupling, as used in the chiral-invariant Georgi-Manohar model [818], was explored in Ref. [817]. While a good description of the  $z$  behavior of the FF is obtained, the magnitude is just about half of typical fit results [817]. Also the Nambu-Jona-Lasinio model [819–821] and a lonlocal chiral quark model [822–824] were used to compute FFs in a spectator approach. Overall one again finds just qualitative agreement with existing fits, which implies that also results for the TMDFFs in such models are qualitative only, even though the results for the transverse momentum dependence may be reasonable. A better phenomenology of spectator models for FFs can be obtained by introducing more free parameters, where often two types of modifications are considered; see, for instance, Refs. [756, 825]. First, a form factor is used for the quark-hadron-spectator vertex. Second, the spectator mass is allowed to vary. Of course such approaches are no longer related to an underlying Lagrange density. In Ref. [825] good results were obtained for integrated pion and kaon FFs in a spectator model with five parameters. Once the parameters are fixed, other (TMD) FFs can be computed. We note in passing that the momentum sum rule for the unpolarized FF has been discussed in Refs. [10, 819, 826] in spectator models.

Spectator models were also used to compute the Collins function, with a first calculation already presented in the original paper by Collins [57]. In that study, a nonzero  $H_1^\perp$  was found by taking into consideration the imaginary part of the propagator of the fragmenting quark.

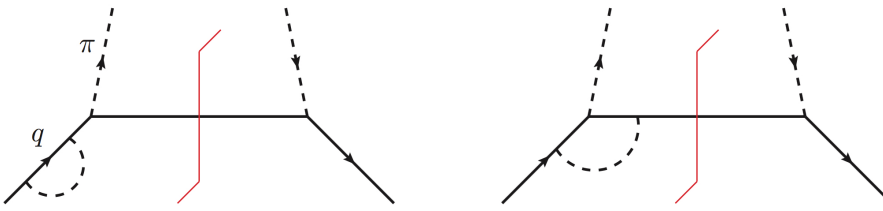


Figure 7.9: One-loop corrections to the fragmentation of a quark into a pion for a pseudoscalar quark-pion coupling. Shown are all the graphs contributing to the Collins function: quark self-energy (left) and vertex correction (right). (Hermitean conjugate diagrams are not shown.)

Despite this result, it was speculated whether the Collins function might actually vanish due to a cancellation between different contributions to the fragmentation process, see, for instance, Ref. [292]. Therefore, in Ref. [815] the aforementioned pseudoscalar quark-pion coupling was used for a complete field-theoretic model calculation. The lowest-order diagrams in Fig. 7.9 provide [815]

$$H_1^{\perp \pi^+/q}(z, z p_T) = -\frac{g_{\pi q}^2}{4\pi^3} \frac{m_\pi}{1-z} \left( \frac{m_q \operatorname{Im} \tilde{\Sigma}(p^2)}{(p^2 - m_q^2)^2} + \frac{\operatorname{Im} \tilde{\Gamma}(p^2)}{p^2 - m_q^2} \right) \Big|_{p^2 = p_T^2 \frac{z}{1-z} + \frac{m_q^2}{1-z} + \frac{m_\pi^2}{z}}, \quad (7.13)$$

with  $\operatorname{Im} \tilde{\Sigma}$  and  $\operatorname{Im} \tilde{\Gamma}$  indicating the imaginary part of the quark self-energy and the vertex correction, respectively. The final result for the Collins function in Eq. (7.13) is nonzero, which gave support to its existence from the theoretical point of view [815]. In the meantime, there exists compelling experimental evidence for a non-vanishing Collins function, see Sec. 5.3.2. In Ref. [817] the Georgi-Manohar model [818] with pion loops was used to calculate the Collins function, while later also gluon loops were considered in different spectator models [825, 827–829]. In such approaches, even predicting the sign of the Collins function is difficult because the individual diagrams can contribute with different signs [828]. In the latest phenomenological papers just gluon loops have been used [825, 829]. In Ref. [825], for instance, the Collins function for pions and kaons was computed, with the model parameters fixed by means of the integrated unpolarized FFs. In the case of pions, reasonable agreement with information from experimental data was obtained. A spectator model was even used to compute the Collins function for  $\Lambda$  hyperons [830].

## 7.7.2 Models for multi-step fragmentation process

The second general class of models for FFs considers hadron production as a multi-step process, with the Feynman-Field model being an important representative [831]. The underlying principle of that approach is shown in Fig. 7.10, namely, a high-energetic quark combines with an antiquark of a  $q\bar{q}$  pair from the vacuum, where the combination process repeats until the remaining energy falls below some cut-off. In the Feynman-Field model, multiple-hadron emission originating from a single parton is given by just one function,  $f(\eta)$ , characterizing a single emission, where  $f(\eta)$  describes the probability that the first hierarchy (rank 1) meson leaves fractional momentum  $\eta$  to the remaining cascade. This model was quite successful in describing data from early  $e^+e^-$  annihilation experiments with a very limited set of parameters [832, 833]. Nowadays the Feynman-Field model can still provide guidance when trying to parametrize FFs at an initial scale.

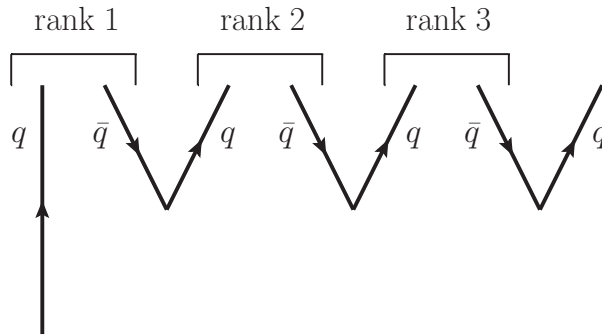


Figure 7.10: Hierarchy of mesons that emerges when an initial quark combines with an antiquark from a produced  $q\bar{q}$  pair to form the meson of rank 1. The leftover quark then combines with an antiquark from another  $q\bar{q}$  pair to form the meson of rank 2 and so on.

A similar approach is the string fragmentation model [834–837], where hadrons are also produced in a hierarchy as indicated in Fig. 7.10, but the treatment of the kinematics differs for the two models. Moreover, in the string model, applied to  $e^+e^-$  annihilation for instance, one considers hadronization of the  $q\bar{q}$  pair as opposed to independent fragmentation of the quark and antiquark employed in the Feynman-Field model. The quark and antiquark lose energy to the color field between them, which is treated as a string-like configuration. Once that energy exceeds a certain threshold, the string breaks up into hadrons.

A string fragmentation model was also used in an attempt to capture the main features of the Collins function [838]. Here we briefly repeat the main idea of that work. Let's consider fragmentation of a transversely polarized quark into a spin-0 particle like a pion. In the string model, it is assumed that a  $q\bar{q}$  pair originating from string breaking has the quantum numbers of the vacuum, that is,  $J^P = 0^+$  [838]. This situation is possible if the pair has spin  $S = 1$  and orbital angular momentum  $L = 1$ , where the spin and orbital angular momentum point in opposite directions. Therefore, a correlation exists between the spin of the antiquark of the  $q\bar{q}$  pair and its orbital angular momentum. Because the antiquark and the original quark form a spin-0 meson, there is also a correlation between the orbital angular momentum of the antiquark, which gets transferred to the meson, and the transverse polarization of the fragmenting quark. This leads to a nonzero Collins effect, namely, that the meson has a preferred direction relative to the plane which is given by the momentum and the spin of the fragmenting quark. Originally, the model was confronted with data for the transverse SSA in processes like  $p^\uparrow p \rightarrow hX$  where it provides the correct sign for the asymmetry [838]. The model also agrees in sign with the Collins function extracted from data in SIDIS and  $e^+e^-$  annihilation. Disfavored fragmentation requires rank 2 (and higher-rank) mesons which, in particular, leads to opposite signs for the favored and disfavored Collins functions [838], in accordance with phenomenology. Further developments of the string fragmentation model for the Collins effect have been discussed in Refs. [839–842].

### 7.7.3 Combining models for FFs

Another line of research in this area combines spectator models with the main idea underlying the Feynman-Field model. Specifically, single-hadron emission is computed in a spectator model defined through a Lagrange density, and then iterated according to the Feynman-Field

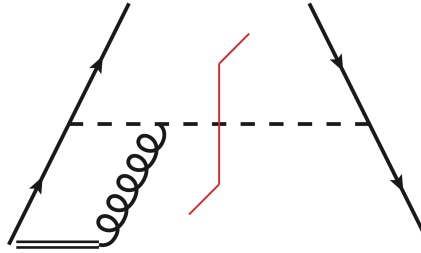


Figure 7.11: Specific contribution to fragmentation correlator for the fragmentation of a quark into a hadron and a spectator particle.

approach. Such calculations for  $D_1(z)$  were carried out in the Nambu- $\bar{\text{A}}\text{S}$ Jona-Lasinio model [819–821] and in a non-local chiral-quark model [822–824], while results for TMDFFs were reported in [829, 843, 844] along with discussion about how model-independent constraints such as the Schäfer-Teryaev sum rule [826, 845] can be satisfied in such a model. A major goal of those works is to obtain quantitative results for FFs with as few parameters as possible. Presently, it is not fully clear if this goal can be met or if more flexible parametrizations for the single-hadron production are needed.

#### 7.7.4 Universality of TMD fragmentation functions

Here we would like to add some discussion about the universality of TMDFFs. We remind the reader that TMDPDFs defined with future-pointing and past-pointing Wilson lines can be related through the parity and time-reversal operations. This led to the crucial finding that T-even TMDPDFs do not depend on the direction of the Wilson line, while T-odd TMDPDFs have reversed signs in the two cases [59]. The question about universality also arises for TMDFFs as for those objects in the SIDIS process, *a priori*, one obtains past-pointing Wilson lines when eikonalizing the relevant propagators, while future-pointing Wilson lines emerge in  $e^+e^-$  annihilation. Since those two definitions can not be related via parity and time reversal, it remained at first unclear whether TMDFFs are universal or not.

To explore this situation, in Ref. [704] a transverse SSA for fragmentation in both SIDIS and  $e^+e^-$  annihilation was computed in a spectator model, including one-loop gluon exchange which is associated with the Wilson line of TMDFFs. The factorized description of the SSA is proportional to the TMDFF  $D_{1T}^\perp$ . The calculation of Ref. [704] can be considered the counterpart of the Brodsky-Hwang-Schmidt calculation of the Sivers SSA for the fragmentation process [58, 133, 711]. It was found that the SSAs in the two processes are identical, suggesting universality of  $D_{1T}^\perp$ .

A more general investigation of the universality of TMDFFs was carried out in Ref. [122]. There it was argued that, when deriving TMD factorization, in the case of the fragmentation process one is actually not sensitive to the direction of the Wilson line. This led to the conclusion that TMDFFs in both aforementioned processes can be defined through, for instance, future-pointing Wilson lines [122] and, hence, they are universal.

To make the argument explicit in a simple example, we consider again a spectator model calculation and evaluate the diagram Fig. 7.11 [846]. Specifically, we just focus on the calculation for the difference between a future-pointing and a past-pointing Wilson line, where the

essential part of the computation is given by

$$\begin{aligned} I_{\text{future}} - I_{\text{past}} &\sim \int d^4l \frac{N(l^+, \mathbf{l}_T)}{[(p-l)^2 - m_q^2 + i0][(p-P_h-l)^2 - m_s^2 + i0][l^2 + i0]} \\ &\quad \times \left( \frac{1}{l^+ + i0} - \frac{1}{l^+ - i0} \right) \\ &= 0. \end{aligned} \tag{7.14}$$

To arrive at this result, we first carried out the  $l^+$  integral by using  $1/(l^+ + i0) - 1/(l^+ - i0) = -2\pi i \delta(l^+)$ . Then the  $l^-$  integral can be evaluated via contour integration. However, since all the  $l^-$  poles are on the same side of the real axis, the integral vanishes. The calculation shows that, for this example, the direction of the Wilson line is irrelevant. Note that the numerator of the integrand,  $N(l^+, \mathbf{l}_T)$ , depends on the TMDFF under consideration. However, for all leading-power TMDFFs this numerator does not depend on  $l^-$ , which is all what matters for the argument to hold. Generally, the fact that TMDFFs are not sensitive to the direction of the Wilson line can be traced back to the specific kinematics of the fragmentation process.

The universality of TMDFFs has also been studied by considering transverse-momentum moments of the TMD correlator. It was found that a potential non-universality of moments of TMDFFs can be related to certain higher-twist collinear (soft-gluon-pole) matrix elements. But, through model-dependent and model-independent analyses, it was concluded that such matrix elements vanish [167, 847–849]; see also Ref. [850]. While those findings further corroborated the universality of TMDFFs, it must be pointed out that the moments were not taken for properly renormalized TMDFFs. As already explained in Sec. 2.9, generally, renormalization and taking transverse-momentum moments generally do not commute. The potential implications of this feature on the results discussed in this paragraph remain to be studied.

## 7.8 Formal Constraints on TMD Functions

In this section we discuss several general results which hold formally for bare TMD functions. While they are generally not considered to be model-dependent, presently it is not known how to prove these relations in terms of renormalized TMD functions. These general constraints are, however, expected to be valid in models and can be used to test model results. In addition, some of these general constraints have been used in phenomenology.

### 7.8.1 Positivity constraints

Cross sections of physical processes must be positive — no matter which spin configurations or azimuthal asymmetries one considers. In order to guarantee this, one can introduce a spin density matrix for the nucleon which is formally related to TMD PDFs and which obeys certain conditions. For a spin- $\frac{1}{2}$  particle like the nucleon, this yields the following inequalities

for the leading quark and antiquark TMD PDFs [499]

$$f_1^a(x, k_T) \geq 0, \quad |g_1^a(x, k_T)| \leq f_1^a(x, k_T), \quad |h_1^a(x, k_T)| \leq f_1^a(x, k_T), \quad (7.15a)$$

$$|h_1^a(x, k_T)| \leq \frac{1}{2} \left( f_1^a(x, k_T) + g_1^a(x, k_T) \right), \quad (7.15b)$$

$$|h_{1T}^{\perp(1)a}(x, k_T)| \leq \frac{1}{2} \left( f_1^a(x, k_T) - g_1^a(x, k_T) \right), \quad (7.15c)$$

$$g_{1T}^{\perp(1)a}(x, k_T)^2 + f_{1T}^{\perp(1)a}(x, k_T)^2 \leq \frac{k_T^2}{4M_N^2} \left( f_1^a(x, k_T)^2 - g_1^a(x, k_T)^2 \right), \quad (7.15d)$$

$$h_{1L}^{\perp(1)a}(x, k_T)^2 + h_{1T}^{\perp(1)a}(x, k_T)^2 \leq \frac{k_T^2}{4M_N^2} \left( f_1^a(x, k_T)^2 - g_1^a(x, k_T)^2 \right). \quad (7.15e)$$

The meaning of the inequalities in (7.15a) is obvious from the partonic interpretation, e.g.,  $f_1^a(x, k_T) \geq 0$  expresses the expectation that a probability (to find a parton carrying fraction  $x$  of nucleon's  $P^+$ -momentum component and  $k_T$ ) can not be negative. Similarly, the difference of probability densities of partons with positive helicities and negative helicities can not exceed their sum which implies  $|g_1^a(x, k_T)| \leq f_1^a(x, k_T)$ , and analogously for transversely polarized quarks. The analog of Eq. (7.15b) for PDFs is known as the Soffer inequality [366] and was generalized to TMD PDFs in [499] where also the inequalities (7.15c-7.15e) were derived. For fragmentation functions analogous inequalities can be derived [499], as well as those for gluon TMD PDFs [148].

Despite being intuitive, the status of such inequalities remains unclear for renormalized TMD functions. It is natural to expect that some positivity constraints should hold also for renormalized TMD functions in order to guarantee the positivity of cross sections. But it is not straightforward to prove this rigorously, see for instance the recent attempt to prove the positivity of  $f_1^a(x, k_T)$  in  $\overline{\text{MS}}$  scheme in [851], and the critical review of this attempt in [145].

In most model studies one typically does not face many of the subtleties occurring in QCD in the definition of TMD PDFs, and the inequalities (7.15a-7.15e) are routinely used to double check the internal consistency of the model calculations. The positivity inequalities have been also implemented in many phenomenological studies, see Chapter 5. For a discussion of the importance of the Soffer bound for the extraction of transversity, we refer to Ref. [375].

### 7.8.2 Burkardt sum rule

A nontrivial constraint in modelling (or fitting) of the Sivers function is given by the Burkardt sum rule [809]. This sum rule states that the average transverse momentum induced in the Sivers effect vanishes after summing over all partons (cf. Eq. (5.25) for the notation for  $k_T$  moments of TMDs),

$$\sum_a \int dx \int d^2 k_T f_{1T}^{\perp(1)a}(x, k_T) = 0. \quad (7.16)$$

Due to its relation to the conservation of (transverse) momentum, the sum rule can also be proven formally through studies of the energy-momentum tensor [852].

Also in the case of this sum rule, it is not obvious how to formulate a rigorous proof in terms of renormalized TMDs. Despite its formal character in QCD, the sum rule was shown to

be valid, e.g., in one-loop calculations in the quark-target model and a scalar diquark model of the nucleon [808] as well as in light-cone constituent quark models [783]. In the bag model the sum rule was found violated by a few percent [780–782] which has been attributed to the fact that the bag states are not good momentum eigenstates. Also in non-relativistic calculations in constituent quark models a small violation of the sum rule was observed due to similar reasons [781, 782].

In the leading order of the large- $N_c$  limit, the Burkardt sum rule is saturated by the Sivers functions of  $u$ - and  $d$ -flavors having the same magnitude but opposite signs with the contributions from gluons and other quark flavors appearing only at subleading order of the large  $N_c$  expansion, see Sec. 7.3.2.

For completeness let us mention the formal connection of the transverse moment of the Sivers function to the collinear twist-3 Qiu-Sterman function [159], see Sec. 2.8, which could allow to study (formally) the scale dependence of the Burkardt sum rule [853].

### 7.8.3 Schäfer-Teryaev sum rule

The Schäfer-Teryaev sum rule is based on the conservation of the transverse momentum acquired by the hadrons during the fragmentation process of a transversely polarized quark,

$$\sum_h (2S_h + 1) \int dz z \int d^2 K_T H_1^{\perp(1)q/h}(z, K_T) = 0. \quad (7.17)$$

The sum rule was proven in [845] on the basis of intuitive momentum conservation arguments. A more rigorous formal proof was given in [826], see also the review article [296] and Ref. [854].

It is difficult to test this sum rule in model calculations. Strictly speaking, it requires the consideration of "all" possible hadrons a quark can fragment into. Nevertheless, the Schäfer-Teryaev sum rule was shown to hold in a Manohar-Georgi type-model study [826], and the quark-jet model of Ref. [844].

## 7.9 Relations in Models

After reviewing model-independent formal constraints, here we discuss relations among TMD PDFs in models. While model-dependent, these relations are nevertheless of interest because they are observed in a wide class of models based on much different dynamics.

### 7.9.1 Independence of TMD PDFs in QCD

In QCD no relations exist among different TMD functions which are independent functions, each of which describing different characteristics of the nucleon structure. This can be established by considering the fully unintegrated quark correlator  $\Phi^q$  for which we will use the definition of Refs. [60, 61] (see the text below Eq. (7.6) for an explanation of the notation).

For a Lorentz-decomposition of the quark correlator, one can make use of four linearly independent 4-vectors: quark momentum  $k^\mu$ , nucleon momentum  $P^\mu$ , nucleon polarization vector  $S^\mu$ , and the gauge-link vector  $v^\mu$ , i.e.  $\Phi^q = \Phi^q(k, P, S, v)$  where we do not indicate that the renormalized correlator would depend also on renormalization and other scales. These four linearly independent vectors allow one to carry out a Lorentz-decomposition of the quark correlator in terms of 32 Lorentz-scalar valued amplitudes: 12  $A_i^q$ -amplitudes and 20  $B_i^q$ -amplitudes. This naming scheme has historical reasons, and will be clarified shortly. The amplitudes depend on the scalars  $P \cdot k$  and  $k^2$  which will not be indicated for brevity in

the following. The fully unintegrated quark-quark correlator can be decomposed according to [131, 706, 707]

$$\begin{aligned}
\Phi^q(k, P, S, v) = & MA_1^q + \not{P}A_2^q + \not{k}A_3^q + \frac{i}{2M} [\not{P}, \not{k}] A_4^q + i(k \cdot S) \gamma_5 A_5^q + M \not{S} \gamma_5 A_6^q + \frac{k \cdot S}{M} \not{P} \gamma_5 A_7^q \\
& + \frac{k \cdot S}{M} \not{k} \gamma_5 A_8^q + \frac{[\not{P}, \not{S}]}{2} \gamma_5 A_9^q + \frac{[\not{k}, \not{S}]}{2} \gamma_5 A_{10}^q + \frac{k \cdot S}{2M^2} [\not{P}, \not{k}] \gamma_5 A_{11}^q + \frac{1}{M} \varepsilon^{\mu\nu\rho\sigma} \gamma_\mu P_\nu k_\rho S_\sigma A_{12}^q \\
& + \frac{M^2}{P \cdot v} \not{\psi} B_1^q + \frac{iM}{2P \cdot v} [\not{P}, \not{\psi}] B_2^q + \frac{iM}{2P \cdot v} [\not{k}, \not{\psi}] B_3^q + \frac{1}{P \cdot v} \varepsilon^{\mu\nu\rho\sigma} \gamma_\mu \gamma_5 P_\nu p_\rho v_\sigma B_4^q \\
& + \frac{1}{P \cdot v} \varepsilon^{\mu\nu\rho\sigma} P_\mu k_\nu v_\rho S_\sigma B_5^q + \frac{iM^2}{P \cdot v} (v \cdot S) \gamma_5 B_6^q + \frac{M}{P \cdot v} \varepsilon^{\mu\nu\rho\sigma} \gamma_\mu P_\nu v_\rho S_\sigma B_7^q \\
& + \frac{M}{P \cdot v} \varepsilon^{\mu\nu\rho\sigma} \gamma_\mu k_\nu v_\rho S_\sigma B_8^q + \frac{p \cdot S}{M(P \cdot v)} \varepsilon^{\mu\nu\rho\sigma} \gamma_\mu P_\nu k_\rho v_\sigma B_9^q + \frac{M(v \cdot S)}{(P \cdot v)^2} \varepsilon^{\mu\nu\rho\sigma} \gamma_\mu P_\nu k_\rho v_\sigma B_{10}^q \\
& + \frac{M}{P \cdot v} (v \cdot S) \not{P} \gamma_5 B_{11}^q + \frac{M}{P \cdot v} (v \cdot S) \not{k} \gamma_5 B_{12}^q + \frac{M}{P \cdot v} (p \cdot S) \not{\psi} \gamma_5 B_{13}^q + \frac{M^3}{(P \cdot v)^2} (v \cdot S) \not{\psi} \gamma_5 B_{14}^q \\
& + \frac{M^2}{2P \cdot v} [\not{\psi}, \not{S}] \gamma_5 B_{15}^q + \frac{p \cdot S}{2P \cdot v} [\not{P}, \not{\psi}] \gamma_5 B_{16}^q + \frac{p \cdot S}{2P \cdot v} [\not{k}, \not{\psi}] \gamma_5 B_{17}^q + \frac{v \cdot S}{2P \cdot v} [\not{P}, \not{k}] \gamma_5 B_{18}^q \\
& + \frac{M^2(v \cdot S)}{2(P \cdot v)^2} [\not{P}, \not{\psi}] \gamma_5 B_{19}^q + \frac{M^2(v \cdot S)}{2(P \cdot v)^2} [\not{k}, \not{\psi}] \gamma_5 B_{20}^q,
\end{aligned} \tag{7.18}$$

where  $\varepsilon^{0123} = 1$  is used. The naming scheme for the amplitudes is such that the  $A_i^q$ -amplitudes in (7.18) are accompanied by Dirac-structures contracted with the 4-vectors  $k^\mu, P^\mu, S^\mu$ , while the  $B_i^q$ -amplitudes are associated in addition to that with the gauge-link vector  $v^\mu$ .

The 32 amplitudes are independent structures, as there is no model-independent way to relate them to each other. At the same time, there are 32 quark TMD PDFs: 8 at leading, 16 at subleading, and 8 at subsubleading order. The subleading functions will be discussed in Sec. 10. The subsubleading functions (associated with the Dirac structures  $\gamma^-$ ,  $\gamma^- \gamma_5$ ,  $i\sigma^\alpha \gamma_5$ ) are of rather academical character [131]. The crucial point is: there are as many independent amplitudes as there are overall (leading, subleading, subsubleading) TMD PDFs which implies that no relations among TMD functions exist in QCD.

### 7.9.2 Quark-model Lorentz-invariance relations

In the early works, the role of the gauge-link vector  $v^\mu$  was not recognized, and the correlator (7.18) was decomposed with the  $B_i^q$  amplitudes missing [60, 61, 129, 460]. As mentioned in Sec. 7.1, calculations in a quark-target model [705] helped to realize and fix this oversight in [706, 707]. (As reviewed in Sec. 7.2, the importance of the gauge link for the understanding of T-odd TMD PDFs was also recognized thanks to a model calculation [58].)

What is an oversight in QCD, however, becomes strictly correct in quark models with no explicit gauge field degrees of freedom. In these models, no gauge link is present in the model expressions and the Lorentz decomposition rightly contains no  $B_i^q$  amplitudes. In quark models without explicit gluons, also T-odd structures are absent, i.e., in addition to  $B_i^q$  amplitudes also the T-odd  $A_i^q$  amplitudes (namely  $A_4^q, A_5^q, A_{12}^q$ ) are absent. One therefore ends up with more TMD functions than amplitudes, and this implies the so-called "quark model Lorentz Invariance Relations" (qLIRs). The qLIRs in general connect leading and subleading

TMD functions. The subleading TMD functions will be discussed in detail in Chapter 10, but it is convenient to include these model relations here for completeness.

More precisely, one has overall 6 leading and 8 subleading TMD PDFs, i.e., 14 functions. At the same time, one has 9 T-even  $A_i^q$  amplitudes in quark models without explicit gauge field degrees of freedom. This implies 5 qLIRs which are given by

$$g_T^q(x) \stackrel{\text{qLIR}}{=} g_1^q(x) + \frac{d}{dx} g_{1T}^{\perp(1)q}(x), \quad (7.19\text{a})$$

$$h_L^q(x) \stackrel{\text{qLIR}}{=} h_1(x) - \frac{d}{dx} h_{1L}^{\perp(1)q}(x), \quad (7.19\text{b})$$

$$h_T^q(x) \stackrel{\text{qLIR}}{=} -\frac{d}{dx} h_{1T}^{\perp(1)q}(x), \quad (7.19\text{c})$$

$$g_L^{\perp q}(x) + \frac{d}{dx} g_T^{\perp(1)q}(x) \stackrel{\text{qLIR}}{=} 0, \quad (7.19\text{d})$$

$$h_T^q(x, k_T) - h_T^{\perp q}(x, k_T) \stackrel{\text{qLIR}}{=} h_{1L}^{\perp q}(x, k_T). \quad (7.19\text{e})$$

The subleading functions  $g_T^q, g_L^{\perp q}, h_L^q, h_T^q, h_T^{\perp q}$  will be defined and discussed in Sec. 10.

Being based on Lorentz invariance, the relations (7.19) must be obeyed in relativistic models without gluons which provides a powerful cross check for the numerics. Care may be in order in models where UV-divergences could spoil the qLIRs. It may [13] or may not [855] be possible to find regularization schemes in a given model which preserve qLIRs. It will be interesting to see whether the qLIRs are supported approximately in phenomenology, and learn about the size of the  $B_i^q$ -amplitudes.

### 7.9.3 Relations among TMDs in quark models

In some quark models with wave functions obeying SU(4) spin-flavor symmetry, the following relation can hold between the unpolarized, helicity, and transversity TMD PDFs

$$\frac{f_1^q(x, k_T)}{N_q} + \frac{g_1^q(x, k_T)}{P_q} = 2 \frac{h_1^q(x, k_T)}{P_q}, \quad (7.20)$$

where the SU(4) spin-flavor factors are given by  $N_u = 2$ ,  $N_d = 1$ ,  $P_u = \frac{4}{3}$ ,  $P_d = -\frac{1}{3}$  for  $N_c = 3$  (below Eq. (7.5) these spin-flavor factors are given for general  $N_c$ ). The model relation (7.20) holds in bag and light-cone constituent models [13, 747]. Its  $k_T$ -integrated analog was discussed in the bag model even earlier in [387, 724, 856].

The following model relation connects the two Kotzinian-Mulders worm-gear functions,

$$g_{1T}^{\perp q}(x, k_T) = -h_{1L}^{\perp q}(x, k_T). \quad (7.21)$$

First observed in the spectator model [756], it holds also in light-cone constituent quark model [747], covariant parton model [726], bag model [13], light-cone quark-diquark model [470], and the light-cone version of the chiral quark-soliton model [751]. The partonic interpretation of (7.21) is that the distributions of longitudinally polarized quarks in a transversely polarized nucleon ( $g_{1T}^{\perp q}$ ) are exactly opposite to the distributions of transversely polarized quarks in a longitudinally polarized nucleon ( $h_{1L}^{\perp q}$ ).

Next, we discuss the interesting model relation which connects helicity, transversity and pretzelosity, namely

$$g_1^q(x, k_T) - h_1^q(x, k_T) = h_{1T}^{\perp(1)q}(x, k_T). \quad (7.22)$$

The relation (7.22) was first observed in the bag model [742]. It is valid also in spectator model [756], different light-cone models [12, 747, 751] and covariant parton model [726]. Recalling the non-relativistic model prediction (7.4), the relation (7.22) implies that in these quark models the transverse moment of pretzelosity can be considered as a "measure" of relativistic effects.

Finally, let us mention the following non-linear relation which connects all three T-even chiral-odd TMD PDFs and is given by

$$h_1^q(x, k_T) h_{1T}^{\perp q}(x, k_T) = -\frac{1}{2} \left[ h_{1L}^{\perp q}(x, k_T) \right]^2. \quad (7.23)$$

This non-linear relation was derived in the covariant parton model [726] and holds also in bag model [742], light-cone constituent quark model [747] or the light-cone version of the chiral quark-soliton model [751]. Interestingly, it holds in the light-cone quark-diquark model [470] for  $d$ - but not for  $u$ -quarks. More linear and non-linear model relations are known when subleading functions are included [730, 742, 754, 755].

The deeper reasons underlying the emergence of these model relations in such a variety of conceptually very different models have been elucidated in Ref. [857]. The common features of these models are that the quarks can basically be considered bound in a mean field, and the nucleon wave functions exhibit spherical symmetry. When these conditions are fulfilled, the relations (7.21–7.23) hold. If one imposes in addition to that SU(4) spin-flavor symmetry of the nucleon wave function, then also the relation (7.20) holds.

Notice that SU(4) spin-flavor symmetry is necessary but not sufficient for Eq. (7.20) to hold, which is valid only in models with nucleon wave-functions constructed from 'flavor-blind' quark wave-functions multiplied by the spin-flavor factors  $N_q$  or  $P_q$ . The SU(4) spin-flavor symmetry can, however, be realized in more sophisticated ways, e.g., in the spectator model of Ref. [756] the SU(4) symmetry is implemented, but (7.20) is spoiled by the different masses of the (scalar, axial-vector) diquarks. In this model, it is possible to restore (7.20) in the large- $N_c$  limit (where the scalar- and axial-vector diquark masses become equal; notice that in general large  $N_c$  does not imply SU(4) spin-flavor symmetry). In nature, SU(4) spin-flavor symmetry is supported only roughly and one should not expect more from (7.20).

Relations connecting only polarized TMDs, like (7.21–7.23), do not require SU(4) spin-flavor symmetry, are supported by a larger class of models, and may be more reliable. The quark-target model [149], though, does not support (7.21–7.23) which is not surprising: including gluonic fields brings us a step closer to QCD where one can not expect such relations to hold. (Notice that even if such relations were valid in QCD at some scale, they would not be valid at other scales because the different functions obey different evolution equations.)

Two relatively robust conclusions concern the signs of the TMD PDFs: the Kotzinian-Mulders worm-gear functions can be expected to have opposite signs based on Eq. (7.21). One can conclude the same about pretzelosity and transversity from (7.23).

It remains to be seen, whether the model relations (7.21–7.23) will turn out to hold at least approximately within some reasonable accuracy in some region of valence-like  $x$ . Future data, phenomenological work and lattice QCD studies will give insights in that respect.

### 7.9.4 Connection of pretzelosity to orbital angular momentum

Since EMC measurements of polarized structure functions triggered the "proton spin crisis", see Sec. 6.2.2 and Ref. [558], one important motivation to go beyond the collinear approximation and study TMD physics was to learn about the quark orbital motion and the role of orbital angular momentum in the spin structure of the nucleon. But how are TMD PDFs related to quark orbital angular momentum?

In QCD, there is no connection between orbital angular momentum and TMD PDFs (though there is one involving generalized transverse momentum dependent parton distribution functions and Wigner functions, see Sec. 11). In quark models the situation is different. In a wide class of quark models incorporating different model dynamics, the following relation of the pretzelosity function  $h_{1T}^{\perp q}$  to quark orbital angular momentum was found

$$L_z^q = - \int dx d^2k_T \frac{k_T^2}{2M_N^2} h_{1T}^{\perp q}(x, k_T^2) = - \int dx h_{1T}^{\perp(1)q}(x) \quad (\text{in quark models}). \quad (7.24)$$

This relation is supported in the spectator model, bag model, light-front constituent quark model, and the light-front version of the chiral quark soliton model restricted to the 3-quark Fock-state sector, or the covariant parton model [12–14, 554, 726, 742]. Despite being supported by many models, the connection of pretzelosity to orbital angular momentum is, for instance, spoiled by the contributions of axial diquarks in the model of [858] and is not valid in the AdS/QCD-based light-front quark-diquark model of Ref. [794].

In the models where it is supported, Eq. (7.24) holds for the expectation values of operators and not on operator level. None of the supporting models has explicit gluonic degrees of freedom. In these models, the spin contribution of a quark of flavor  $q$  to the nucleon spin is given by  $2S_z^q = \int dx g_1^q(x)$  and the nucleon spin budget takes the simple form

$$\sum_q S_z^q + \sum_q L_z^q = \frac{1}{2} \quad (\text{in quark models}). \quad (7.25)$$

In Ref. [859] the origins of the relation (7.24) were elucidated. For the connection between quark orbital angular momentum and the pretzelosity to be valid in a model, a key ingredient is a certain spherical symmetry of the quark wave functions in the nucleon rest frame. It was furthermore shown that the quark orbital angular momentum defined by Eq. (7.24) contains contributions from the transverse center of momentum which cancel out in the total quark orbital angular momentum, i.e., after summing over all quark flavours present in a model.

In QCD, orbital angular momentum can be described in terms of Wigner functions, see Sec. 11. It is an open question whether the model relation of orbital angular momentum and pretzelosity, Eq. (7.24), has a connection to the expression for angular momentum defined in terms of Wigner functions in Eq. (11.22) in Sec. 11. In QCD, no such relation can be expected. But it will be interesting to address this question in models.

While model-dependent, the relation Eq. (7.24) remains the closest connection of TMD PDFs to quark orbital angular momentum uncovered thus far.

## 7.10 Summary and Outlook

Model studies are needed and well motivated, as argued in Sec. 7.1, and had important impact on the progress in TMD physics. For instance, as reviewed in Sec. 7.2, a model

calculation paved the way towards clarifying the QCD foundations of T-odd TMD PDFs. After discussing limits in QCD in Sec. 7.3 (parton model, large- $N_c$ , non-relativistic limit), we reviewed models of T-even (in Sec. 7.4) and T-odd (in Sec. 7.5) TMD PDFs of quarks. The Sec. 7.6 was devoted to gluon TMD PDFs. Model studies of TMD fragmentation functions were discussed in Sec. 7.7. The Sec. 7.8 addressed formal inequalities and sum rules among TMD functions which, while not model-dependent, have not yet been proven rigorously in terms of renormalized TMD functions. Finally, in Sec. 7.9 we have reviewed relations among TMD PDFs valid and supported in a wide class of quark models without explicit gauge field degrees of freedom.

Many model predictions remain to be tested in experiment or lattice QCD. While there are no reasons to believe that, e.g., the model relations among TMD functions are exact, it may well turn out that some of them hold approximately within a good accuracy. In such cases, it will be interesting to understand the exact reasons for that in QCD. At such instances, the understanding of TMDs and nucleon structure is likely to make significant progress. Models are likely to yield future surprises and new, unexpected and unanticipated insights and will continue to contribute their share to the progress in the field.

Before concluding, let us stress that this chapter was not intended to present a detailed and complete review of all model studies in the literature which would require far more space. Our goal was to highlight the important lessons learned from model studies and their applications. As stressed at the beginning of this chapter, progress in TMD physics arises from combined efforts in experiment, perturbative QCD, lattice QCD, phenomenology, *and* models.

# 8 - Small- $x$ TMDs

## 8.1 Gluon Saturation and TMDs at Small $x$

We will begin this section with a discussion of gluon saturation in the Regge asymptotics of QCD and an effective field theory (EFT) description of this regime. This discussion is important because the EFT description, called the Color Glass Condensate (CGC), strongly constrains the structure of small- $x$  TMDs. For instance, as we shall discuss, the BFKL equation that describes the evolution of unintegrated gluon distributions at small  $x$  can be recovered straightforwardly within the CGC EFT. Conversely, small- $x$  TMDs computed by extrapolating the TMD framework to small  $x$  must have a regime of overlap with the CGC EFT which can help test and refine the dynamical assumptions within this framework.

There are compelling theoretical arguments and strong experimental hints that suggest that gluon distributions saturate at small Bjorken- $x$  [860–865]. Gluon saturation occurs when the nonlinear terms in the field strength tensor are of the same magnitude as the kinetic terms which is the case when the gauge fields are  $O(1/g)$ , or when the occupancy of field modes is  $O(1/\alpha_S)$ . In QCD’s Regge limit, a probe with arbitrarily fine resolution  $Q^2 \gg \Lambda_{\text{QCD}}^2$  will encounter such large field strengths at sufficiently small  $x_{\text{Bj}}$ ; the corresponding scale  $Q \rightarrow Q_s(x)$  is appropriately called the saturation scale. This classicalization scale is also the scale which unitarizes the interaction of the probe with the target; the  $S$ -matrix for a probe of inverse size  $\geq 1/Q$  goes rapidly to zero and its unitarization is accompanied by a significant slowing down in the growth rate of the cross section. Since  $Q_s(x) \gg \Lambda_{\text{QCD}}$  in Regge asymptotics, one can have  $\alpha_S(Q_s) \ll 1$ , which self-consistently satisfies the condition of high occupancy.

As the very large  $O(1/g)$  field strengths suggest, gluon saturation at small  $x$  is an emergent non-perturbative phenomenon. Its dynamical origin is due to many-body screening and recombination higher twist effects that become large with increasing energy at fixed resolution and compete with the bremsstrahlung of soft gluons that is the dominant effect for weak field strengths. Because the coupling governing the emergent non-perturbative dynamics is weak, one can systematically study how strong fields dynamically modify the landscape of many-body parton distributions inside a nucleon or nucleus. In particular, in this region of high parton densities, the effective degrees of freedom and their dynamics are qualitatively different from those in the dilute “Bjorken limit” of QCD. In the latter, leading twist DGLAP [36–39] evolution can be employed to understand the QCD evolution of parton distributions.

The necessity for the emergence of gluon saturation can already be deduced from perturbative QCD. The dynamics of QCD evolution in this framework is governed by phase-space logarithms in  $Q^2$  and  $x$ , that arise at each rung of the evolution ladder, and have the generic structure  $\alpha_S \ln(Q^2) \ln(1/x)$ . In the small- $x$  Regge limit of QCD, large logarithms  $\alpha_S \ln(1/x) \sim O(1)$  dominate over the DGLAP logs  $\alpha_S \ln(Q^2)$ , which suggests that the dominant contributions to QCD evolution at small  $x$  are obtained by organizing the perturbative series accordingly to resum such “leading logs in  $x$ ” (LLx) contributions. The renormalization group equation describing this LLx evolution is the BFKL equation [866, 867], the solution of which, as anticipated, demonstrates a very rapid growth of the gluon distribution, far more so than obtained by solving the DGLAP equation which does not fully account for the large

$\alpha_S \ln(1/x)$  contributions.

The  $\alpha_S^{n+1} \ln^n(1/x)$  resummation of next-to-leading logs in  $x$  (NLLx), to each  $n$ th order in perturbation theory generates the NLLx BFKL equation [868, 869]; careful treatment of collinear poles that appear in the kernel of the NLLx BFKL equation leads to robust results that give a significantly slower growth in gluon distributions at small  $x$  relative to the LLx BFKL equation [870]. It is nevertheless significantly faster than DGLAP evolution at small  $x$ , growing at rate that will violate unitarity asymptotically if unchecked. Since this growth leads to growing occupancy of field modes, gluon saturation provides a dynamical self-regulating non-perturbative unitarization mechanism in QCD at weak coupling.

Since first principles perturbative computations quickly run into the problem of dealing with all-order twist contributions [861], an alternate approach is to construct an effective field theory that captures the many-body dynamics of the saturation regime and can be matched to perturbative computations at large- $x$  and momentum resolutions in their overlapping regime of validity. As noted earlier, the EFT describing the gluon saturation regime is the Color Glass Condensate (CGC) [864, 865, 871, 872], whose construction [863] relies on the following ingredients:

1. A Born-Oppenheimer separation between large- $x$  and small- $x$  modes; the former can be treated as heavy static modes on the light front while the latter are dynamical modes [873, 874].
2. Due to large coherence lengths at small- $x$ , the correspondingly large number of colored static modes constitute higher dimensional (classical) representations of color charge. An explicit construction demonstrates that summations over the color charges of large- $x$  modes can be replaced by a path integral over classical color sources whose mean color charge density is zero, but its variance scales as (for a nucleus with atomic number  $A \gg 1$ )  $\sim A^{1/3}$  for  $x \ll A^{-1/3}$  [862, 863, 875].
3. The large- $x$  static color sources (represented by a source density  $\rho$ ) has the most general gauge invariant coupling [876] to the small- $x$  degrees of freedom, represented by the Yang-Mills action.

This CGC EFT implicitly contains a scale  $x_0$  that separates the large- $x$  static degrees of freedom that are distributed according to a non-perturbative gauge invariant weight functional  $W_{x_0}[\rho]$ . As we will discuss shortly, the requirement that physics be independent of this scale generates the small- $x$  renormalization group equations describing QCD evolution in the saturation regime.

But before we discuss these, we note that the CGC effective action has a classical saddle point  $A_{\text{cl.}}^\mu \equiv A_{\text{cl.}}^\mu[\rho]$  which is an explicit functional of  $\rho$  and is of  $O(1/g)$ . In the McLerran-Venugopalan (MV) model [862, 863, 877] for a large nucleus, where  $W_{x_0}[\rho]$  is a Gaussian in  $\rho$ , the non-perturbative classical dynamics of  $n$ -point correlators of saturated gauge fields can be computed explicitly. For example, the number distribution in lightcone gauge is seen straightforwardly to give the Weizsäcker-Williams distribution at large  $k_\perp > Q_S$  but for  $k_\perp \leq Q_S$  demonstrates a softer logarithmic dependence on  $k_\perp$ . Thus even at the classical level in lightcone gauge one sees a clear manifestation, in this non-Abelian Weizsäcker-Williams distribution, of the role of non-linearities in taming the growth of gluon distributions. Since

the Weizsäcker-Williams distribution provides the bremsstrahlung kernel for QCD evolution in the “linear” regime, its tree-level modification due to gluon saturation provides a preview of a qualitatively different corresponding QCD evolution in this regime.

In lightcone gauge, the non-trivial classical gauge fields  $A_{\text{cl}}^i$  are so-called “pure gauge” fields carrying zero field strength that are separated by a discontinuity at  $x^- = 0$  [862, 863], corresponding to highly singular field strengths (transverse electric and magnetic fields) that only have support at  $x^- = 0$ . In contrast, in Lorenz gauge, the only non-zero component of the gauge field is  $A_{\text{cl}}^+$ , which itself is singular at  $x^- = 0$ , and are therefore often called “shock wave” background field configurations [878]. By solving the Dirac equation in such a background, and likewise the Yang-Mills small fluctuation equations, one can construct respectively quark and gluon propagators in this shock wave background [877, 878]. Remarkably, in Lorenz gauge, these quark and gluon propagators have a very simple structure; in momentum space, they can be expressed as the convolution of free propagators with the insertion respectively of non-local momentum-dependent quark and gluon effective vertices [879–881]. These effective vertices are proportional to Fourier transforms of the respective fundamental and adjoint Wilson lines of the shock wave field  $A_{\text{cl}}^{+,a} = -\frac{\rho^a}{\nabla_\perp^2} \delta(x^-)$ . Note that this implies a dependence to all orders in powers of the large- $x$  color charge densities  $\rho$ .

The structure of these effective propagators allows one to establish an exact correspondence [882–887] of the CGC EFT to Lipatov’s Reggeon field theory [888]. The color charge densities  $\rho$  can be related to the Reggeon degrees of freedom [882] and color singlet combinations of these to Pomeron and Odderon degrees of freedom [889, 890]. Historically, such non-perturbative effective degrees of freedom were found to provide successful descriptions of high energy scattering but a first principles understanding from QCD has remained elusive. The correspondence noted here may therefore provide a useful link between the CGC EFT and intrinsically non-perturbative [891] modern approaches to Reggeon/Pomeron physics.

We now turn to the computation of physical observables in the CGC EFT and the renormalization group (RG) evolution equations that emerge from their proper treatment. A simple example is provided by the inclusive structure functions  $F_2$  and  $F_L$ , which in general can be expressed in terms of bilinears of the quark propagators,  $\text{Tr}(S_A(x, y)\gamma^\mu S_A(y, x)\gamma^\nu)$  in arbitrary background fields. In the CGC EFT, the leading order result for  $F_{2,L}$  is obtained by replacing  $A \rightarrow A_{\text{cl}}$ , and  $S_A$  by the shock wave propagators we mentioned earlier. One immediately recovers the Glauber-Mueller dipole model [892], with  $F_{2,L} \propto (1 - \langle \mathcal{S} \rangle)$ , where  $\mathcal{S} = \frac{1}{N_c} \text{Tr} (V(x_\perp)V^\dagger(y_\perp))$  is the dipole S-matrix,  $V(x_\perp) = P \exp \left( i \frac{\rho}{\nabla_\perp^2} (x_\perp) \right)$  and  $\langle \mathcal{S} \rangle = \int [D\rho] W_{x_0}[\rho] \mathcal{S}$ .

For the MV model with Gaussian distributed color sources  $W_{x_0}[\rho]$  with weight  $\mu_A^2$  (corresponding to the color charge squared per unit area), one obtains

$$\langle \mathcal{S} \rangle(r_\perp) = \exp \left( -\frac{r_\perp^2 Q_S^2}{4} \ln \left( \frac{1}{r_\perp^2 \Lambda_{\text{QCD}}^2} \right) \right), \quad (8.1)$$

where  $Q_S^2 = \alpha_S C_F \mu_A^2$  with  $C_F = (N_c^2 - 1)/2N_c$ . For  $r_\perp^2 Q_S^2 \ll 1$ , one recovers the color transparency limit of QCD for the dipole cross section; for  $r_\perp^2 Q_S^2 \gg 1$ ,  $\langle \mathcal{S} \rangle \rightarrow 0$ , corresponding to the “color opacity” or black disc limit of QCD [893].

At next-to-leading order, including the contribution of real and virtual slow gluons in the shock wave background, leads to the relation [878, 894]:

$$\frac{d\langle \mathcal{S} \rangle}{dY} = -\frac{\alpha_s N_c}{2\pi^2} \int d^2 z_\perp \frac{(x_\perp - y_\perp)^2}{(x_\perp - z_\perp)^2(z_\perp - y_\perp)^2} \langle \mathcal{S}(x_\perp, y_\perp) - \mathcal{S}(x_\perp, z_\perp) \mathcal{S}(z_\perp, y_\perp) \rangle, \quad (8.2)$$

where  $Y = \ln(x_0/x)$  denotes the rapidity. In the large  $N_c$  limit, and for  $A \gg 1$ ,  $\langle \mathcal{S} \mathcal{S} \rangle \approx \langle \mathcal{S} \rangle \langle \mathcal{S} \rangle$ , leading to a closed form non-linear equation, the Balitsky-Kovchegov (BK) equation [878, 894], for the dipole S-matrix. When  $\langle \mathcal{S} \rangle \sim 1$ , one can write  $\langle \mathcal{S} \rangle \sim 1 - \langle \mathcal{N} \rangle$ , where the dipole amplitude  $\langle \mathcal{N} \rangle$  ( $\ll 1$ ) satisfies the BFKL equation. In the opposite limit,  $\langle \mathcal{S} \rangle \approx 0$ , the BK equation unitarizes the cross section, as noted previously. In between these two regimes, lies a "geometrical scaling" regime, where the dipole amplitude obeys leading twist shadowing; in other words, it satisfies leading twist BFKL evolution but is still sensitive to the presence of a saturation scale [895]. Interestingly, small- $x$  data from HERA data exhibit this geometric scaling phenomenon [896].

In general, Eq. (8.2) represents the RG equation for the evolution of the two-point correlator of Wilson lines. One can similarly write down the corresponding evolution equation for an arbitrary number of Wilson line correlators, which generates the Balitsky-JIMWLK hierarchy [878, 897–900]. The entire content of this hierarchy, and of the CGC EFT to LLx, can alternatively be written as an evolution equation for the weight functional  $W_Y[\rho]$ :

$$\frac{dW_Y[\rho]}{dY} = \mathcal{H}_{\text{JIMWLK}} \otimes W_Y[\rho], \quad (8.3)$$

where  $\mathcal{H}_{\text{JIMWLK}}$  represents the JIMWLK Hamiltonian. This equation has the structure of a Fokker-Planck equation in the space of functions  $\rho$  and can therefore be equivalently written as a Langevin equation for the Wilson lines  $V$  [901]. This Langevin equation can be solved numerically [902, 903] which allows us to determine the solution to Eq. (8.2) for finite  $N_c$  as well as the evolution equations for higher point Wilson line correlators to LLx accuracy.

Our discussion up to this point can be summarized in Fig. 8.1 which shows the different regimes of QCD evolution at small- $x$ . The line corresponding to the saturation scale  $Q_S^2(Y)$ , as noted corresponds to the boundary where classicalization and unitarization occurs. In nuclei, it is estimated that  $Q_S^2(Y) \sim (A/x)^\delta$ , where  $\delta \approx 0.3$  [904]. At small- $x$ , the CGC EFT predicts that distributions are universal after appropriate scaling of  $Q_S$  with  $A$ . This suggests that saturation effects can be observed precociously in DIS off nuclei at lower energies than in DIS off protons.

This LLx framework in the CGC EFT has now been extended to next-to-leading-log (NLLx) accuracy for both BK [905–907] and JIMWLK evolution [882, 908–911]. In particular, the NLL evolution kernels for the Wilson lines [906], for dipoles [905], for 3-point operators [912] and for quadrupoles [913] have been used to derive the full NLL JIMWLK Hamiltonian [910], which was then confirmed by a more explicit computation [908]. An unanticipated synergy between non-global logarithms and small- $x$  evolution has also enabled one to use computations to NNLO in the former to extract parts of the NNL BK kernel [914]. Complete analytical expressions have been obtained for a varied range of physical observables. The fully inclusive DIS cross section was computed in [915] and in [916], then confirmed in [917]. Semi-inclusive processes have been studied both for  $pA$  collisions in the dilute-dense hybrid factorization

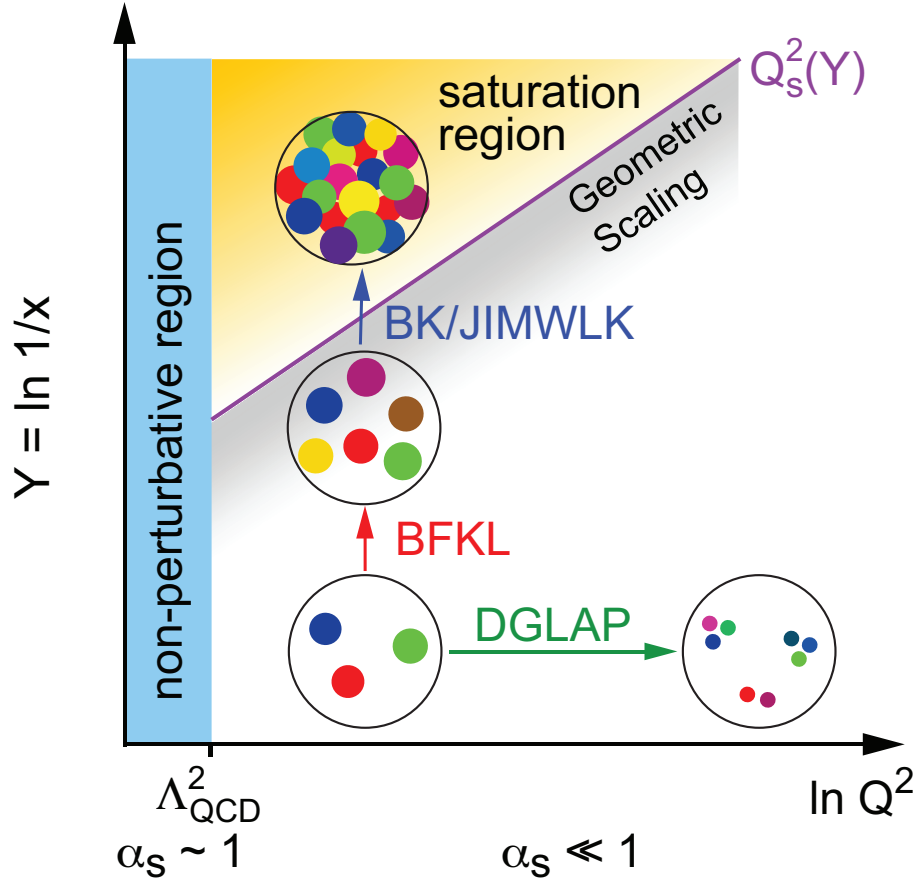


Figure 8.1: The map of high energy QCD in the ( $Q^2$ ,  $Y = \ln(1/x)$ ) plane. (This plot is adopted from Ref. [15]).

ansatz [918, 919], and for  $eA$  collisions [920–922], where the NLO impact factor has been computed for di-jet and photon+di-jet final states. Finally, exclusive  $eA$  collisions have been studied for dijet production [923] and for the production of a light vector meson [924].

This general picture of interactions at small- $x$ , in terms of the RG evolution of the shockwave classical fields, does not depend on the type of scattering reaction. It should therefore be valid for transverse momentum dependent (TMD) processes. The first step of TMD studies at small- $x$  would be the implementation of the available theoretical tools most effectively represented by the CGC formalism to a variety of TMD observables. In particular, there have been important developments that have brought to the fore the connections between the TMD formalism and the small- $x$  CGC formalism in various contexts [925–931]. It was realized for instance that TMD-like hard processes which involve a hard scale  $Q$  in addition to the transverse momenta of the observables offer unique possibilities to probe the saturation regime.

The most important point of convergence is the fact that unintegrated gluon distributions are important ingredients in both the TMD and CGC frameworks. In the latter, there is a classification of scatterings into dilute-dilute, dilute-dense and dense-dense depending on the field strengths of the color sources in the projectile and target and the transverse momenta of interest [871, 932]. Unintegrated distributions appear at small- $x$  in dilute-dilute ( $p + p$

scattering for instance) and dilute-dense ( $p + A$  scattering being a natural example). In the latter case, the unintegrated distributions in the target are sensitive to coherent multi-parton interactions. Several processes have been proposed in the literature to study the unintegrated gluon distributions including semi-inclusive DIS [925], low  $p_T$  Drell-Yan [933], and back-to-back di-hadron correlations in forward  $pA$  processes [934]. Recently, considerable progress has been made in computing Sudakov double logarithms that can be resummed consistently in the small- $x$  formalism [935–939]. These computations provide a solid theoretical foundation for further rigorous investigations that probe the dynamics of the saturation regime with hard processes.

## 8.2 Weizsäcker-Williams and Dipole Gluon Distributions

It is important to emphasize that the properties of the QCD dynamics typical for small  $x$  lead to a very different picture of TMD scattering compared to the standard TMD framework at large  $x$ . Indeed, it was in the context of the CGC framework that the existence of *two* different unintegrated gluon distributions (UGDs) was first proven [940]. This observation is related to the question of *non-universality* for TMD distributions due to the process-dependence of their gauge link structures, since then taken into account in the standard TMD approach [926, 927]. The topic of non-universality at small  $x$  is discussed in great detail in [941].

Two types of gluon TMD distributions are the most common. The first such distribution, the Weizsäcker-Williams (WW) gluon distribution, is calculated from the correlator of two classical gluon fields of relativistic hadrons (the non-Abelian Weizsäcker-Williams fields) [862, 863, 942, 943]. The WW gluon distribution can be defined following the conventional gluon distribution [119, 228]. Following Eq. (2.139), we can define the WW gluon distribution as,

$$xG_{WW}(x, k_\perp) = \int \frac{d\xi^- d^2\xi_\perp}{(2\pi)^3 P^+} e^{-ixP^+\xi^- + ik_\perp \cdot \xi_\perp} \langle P | G^{+i}(\xi^-, \xi_\perp) W_{\square}(\xi^\mu, 0) G^{+i}(0) | P \rangle , \quad (8.4)$$

where  $G^{\mu\nu}$  is the gauge field strength tensor and  $W_{\square}(\xi^\mu, 0)$  represents the gauge link in the adjoint representation and points to the past ( $-\infty$ ). This gluon distribution can also be defined in the fundamental representation [76],

$$\begin{aligned} xG_{WW}(x, k_\perp) &= \frac{2}{P^+} \int \frac{d\xi^- d^2\xi_\perp}{(2\pi)^3} e^{-ixP^+\xi^- + ik_\perp \cdot \xi_\perp} \\ &\quad \times \text{Tr} \langle P | G^{+i}(\xi^-, \xi_\perp) W_{\square}(\xi^\mu, 0) G^{+i}(0^-, 0_\perp) W_{\square}^\dagger(\xi^\mu, 0) | P \rangle . \end{aligned} \quad (8.5)$$

Here,  $W_{\square}(\xi^\mu, 0)$  represents the gauge link in the fundamental representation. We note that for the WW gluon distribution, the two gauge links in the above definition point to the same direction (to  $-\infty$ ). This gluon distribution corresponds to the gluon distributions associated with Higgs Boson production in hadronic collisions as described in Sec. 2.11.2. The above  $G_{WW}(x, k_\perp)$  is referred to as  $f_1^g$  there. If we want to study the gluon distribution associated with semi-inclusive deep inelastic scattering, the gauge links will point to the future ( $+\infty$ ). The universality of the gluon distributions in the different processes will follow the discussions in previous sections, see, e.g., Sec. 2.7.1 and 3.3. In the following, for brevity we do not include explicitly the transverse gauge links which connects the Wilson lines in Eqs. (8.5, 8.4) at  $\xi^- \rightarrow +\infty$ . Also note that all transverse gauge links are subdominant in the small- $x$  regime,

which is why we will neglect them hereafter<sup>30</sup>.

The structure of the WW distribution used in the CGC approach coincides with the gluon TMD distribution at large  $x$  and has a clear physical interpretation as the number density of gluons inside the hadron in light-cone gauge. This makes it the primary candidate to study the transition region between dilute and dense regimes. Since the WW distribution is constructed from semi-infinite future-pointing Wilson lines (and past-pointing lines for the Drell-Yan process) it takes into account only final state interactions (initial state for DY) which occur after (before) the initial interaction of the hard probe with the target.

This makes it qualitatively different from the second gluon distribution, defined as the Fourier transformation of the color dipole cross section:

$$xG_{dip.}(x, k_\perp) = \frac{2}{P^+} \int \frac{d\xi^- d^2\xi_\perp}{(2\pi)^3} e^{-ixP^+\xi^- + ik_\perp \cdot \xi_\perp} \times \text{Tr} \langle P | G^{+i}(\xi^-, \xi_\perp) W_\square(\xi^\mu, 0) G^{+i}(0^-, 0_\perp) W_\square^\dagger(\xi^\mu, 0) | P \rangle, \quad (8.6)$$

where the two gauge links point to the opposite directions and they form a loop. These gauge links stretch between minus and plus infinity and take into account both final and initial interactions, which reflects in the shockwave nature of scattering at small- $x$  and separation of scales between projectile and target. Unlike the WW distribution, the dipole gluon distribution does not have a clear parton interpretation.

Within the CGC framework, the WW gluon distribution can be written in terms of the correlator of four Wilson lines as,

$$xG_{WW}(x, k_\perp) = -\frac{2}{\alpha_S} \int \frac{d^2v_\perp}{(2\pi)^2} \frac{d^2v'_\perp}{(2\pi)^2} e^{-ik_\perp \cdot (v_\perp - v'_\perp)} \left\langle \text{Tr} [\partial_i U(v_\perp)] U^\dagger(v'_\perp) [\partial_i U(v'_\perp)] U^\dagger(v_\perp) \right\rangle_x, \quad (8.7)$$

where the Wilson line  $U(v_\perp)$  is defined as a gauge link from  $(-\infty)$  to  $(+\infty)$ . By using the notation of Eq. (2.43), we have  $U(v_\perp) = W_n(v_\perp, -\infty, +\infty)$ . In the above equation, subscript  $x$  represents the momentum fraction carried by the gluon when we evaluate the matrix element. The precise  $x$  value is determined by the kinematics of the process. In addition, the normalizations of the states are different in the CGC computations. For example, Eq. (8.5) is normalized covariantly and the hadronic state  $|P\rangle$  is relativistically normalized to  $\langle P'|P\rangle = (2\pi)^3 2P^+ \delta(P^+ - P'^+) \delta^{(2)}(P_\perp - P'_\perp)$ , while the average in Eq. (8.7) and Eq. (8.8) below is taken over the CGC wave function and is normalized that  $\langle 1 \rangle_x = 1$ , such as  $\langle \hat{O} \rangle_x = \frac{\langle P|\hat{O}|P\rangle}{\langle P|P\rangle}$ .

Similarly, the dipole gluon distribution can be directly evaluated in the CGC framework,

$$xG_{dip.}(x, k_\perp) = k_\perp^2 \frac{2}{\alpha_S} \int \frac{d^2v_\perp}{(2\pi)^2} \frac{d^2v'_\perp}{(2\pi)^2} e^{-ik_\perp \cdot (v_\perp - v'_\perp)} \left\langle \text{Tr} U(v_\perp) U^\dagger(v'_\perp) \right\rangle_x. \quad (8.8)$$

To make the connections between the CGC results of Eqs. (8.7,8.8) and those in Eqs. (8.5,8.6) more clearly, one can apply the derivative on the Wilson line,

$$\partial_i U(v_\perp) = ig_S \int_{-\infty}^{\infty} dv^- W_n(v_\perp, -\infty, v^-) (\partial_i A^+(v^-, v_\perp)) W_n(v_\perp, v^-, \infty). \quad (8.9)$$

<sup>30</sup>In a singular gauge, such as the light-cone gauge, we need to consider the transverse gauge link contributions at the spatial infinity [46, 944].

Notice that  $(\partial_i A^+(v^-, v_\perp))$  is the leading part of the gauge invariant field strength tensor  $G^{i+}(v_\perp)$  at small- $x$ . Therefore, the above correlator can be written in terms of a gauge invariant matrix element [926, 927],

$$\begin{aligned} & -\langle \text{Tr} [\partial_i U(v_\perp)] U^\dagger(v'_\perp) [\partial_j U(v'_\perp)] U^\dagger(v_\perp) \rangle_x \\ &= g_S^2 \int_{-\infty}^{\infty} dv^- dv'^- \left\langle \text{Tr} [G^{i+}(\vec{v}) W_\square(v, v') G^{j+}(\vec{v}') W_\square^\dagger(v, v')] \right\rangle_x . \end{aligned} \quad (8.10)$$

To recover the gluon distribution function as written in Eq. (8.5), it is necessary to account for the different normalizations used to calculate the average of Wilson lines, see the discussions after Eq. (8.7).

The above two gluon distributions form the fundamental building blocks of all unpolarized TMD gluon distributions at small  $x$  in the planar limit [927, 945]. It was realized that the WW gluon distribution could be directly accessed in the dijet production process in DIS while the photon-jet correlations measurement in  $pA$  collisions can access the dipole gluon distribution directly [926]. More complicated dijet production processes in  $pA$  collisions will involve both of these gluon distributions through a convolution in transverse momentum space [927]. Related phenomena have also been intensively investigated in the TMD factorization framework [76, 222, 223, 946], where the associated parton distributions are found to be non-universal. Detailed analyses [927] have shown that these results in the TMD formalism can be related to the small- $x$  calculations for dijet production [934]. Phenomenological applications of this formalism to the RHIC data of forward di-hadron productions in  $dA/pA$  collisions have been carried out in Refs. [947–950]. More importantly, precision studies of dijet/di-hadron process in DIS at the future EIC will provide a unique perspective to probe the gluon saturation at small  $x$  in large nuclei [15, 951].

In addition, the azimuthal correlated (linearly polarized) TMD gluon distribution has played an important role in describing cross sections in hard processes at small  $x$  [928]. For example, the linearly polarized WW gluon distribution  $xh_{WW}^\perp(x, k_\perp)$  is identical to  $xG_{WW}(x, k_\perp)$  at large transverse momentum and agrees with the perturbative QCD results. For the case  $\Lambda^2 \ll k_\perp^2 \ll Q_s^2$  one finds  $xh_{WW}^\perp(x, k_\perp)$  is suppressed as compared to  $xG_{WW}(x, k_\perp)$ . On the other hand, for the dipole gluon distribution, we have the following simple result,

$$xh_{dip.}^\perp(x, k_\perp) = xG_{dip.}(x, k_\perp) , \quad (8.11)$$

for all  $k_\perp$  region, which means that it has as many linearly polarized gluon pairs as unpolarized gluon pairs. The phenomenological implication of the above discussed linearly polarized gluon distributions have been investigated in a number of papers, in particular, that we may study them in great detail at the future EIC [503, 952–957].

### 8.3 TMD Evolution and Resummation

The QCD evolution effects play an important role in describing the scale dependence of these gluon distributions. This includes the small- $x$  evolution, i.e., the BFKL/BK evolution [878, 958], and the so-called TMD evolution, i.e., the Collins-Soper evolution [86, 119]. With the small- $x$  approximations applied in Eq. (8.7, 8.8), the small- $x$  evolution effects are taken into account with the associated evolution equations. However, from those equations,

the Collins-Soper evolution effects are not explicit. Recent developments have paved the way to perform resummation of large logarithms in the TMD gluon distributions at small  $x$  [935–938, 959, 960]. It has been shown the above two resummations (Sudakov and small  $x$ ) can be performed consistently at the cross section level.

To study the scale dependence of TMDs at small  $x$ , we go back to the full QCD definitions of the TMDs, in which the scale dependence naturally shows up in the associated TMD factorization for hard scattering processes. In the gauge invariant definitions of the gluon distributions, as shown in Eqs. (8.5, 8.6), there are un-cancelled light-cone singularities from high order gluon radiations. The regularization introduces the scheme dependence for the un-subtracted gluon TMDs. However, the final result for the subtracted gluon TMDs will be independent of the rapidity regulator and the scheme, see more discussions in Sec. 2 and 4.

Similar to the case of the hard scattering processes studied in Refs. [935, 936], the most important high order gluon radiation come from two regions: (1) soft gluon and (2) collinear gluon. The soft gluon radiation leads to the Collins-Soper evolution, whereas the collinear gluon contributes to the DGLAP resummation formulated in terms of the integrated parton distributions in the CSS resummation formalism. In the current case, these collinear gluon radiation contributions actually become the small- $x$  evolution contributions, which are described by the associated BK/JIMWLK equations [864, 878, 958, 961]. The above two contributions are well separated in phase space. That is the reason that we can achieve resummations of large logarithms from these two sources consistently. The final results for the TMDs can be written as [938],

$$xG_{WW}(x, k_\perp, \zeta_c = \mu_F = Q) = -\frac{2}{\alpha_s} \int \frac{d^2 v_\perp d^2 v'_\perp}{(2\pi)^4} e^{ik_\perp \cdot r_\perp} \mathcal{H}^{WW}(\alpha_s(Q)) e^{-\mathcal{S}_{sud}(Q^2, r_\perp^2)} \times \mathcal{F}_{Y=\ln 1/x}^{WW}(v_\perp, v'_\perp), \quad (8.12)$$

where  $r_\perp = v_\perp - v'_\perp$ ,  $\zeta_c$  is the regulator for the end-point singularity in the TMD distributions in the Collins 2011 scheme [10], and  $\mu_F$  is the associated factorization scale. In the final factorization formula, these two scales are usually taken as the same as the hard momentum scale  $Q$  in hard scattering processes. Meanwhile,  $\mathcal{F}_Y^{WW}$  is the Fourier transform of the WW gluon distribution, as in Eq. (8.7),

$$\mathcal{F}_Y^{WW}(v_\perp, v'_\perp) = \left\langle \text{Tr} \left[ \partial_\perp^\beta U(v_\perp) U^\dagger(v'_\perp) \partial_\perp^\beta U(v'_\perp) U^\dagger(v_\perp) \right] \right\rangle_x, \quad (8.13)$$

and  $Y$  represents the rapidity of the gluon from the nucleus,  $Y \sim \ln(1/x)$ . The Sudakov form factor contains an all order resummation

$$\mathcal{S}_{sud} = \int_{c_0^2/r_\perp^2}^{Q^2} \frac{d\mu^2}{\mu^2} \left[ A \ln \frac{Q^2}{\mu^2} + B \right], \quad (8.14)$$

where  $c_0 = 2e^{-\gamma_E}$  with  $\gamma_E$  the Euler constant. The hard coefficients  $A$  and  $B$  can be calculated perturbatively [63]:  $A = \sum_{i=1}^{\infty} A^{(i)} \left( \frac{\alpha_s}{\pi} \right)^i$  and  $B = \sum_{i=1}^{\infty} B^{(i)} \left( \frac{\alpha_s}{\pi} \right)^i$ . One-loop results for these coefficients can be found in Ref. [938]. It is interesting to note that  $B^{(1)} = 0$  which is different from the TMD gluon distribution in the collinear framework. Reconciling these two frameworks

has been a theoretical challenge in small- $x$  physics, see discussions in Ref. [929, 935–938]. Similarly, we can write down the result for the dipole-gluon TMD [938],

$$xG_{dip.}(x, k_\perp, \zeta_c = \mu_F = Q) = -\frac{2}{\alpha_s} \int \frac{d^2v_\perp d^2v'_\perp}{(2\pi)^4} e^{ik_\perp \cdot r_\perp} \mathcal{H}^{DP}(\alpha_s(Q)) e^{-\mathcal{S}_{sud}(Q^2, r_\perp^2)} \times \vec{\nabla}_{r_\perp}^2 \mathcal{F}_{Y=\ln 1/x}^{DP}(v_\perp, v'_\perp), \quad (8.15)$$

where  $\mathcal{F}_Y^{DP}(v_\perp, v'_\perp)$  is defined as,

$$\mathcal{F}_Y^{DP}(v_\perp, v'_\perp) = \langle \text{Tr} [U(v_\perp) U^\dagger(v'_\perp)] \rangle_x. \quad (8.16)$$

In the above equations, both  $\mathcal{F}_Y^{WW}$  and  $\mathcal{F}_Y^{DP}$  are the renormalized quadrupole and dipole amplitudes, respectively, which obey the associated small- $x$  evolution equations. The TMD evolution effects are included in the Sudakov factor. The remaining factors,  $\mathcal{H}^{WW}(\alpha_s(Q))$  and  $\mathcal{H}^{DP}(\alpha_s(Q))$ , which are of order 1, are the perturbatively calculable finite hard parts.

## 8.4 Spin-dependent TMDs

The problem of identifying the basic TMD distributions at small  $x$  is of course not limited to the case of unpolarized scattering. In fact, the TMD framework represents the most effective approach to the study of the spin structure of the hadron. A particularly challenging problem is the so-called “spin crisis” which states that while we know the value of the proton’s spin we do not know its origin and how different components of the proton’s dynamics contribute to it, see detailed discussions in Sec. 6.2.2.

A major source of experimental uncertainty is the spin content of the proton at small  $x$ . However, this study is highly non-trivial because, to leading eikonal order, longitudinal spin effects are highly suppressed. For example, the McLerran-Venugopalan (MV) model [862, 863] provides the following solution for the classical field formed by the small- $x$  gluons:

$$A_{\text{cl}}^+(x) = -\frac{1}{\partial_\perp^2} \rho(x_\perp) \delta(x^-); \quad A_{\text{cl}}^- = A_{\text{cl}}^\perp = 0. \quad (8.17)$$

As noted, this solution has the form of a shockwave, with the small- $x$  gluons of the hadron shrunk to a single point  $x^- = 0$ . To study longitudinal spin at small  $x$ , one has to, in general, extend the leading order eikonal solution of Eq. (8.17) to include sub-eikonal effects.

To illustrate this property, let us look at the leading diagram contributing to DIS at small  $x$  presented in Fig. 8.2a. At leading order, the interaction of the virtual photon with the target is realized through the photon splitting into a  $q\bar{q}$  pair which subsequently interacts with a background field formed by partons of the target. Those partons are schematically depicted as vertical lines in Fig. 8.2a. The structure of the background is of course defined by the small- $x$  QCD dynamics of the target and can be characterized by a typical momentum  $l$ . The momentum scale  $p$  of the  $q\bar{q}$  is different and in general is defined by the virtuality of the incoming photon  $Q^2$  (hard scale). As a result, the condition of the strict ordering of longitudinal components of momenta at small  $x$  can be formulated by the condition

$$l^+ \gg p^+, \quad l^- \ll p^-. \quad (8.18)$$

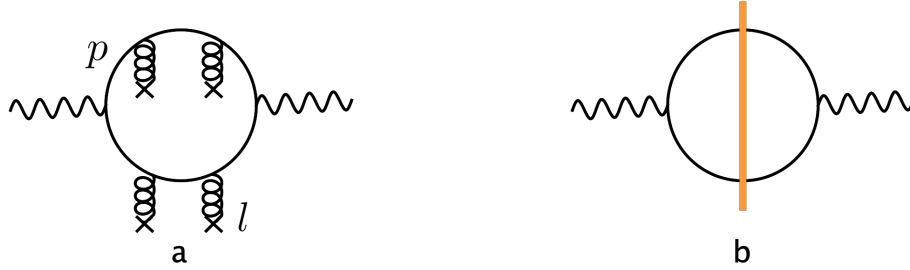


Figure 8.2: a) Current-current correlator in an arbitrary background field; b) The same in the CGC shockwave background, where the spatial separation in  $x^-$  shrinks to a point (represented by the orange vertical bar).

This ordering of momenta can only be realized if the virtuality of the small- $x$  partons is dominated by the transverse momentum component:

$$|l^+l^-| \ll l_\perp^2 \sim Q_s^2. \quad (8.19)$$

There are three types of sub-eikonal corrections to the shockwave approximation, as can be seen in Eq. (8.17). First, there could be a non-trivial dependence on  $x^-$  in lieu of the  $\delta$  function. There could also be non-zero components to  $A_{\text{cl}}$  besides  $A^+$ , and finally there could be a dependence on  $x^+$  as well, which we will not discuss here since it was found to be sub-sub-leading [962]. The first type of correction is taken into account in computations with finite longitudinal size for the background field and is the most straightforward extension of the shockwave picture in Fig. 8.2b. Going beyond the shockwave approximation in this case means that the kinematic conditions in Eq. (8.18) are loosened and there is some transfer of longitudinal momenta from the small- $x$  background to the hard part of the scattering. Loosening these conditions allows for TMD distributions at small  $x$  to be defined with nonzero longitudinal phases, contrary to expressions such as Eqs. (8.7,8.8), and thus overcome the cancellation of spin and angular momentum terms observed at small  $x$  [963]. More frequently, these types of non-eikonal corrections are studied in describing the transition between dilute and dense regions, specifically, the connection between the standard large- $x$  TMD framework and its small- $x$  counterpart we discussed previously [929, 937].

Spin effects are also more naturally described by the second type of non-eikonal corrections which correspond to taking nonzero transverse components of the background field  $A_\perp$  into account while also imposing the kinematic condition in Eq. (8.18). Strictly speaking, this type of non-eikonal correction can only arise in a background of the finite width as well. This makes computations with non-zero  $A_\perp$  extremely difficult because of the competing non-eikonal effects of both first and second types, though there is considerable recent progress in this direction [964–966].

In small- $x$  spin physics, and in its TMD applications, both types of corrections are related to the missing longitudinal phase in Eqs. (8.7)–(8.8), but for formal computations the second type of correction allows one to cast distributions in a form where the non-zero longitudinal width for the background field is not required. Then one can take the formal limit of the zero-width background field while keeping nonzero  $A_\perp$ , thereby taking into account spin effects from the transfer of the polarization from the target in a more obvious way.

These strategies have been applied recently to spin-dependent TMDs and there are two realizations available. The first method [967–974] involves imposing the kinematic constraint at the level of Feynman diagrams. In the second approach [975–977], the shockwave approximation is used. One can in the latter approach identify the structure of the operator describing the transfer of polarization from target to projectile at small  $x$ .

The spin dependent interaction is a sub-eikonal effect which is suppressed at high energies. For this reason the dominant contribution at small  $x$  has to be described by an operator which contains the smallest number of spin dependent interactions. Such an operator has been constructed in [975, 976] by calculating the quark production cross section in SIDIS on a longitudinally polarized proton or a nucleus. Similar to the unpolarized case the latter can be defined as a forward scattering amplitude for a color singlet longitudinally polarized quark-antiquark pair propagating in a background of a polarized target, see Fig. 8.2b. However, now the quark propagation contains exactly one sub-eikonal interaction carrying spin information from the target. As a result a concept of a polarized dipole amplitude can be introduced. This amplitude can be related to the quark helicity TMD, see discussion in [975].

In the operator language this amplitude is defined by a correlator of a trace of a Wilson line which describes eikonal interactions with the target and a so-called polarized Wilson line operator. The latter is an extension of a regular light-cone Wilson line which contains a sub-eikonal helicity-dependent local operator insertion between two semi-infinite eikonal Wilson lines [977]. In the case of gluon exchanges the sub-eikonal insertion is the  $F_{12}$  component of the gluon field strength tensor. This form, which is counterintuitive in terms of TMD distributions since it resembles a very subleading twist distribution while actually appearing at leading twist, can be interpreted as arising from the scalar  $\vec{\mu} \cdot \vec{B} = -\mu_z F^{12}$  for a quark with chromomagnetic moment  $\vec{\mu}$  travelling through the chromomagnetic field  $\vec{B}$ . This operator structure was also obtained in [962, 964, 978, 979].

A significant difference between polarized and unpolarized scattering at small  $x$  is that in the former case contribution of quark exchanges should be included already at the leading order. The helicity-dependent quark exchanges are of the same order as the sub-eikonal spin dependent gluon exchanges. The resulting operator which takes into account both effects [976, 977] is

$$(U^{\text{pol}}(v_\perp))^{ab} = \frac{2i g p^+}{s} \int_{-\infty}^{+\infty} dv^- \left( W_n(v_\perp, +\infty, v^-) G^{12}(v^-, v_\perp) W_n(v_\perp, v^-, -\infty) \right)^{ab} (8.20)$$

$$- \frac{g^2 p^+}{s} \int_{-\infty}^{\infty} dv^- \int_{-\infty}^{v^-} dv'^- W_n^{aa'}(v_\perp, +\infty, v^-) \bar{\psi}(v^-, v_\perp) t^{a'} W_n(v_\perp, v^-, v'^-) \\ \times \frac{1}{2} \gamma^+ \gamma_5 t^{b'} \psi(v'^-, v_\perp) W_n^{b'b}(v_\perp, v'^-, -\infty) - c.c.,$$

Evolving this operator in the shockwave framework one can obtain the small- $x$  helicity evolution equations [975–977]. These equations are analogue to the unpolarized BK/JIMWLK evolution equations. JIMWLK-type treatment of the helicity evolution was constructed in [980].

The large logarithm which is resummed by the helicity evolution equations is  $\alpha_s \ln^2(\frac{1}{x})$ , i.e., two logarithms of energy for each power of the coupling constant. This is very different

from the unpolarized small- $x$  evolution where at the leading order the powers of  $\alpha_s \ln(\frac{1}{x})$  are resummed. Recently a single-logarithmic correction  $\alpha_s \ln(\frac{1}{x})$  to the double-logarithmic kernel of the helicity evolution equations has been calculated as well [981].

The equations were constructed in both flavor singlet and non-singlet channels. In general, the evolution equations are not closed. They contain not only mixing between polarized quark and gluon exchanges but also include non-linear (saturation) terms with higher-order operators in the evolution kernel. Fortunately, the equations become closed in the large  $N_c$  and large  $N_c \& N_f$  limits. The flavour singlet helicity evolution equations were solved numerically and analytically in large  $N_c$  limit [976, 982]. Flavor non-singlet equations at large  $N_c$  were solved analytically in [983]. A numerical solution of the large  $N_c \& N_f$  equations was obtained in [984].

Despite the fact that several methods of calculation of spin effects at small- $x$  are available at different levels of sophistication, the field is still in its infancy. This is illustrated most directly by noting that different results are obtained for the evolution of quark helicity at small- $x$ :

$$\Delta\Sigma(x, Q^2) \sim \left(\frac{1}{x}\right)^\delta, \quad (8.21)$$

where  $\delta = 1.481$  is obtained in the standard Feynman diagram approach [972, 974] while one obtains  $\delta = 0.874$  when  $\alpha_s = 0.3$  with the shockwave technique. This difference between the two results needs to be resolved and will be a focus of future effort.

Meanwhile, the shockwave approximation approach of Refs. [975–977] has been extended to other spin-dependent distributions at small  $x$ , including the quark/gluon orbital angular momentum distribution [985] and the quark transversity distribution [986]. There has already been some progress on the phenomenology front, where a recent analysis of polarized inclusive DIS data incorporated the small- $x$  helicity evolution of the shockwave approach [987]. More developments in this direction will be important to resolve the spin crisis with data from the EIC.

On the other hand, for a transversely polarized nucleon, the spin effects are not sub-eikonal and one finds that the naive-time-reversal-odd dipole gluon distributions can be described by a universal function [988],

$$xf_{1T}^{\perp g} = xh_{1T}^g = xh_{1T}^{\perp g} = \frac{-k_\perp^2 N_c}{4\pi^2 \alpha_s} O_{1T}^\perp(x, k_\perp^2), \quad (8.22)$$

which is related to the so-called spin-dependent odderon  $O_{1T}^\perp(x, k_\perp^2)$ . The latter is defined through the dipole odderon operator of  $\text{Tr} [U^{[\square]}(0_T, y_T) - U^{[\square]\dagger}(0_T, y_T)]$  [889]. The spin-dependent odderon has been considered in this way in [989] and in many studies of elastic scattering [990–992]. Based on these developments, Ref. [993] has proposed to measure the small- $x$  gluon Sivers function through exclusive pion production in unpolarized electron-proton scattering in the forward region due to its connection to the QCD odderon.

An important caveat to the above discussion is the possible role of topological effects due to the chiral anomaly, which has provoked considerable debate in the literature [553, 994, 995]. The role of the chiral anomaly can be deduced from the first moment of  $g_1$ , which is equal to the quark helicity  $\Delta\Sigma(Q^2)$  (plus a nearly constant term arising from a linear combination of iso-triplet and iso-octet axial charges). This quantity is given by the matrix element of the

iso-singlet axial vector current  $J_\mu^5$ , which is not conserved, and in fact satisfies the famous anomaly equation

$$\partial^\mu J_\mu^5 = \frac{n_f \alpha_s}{2\pi} \text{Tr} (F_{\mu\nu} \tilde{F}^{\mu\nu}) , \quad (8.23)$$

with  $n_f$  the number of light flavors,  $F_{\mu\nu}$  the field strength tensor, and  $\tilde{F}_{\mu\nu} = \frac{1}{2}\epsilon^{\mu\nu\rho\sigma}F_{\rho\sigma}$  is its dual. This is a statement of the explicit breaking of the  $U_A(1)$  axial symmetry of QCD by quantum/topological effects. It was first argued by Veneziano that the problem of understanding the quark helicity of the proton is deeply tied to the  $U_A(1)$  problem [996]. Specifically, using anomalous chiral Ward identities, Shore and Veneziano [997, 998] showed that

$$\Delta\Sigma(Q^2) \propto \sqrt{\chi'(0)} , \quad (8.24)$$

where  $\chi'(0)$  is the slope of the QCD topological susceptibility in the forward limit. Phenomenological estimates in this approach using QCD sum rules give estimates for  $\Delta\Sigma$  that are in good agreement with HERMES and COMPASS data [999, 1000]. The computation of  $\chi'$  on the lattice has been discussed previously [1001]; for a recent summary of computations of the topological susceptibility on the lattice, see [1002].

This “topological screening” picture (specifically Eq. (8.24)) was recovered recently in a QFT worldline formalism [1003, 1004]. A remarkable result is that the chiral anomaly dominates  $g_1$  not only in the Bjorken limit (which is consistent with an OPE analysis) but also in the Regge limit of  $x_B \rightarrow 0$ . In this framework, since the anomaly also dominates at small  $x_B$ , it is argued that its coupling to zero modes of the Dirac operator causes a breakdown of the eikonal expansion; instead, the cross-talk between the axial vector and pseudoscalar sectors in the form of a Goldberger-Treiman relation [996, 997], leads to spin diffusion through emergent axion-like dynamics. Here the axion is a primordial  $\bar{\eta}$  meson which, through its coupling to the topological charge density, acquires mass and becomes the physical  $\eta'$  meson. Its dynamics concretely illustrates the connection between the  $U_A(1)$  problem and the spin puzzle.

Saturation at small  $x_B$  introduces a novel twist to this picture. In ’t Hooft’s [1005] formulation of the  $U_A(1)$  problem, instanton-anti-instanton configurations saturate the topological charge density and thereby generate the mass of the  $\eta'$ . However at small  $x_B$ , the topological susceptibility couples to the large density  $\rho$  of color charges. These can cause “over-the-barrier” sphaleron transitions [1006], previously suggested as a mechanism for electroweak baryogenesis [1007]. While sphaleron-like transitions do not affect the  $\eta'$  mass, they introduce a drag effect [1008] that suppresses spin diffusion mediated by the  $\bar{\eta}$ . The sphaleron transition rate is governed by  $Q_S$  [1009], and the corresponding drag on spin diffusion leads to a strong suppression of the isosinglet contribution to  $g_1$  at small  $x_B$  with an exponential dependence on the saturation scale.

This suppression is qualitatively different from Eq. (8.21), which does not presume the existence of topological effects due to the chiral anomaly. Thus in principle, it should be possible to distinguish the two mechanisms at the EIC. If such a suppression is observed at the EIC, and confirmed by other non-inclusive measurements sensitive to the anomaly, it could provide first evidence for the existence of sphaleron transitions in QCD [1004].

## 8.5 Saturation and Multiple Scattering Effects for TMDs

Recent investigations [930, 931] have further extended the correspondence between small- $x$  observables and TMD physics by showing that any dilute-dense low- $x$  observable involving at most two colored particles in the final state can be rewritten entirely in terms of gluon TMD distributions. For example, the inclusive production of a forward dijet in  $pA$  collisions is given as the convolution in transverse momentum transfer  $k_\perp$  of hard scattering amplitudes with 2, 3 or 4 physical gluons with the corresponding 2, 3 and 4 gluon TMD distributions with the appropriate gauge link structures. This correspondence was extended using more fundamental gauge invariance arguments [1010] in a way that can be systematically generalized. It relies on rewriting Wilson line operators into transverse strings built from so-called twisted field strength tensors  $WG^{\mu\nu}(x)W^\dagger$ , where  $W$  is a Wilson line of which  $x$  is an end. In the Regge limit, transverse gluon fields are pure gauges and they are the integrals of twisted  $WG W^\dagger$  tensors:

$$A_\perp^\mu(z_\perp) \equiv \frac{i}{g} U(z_\perp) \partial_\perp^\mu U^\dagger(z_\perp) = \int dz^- [z^-, \infty]_{z_\perp} G^{\mu+}(z^-, z_\perp) [z^-, -\infty]_{z_\perp}. \quad (8.25)$$

As the reader can infer from Eq. 8.9, these quantities are the fundamental building blocks which construct TMD distributions at small longitudinal momentum transfer: for example, the WW gluon distribution is none other than the Fourier transform of  $A_\perp^\mu(x_\perp) A_\perp^\nu(y_\perp)$ . Pairs of Wilson line operators can take the form of transverse strings built from these pure gauge gluons. In the simplest case of a fundamental dipole operator, one has:

$$U(x_\perp) U^\dagger(y_\perp) = \mathcal{P} \exp \left[ ig \int_{y_\perp}^{x_\perp} dz_\perp \cdot A_\perp(z_\perp) \right], \quad (8.26)$$

which defines the transverse string  $[x_\perp, y_\perp]$  built from pure gauge gluons. This relation is the small- $x$  limit of a particular case of the non-Abelian Stokes formula,

$$\mathcal{P} \exp \left[ \oint_C dx_\mu A^\mu(x) \right] = \mathcal{P} \exp \left[ \int_S d\sigma_{\mu\nu} W F^{\mu\nu} W^\dagger \right], \quad (8.27)$$

where  $C$  is the square loop which links the points  $(\infty^+, x_\perp), (-\infty^+, x_\perp), (\infty^+, y_\perp)$  and  $(-\infty^+, y_\perp)$ , and  $S$  is an appropriately chosen surface enclosed in  $C$ <sup>31</sup>. Once we have the transverse strings, we can use simple formulae such as

$$[x_\perp, y_\perp] = 1 + ig \int_{y_\perp}^{x_\perp} dz_\perp \cdot A_\perp(z_\perp) [z_\perp, y_\perp], \quad (8.28)$$

in order to perform an expansion in the powers of  $g A_\perp$ . A remarkable recursive formula for the dipole operator can be deduced from the results of [1010]:

$$\begin{aligned} U(b_\perp + r_\perp) U^\dagger(b_\perp) &= 1 + \int d^2 v_{1\perp} \int \frac{d^2 k_{1\perp}}{(2\pi)^2} e^{ik_{1\perp} \cdot (v_{1\perp} - b_\perp)} ig(r_\perp \cdot A_\perp)(v_{1\perp}) \mathcal{H}_1(k_{1\perp}, r_\perp) \\ &\quad + \int d^2 v_{1\perp} d^2 v_{2\perp} \int \frac{d^2 k_{1\perp}}{(2\pi)^2} \frac{d^2 k_{2\perp}}{(2\pi)^2} e^{ik_{1\perp} \cdot (v_{1\perp} - b_\perp) + ik_{2\perp} \cdot (v_{2\perp} - b_\perp)} \\ &\quad \times ig(r_\perp \cdot A_\perp)(v_{1\perp}) U(v_{1\perp}) U^\dagger(v_{2\perp}) ig(r_\perp \cdot A_\perp)(v_{2\perp}) \mathcal{H}_2(k_{1\perp}, k_{2\perp}, r_\perp), \end{aligned} \quad (8.29)$$

---

<sup>31</sup>See [1010] for details.

with

$$\mathcal{H}_1(k_{1\perp}, r_\perp) = \int_0^1 d\alpha e^{-i\alpha(k_{1\perp} \cdot r_\perp)}, \quad (8.30)$$

and

$$\mathcal{H}_2(k_{1\perp}, k_{2\perp}, r_\perp) = \int_0^1 d\alpha e^{-i\alpha(k_{1\perp} \cdot r_\perp)} \int_0^\alpha d\beta e^{-i\beta(k_{2\perp} \cdot r_\perp)}. \quad (8.31)$$

This recursive relation allows for a straightforward expansion in powers of  $gA_\perp$ . Once squared, it yields the complete rewriting of the quadrupole operator into TMD distributions with infinite power accuracy and takes into account all powers of the transverse momenta and all twist corrections that are not suppressed by a power of the center-of-mass energy.

When discussing power expansions, it is customary to distinguish kinematic effects from genuine higher twist effects. Eq. (8.29) readily distinguishes both kinds of effects: genuine higher twists come from  $gA_\perp$  corrections, whereas kinematic power corrections come from the expansion in the transverse momenta of the gluons  $k_{1\perp}, k_{2\perp}$ ... which are intrinsic transverse momenta in the target hadron. In dense targets, the CGC requires to resum all powers of  $gA_\perp \sim 1$ , while when dealing with dilute targets it is usually assumed to be safe to neglect such powers. In that sense, all dilute frameworks neglect the genuine higher twist corrections which are resummed by the CGC EFT. There are, however, some interesting subtleties when comparing dilute frameworks. Once higher powers of  $gA_\perp$  in the CGC formulas have been neglected, one recovers the so-called small- $x$  improved TMD framework which was constructed in [1011]. The more standard dilute framework known as BFKL can be obtained from the improved TMD (iTMD) limit by switching off all multiple scatterings from the gauge links that define the TMD distributions.

It is actually expected that at large  $k_\perp$ , the gauge link structure of the distributions can be neglected as observed numerically in [1012, 1013] and proven in [931], hence cancelling the first kind of multiple scatterings. As can be observed from the definition of the distributions (8.5) and (8.6), the large  $k_\perp$  regime corresponds to the regime of small transverse separation  $r_\perp \sim 1/k_\perp$  between the physical gluons, while the small (semi-hard)  $k_\perp$  corresponds to the regime of large transverse separation  $r_\perp$ , where the transverse distance will be filled by multiple gluons in the form of a gauge link.

In this sense, the saturation scale  $Q_s$  can be understood as the scale at which the separation  $|r_\perp| \sim 1/|k_\perp|$  starts to be large enough for gauge links to matter in the distributions. Furthermore, the proof in [931] leads to a subtle addition to the notion of the dilute limit articulated in [871]: low- $x$  observables are only dilute at large  $k_\perp$  when one applies the Wandzura-Wilczek approximation [666]. This approximation amounts to neglecting higher genuine twist corrections and thus assuming  $g_s A^\mu \ll 1$  in the projectile/target; this is the essence of the hybrid formalism developed in the context of the phenomenology of  $p + A$  collisions [918, 1014, 1015]. Within the Wandzura-Wilczek approximation, and at small  $k_\perp$ , one should still expect multiple scatterings from the TMD in a dilute target, although the emergence of the gauge link structure would be postponed to lower values of  $k_\perp$ . In the CGC approach, this can be understood as the transition between dilute-dense and dilute-dilute regimes.

The dense-dense regime in the CGC does not have a  $k_\perp$  factorized form [1016]; however, results for single inclusive gluon distributions can be obtained numerically from solutions of

the Yang-Mills equations with appropriate boundary conditions [1017]. A similar transition in the context of quark pair production from dilute-dilute [1018] to dilute-dense [1019, 1020] to dense-dense [1021, 1022] have been worked out explicitly.

The discussion above gives us an example of how powerful small- $x$  twist resummation tools are, and how much insight it gives for TMD physics. The non-universality of distributions can be fully understood as an effect due to multiple scatterings at small momentum transfer, which are very naturally taken into account in the small- $x$  effective theories. The decomposition of small- $x$  physics into different types of twists, which is uniquely written in a QCD gauge invariant way, leads to very interesting reinterpretations of well understood saturation effects, now in terms of TMD distributions. In the CGC, these distributions can correspond to dipoles but also quadrupoles, sextupoles and higher point Wilson line correlators that appear in semi-inclusive processes [927, 1019, 1023]; to leading logs in  $x$ , their evolution in  $x$  can be computed by reformulating the JIMWLK equation as a Langevin equation [901, 903].

## 8.6 Outlook

In summary, there has been great progress in the last few years on TMDs at small- $x$ , mainly on the connection between the TMD factorization and the small- $x$  CGC formalism. The ultimate goal is to extend the theoretical and phenomenological investigations of the two frameworks with the aim of obtaining a unified picture of parton distributions in the high parton density regime. A number of challenging issues need further investigations:

1. *Proton spin at small- $x$ .* Recent progress has generated strong interest in the community to understand the proton spin structure at small- $x$  from the associated small- $x$  evolution equations. More theoretical efforts are needed to resolve the issues raised in these derivations which do not take into account topological effects [974–977, 980] or instead take these into account [1003, 1004]. The final answer to these questions will provide important guidance for novel physics at the future EIC, where proton spin rum rule is a major focus.
2. *Small- $x$  evolution of the TMD gluon distributions [903].* The theoretical framework exists to solve the small- $x$  evolution equations for the dipole and WW gluon distributions. One needs to develop an efficient program to numerically solve these equations and gain insight into the TMD gluon distributions at different  $x$ . The combination of theory developments and phenomenological applications to the experimental data will help clarify the role of parton dynamics relative to those of “dipoles” and “quadrupole” effective degrees of freedom in the high parton density regime.
3. *Systematic study of gluon distributions at small  $x$  to reach a quantitative level.* There has been tremendous progress in small- $x$  phenomenology in the last decade. It is important to continue these studies, but focus on the relevant TMD gluon distributions. In particular, one needs to investigate the role played by the polarization (of the gluon or the target nucleon) in the small- $x$  gluon TMDs. It has been shown that WW distribution of linearly polarized gluons is suppressed at small  $k_\perp$  as compared to the dipole gluon distribution [928]. It was also shown in [931, 953] that at large  $k_\perp$  linearly polarized gluons are extremely important since the unpolarized and Boer-Mulders TMD become

equal in that limit regardless of their gauge link structure<sup>32</sup>. Similarly, the target polarization may also affect the gluon distribution, such as the gluon Sivers function at small  $x$  [1024, 1025]. There is much to explore along these directions, in particular, in light of future experiments at the EIC.

4. *Further exploration of probes for the TMD quark/gluon distributions in the small- $x$  region.* With the EIC on the horizon, one needs to address critical questions concerning direct probes for the TMD gluon distributions at small  $x$ . In particular, one of the key issues is the universality of distributions in the CGC formalism, as well as the matching of computations in the small- $x$  formalism to those in the TMD formalism at large transverse momenta. Next-to-leading order computations are now available for diffractive dijet [924] as well as inclusive photon+dijet production [921, 922] in  $e+A$  collisions: these results will be useful in extending the matching of the two formalisms to higher orders in perturbation theory. A specific example where such matching studies has led to significant phenomenological progress is in quarkonium production at collider energies [1026–1029]. Such studies can be extended to DIS where quantitative predictions and comparisons with data will also provide crucial tests of the universality of QCD dynamics in the saturation regime of the theory.

---

<sup>32</sup>Note that Ref. [953], however, shows a suppression from Sudakov resummations in the TMD evolution.

## 9 - Jet Fragmentation

[1030], collimated showers of energetic final-state particles, have long been regarded as an essential tool to understand hard scattering ( $Q^2 \gg \Lambda_{\text{QCD}}^2$ ) processes in  $e^+e^-$  collisions, semi-inclusive deep inelastic scattering, and hadron-hadron collisions from first principles in QCD. As they are copiously produced [270], jets are easily accessible by experiment, and their discovery has stimulated some of the most important developments in the perturbation theory of strong interactions. At present, cross sections for processes involving jets are routinely calculated at next-to-leading order, and next-to-next-to-leading order results are also becoming available [1031–1034]. This remarkable theoretical accuracy combined with careful uncertainty analysis [1035] has made precision jet studies a promising method to search for new physics beyond the Standard Model at very high energies. In more complex environments, jet observables can differentiate between models and theories of parton shower formation [1036, 1037]. This is exemplified by the recent CMS measurements of the radius dependence of the suppression of inclusive jets [1038].

In addition to inclusive and tagged jet cross sections, studies of provide precision tests of perturbative QCD in high energy processes. They originate from the studies of event shapes in  $e^+e^-$  collisions, which helped test and confirm the gauge structure of QCD [1039–1046]. Accurate event shape calculations have allowed for some of the most precise extractions of the strong coupling constant [236, 1047–1052]. At hadron colliders, due to the presence of beam remnants, underlying event and pileup, the studies of jet observables become much more complicated. Considerable effort and progress have been made in the direction of more efficient jet reconstruction and the development of grooming techniques to achieve this goal [1053]. In the past decades jets have increasingly been used to constrain essential perturbative and non-perturbative aspects of QCD. For example, jets are now routinely used to constrain the PDFs in hadronic collisions [1054, 1055]. They are particularly useful in constraining the large- $x$  gluon distributions [1056].

Jets are not fundamental objects in nature in the way that hadrons are, but are reconstructed by grouping final-state particles via an algorithm. Different , so long as they maintain infrared and collinear safety, provide different opportunities to probe QCD dynamics. It is desirable that such algorithms exhibit reduced sensitivity to the physics of hadronization, are applicable at the detector level, and can be identically implemented for partons and final-state particles. For one of the earliest examples of an analytic calculation with a fixed cone radius see [1030]. It is possible to classify most modern jet algorithms into one of two broad classes: and [1057]. Examples of the former are the Midpoint Cone, Iterative Cone, and Seedless Cone[1058, 1059]. Only the Seedless Cone is infrared and collinear safe. The sequential recombination algorithms include the  $k_T$ , Cambridge/Aachen, and the anti- $k_T$  [1060]. All of these satisfy the above criteria in addition to being clean and simple.

The  $k_T$ -class of algorithms in  $p\bar{p}$  collisions are based on a pair of distance measures,  $d_{ij}$

measuring an inter-particle distance and  $d_{iB}$  measuring a particle-beam distance.

$$d_{ij} = \min(p_{Ti}^{2p}, p_{Tj}^{2p}) \frac{\Delta R_{ij}^2}{R^2}, \quad \text{where } \Delta R_{ij}^2 = (y_i - y_j)^2 + (\phi_i - \phi_j)^2, \quad (9.1)$$

$$d_{iB} = p_{Ti}^{2p},$$

where  $p_T$  is the transverse momentum,  $y$  is the rapidity, and  $\phi$  the azimuthal angle, all with respect to the hadronic beam axis. These measures are designed to be boost-invariant along the beam axis. Here  $p$  is a parameter, which we will choose to be  $p = -1$ , which yields the *anti- $k_t$*  algorithm [1059]. The *anti- $k_t$*  algorithm favors grouping energetic collinear particles with one another first, before collecting soft particles into the jets. By finding the minimum distance measure the particles can recombined or identified as a jet if this minimum is given by  $d_{iB}$ .

What all jets have in common is a finite radius parameter  $R$ , setting a transverse scale  $\omega_J R$ , where  $\omega_J$  is the lightcone energy of the jet. Thus, evaluation of jet production and jet substructure always requires control over the transverse momentum QCD dynamics. One important problem related to the use of jets as probes is to develop improved methods to distinguish quark-initiated from gluon-initiated jets [1061, 1062]. The jet charge is one observable [1063, 1064] that is sensitive to the flavor origin and has recently been measured at the LHC [1065, 1066]. Individual flavor jet charges remain distinct even in collisions with heavy nuclei [1067, 1068] and first steps toward their measurement have been taken in such collisions [1069]. Jet substructure and jet fragmentation functions in particular can be used to probe the non-perturbative physics of hadronization in ways not possible with more inclusive measurements [1070, 1071].

In the presence of nuclear matter, jet production is sensitive to its transport properties. In general, jet substructure observables are primarily dependent on the details of the final state. They allow us to disentangle the initial state cold nuclear matter effects and are cleaner probes of the medium properties when compared to inclusive cross sections [1072]. At the same time, different jet substructure observables are sensitive to radiation at different energy scales. By measuring jet cross sections, jet shapes and jet fragmentation functions, jet masses and particle multiplicities, the in-medium jet formation mechanism across a wide range of energy scales can be examined [1073–1078]. Jet substructure observables and their medium modifications are also highly dependent on the partonic origin of jets.

## 9.1 Jets as Probes of TMD PDFs

Jet production in unpolarized and polarized  $ep$  collisions can be sensitive to the transverse motion of the partons inside the nucleon. For example, recently, production of back-to-back electron+jet in  $ep$  collisions has been proposed as a probe of both unpolarized and polarized TMD PDFs [1079–1082], such as quark Sivers functions. In such a process,  $p(P, S_T) + e(\ell) + \rightarrow J(y_J, P_{JT}) + e(\ell') + X$ , one defines the transverse momentum imbalance,  $q_T = P_{JT} + \ell'_T$  and the average transverse momentum of the electron-jet,  $P_T = (P_{JT} - \ell'_T)/2$ , as shown in Fig. 9.1. In

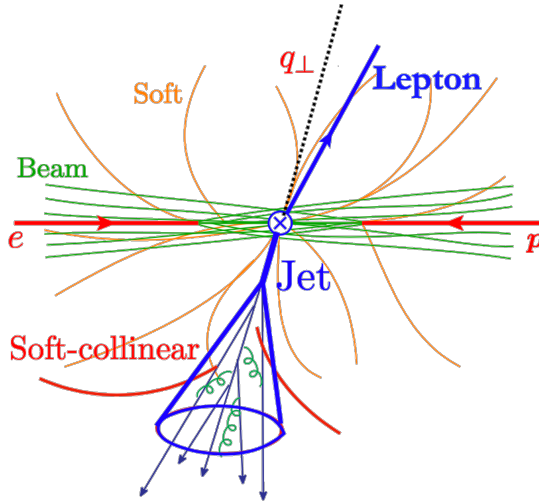


Figure 9.1: Illustration of back-to-back dijet production in transversely polarized  $ep$  collisions:  $p(P, S_T) + e(\ell) \rightarrow J(y_J, P_{JT}) + e(\ell') + X$ . The lepton-jet transverse momentum imbalance is defined as  $q_T = P_{JT} + \ell'_T$ .

the back-to-back region where  $q_T \ll P_T$ , one can derive a TMD factorization as follows [1082],

$$\frac{d\sigma}{dy_J dP_T^2 d^2 q_T} = \hat{\sigma}_0 H(Q, \mu) \sum_q e_q^2 J_q(P_T R, \mu) \int \frac{d^2 b_T}{(2\pi)^2} e^{ib_T \cdot q_T} x \tilde{B}_{q/p}(x, b_T, \mu, \zeta/v^2) \times \tilde{S}_q^{\text{global}}(b_T, \mu, v) \tilde{S}_q^{\text{cs}}(b_T, R, \mu), \quad (9.2)$$

for electron-jet production in  $ep$  collisions. Here,  $\hat{\sigma}_0$  is the Born cross section for the unpolarized electron and quark scattering process, while  $H(Q, \mu)$  is the hard function taking into account virtual corrections at the scale  $Q$ , with  $Q^2 = -(\ell - \ell')^2$  denoting the virtuality of the exchanged photon. On the other hand,  $J_q(P_T R, \mu)$  is the quark jet function [1083] which describes the production of the outgoing jet from a hard interaction.  $\tilde{B}_{q/p}(x, b_T, \mu, \zeta/v^2)$  is the quark beam function given in Eq. (2.29b),  $\tilde{S}_q^{\text{global}}(b_T, \mu, v)$  is a global soft function describing soft gluons of momentum  $\sim q_T$  at arbitrary angles while  $\tilde{S}_q^{\text{cs}}(b_T, R, \mu)$  is the collinear-soft function that describes soft gluon radiation close to the jet direction and able to probe the boundary of radius  $R$ . Note that the global soft function has rapidity divergence as indicated by the  $v$ -dependence, while the collinear-soft function does not.

In general, the above factorization formula is more complex in its structure in comparison with the standard TMD processes such as SIDIS, Drell-Yan and  $e^+e^-$  collisions. In particular, additional soft functions are involved in the formalism where jets are produced, while only a single soft function is required for the standard TMD processes. This provides additional complications in establishing rigorously the relationship between the TMD PDFs probed in the jet process and those standard TMD PDFs, in particular the role of these additional soft functions in the non-perturbative (or small transverse momentum) region. On the other hand it is precisely because of the richer structure in the soft functions that jet production might provide novel insights into TMD dynamics and the TMD PDFs in the non-perturbative region,

which otherwise can not be extracted from the standard TMD processes.

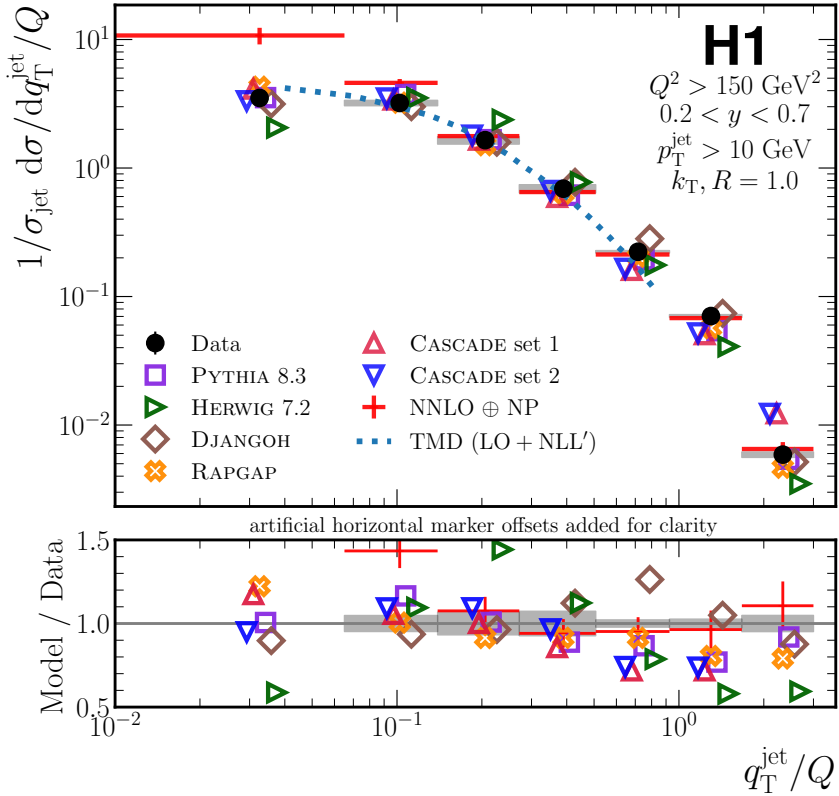


Figure 9.2: Theoretical comparison with the experimental data from HERA for lepton-jet back-to-back production. The prediction of TMD factorization is shown by the dashed blue line. Figure from Ref. [1084].

In the perturbative region ( $1/b_T \gg \Lambda_{\text{QCD}}$ ), one can show that at the next-to-leading order,

$$\tilde{B}_{q/p}(x, \mathbf{b}_T, \mu, \zeta/\nu^2) \tilde{S}_q^{\text{global}}(\mathbf{b}_T, \mu, \nu) = \tilde{f}_{q/p}(x, \mathbf{b}_T, \mu, \zeta) \tilde{S}_q^{\text{global}}(\mathbf{b}_T, \mu), \quad (9.3)$$

where we have used Eq. (2.32) and redefined a global soft function  $\tilde{S}_q^{\text{global}}(\mathbf{b}_T, \mu)$  that is free of rapidity divergence,

$$\tilde{S}_q^{\text{global}}(\mathbf{b}_T, \mu, \nu) = \tilde{S}_q^{\text{global}}(\mathbf{b}_T, \mu) \sqrt{\tilde{S}_{n_a n_b}(b_T, \mu, \nu)}, \quad (9.4)$$

with the standard soft function  $\tilde{S}_{n_a n_b}(b_T, \mu, \nu)$  given in Eq. (2.32) and the NLO expression for  $\tilde{S}_q^{\text{global}}(\mathbf{b}_T, \mu)$  given in [1082]. With such a procedure, we can then rewrite the factorization formula in Eq. (9.2) in terms of a standard TMD PDF  $\tilde{f}_{q/p}(x, \mathbf{b}_T, \mu, \zeta)$  as follows

$$\begin{aligned} \frac{d\sigma}{dy_J dP_T^2 d^2 \mathbf{q}_T} &= \hat{\sigma}_0 H(Q, \mu) \sum_q e_q^2 J_q(P_T R, \mu) \int \frac{d^2 \mathbf{b}_T}{(2\pi)^2} e^{i\mathbf{b}_T \cdot \mathbf{q}_T} x \tilde{f}_{q/p}(x, \mathbf{b}_T, \mu, \zeta) \\ &\quad \times \tilde{S}_q^{\text{global}}(\mathbf{b}_T, \mu) \tilde{S}_q^{\text{cs}}(\mathbf{b}_T, R, \mu). \end{aligned} \quad (9.5)$$

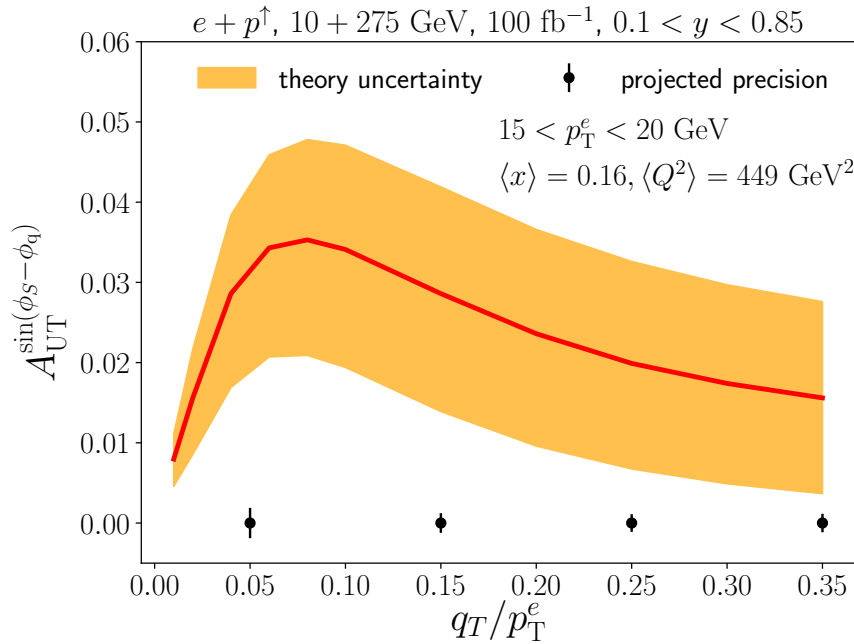


Figure 9.3: Theoretical result for the electron-jet asymmetry sensitive to the Sivers distribution (red). The uncertainty band (orange) displays the current uncertainty of the Sivers function. In addition, we show projections of statistical uncertainties for an EIC measurement (black error bars). Figure from Ref. [1080].

Most recently, the H1 collaboration at HERA has performed the first measurement of lepton-jet momentum imbalance in lepton-proton scattering [1084]. As shown in the dashed curve in Fig. 9.2, the above TMD factorization formula gives a decent description of the experimental data at low momentum imbalance  $q_T$ .

In addition, it has been demonstrated in [1079–1081] that lepton-jet production in  $ep$  collisions also shows great potential in constraining the quark Sivers functions. See a recent study as shown in Fig. 9.3. Here the theoretical uncertainty in the Sivers asymmetry  $A_{UT}^{\sin(\phi_S - \phi_q)}$  is computed using current knowledge of the quark Sivers functions and is shown as the orange band. On the other hand, the projections of statistical uncertainties for the EIC measurements are also shown as black error bars. Obviously there is much room for improvement in the accuracy of the theoretical predictions in order to meet the challenge of the anticipated experimental precision. In order to perform flavor separation for different quark Sivers functions at the EIC, jet charge observables have been proposed in [1085], which shows that jet charge measurements can substantially enhance the sensitivity of spin asymmetries to different partonic flavors in the nucleon.

Besides lepton-jet production in  $ep$  collisions where TMD factorization holds, one can also study back-to-back dijet and vector-boson-jet (such as  $Z + \text{jet}$  or  $\gamma + \text{jet}$ ) production in  $pp$  collisions. These processes are usually even more involved, and TMD factorization typically breaks [222, 223]. Nevertheless, theoretical studies have been performed [1086–1089] and experimental measurements have also been undertaken [1090, 1091] for such processes. This would allow for probing potential TMD factorization breaking, or for constraining TMD PDFs

if the breaking is relatively small.

## 9.2 Jet Substructure and Jet Fragmentation

The momentum distribution of hadrons inside a fully reconstructed jet, commonly referred to as the (JFF) [1070, 1092–1102], has received increasing attention in recent years. The JFF probes the parton-to-hadron fragmentation function at a differential level and can thus provide new insights for the hadronization process. Jet fragmentation functions can be measured for either *inclusive* jet production or *exclusive* jet processes. Single inclusive jet production correspond to the process  $AB \rightarrow \text{jet} + X$ , where incoming particles  $A$  (or  $B$ ) can be either a lepton or a proton, and one sums over all particles in the final state  $X$  besides the observed jet. The factorization formalism for single inclusive jet production has a similar form as that for single inclusive hadron production, where one replaces the usual collinear fragmentation function  $D_{h/i}(z, \mu)$  by a  $J_i(z, p_T R, \mu)$ . For example, the differential cross section for single inclusive jet production in  $pp$  collisions can be written as [1098, 1103]

$$\frac{d\sigma^{pp \rightarrow \text{jet}X}}{dp_T d\eta} = \sum_{a,b,c} \int_{\xi_a^{\min}}^1 \frac{d\xi_a}{\xi_a} f_a(\xi_a, \mu) \int_{\xi_b^{\min}}^1 \frac{d\xi_b}{\xi_b} f_b(\xi_b, \mu) \times \int_{z_c^{\min}}^1 \frac{dz_c}{z_c^2} H_{ab \rightarrow c}(\hat{s}, \hat{p}_T, \hat{\eta}, \mu) J_c(z_c, p_T R, \mu), \quad (9.6)$$

where  $p_T$  and  $\eta$  are the transverse momentum and the rapidity for the jet. The hard function  $H_{ab \rightarrow c}$  depends on the partonic CM energy  $\hat{s} = \xi_a \xi_b s$ , the partonic transverse momentum  $\hat{p}_T = p_T/z_c$  and the partonic rapidity  $\hat{\eta} = \eta - \ln(\xi_a/\xi_b)/2$ . The semi-inclusive jet function  $J_c(z_c, p_T R, \mu)$  describes the transition from a parton  $c$  with transverse momentum  $\hat{p}_T$  to the jet with transverse momentum  $p_T$  and jet radius  $R$ . Note that since the only measured hard momentum scale is the jet  $p_T$ , the process is sensitive to the collinear PDFs  $f_a(\xi_a, \mu)$  and  $f_b(\xi_b, \mu)$ , just like the case for single inclusive hadron production [395].

On the other hand, for exclusive jet processes  $AB \rightarrow n$  jets, one measures a fixed number of signal jets but vetoes additional jets. For example, when measuring dijet production, by selecting the kinematics to be in the back-to-back configuration, we restrict the events to be those with exactly two jets in the selected kinematic region. Just as shown in Sec. 9.1, the factorization formalism for such exclusive jet production processes are different from that of single inclusive jet production. For example, we see clearly that the back-to-back dijet production in  $ep$  collisions is sensitive to the TMD PDFs. One also notices that the semi-inclusive jet function  $J_i(z, p_T R, \mu)$  is replaced with the exclusive jet function  $J_i(p_T R, \mu)$  in Eq. (9.5).

In both single inclusive jet and exclusive jet production cases, one can further measure the distribution of hadrons inside the jet. One usually characterizes such a hadron distribution by the longitudinal momentum fraction  $z_h$  of the jet carried by the hadron and the transverse momentum  $j_\perp$  with respect to the jet direction. For example, for single inclusive jet production in  $pp$  collisions,  $pp \rightarrow (\text{jet}(\eta, p_T, R) h(z_h, j_\perp)) + X$ , one measures the hadron distribution inside the jet

$$F(z_h, j_\perp; \eta, p_T, R) = \frac{d\sigma^{pp \rightarrow (\text{jet} h)X}}{dp_T d\eta dz_h d^2 j_\perp} \Bigg| \frac{d\sigma^{pp \rightarrow \text{jet}X}}{dp_T d\eta}, \quad (9.7)$$

where  $F(z_h, \mathbf{j}_\perp; \eta, p_T, R)$  is commonly referred to as the JFF, and the numerator and denominator are the differential jet cross sections with and without the reconstruction of the hadron  $h$  inside the jet. The large light-cone momentum fraction of the jet carried by the hadron  $h$  is denoted by  $z_h$  and  $\mathbf{j}_\perp$  is the transverse momentum of the hadron with respect to the standard jet axis. The factorization formula for the hadron distribution inside the single inclusive jet production can be written as

$$\frac{d\sigma^{pp \rightarrow (\text{jet } h)X}}{dp_T d\eta dz_h d^2\mathbf{j}_\perp} = \sum_{a,b,c} \int_{\xi_a^{\min}}^1 \frac{d\xi_a}{\xi_a} f_a(\xi_a, \mu) \int_{\xi_b^{\min}}^1 \frac{d\xi_b}{\xi_b} f_b(\xi_b, \mu) \\ \times \int_{z_c^{\min}}^1 \frac{dz_c}{z_c^2} H_{ab \rightarrow c}(\hat{s}, \hat{p}_T, \hat{\eta}, \mu) \mathcal{G}_c^h(z_c, p_T R, z_h, \mathbf{j}_\perp, \mu, \zeta_J). \quad (9.8)$$

In other words, the factorizations for the numerator and the denominator are very similar to each other. For jet production with hadron distribution inside the jet, one simply replaces the semi-inclusive jet function  $J_c(z_c, p_T R, \mu)$  in Eq. (9.6) by the semi-inclusive TMD fragmenting jet function (TMD FJF)  $\mathcal{G}_c^h(z_c, p_T R, z_h, \mathbf{j}_\perp, \mu, \zeta_J)$  in Eq. (9.8) to be defined below. As expected, since this is a TMD observable, we have a Collins-Soper scale  $\zeta_J$ .

Jet fragmentation functions have been measured for single inclusive jets produced in unpolarized proton-proton collisions at the Large Hadron Collider (LHC) for light hadrons [1104, 1105], for open heavy flavor mesons [1106–1108], and for heavy quarkonium [1109, 1110]. Such measurements have already started to constrain the fragmentation functions for open heavy flavor mesons [1071, 1095], and to pin down non-relativistic QCD (NRQCD) long-distance matrix elements, which characterize the hadronization process for heavy quarkonium production [1070, 1101], see Sec. 9.5. At the same time, there are also important exclusive-type jet measurements at the LHC, e.g., exclusive jet production associated with vector bosons. See [1076] for a recent JFF measurement for photon-tagged jets. More recently the LHCb collaboration has measured both longitudinal and transverse momentum distributions of charged hadrons produced inside  $Z$ -tagged jets in the forward rapidity region in proton-proton collisions [1090],  $p + p \rightarrow Z + \text{jet} + X$ . At the same time, there have been recent studies for hadron distributions inside the jet in the back-to-back lepton-jet production in  $e p$  collisions [1080, 1082], a process that is very promising at the future EIC.

### 9.3 Hadron longitudinal distribution inside jets: $z_h$ dependence

If one measures only the longitudinal  $z_h$  distribution of hadrons inside a fully reconstructed jet, with  $z_h = \omega_h/\omega_J$ , where  $\omega_h$  and  $\omega_J$  are the lightcone energy of the identified hadron and jet, respectively, then the JFF is sensitive to the standard collinear fragmentation functions. See an illustration in Fig. 9.4. For inclusive jet production, one further introduces a momentum fraction  $z$  of the initiating parton carried by the jet,  $z = \omega_J/\omega$ , with  $\omega$  representing the lightcone energy of the parton which initiates the jet. In this case, one has the so-called semi-inclusive fragmenting jet function (FJF),  $\mathcal{G}_i^h(z, z_h, \omega_J, R, \mu)$ , whose operator definition is given in [1099]. Note that in the  $pp$  collisions where usually the jet transverse momentum  $p_T$  is measured and particle transverse momenta are used to construct the jets, we have semi-inclusive FJF written as  $\mathcal{G}_i^h(z, z_h, p_T R, \mu)$ , just like in Eqs. (9.6) and (9.8). We will use both conventions below interchangeably. It can be shown [1099] that such a semi-inclusive FJF follows a time-like

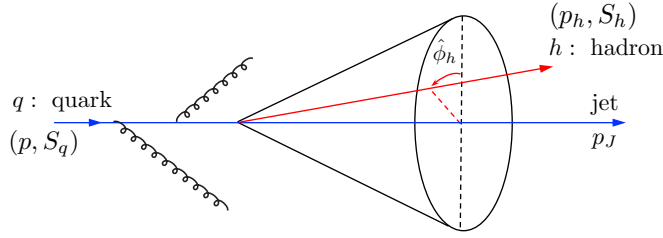


Figure 9.4: Illustration for the distribution of hadrons inside a fully reconstructed jet, that is initiated by a quark.

DGLAP evolution equation, just like the usual collinear fragmentation functions

$$\mu \frac{d}{d\mu} \mathcal{G}_i^h(z, z_h, p_T R, \mu) = \frac{\alpha_s(\mu)}{\pi} \sum_j \int_z^1 \frac{dz'}{z'} P_{ji} \left( \frac{z}{z'} \right) \mathcal{G}_j^h(z', z_h, p_T R, \mu), \quad (9.9)$$

where  $P_{ji}$  are the usual parton splitting functions. At the same time, for the scale  $\mu \gg \Lambda_{\text{QCD}}$ , we can match the semi-inclusive FJF  $\mathcal{G}_i^j(z, z_h, \omega_J, \mu)$  onto the collinear fragmentation functions  $D_i^h(z, \mu)$  as follows:

$$\mathcal{G}_i^h(z, z_h, p_T R, \mu) = \sum_j \int_{z_h}^1 \frac{dz'_h}{z'_h} \mathcal{J}_{ij}^{\text{incl}} \left( z, z'_h, p_T R, \mu \right) D_j^h \left( \frac{z_h}{z'_h}, \mu \right) \left[ 1 + \mathcal{O} \left( \frac{\Lambda_{\text{QCD}}^2}{p_T^2 R^2} \right) \right], \quad (9.10)$$

where the superscript “incl” in the matching coefficients  $\mathcal{J}_{ij}^{\text{incl}}$  emphasizes that they are for the semi-inclusive FJF, to be distinguished from the matching coefficients to be defined below for exclusive FJF. The expressions for  $\mathcal{J}_{ij}^{\text{incl}}$  are different for different jet algorithms and are given in [1099].

In exclusive jet production, one has a similar exclusive fragmenting jet function,  $\mathcal{G}_i^h(z_h, p_T R, \mu)$ . In such a set-up, one identifies only a certain number of signal jets and vetoes any additional jets. The only difference between the semi-inclusive FJF and the exclusive FJF lies in the fact that any out-of-jet radiation is power suppressed in the calculations of the exclusive FJF and can be neglected. Of course, the contribution of such out-of-jet radiation is characterized by the soft functions, see e.g. Eq. (9.5) for exclusive jet production. As a consequence, for the exclusive jet production, the energy of the initiating parton is fully contained inside the final jet, and thus the momentum fraction of the parton carried by the jet,  $z$ , is equal to one. Hence,  $z$  is dropped in the definition and only  $z_h$  is maintained. It can be shown that such exclusive FJF satisfies the following renormalization group equation

$$\mu \frac{d}{d\mu} \mathcal{G}_i^h(z_h, p_T R, \mu) = \gamma_J^i(\mu) \mathcal{G}_i^h(z_h, p_T R, \mu), \quad (9.11)$$

The anomalous dimensions  $\gamma_J^i$  are given by

$$\gamma_J^i(\mu) = \Gamma_{\text{cusp}}^i [\alpha_s(\mu)] \ln \left( \frac{\mu^2}{p_T^2 R^2} \right) + \gamma^i [\alpha_s(\mu)], \quad (9.12)$$

where  $\Gamma_{\text{cusp}}^i$  and  $\gamma^i$  are the cusp and non-cusp anomalous dimensions [1093, 1111–1114] with their expansions defined in Eq. (E.2) and they are the same as those for the exclusive jet functions in Eq. (9.5), also referred to as the unmeasured jet function in [1083, 1115]. The exclusive FJF can also be matched onto the standard collinear fragmentation functions,

$$\mathcal{G}_i^h(z_h, p_T R, \mu) = \sum_j \int_{z_h}^1 \frac{dz'_h}{z'_h} \mathcal{J}_{ij}(z'_h, p_T R, \mu) D_j^h\left(\frac{z_h}{z'_h}, \mu\right) \left[1 + O\left(\frac{\Lambda_{\text{QCD}}^2}{p_T^2 R^2}\right)\right], \quad (9.13)$$

where the matching coefficients  $\mathcal{J}_{ij}$  can be perturbatively computed [1116–1118] and are different from  $\mathcal{J}_{ij}^{\text{incl}}$  in semi-inclusive FJF case in Eq. (9.10).

## 9.4 Hadron transverse momentum distribution inside jets: $j_\perp$ -dependence

If one measures both the longitudinal  $z_h$  and transverse momentum  $j_\perp$  distribution of hadrons inside the jet, such a measurement will be sensitive to the TMD FFs introduced in Sec. 2.6. We again distinguish between inclusive jet production and exclusive jet processes. For single inclusive jet production, one introduces the so-called semi-inclusive TMD fragmenting jet functions (TMD FJFs),  $\mathcal{G}_i^h(z, p_T R, z_h, j_\perp, \mu)$ . In the TMD region where  $j_\perp \ll p_T R$ , we have the following factorized form for  $\mathcal{G}_i^h$  [1119],

$$\begin{aligned} \mathcal{G}_i^h(z, p_T R, z_h, j_\perp, \mu, \zeta_J) &= \mathcal{H}_{c \rightarrow i}(z, p_T R, \mu) \int d^2 k_\perp d^2 \lambda_\perp \delta^2(z_h \lambda_\perp + k_\perp - j_\perp) \\ &\times D_{h/i}(z_h, k_\perp, \mu, \zeta_J/v^2) S_i(\lambda_\perp, \mu, vR), \end{aligned} \quad (9.14)$$

where  $S_i(\lambda_\perp, \mu, vR)$  is a collinear-soft function. One can show at the NLO that the collinear-soft function is related to the standard soft function  $S_i(\lambda_\perp, \mu, v)$  in Eq. (2.78) as follows:

$$S_i(\lambda_\perp, \mu, vR) = \sqrt{S_i(\lambda_\perp, \mu, v)} \Big|_{v \rightarrow vR/2}. \quad (9.15)$$

Taking advantage of this relation, one can eventually show [1082, 1119]

$$\mathcal{G}_i^h(z, p_T R, z_h, j_\perp, \mu, \zeta_J) = C_{i \rightarrow j}(z, p_T R, \mu) D_{h/j}(z_h, j_\perp, \mu, \zeta_J), \quad (9.16)$$

where  $D_{h/j}(z_h, j_\perp, \mu, \zeta_J)$  with  $\zeta_J = p_T^2 R^2$  is the standard TMD FF as probed in the usual semi-inclusive deep inelastic scattering (SIDIS) or  $e^+e^-$  collisions in Sec. 2.7.3. On the other hand,  $C_{i \rightarrow j}$  are the coefficient functions that can be computed perturbatively as long as  $\mu \gg \Lambda_{\text{QCD}}$ . It is important to realize that the semi-inclusive TMD FJFs satisfy the DGLAP evolution equations,

$$\mu \frac{d}{d\mu} \mathcal{G}_i^h(z, p_T R, z_h, j_\perp, \mu, \zeta_J) = \frac{\alpha_s(\mu)}{\pi} \sum_j \int_z^1 \frac{dz'}{z'} P_{ji}\left(\frac{z}{z'}\right) \mathcal{G}_j^h(z', p_T R, z_h, j_\perp, \mu, \zeta_J), \quad (9.17)$$

and thus when one evolves the above equations from the natural scale  $\mu \sim \sqrt{\zeta_J} \sim p_T R$  to the hard scales  $\mu \sim \sqrt{\zeta_J} \sim p_T$ , one resums the series of logs  $\ln R$  for small radius  $R \ll 1$  jets.

On the other hand, for exclusive jet processes, e.g., the hadron transverse momentum distribution inside  $Z$ -tagged jets, where the  $Z$ -boson and the jet are produced back-to-back, one introduces the exclusive TMD fragmenting jet function,  $\mathcal{G}_i^h(p_{TR}, z_h, \mathbf{j}_\perp, \mu)$  [1096]. They follow the same renormalization group equation like  $\mathcal{G}_i^h(z_h, p_{TR}, \mu)$  above,

$$\mu \frac{d}{d\mu} \mathcal{G}_i^h(p_{TR}, z_h, \mathbf{j}_\perp, R, \mu) = \gamma_J^i(\mu) \mathcal{G}_i^h(p_{TR}, z_h, \mathbf{j}_\perp, \mu). \quad (9.18)$$

At the same time, it can be related to the TMD fragmentation functions as follows

$$\mathcal{G}_i^h(z_h, p_{TR}, \mathbf{j}_\perp, \mu, \zeta_J) = D_{h/i}(z_h, \mathbf{j}_\perp, \mu_J, \mu_J^2) \exp \left[ \int_{\mu_J}^\mu \frac{d\mu'}{\mu'} \gamma_J^i(\mu') \right], \quad (9.19)$$

where the exponential factor is simply reflecting the fact that it follows the renormalization group equation as given in Eq. (9.18).

In general, jet substructure can receive contamination from both underlying event and non-global color correlations. Both types of contamination would lead to complications in establishing the relations between TMD FFs probed via jet substructure and those via standard TMD processes. Modern grooming techniques can be applied to remove these sources of contamination [1120]. For example, Refs. [1121, 1122] have investigated how soft-drop grooming can be used to reduce the non-global logarithms. In addition, it has been shown there that the TMD hadron distribution with respect to the groomed jet axis is particularly sensitive to non-perturbative physics of the TMD evolution at low values of  $j_\perp$ , which can be probed in the variation of the cut-off parameter,  $z_{\text{cut}}$ , of the groomer.

#### 9.4.1 Polarized jet fragmentation functions

Our discussion above mainly deals with *unpolarized* hadron distributions inside the jet, which allows us to probe unpolarized collinear FFs or TMD FFs via jets. One can naturally ask questions if jets can also be used to study *polarized* TMD FFs. Ref. [1123] provides a general theoretical framework for studying the distribution of hadrons inside a jet by taking full advantage of the polarization effects. The key development, referred to as polarized jet fragmentation functions, describes the situation where the parton that initiates the jet and the hadron that is inside the jet can both be polarized, as illustrated in Fig. 9.4. For example, with polarized jet fragmentation functions, one could study  $\Lambda$  hyperon polarization inside a jet produced in unpolarized proton-proton collisions, where one would be able to probe the so-called TMD polarized fragmentation functions (TMD PFFs). Such TMD PFFs have been recently measured by the Belle collaboration [1124–1126].

Another well-known example is the so-called Collins hadron asymmetry inside a jet. Here, if one studies the distribution of an unpolarized hadron inside the jet which is initiated by a transversely-polarized quark, then the transverse spin of the quark and the transverse momentum  $\mathbf{j}_\perp$  of the hadron with respect to the jet would be correlated, resulting in a non-trivial azimuthal modulation for the hadron distribution. This was first proposed in [1130] to explore the Collins fragmentation functions, with further developments in [1128, 1131]. The STAR collaboration at RHIC has since studied such a Collins asymmetry for  $\pi^\pm$  production inside jets in transversely-polarized proton-proton collisions. Theoretical predictions from [1127, 1128] with the Collins fragmentation functions taken from a fit of SIDIS and  $e^+e^-$  data has shown to

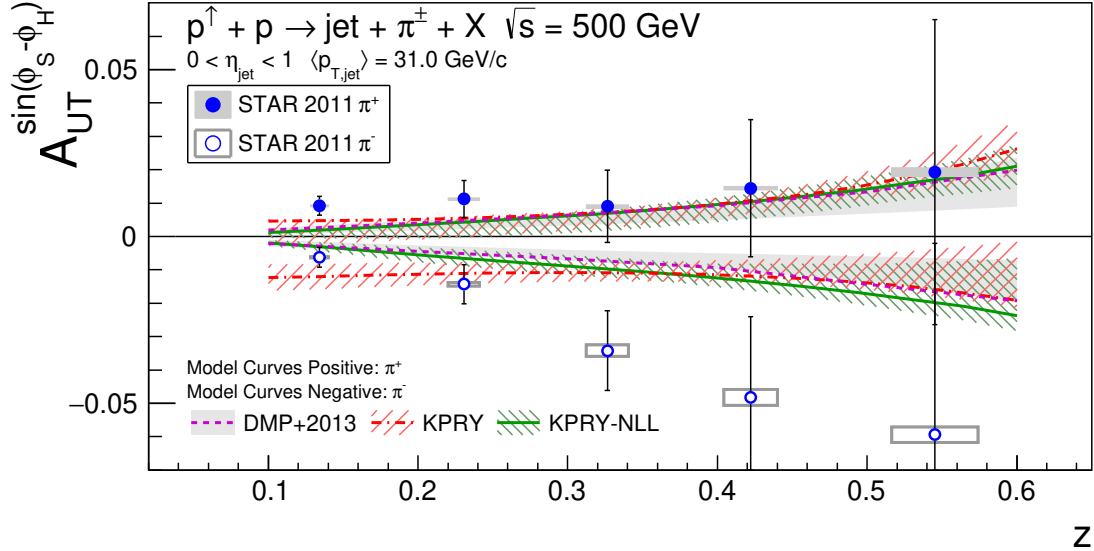


Figure 9.5: Collins asymmetries as a function of pion  $z_h$  for jets reconstructed with  $22.7 < p_T < 55.0$  GeV and rapidity  $0 < \eta < 1$ . The asymmetries are shown in comparison with model calculations from Refs. [1127, 1128]. Plot from [1129].

give a good description of the experimental data. This indicates the universality of the Collins function among SIDIS,  $e^+e^-$ , and  $p\bar{p}$  collisions, although the experimental uncertainty is still quite large. Future measurements with improved statistics have been planned [1132].

## 9.5 Jets with Heavy Quarkonium

are an interesting laboratory in which to apply the formalism for FJFs, as first pointed out in Ref. [1133]. As shown in Eq. (9.10) and Eq. (9.13) the FJF can be written as a convolution of a perturbatively calculable matching coefficient and a fragmentation function. For light hadrons and singly heavy hadrons, the fragmentation functions are nonperturbative and must be extracted from data. An old idea from the 90's is that the factorization formalism (NRQCD) [1134] can be used to calculate heavy quarkonium fragmentation functions because the heavy quark mass provides a large scale justifying the use of perturbation theory [1135–1138]. In NRQCD the conjectured factorization for the fragmentation functions take the form (here we use  $J/\psi$  as an example)

$$D_i^{J/\psi}(z, m_c, \mu) = \sum_n C_i^n(z, \alpha_S, m_c, \mu) \langle O_n^{J/\psi} \rangle \quad (9.20)$$

where  $n$  denotes the color and angular quantum numbers of the heavy charm-anticharm pair produced in the short distance process,  $i \rightarrow c\bar{c}(n) + X$  and  $\langle O_n^{J/\psi} \rangle$  is a describing the nonperturbative transition of the  $c\bar{c}$  in a state of definite color and angular momentum to the final state including the  $J/\psi$ .  $C_i^n(z, \alpha_S, m_c, \mu)$  is a perturbatively calculable function of  $z$ ,  $\alpha_S$ , and  $m_c$ .

If we identify a quarkonium inside a jet, we can combine the FJF formalism with NRQCD calculations of fragmentation functions to predict the distribution in  $z$ , where  $z$  is the fraction

of the energy carried by the quarkonium in the jet. For example, if we wish to calculate the cross section for  $e^+e^-$  to two jets with a  $J/\psi$  carrying a fraction  $z$  of its jet energy, the cross section is

$$\frac{1}{\sigma_0} \frac{d\sigma}{dz} = \sum_{i,j} H_{ij}(\mu) \times J_i(\mu) \times S^{\text{unmeas}}(\mu) \times \int_0^1 \frac{dz'}{z'} S^{\text{meas}}\left(\frac{z}{z'}, \mu\right) G_j^{J/\psi}(z', ER, \mu). \quad (9.21)$$

Here  $H_{ij}(\mu)$  is the hard cross section for producing the partons  $i$  and  $j$  that initiate the jets,  $J_i(\mu)$  is the jet function for the jet not containing the quarkonium,  $S^{\text{unmeas}}(\mu)$  is the soft function describing soft radiation outside the jets,  $S^{\text{meas}}(\mu)$  describes soft radiation in the jet with the quarkonium, and  $G_j^{J/\psi}(z, ER, \mu)$  is the FJF for a jet of energy  $E$  with a  $J/\psi$  with energy fraction  $z$ . (Note that in  $e^+e^-$  collisions the jet energy rather than the jet  $p_T$  is typically measured.) Then Eq. (9.20) is used in Eq. (9.13) to calculate the quarkonium FJF in terms of the LDME. Ref. [1133] showed that the FJF is well approximated by evaluating the NRQCD fragmentation at the scale  $2m_c$  then evolving that fragmentation function up to the jet energy scale. At that scale, perturbative corrections in the matching coefficients in Eq. (9.13) are small.

Various extractions of the LDME exist in the literature, for reviews of the status of quarkonium production theory, see [1139]. Global fits to the world's data on  $J/\psi$  production provide a reasonable fit, but predict transverse polarization of  $J/\psi$  at large  $p_T$  at hadron colliders, which is not seen in experiments [1140, 1141]. Alternative fits which focus extensively on high  $p_T$  data can do a better job of describing  $J/\psi$  production in these experiments [1142, 1143], but at the expense of statistical accuracy as well as ignoring much of the world's data on  $J/\psi$  production. Different NRQCD production mechanisms yield different  $z$  dependence for the  $C_i^n(z, \alpha_S, m_c, \mu)$  so the  $z$  distribution of  $J/\psi$  within a jet is sensitive to the underlying production mechanism. Ref. [1133] proposed the study of quarkonium production within jets as an alternative way to test NRQCD at high  $p_T$  and extract LDMEs.

Ref. [1144] performed analytical studies of heavy mesons and quarkonia produced in jets in an  $e^+e^-$  collider using the FJF formalism. These were compared to the results of Monte Carlo simulations using Herwig and Pythia. The dependence of the cross section on the jet angularities [1145] and the fraction of the energy carried by the heavy meson,  $z$ , were studied. Ref. [1144] found agreement between Monte Carlo and the FJF formalism for heavy mesons. However, the  $z$  dependence of the cross sections for quarkonia in jets is not well reproduced by Monte Carlo. Monte Carlo predicts a much harder distribution than the FJF formalism. This was attributed to incorrect modelling of radiation from color-octet pairs in default Pythia. These results were later confirmed by experiment when the LHCb experiment [1109] measured the distribution of  $J/\psi$  within a jet for the first time.

LHCb [1109] measured the distribution in  $z(J/\psi)$ , where  $z(J/\psi) = p_T^{J/\psi}/p_T^{\text{jet}}$ , shown in Fig. 9.6. The  $z(J/\psi)$  distributions predicted by default Pythia (not shown) were much harder than observed, peaking at  $z(J/\psi) > 0.8$ . A description of the LHCb data obtained in Ref. [1070] is also shown in Fig. 9.6. FJF is the calculation of the  $z(J/\psi)$  distribution using the quarkonium FJF, calculated in the approximation mentioned above of evolving the NRQCD fragmentation function from the scale  $2m_c$  to the jet energy scale. Gluon Fragmentation Improved Pythia GFIP is a modified implementation of Pythia described in Refs. [1070, 1144]. NRQCD LDMEs extracted from high  $p_T$  data did a better job of describing the  $z(J/\psi)$  distributions of  $J/\psi$  in jets than LDMEs from global fits.

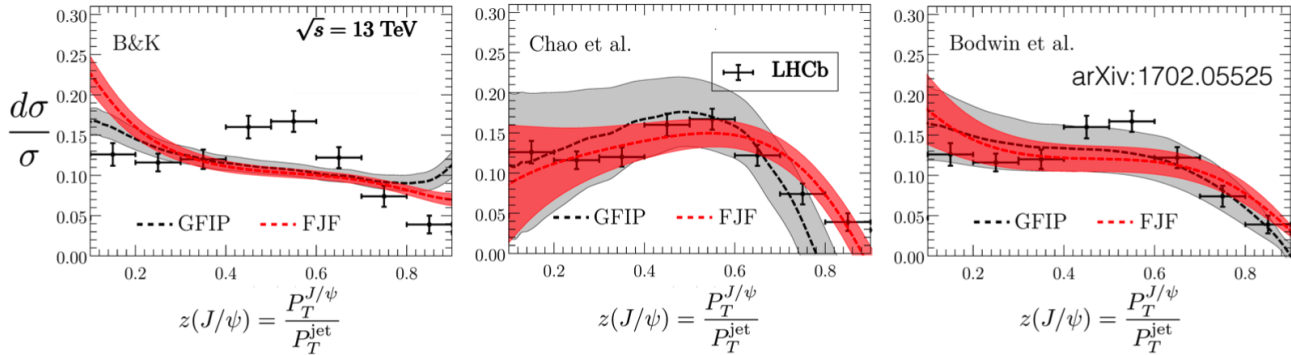


Figure 9.6: Comparisons of  $z(J/\psi)$  measured by LHCb with FJF (red) and GFIP (gray) for three different choice of LDME. Figure from Ref. [1139], the plots originally appeared in Ref. [1070].

Ref. [1146] was the first to consider the transverse momentum of the quarkonium within a jet. The TMD FJFs that appeared in Ref. [1146] are very similar to those discussed in the previous subsections. The transverse momentum is defined relative to the jet axis. RGE and rapidity RGE (RRGE) were used to resum logarithms. Non-perturbative effects were not taken into account in Ref. [1146] and this remains to be done before comparison with experiment can be made. Nonetheless, Ref. [1146] showed that different NRQCD production mechanisms give rise to different  $j_T$  distributions for the quarkonia within the jet, so the  $j_T$  spectrum would allow for novel tests of NRQCD and a framework for extracting LDMEs. At present, the  $j_T$  spectrum of quarkonia within jets has not been measured, but it would be interesting to study in the future.

Finally important recent theoretical developments that merit attention are the , introduced in Refs. [478, 1147], and the TMD fragmentation function for quarkonia [1148]. These objects appear in factorized cross sections that are relevant when the observable is sensitive to soft ( $p \sim m_Q v$ , where  $m_Q$  is the heavy quark mass and  $v$  its velocity) radiation interacting with the heavy quark-antiquark. Ref. [478] studied the process  $pp \rightarrow \eta_c$  with only color-singlet mechanisms. Ref. [1147] studied  $\Upsilon$  to two jets with identified heavy hadrons whose transverse momentum is measured. The TMD fragmentation function was discovered in a study of the transverse momentum distribution of  $J/\psi$  coming from the fragmentation of light partons [1148] in SIDIS. This paper also determined what regions in phase space this process will dominate at the EIC and discusses the role of NRQCD TMD fragmentation. TMD observables featuring quarkonia will figure prominently at the EIC, so the quarkonium shape functions and TMD fragmentation functions will be relevant for future studies. For example, Ref. [1149] studies asymmetries in  $J/\psi$  plus jet production for extracting the gluon TMDs. For other recent work on quarkonium production which utilizes the TMD formalism, see Refs. [1149, 1150].

## 9.6 Transverse Energy-Energy Correlations

are event shape observables that provide new ways to probe TMD dynamics. TEEC at hadronic colliders [1151] is an extension of the [1152] variable introduced decades ago in  $e^+e^-$

collisions to describe the global event shape. It is defined as

$$\text{TEEC} = \sum_{a,b} \int d\sigma_{pp \rightarrow a+b+X} \frac{2E_{T,a}E_{T,b}}{|\sum_i E_{T,i}|^2} \delta(\cos \phi_{ab} - \cos \phi), \quad (9.22)$$

where  $E_{T,i}$  is the transverse energy of hadron  $i$  relative to the collision axis and  $\phi_{ab}$  is the azimuthal angle between hadrons  $a$  and  $b$ . The NLO QCD corrections for the TEEC observable were calculated in Ref. [1153]. In the back-to-back dijet limit TEEC exhibits remarkable perturbative simplicity [1154]. This observable can be generalized to DIS by considering the transverse-energy and transverse-energy correlation between the lepton and hadrons in the final state [1155]

$$\text{TEEC} = \sum_a \int d\sigma_{lp \rightarrow l+a+X} \frac{E_{T,l}E_{T,a}}{E_{T,l} \sum_i E_{T,i}} \delta(\cos \phi_{la} - \cos \phi), \quad (9.23)$$

where the sum runs over all the hadrons in the final state and  $\phi_{la}$  is the azimuthal angle between the final-state lepton  $l$  and hadron  $a$ .

Taking DIS as an example, the underlying partonic Born process is  $e(k_1) + q(k_2) \rightarrow e(k_3) + q(k_4)$  and the first order non-trivial contribution to TEEC begins from one order higher. Similarly to TEEC in hadronic collisions, the cross section in the back-to-back limit is factorized into the convolution of a hard function, beam function, soft function, and jet function. Specifically, up to leading power in SCET in terms of the variable  $\tau = [1 + \cos(\phi)]/2$  the cross section can be written as

$$\begin{aligned} \frac{d\sigma^{(0)}}{d\tau} = & \sum_f \int \frac{d\xi dQ^2}{\xi Q^2} Q_f^2 \sigma_0 \frac{p_T}{\sqrt{\tau}} \int \frac{db}{2\pi} e^{-2ib\sqrt{\tau}p_T} B_{f/N}(b, E_2, \xi, \mu, \nu) H(Q, \mu) \\ & \times S\left(b, \frac{n_2 \cdot n_4}{2}, \mu, \nu\right) J_f(b, E_4, \mu, \nu), \end{aligned} \quad (9.24)$$

where  $\sigma_0 = \frac{2\pi\alpha^2}{Q^2}[1 + (1 - y)^2]$ ,  $b$  is the conjugate variable to  $k_y$ ,  $Q^2$  is the invariant mass of the virtual photon, and  $y = Q^2/(\xi s)$ . Four-vectors  $n_2$  and  $n_4$  represent the momentum directions of the momenta  $k_2$  and  $k_4$ , respectively.  $E_2$  and  $E_4$  are the energies of  $k_2$  and  $k_4$ .  $\nu$  is the rapidity scale associated with the rapidity regulator for which we adopt the exponential regulator introduced in Ref. [105] and reviewed in Sec. 2.4.

The TMD beam functions have been calculated up to three loops for quark beam functions and two loops for gluon beam functions [156, 164, 176, 1156]. The jet function  $J_f$  is defined as the second Mellin moment of the matching coefficients of the TMD fragmentation function. The soft function  $S$  is the same as the TMD soft function. In addition to the close connection to TMD physics, TEEC in DIS has the advantage that it can be computed to high accuracy. The left panel of Fig. 9.7 presents the resummed predictions at NLL, NNLL, and  $N^3\text{LL}$  accuracy in the back-to-back limit with scale uncertainties [1155]. Ref. [1155] finds good perturbative convergence. There is about 30% suppression in the peak region from NLL to NNLL, while it is about 5-6% from NNLL to  $N^3\text{LL}$ . The reason is that these are absolute cross sections rather than ones normalized over a finite  $\tau$  interval. The NLL uncertainty might also be underestimated. In general the non-perturbative (NP) corrections can be important in the infrared region

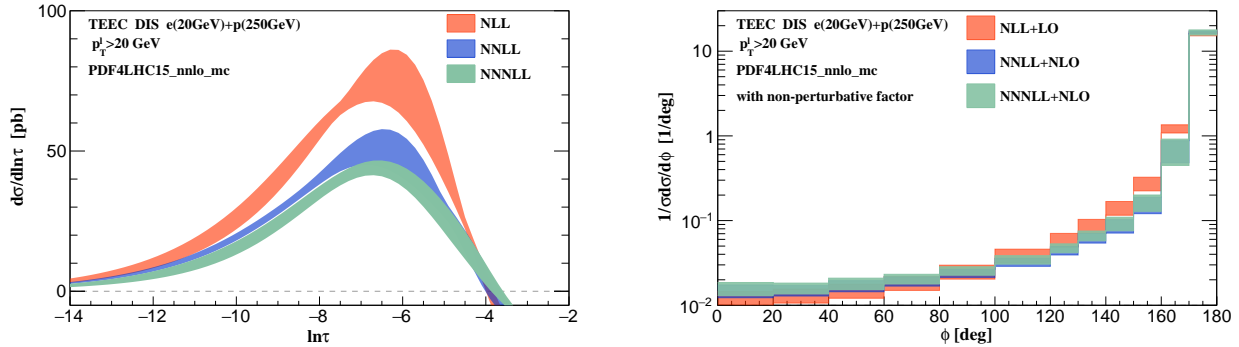


Figure 9.7: Left: resummed distributions in the back-to-back limit up to  $N^3LL$  accuracy. Note that results are not normalized by  $\sigma$  in the  $\tau$  interval shown. Right: TEEC  $\phi$  distribution matched with a nonperturbative model. The orange, blue and green bands are the final predictions with scale uncertainties up to  $N^3LL+NLO$ .

and can be studied with the help of TEEC in DIS. The results for the normalized TEEC  $\phi$  distributions are shown in the right panel of Fig. 9.7, where the non-perturbative Sudakov factor is also implemented [1155]. The matching region is chosen to be  $160^\circ < \phi < 175^\circ$  and for  $\phi < 160^\circ$  the distributions are generated by fixed-order calculations. The fixed-order predictions are calculated with  $\mu_r = \mu_f = \kappa Q$  with  $\kappa = (0.5, 1, 2)$ . In the back-to-back limit, the predictions are significantly improved.

Measurements of QCD observables in DIS are often done in the Breit frame. Recently, a new definition of EEC in the , which is a natural frame for the study of TMD physics [10], was presented [1157]. In this frame, the target hadron moves along  $\hat{z}$  and the virtual photon moves in the opposite direction. The Born-level process is described by the lepton-parton scattering  $e + q_i \rightarrow e + q_f$ , where the outgoing quark  $q_f$  back-scatters in the direction opposite to the proton. Hadronization of the struck quark will form a collimated spray of radiation close to the  $-\hat{z}$  direction. On the other hand, initial state radiation and beam remnants are moving in the opposite direction close to the proton's direction of motion. It is this feature of the Breit frame, which leads to the clean separation of target and current fragmentation that we utilize to construct the novel EEC observable in DIS. The kinematics, together with the contributions from the collinear and soft momenta to the transverse momentum of the hadron  $q_\perp$  is illustrated in Figure 9.8.

We denote the new event shape variable  $\text{EEC}_{\text{DIS}}$  to avoid confusion with the conventional observable. Our definition reads,

$$\text{EEC}_{\text{DIS}} = \sum_a \int \frac{d\sigma_{ep \rightarrow e+a+X}}{\sigma} z_a \delta(\cos \theta_{ap} - \cos \theta) , \quad (9.25)$$

where

$$z_a \equiv \frac{P \cdot p_a}{P \cdot (\sum_i p_i)} , \quad (9.26)$$

and  $p_a^\mu$  and  $P^\mu$  are the momenta of the hadron  $a$  and the incoming proton respectively. The sum over  $i$  includes all final state hadrons, including  $a$ . The angle  $\theta_{ap}$  is the polar angle of

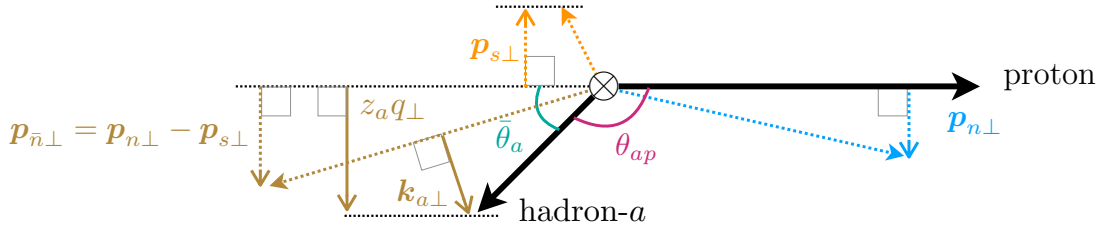


Figure 9.8: Illustration of the measurement of the transverse momentum  $q_{\perp}$  of the hadron- $a$  w.r.t. the proton axis in the Breit frame.

hadron  $a$ , which is measured with respect to the incoming proton. Note that the asymmetric weight function,  $z_a$ , is Lorentz invariant and is suppressed for soft radiation and radiation close to the beam direction. Furthermore, this definition of EEC in the Breit frame naturally separates the contribution to the  $\cos \theta$  spectrum from: i) wide angle soft radiation, ii) initial state radiation and beam remnants, and iii) radiation from the hadronization of the struck quark. This unique feature makes the new observable in the back-to-back limit ( $\theta \rightarrow \pi$ ) insensitive to experimental cuts on the particle pseudorapidity (in the Laboratory frame) due to detector acceptance limitations in the backward and forward regions, making the comparison of theory and experiment in this region even more accurate. This definition of EEC is spherically invariant, however, definitions that are fully Lorentz invariant and can be measured directly in any frame are also possible.

To illustrate the reduced sensitivity of the new observable to kinematics, we present the TEEC<sub>Lab</sub> [1155] and EEC<sub>DIS</sub> distributions predicted by PYTHIA 8 [1158, 1159] in Fig. 9.9. The red, blue, and green lines represent the results with pseudorapidity cuts  $|\eta| < 5.5$ ,  $|\eta| < 4.5$ , and  $|\eta| < 3.5$  in the lab frame, respectively, which imitates detector limitations in the backward and forward regions. In order to compare the results with different pseudorapidity cuts, all the distributions in Fig. 9.9 are normalized by the event number with  $|\eta| < 5.5$ . Because TEEC measures the correlation between hadrons and the final state lepton in the lab frame, pseudorapidity cuts have an impact on the full  $\cos \phi$  range, as shown in left panel of Fig. 9.9. EEC is defined as the correlation between the final state hadrons and incoming proton in the Breit frame, and the pseudorapidity cuts only remove particles in the forward region where the weighted cross section is small. In the backward region the distribution is independent of the pseudorapidity cuts.

## 9.7 Medium Modification of Jets

The key theoretical tool to disentangle the different physics effects on jets and predict each of their contributions to high accuracy is factorization [87]. The cross sections with a jet final state in vacuum can be written in the form [1160, 1161]

$$\sigma = \text{Tr}(HS) \otimes \prod_{i=1}^{n_B} B_i \otimes \prod_{j=1}^N J_j + \text{power corrections}, \quad (9.27)$$

for a process with  $n_B$  incoming hadronic beams and  $N$  outgoing hadronic jets. The hard function  $H$  is perturbative and contains information on the partonic hard scattering of  $n_B$

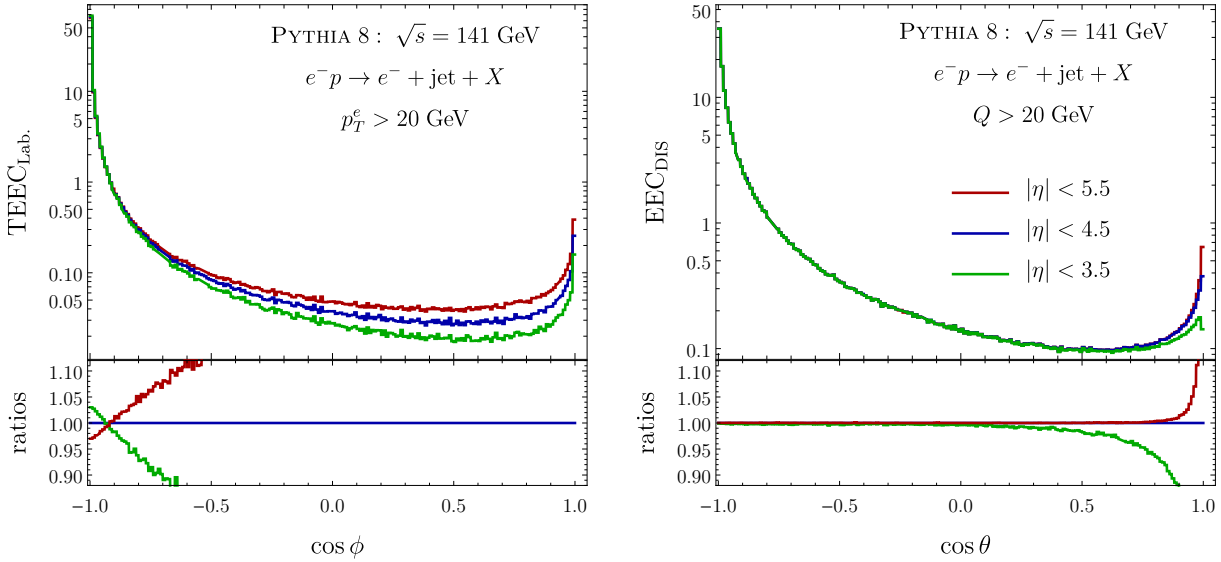


Figure 9.9: TEEC (left) and EEC (right) distributions from PYTHIA 8 with different rapidity cuts in the lab frame. The ratio relative to the  $|\eta| < 4.5$  case is also shown.

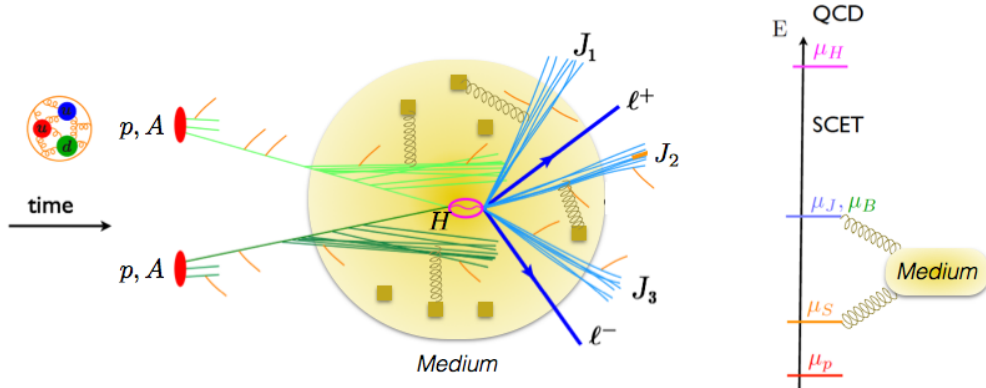


Figure 9.10: Degrees of freedom in jet cross sections in  $p+p$ ,  $p+A$  or  $A+A$  collisions. At short distance there is the partonic hard collision described by the hard function  $H(\mu_H)$ , obtained from matching full QCD onto an EFT of collinear and soft modes. The collinear splitting and emissions of partons in jets are described by jet and beam functions  $J(\mu_J)$ ,  $B(\mu_B)$ . Low energy soft particles connect beams and jets and mediate color exchange, described by the soft function  $S(\mu_S)$ . Nonperturbative dynamics of binding in the initial or final state are described by PDFs or nonperturbative matrix elements at the scale  $\mu_p$ . When a dense medium is created in heavy-ion collisions, interactions between the collinear or soft modes and the quarks/gluons in the medium occur through exchange of Glauber modes, which must be included in the EFT.

incoming and  $N$  outgoing partons, and the soft function  $S$  contains the soft radiation between these hard partons. They are in general color matrices, and the trace is over color indices.

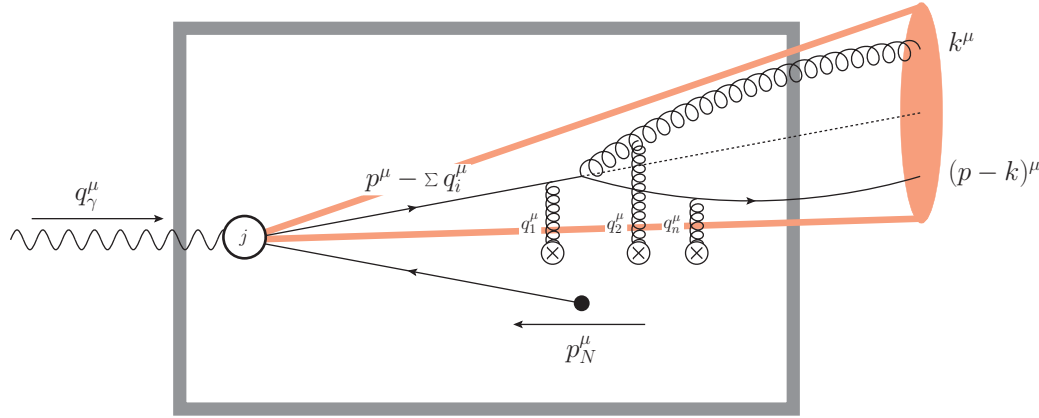


Figure 9.11: Illustration of parton splitting processes in matter for SIDIS case in the Breit frame. The dark box represents the medium and the red cone represents the jet.

The beam functions  $B_i$  contain the PDFs for the colliding hadrons and also the effects of perturbative collinear radiation from them, while the jet functions  $J_j$  contain the collinear splittings of the outgoing hard partons. These functions and the hierarchy of their scales in a typical  $p + p$  or heavy-ion collisions are illustrated in Figure 9.10. The same extension of the perturbative theory can be achieved from  $e + p$  to  $e + A$  collisions.

Historically, first studies in the field focused on the production cross section of energetic particles and jets in high energy reactions with nuclei. This is one of the primary signatures of inelastic parton scattering in dense nuclear matter [1162, 1163]. The rapid development of heavy ion programs at fixed target and collider experiments fueled tremendous interest in processes and radiative in QCD [1164], often discussed in analogy with the for photon emission in QED [1165, 1166]. Radiative energy loss in QCD is synonymous with soft gluon bremsstrahlung, a process in which hard quarks and gluons shed energy in small quanta during propagation in a nuclear medium. As a result, the leading parton always remains the most energetic. This does not preclude the possibility that it may dissipate a sizable fraction of its energy, but this is achieved through multiple gluon emission. All radiative parton energy loss approaches rely on perturbative techniques and treat the interactions of the jet with the quasi-particles of the medium primarily through  $t$ -channel gluon exchanges [1164]. Theoretical calculations differ in their assumptions about the kinematic regimes in which the parton system is produced and the size of the nuclear medium [1167–1176].

In the past decade important progress was made in understanding the full longitudinal and transverse structure of in-medium parton showers. The Altarelli-Parisi splitting functions [38] are the key ingredients in all modern high-precision calculations in QCD and in Monte-Carlo event generators. For jet physics, quark and gluon branching processes play an essential role in understanding the radius dependence of inclusive and tagged jet cross sections and of jet substructure. In Eq. (9.27) the splitting kernels enter into the calculation of beam and jet functions. The collision of ions introduces additional variables, such as the centrality and the nuclear species, in addition to the transverse momentum and rapidity of the jets. More importantly, the vacuum splitting kernels receive medium-induced contributions [1177–1187] which depend on the centrality and the colliding system, see Figure 9.11. To the lowest

non-trivial order for the double differential branching distributions we have

$$\frac{dN^{\text{vac}}(x, \mathbf{k}_\perp)}{dxd^2\mathbf{k}_\perp} \rightarrow \frac{dN^{\text{vac}}(x, \mathbf{k}_\perp)}{dxd^2\mathbf{k}_\perp} + \frac{dN^{\text{med}}(x, \mathbf{k}_\perp)}{dxd^2\mathbf{k}_\perp}, \quad (9.28)$$

where  $x$  is the longitudinal momentum fraction and  $\mathbf{k}_\perp$  is the transverse momentum of the splitting relative to the parent parton direction.

One way of calculating in-medium branching processes is in terms of the correlations between multiple scattering centers, known as the . To first order in opacity defined as  $L/\lambda$ , where  $L$  is the typical medium size and  $\lambda$  is the scattering length, the were explicitly calculated in [1178, 1179] and shown to be gauge invariant:

$$\begin{aligned} \left( \frac{dN^{\text{med}}}{dxd^2\mathbf{k}_\perp} \right)_{q \rightarrow qg} = & \frac{\alpha_s}{2\pi^2} C_F \frac{1 + (1-x)^2}{x} \int \frac{d\Delta z}{\lambda_g(z)} \int d^2\mathbf{q}_\perp \frac{1}{\sigma_{el}} \frac{d\sigma_{el}^{\text{medium}}}{d^2\mathbf{q}_\perp} \left[ \frac{\mathbf{B}_\perp}{\mathbf{B}_\perp^2} \cdot \left( \frac{\mathbf{B}_\perp}{\mathbf{B}_\perp^2} - \frac{\mathbf{C}_\perp}{\mathbf{C}_\perp^2} \right) \right. \\ & \times (1 - \cos[(\Omega_1 - \Omega_2)\Delta z]) + \frac{\mathbf{C}_\perp}{\mathbf{C}_\perp^2} \cdot \left( 2 \frac{\mathbf{C}_\perp}{\mathbf{C}_\perp^2} - \frac{\mathbf{A}_\perp}{\mathbf{A}_\perp^2} - \frac{\mathbf{B}_\perp}{\mathbf{B}_\perp^2} \right) (1 - \cos[(\Omega_1 - \Omega_3)\Delta z]) \\ & + \frac{\mathbf{B}_\perp}{\mathbf{B}_\perp^2} \cdot \frac{\mathbf{C}_\perp}{\mathbf{C}_\perp^2} (1 - \cos[(\Omega_2 - \Omega_3)\Delta z]) + \frac{\mathbf{A}_\perp}{\mathbf{A}_\perp^2} \cdot \left( \frac{\mathbf{D}_\perp}{\mathbf{D}_\perp^2} - \frac{\mathbf{A}_\perp}{\mathbf{A}_\perp^2} \right) (1 - \cos[\Omega_4\Delta z]) \\ & \left. - \frac{\mathbf{A}_\perp}{\mathbf{A}_\perp^2} \cdot \frac{\mathbf{D}_\perp}{\mathbf{D}_\perp^2} (1 - \cos[\Omega_5\Delta z]) + \frac{1}{N_c^2} \frac{\mathbf{B}_\perp}{\mathbf{B}_\perp^2} \cdot \left( \frac{\mathbf{A}_\perp}{\mathbf{A}_\perp^2} - \frac{\mathbf{B}_\perp}{\mathbf{B}_\perp^2} \right) (1 - \cos[(\Omega_1 - \Omega_2)\Delta z]) \right]. \end{aligned} \quad (9.29)$$

Here,  $x$  is the large lightcone momentum fraction taken by the daughter parton. This choice corresponds to having the soft gluon emission limit when  $x \ll 1$ . In Eq. (9.29)  $\lambda_g(z)$  is the scattering length of a gluon in the medium and  $(1/\sigma_{el}) d\sigma_{el}^{\text{medium}}/d^2\mathbf{q}_\perp$  stands for normalized elastic scattering cross section of a parton in nuclear matter. The kinematics of the LO branching processes and interactions with the medium mediated by Glauber gluons enter through

$$\mathbf{A}_\perp = \mathbf{k}_\perp, \quad \mathbf{B}_\perp = \mathbf{k}_\perp + x\mathbf{q}_\perp, \quad \mathbf{C}_\perp = \mathbf{k}_\perp - (1-x)\mathbf{q}_\perp, \quad \mathbf{D}_\perp = \mathbf{k}_\perp - \mathbf{q}_\perp, \quad (9.30)$$

$$\Omega_1 - \Omega_2 = \frac{\mathbf{B}_\perp^2}{p_0^+ x(1-x)}, \quad \Omega_1 - \Omega_3 = \frac{\mathbf{C}_\perp^2}{p_0^+ x(1-x)}, \quad \Omega_2 - \Omega_3 = \frac{\mathbf{C}_\perp^2 - \mathbf{B}_\perp^2}{p_0^+ x(1-x)},$$

$$\Omega_4 = \frac{\mathbf{A}_\perp^2}{p_0^+ x(1-x)}, \quad \Omega_5 = \frac{\mathbf{A}_\perp^2 - \mathbf{D}_\perp^2}{p_0^+ x(1-x)}. \quad (9.31)$$

The medium-induced splitting for  $q \rightarrow gq$  can be obtained from Eq. (9.29) with the substitution

$x \rightarrow 1 - x$ . The gluon splitting kernels are:

$$\begin{aligned} \left( \frac{dN^{\text{med}}}{dxd^2\mathbf{k}_\perp} \right) \left\{ \begin{array}{l} g \rightarrow gg \\ g \rightarrow q\bar{q} \end{array} \right\} &= \left\{ \begin{array}{l} \frac{\alpha_s}{2\pi^2} 2C_A \left( \frac{x}{1-x} + \frac{1-x}{x} + x(1-x) \right) \\ \frac{\alpha_s}{2\pi^2} T_R \left( x^2 + (1-x)^2 \right) \end{array} \right\} \int d\Delta z \left\{ \begin{array}{l} \frac{1}{\lambda_g(z)} \\ \frac{1}{\lambda_q(z)} \end{array} \right\} \\ &\times \int d^2\mathbf{q}_\perp \frac{1}{\sigma_{el}} \frac{d\sigma_{el}^{\text{medium}}}{d^2\mathbf{q}_\perp} \left[ 2 \frac{\mathbf{B}_\perp}{\mathbf{B}_\perp^2} \cdot \left( \frac{\mathbf{B}_\perp}{\mathbf{B}_\perp^2} - \frac{\mathbf{A}_\perp}{\mathbf{A}_\perp^2} \right) (1 - \cos[(\Omega_1 - \Omega_2)\Delta z]) \right. \\ &+ 2 \frac{\mathbf{C}_\perp}{\mathbf{C}_\perp^2} \cdot \left( \frac{\mathbf{C}_\perp}{\mathbf{C}_\perp^2} - \frac{\mathbf{A}_\perp}{\mathbf{A}_\perp^2} \right) (1 - \cos[(\Omega_1 - \Omega_3)\Delta z]) \\ &+ \left\{ \begin{array}{l} -\frac{1}{2} \\ \frac{1}{N_c^2-1} \end{array} \right\} \left( 2 \frac{\mathbf{B}_\perp}{\mathbf{B}_\perp^2} \cdot \left( \frac{\mathbf{C}_\perp}{\mathbf{C}_\perp^2} - \frac{\mathbf{A}_\perp}{\mathbf{A}_\perp^2} \right) (1 - \cos[(\Omega_1 - \Omega_2)\Delta z]) \right. \\ &+ 2 \frac{\mathbf{C}_\perp}{\mathbf{C}_\perp^2} \cdot \left( \frac{\mathbf{B}_\perp}{\mathbf{B}_\perp^2} - \frac{\mathbf{A}_\perp}{\mathbf{A}_\perp^2} \right) (1 - \cos[(\Omega_1 - \Omega_3)\Delta z]) - 2 \frac{\mathbf{C}_\perp}{\mathbf{C}_\perp^2} \cdot \frac{\mathbf{B}_\perp}{\mathbf{B}_\perp^2} (1 - \cos[(\Omega_2 - \Omega_3)\Delta z]) \\ &\left. \left. + 2 \frac{\mathbf{A}_\perp}{\mathbf{A}_\perp^2} \cdot \left( \frac{\mathbf{A}_\perp}{\mathbf{A}_\perp^2} - \frac{\mathbf{D}_\perp}{\mathbf{D}_\perp^2} \right) (1 - \cos[\Omega_4\Delta z]) + 2 \frac{\mathbf{A}_\perp}{\mathbf{A}_\perp^2} \cdot \frac{\mathbf{D}_\perp}{\mathbf{D}_\perp^2} (1 - \cos[\Omega_5\Delta z]) \right) \right], \quad (9.32) \end{aligned}$$

Note that the longitudinal and transverse momentum dependencies of the branching processes in matter do not factorize and for phenomenological applications  $dN^{\text{med}}(x, \mathbf{k}_\perp)/dxd^2\mathbf{k}_\perp$  can only be obtained as numerical grids.

One example that illustrates how medium induced showers can affect the TMD structure of jets is shown in Fig. 9.12. It presents the ratio of the transverse momentum  $k_T$  dependence of the medium-induced splitting kernel to the vacuum Altarelli-Parisi one -  $\frac{dN^{\text{med}}}{dxd^2k_T} / \frac{dN^{\text{vac}}}{dxd^2k_T}$ . The blue and cyan symbols represent calculations to different orders in the interaction of the jet with the medium (opacity) and the grey line is the average. In all parton branching channels  $i \rightarrow jk$  there is distinct broadening in the transverse momentum and, correspondingly, angular distributions of parton showers and jet constituents. These will manifest themselves in jet cross section and jet substructure modification in reactions with nuclei.

### 9.7.1 Jet cross sections

A recently developed framework to calculate jet cross sections is based on semi-inclusive jet functions  $J_i(z, p_T R, \mu)$ , which describe the fragmentation of parton  $i$  into a jet of radius  $R$  [1103]. Since medium induced parton showers emerge from branching processes that have longitudinal and transverse momentum structure different from the one in the vacuum, the essential many-body QCD physics is captured in the ratio of observables measured in nucleus collisions relative to the simpler proton ones.

$$R_{eA}^{\langle O \rangle}(PS) = \langle O_{eA} \rangle(PS) / \langle O_{ep} \rangle(PS) : e + A \text{ relative to } e + p , \quad (9.33)$$

$$R_{AB}^{\langle O \rangle}(PS) = \langle O_{AB} \rangle(PS) / \langle O_{pp} \rangle(PS) : A + B \text{ relative to } p + p , \quad (9.34)$$

where  $\langle O \rangle$  is the observable,  $e$ ,  $p$ ,  $A$  and  $B$  are the incoming leptons, hadrons or nuclei, and  $PS$  is the phase space variable, such as the transverse momentum, rapidity, subject radius or fragmentation fraction. The in-medium splitting functions in Eq. (9.28) have been used to

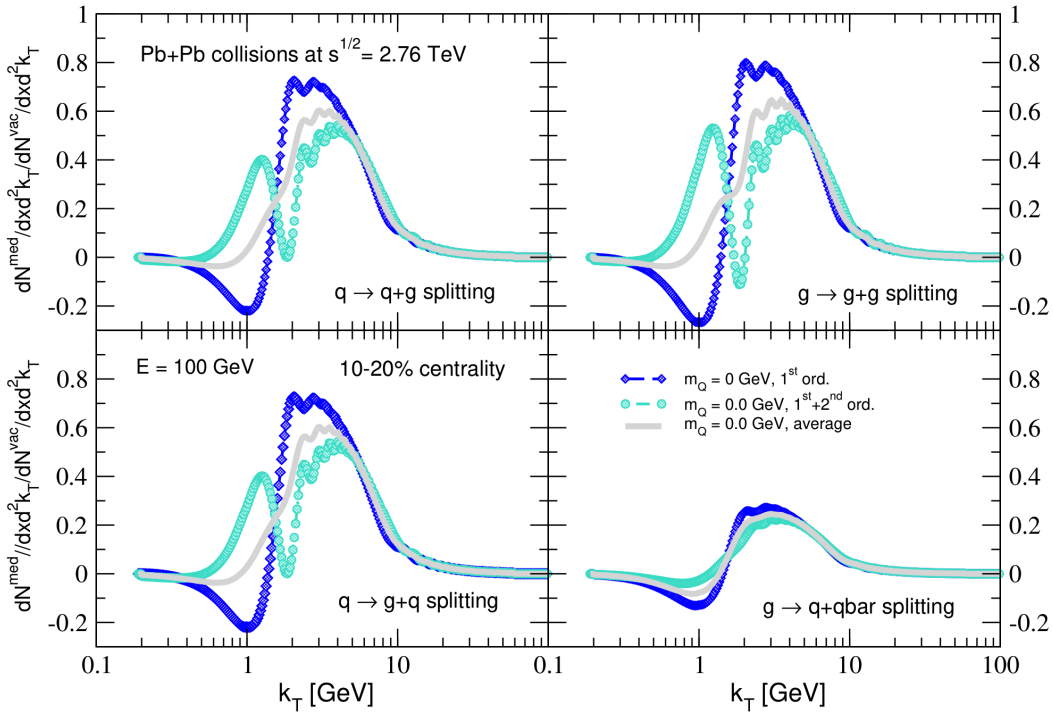


Figure 9.12: The transverse momentum distribution of the medium-induced radiation, as a ratio to the vacuum radiation spectrum. Here the distribution is shown for a 100 GeV jet and  $x = 0.3$ . We have chosen a 10 – 20% centrality cut of  $\sqrt{s_{NN}} = 2.76$  TeV PbPb collisions [1186].

obtain the suppression of inclusive light and heavy meson production in heavy ion collision using fixed-order [1184] and resummed calculations [1118, 1188, 1189]. For the case of jets, the in-medium effects have been included at fixed order in the semi-inclusive jet functions [1190–1193].

If we denote for brevity  $f_{i \rightarrow jk}^{\text{med}}(z, \mathbf{k}_\perp) = dN_{i \rightarrow jk}^{\text{med}}/d^2\mathbf{k}_\perp dz$ , at one loop the medium correction to the semi-inclusive jet functions read

$$J_q^{\text{med}}(z, p_T R, \mu) = \left[ \int_{z(1-z)p_T R}^\mu d^2\mathbf{k}_\perp f_{q \rightarrow qg}^{\text{med}}(z, \mathbf{k}_\perp) \right]_+ + \int_{z(1-z)p_T R}^\mu d^2\mathbf{k}_\perp f_{q \rightarrow gq}^{\text{med}}(z, \mathbf{k}_\perp) , \quad (9.35)$$

$$\begin{aligned} J_g^{\text{med}}(z, p_T R, \mu) = & \left[ \int_{z(1-z)p_T R}^\mu d^2\mathbf{k}_\perp \left( h_{gg}(z, \mathbf{k}_\perp) \left( \frac{z}{1-z} + z(1-z) \right) \right) \right]_+ \\ & + n_f \left[ \int_{z(1-z)p_T R}^\mu d^2\mathbf{k}_\perp f_{g \rightarrow q\bar{q}}(z, \mathbf{k}_\perp) \right]_+ \\ & + \int_{z(1-z)p_T R}^\mu d^2\mathbf{k}_\perp \left( h_{gg}(z, \mathbf{k}_\perp) \left( \frac{1-z}{z} + \frac{z(1-z)}{2} \right) + n_f f_{g \rightarrow q\bar{q}}(z, \mathbf{k}_\perp) \right) . \end{aligned} \quad (9.36)$$

Recall that the plus prescription definition is given in Eq. (2.70). Here we give the gluon

semi-inclusive jet function explicitly and note that

$$h_{gg}(z, \mathbf{k}_\perp) = \frac{f_{g \rightarrow gg}^{\text{med}}(z, \mathbf{k}_\perp)}{\frac{z}{1-z} + \frac{1-z}{z} + z(1-z)}. \quad (9.37)$$

The result for  $J_q^{\text{med}}$ ,  $J_g^{\text{med}}$  written in this form is finite for  $z \rightarrow 1$  and we only need the upper UV cut-off  $\mu$ , which is suitable for numerical implementations and integrations. The contribution of the in-medium shower to jet cross sections depends on its transverse momentum structure.

The formalism of semi-inclusive jet functions in nuclear matter has been applied to light jet cross sections [1190, 1192]. Very recently, the semi-inclusive jet functions for partons fragmenting into heavy flavor jets were computed for proton collisions [1194]. This approach has also been extended to c-jet and b-jet production in heavy ion collisions [1191]. Examples of jet cross section modification in different types of collisions including nuclei is shown in Fig. 9.13. These are defined as

$$R_{AA} = \frac{1}{\langle N_{\text{bin}} \rangle} \frac{d\sigma_{AA}/dydp_T}{d\sigma_{pp}/dydp_T}, \quad R_{eA} = \frac{1}{A} \frac{d\sigma_{eA}/dydp_T}{d\sigma_{ep}/dydp_T}, \quad (9.38)$$

for heavy ion and electron-nucleus reactions. To study cold with jets at the Electron-Ion Collider, it is essential reduce the role of nuclear PDFs and enhance the effects due to final-state interactions. An efficient strategy is to measure the ratio of the modifications with different jet radii,  $R_{eA}(R)/R_{eA}(R = 1)$ , which is also an observable very sensitive to the details of in-medium branching processes [1036] and greatly discriminating with respect to theoretical models [1195]. Furthermore, it is very beneficial to explore smaller center-of-mass energies. Predictions for the ratio of jet cross section suppressions for different radii at the EIC is presented in Fig. 9.13 (left), where the upper and lower panels correspond to results for 10 GeV (e)  $\times$  100 GeV (A) and 18 GeV (e)  $\times$  275 GeV (A) collisions, respectively. The plot in the upper panel is truncated around  $p_T \sim 20$  GeV because of phase space constraints in the lower energy collisions. The red, blue, and green bands denote ratios with  $R = 0.3, 0.5, 0.8$ , respectively. Since medium-induced parton showers are broader than the ones in the vacuum, for smaller jet radii the suppression from final-state interactions is more significant. Even though the scale uncertainties also grow, the nuclear effect is clear and its magnitude is further enhanced by the steeper  $p_T$  spectra at lower  $\sqrt{s}$ .

A different type of nuclear modification is shown in Fig. 9.13 (right) —  $R_{AA}$  in lead-lead collisions at the LHC at  $\sqrt{s} = 2.76$  TeV. Numerical calculations of  $b$ -jet suppression are compared to data [1196] from the CMS collaboration. The properly normalized cross section in A+A relative to p+p collisions denoted  $R_{AA}$  decreases, indicating larger suppression, with increasing collision centrality. The attenuation factor is less dependent on the centrality when compared to the light jet modification. Theoretical predictions agree very well with the data for both the inclusive cross sections and the nuclear modification factors. Importantly, this framework can also be applied to heavy flavor in DIS and provide further insight to the transport properties of large nuclei and the physics of hadronization [1192, 1197].

## 9.7.2 Jet substructure

The transverse and longitudinal structure of parton showers can be studied with jet substructure. One such observable is the average jet charge, defined as the transverse momentum

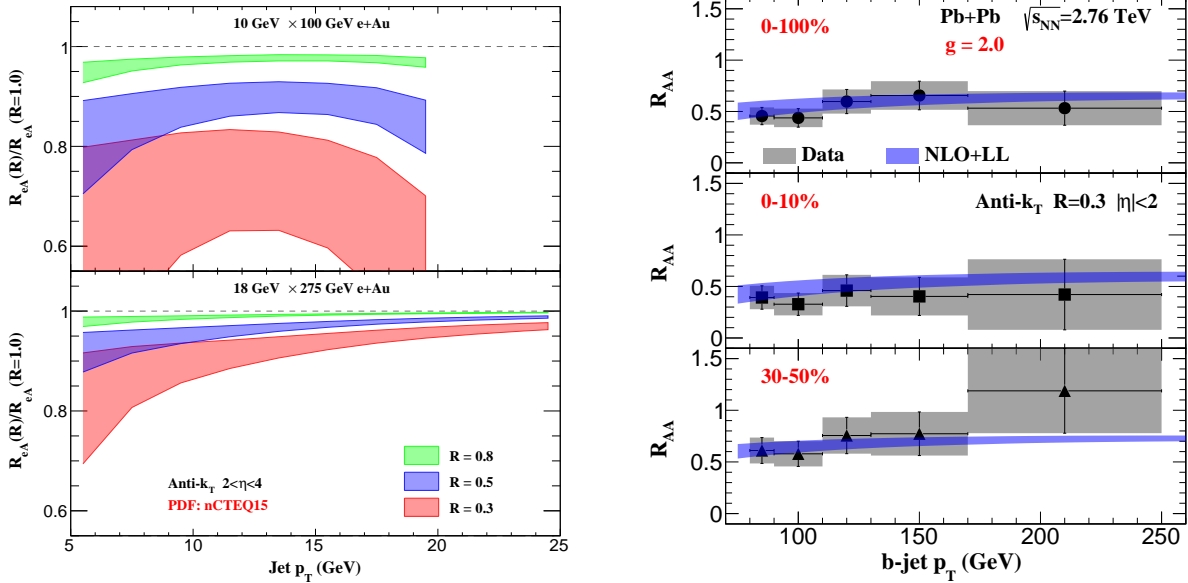


Figure 9.13: Left: ratio of jet cross section modifications for different radii  $R_{eA}(R)/R_{eA}(R = 1.0)$  in  $10 \times 100$  GeV (upper) and  $18 \times 275$  GeV (lower)  $e+Au$  collisions, where the smaller jet radius is  $R=0.3, 0.5$ , and  $0.8$ , and the jet rapidity interval is  $2 < \eta < 4$ . Right: the nuclear modification factor  $R_{AA}$  of  $b$ -jets , defined as the ratio of the inclusive cross section in heavy ion reactions normalized by the number of binary collisions to the cross section in proton collisions, for different centrality classes (0-100%, 0-10% and 30-50% ), as indicated in the legend. Data is from CMS measurements [1196].

$p_T^i$  weighted sum of the charges  $Q_i$  of the jet constituents

$$Q_{\kappa, \text{jet}} = \left( p_T^{\text{jet}} \right)^{-\kappa} \sum_{i \in \text{jet}} Q_i \left( p_T^i \right)^\kappa, \quad \kappa > 0. \quad (9.39)$$

Studies in proton and heavy-ion collisions [1068, 1198, 1199] have found that the jet charge is strongly correlated with the electric charge of the parent parton and can be used to separate quark jets from anti-quark jets and to pinpoint their flavor origin. In the framework of soft-collinear effective theory the average jet charge can be expressed as follows [1068, 1198]:

$$\langle Q_{\kappa, q} \rangle = \frac{\tilde{J}_{qq}(E, R, \kappa, \mu)}{J_q(E, R, \mu)} \tilde{D}_q^Q(\kappa) \exp \left[ \int_{1\text{GeV}}^{\mu} \frac{d\mu'}{\mu'} \frac{\alpha_s(\mu')}{\pi} \tilde{P}_{qq}(\kappa) \right], \quad (9.40)$$

where  $J_q(E, R, \mu)$  is a jet function and  $\tilde{J}_{qq}(E, R, \kappa, \mu)$  is the  $(\kappa + 1)$ -th Mellin moment of the Wilson coefficient for matching the quark fragmenting jet function onto a quark fragmentation function. Note that up to NLO gluons do not contribute to the average jet charge.

Nuclear matter effects on the jet charge were studied in Refs. [1067, 1068] for the case of heavy-ion collisions. Following the derivations in Ref. [1068] the average jet charge at the EIC can also be calculated and written as

$$\langle Q_{q,\kappa} \rangle = \langle Q_{q,\kappa}^{\text{ep}} \rangle \exp \left[ \int_{\mu_0}^{\mu} \frac{d\mu'}{\mu'} \frac{\alpha_s(\mu')}{2\pi^2} (2\pi\mu'^2) \tilde{f}_{qq}^{\text{med}}(\kappa, \mu') \right] \left( 1 + \tilde{J}_{qq}^{\text{med}} - J_q^{\text{med}} \right) + O(\alpha_s^2). \quad (9.41)$$

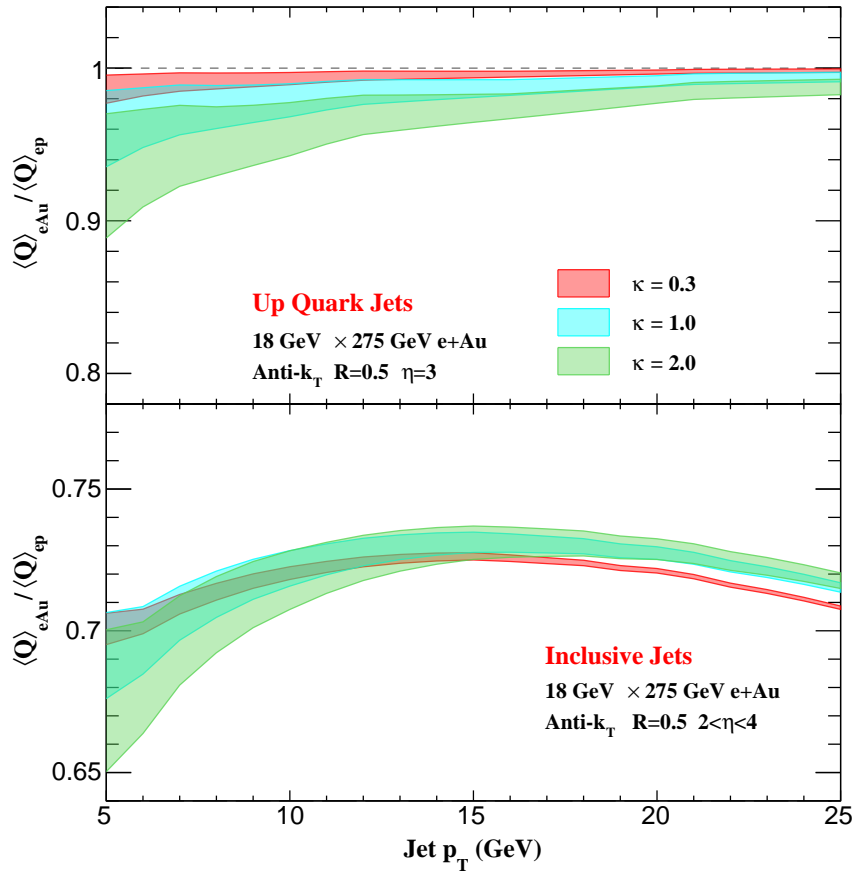


Figure 9.14: Modifications of the jet charge in e+Au collisions. The upper panel is the modification for up-quark jet with  $\eta = 3$  in the lab frame. The lower panel is the results for inclusive jet with  $2 < \eta < 4$  in  $18 \times 275$  GeV e+Au collisions.

Here, the exponential term comes from the medium-modified DGLAP evolution from  $\mu_0 \approx \Lambda_{\text{QCD}}$  to the jet scale and  $\tilde{f}_{qg}^{\text{med}}(\kappa, \mu) = \int_0^1 dx (x^\kappa - 1) f_{qg}^{\text{med}}(x, \mu)$ . Finally, for the medium-induced jet functions contributions in Eq. (9.41) we have explicitly

$$\tilde{\mathcal{J}}_{qg}^{\text{med}} - J_q^{\text{med}} = \int_0^{2Ex(1-x)\tan R/2} d^2\mathbf{k}_\perp f_{q \rightarrow qg}^{\text{med}}(x, \mathbf{k}_\perp). \quad (9.42)$$

Fig. 9.14 presents the jet charge results at the EIC in  $18 \text{ GeV} \times 275 \text{ GeV}$  e+Au collision and for radius parameter  $R = 0.5$ . The red, blue and green bands correspond to the jet charge parameter  $\kappa = 0.3, 1.0, 2.0$ , see Eq. (9.39), respectively. The upper panel shows the modification for the average charge of up-quark initialized jets, where the rapidity is fixed to be  $\eta = 3$ . It is defined as  $\langle Q_{q,\kappa}^{\text{eA}} \rangle / \langle Q_{q,\kappa}^{\text{ep}} \rangle$  and predicted by Eq. (9.41), which is independent of the jet flavor and originates purely from final-state interactions. Flavor separation for jets has been accomplished at the LHC [1065] and can be pursued at the EIC. For a larger  $\kappa$ , the  $(\kappa + 1)$ -th Mellin moment of the splitting function is more sensitive to soft-gluon emission, this is the  $x \sim 1$  region in the splitting function where medium enhancement for soft-gluon radiation

is the largest. As shown in the upper panel of Fig. 9.14, the modification is more significant for larger  $\kappa$ . The overall corrections are of order 10% or smaller and decrease with increasing  $p_T$ . Measurements of jet charge modification in reactions with nuclei open the possibility for direct observation of medium-induced scaling violations in QCD. The modification of the average charge for inclusive jets behaves very differently because there is a cancellation between contributions from jets initiated by different flavor partons, in particular from up quarks and down quarks. The lower panel of Fig. 9.14 shows the ratio of average charges for inclusive jets with  $R = 0.5$  and  $2 < \eta < 4$  for e+A and e+p collisions. The modification is about 30% and the  $\kappa$  dependence is small due to the large difference between up/down quark density between proton and gold PDFs. Precision measurement of the charge for inclusive jets will be an excellent way to constrain isospin effects and the up/down quark PDFs in the nucleus.

Another interesting observable is the  $z_g$  of the two leading subjets inside a reconstructed jet [1200], as it can give first-hand information about the QCD splitting functions. Given a jet reconstructed using the anti- $k_T$  algorithm with radius  $R$ , one reclusters the jet using the Cambridge/Aachen algorithm and goes through the branching history, grooming away the soft branch at each step until the following condition is satisfied,

$$z_{\text{cut}} < \frac{\min(p_{T_1}, p_{T_2})}{p_{T_1} + p_{T_2}} \equiv z_g , \quad (9.43)$$

i.e., the soft branch must carry more than a  $z_{\text{cut}}$  fraction of the sum of the transverse momenta to not be dropped. Note that by definition  $z_{\text{cut}} < z_g < \frac{1}{2}$  and the groomed momentum sharing is not sensitive to soft radiation by design. Due to detector granularity one also demands that the angular separation between the two branches  $\Delta R_{12} \equiv r_g$ , which is also called the groomed jet radius, be greater than the angular detector resolution. More generally, one can also study the subjet distribution as a function of the angular separation  $r_g$  as proposed in [1201]. This generalization provides access to the transverse momentum dependent physics of the branching processes. If one can distinguish the splitting process involving heavy flavor, for example by tagging jets and subjets with leading charm and beauty mesons ( $D, B$ ), such studies can be extended to heavy quark splitting processes [1202, 1203]. It is convenient to rewrite the groomed jet radius  $r_g = \theta_g R$  and the double differential distribution of subjets inside a reconstructed jet of radius  $R$  can be calculated as follows

$$\frac{dN_j^{\text{vac,MLL}}}{dz_g d\theta_g} = \sum_i \left( \frac{dP^{\text{vac}}}{dz_g d\theta_g} \right)_{j \rightarrow i\bar{i}} \underbrace{\exp \left[ - \int_{\theta_g}^1 d\theta \int_{z_{\text{cut}}}^{1/2} dz \sum_i \left( \frac{dN^{\text{vac}}}{dz d\theta} \right)_{j \rightarrow i\bar{i}} \right]}_{\text{Sudakov Factor}} . \quad (9.44)$$

By integrating over the angular variable one can recover the subjet momentum sharing observable Eq. (9.43). In the presence of QCD matter the full splitting functions include both a vacuum and medium-induced components. Fig. 9.15 presents the modifications for jets of different transverse momenta  $p_T$ , defined as the ratio of the  $z_g$  distributions in the medium and the vacuum. The groomed light jet momentum sharing distributions are compared to CMS measurements over different kinematic ranges in 0-10% central Pb+Pb collisions at  $\sqrt{s_{\text{NN}}} = 5.02$  TeV [1204]. Jets are reconstructed using anti- $k_T$  algorithm with  $R = 0.4$  and  $|\eta| < 1.3$  in both p+p and Pb+Pb collisions. Besides the jet  $p_T$  and rapidity cut, an additional cut on the distance between the two subjets  $\Delta R_{12} > 0.1$  is applied due to the detector

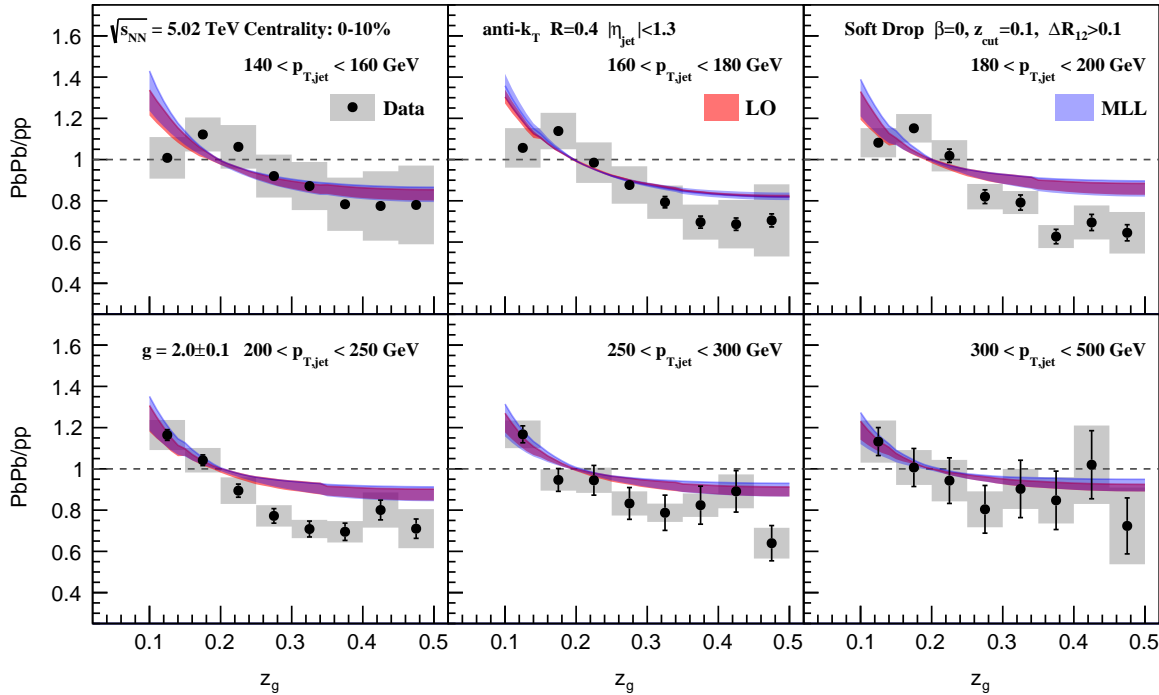


Figure 9.15: Theoretical predictions for the in-medium  $z_g$  distribution modification in Pb+Pb collisions with different jet  $p_T$  intervals at  $\sqrt{s_{NN}} = 5.02$  TeV are compared to CMS measurements [1204].

resolution of the measurements. Thus, the data can be described by both fixed order [1201] and resummed predictions. For heavy flavor jets of relatively small energy, this observable provides a unique opportunity to understand the effects of heavy quark mass on in-medium parton showers [1203].

To gain further insight into the transverse and longitudinal physics of parton showers and fragmentation, calculations of jet substructure in matter can be extended to other observables such as jet shapes or jet fragmentation functions [1068, 1072, 1076–1078, 1205]. We finally point out that an effective field theory of quarkonia in matter, , has been developed [1206, 1207]. Applications to e+A collisions at the EIC are being investigated. Furthermore, an intriguing description of the jet and the medium as an open quantum system has been proposed [?] - a direction that will be further pursued.

## 9.8 Outlook

In this section we discussed production and correlation of jets. We further showed examples of their longitudinal and transverse substructure in more elementary hadronic collisions as well as nuclear collisions.

In the future it will be interesting to study the modification of jet substructure in collisions involving nuclei relative to simpler reactions (for example e+A relative to e+p). Such observables may include jet shapes and transverse to the jet axis distribution of fragmentation functions. The opportunities that the EIC offers in this respect are particularly interesting. In contrast to heavy ion collisions, the energy of the jet's parent parton, which determines the characteristics and relative contribution of the medium-induced parton shower, and the

jet transverse momentum, which determines together with the jet radius the available phase space for jet substructure development, are very different. This, in turn may lead to a very different modification, as was shown for heavy flavor jet splitting functions at the EIC [1193]. Even though jet substructure modification is noticeably smaller than the modification of jet cross sections, we hope that the high-luminosity nature of the future EIC will enable these important measurements.

# 10 - Subleading TMDs

## 10.1 Introduction

**AM:** [Two suggestions for entire chapter: (i) introduce  $q\bar{q}q$  for “quark-gluon-quark” when used first; (ii) different terms contribute to the subleading-power of TMD observables. In Ref. [167] they are referred to as *intrinsic* (matrix elements with just two quark fields but a subleading gamma matrix), *kinematical* (moments of certain leading-power TMDs), and *dynamical* ( $q\bar{q}q$  matrix elements). Should we try to use this (or some other) notation consistently in the chapter? (For instance, *dynamical* power corrections have also been referred to as *genuine* or *pure* higher twist.)] **IS:** I've done both of these below. 2nd marked

In this chapter we consider the subleading-power TMDs (which for brevity we will also refer to as subleading TMDs). Unless stated otherwise, by those quantities we mean what in the literature is often denoted as twist-3 TMDs, that is, functions which appear in semi-inclusive reactions suppressed by one inverse power of the hard scale  $Q$  of the process. (Generally, we indicate that subleading contributions are suppressed by powers of  $\Lambda/Q$ , where  $\Lambda$  is a typical hadronic scale which could be the target mass  $M$ , the mass of a produced hadron  $M_h$ , a transverse momentum  $P_T$ , or  $\Lambda_{QCD}$ . Note also that quark mass effects can always be eliminated through the QCD equation of motion.) We provide an overview of subleading TMDs, discuss some of the relevant observables, and summarize calculations of subleading TMDs and related observables.

Subleading TMDs are important for a number of reasons. First, their understanding is required for a complete description of SIDIS and similar semi-inclusive reactions. Second, they may be relevant for a proper extraction of the leading-power effects from data. Third, subleading TMDs can be as sizeable as leading-power TMDs in some situations. Fourth, those functions are of interest in their own right as they, for instance, can offer new insights into the physics of the largely unexplored quark-gluon-quark correlations which provide novel information about the partonic structure of hadrons. While experimental information from SIDIS on effects related to subleading TMDs is available already, the EIC, with its large kinematical coverage, will be ideal for further groundbreaking progress in this area.

From a historical perspective it is very interesting that the subleading-power  $\cos \phi_h$  azimuthal modulation of the unpolarized SIDIS cross section was important for the development of the TMD field, since one of the earliest discussions of transverse parton momenta in DIS is related to this observable [278, 1208], see also Sec. 5.1 for more details. Generally, although suppressed by  $\Lambda/Q$  with respect to leading-power observables, subleading TMD observables are typically not small, especially in the kinematics of fixed-target experiments. In fact, the first-ever observed SSAs in SIDIS were sizeable power-suppressed longitudinal target SSAs for pion production from the HERMES Collaboration [466, 1209]. Those measurements, which triggered many theoretical studies and preceded the first measurements of the (leading-power) Sivers and Collins SSAs, were critical for the growth of TMD-related research.

The theory for subleading-power TMD observables is challenging and still in the early stage of development in comparison to the current state-of-the-art of leading observables. Treatments in the literature are mostly limited to a tree-level formalism, although recently results based on the SCET and CSS factorization formalisms have appeared. In Sec. 10.2 we

discuss observables in SIDIS which are directly sensitive to subleading TMDs, defining them in terms of general QCD structure functions. In Sec. 10.3 we provide definitions for subleading power TMD distributions, including those arising from quark-gluon-quark correlators (referred to as  $qgq$  correlators), subleading quark distributions, and corrections associated to simple kinematic expansions. **IS:** The  $qgq$  correlator corrections are sometimes referred to as dynamic power corrections, while the subleading quark distributions are called intrinsic power corrections [167]. Only the  $qgq$  correlator corrections introduce new subleading power TMDs, while, as we discuss, all other corrections can be related to leading power TMDs [121? ]. In Sec. 10.4 we present the current status for factorization formula that relate the structure functions to leading and subleading TMDs, and then in Sec. 10.5 we give a review of experimental measurements of subleading power TMD observables. Lattice QCD and model based determinations of subleading TMDs are taken up in Sec. 10.6. Finally, Sec. 10.7 gives a summary and outlook.

## 10.2 Observables for Subleading TMDs

Since the earliest treatments of transverse motion of partons in the nucleon emerged from studies of power-suppressed contributions in SIDIS [278, 279, 1208], we will focus our discussion on the general structure of the subleading-power SIDIS cross section. In so doing, we consider both unpolarized and polarized targets.

The fully differential SIDIS cross section — assuming a one-photon exchange between the lepton and the nucleon, and unpolarized produced hadrons in the final state — can be decomposed into 18 structure functions [121, 1210]. For low transverse momenta of the final-state hadron, eight of those structure functions are leading in a  $\Lambda/Q$  expansion; see Eq. (2.187). Another eight are suppressed by a factor  $\Lambda/Q$ , while the remaining two are suppressed by a factor  $\Lambda^2/Q^2$ . Focusing on the ten subleading contributions we have, in the notation of Refs. [121, 210],

$$\begin{aligned} \frac{d^6\sigma_{\text{subleading}}}{dx dy dz_h d\phi_S d\phi_h dP_{hT}^2} = & \frac{\alpha_{em}^2}{x y Q^2} \left(1 - y + \frac{1}{2}y^2\right) \left\{ p_1 F_{UU,L} + \cos(\phi_h) p_3 F_{UU}^{\cos(\phi_h)} \right. \\ & + \lambda \sin(\phi_h) p_4 F_{LU}^{\sin(\phi_h)} + S_L \sin(\phi_h) p_3 F_{UL}^{\sin(\phi_h)} + \lambda S_L \cos(\phi_h) p_4 F_{LL}^{\cos(\phi_h)} \\ & + S_T \sin(2\phi_h - \phi_S) p_3 F_{UT}^{\sin(2\phi_h - \phi_S)} + S_T \sin(\phi_S) p_3 F_{UT}^{\sin(\phi_S)} \\ & + S_T \sin(\phi_h - \phi_S) p_1 F_{UT,L}^{\sin(\phi_h - \phi_S)} \\ & \left. + \lambda S_T \cos(\phi_S) p_4 F_{LT}^{\cos(\phi_S)} + \lambda S_T \cos(2\phi_h - \phi_S) p_4 F_{LT}^{\cos(2\phi_h - \phi_S)} \right\}, \end{aligned} \quad (10.1)$$

where the kinematic prefactors  $p_i$  in Eq. (10.17) are given in Eq. (2.188). We also refer the reader to Sec. 2.11.3 for more details about the notation. The structure functions  $F_{UU,L}$  and  $F_{UT,L}^{\sin(\phi_h - \phi_S)}$  are of  $\mathcal{O}(\Lambda^2/Q^2)$  for small transverse momenta of the final-state hadron. In this chapter we will focus on the remaining eight which are  $\mathcal{O}(\Lambda/Q)$ .

Although we use the structure functions in Eqs. (10.20)–(10.23) as benchmark observables for subleading-power TMDs, we would like to mention that there are several other observables of that kind. For example, Ref. [1224] addresses the production of polarized hadrons,

e.g., lambda baryons, in SIDIS within the TMD formalism through  $\mathcal{O}(\Lambda/Q)$ . Ref. [1225] even discusses  $\mathcal{O}(\Lambda^2/Q^2)$  effects in SIDIS within the TMD formalism. Observables sensitive to subleading TMDs may also be found in other processes such as the Drell-Yan dilepton production [1226] and electron-positron annihilation into two almost back-to-back hadrons [211? , 212].

In the parton-model approximation, the structure functions in Eq. (10.17) can be expressed through subleading quark TMDs, with more discussion given in the following section. The very fact that we have a considerable amount of data for the structure functions in Eq. (10.17) alone gives a strong justification to study subleading TMDs in detail.

## 10.3 Subleading TMD Distribution Functions

### 10.3.1 Quark-gluon-quark correlators

Beyond leading power we begin to probe the structure of partons inside hadrons in greater depth. For observables that involve quark TMDs at leading power, the most important new operators have a gluon field strength in addition to the two quark fields present at leading power. Matrix elements of these operators give rise to subleading power TMDs which we will refer to as quark-gluon-quark correlators, or  $qgq$  correlators for short. In this section we provide definitions of these subleading TMDs. Since to-date the most complete discussion of factorization in subleading power SIDIS has been carried out using SCET in Ref. [? ], we will introduce a bit of SCET formalism in our presentation.<sup>33</sup> Where appropriate we also provide a translation to the notation for the  $qgq$  correlators used in earlier literature [121, 129–131].

The most general TMD  $qgq$  correlators for PDFs and FFs are defined by the following matrix elements [? ]

$$\begin{aligned}\tilde{\mathcal{B}}_{\mathcal{B} i/p_s}^{\rho \beta \beta'}(x, \xi, \mathbf{b}_T) &= \theta(\omega_a) \langle p(P, S) | [\bar{\chi}_{n_a}^{\beta'i}(b_\perp) T_{n_a}(b_\perp, 0) g \mathcal{B}_{n_a \perp, -\xi \omega_a}^\rho(0) \chi_{n_a, (1-\xi)\omega_a}^{\beta i}(0)]_\tau | p(P, S) \rangle, \\ \tilde{\mathcal{G}}_{\mathcal{B} h/i}^{\rho \alpha' \alpha}(z, \xi, \mathbf{b}_T) &= \frac{1}{2z N_c} \theta(\omega_b) \sum_{X_{\bar{n}}} \text{tr} \langle 0 | [Z_{n_b}^\dagger(b_\perp) \chi_{n_b}^{\alpha'i}(b_\perp)]_\tau | h, X_{\bar{n}} \rangle \\ &\quad \times \langle h, X_{\bar{n}} | [\bar{\chi}_{n_b, -(1-\xi)\omega_b}^{\alpha i}(0) g \mathcal{B}_{n_b \perp, \xi \omega_b}^\rho(0) Z_{n_b}(0_\perp)]_\tau | 0 \rangle,\end{aligned}\tag{10.2}$$

where  $x = \omega_a / (n_b \cdot P)$  and  $z = (n_a \cdot P_h) / \omega_b$ . Here we make use of the SCET building block field for quarks,  $\chi_n$ , which involves the good components of the quark field attached to a Wilson line that extends off to infinity. Likewise, for gluons we have the building block field  $\mathcal{B}_{n \perp}^\rho$ , which involves a gluon field strength and adjoint Wilson line, where the index  $\rho$  is transverse. They are defined by

$$\begin{aligned}\chi_{n_a}^i(x) &= W_{n_b}(\infty, x) \frac{\not{n}_a \not{n}_b}{2} \psi^i(x), & \chi_{n_a, \omega}^i(x) &= [\delta(\omega - in_b \cdot \partial) \chi_{n_a}^i(x)], \\ \mathcal{B}_{n_a \perp}^\rho(x) &= \frac{i}{g} \frac{1}{in_b \cdot \partial} n_{b\nu} G^{B\nu\rho\perp}(x) \mathcal{W}_{n_b}^{BA}(\infty, x) T^A, & \mathcal{B}_{n_a \perp, \omega}^\rho(x) &= [\delta(\omega + in_b \cdot \partial) \mathcal{B}_{n_a \perp}^\rho(x)].\end{aligned}\tag{10.3}$$

All fields here should be considered to be bare even though we have not indicated this explicitly with an extra superscript (0). Expanded in the gluon field,  $\mathcal{B}_{n_a \perp}^\rho = A_\perp^\rho - (i\partial_\perp^\rho / in_b \cdot \partial) n_b \cdot A + \dots$

<sup>33</sup>We continue to follow our conventions, such as the light-like four vectors, so some of the expressions here will differ slightly from Ref. [? ].

Subleading Quark-Gluon-Quark TMDPDFs				Subleading Quark-Gluon-Quark TMDFFs	
		Quark Chirality		Quark Chirality	
		Chiral Even	Chiral Odd	Chiral Even	Chiral Odd
Nucleon Polarization	U	$\tilde{f}^\perp, \tilde{g}^\perp$	$\tilde{e}, \tilde{h}$	$\tilde{D}^\perp, \tilde{G}^\perp$	$\tilde{E}, \tilde{H}$
	L	$\tilde{f}_L^\perp, \tilde{g}_L^\perp$	$\tilde{e}_L, \tilde{h}_L$	$\tilde{D}_L^\perp, \tilde{G}_L^\perp$	$\tilde{E}_L, \tilde{H}_L$
	T	$\tilde{f}_T, \tilde{f}_T^\perp, \tilde{g}_T, \tilde{g}_T^\perp$	$\tilde{e}_T, \tilde{e}_T^\perp, \tilde{h}_T, \tilde{h}_T^\perp$	$\tilde{D}_T, \tilde{D}_T^\perp, \tilde{G}_T, \tilde{G}_T^\perp$	$\tilde{E}_T, \tilde{E}_T^\perp, \tilde{H}_T, \tilde{H}_T^\perp$

Figure 10.1: Table of the subleading quark-gluon-quark (QQQ) TMDPDFs for the nucleon, which are suppressed in observables by the factor  $\Lambda/Q$ . The columns indicate the quark chirality, and rows the nucleon polarization [121, 129–131].

The presence of the extra subscripts  $\omega$  in Eq. (??) indicates that the total  $n_b \cdot p$  component of the product of fields is fixed to  $\omega$ , as shown. In Eq. (??) the momentum  $\omega_a$  gives the overall momentum of the fields at position 0 (and at  $b_\perp$ ), while  $\xi$  determines how this momentum is shared between the quark and gluon fields that are at the same transverse position. The presence of  $\xi$  corresponds in position space to allowing the quark and gluon fields that are at the same transverse position to be at different positions along the light-cone. The results in Eq. (??) are referred to as “quark” correlators since the lowest order term in the field without a momentum subscript would create or annihilate a quark. Analogous formulas also exist for the “anti-quark” case where  $\omega_a < 0$  and  $\omega_b < 0$ . In Eq. (??) the  $\alpha, \alpha', \beta, \beta'$  are spinor indices,  $i$  is a flavor index, and all color indices are traced over. Just like at leading power, the  $[\dots]_\tau$  notation indicates the presence of additional rapidity regulators. Finally, we have transverse Wilson line gauge links  $T_{n_a}(b_\perp, 0) = W[], Z_{n_b}(0_\perp) = W[]$  and  $Z_{n_b}(b_\perp) = W[]$  **IS: [To fix]**.

The configuration space geometry of the quark-gluon-quark correlators is actually fairly similar to that of the TMDs at leading power. For the PDF, comparing to the staple shaped Wilson line path with two quarks on each end shown in Fig. 2.1, the additional ingredient for the quark-gluon-quark correlators is roughly that we add an extra gluon field strength at a new position on one of the light-cone paths. Similarly for the FF, a field strength is also added on one of the light-cone

The most general Lorentz decomposition of the quark-gluon-quark TMD PDF with a polarized spin-1/2 hadron  $H$  was first derived in Ref. [121]. The analysis there was carried out for the correlator integrated over  $\xi$ , so that a quark and gluon field are at the same position, but the decomposition holds equally well for the more general case discussed here. The result

is

$$\begin{aligned} \tilde{B}_{\mathcal{B} i/H}^\rho(x, \xi, \mathbf{b}_T) = & \frac{M}{4P_N^-} \left\{ \left[ -iM(\tilde{f}^{\perp(1)} + i\kappa\tilde{g}^{\perp(1)})b_{\perp\sigma} + (\kappa\tilde{f}_T - i\tilde{g}_T)\epsilon_{\perp\sigma\delta}S_\perp^\delta \right. \right. \\ & - iMS_L(\kappa\tilde{f}_L^{\perp(1)} - i\tilde{g}_L^{\perp(1)})\epsilon_{\perp\sigma\delta}b_\perp^\delta \\ & - \frac{1}{2}M^2(\kappa\tilde{f}_T^{\perp(2)} - i\tilde{g}_T^{\perp(2)})\epsilon_{\perp\sigma\delta}\left(\frac{1}{2}b_\perp^2 S_\perp^\delta - b_\perp \cdot S_\perp b_\perp^\delta\right) \left. \right] (g_\perp^{\rho\sigma} - i\epsilon_\perp^{\rho\sigma}\gamma_5) \\ & - \left[ S_L(\tilde{h}_L - i\kappa\tilde{e}_L) + iM b_\perp \cdot S_\perp (\tilde{h}_T^{\perp(1)} - i\kappa\tilde{e}_T^{\perp(1)}) \right] \gamma_\perp^\rho \gamma_5 \\ & + \left[ (-\kappa\tilde{h} + i\tilde{e}) - iM(h_T^{\perp(1)} + i\kappa\tilde{e}_T^{\perp(1)})\epsilon_\perp^{\sigma\delta}b_{\perp\sigma}S_{\perp\delta} \right] i\gamma_\perp^\rho \\ & \left. \left. + \dots (g_\perp^{\rho\sigma} + i\epsilon_\perp^{\rho\sigma}\gamma_5) \right\} \frac{\not{q}}{2}. \right. \end{aligned} \quad (10.4)$$

**IS:** [fix  $P_N^-$ , check 2's] **LG:** Iain, aren't we naming  $P_N^+ \sim Q$  as the large momentum, power suppressed factor and visa versa for  $P_h^- \sim Q$  for fragmentation... For brevity, we suppress the arguments on the right-hand side, for example  $\tilde{f}^{\perp(1)} \equiv \tilde{f}_{i/H}(x, \xi, b_T, \mu, \zeta_a)$  and likewise for all the other TMDs. Only the displayed terms contribute in the subleading power factorization formula for SIDIS. These sixteen quark-gluon-quark TMD PDFs can be organized by which hadron polarization channel they contribute to, and by the quark chirality of the spinor indices, as shown in Fig. 10.1. In Eq. (??) the  $\kappa = \mp 1$  according to Eq. (??), and indicate the terms that are odd under time-reversal. These terms flip sign when considered considering contributions to the SIDIS versus Drell-Yan processes at subleading power. For SIDIS we can simply set  $\kappa = -1$ .

For the quark-gluon-quark TMD FF with an unpolarized hadron  $h$  we have

$$\begin{aligned} \tilde{G}_{\mathcal{B} h/i}^\rho(z, \xi, \mathbf{b}_T) = & \frac{M_h}{4P_h^+} \left\{ iM_h(\tilde{D}^{\perp(1)} + i\tilde{G}^{\perp(1)})b_{\perp\sigma}(g_\perp^{\rho\sigma} - i\epsilon_\perp^{\rho\sigma}\gamma_5) + (\tilde{H} - i\tilde{E})i\gamma_\perp^\rho \right. \\ & \left. + \dots (g_\perp^{\rho\sigma} + i\epsilon_\perp^{\alpha\sigma}\gamma_5) \right\} \frac{\not{q}}{2}. \end{aligned} \quad (10.5)$$

**IS:** [check sign convention vs choice of using  $n_a/n_b$ ,  $P_h^+$ , 2's] Again, for brevity we suppress the arguments on the right-hand side, so for example  $\tilde{D}^{\perp(1)} \equiv \tilde{D}_{h/i}(z, \xi, b_T, \mu, \zeta_b)$ , and likewise for the all other TMDs. Here only the TMD FFs for a spin-0 or unpolarized final state hadron are shown. A more extensive enumeration of subleading power  $qgq$  TMD FFs is shown in Fig. 10.1, and can be found in Ref. [? ].

- Modify text below to include a discussion of the  $\xi$  integrated quark-gluon-quark correlator, and comparison to notation in the original literature.

**IS:** [This paragraph still needs to updated:] To be specific, we will provide a parton-model definition for tilde TMDs as in Ref. [121]. It is convenient to do so using matrix elements that involve a covariant derivative  $D^\mu = \partial^\mu - igA^\mu$ . We can define a gauge-invariant "D-type" quark-gluon-quark TMD correlator of the nucleon  $\Phi_D^\rho(x, \mathbf{k}_T)$  as well as a fragmentation

correlator  $\Delta_D^\rho(z, \mathbf{p}_T)$  as follows,

$$(\Phi_D^\rho)_{ij}(x, \mathbf{k}_T) = \int \frac{db^- d^2\mathbf{b}_T}{(2\pi)^3} e^{ib \cdot k} \langle p(P, S) | \bar{\psi}_j(0) W_\square iD^\rho(b) \psi_i(b) | p(P, S) \rangle \Big|_{b^+=0}, \quad (10.6)$$

$$\begin{aligned} (\Delta_D^\rho)_{ij}(z, \mathbf{p}_T) &= \frac{1}{2N_c z} \sum_X \int \frac{db^+ d^2\mathbf{b}_T}{(2\pi)^3} e^{ip \cdot b} \langle 0 | W_\square iD^\rho(b) \psi_i(b) | h(P, S); X \rangle \\ &\quad \times \langle h(P, S); X | \bar{\psi}_j(0) W_\neg | 0 \rangle \Big|_{b^-=0}. \end{aligned} \quad (10.7)$$

The form of the Wilson line  $W_\square$  was given in Eq. (2.118) while  $W_\neg, W_\perp$  was defined in Eq. (2.110). The definitions are similar to the ordinary TMD objects  $f_{i/p_s}^{[\Gamma]}(x, \mathbf{k}_T)$  (spin-dependent TMDPDF in Eqs. (2.122), (2.124)) and  $\Delta_{h/i}^{[\Gamma]}(z, -zp'_T)$  (TMDFF in Eqs. (2.132), (2.112)), except for an additional insertion of the covariant derivative. According to Ref. [121] one can obtain a parameterization of the object  $\Phi_D^\rho - \mathbf{k}_T^\rho f_{i/p_s}$  in terms of tilde TMDPDFs,

$$\Phi_D^\rho(x, \mathbf{k}_T) - \mathbf{k}_T^\rho f_{i/p_s}(x, \mathbf{k}_T) = \frac{xM}{4} \left[ (\tilde{f}^\perp - i\tilde{g}^\perp) \frac{\mathbf{k}_{T\alpha}}{M} (g_T^{\rho\alpha} - i\epsilon_T^{\rho\alpha} \gamma_5) + \dots \right] \gamma_-^-. \quad (10.8)$$

The tilde functions that appear in the subleading observables Eqs. (10.20)–(10.23) are then obtained by parameterization of the combinations  $\Delta_D^\rho - \mathbf{p}_T^\rho \Delta$ ,

$$\Delta_D^\rho(z, \mathbf{p}_T) - \mathbf{p}_T^\rho \Delta(z, \mathbf{p}_T) = \frac{m_h}{4z} \left[ (\tilde{D}^\perp - i\tilde{G}^\perp) \frac{\mathbf{p}_{T\alpha}}{m_h} (g_T^{\rho\alpha} + i\epsilon_T^{\rho\alpha} \gamma_5) + (\tilde{H} + i\tilde{E}) i\gamma_T^\rho + \dots \right] \gamma_+^+. \quad (10.9)$$

We return to those functions in the next section.

### 10.3.2 Quark-quark correlators and equations of motion

- Discuss reduction to minimal operator basis from SCET point of view. Use of  $W^\dagger iD_\perp W = P_\perp + g\mathcal{B}_\perp$  to write subleading quark components in terms of  $P_\perp$  and  $\mathcal{B}_\perp$  operators.
- Discuss classification of subleading quark operators, and use of the equations of motion to derive relations between them and the leading power and  $\xi$ -integrated  $qgq$  TMDs.

At subleading power, a total of 16 quark TMDPDFs exists [121, 129–131], and they are listed in Fig. 10.2. These TMDPDFs are obtained by projecting the quark-quark correlator with the Dirac structures **DP: This equation could probably just be put inline.**

$$\Gamma = \{1, i\gamma_5, \gamma^\alpha, \gamma^\alpha \gamma_5, i\sigma^{\alpha\beta} \gamma_5, i\sigma^{+-} \gamma_5, \dots\}. \quad (10.10)$$

### Subleading Quark TMDFFs

		Subleading Quark TMDPDFs		Quark Chirality	
		Quark Chirality		Chiral Even	Chiral Odd
Nucleon Polarization	U	$f^\perp, g^\perp$	$e, h$	$D^\perp, G^\perp$	$E, H$
	L	$f_L^\perp, g_L^\perp$	$e_L, h_L$	$D_L^\perp, G_L^\perp$	$E_L, H_L$
	T	$f_T, f_T^\perp, g_T, g_T^\perp$	$e_T, e_T^\perp, h_T, h_T^\perp$	$D_T, D_T^\perp, G_T, G_T^\perp$	$E_T, E_T^\perp, H_T, H_T^\perp$

Figure 10.2: Table of the subleading quark TMDPDFs and TMDFFs, which are suppressed in observables by the factor  $\Lambda/Q$ . The columns indicate the quark chirality, and rows the hadron polarization [121, 129–131].

To be specific, the subleading TMDs are given by [121, 129–131]

$$f_{i/p_S}^{[1]}(x, \mathbf{k}_T, \mu, \zeta) = \frac{M}{P^+} \left[ e(x, k_T) - \frac{\epsilon_T^{\rho\sigma} k_T \rho S_{T\sigma}}{M} \kappa e_T^\perp(x, k_T) \right], \quad (10.11a)$$

$$f_{i/p_S}^{[i\gamma_5]}(x, \mathbf{k}_T, \mu, \zeta) = \frac{M}{P^+} \left[ S_L \kappa e_L(x, k_T) - \frac{k_T \cdot S_T}{M} \kappa e_T(x, k_T) \right], \quad (10.11b)$$

$$\begin{aligned} f_{i/p_S}^{[\gamma^\alpha]}(x, \mathbf{k}_T, \mu, \zeta) = & \frac{M}{P^+} \left[ \frac{k_T^\alpha}{M} f^\perp(x, k_T) - \epsilon_T^{\alpha\rho} S_{T\rho} \kappa f_T(x, k_T) \right. \\ & \left. - S_L \frac{\epsilon_T^{\alpha\rho} k_T \rho}{M} \kappa f_L^\perp(x, k_T) - \frac{\mathbf{k}_T^2}{M^2} \left( \frac{1}{2} g_T^{\alpha\rho} + \frac{k_T^\alpha k_T^\rho}{\mathbf{k}_T^2} \right) \epsilon_{T\rho\sigma} S_T^\sigma \kappa f_T^\perp(x, k_T) \right], \end{aligned} \quad (10.11c)$$

$$\begin{aligned} f_{i/p_S}^{[\gamma^\alpha\gamma_5]}(x, \mathbf{k}_T, \mu, \zeta) = & \frac{M}{P^+} \left[ S_T^\alpha g_T(x, k_T) + S_L \frac{k_T^\alpha}{M} g_L^\perp(x, k_T) \right. \\ & \left. - \frac{\mathbf{k}_T^2}{M^2} \left( \frac{1}{2} g_T^{\alpha\rho} + \frac{k_T^\alpha k_T^\rho}{\mathbf{k}_T^2} \right) S_{T\rho} g_T^\perp(x, k_T) - \frac{\epsilon_T^{\alpha\rho} k_T \rho}{M} \kappa g^\perp(x, k_T) \right], \end{aligned} \quad (10.11d)$$

$$f_{i/p_S}^{[i\sigma^{\alpha\beta}\gamma_5]}(x, \mathbf{k}_T, \mu, \zeta) = \frac{M}{P^+} \left[ \frac{S_T^\alpha k_T^\beta - S_T^\beta k_T^\alpha}{M} h_T^\perp(x, k_T) - \epsilon_T^{\alpha\beta} \kappa h(x, k_T) \right], \quad (10.11e)$$

$$f_{i/p_S}^{[i\sigma^{+-}\gamma_5]}(x, \mathbf{k}_T, \mu, \zeta) = \frac{M}{P^+} \left[ S_L h_L(x, k_T) - \frac{k_T \cdot S_T}{M} h_T(x, k_T) \right], \quad (10.11f)$$

where for further details about the notation we refer to Sec. 2.7. Among them, 8 are chiral-even and 8 are chiral-odd. Likewise, 8 **PS: leading subleading** quark TMDPDFs are T-even and 8

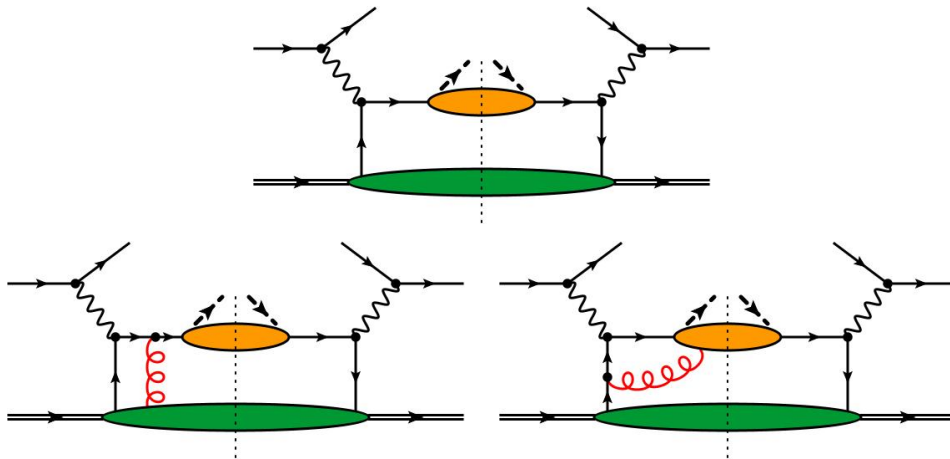


Figure 10.3: SIDIS tree-level diagrams relevant for subleading-power observables. The upper diagram entails intrinsic and kinematical contributions, the lower diagrams dynamical contributions. Also mirror diagrams are to be included.

are T-odd. Note that, unlike in the case of leading TMDs, it is not possible to assign a parton polarization to subleading TMDs as they have no density interpretation. Also, the same number of subleading TMDFFs exists, see Fig. 10.11. Given that the structure of the equations which define TMDPDFs and TMDFFs is very similar — compare Eq. (2.124) and Eq. (2.135) for the leading-power functions — we don't give a set of equations for the subleading TMDFFs but just mention that their definition can be obtained from Eqs. (10.19f)–(10.19f) by replacing on the l.h.s.  $f_{i/p_S}^{[\Gamma]}(x, \mathbf{k}_T, \mu, \zeta)$  by  $\Delta_{h/i}^{[\Gamma]}(z, -zp'_T, \mu, \zeta)$ , and on the r.h.s. the target mass  $M$  by the mass of the produced hadron  $M_h$ , as well as  $k_T$  by  $p'_T$ . Furthermore, the lower case letters for the TMDPDFs become upper case letters for the TMDFFs, with the exception of the projector  $\Gamma = \gamma^\alpha$ , where the symbol  $D$  is used for the FFs (instead of  $F$ ). Recall also that the TMDFFs are functions of  $(z, zp'_T)$ , and that  $\kappa$ , the indicator of a nontrivial universality behavior, is absent for TMDFFs.

It was also found that 16 subleading gluon TMDPDFs and TMDFFs can be identified [148, 1211]. Presently, for those objects not much is known beyond their classification. Finally, for subleading TMDs in the case of spin-1 particles we refer to [1212, 1213].

## 10.4 Factorization for SIDIS with Subleading Power TMDs

### 10.4.1 Status of SIDIS factorization at next-to-leading power

- Discuss classification of all potential contributions to subleading power SIDIS factorization (minimal detail, following SCET classification scheme for subleading power terms)
- Discuss in words the arguments needed to eliminate all non-trivial subleading power soft contributions at  $\mathcal{O}(\Lambda/Q)$ . Mention that such soft contributions are known to contribute at subsubleading power,  $\mathcal{O}(\Lambda^2/Q^2)$ .
- Discuss the missing item needed to fully prove factorization at this order, namely the treatment of Glauber interactions.

### 10.4.2 SIDIS structure functions in terms of next-to-leading power TMDs

- Provide full factorization formula in  $b_T$  space for the unpolarized and longitudinally polarized structure functions in SIDIS. Point to literature for transverse case.
- Explain simplification that occurs when working at lowest order in hard function  $H^{(1)}$  ( $\xi$  integral).
- Provide momentum space factorization formula for one case ??

Unpolarized structure functions.

$$\begin{aligned} W_{UU}^{\cos \phi_h} &= \mathcal{F} \left\{ \frac{q_T}{Q} H(Q^2, \mu) \left[ -\tilde{f}_1 \tilde{D}_1 + \tilde{h}_1^{\perp(1)} \tilde{H}_1^{\perp(1)} \right] \right. \\ &\quad + H(Q^2, \mu) \left[ -\frac{M}{Q} \tilde{f}_1^{(1)} \tilde{D}_1 - \frac{M_h}{Q} \tilde{f}_1 \tilde{D}_1^{(1)} + \frac{M}{Q} \tilde{h}_1^{\perp(0')} \tilde{H}_1^{\perp(1)} + \frac{M_h}{Q} \tilde{h}_1^{\perp(1)} \tilde{H}_1^{\perp(0')} \right] \\ &\quad \left. - H^{(1)}(Q^2, \xi, \mu) \left[ \frac{2xM}{Q} \left( \tilde{f}_1^{\perp(1)} D_1 + \tilde{h}_1^{\perp(1)} \tilde{H}_1^{\perp(1)} \right) + \frac{2M_h}{zQ} \left( \tilde{f}_1 \tilde{D}^{\perp(1)} + \tilde{h}_1^{\perp(1)} \tilde{H} \right) \right] \right\}, \\ W_{LU}^{\sin \phi_h} &= \mathcal{F} \left\{ H^{(1)}(Q^2, \xi, \mu) \left[ \frac{2xM}{Q} \left( \tilde{g}_1^{\perp(1)} \tilde{D}_1 - \tilde{e}_1^{\perp(1)} \tilde{H}_1^{\perp(1)} \right) - \frac{2M_h}{zQ} \left( \tilde{f}_1 \tilde{G}^{\perp(1)} - \tilde{h}_1^{\perp(1)} \tilde{E} \right) \right] \right\}. \end{aligned} \quad (10.12)$$

Longitudinally polarized structure functions.

$$\begin{aligned} W_{UL}^{\sin \phi_h} &= \mathcal{F} \left\{ \frac{q_T}{Q} H(Q^2, \mu) \tilde{h}_{1L}^{\perp(1)} \tilde{H}_1^{\perp(1)} + H(Q^2, \mu) \left( \frac{M}{Q} \tilde{h}_{1L}^{\perp(0')} \tilde{H}_1^{\perp(1)} + \frac{M_h}{Q} \tilde{h}_{1L}^{\perp(1)} \tilde{H}_1^{\perp(0')} \right) \right. \\ &\quad \left. + H^{(1)}(Q^2, \xi, \mu) \left[ \frac{2xM}{Q} \left( \tilde{f}_L^{\perp(1)} \tilde{D}_1 - \tilde{h}_L^{\perp(1)} \tilde{H}_1^{\perp(1)} \right) - \frac{2M_h}{zQ} \left( \tilde{g}_{1L} \tilde{G}^{\perp(1)} + \tilde{h}_{1L}^{\perp(1)} \tilde{H} \right) \right] \right\}, \\ W_{LL}^{\cos \phi_h} &= \mathcal{F} \left\{ -\frac{q_T}{Q} H(Q^2, \mu) \tilde{g}_{1L} \tilde{D}_1 - H(Q^2, \mu) \left( \frac{M}{Q} \tilde{g}_{1L}^{(1)} \tilde{D}_1 + \frac{M_h}{Q} \tilde{g}_{1L} \tilde{D}_1^{(1)} \right) \right. \\ &\quad \left. + H^{(1)}(Q^2, \xi, \mu) \left[ -\frac{2xM}{Q} \left( \tilde{g}_L^{\perp(1)} \tilde{D}_1 - \tilde{e}_L^{\perp(1)} \tilde{H}_1^{\perp(1)} \right) - \frac{2M_h}{zQ} \left( \tilde{g}_{1L} \tilde{D}^{\perp(1)} + \tilde{h}_{1L}^{\perp(1)} \tilde{E} \right) \right] \right\}. \end{aligned} \quad (10.13)$$

Analogous results for the transversely polarized structure functions  $W_{UT}^{\sin \phi_S}$ ,  $W_{UT}^{\sin(2\phi_h - \phi_S)}$ ,  $W_{LT}^{\cos \phi_S}$ , and  $W_{LT}^{\cos(2\phi_h - \phi_S)}$ , can be found in [? ].

Due to the presence of an additional convolution in  $\xi$  we have a slightly modified definition of the convolution integral at NLP, which varies depending on whether or not it is acting on a

function arising from a quark-gluon-quark correlator:

$$\begin{aligned}
\mathcal{F}[\mathcal{H} \tilde{g}^{(n)} \tilde{D}^{(m)}] &= 2z \sum_f \mathcal{H}_f(q^+ q^-) \int_0^\infty \frac{db_T b_T}{2\pi} (Mb_T)^n (-M_h b_T)^m J_{n+m}(b_T q_T) \\
&\quad \times g_f^{(n)}(x, b_T) D_f^{(m)}(z, b_T) + (f \rightarrow \bar{f}), \\
\mathcal{F}[\mathcal{H} \tilde{\tilde{g}}^{(n)} \tilde{D}^{(m)}] &= 2z \sum_f \int d\xi \mathcal{H}_f(q^+ q^-, \xi) \int_0^\infty \frac{db_T b_T}{2\pi} (Mb_T)^n (-M_h b_T)^m J_{n+m}(b_T q_T) \\
&\quad \times \tilde{g}_f^{(n)}(x, \xi, b_T) D_f^{(m)}(z, b_T) + (f \rightarrow \bar{f}), \\
\mathcal{F}[\mathcal{H} \tilde{g}^{(n)} \tilde{\tilde{D}}^{(m)}] &= 2z \sum_f \int d\xi \mathcal{H}_f(q^+ q^-, \xi) \int_0^\infty \frac{db_T b_T}{2\pi} (Mb_T)^n (-M_h b_T)^m J_{n+m}(b_T q_T) \\
&\quad \times g_f^{(n)}(x, b_T) \tilde{D}_f^{(m)}(z, \xi, b_T) + (f \rightarrow \bar{f}). \tag{10.14}
\end{aligned}$$

In this section, we intend to summarize the efforts that have been made in the literature to understand observables within the TMD formalism that require subleading TMD functions, by focusing on SIDIS where by far most of the literature is available. When the transverse hadron momentum  $P_{hT}$  of the final-state hadron is much smaller than  $Q$ , a treatment of the relevant structure functions in a TMD framework is appropriate<sup>34</sup>. For SIDIS, a concise TMD parton model treatment, that is, a leading-order pQCD analysis, has been presented already some time ago in Refs. [121, 129]. As is the case for all power-suppressed observables, the theoretical analysis, even at lowest order, is more involved compared to leading-power observables. A particular complication within a pQCD description is that different subleading effects, for both PDFs and FFs, contribute to the same power-suppressed observable, see, for instance, Ref. [167]. However, one may employ relations based on the QCD equation of motion to re-express certain classes of functions through other subleading functions.

In the following we will discuss four prominent subleading effects in SIDIS that have been measured at HERMES, COMPASS, and Jefferson Lab ([448, 457, 458, 1214–1222], see also Ref. [1223] for a recent review: the structure functions  $F_{UU}^{\cos \phi_h}$  (Cahn effect),  $F_{LU}^{\sin \phi_h}$  (longitudinal beam spin asymmetry (BSA)),  $F_{UL}^{\sin \phi_h}$  (longitudinal target spin asymmetry) and  $F_{UT}^{\sin \phi_s}$ . According to Refs. [121, 129], those structure functions can be ~~PS: factorized within the subleading-power tree-level TMD framework and acquire the form expressed under the assumption of factorization in a subleading-power tree-level TMD framework in the following~~

<sup>34</sup>In a frame in which both the target particle and the final-state hadron have no transverse momentum, one requires  $q_T \ll Q$  for TMD factorization to work, where  $\mathbf{q}_T$  is the transverse momentum of the virtual photon. Since  $q_T = P_{hT}/z$ , from the point of view of power counting the conditions  $q_T \ll Q$  and  $P_{hT} \ll Q$  are equivalent. However, depending on the numerical value for  $z$ , data which satisfy  $P_{hT} \ll Q$  may not satisfy  $q_T \ll Q$  and therefore be difficult to describe in a TMD approach.

form (??)

$$F_{UU}^{\cos \phi_h} = \frac{2M}{Q} C \left[ \frac{\hat{h} \cdot \mathbf{p}_T}{zM_h} \left( x h H_1^\perp + \frac{M_h}{M} f_1 \frac{\tilde{D}^\perp}{z} \right) - \frac{\hat{h} \cdot \mathbf{k}_T}{M} \left( x f^\perp D_1 + \frac{M_h}{M} h_1^\perp \frac{\tilde{H}}{z} \right) \right], \quad (10.15)$$

$$F_{LU}^{\sin \phi_h} = \frac{2M}{Q} C \left[ \frac{\hat{h} \cdot \mathbf{p}_T}{zM_h} \left( x e H_1^\perp + \frac{M_h}{M} f_1 \frac{\tilde{G}^\perp}{z} \right) + \frac{\hat{h} \cdot \mathbf{k}_T}{M} \left( x g^\perp D_1 + \frac{M_h}{M} h_1^\perp \frac{\tilde{E}}{z} \right) \right], \quad (10.16)$$

$$F_{UL}^{\sin \phi_h} = \frac{2M}{Q} C \left[ \frac{\hat{h} \cdot \mathbf{p}_T}{zM_h} \left( x h_L H_1^\perp + \frac{M_h}{M} g_1 \frac{\tilde{G}^\perp}{z} \right) + \frac{\hat{h} \cdot \mathbf{k}_T}{M} \left( x f_L^\perp D_1 - \frac{M_h}{M} h_{1L}^\perp \frac{\tilde{H}}{z} \right) \right], \quad (10.17)$$

$$\begin{aligned} F_{UT}^{\sin \phi_S} = & \frac{2M}{Q} C \left[ x f_T D_1 - \frac{M_h}{M} h_1 \frac{\tilde{H}}{z} \right. \\ & \left. + \frac{\mathbf{p}_T \cdot \mathbf{k}_T}{2zMM_h} \left( x h_T H_1^\perp + \frac{M_h}{M} g_{1T}^\perp \frac{\tilde{G}^\perp}{z} - x h_T^\perp H_1^\perp + \frac{M_h}{M} f_{1T}^\perp \frac{\tilde{D}^\perp}{z} \right) \right], \end{aligned} \quad (10.18)$$

where the convolution of transverse momenta  $C$  is defined as

$$C[w f D] = x \sum_i e_i^2 \int d^2 \mathbf{k}_T d^2 \mathbf{p}_T \delta^{(2)}(z \mathbf{k}_T + \mathbf{p}_T - \mathbf{P}_{hT}) w(\mathbf{p}_T, \mathbf{k}_T) f^q(x, k_T) D^q(z, z p_T). \quad (10.19)$$

Note that the convolution integral in Eq. (10.8) coincides with Eq. (2.172), with  $\mathcal{H} = 1$ . The vector  $\hat{h} \equiv \mathbf{P}_{hT}/|\mathbf{P}_{hT}|$  is a unit vector in the direction of the transverse momentum of the produced hadron.

In order to derive Eqs. (10.20)–(10.23), the tree-level diagrams shown in Fig. 10.12 have to be calculated, see Refs. [121, 129]. The TMD formulas in Eqs. (10.20)–(10.23) indicate that those structure functions are each generated by convolutions of subleading TMDPDFs with leading TMDFFs, and vice versa<sup>35</sup>. TMDs that appear with a tilde, such as  $\tilde{D}^\perp$ , represent matrix elements of quark-gluon-quark correlations. PS: [Two remarks: (i) one can add that all subleading TMDFFs have a tilde, as a consequence of the adopted conventions. (ii) In the Table in Fig. 10.11 no tilde is shown. Perhaps this could be made uniform.]

## 10.5 Experimental Results for NLP TMD Observables

AM: [The following is “raw material” concerning experimental data.]

- Cahn effect: First observation by EMC Collaboration [1214, 1215], also seen at Fermilab [?], and at HERA [? ]. There are measurements at JLab [? ? ], HERMES [? ], and COMPASS [? ].
- Beam-spin asymmetry  $A_{LU}^{\sin \phi_h}$ : COMPASS results in Ref. [? ] (for  ${}^6\text{LiD}$  target, same paper as Cahn effect), JLab (CLAS) [1220? –1222], and HERMES [1217? ? ]
- Longitudinal target SSA  $A_{UL}^{\sin \phi_h}$ : This was seen at HERMES [1217? –1219], JLab [? ? ], and preliminary data from COMPASS [? ].
- Transverse target SSA  $A_{UT}^{\sin \phi_S}$ : COMPASS data [456] and HERMES data [458] (shown in figure below); apparently nothing from JLab on this.

<sup>35</sup>This implies that the structure functions (10.20)–(10.23) may be relevant for an analysis of leading TMDs as well.

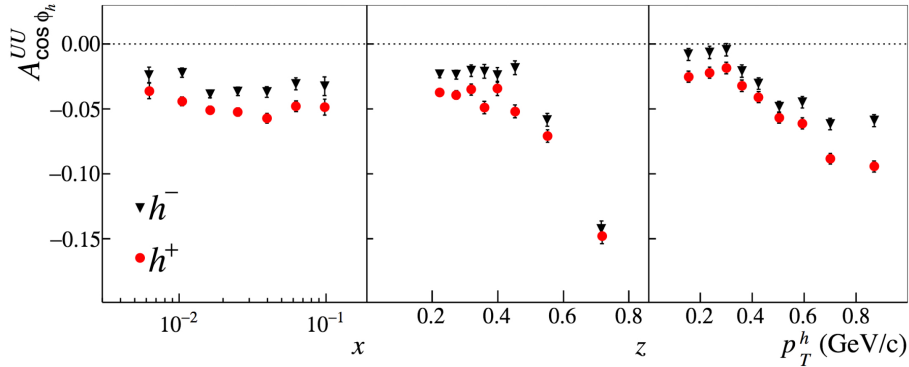


Figure 10.4: COMPASS data, for a  ${}^6\text{LiD}$  target, of the Cahn asymmetry  $A_{\cos \phi_h}^{UU}|_{\text{fig.}} \propto F_{UU}^{\cos \phi_h} / F_{UU}$  for positively and negatively charged hadrons as a function of  $x$ ,  $z$  and  $P_{hT} = p_T^h|_{\text{fig.}}$  [448].

Let us now elaborate a bit more on the experimental significance of power-suppressed TMD observables in SIDIS. We repeat that there has been a tremendous effort to measure the SIDIS structure functions in Eqs. (10.20)–(10.23) at HERMES, COMPASS, and JLab. For example, COMPASS data for the Cahn effect is shown in Fig. 10.13. One can see that the data is very precise, and the Cahn effect is not small at all. Similar observations can be made for CLAS measurements of the longitudinal beam spin asymmetry and HERMES measurements of the target spin asymmetry in Fig. 10.14, as well as for COMPASS measurements of the transverse spin asymmetry in Fig. 10.15. Several other measurements of power-suppressed structure functions have been reported at COMPASS, HERMES and Jlab. More details about the status of measurements for subleading-power TMD effects can also be found in a recent review [1223]. Generally, the data points for those structure functions that have been provided by the experiments are too large and too precise to simply ignore them. On the contrary, they require theoretical efforts and analyses to understand these effects, at least qualitatively. This is the main motivation for studying  $\Lambda/Q$ -suppressed observables within the TMD formalism, as this is basically the only QCD-based approach that can be applied to such observables.

**AM:** [Revisit the following discussion after the discussion about TMD factorization has been settled.] As a final point in this subsection, we briefly summarize the current status of factorization for subleading TMDs. There actually exist only very few papers which address this topic by trying to go beyond the lowest order in pQCD. Early on, model calculations for the beam spin asymmetry  $F_{LU}^{\sin \phi_h}$  [1230] and a corresponding T-odd twist-3 TMDPDF  $g^\perp$  [1231] (cf. Eq. (10.21)) indicated a problem with a light-cone divergence that wouldn't cancel in tree-level formulae. Furthermore, an issue was reported in relation to the  $\cos \phi_h$  modulation of the unpolarized SIDIS cross section [1232], namely that the result for TMD factorization in the intermediate transverse momentum region  $\Lambda_{\text{QCD}} \ll |P_{h\perp}| \ll Q$  does not match with the result from collinear factorization. However, a more recent work argues that this problem can actually be overcome [1233]. A related discussion about subleading-power TMD factorization in Drell-Yan has been presented in Refs. [258, 259, 1234]. In Refs. [258, 259] the TMD factorization breaking effects were analyzed and the form of the power corrections to the TMD factorization formula (2.6) was obtained. It was found that the power corrections have a simple form and in the large- $N_c$  limit can be expressed in terms of the leading-power

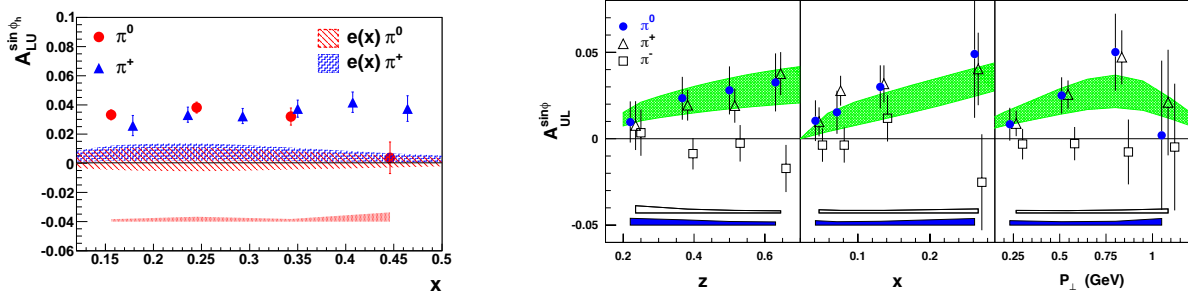


Figure 10.5: **Left:** CLAS data for the beam-spin asymmetry  $A_{LU}^{\sin \phi_h} \propto F_{LU}^{\sin(\phi_h)} / F_{UU}$  for  $\pi^0$  and  $\pi^+$  as a function of  $x$  at an average  $P_{hT} = 0.38$  GeV and for  $0.4 < z < 0.7$  [1221]. The error bars correspond to statistical uncertainties, and the red error band at the bottom of the plot corresponds to systematic uncertainties. The red and blue hatched bands show model calculations involving only the Collins effect for  $\pi^0$  and  $\pi^+$ , respectively. **Right:** HERMES data for the longitudinal target-spin asymmetry  $A_{UL}^{\sin \phi_h} \propto F_{UL}^{\sin(\phi_h)} / F_{UU}$  for pion production [1218]. Error bars include the statistical uncertainties only. The filled (blue) and open (white) bands at the bottom of the panels represent the systematic uncertainties for neutral and charged pions, respectively. The shaded (green) areas show a range of predictions of a model calculation [1227, 1228] applied to the case of  $\pi^0$  production.

TMD distribution functions listed in Fig. 2.5. It was estimated that the power corrections reach a few percent of the leading-twist result at  $|P_{h\perp}|/Q \sim 0.2$ .

Overall, it is very important to further explore the topic of subleading-power TMD factorization in order to get a better understanding of its status.

## 10.6 Estimating Subleading TMDs and Related Observables

We now turn our attention to calculations of subleading TMD effects. As is the case for integrated PDFs, we repeat that subleading TMDs are not necessarily smaller than leading TMDs. While most calculations of TMDs address the leading sector (see Ch. 6 and Ch. 7 for an overview), quite a few estimates exist for subleading TMDs as well. The vast majority of those studies are based on model calculations. Details about the main features of the relevant models can be found in Ch. 7 and references therein.

### 10.6.1 Generalized scalar charge from Lattice QCD

Preliminary information is available for the function  $e(x, k_T)$  from LQCD. The LQCD methodology to evaluate selected TMD observables, described in detail in Sec. 6.4.1, can also be employed to access quantities involving subleading TMDs, in analogy to the leading TMD observables discussed there. In the case of the scalar Dirac structure  $\Gamma = 1$ , the fundamental hadronic matrix element in Eq. (6.55) can be decomposed into Lorentz-invariant amplitudes  $\tilde{A}_i, \tilde{B}_i$  as follows (the complete decomposition is given in Ref. [140]),

$$\frac{1}{2M} \tilde{\Phi}^{[1]} = \tilde{A}_1 + \frac{iM}{v \cdot P} \epsilon^{\mu\nu\rho\sigma} P_\mu b_\nu v_\rho S_\sigma \tilde{B}_5. \quad (10.20)$$

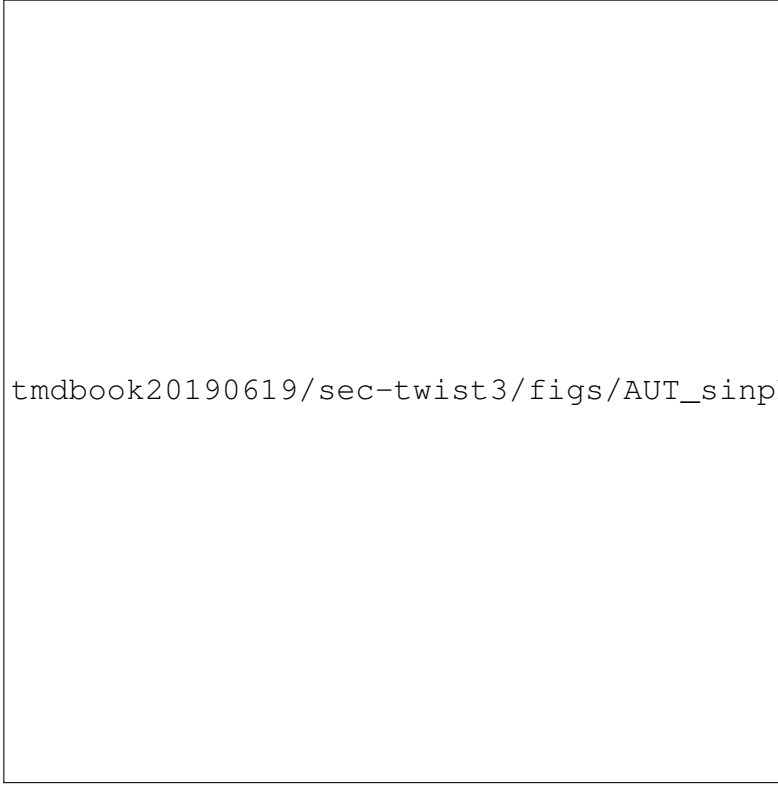


Figure 10.6: HERMES data for charged pions of the  $\sin \phi_S$  modulation of the SIDIS cross section for a proton target [458]. Systematic uncertainties are given as bands. The observable is directly proportional to the structure function  $F_{UT}^{\sin \phi_S}$ .

The Lorentz-invariant amplitudes are closely related to Fourier-transformed TMDs [140], and can thus be utilized to define the chiral-odd generalized scalar charge

$$\frac{\tilde{e}^{[1](0)}}{\tilde{f}_1^{[1](0)}} = \frac{\tilde{A}_1(-b_T^2, b \cdot P = 0, \hat{\zeta}, \eta v \cdot P)}{\tilde{A}_{2B}(-b_T^2, b \cdot P = 0, \hat{\zeta}, \eta v \cdot P)}, \quad (10.21)$$

in analogy to the generalized tensor charge in Eq. (6.63); the arguments  $v$ ,  $\hat{\zeta}$  and  $\eta$  describing the geometry of the staple-shaped gauge link are defined in Sec. 2.10.1. The unpolarized amplitude  $\tilde{A}_{2B}$  in the denominator was introduced in Eq. (6.56). The ratio in Eq. (10.14) is interpreted as a generalized scalar charge because, in the formal  $b_T \rightarrow 0$  limit, i.e., upon complete integration over quark momentum components, the numerator corresponds to the standard scalar charge. It is normalized to the corresponding number of valence quarks by the denominator. It should, however, be emphasized that additional divergences arise in the  $b_T \rightarrow 0$  limit (which corresponds to unrestricted integration over transverse momentum  $k_T$ ) that require further renormalization. As a consequence, the ratio of scalar to vector renormalization constants,  $Z_S/Z_V$ , has to be accounted for when connecting the generalized scalar charge to the standard scalar charge.

In Fig. 10.8 we show results for the generalized scalar charge of the nucleon obtained using a clover fermion ensemble at the pion mass  $m_\pi = 317$  MeV. No appreciable variation is seen as

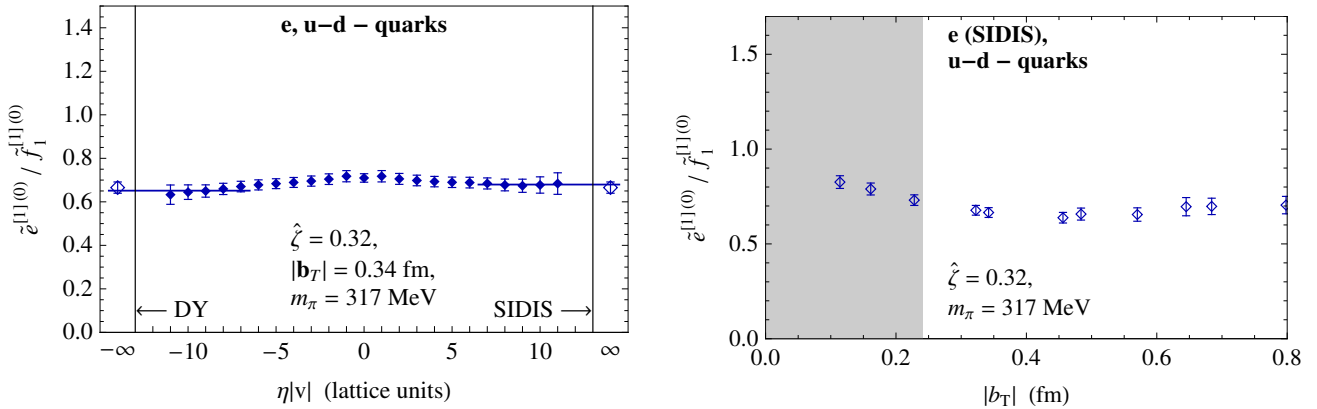


Figure 10.7: Isovector generalized scalar charge in the nucleon, obtained using a clover fermion ensemble at the pion mass  $m_\pi = 317$  MeV. Left: As a function of the staple length  $\eta$  at fixed  $b_T$  and  $\hat{\zeta}$ . Right: SIDIS/DY limit as a function of  $b_T$  for fixed  $\hat{\zeta}$ , also presented previously in Ref. [1223]. The shaded area indicates the region which may be subject to significant lattice artifacts.

a function of the staple length  $\eta$ , indicating that the final-state interaction effects in the scalar and  $\gamma^+$  nucleon matrix elements closely track one another. Also as a function of the quark operator separation  $b_T$  in the SIDIS/DY limit, the variation of the generalized scalar charge appears to be weak. This stands in contrast to the significant variations seen for the Sivers, Boer-Mulders and  $g_{1T}^\perp$  worm-gear shifts exhibited in Sec. 6.4.1.

### 10.6.2 Model calculations of subleading TMDs

Most model calculations of subleading TMDs have been performed in diquark spectator models, where many studies have included both scalar and vector diquarks in order to obtain results for up quarks and down quarks. Analytical results in such a model for all 8 T-even subleading TMDPDFs can be found in Ref. [756]. In Ref. [1231], the subleading T-odd PDF  $g^\perp(x, k_T)$  was computed in the scalar diquark model, with an emphasis on scrutinizing the mere definition of subleading TMDs. It was found that, to lowest nontrivial order in perturbation theory, one encounters a light-cone singularity, a feature which does not show up for the corresponding calculation of leading T-odd PDFs. Moreover, it was argued that actually all T-odd subleading TMDs exhibit a light-cone singularity in the same model and in the quark-target model in QCD. This led to the conclusion that presently we may not have a valid definition of (T-odd) subleading TMDs and that the status of factorization for subleading TMDs is not fully settled. (See also the last paragraph in Sec. 10.7 for more discussion of that point.) **AM:** [Revisit discussion of  $g^\perp(x, k_T)$  in this paragraph after the discussion about TMD factorization has been settled. The same applies to the first part of the following paragraph.]

The subleading beam SSA  $A_{LU}^{\sin\phi_h}$  in SIDIS, which is related to  $g^\perp(x, k_T)$  in a tree-level analysis (see Eq. (10.21)), was also computed in the scalar diquark model [1235]. By assuming factorization to be valid, from the (finite) result for the asymmetry, a finite expression for  $g^\perp(x, k_T)$  was extracted. However, that study did not address the direct calculation of  $g^\perp(x, k_T)$  based on its operator definition, which explains the qualitatively different finding relative to Ref. [1231]. Another computation of  $g^\perp(x, k_T)$  in a diquark spectator model for both up quarks and down quarks is discussed in Ref. [1236], while further spectator model results

for (T-even and T-odd) subleading TMDPDFs can be found in Refs. [1237–1242]. In some papers, subleading FFs were also studied in spectator models. Specifically, calculations of the chiral-odd integrated FF  $E(z)$  have been presented in Refs. [1243, 1244]. Furthermore, (T-odd) subleading TMDFFs, some of which are relevant for the QCD description of transverse SSAs in processes like  $p^\dagger p \rightarrow hX$ , have been addressed in Refs. [1245, 1246].

All T-even subleading TMDPDFs were also computed in the bag model [13]. Like in the case of leading TMDs, the results agree quite well with a Gaussian  $k_T$ -dependence. Another interesting approach for estimating (subleading) TMDs is the light-front constituent model (LFCM). In that framework, the TMDs are first represented through the overlap of light-front wave functions in a model-independent manner. In a second step, one can exploit different models for the wave functions to obtain numerical results for the TMDs. The LFCM was applied to the T-even subleading TMDPDFs for both the nucleon [754] and the pion [755], with the treatment limited to the 3-quark ( $3q$ ) sector. In this approach, the analysis becomes quite cumbersome when including higher Fock states. On the other hand, going beyond the  $3q$  Fock state is expected to be very important in order to find realistic results for subleading TMDs. For  $e(x, k_T)$ , in Ref. [1247] the  $3q + g$  Fock state has actually been included in the analysis in the LFCM. We note that Ref. [754] also contains a discussion of the T-even TMD  $f^\perp(x, k_T)$  in the chiral quark soliton model, which presently is the only available result for a subleading TMD in this model. (Studies of the collinear twist-3 PDFs  $g_T(x)$ ,  $h_L(x)$  and  $e(x)$  in the chiral quark soliton model can be found in Refs. [?? ?? ?? ].) According to Eq. (10.20), this TMD plays a critical role for the understanding of the  $\cos \phi_h$  modulation of the unpolarized SIDIS cross section. Furthermore, results for all T-even subleading TMDPDFs in the covariant parton model have been reported recently in Ref. [730].

Calculations of TMDs (and related observables) in pQCD using the quark-target model are often used to study factorization and TMD evolution. They can also shed light on the status of relations/constraints for TMDs that appear in other models. A calculation of the subleading TMD  $f^\perp(x, k_T)$  in the quark-target model was presented in Ref. [1248], whereas in Ref. [1234] factorization for subleading TMDs for the Drell-Yan process was considered by focusing on the contribution related to  $f^\perp(x, k_T)$ , along with the evolution of that TMD. Related work dealing with the twist-3 functions  $g_T(x)$ ,  $e(x)$  and  $h_L(x)$  in the quark-target model can be found in, for instance, Refs. [663, 665, 705, 1249–1251]. We also want to briefly mention an interesting general feature for subleading parton distributions: They can exhibit singular zero-mode contributions, that is, terms which are proportional to  $\delta(x)$ . Such terms have been identified in model calculations but also in model-independent analyses, see [1247, 1249? ? –1253] and references therein for more details.

(Subleading) TMDs obtained in models without gluonic degrees of freedom may satisfy a number of so-called quark-model Lorentz invariance relations (qLIRs) [60, 129, 463, 464, 1254]. The qLIRs can provide a reasonable approximation for the TMDs and the corresponding subleading-power observables. From a practical point of view, they allow for important cross checks of the analytical and numerical model results. The qLIRs are discussed in more detail in Sec. 7.9.2 to which we refer the reader. They must be distinguished from the LIRs which hold in full QCD and typically involve quark-gluon-quark correlations [167, 850, 1255–1257].

A frequently-used approach for estimating subleading integrated PDFs is the Wandzura-Wilczek (WW) approximation, which was originally derived for  $g_T(x)$  [666] but can also be applied to  $h_L(x)$  [387]. Here one makes use of the fact that, for instance,  $g_T(x)$  can be

decomposed into a term which is fixed by the twist-2 helicity distribution  $g_1(x)$ , plus a term that is given by a  $q\bar{q}$  correlator, where the WW approximation consists of neglecting the latter contribution. At present, we are lacking very robust information about the quality of the WW approximation. (More details about this point can be found in [210] and references therein.) However, for the lowest nontrivial  $x$ -moment of  $g_T$  and  $h_L$  instanton-vacuum model calculations [1258, 1259], as well as a study in LQCD [548], suggest that the WW approximation works very well. It has also been argued that, based on experimental data, a violation of the WW approximation for  $g_T(x)$  at the level of 15–40% is possible [732]. We also point out that the very first calculations of  $g_T(x)$  and  $h_L(x)$  in LQCD are compatible with this finding [630, 664]; see Sec. 6.3.2 for more details.

A very similar approximation, which is typically called WW-type approximation, can be made for subleading TMDs [121, 129]. We refer to [210] for a comprehensive review of the WW-type approximation, where all parton model results for the SIDIS structure functions at low transverse hadron momenta have been expressed in the WW-type approximation. To discuss just one example of this approximation we quote the relation [121, 129]

$$xf^\perp(x) = x\tilde{f}^\perp(x) + f_1(x), \quad (10.22)$$

with  $\tilde{f}^\perp$  representing a dynamical twist-3 term that is defined through a  $q\bar{q}$  correlator. The WW-type approximation for the subleading TMD  $f^\perp$  is then given by

$$xf^\perp(x)|_{\text{WW-type}} = f_1(x). \quad (10.23)$$

The curves in Fig. 10.9 show bag model results for both the twist-3 function  $xf^\perp(x)$  and the twist-2 function  $f_1(x)$ . Obviously, in this model the quality of the WW-type approximation (strongly) depends on  $x$ , with the approximation working best for intermediate to large values of  $x$  which is the region where quark model results are expected to be more reliable. It also depends on the TMD under consideration, where we refer to [13] for more numerical results. The same general features apply to all models [210]. We note in passing that, interestingly, the relation (10.15) is exact in the chiral quark soliton model. Even though in that model very strong (chiral) interactions are present, the function of  $\tilde{f}^\perp$  in Eq. (10.15) is zero in this model [754].

### 10.6.3 Model calculations of subleading-power observables

The calculation of the  $\cos\phi_h$  dependence of the unpolarized SIDIS cross section by Cahn in the framework of a generalized parton model has similarities with applying the WW-type approximation to the tree level expression for  $F_{UU}^{\cos\phi_h}$  in Eq. (10.20) [278, 279]. A very similar approach for this structure function was employed in Ref. [303]. More specifically, the authors of that paper used a Gaussian ansatz for the TMDPDF  $f_1(x, k_T)$  and the TMDFF  $D_1(z, zp'_T)$ , and extracted (approximate) values for the respective average transverse momenta from data of the EMC Collaboration [1260, 1261] and the E665 Collaboration [1262]. (For a related discussion we refer to [304].) They found the values  $\langle k_T^2 \rangle = 0.25 \text{ GeV}^2$  and  $\langle p_T^2 \rangle = 0.20 \text{ GeV}^2$  [303], which compare reasonably well with the widths extracted from leading-power observables; see Sec. 5.2.1.

We repeat that further interest in subleading SIDIS structure functions arose with the first observation of a nonzero longitudinal target SSA, that is, a nonzero result for the structure

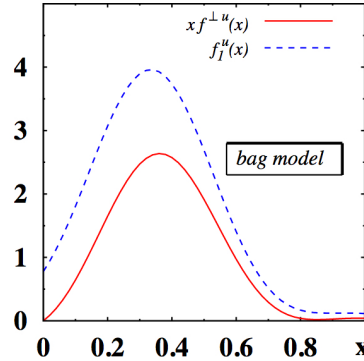


Figure 10.8: Bag model results for the functions  $xf^{\perp u}(x)$  and  $f_1^u(x)$  for up quarks in the proton [13, 1254]. These functions would be equal in the WW-type approximation in Eq. (10.16).

function in Eq. (10.22), for  $\pi^+$  production on a hydrogen target by the HERMES Collaboration [466]. As a consequence of that measurement, this SSA, as well as other subleading effects in SIDIS, were explored in a number of studies which made use of the WW-type approximation in one form or another [472, 473, 1227, 1228, 1263–1275]. The goals of those works included describing the experimental data, extracting information on PDFs and FFs from the data in the WW-type approximation, and making predictions for different kinematics and experiments and/or other structure functions. Recently, in Ref. [210] a comprehensive numerical analysis of the SIDIS structure functions in the WW-type approximation was presented.

Another series of papers made use of spectator models in order to estimate subleading effects in SIDIS [1236, 1238–1242, 1244]. Furthermore, in Ref. [1276] the unpolarized SIDIS cross section was studied through  $\Lambda^2/Q^2$  accuracy, with a particular focus on the  $\cos 2\phi_h$  modulation. Using a generalized parton model in the spirit of the work by Cahn [278, 279] provides an (important) nonzero  $\Lambda^2/Q^2$  contribution to this structure function which is related to the leading unpolarized TMDPDF  $f_1(x, k_T)$  and TMDFF  $D_1(z, zp'_T)$ . However, such a treatment does not lead to a full tree-level result in QCD which was aimed at in Ref. [1276]. Another interesting aspect of that work is a comparison between scattering off a proton versus a nuclear target. Related studies, dealing with subleading-power observables for semi-inclusive reactions and nuclear targets, can be found in Refs. [1277–1279].

Calculations of power-suppressed observables in SIDIS were also instrumental for obtaining a complete list of subleading TMDs. Specifically, Ref. [1280] addressed the structure function  $F_{LU}^{\sin \phi_h}$  in Eq. (10.21) in a scalar diquark model. This work was revisited and extended to the structure function  $F_{UL}^{\sin \phi_h}$  in Eq. (10.22) in Ref. [1230], and based on the results it was argued that the list of subleading TMDs known at that time was incomplete. This development indeed led to the discovery of a new T-odd subleading TMD for an unpolarized target, namely  $g^{\perp}(x, k_T)$ , in Ref. [130]. Later on, further studies uncovered two additional subleading TMDs for a spin- $\frac{1}{2}$  hadron [131], completing the list of the 16 subleading TMDPDFs in the table in Fig. 10.2 above.

## 10.7 Summary and Outlook

So far, the main focus of the TMD community has been on the leading-power TMDs. However, as we have emphasized, subleading TMDs are important as well for several reasons. For a long time, the unclear status of factorization has been a serious impediment in the field of subleading TMDs. But considerable progress in this area has now been reported [Refs.] [expand and briefly mention open points for further research].

These recent developments hold promise to the put the studies of subleading TMDs on very safe ground. They will certainly generate renewed interest in this field and can initiate additional calculations of those functions and related observables in various approaches, including LQCD. It is certainly worthwhile to take a fresh look at what information on subleading TMDs can be extracted from existing data and how future experiments, in particular the EIC, can move this field forward.

We repeat that subleading TMDs are related to quark-gluon-quark correlations which allow for studies of the hadron structure that are complementary to the investigation of parton densities described by leading TMDs. While this alone provides a strong motivation for the field, it is important to try further revealing the physics encoded in the subleading TMDs.

## 10.8 Placeholder: Original Sections 10.2 and 10.3

### 10.8.1 Original 10.2: Overview of subleading TMDs

Since the earliest treatments of transverse motion of partons in the nucleon emerged from studies of power-suppressed contributions in SIDIS [278, 279, 1208], we begin our discussion with the general structure of the subleading-power SIDIS cross section. In so doing, we consider both unpolarized and polarized targets.

The fully differential SIDIS cross section — assuming a one-photon exchange between the lepton and the nucleon, and unpolarized produced hadrons in the final state — can be decomposed into 18 structure functions [121, 1210]. For low transverse momenta of the final-state hadron, eight of those structure functions are leading in a  $\Lambda/Q$  expansion, see Eq. (2.187). Another eight are suppressed by a factor  $\Lambda/Q$ , while the remaining two are suppressed by a factor  $\Lambda^2/Q^2$ . Focusing on the subleading contributions we have, in the notation of Refs. [121, 210]<sup>36</sup>,

$$\begin{aligned} \frac{d^6\sigma_{\text{subleading}}}{dx dy dz_h d\phi_S d\phi_h dP_{hT}^2} = & \frac{\alpha_{em}^2}{x y Q^2} \left(1 - y + \frac{1}{2}y^2\right) \left\{ p_1 F_{UU,L} + \cos(\phi_h) p_3 F_{UU}^{\cos(\phi_h)} \right. \\ & + \lambda \sin(\phi_h) p_4 F_{LU}^{\sin(\phi_h)} + S_L \sin(\phi_h) p_3 F_{UL}^{\sin(\phi_h)} + \lambda S_L \cos(\phi_h) p_4 F_{LL}^{\cos(\phi_h)} \\ & + S_T \sin(2\phi_h - \phi_S) p_3 F_{UT}^{\sin(2\phi_h - \phi_S)} + S_T \sin(\phi_S) p_3 F_{UT}^{\sin(\phi_S)} \\ & + S_T \sin(\phi_h - \phi_S) p_1 F_{UT,L}^{\sin(\phi_h - \phi_S)} \\ & \left. + \lambda S_T \cos(\phi_S) p_4 F_{LT}^{\cos(\phi_S)} + \lambda S_T \cos(2\phi_h - \phi_S) p_4 F_{LT}^{\cos(2\phi_h - \phi_S)} \right\}, \end{aligned} \quad (10.24)$$

<sup>36</sup>The structure functions  $F_{UU,L}$  and  $F_{UT,L}^{\sin(\phi_h - \phi_S)}$  are of  $O(\Lambda^2/Q^2)$  for small transverse momenta of the final-state hadron.

## Subleading Quark TMDPDFs

		Quark Chirality	
		Chiral Even	Chiral Odd
Nucleon Polarization	U	$f^\perp, g^\perp$	$e, h$
	L	$f_L^\perp, g_L^\perp$	$e_L, h_L$
	T	$f_T, f_T^\perp, g_T, g_T^\perp$	$e_T, e_T^\perp, h_T, h_T^\perp$
	S		

Figure 10.9: Table of the subleading quark TMDPDFs for the nucleon, which are suppressed in observables by the factor  $\Lambda/Q$ . The columns indicate the quark chirality, and rows the nucleon polarization [121, 129–131].

where the kinematic prefactors  $p_i$  in Eq. (10.17) are given in Eq. (2.188). We also refer the reader to Sec. 2.11.3 for more details about the notation. In the parton-model approximation, the structure functions in Eq. (10.17) can be expressed through subleading quark TMDs, with more discussion given in the following section. The very fact that we have a considerable amount of data for the structure functions in Eq. (10.17) alone gives a strong justification to study subleading TMDs in detail.

At subleading power, a total of 16 quark TMDPDFs exists [121, 129–131], and they are listed in Fig. 10.10. These TMDPDFs are obtained by projecting the quark-quark correlator with the Dirac structures

$$\Gamma = \{1, i\gamma_5, \gamma^\alpha, \gamma^\alpha\gamma_5, i\sigma^{\alpha\beta}\gamma_5, i\sigma^{+-}\gamma_5, \} . \quad (10.25)$$

## Subleading Quark-Gluon-Quark TMDFFs

		Quark Chirality	
		Chiral Even	Chiral Odd
Unpolarized (or Spin 0) Hadrons		$\tilde{D}^\perp, \tilde{G}^\perp$	$\tilde{E}, \tilde{H}$
	L	$\tilde{D}_L^\perp, \tilde{G}_L^\perp$	$\tilde{E}_L, \tilde{H}_L$
Polarized Hadrons	T	$\tilde{D}_T, \tilde{D}_T^\perp, \tilde{G}_T, \tilde{G}_T^\perp$	$\tilde{E}_T, \tilde{E}_T^\perp, \tilde{H}_T, \tilde{H}_T^\perp$

Figure 10.10: Table for the subleading quark TMDFFs, which are suppressed in observables by the factor  $\Lambda/Q$ . The columns indicate the quark chirality, and rows the hadron polarization.

To be specific, the subleading TMDs are given by [121, 129–131]

$$f_{i/p_S}^{[1]}(x, \mathbf{k}_T, \mu, \zeta) = \frac{M}{P^+} \left[ e(x, k_T) - \frac{\epsilon_T^{\rho\sigma} k_{T\rho} S_{T\sigma}}{M} \kappa e_T^\perp(x, k_T) \right], \quad (10.26a)$$

$$f_{i/p_S}^{[\gamma_5]}(x, \mathbf{k}_T, \mu, \zeta) = \frac{M}{P^+} \left[ S_L \kappa e_L(x, k_T) - \frac{k_T \cdot S_T}{M} \kappa e_T(x, k_T) \right], \quad (10.26b)$$

$$\begin{aligned} f_{i/p_S}^{[\gamma^\alpha]}(x, \mathbf{k}_T, \mu, \zeta) = & \frac{M}{P^+} \left[ \frac{k_T^\alpha}{M} f^\perp(x, k_T) - \epsilon_T^{\alpha\rho} S_{T\rho} \kappa f_T(x, k_T) \right. \\ & \left. - S_L \frac{\epsilon_T^{\alpha\rho} k_{T\rho}}{M} \kappa f_L^\perp(x, k_T) - \frac{\mathbf{k}_T^2}{M^2} \left( \frac{1}{2} g_T^{\alpha\rho} + \frac{k_T^\alpha k_T^\rho}{\mathbf{k}_T^2} \right) \epsilon_{T\rho\sigma} S_T^\sigma \kappa f_T^\perp(x, k_T) \right], \end{aligned} \quad (10.26c)$$

$$\begin{aligned} f_{i/p_S}^{[\gamma^\alpha \gamma_5]}(x, \mathbf{k}_T, \mu, \zeta) = & \frac{M}{P^+} \left[ S_T^\alpha g_T(x, k_T) + S_L \frac{k_T^\alpha}{M} g_L^\perp(x, k_T) \right. \\ & \left. - \frac{\mathbf{k}_T^2}{M^2} \left( \frac{1}{2} g_T^{\alpha\rho} + \frac{k_T^\alpha k_T^\rho}{\mathbf{k}_T^2} \right) S_{T\rho} g_T^\perp(x, k_T) - \frac{\epsilon_T^{\alpha\rho} k_{T\rho}}{M} \kappa g^\perp(x, k_T) \right], \end{aligned} \quad (10.26d)$$

$$f_{i/p_S}^{[i \sigma^{\alpha\beta} \gamma_5]}(x, \mathbf{k}_T, \mu, \zeta) = \frac{M}{P^+} \left[ \frac{S_T^\alpha k_T^\beta - S_T^\beta k_T^\alpha}{M} h_T^\perp(x, k_T) - \epsilon_T^{\alpha\beta} \kappa h(x, k_T) \right], \quad (10.26e)$$

$$f_{i/p_S}^{[i \sigma^{+-} \gamma_5]}(x, \mathbf{k}_T, \mu, \zeta) = \frac{M}{P^+} \left[ S_L h_L(x, k_T) - \frac{k_T \cdot S_T}{M} h_T(x, k_T) \right], \quad (10.26f)$$

where for further details about the notation we refer to Sec. 2.7. Among them, 8 are chiral-even

and 8 are chiral-odd. Likewise, 8 leading quark TMDPDFs are T-even and 8 are T-odd. Note that, unlike in the case of leading TMDs, it is not possible to assign a parton polarization to subleading TMDs as they have no density interpretation. Also, the same number of subleading TMDFFs exists; see Fig. 10.11. Given that the structure of the equations which define TMDPDFs and TMDFFs is very similar — compare Eq. (2.124) and Eq. (2.135) for the leading-power functions — we don't give a set of equations for the subleading TMDFFs but just mention that their definition can be obtained from Eqs. (10.19f)–(10.19f) by replacing on the l.h.s.  $f_{i/p_s}^{[\Gamma]}(x, \mathbf{k}_T, \mu, \zeta)$  by  $\Delta_{h/i}^{[\Gamma]}(z, -zp'_T, \mu, \zeta)$ , and on the r.h.s. the target mass  $M$  by the mass of the produced hadron  $M_h$ , as well as  $k_T$  by  $p'_T$ . Furthermore, the lower case letters for the TMDPDFs become upper case letters for the TMDFFs, with the exception of the projector  $\Gamma = \gamma^\alpha$ , where the symbol  $D$  is used for the FFs (instead of  $F$ ). Recall also that the TMDFFs are functions of  $(z, zp'_T)$ , and that  $\kappa$ , the indicator of a nontrivial universality behavior, is absent for TMDFFs.

It was also found that 16 subleading gluon TMDPDFs and TMDFFs can be identified [148, 1211]. Presently, for those objects not much is known beyond their classification. Finally, for subleading TMDs in the case of spin-1 particles we refer to [1212, 1213].

### 10.8.2 Original 10.3: Observables for subleading TMDs

In this section, we intend to summarize the efforts that have been made in the literature to understand observables within the TMD formalism that require subleading TMD functions, by focusing on SIDIS where by far most of the literature is available. When the transverse hadron momentum  $P_{hT}$  of the final-state hadron is much smaller than  $Q$ , a treatment of the relevant structure functions in a TMD framework is appropriate<sup>37</sup>. For SIDIS, a concise TMD parton model treatment, that is, a leading-order pQCD analysis, has been presented already some time ago in Refs. [121, 129]. As is the case for all power-suppressed observables, the theoretical analysis, even at lowest order, is more involved compared to leading-power observables. A particular complication within a pQCD description is that different subleading effects, for both PDFs and FFs, contribute to the same power-suppressed observable; see, for instance, Ref. [167]. However, one may employ relations based on the QCD equation of motion to re-express certain classes of functions through other subleading functions.

In the following we will discuss four prominent subleading effects in SIDIS that have been measured at HERMES, COMPASS, and Jefferson Lab ([448, 457, 458, 1214–1222]; see also Ref. [1223] for a recent review: the structure functions  $F_{UU}^{\cos\phi_h}$  (Cahn effect),  $F_{LU}^{\sin\phi_h}$  (longitudinal beam spin asymmetry (BSA)),  $F_{UL}^{\sin\phi_h}$  (longitudinal target spin asymmetry) and  $F_{UT}^{\sin\phi_s}$ . According to Refs. [121, 129], those structure functions can be factorized within the subleading-power

<sup>37</sup>In a frame in which both the target particle and the final-state hadron have no transverse momentum, one requires  $q_T \ll Q$  for TMD factorization to work, where  $\mathbf{q}_T$  is the transverse momentum of the virtual photon. Since  $q_T = P_{hT}/z$ , from the point of view of power counting the conditions  $q_T \ll Q$  and  $P_{hT} \ll Q$  are equivalent. However, depending on the numerical value for  $z$ , data which satisfy  $P_{hT} \ll Q$  may not satisfy  $q_T \ll Q$  and therefore be difficult to describe in a TMD approach.

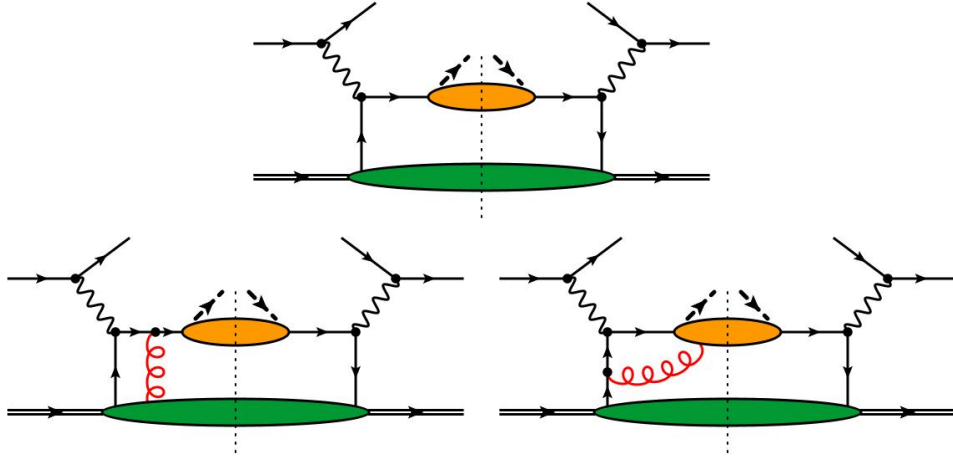


Figure 10.11: SIDIS tree-level diagrams relevant for subleading-power observables. The upper diagram entails intrinsic and kinematical contributions, the lower diagrams dynamical contributions. Also mirror diagrams are to be included.

tree-level TMD framework and acquire the form

$$F_{UU}^{\cos \phi_h} = \frac{2M}{Q} C \left[ \frac{\hat{h} \cdot p_T}{zM_h} \left( x h H_1^\perp + \frac{M_h}{M} f_1 \tilde{D}^\perp \right) - \frac{\hat{h} \cdot k_T}{M} \left( x f^\perp D_1 + \frac{M_h}{M} h_1^\perp \tilde{H} \right) \right], \quad (10.27)$$

$$F_{LU}^{\sin \phi_h} = \frac{2M}{Q} C \left[ \frac{\hat{h} \cdot p_T}{zM_h} \left( x e H_1^\perp + \frac{M_h}{M} f_1 \tilde{G}^\perp \right) + \frac{\hat{h} \cdot k_T}{M} \left( x g^\perp D_1 + \frac{M_h}{M} h_1^\perp \tilde{E} \right) \right], \quad (10.28)$$

$$F_{UL}^{\sin \phi_h} = \frac{2M}{Q} C \left[ \frac{\hat{h} \cdot p_T}{zM_h} \left( x h_L H_1^\perp + \frac{M_h}{M} g_1 \tilde{G}^\perp \right) + \frac{\hat{h} \cdot k_T}{M} \left( x f_L^\perp D_1 - \frac{M_h}{M} h_{1L}^\perp \tilde{H} \right) \right], \quad (10.29)$$

$$\begin{aligned} F_{UT}^{\sin \phi_S} = & \frac{2M}{Q} C \left[ x f_T D_1 - \frac{M_h}{M} h_1 \tilde{H} \right. \\ & \left. + \frac{\mathbf{p}_T \cdot \mathbf{k}_T}{2zMM_h} \left( x h_T H_1^\perp + \frac{M_h}{M} g_{1T}^\perp \tilde{G}^\perp - x h_T^\perp H_1^\perp + \frac{M_h}{M} f_{1T}^\perp \tilde{D}^\perp \right) \right], \end{aligned} \quad (10.30)$$

where the convolution of transverse momenta  $C$  is defined as

$$C[w f D] = x \sum_i e_i^2 \int d^2 \mathbf{k}_T d^2 \mathbf{p}_T \delta^{(2)}(z \mathbf{k}_T + \mathbf{p}_T - \mathbf{P}_{hT}) w(\mathbf{p}_T, \mathbf{k}_T) f^q(x, \mathbf{k}_T) D^q(z, z \mathbf{p}_T). \quad (10.31)$$

Note that the convolution integral in Eq. (10.24) coincides with Eq. (2.172), with  $\mathcal{H} = 1$ . The vector  $\hat{h} \equiv \mathbf{P}_{hT}/|\mathbf{P}_{hT}|$  is a unit vector in the direction of the transverse momentum of the produced hadron. In order to derive Eqs. (10.20)–(10.23), the tree-level diagrams shown in Fig. 10.12 have to be calculated; see Refs. [121, 129]. The TMD formulas in Eqs. (10.20)–(10.23) indicate that those structure functions are each generated by convolutions of subleading TMDPDFs with leading TMDFFs, and vice versa<sup>38</sup>. TMDs that appear with a tilde, such as  $\tilde{D}^\perp$ , represent matrix elements of quark-gluon-quark correlations. To be specific, we will

<sup>38</sup>This implies that the structure functions (10.20)–(10.23) may be relevant for an analysis of leading TMDs as well.

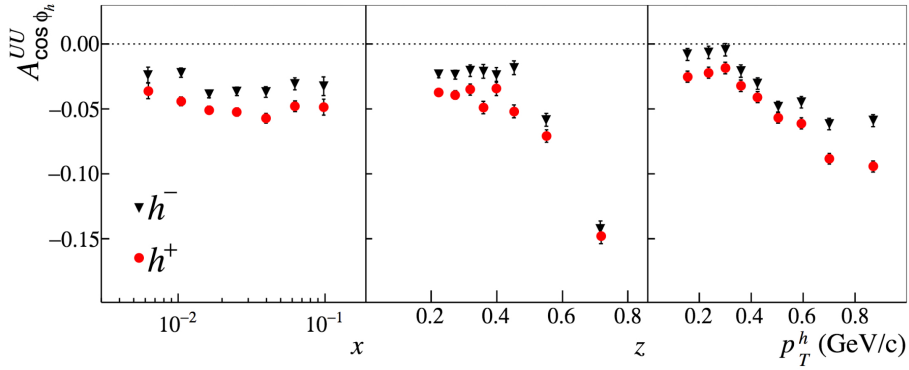


Figure 10.12: COMPASS data for the Cahn asymmetry  $A_{\cos \phi_h}^{UU}|_{\text{fig.}} \propto F_{UU}^{\cos \phi_h}/F_{UU}$  for positively and negatively charged hadrons as a function of  $x$ ,  $z$  and  $P_{hT} = p_T^h|_{\text{fig.}}$  [448].

provide a parton-model definition for tilde TMDs as in Ref. [121]. It is convenient to do so using matrix elements that involve a covariant derivative  $D^\mu = \partial^\mu - igA^\mu$ . We can define a gauge-invariant "D-type" quark-gluon-quark TMD correlator of the nucleon  $\Phi_D^\rho(x, \mathbf{k}_T)$  as well as a fragmentation correlator  $\Delta_D^\rho(z, \mathbf{p}_T)$  as follows,

$$(\Phi_D^\rho)_{ij}(x, \mathbf{k}_T) = \int \frac{db^- d^2 b_T}{(2\pi)^3} e^{ib \cdot k} \langle p(P, S) | \bar{\psi}_j(0) W_\square iD^\rho(b) \psi_i(b) | p(P, S) \rangle \Big|_{b^+=0} \quad (10.32)$$

$$\begin{aligned} (\Delta_D^\rho)_{ij}(z, \mathbf{p}_T) &= \frac{1}{2N_c z} \sum_X \int \frac{db^+ d^2 b_T}{(2\pi)^3} e^{ip \cdot b} \langle 0 | W_\perp iD^\rho(b) \psi_i(b) | h(P, S); X \rangle \\ &\quad \times \langle h(P, S); X | \bar{\psi}_j(0) W_\perp | 0 \rangle \Big|_{b^-=0}. \end{aligned} \quad (10.33)$$

The form of the Wilson line  $W_\square$  was given in Eq. (2.118) while  $W_\perp$ ,  $W_\perp$  was defined in Eq. (2.110). The definitions are similar to the ordinary TMD objects  $f_{i/p_s}^{[\Gamma]}(x, \mathbf{k}_T)$  (spin-dependent TMDPDF in Eqs. (2.122), (2.124)) and  $\Delta_{h/i}^{[\Gamma]}(z, -z\mathbf{p}'_T)$  (TMDFF in Eqs. (2.132), (2.112)), except for an additional insertion of the covariant derivative. According to Ref. [121] one can obtain a parameterization of the object  $\Phi_D^\rho - \mathbf{k}_T^\rho f_{i/p_s}$  in terms of tilde TMDPDFs,

$$\Phi_D^\rho(x, \mathbf{k}_T) - \mathbf{k}_T^\rho f_{i/p_s}(x, \mathbf{k}_T) = \frac{xM}{4} \left[ (\tilde{f}^\perp - i\tilde{g}^\perp) \frac{\mathbf{k}_{T\alpha}}{M} (g_T^{\rho\alpha} - i\epsilon_T^{\rho\alpha} \gamma_5) + \dots \right] \gamma_-^\perp. \quad (10.34)$$

The tilde functions that appear in the subleading observables Eqs. (10.20)–(10.23) are then obtained by parameterization of the combinations  $\Delta_D^\rho - \mathbf{p}_T^\rho \Delta$ ,

$$\Delta_D^\rho(z, \mathbf{p}_T) - \mathbf{p}_T^\rho \Delta(z, \mathbf{p}_T) = \frac{m_h}{4z} \left[ (\tilde{D}^\perp - i\tilde{G}^\perp) \frac{\mathbf{p}_{T\alpha}}{m_h} (g_T^{\rho\alpha} + i\epsilon_T^{\rho\alpha} \gamma_5) + (\tilde{H} + i\tilde{E}) i\gamma_T^\rho + \dots \right] \gamma_-^\perp \quad (10.35)$$

We return to those functions in the next section.

Although we use the structure functions in Eqs. (10.20)–(10.23) as benchmark observables for subleading-power TMDs, we would like to mention that there are several other observables of that kind. For example, Ref. [1224] addresses the production of polarized hadrons, e.g., lambda baryons, in SIDIS within the TMD formalism through  $\mathcal{O}(\Lambda/Q)$ . Ref. [1225] even

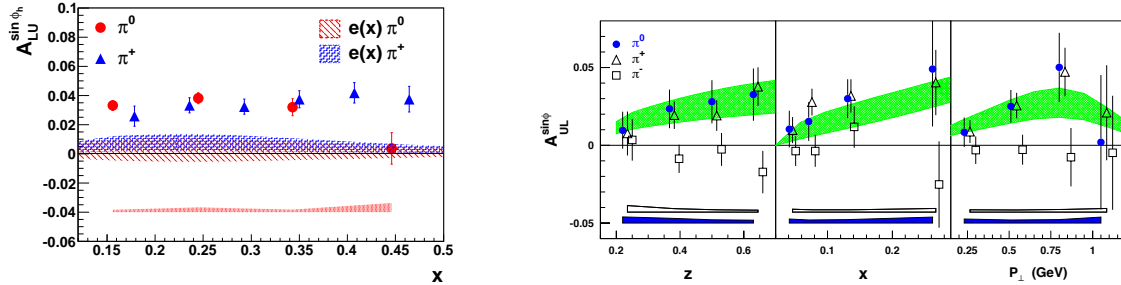


Figure 10.13: **Left:** CLAS data for the beam-spin asymmetry  $A_{LU}^{\sin \phi_h} \propto F_{LU}^{\sin(\phi_h)} / F_{UU}$  for  $\pi^0$  and  $\pi^+$  as a function of  $x$  at an average  $P_{hT} = 0.38$  GeV and for  $0.4 < z < 0.7$  [1221]. The error bars correspond to statistical uncertainties, and the red error band at the bottom of the plot corresponds to systematic uncertainties. The red and blue hatched bands show model calculations involving only the Collins effect for  $\pi^0$  and  $\pi^+$ , respectively. **Right:** HERMES data DP: HERMES now has updated measurements. **AM:** (This will be addressed) for the longitudinal target-spin asymmetry  $A_{UL}^{\sin \phi_h} \propto F_{UL}^{\sin(\phi_h)} / F_{UU}$  for pion production. Error bars include the statistical uncertainties only. The filled (blue) and open (white) bands at the bottom of the panels represent the systematic uncertainties for neutral and charged pions, respectively. The shaded (green) areas show a range of predictions of a model calculation [1227, 1228] applied to the case of  $\pi^0$  electroproduction.

discusses  $O(\Lambda^2/Q^2)$  effects in SIDIS within the TMD formalism. Observables sensitive to subleading TMDPDFs may also be found in other processes such as the Drell-Yan dilepton production [1226]. **AM:** [Include Amsterdam papers for DY and electron-positron annihilation, and perhaps others.]

Let us now elaborate a bit more on the experimental significance of power-suppressed TMD observables in SIDIS. We repeat that there has been a tremendous effort to measure the SIDIS structure functions in Eqs. (10.20)–(10.23) at HERMES, COMPASS, and JLab. For example, COMPASS data for the Cahn effect is shown in Fig. 10.13. One can see that the data is very precise, and the Cahn effect is not small at all. Similar observations can be made for CLAS measurements of the longitudinal beam spin asymmetry and HERMES measurements of the target spin asymmetry in Fig. 10.14, as well as for COMPASS measurements of the transverse spin asymmetry in Fig. 10.15. Several other measurements of power-suppressed structure functions have been reported at COMPASS, HERMES and Jlab. More details about the status of measurements for subleading-power TMD effects can also be found in a recent review [1223]. Generally, the data points for those structure functions that have been provided by the experiments are too large and too precise to simply ignore them. On the contrary, they require theoretical efforts and analyses to understand these effects, at least qualitatively. This is the main motivation for studying  $\Lambda/Q$ -suppressed observables within the TMD formalism, as this is basically the only QCD-based approach that can be applied to such observables.

As a final point in this subsection, we briefly summarize the current status of factorization for subleading TMDs. **AT:** More details here **AM:** (This paragraph needs to be reworked significantly, by paying also attention to the recent work in Ref. [1229]. Perhaps the discussion of this point in the end deserves its own subsection.) There actually exist only very few papers which address this topic by trying to go beyond the lowest order in pQCD. Early on, model calculations for the beam spin asymmetry  $F_{LU}^{\sin \phi_h}$  [1230] and a corresponding T-odd twist-3

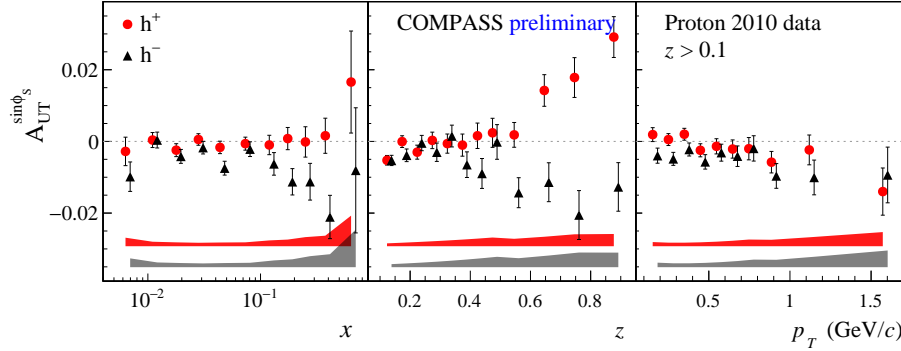


Figure 10.14: COMPASS data for the transverse target spin asymmetry  $A_{UT}^{\sin\phi_s} \propto F_{UT}^{\sin(\phi_s)} / F_{UU}$  for positively and negatively charged hadrons as a function of  $x$ ,  $z$  and  $|\mathbf{P}_{h\perp}|$  [358, 457]. Error bars indicate statistical errors, the red and green error bands at the bottom represent systematical errors, for positively and negatively charged hadrons, respectively. **DP:** HERMES now also has published data for this. **AM:** (This will be addressed.)

TMDPDF  $g^\perp$  [1231] (cf. Eq. (10.21)) indicated a problem with a light-cone divergence that wouldn't cancel in tree-level formulae. Furthermore, an issue was reported in relation to the  $\cos\phi_h$  modulation of the unpolarized SIDIS cross section [1232], namely that the result for TMD factorization in the intermediate transverse momentum region  $\Lambda_{\text{QCD}} \ll |\mathbf{P}_{h\perp}| \ll Q$  does not match with the result from collinear factorization. However, a more recent work argues that this problem can actually be overcome [1233]. A related discussion about subleading-power TMD factorization in Drell-Yan has been presented in Refs. [258, 259, 1234]. In Refs. [258, 259] the TMD factorization breaking effects were analyzed and the form of the power corrections to the TMD factorization formula (2.6) was obtained. It was found that the power corrections have a simple form and in the large- $N_c$  limit can be expressed in terms of the leading-power TMD distribution functions listed in Fig. 2.5. It was estimated that the power corrections reach a few percent of the leading-twist result at  $|\mathbf{P}_{h\perp}|/Q \sim 0.2$ .

**LG:** Very recently in a talk given by Gao [SCET 2021] a solution to the subleading-power factorization has been presented where the conjecture that the soft factor is the same as for the leading power [1233] is found to be true, and that the rapidity anomalous dimension is the same as the leading power. However the **LG:** momentum dependence of the hard factor and in the subleading-power TMDs is "non-trivial"—ask Iain about this...

**IS:** [I will help edit the above, including also the structure of Hard factors at subleading power, and will add a list of open issues and questions.]

Overall, it is very important to further explore the topic of subleading-power TMD factorization in order to get a better understanding of its status.

# 11 - Generalized TMDs and Wigner Phase Space Distributions

TMDs provide, on the one hand, the most complete description of hadronic structure as far as its dependence on quark and gluon longitudinal and transverse momentum components is concerned. On the other hand, however, a full representation of hadron dynamics is only attained by addressing, in addition to the quark and gluon 3D momentum structure, the correlation between their momenta and spatial coordinates. Through this correlation we can study rotational motion and, in particular, angular momentum as well as other mechanical properties of the proton.

The idea of a phase-space distribution for a quantum mechanical system was first introduced by Wigner [1289]. Wigner distributions based approaches were subsequently applied to a large variety of systems; in the context of nuclear physics, this includes the description of parton showers [? ] and heavy ion collisions [? ]. To study the structure of the proton an approach was developed in [1288] where it was shown that Wigner distributions can reduce to positive definite, probability density distributions in particular limits. As we explain in detail in what follows, by taking the integral of the Wigner distribution over transverse momentum, one obtains a so-called impact parameter distribution (IPD) [1284, 1285] describing the longitudinal momentum fraction  $x$  distribution of partons located at a given transverse distance from the hadron center of momentum.<sup>39</sup> Furthermore, performing a Fourier transform with respect to the transverse coordinate variable, one obtains a generalized parton distribution (GPD). GPDs bring the study of momentum-coordinate-space correlations inside the proton within experimental grasp since, as first observed by Ji [551, 1281], they are key observables parametrizing the matrix elements of deeply virtual exclusive scattering experiments. The prototype of deeply virtual exclusive scattering experiments is deeply virtual Compton scattering (DVCS), where a photon is produced in the hard scattering while the initial proton recoils intact Figure 11.1. While Ji provided a connection between angular momentum as described by the matrix elements of the QCD energy momentum tensor, and the DVCS scattering amplitude, similar formal structures initially called “non-forward distributions” were also derived in Refs. [? ? ] to describe the DVCS matrix elements. Other deeply virtual exclusive experiments include meson electroproduction and crossed channel experiments such as timelike Compton scattering.

GPDs can be viewed as hybrid objects that, on the one hand, similarly to the collinear PDFs, describe quark and gluon distributions in the longitudinal momentum fraction,  $x$ , at a given scale,  $Q^2$ . On the other hand, similarly to the nucleon elastic form factors, they give insight into the internal spatial distribution of the quark and gluon constituents through two additional kinematic variables:  $\xi$ , known as the skewness parameter, and the Mandelstam invariant  $t$ . These, respectively, describe the longitudinal and transverse components of the proton momentum transfer variable,  $\Delta = P' - P$ . GPDs parametrize the following collinear

<sup>39</sup>The “impact parameter” entering the Wigner distribution must be distinguished from the coordinate  $\mathbf{b}_T$  introduced for TMDs in this handbook. In the present treatment, we use the notation  $\mathbf{r}_T$  for the impact parameter to avoid confusion with the coordinate space quantity  $\mathbf{b}_T$  conjugate to  $\mathbf{k}_T$  used throughout.

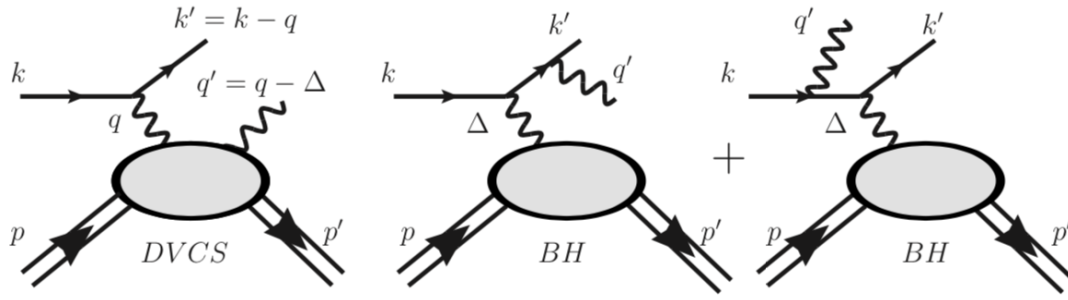


Figure 11.1: (adapted from Ref. [1283]) Exclusive electroproduction of a photon through the DVCS and Bethe-Heitler processes.

correlation function,

$$\mathcal{F}_{S',S}^{q[\Gamma]} = \frac{1}{2} \int \frac{db^-}{2\pi} e^{ix(P^+ + P'^+)b^-/2} \left\langle p(P', S') \left| \bar{\psi}_q(b^{out}) \Gamma W(b^{out}, b^{in}) \psi_q(b^{in}) \right| p(P, S) \right\rangle \Big|_{b_T=0, b^+=0}, \quad (11.1)$$

where  $\Gamma = \gamma^+, \gamma^+ \gamma_5, \dots$  and the Wilson line  $W$  takes a straight path between  $b^{in}$  and  $b^{out}$  on the light cone. For detailed reviews on GPDs and their experimental access, we refer the reader to Refs. [1282, 1286? ?, 1287].

TMDs represent another limit of the Wigner distribution obtained by integrating over the transverse coordinate,  $\mathbf{r}_T$ . TMDs and GPDs can be seen, therefore, as different “slices” of Wigner distributions, giving complementary information on the distributions of partonic transverse momentum on the one hand, and transverse spatial coordinates on the other.

Two sets of coordinate space quantities are needed to describe a phase-space distribution in QCD:  $\mathbf{r}_T = (\mathbf{b}_T^{in} + \mathbf{b}_T^{out})/2$ , which is Fourier conjugate to  $\Delta_T$ , and  $\mathbf{b}_T = \mathbf{b}_T^{in} - \mathbf{b}_T^{out}$ , which is Fourier conjugate to the transverse momentum,  $\mathbf{k}_T$ . All quantities are measured with respect to the proton center of momentum (CoM). By considering the collinear  $\mathbf{k}_T$  integrated quantity, setting  $\mathbf{b}_T = 0$  as in Eq. (11.1), one has that  $\mathbf{r}_T$  can be interpreted as the average position of the parton inside the proton with respect to the CoM. Quark and gluon spatial probability distributions in the transverse coordinate,  $\mathbf{r}_T$ ,  $f(x, \mathbf{r}_T)$ , are obtained by Fourier transformation with respect to the transverse component  $\Delta_T$ , where  $\Delta_T^2 = -t$  by setting the skewness parameter,  $\xi = 0$ . The transverse coordinate space variables for the GPD correlator are shown in Figure 11.2.

Wigner distributions encompass both types of distributions, TMDs and GPDs. In what follows, we elaborate on the complementary role of TMDs and GPDs using the concept of Wigner distributions as illustrated in the scheme in Figure 11.3.

## 11.1 Wigner Distributions

Wigner distributions were first introduced in non-relativistic quantum mechanics [1289]. For quantum particles, they are also known as quasi-distributions<sup>40</sup> since they are affected by the uncertainty principle; in general, they are not positive definite, and therefore they do

<sup>40</sup>Note this is a different concept than the quasi-distributions introduced in Chapter 6.

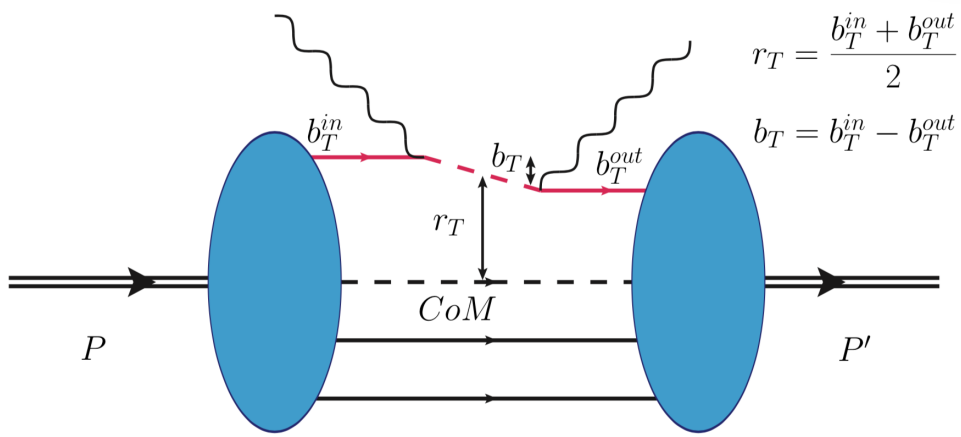


Figure 11.2: Transverse spatial coordinates entering the definition of GPDs through the correlation function in Eq. (11.1).

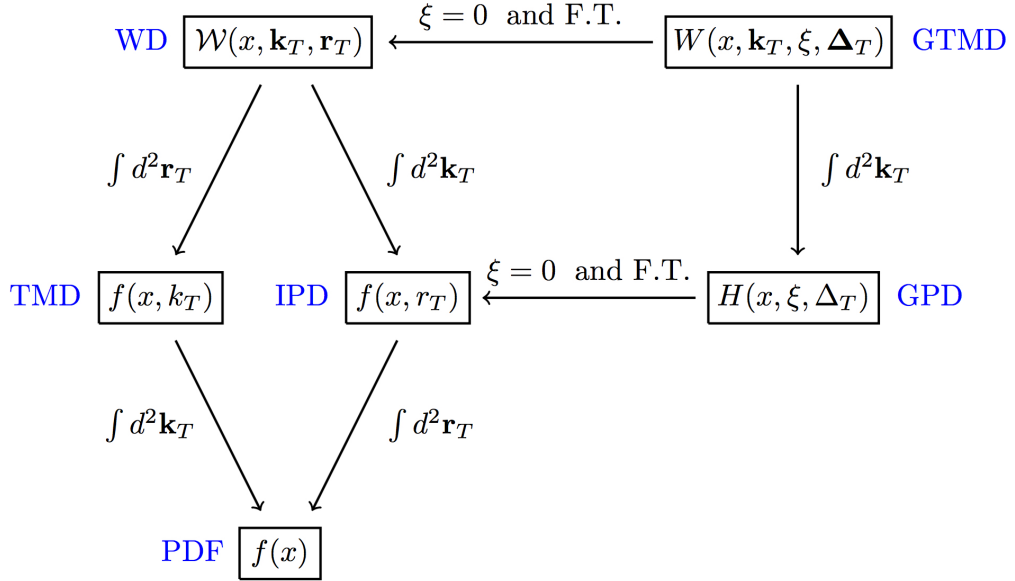


Figure 11.3: Quantities characterizing the multi-dimensional parton structure of hadrons and the relations between them. In order to arrive through a Fourier transform (F.T.) from GPDs and GTMDs, which (in principle) can be measured, at impact parameter distributions (IPDs) and Wigner distributions (WDs), respectively, an extrapolation to the kinematical point  $\xi = 0$  is needed.

not have a straightforward probability interpretation. For a 1D system, the relation between a Wigner distribution and the wave function in position space or momentum space reads [1290],

$$\mathcal{W}(x, k) = \int \frac{dx'}{2\pi} e^{ik'x'} \psi^*\left(x + \frac{x'}{2}\right) \psi\left(x - \frac{x'}{2}\right) = \int \frac{dk'}{2\pi} e^{-ik'x} \tilde{\psi}^*\left(k + \frac{k'}{2}\right) \tilde{\psi}\left(k - \frac{k'}{2}\right), \quad (11.2)$$

which readily implies that integrating the Wigner distribution  $\mathcal{W}(x, k)$  upon  $k$  gives the position space density  $|\psi(x)|^2$ , while integrating upon  $x$  gives the momentum space density  $|\tilde{\psi}(k)|^2$ . The calculation of the expectation value of an observable  $O$  is very appealing in the Wigner distribution framework. In particular,

$$\langle O \rangle = \int dx dk O(x, k) \mathcal{W}(x, k), \quad (11.3)$$

which is identical to the calculation of an expectation value using a classical phase space distribution. In other areas of physics, such as quantum optics, Wigner distributions have been frequently used. They can give deeper insights into the relation between quantum mechanics and classical mechanics. The generalization from 1D to 3D is straightforward in non-relativistic quantum mechanics and leads to 6D Wigner distributions.

Partonic Wigner distributions can be defined in quantum field theory in terms of correlation functions in analogy to Eq. (11.2). To this end, we consider the Wigner operator [554, 1288, 1291]

$$\widehat{\mathcal{W}}^{q[\Gamma]W}(x, \mathbf{k}_T, \mathbf{r}_T) = \int \frac{db^- d^2\mathbf{b}_T}{2(2\pi)^3} e^{-ik \cdot b} \bar{\psi}_q\left(\mathbf{r}_T + \frac{b}{2}\right) \Gamma W_{\exists\eta}^v\left(\mathbf{r}_T + \frac{b}{2}, \mathbf{r}_T - \frac{b}{2}\right) \psi_q\left(\mathbf{r}_T - \frac{b}{2}\right) \Big|_{b^+=0}, \quad (11.4)$$

where the analogy to Eq. (11.2) is obvious. This operator depends on the longitudinal and transverse parton momenta, the transverse parton position  $\mathbf{r}_T$  (impact parameter), the Dirac structure  $\Gamma$ , and on the path of the Wilson line, denoted by the superscript  $W$  on the left-hand side of Eq. (11.4). Note that, in the description of the Wilson line, the flexible notation of Eq. (2.163) is adopted, which includes the option of choosing a straight path between the quark operators, by setting  $\eta = 0$ . The reason is that, in the context of Wigner distributions and GTMDs, both staple-shaped and straight Wilson line paths constitute physically interesting cases, as will be discussed further in Sec. 11.4 in the context of quark Orbital Angular Momentum (OAM).

We limit our description to 2D spatial Wigner distributions which can be unambiguously extracted from experiment through Fourier transformation in the transverse momentum transfer  $\Delta_T$ . It is well known that a full 3D spatial description is hampered by relativistic proton recoil effects [? ?], while these effects are mitigated in a heavy nucleus. Whether it is possible to define meaningful 6D Wigner distributions for partons has generated an intense debate with various approaches addressing this problem [554, 1288].

The Wigner operator in Eq. (11.4) can now be used to define the correlator for 5D Wigner distributions of quarks [554, 1288, 1291],

$$\mathcal{W}_{S',S}^{q[\Gamma]W}(x, \mathbf{k}_T, \mathbf{r}_T) = \int \frac{d^2\Delta_T}{(2\pi)^2} \left\langle p(P', S') \left| \widehat{\mathcal{W}}^{q[\Gamma]W}(x, \mathbf{k}_T, \mathbf{r}_T) \right| p(P, S) \right\rangle \quad (11.5)$$

where  $S'$ ,  $S$  denote the spins of the external states, the average proton momentum  $\bar{P} = (P' + P)/2$  defines the longitudinal direction, and the momentum transfer is purely transverse,  $P' = \bar{P} + \Delta_T/2$ ,  $P = \bar{P} - \Delta_T/2$ .

The full 5D information contained in the Wigner distribution can be reduced in several

ways by integrating out some of the variables. In particular, one can extract

$$\mathcal{F}_{S',S}^{q[\Gamma]}(x, \mathbf{r}_T) = \int d^2\mathbf{k}_T \mathcal{W}_{S',S}^{q[\Gamma]W}(x, \mathbf{k}_T, \mathbf{r}_T), \quad (11.6)$$

$$\Phi_{S',S}^{q[\Gamma]W}(x, \mathbf{k}_T) = \int d^2\mathbf{r}_T \mathcal{W}_{S',S}^{q[\Gamma]W}(x, \mathbf{k}_T, \mathbf{r}_T), \quad (11.7)$$

$$\langle O \rangle_{S',S}^{[\Gamma]W} = \int dx d^2\mathbf{k}_T d^2\mathbf{r}_T O(x, \mathbf{k}_T, \mathbf{r}_T) \mathcal{W}_{S',S}^{q[\Gamma]W}(x, \mathbf{k}_T, \mathbf{r}_T), \quad (11.8)$$

where  $\mathcal{F}_{S',S}^{q[\Gamma]}(x, \mathbf{r}_T)$  is the density of quarks in longitudinal momentum and transverse position space, while  $\Phi_{S',S}^{q[\Gamma]W}(x, \mathbf{k}_T)$  is the density in momentum space. The quantity  $\mathcal{F}_{S',S}^{q[\Gamma]}(x, \mathbf{r}_T)$  is what defines the so-called impact parameter distributions  $f_{S',S}(x, \mathbf{r}_T)$ , cf. [1284], which are related to GPDs, taken at  $\xi = 0$ , through a Fourier transform [1285]. Note that, upon taking the  $\mathbf{k}_T$  integral in Eq. (11.6), the dependence on the path of the Wilson line disappears. We also point out that, strictly speaking, in this relation the same complications can arise that one has when integrating TMDs in order to get to PDFs. In particular, these relations are true at a bare level and must be reconsidered after renormalization has been carried out, cf. the detailed discussion of the relation between TMDs and PDFs given in Sec. 2.9. Note the very close analogy of Eqs. (11.6)-(11.8) with the situation in non-relativistic quantum mechanics. In Sec. 11.4, we return to Eq. (11.8) in the context of partonic orbital angular momentum and spin-orbit correlations.

The range of physical information contained in the full set of leading-twist nucleon Wigner distributions, including, in particular, the dependence on the nucleon spins  $S'$ ,  $S$  and the quark polarization encoded in the  $\Gamma$  structure, has been further elucidated in Ref. [1292]. By decomposing these Wigner distributions into multipoles in the transverse phase space, correlations between target polarization, quark polarization and quark orbital angular momentum can be isolated and exhibited, and the structure of the different components visualized.

## 11.2 Momentum Space Definition – Generalized TMDs (GTMDs)

Similar to the relationship between impact parameter distributions and GPDs already mentioned above, the full Wigner distributions defined in Eq. (11.5) can be connected to distributions that depend on transverse momentum transfer,  $\Delta_T$ , through Fourier transformation,

$$\mathbb{W}_{S',S}^{q[\Gamma]W}(\bar{P}, \Delta, x, \mathbf{k}_T) \Big|_{\xi=0} = \int \frac{d^2\Delta_T}{(2\pi)^2} e^{i\Delta_T \cdot \mathbf{r}_T} \mathcal{W}_{S',S}^{q[\Gamma]W}(x, \mathbf{k}_T, \mathbf{r}_T). \quad (11.9)$$

Note that in Eq. (11.9) the Wigner operator is evaluated between states which have the same plus-momentum, that is, for  $\xi = 0$ . On the other hand, the correlator on the left-hand side,  $\mathbb{W}_{S',S}^{q[\Gamma]W}$ , can be defined for general momentum transfer  $\Delta = P' - P$ , including a longitudinal component, cf. Eq. (11.10) below; only its  $\xi = 0$  limit enters the relation (11.9). Also the dependence on the average hadron momentum  $\bar{P} = (P' + P)/2$  has been made explicit on the left-hand side.

The correlator  $\mathbb{W}_{S',S}^{q[\Gamma]W}$  serves to define generalized TMDs (GTMDs) [707, 785], which can be considered a natural extension of the concept of TMDs. As will be discussed below, GTMDs are important for the definition of Orbital Angular Momentum (OAM) carried by partons.

Although no measurements related to these quantities have been performed to date, Sec. 11.3 highlights initial progress towards identifying scattering processes from which GTMDs can be extracted.

For a spin- $\frac{1}{2}$ -target, the GTMD correlator in the quark sector in a helicity basis, i.e., in terms of longitudinal spin components  $S'_L, S_L$  can be written as [707], cf. Eqs. (11.4) and (11.5),

$$\mathbb{W}_{S'_L, S_L}^{q[\Gamma]W}(\bar{P}, \Delta, x, \mathbf{k}_T) = \int \frac{db^- d^2\mathbf{b}_T}{2(2\pi)^3} e^{-ik \cdot b} \langle p(P', S'_L) | \bar{\psi}_q(\frac{b}{2}) \Gamma W_{\square\eta}^v(\frac{b}{2}, -\frac{b}{2}) \psi_q(-\frac{b}{2}) | p(P, S_L) \rangle \Big|_{b^+=0} \quad (11.10)$$

with  $q$  indicating the quark flavor,  $\Gamma$  a generic gamma matrix, and the superscript  $W$  the dependence on the choice of the Wilson line  $W_{\square\eta}^v(b/2, -b/2)$ . Similar to the definition of GPDs, the matrix element is taken between states with, in general, different four-momenta and spins. The correlator in Eq. (11.10) can be parametrized in terms of Dirac bilinears multiplied by GTMDs, where at leading power ( $\Gamma = \gamma^+, \gamma^+ \gamma_5, i\sigma^{i+} \gamma_5, i=1,2$ ) a total of 16 quark GTMDs exist for a spin- $\frac{1}{2}$  hadron [707, 1211]. As examples, we list the expressions for the vector and the axial-vector operators [707],<sup>41</sup>

$$\mathbb{W}_{S'_L, S_L}^{q[\gamma^+]W} = \frac{1}{2M} \bar{u}(P', S'_L) \left[ F_{1,1}^{qW} + \frac{i\sigma^{i+} k_T^i}{P^+} F_{1,2}^{qW} + \frac{i\sigma^{i+} \Delta_T^i}{P^+} F_{1,3}^{qW} + \frac{i\sigma^{ij} k_T^i \Delta_T^j}{M^2} F_{1,4}^{qW} \right] u(P, S_L), \quad (11.11)$$

$$\mathbb{W}_{S'_L, S_L}^{q[\gamma^+ \gamma_5]W} = \frac{1}{2M} \bar{u}(P', S'_L) \left[ -\frac{i\varepsilon^{ij} k_T^i \Delta_T^j}{M^2} G_{1,1}^{qW} + \frac{i\sigma^{i+} \gamma_5 k_T^i}{P^+} G_{1,2}^{qW} + \frac{i\sigma^{i+} \gamma_5 \Delta_T^i}{P^+} G_{1,3}^{qW} + i\sigma^{+-} \gamma_5 G_{1,4}^{qW} \right] u(P, S_L), \quad (11.12)$$

where the indices  $i, j = 1, 2$  represent transverse components;  $F_{1,1}^{qW}, F_{1,2}^{qW}, F_{1,3}^{qW}, F_{1,4}^{qW}$  and  $G_{1,1}^{qW}, G_{1,2}^{qW}, G_{1,3}^{qW}, G_{1,4}^{qW}$  are the quark GTMDs. A generic GTMD  $X(x, \mathbf{k}_T, \xi, \Delta_T)$  depends on the (average) longitudinal ( $x$ ) and transverse ( $\mathbf{k}_T$ ) parton momentum, as well as the longitudinal ( $\xi$ ) and transverse ( $\Delta_T$ ) momentum transfer to the target. We point out that, in general, GTMDs are complex functions, where the real part is invariant ( $T$ -even) under reversal of the staple direction,  $\eta \rightarrow -\eta$ , whereas the imaginary part is  $T$ -odd, i.e., changes sign under reversal of the staple direction, cf. also the corresponding discussion of  $T$ -even vs.  $T$ -odd TMDs in Sec. 2.7. In Ref. [707], the real and imaginary parts of the GTMD  $X$  are correspondingly denoted as  $X = X^e + iX^o$ . For a straight gauge link,  $\eta = 0$ , the imaginary parts of the GTMDs vanish. For gluons, 16 leading-power GTMDs also exist [1211]. Furthermore, the subleading quark and gluon GTMDs have been classified as well [707, 1211].

As in the case of TMDs, the subtraction of a soft factor is required in Eq. (11.10) for a proper definition of GTMDs, in extension of the detailed discussion in Ch. 2. In Ref. [1293], it was shown that the soft factor used for TMDs is also appropriate for GTMDs for  $\xi = 0$ , while the case of nonzero  $\xi$  still needs to be explored. Note also that, for brevity, we omitted two auxiliary scales in Eq. (11.10) that are needed in QCD. Studies of the scale dependence of GTMDs can be found in Refs. [1293, 1294].

<sup>41</sup>For ease of notation, in Eqs. (11.11), (11.12) we suppress the arguments of the GTMD correlators and the GTMDs.

The reductions of Wigner distributions exhibited in Eqs. (11.6) and (11.7) have counterparts in momentum space, as a result of which all GPDs and TMDs are projections of certain GTMDs. Therefore, GTMDs, and Wigner distributions, can be considered partonic “mother functions”, where it should be emphasized that only the GTMDs include a dependence on the skewness  $\xi$  and therefore generate the full GPDs upon integrating out transverse momenta; by contrast, the Wigner distributions, because of their restriction to the 2D transverse spatial plane, only generate the GPDs evaluated specifically at  $\xi = 0$ .

On the other hand, it should also be noted that various GTMDs (or Wigner distributions) disappear due to symmetry constraints when taking the GPD limit or the TMD limit of the respective correlator [707, 785, 1211]. One important example is the GTMD  $F_{1,4}^{qW}$ , which is closely related to the orbital angular momentum of partons, as will be discussed further in Sec. 11.4. Therefore, GTMDs (or Wigner distributions) contain considerably more information than their GPD and TMD projections alone. They provide 6D (or 5D) images of hadrons, even though such images have to be interpreted with some care; see Sec. 11.6 below. The relationship between the various quantities characterizing the (multi-dimensional) parton structure of hadrons is displayed in Fig. 11.3.

The fact that all GPDs and TMDs are kinematical projections of GTMDs was used in Refs. [707, 785] to explore possible nontrivial relations between TMDs and GPDs that can be seen to hold in semi-classical approaches [788] and in certain spectator model calculations [149, 710, 777]. The relation between the quark Sivers function  $f_{1T}^{\perp q}$  and the GPD  $E^q$  is the best known example of such a connection [788], cf. the discussion in Sec. 7.5.4. Several additional nontrivial relations can be identified as well [149]. However, since the involved TMDs and GPDs appear as projections of different GTMDs, none of those relations is model-independent [707, 785]. Indeed, these relations typically break down in more sophisticated model calculations [149, 793]. On the other hand, such relations reveal some general qualitative features of certain TMDs and GPDs, and of observables in which those functions appear [788].

### 11.3 Observables for GTMDs

After the first discussion of partonic Wigner distributions appeared in Refs. [1288, 1291], it took more than a decade until a scattering process was identified in which GTMDs could be measured directly [1295]; see also Ref. [1296]. Specifically, in Ref. [1295] it was shown that gluon GTMDs at small  $x$  can be accessed through hard exclusive diffractive di-jet production in DIS, a reaction which in the future should be measurable at the EIC. That work on observables for GTMDs was followed by several related studies [956, 963, 993, 1297–1301, 1303? , 1304], all of which deal with gluon GTMDs, and all but one [1298] focus on the small- $x$  region. In the following we provide some details of the analysis presented in Ref. [1295] and briefly summarize what is presently known about observables for quark GTMDs.

To begin with, we note that in analogy to the quark Wigner distributions defined above, the gluon Wigner distributions are defined through the matrix element

$$\begin{aligned} x\mathcal{W}^g(x, \mathbf{k}_T; \mathbf{r}_T) &= \int \frac{db^- d^2\mathbf{b}_T}{(2\pi)^3 P^+} \int \frac{d^2\Delta_T}{(2\pi)^2} e^{-ixP^+ b^- - i\mathbf{k}_T \cdot \mathbf{b}_T} \left\langle p(P') \middle| G^{+i} \left( \mathbf{r}_T + \frac{b}{2} \right) \right. \\ &\quad \times W_{\square} \left( \mathbf{r}_T + \frac{b}{2}, \mathbf{r}_T - \frac{b}{2} \right) G^{+i} \left( \mathbf{r}_T - \frac{b}{2} \right) W_{\square}^\dagger \left( \mathbf{r}_T + \frac{b}{2}, \mathbf{r}_T - \frac{b}{2} \right) \left. \middle| p(P) \right\rangle_{b^+=0}, \end{aligned} \quad (11.13)$$

where, as previously,  $P' = \bar{P} + \Delta_T/2$ ,  $P = \bar{P} - \Delta_T/2$ . Here we consider unpolarized gluons and no target polarization.  $G^{\mu\nu}$  represents the gluon field strength tensor,  $x$  and  $\mathbf{k}_T$  the (average) longitudinal momentum fraction and the transverse momentum for the gluon, respectively, and  $\mathbf{r}_T$  the coordinate space variable (gluon impact parameter). As in the case of quarks discussed above, the Fourier transforms of gluon Wigner distributions w.r.t.  $\mathbf{r}_T$  are GTMDs for gluons [707, 1211], where in Eq. (11.13) the gauge links associated with the gluon fields are such that one obtains the dipole gluon GTMD (see Ch. 8 for more discussion) that is needed for the present purposes.

The dipole gluon GTMD correlator takes the form

$$\begin{aligned} xG_{dip.}(x, \mathbf{k}_T, \Delta_T) &= 2 \int \frac{db^- d^2\mathbf{b}_T}{(2\pi)^3 P^+} e^{-ixP^+ b^- - i\mathbf{k}_T \cdot \mathbf{b}_T} \\ &\quad \times \langle p(P') | \text{Tr} [G^{+i}(b/2) W_{\square}(b/2, -b/2) G^{+i}(-b/2) W_{\square}^\dagger(b/2, -b/2)] | p(P) \rangle, \end{aligned} \quad (11.14)$$

which, following the derivations in Ch. 8, in the small- $x$  region reduces to

$$\begin{aligned} xG_{dip.}(x, \mathbf{k}_T, \Delta_T) &= \frac{2N_c}{\alpha_s} \int \frac{d^2\mathbf{R}_T d^2\mathbf{R}'_T}{(2\pi)^4} e^{i\mathbf{k}_T \cdot (\mathbf{R}_T - \mathbf{R}'_T) + i\frac{\Delta_T}{2} \cdot (\mathbf{R}_T + \mathbf{R}'_T)} \\ &\quad \times (\nabla_{\mathbf{R}_T} \cdot \nabla_{\mathbf{R}'_T}) \frac{1}{N_c} \langle \text{Tr} [U(\mathbf{R}_T) U^\dagger(\mathbf{R}'_T)] \rangle_x. \end{aligned} \quad (11.15)$$

In Eq. (11.15) we have used the Wilson line  $U(\mathbf{R}_T) = W_n(\mathbf{R}_T, -\infty, +\infty)$ , while the subscript  $x$  indicates the momentum fraction of the gluon at which the matrix element is evaluated. (For more information about the averaging procedure in the small- $x$  CGC formalism, indicated by  $\langle \dots \rangle_x$ , we refer to the paragraph after Eq. (8.7).) The last factor in Eq. (11.15) is the well-known impact-parameter-dependent dipole amplitude. Defining its double Fourier transform through

$$\frac{1}{N_c} \text{Tr} \left[ U \left( \mathbf{r}_T + \frac{\mathbf{b}_T}{2} \right) U^\dagger \left( \mathbf{r}_T - \frac{\mathbf{b}_T}{2} \right) \right] \equiv \int d^2\mathbf{k}_T d^2\Delta_T e^{-i\mathbf{k}_T \cdot \mathbf{b}_T - i\Delta_T \cdot \mathbf{r}_T} \mathcal{F}_x(\mathbf{k}_T, \Delta_T), \quad (11.16)$$

allows us to write

$$xG_{dip.}(x, \mathbf{k}_T, \Delta_T) = (\mathbf{k}_T^2 - \Delta_T^2/4) \frac{2N_c}{\alpha_s} \mathcal{F}_x(\mathbf{k}_T, \Delta_T). \quad (11.17)$$

It is  $\mathcal{F}_x(\mathbf{k}_T, \Delta_T)$  which shows up in the cross section for diffractive di-jet production in electron-ion collisions. Such processes probe the dipole gluon GTMD in the small- $x$  limit where the quark contribution is negligible [1295]. For the calculation of the cross section, one requires that the final-state quark-antiquark pair (see Fig. 11.4 (left)) forms a color singlet state, leading to

$$\begin{aligned} \frac{d\sigma^{\gamma_T^* A \rightarrow q\bar{q} X}}{dy_1 d^2\mathbf{q}_{1T} dy_2 d^2\mathbf{q}_{2T}} &= 2N_c \alpha_{em} e_q^2 \delta(x_{\gamma^*} - 1) z(1-z)[z^2 + (1-z)^2] \\ &\quad \times \int d^2\mathbf{k}_T d^2\mathbf{k}'_T \mathcal{F}_x(\mathbf{k}_T, \Delta_T) \mathcal{F}_x(\mathbf{k}'_T, \Delta_T) \\ &\quad \times \left[ \frac{\mathbf{P}_T}{\mathbf{P}_T^2 + \epsilon_f^2} - \frac{\mathbf{P}_T - \mathbf{k}_T}{(\mathbf{P}_T - \mathbf{k}_T)^2 + \epsilon_f^2} \right] \cdot \left[ \frac{\mathbf{P}_T}{\mathbf{P}_T^2 + \epsilon_f^2} - \frac{\mathbf{P}_T - \mathbf{k}'_T}{(\mathbf{P}_T - \mathbf{k}'_T)^2 + \epsilon_f^2} \right], \end{aligned} \quad (11.18)$$

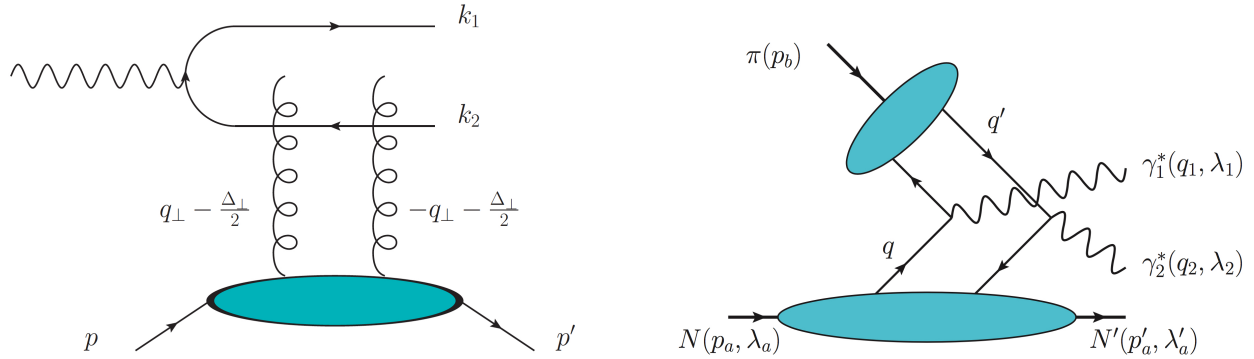


Figure 11.4: Processes that can provide information on GTMDs. Left: Sketch of exclusive diffractive di-jet production which is sensitive to gluon GTMDs; figure from Ref. [1295]. (The conventions for the momenta in the figure differ from the text. In particular, the 4-momenta of the produced quark and antiquark are  $q_1 = k_1|_{\text{fig.}}$  and  $q_2 = k_2|_{\text{fig.}}$ , respectively. Moreover, the average transverse gluon momentum is  $\mathbf{k}_T = \mathbf{q}_{\perp}|_{\text{fig.}}$ .) Right: One of two lowest-order diagrams for the exclusive pion-nucleon double Drell-Yan process which is sensitive to quark GTMDs; figure from Ref. [1302].

for transversely polarized photons, where  $A$  indicates the target which can be a proton or any nucleus. In Eq. (11.18),  $x_{\gamma^*} = z_q + z_{\bar{q}}$  with  $z_q = z$  and  $z_{\bar{q}} = 1 - z$  the momentum fractions of the virtual photon carried by the quark and antiquark, respectively. Furthermore,  $y_{1,2}$  and  $\mathbf{q}_{1,2T}$  are the rapidities and transverse momenta of the quark and antiquark jets, respectively, defined in the center of mass frame of the incoming photon and target, whereas  $\mathbf{P}_T \equiv \frac{1}{2}(\mathbf{q}_{2T} - \mathbf{q}_{1T})$  represents the typical di-jet transverse momentum, and  $e_f^2 \equiv z(1 - z)Q^2$ . We are interested in the back-to-back kinematic region for the two jets where  $|\mathbf{P}_T| \gg |\mathbf{q}_{1T} + \mathbf{q}_{2T}|$ . Suppose that  $e_f^2$  is not too large as compared to  $\mathbf{P}_T^2$ , then we expect that the  $\mathbf{k}_T$  integrals in Eq. (11.18) are dominated by the region  $\mathbf{k}_T \sim \mathbf{P}_T$  and the cross section is roughly proportional to  $\mathcal{F}_x^2(\mathbf{P}_T, \Delta_T)$ . Thus, the diffractive di-jet production will be sensitive to the correlations between  $\mathbf{P}_T$  and  $\Delta_T$ . Of particular interest is the angular correlation of the form  $\cos 2(\phi_{\mathbf{P}_T} - \phi_{\Delta_T})$ , which originates from the  $\cos 2\phi$  correlation in the GTMD and the Wigner distribution. With the detector capability at the EIC [15, 513], we will be able to identify both  $\mathbf{P}_T$  and  $\Delta_T$  and measure the angular correlation between them.

Later on, the same process was considered in the small- $x$  region for a (longitudinally) polarized nucleon [963] — see also the recent update discussed in Ref. [? ]. The specific interest of that work was the gluon GTMD  $F_{1,4}^g$ , which is directly related to the orbital angular momentum of gluons, as discussed in detail in the following section. Interestingly, in Ref. [1298] it was argued that di-jet production could even be used to address  $F_{1,4}^g$  and, therefore, the gluon orbital angular momentum at moderate  $x$ .

In Refs. [956, 1304], the small- $x$  JIMWLK evolution effects for the dipole scattering amplitude and the associated diffractive di-jet production have been investigated. It was found that the elliptic angular correlation is sensitive to the small- $x$  evolution effects. This leads to an interesting probe for the small- $x$  physics at the future EIC.

In a very interesting recent work, a small- $x$  model for gluon GTMDs was fitted to HERA data on diffractive di-jet production in electron-proton collisions [? ]. The data were described well with a small number of fit parameters, and predictions were made for both photo-production

and electro-production at the EIC.

GTMDs for gluons can also play an important role in exclusive  $\pi^0$  production at high energies [993]. It was shown that this process is related to a particular gluon GTMD, which in the forward limit reduces to the gluon Sivers function  $f_{1T}^{\perp g}$ . In turn, at small  $x$ , the latter is intimately related to the QCD odderon [989].

Let us finally discuss potential observables for quark GTMDs. Presently, the only known process that is sensitive to quark GTMDs is the exclusive pion-nucleon double Drell-Yan reaction,  $\pi N \rightarrow (\ell_1^- \ell_1^+) (\ell_2^- \ell_2^+) N'$  [1302]; see Fig. 11.4 (right). (Note that for the exclusive nucleon-nucleon double Drell-Yan process, spectator-spectator interactions enter which pose a challenge for factorization.) At leading order, the process would allow one to probe the Efremov-Radyushkin-Brodsky-Lepage region [1305, 1306] of GTMDs which is characterized by  $-\xi < x < \xi$ , while the DGLAP region ( $x \leq -\xi$  or  $x \geq \xi$ ) is not accessible [1302]. Through the double Drell-Yan process, in principle, all leading-power quark GTMDs could be addressed by making use of suitable polarization observables [1302]. However, the count rate for this reaction is very small since the cross section is proportional to  $\alpha_{\text{em}}^4$ . Furthermore, higher-order corrections for this process need to be computed for a thorough test of factorization. Closely related work [1307, 1308] deals with addressing gluon GTMDs through double production of charge-parity even quarkonia such as the  $\eta_c$  and  $\eta_b$ . While those reactions have sufficiently large count rates and may allow study of gluon GTMDs at moderate  $x$  [1307], detecting charge-parity even quarkonia is very challenging.

## 11.4 Connection with Orbital Angular Momentum of Partons

As introduced in Sec. 6.2.2, the proton's total momentum and angular momentum are encoded in the matrix elements of the QCD energy momentum tensor (EMT) between proton helicity states. The latter are parametrized in terms of form factors which are functions of the four-momentum transfer squared,  $t = \Delta^2 = (P' - P)^2$ , between the initial,  $P$ , and final,  $P'$ , proton momenta [551]. In 1996 Ji [551] made the key observation that the form factors of the EMT can be accessed experimentally since they coincide, through the operator product expansion (OPE), with the expressions for the second Mellin moments of GPDs. This led to the definition of the Ji sum rule describing the proton angular momentum in terms of parton distributions, already introduced in Sec. 6.2.2,

$$J_q + J_g = \frac{1}{2} \sum_{i=q,g} (A_i + B_i) = \frac{1}{2} \sum_{i=q,g} \int dx x (H_i(x, 0, 0) + E_i(x, 0, 0)) = \frac{1}{2} \quad (11.19)$$

where  $H_{q,g}$  and  $E_{q,g}$  are GPDs corresponding to different quark/gluon-proton helicity configurations. Remarkably, the first moment of  $H + E$  is given by the magnetic form factor,  $G_M = F_1 + F_2$ , thus uncovering an interesting connection between partonic angular momentum and the magnetization density of the nucleon. Moreover,  $F_1$  and  $F_2$  are comparatively well-determined from experiment, which can be useful in constraining phenomenological models for  $H$  and  $E$ . A similar relation is found for partonic angular momentum in a spin one target, *e.g.*, the deuteron [? ].

Differently from the parton momentum sum rule that has an immediate dynamical interpretation in terms of the average longitudinal momentum carried by the quark and gluon components, the analysis of angular momentum requires, on one side, to identify the respec-

tive operators for spin and orbital angular momentum (OAM), and on the other, to give a physical interpretation of the components of the sum rule while simultaneously preserving the gauge invariance of the theory.

We recall, in what follows, the two main frameworks which have been adopted for the decomposition of the total quark and gluon angular momenta,  $J^q$ , and  $J^g$ , into their respective spin and orbital components (a discussion related to the evaluation of these terms in lattice QCD was already given in Sec.6). In the quark sector the focus of most studies and measurements has been on the longitudinal/helicity components, where both the spin and the longitudinal partonic OAM can be obtained directly from the quark-quark correlation function [554], by evaluating the moments in both  $x$  and transverse momentum,  $k_T$ , of the generalized transverse momentum-dependent parton distribution (GTMD)  $F_{14}$  [707]. Transverse angular momentum is more subtle. First of all, transverse boosts become dynamical and the definition of OAM depends specifically on the point about which it is evaluated. Secondly, transverse spin is represented by a twist three structure function,  $g_T$ , with a non-trivial  $qgq$  structure (Section 7). For these reasons, transverse angular momentum is still an intensely debated subject at present. For ongoing studies and literature on the subject we refer the reader to [559, 560, 700, 1315, 1321] and references therein.

Restricting our discussion to the longitudinal sector, we see that on one side, the Ji decomposition reads[551],

$$\frac{1}{2}\Delta\Sigma + L_z^{q(Ji)} + J_g = \frac{1}{2}, \quad (11.20)$$

while, on the other, the Jaffe and Manohar (JM) decomposition [553] is,

$$\frac{1}{2} = \frac{1}{2}\Delta\Sigma + L_z^{q(JM)} + \Delta G + L_g^{JM}. \quad (11.21)$$

In Ji's picture a fully gauge invariant decomposition is sought thus yielding the result that, while  $J_q$  can be decomposed into spin and OAM, a further decomposition of the gluon part into its orbital and spin components can not be obtained while satisfying the gauge invariance principle [? ]. On the other side, the JM decomposition follows a parton model picture where, in the light-cone gauge,  $A^+ = 0$ , for  $P^+ \rightarrow \infty$ , gluon helicity,  $\Delta G$ , can be defined unambiguously, and it can be, therefore, measured experimentally. It should be stressed that the decompositions are at variance with one another in all terms, except for the quark spin term,  $\Delta\Sigma$ .

Various other pictures have been given in the literature that can be seen as variations of the two main frameworks represented by Eqs.(11.20) and (11.21). In Ref.[1309], for instance,  $L_q^{Ji}$  is further decomposed into a potential term attributed to gluon angular momentum. On the other side, in Ref.[? ], a gauge invariant extension of Eq.(11.21) was proposed that led to several further developments. For reviews of the various decompositions we refer the reader to Refs.[558? ? ].

Presently, proton angular momentum including its theoretical investigation and measurability are intensely investigated subjects. A more thorough understanding of the quark component,  $L_q$ , was obtained in recent years through the study of the spatial and momentum correlations provided by Wigner distributions which play a fundamental role in the quest for understanding OAM.

In Ref.[1288] it was observed that the correlation between coordinate space and momentum components describing OAM can be written in terms of Wigner distributions. In Refs. [554, 1310] it was subsequently observed that the specific GTMDs obtained by Fourier transforming the quantities defined in [1288] could be identified with the functions given in the general parametrization of correlation functions given in Ref.[707]. The derivation in [554, 1310] was limited to the longitudinal component of OAM,  $L_z$ , in the quark sector which is more straightforward since the angular momentum components lie on the transverse plane with respect to the proton momentum. As shown in [1284], the transverse plane thus defined is invariant under longitudinal boosts. The significance of this observation is that transformations in the transverse plane can be effectively described by the Galilean group in 2D. The decomposition of the transverse component of angular momentum,  $J_T$  into its orbital and spin components can also be evaluated as we explain in what follows, although with a more complicated structure since components off the transverse plane are involved in this case.

It should be stressed that, in order to validate the QCD description of angular momentum decomposition in the quark sector described in this handbook, one needs three separate evaluations and/or experimental observations for  $J_q$ ,  $L_q$  and  $S_q$ , respectively. While Section 6 was dedicated to the evaluation of  $J_{q(g)}$  and spin (check notation) in various lattice QCD approaches, from which the orbital component,  $L_q$  was obtained by subtraction, here we address an independent evaluation of this quantity.

The longitudinal OAM distribution in the quark sector is identified with a Wigner distribution weighted by the cross product of position and momentum in the transverse plane,  $\mathbf{r}_T \times \mathbf{k}_T$  [554, 1310],

$$L_z^{q,W} = \int dx \int d^2\mathbf{k}_T \int d^2\mathbf{r}_T (\mathbf{r}_T \times \mathbf{k}_T)_z \frac{1}{2} \left( \mathcal{W}_{++}^{q[\gamma^+]W} - \mathcal{W}_{--}^{q[\gamma^+]W} \right). \quad (11.22)$$

This is related to the corresponding GTMD description by a 2D Fourier transform in  $\mathbf{r}_T$  [554, 1311],

$$L_z^{q,W} = \int dx \int d^2\mathbf{k}_T \left( \mathbf{k}_T \times i \frac{\partial}{\partial \Delta_T} \right)_z \frac{1}{2} \left( \mathbb{W}_{++}^{q[\gamma^+]W} - \mathbb{W}_{--}^{q[\gamma^+]W} \right) \Big|_{\Delta=0} \quad (11.23)$$

$$= - \int dx \int d^2\mathbf{k}_T \frac{\mathbf{k}_T^2}{M^2} F_{14}^{q,W} \Big|_{\Delta=0}, \quad (11.24)$$

where  $\mathbb{W}_{\lambda\lambda'}^{[\Gamma]}$  was defined in Eq. (11.11). Note that the distributions are evaluated in the forward limit; below, this specification will be omitted for conciseness of notation. Eq. (??) on one side provides a very intuitive definition of OAM while, on the other, it corresponds to a specific parton helicity configuration which can be calculated on the lattice (Sections 2.10.1, 11.5), and, in principle, measured in experiments (Section 11.3). In Ref.[1326] it was observed that, in analogy with the Sivers function, the  $k_T^2$  moment of  $F_{14}$  depends on the gauge link structure entering its evaluation: in particular, for a straight link one obtains the OAM term entering Ji's definition, while a staple link yields JM's definition. In other words, Ji's picture gives the intrinsic quark angular momentum, independent from spectator interactions, while JM's picture includes interactions with the spectators. The representation of OAM through Eq. (11.22) can also be used to obtain an intuitive semi-classical interpretation of the difference

$L_{\text{JM}}^q - L_{\text{Ji}}^q$  as the torque acting on the active quark due to its interaction with the spectator partons of the target [1326]. Formally, the additional term is equivalent to a Qiu-Sterman type term for a longitudinally polarized proton [1311, 1313].

In a recent development [1312, 1313], the decomposition of angular momentum was obtained using generalized LIR relations, *i.e.* LIRs similar to the ones introduced in Section 10, but involving off-forward proton states with  $P \neq P'$ . The following relation was derived for  $F_{14}^q$

$$L_z^q(x) = - \int d^2 k_T \frac{k_T^2}{M^2} F_{14}^q = \int_x^1 dy \left( \tilde{E}_{2T}^q + H_q + E_q + \mathcal{A}_{F_{14}} \right) \quad (11.25)$$

where, following the notation of Ref. [707], the *rhs* involves the twist-2 GPD combination,  $H_q + E_q$ , and introduced the twist-3 GPD,  $\tilde{E}_{2T}$ . Furthermore,  $\mathcal{A}_{F_{14}}$  is an explicit  $qgq$  term describing the gauge link structure of the equation, whose form is given in detail below. All expressions are given in the forward limit  $(\xi, t) \rightarrow 0$ , similarly to the integrands in the sum rule in Eq.(6.20), although these relations are valid point by point in the kinematic variables  $x$  and  $t$  and can be easily extended to the  $\xi \neq 0$  case [1315]. Note that the combination,  $\tilde{E}_{2T}^q + H_q + E_q$ , is expressed in an analogous format as in the original Wandzura Wilczek (WW) relation where the twist-3 PDF,  $g_T$  was decomposed into a twist-2 PDF,  $g_1$ , and a twist-3 PDF,  $g_2$ , as:  $g_T = g_1 + g_2$  [62, 666]. In the off-forward case considered here, we have the decomposition into the twist-2 combination,  $(H_q + E_q) \leftrightarrow g_1$ , and the twist-3 GPD,  $\tilde{E}_{2T}^q \leftrightarrow g_T$ .

Eq. (11.23) establishes a relation between the  $k_T^2$  moment of  $F_{14}^q$ , representing quark OAM, and the twist-3 GPD  $\tilde{E}_{2T}$ . The latter had been previously identified with OAM in Refs. [1311, 1316], within a derivation using OPE [1317, 1318], showing that the second Mellin moment of the twist-3 GPD defined as:  $G_2 = -(\tilde{E}_{2T}^q + H_q + E_q)$  in Ref.[1316], yields  $J_z^q - (1/2)\Sigma_q \equiv L_z^q$ .

Using the equations of motion, in Refs.[1312, 1313] it was shown that the decomposition of longitudinal angular momentum for a proton target in the quark sector was written both in terms of the GTMD  $F_{14}^q$  and the twist-3 GPD,  $\tilde{E}_{2T}^q$ , as,

$$\begin{aligned} J_z &= L_z + S_z \\ \frac{1}{2} \int dx x (H_q + E_q) &= \int dx x (\tilde{E}_{2T}^q + H_q + E_q) + \frac{1}{2} \int dx \tilde{H}_q \end{aligned} \quad (11.26)$$

$$= - \int dx \int d^2 k_T \frac{k_T^2}{M^2} F_{14}^q + \frac{1}{2} \int dx \tilde{H}_q. \quad (11.27)$$

The work in Refs. [1312, 1313] describes the connection between the two descriptions while introducing the following generalized WW relation for  $\tilde{E}_{2T}^q$ , obtained by extending to the off-forward case the set of QCD relations involving transverse momentum first introduced in Refs. [129, 460], and using the equations of motion,

$$\begin{aligned} \tilde{E}_{2T}^q(x) &= - \int_x^1 \frac{dy}{y} (H_q(y) + E_q(y)) - \left[ \frac{\tilde{H}_q(x)}{x} - \int_x^1 \frac{dy}{y^2} \tilde{H}_q(y) \right] - \left[ \frac{1}{x} \mathcal{M}_{F_{14}^q} - \int_x^1 \frac{dy}{y^2} \mathcal{M}_{F_{14}^q} \right] \\ &- \int_x^1 \frac{dy}{y} \mathcal{A}_{F_{14}^q}(y) \end{aligned} \quad (11.28)$$

In Eq.(11.26),  $\mathcal{M}_{F_{14}}$  is the  $qgq$  interaction term stemming from the equations of motion  $A$  field, namely,

$$\begin{aligned} \mathcal{M}_{\lambda'\lambda}^{i,S} &= -\frac{i}{4} \int \frac{dz^- d^2 z_T}{(2\pi)^3} e^{ixP^+z^- - ik_T \cdot z_T} \\ &\times \left\langle p', \lambda' \left| \bar{\psi} \left( -\frac{z}{2} \right) \left[ (\vec{\partial} - ig\mathcal{A}) W \Gamma \right]_{-z/2} + \Gamma W (\vec{\partial} + ig\mathcal{A}) \right|_{z/2} \right| \psi \left( \frac{z}{2} \right) \right\rangle_{z^+=0} p, \lambda \end{aligned} \quad (11.29)$$

with  $\Gamma = i\sigma^{i+}\gamma^5$ . For  $F_{14}$  one needs the combination,

$$\mathcal{M}_{F_{14}}(x) = \int d^2 k_T \frac{\Delta_1}{\Delta_T^2} (\mathcal{M}_{++}^{1,S} - \mathcal{M}_{--}^{1,S}) + \frac{\Delta_2}{\Delta_T^2} (\mathcal{M}_{++}^{2,S} - \mathcal{M}_{--}^{2,S}) \quad (11.30)$$

where  $\Delta_T^2 = \Delta_1^2 + \Delta_2^2$ .  $\mathcal{A}_{F_{14}}^q$  is the gauge link representing either a staple or a straight link for  $\mathcal{A}_{F_{14}} = 0$ . The general structure of this term is given in term of unintegrated in  $k^-$  amplitudes [707] as [1313],

$$\begin{aligned} \mathcal{A}_{F_{14}} &= v^- \frac{(2P^+)^2}{M^2} \int d^2 k_T \int dk^- \\ &\left[ \frac{k_T \cdot \Delta_T}{\Delta_T^2} (A_{11}^F + x A_{12}^F) + A_{14}^F + \frac{k_T^2 \Delta_T^2 - (k_T \cdot \Delta_T)^2}{\Delta_T^2} \left( \frac{\partial A_8^F}{\partial(k \cdot v)} + x \frac{\partial A_9^F}{\partial(k \cdot v)} \right) \right] \end{aligned} \quad (11.31)$$

where the 4-vector  $v = (0, v^-, 0, 0)$  describes the direction of the staple, which here is taken to extend along the light cone. The completely unintegrated amplitudes named,  $A_j$ , were introduced from the inception [62], and are essential to the derivation as they underline the common structures in the twist-2 and twist-3 distributions. A detailed description for both thew staple and straight link cases is given in Refs.[707, 1313]. The relation between Ji and JM OAM using a straight and a staple link, respectively, can be evaluated through Eq.(11.29). An explicitly calculable form of the difference between the two definitions was obtained in Ref.[1313] as a function of  $\mathcal{M}$  and  $\mathcal{A}$  as,

$$L^{JM}(x) - L^{Ji}(x) = \mathcal{M}_{F_{14}} - \mathcal{M}_{F_{14}} \Big|_{v=0} = - \int_x^1 dy \mathcal{A}_{F_{14}}(y). \quad (11.32)$$

An important finding stems from the similarity found with the composition of the intrinsic  $qgq$  twist three contribution to the twist three structure functions already raised in Ref. [732] for the twist-3 PDF,  $g_2$ . The two different contributions singled out in [732] are  $\hat{g}_T$  and  $\tilde{g}_T$ . While representing two different projections of the two-dimensional twist three term, they can not be separated in experiments involving only collinear PDFs. Similarly, for OAM, experimental measurements of twist-3 GPDs do not allow us to obtain separately,  $\mathcal{M}_{F_{14}}$  and  $\mathcal{A}_{F_{14}}$ , the immediate consequence being that an experimental determination of the difference between JM and Ji OAM, described by  $\mathcal{A}_{F_{14}}$ , is possible only by measuring separately the GPDs  $\tilde{E}_{2T}$ ,  $H$  and  $E$ , and the GTMD  $F_{14}$ , using Eq.(11.26).

GTMDs and Wigner distributions are also fundamental for investigating spin-orbit correlations. The correlation between the quark longitudinal spin and OAM denoted by  $C_z^q$  in Ref. [554], can be computed according to [554, 1319]

$$\begin{aligned} \langle C_z^{q,W} \rangle &= \int dx \int d^2\mathbf{k}_T \int d^2\mathbf{r}_T (\mathbf{r}_T \times \mathbf{k}_T)_z W_{++}^{q[\gamma^+\gamma_5]W}(x, \mathbf{k}_T, \mathbf{r}_T) \\ &= \int dx \int d^2\mathbf{k}_T \frac{\mathbf{k}_T^2}{M^2} G_{1,1}^{q,W}(x, \mathbf{k}_T, \xi, \Delta_T) |_{\Delta=0}. \end{aligned} \quad (11.33)$$

By definition, this correlation shows a close analogy to the correlation between the spin and the OAM of the electron in the hydrogen atom. In Ref.[1313] an analogous derivation to the OAM components was obtained for  $C_z$ , namely,

$$(L_z S_z)_q(x) = \int d^2k_T \frac{k_T^2}{M^2} G_{11}^q = \int_x^1 dy \left( 2\tilde{H}'_{2T} + E'_{2T} + \tilde{H} - \mathcal{A}_{G_{11}^{q,W}} \right), \quad (11.34)$$

where the "o" superscript on  $F_{12}$  denotes the imaginary part of the GTMD (Sec.11.2);  $\mathcal{A}_{G_{11}^{q,W}}$  is a gauge link term that can be evaluated similarly to the OAM one in Eq.(11.29).

Finally, similar relations can be derived to identify the OAM component in the proton transverse spin decomposition [791, 1315, 1321, 1322] by working out similar relations involving transverse polarization. For example, the off-forward generalization of the Sivers shift [132], reads

$$\int d^2k_T \frac{k_T^2}{M^2} F_{12}^o \equiv -f_{1T}^{\perp(1)} = -\mathcal{M}_{F_{12}}|_{\Delta_T=0} \quad (11.35)$$

where the term  $\mathcal{M}_{F_{12}}$  on the *rhs* is an off-forward/generalized analogue of the Qiu-Sterman  $T_q(x, x)$  term [159]. The Sivers shift was evaluated in lattice QCD calculations in [141, 142]. Additional spin-orbit correlations can be identified when considering transverse polarization effects [1320].

In conclusion, while  $J_{q,g}$  and OAM measurements of collinear GPDs are in progress, GTMDs, providing in principle the density distributions for OAM, remain experimentally more difficult to extract since they require exclusive measurements of particles in the two distinct hadronic planes disentangling the  $k_T$  and  $r_T$  (or  $\Delta_T$ ) directions [1302, 1323, 1324]. Twist-2 and twist-3 GPDs and GTMDs can now be evaluated in ab initio calculations [557] as illustrated in the following Section.

## 11.5 GTMD observables from LQCD: Quark orbital angular momentum in the proton

Lattice QCD calculations of TMD observables were discussed in Sec. 6.4. They are based on evaluating the fundamental matrix element in Eq. (6.55) in the forward limit,  $P' = P$ . By generalizing such calculations to include a momentum transfer  $\Delta_T = P' - P$  in the transverse direction, one can furthermore access GTMD observables; since  $\Delta_T$  is Fourier conjugate to the impact parameter  $\mathbf{r}_T$  of the struck quark in a deep inelastic scattering process, one thus supplements the transverse momentum information with transverse position information.

In effect, one can access information about Wigner distributions  $\mathcal{W}^{q[\Gamma]W}(x, \mathbf{k}_T, \mathbf{r}_T)$  simultaneously characterizing quark position and momentum. As discussed in Sec. 11.4, a prime application immediately offering itself is the direct evaluation of quark orbital angular momentum (OAM) in the proton, associated with the GTMD  $F_{1,4}^{qW}$ , cf. Eq. (11.22). Casting this, via Eq. (11.11), in terms of the matrix element in Eq. (6.55) [556], one can evaluate the longitudinal component  $L_z^{q,W}$  of quark OAM in a longitudinally polarized proton, normalized to the number of valence quarks  $n$ , in the form [556, 557]

$$\frac{L_z^{q,W}}{n} = \frac{-\epsilon_{jk} \frac{\partial}{\partial b_{T,j}} \frac{\partial}{\partial \Delta_{T,k}} \langle p(P', S_L) | \bar{\psi}_i^0(\frac{b}{2}) \gamma^+ W_{\square\eta}^v(\frac{b}{2}, -\frac{b}{2}) \psi_i^0(-\frac{b}{2}) | p(P, S_L) \rangle \Big|_{b^+=b^-=0, \Delta_T=0, \mathbf{b}_T \rightarrow 0}}{\langle p(P', S_L) | \bar{\psi}_i^0(\frac{b}{2}) \gamma^+ W_{\square\eta}^v(\frac{b}{2}, -\frac{b}{2}) \psi_i^0(-\frac{b}{2}) | p(P, S_L) \rangle \Big|_{b^+=b^-=0, \Delta_T=0, \mathbf{b}_T \rightarrow 0}} \quad (11.36)$$

where the index  $i$  specifies the quark flavor under consideration. The ratio (11.34) serves to cancel soft factors associated with the gauge links, in analogy to the TMD studies described in Sec. 6.4.1. The limit  $\mathbf{b}_T \rightarrow 0$  has to be taken with care, since it engenders additional divergences; this is analogous to the subtlety involved in relating TMDs to PDFs discussed in detail in Sec 2.9. Through its dependence on the gauge link<sup>42</sup>  $W_{\square\eta}^v$ , the ratio (11.34) allows one to access both the quark OAM of the Ji decomposition of proton spin (by choosing zero staple length  $\eta$  in Fig. 2.11, i.e., a straight gauge link between the quark operators) as well as the quark OAM of the Jaffe-Manohar decomposition of proton spin (by choosing infinite staple length  $\eta$ ) [554, 1311, 1325, 1326]. As far as LQCD calculations are concerned, this formulation thus offers the opportunity to go beyond previous work, which has been restricted to Ji quark OAM, evaluated as  $L = J - S$  via Ji's sum rule [551] (LQCD calculations employing Ji's sum rule are discussed in Sec. 6.2.2). Fig. 11.5 shows results for Ji OAM using the GTMD approach, compared with the Ji sum rule value, as well as a continuous, gauge-invariant interpolation between Ji OAM and Jaffe-Manohar OAM, achieved by varying the staple length  $\eta$ .

An important technical aspect encountered in carrying out such calculations is the need to construct an unbiased estimate of the derivative with respect to transverse momentum transfer  $\Delta_T$  in Eq. (11.34). In the initial exploration [556], the derivative was evaluated as a finite difference using a rather large interval in  $\Delta_T$ , which led to a significant systematic bias, and consequently a discrepancy between the value obtained for Ji OAM from Eq. (11.34) and the one obtained from the Ji sum rule. The data shown in Fig. 11.5, taken from Ref. [557], were instead obtained using a direct derivative method [1327] which eliminates this bias; essentially, one samples directly the  $\Delta_T$ -derivative of the proton matrix element instead of evaluating the proton matrix element itself and numerically extracting its derivative a posteriori (details are given in Ref. [557]). With this methodological improvement, agreement between the results obtained using Eq. (11.34) and using the Ji sum rule is indeed achieved, as shown in Fig. 11.5 (left).

Since, as already noted in Sec. 11.4, a staple-shaped gauge link incorporates the final state interactions experienced by the struck quark in a deep-inelastic scattering process, the data shown in Fig. 11.5 (right) elucidate the consequent torque [1326] experienced by a struck quark leaving the proton remnant, beginning with Ji OAM and approaching Jaffe-Manohar

<sup>42</sup>In the GTMD case, the Collins-Soper type evolution parameter  $\hat{\zeta}$  characterizing the staple direction  $v$  of the gauge link is defined using the average hadron momentum  $\bar{P} = (P' + P)/2$  as  $\hat{\zeta} = v \cdot \bar{P}/(\sqrt{|v^2|} \sqrt{\bar{P}^2})$ .

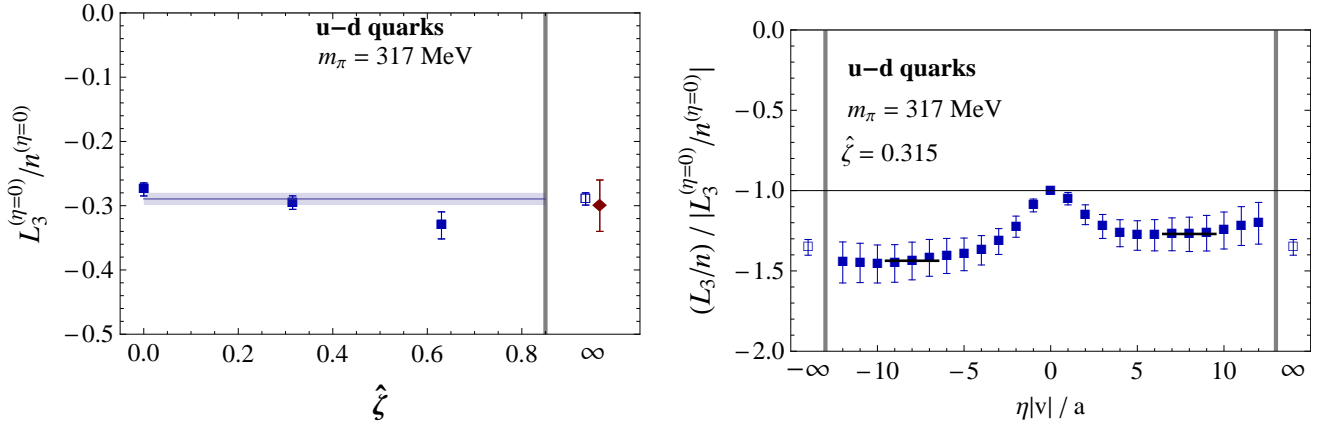


Figure 11.5: Isovector ( $u - d$  quark) longitudinal orbital angular momentum in the proton in units of the number of valence quarks  $n$ , cf. the definition (11.34), obtained using a clover fermion ensemble at  $m_\pi = 317$  MeV; from [557]. Left: Ji OAM obtained using a straight gauge link; in this case,  $\hat{\zeta}$  essentially quantifies the proton momentum in the 3-direction (the direction in which the staple link also extends once the staple length is varied), but the obtained results can not in fact depend on  $\hat{\zeta}$ , since there is no physical staple direction  $v$  in the straight-link case. Fitting, therefore, a constant value to the data yields the extrapolated blue data point. The red data point is the value obtained from Ji's sum rule at the same pion mass (since this value was not available on the same ensemble, an interpolation of data from [575] was used instead). Right: Varying the staple length  $\eta$  allows for a continuous, gauge-invariant interpolation between Ji OAM ( $\eta = 0$ ) and Jaffe-Manohar OAM ( $|\eta| \rightarrow \infty$ ). Data are shown in units of the magnitude of Ji OAM. The sign of this ratio reflects the fact that isovector quark OAM is negative.

OAM at asymptotic distances. The difference between Jaffe-Manohar and Ji OAM, i.e., the accumulated torque, can be clearly resolved and is sizeable, amounting to roughly 1/3 of the originally present Ji OAM at the pion mass  $m_\pi \approx 317$  MeV. The torque is directed such as to enhance OAM as the quark leaves the proton.

Besides the above Wigner function approach and Ji's sum rule, a third avenue of accessing Ji quark OAM in the proton is via the twist-3 GPD  $\tilde{E}_{2T}^q$  [1312, 1313, 1316], cf. the discussion in Sec. 11.4, or its twist-3 GTMD “mother distributions”  $F_{2,7}^{qW}$  and  $F_{2,8}^{qW}$ , cf. [707]. In this case, one is led to evaluate a correlator of the type in Eq. (6.55) specifically for  $\Gamma = \gamma^i$ , where  $i$  denotes one of the transverse directions. A preliminary analysis of corresponding lattice data as of this writing indicates that this avenue is feasible and yields results compatible with the other methods, albeit with larger numerical uncertainties at comparable numerical effort.

The study of GTMD observables using LQCD can moreover be extended to encompass further characteristics of the nucleon, such as the quark spin-orbit correlations quantified by the GTMD  $G_{1,1}^{qW}$ , cf. Eq. (11.31) and the associated discussion. This case again requires employing the direct derivative method mentioned above, in order to evaluate a derivative with respect to momentum transfer. A first calculation in this direction, reported in [?], employs the domain wall fermion (DWF) discretization, which mitigates possible operator mixing effects by preserving chiral symmetry, as discussed in Sec. 6.4.1.

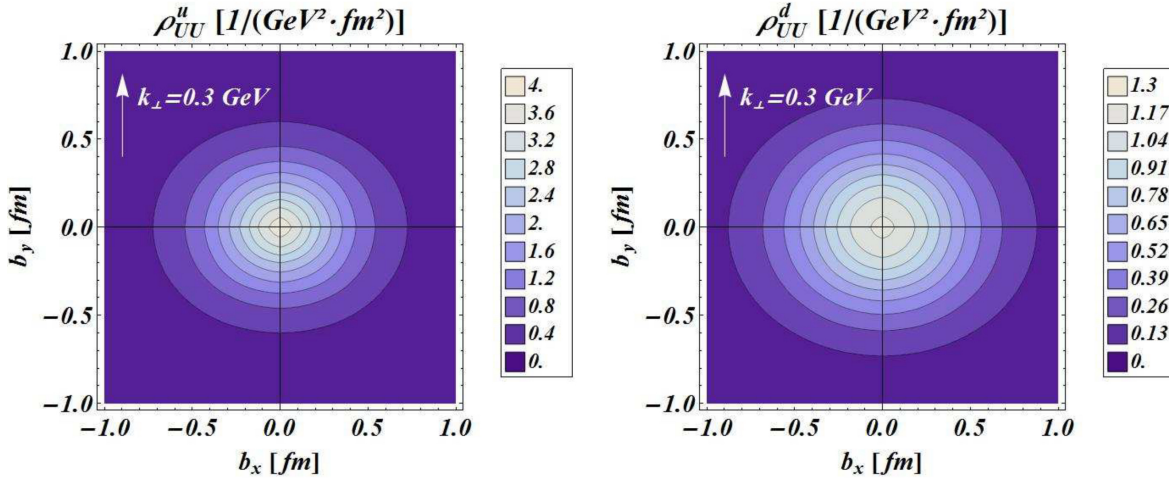


Figure 11.6: Wigner distributions for unpolarized up quarks (left) and down quarks (right), as defined in Eq. (11.35), in a light-front constituent quark model; figure from Ref. [554]. The results are shown for a fixed  $\mathbf{k}_T$  with  $k_T = 0.3 \text{ GeV}$  and pointing in the positive  $y$ -direction, as a function of  $r_x = b_x|_{\text{fig.}}$  and  $r_y = b_y|_{\text{fig.}}$ . Comparing up quarks and down quarks, the same color corresponds to different values of the Wigner distributions.

## 11.6 Model results and their interpretation

GTMDs and Wigner distributions of the nucleon have been computed in different models, including diquark spectator models [707, 1314, 1328? ? ? ], light-front quark models [554, 751? ], the light-cone version of the chiral quark-soliton model [554, 751], the quark-target model [1314, 1329? ? ? ? –1331], the bag model [? ], and models which make use of the AdS/QCD correspondence [? ? ? ]. Model calculations of those quantities for the pion are available as well [785? ? ? ? ]. We refer to Ch. 7 for the salient features of the pertinent models and for further related references. Moreover, there exist various papers on (model) calculations of gluon GTMDs and Wigner distributions in the small- $x$  region [956, 963, 993, 1295, 1297, 1301, 1308, 1323? ? ? ? ? ]. Several of those studies are closely related to treatments of gluon TMDs at small  $x$  which are discussed in Ch. 8.

As one example, Fig. 11.6 displays results for the Wigner distribution of unpolarized quarks in an unpolarized proton, obtained in a light-front constituent quark model [554]. To be precise, the figure shows the quantity

$$\rho_{UU}^q(\mathbf{k}_T, \mathbf{r}_T) = \int dx \mathcal{F}_{1,1}^q(x, \mathbf{k}_T, \mathbf{r}_T), \quad (11.37)$$

where  $\mathcal{F}_{1,1}^q$  is the Wigner distribution which is the Fourier transform of the GTMD  $F_{1,1}^q$ . (Here we have dropped the dependence of the Wigner distribution and the GTMD on the Wilson line since the model employed in Ref. [554] does not contain gluons.) The distributions for up quarks and down quarks, with a fixed transverse momentum in the  $y$ -direction, are plotted as a function of  $(r_x, r_y)$ . The most important qualitative result is that the distributions are not axially symmetric. Interpreting the results as densities, one concludes that a configuration with large  $\mathbf{r}_T \perp \mathbf{k}_T$  is more likely than a configuration with large  $\mathbf{r}_T \parallel \mathbf{k}_T$ , which can be understood based on the finite extension of the proton [554]. The left-right symmetry of the

densities is a model-independent result while the top-bottom symmetry could be traced back to the lack of gluons in the model [554]. Note also that the spread of the distributions is smaller for up quarks than for down quarks, reflecting the fact that up quarks are more concentrated at the center of the proton than down quarks.

While the results of the previous paragraph and other similar findings suggest that Wigner distributions can be used for 5D imaging of hadrons, one must exercise some care in this context. (For discussions concerning 6D imaging of hadrons we refer to [1288, 1291? ? ] and references therein.) It is already known from non-relativistic quantum mechanics that Wigner distributions are quasi-probability distributions only, and as such they can become negative. Considering the quark-target model to lowest nontrivial order in pQCD, it has been made explicit that partonic Wigner distributions can also become negative [1330] which implies that interpretations of results for Wigner distributions in the sense of multi-dimensional densities are not always straightforward. In order to address this shortcoming, the authors of Ref. [1330] suggested to use the so-called Husimi distribution [1332] instead of the Wigner distribution. Like the Wigner distribution, the Husimi phase space distribution is used in non-relativistic quantum mechanics. The main underlying idea is a Gaussian smearing for both position and momentum in such a manner that positivity of the distribution is maintained. (It is expected that also partonic Husimi distributions are positive semi-definite, but a rigorous proof of this property is still lacking [1330].) The Gaussian smearing, however, implies that for Husimi distributions the connections to the densities in position and momentum space are lost, in contrast to Wigner distributions where these connections are expressed through Eqs. (11.6) and (11.7). Further research is required in order to better understand the opportunities as well as the limitations of a 5D imaging of hadrons.

## 12 - Summary and Outlook

Deep inelastic scattering (DIS) experiments in the early 1970s first revealed the internal structure of the nucleon through the phenomenon of Bjorken scaling. The parton model gave an intuitive explanation of this phenomenon as the consequence of the nucleon being constituted of quasi-free partons, now known to be quarks and gluons. The form factors measured in DIS were calculated in terms parton distribution function (PDFs) which described the distribution in the fraction,  $x$ , of the nucleon's momentum carried by each parton. Initially only the momentum of the parton along the light-like direction of the large component of the nucleon was considered. As QCD developed it became apparent the PDFs were scale dependent and obeyed evolution (DGLAP) equations which allow one to calculate how the PDFs change as the scale at which they are probed is varied. The ability to measure the PDFs in experiments across a wide range scales and successfully describe the evolution of the PDFs using DGLAP is a major achievement of QCD. Collinear factorization - convolving collinear PDFs with perturbatively calculable hard cross sections - has been the main tool for making predictions for high energy physics experiments for decades. Today most cross sections for searches for new physics at the LHC, for example, are calculated in the collinear factorization approximation.

However, neglecting the transverse motion of the quarks within the nucleon misses much of the rich internal structure of the proton. It is like studying the Solar System and knowing only the average distance of each planet from the sun and not the shapes or periods of their orbits. In the last couple of decades a huge amount of both experimental and theoretical work has gone into studying the transverse structure of the nucleons and nuclei. The relevant PDFs which depend on the light-like momentum fraction and the transverse momentum of the partons,  $k_T$ , are called transverse momentum dependent PDFs (TMD PDFs). The TMD PDFs along with the transverse momentum dependent fragmentation functions (TMD FFs), collectively known as TMDs, are the main subject of this handbook.

Processes which are sensitive to the  $k_T$  dependence of the hadron are necessarily less inclusive than DIS. They also involve at least two scales a hard scale justifying the application of perturbation theory along with the transverse momentum which can typically be much closer to  $\Lambda_{\text{QCD}}$ . The three main processes for which TMD factorization is relevant are: semi inclusive DIS (SIDIS), in which a specific hadron in the final state is measured, the Drell Yan process in which the transverse momentum of the lepton pair is measured, and di-hadron production in  $e^+e^-$  collisions. The factorization theorems for these processes each involve different TMD PDFs and TMD FFs. SIDIS involves a TMD PDF for the initial state proton and a TMD FF for the final state hadron, Drell-Yan involves two TMD PDFs for the initial state hadrons and di-hadron production involves two TMD FFs for each final state hadron. These processes were studied in detail in the first five chapters of the Handbook. Chapter 1 gave an overview of the field some as well as some cross section formulae for SIDIS, Drell-Yan, and di-hadron production. Chapter 2 covers the definition of TMDs. This is a rather involved topic as unlike collinear PDFs the TMD PDFs have both ultraviolet and rapidity divergences when computed in perturbation theory. A one-loop calculation exhibiting these divergences is performed in this chapter. Subtraction of soft Wilson lines are needed to properly define the TMD PDFs. There are number of approaches to defining the TMDs and these reviewed here. The leading eight leading TMD PDFs and TMD FFs for both quarks and gluons are

given here and full cross section formulae for SIDIS, Drell-Yan, and di-hadron production are given in this chapter as well. Chapter 3 sketches the proof of the factorization theorems given in the previous Chapter. Chapter 4 discusses the solution of the renormalization group equations (RGE) and rapidity renormalization group equations (RRGE) and their application to resumming large logarithms. Chapter 5 gives a thorough review of the phenomenology and extraction of TMDs from data. A striking observation in this chapter is that early fits with simplistic models of TMDs, e.g., the collinear PDF times a Gaussian in  $k_T$ , have given way to more sophisticated parametrizations that are consistent with the evolution discussed in Chapter 4. It is clear that we have made substantial progress in extracting quark TMDs from the abundant data from a variety of colliders. An important issue going forward is the extraction of gluon TMDs.

A very important development in recent years is the application of the lattice to both collinear and TMD PDFs. For a long time it was thought the only relevant calculation one could calculate on the lattice was to compute matrix elements of local operators that corresponded to moments of the collinear PDFs. It has been recently realized that by computing euclidean matrix elements in highly boosted states one could access the collinear PDFs via a matching calculation. For a while it was thought that it would be difficult to extract the soft matrix elements with more than one light-like Wilson line need for computing TMD PDFs but this problem has recently been solved. There are variety of different schemes for doing these calculations. Progress in theory and comparison with experimentally determined collinear PDFs and TMD PDFs is discussed in Chapter 6.

An interesting aspect of TMD physics are the so called T-odd distribution. Originally, thought to be vanishing because of the time reversal invariance of QCD, it was later realized because the time reversal operation reverses the orientation of the Wilson line that these functions are non zero and take the opposite sign in Drell-Yan and SIDIS. The Sivers asymmetry is an example of this and this prediction is frequently checked experimentally. That QCD could generate such an asymmetry was realized in a model calculation that is described in Chapter 7. Other models for TMDs are described in this chapter as well. These are useful for estimating the size and sign of asymmetries and testing conjectured relations between TMDs.

## 13 - Acknowledgement

We would like to thank Tatiana Donskova for designing the logo of the TMD Collaboration. This work has been supported in part by the National Science Foundation under Grants No. PHY-2011763 (Pitonyak), No. PHY-2012002 (Prokudin), No. PHY 2111490 (Schweitzer). This work has been supported in part by the U.S. Department of Energy, under contracts No. DE-FG02-07ER41460 (Gamberg), No. DE-SC0011090 (Detmold, Negele, and Stewart), No. DE-AC05-06OR23177 (Prokudin), No. DE-FG02-96ER40965 (Burkardt, Engelhardt), No. DE-FG02-04ER41338 (Fleming), No. DE-SC0004286 (Tarasov), No. DE-SC0020405 (Constantinou), and No. DE-FG02- 05ER41367 (Mehen) under which Jefferson Science Associates, LLC, manages and operates Jefferson Lab; through the DOE Office of Nuclear Physics and the LDRD Program of Los Alamos National Laboratory, which is operated by Triad National Security, LLC, for the National Nuclear Security Administration under contract No. 89233218CNA00001 (Lee, Vitev); and within the framework of the TMD Topical Collaboration. Stewart was also supported in part by the Simons Foundation through the Investigator grant 327942.

## A - Glossary

This appendix will discuss notation and relations to the literature.

Notation decisions:

1. use  $\mathbf{q}_T$  for Euclidean transverse momentum,  $\mathbf{b}_T$  for Euclidean transverse coordinate, and non-bold face for Minkowski four vector,  $q_T$  etc.
2. Use  $\mathbf{k}_T$  for transverse momentum in TMDPDF, and  $\mathbf{p}_T$  for that in TMDFF, saving  $\mathbf{q}_T$  for leptonic transverse momentum.
3. use  $Y$  for lepton rapidity, and small  $y$  with subscripts for other rapidities
4. Use both  $i/H$  or  $i/p$  for hadron or proton depending on context
5.  $f_{i/p}(x, \mathbf{b}_T, \mu, \zeta)$  for renormalized TMDPDF  
 $f_{i/p}^{0(u)} (= B_{i/p}^{0\text{naive}})$  for bare unsubtracted TMDPDF (equal to bare naive beam function)  
 $B_{i/p}^0$  for bare beam function, where  $B_{i/p}^0 = f_{i/p}^{0(u)}/S_i^{0\text{subt}}$   
 $B_{i/p}(x, \mathbf{b}_T, \mu, \zeta/\nu^2)$  for renormalized beam function  
 $S_i^0$  for bare soft function  
 $S_i^{0\text{subt}}$  for overlap factor = soft subtraction factor
6. Light-cone variable conventions
7. Wilson lines  $W_n(a, b)$  where  $n$  is the direction and  $(a, b)$  are the path endpoints.
8. Use  $\psi$  for the fermion field.
9. Use the notation  $|H(P, S)\rangle$  for a hadron  $H$  with momentum  $P^\mu$  and spin  $S$ .
10. Use  $b_0 = 2e^{-\gamma_E}$

## B - Feynman rules

In order to evaluate Eq. (2.57) perturbatively, we need to know the Feynman rules of the Wilson line  $W_\square(b^\mu, 0)$ . Since it is composed of several straight Wilson line segments, it suffices to consider the straight Wilson line defined in Eq. (2.43). We can perturbatively expand it as

$$\begin{aligned} W_n(x; a, b) &= P \exp \left[ -ig_0 \int_a^b ds n \cdot A^{\mu 0} (x^\mu + sn^\mu) t^\mu \right] \\ &= 1 - ig_0 n^\mu t^\mu \int_a^b ds A_\mu^{\mu 0} (x^\mu + sn^\mu) + O(g_0^2). \end{aligned} \quad (\text{B.1})$$

At this order, the path ordering  $P$  has no effect. The corresponding Feynman rule can be obtained using standard techniques for the Feynman rules of the gluon field  $A_\mu^a$  itself. We obtain

$$\begin{aligned} \overset{x+a}{\overbrace{\overset{n}{\overbrace{\overset{k}{\overbrace{\text{gl}}}}}}} \overset{x+b}{n} &= -ig_0 n^\mu t^a \int_a^b ds e^{-ik \cdot (x+sn)} \\ &= g_0 n^\mu t^a e^{-ik \cdot x} \frac{e^{-ib(k \cdot n)} - e^{-ia(k \cdot n)}}{k \cdot n}. \end{aligned} \quad (\text{B.2})$$

Care has to be taken when taking the limit of either  $a \rightarrow \infty$  or  $b \rightarrow \infty$ , in which case one has to give momentum  $k$  a small imaginary part to make the pure phase vanish. For concreteness, the one-loop Wilson rules for the linear segments in Eq. (2.43) are given by

$$\begin{aligned} W_{n_b}(b^\mu; -\infty, 0) : & -g_0 n_b^\mu t^a \frac{1}{k^+ + i0} e^{-ik \cdot b}, \\ W_{n_b}^\dagger(0; -\infty, 0) : & +g_0 n_b^\mu t^a \frac{1}{k^+ - i0}, \end{aligned} \quad (\text{B.3})$$

and the transverse Wilson vanishes at lightcone infinity. The relative sign between the two results reflects the inverse direction of  $W_{n_b}$  and  $W_{n_b}^\dagger$ . The  $\pm i0$  in the denominator arises to take the limit to lightcone infinity, but will not be crucial in our following calculation.

## C - Fourier transforms

Here, we collect some useful definitions and identities for Fourier transforms in transverse space. As discussed in Sec. 2, the sign convention of the Fourier transform differs between TMD PDFs and TMD FFs, and thus we will discuss both cases separately.

### C.1 Conventions for the TMD PDF

In the case of the TMD PDF, our convention for the Fourier transform and its inverse is

$$\tilde{f}(\mathbf{b}_T) = \int d^2 \mathbf{p}_T e^{-i\mathbf{b}_T \cdot \mathbf{p}_T} f(\mathbf{p}_T), \quad f(\mathbf{p}_T) = \int \frac{d^2 \mathbf{b}_T}{(2\pi)^2} e^{+i\mathbf{b}_T \cdot \mathbf{p}_T} \tilde{f}(\mathbf{b}_T), \quad (\text{C.1})$$

where  $\tilde{f}(\mathbf{b}_T)$  is the function in Fourier or position space, and  $f(\mathbf{p}_T)$  is the function in momentum space. If  $f(\mathbf{p}_T)$  is independent of the azimuthal angle, i.e.  $f(\mathbf{p}_T) \equiv f(|\mathbf{p}_T|)$ , then one can use the identity

$$\tilde{f}(b_T) = \int_0^\infty dp_T p_T \int_0^{2\pi} d\phi e^{-ib_T p_T \cos \phi} f(p_T) = 2\pi \int_0^\infty dp_T p_T J_0(b_T p_T) f(p_T), \quad (\text{C.2})$$

where  $J_0(x)$  is the 0-th order Bessel function of the first kind. In this case,  $\tilde{f}(\mathbf{b}_T) \equiv \tilde{f}(b_T)$  is independent of the azimuthal angle as well, which yields the corresponding identity for the inverse transform

$$f(p_T) = \frac{1}{(2\pi)^2} \int_0^\infty db_T b_T \int_0^{2\pi} d\phi e^{ib_T p_T \cos \phi} \tilde{f}(b_T) = \frac{1}{2\pi} \int_0^\infty db_T b_T J_0(b_T p_T) \tilde{f}(b_T). \quad (\text{C.3})$$

From Eqs. (C.2) and (C.3), it is clear that the Fourier transform  $\tilde{f}(b_T)$  of a real function  $f(p_T)$  is real, and likewise for the inverse Fourier transform.

A key feature of the Fourier transform is that it turns convolutions in momentum space into simple products,

$$\int d^2\mathbf{k}_1 d^2\mathbf{k}_2 \delta^{(2)}(\mathbf{p}_T - \mathbf{k}_1 - \mathbf{k}_2) f(\mathbf{k}_1) g(\mathbf{k}_2) = \int \frac{d^2\mathbf{b}_T}{(2\pi)^2} e^{i\mathbf{b}_T \cdot \mathbf{p}_T} \tilde{f}(\mathbf{b}_T) \tilde{g}(\mathbf{b}_T), \quad (\text{C.4})$$

which can be easily seen by inserting Eq. (C.1) together with the distributional identity

$$\delta^{(2)}(\mathbf{p}_T - \mathbf{k}_1 - \mathbf{k}_2) = \int \frac{d^2\mathbf{b}_T}{(2\pi)^2} e^{i\mathbf{b}_T \cdot (\mathbf{p}_T - \mathbf{k}_1 - \mathbf{k}_2)}. \quad (\text{C.5})$$

In Sec. 2.7, we also need Fourier transforms of functions of the form  $p_T^\mu f(p_T)$ , which can be obtained as

$$\begin{aligned} \int d^2\mathbf{p}_T e^{-i\mathbf{p}_T \cdot \mathbf{b}_T} (p_T^\mu \cdots p_T^\nu) f(p_T) &= \left(-i \frac{\partial}{\partial b_{T\mu}}\right) \cdots \left(-i \frac{\partial}{\partial b_{T\nu}}\right) \int d^2\mathbf{p}_T e^{-i\mathbf{p}_T \cdot \mathbf{b}_T} f(p_T) \\ &= (-i\partial^\mu) \cdots (-i\partial^\nu) \tilde{f}(b_T) \\ &= (-i\partial^\mu) \cdots (-i\partial^\nu) 2\pi \int_0^\infty dp_T p_T J_0(b_T p_T) f(p_T). \end{aligned} \quad (\text{C.6})$$

By acting with the partial derivative

$$\partial^\mu \equiv \frac{\partial}{\partial b_{T\mu}} = -\frac{b_T^\mu}{b_T} \frac{\partial}{\partial b_T} \quad (\text{C.7})$$

on the exponential phase, one induces the desired tensor structure  $p_T^\mu \cdots p_T^\nu$  in the Fourier integral. (Recall that  $\mathbf{p}_T \cdot \mathbf{b}_T = -p_T^\mu b_{T\mu}$ , which fixes the sign of the derivative factors.) Thus, we can conveniently express this Fourier transform as derivatives acting on the Fourier transform  $\tilde{f}(b_T)$ , which in the last line was expressed using Eq. (C.2). Using Eq. (C.6) together with the Bessel function identity

$$\frac{d}{dz} z^{-m} J_m(z) = -z^{-m} J_{m+1}(z), \quad (\text{C.8})$$

we easily obtain the explicit results

$$\begin{aligned} \int d^2\mathbf{p}_T e^{-i\mathbf{p}_T \cdot \mathbf{b}_T} \frac{p_T^\mu}{p_T} f(p_T) &= (-i) \frac{b_T^\mu}{b_T} \times 2\pi \int_0^\infty dp_T p_T J_1(b_T p_T) f(p_T), \\ \int d^2\mathbf{p}_T e^{-i\mathbf{p}_T \cdot \mathbf{b}_T} \left(\frac{g_T^{\mu\nu}}{2} + \frac{p_T^\mu p_T^\nu}{\mathbf{p}_T^2}\right) f(p_T) &= (-i)^2 \left(\frac{g_T^{\mu\nu}}{2} + \frac{b_T^\mu b_T^\nu}{\mathbf{b}_T^2}\right) \times 2\pi \int_0^\infty dp_T p_T J_2(b_T p_T) f(p_T). \end{aligned} \quad (\text{C.9})$$

The integrals over  $p_T$  have the same structure as in Eq. (C.2), up to exchanging  $J_0(x)$  by  $J_1(x)$  and  $J_2(x)$ , respectively. From Eq. (C.9), we easily obtain the relations

$$\begin{aligned} \int d^2\mathbf{p}_T e^{-i\mathbf{p}_T \cdot \mathbf{b}_T} \frac{p_T^\mu}{M} f(p_T) &= (-i) b_T^\mu M \tilde{f}^{(1)}(b_T), \\ \int d^2\mathbf{p}_T e^{-i\mathbf{p}_T \cdot \mathbf{b}_T} \frac{\mathbf{p}_T^2}{M^2} \left(\frac{g_T^{\mu\nu}}{2} + \frac{p_T^\mu p_T^\nu}{\mathbf{p}_T^2}\right) f(p_T) &= \frac{(-i)^2}{2} b_T^2 M^2 \left(\frac{g_T^{\mu\nu}}{2} + \frac{b_T^\mu b_T^\nu}{\mathbf{b}_T^2}\right) \tilde{f}^{(2)}(b_T), \end{aligned} \quad (\text{C.10})$$

where the  $\tilde{f}^{(n)}$  denote derivatives with respect to  $b_T$  as defined in Eq. (2.129),

$$\tilde{f}^{(n)}(b_T) \equiv n! \left( \frac{-1}{M^2 b_T} \partial_{b_T} \right)^n \tilde{f}(b_T) = \frac{2\pi n!}{(b_T M)^n} \int_0^\infty dp_T p_T \left( \frac{p_T}{M} \right)^n J_n(b_T p_T) f(p_T). \quad (\text{C.11})$$

The equality in the second step follows directly from Eq. (C.8). The factor of  $n!$  arises from following the convention of [139]. Also note that the Eq. (C.11) is manifestly real if  $f(p_T)$  is real, and hence the explicit factors of  $i$  have been extracted in Eq. (C.10).

For the gluon TMD, we also need the Fourier transform

$$\begin{aligned} \int d^2 \mathbf{p}_T e^{-i \mathbf{p}_T \cdot \mathbf{b}_T} \frac{p_T^\mu p_T^\nu p_T^\sigma}{p_T^3} f(p_T) &= \frac{1}{b_T} (b_T^\mu g_\perp^{\nu\sigma} + b_T^\nu g_\perp^{\sigma\mu} + b_T^\sigma g_\perp^{\mu\nu}) 2\pi(-i)^3 \int_0^\infty dp_T p_T \frac{J_2(b_T p_T)}{p_T b_T} f(p_T) \\ &\quad + \frac{b_T^\nu b_T^\sigma b_T^\mu}{b_T^3} 2\pi(-i)^3 \int_0^\infty dp_T p_T J_3(b_T p_T) f(p_T). \end{aligned} \quad (\text{C.12})$$

More precisely, we will only need the second term, while the first one that is completely symmetry under exchange of the indices  $\mu, \nu, \sigma$  will drop out. Then, using Eq. (C.11), we have

$$\int d^2 \mathbf{p}_T e^{-i \mathbf{p}_T \cdot \mathbf{b}_T} \frac{p_T^\mu p_T^\nu p_T^\sigma}{M^3} f(p_T) = \frac{(-i)^3}{6} M^3 b_T^\nu b_T^\sigma b_T^\mu \tilde{f}^{(3)}(b_T) + (\text{symmetric in } \mu, \nu, \sigma). \quad (\text{C.13})$$

Eq. (C.11) can be inverted using the orthogonality relation of Bessel functions,

$$\int_0^\infty db_T b_T J_n(p_T b_T) J_n(p'_T b_T) = \frac{1}{p_T} \delta(p_T - p'_T), \quad (\text{C.14})$$

from which one easily finds that

$$f(p_T) = \frac{M^{2n}}{2\pi n!} \int_0^\infty db_T b_T \left( \frac{b_T}{p_T} \right)^n J_n(b_T p_T) \tilde{f}^{(n)}(b_T). \quad (\text{C.15})$$

## C.2 Conventions for the TMD FF

In the case of the TMD FF, our convention for the Fourier transform and its inverse is

$$\tilde{D}(\mathbf{b}_T) = \int d^2 \mathbf{k}_T e^{+i \mathbf{b}_T \cdot \mathbf{k}_T} D(\mathbf{k}_T), \quad D(\mathbf{k}_T) = \int \frac{d^2 \mathbf{b}_T}{(2\pi)^2} e^{-i \mathbf{b}_T \cdot \mathbf{k}_T} \tilde{D}(\mathbf{b}_T), \quad (\text{C.16})$$

where  $\tilde{D}(\mathbf{b}_T)$  is the function in Fourier or position space. Compared to the convention for the TMD PDF in Eq. (C.1), this differs by the sign of the Fourier phase. Thus, all identities derived in appendix C.1 can be applied to the TMD FF by simply letting  $\mathbf{b}_T \rightarrow -\mathbf{b}_T$ . Also note that the Fourier transform of the TMD FF is defined with respect to the hadron frame, i.e.  $\mathbf{k}_T$  is the transverse momentum of the parton fragmenting into a hadron relative to the hadron momenta, see Sec. 2.6 for more details.

# D - Explicit definitions of TMD PDFs

In the following, we give more details on all rapidity regulators employed in the literature that give rise to the result in Eq. (2.80), i.e. those that correspond to the  $\overline{\text{MS}}$  scheme. We do not give explicit results for the regulated results of the bare unsubtracted TMD PDF and soft function, but these can be found in [104] for all considered regulators.

## D.1 Wilson lines off the light-cone

In the modern definition by Collins [89], the lightlike direction  $n_a$  and  $n_b$  defined in Eq. (2.19) are replaced by spacelike reference vectors,

$$\begin{aligned} n_a^\mu &= \frac{1}{\sqrt{2}}(1, 0, 0, +1) \quad \rightarrow \quad n_A^\mu(y_A) \equiv n_a^\mu - e^{-2y_A} n_b^\mu = (1, -e^{-2y_A}, \mathbf{0}_T), \\ n_b^\mu &= \frac{1}{\sqrt{2}}(1, 0, 0, -1) \quad \rightarrow \quad n_B^\mu(y_B) \equiv n_b^\mu - e^{+2y_B} n_a^\mu = (-e^{+2y_B}, 1, \mathbf{0}_T). \end{aligned} \quad (\text{D.1})$$

The bare unsubtracted TMD PDF in Eq. (2.37) for a proton close to the  $n_a$  direction is then defined by replacing  $n_b \rightarrow n_B(y_B)$ ,

$$\begin{aligned} f_{i/P}^{0(\text{u})}(x, \mathbf{b}_T, \epsilon, y_B, xP^-) &= \int \frac{db^+}{2\pi} e^{-ib^+(xP^-)} \langle p(P) | \bar{q}(b^\mu) W_{n_B(y_B)}(b^\mu; -\infty, 0) \frac{\gamma^-}{2} W_{n_\perp}(-\infty n_B(y_B), b_T, 0) \\ &\quad \times W_{n_B(y_B)}^\dagger(0; -\infty, 0) q(0) | p(P) \rangle. \end{aligned} \quad (\text{D.2})$$

Similarly, the soft function in Eq. (2.38) is modified as

$$\begin{aligned} S_{n_a n_b}^0(b_T, \epsilon, y_A - y_B) &= \frac{1}{N_c} \langle 0 | \text{Tr}[W_{n_A(y_A)}^\dagger(\mathbf{b}_T; -\infty, 0) W_{n_B(y_B)}(\mathbf{b}_T; -\infty, 0) W_{n_\perp}(-\infty n_B(y_B); b_T, 0) \\ &\quad \times W_{n_B(y_B)}^\dagger(\mathbf{b}_T; -\infty, 0) W_{n_A(y_A)}(\mathbf{b}_T; -\infty, 0) W_{n_\perp}^\dagger(-\infty n_A(y_A); b_T, 0)]_T | 0 \rangle. \end{aligned} \quad (\text{D.3})$$

By Lorentz invariance, the regulated bare soft function only depends on the difference  $y_A - y_B$  [113]. The renormalized TMD PDF is finally constructed as [89]

$$\begin{aligned} f_{i/P}(x, \mathbf{b}_T, \mu, \zeta) &= \lim_{\substack{y_A \rightarrow +\infty \\ y_B \rightarrow -\infty}} Z_{\text{uv}} f_{i/P}^{0(\text{u})}(x, \mathbf{b}_T, \epsilon, y_B, xP^-) \sqrt{\frac{S_{n_a n_b}^0(b_T, \epsilon, y_A - y_B)}{S_{n_a n_b}^0(b_T, \epsilon, y_A - y_B) S_{n_a n_b}^0(b_T, \epsilon, y_n - y_B)}} \\ &= \lim_{y_B \rightarrow -\infty} Z_{\text{uv}} \frac{f_{i/P}^{0(\text{u})}(x, \mathbf{b}_T, \epsilon, y_B, xP^-)}{\sqrt{S_{n_a n_b}^0(b_T, \epsilon, 2y_n - 2y_B)}}, \end{aligned} \quad (\text{D.4})$$

where the result in the last line was derived in [113]. The UV renormalization factor  $Z_{\text{uv}}$  is often further split into a field strength renormalization  $Z_2$  and the operator renormalization  $Z_F$ , i.e.  $Z_{\text{uv}} = Z_2 Z_F$ . In Eq. (D.4),  $y_{A,B}$  are the Wilson line rapidities as defined in Eq. (D.1), and  $y_n$  is an additional rapidity parameter that controls the split of soft radiation into the two TMD PDFs. The  $\zeta$  scale is defined as

$$\zeta = (xP^- e^{-y_n})^2 = (xm_P e^{y_P - y_n})^2, \quad (\text{D.5})$$

where  $y_P$  is the rapidity of the proton.

## D.2 $\delta$ regulator

The  $\delta$  regulator was introduced by Echevarria, Idilbi and Scimemi (EIS) for TMD PDFs in [99] and used to defined TMD PDFs in the notation of Sec. 2.3 in [100]. Here, we briefly present the  $\delta$  regulator as modified in [114–116], which is necessary to be applicable beyond next-to-leading order. For more details on the regulator, we refer to [115].

The  $\delta$  regularization scheme consists of modifying the lightlike Wilson lines appearing in the collinear and soft matrix elements, while the transverse gauge links are not modified. The Wilson lines  $W_n$  appearing in the unsubtracted TMD PDF, see Eq. (2.37), are modified as

$$W_n(x^\mu; -\infty, 0) = P \exp \left[ -ig_s \int_{-\infty}^0 ds n \cdot A^{a0}(x^\mu + sn^\mu) t^a e^{\delta^- s x} \right]. \quad (\text{D.6})$$

Here,  $\delta^-$  is the regulator, which plays the role of  $\tau$  in the unsubtracted TMD PDF  $f_{i/p}^{0(u)}(x, \mathbf{b}_T, \epsilon, \tau, xP^-)$ , and the  $x$  in  $e^{\delta^- s x}$  is the Bjorken momentum fraction of the struck parton. In the soft function defined in Eq. (2.38), the lightlike Wilson lines originally defined in Eq. (2.43) are changed as

$$\begin{aligned} W_n(x^\mu; -\infty, 0) &= P \exp \left[ -ig_s \int_{-\infty}^0 ds n \cdot A^{a0}(x^\mu + sn^\mu) t^a \right] \\ &\rightarrow P \exp \left[ -ig_s \int_{-\infty}^0 ds n \cdot A^{a0}(x^\mu + sn^\mu) t^a e^{\delta^- s} \right], \end{aligned} \quad (\text{D.7})$$

and likewise for the other lightlike Wilson line  $W_{\bar{n}}$ , up to replacing  $\delta^- \rightarrow \delta^+$ .

Note that the  $\delta$  regulator violates gauge invariance, but gauge violation is power suppressed in  $\delta^\pm$  and thus gauge invariance holds as long as  $\delta^\pm$  is kept infinitesimal. In perturbation theory, this regularization procedures amounts to shifting Wilson line vertices as

$$\frac{1}{(k_1^- + i0)(k_2^- + i0)\dots} \rightarrow \frac{1}{(k_1^- + i\delta^-)(k_2^- + 2i\delta^-)\dots}, \quad (\text{D.8})$$

where the  $k_i$  are the momenta of the gluons emitted from a Wilson line  $W_n$ , ordered such that  $k_1$  is closest to  $-\infty$ . The shift in these propagators fully regulates rapidity divergences, such as those in the example integrals in Eqs. (2.71) and (2.78) are regulated. Note that the exponential form of introducing  $\delta^-$  in Eq. (D.7) is crucial for important properties such as non-Abelian exponentiation, see [115] for more details.

With the  $\delta$  regulator, the soft function can be symmetrically split into  $n$ -collinear and  $\bar{n}$ -collinear component as

$$S_{\text{EIS}}^q(b_T, \epsilon, \sqrt{\delta^+ \delta^-}) = \sqrt{S_{\text{EIS}}^q(b_T, \epsilon, \delta^- e^{-y_n})} \sqrt{S_{\text{EIS}}^q(b_T, \epsilon, \delta^+ e^{+y_n})}. \quad (\text{D.9})$$

Here,  $y_n$  is an arbitrary parameter that governs the split of the soft function into the two beam directions. With this regulator, the zero-bin subtraction is equal to the soft function itself,  $S^{0\text{subt}} = S^0$ , and hence one can define the TMD PDF by

$$f_{i/p}(x, \mathbf{b}_T, \mu, \zeta) = \lim_{\substack{\epsilon \rightarrow 0 \\ \delta^- \rightarrow 0}} Z_{uv}^i(\mu, \zeta, \epsilon) \frac{f_{i/p}^{0(u)}(x, \mathbf{b}_T, \epsilon, \delta^-/(xP^-))}{\sqrt{S_{\text{EIS}}^q(b_T, \epsilon, \delta^- e^{-y_n})}}, \quad (\text{D.10})$$

and likewise for the other proton. The Collins-Soper scales are defined as

$$\zeta_a = (x_a P_a^- e^{-y_n})^2, \quad \zeta_b = (x_b P_b^+ e^{+y_n})^2, \quad \zeta_a \zeta_b = Q^4, \quad (\text{D.11})$$

where  $x_{a,b}$  and  $P_{a,b}$  are the momentum fractions and proton momenta entering the two two TMD PDFs, see Eq. (2.29). To relate these results to the generic notation used in Sec. 2.3, one can identify  $1/\tau = \ln(\delta^- e^{-y_n})$ .

### D.3 $\eta$ regulator

The  $\eta$  regulator was introduced by Chiu, Jain, Neill and Rothstein (CJNR) in [102, 109]. It is defined to modify Wilson lines in momentum space, i.e. the Fourier transforms of Eq. (2.43). The lightlike Wilson lines entering in the unsubtracted beam function and soft functions, Eqs. (2.37) and (2.38), are modified as

$$\begin{aligned} f_{i/P}^{0(u)} : \quad W_n &\rightarrow \sum_{\text{perms}} \exp \left[ -g_s w^2 \frac{|\bar{n} \cdot \mathcal{P}_g|^{-\eta}}{\nu^{-\eta}} \frac{\bar{n} \cdot A_n}{\bar{n} \cdot \mathcal{P}} \right], \quad R(k, \eta) = w^2 \left| \frac{k^-}{\nu} \right|^{-\eta}, \\ S_{n_a n_b}^0 : \quad W_n &\rightarrow \sum_{\text{perms}} \exp \left[ -g_s w \frac{|2\mathcal{P}_{g3}|^{-\eta/2}}{\nu^{-\eta/2}} \frac{n \cdot A_s}{n \cdot \mathcal{P}} \right], \quad R(k, \eta) = w \left| \frac{k^z}{\nu} \right|^{-\eta/2}. \end{aligned} \quad (\text{D.12})$$

Here, the function  $R(k, \eta)$  shows the resulting regulating factor as entering the examples in Eqs. (2.71) and (2.78). In Eq. (D.12), the momentum operator  $\mathcal{P}$  picks up the momentum of the gluon fields  $A$ , and  $\eta$  is the rapidity regulator with an associated rapidity scale  $\nu$ . The different powers of  $\eta$  arise because the soft function involves double the number of Wilson lines than the beam function.

A key feature of this regulator is that rapidity divergences manifest themselves as poles in  $1/\eta$  as  $\eta \rightarrow 0$ , which can be removed with a counterterm at the cost of leaving a dependence on the “rapidity scale”  $\nu$ . This is analogous the ultraviolet renormalization, where poles in  $1/\epsilon$  are removed, giving rise to the  $\mu$  dependence. The bookkeeping parameter  $w$  in Eq. (D.12) plays the role of running coupling, and will be set to  $w \rightarrow 1$  after renormalization. In this approach, the Collins-Soper evolution is identical to the evolution in  $\nu$ , and the CS kernel is obtained as the anomalous dimension associated with removing poles in  $\eta$ .

In the  $\eta$  regulator, the soft zero-bin subtraction is absent, as  $S_{n_a n_b}^{0\text{subt}} = 1$ . In terms of the notation of Sec. 2.2, we have

$$\eta = \tau, \quad \zeta = (x P^-)^2, \quad y_n = 0. \quad (\text{D.13})$$

The choice of fixing  $y_n = 0$  arises because of the symmetric treatment of the two beam functions, but can be relaxed as in the other definitions if so desired.

Finally, we remark that while the  $\eta$  regulator can be used to combine unsubtracted beam and soft functions into the TMD PDF, as in Eq. (2.33), it is usually applied such that these functions are renormalized separately, see Eqs. (2.34) and (2.35).

### D.4 Exponential regulator

In contrast to the previous regulators, the exponential regulator introduced in [105] does not directly modify the lightlike Wilson lines appearing in Eqs. (2.37) and (2.38), but modifies

the phase space of each real emissions in the perturbative calculation by a factor

$$R(k, \tau) = \exp[-k^0 \tau e^{-\gamma_E}]. \quad (\text{D.14})$$

One then takes the  $\tau \rightarrow 0$  limit, keeping only divergent terms. The individual beam and soft functions obtained in this manner are not  $\tau$  independent. Instead, the  $\tau$  evolution is identical to the rapidity RGE of the  $\eta$  regulator. Hence, similar to a Wilsonian approach, the cutoff  $\tau$  plays both the role of regulating divergences and being the evolution variable. Of course, as usual the  $\tau$  dependence cancels after combining beam and soft functions into the TMD PDF, exposing the standard CS evolution.

The exponential regulator can also be viewed as extending the unsubtracted TMD PDF and soft functions in position space, which only depend on  $(b^+, \mathbf{b}_T)$  and  $\mathbf{b}_T$ , respectively, to depend on the full fourvector  $b^\mu$ . To be precise, for the soft function one can write

$$S_{n_a n_b}^0(b_T, \epsilon, \tau) = \lim_{\tau \rightarrow 0} S_{n_a n_b}^0(b^+ = i\tau e^{-\gamma_E}, b^- = i\tau e^{-\gamma_E}, b_T, \epsilon, \tau), \quad (\text{D.15})$$

where the soft function of the right-hand sides depends on  $b^\mu = (b^+, b^-, \mathbf{b}_T)$ , and one takes the lightcone momenta to zero. Its definition is analogous to that in Eq. (2.38), but with all Wilson lines ending at  $\mathbf{b}_T$  now being shifted to  $b^\mu$ . A similar equation holds for the unsubtracted TMD PDF, where the matrix element is extended to the  $b^+ = i\tau e^{-\gamma_E}$  direction. In this approach, it is clear that the  $\tau$  regulator is equivalent to modifying Wilson lines, and thus by construction is gauge-invariant even before taking the limit  $\tau \rightarrow 0$ .

Another advantage of Eq. (D.15) is that it connects the TMD soft function to the fully-differential soft function, which allowed for the calculation of the soft function using the exponential regulator to three loops [155]. Recently, also the quark beam functions has been calculated at N<sup>3</sup>LO in this regulator [156], completing the three-loop calculation of the TMD PDF.

## D.5 Analytic and pure rapidity regulator

The analytic regulator was first introduced in Becher and Neubert (BN) in [96] for TMDs and later modified in [117]. In the latter formulation, it is implemented by modifying the phase space for all real emissions by

$$R(k, \alpha) = \left(\frac{\nu}{k^+}\right)^\alpha, \quad (\text{D.16})$$

and then letting  $\alpha \rightarrow 0$ , which exposes poles in  $1/\alpha$ . In this approach, the soft function is absent,  $S_{n_a n_b}^0 \equiv 1$  to all orders in perturbation theory. Thus, in order to obtain a well-defined TMD PDF, one has to calculate both the  $n_a$ -collinear and  $n_b$ -collinear unsubtracted TMD PDFs, which can be combined to obtain the physical TMD PDFs,

$$\begin{aligned} & \lim_{\substack{\epsilon \rightarrow 0 \\ \alpha \rightarrow 0}} \left[ f_{q/n_a}^{0(u), \text{BN}}(x_1, \mathbf{b}_T, \epsilon, \alpha) f_{q/n_b}^{0(u), \text{BN}}(x_2, \mathbf{b}_T, \epsilon, \alpha) \right] \\ &= \left( \frac{b_T^2 Q^2}{b_0^2} \right)^{-\gamma_\zeta^q(\mu, b_T)} f_{q/n_a}^{\text{BN}}(x_1, \mathbf{b}_T, \mu) f_{q/n_b}^{\text{BN}}(x_2, \mathbf{b}_T, \mu). \end{aligned} \quad (\text{D.17})$$

Note that in this formulation, the TMD PDFs are explicitly independent of  $\zeta$ , as the combined  $\zeta$  dependence is pulled out in the form of the prefactor depending on  $Q^2 = \sqrt{\zeta_a \zeta_b}$ . In the language of [96], the origin of this factor is attributed to the collinear anomaly, which is equivalent to the occurrence of rapidity divergences.

Since Eq. (D.16) only depends on  $k^+$ , not on  $k^-$ , the resulting TMD PDFs  $f_{q/n_a}^{0(u),BN}$  and  $f_{q/n_b}^{0(u),BN}$  are not symmetric. A symmetric formulation of Eq. (D.16) was given in [118] as

$$R(k, \eta) = w^2 v^2 \left| \frac{k^+}{k^-} \right|^{-\eta/2}. \quad (\text{D.18})$$

This regulator was named “pure rapidity regulator”, as the combination  $y_k = \frac{1}{2} \ln(k^+/k^-)$  precisely corresponds to the rapidity of a real emission with momentum  $k$ . Employing Eq. (D.18), one obtains symmetric results for the TMD PDFs in the  $n_a$  and  $n_b$  direction, and poles in  $1/\eta$  as  $\eta \rightarrow 0$  can be renormalized, which yields TMD PDFs to obtain TMD PDFs identical to those of Eq. (D.12).

## E - Expansions for evolution kernels

In this appendix we collect formulas for perturbative expansions of the evolution kernels that enter the solution of RGEs and RRGEs in Sec. 4. They are conveniently expressed in terms of the integrals of anomalous dimensions:

$$\begin{aligned} K_\Gamma(\mu_L, \mu) &= \int_{\mu_L}^\mu \frac{d\mu'}{\mu'} \Gamma_{\text{cusp}}[\alpha_s(\mu')] \ln \frac{\mu'}{\mu_L} \\ \eta_\Gamma(\mu_L, \mu) &= \int_{\mu_L}^\mu \frac{d\mu'}{\mu'} \Gamma_{\text{cusp}}[\alpha_s(\mu')], \quad K_\gamma(\mu_L, \mu) = \int_{\mu_L}^\mu \frac{d\mu'}{\mu'} \gamma[\alpha_s(\mu')]. \end{aligned} \quad (\text{E.1})$$

Direct integration of these expressions is complicated by the  $\mu$  evolution of  $\alpha_s(\mu)$ , which must be taken into account to all orders when there are large logs. The cusp and non-cusp anomalous dimensions themselves have the expansions

$$\Gamma_{\text{cusp}}[\alpha_s(\mu)] = \sum_{n=0}^{\infty} \left( \frac{\alpha_s(\mu)}{4\pi} \right)^{n+1} \Gamma_n, \quad \gamma[\alpha_s(\mu)] = \sum_{n=0}^{\infty} \left( \frac{\alpha_s(\mu)}{4\pi} \right)^{n+1} \gamma_n, \quad (\text{E.2})$$

where the coefficients  $\Gamma_n, \gamma_n$  are constants, equivalently in the notation of CSS in Table 4.1 for quarks,

$$\gamma_K = \sum_{n=1}^{\infty} \gamma_K^{(n)} \left( \frac{\alpha_s}{\pi} \right)^n, \quad \gamma_q = \sum_{n=1}^{\infty} \gamma_q^{(n)} \left( \frac{\alpha_s}{\pi} \right)^n. \quad (\text{E.3})$$

The accuracy of resummation is achieved by including anomalous dimensions in evolution kernels to the orders given in Table 4.2; for instance, to next-to-leading-log (NLL) accuracy the required anomalous dimension coefficients are:  $\gamma_K^{(1)}, \gamma_K^{(2)}$  and  $\gamma_i^{(1)}$ . They are spin-independent [63, 83, 171, 240, 243, 309, 1113, 1334, 1335], and are given for quark TMD PDFs

by

$$\gamma_K^{(1)} = \frac{\Gamma_0^q}{2} = 2C_F, \quad \gamma_K^{(2)} = \frac{\Gamma_1^q}{8} = C_F \left[ C_A \left( \frac{67}{18} - \frac{\pi^2}{6} \right) - \frac{10}{9} T_F n_f \right], \quad \gamma_q^{(1)} = \frac{\gamma_\mu^{q,0}}{4} = \frac{3}{2} C_F, \quad (\text{E.4})$$

where  $C_F = 4/3$ ,  $C_A = 3$ ,  $T_F = 1/2$  and  $n_f$  is the number of active flavors. Higher-order coefficients and results for gluons TMD PDFs are given below.

The integrals over  $\mu$  in Eq. (E.1) can be evaluated nicely in closed form at each order of resummed accuracy by changing integration variables<sup>43</sup> in Eq. (E.1) [236, 253]:

$$\frac{d\mu}{\mu} = \frac{d\alpha_s}{\beta[\alpha_s]}, \quad \ln \frac{\mu}{\mu_L} = \int_{\alpha_s(\mu_L)}^{\alpha_s(\mu)} \frac{d\alpha_s}{\beta[\alpha_s]}. \quad (\text{E.5})$$

The  $\beta$  function has the expansion

$$\beta[\alpha_s(\mu)] = -2\alpha_s(\mu) \sum_{n=0}^{\infty} \left( \frac{\alpha_s(\mu)}{4\pi} \right)^{n+1} \beta_n. \quad (\text{E.6})$$

Using these expansions, we can evaluate Eq. (E.1) order by order (see, e.g., [236, 237, 254]):

$$\begin{aligned} K_\Gamma(\mu_L, \mu) = & \frac{\Gamma_0}{4\beta_0^2} \left\{ \frac{4\pi}{\alpha_s(\mu_L)} \left( \ln r + \frac{1}{r} - 1 \right) + \left( \frac{\Gamma_1}{\Gamma_0} - \frac{\beta_1}{\beta_0} \right) (r - 1 - \ln r) - \frac{\beta_1}{2\beta_0} \ln^2 r \right. \\ & + \frac{\alpha_s(\mu_L)}{4\pi} \left[ B_2 \left( \frac{r^2 - 1}{2} - \ln r \right) + \left( \frac{\beta_1 \Gamma_1}{\beta_0 \Gamma_0} - \frac{\beta_1^2}{\beta_0^2} \right) (r - 1 - r \ln r) + \left( \frac{\Gamma_2}{\Gamma_0} - \frac{\beta_1 \Gamma_1}{\beta_0 \Gamma_0} \right) \frac{(1-r)^2}{2} \right] \\ & + \left( \frac{\alpha_s(\mu_L)}{4\pi} \right)^2 \left[ \left( \frac{\Gamma_3}{\Gamma_0} - \frac{\Gamma_2 \beta_1}{\Gamma_0 \beta_0} + \frac{\Gamma_1}{\Gamma_0} B_2 + B_3 \right) \frac{r^3 - 1}{3} - \frac{B_3}{2} \ln r - B_2 \left( \frac{\Gamma_1}{\Gamma_0} - \frac{\beta_1}{\beta_0} \right) (r - 1) \right. \\ & \left. - \frac{\beta_1}{2\beta_0} \left( \frac{\Gamma_2}{\Gamma_0} - \frac{\Gamma_1 \beta_1}{\Gamma_0 \beta_0} + B_2 \right) r^2 \ln r + \left( -\frac{2\Gamma_3}{\Gamma_0} + \frac{3\Gamma_2 \beta_1}{\Gamma_0 \beta_0} - \frac{\Gamma_1 \beta_1^2}{\Gamma_0 \beta_0^2} + \frac{\beta_3}{\beta_0} - \frac{\beta_1 \beta_2}{\beta_0^2} \right) \frac{r^2 - 1}{4} \right] + \dots \right\}. \end{aligned} \quad (\text{E.7})$$

organized in groups of terms of order  $1/\alpha_s$  (LL),  $1$  (NLL),  $\alpha_s$  (NNLL), and  $\alpha_s^2$  ( $N^3LL$ ) in log counting, with the  $\dots$  denoting terms of higher order. Large logs of  $\mu/\mu_L$  are essentially captured in the ratio  $r$ :

$$r \equiv r(\mu_L, \mu) = \frac{\alpha_s(\mu)}{\alpha_s(\mu_L)}. \quad (\text{E.8})$$

In Eq. (E.7), the coefficients  $B_{2,3}$  are given by

$$B_2 \equiv \frac{\beta_1^2}{\beta_0^2} - \frac{\beta_2}{\beta_0}, \quad B_3 \equiv -\frac{\beta_1^3}{\beta_0^3} + \frac{2\beta_1 \beta_2}{\beta_0^2} - \frac{\beta_3}{\beta_0}, \quad (\text{E.9})$$

---

<sup>43</sup>See [254, 1336] for commentary on how using Eq. (E.5) at a truncated perturbative order may affect explicit RG invariance (i.e.  $\mu$  independence) of a resummed cross section using resulting expansions of Eq. (E.1). See also [1333] [add details].

which come from expanding  $1/\beta[\alpha_s]$  in Eq. (E.5). Meanwhile the  $\eta_\Gamma$  kernel has the expansion:

$$\begin{aligned}\eta_\Gamma(\mu_L, \mu) = & -\frac{\Gamma_0}{2\beta_0} \left[ \ln r + \frac{\alpha_s(\mu_L)}{4\pi} \left( \frac{\Gamma_1}{\Gamma_0} - \frac{\beta_1}{\beta_0} \right) (r-1) + \left( \frac{\alpha_s(\mu_L)}{4\pi} \right)^2 \left( B_2 + \frac{\Gamma_2}{\Gamma_0} - \frac{\Gamma_1\beta_1}{\Gamma_0\beta_0} \right) \frac{r^2-1}{2} \right. \\ & \left. + \left( \frac{\alpha_s(\mu_L)}{4\pi} \right)^3 \left( B_3 + \frac{\Gamma_1}{\Gamma_0} B_2 - \frac{\Gamma_2\beta_1}{\Gamma_0\beta_0} + \frac{\Gamma_3}{\Gamma_0} \right) \frac{r^3-1}{3} + \dots \right].\end{aligned}\quad (\text{E.10})$$

The terms in this expression are one power of  $\alpha_s$  smaller than the corresponding terms in  $K_\Gamma$  in Eq. (E.7), but should be kept to the same corresponding order, i.e. in  $\eta_\Gamma$ , we keep the  $\mathcal{O}(1)$  term at LL, the  $\mathcal{O}(\alpha_s)$  terms at NLL,  $\mathcal{O}(\alpha_s^2)$  at NNLL, and  $\mathcal{O}(\alpha_s^3)$  at N<sup>3</sup>LL. This is because of the way the combination of  $K_\Gamma$  and  $\eta_\Gamma$  appears in the evolution kernels, e.g. Eq. (4.65) or Eq. (4.69), with  $\eta_\Gamma$  always multiplied by another log. See also [237].

The non-cusp kernel  $K_\gamma$  in Eq. (E.1) has the same expansion as Eq. (E.10) with  $\Gamma_n \rightarrow \gamma_n$ . For  $K_\gamma$ , the expansion can be truncated according to the standard counting,  $\mathcal{O}(1/\alpha_s)$  at LL (in this case, zero),  $\mathcal{O}(1)$  at NLL,  $\mathcal{O}(\alpha_s)$  at NNLL, etc.

*[to add more]*

# List of acronyms

AdS	Anti-DeSitter
BFKL	Balitsky-Fadin-Kuraev-Lipatov
BH	Bethe-Heitler
BN	Becher-Neubert
CGC	Color glass condensate
CM	Center of momentum
CJNR	Chiu-Jain-Neill-Rothstein
CSS	Collins-Soper-Sterman
CS	Collins-Soper
DGLAP	Dokshitzer-Gribov-Lipatov-Altarelli-Parisi
DA	Distribution amplitude
dof	Degrees of freedom
DVCS	Deeply virtual Compton scattering
DWF	Domain wall fermion
DY	Drell-Yan
EEC	Energy-energy-correlations
EIC	Electron-Ion collider
EIS	Echevarria-Idilbi-Scimemi
EMSTVZ	Ebert-Moult-Stewart-Tackmann-Vita-Zhu
EMT	Energy-momentum tensor
FF	Fragmentation function
FJF	Fragmenting Jet Function
GFIP	Gluon Fragmentation Improved PYTHIA
GPD	Generalized parton distribution function
CTMD	Generalized transverse momentum dependent parton distribution function
ITD	Ioffe time distribution
iTMD	improved TMD
IPD	Impact parameter distribution
JFF	Jet Fragmentation Function
JIMWLK	Jalilian-Marian-Iancu-McLerran-Weigert-Leonidov-Kovner
JM	Jaffe-Manohar
JMY	Ji-Ma-Yuan
LaMET	large-momentum effective theory
LCWF	Light-cone wave function
LCS	Lattice cross sections
LDME	Long distance matrix elements
LFCM	Light front constituent model
LIR	Lorentz-invariance relation
LL	Leading log
LLx	Leading Log in x
LNZ	Li-Neill-Zhu

---

LO	Leading order
LQCD	Lattice Quantum Chromodynamics
MHENS	Musch-Hägler-Engelhardt-Negele-Schäfer
MS ( $\overline{\text{MS}}$ )	Minimal Subtraction (MS-bar)
MV	McLerran-Venugopalan
NLL	Next-to-leading log
NLLx	Next-to-leading log in
NNLL	Next-to-next-to-leading log
$\text{N}^3\text{LL}$	Next-to-next-to-next-to-leading log
NLO	Next-to-leading order
NNLO	Next-to-next-to-leading order
N3LO	Next-to-next-to-next-to-leading order
NRQCD	Non-relativistic QCD
nTMDs	nuclear TMDs
OAM	Orbital angular momentum
OPE	Operator product expansion
PDF	Parton distribution function
pQCD	perturbative quantum chromodynamics
QCD	quantum chromodynamics
qLIR	Quark model Lorentz invariance relations
QS	Qiu-Sterman (function)
QGP	Quark-gluon plasma
RI/MOM	regularization independent momentum subtraction
RGE	Renormalization group equation
RRGE	Rapidity RGE
SCET	Soft-Collinear Effective Theory
SIDIS	Semi-inclusive deep-inelastic scattering
SISCone	SeedlessCone
SSA	Single-spin asymmetry
TEEC	Transverse-energy-energy-correlations
TMD	Tranverse momentum dependent
TMD FJFs	TMD Fragmenting jet functions
TMD PFFs	TMD Polarized fragmentation functions
TMDs	Transverse momentum dependent distributions
UGD	Unintegrated gluon distributions
WW	Wandzura-Wilczek

# Errata and Chapter Contacts

Please report any typos or errors that you spot in the Handbook in this Google Document.

For questions and comments on specific chapters in the handbook, which are not just typos, please use the following links:

Chapter 1: Send email to Sean Fleming and Jian-Wei Qiu

Chapter 2: Send email to Markus Ebert, Alexei Prokudin, and Iain Stewart

Chapter 3: Send email to Iain Stewart

Chapter 4: Send email to Leonard Gamberg, Christopher Lee, and Thomas Mehen

Chapter 5: Send email to Zhong-Bo Kang, Daniel Pitonyak, Alexei Prokudin, and Marc Schlegel

Chapter 6: Send email to Martha Constantinou, William Detmold, Michael Engelhardt, Keh-Fei Liu, Phiala Shanahan, and Yong Zhao

Chapter 7: Send email to Matthias Burkardt, Andreas Metz, and Peter Schweitzer

Chapter 8: Send email to Renaud Boussarie, Andrey Tarasov, Raju Venugopalan, and Feng Yuan

Chapter 9: Send email to Zhong-Bo Kang, Thomas Mehen, and Ivan Vitev

Chapter 10: Send email to Leonard Gamberg, Andreas Metz, Marc Schlegel, and Iain Stewart

Chapter 11: Send email to Michael Engelhardt, Simonetta Liuti, Andreas Metz, and Feng Yuan

General: Send email to Thomas Mehen and Iain Stewart

# Index

AdS/QCD model	240	lensing function	247
bag model	239	lightfront constituent models	239
Breit frame	295	long-distance matrix element (LDME)	291
Burkardt sum rule	256	medium-induced bremsstrahlung	298
Cahn effect	149, 175	models	233–262
chiral quark soliton model	241	multi-step fragmentation	252
Collins-Soper evolution kernel		Nambu–Jona-Lasinio model	240, 251
Lattice calculations	229–231	non-relativistic limit	236
cone algorithms	281	Non-Relativistic QCD	291
covariant parton model	237	NRQCD with Glauber gluons	306
deeply virtual Compton scattering (DVCS)	334	nuclear matter transport properties	302
diffractive di-jet production	340	opacity expansion	299
Efremov-Teryaev-Qiu-Sterman matrix element		orbital angular momentum (OAM)	261, 342,
149		343, 348	
electron-ion collider (EIC)	340	parton energy loss	298
energy-energy correlation (EEC)	293	parton model	235
final state interactions	349	positivity	255
GPD	334, 335	Proton spin crisis	197
groomed soft-dropped momentum sharing		Pseudo-PDF	212–213
distribution	305	Qiu-Sterman (QS) function	161–173
GTMD	83, 338	Quark-model Lorentz-invariance relations	
Hadronic jets	281	(qLIRs)	258
Heavy quarkonia	291	quark-target model	246
Husimi distribution	352	Quasi-PDF	203
impact parameter distribution	334, 338	Schäfer-Teryaev sum rule	257
in-medium splitting kernels	299	semi-inclusive jet function	286
instantons	248	sequential clustering algorithms	281
jet algorithms	281	small-x region	340
jet fragmentation function	286	soft factor	339
jet substructure	281	spectator model	240, 250
jet-medium interactions	282	Spin decomposition	
Landau-Pomeranchuk-Migdal effect	298	Jaffe-Manohar	196, 349
large- $N_c$ limit	236	Ji	196, 198, 349
Large-momentum effective theory	203	spin-orbit correlation	348, 350
Lattice QCD	190–193	TMD quarkonium shape function	293
Lattice QCD calculations		Transverse-energy-energy correlations (TEEC)	
GTMDs	348	293	
TMDs	216	universality	254
twist-3 TMDs	320	Wigner distribution	335, 351

# References

- [1] K. G. Wilson, *Confinement of Quarks*, *Phys. Rev.* **D10** (1974) 2445.
- [2] N. Brambilla et al., *QCD and Strongly Coupled Gauge Theories: Challenges and Perspectives*, *Eur. Phys. J.* **C74** (2014) 2981 [[1404.3723](#)].
- [3] D. J. Gross and F. Wilczek, *Ultraviolet Behavior of Nonabelian Gauge Theories*, *Phys. Rev. Lett.* **30** (1973) 1343.
- [4] H. D. Politzer, *Reliable Perturbative Results for Strong Interactions?*, *Phys. Rev. Lett.* **30** (1973) 1346.
- [5] J. C. Collins, D. E. Soper and G. F. Sterman, *Factorization of Hard Processes in QCD*, *Adv.Ser.Direct.High Energy Phys.* **5** (1988) 1 [[hep-ph/0409313](#)].
- [6] M. Bartusiak, *Who ordered the Muon?*,  
<https://www.nytimes.com/1987/09/27/books/science-technology-who-ordered-the-muon.html>
- [7] E. D. Bloom et al., *High-Energy Inelastic e p Scattering at 6-Degrees and 10-Degrees*, *Phys. Rev. Lett.* **23** (1969) 930.
- [8] R. P. Feynman, *Very high-energy collisions of hadrons*, *Phys. Rev. Lett.* **23** (1969) 1415.
- [9] S. Drell and T.-M. Yan, *Massive Lepton Pair Production in Hadron-Hadron Collisions at High-Energies*, *Phys. Rev. Lett.* **25** (1970) 316.
- [10] J. Collins, *Foundations of perturbative QCD*, *Cambridge monographs on particle physics, nuclear physics, and cosmology* **32** (2011) 1.
- [11] M. Constantinou et al., *Parton distributions and lattice QCD calculations: toward 3D structure*, [2006.08636](#).
- [12] J. She, J. Zhu and B.-Q. Ma, *Pretzelosity  $h(1T)^{**}$ perpendicular and quark orbital angular momentum*, *Phys. Rev.* **D79** (2009) 054008 [[0902.3718](#)].
- [13] H. Avakian, A. V. Efremov, P. Schweitzer and F. Yuan, *The transverse momentum dependent distribution functions in the bag model*, *Phys. Rev.* **D81** (2010) 074035 [[1001.5467](#)].
- [14] A. Efremov, P. Schweitzer, O. Teryaev and P. Zavada, *Images of Quark Intrinsic Motion in Covariant Parton Model*, *PoS DIS2010* (2010) 253 [[1008.3827](#)].
- [15] A. Accardi et al., *Electron Ion Collider: The Next QCD Frontier*, *Eur. Phys. J.* **A52** (2016) 268 [[1212.1701](#)].
- [16] J. C. Collins and D. E. Soper, *Back-To-Back Jets: Fourier Transform from B to K-Transverse*, *Nucl.Phys.* **B197** (1982) 446.

- [17] JEFFERSON LAB ANGULAR MOMENTUM collaboration, J. Cammarota, L. Gamberg, Z.-B. Kang, J. A. Miller, D. Pitonyak, A. Prokudin et al., *Origin of single transverse-spin asymmetries in high-energy collisions*, *Phys. Rev. D* **102** (2020) 054002 [2002.08384].
- [18] A. Bacchetta, U. D'Alesio, M. Diehl and C. Miller, *Single-spin asymmetries: The Trento conventions*, *Phys. Rev. D* **70** (2004) 117504 [hep-ph/0410050].
- [19] Y. Aoki et al., *FLAG Review 2021*, 2111.09849.
- [20] K.-F. Liu and S.-J. Dong, *Origin of difference between anti-d and anti-u partons in the nucleon*, *Phys. Rev. Lett.* **72** (1994) 1790 [hep-ph/9306299].
- [21] K.-F. Liu, *Parton degrees of freedom from the path integral formalism*, *Phys. Rev. D* **62** (2000) 074501 [hep-ph/9910306].
- [22] K.-F. Liu, *Parton Distribution Function from the Hadronic Tensor on the Lattice*, PoS **LATTICE2015** (2016) 115 [1603.07352].
- [23] U. Aglietti, M. Ciuchini, G. Corbo, E. Franco, G. Martinelli and L. Silvestrini, *Model independent determination of the light cone wave functions for exclusive processes*, *Phys. Lett. B* **441** (1998) 371 [hep-ph/9806277].
- [24] A. Abada, P. Boucaud, G. Herdoiza, J. P. Leroy, J. Micheli, O. Pene et al., *Preliminaries on a lattice analysis of the pion light cone wave function: A Partonic signal?*, *Phys. Rev. D* **64** (2001) 074511 [hep-ph/0105221].
- [25] W. Detmold and C. D. Lin, *Deep-inelastic scattering and the operator product expansion in lattice QCD*, *Phys. Rev. D* **73** (2006) 014501 [hep-lat/0507007].
- [26] V. Braun and D. MÄijller, *Exclusive processes in position space and the pion distribution amplitude*, *Eur. Phys. J. C* **55** (2008) 349 [0709.1348].
- [27] B. U. Musch, P. Hagler, J. W. Negele and A. Schafer, *Exploring quark transverse momentum distributions with lattice QCD*, *Phys. Rev. D* **83** (2011) 094507 [1011.1213].
- [28] X. Ji, *Parton Physics on a Euclidean Lattice*, *Phys. Rev. Lett.* **110** (2013) 262002 [1305.1539].
- [29] X. Ji, *Parton Physics from Large-Momentum Effective Field Theory*, *Sci.China Phys.Mech.Astron.* **57** (2014) 1407 [1404.6680].
- [30] X. Ji, Y.-S. Liu, Y. Liu, J.-H. Zhang and Y. Zhao, *Large-Momentum Effective Theory*, 2004.03543.
- [31] A. V. Radyushkin, *Quasi-parton distribution functions, momentum distributions, and pseudo-parton distribution functions*, *Phys. Rev. D* **96** (2017) 034025 [1705.01488].
- [32] A. J. Chambers, R. Horsley, Y. Nakamura, H. Perlt, P. E. L. Rakow, G. Schierholz et al., *Nucleon Structure Functions from Operator Product Expansion on the Lattice*, *Phys. Rev. Lett.* **118** (2017) 242001 [1703.01153].

- [33] Y.-Q. Ma and J.-W. Qiu, *Exploring Partonic Structure of Hadrons Using ab initio Lattice QCD Calculations*, *Phys. Rev. Lett.* **120** (2018) 022003 [[1709.03018](#)].
- [34] Y.-Q. Ma and J.-W. Qiu, *Extracting Parton Distribution Functions from Lattice QCD Calculations*, *Phys. Rev.* **D98** (2018) 074021 [[1404.6860](#)].
- [35] C. W. Gardiner and D. P. Majumdar, *Effect of a transverse momentum distribution in the parton model*, *Phys. Rev.* **D2** (1970) 2040.
- [36] V. N. Gribov and L. N. Lipatov, *Deep inelastic e p scattering in perturbation theory*, *Sov. J. Nucl. Phys.* **15** (1972) 438.
- [37] L. N. Lipatov, *The parton model and perturbation theory*, *Sov. J. Nucl. Phys.* **20** (1975) 94.
- [38] G. Altarelli and G. Parisi, *Asymptotic Freedom in Parton Language*, *Nucl. Phys.* **B126** (1977) 298.
- [39] Y. L. Dokshitzer, *Calculation of the Structure Functions for Deep Inelastic Scattering and e+e- Annihilation by Perturbation Theory in Quantum Chromodynamics.*, *Sov. Phys. JETP* **46** (1977) 641.
- [40] J. C. Collins, *What exactly is a parton density?*, *Acta Phys. Polon.* **B34** (2003) 3103 [[hep-ph/0304122](#)].
- [41] D. E. Soper, *Partons and Their Transverse Momenta in QCD*, *Phys. Rev. Lett.* **43** (1979) 1847.
- [42] J. P. Ralston and D. E. Soper, *Drell-Yan model at measured  $Q_T$ : Asymptotic smallness of one loop corrections*, *Nucl. Phys.* **B172** (1980) 445.
- [43] J. C. Collins, *Algorithm to compute corrections to the Sudakov form-factor*, *Phys. Rev.* **D22** (1980) 1478.
- [44] J. C. Collins, D. E. Soper and G. Sterman, *Does the Drell-Yan cross-section factorize?*, *Phys. Lett.* **B109** (1982) 388.
- [45] J. C. Collins, D. E. Soper and G. F. Sterman, *Factorization for One Loop Corrections in the Drell-Yan Process*, *Nucl. Phys.* **B223** (1983) 381.
- [46] A. V. Belitsky, X. Ji and F. Yuan, *Final state interactions and gauge invariant parton distributions*, *Nucl. Phys.* **B656** (2003) 165 [[hep-ph/0208038](#)].
- [47] D. W. Sivers, *Single spin production asymmetries from the hard scattering of point-like constituents*, *Phys. Rev.* **D41** (1990) 83.
- [48] R. Klem, J. Bowers, H. Courant, H. Kagan, M. Marshak, E. Peterson et al., *Measurement of Asymmetries of Inclusive Pion Production in Proton Proton Interactions at 6-GeV/c and 11.8-GeV/c*, *Phys. Rev. Lett.* **36** (1976) 929.

- [49] W. Dragoset, J. Roberts, J. Bowers, H. Courant, H. Kagan et al., *Asymmetries in Inclusive Proton-Nucleon Scattering at 11.75-GeV/c*, *Phys.Rev.* **D18** (1978) 3939.
- [50] J. Antille, L. Dick, L. Madansky, D. Perret-Gallix, M. Werlen et al., *spin dependence of the inclusive reaction p p (polarized) to pi0 X at 24-GeV/c for high p(t) pi0 produced in the central region*, *Phys.Lett.* **B94** (1980) 523.
- [51] V. Apokin, Y. Aretev, O. Astafev, N. Belikov, B. Chuiko et al., *Observation of significant spin effects in hard collisions at 40-GeV/c*, *Phys.Lett.* **B243** (1990) 461.
- [52] S. Saroff, B. Baller, G. Blazey, H. Courant, K. J. Heller et al., *Single spin asymmetry in inclusive reactions: polarized p,p goes to pi+, pi-, and p at high p(t) at 13.3-GeV/c and 18.5-GeV/c*, *Phys.Rev.Lett.* **64** (1990) 995.
- [53] E581 COLLABORATION, E704 COLLABORATION collaboration, D. Adams et al., *Comparison of spin asymmetries and cross-sections in pi0 production by 200-GeV polarized anti-protons and protons*, *Phys.Lett.* **B261** (1991) 201.
- [54] FNAL-E704 collaboration, D. L. Adams et al., *Analyzing power in inclusive pi+ and pi- production at high x(F) with a 200-GeV polarized proton beam*, *Phys. Lett.* **B264** (1991) 462.
- [55] C. A. Aidala, S. D. Bass, D. Hasch and G. K. Mallot, *The Spin Structure of the Nucleon*, *Rev. Mod. Phys.* **85** (2013) 655 [[1209.2803](#)].
- [56] J.-P. Chen, *QCD evolution and TMD/Spin experiments*, *Int.J.Mod.Phys.Conf.Ser.* **20** (2012) 45.
- [57] J. C. Collins, *Fragmentation of transversely polarized quarks probed in transverse momentum distributions*, *Nucl.Phys.* **B396** (1993) 161 [[hep-ph/9208213](#)].
- [58] S. J. Brodsky, D. S. Hwang and I. Schmidt, *Final-state interactions and single-spin asymmetries in semi-inclusive deep inelastic scattering*, *Phys. Lett.* **B530** (2002) 99 [[hep-ph/0201296](#)].
- [59] J. C. Collins, *Leading twist single transverse-spin asymmetries: Drell-Yan and deep inelastic scattering*, *Phys.Lett.* **B536** (2002) 43 [[hep-ph/0204004](#)].
- [60] D. Boer and P. J. Mulders, *Time reversal odd distribution functions in lepto-production*, *Phys. Rev.* **D57** (1998) 5780 [[hep-ph/9711485](#)].
- [61] R. D. Tangerman and P. J. Mulders, *Intrinsic transverse momentum and the polarized Drell-Yan process*, *Phys. Rev.* **D51** (1995) 3357 [[hep-ph/9403227](#)].
- [62] P. J. Mulders and R. D. Tangerman, *The complete tree-level result up to order 1/Q for polarized deep-inelastic lepto-production*, *Nucl. Phys.* **B461** (1996) 197 [[hep-ph/9510301](#)].
- [63] J. C. Collins, D. E. Soper and G. Sterman, *Transverse Momentum Distribution in Drell-Yan Pair and W and Z Boson Production*, *Nucl. Phys.* **B250** (1985) 199.

- [64] D. de Florian and M. Grazzini, *Next-to-next-to-leading logarithmic corrections at small transverse momentum in hadronic collisions*, *Phys. Rev. Lett.* **85** (2000) 4678 [[hep-ph/0008152](#)].
- [65] D. de Florian and M. Grazzini, *The Structure of large logarithmic corrections at small transverse momentum in hadronic collisions*, *Nucl. Phys.* **B616** (2001) 247 [[hep-ph/0108273](#)].
- [66] S. Catani, D. de Florian and M. Grazzini, *Universality of nonleading logarithmic contributions in transverse momentum distributions*, *Nucl.Phys.* **B596** (2001) 299 [[hep-ph/0008184](#)].
- [67] S. Catani, L. Cieri, G. Ferrera, D. de Florian and M. Grazzini, *Vector boson production at hadron colliders: a fully exclusive QCD calculation at NNLO*, *Phys. Rev. Lett.* **103** (2009) 082001 [[0903.2120](#)].
- [68] S. Catani, L. Cieri, D. de Florian, G. Ferrera and M. Grazzini, *Vector boson production at hadron colliders: hard-collinear coefficients at the NNLO*, *Eur. Phys. J.* **C72** (2012) 2195 [[1209.0158](#)].
- [69] G. Bozzi, S. Catani, G. Ferrera, D. de Florian and M. Grazzini, *Production of Drell-Yan lepton pairs in hadron collisions: Transverse-momentum resummation at next-to-next-to-leading logarithmic accuracy*, *Phys. Lett.* **B696** (2011) 207 [[1007.2351](#)].
- [70] S. Catani, L. Cieri, D. de Florian, G. Ferrera and M. Grazzini, *Universality of transverse-momentum resummation and hard factors at the NNLO*, *Nucl. Phys.* **B881** (2014) 414 [[1311.1654](#)].
- [71] J. C. Collins and F. Hautmann, *Infrared divergences and non-lightlike eikonal lines in Sudakov processes*, *Phys. Lett.* **B472** (2000) 129 [[hep-ph/9908467](#)].
- [72] D. Boer, P. J. Mulders and F. Pijlman, *Universality of t-odd effects in single spin and azimuthal asymmetries*, *Nucl. Phys.* **B667** (2003) 201 [[hep-ph/0303034](#)].
- [73] C. Bomhof, P. Mulders and F. Pijlman, *Gauge link structure in quark-quark correlators in hard processes*, *Phys.Lett.* **B596** (2004) 277 [[hep-ph/0406099](#)].
- [74] X.-d. Ji, J.-p. Ma and F. Yuan, *QCD factorization for semi-inclusive deep-inelastic scattering at low transverse momentum*, *Phys.Rev.* **D71** (2005) 034005 [[hep-ph/0404183](#)].
- [75] X.-d. Ji, J.-P. Ma and F. Yuan, *QCD factorization for spin-dependent cross sections in DIS and Drell-Yan processes at low transverse momentum*, *Phys. Lett. B* **597** (2004) 299 [[hep-ph/0405085](#)].
- [76] C. Bomhof, P. Mulders and F. Pijlman, *The Construction of gauge-links in arbitrary hard processes*, *Eur.Phys.J.* **C47** (2006) 147 [[hep-ph/0601171](#)].
- [77] I. Cherednikov and N. Stefanis, *New results on gauge-invariant TMD PDFs in QCD*, 0809.1315.

- [78] I. Cherednikov and N. Stefanis, *Renormalization, Wilson lines, and transverse-momentum dependent parton distribution functions*, *Phys. Rev.* **D77** (2008) 094001 [[0710.1955](#)].
- [79] I. Cherednikov and N. Stefanis, *Wilson lines and transverse-momentum dependent parton distribution functions: A renormalization-group analysis*, *Nucl. Phys.* **B802** (2008) 146 [[0802.2821](#)].
- [80] F. Hautmann, *Endpoint singularities in unintegrated parton distributions*, *Phys.Lett.* **B655** (2007) 26 [[hep-ph/0702196](#)].
- [81] J. Collins, *Rapidity divergences and valid definitions of parton densities*, *PoS LC2008* (2008) 028 [[0808.2665](#)].
- [82] F. Hautmann, *Unintegrated parton distributions and applications to jet physics*, *Acta Phys.Polon.* **B40** (2009) 2139.
- [83] S. Aybat and T. C. Rogers, *TMD Parton Distribution and Fragmentation Functions with QCD Evolution*, *Phys.Rev.* **D83** (2011) 114042 [[1101.5057](#)].
- [84] M. A. Ebert and F. J. Tackmann, *Impact of isolation and fiducial cuts on  $q_T$  and N-jettiness subtractions*, *JHEP* **03** (2020) 158 [[1911.08486](#)].
- [85] M. A. Ebert, J. K. Michel, I. W. Stewart and F. J. Tackmann, *Drell-Yan  $q_T$  Resummation of Fiducial Power Corrections at  $N^3LL$* , [2006.11382](#).
- [86] J. C. Collins and D. E. Soper, *Back-To-Back Jets in QCD*, *Nucl. Phys.* **B193** (1981) 381.
- [87] J. C. Collins, D. E. Soper and G. F. Sterman, *Factorization for Short Distance Hadron - Hadron Scattering*, *Nucl.Phys.* **B261** (1985) 104.
- [88] J. C. Collins, D. E. Soper and G. F. Sterman, *Soft Gluons and Factorization*, *Nucl. Phys.* **B308** (1988) 833.
- [89] J. Collins, *Foundations of perturbative QCD*, Cambridge monographs on particle physics, nuclear physics, and cosmology. Cambridge Univ. Press, New York, NY, 2011.
- [90] M. Diehl, J. R. Gaunt, D. Ostermeier, P. Plößl and A. Schäfer, *Cancellation of Glauber gluon exchange in the double Drell-Yan process*, *JHEP* **01** (2016) 076 [[1510.08696](#)].
- [91] S. Catani and M. Grazzini, *QCD transverse-momentum resummation in gluon fusion processes*, *Nucl. Phys.* **B845** (2011) 297 [[1011.3918](#)].
- [92] C. W. Bauer, S. Fleming and M. E. Luke, *Summing Sudakov logarithms in  $B \rightarrow X_s \gamma$  in effective field theory*, *Phys.Rev.* **D63** (2000) 014006 [[hep-ph/0005275](#)].
- [93] C. W. Bauer, S. Fleming, D. Pirjol and I. W. Stewart, *An Effective field theory for collinear and soft gluons: Heavy to light decays*, *Phys.Rev.* **D63** (2001) 114020 [[hep-ph/0011336](#)].
- [94] C. W. Bauer and I. W. Stewart, *Invariant operators in collinear effective theory*, *Phys.Lett.* **B516** (2001) 134 [[hep-ph/0107001](#)].

- [95] C. W. Bauer, D. Pirjol and I. W. Stewart, *Soft collinear factorization in effective field theory*, *Phys.Rev.* **D65** (2002) 054022 [[hep-ph/0109045](#)].
- [96] T. Becher and M. Neubert, *Drell-Yan Production at Small  $q_T$ , Transverse Parton Distributions and the Collinear Anomaly*, *Eur.Phys.J.* **C71** (2011) 1665 [[1007.4005](#)].
- [97] T. Becher, M. Neubert and D. Wilhelm, *Electroweak Gauge-Boson Production at Small  $q_T$ : Infrared Safety from the Collinear Anomaly*, *JHEP* **02** (2012) 124 [[1109.6027](#)].
- [98] T. Becher, M. Neubert and D. Wilhelm, *Higgs-Boson Production at Small Transverse Momentum*, *JHEP* **05** (2013) 110 [[1212.2621](#)].
- [99] M. G. Echevarria, A. Idilbi and I. Scimemi, *Factorization Theorem For Drell-Yan At Low  $q_T$  And Transverse Momentum Distributions On-The-Light-Cone*, *JHEP* **1207** (2012) 002 [[1111.4996](#)].
- [100] M. G. Echevarria, A. Idilbi and I. Scimemi, *Soft and Collinear Factorization and Transverse Momentum Dependent Parton Distribution Functions*, *Phys.Lett.* **B726** (2013) 795 [[1211.1947](#)].
- [101] M. G. Echevarria, A. Idilbi and I. Scimemi, *Unified treatment of the QCD evolution of all (un-)polarized transverse momentum dependent functions: Collins function as a study case*, *Phys.Rev.* **D90** (2014) 014003 [[1402.0869](#)].
- [102] J.-Y. Chiu, A. Jain, D. Neill and I. Z. Rothstein, *A Formalism for the Systematic Treatment of Rapidity Logarithms in Quantum Field Theory*, *JHEP* **1205** (2012) 084 [[1202.0814](#)].
- [103] J. Collins and T. C. Rogers, *Connecting Different TMD Factorization Formalisms in QCD*, *Phys. Rev.* **D96** (2017) 054011 [[1705.07167](#)].
- [104] M. A. Ebert, I. W. Stewart and Y. Zhao, *Towards Quasi-Transverse Momentum Dependent PDFs Computable on the Lattice*, [1901.03685](#).
- [105] Y. Li, D. Neill and H. X. Zhu, *An Exponential Regulator for Rapidity Divergences*, [1604.00392](#).
- [106] I. W. Stewart, F. J. Tackmann and W. J. Waalewijn, *Factorization at the LHC: From PDFs to Initial State Jets*, *Phys. Rev. D* **81** (2010) 094035 [[0910.0467](#)].
- [107] A. V. Manohar and I. W. Stewart, *The Zero-Bin and Mode Factorization in Quantum Field Theory*, *Phys. Rev.* **D76** (2007) 074002 [[hep-ph/0605001](#)].
- [108] J. C. Collins and F. V. Tkachov, *Breakdown of dimensional regularization in the Sudakov problem*, *Phys. Lett.* **B294** (1992) 403 [[hep-ph/9208209](#)].
- [109] J.-y. Chiu, A. Jain, D. Neill and I. Z. Rothstein, *The Rapidity Renormalization Group*, *Phys. Rev. Lett.* **108** (2012) 151601 [[1104.0881](#)].
- [110] X.-d. Ji and F. Yuan, *Parton distributions in light cone gauge: Where are the final state interactions?*, *Phys. Lett.* **B543** (2002) 66 [[hep-ph/0206057](#)].

- [111] A. Idilbi and I. Scimemi, *Singular and Regular Gauges in Soft Collinear Effective Theory: The Introduction of the New Wilson Line T*, *Phys. Lett.* **B695** (2011) 463 [[1009.2776](#)].
- [112] M. Garcia-Echevarria, A. Idilbi and I. Scimemi, *SCET, Light-Cone Gauge and the T-Wilson Lines*, *Phys. Rev.* **D84** (2011) 011502 [[1104.0686](#)].
- [113] M. G. A. Buffing, M. Diehl and T. Kasemets, *Transverse momentum in double parton scattering: factorisation, evolution and matching*, *JHEP* **01** (2018) 044 [[1708.03528](#)].
- [114] M. G. Echevarria, I. Scimemi and A. Vladimirov, *Transverse momentum dependent fragmentation function at next-to-next-to-leading order*, *Phys. Rev.* **D93** (2016) 011502 [[1509.06392](#)].
- [115] M. G. Echevarria, I. Scimemi and A. Vladimirov, *Universal transverse momentum dependent soft function at NNLO*, *Phys. Rev.* **D93** (2016) 054004 [[1511.05590](#)].
- [116] M. G. Echevarria, I. Scimemi and A. Vladimirov, *Unpolarized Transverse Momentum Dependent Parton Distribution and Fragmentation Functions at next-to-next-to-leading order*, *JHEP* **09** (2016) 004 [[1604.07869](#)].
- [117] T. Becher and G. Bell, *Analytic Regularization in Soft-Collinear Effective Theory*, *Phys. Lett.* **B713** (2012) 41 [[1112.3907](#)].
- [118] M. A. Ebert, I. Moult, I. W. Stewart, F. J. Tackmann, G. Vita and H. X. Zhu, *Subleading power rapidity divergences and power corrections for  $q_T$* , *JHEP* **04** (2019) 123 [[1812.08189](#)].
- [119] J. C. Collins and D. E. Soper, *Parton Distribution and Decay Functions*, *Nucl.Phys.* **B194** (1982) 445.
- [120] M. Boglione, A. Dotson, L. Gamberg, S. Gordon, J. O. Gonzalez-Hernandez, A. Prokudin et al., *Mapping the Kinematical Regimes of Semi-Inclusive Deep Inelastic Scattering*, *JHEP* **10** (2019) 122 [[1904.12882](#)].
- [121] A. Bacchetta, M. Diehl, K. Goeke, A. Metz, P. J. Mulders and M. Schlegel, *Semi-inclusive deep inelastic scattering at small transverse momentum*, *JHEP* **02** (2007) 093 [[hep-ph/0611265](#)].
- [122] J. C. Collins and A. Metz, *Universality of soft and collinear factors in hard-scattering factorization*, *Phys.Rev.Lett.* **93** (2004) 252001 [[hep-ph/0408249](#)].
- [123] J. B. Kogut and D. E. Soper, *Quantum Electrodynamics in the Infinite Momentum Frame*, *Phys. Rev. D* **1** (1970) 2901.
- [124] C. W. Bauer, S. Fleming, D. Pirjol, I. Z. Rothstein and I. W. Stewart, *Hard scattering factorization from effective field theory*, *Phys. Rev. D* **66** (2002) 014017 [[hep-ph/0202088](#)].
- [125] M. Anselmino, M. Boglione, U. D'Alesio, E. Leader, S. Melis and F. Murgia, *The general partonic structure for hadronic spin asymmetries*, *Phys. Rev. D* **73** (2006) 014020 [[hep-ph/0509035](#)].

- [126] U. D'Alesio and F. Murgia, *Azimuthal and Single Spin Asymmetries in Hard Scattering Processes*, *Prog. Part. Nucl. Phys.* **61** (2008) 394 [[0712.4328](#)].
- [127] M. Anselmino, M. Boglione, U. D'Alesio, S. Melis, F. Murgia, E. R. Nocera et al., *General Helicity Formalism for Polarized Semi-Inclusive Deep Inelastic Scattering*, *Phys. Rev. D* **83** (2011) 114019 [[1101.1011](#)].
- [128] J. P. Ralston and D. E. Soper, *Production of Dimuons from High-Energy Polarized Proton Proton Collisions*, *Nucl. Phys. B* **152** (1979) 109.
- [129] P. J. Mulders and R. D. Tangerman, *The Complete tree level result up to order 1/Q for polarized deep inelastic leptoproduction*, *Nucl. Phys. B* **461** (1996) 197 [[hep-ph/9510301](#)].
- [130] A. Bacchetta, P. J. Mulders and F. Pijlman, *New observables in longitudinal single-spin asymmetries in semi-inclusive DIS*, *Phys. Lett. B* **595** (2004) 309 [[hep-ph/0405154](#)].
- [131] K. Goeke, A. Metz and M. Schlegel, *Parameterization of the quark-quark correlator of a spin-1/2 hadron*, *Phys. Lett. B* **618** (2005) 90 [[hep-ph/0504130](#)].
- [132] D. W. Sivers, *Single spin production asymmetries from the hard scattering of point - like constituents*, *Phys. Rev. D* **41** (1990) 83.
- [133] S. J. Brodsky, D. S. Hwang and I. Schmidt, *Initial state interactions and single spin asymmetries in Drell-Yan processes*, *Nucl. Phys. B* **642** (2002) 344 [[hep-ph/0206259](#)].
- [134] A. Kotzinian and P. Mulders, *Probing transverse quark polarization via azimuthal asymmetries in leptoproduction*, *Phys. Lett. B* **406** (1997) 373 [[hep-ph/9701330](#)].
- [135] A. Kotzinian and P. Mulders, *Longitudinal quark polarization in transversely polarized nucleons*, *Phys. Rev. D* **54** (1996) 1229 [[hep-ph/9511420](#)].
- [136] G. A. Miller, *Shapes of the proton*, *Phys. Rev. C* **68** (2003) 022201 [[nucl-th/0304076](#)].
- [137] K. Chang, "It's a ball. no, it's a pretzel. must be a proton.."   
<https://www.nytimes.com/2003/05/06/science/it-s-a-ball-no-it-s-a-pretzel-must-be-a-proton.html>, May, 2003.
- [138] Z.-B. Kang and J.-W. Qiu, *Testing the Time-Reversal Modified Universality of the Sivers Function*, *Phys. Rev. Lett.* **103** (2009) 172001 [[0903.3629](#)].
- [139] D. Boer, L. Gamberg, B. Musch and A. Prokudin, *Bessel-Weighted Asymmetries in Semi Inclusive Deep Inelastic Scattering*, *JHEP* **1110** (2011) 021 [[1107.5294](#)].
- [140] B. Musch, P. Hagler, M. Engelhardt, J. Negele and A. Schafer, *Sivers and Boer-Mulders observables from lattice QCD*, *Phys. Rev. D* **85** (2012) 094510 [[1111.4249](#)].
- [141] M. Engelhardt, P. Hägler, B. Musch, J. Negele and A. Schäfer, *Lattice QCD study of the Boer-Mulders effect in a pion*, *Phys. Rev. D* **93** (2016) 054501 [[1506.07826](#)].

- [142] B. Yoon, M. Engelhardt, R. Gupta, T. Bhattacharya, J. R. Green, B. U. Musch et al., *Nucleon Transverse Momentum-dependent Parton Distributions in Lattice QCD: Renormalization Patterns and Discretization Effects*, *Phys. Rev.* **D96** (2017) 094508 [1706.03406].
- [143] I. Scimemi and A. Vladimirov, *Matching of transverse momentum dependent distributions at twist-3*, *Eur. Phys. J. C* **78** (2018) 802 [1804.08148].
- [144] D. Gutiérrez-Reyes, I. Scimemi and A. A. Vladimirov, *Twist-2 matching of transverse momentum dependent distributions*, *Phys. Lett. B* **769** (2017) 84 [1702.06558].
- [145] J. Collins, T. C. Rogers and N. Sato, *Positivity and renormalization of parton densities*, 2111.01170.
- [146] M. G. A. Buffing, A. Mukherjee and P. J. Mulders, *Generalized Universality of Definite Rank Gluon Transverse Momentum Dependent Correlators*, *Phys. Rev. D* **88** (2013) 054027 [1306.5897].
- [147] D. Boer, C. Lorcé, C. Pisano and J. Zhou, *The gluon Sivers distribution: status and future prospects*, *Adv. High Energy Phys.* **2015** (2015) 371396 [1504.04332].
- [148] P. Mulders and J. Rodrigues, *Transverse momentum dependence in gluon distribution and fragmentation functions*, *Phys. Rev. D* **63** (2001) 094021 [hep-ph/0009343].
- [149] S. Meissner, A. Metz and K. Goeke, *Relations between generalized and transverse momentum dependent parton distributions*, *Phys. Rev. D* **76** (2007) 034002 [hep-ph/0703176].
- [150] V. E. Lyubovitskij and I. Schmidt, *New findings in gluon TMD physics*, *Phys. Rev. D* **104** (2021) 014001 [2105.07842].
- [151] M. G. Echevarria, T. Kasemets, P. J. Mulders and C. Pisano, *QCD evolution of (un)polarized gluon TMDPDFs and the Higgs  $q_T$ -distribution*, 1502.05354.
- [152] S. Catani and M. Grazzini, *Higgs Boson Production at Hadron Colliders: Hard-Collinear Coefficients at the NNLO*, *Eur. Phys. J. C* **72** (2012) 2013 [1106.4652].
- [153] T. Gehrmann, T. Luebbert and L. L. Yang, *Calculation of the transverse parton distribution functions at next-to-next-to-leading order*, *JHEP* **06** (2014) 155 [1403.6451].
- [154] T. Lübbert, J. Oredsson and M. Stahlhofen, *Rapidity renormalized TMD soft and beam functions at two loops*, *JHEP* **03** (2016) 168 [1602.01829].
- [155] Y. Li and H. X. Zhu, *Bootstrapping Rapidity Anomalous Dimensions for Transverse-Momentum Resummation*, *Phys. Rev. Lett.* **118** (2017) 022004 [1604.01404].
- [156] M.-x. Luo, T.-Z. Yang, H. X. Zhu and Y. J. Zhu, *Quark Transverse Parton Distribution at the Next-to-Next-to-Next-to-Leading Order*, 1912.05778.

- [157] M. A. Ebert, B. Mistlberger and G. Vita, *Transverse momentum dependent PDFs at  $N^3LO$* , 2006.05329.
- [158] M.-x. Luo, T.-Z. Yang, H. X. Zhu and Y. J. Zhu, *Unpolarized Quark and Gluon TMD PDFs and FFs at  $N^3LO$* , 2012.03256.
- [159] J.-w. Qiu and G. F. Sterman, *Single transverse spin asymmetries*, *Phys. Rev. Lett.* **67** (1991) 2264.
- [160] V. Braun, A. Manashov and B. Pirnay, *Scale dependence of twist-three contributions to single spin asymmetries*, *Phys. Rev. D* **80** (2009) 114002 [0909.3410].
- [161] M. A. Ebert, B. Mistlberger and G. Vita, *TMD Fragmentation Functions at  $N^3LO$* , 2012.07853.
- [162] V. Moos and A. Vladimirov, *Calculation of transverse momentum dependent distributions beyond the leading power*, *JHEP* **12** (2020) 145 [2008.01744].
- [163] I. I. Balitsky and V. M. Braun, *The Nonlocal operator expansion for inclusive particle production in  $e+e-$  annihilation*, *Nucl. Phys. B* **361** (1991) 93.
- [164] M.-X. Luo, X. Wang, X. Xu, L. L. Yang, T.-Z. Yang and H. X. Zhu, *Transverse Parton Distribution and Fragmentation Functions at NNLO: the Quark Case*, *JHEP* **10** (2019) 083 [1908.03831].
- [165] H. Chen, T.-Z. Yang, H. X. Zhu and Y. J. Zhu, *Analytic Continuation and Reciprocity Relation for Collinear Splitting in QCD*, 2006.10534.
- [166] A. Bacchetta and A. Prokudin, *Evolution of the helicity and transversity Transverse-Momentum-Dependent parton distributions*, *Nucl. Phys. B* **875** (2013) 536 [1303.2129].
- [167] K. Kanazawa, Y. Koike, A. Metz, D. Pitonyak and M. Schlegel, *Operator Constraints for Twist-3 Functions and Lorentz Invariance Properties of Twist-3 Observables*, *Phys. Rev. D* **93** (2016) 054024 [1512.07233].
- [168] X. Ji, J.-W. Qiu, W. Vogelsang and F. Yuan, *A Unified picture for single transverse-spin asymmetries in hard processes*, *Phys. Rev. Lett.* **97** (2006) 082002 [hep-ph/0602239].
- [169] X. Ji, J.-w. Qiu, W. Vogelsang and F. Yuan, *Single Transverse-Spin Asymmetry in Drell-Yan Production at Large and Moderate Transverse Momentum*, *Phys. Rev. D* **73** (2006) 094017 [hep-ph/0604023].
- [170] Y. Koike, W. Vogelsang and F. Yuan, *On the Relation Between Mechanisms for Single-Transverse-Spin Asymmetries*, *Phys. Lett. B* **659** (2008) 878 [0711.0636].
- [171] Z.-B. Kang, B.-W. Xiao and F. Yuan, *QCD Resummation for Single Spin Asymmetries*, *Phys. Rev. Lett.* **107** (2011) 152002 [1106.0266].

- [172] P. Sun and F. Yuan, *Transverse momentum dependent evolution: Matching semi-inclusive deep inelastic scattering processes to Drell-Yan and W/Z boson production*, *Phys. Rev.* **D88** (2013) 114012 [[1308.5003](#)].
- [173] L.-Y. Dai, Z.-B. Kang, A. Prokudin and I. Vitev, *Next-to-leading order transverse momentum-weighted Sivers asymmetry in semi-inclusive deep inelastic scattering: the role of the three-gluon correlator*, *Phys. Rev. D* **92** (2015) 114024 [[1409.5851](#)].
- [174] I. Scimemi, A. Tarasov and A. Vladimirov, *Collinear matching for Sivers function at next-to-leading order*, *JHEP* **05** (2019) 125 [[1901.04519](#)].
- [175] D. Gutierrez-Reyes, I. Scimemi and A. Vladimirov, *Transverse momentum dependent transversely polarized distributions at next-to-next-to-leading-order*, *JHEP* **07** (2018) 172 [[1805.07243](#)].
- [176] M.-X. Luo, T.-Z. Yang, H. X. Zhu and Y. J. Zhu, *Transverse Parton Distribution and Fragmentation Functions at NNLO: the Gluon Case*, *JHEP* **01** (2020) 040 [[1909.13820](#)].
- [177] D. Gutierrez-Reyes, S. Leal-Gomez, I. Scimemi and A. Vladimirov, *Linearly polarized gluons at next-to-next-to leading order and the Higgs transverse momentum distribution*, *JHEP* **11** (2019) 121 [[1907.03780](#)].
- [178] J.-w. Qiu and X.-f. Zhang, *Role of the nonperturbative input in QCD resummed Drell-Yan  $Q_T$  distributions*, *Phys. Rev. D* **63** (2001) 114011 [[hep-ph/0012348](#)].
- [179] E. L. Berger and J.-w. Qiu, *Differential cross-section for Higgs boson production including all orders soft gluon resummation*, *Phys. Rev. D* **67** (2003) 034026 [[hep-ph/0210135](#)].
- [180] M. A. Ebert, J. K. L. Michel, I. W. Stewart and Z. Sun, *Disentangling Long and Short Distances in Momentum-Space TMDs*, to appear. See [https://indico.desy.de/event/28334/contributions/112377/attachments/69829/88644/REFtalkslides\\_ZS.pdf](https://indico.desy.de/event/28334/contributions/112377/attachments/69829/88644/REFtalkslides_ZS.pdf).
- [181] P. Hagler, B. Musch, J. Negele and A. Schafer, *Intrinsic quark transverse momentum in the nucleon from lattice QCD*, *Europhys.Lett.* **88** (2009) 61001 [[0908.1283](#)].
- [182] B. Yoon, T. Bhattacharya, M. Engelhardt, J. Green, R. Gupta, P. Hägler et al., *Lattice QCD calculations of nucleon transverse momentum-dependent parton distributions using clover and domain wall fermions*, in *Proceedings, 33rd International Symposium on Lattice Field Theory (Lattice 2015): Kobe, Japan, July 14-18, 2015*, SISSA, SISSA, 2015, [1601.05717](#).
- [183] X. Ji, P. Sun, X. Xiong and F. Yuan, *Soft factor subtraction and transverse momentum dependent parton distributions on the lattice*, *Phys. Rev. D* **91** (2015) 074009 [[1405.7640](#)].
- [184] X. Ji, L.-C. Jin, F. Yuan, J.-H. Zhang and Y. Zhao, *Transverse Momentum Dependent Quasi-Parton-Distributions*, *Phys. Rev. D* **99** (2019) 114006 [[1801.05930](#)].
- [185] M. A. Ebert, I. W. Stewart and Y. Zhao, *Determining the Nonperturbative Collins-Soper Kernel From Lattice QCD*, *Phys. Rev. D* **99** (2019) 034505 [[1811.00026](#)].

- [186] M. A. Ebert, I. W. Stewart and Y. Zhao, *Renormalization and Matching for the Collins-Soper Kernel from Lattice QCD*, 1910.08569.
- [187] X. Ji, Y. Liu and Y.-S. Liu, *TMD soft function from large-momentum effective theory*, *Nucl. Phys. B* **955** (2020) 115054 [1910.11415].
- [188] X. Ji, Y. Liu and Y.-S. Liu, *Transverse-momentum-dependent parton distribution functions from large-momentum effective theory*, *Phys. Lett. B* **811** (2020) 135946 [1911.03840].
- [189] A. A. Vladimirov and A. Schäfer, *Transverse momentum dependent factorization for lattice observables*, *Phys. Rev. D* **101** (2020) 074517 [2002.07527].
- [190] M. A. Ebert, S. T. Schindler, I. W. Stewart and Y. Zhao, *One-loop Matching for Spin-Dependent Quasi-TMDs*, *JHEP* **09** (2020) 099 [2004.14831].
- [191] X. Ji, Y. Liu, A. Schäfer and F. Yuan, *Single Transverse-Spin Asymmetry and Sivers Function in Large Momentum Effective Theory*, 2011.13397.
- [192] P. Shanahan, M. Wagman and Y. Zhao, *Nonperturbative renormalization of staple-shaped Wilson line operators in lattice QCD*, 1911.00800.
- [193] J. C. Collins and D. E. Soper, *Angular Distribution of Dileptons in High-Energy Hadron Collisions*, *Phys. Rev. D* **16** (1977) 2219.
- [194] S. Bastami, L. Gamberg, B. Parsamyan, B. Pasquini, A. Prokudin and P. Schweitzer, *The Drell-Yan process with pions and polarized nucleons*, 2005.14322.
- [195] S. Arnold, A. Metz and M. Schlegel, *Dilepton production from polarized hadron hadron collisions*, *Phys. Rev. D* **79** (2009) 034005 [0809.2262].
- [196] COMPASS collaboration, M. Aghasyan et al., *First measurement of transverse-spin-dependent azimuthal asymmetries in the Drell-Yan process*, *Phys. Rev. Lett.* **119** (2017) 112002 [1704.00488].
- [197] ATLAS collaboration, G. Aad et al., *Measurements of fiducial and differential cross sections for Higgs boson production in the diphoton decay channel at  $\sqrt{s} = 8$  TeV with ATLAS*, *JHEP* **09** (2014) 112 [1407.4222].
- [198] ATLAS collaboration, G. Aad et al., *Fiducial and differential cross sections of Higgs boson production measured in the four-lepton decay channel in pp collisions at  $\sqrt{s}=8$  TeV with the ATLAS detector*, *Phys. Lett. B* **738** (2014) 234 [1408.3226].
- [199] ATLAS collaboration, G. Aad et al., *Measurement of fiducial differential cross sections of gluon-fusion production of Higgs bosons decaying to  $WW^* \rightarrow e\nu\mu\nu$  with the ATLAS detector at  $\sqrt{s} = 8$  TeV*, *JHEP* **08** (2016) 104 [1604.02997].
- [200] ATLAS collaboration, M. Aaboud et al., *Measurement of inclusive and differential cross sections in the  $H \rightarrow ZZ^* \rightarrow 4\ell$  decay channel in pp collisions at  $\sqrt{s} = 13$  TeV with the ATLAS detector*, *JHEP* **10** (2017) 132 [1708.02810].

- [201] ATLAS collaboration, M. Aaboud et al., *Measurements of Higgs boson properties in the diphoton decay channel with  $36 \text{ fb}^{-1}$  of  $pp$  collision data at  $\sqrt{s} = 13 \text{ TeV}$  with the ATLAS detector*, *Phys. Rev.* **D98** (2018) 052005 [[1802.04146](#)].
- [202] ATLAS collaboration, G. Aad et al., *Measurements of the Higgs boson inclusive and differential fiducial cross sections in the  $4\ell$  decay channel at  $\sqrt{s} = 13 \text{ TeV}$* , *Submitted to: Eur. Phys. J.* (2020) [[2004.03969](#)].
- [203] CMS collaboration, V. Khachatryan et al., *Measurement of differential cross sections for Higgs boson production in the diphoton decay channel in  $pp$  collisions at  $\sqrt{s} = 8 \text{ TeV}$* , *Eur. Phys. J.* **C76** (2016) 13 [[1508.07819](#)].
- [204] CMS collaboration, V. Khachatryan et al., *Measurement of differential and integrated fiducial cross sections for Higgs boson production in the four-lepton decay channel in  $pp$  collisions at  $\sqrt{s} = 7$  and  $8 \text{ TeV}$* , *JHEP* **04** (2016) 005 [[1512.08377](#)].
- [205] CMS collaboration, V. Khachatryan et al., *Measurement of the transverse momentum spectrum of the Higgs boson produced in  $pp$  collisions at  $\sqrt{s} = 8 \text{ TeV}$  using  $H \rightarrow WW$  decays*, *Submitted to: JHEP* (2016) [[1606.01522](#)].
- [206] CMS collaboration, A. M. Sirunyan et al., *Measurement of inclusive and differential Higgs boson production cross sections in the diphoton decay channel in proton-proton collisions at  $\sqrt{s} = 13 \text{ TeV}$* , *JHEP* **01** (2019) 183 [[1807.03825](#)].
- [207] CMS collaboration, A. M. Sirunyan et al., *Measurement and interpretation of differential cross sections for Higgs boson production at  $\sqrt{s} = 13 \text{ TeV}$* , *Phys. Lett. B* **792** (2019) 369 [[1812.06504](#)].
- [208] S. Mantry and F. Petriello, *Factorization and Resummation of Higgs Boson Differential Distributions in Soft-Collinear Effective Theory*, *Phys. Rev.* **D81** (2010) 093007 [[0911.4135](#)].
- [209] Z.-B. Kang, A. Prokudin, P. Sun and F. Yuan, *Extraction of Quark Transversity Distribution and Collins Fragmentation Functions with QCD Evolution*, *Phys. Rev.* **D93** (2016) 014009 [[1505.05589](#)].
- [210] S. Bastami et al., *Semi-Inclusive Deep Inelastic Scattering in Wandzura-Wilczek-type approximation*, *JHEP* **06** (2019) 007 [[1807.10606](#)].
- [211] D. Boer, R. Jakob and P. J. Mulders, *Asymmetries in polarized hadron production in  $e+e-$  annihilation up to order  $1/Q$* , *Nucl. Phys.* **B504** (1997) 345 [[hep-ph/9702281](#)].
- [212] D. Boer, *Angular dependences in inclusive two-hadron production at BELLE*, *Nucl. Phys.* **B806** (2009) 23 [[0804.2408](#)].
- [213] D. Pitonyak, M. Schlegel and A. Metz, *Polarized hadron pair production from electron-positron annihilation*, *Phys. Rev.* **D89** (2014) 054032 [[1310.6240](#)].

- [214] I. Z. Rothstein and I. W. Stewart, *An Effective Field Theory for Forward Scattering and Factorization Violation*, *JHEP* **08** (2016) 025 [[1601.04695](#)].
- [215] S. B. Libby and G. Sterman, *Mass divergences in two-particle inelastic scattering*, *Phys. Rev.* **D18** (1978) 4737.
- [216] R. J. Glauber, *Cross-sections in deuterium at high-energies*, *Phys. Rev.* **100** (1955) 242.
- [217] J. C. Collins, D. E. Soper and G. F. Sterman, *Factorization is not violated*, *Phys. Lett.* **B438** (1998) 184 [[hep-ph/9806234](#)].
- [218] V. A. Khoze, A. D. Martin and M. Ryskin, *The Compatibility of diffractive hard scattering in  $p\bar{p}$  and  $ep$  collisions*, *Phys.Lett.* **B502** (2001) 87 [[hep-ph/0007083](#)].
- [219] A. Kaidalov, V. A. Khoze, A. D. Martin and M. Ryskin, *Probabilities of rapidity gaps in high-energy interactions*, *Eur.Phys.J.* **C21** (2001) 521 [[hep-ph/0105145](#)].
- [220] M. Klasen and G. Kramer, *Review of factorization breaking in diffractive photoproduction of dijets*, *Mod.Phys.Lett.* **A23** (2008) 1885 [[0806.2269](#)].
- [221] A. Kaidalov, V. Khoze, A. Martin and M. Ryskin, *Factorization breaking in diffractive dijet photoproduction at HERA*, *Eur.Phys.J.* **C66** (2010) 373 [[0911.3716](#)].
- [222] J. Collins and J.-W. Qiu,  *$k_T$  factorization is violated in production of high-transverse-momentum particles in hadron-hadron collisions*, *Phys. Rev.* **D75** (2007) 114014 [[0705.2141](#)].
- [223] T. C. Rogers and P. J. Mulders, *No Generalized TMD-Factorization in Hadro-Production of High Transverse Momentum Hadrons*, *Phys. Rev. D* **81** (2010) 094006 [[1001.2977](#)].
- [224] P. Mulders and T. Rogers, *Gauge Links, TMD-Factorization, and TMD-Factorization Breaking*, [1102.4569](#).
- [225] T. C. Rogers and P. J. Mulders, *No Generalized TMD-Factorization in Hadro-Production of High Transverse Momentum Hadrons*, *Phys.Rev.* **D81** (2010) 094006 [[1001.2977](#)].
- [226] I. Z. Rothstein and I. W. Stewart, *A Proof of Factorization for Drell-Yan with SCET*, to appear. See [https://indico.ph.ed.ac.uk/event/63/contributions/1040/attachments/799/980/Ira\\_Rothstein.pdf](https://indico.ph.ed.ac.uk/event/63/contributions/1040/attachments/799/980/Ira_Rothstein.pdf).
- [227] S. Fleming, *The role of Glauber exchange in soft collinear effective theory and the Balitsky–Fadin–Kuraev–Lipatov Equation*, *Phys. Lett. B* **735** (2014) 266 [[1404.5672](#)].
- [228] X.-d. Ji, J.-P. Ma and F. Yuan, *Transverse-momentum-dependent gluon distributions and semi-inclusive processes at hadron colliders*, *JHEP* **07** (2005) 020 [[hep-ph/0503015](#)].
- [229] S. M. Aybat, A. Prokudin and T. C. Rogers, *Calculation of TMD Evolution for Transverse Single Spin Asymmetry Measurements*, *Phys.Rev.Lett.* **108** (2012) 242003 [[1112.4423](#)].

- [230] A. H. Mueller, *On the Asymptotic Behavior of the Sudakov Form-factor*, *Phys. Rev. D* **20** (1979) 2037.
- [231] A. Sen, *Asymptotic Behavior of the Sudakov Form-Factor in QCD*, *Phys. Rev. D* **24** (1981) 3281.
- [232] H. Contopanagos, E. Laenen and G. F. Sterman, *Sudakov factorization and resummation*, *Nucl. Phys. B* **484** (1997) 303 [[hep-ph/9604313](#)].
- [233] G. Altarelli, R. K. Ellis, M. Greco and G. Martinelli, *Vector Boson Production at Colliders: A Theoretical Reappraisal*, *Nucl. Phys. B* **246** (1984) 12.
- [234] C. Davies and W. J. Stirling, *Nonleading Corrections to the Drell-Yan Cross-Section at Small Transverse Momentum*, *Nucl.Phys. B* **244** (1984) 337.
- [235] P. B. Arnold and R. P. Kauffman, *W and Z production at next-to-leading order: From large  $q(t)$  to small*, *Nucl. Phys. B* **349** (1991) 381.
- [236] R. Abbate, M. Fickinger, A. H. Hoang, V. Mateu and I. W. Stewart, *Thrust at  $N^3LL$  with Power Corrections and a Precision Global Fit for  $\alpha_s(m_Z)$* , *Phys. Rev. D* **83** (2011) 074021 [[1006.3080](#)].
- [237] L. G. Almeida, S. D. Ellis, C. Lee, G. Sterman, I. Sung et al., *Comparing and counting logs in direct and effective methods of QCD resummation*, *JHEP* **1404** (2014) 174 [[1401.4460](#)].
- [238] I. Scimemi and A. Vladimirov, *Systematic analysis of double-scale evolution*, *JHEP* **08** (2018) 003 [[1803.11089](#)].
- [239] J. Collins, *CSS Equation, etc, Follow from Structure of TMD Factorization*, [1212.5974](#).
- [240] J. Collins and T. Rogers, *Understanding the large-distance behavior of TMD parton densities and the Collins-Soper evolution kernel*, [1412.3820](#).
- [241] A. Idilbi, X.-d. Ji, J.-P. Ma and F. Yuan, *Collins-Soper equation for the energy evolution of transverse-momentum and spin dependent parton distributions*, *Phys. Rev. D* **70** (2004) 074021 [[hep-ph/0406302](#)].
- [242] G. Bozzi, S. Catani, D. de Florian and M. Grazzini, *Transverse-momentum resummation and the spectrum of the Higgs boson at the LHC*, *Nucl. Phys. B* **737** (2006) 73 [[hep-ph/0508068](#)].
- [243] J.-W. Qiu and X.-f. Zhang, *QCD prediction for heavy boson transverse momentum distributions*, *Phys.Rev.Lett.* **86** (2001) 2724 [[hep-ph/0012058](#)].
- [244] P. M. Nadolsky, D. R. Stump and C. P. Yuan, *Semiinclusive hadron production at HERA: The Effect of QCD gluon resummation*, *Phys. Rev. D* **61** (2000) 014003 [[hep-ph/9906280](#)].
- [245] Y. Koike, J. Nagashima and W. Vogelsang, *Resummation for polarized semi-inclusive deep-inelastic scattering at small transverse momentum*, *Nucl.Phys. B* **744** (2006) 59 [[hep-ph/0602188](#)].

- [246] T. C. Rogers, *An Overview of Transverse Momentum Dependent Factorization and Evolution*, *Eur. Phys. J.* **A52** (2016) 153 [[1509.04766](#)].
- [247] A. Bacchetta, M. G. Echevarria, P. J. G. Mulders, M. Radici and A. Signori, *Effects of TMD evolution and partonic flavor on  $e^+e^-$  annihilation into hadrons*, *JHEP* **11** (2015) 076 [[1508.00402](#)].
- [248] A. Bacchetta, F. Delcarro, C. Pisano, M. Radici and A. Signori, *Extraction of partonic transverse momentum distributions from semi-inclusive deep-inelastic scattering, Drell-Yan and Z-boson production*, *JHEP* **06** (2017) 081 [[1703.10157](#)].
- [249] J. Collins, L. Gamberg, A. Prokudin, T. C. Rogers, N. Sato and B. Wang, *Relating Transverse Momentum Dependent and Collinear Factorization Theorems in a Generalized Formalism*, *Phys. Rev.* **D94** (2016) 034014 [[1605.00671](#)].
- [250] J. Collins, L. Gamberg, A. Prokudin, T. Rogers, N. Sato and B. Wang, *Combining TMD factorization and collinear factorization*, in *22nd International Symposium on Spin Physics*, 2, 2017, [1702.00387](#).
- [251] E. Laenen, G. F. Sterman and W. Vogelsang, *Higher order QCD corrections in prompt photon production*, *Phys. Rev. Lett.* **84** (2000) 4296 [[hep-ph/0002078](#)].
- [252] A. Kulesza, G. F. Sterman and W. Vogelsang, *Joint resummation in electroweak boson production*, *Phys. Rev.* **D66** (2002) 014011 [[hep-ph/0202251](#)].
- [253] Z. Ligeti, I. W. Stewart and F. J. Tackmann, *Treating the b quark distribution function with reliable uncertainties*, *Phys. Rev. D* **78** (2008) 114014 [[0807.1926](#)].
- [254] G. Bell, A. Hornig, C. Lee and J. Talbert,  *$e^+e^-$  angularity distributions at NNLL' accuracy*, *JHEP* **01** (2019) 147 [[1808.07867](#)].
- [255] P. F. Monni, E. Re and P. Torrielli, *Higgs Transverse-Momentum Resummation in Direct Space*, *Phys. Rev. Lett.* **116** (2016) 242001 [[1604.02191](#)].
- [256] M. A. Ebert and F. J. Tackmann, *Resummation of Transverse Momentum Distributions in Distribution Space*, *JHEP* **02** (2017) 110 [[1611.08610](#)].
- [257] D. Kang, C. Lee and V. Vaidya, *A fast and accurate method for perturbative resummation of transverse momentum-dependent observables*, *JHEP* **04** (2018) 149 [[1710.00078](#)].
- [258] I. Balitsky and A. Tarasov, *Higher-twist corrections to gluon TMD factorization*, *JHEP* **07** (2017) 095 [[1706.01415](#)].
- [259] I. Balitsky and A. Tarasov, *Power corrections to TMD factorization for Z-boson production*, *JHEP* **05** (2018) 150 [[1712.09389](#)].
- [260] M. Boglione, J. O. G. Hernandez, S. Melis and A. Prokudin, *A study on the interplay between perturbative QCD and CSS/TMD formalism in SIDIS processes*, *JHEP* **1502** (2015) 095 [[1412.1383](#)].

- [261] L. Gamberg, A. Metz, D. Pitonyak and A. Prokudin, *Connections between collinear and transverse-momentum-dependent polarized observables within the Collins–Soper–Sterman formalism*, *Phys. Lett. B* **781** (2018) 443 [[1712.08116](#)].
- [262] G. Bozzi, S. Catani, D. de Florian and M. Grazzini, *The  $q(T)$  spectrum of the Higgs boson at the LHC in QCD perturbation theory*, *Phys.Lett. B* **564** (2003) 65 [[hep-ph/0302104](#)].
- [263] C. F. Berger, C. Marcantonini, I. W. Stewart, F. J. Tackmann and W. J. Waalewijn, *Higgs Production with a Central Jet Veto at NNLL+NNLO*, *JHEP* **04** (2011) 092 [[1012.4480](#)].
- [264] D. Neill, I. Z. Rothstein and V. Vaidya, *The Higgs Transverse Momentum Distribution at NNLL and its Theoretical Errors*, *JHEP* **12** (2015) 097 [[1503.00005](#)].
- [265] A. Banfi, G. P. Salam and G. Zanderighi, *Principles of general final-state resummation and automated implementation*, *JHEP* **03** (2005) 073 [[hep-ph/0407286](#)].
- [266] A. Banfi, H. McAslan, P. F. Monni and G. Zanderighi, *A general method for the resummation of event-shape distributions in  $e^+e^-$  annihilation*, *JHEP* **05** (2015) 102 [[1412.2126](#)].
- [267] W. Bizon, P. F. Monni, E. Re, L. Rottoli and P. Torrielli, *Momentum-space resummation for transverse observables and the Higgs  $p_\perp$  at N<sup>3</sup>LL+NNLO*, *JHEP* **02** (2018) 108 [[1705.09127](#)].
- [268] A. Banfi, G. P. Salam and G. Zanderighi, *NLL+NNLO predictions for jet-veto efficiencies in Higgs-boson and Drell-Yan production*, *JHEP* **06** (2012) 159 [[1203.5773](#)].
- [269] R. P. Feynman, R. D. Field and G. C. Fox, *Correlations Among Particles and Jets Produced with Large Transverse Momenta*, *Nucl. Phys.* **B128** (1977) 1.
- [270] R. P. Feynman, R. D. Field and G. C. Fox, *A Quantum Chromodynamic Approach for the Large Transverse Momentum Production of Particles and Jets*, *Phys. Rev. D* **18** (1978) 3320.
- [271] M. Anselmino, M. Boglione and F. Murgia, *Single spin asymmetry for  $p$  (polarized)  $p \rightarrow pi X$  in perturbative QCD*, *Phys. Lett. B* **362** (1995) 164 [[hep-ph/9503290](#)].
- [272] M. Anselmino, M. Boglione and F. Murgia, *Phenomenology of single spin asymmetries in  $p$  - polarized  $p \rightarrow pi X$* , *Phys. Rev. D* **60** (1999) 054027 [[hep-ph/9901442](#)].
- [273] M. Boglione and E. Leader, *Reassessment of the Collins mechanism for single spin asymmetries and the behavior of Delta d(x) at large x*, *Phys. Rev. D* **61** (2000) 114001 [[hep-ph/9911207](#)].
- [274] M. Anselmino, M. Boglione, U. D'Alesio, E. Leader and F. Murgia, *Accessing Sivers gluon distribution via transverse single spin asymmetries in  $p$ (transv. polarized)  $p \rightarrow D X$  processes at RHIC*, *Phys. Rev. D* **70** (2004) 074025 [[hep-ph/0407100](#)].
- [275] H. Georgi and H. D. Politzer, *Clean Tests of QCD in mu p Scattering*, *Phys. Rev. Lett.* **40** (1978) 3.

- [276] A. Mendez, *QCD Predictions for Semiinclusive and Inclusive Leptoproduction*, *Nucl. Phys.* **B145** (1978) 199.
- [277] G. L. Kane, J. Pumplin and W. Repko, *Transverse Quark Polarization in Large  $p(T)$  Reactions,  $e^+e^-$  Jets, and Leptoproduction: A Test of QCD*, *Phys. Rev. Lett.* **41** (1978) 1689.
- [278] R. N. Cahn, *Azimuthal Dependence in Leptoproduction: A Simple Parton Model Calculation*, *Phys. Lett. B* **78** (1978) 269.
- [279] R. Cahn, *Critique of Parton Model Calculations of Azimuthal Dependence in Leptoproduction*, *Phys. Rev. D* **40** (1989) 3107.
- [280] A. Kotzinian, *New quark distributions and semiinclusive electroproduction on the polarized nucleons*, *Nucl. Phys.* **B441** (1995) 234 [[hep-ph/9412283](#)].
- [281] R. D. Tangerman and P. J. Mulders, *Probing transverse quark polarization in deep inelastic leptoproduction*, *Phys. Lett. B* **352** (1995) 129 [[hep-ph/9501202](#)].
- [282] A. Efremov and O. Teryaev, *On Spin Effects in Quantum Chromodynamics*, *Sov. J. Nucl. Phys.* **36** (1982) 140.
- [283] A. V. Efremov and O. V. Teryaev, *THE TRANSVERSAL POLARIZATION IN QUANTUM CHROMODYNAMICS*, *Sov. J. Nucl. Phys.* **39** (1984) 962.
- [284] J.-w. Qiu and G. F. Sterman, *Single transverse spin asymmetries in hadronic pion production*, *Phys. Rev. D* **59** (1999) 014004 [[hep-ph/9806356](#)].
- [285] J.-W. Qiu and G. Sterman, *Single transverse spin asymmetries in direct photon production*, *Nucl. Phys.* **B378** (1992) 52.
- [286] D. W. Sivers, *Hard scattering scaling laws for single spin production asymmetries*, *Phys. Rev. D* **43** (1991) 261.
- [287] O. Nachtmann, *A New Tool for the Study of Fundamental Interactions: Parity Odd Correlations in Quark Fragmentation*, *Nucl. Phys. B* **127** (1977) 314.
- [288] R. H. Dalitz, G. R. Goldstein and R. Marshall, *On the Helicity of Charm Jets*, *Z. Phys. C* **42** (1989) 441.
- [289] R. H. Dalitz, G. R. Goldstein and R. Marshall, *Heavy Quark Spin Correlations in  $e^+e^-$  Annihilations*, *Phys. Lett. B* **215** (1988) 783.
- [290] A. V. Efremov, L. Mankiewicz and N. A. Tornqvist, *Jet handedness as a measure of quark and gluon polarization*, *Phys. Lett. B* **284** (1992) 394.
- [291] J. C. Collins, S. F. Heppelmann and G. A. Ladinsky, *Measuring transversity densities in singly polarized hadron hadron and lepton - hadron collisions*, *Nucl. Phys.* **B420** (1994) 565 [[hep-ph/9305309](#)].

- [292] R. L. Jaffe, X.-m. Jin and J. Tang, *Interference fragmentation functions and the nucleon's transversity*, *Phys. Rev. Lett.* **80** (1998) 1166 [[hep-ph/9709322](#)].
- [293] A. Bianconi, S. Boffi, R. Jakob and M. Radici, *Two hadron interference fragmentation functions. Part 1. General framework*, *Phys. Rev. D* **62** (2000) 034008 [[hep-ph/9907475](#)].
- [294] M. Radici, R. Jakob and A. Bianconi, *Accessing transversity with interference fragmentation functions*, *Phys. Rev. D* **65** (2002) 074031 [[hep-ph/0110252](#)].
- [295] A. Bacchetta and M. Radici, *Partial wave analysis of two hadron fragmentation functions*, *Phys. Rev. D* **67** (2003) 094002 [[hep-ph/0212300](#)].
- [296] A. Metz and A. Vossen, *Parton Fragmentation Functions*, *Prog. Part. Nucl. Phys.* **91** (2016) 136 [[1607.02521](#)].
- [297] A. Bacchetta, *Where do we stand with a 3-D picture of the proton?*, *Eur. Phys. J. A* **52** (2016) 163 [[2107.06772](#)].
- [298] E. C. Aschenauer, U. D'Alesio and F. Murgia, *TMDs and SSAs in hadronic interactions*, *Eur. Phys. J. A* **52** (2016) 156 [[1512.05379](#)].
- [299] M. Boglione and A. Prokudin, *Phenomenology of transverse spin: past, present and future*, *Eur. Phys. J. A* **52** (2016) 154 [[1511.06924](#)].
- [300] H. Avakian, A. Bressan and M. Contalbrigo, *Experimental results on TMDs*, *Eur. Phys. J. A* **52** (2016) 150.
- [301] HERMES collaboration, A. Airapetian et al., *Multiplicities of charged pions and kaons from semi-inclusive deep-inelastic scattering by the proton and the deuteron*, *Phys. Rev. D* **87** (2013) 074029 [[1212.5407](#)].
- [302] COMPASS collaboration, M. Aghasyan et al., *Transverse-momentum-dependent Multiplicities of Charged Hadrons in Muon-Deuteron Deep Inelastic Scattering*, *Phys. Rev. D* **97** (2018) 032006 [[1709.07374](#)].
- [303] M. Anselmino, M. Boglione, U. D'Alesio, A. Kotzinian, F. Murgia and A. Prokudin, *The Role of Cahn and sivers effects in deep inelastic scattering*, *Phys. Rev. D* **71** (2005) 074006 [[hep-ph/0501196](#)].
- [304] P. Schweitzer, T. Teckentrup and A. Metz, *Intrinsic transverse parton momenta in deeply inelastic reactions*, *Phys. Rev. D* **81** (2010) 094019 [[1003.2190](#)].
- [305] M. Anselmino, M. Boglione, J. O. Gonzalez Hernandez, S. Melis and A. Prokudin, *Unpolarised Transverse Momentum Dependent Distribution and Fragmentation Functions from SIDIS Multiplicities*, *JHEP* **04** (2014) 005 [[1312.6261](#)].
- [306] A. Signori, A. Bacchetta, M. Radici and G. Schnell, *Investigations into the flavor dependence of partonic transverse momentum*, *JHEP* **11** (2013) 194 [[1309.3507](#)].

- [307] LHPC collaboration, B. U. Musch, P. Hagler, A. Schafer, M. Gockeler, D. B. Renner and J. W. Negele, *Transverse momentum distributions of quarks from the lattice using extended gauge links*, PoS **LATTICE2007** (2007) 155 [[0710.4423](#)].
- [308] K. Orginos, A. Radyushkin, J. Karpie and S. Zafeiropoulos, *Lattice QCD exploration of parton pseudo-distribution functions*, Phys. Rev. **D96** (2017) 094503 [[1706.05373](#)].
- [309] F. Landry, R. Brock, P. M. Nadolsky and C. Yuan, *Tevatron Run-1 Z boson data and Collins-Soper-Sterman resummation formalism*, Phys. Rev. **D67** (2003) 073016 [[hep-ph/0212159](#)].
- [310] P. Sun, J. Isaacson, C. P. Yuan and F. Yuan, *Nonperturbative functions for SIDIS and Drell-Yan processes*, Int. J. Mod. Phys. **A33** (2018) 1841006 [[1406.3073](#)].
- [311] A. Kulesza, G. F. Sterman and W. Vogelsang, *Joint resummation for Higgs production*, Phys. Rev. **D69** (2004) 014012 [[hep-ph/0309264](#)].
- [312] S. Catani, D. de Florian, M. Grazzini and P. Nason, *Soft gluon resummation for Higgs boson production at hadron colliders*, JHEP **0307** (2003) 028 [[hep-ph/0306211](#)].
- [313] V. Bertone, I. Scimemi and A. Vladimirov, *Extraction of unpolarized quark transverse momentum dependent parton distributions from Drell-Yan/Z-boson production*, [1902.08474](#).
- [314] I. Scimemi and A. Vladimirov, *Non-perturbative structure of semi-inclusive deep-inelastic and Drell-Yan scattering at small transverse momentum*, JHEP **06** (2020) 137 [[1912.06532](#)].
- [315] A. A. Vladimirov, *Self-contained definition of the Collins-Soper kernel*, Phys. Rev. Lett. **125** (2020) 192002 [[2003.02288](#)].
- [316] A. V. Konychev and P. M. Nadolsky, *Universality of the Collins-Soper-Sterman nonperturbative function in gauge boson production*, Phys. Lett. **B633** (2006) 710 [[hep-ph/0506225](#)].
- [317] C. Aidala, B. Field, L. Gamberg and T. Rogers, *Limits on TMD Evolution From Semi-Inclusive Deep Inelastic Scattering at Moderate Q*, Phys. Rev. **D89** (2014) 094002 [[1401.2654](#)].
- [318] A. Vladimirov, *Pion-induced Drell-Yan processes within TMD factorization*, JHEP **10** (2019) 090 [[1907.10356](#)].
- [319] A. A. Vladimirov, *Correspondence between Soft and Rapidity Anomalous Dimensions*, Phys. Rev. Lett. **118** (2017) 062001 [[1610.05791](#)].
- [320] I. Scimemi and A. Vladimirov, *Analysis of vector boson production within TMD factorization*, Eur. Phys. J. **C78** (2018) 89 [[1706.01473](#)].

- [321] A. Bacchetta, V. Bertone, C. Bissolotti, G. Bozzi, F. Delcarro, F. Piacenza et al., *Transverse-momentum-dependent parton distributions up to  $N^3LL$  from Drell-Yan data*, JHEP **07** (2020) 117 [[1912.07550](#)].
- [322] M. G. Echevarria, A. Idilbi, Z.-B. Kang and I. Vitev, *QCD Evolution of the Sivers Asymmetry*, Phys. Rev. **D89** (2014) 074013 [[1401.5078](#)].
- [323] G. Moreno et al., *Dimuon production in proton - copper collisions at  $\sqrt{s} = 38.8\text{-GeV}$* , Phys. Rev. D **43** (1991) 2815.
- [324] A. Ito et al., *Measurement of the Continuum of Dimuons Produced in High-Energy Proton - Nucleus Collisions*, Phys. Rev. D **23** (1981) 604.
- [325] CDF collaboration, T. Affolder et al., *The transverse momentum and total cross section of  $e^+e^-$  pairs in the Z boson region from  $p\bar{p}$  collisions at  $\sqrt{s} = 1.8\text{ TeV}$* , Phys. Rev. Lett. **84** (2000) 845 [[hep-ex/0001021](#)].
- [326] CDF collaboration, T. Aaltonen et al., *Transverse momentum cross section of  $e^+e^-$  pairs in the Z-boson region from  $p\bar{p}$  collisions at  $\sqrt{s} = 1.96\text{ TeV}$* , Phys. Rev. D **86** (2012) 052010 [[1207.7138](#)].
- [327] D0 collaboration, B. Abbott et al., *Measurement of the inclusive differential cross section for Z bosons as a function of transverse momentum in  $\bar{p}p$  collisions at  $\sqrt{s} = 1.8\text{ TeV}$* , Phys. Rev. D **61** (2000) 032004 [[hep-ex/9907009](#)].
- [328] D0 collaboration, V. Abazov et al., *Measurement of the shape of the boson transverse momentum distribution in  $p\bar{p} \rightarrow Z/\gamma^* \rightarrow e^+e^- + X$  events produced at  $\sqrt{s}=1.96\text{-TeV}$* , Phys. Rev. Lett. **100** (2008) 102002 [[0712.0803](#)].
- [329] D0 collaboration, V. M. Abazov et al., *Measurement of the Normalized  $Z/\gamma^* \rightarrow \mu^+\mu^-$  Transverse Momentum Distribution in  $p\bar{p}$  Collisions at  $\sqrt{s} = 1.96\text{ TeV}$* , Phys. Lett. B **693** (2010) 522 [[1006.0618](#)].
- [330] LHCb collaboration, R. Aaij et al., *Measurement of the forward Z boson production cross-section in  $pp$  collisions at  $\sqrt{s} = 7\text{ TeV}$* , JHEP **08** (2015) 039 [[1505.07024](#)].
- [331] LHCb collaboration, R. Aaij et al., *Measurement of forward W and Z boson production in  $pp$  collisions at  $\sqrt{s} = 8\text{ TeV}$* , JHEP **01** (2016) 155 [[1511.08039](#)].
- [332] LHCb collaboration, R. Aaij et al., *Measurement of the forward Z boson production cross-section in  $pp$  collisions at  $\sqrt{s} = 13\text{ TeV}$* , JHEP **09** (2016) 136 [[1607.06495](#)].
- [333] CMS collaboration, S. Chatrchyan et al., *Measurement of the Rapidity and Transverse Momentum Distributions of Z Bosons in  $pp$  Collisions at  $\sqrt{s} = 7\text{ TeV}$* , Phys. Rev. **D85** (2012) 032002 [[1110.4973](#)].
- [334] CMS collaboration, V. Khachatryan et al., *Measurement of the transverse momentum spectra of weak vector bosons produced in proton-proton collisions at  $\sqrt{s} = 8\text{ TeV}$* , JHEP **02** (2017) 096 [[1606.05864](#)].

- [335] ATLAS collaboration, G. Aad et al., *Measurement of the transverse momentum and  $\phi_\eta^*$  distributions of Drell–Yan lepton pairs in proton–proton collisions at  $\sqrt{s} = 8$  TeV with the ATLAS detector*, *Eur. Phys. J.* **C76** (2016) 291 [1512.02192].
- [336] D. Boer, M. Diehl, R. Milner, R. Venugopalan, W. Vogelsang et al., *Gluons and the quark sea at high energies: Distributions, polarization, tomography*, 1108.1713.
- [337] J. Dudek et al., *Physics Opportunities with the 12 GeV Upgrade at Jefferson Lab*, *Eur. Phys. J.* **A48** (2012) 187 [1208.1244].
- [338] E.-C. Aschenauer, A. Bazilevsky, M. Diehl, J. Drachenberg, K. O. Eyser et al., *The RHIC SPIN Program: Achievements and Future Opportunities*, 1501.01220.
- [339] COMPASS collaboration, F. Gautheron et al., *COMPASS-II Proposal*, .
- [340] COMPASS collaboration, F. Bradamante, *The future SIDIS measurement on transversely polarized deuterons by the COMPASS Collaboration*, *PoS SPIN2018* (2018) 045 [1812.07281].
- [341] M. Anselmino, M. Boglione, U. D'Alesio, S. Melis, F. Murgia and A. Prokudin, *New insight on the Sivers transverse momentum dependent distribution function*, *J. Phys. Conf. Ser.* **295** (2011) 012062 [1012.3565].
- [342] M. Anselmino, M. Boglione, U. D'Alesio, A. Kotzinian, F. Murgia and A. Prokudin, *Extracting the Sivers function from polarized SIDIS data and making predictions*, *Phys. Rev.* **D72** (2005) 094007 [hep-ph/0507181].
- [343] M. Anselmino et al., *Comparing extractions of Sivers functions*, in *Transversity. Proceedings, Workshop, Como, Italy, September 7-10, 2005*, pp. 236–243, 2005, hep-ph/0511017, DOI.
- [344] J. Collins, A. Efremov, K. Goeke, S. Menzel, A. Metz et al., *Sivers effect in semi-inclusive deeply inelastic scattering*, *Phys. Rev.* **D73** (2006) 014021 [hep-ph/0509076].
- [345] W. Vogelsang and F. Yuan, *Single-transverse spin asymmetries: From DIS to hadronic collisions*, *Phys. Rev.* **D72** (2005) 054028 [hep-ph/0507266].
- [346] M. Anselmino, M. Boglione, U. D'Alesio, A. Kotzinian, S. Melis, F. Murgia et al., *Sivers Effect for Pion and Kaon Production in Semi-Inclusive Deep Inelastic Scattering*, *Eur. Phys. J.* **A39** (2009) 89 [0805.2677].
- [347] A. Bacchetta and M. Radici, *Constraining quark angular momentum through semi-inclusive measurements*, *Phys. Rev. Lett.* **107** (2011) 212001 [1107.5755].
- [348] A. Bacchetta, F. Delcarro, C. Pisano and M. Radici, *The three-dimensional distribution of quarks in momentum space*, 2004.14278.
- [349] M. G. Echevarria, Z.-B. Kang and J. Terry, *Global analysis of the Sivers functions at NLO+NNLL in QCD*, *JHEP* **01** (2021) 126 [2009.10710].

- [350] M. Bury, A. Prokudin and A. Vladimirov, *Extraction of the Sivers Function from SIDIS, Drell-Yan, and  $W^\pm/Z$  Data at Next-to-Next-to-Next-to Leading Order*, *Phys. Rev. Lett.* **126** (2021) 112002 [2012.05135].
- [351] HERMES collaboration, A. Airapetian et al., *Observation of the Naive-T-odd Sivers Effect in Deep-Inelastic Scattering*, *Phys. Rev. Lett.* **103** (2009) 152002 [0906.3918].
- [352] HERMES collaboration, A. Airapetian et al., *Azimuthal single- and double-spin asymmetries in semi-inclusive deep-inelastic lepton scattering by transversely polarized protons*, 2007.07755.
- [353] COMPASS collaboration, M. Alekseev et al., *Collins and Sivers asymmetries for pions and kaons in muon-deuteron DIS*, *Phys. Lett.* **B673** (2009) 127 [0802.2160].
- [354] COMPASS collaboration, C. Adolph et al., *Collins and Sivers asymmetries in muonproduction of pions and kaons off transversely polarised protons*, *Phys. Lett.* **B744** (2015) 250 [1408.4405].
- [355] JEFFERSON LAB HALL A collaboration, X. Qian et al., *Single Spin Asymmetries in Charged Pion Production from Semi-Inclusive Deep Inelastic Scattering on a Transversely Polarized  $^3\text{He}$  Target*, *Phys. Rev. Lett.* **107** (2011) 072003 [1106.0363].
- [356] STAR collaboration, L. Adamczyk et al., *Measurement of the transverse single-spin asymmetry in  $p^\uparrow + p \rightarrow W^\pm/Z^0$  at RHIC*, *Phys. Rev. Lett.* **116** (2016) 132301 [1511.06003].
- [357] JEFFERSON LAB HALL A collaboration, Y. X. Zhao et al., *Single spin asymmetries in charged kaon production from semi-inclusive deep inelastic scattering on a transversely polarized  $^3\text{He}$  target*, *Phys. Rev.* **C90** (2014) 055201 [1404.7204].
- [358] COMPASS collaboration, C. Adolph et al., *Sivers asymmetry extracted in SIDIS at the hard scales of the Drell-Yan process at COMPASS*, *Phys. Lett.* **B770** (2017) 138 [1609.07374].
- [359] M. Anselmino, M. Boglione, U. D'Alesio, F. Murgia and A. Prokudin, *Study of the sign change of the Sivers function from STAR Collaboration  $W/Z$  production data*, *JHEP* **04** (2017) 046 [1612.06413].
- [360] M. Boglione, U. D'Alesio, C. Flore and J. Gonzalez-Hernandez, *Assessing signals of TMD physics in SIDIS azimuthal asymmetries and in the extraction of the Sivers function*, *JHEP* **07** (2018) 148 [1806.10645].
- [361] M. Bury, A. Prokudin and A. Vladimirov, *Extraction of the Sivers function from SIDIS, Drell-Yan, and  $W^\pm/Z$  boson production data with TMD evolution*, *JHEP* **05** (2021) 151 [2103.03270].
- [362] J.-W. Qiu, T. C. Rogers and B. Wang, *Intrinsic Transverse Momentum and Evolution in Weighted Spin Asymmetries*, *Phys. Rev. D* **101** (2020) 116017 [2004.13193].

- [363] R. L. Jaffe and X.-D. Ji, *Chiral odd parton distributions and polarized Drell-Yan*, *Phys. Rev. Lett.* **67** (1991) 552.
- [364] G. R. Goldstein and M. J. Moravcsik, *Optimally Simple Connection Between the Reaction Matrix and the Observables*, *Annals Phys.* **98** (1976) 128.
- [365] X. Artru and M. Mekhfi, *Transversely Polarized Parton Densities, their Evolution and their Measurement*, *Z. Phys. C* **45** (1990) 669.
- [366] J. Soffer, *Positivity constraints for spin dependent parton distributions*, *Phys. Rev. Lett.* **74** (1995) 1292 [[hep-ph/9409254](#)].
- [367] V. Barone, *On the QCD evolution of the transversity distribution*, *Phys. Lett. B* **409** (1997) 499 [[hep-ph/9703343](#)].
- [368] W. Vogelsang, *Next-to-leading order evolution of transversity distributions and Soffer's inequality*, *Phys. Rev. D* **57** (1998) 1886 [[hep-ph/9706511](#)].
- [369] HERMES collaboration, A. Airapetian et al., *Effects of transversity in deep-inelastic scattering by polarized protons*, *Phys. Lett. B* **693** (2010) 11 [[1006.4221](#)].
- [370] Z.-B. Kang, A. Prokudin, P. Sun and F. Yuan, *Nucleon tensor charge from Collins azimuthal asymmetry measurements*, *Phys. Rev. D* **91** (2015) 071501 [[1410.4877](#)].
- [371] M. Anselmino, M. Boglione, U. D'Alesio, S. Melis, F. Murgia et al., *Simultaneous extraction of transversity and Collins functions from new SIDIS and  $e^+e^-$  data*, *Phys. Rev. D* **87** (2013) 094019 [[1303.3822](#)].
- [372] M. Anselmino, M. Boglione, U. D'Alesio, J. O. Gonzalez Hernandez, S. Melis, F. Murgia et al., *Collins functions for pions from SIDIS and new  $e^+e^-$  data: a first glance at their transverse momentum dependence*, *Phys. Rev. D* **92** (2015) 114023 [[1510.05389](#)].
- [373] M. Radici and A. Bacchetta, *First Extraction of Transversity from a Global Analysis of Electron-Proton and Proton-Proton Data*, *Phys. Rev. Lett.* **120** (2018) 192001 [[1802.05212](#)].
- [374] J. Benel, A. Courtoy and R. Ferro-Hernandez, *A constrained fit of the valence transversity distributions from dihadron production*, *Eur. Phys. J. C* **80** (2020) 465 [[1912.03289](#)].
- [375] U. D'Alesio, C. Flore and A. Prokudin, *Role of the Soffer bound in determination of transversity and the tensor charge*, *Phys. Lett. B* **803** (2020) 135347 [[2001.01573](#)].
- [376] COMPASS collaboration, V. Y. Alexakhin et al., *First measurement of the transverse spin asymmetries of the deuteron in semi-inclusive deep inelastic scattering*, *Phys. Rev. Lett.* **94** (2005) 202002 [[hep-ex/0503002](#)].
- [377] BELLE collaboration, R. Seidl et al., *Measurement of Azimuthal Asymmetries in Inclusive Production of Hadron Pairs in  $e^+e^-$  Annihilation at  $s^{**}(1/2) = 10.58\text{-GeV}$* , *Phys. Rev. D* **78** (2008) 032011 [[0805.2975](#)].

- [378] BABAR collaboration, J. P. Lees et al., *Measurement of Collins asymmetries in inclusive production of charged pion pairs in  $e^+e^-$  annihilation at BABAR*, *Phys. Rev.* **D90** (2014) 052003 [[1309.5278](#)].
- [379] J. Wan, C. Tan and Z. Lu, *The  $\cos 2\phi$  azimuthal asymmetry in  $e^+e^- \rightarrow \pi^+\pi^- X$  process*, *Phys. Lett. B* **811** (2020) 135884.
- [380] A. V. Efremov, K. Goeke and P. Schweitzer, *Collins effect in semi-inclusive deeply inelastic scattering and in  $e^+e^-$  annihilation*, *Phys. Rev. D* **73** (2006) 094025 [[hep-ph/0603054](#)].
- [381] G. R. Goldstein, J. O. Gonzalez Hernandez and S. Liuti, *Flavor dependence of chiral odd generalized parton distributions and the tensor charge from the analysis of combined  $\pi^0$  and  $\eta$  exclusive electroproduction data*, [1401.0438](#).
- [382] M. Radici, A. Courtoy, A. Bacchetta and M. Guagnelli, *Improved extraction of valence transversity distributions from inclusive dihadron production*, *JHEP* **05** (2015) 123 [[1503.03495](#)].
- [383] R. Gupta, Y.-C. Jang, B. Yoon, H.-W. Lin, V. Cirigliano and T. Bhattacharya, *Isovector Charges of the Nucleon from 2+1+1-flavor Lattice QCD*, *Phys. Rev. D* **98** (2018) 034503 [[1806.09006](#)].
- [384] N. Hasan, J. Green, S. Meinel, M. Engelhardt, S. Krieg, J. Negele et al., *Nucleon axial, scalar, and tensor charges using lattice QCD at the physical pion mass*, *Phys. Rev. D* **99** (2019) 114505 [[1903.06487](#)].
- [385] C. Alexandrou, S. Bacchio, M. Constantinou, J. Finkenrath, K. Hadjyiannakou, K. Jansen et al., *Nucleon axial, tensor, and scalar charges and  $\sigma$ -terms in lattice QCD*, *Phys. Rev. D* **102** (2020) 054517 [[1909.00485](#)].
- [386] M. Pitschmann, C.-Y. Seng, C. D. Roberts and S. M. Schmidt, *Nucleon tensor charges and electric dipole moments*, *Phys. Rev. D* **91** (2015) 074004 [[1411.2052](#)].
- [387] R. L. Jaffe and X.-D. Ji, *Chiral odd parton distributions and Drell-Yan processes*, *Nucl. Phys. B* **375** (1992) 527.
- [388] J. L. Cortes, B. Pire and J. P. Ralston, *Measuring the transverse polarization of quarks in the proton*, *Z. Phys. C* **55** (1992) 409.
- [389] L. P. Gamberg and G. R. Goldstein, *Flavor spin symmetry estimate of the nucleon tensor charge*, *Phys. Rev. Lett.* **87** (2001) 242001 [[hep-ph/0107176](#)].
- [390] A. Courtoy, S. Baessler, M. González-Alonso and S. Liuti, *Beyond-Standard-Model Tensor Interaction and Hadron Phenomenology*, *Phys. Rev. Lett.* **115** (2015) 162001 [[1503.06814](#)].
- [391] N. Yamanaka, B. K. Sahoo, N. Yoshinaga, T. Sato, K. Asahi and B. P. Das, *Probing exotic phenomena at the interface of nuclear and particle physics with the electric dipole moments of diamagnetic atoms: A unique window to hadronic and semi-leptonic CP violation*, *Eur. Phys. J. A* **53** (2017) 54 [[1703.01570](#)].

- [392] T. Liu, Z. Zhao and H. Gao, *Experimental constraint on quark electric dipole moments*, *Phys. Rev. D* **97** (2018) 074018 [[1704.00113](#)].
- [393] M. González-Alonso, O. Naviliat-Cuncic and N. Severijns, *New physics searches in nuclear and neutron  $\beta$  decay*, *Prog. Part. Nucl. Phys.* **104** (2019) 165 [[1803.08732](#)].
- [394] JLQCD collaboration, N. Yamanaka, S. Hashimoto, T. Kaneko and H. Ohki, *Nucleon charges with dynamical overlap fermions*, *Phys. Rev. D* **98** (2018) 054516 [[1805.10507](#)].
- [395] J. F. Owens, *Large Momentum Transfer Production of Direct Photons, Jets, and Particles*, *Rev. Mod. Phys.* **59** (1987) 465.
- [396] C. Kouvaris, J.-W. Qiu, W. Vogelsang and F. Yuan, *Single transverse-spin asymmetry in high transverse momentum pion production in  $p\ p$  collisions*, *Phys. Rev. D* **74** (2006) 114013 [[hep-ph/0609238](#)].
- [397] Z.-B. Kang, I. Vitev and H. Xing, *Multiple scattering effects on inclusive particle production in the large- $x$  regime*, *Phys. Rev. D* **88** (2013) 054010 [[1307.3557](#)].
- [398] A. Efremov and O. Teryaev, *QCD Asymmetry and Polarized Hadron Structure Functions*, *Phys.Lett. B* **150** (1985) 383.
- [399] H. Eguchi, Y. Koike and K. Tanaka, *Single Transverse Spin Asymmetry for Large- $p(T)$  Pion Production in Semi-Inclusive Deep Inelastic Scattering*, *Nucl.Phys. B* **752** (2006) 1 [[hep-ph/0604003](#)].
- [400] H. Eguchi, Y. Koike and K. Tanaka, *Twist-3 Formalism for Single Transverse Spin Asymmetry Reexamined: Semi-Inclusive Deep Inelastic Scattering*, *Nucl.Phys. B* **763** (2007) 198 [[hep-ph/0610314](#)].
- [401] Y. Koike and T. Tomita, *Soft-fermion-pole contribution to single-spin asymmetry for pion production in  $pp$  collisions*, *Phys.Lett. B* **675** (2009) 181 [[0903.1923](#)].
- [402] A. Metz and D. Pitonyak, *Fragmentation contribution to the transverse single-spin asymmetry in proton-proton collisions*, *Phys.Lett. B* **723** (2013) 365 [[1212.5037](#)].
- [403] H. Beppu, K. Kanazawa, Y. Koike and S. Yoshida, *Three-gluon contribution to the single spin asymmetry for light hadron production in  $pp$  collision*, *Phys. Rev. D* **89** (2014) 034029 [[1312.6862](#)].
- [404] STAR collaboration, J. Adam et al., *Measurement of transverse single-spin asymmetries of  $\pi^0$  and electromagnetic jets at forward rapidity in 200 and 500 GeV transversely polarized proton-proton collisions*, [2012.11428](#).
- [405] S. M. Aybat, J. C. Collins, J.-W. Qiu and T. C. Rogers, *The QCD Evolution of the Sivers Function*, *Phys.Rev. D* **85** (2012) 034043 [[1110.6428](#)].
- [406] Y. Kanazawa and Y. Koike, *Chiral odd contribution to single transverse spin asymmetry in hadronic pion production*, *Phys.Lett. B* **478** (2000) 121 [[hep-ph/0001021](#)].

- [407] L. Gamberg, Z.-B. Kang, D. Pitonyak and A. Prokudin, *Phenomenological constraints on  $A_N$  in  $p^\uparrow p \rightarrow \pi X$  from Lorentz invariance relations*, *Phys. Lett. B* **770** (2017) 242 [1701.09170].
- [408] BRAHMS collaboration, J. Lee and F. Videbaek, *Single spin asymmetries of identified hadrons in polarized  $p + p$  at  $s^{**}(1/2) = 62.4$  and 200-GeV*, *AIP Conf. Proc.* **915** (2007) 533.
- [409] STAR collaboration, J. Adams et al., *Cross-sections and transverse single spin asymmetries in forward neutral pion production from proton collisions at  $s^{**}(1/2) = 200$ - GeV*, *Phys. Rev. Lett.* **92** (2004) 171801 [hep-ex/0310058].
- [410] STAR collaboration, B. Abelev et al., *Forward Neutral Pion Transverse Single Spin Asymmetries in  $p+p$  Collisions at  $s^{**}(1/2) = 200$ -GeV*, *Phys. Rev. Lett.* **101** (2008) 222001 [0801.2990].
- [411] STAR collaboration, L. Adamczyk et al., *Transverse Single-Spin Asymmetry and Cross-Section for  $\pi^0$  and  $\eta$  Mesons at Large Feynman- $x$  in Polarized  $p + p$  Collisions at  $\sqrt{s} = 200$  GeV*, *Phys. Rev. D* **86** (2012) 051101 [1205.6826].
- [412] G. Bunce, R. Handler, R. March, P. Martin, L. Pondrom et al., *Lambda0 Hyperon Polarization in Inclusive Production by 300-GeV Protons on Beryllium.*, *Phys. Rev. Lett.* **36** (1976) 1113.
- [413] K. Krueger et al., *Large analyzing power in inclusive  $\pi^+$ - production at high  $x(F)$  with a 22-GeV/c polarized proton beam*, *Phys. Lett. B* **459** (1999) 412.
- [414] C. Allgower et al., *Measurement of analyzing powers of  $\pi^+$  and  $\pi^-$  produced on a hydrogen and a carbon target with a 22-GeV/c incident polarized proton beam*, *Phys. Rev. D* **65** (2002) 092008.
- [415] PHENIX collaboration, S. Adler et al., *Measurement of transverse single-spin asymmetries for mid-rapidity production of neutral pions and charged hadrons in polarized  $p+p$  collisions at  $s^{**}(1/2) = 200$ -GeV*, *Phys. Rev. Lett.* **95** (2005) 202001 [hep-ex/0507073].
- [416] BRAHMS collaboration, I. Arsene et al., *Single Transverse Spin Asymmetries of Identified Charged Hadrons in Polarized  $p+p$  Collisions at  $s^{**}(1/2) = 62.4$ -GeV*, *Phys. Rev. Lett.* **101** (2008) 042001 [0801.1078].
- [417] STAR collaboration, L. Adamczyk et al., *Longitudinal and transverse spin asymmetries for inclusive jet production at mid-rapidity in polarized  $p + p$  collisions at  $\sqrt{s} = 200$  GeV*, *Phys. Rev. D* **86** (2012) 032006 [1205.2735].
- [418] ANDY collaboration, L. Bland et al., *Cross Sections and Transverse Single-Spin Asymmetries in Forward Jet Production from Proton Collisions at  $\sqrt{s} = 500$  GeV*, *Phys. Lett. B* **750** (2015) 660 [1304.1454].
- [419] PHENIX collaboration, A. Adare et al., *Measurement of transverse-single-spin asymmetries for midrapidity and forward-rapidity production of hadrons in polarized  $p+p$  collisions at  $\sqrt{s} = 200$  and 62.4 GeV*, *Phys. Rev. D* **90** (2014) 012006 [1312.1995].

- [420] PHENIX collaboration, A. Adare et al., *Cross section and transverse single-spin asymmetry of  $\eta$  mesons in  $p^\uparrow + p$  collisions at  $\sqrt{s} = 200$  GeV at forward rapidity*, *Phys. Rev. D* **90** (2014) 072008 [[1406.3541](#)].
- [421] PHENIX collaboration, U. Acharya et al., *Transverse momentum dependent forward neutron single spin asymmetries in transversely polarized  $p+p$  collisions at  $\sqrt{s} = 200$  GeV*, [2011.14187](#).
- [422] K. Kanazawa, Y. Koike, A. Metz and D. Pitonyak, *Towards an explanation of transverse single-spin asymmetries in proton-proton collisions: the role of fragmentation in collinear factorization*, *Phys. Rev. D* **89** (2014) 111501 [[1404.1033](#)].
- [423] D. Boer, *Investigating the origins of transverse spin asymmetries at RHIC*, *Phys. Rev. D* **60** (1999) 014012 [[hep-ph/9902255](#)].
- [424] D. Boer and W. Vogelsang, *Drell-Yan lepton angular distribution at small transverse momentum*, *Phys. Rev. D* **74** (2006) 014004 [[hep-ph/0604177](#)].
- [425] C. Lam and W.-K. Tung, *A Systematic Approach to Inclusive Lepton Pair Production in Hadronic Collisions*, *Phys. Rev. D* **18** (1978) 2447.
- [426] C. Lam and W.-K. Tung, *A Parton Model Relation Sans {QCD} Modifications in Lepton Pair Productions*, *Phys. Rev. D* **21** (1980) 2712.
- [427] J. C. Collins, *Simple Prediction of {QCD} for Angular Distribution of Dileptons in Hadron Collisions*, *Phys. Rev. Lett.* **42** (1979) 291.
- [428] E. Mirkes and J. Ohnemus, *Angular distributions of Drell-Yan lepton pairs at the Tevatron: Order  $\alpha - s^2$  corrections and Monte Carlo studies*, *Phys. Rev. D* **51** (1995) 4891 [[hep-ph/9412289](#)].
- [429] R. Gauld, A. Gehrmann-De Ridder, T. Gehrmann, E. W. N. Glover and A. Huss, *Precise predictions for the angular coefficients in Z-boson production at the LHC*, *JHEP* **11** (2017) 003 [[1708.00008](#)].
- [430] NA10 collaboration, S. Falciano et al., *Angular Distributions of Muon Pairs Produced by 194-{GeV}/c Negative Pions*, *Z. Phys. C* **31** (1986) 513.
- [431] NA10 collaboration, M. Guanziroli et al., *Angular Distributions of Muon Pairs Produced by Negative Pions on Deuterium and Tungsten*, *Z. Phys. C* **37** (1988) 545.
- [432] J. Conway et al., *Experimental Study of Muon Pairs Produced by 252-GeV Pions on Tungsten*, *Phys. Rev. D* **39** (1989) 92.
- [433] NuSea collaboration, L. Zhu et al., *Measurement of Angular Distributions of Drell-Yan Dimuons in  $p + d$  Interaction at 800-GeV/c*, *Phys. Rev. Lett.* **99** (2007) 082301 [[hep-ex/0609005](#)].

- [434] NuSEA collaboration, L. Zhu et al., *Measurement of Angular Distributions of Drell-Yan Dimuons in  $p + p$  Interactions at 800-GeV/c*, *Phys. Rev. Lett.* **102** (2009) 182001 [0811.4589].
- [435] CDF collaboration, T. Aaltonen et al., *First Measurement of the Angular Coefficients of Drell-Yan  $e^+e^-$  pairs in the Z Mass Region from  $p\bar{p}$  Collisions at  $\sqrt{s} = 1.96$  TeV*, *Phys. Rev. Lett.* **106** (2011) 241801 [1103.5699].
- [436] CMS collaboration, V. Khachatryan et al., *Angular coefficients of Z bosons produced in pp collisions at  $\sqrt{s} = 8$  TeV and decaying to  $\mu^+\mu^-$  as a function of transverse momentum and rapidity*, *Phys. Lett. B* **750** (2015) 154 [1504.03512].
- [437] B. Zhang, Z. Lu, B.-Q. Ma and I. Schmidt, *Extracting Boer-Mulders functions from  $p+D$  Drell-Yan processes*, *Phys. Rev. D* **77** (2008) 054011 [0803.1692].
- [438] Z. Lu and I. Schmidt, *Updating Boer-Mulders functions from unpolarized pd and pp Drell-Yan data*, *Phys. Rev. D* **81** (2010) 034023 [0912.2031].
- [439] M. Lambertsen and W. Vogelsang, *Drell-Yan lepton angular distributions in perturbative QCD*, *Phys. Rev. D* **93** (2016) 114013 [1605.02625].
- [440] J.-C. Peng, W.-C. Chang, R. E. McClellan and O. Teryaev, *Interpretation of Angular Distributions of Z-boson Production at Colliders*, *Phys. Lett. B* **758** (2016) 384 [1511.08932].
- [441] W.-C. Chang, R. E. McClellan, J.-C. Peng and O. Teryaev, *Dependencies of lepton angular distribution coefficients on the transverse momentum and rapidity of Z bosons produced in pp collisions at the LHC*, *Phys. Rev. D* **96** (2017) 054020 [1708.05807].
- [442] J.-C. Peng, D. Boer, W.-C. Chang, R. E. McClellan and O. Teryaev, *On the rotational invariance and non-invariance of lepton angular distributions in Drell-Yan and quarkonium production*, *Phys. Lett. B* **789** (2019) 356 [1808.04398].
- [443] W.-C. Chang, R. E. McClellan, J.-C. Peng and O. Teryaev, *Lepton Angular Distributions of Fixed-target Drell-Yan Experiments in Perturbative QCD and a Geometric Approach*, *Phys. Rev. D* **99** (2019) 014032 [1811.03256].
- [444] Y. Lyu, W.-C. Chang, R. E. McClellan, J.-C. Peng and O. Teryaev, *Lepton Angular Distribution of W Boson Productions*, 2010.01826.
- [445] CLAS collaboration, M. Osipenko et al., *Measurement of unpolarized semi-inclusive pi+ electroproduction off the proton*, *Phys. Rev. D* **80** (2009) 032004 [0809.1153].
- [446] JEFFERSON LAB HALL A collaboration, X. Yan et al., *First measurement of unpolarized semi-inclusive deep-inelastic scattering cross sections from a  ${}^3\text{He}$  target*, *Phys. Rev. C* **95** (2017) 035209 [1610.02350].
- [447] HERMES collaboration, A. Airapetian et al., *Azimuthal distributions of charged hadrons, pions, and kaons produced in deep-inelastic scattering off unpolarized protons and deuterons*, *Phys. Rev. D* **87** (2013) 012010 [1204.4161].

- [448] COMPASS collaboration, C. Adolph et al., *Measurement of azimuthal hadron asymmetries in semi-inclusive deep inelastic scattering off unpolarised nucleons*, *Nucl. Phys.* **B886** (2014) 1046 [[1401.6284](#)].
- [449] COMPASS collaboration, A. Moretti, *Azimuthal asymmetries of hadrons produced in unpolarized SIDIS at COMPASS*, *J. Phys. Conf. Ser.* **1435** (2020) 012043.
- [450] V. Barone, S. Melis and A. Prokudin, *The Boer-Mulders effect in unpolarized SIDIS: An Analysis of the COMPASS and HERMES data on the cos 2 phi asymmetry*, *Phys. Rev.* **D81** (2010) 114026 [[0912.5194](#)].
- [451] V. Barone, S. Melis and A. Prokudin, *Azimuthal asymmetries in unpolarized Drell-Yan processes and the Boer-Mulders distributions of antiquarks*, *Phys. Rev.* **D82** (2010) 114025 [[1009.3423](#)].
- [452] V. Barone, M. Boglione, J. O. Gonzalez Hernandez and S. Melis, *Phenomenological analysis of azimuthal asymmetries in unpolarized semi-inclusive deep inelastic scattering*, *Phys. Rev.* **D91** (2015) 074019 [[1502.04214](#)].
- [453] E. Christova, E. Leader and M. Stoilov, *Consistency tests for the extraction of the Boer-Mulders and Sivers functions*, *Phys. Rev. D* **97** (2018) 056018 [[1705.10613](#)].
- [454] E. Christova, D. Kotlorz and E. Leader, *New study of the Boer-Mulders function: Implications for the quark and hadron transverse momenta*, *Phys. Rev. D* **102** (2020) 014035 [[2004.02117](#)].
- [455] S. Bhattacharya, Z.-B. Kang, A. Metz, G. Penn and D. Pitonyak, *First global QCD analysis of the TMD  $g_{1T}$  from semi-inclusive DIS data*, [2110.10253](#).
- [456] COMPASS collaboration, C. Adolph et al., *Sivers asymmetry extracted in SIDIS at the hard scales of the Drell-Yan process at COMPASS*, *Phys. Lett. B* **770** (2017) 138 [[1609.07374](#)].
- [457] B. Parsamyan, *Measurement of target-polarization dependent azimuthal asymmetries in SIDIS and Drell-Yan processes at COMPASS experiment*, *PoS QCDEV2017* (2018) 042.
- [458] HERMES collaboration, A. Airapetian et al., *Azimuthal single- and double-spin asymmetries in semi-inclusive deep-inelastic lepton scattering by transversely polarized protons*, *JHEP* **12** (2020) 010 [[2007.07755](#)].
- [459] JEFFERSON LAB HALL A collaboration, J. Huang et al., *Beam-Target Double Spin Asymmetry  $A_{LT}$  in Charged Pion Production from Deep Inelastic Scattering on a Transversely Polarized  ${}^3\text{He}$  Target at  $1.4 < Q^2 < 2.7 \text{ GeV}^2$* , *Phys. Rev. Lett.* **108** (2012) 052001 [[1108.0489](#)].
- [460] R. Tangerman and P. Mulders, *Polarized twist - three distributions  $g(T)$  and  $h(L)$  and the role of intrinsic transverse momentum*, [hep-ph/9408305](#).
- [461] A. Kotzinian, B. Parsamyan and A. Prokudin, *Predictions for double spin asymmetry  $A(LT)$  in semi inclusive DIS*, *Phys. Rev. D* **73** (2006) 114017 [[hep-ph/0603194](#)].

- [462] H. Avakian, A. Efremov, K. Goeke, A. Metz, P. Schweitzer and T. Teckentrup, *Are there approximate relations among transverse momentum dependent distribution functions?*, *Phys. Rev. D* **77** (2008) 014023 [[0709.3253](#)].
- [463] A. Metz, P. Schweitzer and T. Teckentrup, *Lorentz invariance relations between parton distributions and the Wandzura-Wilczek approximation*, *Phys. Lett. B* **680** (2009) 141 [[0810.5212](#)].
- [464] T. Teckentrup, A. Metz and P. Schweitzer, *Lorentz invariance relations and Wandzura-Wilczek approximation*, *Mod. Phys. Lett. A* **24** (2009) 2950 [[0910.2567](#)].
- [465] P. V. Pobylitsa, *Transverse momentum dependent parton distributions in large N(c) QCD*, [hep-ph/0301236](#).
- [466] HERMES collaboration, A. Airapetian et al., *Observation of a single spin azimuthal asymmetry in semiinclusive pion electro production*, *Phys. Rev. Lett.* **84** (2000) 4047 [[hep-ex/9910062](#)].
- [467] HERMES collaboration, A. Airapetian et al., *Measurement of single spin azimuthal asymmetries in semiinclusive electroproduction of pions and kaons on a longitudinally polarized deuterium target*, *Phys. Lett.* **B562** (2003) 182 [[hep-ex/0212039](#)].
- [468] CLAS collaboration, H. Avakian et al., *Measurement of Single and Double Spin Asymmetries in Deep Inelastic Pion Electroproduction with a Longitudinally Polarized Target*, *Phys. Rev. Lett.* **105** (2010) 262002 [[1003.4549](#)].
- [469] Z. Lu, B.-Q. Ma and J. She, *The  $\sin 2\phi$  azimuthal asymmetry in single longitudinally polarized  $\pi N$  Drell-Yan process*, *Phys. Rev. D* **84** (2011) 034010 [[1104.5410](#)].
- [470] J. Zhu and B.-Q. Ma, *Proposal for measuring new transverse momentum dependent parton distributions  $g_{1T}$  and  $h_{1L}^\perp$  through semi-inclusive deep inelastic scattering*, *Phys. Lett.* **B696** (2011) 246 [[1104.4564](#)].
- [471] S. Boffi, A. V. Efremov, B. Pasquini and P. Schweitzer, *Azimuthal spin asymmetries in light-cone constituent quark models*, *Phys. Rev. D* **79** (2009) 094012 [[0903.1271](#)].
- [472] B.-Q. Ma, I. Schmidt and J.-J. Yang, *Nucleon transversity distribution from azimuthal spin asymmetry in pion electro production*, *Phys. Rev. D* **63** (2001) 037501 [[hep-ph/0009297](#)].
- [473] B.-Q. Ma, I. Schmidt and J.-J. Yang, *Azimuthal spin asymmetries of pion electro production*, *Phys. Rev. D* **65** (2002) 034010 [[hep-ph/0110324](#)].
- [474] H. Li and Z. Lu, *The  $\sin 2\phi_h$  azimuthal asymmetry of pion production in SIDIS within TMD factorization*, [2111.03840](#).
- [475] C. Lefky and A. Prokudin, *Extraction of the distribution function  $h_{1T}^\perp$  from experimental data*, *Phys. Rev. D* **91** (2015) 034010 [[1411.0580](#)].

- [476] S.-C. xue, X. Wang, D.-M. Li and Z. Lu, *Weighted  $\sin(3\phi h - \phi S)$  asymmetry from pretzelosity in SIDIS at electron ion colliders*, *Phys. Lett. B* **820** (2021) 136598 [2104.05173].
- [477] R. Angeles-Martinez et al., *Transverse Momentum Dependent (TMD) parton distribution functions: status and prospects*, *Acta Phys. Polon. B* **46** (2015) 2501 [1507.05267].
- [478] M. G. Echevarria, *Proper TMD factorization for quarkonia production:  $pp \rightarrow \eta_{c,b}$  as a study case*, *JHEP* **10** (2019) 144 [1907.06494].
- [479] C. Balazs, E. L. Berger, P. M. Nadolsky and C. P. Yuan, *All-orders resummation for diphoton production at hadron colliders*, *Phys. Lett. B* **637** (2006) 235 [hep-ph/0603037].
- [480] P. M. Nadolsky, C. Balazs, E. L. Berger and C. P. Yuan, *Gluon-gluon contributions to the production of continuum diphoton pairs at hadron colliders*, *Phys. Rev. D* **76** (2007) 013008 [hep-ph/0702003].
- [481] J.-W. Qiu, M. Schlegel and W. Vogelsang, *Probing Gluonic Spin-Orbit Correlations in Photon Pair Production*, *Phys. Rev. Lett.* **107** (2011) 062001 [1103.3861].
- [482] D. Boer, W. J. den Dunnen, C. Pisano, M. Schlegel and W. Vogelsang, *Linearly Polarized Gluons and the Higgs Transverse Momentum Distribution*, *Phys. Rev. Lett.* **108** (2012) 032002 [1109.1444].
- [483] P. Sun, B.-W. Xiao and F. Yuan, *Gluon Distribution Functions and Higgs Boson Production at Moderate Transverse Momentum*, *Phys. Rev. D* **84** (2011) 094005 [1109.1354].
- [484] D. Boer, W. J. den Dunnen, C. Pisano and M. Schlegel, *Determining the Higgs spin and parity in the diphoton decay channel*, *Phys. Rev. Lett.* **111** (2013) 032002 [1304.2654].
- [485] D. Boer and C. Pisano, *Polarized gluon studies with charmonium and bottomonium at LHCb and AFTER*, *Phys. Rev. D* **86** (2012) 094007 [1208.3642].
- [486] J. P. Ma, J. X. Wang and S. Zhao, *Transverse momentum dependent factorization for quarkonium production at low transverse momentum*, *Phys. Rev. D* **88** (2013) 014027 [1211.7144].
- [487] J. P. Ma, J. X. Wang and S. Zhao, *Breakdown of QCD Factorization for P-Wave Quarkonium Production at Low Transverse Momentum*, *Phys. Lett. B* **737** (2014) 103 [1405.3373].
- [488] W. J. den Dunnen, J.-P. Lansberg, C. Pisano and M. Schlegel, *Accessing the Transverse Dynamics and Polarization of Gluons inside the Proton at the LHC*, *Phys. Rev. Lett.* **112** (2014) 212001 [1401.7611].
- [489] J.-P. Lansberg, C. Pisano and M. Schlegel, *Associated production of a dilepton and a  $\Upsilon(J/\psi)$  at the LHC as a probe of gluon transverse momentum dependent distributions*, *Nucl. Phys. B* **920** (2017) 192 [1702.00305].

- [490] J.-P. Lansberg, C. Pisano, F. Scarpa and M. Schlegel, *Pinning down the linearly-polarised gluons inside unpolarised protons using quarkonium-pair production at the LHC*, *Phys. Lett. B* **784** (2018) 217 [[1710.01684](#)].
- [491] F. Scarpa, D. Boer, M. G. Echevarria, J.-P. Lansberg, C. Pisano and M. Schlegel, *Studies of gluon TMDs and their evolution using quarkonium-pair production at the LHC*, [1909.05769](#).
- [492] F. Yuan, *Heavy Quarkonium Production in Single Transverse Polarized High Energy Scattering*, *Phys. Rev. D* **78** (2008) 014024 [[0801.4357](#)].
- [493] D. Boer and W. J. den Dunnen, *TMD evolution and the Higgs transverse momentum distribution*, *Nucl. Phys. B* **886** (2014) 421 [[1404.6753](#)].
- [494] LHCb collaboration, R. Aaij et al., *Measurement of the  $J/\psi$  pair production cross-section in  $pp$  collisions at  $\sqrt{s} = 13$  TeV*, *JHEP* **06** (2017) 047 [[1612.07451](#)].
- [495] LHCb collaboration, R. Aaij et al., *Observation of  $J/\psi$  pair production in  $pp$  collisions at  $\sqrt{s} = 7$  TeV*, *Phys. Lett. B* **707** (2012) 52 [[1109.0963](#)].
- [496] CMS collaboration, V. Khachatryan et al., *Measurement of Prompt  $J/\psi$  Pair Production in  $pp$  Collisions at  $\sqrt{s} = 7$  TeV*, *JHEP* **09** (2014) 094 [[1406.0484](#)].
- [497] ATLAS collaboration, M. Aaboud et al., *Measurement of the prompt  $J/\psi$  pair production cross-section in  $pp$  collisions at  $\sqrt{s} = 8$  TeV with the ATLAS detector*, *Eur. Phys. J. C* **77** (2017) 76 [[1612.02950](#)].
- [498] D0 collaboration, V. M. Abazov et al., *Observation and Studies of Double  $J/\psi$  Production at the Tevatron*, *Phys. Rev. D* **90** (2014) 111101 [[1406.2380](#)].
- [499] A. Bacchetta, M. Boglione, A. Henneman and P. J. Mulders, *Bounds on transverse momentum dependent distribution and fragmentation functions*, *Phys. Rev. Lett.* **85** (2000) 712 [[hep-ph/9912490](#)].
- [500] C. Hadjidakis et al., *A Fixed-Target Programme at the LHC: Physics Case and Projected Performances for Heavy-Ion, Hadron, Spin and Astroparticle Studies*, [1807.00603](#).
- [501] D. Kikoła, M. G. Echevarria, C. Hadjidakis, J.-P. Lansberg, C. Lorcé, L. Massacrier et al., *Feasibility Studies for Single Transverse-Spin Asymmetry Measurements at a Fixed-Target Experiment Using the LHC Proton and Lead Beams (AFTER@LHC)*, *Few Body Syst.* **58** (2017) 139 [[1702.01546](#)].
- [502] C. A. Aidala et al., *The LHCSpin Project*, [1901.08002](#).
- [503] D. Boer, S. J. Brodsky, P. J. Mulders and C. Pisano, *Direct Probes of Linearly Polarized Gluons inside Unpolarized Hadrons*, *Phys. Rev. Lett.* **106** (2011) 132001 [[1011.4225](#)].
- [504] Z.-B. Kang, J. Reiten, D. Y. Shao and J. Terry, *QCD evolution of the gluon Sivers function in heavy flavor dijet production at the Electron-Ion Collider*, *JHEP* **05** (2021) 286 [[2012.01756](#)].

- [505] R. F. del Castillo, M. G. Echevarria, Y. Makris and I. Scimemi, *TMD factorization for dijet and heavy-meson pair in DIS*, *JHEP* **01** (2021) 088 [[2008.07531](#)].
- [506] G.-P. Zhang, *Back-to-back heavy quark pair production in Semi-inclusive DIS*, *JHEP* **11** (2017) 069 [[1709.08970](#)].
- [507] L. Zheng, E. C. Aschenauer, J. H. Lee, B.-W. Xiao and Z.-B. Yin, *Accessing the gluon Sivers function at a future electron-ion collider*, *Phys. Rev. D* **98** (2018) 034011 [[1805.05290](#)].
- [508] A. Mukherjee and S. Rajesh,  *$J/\psi$  production in polarized and unpolarized ep collision and Sivers and  $\cos 2\phi$  asymmetries*, *Eur. Phys. J. C* **77** (2017) 854 [[1609.05596](#)].
- [509] R. Kishore and A. Mukherjee, *Accessing linearly polarized gluon distribution in  $J/\psi$  production at the electron-ion collider*, *Phys. Rev. D* **99** (2019) 054012 [[1811.07495](#)].
- [510] R. Kishore, A. Mukherjee and S. Rajesh, *Sivers asymmetry in the photoproduction of a  $J/\psi$  and a jet at the EIC*, *Phys. Rev. D* **101** (2020) 054003 [[1908.03698](#)].
- [511] U. D'Alesio, F. Murgia, C. Pisano and P. Taels, *Azimuthal asymmetries in semi-inclusive  $J/\psi$  + jet production at an EIC*, *Phys. Rev. D* **100** (2019) 094016 [[1908.00446](#)].
- [512] EUROPEAN MUON collaboration, J. J. Aubert et al., *The ratio of the nucleon structure functions  $F_{2n}$  for iron and deuterium*, *Phys. Lett. B* **123** (1983) 275.
- [513] R. Abdul Khalek et al., *Science Requirements and Detector Concepts for the Electron-Ion Collider: EIC Yellow Report*, [2103.05419](#).
- [514] W. J. Stirling and M. R. Whalley, *A Compilation of Drell-Yan cross-sections*, *J. Phys. G* **19** (1993) D1.
- [515] HERMES collaboration, A. Airapetian et al., *Hadronization in semi-inclusive deep-inelastic scattering on nuclei*, *Nucl. Phys. B* **780** (2007) 1 [[0704.3270](#)].
- [516] V. D. Burkert, *CLAS12 and its initial Science Program at the Jefferson Lab Upgrade*, in *CLAS 12 RICH Detector Workshop*, 10, 2008, [0810.4718](#).
- [517] CLAS collaboration, S. Moran et al., *Measurement of charged-pion production in deep-inelastic scattering off nuclei with the CLAS detector*, [2109.09951](#).
- [518] NuSEA collaboration, M. A. Vasilev et al., *Parton energy loss limits and shadowing in Drell-Yan dimuon production*, *Phys. Rev. Lett.* **83** (1999) 2304 [[hep-ex/9906010](#)].
- [519] D. M. Alde et al., *Nuclear dependence of dimuon production at 800-GeV FNAL-772 experiment*, *Phys. Rev. Lett.* **64** (1990) 2479.
- [520] PHENIX collaboration, Y. H. Leung, *PHENIX measurements of charm, bottom, and Drell-Yan via dimuons in p+p and p+Au collisions at  $\sqrt{s_{NN}} = 200$  GeV*, *PoS HardProbes2018* (2018) 160.

- [521] CMS collaboration, V. Khachatryan et al., *Study of Z boson production in pPb collisions at  $\sqrt{s_{NN}} = 5.02 \text{ TeV}$* , *Phys. Lett. B* **759** (2016) 36 [[1512.06461](#)].
- [522] ATLAS collaboration, G. Aad et al., *Z boson production in p+Pb collisions at  $\sqrt{s_{NN}} = 5.02 \text{ TeV}$  measured with the ATLAS detector*, *Phys. Rev. C* **92** (2015) 044915 [[1507.06232](#)].
- [523] M. Alrashed, D. Anderle, Z.-B. Kang, J. Terry and H. Xing, *Three-dimensional imaging in nuclei*, [2107.12401](#).
- [524] T. Liu, W. Melnitchouk, J.-W. Qiu and N. Sato, *Factorized approach to radiative corrections for inelastic lepton-hadron collisions*, *Phys. Rev. D* **104** (2021) 094033 [[2008.02895](#)].
- [525] T. Liu, W. Melnitchouk, J.-W. Qiu and N. Sato, *A new approach to semi-inclusive deep-inelastic scattering with QED and QCD factorization*, *JHEP* **11** (2021) 157 [[2108.13371](#)].
- [526] J.-w. Qiu and G. F. Sterman, *Power corrections to hadronic scattering. 2. Factorization*, *Nucl. Phys. B* **353** (1991) 137.
- [527] H. J. Rothe, *Lattice gauge theories: An Introduction*, *World Sci. Lect. Notes Phys.* **43** (1992) 1.
- [528] C. Gattringer and C. B. Lang, *Quantum chromodynamics on the lattice*, *Lect. Notes Phys.* **788** (2010) 1.
- [529] W. Celmaster, *Gauge Theories on the Body - Centered Hypercubic Lattice*, *Phys. Rev.* **D26** (1982) 2955.
- [530] J. B. Kogut and L. Susskind, *Hamiltonian Formulation of Wilson's Lattice Gauge Theories*, *Phys. Rev.* **D11** (1975) 395.
- [531] R. Frezzotti and G. C. Rossi, *Chirally improving Wilson fermions. 1. O(a) improvement*, *JHEP* **08** (2004) 007 [[hep-lat/0306014](#)].
- [532] D. B. Kaplan, *A Method for simulating chiral fermions on the lattice*, *Phys. Lett.* **B288** (1992) 342 [[hep-lat/9206013](#)].
- [533] R. Narayanan and H. Neuberger, *A Construction of lattice chiral gauge theories*, *Nucl. Phys.* **B443** (1995) 305 [[hep-th/9411108](#)].
- [534] B. Sheikholeslami and R. Wohlert, *Improved Continuum Limit Lattice Action for QCD with Wilson Fermions*, *Nucl. Phys.* **B259** (1985) 572.
- [535] S. Duane, A. Kennedy, B. Pendleton and D. Roweth, *Hybrid Monte Carlo*, *Phys. Lett. B* **195** (1987) 216.
- [536] FLAVOUR LATTICE AVERAGING GROUP collaboration, S. Aoki et al., *FLAG Review 2019: Flavour Lattice Averaging Group (FLAG)*, *Eur. Phys. J. C* **80** (2020) 113 [[1902.08191](#)].
- [537] S. Capitani, *Lattice perturbation theory*, *Phys. Rept.* **382** (2003) 113 [[hep-lat/0211036](#)].

- [538] G. Martinelli, C. Pittori, C. T. Sachrajda, M. Testa and A. Vladikas, *A General method for nonperturbative renormalization of lattice operators*, *Nucl. Phys.* **B445** (1995) 81 [[hep-lat/9411010](#)].
- [539] G. Martinelli, G. Parisi, R. Petronzio and F. Rapuano, *The Proton and Neutron Magnetic Moments in Lattice QCD*, *Phys. Lett. B* **116** (1982) 434.
- [540] F. Fucito, G. Parisi and S. Petrarca, *FIRST EVALUATION OF  $G(A)/G(V)$  IN LATTICE QCD IN THE QUENCHED APPROXIMATION*, *Phys. Lett. B* **115** (1982) 148.
- [541] G. Martinelli and C. T. Sachrajda, *Pion Structure Functions From Lattice QCD*, *Phys. Lett. B* **196** (1987) 184.
- [542] G. Martinelli and C. T. Sachrajda, *A Lattice Study of Nucleon Structure*, *Nucl.Phys.* **B316** (1989) 355.
- [543] G. Martinelli and C. T. Sachrajda, *The Quark Distribution Amplitude of the Proton: A Lattice Computation of the Lowest Two Moments*, *Phys. Lett. B* **217** (1989) 319.
- [544] FLAVOUR LATTICE AVERAGING GROUP collaboration, S. Aoki et al., *FLAG Review 2019: Flavour Lattice Averaging Group (FLAG)*, *Eur. Phys. J. C* **80** (2020) 113 [[1902.08191](#)].
- [545] USQCD collaboration, A. S. Kronfeld, D. G. Richards, W. Detmold, R. Gupta, H.-W. Lin, K.-F. Liu et al., *Lattice QCD and Neutrino-Nucleus Scattering*, *Eur. Phys. J. A* **55** (2019) 196 [[1904.09931](#)].
- [546] H.-W. Lin et al., *Parton distributions and lattice QCD calculations: a community white paper*, *Prog. Part. Nucl. Phys.* **100** (2018) 107 [[1711.07916](#)].
- [547] G. Martinelli, *Hadronic weak interactions of light quarks*, *Nucl. Phys. Proc. Suppl.* **73** (1999) 58 [[hep-lat/9810013](#)].
- [548] M. Gockeler, R. Horsley, W. Kurzinger, H. Oelrich, D. Pleiter, P. E. Rakow et al., *A Lattice calculation of the nucleon's spin dependent structure function  $g(2)$  revisited*, *Phys. Rev. D* **63** (2001) 074506 [[hep-lat/0011091](#)].
- [549] G. Martinelli and C. T. Sachrajda, *On the difficulty of computing higher twist corrections*, *Nucl. Phys.* **B478** (1996) 660 [[hep-ph/9605336](#)].
- [550] Z. Davoudi and M. J. Savage, *Restoration of Rotational Symmetry in the Continuum Limit of Lattice Field Theories*, *Phys.Rev. D* **86** (2012) 054505 [[1204.4146](#)].
- [551] X.-D. Ji, *Gauge-Invariant Decomposition of Nucleon Spin*, *Phys.Rev.Lett.* **78** (1997) 610 [[hep-ph/9603249](#)].
- [552] O. V. Teryaev, *Spin structure of nucleon and equivalence principle*, [hep-ph/9904376](#).
- [553] R. Jaffe and A. Manohar, *The G(1) Problem: Fact and Fantasy on the Spin of the Proton*, *Nucl.Phys.* **B337** (1990) 509.

- [554] C. Lorce and B. Pasquini, *Quark Wigner Distributions and Orbital Angular Momentum*, *Phys. Rev.* **D84** (2011) 014015 [[1106.0139](#)].
- [555] Y. Zhao, K.-F. Liu and Y. Yang, *Orbital Angular Momentum and Generalized Transverse Momentum Distribution*, *Phys. Rev.* **D93** (2016) 054006 [[1506.08832](#)].
- [556] M. Engelhardt, *Quark orbital dynamics in the proton from Lattice QCD – from Ji to Jaffe-Manohar orbital angular momentum*, *Phys. Rev.* **D95** (2017) 094505 [[1701.01536](#)].
- [557] M. Engelhardt, J. Green, N. Hasan, S. Krieg, S. Meinel, J. Negele et al., *From Ji to Jaffe-Manohar orbital angular momentum in Lattice QCD using a direct derivative method*, *Phys. Rev. D* **102** (2020) 074505 [[2008.03660](#)].
- [558] E. Leader and C. Lorcé, *The angular momentum controversy: What is it all about and does it matter?*, *Phys.Rept.* **541** (2014) 163 [[1309.4235](#)].
- [559] K.-F. Liu and C. Lorce, *The Parton Orbital Angular Momentum: Status and Prospects*, *Eur. Phys. J.* **A52** (2016) 160 [[1508.00911](#)].
- [560] X. Ji, F. Yuan and Y. Zhao, *What we know and what we don't know about the proton spin after 30 years*, *Nature Rev. Phys.* **3** (2021) 27 [[2009.01291](#)].
- [561] EUROPEAN MUON collaboration, J. Ashman et al., *A Measurement of the Spin Asymmetry and Determination of the Structure Function  $g(1)$  in Deep Inelastic Muon-Proton Scattering*, *Phys. Lett.* **B206** (1988) 364.
- [562] D. de Florian, R. Sassot, M. Stratmann and W. Vogelsang, *Extraction of Spin-Dependent Parton Densities and Their Uncertainties*, *Phys. Rev.* **D80** (2009) 034030 [[0904.3821](#)].
- [563] S.-J. Dong and K.-F. Liu, *Stochastic estimation with Z(2) noise*, *Phys. Lett.* **B328** (1994) 130 [[hep-lat/9308015](#)].
- [564] D. de Florian, R. Sassot, M. Stratmann and W. Vogelsang, *Evidence for polarization of gluons in the proton*, *Phys. Rev. Lett.* **113** (2014) 012001 [[1404.4293](#)].
- [565] NNPDF collaboration, E. R. Nocera, R. D. Ball, S. Forte, G. Ridolfi and J. Rojo, *A first unbiased global determination of polarized PDFs and their uncertainties*, *Nucl. Phys.* **B887** (2014) 276 [[1406.5539](#)].
- [566] STAR collaboration, P. Djawotho, *Gluon polarization and jet production at STAR*, *Nuovo Cim.* **C036** (2013) 35 [[1303.0543](#)].
- [567] PHENIX collaboration, A. Adare et al., *Inclusive double-helicity asymmetries in neutral-pion and eta-meson production in  $\vec{p} + \vec{p}$  collisions at  $\sqrt{s} = 200$  GeV*, *Phys. Rev.* **D90** (2014) 012007 [[1402.6296](#)].
- [568] X. Ji, J.-H. Zhang and Y. Zhao, *Physics of the Gluon-Helicity Contribution to Proton Spin*, *Phys. Rev. Lett.* **111** (2013) 112002 [[1304.6708](#)].

- [569] Y. Hatta, X. Ji and Y. Zhao, *Gluon helicity  $\Delta G$  from a universality class of operators on a lattice*, *Phys. Rev.* **D89** (2014) 085030 [[1310.4263](#)].
- [570] X. Ji, J.-H. Zhang and Y. Zhao, *Justifying the Naive Partonic Sum Rule for Proton Spin*, *Phys. Lett.* **B743** (2015) 180 [[1409.6329](#)].
- [571] X.-S. Chen, X.-F. Lu, W.-M. Sun, F. Wang and T. Goldman, *Spin and orbital angular momentum in gauge theories: Nucleon spin structure and multipole radiation revisited*, *Phys. Rev. Lett.* **100** (2008) 232002 [[0806.3166](#)].
- [572] Y.-B. Yang, R. S. Sufian, A. Alexandru, T. Draper, M. J. Glatzmaier, K.-F. Liu et al., *Glue Spin and Helicity in the Proton from Lattice QCD*, *Phys. Rev. Lett.* **118** (2017) 102001 [[1609.05937](#)].
- [573] N. Mathur, S. J. Dong, K. F. Liu, L. Mankiewicz and N. C. Mukhopadhyay, *Quark orbital angular momentum from lattice QCD*, *Phys. Rev.* **D62** (2000) 114504 [[hep-ph/9912289](#)].
- [574] LHPC, SESAM collaboration, P. Hagler, J. W. Negele, D. B. Renner, W. Schroers, T. Lippert and K. Schilling, *Moments of nucleon generalized parton distributions in lattice QCD*, *Phys. Rev.* **D68** (2003) 034505 [[hep-lat/0304018](#)].
- [575] LHPC collaboration, J. D. Bratt et al., *Nucleon structure from mixed action calculations using 2+1 flavors of asqtad sea and domain wall valence fermions*, *Phys. Rev.* **D82** (2010) 094502 [[1001.3620](#)].
- [576] Y.-B. Yang, J. Liang, Y.-J. Bi, Y. Chen, T. Draper, K.-F. Liu et al., *Proton Mass Decomposition from the QCD Energy Momentum Tensor*, *Phys. Rev. Lett.* **121** (2018) 212001 [[1808.08677](#)].
- [577] C. Alexandrou, M. Constantinou, K. Hadjyiannakou, K. Jansen, C. Kallidonis, G. Koutsou et al., *Nucleon Spin and Momentum Decomposition Using Lattice QCD Simulations*, *Phys. Rev. Lett.* **119** (2017) 142002 [[1706.02973](#)].
- [578] C. Alexandrou, S. Bacchio, M. Constantinou, J. Finkenrath, K. Hadjyiannakou, K. Jansen et al., *Complete flavor decomposition of the spin and momentum fraction of the proton using lattice QCD simulations at physical pion mass*, *Phys. Rev. D* **101** (2020) 094513 [[2003.08486](#)].
- [579] XQCD collaboration, Y.-B. Yang, *A Lattice Story of Proton Spin*, PoS **LATTICE2018** (2019) 017 [[1904.04138](#)].
- [580] K. F. Liu, S. J. Dong, T. Draper, D. Leinweber, J. H. Sloan, W. Wilcox et al., *Valence QCD: Connecting QCD to the quark model*, *Phys. Rev.* **D59** (1999) 112001 [[hep-ph/9806491](#)].
- [581] U. Aglietti, M. Ciuchini, G. Corbo, E. Franco, G. Martinelli and L. Silvestrini, *Model independent determination of the shape function for inclusive B decays and of the structure functions in DIS*, *Phys. Lett.* **B432** (1998) 411 [[hep-ph/9804416](#)].

- [582] K. Can et al., *Lattice QCD evaluation of the Compton amplitude employing the Feynman-Hellmann theorem*, *Phys. Rev. D* **102** (2020) 114505 [2007.01523].
- [583] A. J. Chambers et al., *Disconnected contributions to the spin of the nucleon*, *Phys. Rev.* **D92** (2015) 114517 [1508.06856].
- [584] R. Bryan *European Biophysics Journal* **18** (1990) 165.
- [585] M. Jarrell and J. E. Gubernatis, *Bayesian inference and the analytic continuation of imaginary-time quantum Monte Carlo data*, *Phys. Rept.* **269** (1996) 133.
- [586] Y. Burnier and A. Rothkopf, *Bayesian Approach to Spectral Function Reconstruction for Euclidean Quantum Field Theories*, *Phys. Rev. Lett.* **111** (2013) 182003 [1307.6106].
- [587] G. Backus and F. Gilbert *Geophysical Journal of the Royal Astronomical Society* **16** (1968) 169.
- [588] XQCD collaboration, J. Liang, T. Draper, K.-F. Liu, A. Rothkopf and Y.-B. Yang, *Towards the nucleon hadronic tensor from lattice QCD*, 1906.05312.
- [589] W. Detmold, A. V. Grebe, I. Kanamori, C. J. D. Lin, S. Mondal, R. J. Perry et al., *A Preliminary Determination of the Second Mellin Moment of the Pion's Distribution Amplitude Using the Heavy Quark Operator Product Expansion*, in *Asia-Pacific Symposium for Lattice Field Theory*, 9, 2020, 2009.09473.
- [590] HOPE collaboration, W. Detmold, A. V. Grebe, I. Kanamori, C. J. D. Lin, R. J. Perry and Y. Zhao, *Parton physics from a heavy-quark operator product expansion: Formalism and Wilson coefficients*, *Phys. Rev. D* **104** (2021) 074511 [2103.09529].
- [591] W. Detmold, I. Kanamori, C. J. D. Lin, S. Mondal and Y. Zhao, *Moments of pion distribution amplitude using operator product expansion on the lattice*, *PoS LATTICE2018* (2018) 106 [1810.12194].
- [592] W. Detmold, A. Grebe, I. Kanamori, C. J. D. Lin, S. Mondal, R. Perry et al., *Parton physics from a heavy-quark operator product expansion: Lattice QCD calculation of the second moment of the pion distribution amplitude*, 2109.15241.
- [593] QCDSF, UKQCD collaboration, R. Horsley, R. Millo, Y. Nakamura, H. Perlt, D. Pleiter, P. E. L. Rakow et al., *A Lattice Study of the Glue in the Nucleon*, *Phys. Lett.* **B714** (2012) 312 [1205.6410].
- [594] K. Cichy and M. Constantinou, *A guide to light-cone PDFs from Lattice QCD: an overview of approaches, techniques and results*, *Adv. High Energy Phys.* **2019** (2019) 3036904 [1811.07248].
- [595] M. Constantinou, *The  $x$ -dependence of hadronic parton distributions: A review on the progress of lattice QCD*, *Eur. Phys. J. A* **57** (2021) 77 [2010.02445].
- [596] X. Xiong, X. Ji, J.-H. Zhang and Y. Zhao, *One-loop matching for parton distributions: Nonsinglet case*, *Phys. Rev.* **D90** (2014) 014051 [1310.7471].

- [597] T. Izubuchi, X. Ji, L. Jin, I. W. Stewart and Y. Zhao, *Factorization Theorem Relating Euclidean and Light-Cone Parton Distributions*, *Phys. Rev.* **D98** (2018) 056004 [1801.03917].
- [598] J.-W. Chen, S. D. Cohen, X. Ji, H.-W. Lin and J.-H. Zhang, *Nucleon Helicity and Transversity Parton Distributions from Lattice QCD*, *Nucl. Phys.* **B911** (2016) 246 [1603.06664].
- [599] V. M. Braun, A. Vladimirov and J.-H. Zhang, *Power corrections and renormalons in parton quasidistributions*, *Phys. Rev.* **D99** (2019) 014013 [1810.00048].
- [600] X. Ji, Y. Liu, A. Schäfer, W. Wang, Y.-B. Yang, J.-H. Zhang et al., *A Hybrid Renormalization Scheme for Quasi Light-Front Correlations in Large-Momentum Effective Theory*, 2008.03886.
- [601] W. Wang, J.-H. Zhang, S. Zhao and R. Zhu, *A Complete Matching for Quasi-distribution Functions in Large Momentum Effective Theory*, 1904.00978.
- [602] Y.-S. Liu, W. Wang, J. Xu, Q.-A. Zhang, J.-H. Zhang, S. Zhao et al., *Matching generalized parton quasidistributions in the RI/MOM scheme*, *Phys. Rev.* **D100** (2019) 034006 [1902.00307].
- [603] V. Dotsenko and S. Vergeles, *Renormalizability of Phase Factors in the Nonabelian Gauge Theory*, *Nucl. Phys. B* **169** (1980) 527.
- [604] N. S. Craigie and H. Dorn, *On the Renormalization and Short Distance Properties of Hadronic Operators in QCD*, *Nucl. Phys. B* **185** (1981) 204.
- [605] H. Dorn, *Renormalization of Path Ordered Phase Factors and Related Hadron Operators in Gauge Field Theories*, *Fortsch. Phys.* **34** (1986) 11.
- [606] X. Ji, J.-H. Zhang and Y. Zhao, *Renormalization in Large Momentum Effective Theory of Parton Physics*, *Phys. Rev. Lett.* **120** (2018) 112001 [1706.08962].
- [607] J. Green, K. Jansen and F. Steffens, *Nonperturbative Renormalization of Nonlocal Quark Bilinears for Parton Quasidistribution Functions on the Lattice Using an Auxiliary Field*, *Phys. Rev. Lett.* **121** (2018) 022004 [1707.07152].
- [608] T. Ishikawa, Y.-Q. Ma, J.-W. Qiu and S. Yoshida, *Renormalizability of quasiparton distribution functions*, *Phys. Rev.* **D96** (2017) 094019 [1707.03107].
- [609] J.-H. Zhang, X. Ji, A. Schäfer, W. Wang and S. Zhao, *Accessing Gluon Parton Distributions in Large Momentum Effective Theory*, *Phys. Rev. Lett.* **122** (2019) 142001 [1808.10824].
- [610] Z.-Y. Li, Y.-Q. Ma and J.-W. Qiu, *Multiplicative Renormalizability of Operators defining Quasiparton Distributions*, *Phys. Rev. Lett.* **122** (2019) 062002 [1809.01836].
- [611] T. Ishikawa, Y.-Q. Ma, J.-W. Qiu and S. Yoshida, *Practical quasi parton distribution functions*, 1609.02018.

- [612] X. Xiong, T. Luu and U.-G. Meißner, *Quasi-Parton Distribution Function in Lattice Perturbation Theory*, 1705.00246.
- [613] M. Constantinou and H. Panagopoulos, *Perturbative renormalization of quasi-parton distribution functions*, *Phys. Rev.* **D96** (2017) 054506 [1705.11193].
- [614] L.-B. Chen, W. Wang and R. Zhu, *Quasi parton distribution functions at NNLO: flavor non-diagonal quark contributions*, 2005.13757.
- [615] L.-B. Chen, W. Wang and R. Zhu, *Master Integrals for two-loop QCD corrections to Quasi PDFs*, 2006.10917.
- [616] Z.-Y. Li, Y.-Q. Ma and J.-W. Qiu, *Extraction of Next-to-Next-to-Leading-Order PDFs from Lattice QCD Calculations*, 2006.12370.
- [617] L.-B. Chen, W. Wang and R. Zhu, *Next-to-next-to-leading order corrections to quark Quasi parton distribution functions*, 2006.14825.
- [618] V. M. Braun, K. G. Chetyrkin and B. A. Kniehl, *Renormalization of parton quasi-distributions beyond the leading order: spacelike vs. timelike*, *JHEP* **07** (2020) 161 [2004.01043].
- [619] J.-H. Zhang, J.-W. Chen, X. Ji, L. Jin and H.-W. Lin, *Pion Distribution Amplitude from Lattice QCD*, *Phys. Rev.* **D95** (2017) 094514 [1702.00008].
- [620] J. R. Green, K. Jansen and F. Steffens, *Improvement, generalization, and scheme conversion of Wilson-line operators on the lattice in the auxiliary field approach*, *Phys. Rev. D* **101** (2020) 074509 [2002.09408].
- [621] C. Alexandrou, K. Cichy, M. Constantinou, J. R. Green, K. Hadjiyiannakou, K. Jansen et al., *Lattice continuum-limit study of nucleon quasi-PDFs*, 2011.00964.
- [622] C. Alexandrou, K. Cichy, M. Constantinou, K. Hadjiyiannakou, K. Jansen, H. Panagopoulos et al., *A complete non-perturbative renormalization prescription for quasi-PDFs*, *Nucl. Phys.* **B923** (2017) 394 [1706.00265].
- [623] I. W. Stewart and Y. Zhao, *Matching the quasiparton distribution in a momentum subtraction scheme*, *Phys. Rev.* **D97** (2018) 054512 [1709.04933].
- [624] J.-W. Chen, T. Ishikawa, L. Jin, H.-W. Lin, Y.-B. Yang, J.-H. Zhang et al., *Parton distribution function with nonperturbative renormalization from lattice QCD*, *Phys. Rev.* **D97** (2018) 014505 [1706.01295].
- [625] J.-W. Chen, T. Ishikawa, L. Jin, H.-W. Lin, Y.-B. Yang, J.-H. Zhang et al., *Symmetry Properties of Nonlocal Quark Bilinear Operators on a Lattice*, 1710.01089.
- [626] Y. Zhao, *Unraveling high-energy hadron structures with lattice QCD*, *Int. J. Mod. Phys.* **A33** (2019) 1830033 [1812.07192].

- [627] C. Alexandrou, K. Cichy, M. Constantinou, K. Hadjyiannakou, K. Jansen, A. Scapellato et al., *Systematic uncertainties in parton distribution functions from lattice QCD simulations at the physical point*, *Phys. Rev.* **D99** (2019) 114504 [[1902.00587](#)].
- [628] C. Alexandrou, K. Cichy, M. Constantinou, K. Jansen, A. Scapellato and F. Steffens, *Light-Cone Parton Distribution Functions from Lattice QCD*, *Phys. Rev. Lett.* **121** (2018) 112001 [[1803.02685](#)].
- [629] C. Alexandrou, K. Cichy, M. Constantinou, K. Jansen, A. Scapellato and F. Steffens, *Transversity parton distribution functions from lattice QCD*, *Phys. Rev.* **D98** (2018) 091503 [[1807.00232](#)].
- [630] S. Bhattacharya, K. Cichy, M. Constantinou, A. Metz, A. Scapellato and F. Steffens, *Insights on proton structure from lattice QCD: The twist-3 parton distribution function  $g_T(x)$* , *Phys. Rev. D* **102** (2020) 111501 [[2004.04130](#)].
- [631] C. Alexandrou, M. Constantinou, K. Hadjyiannakou, K. Jansen and F. Manigrasso, *Flavor decomposition for the proton helicity parton distribution functions*, [2009.13061](#).
- [632] Y.-S. Liu, J.-W. Chen, L. Jin, H.-W. Lin, Y.-B. Yang, J.-H. Zhang et al., *Unpolarized quark distribution from lattice QCD: A systematic analysis of renormalization and matching*, [1807.06566](#).
- [633] Y.-S. Liu, W. Wang, J. Xu, Q.-A. Zhang, S. Zhao and Y. Zhao, *Matching the meson quasidistribution amplitude in the RI/MOM scheme*, *Phys. Rev.* **D99** (2019) 094036 [[1810.10879](#)].
- [634] LP3 collaboration, H.-W. Lin, J.-W. Chen, T. Ishikawa and J.-H. Zhang, *Improved parton distribution functions at the physical pion mass*, *Phys. Rev.* **D98** (2018) 054504 [[1708.05301](#)].
- [635] J.-W. Chen, L. Jin, H.-W. Lin, Y.-S. Liu, A. Schäfer, Y.-B. Yang et al., *First direct lattice-QCD calculation of the  $x$ -dependence of the pion parton distribution function*, [1804.01483](#).
- [636] R. Zhang, C. Honkala, H.-W. Lin and J.-W. Chen, *Pion and Kaon Distribution Amplitudes in the Continuum Limit*, [2005.13955](#).
- [637] Z. Fan, X. Gao, R. Li, H.-W. Lin, N. Karthik, S. Mukherjee et al., *Isovector parton distribution functions of the proton on a superfine lattice*, *Phys. Rev. D* **102** (2020) 074504 [[2005.12015](#)].
- [638] R. Zhang, H.-W. Lin and B. Yoon, *Probing nucleon strange and charm distributions with lattice QCD*, [2005.01124](#).
- [639] H.-W. Lin, J.-W. Chen, Z. Fan, J.-H. Zhang and R. Zhang, *The Valence-Quark Distribution of the Kaon from Lattice QCD*, [2003.14128](#).

- [640] H.-W. Lin, J.-W. Chen and R. Zhang, *Lattice Nucleon Isovector Unpolarized Parton Distribution in the Physical-Continuum Limit*, 2011.14971.
- [641] LATTICE PARTON COLLABORATION (LPC) collaboration, Y.-K. Huo et al., *Self-renormalization of quasi-light-front correlators on the lattice*, *Nucl. Phys. B* **969** (2021) 115443 [2103.02965].
- [642] C. Monahan and K. Orginos, *Quasi parton distributions and the gradient flow*, *JHEP* **03** (2017) 116 [1612.01584].
- [643] C. Monahan, *Smeared quasidistributions in perturbation theory*, *Phys. Rev.* **D97** (2018) 054507 [1710.04607].
- [644] H.-W. Lin, J.-W. Chen, S. D. Cohen and X. Ji, *Flavor Structure of the Nucleon Sea from Lattice QCD*, *Phys. Rev.* **D91** (2015) 054510 [1402.1462].
- [645] C. Alexandrou, K. Cichy, V. Drach, E. Garcia-Ramos, K. Hadjyiannakou et al., *First results with twisted mass fermions towards the computation of parton distribution functions on the lattice*, *PoS LATTICE2014* (2014) 135 [1411.0891].
- [646] C. Alexandrou, K. Cichy, V. Drach, E. Garcia-Ramos, K. Hadjyiannakou, K. Jansen et al., *Lattice calculation of parton distributions*, *Phys. Rev.* **D92** (2015) 014502 [1504.07455].
- [647] H.-W. Lin, J.-W. Chen, X. Ji, L. Jin, R. Li, Y.-S. Liu et al., *Proton Isovector Helicity Distribution on the Lattice at Physical Pion Mass*, *Phys. Rev. Lett.* **121** (2018) 242003 [1807.07431].
- [648] ALPHA collaboration, R. Frezzotti, P. A. Grassi, S. Sint and P. Weisz, *Lattice QCD with a chirally twisted mass term*, *JHEP* **08** (2001) 058 [hep-lat/0101001].
- [649] A. Shindler, *Twisted mass lattice qcd*, *Physics Reports* **461** (2008) 37–110.
- [650] S. Alekhin, J. Blümlein, S. Moch and R. Placakyte, *Parton distribution functions,  $\alpha_s$ , and heavy-quark masses for LHC Run II*, *Phys. Rev. D* **96** (2017) 014011 [1701.05838].
- [651] NNPDF collaboration, R. D. Ball et al., *Parton distributions from high-precision collider data*, *Eur. Phys. J.* **C77** (2017) 663 [1706.00428].
- [652] A. Accardi, L. T. Brady, W. Melnitchouk, J. F. Owens and N. Sato, *Constraints on large- $x$  parton distributions from new weak boson production and deep-inelastic scattering data*, *Phys. Rev.* **D93** (2016) 114017 [1602.03154].
- [653] J. J. Ethier, N. Sato and W. Melnitchouk, *First simultaneous extraction of spin-dependent parton distributions and fragmentation functions from a global QCD analysis*, *Phys. Rev. Lett.* **119** (2017) 132001 [1705.05889].
- [654] H.-W. Lin, W. Melnitchouk, A. Prokudin, N. Sato and H. Shows, *First Monte Carlo Global Analysis of Nucleon Transversity with Lattice QCD Constraints*, *Phys. Rev. Lett.* **120** (2018) 152502 [1710.09858].

- [655] M. Constantinou et al., *Parton distributions and lattice-QCD calculations: Toward 3D structure*, *Prog. Part. Nucl. Phys.* **121** (2021) 103908 [2006.08636].
- [656] J. Karpie, K. Orginos, A. Rothkopf and S. Zafeiropoulos, *Reconstructing parton distribution functions from Ioffe time data: from Bayesian methods to Neural Networks*, *JHEP* **04** (2019) 057 [1901.05408].
- [657] T. Izubuchi, L. Jin, C. Kallidonis, N. Karthik, S. Mukherjee, P. Petreczky et al., *Valence parton distribution function of pion from fine lattice*, *Phys. Rev. D* **100** (2019) 034516 [1905.06349].
- [658] X. Gao, L. Jin, C. Kallidonis, N. Karthik, S. Mukherjee, P. Petreczky et al., *Valence parton distribution of pion from lattice QCD: Approaching continuum*, 2007.06590.
- [659] Y. Chai et al., *Parton distribution functions of  $\Delta^+$  on the lattice*, *Phys. Rev. D* **102** (2020) 014508 [2002.12044].
- [660] H.-W. Lin and R. Zhang, *Lattice finite-volume dependence of the nucleon parton distributions*, *Phys. Rev. D* **100** (2019) 074502.
- [661] C. Alexandrou, M. Constantinou, K. Hadjyiannakou, K. Jansen and F. Manigrasso, *Flavor decomposition of the nucleon unpolarized, helicity, and transversity parton distribution functions from lattice QCD simulations*, *Phys. Rev. D* **104** (2021) 054503 [2106.16065].
- [662] A. Buckley, J. Ferrando, S. Lloyd, K. Nordström, B. Page, M. Rüfenacht et al., *LHAPDF6: parton density access in the LHC precision era*, *Eur. Phys. J. C* **75** (2015) 132 [1412.7420].
- [663] S. Bhattacharya, K. Cichy, M. Constantinou, A. Metz, A. Scapellato and F. Steffens, *One-loop matching for the twist-3 parton distribution  $g_T(x)$* , *Phys. Rev. D* **102** (2020) 034005 [2005.10939].
- [664] S. Bhattacharya, K. Cichy, M. Constantinou, A. Metz, A. Scapellato and F. Steffens, *Parton distribution functions beyond leading twist from lattice QCD: The  $h_L(x)$  case*, 2107.02574.
- [665] S. Bhattacharya, K. Cichy, M. Constantinou, A. Metz, A. Scapellato and F. Steffens, *The role of zero-mode contributions in the matching for the twist-3 PDFs  $e(x)$  and  $h_L(x)$* , *Phys. Rev. D* **102** (2020) 114025 [2006.12347].
- [666] S. Wandzura and F. Wilczek, *Sum Rules for Spin Dependent Electroporation: Test of Relativistic Constituent Quarks*, *Phys. Lett.* **72B** (1977) 195.
- [667] C. Alexandrou, K. Cichy, M. Constantinou, K. Hadjyiannakou, K. Jansen, A. Scapellato et al., *Unpolarized and helicity generalized parton distributions of the proton within lattice QCD*, *Phys. Rev. Lett.* **125** (2020) 262001 [2008.10573].
- [668] C. Alexandrou, K. Cichy, M. Constantinou, K. Hadjyiannakou, K. Jansen, A. Scapellato et al., *Transversity GPDs of the proton from lattice QCD*, 2108.10789.

- [669] S. Bhattacharya, K. Cichy, M. Constantinou, J. Dodson, A. Metz, A. Scapellato et al., *First Lattice QCD Study of Proton Twist-3 GPDs*, 2021.
- [670] A. Radyushkin, *Nonperturbative Evolution of Parton Quasi-Distributions*, *Phys. Lett.* **B767** (2017) 314 [1612.05170].
- [671] A. Radyushkin, *Target Mass Effects in Parton Quasi-Distributions*, *Phys. Lett.* **B770** (2017) 514 [1702.01726].
- [672] B. L. Ioffe, *Space-time picture of photon and neutrino scattering and electroproduction cross-section asymptotics*, *Phys. Lett.* **30B** (1969) 123.
- [673] A. Radyushkin, *One-loop evolution of parton pseudo-distribution functions on the lattice*, *Phys. Rev.* **D98** (2018) 014019 [1801.02427].
- [674] J.-H. Zhang, J.-W. Chen and C. Monahan, *Parton distribution functions from reduced Ioffe-time distributions*, *Phys. Rev.* **D97** (2018) 074508 [1801.03023].
- [675] A. V. Radyushkin, *Structure of parton quasi-distributions and their moments*, *Phys. Lett.* **B788** (2019) 380 [1807.07509].
- [676] A. Radyushkin, *Quasi-PDFs and pseudo-PDFs*, *PoS QCDEV2017* (2017) 021 [1711.06031].
- [677] J. Karpie, K. Orginos, A. Radyushkin and S. Zafeiropoulos, *Parton distribution functions on the lattice and in the continuum*, *EPJ Web Conf.* **175** (2018) 06032 [1710.08288].
- [678] J. Karpie, K. Orginos and S. Zafeiropoulos, *Moments of Ioffe time parton distribution functions from non-local matrix elements*, *JHEP* **11** (2018) 178 [1807.10933].
- [679] B. JoÅŸ, J. Karpie, K. Orginos, A. V. Radyushkin, D. G. Richards, R. S. Sufian et al., *Pion Valence Structure from Ioffe Time Pseudo-Distributions*, *Phys. Rev.* **D100** (2019) 114512 [1909.08517].
- [680] B. JoÅŸ, J. Karpie, K. Orginos, A. Radyushkin, D. Richards and S. Zafeiropoulos, *Parton Distribution Functions from Ioffe time pseudo-distributions*, *JHEP* **12** (2019) 081 [1908.09771].
- [681] B. Joó, J. Karpie, K. Orginos, A. V. Radyushkin, D. G. Richards and S. Zafeiropoulos, *Parton Distribution Functions from Ioffe Time Pseudodistributions from Lattice Calculations: Approaching the Physical Point*, *Phys. Rev. Let.* (2020) [2004.01687].
- [682] A. Martin, W. Stirling, R. Thorne and G. Watt, *Parton distributions for the LHC*, *Eur. Phys. J. C* **63** (2009) 189 [0901.0002].
- [683] M. Bhat, K. Cichy, M. Constantinou and A. Scapellato, *Parton distribution functions from lattice QCD at physical quark masses via the pseudo-distribution approach*, 2005.02102.
- [684] G. S. Bali et al., *Pion distribution amplitude from Euclidean correlation functions*, *Eur. Phys. J. C* **78** (2018) 217 [1709.04325].

- [685] G. S. Bali, V. M. Braun, B. Glädel, M. Gückeler, M. Gruber, F. Hutzler et al., *Pion distribution amplitude from Euclidean correlation functions: Exploring universality and higher-twist effects*, *Phys. Rev.* **D98** (2018) 094507 [[1807.06671](#)].
- [686] Y.-Q. Ma and J.-W. Qiu, *QCD Factorization and PDFs from Lattice QCD Calculation*, *Int.J.Mod.Phys.Conf.Ser.* **37** (2015) 0041 [[1412.2688](#)].
- [687] R. S. Sufian, J. Karpie, C. Egerer, K. Orginos, J.-W. Qiu and D. G. Richards, *Pion Valence Quark Distribution from Matrix Element Calculated in Lattice QCD*, *Phys. Rev.* **D99** (2019) 074507 [[1901.03921](#)].
- [688] R. S. Sufian, C. Egerer, J. Karpie, R. G. Edwards, B. Joá, Y.-Q. Ma et al., *Pion Valence Quark Distribution at Large  $x$  from Lattice QCD*, [2001.04960](#).
- [689] M. Aicher, A. Schafer and W. Vogelsang, *Soft-gluon resummation and the valence parton distribution function of the pion*, *Phys. Rev. Lett.* **105** (2010) 252003 [[1009.2481](#)].
- [690] L. Chang, C. Mezrag, H. Moutarde, C. D. Roberts, J. Rodríguez-Quintero and P. C. Tandy, *Basic features of the pion valence-quark distribution function*, *Phys. Lett. B* **737** (2014) 23 [[1406.5450](#)].
- [691] D. Boer, M.Buffing and P. Mulders, *Operator analysis of  $p_T$ -widths of TMDs*, *JHEP* **08** (2015) 053 [[1503.03760](#)].
- [692] R. A. Briceño, J. V. Guerrero, M. T. Hansen and C. J. Monahan, *Finite-volume effects due to spatially nonlocal operators*, *Phys. Rev. D* **98** (2018) 014511 [[1805.01034](#)].
- [693] G. S. Bali, B. Lang, B. U. Musch and A. Schäfer, *Novel quark smearing for hadrons with high momenta in lattice QCD*, *Phys. Rev. D* **93** (2016) 094515 [[1602.05525](#)].
- [694] M. Constantinou, H. Panagopoulos and G. Spanoudes, *One-loop renormalization of staple-shaped operators in continuum and lattice regularizations*, *Phys. Rev. D* **99** (2019) 074508 [[1901.03862](#)].
- [695] M. Engelhardt, J. R. Green, N. Hasan, T. Izubuchi, C. Kallidonis, S. Krieg et al., *to be published*.
- [696] M. Engelhardt, J. R. Green, S. Krieg, S. Meinel, J. Negele, A. Pochinsky et al., *to be published*.
- [697] A. Bacchetta, G. Bozzi, M. Radici, M. Ritzmann and A. Signori, *Effect of Flavor-Dependent Partonic Transverse Momentum on the Determination of the W Boson Mass in Hadronic Collisions*, *Phys. Lett. B* **788** (2019) 542 [[1807.02101](#)].
- [698] LATTICE PARTON collaboration, Q.-A. Zhang et al., *Lattice QCD Calculations of Transverse-Momentum-Dependent Soft Function through Large-Momentum Effective Theory*, *Phys. Rev. Lett.* **125** (2020) 192001 [[2005.14572](#)].
- [699] Y. Li et al., *Systematic study of transverse-momentum dependent soft function from lattice QCD*, [2106.13027](#).

- [700] X. Ji and Y. Liu, *Computing Light-Front Wave Functions Without Light-Front Quantization: A Large-Momentum Effective Theory Approach*, 2106.05310.
- [701] P. Shanahan, M. Wagman and Y. Zhao, *Collins-Soper Kernel for TMD Evolution from Lattice QCD*, 2003.06063.
- [702] P. Shanahan, M. Wagman and Y. Zhao, *Lattice QCD calculation of the Collins-Soper kernel from quasi TMDPDFs*, 2107.11930.
- [703] M. Schlemmer, A. Vladimirov, C. Zimmermann, M. Engelhardt and A. Schäfer, *Determination of the Collins-Soper Kernel from Lattice QCD*, 2103.16991.
- [704] A. Metz, *Gluon-exchange in spin-dependent fragmentation*, *Phys. Lett. B* **549** (2002) 139 [hep-ph/0209054].
- [705] R. Kundu and A. Metz, *Higher twist and transverse momentum dependent parton distributions: A Light front Hamiltonian approach*, *Phys. Rev. D* **65** (2002) 014009 [hep-ph/0107073].
- [706] K. Goeke, A. Metz, P. Pobylitsa and M. Polyakov, *Lorentz invariance relations among parton distributions revisited*, *Phys. Lett. B* **567** (2003) 27 [hep-ph/0302028].
- [707] S. Meissner, A. Metz and M. Schlegel, *Generalized parton correlation functions for a spin-1/2 hadron*, *JHEP* **0908** (2009) 056 [0906.5323].
- [708] H. Avakian, H. Matevosyan, B. Pasquini and P. Schweitzer, *Studying the information content of TMDs using Monte Carlo generators*, *J. Phys. G* **42** (2015) 034015.
- [709] A. O. Barut and C. Fronsdal, *Spin-Orbit Correlations in mu-e and e-e- Scattering*, *Phys. Rev.* **120** (1960) 1871.
- [710] M. Burkardt and D. S. Hwang, *Sivers asymmetry and generalized parton distributions in impact parameter space*, *Phys. Rev. D* **69** (2004) 074032 [hep-ph/0309072].
- [711] S. J. Brodsky, D. S. Hwang, Y. V. Kovchegov, I. Schmidt and M. D. Sievert, *Single-Spin Asymmetries in Semi-inclusive Deep Inelastic Scattering and Drell-Yan Processes*, *Phys. Rev. D* **88** (2013) 014032 [1304.5237].
- [712] R. P. Feynman, *Photon-hadron interactions*, .
- [713] D. J. Gross and F. Wilczek, *ASYMPTOTICALLY FREE GAUGE THEORIES. 2.*, *Phys. Rev. D* **9** (1974) 980.
- [714] H. D. Politzer, *Setting the scale for predictions of asymptotic freedom*, *Phys. Rev. D* **9** (1974) 2174.
- [715] R. K. Ellis, H. Georgi, M. Machacek, H. D. Politzer and G. G. Ross, *Perturbation Theory and the Parton Model in QCD*, *Nucl. Phys. B* **152** (1979) 285.
- [716] G. 't Hooft, *A Planar Diagram Theory for Strong Interactions*, *Nucl. Phys. B* **72** (1974) 461.

- [717] E. Witten, *Baryons in the 1/n Expansion*, *Nucl. Phys.* **B160** (1979) 57.
- [718] E. Witten, *Current Algebra, Baryons, and Quark Confinement*, *Nucl. Phys. B* **223** (1983) 433.
- [719] P. V. Pobylitsa and M. V. Polyakov, *New positivity bounds on parton distributions in multicolored QCD*, *Phys. Rev. D* **62** (2000) 097502 [[hep-ph/0004094](#)].
- [720] A. V. Efremov, K. Goeke, S. Menzel, A. Metz and P. Schweitzer, *Sivers effect in semi-inclusive DIS and in the Drell-Yan process*, *Phys. Lett.* **B612** (2005) 233 [[hep-ph/0412353](#)].
- [721] A. V. Efremov, K. Goeke and P. V. Pobylitsa, *Gluon and quark distributions in large N(c) QCD: Theory versus phenomenology*, *Phys. Lett.* **B488** (2000) 182 [[hep-ph/0004196](#)].
- [722] S. J. Brodsky and S. Gardner, *Evidence for the Absence of Gluon Orbital Angular Momentum in the Nucleon*, *Phys. Lett.* **B643** (2006) 22 [[hep-ph/0608219](#)].
- [723] M. Anselmino, U. D'Alesio, S. Melis and F. Murgia, *Constraints on the gluon Sivers distribution via transverse single spin asymmetries at mid-rapidity in p(up) p → pi0 X processes at RHIC*, *Phys. Rev.* **D74** (2006) 094011 [[hep-ph/0608211](#)].
- [724] V. Barone, A. Drago and P. G. Ratcliffe, *Transverse polarisation of quarks in hadrons*, *Phys. Rept.* **359** (2002) 1 [[hep-ph/0104283](#)].
- [725] G. Karl and J. E. Paton, *Naive Quark Model for an Arbitrary Number of Colors*, *Phys. Rev.* **D30** (1984) 238.
- [726] A. V. Efremov, P. Schweitzer, O. V. Teryaev and P. Zavada, *Transverse momentum dependent distribution functions in a covariant parton model approach with quark orbital motion*, *Phys. Rev.* **D80** (2009) 014021 [[0903.3490](#)].
- [727] P. Zavada, *The Structure functions and parton momenta distribution in the hadron rest system*, *Phys. Rev. D* **55** (1997) 4290 [[hep-ph/9609372](#)].
- [728] P. Zavada, *Generalized Cahn effect and parton 3D motion in a covariant approach*, *Phys. Rev. D* **83** (2011) 014022 [[0908.2316](#)].
- [729] A. V. Efremov, P. Schweitzer, O. V. Teryaev and P. Zavada, *The relation between TMDs and PDFs in the covariant parton model approach*, *Phys. Rev.* **D83** (2011) 054025 [[1012.5296](#)].
- [730] S. Bastami, A. Efremov, P. Schweitzer, O. Teryaev and P. Zavada, *Structure of the nucleon at leading and subleading twist in the covariant parton model*, [2011.06203](#).
- [731] F. Aslan, S. Bastami, Schweitzer and et al., *The parton model of the nucleon*, (forthcoming) (2021).
- [732] A. Accardi, A. Bacchetta, W. Melnitchouk and M. Schlegel, *What can break the Wandzura-Wilczek relation?*, *JHEP* **11** (2009) 093 [[0907.2942](#)].

- [733] J. D. Jackson, G. G. Ross and R. G. Roberts, *Polarized Structure Functions in the Parton Model*, *Phys. Lett. B* **226** (1989) 159.
- [734] R. G. Roberts and G. G. Ross, *Quark model description of polarized deep inelastic scattering and the prediction of  $g(2)$* , *Phys. Lett. B* **373** (1996) 235 [[hep-ph/9601235](#)].
- [735] C. Bourrely, J. Soffer and F. Buccella, *The Extension to the transverse momentum of the statistical parton distributions*, *Mod. Phys. Lett. A* **21** (2006) 143 [[hep-ph/0507328](#)].
- [736] C. Bourrely, F. Buccella and J. Soffer, *Semiinclusive DIS cross sections and spin asymmetries in the quantum statistical parton distributions approach*, *Phys. Rev. D* **83** (2011) 074008 [[1008.5322](#)].
- [737] U. D'Alesio, E. Leader and F. Murgia, *On the importance of Lorentz structure in the parton model: Target mass corrections, transverse momentum dependence, positivity bounds*, *Phys. Rev. D* **81** (2010) 036010 [[0909.5650](#)].
- [738] J. Blumlein and N. Kochelev, *On the twist-2 contributions to polarized structure functions and new sum rules*, *Phys. Lett. B* **381** (1996) 296 [[hep-ph/9603397](#)].
- [739] J. Blumlein and N. Kochelev, *On the twist -2 and twist - three contributions to the spin dependent electroweak structure functions*, *Nucl. Phys. B* **498** (1997) 285 [[hep-ph/9612318](#)].
- [740] J. Soffer and O. V. Teryaev, *Gluon polarization in transversely polarized nucleons and jet spin asymmetries at RHIC*, *Phys. Rev. D* **56** (1997) R1353 [[hep-ph/9702352](#)].
- [741] J. Blumlein and A. Tkabladze, *Target mass corrections for polarized structure functions and new sum rules*, *Nucl. Phys. B* **553** (1999) 427 [[hep-ph/9812478](#)].
- [742] H. Avakian, A. V. Efremov, P. Schweitzer and F. Yuan, *Transverse momentum dependent distribution function  $h_{1T}^\perp$  and the single spin asymmetry  $A_{UT}^{\sin(3\phi-3S)}$* , *Phys. Rev. D* **78** (2008) 114024 [[0805.3355](#)].
- [743] A. W. Thomas, *Chiral Symmetry and the Bag Model: A New Starting Point for Nuclear Physics*, *Adv. Nucl. Phys.* **13** (1984) 1.
- [744] A. I. Signal and F. G. Cao, *Transverse Momentum and Transverse Momentum Distributions in the MIT Bag Model*, [2108.12116](#).
- [745] S. J. Brodsky, D. S. Hwang, B.-Q. Ma and I. Schmidt, *Light cone representation of the spin and orbital angular momentum of relativistic composite systems*, *Nucl. Phys. B* **593** (2001) 311 [[hep-th/0003082](#)].
- [746] X.-d. Ji, J.-P. Ma and F. Yuan, *Three quark light cone amplitudes of the proton and quark orbital motion dependent observables*, *Nucl. Phys. B* **652** (2003) 383 [[hep-ph/0210430](#)].
- [747] B. Pasquini, S. Cazzaniga and S. Boffi, *Transverse momentum dependent parton distributions in a light-cone quark model*, *Phys. Rev. D* **78** (2008) 034025 [[0806.2298](#)].

- [748] B. Pasquini, S. Boffi and P. Schweitzer, *The Spin Structure of the Nucleon in Light-Cone Quark Models*, *Mod. Phys. Lett.* **A24** (2009) 2903 [[0910.1677](#)].
- [749] G. A. Miller, *Densities, Parton Distributions, and Measuring the Non-Spherical Shape of the Nucleon*, *Phys. Rev.* **C76** (2007) 065209 [[0708.2297](#)].
- [750] M. Burkardt, *Spin-orbit correlations and single-spin asymmetries*, in *Workshop on Exclusive Reactions at High Momentum Transfer*, 9, 2007, 0709.2966, DOI.
- [751] C. Lorce, B. Pasquini and M. Vanderhaeghen, *Unified framework for generalized and transverse-momentum dependent parton distributions within a 3Q light-cone picture of the nucleon*, *JHEP* **05** (2011) 041 [[1102.4704](#)].
- [752] B. Pasquini and P. Schweitzer, *Naive time-reversal odd phenomena in semi-inclusive deep-inelastic scattering from light-cone constituent quark models*, *Phys. Rev.* **D83** (2011) 114044 [[1103.5977](#)].
- [753] B. Pasquini and P. Schweitzer, *Pion transverse momentum dependent parton distributions in a light-front constituent approach, and the Boer-Mulders effect in the pion-induced Drell-Yan process*, *Phys. Rev.* **D90** (2014) 014050 [[1406.2056](#)].
- [754] C. Lorcé, B. Pasquini and P. Schweitzer, *Unpolarized transverse momentum dependent parton distribution functions beyond leading twist in quark models*, *JHEP* **01** (2015) 103 [[1411.2550](#)].
- [755] C. Lorcé, B. Pasquini and P. Schweitzer, *Transverse pion structure beyond leading twist in constituent models*, *Eur. Phys. J.* **C76** (2016) 415 [[1605.00815](#)].
- [756] R. Jakob, P. J. Mulders and J. Rodrigues, *Modeling quark distribution and fragmentation functions*, *Nucl. Phys.* **A626** (1997) 937 [[hep-ph/9704335](#)].
- [757] L. P. Gamberg, G. R. Goldstein and K. A. Oganessyan, *Novel transversity properties in semiinclusive deep inelastic scattering*, *Phys. Rev.* **D67** (2003) 071504 [[hep-ph/0301018](#)].
- [758] A. Bacchetta, F. Conti and M. Radici, *Transverse-momentum distributions in a diquark spectator model*, *Phys. Rev.* **D78** (2008) 074010 [[0807.0323](#)].
- [759] Z. Lu and I. Schmidt, *Orbital structure of quarks inside the nucleon in the light-cone diquark model*, *Phys. Rev.* **D82** (2010) 094005 [[1008.2684](#)].
- [760] D. MÄijller and D. S. Hwang, *The concept of phenomenological light-front wave functions – Regge improved diquark model predictions*, [1407.1655](#).
- [761] X. Liu, W. Mao, X. Wang and B.-Q. Ma, *Leading and higher twist transverse momentum dependent parton distribution functions in the spectator model*, *Phys. Rev. D* **104** (2021) 094043 [[2110.14070](#)].
- [762] I. C. Cloet, W. Bentz and A. W. Thomas, *Transversity quark distributions in a covariant quark-diquark model*, *Phys. Lett.* **B659** (2008) 214 [[0708.3246](#)].

- [763] Y. Ninomiya, W. Bentz and I. C. CloÁnt, *Transverse-momentum-dependent quark distribution functions of spin-one targets: Formalism and covariant calculations*, *Phys. Rev.* **C96** (2017) 045206 [[1707.03787](#)].
- [764] C. Shi and I. C. CloÁnt, *Intrinsic Transverse Motion of the PionâŽs Valence Quarks*, *Phys. Rev. Lett.* **122** (2019) 082301 [[1806.04799](#)].
- [765] S. J. Brodsky and G. F. de Teramond, *Hadronic spectra and light-front wavefunctions in holographic QCD*, *Phys. Rev. Lett.* **96** (2006) 201601 [[hep-ph/0602252](#)].
- [766] T. Maji, C. Mondal, D. Chakrabarti and O. V. Teryaev, *Relating transverse structure of various parton distributions*, *JHEP* **01** (2016) 165 [[1506.04560](#)].
- [767] T. Maji and D. Chakrabarti, *Transverse structure of a proton in a light-front quark-diquark model*, *Phys. Rev.* **D95** (2017) 074009 [[1702.04557](#)].
- [768] A. Bacchetta, S. Cotogno and B. Pasquini, *The transverse structure of the pion in momentum space inspired by the AdS/QCD correspondence*, *Phys. Lett.* **B771** (2017) 546 [[1703.07669](#)].
- [769] T. Maji, D. Chakrabarti and O. V. Teryaev, *Model predictions for azimuthal spin asymmetries for HERMES and COMPASS kinematics*, *Phys. Rev.* **D96** (2017) 114023 [[1711.01746](#)].
- [770] T. Maji, D. Chakrabarti and A. Mukherjee, *Sivers and  $\cos 2\phi$  asymmetries in semi-inclusive deep inelastic scattering in light-front holographic model*, *Phys. Rev.* **D97** (2018) 014016 [[1711.02930](#)].
- [771] P. Schweitzer, M. Strikman and C. Weiss, *Intrinsic transverse momentum and parton correlations from dynamical chiral symmetry breaking*, *JHEP* **1301** (2013) 163 [[1210.1267](#)].
- [772] M. Wakamatsu, *Transverse momentum distributions of quarks in the nucleon from the Chiral Quark Soliton Model*, *Phys. Rev.* **D79** (2009) 094028 [[0903.1886](#)].
- [773] F. A. Ceccopieri, A. Courtoy, S. Noguera and S. Scopetta, *Pion nucleus Drell–Yan process and parton transverse momentum in the pion*, *Eur. Phys. J. C* **78** (2018) 644 [[1801.07682](#)].
- [774] J. Arrington, D. W. Higinbotham, G. Rosner and M. Sargsian, *Hard probes of short-range nucleon-nucleon correlations*, *Prog. Part. Nucl. Phys.* **67** (2012) 898 [[1104.1196](#)].
- [775] P. V. Pobylitsa, *T odd quark distributions: QCD versus chiral models*, [hep-ph/0212027](#).
- [776] G. R. Goldstein and L. Gamberg, *Transversity and meson photoproduction*, in *High energy physics. Proceedings, 31st International Conference, ICHEP 2002, Amsterdam, Netherlands, July 25-31, 2002*, pp. 452–454, 2002, [hep-ph/0209085](#).
- [777] Z. Lu and I. Schmidt, *Connection between the Sivers function and the anomalous magnetic moment*, *Phys. Rev.* **D75** (2007) 073008 [[hep-ph/0611158](#)].

- [778] L. P. Gamberg, G. R. Goldstein and M. Schlegel, *Transverse Quark Spin Effects and the Flavor Dependence of the Boer-Mulders Function*, *Phys. Rev.* **D77** (2008) 094016 [0708.0324].
- [779] J. R. Ellis, D. S. Hwang and A. Kotzinian, *Sivers Asymmetries for Inclusive Pion and Kaon Production in Deep-Inelastic Scattering*, *Phys. Rev.* **D80** (2009) 074033 [0808.1567].
- [780] F. Yuan, *Sivers function in the MIT bag model*, *Phys. Lett.* **B575** (2003) 45 [hep-ph/0308157].
- [781] A. Courtoy, S. Scopetta and V. Vento, *Model calculations of the Sivers function satisfying the Burkardt Sum Rule*, *Phys. Rev.* **D79** (2009) 074001 [0811.1191].
- [782] A. Courtoy, S. Scopetta and V. Vento, *Analyzing the Boer-Mulders function within different quark models*, *Phys. Rev.* **D80** (2009) 074032 [0909.1404].
- [783] B. Pasquini and F. Yuan, *Sivers and Boer-Mulders functions in Light-Cone Quark Models*, *Phys. Rev.* **D81** (2010) 114013 [1001.5398].
- [784] Z. Lu and B.-Q. Ma, *Non-zero transversity distribution of the pion in a quark-spectator-antiquark model*, *Phys. Rev. D* **70** (2004) 094044 [hep-ph/0411043].
- [785] S. Meissner, A. Metz, M. Schlegel and K. Goeke, *Generalized parton correlation functions for a spin-0 hadron*, *JHEP* **08** (2008) 038 [0805.3165].
- [786] L. Gamberg and M. Schlegel, *Final state interactions and the transverse structure of the pion using non-perturbative eikonal methods*, *Phys. Lett.* **B685** (2010) 95 [0911.1964].
- [787] A. Courtoy, F. Fratini, S. Scopetta and V. Vento, *A Quark model analysis of the Sivers function*, *Phys. Rev.* **D78** (2008) 034002 [0801.4347].
- [788] M. Burkardt, *Impact parameter dependent parton distributions and transverse single spin asymmetries*, *Phys. Rev.* **D66** (2002) 114005 [hep-ph/0209179].
- [789] M. Burkardt, *Chromodynamic lensing and transverse single spin asymmetries*, *Nucl. Phys.* **A735** (2004) 185 [hep-ph/0302144].
- [790] M. Diehl and P. Hagler, *Spin densities in the transverse plane and generalized transversity distributions*, *Eur. Phys. J. C* **44** (2005) 87 [hep-ph/0504175].
- [791] M. Burkardt, *Transverse deformation of parton distributions and transversity decomposition of angular momentum*, *Phys. Rev. D* **72** (2005) 094020 [hep-ph/0505189].
- [792] M. Burkardt and B. Pasquini, *Modelling the nucleon structure*, *Eur. Phys. J. A* **52** (2016) 161 [1510.02567].
- [793] B. Pasquini, S. Rodini and A. Bacchetta, *Revisiting model relations between T-odd transverse-momentum dependent parton distributions and generalized parton distributions*, *Phys. Rev. D* **100** (2019) 054039 [1907.06960].

- [794] B. Gurjar, D. Chakrabarti, P. Choudhary, A. Mukherjee and P. Talukdar, *Relations between generalized parton distributions and transverse momentum dependent parton distributions*, *Phys. Rev. D* **104** (2021) 076028 [[2107.02216](#)].
- [795] S. J. Brodsky, B. Pasquini, B.-W. Xiao and F. Yuan, *Phases of Augmented Hadronic Light-Front Wave Functions*, *Phys. Lett. B* **687** (2010) 327 [[1001.1163](#)].
- [796] L. Gamberg and M. Schlegel, *Final State Interactions and the Transverse Structure of the Pion*, *Mod. Phys. Lett. A* **24** (2009) 2960 [[0912.5399](#)].
- [797] D. Ostromsky and E. Shuryak, *Instanton-induced azimuthal spin asymmetry in deep inelastic scattering*, *Phys. Rev. D* **71** (2005) 014037 [[hep-ph/0409253](#)].
- [798] I. O. Cherednikov, U. D'Alesio, N. I. Kochelev and F. Murgia, *Instanton contribution to the Sivers function*, *Phys. Lett. B* **642** (2006) 39 [[hep-ph/0606238](#)].
- [799] Y. Qian and I. Zahed, *Single Spin Asymmetry through QCD Instantons*, *Phys. Rev. D* **86** (2012) 014033 [[1112.4552](#)].
- [800] P. Hoyer and M. Jarvinen, *Soft rescattering in DIS: Effects of helicity flip*, *JHEP* **10** (2005) 080 [[hep-ph/0509058](#)].
- [801] A. Drago, *Time-reversal odd distribution functions in chiral models with vector mesons*, *Phys. Rev. D* **71** (2005) 057501 [[hep-ph/0501282](#)].
- [802] F. He and P. Wang, *Sivers distribution functions of sea quark in proton with chiral Lagrangian*, *Phys. Rev. D* **100** (2019) 074032 [[1904.06815](#)].
- [803] M. Gluck, E. Reya and A. Vogt, *Dynamical parton distributions of the proton and small x physics*, *Z. Phys. C* **67** (1995) 433.
- [804] M. Glück, E. Reya and A. Vogt, *Dynamical parton distributions revisited*, *Eur. Phys. J. C* **5** (1998) 461 [[hep-ph/9806404](#)].
- [805] M. Gluck, E. Reya, M. Stratmann and W. Vogelsang, *Next-to-leading order radiative parton model analysis of polarized deep inelastic lepton - nucleon scattering*, *Phys. Rev. D* **53** (1996) 4775 [[hep-ph/9508347](#)].
- [806] M. Gluck, E. Reya, M. Stratmann and W. Vogelsang, *Models for the polarized parton distributions of the nucleon*, *Phys. Rev. D* **63** (2001) 094005 [[hep-ph/0011215](#)].
- [807] M. Gluck, P. Jimenez-Delgado and E. Reya, *Dynamical parton distributions of the nucleon and very small-x physics*, *Eur. Phys. J. C* **53** (2008) 355 [[0709.0614](#)].
- [808] K. Goeke, S. Meissner, A. Metz and M. Schlegel, *Checking the Burkardt sum rule for the Sivers function by model calculations*, *Phys. Lett. B* **637** (2006) 241 [[hep-ph/0601133](#)].
- [809] M. Burkardt, *Sivers mechanism for gluons*, *Phys. Rev. D* **69** (2004) 091501 [[hep-ph/0402014](#)].

- [810] Z. Lu and B.-Q. Ma, *Gluon Sivers function in a light-cone spectator model*, *Phys. Rev. D* **94** (2016) 094022 [[1611.00125](#)].
- [811] J. Rodrigues, *Modelling quark and gluon correlation functions*, Ph.D. thesis, Vrije Univ. Amsterdam, Amsterdam, 2001.
- [812] A. Bacchetta, F. G. Celiberto, M. Radici and P. Taels, *Transverse-momentum-dependent gluon distribution functions in a spectator model*, *Eur. Phys. J. C* **80** (2020) 733 [[2005.02288](#)].
- [813] A. Bacchetta, F. G. Celiberto and M. Radici, *Toward twist-2 T-odd transverse-momentum-dependent gluon distributions: the f-type Sivers function*, in *European Physical Society Conference on High Energy Physics 2021*, 11, 2021, [2111.01686](#).
- [814] V. E. Lyubovitskij and I. Schmidt, *Gluon parton densities in soft-wall AdS/QCD*, [2012.01334](#).
- [815] A. Bacchetta, R. Kundu, A. Metz and P. J. Mulders, *The Collins fragmentation function: A Simple model calculation*, *Phys. Lett. B* **506** (2001) 155 [[hep-ph/0102278](#)].
- [816] J. C. Collins and G. A. Ladinsky, *On pi - pi correlations in polarized quark fragmentation using the linear sigma model*, [hep-ph/9411444](#).
- [817] A. Bacchetta, R. Kundu, A. Metz and P. J. Mulders, *Estimate of the Collins fragmentation function in a chiral invariant approach*, *Phys. Rev. D* **65** (2002) 094021 [[hep-ph/0201091](#)].
- [818] A. Manohar and H. Georgi, *Chiral Quarks and the Nonrelativistic Quark Model*, *Nucl. Phys. B* **234** (1984) 189.
- [819] T. Ito, W. Bentz, I. C. Cloet, A. W. Thomas and K. Yazaki, *The NJL-jet model for quark fragmentation functions*, *Phys. Rev. D* **80** (2009) 074008 [[0906.5362](#)].
- [820] H. H. Matevosyan, A. W. Thomas and W. Bentz, *Calculating Kaon Fragmentation Functions from NJL-Jet Model*, *Phys. Rev. D* **83** (2011) 074003 [[1011.1052](#)].
- [821] H. H. Matevosyan, A. W. Thomas and W. Bentz, *Monte Carlo Simulations of Hadronic Fragmentation Functions using NJL-Jet Model*, *Phys. Rev. D* **83** (2011) 114010 [[1103.3085](#)].
- [822] S.-i. Nam and C.-W. Kao, *Fragmentation functions and parton distribution functions for the pion with the nonlocal interactions*, *Phys. Rev. D* **85** (2012) 034023 [[1111.4444](#)].
- [823] S.-i. Nam and C.-W. Kao, *Fragmentation and quark distribution functions for the pion and kaon with explicit flavor-SU(3)-symmetry breaking*, *Phys. Rev. D* **85** (2012) 094023 [[1202.3281](#)].
- [824] D. J. Yang, F. J. Jiang, C. W. Kao and S. i. Nam, *Quark-jet contribution to the fragmentation functions for the pion and kaon with the nonlocal interactions*, *Phys. Rev. D* **87** (2013) 094007 [[1304.0525](#)].

- [825] A. Bacchetta, L. P. Gamberg, G. R. Goldstein and A. Mukherjee, *Collins fragmentation function for pions and kaons in a spectator model*, *Phys. Lett.* **B659** (2008) 234 [[0707.3372](#)].
- [826] S. Meissner, A. Metz and D. Pitonyak, *Momentum sum rules for fragmentation functions*, *Phys. Lett.* **B690** (2010) 296 [[1002.4393](#)].
- [827] A. Bacchetta, A. Metz and J.-J. Yang, *Collins fragmentation function from gluon rescattering*, *Phys. Lett.* **B574** (2003) 225 [[hep-ph/0307282](#)].
- [828] D. Amrath, A. Bacchetta and A. Metz, *Reviewing model calculations of the Collins fragmentation function*, *Phys. Rev.* **D71** (2005) 114018 [[hep-ph/0504124](#)].
- [829] H. H. Matevosyan, A. W. Thomas and W. Bentz, *Collins Fragmentation Function within NJL-jet Model*, *Phys. Rev.* **D86** (2012) 034025 [[1205.5813](#)].
- [830] X. Wang, Y. Yang and Z. Lu, *Double Collins effect in  $e^+e^- \rightarrow \Lambda\bar{\Lambda}X$  process in a diquark spectator model*, *Phys. Rev. D* **97** (2018) 114015 [[1802.01843](#)].
- [831] R. D. Field and R. P. Feynman, *A Parametrization of the Properties of Quark Jets*, *Nucl. Phys.* **B136** (1978) 1.
- [832] P. Hoyer, P. Osland, H. G. Sander, T. F. Walsh and P. M. Zerwas, *Quantum Chromodynamics and Jets in  $e^+ e^-$* , *Nucl. Phys.* **B161** (1979) 349.
- [833] A. Ali, E. Pietarinen, G. Kramer and J. Willrodt, *A QCD Analysis of the High-Energy  $e^+ e^-$  Data from PETRA*, *Phys. Lett.* **93B** (1980) 155.
- [834] X. Artru and G. Mennessier, *String model and multiproduction*, *Nucl. Phys.* **B70** (1974) 93.
- [835] M. G. Bowler,  *$e^+ e^-$  Production of Heavy Quarks in the String Model*, *Z. Phys.* **C11** (1981) 169.
- [836] B. Andersson, G. Gustafson and B. Soderberg, *A General Model for Jet Fragmentation*, *Z. Phys.* **C20** (1983) 317.
- [837] B. Andersson, G. Gustafson, G. Ingelman and T. Sjostrand, *Parton Fragmentation and String Dynamics*, *Phys. Rept.* **97** (1983) 31.
- [838] X. Artru, J. Czyzewski and H. Yabuki, *Single spin asymmetry in inclusive pion production, Collins effect and the string model*, *Z. Phys.* **C73** (1997) 527 [[hep-ph/9508239](#)].
- [839] J. Czyzewski, *Single spin asymmetry of vector meson production in the string model*, *Acta Phys. Polon.* **27** (1996) 1759 [[hep-ph/9606390](#)].
- [840] X. Artru, *Recursive fragmentation model with quark spin. Application to quark polarimetry*, [1001.1061](#).
- [841] A. Kerbizi, X. Artru, Z. Belghobsi, F. Bradamante and A. Martin, *Recursive model for the fragmentation of polarized quarks*, *Phys. Rev. D* **97** (2018) 074010 [[1802.00962](#)].

- [842] A. Kerbizi, X. Artru, Z. Belghobsi and A. Martin, *Simplified recursive  ${}^3P_0$  model for the fragmentation of polarized quarks*, *Phys. Rev. D* **100** (2019) 014003 [[1903.01736](#)].
- [843] H. H. Matevosyan, W. Bentz, I. C. Cloet and A. W. Thomas, *Transverse Momentum Dependent Fragmentation and Quark Distribution Functions from the NJL-jet Model*, *Phys. Rev. D* **85** (2012) 014021 [[1111.1740](#)].
- [844] W. Bentz, A. Kotzinian, H. H. Matevosyan, Y. Ninomiya, A. W. Thomas and K. Yazaki, *Quark-Jet model for transverse momentum dependent fragmentation functions*, *Phys. Rev. D* **94** (2016) 034004 [[1603.08333](#)].
- [845] A. Schafer and O. V. Teryaev, *Sum rules for the  $T$ -odd fragmentation functions*, *Phys. Rev. D* **61** (2000) 077903 [[hep-ph/9908412](#)].
- [846] J. Collins and A. Metz, *unpublished*.
- [847] L. P. Gamberg, A. Mukherjee and P. J. Mulders, *Spectral analysis of gluonic pole matrix elements for fragmentation*, *Phys. Rev. D* **77** (2008) 114026 [[0803.2632](#)].
- [848] S. Meissner and A. Metz, *Partonic pole matrix elements for fragmentation*, *Phys. Rev. Lett.* **102** (2009) 172003 [[0812.3783](#)].
- [849] L. P. Gamberg, A. Mukherjee and P. J. Mulders, *A model independent analysis of gluonic pole matrix elements and universality of TMD fragmentation functions*, *Phys. Rev. D* **83** (2011) 071503 [[1010.4556](#)].
- [850] A. V. Belitsky, *Leading order analysis of twist-3 space- and time-like cut vertices in QCD*, *Int. J. Mod. Phys. A* **32** (2017) 1730018 [[hep-ph/9703432](#)].
- [851] A. Candido, S. Forte and F. Hekhorn, *Can  $\overline{\text{MS}}$  parton distributions be negative?*, *JHEP* **11** (2020) 129 [[2006.07377](#)].
- [852] C. Lorcé, *The light-front gauge-invariant energy-momentum tensor*, *JHEP* **08** (2015) 045 [[1502.06656](#)].
- [853] J. Zhou, *Note on the scale dependence of the Burkardt sum rule*, *Phys. Rev. D* **92** (2015) 074016 [[1507.02819](#)].
- [854] A. Accardi and A. Signori, *Quark fragmentation as a probe of dynamical mass generation*, *Phys. Lett. B* **798** (2019) 134993 [[1903.04458](#)].
- [855] F. Aslan and T. C. Rogers, *The parton model of the nucleon*, (work in preparation) (2021).
- [856] A. I. Signal, *Calculations of higher twist distribution functions in the MIT bag model*, *Nucl. Phys. B* **497** (1997) 415 [[hep-ph/9610480](#)].
- [857] C. Lorce and B. Pasquini, *On the Origin of Model Relations among Transverse-Momentum Dependent Parton Distributions*, *Phys. Rev. D* **84** (2011) 034039 [[1104.5651](#)].

- [858] T. Liu and B.-Q. Ma, *Quark angular momentum in a spectator model*, *Phys. Lett. B* **741** (2015) 256 [[1501.00062](#)].
- [859] C. Lorce and B. Pasquini, *Pretzelosity TMD and Quark Orbital Angular Momentum*, *Phys. Lett. B* **710** (2012) 486 [[1111.6069](#)].
- [860] L. Gribov, E. Levin and M. Ryskin, *Semihard Processes in QCD*, *Phys.Rept.* **100** (1983) 1.
- [861] A. H. Mueller and J.-W. Qiu, *Gluon Recombination and Shadowing at Small Values of  $x$* , *Nucl.Phys.* **B268** (1986) 427.
- [862] L. D. McLerran and R. Venugopalan, *Computing quark and gluon distribution functions for very large nuclei*, *Phys.Rev.* **D49** (1994) 2233 [[hep-ph/9309289](#)].
- [863] L. D. McLerran and R. Venugopalan, *Gluon distribution functions for very large nuclei at small transverse momentum*, *Phys. Rev.* **D49** (1994) 3352 [[hep-ph/9311205](#)].
- [864] E. Iancu and R. Venugopalan, *The Color glass condensate and high-energy scattering in QCD*, [hep-ph/0303204](#).
- [865] Y. V. Kovchegov and E. Levin, *Quantum chromodynamics at high energy*, *Camb. Monogr. Part. Phys. Nucl. Phys. Cosmol.* **33** (2012) 1.
- [866] E. A. Kuraev, L. N. Lipatov and V. S. Fadin, *The Pomeranchuk Singularity in Nonabelian Gauge Theories*, *Sov. Phys. JETP* **45** (1977) 199.
- [867] I. I. Balitsky and L. N. Lipatov, *The Pomeranchuk Singularity in Quantum Chromodynamics*, *Sov. J. Nucl. Phys.* **28** (1978) 822.
- [868] V. S. Fadin and L. N. Lipatov, *BFKL pomeron in the next-to-leading approximation*, *Phys. Lett. B* **429** (1998) 127 [[hep-ph/9802290](#)].
- [869] M. Ciafaloni and G. Camici, *Energy scale(s) and next-to-leading BFKL equation*, *Phys. Lett. B* **430** (1998) 349 [[hep-ph/9803389](#)].
- [870] M. Ciafaloni, D. Colferai, G. P. Salam and A. M. Stasto, *Renormalization group improved small  $x$  Green's function*, *Phys. Rev. D* **68** (2003) 114003 [[hep-ph/0307188](#)].
- [871] F. Gelis, E. Iancu, J. Jalilian-Marian and R. Venugopalan, *The Color Glass Condensate*, *Ann. Rev. Nucl. Part. Sci.* **60** (2010) 463 [[1002.0333](#)].
- [872] J.-P. Blaizot, *High gluon densities in heavy ion collisions*, *Rept. Prog. Phys.* **80** (2017) 032301 [[1607.04448](#)].
- [873] L. Susskind, *Model of selfinduced strong interactions*, *Phys. Rev.* **165** (1968) 1535.
- [874] K. Bardakci and M. B. Halpern, *Theories at infinite momentum*, *Phys. Rev.* **176** (1968) 1686.

- [875] S. Jeon and R. Venugopalan, *Random walks of partons in  $SU(N(c))$  and classical representations of color charges in QCD at small  $x$* , *Phys. Rev. D* **70** (2004) 105012 [[hep-ph/0406169](#)].
- [876] J. Jalilian-Marian, S. Jeon and R. Venugopalan, *Wong's equations and the small  $x$  effective action in QCD*, *Phys. Rev. D* **63** (2001) 036004 [[hep-ph/0003070](#)].
- [877] L. D. McLerran and R. Venugopalan, *Green's functions in the color field of a large nucleus*, *Phys. Rev. D* **50** (1994) 2225 [[hep-ph/9402335](#)].
- [878] I. Balitsky, *Operator expansion for high-energy scattering*, *Nucl. Phys.* **B463** (1996) 99 [[hep-ph/9509348](#)].
- [879] L. D. McLerran and R. Venugopalan, *Fock space distributions, structure functions, higher twists and small  $x$* , *Phys. Rev. D* **59** (1999) 094002 [[hep-ph/9809427](#)].
- [880] A. Ayala, J. Jalilian-Marian, L. D. McLerran and R. Venugopalan, *Quantum corrections to the Weizsäcker-Williams gluon distribution function at small  $x$* , *Phys. Rev. D* **53** (1996) 458 [[hep-ph/9508302](#)].
- [881] I. I. Balitsky and A. V. Belitsky, *Nonlinear evolution in high density QCD*, *Nucl. Phys.* **B629** (2002) 290 [[hep-ph/0110158](#)].
- [882] S. Caron-Huot, *When does the gluon reggeize?*, *JHEP* **05** (2015) 093 [[1309.6521](#)].
- [883] S. Bondarenko, L. Lipatov, S. Pozdnyakov and A. Prygarin, *One loop light-cone QCD, effective action for reggeized gluons and QCD RFT calculus*, *Eur. Phys. J.* **C77** (2017) 630 [[1708.05183](#)].
- [884] A. Ayala, M. Hentschinski, J. Jalilian-Marian and M. E. Tejeda-Yeomans, *Spinor helicity methods in high-energy factorization: efficient momentum-space calculations in the Color Glass Condensate formalism*, *Nucl. Phys.* **B920** (2017) 232 [[1701.07143](#)].
- [885] M. Hentschinski, *Color glass condensate formalism, Balitsky-JIMWLK evolution, and Lipatov's high energy effective action*, *Phys. Rev. D* **97** (2018) 114027 [[1802.06755](#)].
- [886] S. Bondarenko and S. Pozdnyakov, *S-matrix and production amplitudes in high energy QCD*, *Phys. Lett. B* **783** (2018) 207 [[1803.04131](#)].
- [887] S. Bondarenko and S. Pozdnyakov, *On correlators of Reggeon fields and operators of Wilson lines in high energy QCD*, *Int. J. Mod. Phys. A* **33** (2018) 1850204 [[1806.02563](#)].
- [888] L. N. Lipatov, *Small  $x$  physics in perturbative QCD*, *Phys. Rept.* **286** (1997) 131 [[hep-ph/9610276](#)].
- [889] Y. Hatta, E. Iancu, K. Itakura and L. McLerran, *Odderon in the color glass condensate*, *Nucl. Phys.* **A760** (2005) 172 [[hep-ph/0501171](#)].
- [890] S. Jeon and R. Venugopalan, *A Classical Odderon in QCD at high energies*, *Phys. Rev. D* **71** (2005) 125003 [[hep-ph/0503219](#)].

- [891] R. C. Brower, J. Polchinski, M. J. Strassler and C.-I. Tan, *The Pomeron and gauge/string duality*, *JHEP* **12** (2007) 005 [[hep-th/0603115](#)].
- [892] A. H. Mueller, *Small x Behavior and Parton Saturation: A QCD Model*, *Nucl. Phys. B* **335** (1990) 115.
- [893] L. Frankfurt, V. Guzey and M. Strikman, *Leading Twist Nuclear Shadowing Phenomena in Hard Processes with Nuclei*, *Phys. Rept.* **512** (2012) 255 [[1106.2091](#)].
- [894] Y. V. Kovchegov and A. H. Mueller, *Gluon production in current nucleus and nucleon - nucleus collisions in a quasiclassical approximation*, *Nucl.Phys. B* **529** (1998) 451 [[hep-ph/9802440](#)].
- [895] E. Iancu, K. Itakura and L. McLerran, *Geometric scaling above the saturation scale*, *Nucl. Phys. A* **708** (2002) 327 [[hep-ph/0203137](#)].
- [896] A. M. Stasto, K. J. Golec-Biernat and J. Kwiecinski, *Geometric scaling for the total gamma\* p cross-section in the low x region*, *Phys. Rev. Lett.* **86** (2001) 596 [[hep-ph/0007192](#)].
- [897] J. Jalilian-Marian, A. Kovner, A. Leonidov and H. Weigert, *The Wilson renormalization group for low x physics: Towards the high density regime*, *Phys. Rev. D* **59** (1998) 014014 [[hep-ph/9706377](#)].
- [898] J. Jalilian-Marian, A. Kovner and H. Weigert, *The Wilson renormalization group for low x physics: Gluon evolution at finite parton density*, *Phys. Rev. D* **59** (1998) 014015 [[hep-ph/9709432](#)].
- [899] E. Iancu, A. Leonidov and L. D. McLerran, *Nonlinear gluon evolution in the color glass condensate. 1.*, *Nucl. Phys. A* **692** (2001) 583 [[hep-ph/0011241](#)].
- [900] E. Ferreiro, E. Iancu, A. Leonidov and L. McLerran, *Nonlinear gluon evolution in the color glass condensate. 2.*, *Nucl. Phys. A* **703** (2002) 489 [[hep-ph/0109115](#)].
- [901] J.-P. Blaizot, E. Iancu and H. Weigert, *Nonlinear gluon evolution in path integral form*, *Nucl. Phys. A* **713** (2003) 441 [[hep-ph/0206279](#)].
- [902] K. Rummukainen and H. Weigert, *Universal features of JIMWLK and BK evolution at small x*, *Nucl. Phys. A* **739** (2004) 183 [[hep-ph/0309306](#)].
- [903] A. Dumitru, J. Jalilian-Marian, T. Lappi, B. Schenke and R. Venugopalan, *Renormalization group evolution of multi-gluon correlators in high energy QCD*, *Phys.Lett. B* **706** (2011) 219 [[1108.4764](#)].
- [904] H. Kowalski, T. Lappi and R. Venugopalan, *Nuclear enhancement of universal dynamics of high parton densities*, *Phys. Rev. Lett.* **100** (2008) 022303 [[0705.3047](#)].
- [905] I. Balitsky and G. A. Chirilli, *Next-to-leading order evolution of color dipoles*, *Phys. Rev. D* **77** (2008) 014019 [[0710.4330](#)].

- [906] I. Balitsky and G. A. Chirilli, *Rapidity evolution of Wilson lines at the next-to-leading order*, *Phys. Rev.* **D88** (2013) 111501 [[1309.7644](#)].
- [907] Y. V. Kovchegov and H. Weigert, *Triumvirate of Running Couplings in Small- $x$  Evolution*, *Nucl. Phys.* **A784** (2007) 188 [[hep-ph/0609090](#)].
- [908] M. Lublinsky and Y. Mulian, *High Energy QCD at NLO: from light-cone wave function to JIMWLK evolution*, *JHEP* **05** (2017) 097 [[1610.03453](#)].
- [909] A. Kovner, M. Lublinsky and Y. Mulian, *Jalilian-Marian, Iancu, McLerran, Weigert, Leonidov, Kovner evolution at next to leading order*, *Phys. Rev.* **D89** (2014) 061704 [[1310.0378](#)].
- [910] A. Kovner, M. Lublinsky and Y. Mulian, *NLO JIMWLK evolution unabridged*, *JHEP* **08** (2014) 114 [[1405.0418](#)].
- [911] A. V. Grabovsky, *Connected contribution to the kernel of the evolution equation for 3-quark Wilson loop operator*, *JHEP* **09** (2013) 141 [[1307.5414](#)].
- [912] I. Balitsky and A. V. Grabovsky, *NLO evolution of 3-quark Wilson loop operator*, *JHEP* **01** (2015) 009 [[1405.0443](#)].
- [913] A. V. Grabovsky, *On the low- $x$  NLO evolution of 4 point colorless operators*, *JHEP* **09** (2015) 194 [[1507.08622](#)].
- [914] S. Caron-Huot, *Resummation of non-global logarithms and the BFKL equation*, *JHEP* **03** (2018) 036 [[1501.03754](#)].
- [915] I. Balitsky and G. A. Chirilli, *Photon impact factor in the next-to-leading order*, *Phys. Rev. D* **83** (2011) 031502 [[1009.4729](#)].
- [916] G. Beuf, *Dipole factorization for DIS at NLO: Combining the  $q\bar{q}$  and  $q\bar{q}g$  contributions*, *Phys. Rev. D* **96** (2017) 074033 [[1708.06557](#)].
- [917] H. Hänninen, T. Lappi and R. Paatelainen, *One-loop corrections to light cone wave functions: the dipole picture DIS cross section*, *Annals Phys.* **393** (2018) 358 [[1711.08207](#)].
- [918] G. A. Chirilli, B.-W. Xiao and F. Yuan, *One-loop Factorization for Inclusive Hadron Production in  $pA$  Collisions in the Saturation Formalism*, *Phys. Rev. Lett.* **108** (2012) 122301 [[1112.1061](#)].
- [919] T. Altinoluk, N. Armesto, G. Beuf, A. Kovner and M. Lublinsky, *Single-inclusive particle production in proton-nucleus collisions at next-to-leading order in the hybrid formalism*, *Phys. Rev. D* **91** (2015) 094016 [[1411.2869](#)].
- [920] P. Caucal, F. Salazar and R. Venugopalan, *Dijet impact factor in DIS at next-to-leading order in the Color Glass Condensate*, [2108.06347](#).
- [921] K. Roy and R. Venugopalan, *NLO impact factor for inclusive photon+dijet production in  $e + A$  DIS at small  $x$* , *Phys. Rev. D* **101** (2020) 034028 [[1911.04530](#)].

- [922] K. Roy and R. Venugopalan, *Extracting many-body correlators of saturated gluons with precision from inclusive photon+dijet final states in deeply inelastic scattering*, *Phys. Rev. D* **101** (2020) 071505 [[1911.04519](#)].
- [923] R. Boussarie, A. V. Grabovsky, L. Szymanowski and S. Wallon, *On the one loop  $\gamma^{(*)} \rightarrow q\bar{q}$  impact factor and the exclusive diffractive cross sections for the production of two or three jets*, *JHEP* **11** (2016) 149 [[1606.00419](#)].
- [924] R. Boussarie, A. V. Grabovsky, D. Yu. Ivanov, L. Szymanowski and S. Wallon, *Next-to-Leading Order Computation of Exclusive Diffractive Light Vector Meson Production in a Saturation Framework*, *Phys. Rev. Lett.* **119** (2017) 072002 [[1612.08026](#)].
- [925] C. Marquet, B.-W. Xiao and F. Yuan, *Semi-inclusive Deep Inelastic Scattering at small  $x$* , *Phys.Lett.* **B682** (2009) 207 [[0906.1454](#)].
- [926] F. Dominguez, B.-W. Xiao and F. Yuan,  *$k_t$ -factorization for Hard Processes in Nuclei*, *Phys.Rev.Lett.* **106** (2011) 022301 [[1009.2141](#)].
- [927] F. Dominguez, C. Marquet, B.-W. Xiao and F. Yuan, *Universality of Unintegrated Gluon Distributions at small  $x$* , *Phys. Rev.* **D83** (2011) 105005 [[1101.0715](#)].
- [928] A. Metz and J. Zhou, *Distribution of linearly polarized gluons inside a large nucleus*, *Phys.Rev.* **D84** (2011) 051503 [[1105.1991](#)].
- [929] I. Balitsky and A. Tarasov, *Gluon TMD in particle production from low to moderate  $x$* , *JHEP* **06** (2016) 164 [[1603.06548](#)].
- [930] T. Altinoluk, R. Boussarie and P. Kotko, *Interplay of the CGC and TMD frameworks to all orders in kinematic twist*, *JHEP* **05** (2019) 156 [[1901.01175](#)].
- [931] T. Altinoluk and R. Boussarie, *Low  $x$  physics as an infinite twist (G)TMD framework: unravelling the origins of saturation*, [1902.07930](#).
- [932] F. Gelis, T. Lappi and R. Venugopalan, *High energy scattering in Quantum Chromodynamics*, *Int. J. Mod. Phys.* **E16** (2007) 2595 [[0708.0047](#)].
- [933] R. Baier, A. Mueller and D. Schiff, *Saturation and shadowing in high-energy proton nucleus dilepton production*, *Nucl.Phys.* **A741** (2004) 358 [[hep-ph/0403201](#)].
- [934] C. Marquet, *Forward inclusive dijet production and azimuthal correlations in  $p(A)$  collisions*, *Nucl.Phys.* **A796** (2007) 41 [[0708.0231](#)].
- [935] A. Mueller, B.-W. Xiao and F. Yuan, *Sudakov Resummation in Small- $x$  Saturation Formalism*, *Phys.Rev.Lett.* **110** (2013) 082301 [[1210.5792](#)].
- [936] A. H. Mueller, B.-W. Xiao and F. Yuan, *Sudakov double logarithms resummation in hard processes in the small- $x$  saturation formalism*, *Phys. Rev.* **D88** (2013) 114010 [[1308.2993](#)].
- [937] I. Balitsky and A. Tarasov, *Rapidity evolution of gluon TMD from low to moderate  $x$* , *JHEP* **10** (2015) 017 [[1505.02151](#)].

- [938] B.-W. Xiao, F. Yuan and J. Zhou, *Transverse Momentum Dependent Parton Distributions at Small- $x$* , *Nucl. Phys. B* **921** (2017) 104 [[1703.06163](#)].
- [939] I. Balitsky, *Gauge-invariant TMD factorization for Drell-Yan hadronic tensor at small  $x$* , [2012.01588](#).
- [940] D. Kharzeev, Y. V. Kovchegov and K. Tuchin, *Cronin effect and high  $p(T)$  suppression in  $pA$  collisions*, *Phys. Rev. D* **68** (2003) 094013 [[hep-ph/0307037](#)].
- [941] E. Petreska, *TMD gluon distributions at small  $x$  in the CGC theory*, *Int. J. Mod. Phys. E* **27** (2018) 1830003 [[1804.04981](#)].
- [942] J. Jalilian-Marian, A. Kovner, L. D. McLerran and H. Weigert, *The Intrinsic glue distribution at very small  $x$* , *Phys. Rev. D* **55** (1997) 5414 [[hep-ph/9606337](#)].
- [943] Y. V. Kovchegov, *NonAbelian Weizsäcker-Williams field and a two-dimensional effective color charge density for a very large nucleus*, *Phys. Rev. D* **54** (1996) 5463 [[hep-ph/9605446](#)].
- [944] Y. Hatta, *CGC formalism with two sources*, *Nucl. Phys. A* **781** (2007) 104 [[hep-ph/0607126](#)].
- [945] F. Dominguez, C. Marquet, A. M. Stasto and B.-W. Xiao, *Universality of multiparticle production in QCD at high energies*, *Phys. Rev. D* **87** (2013) 034007 [[1210.1141](#)].
- [946] W. Vogelsang and F. Yuan, *Hadronic Dijet Imbalance and Transverse-Momentum Dependent Parton Distributions*, *Phys. Rev. D* **76** (2007) 094013 [[0708.4398](#)].
- [947] J. L. Albacete and C. Marquet, *Azimuthal correlations of forward di-hadrons in  $d+Au$  collisions at RHIC in the Color Glass Condensate*, *Phys. Rev. Lett.* **105** (2010) 162301 [[1005.4065](#)].
- [948] A. Stasto, B.-W. Xiao and F. Yuan, *Back-to-Back Correlations of Di-hadrons in  $dAu$  Collisions at RHIC*, *Phys. Lett. B* **716** (2012) 430 [[1109.1817](#)].
- [949] A. Stasto, S.-Y. Wei, B.-W. Xiao and F. Yuan, *On the Dihadron Angular Correlations in Forward  $pA$  collisions*, *Phys. Lett. B* **784** (2018) 301 [[1805.05712](#)].
- [950] J. L. Albacete, G. Giacalone, C. Marquet and M. Matas, *Forward dihadron back-to-back correlations in  $pA$  collisions*, *Phys. Rev. D* **99** (2019) 014002 [[1805.05711](#)].
- [951] L. Zheng, E. Aschenauer, J. Lee and B.-W. Xiao, *Probing Gluon Saturation through Dihadron Correlations at an Electron-Ion Collider*, *Phys. Rev. D* **89** (2014) 074037 [[1403.2413](#)].
- [952] D. Boer, P. J. Mulders, C. Pisano and J. Zhou, *Asymmetries in Heavy Quark Pair and Dijet Production at an EIC*, *JHEP* **08** (2016) 001 [[1605.07934](#)].
- [953] D. Boer, P. J. Mulders, J. Zhou and Y.-j. Zhou, *Suppression of maximal linear gluon polarization in angular asymmetries*, *JHEP* **10** (2017) 196 [[1702.08195](#)].

- [954] A. Dumitru, T. Lappi and V. Skokov, *Distribution of Linearly Polarized Gluons and Elliptic Azimuthal Anisotropy in Deep Inelastic Scattering Dijet Production at High Energy*, *Phys. Rev. Lett.* **115** (2015) 252301 [[1508.04438](#)].
- [955] A. Dumitru, V. Skokov and T. Ullrich, *Measuring the Weizsäcker-Williams distribution of linearly polarized gluons at an electron-ion collider through dijet azimuthal asymmetries*, *Phys. Rev. C* **99** (2019) 015204 [[1809.02615](#)].
- [956] H. Mäntysaari, N. Mueller and B. Schenke, *Diffractive Dijet Production and Wigner Distributions from the Color Glass Condensate*, *Phys. Rev. D* **99** (2019) 074004 [[1902.05087](#)].
- [957] H. Mäntysaari, N. Mueller, F. Salazar and B. Schenke, *Multigluon Correlations and Evidence of Saturation from Dijet Measurements at an Electron-Ion Collider*, *Phys. Rev. Lett.* **124** (2020) 112301 [[1912.05586](#)].
- [958] Y. V. Kovchegov, *Small  $x$   $F(2)$  structure function of a nucleus including multiple pomeron exchanges*, *Phys. Rev. D* **60** (1999) 034008 [[hep-ph/9901281](#)].
- [959] J. Zhou, *The evolution of the small  $x$  gluon TMD*, *JHEP* **06** (2016) 151 [[1603.07426](#)].
- [960] S. Marzani, *Combining  $Q_T$  and small- $x$  resummations*, *Phys. Rev. D* **93** (2016) 054047 [[1511.06039](#)].
- [961] J. Jalilian-Marian, A. Kovner, A. Leonidov and H. Weigert, *The BFKL equation from the Wilson renormalization group*, *Nucl. Phys. B* **504** (1997) 415 [[hep-ph/9701284](#)].
- [962] G. A. Chirilli, *Sub-eikonal corrections to scattering amplitudes at high energy*, *JHEP* **01** (2019) 118 [[1807.11435](#)].
- [963] Y. Hatta, Y. Nakagawa, F. Yuan, Y. Zhao and B. Xiao, *Gluon orbital angular momentum at small- $x$* , *Phys. Rev. D* **95** (2017) 114032 [[1612.02445](#)].
- [964] T. Altinoluk, N. Armesto, G. Beuf, M. Martínez and C. A. Salgado, *Next-to-eikonal corrections in the CGC: gluon production and spin asymmetries in  $pA$  collisions*, *JHEP* **07** (2014) 068 [[1404.2219](#)].
- [965] T. Altinoluk, N. Armesto, G. Beuf and A. Moscoso, *Next-to-next-to-eikonal corrections in the CGC*, *JHEP* **01** (2016) 114 [[1505.01400](#)].
- [966] P. Agostini, T. Altinoluk and N. Armesto, *Non-eikonal corrections to multi-particle production in the Color Glass Condensate*, *Eur. Phys. J. C* **79** (2019) 600 [[1902.04483](#)].
- [967] R. Kirschner and L. n. Lipatov, *Double Logarithmic Asymptotics and Regge Singularities of Quark Amplitudes with Flavor Exchange*, *Nucl. Phys. B* **213** (1983) 122.
- [968] R. Kirschner, *Reggeon interactions in perturbative QCD*, *Z. Phys. C* **65** (1995) 505 [[hep-th/9407085](#)].

- [969] R. Kirschner, *Regge asymptotics of scattering with flavor exchange in QCD*, *Z. Phys. C* **67** (1995) 459 [[hep-th/9404158](#)].
- [970] J. Blumlein and A. Vogt, *On the behavior of nonsinglet structure functions at small  $x$* , *Phys. Lett. B* **370** (1996) 149 [[hep-ph/9510410](#)].
- [971] J. Bartels, B. I. Ermolaev and M. G. Ryskin, *Nonsinglet contributions to the structure function  $g1$  at small  $x$* , *Z. Phys. C* **70** (1996) 273 [[hep-ph/9507271](#)].
- [972] J. Bartels, B. I. Ermolaev and M. G. Ryskin, *Flavor singlet contribution to the structure function  $G(1)$  at small  $x$* , *Z. Phys. C* **72** (1996) 627 [[hep-ph/9603204](#)].
- [973] J. Blumlein and A. Vogt, *The Singlet contribution to the structure function  $g1(x, Q^{**2})$  at small  $x$* , *Phys. Lett. B* **386** (1996) 350 [[hep-ph/9606254](#)].
- [974] R. Boussarie, Y. Hatta and F. Yuan, *Proton Spin Structure at Small- $x$* , *Phys. Lett. B* **797** (2019) 134817 [[1904.02693](#)].
- [975] Y. V. Kovchegov, D. Pitonyak and M. D. Sievert, *Helicity Evolution at Small- $x$* , *JHEP* **01** (2016) 072 [[1511.06737](#)].
- [976] Y. V. Kovchegov, D. Pitonyak and M. D. Sievert, *Small- $x$  asymptotics of the quark helicity distribution*, *Phys. Rev. Lett.* **118** (2017) 052001 [[1610.06188](#)].
- [977] Y. V. Kovchegov and M. D. Sievert, *Small- $x$  Helicity Evolution: an Operator Treatment*, *Phys. Rev. D* **99** (2019) 054032 [[1808.09010](#)].
- [978] J. Jalilian-Marian, *Elastic scattering of a quark from a color field: longitudinal momentum exchange*, *Phys. Rev. D* **96** (2017) 074020 [[1708.07533](#)].
- [979] A. Tarasov and R. Venugopalan, *Structure functions at small  $x$  from worldlines: Unpolarized distributions*, *Phys. Rev. D* **100** (2019) 054007 [[1903.11624](#)].
- [980] F. Cougoulic and Y. V. Kovchegov, *Helicity-dependent generalization of the JIMWLK evolution*, *Phys. Rev. D* **100** (2019) 114020 [[1910.04268](#)].
- [981] Y. V. Kovchegov, A. Tarasov and Y. Tawabutr, *Helicity Evolution at Small  $x$ : the Single-Logarithmic Contribution*, [2104.11765](#).
- [982] Y. V. Kovchegov, D. Pitonyak and M. D. Sievert, *Small- $x$  Asymptotics of the Quark Helicity Distribution: Analytic Results*, *Phys. Lett. B* **772** (2017) 136 [[1703.05809](#)].
- [983] Y. V. Kovchegov, D. Pitonyak and M. D. Sievert, *Helicity Evolution at Small  $x$ : Flavor Singlet and Non-Singlet Observables*, *Phys. Rev. D* **95** (2017) 014033 [[1610.06197](#)].
- [984] Y. V. Kovchegov and Y. Tawabutr, *Helicity at Small  $x$ : Oscillations Generated by Bringing Back the Quarks*, *JHEP* **08** (2020) 014 [[2005.07285](#)].
- [985] Y. V. Kovchegov, *Orbital Angular Momentum at Small  $x$* , *JHEP* **03** (2019) 174 [[1901.07453](#)].

- [986] Y. V. Kovchegov and M. D. Sievert, *Valence Quark Transversity at Small x*, *Phys. Rev. D* **99** (2019) 054033 [[1808.10354](#)].
- [987] D. Adamiak, Y. V. Kovchegov, W. Melnitchouk, D. Pitonyak, N. Sato and M. D. Sievert, *First analysis of world polarized DIS data with small-x helicity evolution*, [2102.06159](#).
- [988] D. Boer, M. G. Echevarria, P. Mulders and J. Zhou, *Single spin asymmetries from a single Wilson loop*, *Phys. Rev. Lett.* **116** (2016) 122001 [[1511.03485](#)].
- [989] J. Zhou, *Transverse single spin asymmetries at small x and the anomalous magnetic moment*, *Phys. Rev. D* **89** (2014) 074050 [[1308.5912](#)].
- [990] M. G. Ryskin, *Odderon and Polarization Phenomena in QCD*, *Sov. J. Nucl. Phys.* **46** (1987) 337.
- [991] N. H. Buttimore, B. Z. Kopeliovich, E. Leader, J. Soffer and T. L. Trueman, *The spin dependence of high-energy proton scattering*, *Phys. Rev. D* **59** (1999) 114010 [[hep-ph/9901339](#)].
- [992] E. Leader and T. L. Trueman, *The Odderon and spin dependence of high-energy proton proton scattering*, *Phys. Rev. D* **61** (2000) 077504 [[hep-ph/9908221](#)].
- [993] R. Boussarie, Y. Hatta, L. Szymanowski and S. Wallon, *Probing the Gluon Sivers Function with an Unpolarized Target: GTMD Distributions and the Odderons*, *Phys. Rev. Lett.* **124** (2020) 172501 [[1912.08182](#)].
- [994] G. Altarelli and G. G. Ross, *The Anomalous Gluon Contribution to Polarized Leptoproduction*, *Phys. Lett. B* **212** (1988) 391.
- [995] R. D. Carlitz, J. C. Collins and A. H. Mueller, *The Role of the Axial Anomaly in Measuring Spin Dependent Parton Distributions*, *Phys. Lett. B* **214** (1988) 229.
- [996] G. Veneziano, *Is There a QCD Spin Crisis?*, *Mod. Phys. Lett. A* **4** (1989) 1605.
- [997] G. M. Shore and G. Veneziano, *The U(1) Goldberger-Treiman Relation and the Two Components of the Proton 'Spin'*, *Phys. Lett. B* **244** (1990) 75.
- [998] G. M. Shore and G. Veneziano, *The U(1) Goldberger-Treiman relation and the proton 'spin': A Renormalization group analysis*, *Nucl. Phys. B* **381** (1992) 23.
- [999] S. Narison, G. M. Shore and G. Veneziano, *Topological charge screening and the 'proton spin' beyond the chiral limit*, *Nucl. Phys. B* **546** (1999) 235 [[hep-ph/9812333](#)].
- [1000] S. Narison, *Slope of the topological charge, proton spin and  $0^{-+}$  pseudoscalar di-gluonia spectra*, [2111.02873](#).
- [1001] L. Giusti, G. C. Rossi, M. Testa and G. Veneziano, *The  $U(A)(1)$  problem on the lattice with Ginsparg-Wilson fermions*, *Nucl. Phys. B* **628** (2002) 234 [[hep-lat/0108009](#)].

- [1002] RQCD collaboration, G. S. Bali, V. Braun, S. Collins, A. Schäfer and J. Simeth, *Masses and decay constants of the  $\eta$  and  $\eta'$  mesons from lattice QCD*, *JHEP* **08** (2021) 137 [2106.05398].
- [1003] A. Tarasov and R. Venugopalan, *The role of the chiral anomaly in polarized deeply inelastic scattering I: Finding the triangle graph inside the box diagram in Bjorken and Regge asymptotics*, *Phys. Rev. D* **102** (2020) 114022 [2008.08104].
- [1004] A. Tarasov and R. Venugopalan, *The role of the chiral anomaly in polarized deeply inelastic scattering II: Topological screening and transitions from emergent axion-like dynamics*, 2109.10370.
- [1005] G. 't Hooft, *Computation of the Quantum Effects Due to a Four-Dimensional Pseudoparticle*, *Phys. Rev. D* **14** (1976) 3432.
- [1006] F. R. Klinkhamer and N. S. Manton, *A Saddle Point Solution in the Weinberg-Salam Theory*, *Phys. Rev. D* **30** (1984) 2212.
- [1007] V. A. Kuzmin, V. A. Rubakov and M. E. Shaposhnikov, *On the Anomalous Electroweak Baryon Number Nonconservation in the Early Universe*, *Phys. Lett. B* **155** (1985) 36.
- [1008] L. D. McLerran, E. Mottola and M. E. Shaposhnikov, *Sphalerons and Axion Dynamics in High Temperature QCD*, *Phys. Rev. D* **43** (1991) 2027.
- [1009] M. Mace, S. Schlichting and R. Venugopalan, *Off-equilibrium sphaleron transitions in the Glasma*, *Phys. Rev. D* **93** (2016) 074036 [1601.07342].
- [1010] R. Boussarie and Y. Mehtar-Tani, *On gauge invariance of transverse momentum dependent distributions at small  $x$* , *Phys. Rev. D* **103** (2021) 094012 [2001.06449].
- [1011] P. Kotko, K. Kutak, C. Marquet, E. Petreska, S. Sapeta and A. van Hameren, *Improved TMD factorization for forward dijet production in dilute-dense hadronic collisions*, *JHEP* **09** (2015) 106 [1503.03421].
- [1012] C. Marquet, E. Petreska and C. Roiesnel, *Transverse-momentum-dependent gluon distributions from JIMWLK evolution*, *JHEP* **10** (2016) 065 [1608.02577].
- [1013] C. Marquet, C. Roiesnel and P. Taels, *Linearly polarized small- $x$  gluons in forward heavy-quark pair production*, *Phys. Rev. D* **97** (2018) 014004 [1710.05698].
- [1014] A. Dumitru, A. Hayashigaki and J. Jalilian-Marian, *The Color glass condensate and hadron production in the forward region*, *Nucl. Phys. A* **765** (2006) 464 [hep-ph/0506308].
- [1015] G. A. Chirilli, B.-W. Xiao and F. Yuan, *Inclusive Hadron Productions in  $pA$  Collisions*, *Phys. Rev. D* **86** (2012) 054005 [1203.6139].
- [1016] F. Gelis, T. Lappi and R. Venugopalan, *High energy factorization in nucleus-nucleus collisions*, *Phys. Rev. D* **78** (2008) 054019 [0804.2630].

- [1017] A. Krasnitz and R. Venugopalan, *Nonperturbative computation of gluon minijet production in nuclear collisions at very high-energies*, *Nucl. Phys. B* **557** (1999) 237 [[hep-ph/9809433](#)].
- [1018] F. Gelis and R. Venugopalan, *Large mass  $q$  anti- $q$  production from the color glass condensate*, *Phys. Rev. D* **69** (2004) 014019 [[hep-ph/0310090](#)].
- [1019] J. P. Blaizot, F. Gelis and R. Venugopalan, *High-energy  $pA$  collisions in the color glass condensate approach. 2. Quark production*, *Nucl. Phys. A* **743** (2004) 57 [[hep-ph/0402257](#)].
- [1020] H. Fujii, F. Gelis and R. Venugopalan, *Quark pair production in high energy  $pA$  collisions: General features*, *Nucl. Phys. A* **780** (2006) 146 [[hep-ph/0603099](#)].
- [1021] F. Gelis, K. Kajantie and T. Lappi, *Production of quark pairs from classical gluon fields*, *Eur. Phys. J. A* **29** (2006) 89 [[hep-ph/0509363](#)].
- [1022] F. Gelis and N. Tanji, *Quark production in heavy ion collisions: formalism and boost invariant fermionic light-cone mode functions*, *JHEP* **02** (2016) 126 [[1506.03327](#)].
- [1023] J. Jalilian-Marian and Y. V. Kovchegov, *Inclusive two-gluon and valence quark-gluon production in DIS and  $pA$* , *Phys. Rev. D* **70** (2004) 114017 [[hep-ph/0405266](#)].
- [1024] Y. V. Kovchegov and M. D. Sievert, *Sivers function in the quasiclassical approximation*, *Phys. Rev. D* **89** (2014) 054035 [[1310.5028](#)].
- [1025] Y. V. Kovchegov and M. G. Santiago, *Lensing mechanism meets small-  $x$  physics: Single transverse spin asymmetry in  $p^\uparrow + p$  and  $p^\uparrow + A$  collisions*, *Phys. Rev. D* **102** (2020) 014022 [[2003.12650](#)].
- [1026] Z.-B. Kang, Y.-Q. Ma and R. Venugopalan, *Quarkonium production in high energy proton-nucleus collisions: CGC meets NRQCD*, *JHEP* **01** (2014) 056 [[1309.7337](#)].
- [1027] Y.-Q. Ma and R. Venugopalan, *Comprehensive Description of  $J/\psi$  Production in Proton-Proton Collisions at Collider Energies*, *Phys. Rev. Lett.* **113** (2014) 192301 [[1408.4075](#)].
- [1028] Y.-Q. Ma, R. Venugopalan and H.-F. Zhang,  *$J/\psi$  production and suppression in high energy proton-nucleus collisions*, *Phys. Rev. D* **92** (2015) 071901 [[1503.07772](#)].
- [1029] J.-W. Qiu, P. Sun, B.-W. Xiao and F. Yuan, *Universal Suppression of Heavy Quarkonium Production in  $pA$  Collisions at Low Transverse Momentum*, *Phys. Rev. D* **89** (2014) 034007 [[1310.2230](#)].
- [1030] G. Sterman and S. Weinberg, *Jets from Quantum Chromodynamics*, *Phys. Rev. Lett.* **39** (1977) 1436.
- [1031] J. M. Campbell, J. W. Huston and W. J. Stirling, *Hard Interactions of Quarks and Gluons: A Primer for LHC Physics*, *Rept. Prog. Phys.* **70** (2007) 89 [[hep-ph/0611148](#)].

- [1032] S. D. Ellis, J. Huston, K. Hatakeyama, P. Loch and M. Tonnesmann, *Jets in hadron-hadron collisions*, *Prog. Part. Nucl. Phys.* **60** (2008) 484 [[0712.2447](#)].
- [1033] R. Boughezal, J. M. Campbell, R. K. Ellis, C. Focke, W. T. Giele, X. Liu et al., *Z-boson production in association with a jet at next-to-next-to-leading order in perturbative QCD*, *Phys. Rev. Lett.* **116** (2016) 152001 [[1512.01291](#)].
- [1034] R. Boughezal, F. Caola, K. Melnikov, F. Petriello and M. Schulze, *Higgs boson production in association with a jet at next-to-next-to-leading order*, *Phys. Rev. Lett.* **115** (2015) 082003 [[1504.07922](#)].
- [1035] F. I. Olness and D. E. Soper, *Correlated theoretical uncertainties for the one-jet inclusive cross section*, *Phys. Rev.* **D81** (2010) 035018 [[0907.5052](#)].
- [1036] I. Vitev, S. Wicks and B.-W. Zhang, *A Theory of jet shapes and cross sections: From hadrons to nuclei*, *JHEP* **11** (2008) 093 [[0810.2807](#)].
- [1037] I. Vitev and B.-W. Zhang, *Jet tomography of high-energy nucleus-nucleus collisions at next-to-leading order*, *Phys. Rev. Lett.* **104** (2010) 132001 [[0910.1090](#)].
- [1038] M. T. for the CMS Collaboration, *Mapping the redistribution of jet energy in PbPb collisions using jets with various radius parameters with CMS*, *Quark Matter 2019 proceedings* (2019) .
- [1039] E. Farhi, *A QCD Test for Jets*, *Phys.Rev.Lett.* **39** (1977) 1587.
- [1040] H. Georgi and M. Machacek, *A Simple QCD Prediction of Jet Structure in e+ e- Annihilation*, *Phys.Rev.Lett.* **39** (1977) 1237.
- [1041] G. C. Fox and S. Wolfram, *Observables for the analysis of event shapes in e+e- annihilation and other processes*, *Phys. Rev. Lett.* **41** (1978) 1581.
- [1042] C. L. Basham, L. S. Brown, S. D. Ellis and S. T. Love, *Energy correlations in electron-positron annihilation: Testing quantum chromodynamics*, *Phys. Rev. Lett.* **41** (1978) 1585.
- [1043] ALEPH COLLABORATION collaboration, A. Heister et al., *Studies of QCD at e+ e- centre-of-mass energies between 91-GeV and 209-GeV*, *Eur.Phys.J.* **C35** (2004) 457.
- [1044] DELPHI COLLABORATION collaboration, J. Abdallah et al., *A Study of the energy evolution of event shape distributions and their means with the DELPHI detector at LEP*, *Eur.Phys.J.* **C29** (2003) 285 [[hep-ex/0307048](#)].
- [1045] L3 COLLABORATION collaboration, P. Achard et al., *Studies of hadronic event structure in e+e- annihilation from 30-GeV to 209-GeV with the L3 detector*, *Phys.Rept.* **399** (2004) 71 [[hep-ex/0406049](#)].
- [1046] OPAL COLLABORATION collaboration, G. Abbiendi et al., *Measurement of event shape distributions and moments in e+ e- of hadrons at 91-GeV - 209-GeV and a determination of alpha(s)*, *Eur.Phys.J.* **C40** (2005) 287 [[hep-ex/0503051](#)].

- [1047] T. Becher and M. D. Schwartz, *A precise determination of  $\alpha_s$  from LEP thrust data using effective field theory*, *JHEP* **0807** (2008) 034 [[0803.0342](#)].
- [1048] Y.-T. Chien and M. D. Schwartz, *Resummation of heavy jet mass and comparison to LEP data*, *JHEP* **1008** (2010) 058 [[1005.1644](#)].
- [1049] R. Davison and B. Webber, *Non-Perturbative Contribution to the Thrust Distribution in  $e+e-$  Annihilation*, *Eur.Phys.J.* **C59** (2009) 13 [[0809.3326](#)].
- [1050] T. Gehrmann, G. Luisoni and P. F. Monni, *Power corrections in the dispersive model for a determination of the strong coupling constant from the thrust distribution*, *Eur. Phys. J. C* **73** (2013) 2265 [[1210.6945](#)].
- [1051] A. H. Hoang, D. W. Kolodrubetz, V. Mateu and I. W. Stewart, *Precise determination of  $\alpha_s$  from the C-parameter distribution*, *Phys. Rev. D* **91** (2015) 094018 [[1501.04111](#)].
- [1052] A. Kardos, S. Kluth, G. Somogyi, Z. Tulipánt and A. Verbytskyi, *Precise determination of  $\alpha_s(M_Z)$  from a global fit of energy-energy correlation to NNLO+NNLL predictions*, *Eur. Phys. J. C* **78** (2018) 498 [[1804.09146](#)].
- [1053] A. Altheimer, A. Arce, L. Asquith, J. Backus Mayes, E. Bergeaas Kuutmann et al., *Boosted objects and jet substructure at the LHC*, [1311.2708](#).
- [1054] R. D. Ball, L. Del Debbio, S. Forte, A. Guffanti, J. I. Latorre, J. Rojo et al., *A first unbiased global NLO determination of parton distributions and their uncertainties*, *Nucl. Phys.* **B838** (2010) 136 [[1002.4407](#)].
- [1055] S. Dulat, T.-J. Hou, J. Gao, M. Guzzi, J. Huston, P. Nadolsky et al., *New parton distribution functions from a global analysis of quantum chromodynamics*, *Phys. Rev. D* **93** (2016) 033006 [[1506.07443](#)].
- [1056] D. Stump, J. Huston, J. Pumplin, W.-K. Tung, H. L. Lai, S. Kuhlmann et al., *Inclusive jet production, parton distributions, and the search for new physics*, *JHEP* **10** (2003) 046 [[hep-ph/0303013](#)].
- [1057] M. Cacciari, G. P. Salam and G. Soyez, *FastJet User Manual*, *Eur. Phys. J. C* **72** (2012) 1896 [[1111.6097](#)].
- [1058] G. P. Salam and G. Soyez, *A Practical Seedless Infrared-Safe Cone jet algorithm*, *JHEP* **05** (2007) 086 [[0704.0292](#)].
- [1059] M. Cacciari, G. P. Salam and G. Soyez, *The anti- $k_t$  jet clustering algorithm*, *JHEP* **04** (2008) 063 [[0802.1189](#)].
- [1060] S. Catani, Y. L. Dokshitzer, M. H. Seymour and B. R. Webber, *Longitudinally invariant  $K_t$  clustering algorithms for hadron hadron collisions*, *Nucl. Phys. B* **406** (1993) 187.
- [1061] J. Gallicchio and M. D. Schwartz, *Quark and Gluon Tagging at the LHC*, *Phys.Rev.Lett.* **107** (2011) 172001 [[1106.3076](#)].

- [1062] J. Gallicchio and M. D. Schwartz, *Quark and Gluon Jet Substructure*, *JHEP* **1304** (2013) 090 [[1211.7038](#)].
- [1063] J. P. Berge et al., *Quark Jets from anti-neutrino Interactions. 1. Net Charge and Factorization in the Quark Jets*, *Nucl. Phys.* **B184** (1981) 13.
- [1064] EUROPEAN MUON collaboration, J. P. Albanese et al., *Quark Charge Retention in Final State Hadrons From Deep Inelastic Muon Scattering*, *Phys. Lett.* **144B** (1984) 302.
- [1065] ATLAS collaboration, G. Aad et al., *Measurement of jet charge in dijet events from  $\sqrt{s}=8$  TeV pp collisions with the ATLAS detector*, *Phys. Rev.* **D93** (2016) 052003 [[1509.05190](#)].
- [1066] CMS collaboration, A. M. Sirunyan et al., *Measurements of jet charge with dijet events in pp collisions at  $\sqrt{s} = 8$  TeV*, *JHEP* **10** (2017) 131 [[1706.05868](#)].
- [1067] S.-Y. Chen, B.-W. Zhang and E.-K. Wang, *Jet charge in high energy nuclear collisions*, [1908.01518](#).
- [1068] H. T. Li and I. Vitev, *Jet charge modification in dense QCD matter*, *Phys. Rev. D* **101** (2020) 076020 [[1908.06979](#)].
- [1069] D. H. for the CMS Collaboration, *Studies of Quark and Gluon Contributions to Jets using Jet Charge Measurements in pp and PbPb Collisions*, *Quark Matter 2019 proceedings* (2019) .
- [1070] R. Bain, L. Dai, A. Leibovich, Y. Makris and T. Mehen, *NRQCD Confronts LHCb Data on Quarkonium Production within Jets*, *Phys. Rev. Lett.* **119** (2017) 032002 [[1702.05525](#)].
- [1071] D. P. Anderle, T. Kaufmann, M. Stratmann, F. Ringer and I. Vitev, *Using hadron-in-jet data in a global analysis of  $D^*$  fragmentation functions*, *Phys. Rev.* **D96** (2017) 034028 [[1706.09857](#)].
- [1072] Y.-T. Chien and I. Vitev, *Towards the understanding of jet shapes and cross sections in heavy ion collisions using soft-collinear effective theory*, *JHEP* **05** (2016) 023 [[1509.07257](#)].
- [1073] STAR collaboration, L. Adamczyk et al., *Measurements of jet quenching with semi-inclusive hadron+jet distributions in Au+Au collisions at  $\sqrt{s_{NN}} = 200$  GeV*, *Phys. Rev.* **C96** (2017) 024905 [[1702.01108](#)].
- [1074] CMS collaboration, A. M. Sirunyan et al., *Measurement of the groomed jet mass in PbPb and pp collisions at  $\sqrt{s_{NN}} = 5.02$  TeV*, *JHEP* **10** (2018) 161 [[1805.05145](#)].
- [1075] CMS collaboration, A. M. Sirunyan et al., *Observation of Medium-Induced Modifications of Jet Fragmentation in Pb-Pb Collisions at  $\sqrt{s_{NN}} = 5.02$  TeV Using Isolated Photon-Tagged Jets*, *Phys. Rev. Lett.* **121** (2018) 242301 [[1801.04895](#)].
- [1076] ATLAS collaboration, M. Aaboud et al., *Comparison of fragmentation functions for light-quark- and gluon-dominated jets from pp and Pb+Pb collisions in ATLAS*, *Submitted to: Phys. Rev. Lett.* (2019) [[1902.10007](#)].

- [1077] CMS collaboration, A. M. Sirunyan et al., *Jet Shapes of Isolated Photon-Tagged Jets in Pb-Pb and pp Collisions at  $\sqrt{s_{NN}} = 5.02 \text{ TeV}$* , *Phys. Rev. Lett.* **122** (2019) 152001 [1809.08602].
- [1078] ATLAS collaboration, M. Aaboud et al., *Measurement of jet fragmentation in Pb+Pb and pp collisions at  $\sqrt{s_{NN}} = 5.02 \text{ TeV}$  with the ATLAS detector*, *Phys. Rev. C* **98** (2018) 024908 [1805.05424].
- [1079] X. Liu, F. Ringer, W. Vogelsang and F. Yuan, *Lepton-jet Correlations in Deep Inelastic Scattering at the Electron-Ion Collider*, *Phys. Rev. Lett.* **122** (2019) 192003 [1812.08077].
- [1080] M. Arratia, Z.-B. Kang, A. Prokudin and F. Ringer, *Jet-based measurements of Sivers and Collins asymmetries at the future electron-ion collider*, *Phys. Rev. D* **102** (2020) 074015 [2007.07281].
- [1081] X. Liu, F. Ringer, W. Vogelsang and F. Yuan, *Lepton-jet Correlation in Deep Inelastic Scattering*, *Phys. Rev. D* **102** (2020) 094022 [2007.12866].
- [1082] Z.-B. Kang, K. Lee, D. Y. Shao and F. Zhao, *Spin asymmetries in electron-jet production at the future electron ion collider*, *JHEP* **11** (2021) 005 [2106.15624].
- [1083] S. D. Ellis, C. K. Vermilion, J. R. Walsh, A. Hornig and C. Lee, *Jet Shapes and Jet Algorithms in SCET*, *JHEP* **11** (2010) 101 [1001.0014].
- [1084] H1 collaboration, V. Andreev et al., *Measurement of lepton-jet correlation in deep-inelastic scattering with the H1 detector using machine learning for unfolding*, 2108.12376.
- [1085] Z.-B. Kang, X. Liu, S. Mantry and D. Y. Shao, *Jet Charge: A Flavor Prism for Spin Asymmetries at the EIC*, *Phys. Rev. Lett.* **125** (2020) 242003 [2008.00655].
- [1086] M. G. A. Buffing, Z.-B. Kang, K. Lee and X. Liu, *A transverse momentum dependent framework for back-to-back photon+jet production*, 1812.07549.
- [1087] Y.-T. Chien, D. Y. Shao and B. Wu, *Resummation of Boson-Jet Correlation at Hadron Colliders*, *JHEP* **11** (2019) 025 [1905.01335].
- [1088] Z.-B. Kang, K. Lee, D. Y. Shao and J. Terry, *The Sivers Asymmetry in Hadronic Dijet Production*, *JHEP* **02** (2021) 066 [2008.05470].
- [1089] X. Liu, F. Ringer, W. Vogelsang and F. Yuan, *Factorization and its Breaking in Dijet Single Transverse Spin Asymmetries in pp Collisions*, *Phys. Rev. D* **102** (2020) 114012 [2008.03666].
- [1090] LHCb collaboration, R. Aaij et al., *Measurement of charged hadron production in Z-tagged jets in proton-proton collisions at  $\sqrt{s} = 8 \text{ TeV}$* , *Phys. Rev. Lett.* **123** (2019) 232001 [1904.08878].
- [1091] H. Liu, *Talk given at RIKEN BNL Workshop Jet Observables at the Electron-Ion Collider*, 2020.

- [1092] M. Procura and I. W. Stewart, *Quark Fragmentation within an Identified Jet*, *Phys. Rev.* **D81** (2010) 074009 [[0911.4980](#)].
- [1093] A. Jain, M. Procura and W. J. Waalewijn, *Parton Fragmentation within an Identified Jet at NNLL*, *JHEP* **05** (2011) 035 [[1101.4953](#)].
- [1094] A. Jain, M. Procura and W. J. Waalewijn, *Fully-Unintegrated Parton Distribution and Fragmentation Functions at Perturbative  $k_T$* , *JHEP* **04** (2012) 132 [[1110.0839](#)].
- [1095] Y.-T. Chien, Z.-B. Kang, F. Ringer, I. Vitev and H. Xing, *Jet fragmentation functions in proton-proton collisions using soft-collinear effective theory*, *JHEP* **05** (2016) 125 [[1512.06851](#)].
- [1096] Z.-B. Kang, K. Lee, J. Terry and H. Xing, *Jet fragmentation functions for Z-tagged jets*, [1906.07187](#).
- [1097] F. Arleo, M. Fontannaz, J.-P. Guillet and C. L. Nguyen, *Probing fragmentation functions from same-side hadron-jet momentum correlations in p-p collisions*, *JHEP* **04** (2014) 147 [[1311.7356](#)].
- [1098] T. Kaufmann, A. Mukherjee and W. Vogelsang, *Hadron Fragmentation Inside Jets in Hadronic Collisions*, *Phys. Rev. D* **92** (2015) 054015 [[1506.01415](#)].
- [1099] Z.-B. Kang, F. Ringer and I. Vitev, *Jet substructure using semi-inclusive jet functions in SCET*, *JHEP* **11** (2016) 155 [[1606.07063](#)].
- [1100] L. Dai, C. Kim and A. K. Leibovich, *Fragmentation of a Jet with Small Radius*, *Phys. Rev. D* **94** (2016) 114023 [[1606.07411](#)].
- [1101] Z.-B. Kang, J.-W. Qiu, F. Ringer, H. Xing and H. Zhang,  *$J/\psi$  production and polarization within a jet*, *Phys. Rev. Lett.* **119** (2017) 032001 [[1702.03287](#)].
- [1102] L. Wang, Z.-B. Kang, H. Xing and B.-W. Zhang, *Semi-inclusive jet functions and jet substructure in  $J_{ET}^{(I)}$  and  $J_{ET}^{(II)}$  algorithms*, *Phys. Rev. D* **103** (2021) 054043 [[2003.03796](#)].
- [1103] Z.-B. Kang, F. Ringer and I. Vitev, *The semi-inclusive jet function in SCET and small radius resummation for inclusive jet production*, *JHEP* **10** (2016) 125 [[1606.06732](#)].
- [1104] ATLAS collaboration, G. Aad et al., *Measurement of the jet fragmentation function and transverse profile in proton-proton collisions at a center-of-mass energy of 7 TeV with the ATLAS detector*, *Eur. Phys. J.* **C71** (2011) 1795 [[1109.5816](#)].
- [1105] ATLAS collaboration, M. Aaboud et al., *Measurement of jet fragmentation in 5.02 TeV proton-lead and proton-proton collisions with the ATLAS detector*, *Nucl. Phys.* **A978** (2018) 65 [[1706.02859](#)].
- [1106] ATLAS collaboration, G. Aad et al., *Measurement of  $D^{*+/-}$  meson production in jets from pp collisions at  $\text{sqrt}(s) = 7 \text{ TeV}$  with the ATLAS detector*, *Phys. Rev.* **D85** (2012) 052005 [[1112.4432](#)].

- [1107] CMS collaboration, C. Collaboration, *Measurement of the radial profile of  $D^0$  mesons in jets produced in  $pp$  and  $PbPb$  collisions at 5.02 TeV*, .
- [1108] ALICE collaboration, S. Acharya et al., *Measurement of the production of charm jets tagged with  $D^0$  mesons in  $pp$  collisions at  $\sqrt{s} = 7$  TeV*, 1905.02510.
- [1109] LHCb collaboration, R. Aaij et al., *Study of  $J/\psi$  Production in Jets*, *Phys. Rev. Lett.* **118** (2017) 192001 [1701.05116].
- [1110] CMS collaboration, C. Collaboration, *Production of prompt and nonprompt  $J/\psi$  mesons in jets in  $pp$  collisions at  $\sqrt{s} = 5.02$  TeV*, .
- [1111] T. Becher, M. Neubert and B. D. Pecjak, *Factorization and Momentum-Space Resummation in Deep-Inelastic Scattering*, *JHEP* **01** (2007) 076 [hep-ph/0607228].
- [1112] T. Becher and M. D. Schwartz, *Direct photon production with effective field theory*, *JHEP* **02** (2010) 040 [0911.0681].
- [1113] M. G. Echevarria, A. Idilbi, A. Schäfer and I. Scimemi, *Model-Independent Evolution of Transverse Momentum Dependent Distribution Functions (TMDs) at NNLL*, *Eur.Phys.J.* **C73** (2013) 2636 [1208.1281].
- [1114] S. Moch, J. A. M. Vermaseren and A. Vogt, *The Three loop splitting functions in QCD: The Nonsinglet case*, *Nucl. Phys.* **B688** (2004) 101 [hep-ph/0403192].
- [1115] Y.-T. Chien, A. Hornig and C. Lee, *Soft-collinear mode for jet cross sections in soft collinear effective theory*, *Phys. Rev. D* **93** (2016) 014033 [1509.04287].
- [1116] M. Procura and W. J. Waalewijn, *Fragmentation in Jets: Cone and Threshold Effects*, *Phys. Rev.* **D85** (2012) 114041 [1111.6605].
- [1117] W. J. Waalewijn, *Calculating the Charge of a Jet*, *Phys. Rev. D* **86** (2012) 094030 [1209.3019].
- [1118] Y.-T. Chien, A. Emerman, Z.-B. Kang, G. Ovanesyan and I. Vitev, *Jet Quenching from QCD Evolution*, *Phys. Rev. D* **93** (2016) 074030 [1509.02936].
- [1119] Z.-B. Kang, X. Liu, F. Ringer and H. Xing, *The transverse momentum distribution of hadrons within jets*, *JHEP* **11** (2017) 068 [1705.08443].
- [1120] A. J. Larkoski, S. Marzani, G. Soyez and J. Thaler, *Soft Drop*, *JHEP* **05** (2014) 146 [1402.2657].
- [1121] Y. Makris, D. Neill and V. Vaidya, *Probing Transverse-Momentum Dependent Evolution With Groomed Jets*, *JHEP* **07** (2018) 167 [1712.07653].
- [1122] D. Gutierrez-Reyes, Y. Makris, V. Vaidya, I. Scimemi and L. Zoppi, *Probing Transverse-Momentum Distributions With Groomed Jets*, *JHEP* **08** (2019) 161 [1907.05896].

- [1123] Z.-B. Kang, K. Lee and F. Zhao, *Polarized jet fragmentation functions*, *Phys. Lett. B* **809** (2020) 135756 [2005.02398].
- [1124] BELLE collaboration, Y. Guan et al., *Observation of Transverse  $\Lambda/\bar{\Lambda}$  Hyperon Polarization in  $e^+e^-$  Annihilation at Belle*, *Phys. Rev. Lett.* **122** (2019) 042001 [1808.05000].
- [1125] D. Callos, Z.-B. Kang and J. Terry, *Extracting the transverse momentum dependent polarizing fragmentation functions*, *Phys. Rev. D* **102** (2020) 096007 [2003.04828].
- [1126] U. D'Alesio, F. Murgia and M. Zaccheddu, *First extraction of the  $\Lambda$  polarizing fragmentation function from Belle  $e^+e^-$  data*, *Phys. Rev. D* **102** (2020) 054001 [2003.01128].
- [1127] U. D'Alesio, F. Murgia and C. Pisano, *Testing the universality of the Collins function in pion-jet production at RHIC*, *Phys. Lett. B* **773** (2017) 300 [1707.00914].
- [1128] Z.-B. Kang, A. Prokudin, F. Ringer and F. Yuan, *Collins azimuthal asymmetries of hadron production inside jets*, *Phys. Lett. B* **774** (2017) 635 [1707.00913].
- [1129] STAR collaboration, L. Adamczyk et al., *Azimuthal transverse single-spin asymmetries of inclusive jets and charged pions within jets from polarized-proton collisions at  $\sqrt{s} = 500$  GeV*, *Phys. Rev. D* **97** (2018) 032004 [1708.07080].
- [1130] F. Yuan, *Azimuthal asymmetric distribution of hadrons inside a jet at hadron collider*, *Phys. Rev. Lett.* **100** (2008) 032003 [0709.3272].
- [1131] U. D'Alesio, F. Murgia and C. Pisano, *Azimuthal asymmetries for hadron distributions inside a jet in hadronic collisions*, *Phys. Rev. D* **83** (2011) 034021 [1011.2692].
- [1132] E.-C. Aschenauer et al., *The RHIC Cold QCD Plan for 2017 to 2023: A Portal to the EIC*, 1602.03922.
- [1133] M. Baumgart, A. K. Leibovich, T. Mehen and I. Z. Rothstein, *Probing Quarkonium Production Mechanisms with Jet Substructure*, *JHEP* **11** (2014) 003 [1406.2295].
- [1134] G. T. Bodwin, E. Braaten and G. Lepage, *Rigorous QCD analysis of inclusive annihilation and production of heavy quarkonium*, *Phys. Rev. D* **51** (1995) 1125 [hep-ph/9407339].
- [1135] E. Braaten and T. C. Yuan, *Gluon fragmentation into heavy quarkonium*, *Phys. Rev. Lett.* **71** (1993) 1673 [hep-ph/9303205].
- [1136] E. Braaten, K.-m. Cheung and T. C. Yuan, *Z0 decay into charmonium via charm quark fragmentation*, *Phys. Rev. D* **48** (1993) 4230 [hep-ph/9302307].
- [1137] E. Braaten, K.-m. Cheung and T. C. Yuan, *Perturbative QCD fragmentation functions for  $B_c$  and  $B_c^*$  production*, *Phys. Rev. D* **48** (1993) 5049 [hep-ph/9305206].
- [1138] E. Braaten and T. C. Yuan, *Gluon fragmentation into P wave heavy quarkonium*, *Phys. Rev. D* **50** (1994) 3176 [hep-ph/9403401].

- [1139] E. Chapon et al., *Prospects for quarkonium studies at the high-luminosity LHC*, *Prog. Part. Nucl. Phys.* **122** (2022) 103906 [2012.14161].
- [1140] M. Butenschoen and B. A. Kniehl, *World data of J/psi production consolidate NRQCD factorization at NLO*, *Phys. Rev. D* **84** (2011) 051501 [1105.0820].
- [1141] M. Butenschoen and B. A. Kniehl, *Next-to-leading-order tests of NRQCD factorization with J/psi yield and polarization*, *Mod. Phys. Lett. A* **28** (2013) 1350027 [1212.2037].
- [1142] K.-T. Chao, Y.-Q. Ma, H.-S. Shao, K. Wang and Y.-J. Zhang, *J/psi Polarization at Hadron Colliders in Nonrelativistic QCD*, *Phys.Rev.Lett.* **108** (2012) 242004 [1201.2675].
- [1143] G. T. Bodwin, H. S. Chung, U.-R. Kim and J. Lee, *Fragmentation contributions to J/psi production at the Tevatron and the LHC*, *Phys. Rev. Lett.* **113** (2014) 022001 [1403.3612].
- [1144] R. Bain, L. Dai, A. Hornig, A. K. Leibovich, Y. Makris and T. Mehen, *Analytic and Monte Carlo Studies of Jets with Heavy Mesons and Quarkonia*, *JHEP* **06** (2016) 121 [1603.06981].
- [1145] C. F. Berger, T. Kucs and G. F. Sterman, *Event shape / energy flow correlations*, *Phys. Rev. D* **68** (2003) 014012 [hep-ph/0303051].
- [1146] R. Bain, Y. Makris and T. Mehen, *Transverse Momentum Dependent Fragmenting Jet Functions with Applications to Quarkonium Production*, *JHEP* **11** (2016) 144 [1610.06508].
- [1147] S. Fleming, Y. Makris and T. Mehen, *An effective field theory approach to quarkonium at small transverse momentum*, *JHEP* **04** (2020) 122 [1910.03586].
- [1148] M. G. Echevarria, Y. Makris and I. Scimemi, *Quarkonium TMD fragmentation functions in NRQCD*, *JHEP* **10** (2020) 164 [2007.05547].
- [1149] D. Boer, U. D'Alesio, F. Murgia, C. Pisano and P. Taels, *J/psi meson production in SIDIS: matching high and low transverse momentum*, *JHEP* **09** (2020) 040 [2004.06740].
- [1150] U. D'Alesio, L. Maxia, F. Murgia, C. Pisano and S. Rajesh, *Process dependence of the gluon Sivers function in  $p^\uparrow p \rightarrow J/\psi + X$  within a TMD scheme in NRQCD*, *Phys. Rev. D* **102** (2020) 094011 [2007.03353].
- [1151] A. Ali, E. Pietarinen and W. Stirling, *Transverse Energy-energy Correlations: A Test of Perturbative QCD for the Proton - Anti-proton Collider*, *Phys. Lett. B* **141** (1984) 447.
- [1152] C. Basham, L. S. Brown, S. D. Ellis and S. T. Love, *Energy Correlations in electron - Positron Annihilation: Testing QCD*, *Phys. Rev. Lett.* **41** (1978) 1585.
- [1153] A. Ali, F. Barreiro, J. Llorente and W. Wang, *Transverse Energy-Energy Correlations in Next-to-Leading Order in  $\alpha_s$  at the LHC*, *Phys. Rev. D* **86** (2012) 114017 [1205.1689].

- [1154] A. Gao, H. T. Li, I. Moult and H. X. Zhu, *Precision QCD Event Shapes at Hadron Colliders: The Transverse Energy-Energy Correlator in the Back-to-Back Limit*, *Phys. Rev. Lett.* **123** (2019) 062001 [[1901.04497](#)].
- [1155] H. T. Li, I. Vitev and Y. J. Zhu, *Transverse-Energy-Energy Correlations in Deep Inelastic Scattering*, *JHEP* **11** (2020) 051 [[2006.02437](#)].
- [1156] T. Lübbert, J. Oredsson and M. Stahlhofen, *Rapidity renormalized TMD soft and beam functions at two loops*, *JHEP* **03** (2016) 168 [[1602.01829](#)].
- [1157] H. T. Li, Y. Makris and I. Vitev, *Energy-energy correlators in Deep Inelastic Scattering*, *Phys. Rev. D* **103** (2021) 094005 [[2102.05669](#)].
- [1158] T. Sjostrand, S. Mrenna and P. Z. Skands, *A Brief Introduction to PYTHIA 8.1*, *Comput. Phys. Commun.* **178** (2008) 852 [[0710.3820](#)].
- [1159] T. Sjöstrand, S. Ask, J. R. Christiansen, R. Corke, N. Desai, P. Ilten et al., *An Introduction to PYTHIA 8.2*, *Comput. Phys. Commun.* **191** (2015) 159 [[1410.3012](#)].
- [1160] C. W. Bauer, S. Fleming, C. Lee and G. Sterman, *Factorization of  $e^+e^-$  event shape distributions with hadronic final states in Soft Collinear Effective Theory*, *Phys. Rev. D* **78** (2008) 034027 [[0801.4569](#)].
- [1161] T. T. Jouttenus, I. W. Stewart, F. J. Tackmann and W. J. Waalewijn, *The Soft Function for Exclusive N-Jet Production at Hadron Colliders*, *Phys. Rev. D* **83** (2011) 114030 [[1102.4344](#)].
- [1162] M. Gyulassy and M. Plumer, *Jet Quenching in Dense Matter*, *Phys. Lett. B* **243** (1990) 432.
- [1163] M. Gyulassy, I. Vitev, X.-N. Wang and B.-W. Zhang, *Jet quenching and radiative energy loss in dense nuclear matter*, [nucl-th/0302077](#).
- [1164] M. Gyulassy and X.-n. Wang, *Multiple collisions and induced gluon Bremsstrahlung in QCD*, *Nucl. Phys. B* **420** (1994) 583 [[nucl-th/9306003](#)].
- [1165] L. D. Landau and I. Pomeranchuk, *Limits of applicability of the theory of bremsstrahlung electrons and pair production at high-energies*, *Dokl. Akad. Nauk Ser. Fiz.* **92** (1953) 535.
- [1166] A. B. Migdal, *Bremsstrahlung and pair production in condensed media at high-energies*, *Phys. Rev.* **103** (1956) 1811.
- [1167] B. Zakharov, *Fully quantum treatment of the Landau-Pomeranchuk-Migdal effect in QED and QCD*, *JETP Lett.* **63** (1996) 952 [[hep-ph/9607440](#)].
- [1168] B. G. Zakharov, *Radiative energy loss of high-energy quarks in finite size nuclear matter and quark - gluon plasma*, *JETP Lett.* **65** (1997) 615 [[hep-ph/9704255](#)].
- [1169] R. Baier, Y. L. Dokshitzer, A. H. Mueller, S. Peigne and D. Schiff, *Radiative energy loss and  $p(T)$ -broadening of high energy partons in nuclei*, *Nucl. Phys. B* **484** (1997) 265 [[hep-ph/9608322](#)].

- [1170] R. Baier, Y. L. Dokshitzer, A. H. Mueller and D. Schiff, *Medium induced radiative energy loss: Equivalence between the BDMPS and Zakharov formalisms*, *Nucl. Phys.* **B531** (1998) 403 [[hep-ph/9804212](#)].
- [1171] P. B. Arnold, G. D. Moore and L. G. Yaffe, *Photon and gluon emission in relativistic plasmas*, *JHEP* **06** (2002) 030 [[hep-ph/0204343](#)].
- [1172] M. Gyulassy, P. Levai and I. Vitev, *Jet quenching in thin quark gluon plasmas. 1. Formalism*, *Nucl. Phys.* **B571** (2000) 197 [[hep-ph/9907461](#)].
- [1173] M. Gyulassy, P. Levai and I. Vitev, *NonAbelian energy loss at finite opacity*, *Phys.Rev.Lett.* **85** (2000) 5535 [[nucl-th/0005032](#)].
- [1174] M. Gyulassy, P. Levai and I. Vitev, *Reaction operator approach to nonAbelian energy loss*, *Nucl.Phys.* **B594** (2001) 371 [[nucl-th/0006010](#)].
- [1175] X.-N. Wang and X.-f. Guo, *Multiple parton scattering in nuclei: Parton energy loss*, *Nucl. Phys.* **A696** (2001) 788 [[hep-ph/0102230](#)].
- [1176] Y. Guo, B.-W. Zhang and E. Wang, *Parton Energy Loss at Twist-Six in Deeply Inelastic e-A Scattering*, *Phys. Lett.* **B641** (2006) 38 [[hep-ph/0606312](#)].
- [1177] W.-t. Deng and X.-N. Wang, *Multiple Parton Scattering in Nuclei: Modified DGLAP Evolution for Fragmentation Functions*, *Phys. Rev.* **C81** (2010) 024902 [[0910.3403](#)].
- [1178] G. Ovanesyan and I. Vitev, *An effective theory for jet propagation in dense QCD matter: jet broadening and medium-induced bremsstrahlung*, *JHEP* **06** (2011) 080 [[1103.1074](#)].
- [1179] G. Ovanesyan and I. Vitev, *Medium-induced parton splitting kernels from Soft Collinear Effective Theory with Glauber gluons*, *Phys.Lett.* **B706** (2012) 371 [[1109.5619](#)].
- [1180] J.-P. Blaizot, F. Dominguez, E. Iancu and Y. Mehtar-Tani, *Medium-induced gluon branching*, *JHEP* **01** (2013) 143 [[1209.4585](#)].
- [1181] M. Fickinger, G. Ovanesyan and I. Vitev, *Angular distributions of higher order splitting functions in the vacuum and in dense QCD matter*, *JHEP* **07** (2013) 059 [[1304.3497](#)].
- [1182] L. Apolinerio, N. Armesto, J. G. Milhano and C. A. Salgado, *Medium-induced gluon radiation and colour decoherence beyond the soft approximation*, *JHEP* **02** (2015) 119 [[1407.0599](#)].
- [1183] G. Ovanesyan, F. Ringer and I. Vitev, *Initial-state splitting kernels in cold nuclear matter*, *Phys. Lett.* **B760** (2016) 706 [[1512.00006](#)].
- [1184] Z.-B. Kang, F. Ringer and I. Vitev, *Effective field theory approach to open heavy flavor production in heavy-ion collisions*, *JHEP* **03** (2017) 146 [[1610.02043](#)].
- [1185] M. D. Sievert and I. Vitev, *Quark branching in QCD matter to any order in opacity beyond the soft gluon emission limit*, *Phys. Rev.* **D98** (2018) 094010 [[1807.03799](#)].

- [1186] M. D. Sievert, I. Vitev and B. Yoon, *A complete set of in-medium splitting functions to any order in opacity*, *Phys. Lett.* **B795** (2019) 502 [1903.06170].
- [1187] A. V. Sadofyev, M. D. Sievert and I. Vitev, *Ab Initio Coupling of Jets to Collective Flow in the Opacity Expansion Approach*, 2104.09513.
- [1188] N.-B. Chang, W.-T. Deng and X.-N. Wang, *Initial conditions for the modified evolution of fragmentation functions in the nuclear medium*, *Phys. Rev.* **C89** (2014) 034911 [1401.5109].
- [1189] Z.-B. Kang, R. Lashof-Regas, G. Ovanesyan, P. Saad and I. Vitev, *Jet quenching phenomenology from soft-collinear effective theory with Glauber gluons*, *Phys. Rev. Lett.* **114** (2015) 092002 [1405.2612].
- [1190] Z.-B. Kang, F. Ringer and I. Vitev, *Inclusive production of small radius jets in heavy-ion collisions*, *Phys. Lett.* **B769** (2017) 242 [1701.05839].
- [1191] H. T. Li and I. Vitev, *Inclusive heavy flavor jet production with semi-inclusive jet functions: from proton to heavy-ion collisions*, 1811.07905.
- [1192] H. T. Li and I. Vitev, *Nuclear matter effects on jet production at electron-ion colliders*, 2010.05912.
- [1193] H. T. Li, Z. L. Liu and I. Vitev, *Heavy flavor jet production and substructure in electron-nucleus collisions*, 2108.07809.
- [1194] L. Dai, C. Kim and A. K. Leibovich, *Heavy Quark Jet Fragmentation*, *JHEP* **09** (2018) 109 [1805.06014].
- [1195] CMS collaboration, C. Collaboration, *Measurement of Jet Nuclear Modification Factor in PbPb Collisions at  $\sqrt{s_{NN}} = 5.02 \text{ TeV}$  with CMS*, .
- [1196] CMS collaboration, S. Chatrchyan et al., *Evidence of b-Jet Quenching in PbPb Collisions at  $\sqrt{s_{NN}} = 2.76 \text{ TeV}$* , *Phys. Rev. Lett.* **113** (2014) 132301 [1312.4198].
- [1197] H. T. Li, Z. L. Liu and I. Vitev, *Heavy meson tomography of cold nuclear matter at the electron-ion collider*, 2007.10994.
- [1198] D. Krohn, M. D. Schwartz, T. Lin and W. J. Waalewijn, *Jet Charge at the LHC*, *Phys. Rev. Lett.* **110** (2013) 212001 [1209.2421].
- [1199] CMS collaboration, A. M. Sirunyan et al., *Measurement of quark- and gluon-like jet fractions using jet charge in PbPb and pp collisions at 5.02 TeV*, *JHEP* **07** (2020) 115 [2004.00602].
- [1200] A. Larkoski, S. Marzani, J. Thaler, A. Tripathee and W. Xue, *Exposing the QCD Splitting Function with CMS Open Data*, 1704.05066.
- [1201] Y.-T. Chien and I. Vitev, *Probing the Hardest Branching within Jets in Heavy-Ion Collisions*, *Phys. Rev. Lett.* **119** (2017) 112301 [1608.07283].

- [1202] P. Ilten, N. L. Rodd, J. Thaler and M. Williams, *Disentangling Heavy Flavor at Colliders*, *Phys. Rev.* **D96** (2017) 054019 [[1702.02947](#)].
- [1203] H. T. Li and I. Vitev, *Inverting the mass hierarchy of jet quenching effects with prompt b-jet substructure*, *Phys. Lett.* **B793** (2019) 259 [[1801.00008](#)].
- [1204] CMS collaboration, A. M. Sirunyan et al., *Measurement of the splitting function in pp and PbPb collisions at  $\sqrt{s_{\text{NN}}} = 5.02 \text{ TeV}$* , [1708.09429](#).
- [1205] ALICE collaboration, S. Acharya et al., *Jet fragmentation transverse momentum measurements from di-hadron correlations in  $\sqrt{s} = 7 \text{ TeV}$  pp and  $\sqrt{s_{\text{NN}}} = 5.02 \text{ TeV}$  p-Pb collisions*, *JHEP* **03** (2019) 169 [[1811.09742](#)].
- [1206] Y. Makris and I. Vitev, *An Effective Theory of Quarkonia in QCD Matter*, *JHEP* **10** (2019) 111 [[1906.04186](#)].
- [1207] Y. Makris and I. Vitev, *An Effective Theory of Quarkonia in QCD Matter*, *Nucl. Phys. A* **1005** (2021) 121848 [[1912.08008](#)].
- [1208] F. Ravndal, *On the azimuthal dependence of semiinclusive, deep inelastic electroproduction cross-sections*, *Phys. Lett. B* **43** (1973) 301.
- [1209] HERMES collaboration, A. Airapetian et al., *Single spin azimuthal asymmetries in electroproduction of neutral pions in semiinclusive deep inelastic scattering*, *Phys. Rev. D* **64** (2001) 097101 [[hep-ex/0104005](#)].
- [1210] M. Diehl and S. Sapeta, *On the analysis of lepton scattering on longitudinally or transversely polarized protons*, *Eur. Phys. J. C* **41** (2005) 515 [[hep-ph/0503023](#)].
- [1211] C. Lorcé and B. Pasquini, *Structure analysis of the generalized correlator of quark and gluon for a spin-1/2 target*, *JHEP* **09** (2013) 138 [[1307.4497](#)].
- [1212] K.-b. Chen, S.-y. Wei, W.-h. Yang and Z.-t. Liang, *Three dimensional fragmentation functions from the quark-quark correlator*, [1505.02856](#).
- [1213] S. Kumano and Q.-T. Song, *Transverse-momentum-dependent parton distribution functions up to twist 4 for spin-1 hadrons*, [2011.08583](#).
- [1214] EUROPEAN MUON collaboration, J. J. Aubert et al., *Measurement of Hadronic Azimuthal Distributions in Deep Inelastic Muon Proton Scattering*, *Phys. Lett. B* **130** (1983) 118.
- [1215] EUROPEAN MUON collaboration, M. Arneodo et al., *Measurement of Hadron Azimuthal Distributions in Deep Inelastic Muon Proton Scattering*, *Z. Phys. C* **34** (1987) 277.
- [1216] HERMES collaboration, H. Avakian, *Azimuthal single spin asymmetries in semiinclusive DIS from HERMES*, *Nucl. Phys. B Proc. Suppl.* **79** (1999) 523.
- [1217] HERMES collaboration, A. Airapetian et al., *Observation of a single spin azimuthal asymmetry in semiinclusive pion electro production*, *Phys. Rev. Lett.* **84** (2000) 4047 [[hep-ex/9910062](#)].

- [1218] HERMES collaboration, A. Airapetian et al., *Single spin azimuthal asymmetries in electroproduction of neutral pions in semiinclusive deep inelastic scattering*, *Phys. Rev. D* **64** (2001) 097101 [[hep-ex/0104005](#)].
- [1219] HERMES collaboration, A. Airapetian et al., *Measurement of single spin azimuthal asymmetries in semiinclusive electroproduction of pions and kaons on a longitudinally polarized deuterium target*, *Phys. Lett. B* **562** (2003) 182 [[hep-ex/0212039](#)].
- [1220] CLAS collaboration, H. Avakian et al., *Measurement of beam-spin asymmetries for  $\pi^+$  electroproduction above the baryon resonance region*, *Phys. Rev. D* **69** (2004) 112004 [[hep-ex/0301005](#)].
- [1221] M. Aghasyan et al., *Precise measurements of beam spin asymmetries in semi-inclusive  $\pi^0$  production*, *Phys. Lett. B* **704** (2011) 397 [[1106.2293](#)].
- [1222] CLAS collaboration, W. Gohn et al., *Beam-spin asymmetries from semi-inclusive pion electroproduction*, *Phys. Rev. D* **89** (2014) 072011 [[1402.4097](#)].
- [1223] H. Avakian, B. Parsamyan and A. Prokudin, *Spin orbit correlations and the structure of the nucleon*, *Riv. Nuovo Cim.* **42** (2019) 1 [[1909.13664](#)].
- [1224] Y. Yang and Z. Lu, *Polarized  $\Lambda$  hyperon production in semi-inclusive deep inelastic scattering off an unpolarized nucleon target*, *Phys. Rev. D* **95** (2017) 074026 [[1611.07755](#)].
- [1225] S.-y. Wei, Y.-k. Song, K.-b. Chen and Z.-t. Liang, *Twist-4 contributions to semi-inclusive deeply inelastic scatterings with polarized beam and target*, *Phys. Rev. D* **95** (2017) 074017 [[1611.08688](#)].
- [1226] Z. Lu and I. Schmidt, *Transverse momentum dependent twist-three result for polarized Drell-Yan processes*, *Phys. Rev. D* **84** (2011) 114004 [[1109.3232](#)].
- [1227] K. Oganessian, H. Avakian, N. Bianchi and A. Kotzinian, *Sin(phi) azimuthal asymmetry in semiinclusive electroproduction on longitudinally polarized nucleon*, in *8th International Conference on the Structure of Baryons*, pp. 320–324, 8, 1998, [hep-ph/9808368](#).
- [1228] E. De Sanctis, W. Nowak and K. Oganesian, *Single spin azimuthal asymmetries in the ‘Reduced twist - three approximation’*, *Phys. Lett. B* **483** (2000) 69 [[hep-ph/0002091](#)].
- [1229] A. Vladimirov, V. Moos and I. Scimemi, *Transverse momentum dependent operator expansion at next-to-leading power*, [2109.09771](#).
- [1230] A. Metz and M. Schlegel, *Twist three single spin asymmetries in semiinclusive deep inelastic scattering*, *Eur. Phys. J. A* **22** (2004) 489 [[hep-ph/0403182](#)].
- [1231] L. P. Gamberg, D. S. Hwang, A. Metz and M. Schlegel, *Light-cone divergence in twist-3 correlation functions*, *Phys. Lett. B* **639** (2006) 508 [[hep-ph/0604022](#)].
- [1232] A. Bacchetta, D. Boer, M. Diehl and P. J. Mulders, *Matches and mismatches in the descriptions of semi-inclusive processes at low and high transverse momentum*, *JHEP* **08** (2008) 023 [[0803.0227](#)].

- [1233] A. Bacchetta, G. Bozzi, M. G. Echevarria, C. Pisano, A. Prokudin and M. Radici, *Azimuthal asymmetries in unpolarized SIDIS and Drell-Yan processes: a case study towards TMD factorization at subleading twist*, 1906.07037.
- [1234] A. Chen and J. Ma, *Light-Cone Singularities and Transverse-Momentum-Dependent Factorization at Twist-3*, *Phys. Lett. B* **768** (2017) 380 [1610.08634].
- [1235] A. V. Afanasev and C. E. Carlson, *Beam Single-Spin Asymmetry in Semi-Inclusive Deep Inelastic Scattering*, *Phys. Rev. D* **74** (2006) 114027 [hep-ph/0603269].
- [1236] W. Mao and Z. Lu, *Beam single spin asymmetry of neutral pion production in semi-inclusive deep inelastic scattering*, *Phys. Rev. D* **87** (2013) 014012 [1210.4790].
- [1237] Z. Lu and I. Schmidt, *T-odd quark-gluon-quark correlation function in the diquark model*, *Phys. Lett. B* **712** (2012) 451 [1202.0700].
- [1238] W. Mao, Z. Lu and B.-Q. Ma, *Transverse single-spin asymmetries of pion production in semi-inclusive DIS at subleading twist*, *Phys. Rev. D* **90** (2014) 014048 [1405.3876].
- [1239] W. Mao, Z. Lu, B.-Q. Ma and I. Schmidt, *Double spin asymmetries  $A_{LT}^{\cos \phi_S}$  and  $A_{LT}^{\cos(2\phi_h - \phi_S)}$  in semi-inclusive DIS*, *Phys. Rev. D* **91** (2015) 034029 [1412.7390].
- [1240] Z. Lu, *Single-spin asymmetries in electroproduction of pions on the longitudinally polarized nucleon targets*, *Phys. Rev. D* **90** (2014) 014037 [1404.4229].
- [1241] W. Mao, X. Wang, X. Du, Z. Lu and B.-Q. Ma, *On the  $\cos \phi_h$  asymmetry in electroproduction of pions in double longitudinally polarized process*, *Nucl. Phys. A* **945** (2016) 153.
- [1242] Y. Yang, W. Mao and Z. Lu, *Single spin asymmetry in transverse polarized proton production and  $\Lambda$  production in semi-inclusive DIS at twist-3*, *Eur. Phys. J. Plus* **134** (2019) 259 [1808.10565].
- [1243] X.-D. Ji and Z.-K. Zhu, *Quark fragmentation functions in low-energy chiral theory*, hep-ph/9402303.
- [1244] L. P. Gamberg, D. S. Hwang and K. A. Oganessyan, *Chiral odd fragmentation functions in single pion inclusive electroproduction*, *Phys. Lett. B* **584** (2004) 276 [hep-ph/0311221].
- [1245] Z. Lu and I. Schmidt, *Twist-3 fragmentation functions in a spectator model with gluon rescattering*, *Phys. Lett. B* **747** (2015) 357 [1501.04379].
- [1246] Y. Yang, Z. Lu and I. Schmidt, *Twist-3 T-odd fragmentation functions  $G^\perp$  and  $\tilde{G}^\perp$  in a spectator model*, *Phys. Lett. B* **761** (2016) 333 [1607.01638].
- [1247] B. Pasquini and S. Rodini, *The twist-three distribution  $e^q(x, k_\perp)$  in a light-front model*, *Phys. Lett. B* **788** (2019) 414 [1806.10932].
- [1248] A. Mukherjee and R. Korrapati, *Twist Three Distribution  $f_\perp(x, k^\perp)$  in Light-front Hamiltonian Approach*, *Mod. Phys. Lett. A* **26** (2011) 2653 [1005.2830].

- [1249] M. Burkardt and Y. Koike, *Violation of sum rules for twist three parton distributions in QCD*, *Nucl. Phys. B* **632** (2002) 311 [[hep-ph/0111343](#)].
- [1250] F. Aslan and M. Burkardt, *Singularities in Twist-3 Quark Distributions*, *Phys. Rev. D* **101** (2020) 016010 [[1811.00938](#)].
- [1251] S. Bhattacharya and A. Metz, *Burkhardt-Cottingham-type sum rules for light-cone and quasi-PDFs*, [2105.07282](#).
- [1252] M. Burkardt, *On the possible violation of sum rules for higher twist parton distributions*, *Phys. Rev. D* **52** (1995) 3841 [[hep-ph/9505226](#)].
- [1253] A. V. Efremov and P. Schweitzer, *The Chirally odd twist 3 distribution  $e(a)(x)$* , *JHEP* **08** (2003) 006 [[hep-ph/0212044](#)].
- [1254] H. Avakian, A. Efremov, P. Schweitzer, O. Teryaev, F. Yuan and P. Zavada, *Insights on non-perturbative aspects of TMDs from models*, *Mod. Phys. Lett. A* **24** (2009) 2995 [[0910.3181](#)].
- [1255] A. P. Bukhvostov, E. A. Kuraev and L. N. Lipatov, *Deep inelastic scattering by a polarized target in quantum chromodynamics*, *Sov. Phys. JETP* **60** (1984) 22.
- [1256] A. P. Bukhvostov, E. A. Kuraev and L. N. Lipatov, *Deep inelastic scattering on a polarized target in Abelian gauge theory*, *Sov. J. Nucl. Phys.* **39** (1984) 121.
- [1257] A. V. Belitsky and D. Mueller, *Scale dependence of the chiral odd twist - three distributions  $h\text{-}L(x)$  and  $e(x)$* , *Nucl. Phys. B* **503** (1997) 279 [[hep-ph/9702354](#)].
- [1258] J. Balla, M. V. Polyakov and C. Weiss, *Nucleon matrix elements of higher twist operators from the instanton vacuum*, *Nucl. Phys. B* **510** (1998) 327 [[hep-ph/9707515](#)].
- [1259] B. Dressler and M. V. Polyakov, *On the twist - three contribution to  $h(L)$  in the instanton vacuum*, *Phys. Rev. D* **61** (2000) 097501 [[hep-ph/9912376](#)].
- [1260] EUROPEAN MUON collaboration, J. J. Aubert et al., *Measurement of Hadronic Azimuthal Distributions in Deep Inelastic Muon Proton Scattering*, *Phys. Lett.* **130B** (1983) 118.
- [1261] EUROPEAN MUON collaboration, M. Arneodo et al., *Measurement of Hadron Azimuthal Distributions in Deep Inelastic Muon Proton Scattering*, *Z. Phys. C* **34** (1987) 277.
- [1262] E665 collaboration, M. R. Adams et al., *Perturbative QCD effects observed in 490-GeV deep inelastic muon scattering*, *Phys. Rev. D* **48** (1993) 5057.
- [1263] A. Kotsinian, K. Oganesian, H. Avakian and E. De Sanctis, *Single target spin asymmetries in semiinclusive pion electroproduction on longitudinally polarized protons*, *Nucl. Phys. B Proc. Suppl.* (1999) [[hep-ph/9908466](#)].
- [1264] M. Boglione and P. Mulders, *Azimuthal spin asymmetries in semiinclusive production from positron proton scattering*, *Phys. Lett. B* **478** (2000) 114 [[hep-ph/0001196](#)].

- [1265] K. Oganessian, N. Bianchi, E. De Sanctis and W. Nowak, *Investigation of single spin asymmetries in  $\pi^+$  electroproduction*, *Nucl. Phys. A* **689** (2001) 784 [[hep-ph/0010261](#)].
- [1266] A. Efremov, K. Goeke and P. Schweitzer, *Azimuthal asymmetry in electroproduction of neutral pions in semiinclusive DIS*, *Phys. Lett. B* **522** (2001) 37 [[hep-ph/0108213](#)].
- [1267] A. Efremov, K. Goeke and P. Schweitzer, *Predictions for azimuthal asymmetries in pion and kaon production in SIDIS off a longitudinally polarized deuterium target at HERMES*, *Eur. Phys. J. C* **24** (2002) 407 [[hep-ph/0112166](#)].
- [1268] K. Oganessyan, P. Mulders and E. De Sanctis, *Double spin cos phi asymmetry in semiinclusive electroproduction*, *Phys. Lett. B* **532** (2002) 87 [[hep-ph/0201061](#)].
- [1269] A. Efremov, K. Goeke and P. Schweitzer, *Azimuthal asymmetries at CLAS: extraction of  $e^{**}a(x)$  and prediction of  $A(UL)$* , *Phys. Rev. D* **67** (2003) 114014 [[hep-ph/0208124](#)].
- [1270] K. Oganessyan, L. Asilyan, M. Anselmino and E. De Sanctis, *Spin independent and double spin cos phi asymmetries in semiinclusive pion electroproduction*, *Phys. Lett. B* **564** (2003) 60 [[hep-ph/0208208](#)].
- [1271] B.-Q. Ma, I. Schmidt and J.-J. Yang, *Reanalysis of azimuthal spin asymmetries of meson electroproduction*, *Phys. Rev. D* **66** (2002) 094001 [[hep-ph/0209114](#)].
- [1272] A. Efremov, K. Goeke and P. Schweitzer, *Sivers versus Collins effect in azimuthal single spin asymmetries in pion production in SIDIS*, *Phys. Lett. B* **568** (2003) 63 [[hep-ph/0303062](#)].
- [1273] A. Efremov, K. Goeke and P. Schweitzer, *Collins effect and single spin azimuthal asymmetries in the HERMES and COMPASS experiments*, *Eur. Phys. J. C* **32** (2003) 337 [[hep-ph/0309209](#)].
- [1274] F. Yuan, *The Beam single spin asymmetry in semiinclusive deep inelastic scattering*, *Phys. Lett. B* **589** (2004) 28 [[hep-ph/0310279](#)].
- [1275] P. Schweitzer and A. Bacchetta, *Azimuthal single spin asymmetries in SIDIS in the light of chiral symmetry breaking*, *Nucl. Phys. A* **732** (2004) 106 [[hep-ph/0310318](#)].
- [1276] Y.-k. Song, J.-h. Gao, Z.-t. Liang and X.-N. Wang, *Twist-4 contributions to the azimuthal asymmetry in SIDIS*, *Phys. Rev. D* **83** (2011) 054010 [[1012.4179](#)].
- [1277] J.-H. Gao, A. Schafer and J. Zhou, *Azimuthal asymmetry in SIDIS off nuclei as probe for  $\hat{q}$* , *Phys. Rev. D* **85** (2012) 074027 [[1111.1633](#)].
- [1278] Y.-k. Song, J.-h. Gao, Z.-t. Liang and X.-N. Wang, *Azimuthal asymmetries in semi-inclusive DIS with polarized beam and/or target and their nuclear dependences*, *Phys. Rev. D* **89** (2014) 014005 [[1308.1159](#)].
- [1279] L. Chen, J.-h. Gao and Z.-t. Liang, *Nuclear dependencies of azimuthal asymmetries in the Drell-Yan process*, *Phys. Rev. C* **89** (2014) 035204 [[1308.3746](#)].

- [1280] A. Afanasev and C. E. Carlson, *Single spin beam asymmetry in semiexclusive deep inelastic electroproduction*, in *Intersections of particle and nuclear physics. Proceedings, 8th Conference, CIPANP 2003, New York, USA, May 19-24, 2003*, hep-ph/0308163.
- [1281] X.-D. Ji, *Deeply virtual Compton scattering*, *Phys. Rev. D* **55** (1997) 7114 [hep-ph/9609381].
- [1282] K. Kumericki, S. Liuti and H. Moutarde, *GPD phenomenology and DVCS fitting - Entering the high-precision era*, 1602.02763.
- [1283] B. Kriesten, S. Liuti, L. Calero-Diaz, D. Keller, A. Meyer, G. R. Goldstein et al., *Extraction of generalized parton distribution observables from deeply virtual electron proton scattering experiments*, *Phys. Rev. D* **101** (2020) 054021 [1903.05742].
- [1284] D. E. Soper, *The Parton Model and the Bethe-Salpeter Wave Function*, *Phys. Rev. D* **15** (1977) 1141.
- [1285] M. Burkardt, *Impact parameter dependent parton distributions and off forward parton distributions for  $\zeta \rightarrow 0$* , *Phys. Rev. D* **62** (2000) 071503 [hep-ph/0005108].
- [1286] M. Diehl, *Generalized parton distributions*, *Phys. Rept.* **388** (2003) 41 [hep-ph/0307382].
- [1287] A. Belitsky and A. Radyushkin, *Unraveling hadron structure with generalized parton distributions*, *Phys. Rept.* **418** (2005) 1 [hep-ph/0504030].
- [1288] A. V. Belitsky, X.-d. Ji and F. Yuan, *Quark imaging in the proton via quantum phase space distributions*, *Phys. Rev. D* **69** (2004) 074014 [hep-ph/0307383].
- [1289] E. P. Wigner, *On the quantum correction for thermodynamic equilibrium*, *Phys. Rev.* **40** (1932) 749.
- [1290] M. Hillery, R. F. O'Connell, M. O. Scully and E. P. Wigner, *Distribution functions in physics: Fundamentals*, *Phys. Rept.* **106** (1984) 121.
- [1291] X.-d. Ji, *Viewing the proton through 'color' filters*, *Phys. Rev. Lett.* **91** (2003) 062001 [hep-ph/0304037].
- [1292] C. Lorcé and B. Pasquini, *Multipole decomposition of the nucleon transverse phase space*, *Phys. Rev. D* **93** (2016) 034040 [1512.06744].
- [1293] M. G. Echevarria, A. Idilbi, K. Kanazawa, C. Lorcé, A. Metz, B. Pasquini et al., *Proper definition and evolution of generalized transverse momentum dependent distributions*, *Phys. Lett. B* **759** (2016) 336 [1602.06953].
- [1294] I. Balitsky and G. A. Chirilli, *Conformal invariance of transverse-momentum dependent parton distributions rapidity evolution*, *Phys. Rev. D* **100** (2019) 051504 [1905.09144].
- [1295] Y. Hatta, B.-W. Xiao and F. Yuan, *Probing the Small-  $x$  Gluon Tomography in Correlated Hard Diffractive Dijet Production in Deep Inelastic Scattering*, *Phys. Rev. Lett.* **116** (2016) 202301 [1601.01585].

- [1296] T. Altinoluk, N. Armesto, G. Beuf and A. H. Rezaeian, *Diffractive Dijet Production in Deep Inelastic Scattering and Photon-Hadron Collisions in the Color Glass Condensate*, *Phys. Lett. B* **758** (2016) 373 [[1511.07452](#)].
- [1297] J. Zhou, *Elliptic gluon generalized transverse-momentum-dependent distribution inside a large nucleus*, *Phys. Rev. D* **94** (2016) 114017 [[1611.02397](#)].
- [1298] X. Ji, F. Yuan and Y. Zhao, *Hunting the Gluon Orbital Angular Momentum at the Electron-Ion Collider*, *Phys. Rev. Lett.* **118** (2017) 192004 [[1612.02438](#)].
- [1299] Y. Hagiwara, Y. Hatta, B.-W. Xiao and F. Yuan, *Elliptic Flow in Small Systems due to Elliptic Gluon Distributions?*, *Phys. Lett. B* **771** (2017) 374 [[1701.04254](#)].
- [1300] E. Iancu and A. H. Rezaeian, *Elliptic flow from color-dipole orientation in pp and pA collisions*, *Phys. Rev. D* **95** (2017) 094003 [[1702.03943](#)].
- [1301] Y. Hagiwara, Y. Hatta, R. Pasechnik, M. Tasevsky and O. Teryaev, *Accessing the gluon Wigner distribution in ultraperipheral pA collisions*, *Phys. Rev. D* **96** (2017) 034009 [[1706.01765](#)].
- [1302] S. Bhattacharya, A. Metz and J. Zhou, *Generalized TMDs and the exclusive double Drell-Yan process*, *Phys. Lett. B* **771** (2017) 396 [[1702.04387](#)].
- [1303] Y. Hagiwara, C. Zhang, J. Zhou and Y.-j. Zhou, *Probing the gluon tomography in photoproduction of dipion*, *Phys. Rev. D* **104** (2021) 094021.
- [1304] F. Salazar and B. Schenke, *Diffractive dijet production in impact parameter dependent saturation models*, *Phys. Rev. D* **100** (2019) 034007 [[1905.03763](#)].
- [1305] A. V. Efremov and A. V. Radyushkin, *Factorization and Asymptotical Behavior of Pion Form-Factor in QCD*, *Phys. Lett. B* **94B** (1980) 245.
- [1306] G. P. Lepage and S. J. Brodsky, *Exclusive Processes in Quantum Chromodynamics: Evolution Equations for Hadronic Wave Functions and the Form-Factors of Mesons*, *Phys. Lett. B* **87B** (1979) 359.
- [1307] S. Bhattacharya, A. Metz, V. K. Ojha, J.-Y. Tsai and J. Zhou, *Exclusive double quarkonium production and generalized TMDs of gluons*, [1802.10550](#).
- [1308] R. Boussarie, Y. Hatta, B.-W. Xiao and F. Yuan, *Probing the Weizsäcker-Williams gluon Wigner distribution in pp collisions*, *Phys. Rev. D* **98** (2018) 074015 [[1807.08697](#)].
- [1309] M. Wakamatsu, *Chiral odd distribution functions in the chiral quark soliton model*, *Phys. Lett. B* **509** (2001) 59 [[hep-ph/0012331](#)].
- [1310] C. Lorce, B. Pasquini, X. Xiong and F. Yuan, *The quark orbital angular momentum from Wigner distributions and light-cone wave functions*, *Phys. Rev. D* **85** (2012) 114006 [[1111.4827](#)].

- [1311] Y. Hatta, *Notes on the orbital angular momentum of quarks in the nucleon*, *Phys.Lett.* **B708** (2012) 186 [1111.3547].
- [1312] A. Rajan, A. Courtoy, M. Engelhardt and S. Liuti, *Parton Transverse Momentum and Orbital Angular Momentum Distributions*, *Phys. Rev.* **D94** (2016) 034041 [1601.06117].
- [1313] A. Rajan, M. Engelhardt and S. Liuti, *Lorentz Invariance and QCD Equation of Motion Relations for Generalized Parton Distributions and the Dynamical Origin of Proton Orbital Angular Momentum*, *Phys. Rev.* **D98** (2018) 074022 [1709.05770].
- [1314] K. Kanazawa, C. Lorcé, A. Metz, B. Pasquini and M. Schlegel, *Twist-2 generalized transverse-momentum dependent parton distributions and the spin/orbital structure of the nucleon*, *Phys.Rev.* **D90** (2014) 014028 [1403.5226].
- [1315] M. E. A. Rajan, O. Alkasassbeh and S. Liuti, *Transverse Spin Sum Rule*, 2022.
- [1316] D. Kiptily and M. Polyakov, *Genuine twist three contributions to the generalized parton distributions from instantons*, *Eur. Phys. J.* **C37** (2004) 105 [hep-ph/0212372].
- [1317] I. I. Balitsky and V. M. Braun, *Evolution Equations for QCD String Operators*, *Nucl. Phys. B* **311** (1989) 541.
- [1318] N. Kivel, M. V. Polyakov, A. Schafer and O. V. Teryaev, *On the Wandzura-Wilczek approximation for the twist - three DVCS amplitude*, *Phys. Lett. B* **497** (2001) 73 [hep-ph/0007315].
- [1319] C. Lorcé, *Spin-Orbit correlations in the nucleon*, *Phys. Lett.* **B735** (2014) 344 [1401.7784].
- [1320] A. Bhoonah and C. Lorcé, *Quark transverse spin-orbit correlations*, *Phys. Lett. B* **774** (2017) 435 [1703.08322].
- [1321] Y. Guo, X. Ji and K. Shiells, *Novel twist-three transverse-spin sum rule for the proton and related generalized parton distributions*, *Nucl. Phys. B* **969** (2021) 115440 [2101.05243].
- [1322] X. Ji, X. Xiong and F. Yuan, *Transverse Polarization of the Nucleon in Parton Picture*, *Phys. Lett. B* **717** (2012) 214 [1209.3246].
- [1323] Y. Hagiwara, Y. Hatta and T. Ueda, *Wigner, Husimi, and generalized transverse momentum dependent distributions in the color glass condensate*, *Phys. Rev. D* **94** (2016) 094036 [1609.05773].
- [1324] S. Liuti, *DVCS and TCS in New Helicity Amplitudes Formalism*, in *Workshop on High-Intensity Photon Sources*, pp. 48–50, 4, 2017.
- [1325] X. Ji, X. Xiong and F. Yuan, *Proton Spin Structure from Measurable Parton Distributions*, *Phys. Rev. Lett.* **109** (2012) 152005 [1202.2843].
- [1326] M. Burkardt, *Parton Orbital Angular Momentum and Final State Interactions*, *Phys.Rev.* **D88** (2013) 014014 [1205.2916].

- [1327] G. M. de Divitiis, R. Petronzio and N. Tantalo, *On the extraction of zero momentum form factors on the lattice*, *Phys. Lett.* **B718** (2012) 589 [[1208.5914](#)].
- [1328] T. Liu, *Quark orbital motions from Wigner distributions*, [1406.7709](#).
- [1329] A. Mukherjee, S. Nair and V. K. Ojha, *Quark Wigner Distributions and Orbital Angular Momentum in Light-front Dressed Quark Model*, *Phys. Rev. D* **90** (2014) 014024 [[1403.6233](#)].
- [1330] Y. Hagiwara and Y. Hatta, *Use of the Husimi distribution for nucleon tomography*, *Nucl. Phys.* **A940** (2015) 158 [[1412.4591](#)].
- [1331] A. Mukherjee, S. Nair and V. K. Ojha, *Wigner distributions for gluons in a light-front dressed quark model*, *Phys. Rev. D* **91** (2015) 054018 [[1501.03728](#)].
- [1332] K. Husimi, *Some formal aspects of the density matrix*, *Proc. Phys. Math. Soc. Jpn.* **22** (1940) 264.
- [1333] M. A. Ebert, *Analytic results for Sudakov form factors in QCD*, [2110.11360](#).
- [1334] S. Moch, J. A. M. Vermaseren and A. Vogt, *The Quark form-factor at higher orders*, *JHEP* **08** (2005) 049 [[hep-ph/0507039](#)].
- [1335] A. Grozin, J. M. Henn, G. P. Korchemsky and P. Marquard, *Three Loop Cusp Anomalous Dimension in QCD*, *Phys. Rev. Lett.* **114** (2015) 062006 [[1409.0023](#)].
- [1336] G. Billis, F. J. Tackmann and J. Talbert, *Higher-Order Sudakov Resummation in Coupled Gauge Theories*, *JHEP* **03** (2020) 182 [[1907.02971](#)].